INAF
ISTITUTO NAZIONALE
DI ASTROFISICA
NATIONAL INSTITUTE
FOR ASTROPHYSICS

Publication Year	2015
Acceptance in OA	2020-04-15T16:04:46Z
Title	Advancing Astrophysics with the Square Kilometre Array (AASKA14)
Authors	Bourke, Tyler. L., Braun, Robert, Fender, Rob, GOVONI, FEDERICA, Green, Jimi, Hoare, Melvin, Jarvis, Matt, Johnston-Hollitt, Melanie, Keane, Evan, Koopmans, Leon, Kramer, Michael, Maartens, Roy, Macquart, Jean-Pierre, Mellema, Garrelt, Oosterloo, Tom, PRANDONI, ISABELLA, Pritchard, Jonathan, Santos, Mario, Seymour, Nick, Stappers, Ben, Staveley-Smith, Lister, Wu Tian, Wen, UMANA, Grazia Maria Gloria, Wagg, Jeff
Handle	http://hdl.handle.net/20.500.12386/24059
Journal	POS PROCEEDINGS OF SCIENCE
Volume	215

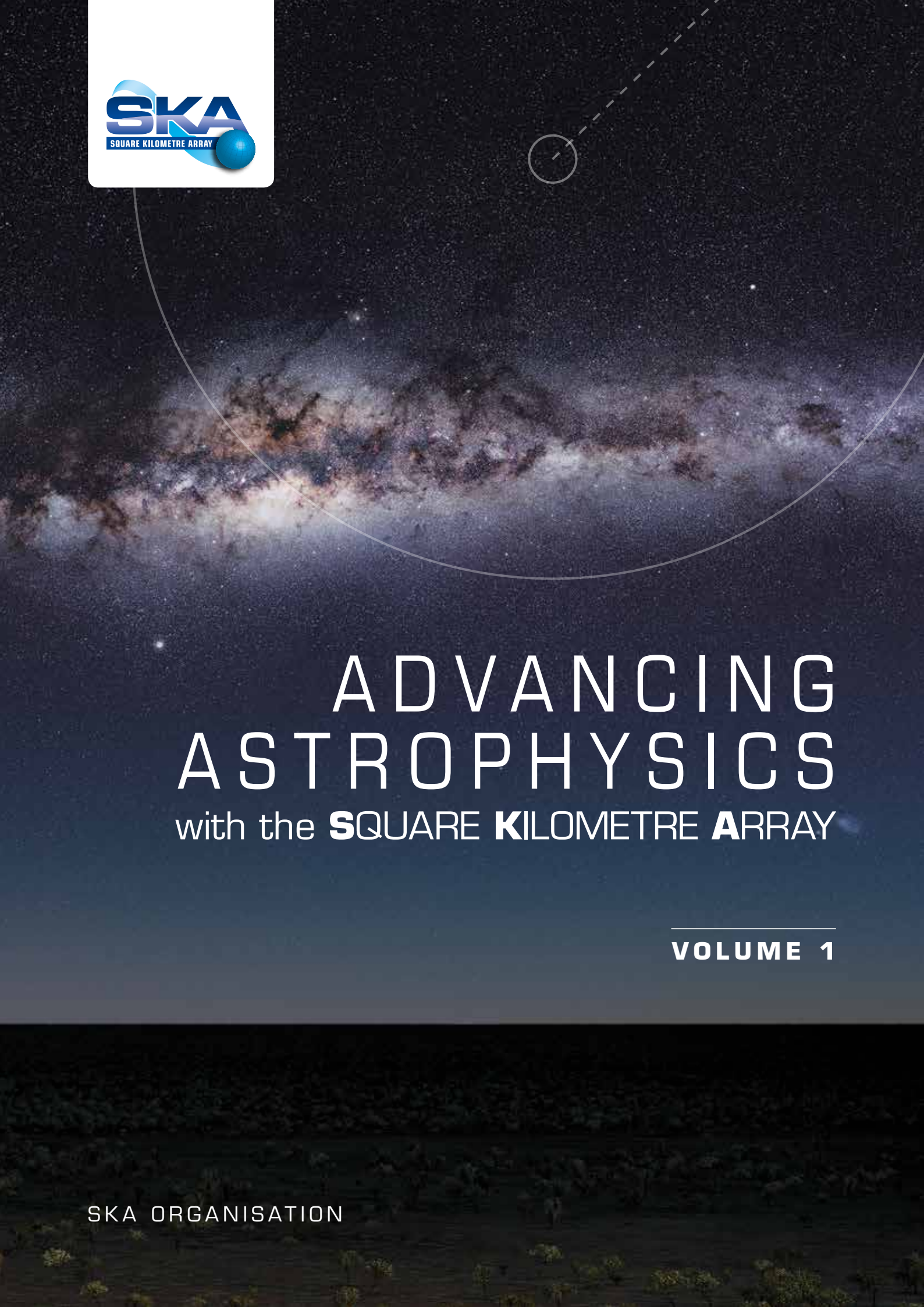

ADVANCING ASTROPHYSICS

with the SQUARE KILOMETRE ARRAY

VOLUME 1

SKA ORGANISATION

Advancing Astrophysics with the Square Kilometre Array

Volume 1

ISBN: 978-1-909204-70-6

Cover design: Carbon Creative | www.carboncreative.net
Cover: Artist impression of the SKA sites at night, Credit: SKA Organisation; The Milky Way panorama, Credit: ESO/S. Brunier

Design, layout and production by Bookcreateservice Ltd
for the SKA Organisation Communications, Outreach and Education Office.

First published in 2015 by Dolman Scott Ltd for SKA Organisation.

©Copyright of the papers owned by the author(s) under the terms of the Creative Commons Attribution-Non Commercial-Share Alike Licence.

Advancing Astrophysics with the Square Kilometre Array © 2015 by SKA Organisation.

All rights reserved. No part of this publication may be copied, stored in a retrieval system, or transmitted in any form, or by any means electronic, mechanical, optical, or otherwise except with written permission of the publisher. Except for review purposes only.

About the SKA

The Square Kilometre Array (SKA) project is an international collaboration to build the world's largest radio telescope. The SKA aims to conduct transformational science that will improve our understanding of the Universe and the laws of fundamental physics. It will monitor the sky in unprecedented detail and map it hundreds of times faster than any current facility.

The SKA is not a single telescope but a collection of telescopes called an array, working together over long distances – tens to hundreds of kilometres and eventually thousands of kilometres. The SKA's construction is divided into two phases: Phase 1 in Australia for SKA1-LOW and South Africa for SKA1-MID; and Phase 2 for SKA2 expanding further in Australia and South Africa as well as into other African countries. Scientific operations are scheduled to begin in the early 2020s.

Supported by 20 countries around the world, the SKA is being designed by more than 500 of the world's finest scientists and engineers drawn from more than 100 companies and research institutions.

Panorama of the Murchison from the SKA site in Australia. Credit: CSIRO

Panorama of the Karoo near the SKA site in South Africa. Credit: Rob Millenaar (ASTRON)

Preface

In 2014 it was 10 years since the publication of the comprehensive *Science with the Square Kilometre Array* book and 15 years since the first such volume appeared in 1999. In that time numerous and unexpected advances have been made in the fields of astronomy and physics relevant to the capabilities of the Square Kilometre Array (SKA). The SKA itself progressed from an idea to a developing reality with a Phase 1 design (SKA1) now well-advanced and scientific operations scheduled to begin in the early 2020s.

To facilitate the publication of a new, updated science book relevant to the current astrophysical context, the meeting *Advancing Astrophysics with the Square Kilometre Array* was held from 9 - 13 June, 2014, in Giardini Naxos, Sicily.

Articles were solicited from the scientific community for that meeting to document the scientific advances enabled by the first phase of the SKA and those pertaining to future SKA deployments. The chapters reproduced in these volumes are the direct result of that meeting.

The papers are published online in the Proceedings of Science (PoS) at:

http://pos.sissa.it/

This book is available in electronic format on the SKA website at

www.skatelescope.org/books/

The conference was considered by all participants to have been a major success and the organisers would like to thank the following event sponsors for their generous support of the event:

The research leading to these results has received funding from the European Commission Seventh Framework Programme (FP/2007-2013) under grant agreement No 283393 (RadioNet3).

The editorial board

Tyler L. Bourke, Robert Braun, Rob Fender, Federica Govoni, Jimi Green, Melvin Hoare, Matt Jarvis, Melanie Johnston-Hollitt, Evan Keane, Leon Koopmans, Michael Kramer, Roy Maartens, Jean-Pierre Macquart, Garrelt Mellema, Tom Oosterloo, Isabella Prandoni, Jonathan Pritchard, Mario Santos, Nick Seymour, Ben Stappers, Lister Staveley-Smith, Wen Wu Tian, Grazia Umana, Jeff Wagg.

27 July 2015

Contents
Volume 1

Introduction

Advancing Astrophysics with the Square Kilometre Array
R. Braun , T.L Bourke, J.A Green, E. Keane and J. Wagg 3

The Cradle of Life

SKA and the Cradle of Life
M. Hoare, L Perez, T.L Bourke, L Testi, I Jimenez-Serra, P Zarka, A.P.V. Siemion, H.J. van-Langevelde, L Loinard, G Anglada, A Belloche, P Bergman, R. Booth, P Caselli, C.J Chandler, C Codella, G Hallinan, J Lazio, I.S Morrison, L Podio, A Remijan and J Tarter 15

Searching for Extraterrestrial Intelligence with the Square Kilometre Array
A. Siemion, J. Benford, J. Cheng-Jin, J. Chennamangalam, J.M. Cordes, H.D.E. Falcke, S.T. Garrington, M.A. Garrett, L. Gurvits, M. Hoare, E. Korpela, J. Lazio, D. Messerschmitt, I. Morrison, T. O'Brien, Z. Paragi, A. Penny, L. Spitler, J. Tarter and D. Werthimer 27

Protoplanetary disks and the dawn of planets with SKA
L. Testi, L Perez, I Jimenez-Serra, M.G Hoare, A Boley, T.L Bourke, J.R Brucato, P Caselli, C.J Chandler, A Isella, J Lazio, M.E Palumbo, L Podio, A Remijan, J Tarter and D.J Wilner 43

The impact of SKA on Galactic Radioastronomy: continuum observations
G. Umana, C. Trigilio, L. Cerrigone, R. Cesaroni, A.A Zijlstra, M. Hoare, K. Weis, A. Beasley, D. Bomans, G. Hallinan, S. Molinari, R. Taylor, L. Testi and M. Thompson 55

Maser Astrometry with VLBI and the SKA
J. Green, H.J. Van Langevelde, A. Brunthaler, S. Ellingsen, H. Imai, W.H.T. Vlemmings, M.J. Reid and A.M.S. Richards 73

Magnetospheric Radio Emissions from Exoplanets with the SKA
P. Zarka, J. Lazio and G. Hallinan 83

Radio Jets in Young Stellar Objects with the SKA
G. Anglada, L.F. Rodríguez and C. Carrasco-Gonzalez 101

Complex organic molecules in protostellar environments in the SKA era
C. Codella, L Podio, F Fontani, I Jimenez-Serra, P Caselli, M.E Palumbo, A Lopez-Sepulcre, M.T Beltran, B Lefloch, J.R Brucato, S Viti and L Testi 109

Studies of Anomalous Microwave Emission (AME) with the SKA
C. Dickinson, Y. Ali-Hamoud, R.J. Beswick, S. Casassus, K. Cleary, B. Draine, R. Genova-Santos, K. Grainge, T.C Hoang, A. Lazarian, E. Murphy, R. Paladini, M.W Peel, Y. Perrott, J.A. Rubino-Martin, A. Scaife, C. Tibbs, L. Verstraete, M. Vidal, R.A. Watson and N. Ysard 127

OH masers in the Milky Way and Local Group galaxies in the SKA era
S. Etoka, D. Engels, H. Imai, J. Dawson, S. Ellingsen, L. Sjouwerman and H. van Langevelde 139

The ionised,radical and molecular Milky Way: spectroscopic surveys with the SKA
M. Thompson, H. Beuther, C. Dickinson, J. Mottram, P. Klaassen, A. Ginsburg,S. Longmore, A. Remijan and K.M. Menten 153

SKA tomography of Galactic star-forming regions and spiral arms
L. Loinard, M. Thompson, M. Hoare, H.J. van Langevelde, S. Ellingsen, A. Brunthaler, J. Forbrich, K. Rygl, L.F Rodriguez, A.J Mioduszewski, R.M Torres-Lopez, S.A Dzib, G.N Ortiz-Leon, T.L Bourke and J.A Green 163

Fundamental Physics with Pulsars

Pulsar Science with the SKA
M. Kramer and B. Stappers 173

Gravitational Wave Astronomy with the SKA
G. Janssen, G. Hobbs, M. McLaughlin, C. Bassa, A. Deller, M. Kramer, K. Lee, C. Mingarelli, P. Rosado, S. Sanidas, A. Sesana, L. Shao, I. Stairs, B. Stappers and J. Verbiest 185

Understanding pulsar magnetospheres with the SKA
A. Karastergiou, S. Johnston, A Karastergiou, S Johnston, N Andersson, R Breton, P Brook, C Gwinn, N Lewandowska, E Keane, M Kramer, J.P Macquart, M Serylak, R Shannon, B Stappers, J van Leeuwen, J Verbiest, P Weltevrede and G Wright 205

Understanding the Neutron Star Population with the SKA
T.M Tauris, V.M Kaspi, R.P Breton, A.T Deller, E.F Keane, M Kramer, D.R Lorimer, M.A McLaughlin, A Possenti, P.S Ray, B.W Stappers and P Weltevrede 225

A Cosmic Census of Radio Pulsars with the SKA
E.F Keane, B Bhattacharyya, M Kramer, B.W Stappers, S.D Bates, M Burgay, S Chatterjee, D.J Champion, R.P Eatough, J.W.T Hessels, G Janssen, K.J Lee, J van Leeuwen, J. Margueron, M Oertel, A Possenti, S Ransom, G. Theureau and P Torne 251

Three-dimensional Tomography of the Galactic and Extragalactic Magnetoionic Medium with the SKA
J. Han, W. van Straten, J. Lazio, A. Deller, C. Sobey, J. Xu, D. Schnitzeler, H. Imai, S. Chatterjee, J.P. Macquart, M. Kramer and J.M. Cordes 273

Testing Gravity with Pulsars in the SKA Era
L. Shao, I. Stairs, J. Antoniadis, A. Deller, P. Freire, J. Hessels, G. Janssen, M. Kramer, J. Kunz, C. Laemmerzahl, V. Perlick, A. Possenti, S. Ransom, B. Stappers and W. van Straten 289

Probing the neutron star interior and the Equation of State of cold dense matter with the SKA
A. Watts, C.M. Espinoza, R. Xu, N. Andersson, J. Antoniadis, D. Antonopoulou, S. Buchner, S. Datta, P. Demorest, P. Freire, J. Hessels, J. Margueron, M. Oertel, A. Patruno, A. Possenti, S. Ransom, I. Stairs and B. Stappers 309

Observing Radio Pulsars in the Galactic Centre with the Square Kilometre Array
R. Eatough, T.J.W Lazio, J Casanellas, S Chatterjee, J.M Cordes, P.B Demorest, M Kramer, K.J Lee, K Liu, S.M Ransom and N Wex 331

Pulsar Wind Nebulae in the SKA era
J. Gelfand, R. Breton, C.U. Ng, J. Hessels, B. Stappers, M. Roberts and A. Possenti 345

Pulsars in Globular Clusters with the SKA
J. Hessels, A Possenti, M Bailes, C. Bassa, P.C.C Freire, D.R Lorimer, R Lynch, S.M Ransom and I.H Stairs 355

Magnetism

Using SKA Rotation Measures to Reveal the Mysteries of the Magnetised Universe
M. Johnston-Hollitt, F. Govoni, R. Beck, S. Dehghan, L. Pratley, T. Akahori, G. Heald, I. Agudo, A. Bonafede, E. Carretti, T. Clarke, S. Colafrancesco, T.A. Ensslin, L. Feretti, B. Gaensler, M. Haverkorn, S.A. Mao, N. Oppermann, L. Rudnick, A. Scaife, D. Schnitzeler, J. Stil, A.R. Taylor and V. Vacca 371

Studies of Relativistic Jets in Active Galactic Nuclei with SKA
I. Agudo, M. Boettcher, H.D.E. Falcke, M. Georganopoulos, G. Ghisellini, G. Giovannini, M. Giroletti, L. Gurvits, J.L. Gómez, R. Laing, M. Lister, J.M. Martí, E. Meyer, Y. Mizuno, S. O'Sullivan, P. Padovani, Z. Paragi, M. Perucho, D. Schleicher, L. Stawarz, N. Vlahakis and J. Wardle 389

Structure, dynamical impact and origin of magnetic fields in nearby galaxies in the SKA era
R. Beck, D. Bomans, S. Colafrancesco, R.J. Dettmar, K. Ferrière, A. Fletcher, G. Heald, V. Heesen, C. Horellou, M. Krause, Y.Q. Lou, S.A. Mao, R. Paladino, E. Schinnerer, D. Sokoloff, J. Stil and F. Tabatabaei 407

Unravelling the origin of large-scale magnetic fields in galaxy clusters and beyond through Faraday Rotation Measures with the SKA
A. Bonafede, F. Vazza, M. Brüggen, T. Akahori, E. Carretti, S. Colafrancesco, L. Feretti, C. Ferrari, G. Giovannini, F. Govoni, M. Johnston-Hollitt, M. Murgia, A. Scaife, V. Vacca, F. Govoni, L. Rudnick and A. Scaife 425

Measuring magnetism in the Milky Way with the Square Kilometre Array
M. Haverkorn, T. Akahori, E. Carretti, K. Ferrière, P. Frick, B. Gaensler, G. Heald, M. Johnston-Hollitt, D. Jones, T. Landecker, S.A. Mao, A. Noutsos, N. Oppermann, W. Reich, T. Robishaw, A. Scaife, D. Schnitzeler, R. Stepanov, X. Sun and R. Taylor 435

Filaments of the radio cosmic web: opportunities and challenges for SKA
F. Vazza, C. Ferrari, A. Bonafede, M. Brüggen, C. Gheller, R. Braun and S. Brown 453

Probing the nature of Dark Matter with the SKA
S. Colafrancesco, M. Regis, P. Marchegiani, G. Beck, R. Beck, H. Zechlin, A. Lobanov and D. Horns 463

Using Tailed Radio Galaxies to Probe the Environment and Magnetic Field of Galaxy Clusters in the SKA Era
M. Johnston-Hollitt, S. Dehghan and L. Pratley 473

SKA studies of in situ synchrotron radiation from molecular clouds
C. Dickinson, R. Beck, R. Crocker, R.M Crutcher, R.D. Davies, K. Ferrière, G. Fuller, T.R. Jaffe, D. Jones, P. Leahy, E. Murphy, M.W Peel, E. Orlando, T. Porter, R.J Protheroe, A. Strong, T. Robishaw, R.A. Watson and F. Yusef-Zadeh 483

Broadband Polarimetry with the Square Kilometre Array: A Unique Astrophysical Probe
B. Gaensler, I. Agudo, T. Akahori, J. Banfield, R. Beck, E. Carretti, J. Farnes, M. Haverkorn, G. Heald, D. Jones, T. Landecker, S.A. Mao, R. Norris, S. O'Sullivan, L. Rudnick, D. Schnitzeler, N. Seymour and X. Sun 493

Mega-parsec scale magnetic fields in low density regions in the SKA era: filaments connecting galaxy clusters and groups
G. Giovannini, A. Bonafede, S. Brown, L. Feretti, C. Ferrari, M. Gitti, F. Govoni, M. Murgia and V. Vacca 505

Cluster magnetic fields through the study of polarized radio halos in the SKA era
F. Govoni, M. Murgia, H. Xu, H. Li, M. Norman, L. Feretti, G. Giovannini, V. Vacca, G. Bernardi, A. Bonafede, G. Brunetti, E. Carretti, S. Colafrancesco, J. Donnert, C. Ferrari, M. Gitti, L. Iapichino, M. Johnston-Hollitt, R. Pizzo and L. Rudnick..... 515

Magnetic Field Tomography in Nearby Galaxies with the Square Kilometre Array
G. Heald, R. Beck, W.J.G. de Blok, R.J. Dettmar, A. Fletcher, B. Gaensler, M. Haverkorn, V. Heesen, C. Horellou, M. Krause, S.A. Mao, N. Oppermann, A. Scaife, D. Sokoloff, J. Stil, F. Tabatabaei, K. Takahashi, A.R. Taylor and A. Williams 525

Kinematics and Dynamics of kiloparsec-scale Jets in Radio Galaxies with SKA
R. Laing..... 537

Giant radio galaxies as probes of the ambient WHIM in the era of the SKA
B. Peng, R.R. Chen and R. Strom..... 547

Measuring Magnetic Fields Near and Far with the SKA via the Zeeman Effect
T. Robishaw, J. Green, G. Surcis, W.H.T. Vlemmings, A.M.S. Richards, S. Etoka, T.L Bourke, V. Fish, M.D Gray, H. Imai, B. Kramer, J. McBride, E. Momjian, A.P. Sarma and A.A Zijlstra..... 557

Stacking for Cosmic Magnetism with SKA Surveys
J. Stil and B. Keller..... 569

SKA Deep Polarization and Cosmic Magnetism
R. Taylor, I. Agudo, T. Akahori, R. Beck, B. Gaensler, G. Heald, M. Johnston-Hollitt, M. Langer, L. Rudnick, A. Scaife, D. Schleicher, J. Stil and D. Ryu..... 579

Statistical methods for the analysis of rotation measure grids in large scale structures in the SKA era
V. Vacca, N. Oppermann, T.A. Ensslin, M. Selig, H. Junklewitz, M. Greiner, J. Jasche, C.A Hales, M. Reneicke, E. Carretti, L. Feretti, C. Ferrari, G. Giovannini, F. Govoni, C. Horellou, S. Ideguchi, M. Johnston-Hollitt, M. Murgia, R. Paladino, R. Pizzo and A. Scaife..... 589

The Hydrogen Universe

HI Science with the Square Kilometre Array
L. Staveley-Smith and T. Oosterloo 601

Exploring Neutral Hydrogen and Galaxy Evolution with the SKA
S. Blyth, T.M. van der Hulst, M.A.W. Verheijen, B. Catinella, F. Fraternali, M.P. Haynes, K.M. Hess, B. Koribalski, C. Lagos, M. Meyer, D. Obreschkow, A. Popping, C. Power, L.L. Verdes-Montenegro and M. Zwaan 611

The SKA view of the Neutral Interstellar Medium in Galaxies
E. de Blok, F. Fraternali, G. Heald, B. Adams, A. Bosma and B. Koribalski 633

Galactic and Magellanic Evolution with the SKA
N.M. McClure-Griffiths, S. Stanimirovic, C. Murray, D. Li, J.M Dickey, E. Vazquez-Semadeni, J.E.G. Peek, M. Putman, S.E. Clark, M.A. Miville-Deschenes, J. Bland-Hawthorn and L. Staveley-Smith 655

Connecting the Baryons: Multiwavelength Data for SKA HI Surveys
M. Meyer, A. Robotham, D. Obreschkow, S. Driver, L. Staveley-Smith and M. Zwaan 679

Observations of the Intergalactic Medium and the Cosmic Web in the SKA era
A. Popping, M. Meyer, L. Staveley-Smith, D. Obreschkow, G. Jozsa and D.J. Pisano 695

Galaxy Formation & Dark Matter Modelling in the Era of the Square Kilometre Array
C. Power, C. Lagos, B. Qin, C. Baugh, D. Cunnama, J. Fu, H. Kim, C. Lacey, L. Li, D. Obreschkow, J. Wang, Y. Wang and M. Zhu 715

Cool Outflows and HI absorbers with SKA
R. Morganti, E.M. Sadler and S. Curran 733

The SKA as a Doorway to Angular Momentum
D. Obreschkow, M. Meyer, A. Popping, C. Power, P. Quinn and L. Staveley-Smith 751

The Physics of the Cold Neutral Medium: Low-frequency Radio Recombination Lines with the Square Kilometre Array
R. Oonk, L. Morabito, F. Salgado, M.C. Toribio, R.J. van Weeren, A.G.G.M. Tielens and H.J.A. Rottgering 765

The Transient Universe

The Transient Universe with the Square Kilometre Array
R. Fender, A. Stewart, J.P. Macquart, I. Donnarumma, T. Murphy, A. Deller, Z. Paragi and S. Chatterjee 781

The SKA View of Gamma-Ray Bursts
D. Burlon, G. Ghirlanda, A. van der Horst, T. Murphy, R.A.M.J. Wijers, B. Gaensler, G. Ghisellini and I. Prandoni 803

Incoherent transient radio emission from stellar-mass compact objects in the SKA era
S. Corbel, J.C.A. Miller-Jones, R. Fender, E. Gallo, T. Maccarone, T. O'Brien, Z. Paragi, M. Rupen, A. Rushton, S. Sabatini, G. Sivakoff, J. Strader and P.A. Woudt 821

SKA as a powerful hunter of jetted Tidal Disruption Events
I. Donnarumma, E.M Rossi, R Fender, S Komossa, Z Paragi, S Van Velzen and I Prandoni 841

Fast Transients at Cosmological Distances with the SKA
J.P. Macquart, E. Keane, K. Grainge, M. McQuinn, R. Fender, J. Hessels, A. Deller, R. Bhat, R. Breton, S. Chatterjee, C. Law, D. Lorimer, E.O. Ofek, M. Pietka, L. Spitler, B. Stappers and C.Trott 857

The SKA contribution to GRB cosmology
L. Amati, S. Capozziello, A.C. Ruggeri, M. De Laurentis, M. Della Valle, O. Luongo and G. Stratta 873

Time domain studies of Active Galactic Nuclei with the Square Kilometre Array
H.E. Bignall, S.D. Croft, T. Hovatta, J.Y. Koay, J. Lazio, J.P. Macquart and C. Reynolds 885

Core-collapse and Type Ia supernovae with the SKA
M. Perez Torres, A Alberdi, R.J. Beswick, P Lundqvist, R Herrero-Illana, C Romero-Canizales, S Ryder, M della Valle, J Conway, J.M. Marcaide, S Mattila, T Murphy and E. Ros 905

Thermal radio emission from novae & symbiotics with the Square Kilometre Array
T. O'Brien, M. Rupen, L. Chomiuk, V. Ribeiro, M. Bode, J. Sokoloski and P.A. Woudt 921

Investigations of supernovae and supernova remnants in the era of SKA
L. Wang, X. Cui, H. Zhu and W. Tian 933

The SKA and the Unknown Unknowns
P. Wilkinson 943

Early Phase Detection and Coverage of Extragalactic and Galactic Black Hole X-ray Transients with SKA
W. Yu, H. Zhang, Z. Yan and W. Zhang 951

Lunar detection of ultra-high-energy cosmic rays and neutrinos with the Square Kilometre Array
J. Bray, J. Alvarez-Muniz, S. Buitink, R. Dagkesamanskii, R.D Ekers, H.D.E. Falcke, K. Gayley, T. Huege, C. James, M. Mevius, R. Mutel, R.J Protheroe, O. Scholten, F. Schroeder, R.E. Spencer and S. ter Veen 961

Precision measurements of cosmic ray air showers with the SKA
T. Huege, J. Bray, S. Buitink, R. Dallier, R.D Ekers, H.D.E. Falcke, C. James, L. Martin, B. Revenu, O. Scholten and F. Schroeder 979

Contents
Volume 2

The Continuum Universe

Revealing the Physics and Evolution of Galaxies and Galaxy Clusters with SKA Continuum Surveys
I. Prandoni and N. Seymour 991

The star-formation history of the Universe with the SKA
M. Jarvis, N. Seymour, J. Afonso, P. Best, R. Beswick, M. Huynh, E. Murphy, I. Prandoni, E. Schinnerer, C. Simpson, M. Vaccari, S. White and I. Heywood 1009

Exploring AGN Activity over Cosmic Time with the SKA
V. Smolcic, P. Padovani, J. Delhaize, I. Prandoni, N. Seymour, M. Jarvis, J. Afonso, M. Magliocchetti, M. Huynh, M. Vaccari and A. Karim 1027

SKA studies of nearby galaxies: star-formation, accretion processes and molecular gas across all environments
R. Beswick, E. Brinks, M. Perez Torres, A.M.S. Richards, S. Aalto, A. Alberdi, M.K. Argo, I. van Bemmel, J.E. Conway, C. Dickinson, D. Fenech, M.D Gray, H.R. Kloeckner, E. Murphy, T.W.B. Muxlow, M.W Peel, A. Rushton and E. Schinnerer 1041

Identifying the first generation of radio powerful AGN in the Universe with the SKA
J. Afonso, J. Casanellas, I. Prandoni, M. Jarvis, S. Lorenzoni, M. Magliocchetti and N. Seymour 1063

Cluster Radio Halos at the crossroads between astrophysics and cosmology in the SKA era
R. Cassano, G. Bernardi, G. Brunetti, M. Brüggen, T. Clarke, D. Dallacasa, K. Dolag, S. Ettori, S. Giacintucci, C. Giocoli, M. Gitti, M. Johnston-Hollitt, R. Kale, M. Markevich, R. Norris, M.P. Pommier, G. Pratt, H.J.A. Rottgering and T. Venturi 1073

Non-thermal emission from galaxy clusters: feasibility study with SKA
C. Ferrari, A. Dabbech, O. Smirnov, S. Makhathini, J.S. Kenyon, M. Murgia, F. Govoni, D. Mary, E. Slezak, F. Vazza, A. Bonafede, M. Brugger, M. Johnston-Hollitt, S. Dehghan, L. Feretti, G. Giovannini, V. Vacca, M.W. Wise, M. Gitti, M. Arnaud, G. Pratt, K. Zarb Adami and S. Colafrancesco 1087

The SKA view of cool-core clusters: evolution of radio mini-halos and AGN feedback
M. Gitti, P. Tozzi, G. Brunetti, R. Cassano, D. Dallacasa, A. Edge, S. Ettori, L. Feretti, C. Ferrari, S. Giacintucci, G. Giovannini, M. Hogan and T. Venturi 1097

Morphological classification of radio sources for galaxy evolution and cosmology with the SKA
S. Makhathini, M. Jarvis, O. Smirnov and I. Heywood 1115

Radio Observations of Star Forming Galaxies in the SKA era
C. Mancuso, A. Lapi, Z.Y. Cai, M. Negrello, G. De Zotti, F. Perrotta and L. Danese 1127

The SKA view of the Interplay between SF and AGN Activity and its role in Galaxy Evolution
K. McAlpine, I. Prandoni, M. Jarvis, N. Seymour, P. Padovani, P. Best, C. Simpson, D. Guidetti, E. Murphy, M. Huynh, M. Vaccari, S. White, R. Beswick, J. Afonso, M. Magliocchetti and M. Bondi 1137

Strong Gravitational Lensing with the SKA
J. McKean, N. Jackson, S Vegetti, M Rybak, S Serjeant, L.V.E. Koopmans, R.B Metcalf, C. Fassnacht, P.J Marshall and M Pandey-Pommier..... 1151

The Astrophysics of Star Formation Across Cosmic Time at >10 GHz with the Square Kilometre Array
E. Murphy, M. Sargent, R. Beswick, C. Dickinson, L. Hunt, M. Huynh, M. Jarvis, A. Karim, M. Krause, I. Prandoni, N. Seymour, E. Schinnerer, F. Tabatabaei, J. Wagg and I. Heywood..... 1169

The SKA Mid-frequency All-sky Continuum Survey: Discovering the unexpected and transforming radio-astronomy
R. Norris, K. Basu, M. Brown, E. Carretti, A.D Kapinska, I. Prandoni, L. Rudnick and N. Seymour.....1183

The physics of the radio emission in the quiet side of the AGN population with the SKA
M. Orienti, F. D'Ammando, M. Giroletti, G. Giovannini and F. Panessa 1201

Radio investigation of Ultra-Luminous X-ray (ULX) Sources in the SKA Era
A. Wolter, A. Rushton, M. Mezcua, D. Cseh, F. Pintore, I. Prandoni, Z. Paragi and L. Zampieri 1209

The SKA and Galaxy Cluster Science with the Sunyaev-Zel'dovich Effect
K. Grainge, S. Borgani, S. Colafrancesco, C. Ferrari, A. Scaife, P. Marchegiani, S. Emritte and J. Weller..... 1221

Astronomy Below the Survey Threshold in the SKA Era
J. Zwart, J. Wall, A. Karim, C. Jackson, R. Norris, J. Condon, J. Afonso, M. Jarvis, F. Navarrete, I. Prandoni, E. Rigby, H.J.A. Rottgering, M. Santos, M. Sargent, N. Seymour, R. Taylor, T. Vernstrom and I. Heywood..... 1233

Unravelling lifecycles and physics of radio-loud AGN in the SKA Era
A.D Kapinska, M. Hardcastle, C. Jackson, T. An, W. Baan and M. Jarvis..... 1247

Cosmology

Overview of Cosmology with the SKA
R. Maartens, F.B. Abdalla, M. Jarvis and M.G Santos..... 1271

Cosmology from HI galaxy surveys with the SKA
F.B. Abdalla, P. Bull, S. Camera, A. Benoit Levy, B. Joachimi, D. Kirk, H.R. Kloeckner, R. Maartens, A. Raccanelli, M.G Santos and G.B. Zhao 1283

Cosmology with SKA Radio Continuum Surveys
M. Jarvis, D. Bacon, C. Blake, M. Brown, S. Lindsay, A. Raccanelli, M. Santos and D.J. Schwarz 1299

Cosmology from a SKA HI intensity mapping survey
M. Santos, P. Bull, D. Alonso, S. Camera, P. Ferreira, G. Bernardi, R. Maartens, M. Viel, F. Villaescusa-Navarro, F.B. Abdalla, M. Jarvis, R.B. Metcalf, A. Pourtsidou and L. Wolz 1315

Cross correlation surveys with the Square Kilometre Array
D. Kirk, F.B. Abdalla, A. Benoit Levy, P. Bull and B. Joachimi 1341

HI galaxy simulations for the SKA: number counts and bias
M. Santos, D. Alonso, P. Bull, M.B. Silva and S. Yahya 1353

Weak gravitational lensing with the Square Kilometre Array
M. Brown, D. Bacon, S. Camera, I. Harrison, B. Joachimi, R.B. Metcalf, A. Pourtsidou, K. Takahashi, J. Zuntz, F.B. Abdalla, S. Bridle, M. Jarvis, T. Kitching, L. Miller and P. Patel 1365

Measuring baryon acoustic oscillations with future SKA surveys
P. Bull, S. Camera, A. Raccanelli, C. Blake, P. Ferreira, M. Santos and D.J. Schwarz 1383

Cosmology on the Largest Scales with the SKA
S. Camera, A. Raccanelli, P. Bull, D. Bertacca, X. Chen, P. Ferreira, M. Kunz, R. Maartens, Y. Mao, M. Santos, P.R. Shapiro, M. Viel and Y. Xu 1399

Real time cosmology - A direct measure of the expansion rate of the Universe with the SKA
H.R. Kloeckner, D. Obreschkow, C. Martins, A. Raccanelli, D. Champion, A.L. Roy, A. Lobanov, J. Wagner and R. Keller 1417

Weak Lensing Simulations for the SKA
P. Patel, I. Harrison, S. Makhathini, F.B. Abdalla, D. Bacon, M. Brown, M. Jarvis, O. Smirnov and I. Heywood 1427

Measuring redshift-space distortion with future SKA surveys
A. Raccanelli, P. Bull, S. Camera, C. Blake, P. Ferreira, R. Maartens, M. Santos, P. Bull, D. Bacon, O. Dore, P. Ferreira, M.G Santos, M. Viel and G.B. Zhao 1445

Testing foundations of modern cosmology with SKA all-sky surveys
D.J. Schwarz, D. Bacon, S. Chen, C. Clarkson, D. Huterer, M. Kunz, R. Maartens, A. Raccanelli, M. Rubart and J.L. Starck 1461

Topology of neutral hydrogen distribution with the Square Kilometre Array
Y. Wang, Y. Xu, F. Wu, X. Chen, X. Wang, J. Kim, C. Park, K.G. Lee and R. Cen 1473

Cosmology with galaxy clusters: studying the Dark Ages and the Epoch of Reionization in the SKA era
S. Colafrancesco, P. Marchegiani and M.S. Emritte 1483

Foreground Subtraction in Intensity Mapping with the SKA
L. Wolz, F.B. Abdalla, D. Alonso, C. Blake, P. Bull, T.C. Chang, P. Ferreira, C.Y. Kuo, M. Santos and J.R. Shaw 1493

Model-independent constraints on dark energy and modified gravity with the SKA
G. Zhao, D. Bacon, R. Maartens, M. Santos and A. Raccanelli 1507

Stacking of SKA data: comparing uv-plane and and image-plane stacking .
K.K. Knudsen, L. Lindroos, W.H.T. Vlemmings, J.E. Conway and I. Marti-Vidal 1519

Epoch of Reionisation

The Cosmic Dawn and Epoch of Reionisation with SKA
L. Koopmans, J Pritchard, G Mellema, J Aguirre, K Ahn, R Barkana, I van Bemmel, G Bernardi, A Bonaldi, F Briggs, A.G. de Bruyn, T.C. Chang, E Chapman, X Chen, B Ciardi, P. Dayal, A. Ferrara, A. Fialkov, F Fiore, K. Ichiki, I.T. Illiev, S Inoue, V Jelic, M Jones, J Lazio, U Maio, S Majumdar, K.J. Mack, A. Mesinger, M.F. Morales, A. Parsons, U.L. Pen, M Santos, R Schneider, B Semelin, R.S de Souza, R Subrahmanyan, T Takeuchi, H Vedantham, J Wagg, R Webster, S Wyithe, K.K. Datta and C. Trott 1529

Probing the First Galaxies and Their Impact on the Intergalactic Medium through 21-cm Observations of the Cosmic Dawn with the SKA
K. Ahn, A. Mesinger, M.A Alvarez and X. Chen 1557

Synergy of CO/[CII]/Lya Line Intensity Mapping with the SKA
T.C. Chang, Y. Gong, M. Santos, M.B. Silva, J. Aguirre, O. Dore and J. Pritchard 1567

Cosmic Dawn and Epoch of Reionization Foreground Removal with the SKA
E. Chapman, A. Bonaldi, G. Harker, V. Jelic, F.B. Abdalla, G. Bernardi, J. Bobin, F. Dulwich, B. Mort, M. Santos and J.L. Starck 1577

21-cm forest with the SKA
B. Ciardi, S. Inoue, K. Mack, Y. Xu and G. Bernardi 1595

Epoch of Reionization modelling and simulations for SKA
I. Iliev, M. Santos, A. Mesinger, S. Majumdar and G. Mellema 1605

SKA - EoR correlations and cross-correlations: kSZ, radio galaxies, and NIR background
V. Jelic, B. Ciardi, E. Fernandez, H. Tashiro and D. Vrbanec 1617

Bulk Flows and End of the Dark Ages with the SKA
U. Maio, B. Ciardi and L. Koopmans 1627

HI tomographic imaging of the Cosmic Dawn and Epoch of Reionization with SKA
G. Mellema, L. Koopmans, H. Shukla, K.K. Datta, A. Mesinger and S. Majumdar 1637

Constraining the Astrophysics of the Cosmic Dawn and the Epoch of Reionization with the SKA .
A. Mesinger, A. Ferrara, B. Greig, I. Iliev, G. Mellema, J. Pritchard and M. Santos 1651

Cosmology from EoR/Cosmic Dawn with the SKA
J. Pritchard, K. Ichiki, A. Mesinger, R.B. Metcalf, A. Pourtsidou, M. Santos, F.B. Abdalla, T.C. Chang, X. Chen, J. Weller and S. Zaroubi 1665

The physics of Reionization: processes relevant for SKA observations
B. Semelin and I. Iliev 1683

All-sky signals from recombination to reionization with the SKA
R. Subrahmanyan, U.N Shankar, J. Pritchard and H.K Vedantham 1693

Imaging HII Regions from Galaxies and Quasars During Reionisation with SKA
S. Wyithe, P. Geil and H. Kim 1705

Synergies and Other Science

Very Long Baseline Interferometry with the SKA
Z. Paragi, L. Godfrey, C. Reynolds, M.J. Rioja, A. Deller, B. Zhang, L. Gurvits, et al. 1719

Synergy between the Large Synoptic Survey Telescope and the Square Kilometre Array
D. Bacon, S. Bridle, F.B. Abdalla, M. Brown, P. Bull, S. Camera, R. Fender, K. Grainge, Z. Ivezic, M. Jarvis, N. Jackson, D. Kirk, B. Mann, J. McEwen, J. McKean, J.A. Newman, A. Raccanelli, M. Sahlen, M. Santos, T. Tyson and G. Zhao 1739

Euclid & SKA Synergies
T. Kitching, D. Bacon, M. Brown, P. Bull, J. McEwen, M. Oguri, R. Scaramella, K. Takahashi, K. Wu and D. Yamauchi 1761

SKA synergy with Microwave Background studies
C. Burigana, P. Alexander, C. Baccigalupi, D.S. Barbosa, A. Blanchard, A. De Rosa, G. De Zotti, F. Finelli, A. Gruppuso, M. Jones, S. Matarrese, A. Melchiorri, D. Molinari, M. Negrello, D. Paoletti, F. Perrotta, R. Scaramella and T. Trombetti 1777

Synergistic science with Euclid and SKA: the nature and history of Star Formation
P. Ciliegi and S. Bardelli 1793

Multiple supermassive black hole systems: SKA's future leading role
R. Deane, Z. Paragi, M. Jarvis, M. Coriat, G. Bernardi, S. Frey, H.R. Kloeckner and I. Heywood 1805

Star and Stellar Cluster Formation: ALMA-SKA Synergies
G. Fuller, J. Forbrich, J. Rathborne, S. Longmore and S. Molinari 1817

The connection between radio and high energy emission in black hole powered systems in the SKA era
M. Giroletti, M. Orienti, F. D'Ammando, F. Massaro, G. Tosti, R. LICO, G. Giovannini, I. Agudo, A. Alberdi, H.E. Bignall, M.P. Pommier and A. Wolter 1829

Synergies between SKA and ALMA: observations of Nearby Galaxies
R. Paladino, E.O. Orru, J. Brand, V. Casasola, E. Liuzzo, M. Massardi and A. Mignano 1841

Multi-wavelength, Multi-Messenger Pulsar Science in the SKA Era
J. Antoniadis, L. Guillemot, A. Possenti, S. Bogdanov, J. Gelfand, M. Kramer, R. Mignani, B. Stappers and P. Torne 1849

Overview of Complementarity and Synergy with Other Wavelengths in Cosmology in the SKA era
K. Takahashi, M. Brown, C. Burigana, C. Jackson, M. Jarvis, K.D Thomas D. Kitching, J.P. Jean-Paul Kneib, M. Masamune Oguri, S. Prunet, H. Shan, J.L. Starck and D. Yamauchi 1863

Solar and Heliospheric Physics with the Square Kilometre Array
V. Nakariakov, M.M Bisi, P.K Browning, D. Maia, E.P Kontar, D. Oberoi, P.T. Gallagher, I.H Cairns and H. Ratcliffe 1875

Extragalactic jets in the SKA era: solving the mystery of Ultra High Energy Cosmic Rays?
S. Turriziani 1889

Enabling the next generation of cm-wavelength studies of high-redshift molecular gas with the SKA
J. Wagg, E. da Cunha, C. Carilli, F. Walter, M. Aravena, J. Hodge, E. Murphy, D. Riechers, M. Sargent, R. Wang and I. Heywood 1901

Enhancing Science from Future Space Missions and Planetary Radar with the SKA
D. Jones and J. Lazio 1911

Delivering SKA Science
P. Quinn, T Axelrod, I Bird, R Dodson, A Szalay and A Wicenec 1921

Summary and Future Directions

Square Kilometre Array key science: a progressive retrospective
C. Carilli 1949

Introduction

PROCEEDINGS OF SCIENCE

Advancing Astrophysics with the Square Kilometre Array

Robert Braun, Tyler L. Bourke, James A. Green, Evan F. Keane & Jeff Wagg
SKA Organisation, Jodrell Bank, UK
E-mail: r.braun@skatelescope.org

The Square Kilometre Array concept has grown from the answer to a simple question: What size radio telescope would it take to permit us to read the history of the Universe as written in the language of its most abundant constituent, Hydrogen? What has also become apparent, is that the same radio telescope that will answer fundamental questions about our cosmic origins and fate will permit a wealth of other discoveries to be made, in areas as diverse as the formation of planets similar to the Earth, detection of gravitational distortions of Space-Time, the origin of cosmic magnetic fields and understanding the formation and growth of Black Holes. In this paper we discuss a few of these headline science topics and refer the reader to the overview chapters within these proceedings for more details on the broad areas of anticipated impact, as well as the individual contributed chapters that focus on specific topics.

Advancing Astrophysics with the Square Kilometre Array
June 8-13, 2014
Giardini Naxos, Sicily, Italy

PoS(AASKA14)174

1. Introduction

The Square Kilometre Array (SKA) concept is the result of answering the question: How large should the collecting area of a radio telescope be to enable the study of the history of the Universe via its most abundant constituent, Hydrogen? The answer is about one square kilometre. What's surprising about this answer is that it applies to such a wide range of cosmic time. An SKA-sized telescope is needed to:

1. See back to the Cosmic Dawn, when the very first stars formed in a Universe that was only 100 million years old,

2. Witness the epoch of galaxy formation at 1 billion years of age, as well as,

3. Understand the current epoch of accelerating expansion, 13.7 billion years after the Big Bang, driven by the mysterious force of Dark Energy.

This same telescope will permit a wealth of other discoveries to be made, in areas as diverse as the formation of Earth-like planets, the detection of gravitational distortions of Space-Time, the origin of cosmic magnetic fields, and the formation and growth of Black Holes. A selection of the most significant contributions anticipated within the eight different areas represented by the current SKA Science Working Groups are summarised in Figure 1. We consider just a few of these many areas briefly below, ordered by their relative distances, and refer the reader to the overview chapters within these proceedings referenced in Figure 1 for more details on the broad areas of anticipated impact, as well as the many individual contributed chapters that focus on an even more diverse set of specific topics. The current SKA Science programme builds on the strong foundations put in place previously in "Science with the Square Kilometre Array" edited by Carilli and Rawlings (2004), which builds in turn on the original compilation of the same name edited by Taylor and Braun (1999).

2. Planet Formation

Since the discovery of the first planetary body outside of the solar system in 1988 there have been almost 2000 planets discovered around more than 1000 stars. Planets have been found with the most diverse properties, ranging in size from half that of the Earth to about twice that of Jupiter and in density from half that of freshly fallen snow to twice that of lead. A particularly vexing problem facing planetary astronomers is understanding how the small pebbles in the disk surrounding a young star are able to stick together to form the boulders that ultimately coalesce into planets. At both smaller and larger sizes, the growth mechanisms are understood, but this key step in the planet formation process is still shrouded in mystery. The SKA will uniquely enable direct observation of this phase of planet assembly by observing at exactly those radio wavelengths that are matched to the size of coalescing particles, from cm-scales to metres, and it will do so with enough resolution to watch the assembly of planets in earth-like orbits about their parent stars.

PoS(AASKA14)174

	SKA1	SKA2
The Cradle of Life & Astrobiology Hoare, M. et al. 2015 PoS(AASKA14)115	Proto-planetary disks; imaging snow/ice line (@ < 100pc), Searches for amino acids.	Proto-planetary disks; sub-AU imaging (@ < 150 pc), Studies of amino acids.
	Targeted SETI: airport radar 10^4 nearby stars.	Ultra-sensitive SETI: airport radar 10^5 nearby star, TV ~10 stars.
Strong-field Tests of Gravity with Pulsars and Black Holes Kramer, M. & Stappers, B. 2015 PoS(AASKA14)036	1st detection of nHz-stochastic gravitational wave background.	Gravitational wave astronomy of discrete sources: constraining galaxy evolution, cosmological GWs and cosmic strings.
	Discover and use NS-NS and PSR-BH binaries to provide the best tests of gravity theories and General Relativity.	Find all ~40,000 visible pulsars in the Galaxy, use the most relativistic systems to test cosmic censorship and the no-hair theorem.
The Origin and Evolution of Cosmic Magnetism Johnston-Hollitt, M. et al. 2015 PoS(AASKA14)092	The role of magnetism from sub-galactic to Cosmic Web scales, the RM-grid @ 300/deg^2.	The origin and amplification of cosmic magnetic fields, the RM-grid @ 5000/deg^2.
	Faraday tomography of extended sources, 100pc resolution at 14Mpc, 1 kpc @ $z \approx 0.04$.	Faraday tomography of extended sources, 100pc resolution at 50Mpc, 1 kpc @ $z \approx 0.13$.
Galaxy Evolution probed by Neutral Hydrogen Staveley-Smith, L. & Oosterloo, T. 2015, PoS(AASKA14)167	Gas properties of 10^7 galaxies, $\langle z \rangle \approx 0.3$, evolution to $z \approx 1$, BAO complement to Euclid.	Gas properties of 10^9 galaxies, $\langle z \rangle \approx 1$, evolution to $z \approx 5$, world-class precision cosmology.
	Detailed interstellar medium of nearby galaxies (3 Mpc) at 50pc resolution, diffuse IGM down to $N_H < 10^{17}$ at 1 kpc.	Detailed interstellar medium of nearby galaxies (10 Mpc) at 50pc resolution, diffuse IGM down to $N_H < 10^{17}$ at 1 kpc.
The Transient Radio Sky Fender, R. et al. 2015 PoS(AASKA14)051	Use fast radio bursts to uncover the missing "normal" matter in the universe.	Fast radio bursts as unique probes of fundamental cosmological parameters and intergalactic magnetic fields.
	Study feedback from the most energetic cosmic explosions and the disruption of stars by super-massive black holes.	Exploring the unknown: new exotic astrophysical phenomena in discovery phase space.
Galaxy Evolution probed in the Radio Continuum Prandoni, I. & Seymour, N. 2015 PoS(AASKA14)067	Star formation rates (10 $M_\odot$/yr to $z \sim 4$).	Star formation rates (10 $M_\odot$/yr to $z \sim 10$).
	Resolved star formation astrophysics (sub-kpc active regions at $z \sim 1$).	Resolved star formation astrophysics (sub-kpc active regions at $z \sim 6$).
Cosmology & Dark Energy Maartens, R. et al. 2015 PoS(AASKA14)016	Constraints on DE, modified gravity, the distribution & evolution of matter on super-horizon scales: competitive to Euclid.	Constraints on DE, modified gravity, the distribution & evolution of matter on super-horizon scales: redefines state-of-art.
	Primordial non-Gaussianity and the matter dipole: 2× Euclid.	Primordial non-Gaussianity and the matter dipole: 10× Euclid.
Cosmic Dawn and the Epoch of Reionization Koopmans, L. et al. 2015 PoS(AASKA14)001	Direct imaging of EoR structures ($z = 6 - 12$).	Direct imaging of Cosmic Dawn structures ($z = 12 - 30$).
	Power spectra of Cosmic Dawn down to arcmin scales, possible imaging at 10 arcmin.	First glimpse of the Dark Ages ($z > 30$).

Figure 1: An overview of some of the key science applications of the Square Kilometre Array, both in its early deployment phase, SKA1, and as the fully scoped, SKA2. Scientific topics are ordered by their increasing distance from the Earth. Definitions of abbreviations are given in the references.

PoS(AASKA14)174

3. Gravitational Waves

When Einstein's General Theory of Relativity was published in 1915, it made some of the most surprising predictions about the nature of space and time; predictions that continue to be confirmed with increasing precision to this day. Although this might be considered reassuring, it actually is not, since the theory is known to be fundamentally incomplete, at least at quantum scales. When will this theory, which constitutes a fundamental building block of modern physics, finally break down and what lies beyond? One of the as yet unconfirmed predictions of the theory is that the rapid relative motion of very massive compact objects, such as are thought to exist at the centre of most galaxies today, will lead to a propagating Space-Time distortion of the Universe; a phenomenon termed Gravitational Waves. The only method yet proposed to measure long period Gravitational Waves makes use of our entire Galaxy as a detector. Rapidly spinning neutron stars with pairs of radio beams emanating from their poles known as millisecond pulsars serve as a system of high precision clocks. By accurately measuring the pulse arrival times from many of these clocks over the course of several years the SKA will create a Gravitational Wave Telescope. The first goal will be the detection of the general Gravitational Wave background due to sources from all directions and distances, but with higher precision it should become possible to identify individual sources of such waves and begin to conduct Gravitational Wave Astronomy for the first time. Just as important would be the absence of detection of such characteristic Space-Time distortions at all. Since current limits are already constraining our understanding of Gravity and massive Black Hole growth, a non-detection would signal the need for a new theory.

4. Cosmic Magnetism

Most of us only encounter magnetism in conjunction with a compass that aligns itself with the Earth's magnetic field. While this has undoubtedly proven useful for centuries to navigators sailing the seas, it may seem quite a subtle phenomenon with only limited relevance to humanity. On the contrary, the Earth's magnetic field plays a key role in sustaining life on the surface by deflecting highly energetic charged particles originating from the Sun and beyond, that would otherwise damage the DNA of many organisms. Similarly, we are beginning to understand that magnetic fields play an important role throughout the Universe on all scales yet studied. The energy contained in magnetic fields appears to be comparable to that due to the heat of the material constituents and it may well play a key role in regulating a whole range of processes, from the formation of planets and stars to both the accumulation and the dispersal of material on the scales of galaxies and clusters of galaxies. The challenge facing astrophysicists today is explaining how and when magnetic fields arose to achieve their current prominence. What is particularly puzzling is the strength of those fields on the largest scales. Current theories fall short of explaining the observed field strengths by factors of a million or more. The only way to solve this puzzle is with a much better sampling of our magnetic environment, so that the sources of magnetic enrichment become apparent as well as the timescales over which they operate. What the SKA will enable is the first three dimensional magnetic map of the Universe. This will be achieved by measuring the individual magnetic components toward extremely large samples of sources distributed in all directions on the sky and at

PoS(AASKA14)174

varying distances. In this way, we will form the first detailed magnetic map of our own Galaxy, as well as the much larger volume around us, reaching back in time to the birth of the first galaxies.

5. Galaxy Evolution

For most of human history it was believed that our Solar system, surrounded by its starry firmament, made up the entire Universe. It wasn't until 1734 that the suggestion was made that our Sun was just one of many stars which together make up our Galaxy, an Island Universe within an otherwise empty void. That belief was replaced in 1920 with the understanding that ours was but one of many galaxies, both larger and smaller in size. The recognition that galaxies and even the Universe itself were ephemeral objects that have a finite lifetime, with a distinct birth, life cycle and ultimate death subsequently emerged in the 1960s. And only within the last few years have we begun to appreciate just how closely the life cycle of an individual galaxy can be coupled to that of the Universe itself. The SKA will finally give us a front row seat to witness such galaxy evolution, as traced by the accumulation and utilisation of atomic Hydrogen – the ultimate galactic power source – throughout cosmic time. The major challenge that the SKA overcomes is that of raw sensitivity. Although Hydrogen is the most abundant element in the cosmos, it is only visible as a faint radio glow in the sky and that intrinsic faintness is exacerbated by large distances. As noted at the outset, it was the desire to study Hydrogen even in the distant, early Universe that originally motivated the concept of a radio telescope comprising one square kilometre of total collecting area. What will ultimately be achieved is the most complete galaxy census ever contemplated, reaching one billion individual galaxies and covering 12.5 billion years of cosmic history. This sample will provide the most precise determination of the properties of Dark Energy yet conceived. Even in its early deployment phase, the SKA will already provide samples of 10 million galaxies spanning 8 billion years of evolution, which will greatly advance our understanding of the galaxy life cycle.

6. The Bursting Sky

Changes in the night sky have traditionally been viewed with a mixture of awe and concern in previous millennia. But for at least the past 100 years such events have instead proven to be valuable tools in recognising our place in the cosmos. First via distance estimates of variable stars that established the distinction between our Galaxy and other external galaxies, and since 1990 in allowing the deduction of an accelerating expansion of the Universe via distance estimates of Supernovae in very distant galaxies. The insights provided by such time variable phenomena show no signs of diminishing returns on an investment in their study. One such class of source is the Gamma-Ray Bursts; first witnessed in the 1960s by satellites designed to detect nuclear weapon detonations on the Earth, these events are now believed to originate in the supernovae of particularly massive stars in the distant Universe. The very high brightness of these events allows them to be seen to very great distances, and this provides an opportunity, at least temporarily, to detect any translucent material along the sightline. What may well be a similar phenomenon, the Fast Radio Bursts, was first discovered in 2007 and only established as a population in 2013. While we are still awaiting the first identification of a long-lived counterpart or galaxy host for the Fast Radio Burst phenomenon, it is quite possible that they reside in extremely distant galaxies.

PoS(AASKA14)174

What makes this plausible is that the radio waves reaching us from these sources have traversed a very substantial amount of ionised plasma, comparable to that seen between the Earth and the very centre of our Galaxy; despite the fact that these events are seen in entirely different directions where our Galaxy's plasma content is minimal. The intervening plasma results in a time delay for lower radio frequencies to reach us compared to the higher radio frequencies of about one second. The length of this time delay provides an accurate measurement of exactly how much plasma there is along the sightline. The SKA will enable us to associate thousands of individual bursts with the objects that host them, allowing us to map out the Universe's plasma content and how it evolves with time in a way that was never previously possible. This is particularly important since we believe that about 70% of all normal matter in the Universe today is in the form of such plasma, but we only have direct measurements of about 10%. The study of Fast Radio Bursts with the SKA will open a completely new window on the cosmos.

7. Forming Stars through Cosmic Time

The realisation that stars like our Sun have a finite lifetime emerged in the early 1900s. This was followed by the comforting conjecture that the Universe was essentially in a "steady state" with a constant rate of stars ageing and being replaced. What instead became apparent in the late 1990's is that the rate at which stars are formed has varied dramatically with time. That rate has increased from a low level in the early Universe to a major peak at some 3 billion years of age, followed by a continuous decline to the rather low rates that apply today. In very broad terms this pattern can be explained by the changing balance between two competing forces of Nature, gravitational attraction which dominates in the first few billion years and Dark Energy driven repulsion which dominates today. While gravity dominated, large quantities of Hydrogen were pulled together from the environments of the early galaxies to fuel a spectacular epoch of star-forming fireworks. Since Dark Energy has become dominant it is increasingly difficult to pull together any additional fuel to sustain future generations of stars. While the quantity of such fuel is still extensive, with only about 25% having been consumed, it has become essentially inaccessible. Although the basic pattern of growth and decline of star formation with time has been established, there are still many unanswered questions. We have evidence that the basic mode of star formation was fundamentally different in the early Universe, often occurring within intense concentrations of "super star clusters" that have few, if any, counterparts today. When and where did this mode first arise and how and why did it come to disappear again? The SKA will play a key role in answering these questions, since it's likely that such events are so deeply enshrouded by material that they can only be seen at radio frequencies that can penetrate the shroud. The SKA will ultimately allow detections of such Super Star Clusters back to when the Universe was only 0.5 billion years old and resolved images of such structures to be made back to 1 billion years of age. Even in its first deployment phase the SKA will permit detection back to 1.5 billion years and imaging back to 6 billion years of age.

8. Cosmology and Dark Energy

Its remarkable how the Universe seems to have an endless capacity to surprise those who study it. One of the biggest surprises to emerge in the past century was that normal matter, of the kind

PoS(AASKA14)174

described in the periodic table of the elements, is only a minor constituent of our Universe and is outweighed more than five to one by some form of invisible Dark Matter. We see evidence for such Dark Matter, in the form of excess gravitational attraction, on all scales between about 300 light years and 300 million light years. The gravitational attraction of Dark Matter has played a crucial role in shaping the Universe we inhabit, locally overcoming the general expansion imparted by the Big Bang and pulling together enough normal matter to allow stars and galaxies to form. But even Dark Matter is now dwarfed by the three times larger effects of Dark Energy. Dark Energy is in many respects the antithesis of Dark Matter, exerting a repulsive rather than attractive force that seems to grow in proportion to the volume of the Universe. During the first 3 billion years following the Big Bang it was Dark Matter that reigned supreme, but since that time, Dark Energy has taken over the dominant role. Establishing the true nature of these Universe-shaping quantities is a key motivation for cosmologists today. Since neither of these constituents was anticipated by current theories, we are still desperately in need of enhancing our observational constraints to inform a more fundamental physical theory. When confronted with such unexpected phenomena it is usual to begin with the simplest possible description of the effect, captured by a single parameter that does not change with cosmic time. This is the current state of affairs for our understanding of the Dark Energy phenomenon. As more extensive observations become available, it becomes possible to extend this practical description of the Universe with both a larger number of parameters and allowing for the possibility that they may change with time. Once such a higher level description becomes sufficiently detailed, it should finally be possible to derive a new physical theory that both explains Dark Energy and makes new predictions about other phenomena. It is anticipated that the SKA will fundamentally advance our understanding of Dark Energy by allowing for as many as ten parameters to describe both the nature and time evolution of this mysterious phenomenon. This is in contrast to other facilities operating on the same timescale that are only anticipated to permit three parameters to be meaningfully constrained. Even in its early deployment phase, the SKA should already permit as many as five Dark Energy parameters to be derived, making major progress toward the goal of enabling precision cosmology.

9. Cosmic Dawn and the Epoch of Re-ionisation

Many of us have become familiar with images, of ever increasing resolution and sensitivity, of the Cosmic Microwave Background; the surface surrounding us that represents the boundary of the visible Universe at only 380,000 years of age and a temperature of 3000 degrees Kelvin. Imprinted on that surface are the small density enhancements that will grow to become galaxies and clusters of galaxies as well as the small density decrements that will evolve to become large empty voids. However, the next 700 million years of evolution, before the birth of the most distant galaxies yet identified, are still shrouded in mystery. It's thought that the Universe's normal matter, which at the time still consists of about 92% Hydrogen, 8% Helium and only rare traces of heavier elements, quietly cools down to temperatures below 100 K. This period is known as the Dark Ages and it lasts until the first stars begin to provide localised heating at about 100 million years of age. This heralds the onset of Cosmic Dawn, characterised by the first signs of temperature contrast between heated and unheated regions, even though essentially all of the Hydrogen is still relatively cold and neutral. The next major era is termed the Epoch of Reionisation lasting from about 370

PoS(AASKA14)174

to 800 million years of age. The heat sources have now become so intense and well distributed that Hydrogen is heated to more than 1000 K, becomes fully ionised and eventually the individual ionised bubbles grow to the point of completely overlapping one another. What the SKA will uniquely enable is measurement of a complete time sequence of images from the onset of Cosmic Dawn to the end of Reionisation using the faint radio light coming directly from the Hydrogen itself. The resulting movie of the Universe's first 700 million years will answer a multitude of questions. When exactly did the first stars form? Were individual stars, large stellar clusters or even early black holes the most important source of heating and ionisation of the Universe? How exactly did the process unfold; was there a single progression from dark to light or were there multiple fits and starts with different heating populations dominating at different times? This vital chapter in the history of the Universe was written long ago, but is now waiting to be read.

10. The SKA Observatory

The SKA Observatory that will make these and a wide range of other discoveries possible will be deployed in two phases; an early deployment phase termed SKA1 of 10 – 20% of the complete system, followed by the fully scoped SKA2. The detailed design of SKA1 is currently underway, building on the preliminary design work toward the original Baseline Design (Dewdney et al., 2013). The scope of the SKA1 deployment has been adjusted in the first quarter of 2015 to match the budget established by the SKA Board of Directors. The updated Baseline Design, the Top Level Science Requirements and the associated System Level Requirements can be found in Cornwell et al. (2015), Braun et al. (2015) and Turner et al. (2015) respectively. The rescope has meant some reduction in the early science capabilities of the Observatory with respect to that envisaged in the original design. Fortunately, the updated SKA1 design preserves a transformational enhancement of capabilities over today's state-of-the-art across the full range of radio frequencies being targeted. The entire suite of high priority scientific objectives identified for the SKA1 still remains viable, albeit with some adjustments of approach. Although the extremely wide-field capabilities that had been planned for the SKA1-Survey facility are not part of the initial deployment, the enabling technology of Phased Array Feeds will be a high priority component of an accelerated research and development program, funded from the SKA1 construction budget, to enable scientific deployment within the SKA at the earliest possible opportunity.

Acknowledgements The tireless efforts of the entire Editorial Board of these proceedings, namely the five authors of this overview together with Rob Fender, Federica Govoni, Melvin Hoare, Melanie Johnston-Hollitt, Leon Koopmans, Michael Kramer, Roy Maartens, Tom Oosterloo, Isabella Prandoni, Nick Seymour, Ben Stappers, Lister Stavely-Smith, Wen Wu Tian and Grazia Umana, are gratefully acknowledged. We also recognise the excellent choice of conference venue and organisational support provided by our Italian colleagues.

PoS(AASKA14)174

References

Braun, R., et al. 2015, "SKA1 Science (Level 0) Requirements", SKA-TEL-SKO-0000007 Rev 2

Carilli, C. & Rawlings, S., 2004, "Science with the Square Kilometre Array", New Astr. Rev. 48, 979 – 1605

Cornwell, T., et al. 2015, "SKA1 Baseline Design", SKA-TEL-SKO-0000002 Rev 2

Dewdney, P., et al. 2013, "SKA1 Baseline Design", SKA-TEL-SKO-0000002 Rev 1

Fender, R. et al. 2015, "The Transient Universe with the Square Kilometre Array", in *Advancing Astrophysics with a Square Kilometre Array*, PoS(AASKA14)051

Hoare, M. et al. 2015, "SKA and the Cradle of Life", in *Advancing Astrophysics with a Square Kilometre Array*, PoS(AASKA14)115

Johnston-Hollitt, M. et al. 2015, "Using SKA Rotation Measures to Reveal the Mysteries of the Magnetised Universe", in *Advancing Astrophysics with a Square Kilometre Array*, PoS (AASKA14)092

Koopmans, L. et al. 2015, "The Cosmic Dawn and Epoch of Reionisation with SKA", in *Advancing Astrophysics with a Square Kilometre Array*, PoS(AASKA14)001

Kramer, M. & Stappers, B., 2015, "An overview of pulsar science with the SKA", in *Advancing Astrophysics with a Square Kilometre Array*, PoS(AASKA14)036

Maartens, R. et al. 2015, "Overview of Cosmology with the SKA", in *Advancing Astrophysics with a Square Kilometre Array*, PoS(AASKA14)016

Prandori, I. & Seymour, N., 2015, "Revealing the Physics and Evolution of Galaxies and Galaxy Clusters with SKA Continuum Surveys", in *Advancing Astrophysics with a Square Kilometre Array*, PoS(AASKA14)067

Staveley-Smith, L. & Oosterloo, T., 2015, "HI Science with the Square Kilometre Array", in *Advancing Astrophysics with a Square Kilometre Array*, PoS(AASKA14)092

Taylor, A.R. & Braun, R., 1999, "Science with the Square Kilometre Array", `https://www.skatelescope.org/uploaded/55267_scienceSKA.pdf`

Turner, W., et al. 2015, "SKA1 System (Level 1) Requirements", SKA-TEL-SKO-0000008 Rev 8

PoS(AASKA14)174

The Cradle of Life

PROCEEDINGS OF SCIENCE

The Cradle of Life and the SKA

M. G. Hoare*[1], L. Perez[2], T. L. Bourke[3], L. Testi[4,5,6], I. Jimenez-Serra[5,7], P. Zarka[8], A. P. V. Siemion[9,10,11], H. J. v. Langevelde[12,13], L. Loinard[14], G. Anglada[15], A. Belloche[16], P. Bergman[17], R. Booth[18,17] P. Caselli[19], C. J. Chandler[2], C. Codella[4], G. Hallinan[20], J. Lazio[21], I. S. Morrison[22,23], L. Podio[4], A. Remijan[2], J. Tarter[24],

[1]*School of Physics and Astronomy, University of Leeds, Leeds, UK;* [2]*National Radio Astronomy Observatory, USA;* [3]*SKA Organisation, Jodrell Bank Observatory, UK;* [4]*INAF-Osservatorio Astrofisico di Arcetri, Firenze, Italy;* [5]*European Southern Observatory, Garching, Germany;* [6]*Excellence Cluster Universe, Garching, Germany;* [7]*University College London, London, UK;* [8]*LESIA, CNRS - Obs. Paris, Meudon, France;* [9]*ASTRON, NL;* [10]*Radboud University, NL;* [11]*University of California, Berkeley, USA;* [12]*JIVE, NL;* [13]*Sterrewacht Leiden, Leiden University, NL;* [14]*CRyA-UNAM, Morelia, Mexico;* [15]*Instituto de Astrofísica de Andalucía, CSIC, Spain;* [16]*MPIfR, Bonn, Germany;* [17]*OSO, Chalmers University of Technology, Sweden;* [18]*University of Pretoria; Pretoria, South Africa;* [19]*MPE, Garching, Germany;* [20]*California Institute of Technology, Pasadena, USA;* [21]*JPL, California Institute of Technology, Pasadena, USA;* [22]*University of New South Wales, Australia;* [23]*Swinburne University of Technology, Australia;* [24]*SETI Institute, Mountain View, USA;*

E-mail: m.g.hoare@leeds.ac.uk

We provide an overview of the exciting capabilities of the SKA in the Cradle of Life theme. With the deployment of the high frequency band 5 receivers, the phase 1 of the SKA can conduct headline science in the study of the earliest stages of grain growth in proto-planetary disks. SKA1-MID can map the 2 cm continuum emission at a resolution of 4 au in the nearest systems and therefore begin to probe the distribuion of cm-sized particles across the snow line. This frequency range will also enable deep searches for pre-biotic molecules such as amino acids from pre-stellar cores to the cold, outer regions of proto-planetary disks where cometary material forms. The lowest frequency capabilities of SKA1 can be used to examine the magnetic fields of exo-planets via their auroral radio emission. This gives unique insight into their interiors and could potentially detect exo-moons. Across the full frequency range, the SKA1 will also carry out systematic, volume-limited searches of exo-planet systems for signals from technologically advanced civilizations. The sensitivity of SKA1 means that these only need to be at the level of typical airport radar signals in the nearest systems. Hence, the SKA1 can conduct high impact science from the first steps on the road to planets and life, through areas affecting the habitability of planets, and ultimately, to whether we are alone in the Galaxy. These inspirational themes will greatly help in the effort to bring SKA1 science to a wide audience and to ensure the progression to the full SKA.

Advancing Astrophysics with the Square Kilometre Array
June 8-13, 2014
Giardini Naxos, Italy

*Speaker.

PoS(AASKA14)115

1. Introduction

The origin of life is as great a question as the origin of the universe. In terms of the interests of the general public it is probably second to none. A suitably equipped SKA will yield new and unique insights into the different stages of the origin and existence of life elsewhere in the Galaxy.

First, the combination of sensitivity and resolution of SKA1-MID equipped with band 5 receivers will probe the first steps on the road to forming habitable planets. Only cm-wave instruments can directly track the growth of dust grains through the important cm-sized regime. For the nearest proto-planetary disk systems SKA1-MID can start to study grain growth processes inside the snow line, which is the realm of rocky planet formation.

Secondly, SKA1-MID can detect the presence of molecules that are of biological interest such as amino acids. These heavy molecules that are the very building blocks of life have detectable transitions in the band 5 frequency range. The sensitivity and resolution of the core of SKA1-MID will enable searches for these pre-biotic molecules in the outer regions of proto-planetary disks free from the line crowding and strong dust emission at millimetre wavebands. It is in these cold outer disk regions where their incorporation into comets could allow the possibility of delivery on to rocky inner region planets.

The next stage of the origins story is the characterization of the planets themselves. A unique contribution of radio observations is the study of planetary magnetic fields via auroral emission. Not only do magnetic fields give clues to the nature of planetary interiors, but they also play a role in protecting planetary surfaces from the high energy stellar wind particles that give rise to the aurorae in the first place. SKA1-LOW has the potential to study the magnetic fields of Jupiter-like planets at moderate distances from their host stars. Modulations of these radio emissions will expand the field of comparative magnetspheric physics to a much broader range of star-planet interactions than in our solar system. They may also indicate the presence of potentially habitable exo-moons.

Last, but by no means least, is the potential for the SKA to detect directly the existence of intelligent life via technologically produced radio signals. Such a discovery would of course be momentous in the history of humankind. However, the sensitivity of the SKA1 is such that interesting conclusions can be drawn from upper limits on targetted samples of the ever growing numbers of known exo-planet systems. The ability to detect typical levels of leakage radiation produced by technological civilizations like ourselves takes the search for extra-terrestrial intelligence to a whole new level. Commensal observing modes with the SKA will enable searches of much larger areas of parameter space for such signals than has ever been possible before.

2. Grain Growth in Proto-Planetary Disks

The unique value of the SKA in this context is that the only unambiguous way of detecting the presence of cm-sized particles is to measure the strength and the spectral index of the continuum emission at cm wavelengths as shown in Figure 1. In principle, the longer the wavelength we can use the better, to probe ever larger grains, but of course the flux is falling off at least as fast as λ^{-2} and so there is a big trade off with sensitivity. Several studies have shown evidence for a flattening in the spectral index of the overall SED showing that grain growth is taking place somewhere in the proto-planetary disk (e.g. Ricci et al. 2010).

PoS(AASKA14)115

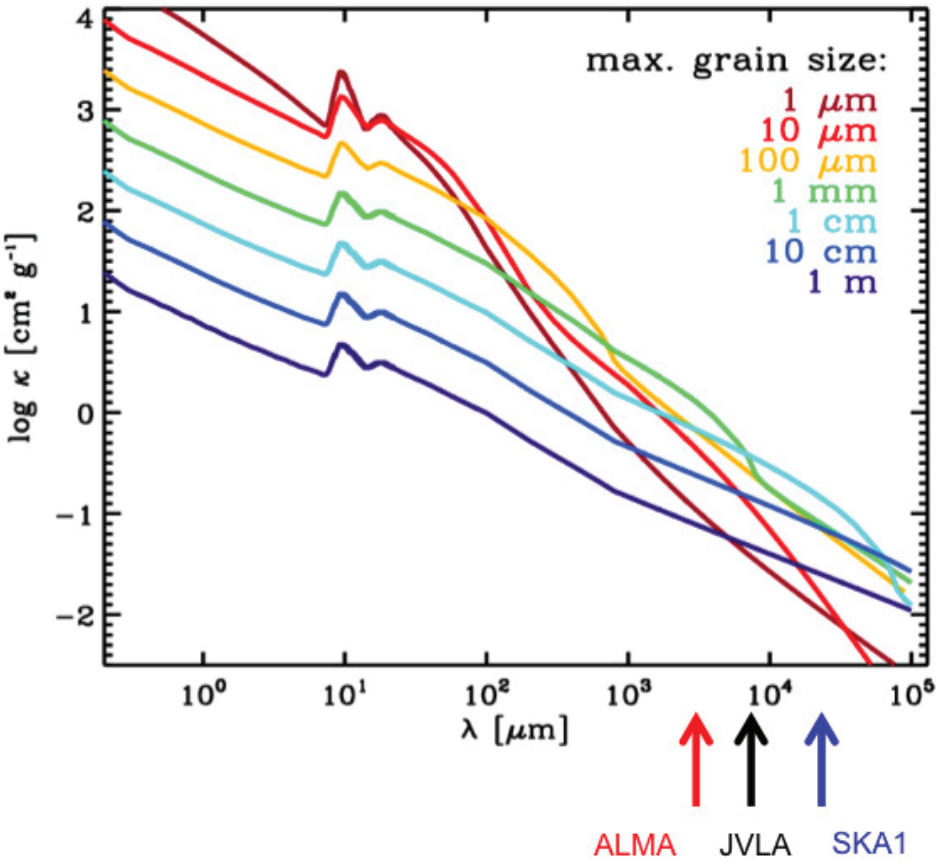

Figure 1: Opacity curves for grains of different sizes showing the flattening of the slope at cm wavelengths as the grains become cm-sized. The wavelengths at which ALMA, JVLA and SKA1-MID can deliver matching-beam data with a resolution of 40 mas are indicated. This corresponds to the ∼4 au radius of the snow line in the nearest proto-planetary disks.

The challenge now is to find out where and how grain growth proceeds as this is the first crucial step on the road to planet formation. As discussed in Testi et al. (2015; these proceedings) there are considerable challenges involved in grains growing through the cm size regime and that growth may only occur in particular locations within disks where dust becomes trapped. Investigating these phenomena requires high spatial resolution at cm wavelengths (e.g. Pérez et al. 2012).

Another key related question is which mechanisms lead to the formation of the very different terrestrial and Jovian planets. This will require studies of grain growth either side of the snow line for water ice, which is located at a radius of a few au from the star. As discussed by Kretke & Lin (2007) the interplay of the additional opacity at the snow line with the formation of dead zones in the turbulence due to the magneto-rotational instability can overcome the barriers to grain growth. For typical proto-planetary disks around solar-type stars the snow line is expected to be at a radius somewhere in the range of 1 to 10 au depending on the accretion rate. The snow line in the well-studied TW Hya disk is deduced from observations to be at a radius of around 4 au (Zhang et al. 2013). Therefore at the typical 100 pc distances of the nearest proto-planetary disks this requires

PoS(AASKA14)115

a spatial resolution of about 40 mas to resolve the snow line. This is precisely the resolution of SKA1-MID operating at the top end of the band 5 frequency range.

The size of the large grains in a proto-planetary disk are deduced from the shape of the spectral energy distribution at each location in the disk. This is best done across a broad spectral range all the way from mm through to cm wavelengths. At the resolution needed to resolve the snowline this can be achieved with SKA1-MID operating at 2.5 cm in combination with the JVLA at 7 mm and ALMA at 3 mm as is illustrated in Figure 1.

To demonstrate the feasibility of such an experiment we show a simulated 11.3 GHz continuum observation of a typical proto-planetary disk model in Figure 2. The model is based on that presented by Isella et al. (2009) for a disk with a symmetric distribution of $0.01 M_{\odot}$ of material as in the minimum mass solar nebula surrounding a $1 M_{\odot}$ star. The disk has a radius of 120 au and is viewed at an angle of 45° at a distance of 125 pc. Dust in the disk has an emissivity law slope of $\beta = 0.5$ and has a total flux of 180 μJy. Here it is imaged at the full resolution of SKA1-MID where the unifrom weighted beam has a size of 35×40 mas. This simulation was for a 1000 hour deep field integration and clearly maps out the dust emission at this high resolution. The peak intensity is 4 μJy/beam, equivalent to a brightness temperature of 30 K, and the noise level is 0.07μJy/beam (0.5 K). Hence, SKA1-MID can clearly make a high impact in the mapping out of grain growth in proto-planetary disks at high resolution in targeted regions.

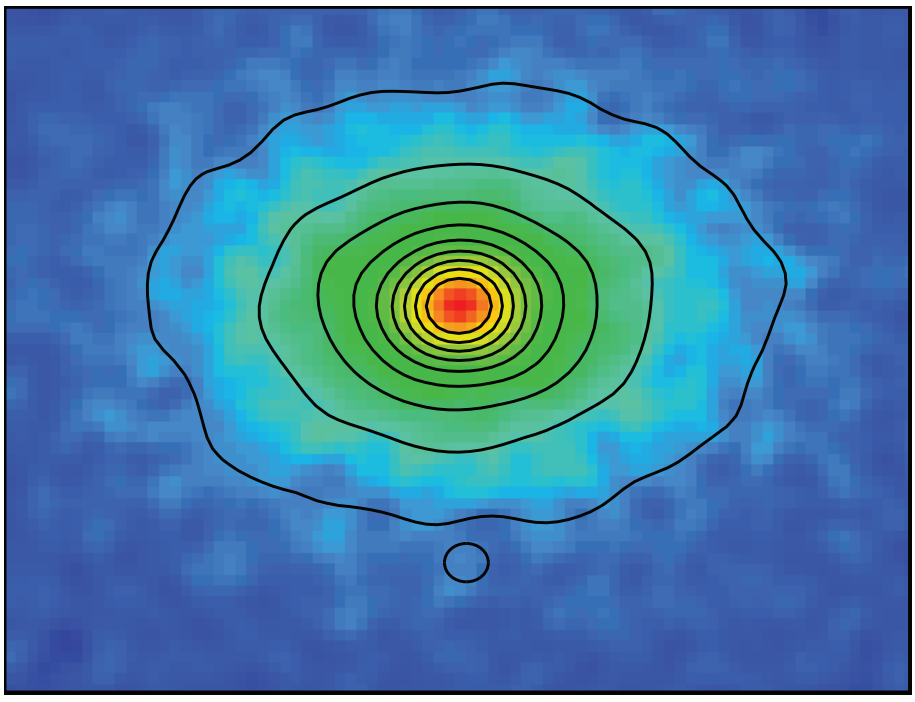

Figure 2: Simulated continuum image of a proto-planetary disk using a 2 × 2.5 GHz bandwidth from 8.8 to 13.8 GHz. Contours run from 5, 10, 15, ...,45 times the 0.07μJy/beam noise level. The image is about 0.85 × 0.65 arcseconds in size and the 35 × 40 mas beam is indicated. See text for details. Note that real disks are likely to have significant structure in them as in Figure 1 of Testi et al. (2015).

PoS(AASKA14)115

3. Pre-Biotic Molecules

As discussed by Testi et al. and Codella et al. in these proceedings another potential high impact area for SKA1-MID operating at band 5 is the detection of pre-biotic molecules in both proto-planetary disks, outflows and pre-stellar cores. The high sensitivity over a large range of angular scales of the SKA1-MID configuration is well suited to the search for these building blocks of life. The concentrated 1 km core results in a good brightness temperature sensitivity on the several arcsecond scales necessary to detect molecules in the pre-stellar core sources. For the cold, outer regions of proto-planetary disks then a resolution of around an arcsecond is well-matched to the 100 au spatial scale. In this way SKA1-MID can attempt to track the origin and evolution of pre-biotic molecules and trace their journey from the interstellar medium into the regions where they could be incorporated into cometary material at the outer edges of young planet forming systems (e.g. Ceccarelli et al. 2014).

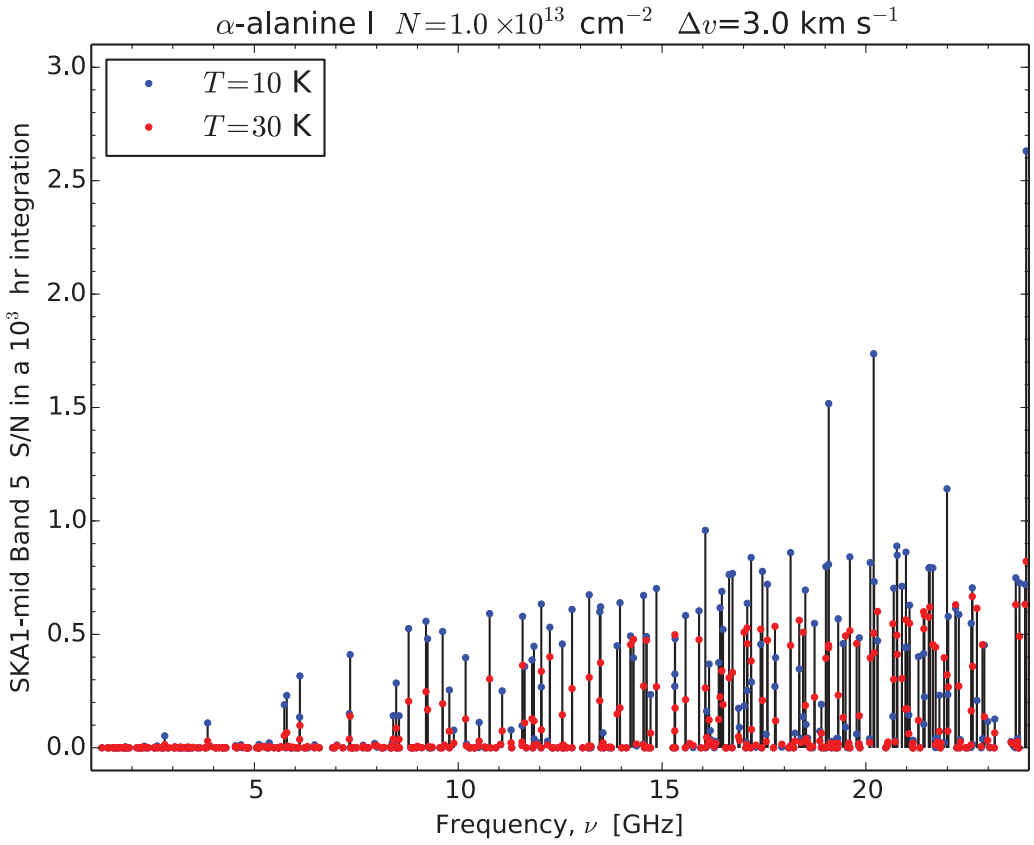

Figure 3: Simulated signal-to-noise ratio that would be achieved with a deep, 1000 hour integration with a 190 dish SKA1-MID for the emission from the spectral lines of the conformer I of α-alanine in LTE for two different temperatures. The frequency range covered includes the baseline design band 5 range from 4.6 to 13.8 GHz as well as the possible extension up to around 24 GHz being considered in the SKA's Advanced Instrumentation Programme. Note that the assumptions here indicate that these lines are not quite detectable, but see text for additional considerations.

PoS(AASKA14)115

Testi et al. and Codella et al. demonstrated that detections of the simplest amino acid glycine are possible with SKA1-MID in band 5. In Figure 3 we show the expected LTE strength of lines from the next most complicated amino acid, alanine. The column density assumed here would correspond to an abundance of alanine of about 10^{-12} relative to hydrogen in a proto-planetary disk like that in TW Hya where the gas surface density is about 15 g cm^{-2} or the hydrogen column density is 6×10^{24} cm^{-2} (Andrews et al. 2012). This is compared to the abundance of 10^{-11} that Testi et al. assumed for glycine. Figure 3 indicates that if alanine is similarly abundant then it would be detectable by SKA1-MID if it was emitting in LTE in the cold mid-plane of the outer regions of a proto-planetary disk. However, as shown by Faure et al. (2014), these cm-wave transitions from such molecules may well undergo boosting by NLTE effects, i.e. they might be weakly masing. Although this would make their interpretation difficult as stated by Testi et al., it would help the detection and identification of these important pre-biotic molecules.

4. A Young Cluster Deep Field

It is clear from Testi et al. and Codella et al. that both the high resolution grain growth study and the search for amino acids will require very deep integrations of order 1000 hours with SKA1-MID. Fortunately, the study of grain growth and pre-biotic molecules in proto-planetary disks could be done simultaneously. The rebaselined design specifies 64 000 channels per IF, which means that the full 2 x 2.5 GHz bandwidth can be observed with a channel spacing of around 1 kms^{-1} in the 8.8 to 13.8 GHz range. This matches the line width in outer disk regions (Qi et al. 2004) and is therefore adequate for line detection experiments, although detailed confirmation and kinematics would require higher spectral resolution follow-ups. A reasonable spectral resolution is also required for the continuum spectral index measurement since it is important to ensure that low level line contamination is corrected for.

The fact that most young stars and their proto-planetary disks form in clusters also gives a significant multiplex advantage due to the large field of view of the SKA dishes. In typical young clusters about 10 targets will be available in the 6 arcminute field of view at the high frequency end of band 5 (e.g. Gutermuth et al. 2009). One rich region would be the centre of the ρ Oph A cluster (Figure 4). This pointing would contain 7 class I sources and 10 class II young stellar objects (Gutermuth et al. 2009) so that different evolutionary stages can be studied at the same time as well as a range of stellar masses.

A deep field experiment on a single pointing at the centre of a rich young cluster would also enable other important science goals to be achieved with the same dataset. The younger sources invariably drive ionized jets as discussed by Anglada et al. (these proceedings). A deep, high resolution image will easily provide a very detailed view of the free-free continuum and the radio recombination line emission from the jets. A high resolution spectral index and/or recombination line map will allow the separation of the ionized gas emission from the dust emission in the disk and is another important pre-requisite to the study of grain growth in the innermost regions.

To build up such a deep field will of course require many repeat visits to the target region. The cadence of such observations could then enable the time monitoring of the ionized gas emission from the young cluster sources. For the thermal jets this will allow the study of variability in jet morphology and proper motion measurements to characterise the mass-loss rate and test driving

PoS(AASKA14)115

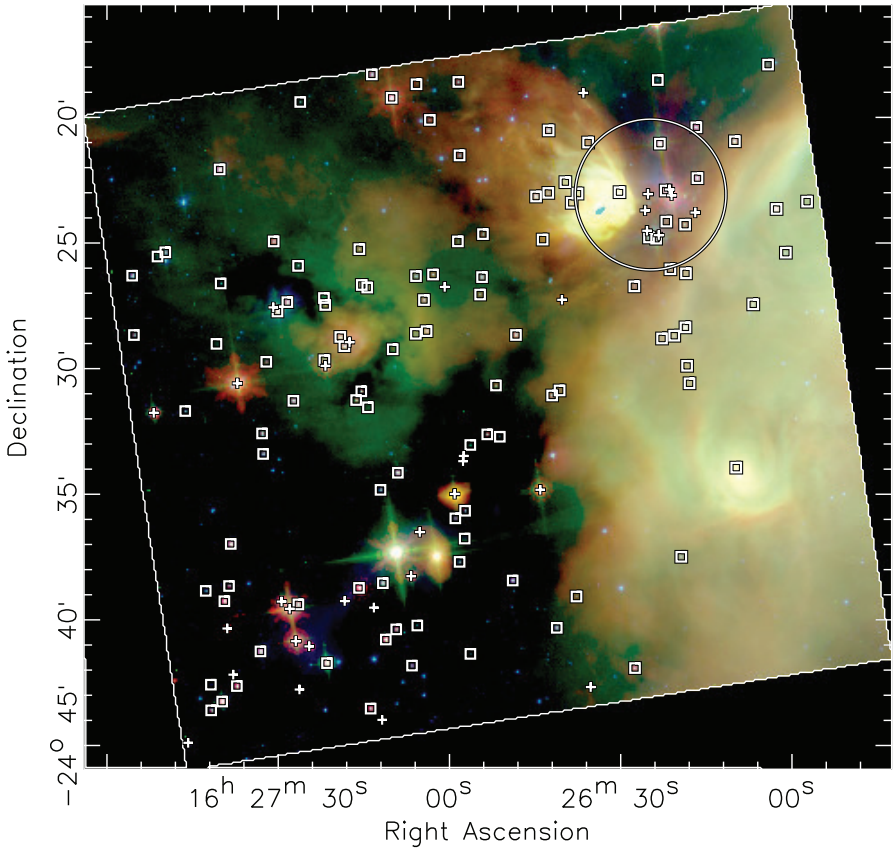

Figure 4: Spitzer three-colour image (3.6μm (blue), 8.0μm (green), 24μm (red)) of the L1688 region of ρ Oph star forming region. Class I and II young stellar objects are indicated by the plusses and squares respectively. Note the clustering of young sources that enables many sources to be studied in one deep pointing with SKA1-MID. One 6 arcminute field of view centred on the ρ Oph A cluster is indicated at the top right.

mechanism models. Variability may also help identify regions of the disk that are contaminated by jet emission as, in general, this is expected to vary on more rapid timescales than the dust emission from the disk. Furthermore, the long duration monitoring will provide a wealth of data with which to study the magnetic flaring activity in the innermost regions where the protoplanetary disk is expected to be disrupted by the magnetic field (e.g. Liu et al. 2014). These highly energetic events have been proposed as being responsible for the chondrules found in meteorites (Shu et al. 2001) and so may help complete the picture of the make-up of planet forming material.

Finally, if some of these observations over the period of a year or so are combined with VLBI runs then the 3D tomography of non-thermal sources in the targeted young cluster can be completed simultaneously as well. As discussed by Loinard et al. (these proceedings) knowledge of the 3D structure and kinematics, via proper motions and radial velocity, will provide stringent tests of cluster formation models. The VLBI resolution will also be able to locate accurately where in the proto-planetary disk the non-thermal emission originates. This will further help elucidate its role

PoS(AASKA14)115

in the thermal and chemical processing of the solid material in the planet formation zone. Overall, such a young cluster deep field experiment could yield a wealth of information on star and planet formation processes and the origins of pre-biotic molecules.

5. Planetary Magnetic Fields and Habitability

Another key question in the Cradle of Life theme is the habitability of planets once they are formed. Many aspects make up this question of course, although the starting point is the presence of liquid water, and usually this means a planet in the habitable zone. Other important aspects of habitability can be probed uniquely by the magnetic properties of the planet. As described in detail by Zarka et al. (2015; these proceedings) the existence and properties of a planet's magnetic field can be diagnosed using the lowest frequencies of the SKA.

A planet only has a magnetic field if dynamo action can generate such a field through the combination of differential rotation and convection in a conducting fluid in the planet's interior. For rocky terrestrial planets this means a liquid iron core. This in turn has implications for geological activity on the planet and the recycling of volatile gases via volcanic outgassing affecting the planet's atmospheric composition. For icy moons such as Jupiter's Ganymede, the conducting medium is thought to be a mineral rich, sub-surface ocean. Given the increasing evidence for extremophiles found in sub-glacial Antartic lakes (Christner et al. 2014), such icy exo-moons could in principle harbour biological activity beneath their surfaces. These exo-moons do not need to be in the traditional habitable zone as the extra heat required to melt the water ice is provided by the tidal heating by its large planetary host.

The probing of planetary magnetic fields via radio studies also impinges on other aspects of habitability. Such fields protect both the planet's atmosphere and surface from high energy particles coming in from either cosmic rays or the host star's solar wind. Such a wind can play a role in eroding a planet's atmosphere over time as well as other effects on atmospheric composition (Brain et al. 2013). Modulation of the auroral radio signals will enable determination of the planets rotation period, which is important in setting day/night temperature differences. Measurements of the inclination of the planet's rotation axis to its orbital plane will reveal whether the planet experiences seasonal changes. Such aspects may well be important in the emergence of life on Earth-like planets.

The SKA is unlikely to be able to detect magnetic fields on terrestrial planets if they are of similar strength to the Earth's since they will emit at too low a frequency. Much more likely are detections of Jovian planets. Here there is considerable interest in the potential to detect exo-moons that are difficult to detect in any other way. Jovian moons leave an imprint on the pattern of auroral emission, which is then revealed as periodic modulation of the radio emission. This can be the case whether the exo-moon itself has a magnetic field (e.g. Ganymede) or not (e.g. Io). If the exo-moons are icy and magnetic then they also hold out the prospect of hosting biological activity. On the timescale of SKA2 we will be learning much more about these prospects via ESA's JUICE mission (Grasset et al. 2013).

PoS(AASKA14)115

6. Search for Extra-terrestrial Intelligence

Of course, the greatest question of them all perhaps is not just whether life can exist on other planetary systems, but whether it can evolve into intelligent life that is technologically advanced. As described by Siemion et al. (2015 these proceedings), searches in the radio waveband for such extra-terrestrial intelligence (SETI) has a long tradition, much of it privately funded. Since the beginnings of the SKA project SETI has formed part of the core science case (Tarter et al. 2004). In the mean time the reasons why SETI is now 'mainstream' have become even stronger. The Kepler mission has now shown that basically every star has a planetary system (Dressing & Charbonneau 2013). Furthermore, a number of Earth-like planets in the habitable zone are known and this number will only increase (e.g. Quintana et al. 2014). So the uncertainty over the widespread availability of planetary hosts has been removed.

The other aspect of the SKA that means SETI searches should be central to its science programme is its sheer sensitivity. The fact that the SKA can detect the typical types of radio signals we on Earth emit as we go about our 'everyday business' means that well-defined questions can be addressed. also opens the possibility of detecting deliberate transmissions from sources of lower power (or at greater distances) than ever before. The large frequency coverage and flexibility of the SKA also make it the ultimate SETI machine.

As detailed by Siemion et al. a complete volume-limited search of the nearest one thousand stars (and hence, their planetary systems) within about 15 pc down to the levels of typical airport radar signals is easily possible in 1000 hours of observing with SKA1. Of course, these targets are exactly the same as those to be searched for auroral emissions from planetary magnetic fields as described above. So on SKA1-LOW these targetted searches can be done in parallel. On SKA1-MID the SETI observations can very naturally be carried out in combination with a wide variety of other large area surveys, using one beam to target a nearby star in the field of view, whilst a few other beams are used to exclude terrestrial origins for any signal detected. As with the transient and pulsar cases, the more commensality that can be achieved with SKA observations the more science can be delivered. With the kind of sensitive, volume-limited search outlined above we can start to make significant progress into evaluating the probability of intelligent life evolving on other planets in the Galaxy.

7. Summary

Overall the rebaselined SKA1 will enable a wide range of exciting discoveries under the Cradle of Life heading. SKA1-MID with its high frequency capability will examine the tricky first steps of building terrestrial planets up from small grains through to rocks. In addition, it will conduct sensitive searches for the large molecules that are the very building blocks of life in the cold, dark places where stars and planets form. At the other end of the SKA1 frequency range, SKA1-LOW will study the magnetic fields of the exo-planets themselves, providing insights into the habitability of these worlds. At the same time the full range of SKA1 frequencies will be systematically searched for any signs of intelligent life on the nearby exo-planets and beyond. Each of these areas is of great interest to the general public. These topics are simple to convey and are especially good for getting young people interested in the science enabled by the SKA. Hence, we expect the Cradle

PoS(AASKA14)115

of Life area to play a major role in the wider impact of the SKA on the general public. This in turn will greatly assist in garnering the funding required for both Phase 1 and beyond.

Acknowledgments

We thank R. Gutermuth for providing Figure 4. Part of this research was carried out at the Jet Propulsion Laboratory, California Institute of Technology, under a contract with the National Aeronautics and Space Administration. GA acknowledges support from MICINN (Spain) grant AYA2011-30228-C03 (co-funded with FEDER funds).

References

Andrews, S. M., et al., 2012, ApJ, 744, 162

Anglada, G., et al., 2015, “Radio Jets in Young Stellar Objects with the SKA”, in proceedings of "Advancing Astrophysics with the Square Kilometre Array", PoS(AASKA14)121

Brain, D. A., Leblanc, F., Luhmann, J. G., Moore, T. E., Tian, F., 2013, in Comparative Climatology of Terrestrial Planets, Stephen J. Mackwell, Amy A. Simon-Miller, Jerald W. Harder, and Mark A. Bullock (eds.), University of Arizona Press, Tucson, p.487

Ceccarelli, C., Caselli, P., Bockelée-Morvan, D., Mousis, O., Pizzarello, S., Robert, F., Semenov, D., 2014, in Protostars and Planets VI, Henrik Beuther, Ralf S. Klessen, Cornelis P. Dullemond, and Thomas Henning (eds.), University of Arizona Press, Tucson, 914 pp., p.859-882

Christner, B. C., et al. 2014, Nature, 512, 310

Codella, C., et al., 2015, “Complex organic molecules in protostellar environments in the SKA era”, in proceedings of "Advancing Astrophysics with the Square Kilometre Array", PoS(AASKA14)123

Dressing, C. D., Charbonneau, D., 2013, ApJ, 767, 95

Faure, A., Remijan, A. J., Szalewicz, K., Wiesenfeld, L., 2014, ApJ, 783, 72

Grasset, O., et al. 2013, P&SS, 78, 1

Gutermuth, R. A., Megeath, S. T., Myers, P. C., Allen, L. E., Pipher, J. L., Fazio, G. G., 2009, ApJS, 184, 18

Isella, Andrea, Carpenter, John M., Sargent, Anneila I., 2009, ApJ, 701, 260

Kretke, K. A., & Lin, D. N. C. 2007, ApJ, 664, L55

Loinard, L. et al., 2015, “SKA tomography of Galactic star-forming regions and spiral arms”, in proceedings of "Advancing Astrophysics with the Square Kilometre Array", PoS(AASKA14)166

Liu, H. B., et al., 2014, ApJ, 780, 155

Pérez, L. M., et al. 2012, ApJ, 760, L17

Qi, C., et al. 2004, ApJ, 616, L11

Quintana, E. V. et al., 2014, Science, 344, 277

Ricci, L., Testi, L., Natta, A., Brooks, K. J., 2010, A&A, 521, 66

Shu, F. H., Shang, H., Gounelle, M., Glassgold, A. E., Lee, T., 2001, ApJ, 548, 1029

Siemion, A. P. V. et al., 2015, “Searching for Extraterrestrial Intelligence with the Square Kilometre Array”, in proceedings of "Advancing Astrophysics with the Square Kilometre Array", PoS(AASKA14)116

Tarter, J. C., 2004, NewAR, 48, 1543

PoS(AASKA14)115

Testi, L. et al., 2015, “Protoplanetary disks and the dawn of planets with SKA”, in proceedings of "Advancing Astrophysics with the Square Kilometre Array", PoS(AASKA14)117

Zarka, P., et al., 2015, “Magnetospheric Radio Emissions from Exoplanets with the SKA”, in proceedings of "Advancing Astrophysics with the Square Kilometre Array", PoS(AASKA14)120

Zhang, K., Pontoppidan, K. M., Salyk, C., Blake, G. A., 2013, ApJ, 766, 82

PoS(AASKA14)115

PROCEEDINGS OF SCIENCE

Searching for Extraterrestrial Intelligence with the Square Kilometre Array

Andrew P. V. Siemion[*1,2,3], **James Benford**[4], **Jin Cheng-Jin**[5], **Jayanth Chennamangalam**[6,7], **James Cordes**[8], **Heino Falcke**[2,1,7,9], **Simon Garrington**[10], **Mike Garrett**[1,11], **Leonid Gurvits**[12,13], **Melvin Hoare**[14], **Eric J. Korpela**[3], **Joseph Lazio**[15], **David Messerschmitt**[3], **Ian Morrison**[16], **Tim O'Brien**[10], **Zsolt Paragi**[12], **Alan Penny**[17], **Laura Spitler**[7], **Jill Tarter**[18], **Dan Werthimer**[3]

[1]*ASTRON, NL;* [2]*Radboud University, NL;* [3]*University of California, Berkeley, USA;* [4]*Microwave Sciences, USA;* [5]*NAOC, China;* [6]*Oxford University, UK;* [7]*MPIfR, Germany;* [8]*Cornell University, USA;* [9]*NIKHEF, NL;* [10]*Jodrell Bank Observatory, UK;* [11]*Leiden University, NL;* [12]*JIVE, NL;* [13]*Delft University of Technology, NL* [14]*University of Leeds, UK;* [15]*Jet Propulsion Laboratory, California Inst. of Technology, USA;* [16]*University of New South Wales;* [17]*University of St. Andrews, UK;* [18]*SETI Inst., USA*

E-mail: siemion at astron.nl

The vast collecting area of the Square Kilometre Array (SKA), harnessed by sensitive receivers, flexible digital electronics and increased computational capacity, could permit the most sensitive and exhaustive search for technologically-produced radio emission from advanced extraterrestrial intelligence (SETI) ever performed. For example, SKA1-MID will be capable of detecting a source roughly analogous to terrestrial high-power radars (e.g. air route surveillance or ballistic missile warning radars, EIRP[†]$\sim 10^{17}$ erg sec^{-1}) at 10 pc in less than 15 minutes, and with a modest four beam SETI observing system could, in one minute, search every star in the primary beam out to $\sim$100 pc for radio emission comparable to that emitted by the Arecibo Planetary Radar (EIRP $\sim$ 2 x 10^{20} erg sec^{-1})[‡]. The flexibility of the signal detection systems used for SETI searches with the SKA will allow new algorithms to be employed that will provide sensitivity to a much wider variety of signal types than previously searched for.

Here we discuss the astrobiological and astrophysical motivations for radio SETI and describe how the technical capabilities of the SKA will explore the radio SETI parameter space. We detail several conceivable SETI experimental programs on all components of SKA1, including commensal, primary-user, targeted and survey programs and project the enhancements to them possible with SKA2. We also discuss target selection criteria for these programs, and in the case of commensal observing, how the varied use cases of other primary observers can be used to full advantage for SETI.

Advancing Astrophysics with the Square Kilometre Array
June 8-13, 2014
Giardini Naxos, Sicily, Italy

[*]Speaker.
[†]EIRP = equivalent isotropic radiated power
[‡]Both for Band 1

PoS(AASKA14)116

1. Background

1.1 Signatures of Life

Whether or not life occurs elsewhere in the universe is one of the most profound questions science can ask. As of this moment, we know of only a single example of the emergence of life, despite evidence that the necessary abiotic precursors and environmental conditions are common. Earth-like planets (Petigura et al. 2013), water (Hogerheijde et al. 2011) and complex chemistry (Herbst & van Dishoeck 2009) have now been found in abundance, emboldening the field of astrobiology and underscoring the allure of extraterrestrial life. Knowing that extraterrestrial life *could* exist, the race is on to discover whether or not it, in fact, *does exist*. Yet more compelling is the possibility that extraterrestrial evolution may have followed a similar track as on the Earth, and brought forth a life form possessing intelligence and a technological capability perhaps far exceeding our own.

Although spectroscopy of extrasolar planet atmospheres or in-situ sampling missions in our Solar System may soon yield indirect evidence for life beyond Earth, the deeper question of the parameters of life's evolution that might lead to intelligence is addressable only by much more select means. The creation of technology, and specifically environmental modification by that technology, is the only known tracer of intelligence detectable over interstellar distances. However, while many chemical tracers of basic life can be ambiguous (Krasnopolsky et al. 2004; Rein et al. 2014), there exist types of electromagnetic emissions that could plausibly be generated by advanced technology but are not known to ever arise naturally. As far as we know, these emissions are definite and conclusive indicators of advanced technology, and presumably its intelligent creator. Radio communication in particular is a superb example of such a probe of extraterrestrial technology and is in fact the most detectable distant signature of our own technology.

Radio astronomy has long played a prominent role in searches for extraterrestrial intelligence (SETI), beginning with the first suggestions by Cocconi & Morrison (1959) that narrow-band radio signals near 1420 MHz might be effective tracers of advanced technology and early experiments along these lines by Drake (1961), continuing through to more recent investigations searching for a variety of coherent radio signals indicative of technology at a wider range of frequencies, e.g. Tarter et al. (1980); Horowitz et al. (1986); Horowitz & Sagan (1993); Leigh (1998); Korpela et al. (2001); Gray & Ellingsen (2002); Rampadarath et al. (2012); Siemion et al. (2010, 2013). The motivation for radio searches for extraterrestrial intelligence has been throughly discussed in the literature (Oliver & Billingham 1971; Tarter 2003), but the salient arguments are the following: 1. coherent radio emission is commonly produced by advanced technology (judging by Earth's technological development), 2. electromagnetic radiation can convey information at the maximum velocity currently known to be possible, 3. radio photons are energetically cheap to produce, 4. certain types of coherent radio emissions are easily distinguished from astrophysical background sources, 5. these emissions can transit vast regions of interstellar space relatively unaffected by gas, plasma and dust. These arguments are unaffected by varying assumptions about the motivation of the transmitting intelligence, e.g. whether the signal transmitted is intentional or unintentional, and can be applied roughly equally to a variety of potential signal types or modulation schemes.

PoS(AASKA14)116

1.2 Artificial Radio Emission

The first modern radio SETI experiments, including Frank Drake's pioneering work described in Drake (1961), focused on identifying continuous narrow-band emission. In the SETI context, "narrow-band" emission is defined as electromagnetic emission that is spectrally narrower than natural astrophysical sources. In the radio regime, the spectrally narrowest natural sources are astrophysical masers, with a spectral width no narrower than $\sim$ 500 Hz. The vast majority of radio SETI searches conducted since have continued this paradigm. The motivations for searching for signals of this type are numerous, but prominent among them are that narrow-band signals are readily distinguishable from natural sources, are relatively simple and are easy to detect with current technology. Were an advanced civilization interested in intentionally signaling another species, these properties would be very valuable. Narrow-band sinusoids are also a prominent component of many of our terrestrial radio communication and ranging systems, e.g. carrier tones and continuous-wave (CW) radar, but this is changing as terrestrial technology becomes more sophisticated.

More recently, it has been suggested that various other types of signals possess merit as well. Several authors have presented variations on the idea that a plausible signal from a very advanced civilization might appear to be a subtle variation on natural emission, either to make use of a natural source's inherent luminosity or to attract the attention of other astronomers (Cordes 1993; Lemarchand 1994; Cordes & Sullivan 1995; Sullivan & Cordes 1995; Chennamangalam et al. 2015). Benford (2010); Benford et al. (2010a,b) have argued that the terrestrial economics of beacon transmitter construction and operation imply that broadband rather than narrow-band systems might be preferred. Fridman (2011) concluded that broadband emission employing frequency-shift keying (FSK) would be preferred by energy-conscious civilizations seeking to transmit information-bearing signals using similar capabilities to our own. Messerschmitt (2012); Messerschmitt & Morrison (2012) similarly arrived at the idea that broadband communication might be preferable by considering robustness to radio frequency interference (RFI), and further deduced that this emission may have time-bandwidth extents influenced by the properties of the interstellar medium (ISM). In other words, the coherence of a modulated information-bearing signal would be limited in time or bandwidth extent by the combined effects of the relative motion of the source and receiver and the inhomogenous plasma occupying the intervening space. Depending on the degree to which these effects can be corrected for, they define either limits or search parameters of any algorithm used to detect information bearing radio emission sent over interstellar distances.

In addition to changing ideas about signal types, there has been steady growth in the number and diversity of suggestions of preferred frequencies for radio SETI. The so-called "terrestrial microwave window" (TMW, Figure 1), the spectral region of relatively low natural noise between the galactic synchrotron background and emission and absorption by water and oxygen in the Earth's atmosphere, was identified early as an ideal band to conduct radio SETI (Morrison et al. 1977). Faced with technological limitations that made it very difficult to search the entire $\sim$1$-$15 GHz window, early SETI experiments developed the notion of the "water-hole," an especially attractive region of spectrum at the bottom of the TMW trough bound by the frequencies of hyperfine transitions of neutral hydrogen (H, $f_{\rm H} \approx 1.42$ GHz) and the hydroxyl radical (OH, $f_{\rm OH} \approx 1.67$ GHz). In addition to the romantic allusion to terrestrial desert oases where life in a barren land gathers to

PoS(AASKA14)116

sate, there was a convenient supply of large telescopes and sensitive radio receivers operating in that range already. As time progressed, other "special frequencies" were identified. Blair & Zadnik (1993) lists 55 individual "interstellar communication channel" frequencies between 500 MHz and 25 GHz based on scaling[1] the rest frequencies of H and OH hyperfine transitions by mathematically special "civilization signature constants," e.g. $\pi, \pi/2, 2\pi, e, \pi e, e^e$. Gindilis et al. (1993) identified additional preferred frequencies based on hyperfine transitions of neutral hydrogen in the $n = 2$ excited state.

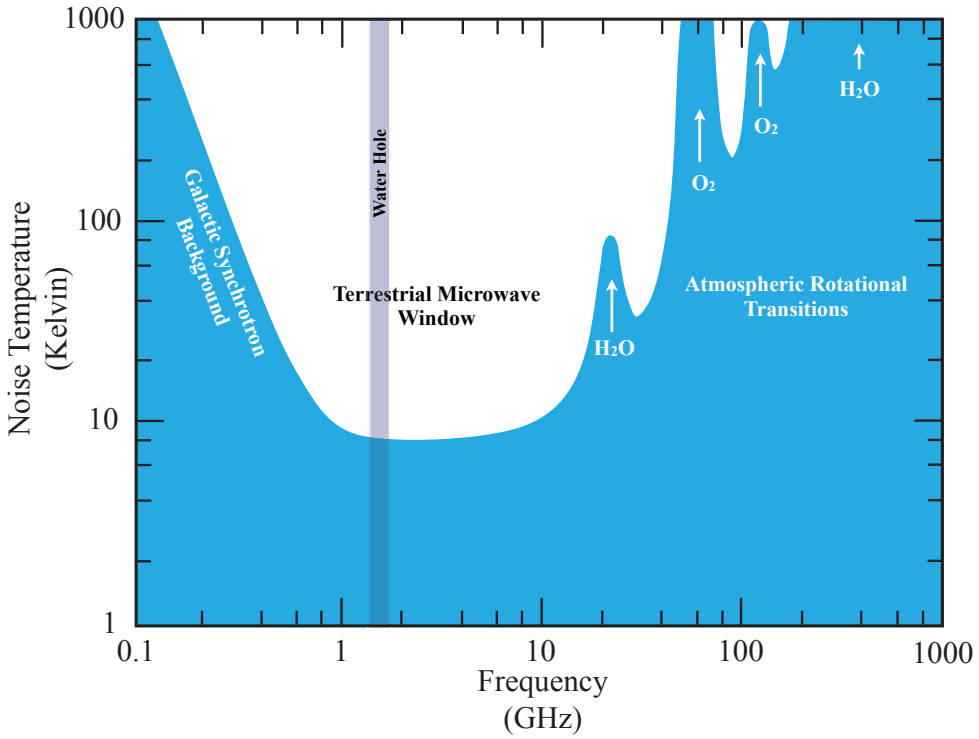

Figure 1: The "terrestrial microwave window": a relatively quiet radio window between non-thermal galactic synchrotron emission and molecular rotational transitions in the Earth's atmosphere. Also indicated on the figure is the so-called "Water Hole" bound by the frequencies of hyperfine transitions of neutral hydrogen (H, $f_{\rm H} \approx 1.42$ GHz) and the hydroxyl radical (OH, $f_{\rm OH} \approx 1.67$ GHz)

Bands above and below the TMW present compelling opportunities as well. Loeb & Zaldarriaga (2007) have detailed a number of reasons why the band between 50−300 MHz might be worthwhile, including the fact that some of the Earth's most detectable emission is leaked at these frequencies. While observations that encroach on the upper end of the TMW tend to become more difficult and less sensitive due to increased atmospheric noise, radio transmissions at these frequencies are less affected by the interstellar and interplanetary plasma and might be more easily produced at very high luminosities (Benford 2010; Benford et al. 2010b,a). Gindilis (1973) pointed out that the received signal to noise ratio (SNR) for pulse communication with delay compensation increases by more than an order of magnitude between 1 and 10 GHz, reaching a peak around 56 GHz. Kardashev (1979) argued that advanced civilizations transmitting deliberate beacons might

[1] e.g. $f_{\rm H}\pi$ =4.462336273 GHz as given in the reference

PoS(AASKA14)116

generally prefer frequencies higher than a few GHz due to less impairment from the ISM, and identified several particular "magic frequencies" related to the cosmic microwave background temperature and hyperfine transitions in the positronium atom around 200 GHz. Fortunately modern radio astronomy technology allows searches over many hundreds of MHz to GHz of instantaneous bandwidth, lessening the extent to which these "magic frequencies" need be considered.

As our own radio technology advances, we will undoubtedly develop new ideas about what type of emission we might expect from similar technology at work on another world. Though there are certain frequencies and signal types that have been particularly advocated to-date, an ideal terrestrial radio SETI observatory would provide near continuous frequency coverage over a significant fractional bandwidth, and flexible signal detection systems that could be programmed to use multiple search algorithms. Such a system is precisely what the SKA will provide - through an open and extensible digital signal processing backend, the SKA will enable SETI observers to readily program flexible compute elements with their own algorithms, and optionally attach user-supplied custom hardware if necessary. The world's most sensitive radio telescope will thus be perfectly suited to conducting novel SETI observations, and as we detail below, will permit the most sensitive search for artificial radio emission ever conducted.

2. SETI Observations on the SKA

2.1 Commensality

Since the inception of modern radio SETI, observers have grappled with a fundamental problem. The SETI search space is so broad in many dimensions, crucially including both frequency and sky location, that a proper search requires very large amounts of telescope time. However, the dedication of significant amounts of observing time on the largest publicly-funded radio telescopes to a single science program, let alone one as speculative as SETI, is simply not possible. More than 30 years ago, SETI astronomers devised a solution that they dubbed "parasitic SETI" (Bowyer et al. 1983). By taking advantage of the fact that the amplified sky signal from a radio telescope can be duplicated many times over with very little added noise or loss of sensitivity, SETI astronomers could "piggy-back" on other users' observations to conduct vast sky surveys for signs of intelligent life without ever billing a minute of primary-user time. Now given the friendly and more accurate name "commensal observing," this technique is enabling the Search for Extraterrestrial Radio Emission from Nearby Developed Intelligent Populations (SERENDIP), SETI@home and AstroPulse projects to use the Arecibo Observatory to conduct SETI observations for thousands of hours per year. Astronomers of all stripes have now begun to recognize the efficacy of commensal observing for a wide range of science programs that can take advantage of very large amounts of observing time without rigorous constraints on integration period or the need to target specific objects or fields. Commensal searches for radio transients are now routinely conducted with the VLBA (Wayth et al. 2011), and other commensal transient and SETI pipelines are in development or early operation at the JVLA, GBT, LOFAR (Serylak et al. 2013), Jodrell Bank and elsewhere.

Support for commensal observations will be critical for the SKA SETI program. For the discussion here, we define commensal observations to mean two or more users using the observatory largely independently, sharing only the primary field(s) of view chosen by the primary observers.

PoS(AASKA14)116

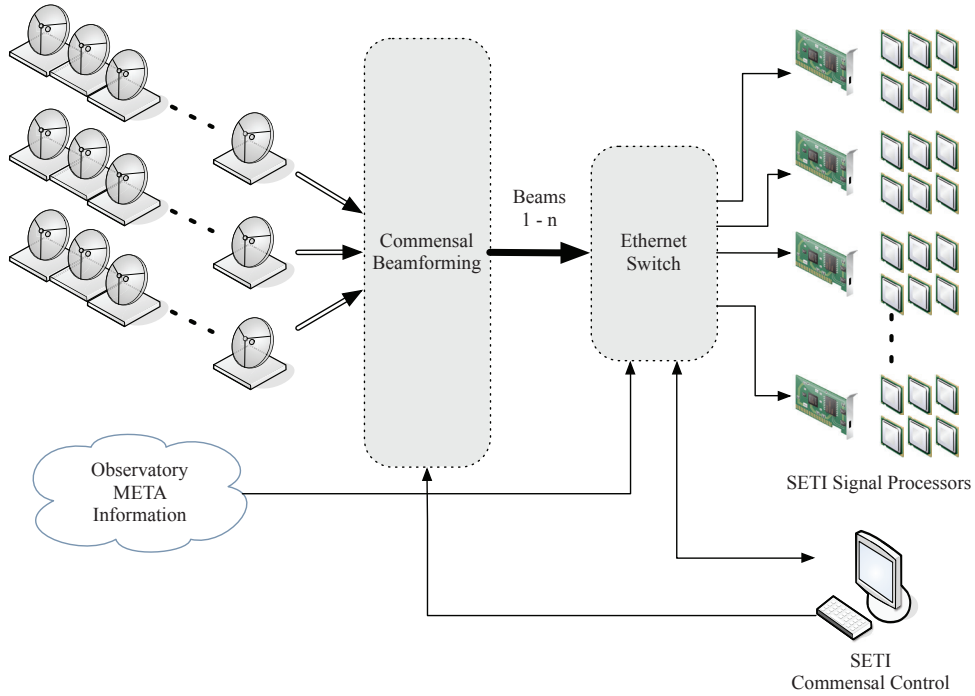

Figure 2: Schematic Diagram of Commensal Observation on the SKA: a SETI observer employs an independent beamforming capability to form phased-array beams within the current primary field(s) of view based on observatory meta information, and directs the unprocessed digital voltage data for those beams to SETI signal processor via Ethernet

From a SETI perspective, we envision an observing system in which multiple phased array beams can be independently steered within the primary field-of-view and fed to dedicated signal processing hardware where SETI specific algorithms are implemented. The Allen Telescope Array's designed mode of operation is an excellent schematic prototype for the way in which such a system can function (Welch et al. 2009). Figure 2 illustrates this scheme: a SETI observer employs an independent beamforming capability to form phased-array beams within the current primary field(s) of view based on observatory meta information, and directs the unprocessed digital voltage data for those beams to SETI signal processors that perform interference excision and signal detection. Using a technology such as Ethernet, multiple copies of a single beam can be directed to multiple signal processors for analysis using multiple techniques. The most sensitive SETI observations with the SKA will be conducted in this phased-array mode, but it is worth pointing out that there are additional opportunities for conducting parallel SETI analysis on imaging and raw u-v data products as well.

2.2 Signal Processing

Signal detection in current SETI experiments is essentially an exercise in matched filtering, in which the filter template is defined by the assumed characteristics of the transmitter. As discussed in Section 1.2, most radio SETI experiments focus on narrow-band emission, and thus the appropriate matched filter is a high resolution Fourier transform, combined with an additional step to account for the unknown relative acceleration between transmitter and receiver. A suite of other

PoS(AASKA14)116

algorithms might be effectively employed in a SETI experiment, including principal component analysis (Biraud 1983; Maccone 1991), autocorrelation (Gardner & Spooner 1992), symbol-wise autocorrelation (SWAC) (Morrison 2012) and automatic modulation classification (AMC) (Aslam & Nandi 2010) and references therein, but are not yet in widespread use largely due to their computational cost. SETI experiments on the SKA will benefit from significant increases in computational performance thanks to the continuing Moore's law growth in the electronics industry (Moore 1965), and thus will be able to consider implementing some of these techniques using the SKA's flexible signal detection systems. Moreover, for the most part these techniques are "embarrassingly parallel" and can readily be scaled to accommodate enhanced capabilities.

Here we will use the case of narrow-band detection as an illustrative example of SETI signal processing and for calculating the sensitivity of SKA SETI observations. Although the sensitivity to sources of a given luminosity would vary somewhat for algorithms detecting other types of signals, the sensitivity expressions and calculations used here are roughly correct for other incoherent or weakly-coherent detection schemes (Sullivan & Mighell 1984; Gulkis 1984).

The minimum incoherently detectable flux, F_i, of a narrow band signal in one polarization is given by:

$$F_i = S_i \Delta b_i = \sigma_{\rm thresh} S_{\rm sys} \sqrt{\frac{\Delta b}{t}} \tag{2.1}$$

Where S_i is the intrinsic flux density of the transmitter, Δb_i the intrinsic bandwidth of the transmitter, $\sigma_{\rm thresh}$ is the SNR, $S_{\rm sys}$ is the system equivalent flux density (SEFD) of the receiving telescope, Δb is the spectral channel bandwidth and t the integration time. Here we assume $\Delta b_i < \Delta b$, and have expressed F_i in terms of flux rather than flux density to more intuitively relate experimental sensitivity to terrestrial transmitter power levels, which are commonly described by total apparent luminosity (or EIRP).

For narrowband signals, the "Doppler drift," or changing apparent frequency due to the relative acceleration between the transmitter and receiver is given simply by:

$$\dot{f} = \frac{d\overrightarrow{V}}{dt} \frac{f_{\rm rest}}{c} \tag{2.2}$$

where $\overrightarrow{V}$ is the line of sight relative velocity between receiver and source, $f_{apparent}$ is the apparent frequency of the transmitter for constant velocity and c the speed of light. Because we are searching for emission at an unknown frequency, the overall Doppler shift imposed on a signal due to some unknown constant relative velocity is unimportant for detection. As points of reference, the maximum contribution from the Earth's orbital motion at 1 GHz is $\sim \pm 0.02$ Hz s^{-1}, and from the Earth's rotation is[2] ~ -0.1 Hz s^{-1}.

Narrow band signals are spectrally broadened by both the ISM and interplanetary medium (IPM), with a magnitude equal to (Cordes & Lazio 1991; Siemion et al. 2013):

$$\Delta\nu_{\rm broad-ISM} = 0.097 \text{ Hz } \nu_{\rm GHz}^{-6/5} \left(\frac{V_\perp}{100}\right) {\rm SM}^{3/5} \tag{2.3}$$

and

$$\Delta\nu_{\rm broad-IPM} = 300 \text{ Hz } \nu_{\rm GHz}^{-6/5} \left(\frac{R}{R_\odot}\right)^{-9/5} \tag{2.4}$$

[2]The maximum rotational contribution is negative because it occurs for a source observed from the equator at zenith.

PoS(AASKA14)116

Where $\nu_{\rm GHz}$ is the observing frequency in GHz, R is the Solar impact distance, $V_\perp$ is the transverse (perpendicular to the line of sight) velocity of the source in km/sec and SM the direction dependent scattering measure, a measure of the electron density fluctuations (c.f. Rickett 1990) integrated along the line of sight. For most lines of sight with $R >\sim 100\ R_\odot$ out to several kpc, the total spectral broadening is no more than[3] ~ 0.1 Hz $\nu_{\rm GHz}^{-6/5}$

The combined influence of the above effects thus dictate the parameters of an optimal search for narrow-band transmitters. Around 1 GHz for example, frequency resolutions of order 0.1 Hz and (unknown) drift correction up to a few Hz/sec would permit optimum detection of equatorial transmitters on a planet up to five times larger and rotating five times faster than the Earth at distances of around 1 kpc. Algorithms used to detect other types of signals will be similarly parameterized, in that they will search or average over similar parameters and will also be constrained based on the expected properties of the signal and communication channel.

2.3 Target Selection

Generally speaking there are two possible SETI observing strategies, targeted observations of individual objects or fields thought to be especially likely to host intelligent life or blind surveys of large swaths of the sky. Occasionally hybrid approaches are employed, e.g. surveys of the *Kepler* Field (Siemion et al. 2013) or the Galactic Center region (Shostak & Tarter 1985). The relative merit of these two approaches depends strongly on the luminosity function of artificial radio transmitters, which at present is largely unconstrained (Tarter 2004), although some insight can be drawn from examining the luminosity distribution of terrestrial transmitters (See Section 2.4). This fact, combined with many other unknowns, will lead to a wide range of views regarding how SETI observations should be conducted on the SKA. As is the case with any science program, these proposals should be subject to peer review and those targets deemed most compelling will be observed with highest priority. Tarter (2001) and references therein detail the varied proposed approaches to SETI target selection in detail.

In practice, the vast majority of SETI observing on the SKA will be conducted commensally with other science programs, employing a signal processing system that will be capable of conducting searches using multiple phased-array beams over only a fraction of the primary beam. Thus an all-sky catalog providing a number of targets per primary field of view, at the highest frequencies, at least equal to the number of phased-array SETI beams ($2-4$ in the minimal case), is required. Such a catalog would consist of $\sim$ 25M targets, and could be readily constructed from the expected results of *GAIA* (Perryman et al. 2001) following a prescription similar to that used in the "HabCat" catalogue of habitable stars (Turnbull & Tarter 2003a,b). That is, essentially choosing stars and exoplanet systems that appear most conducive to life as we know it, or in other words are similar to our own Solar system.

However, a HabCat-like catalog should be supplemented using additional strategies. For example, a simple isotropic volume-selected sample of stars is an ideal target set for a SETI experiment for a number of reasons. Most importantly, it ameliorates the inherent anthropocentric bias that can lead us to concentrate SETI efforts on environments similar to our own planetary system. A search of a blind volume-limited sample of stars is premised only on the notion that intelligent

[3] $V_\perp$ = 25 km/sec, SM from Cordes & Lazio (2002)

PoS(AASKA14)116

life requires a stellar host in order to develop. It also probes a diverse nearby stellar population that is exceedingly well studied at many wavelengths. In the event of a non detection, these attributes of the sample will allow us to place strong and broadly applicable limits on the presence of technologically-produced radio emission. It also allows us to search very deeply, which may be important if the artificial radio transmitter luminosity function declines steeply much past our own technologically produced radio luminosity.

The plethora of multi-planet exoplanet systems now known present a unique opportunity for performing SETI searches at particularly advantageous times - epochs of conjunction along a line of sight to the Earth (See Figure 3). Extrapolating from humanity's exploration of space, it is likely that a more advanced civilization having similar proclivities would explore and perhaps colonize multiple planets in their star system. These explorations could very easily include planet-planet communication, radar imaging or radar mapping of orbital debris, perhaps similar to the way in which we use the Arecibo Planetary Radar to image objects in our own Solar System. Observing these systems during alignments would allow us to potentially eavesdrop on this emission. The published ephemerides of these known systems readily enable calculation of conjunction times, and many more such systems are expected to be discovered in the coming decades.

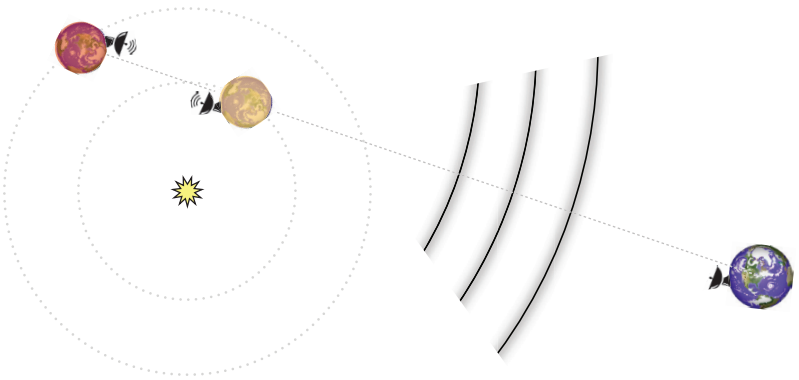

Figure 3: An illustration of a 2-planet conjunction in an extrasolar planetary system along a line of sight to the Earth.

Another idea that may inform the construction of an SKA SETI catalog is the notion that perhaps there are preferred regions of the galaxy for the development of complex life, so-called "galactic habitable zones" (GHZ), e.g. based on stellar population similarity to the Sun or a low rate and proximity of supernovae (Lineweaver et al. 2004). Figure 4 depicts one possible realization of such a GHZ from Morrison & Gowanlock (2014). For each pixel shown, the plotted metric (arbitrary units) is proportional to the accumulated time available for intelligence to evolve across all habitable planets within that pixel out to a maximum range of 5 kpc from Earth, summed over all epochs. The available times for intelligence to putatively emerge occur during gaps between nearby supernova events. As shown, this work suggests that a region of the sky centered on the galactic centre and spanning approximately 60° of longitude and 30° of latitude is especially attractive. Other additions to a SKA SETI target list might include natural sources that could serve either as signposts or natural amplifiers, e.g. using a maser filament to amplify a narrow-band signal transmitted at a specific maser transition frequency (Cordes 1993; Cordes & Sullivan 1995).

PoS(AASKA14)116

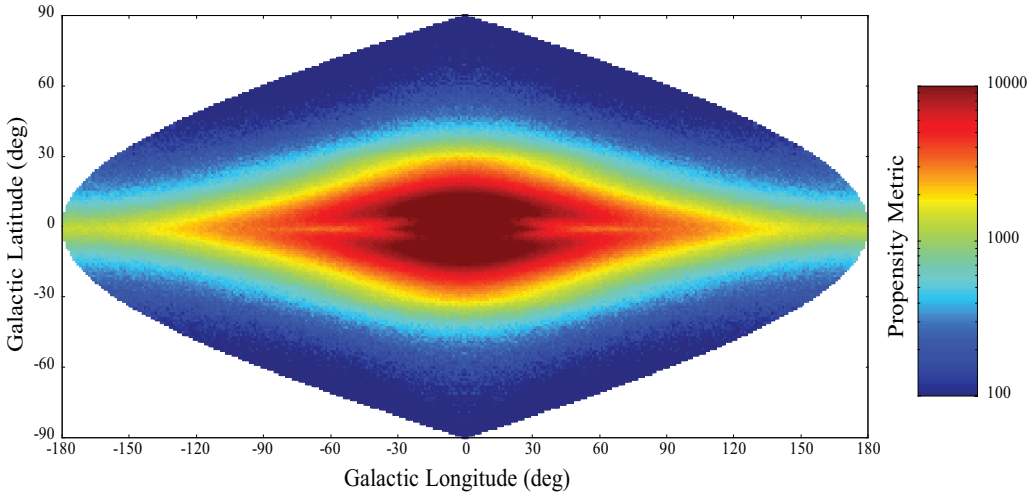

Figure 4: Contour map plot of the relative propensity for the emergence of intelligence as a function of telescope pointing direction in galactic coordinates, based on supernova event rates. An equal-area sinusoidal projection is employed, where each pixel represents approximately one square degree on the sky. For each pixel, the plotted metric (arbitrary units) is proportional to the accumulated time available for intelligence to evolve across all habitable planets within that pixel out to a maximum range of 5 kpc from Earth, summed over all epochs. The available times for intelligence to emerge occur during gaps between nearby supernova events. Only gap times exceeding a minimum threshold are included in the summations. For this plot, a threshold of 2.15 Gyr is employed, consisting of 1.55 Gyr (the assumed time for land-based complex life to evolve) plus 0.6 Gyr (the assumed minimum time for complex life to further evolve to intelligence).

2.4 Sensitivity

Absent of the actual detection of an artificial extraterrestrial radio transmitter, our best points of reference for the sensitivity of radio SETI experiments, and the luminosities of sources we might detect, come from our own terrestrial technology. Figure 5 lists several terrestrial transmitters that produce emission in the bands probed by the SKA, along with their pseudo-luminosities as described by their equivalent isotropically radiated power (EIRP). The approximate number of such transmitters on the Earth is also listed. These terrestrial analogs of artificial transmitters are included simply to describe the energetics of transmitters that SKA SETI experiments might be sensitive to in an intuitive way. Although in many cases these transmitters produce emission precisely alike that searched for in radio SETI experiments, in other cases they modulate their output power in such a way that they would not be as detectable as is implied by considering their transmissions as a simple sinusoid.

Figure 6 depicts the sensitivity of each component of the SKA to narrow-band transmitters at 15 pc, as compared with other facilities actively performing SETI searches over the same band. Search parameter assumptions here match roughly what might be expected for a significant fraction of commensal observations, namely a maximum integration time of 10 minutes. As shown, with appropriate signal detection systems the raw sensitivity of the SKA can be leveraged to create the most sensitive SETI system in the world. In Figure 6, a transmitter is detectable if its EIRP is above the curve for a given telescope. Thus in the observing scenario presented, a transmitter with an EIRP of 2 x 10^{20} ergs/sec (planetary radar) is detectable with all of the telescopes shown, while a transmitter with an EIRP of 1 x 10^{17} ergs/sec (airport radar) is detectable only with SKA2.

PoS(AASKA14)116

Transmitter Type	Luminosity (EIRP) (ergs/sec)	Number on Earth
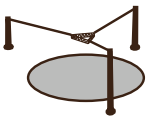 Interplanetary Radar	~2 x 10^{20}	Few
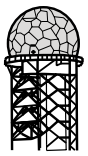 Long Range Aircraft Radar	~1 x 10^{17}	Dozens
High Power TV and Radio	~5 x 10^{12}	Hundreds

Figure 5: A table of terrestrial analogs of artificial extraterrestrial radio sources, including the pseudo-luminosity, as expressed by the equivalent isotropically radiated power (EIRP) and the approximate number of such transmitters present on Earth.

Figure 7 depicts what sensitivities could be attained in a more optimistic scenario, in which SETI was the primary observing purpose or commensal observations were performed with another science case very well matched to SETI. Here we assume an integration time of 60 minutes, and the minimum channelization bandwidth permitted by ISM and IPM effects. As shown, with SKA1, radio transmitter luminosities similar to our high power radars will be detectable from tens of thousands of stars across the entire terrestrial microwave window, and with SKA2 these signals will be detectable from hundreds of thousands of stars. Further, with SKA2 we will for the first time have the sensitivity to detect radio emission similar in power to our own TV and radio stations from a few of our nearest neighbors.

As is the case with many large scientific facilities, we expect the full capabilities of the SKA to emerge over time. SETI is very well suited to conducting early deployment science, as the breadth of unexplored parameter space in SETI is quite large in terms of frequency coverage and raw sensitivity. Although increased sensitivity and digital capabilities, especially the availability of additional phased-array beams, will increase the depth and breadth of SETI on the SKA, with 50% build-out of SKA1 across the board a SETI program could begin to probe the nearer targets in a luminosity-limited survey. More distant targets could be reserved for full sensitivity. However, it is worth pointing out, as shown in Figure 7, that only SKA2 has the ability to detect TV and radio station-like transmitters. With the expected number of planetary systems for which it would be sensitive to these in the single digits, any reduction in sensitivity of SKA2 could render a nearby human-like civilization invisible.

3. Summary

SETI searches with the SKA1 facilities will build from an active base of theoretical and experimental work being done in the field with existing large-scale facilities, but the combination

PoS(AASKA14)116

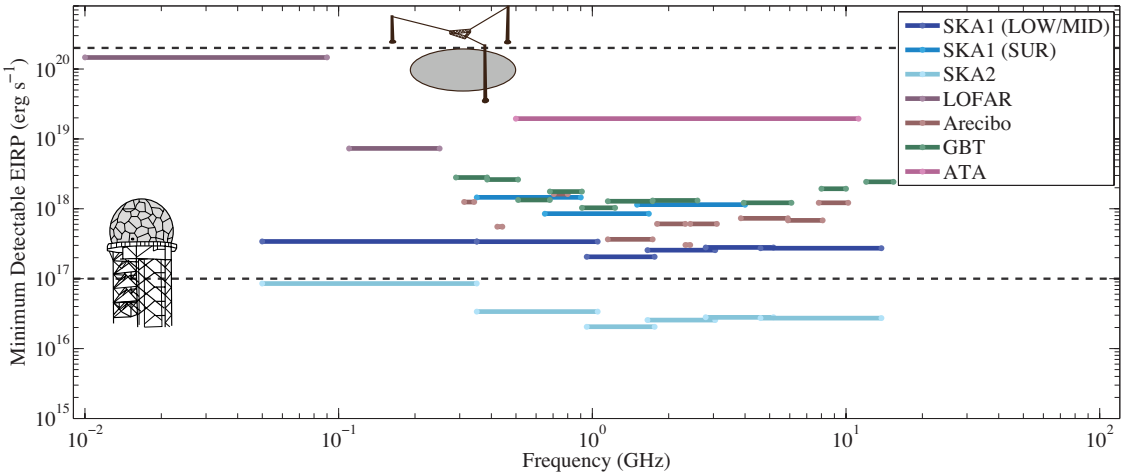

Figure 6: Sensitivity of each component of the SKA to narrow-band transmitters at 15 pc, as compared with other facilities actively performing SETI searches over the same band. Here we assume a significance threshold $\sigma = 15$, bandwidth $\Delta b = 0.5$ Hz and integration time $t = 10$ minutes. A transmitter is detectable if its EIRP is above the curve for a given telescope. Thus a transmitter with an EIRP of 2 x 10^{20} ergs/sec (planetary radar) is detectable with all of the telescopes shown, while a transmitter with an EIRP of 1 x 10^{17} ergs/sec (airport radar) is detectable only with SKA2. Sensitivities for the Green Bank Telescope (GBT), Arecibo and LOFAR were taken from those facilities' observing guides. For LOFAR we assume only core stations are used. Allen Telescope Array (ATA) sensitivity was taken from van Leeuwen et al. (2009).

of raw sensitivity, flexible electronics and increased computational capacity will enable orders-of-magnitude improvement in the speed, depth and breadth of previous SETI experiments. The most thorough targeted SETI search previously conducted surveyed 1000 stars over 1−3 GHz to a luminosity limit of ∼2 x 10^{19} ergs/sec Backus (1998). In a five year commensal campaign, SKA1 could survey every star in its declination range within 60 pc − more than ten thousand stars − to a luminosity limit an order of magnitude fainter, $\sim 10^{18}$ ergs/sec, over a larger band. Conservatively, in ten years SKA2 could survey every star within 60 pc to a luminosity limit equal to the EIRP of terrestrial aircraft radars over the entire terrestrial microwave window.

Historically, performing SETI experiments effectively with large telescopes has been technically and politically difficult. SKA will be the first world-class telescope ever constructed for which SETI observations are a conscious part of the design process and are available as a facility observing mode. Our most powerful tool to search for other intelligent life in the cosmos will be available and accessible to astronomers around the world, infusing new people and ideas in to the field of SETI and maximizing the scientific return of the SKA. Searches for life beyond Earth, especially searches for intelligent life, have a remarkable ability to spark the imagination of the public, and this component of the SKA science case will offer ample opportunity for outreach and public engagement. From a purely scientific standpoint, the discovery of an independent genesis of life on another world would provide strong evidence that life is common, and its intelligence would suggest that evolution proceeds towards this end easily. Were an information-containing transmission to be received and decoded, we can only conjecture what thoughts and ideas might be contained therein, but surely our human culture would be enriched in unimaginable ways.

PoS(AASKA14)116

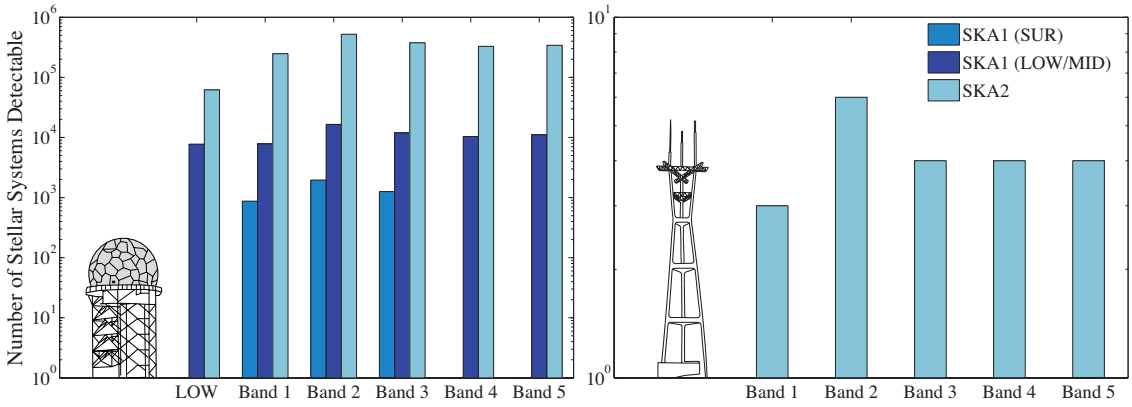

Figure 7: The number of stars in the solar neighborhood from which narrow-band emission would be detectable at two luminosity levels. Here we assume a stellar number density of $n_* = 0.1$ pc^{-3}, significance threshold $\sigma = 12$ and integration time $t = 60$ minutes. For luminosities similar to our terrestrial aircraft radars we assume bandwidth $\Delta b = 0.01$ Hz and for luminosities similar to terrestrial TV/radio-like signals (right) we assume fully coherent integration ($\Delta b = t^{-1}$). The search parameters shown here, namely the smaller value of Δb than discussed in Section 2.2, reflect the relative proximity of these nearby stars and by extension their less scattered lines of sight.

Acknowledgements Part of this research was carried out at the Jet Propulsion Laboratory, California Institute of Technology, under a contract with the National Aeronautics and Space Administration. A. P. V. S., E. J. K. and D. W. received partial support from a competitive grant awarded by the John Templeton Foundation.

References

Aslam, M. & Nandi, A. 2010, in IEEE International Workshop on Machine Learning for Signal Processing, 391–396

Backus, P. R. 1998, Acta Astronautica, 42, 651

Benford, G., Benford, J., & Benford, D. 2010a, Astrobiology, 10, 491

Benford, J. 2010, arXiv, astro-ph.IM:1003.5938

Benford, J., Benford, G., & Benford, D. 2010b, Astrobiology, 10, 475

Biraud, F. 1983, Acta Astronautica, 10, 759

Blair, D. G. & Zadnik, M. G. 1993, Astronomy and Astrophysics, 278, 669

Bowyer, S., Zeitlin, G., Tarter, J., Lampton, M., & Welch, W. J. 1983, Icarus, 53, 147

Chennamangalam, J., Siemion, A. P. V., Lorimer, D. R., & Werthimer, D. 2015, New Astronomy, 34, 245

Cocconi, G. & Morrison, P. 1959, Nature, 184, 844

Cordes, J. 1993, Third Decennial US-USSR Conference on SETI. ASP Conference Series, 47, 257

Cordes, J. & Sullivan, W. I. 1995, Progress in the Search for Extraterrestrial Life, 74, 325

Cordes, J. M. & Lazio, T. J. 1991, Astrophysical Journal, 376, 123

Cordes, J. M. & Lazio, T. J. W. 2002, arXiv:0207156v3

Drake, F. D. 1961, Physics Today, 14, 40

PoS(AASKA14)116

Fridman, P. A. 2011, Acta Astronautica, 69, 777
Gardner, W. A. & Spooner, C. M. 1992, IEEE Transactions on Communications, 40, 149
Gindilis, L., Davydov, V., & Strelnitski, V. 1993, in Third Decennial US-USSR Conference on SETI, ed. G. S. Shostak, 161–163
Gindilis, L. M. 1973, Radiophysics and Quantum Electronics, 16, 1118
Gray, R. H. & Ellingsen, S. 2002, The Astrophysical Journal, 578, 967
Gulkis, S. 1984, Note on the Optimum Search Strategy for Uniformly Distributed CW Transmitters, Tech. Rep. NASA TDA 42-77
Herbst, E. & van Dishoeck, E. F. 2009, Annual Review of Astronomy & Astrophysics, 47, 427
Hogerheijde, M. R., Bergin, E. A., Brinch, C., et al. 2011, Science, 334, 338
Horowitz, P., Matthews, B. S., Forster, J., et al. 1986, Icarus, 67, 525
Horowitz, P. & Sagan, C. 1993, The Astrophysical Journal, 415, 218
Kardashev, N. S. 1979, Nature, 278, 28
Korpela, E., Werthimer, D., Anderson, D., Cobb, J., & Lebofsky, M. 2001, Computing in Science and Engineering, 3, 78
Krasnopolsky, V. A., Maillard, J. P., & Owen, T. C. 2004, Icarus, 172, 537
Leigh, D. 1998, PhD thesis, Harvard University, Cambridge, MA
Lemarchand, G. A. 1994, Astrophysics and Space Science, 214, 209
Lineweaver, C. H., Fenner, Y., & Gibson, B. K. 2004, Science, 303, 59
Loeb, A. & Zaldarriaga, M. 2007, Journal of Cosmology and Astroparticle Physics, 2007, 1
Maccone, C. 1991, in The Exploration Broadens: Proceedings of the Third International Symposium on Bioastronomy, ed. J. Heidmann & M. J. Klein, 247–253
Messerschmitt, D. G. 2012, Acta Astronautica, 81, 227
Messerschmitt, D. G. & Morrison, I. S. 2012, Acta Astronautica, 78, 80
Moore, G. E. 1965, Electronics, 114
Morrison, I. 2012, Acta Astronautica, 78, 90
Morrison, I. S. & Gowanlock, M. G. 2014, submitted to Astrobiology
Morrison, P., Billingham, J., & Wolfe, J., eds. 1977, The Search for Extraterrestrial Intelligence (NASA)
Oliver, B. M. & Billingham, J., eds. 1971, Project Cyclops: A Design Study of a System for Detecting Extraterrestrial Intelligent Life (NASA)
Perryman, M. A. C., de Boer, K. S., Gilmore, G., et al. 2001, Astronomy and Astrophysics, 369, 339
Petigura, E. A., Howard, A. W., & Marcy, G. W. 2013, Proceedings of the National Academy of Sciences, 110, 19273
Rampadarath, H., Morgan, J. S., Tingay, S. J., & Trott, C. M. 2012, The Astronomical Journal, 144, 38
Rein, H., Fujii, Y., & Spiegel, D. S. 2014, in Proceedings of the National Academy of Sciences, 6871–6875
Rickett, B. J. 1990, Annual Review of Astronomy & Astrophysics, 28, 561
Serylak, M., Karastergiou, A., Williams, C., et al. 2013, in Proceedings of the International Astronomical Union, 492–494
Shostak, G. S. & Tarter, J. 1985, Acta Astronautica, 12, 369

PoS(AASKA14)116

Siemion, A., Korff, J. V., McMahon, P., et al. 2010, Acta Astronautica, 67, 1342
Siemion, A. P. V., Demorest, P., Korpela, E., et al. 2013, The Astrophysical Journal, 767, 94
Sullivan, W. I. & Cordes, J. 1995, Progress in the Search for Extraterrestrial Life, 74, 337
Sullivan, III, W. T. & Mighell, K. J. 1984, Icarus, 60, 675
Tarter, J. 2003, Annual Reviews of Astronomy and Astrophysics, 39, 511
Tarter, J., Cuzzi, J., Black, D., & Clark, T. 1980, Icarus, 42, 136
Tarter, J. C. 2001, in Photonics West 2001 - LASE, ed. S. A. Kingsley & R. Bhathal (SPIE), 93–103
Tarter, J. C. 2004, New Astronomy Reviews, 48, 1543
Turnbull, M. C. & Tarter, J. C. 2003a, The Astrophysical Journal Supplement Series, 145, 181
—. 2003b, The Astrophysical Journal Supplement Series, 149, 423
van Leeuwen, J., Blitz, L., Bock, D., et al. 2009, in Panoramic Radio Astronomy: Wide-field 1-2 GHz research on galaxy evolution, 5
Wayth, R. B., Brisken, W. F., Deller, A. T., Majid, W. A., Thompson, D. R., Tingay, S. J., & Wagstaff, K. L. 2011, The Astrophysical Journal, 735, 97
Welch, J., Backer, D., Blitz, L., et al. 2009, in Proceedings of the IEEE, 1438–1447

PoS(AASKA14)116

PROCEEDINGS OF SCIENCE

Protoplanetary disks and the dawn of planets with SKA

L. Testi[*1,2,3], **L. Perez**[4], **I. Jimenez-Serra**[2], **M. Hoare**[5], **A. Boley**[6], **T.L. Bourke**[7], **J.R. Brucato**[1], **P. Caselli**[8], **C. Chandler**[4], **C. Codella**[1], **A. Isella**[9], **J. Lazio**[10], **M.E. Palumbo**[11], **L. Podio**[1], **A. Remijan**[4], **J. Tarter**[12], **D.J. Wilner**[13]

[1]*INAF-Osservatorio Astrofisico di Arcetri, Firenze, Italy;* [2]*European Southern Observatory, Garching, Germany;* [3]*Excellence Cluster Universe, Garching, Germany;* [4]*National Radio Astronomy Observatory, USA;* [5]*University of Leeds, Leeds, UK;* [6]*University of British Columbia, Canada;* [7]*SKA Organization, Jodrell Bank, UK;* [8]*Max Planck Institut fuer Extraterrestrische Physik, Garching, Germany;* [9]*Rice University, Houston TX, USA;* [10]*Jet Propulsion Laboratory, California Institute of Technology, Pasadena, CA;* [11]*INAF-Osservatorio Astrofisico di Catania, Catania, Italy;* [12]*SETI Institute, Mountain View CA, USA;* [13]*Harvard-Smithsonian Center for Astrophysics, Cambridge MA, USA*

E-mail: lt@arcetri.inaf.it, ltesti@eso.org

Protoplanetary disks are formed as a consequence of angular momentum conservation during star formation. Planetary systems are expected to form within the disks during the first few Myrs of evolution of the system. The SKA1, in combination with ALMA and E-ELT, can provide unique constraints on the physical and chemical processes associated with planet formation. In this contribution we investigate the key areas in which SKA1 and its future extensions will advance our understanding of planetary system formation and the delivery of complex and pre-biotic molecules on the proto-planets. We focus mainly on three aspects: the growth of solids and the first steps towards the rocky cores of planets, the detectability of pre-biotic molecules in the gas phase in disks, and the effects of the central star on the disk chemistry. For each area, we discuss which SKA1 science requirements need to be fullfilled to allow this science to be carried out. It emerges that, if the high frequency bands are deployed, SKA1 has the potential of delivering unique and transformational science in the field of planet formation. Key science contributions are also possible with a SKA1 without Band 5, but the impact will be significantly reduced. We also identify the limitations of SKA1 and the expansion of capabilities that will be required in the future.

Advancing Astrophysics with the Square Kilometre Array
June 8-13, 2014
Giardini Naxos, Italy

*Speaker.

PoS(AASKA14)117

1. Introduction

Disks form as a consequence of angular momentum conservation during the star formation process (e.g. Shu et al. 1987). In the early stages of the star formation process the disk mediates accretion from the parental core to the forming protostar, while at later stages it provides the natural location and material for the planet formation process. The observational study of the properties and evolution of protoplanetary disks is thus a direct probe of the initial conditions for planet formation. The presence of protoplanetary disks around young stars was originally inferred from the emission in excess to the stellar photosphere at infrared and submillimetre wavelengths (eg. Beckwith et al. 1990; Beckwith & Sargent 1991). It was very rapidly understood that the excess emission was likely due to a disk-like distribution of dust located around and heated by the young star at the centre. This was also consistent with the dynamics of the molecular gas, which resembled Keplerian rotation around the central object. The inferred sizes (up to few times 100 AU in radius, corresponding to a few arcsec at the distance of the nearby star forming regions) and masses (up to 10-20% of the central star mass) were also consistent with the expected values for a pre-solar nebula. These ideas were then spectacularly confirmed by the HST silhouette optical absorption images a few years later (O'dell et al. 1993). Following these initial observations, protoplanetary disks around young solar analogs have been extensively studied in nearby star forming regions. The recent review by Williams & Cieza (2011) summarizes most of our current knowledge of the general properties of protoplanetary disk populations in nearby star forming regions.

Due to the connection with planet formation, the physical and chemical evolution of protoplanetary disks are of fundamental importance to understand the formation of planetary systems in general and of our own Solar System in particular. Most of the research in the last few years has focused in understanding the global disk population properties and evolution with mass and environment and the evolution of dust and gas under the competing effects of planet formation and photoevaporation from the central star.

The study of protoplanetary disks is one of the main science drivers of ALMA, JWST and the E-ELT. These facilities will advance significantly our understanding of the physics of disks and planet formation, especially in combination with longer wavelength radio observations. The SKA1 will enable unique observations for constraining the physics of planet formation and disk dissipation mechanisms. Studies of disks in the frequency range below 15 GHz have been severely hampered by the limited sensitivity of existing radio facilities. The upgraded VLA is providing tantalizing results that show the potential of SKA1. Wilner (2004) discussed in some detail the case for observing protoplanetary disks with the SKA, here we provide an extension of that case, taking into account the advances in the last decade and especially considering the most recent observational results at millimetre and submillimetre wavelengths. We discuss detailed sensitivity limits, frequency ranges, and spectral resolution requirements for SKA1 and its future extensions, as well as observational strategies and constraints for important new experiments in this field.

In the continuum, the main emission mechanisms are related to three separate phenomena that can be disentangled by monitoring observations at different wavelengths in the 1-15 GHz range: thermal emission from dust, thermal emission from ionized winds, and strongly variable thermal and non-thermal emission arising close to the stellar surface from accretion and magnetic activity. Key SKA observations of protoplanetary disks will focus on (1) the growth of dust grains towards

PoS(AASKA14)117

planetesimals, which can be constrained only by gaining access to centimetre-wave emission from large dust grains and pebbles, (2) the disk cold gas component and its possible pre-biotic molecular species, and (3) the disk-star interaction traced by the emission of photoevaporative and disk winds, which regulate angular momentum transport in disks and the origin of outflows, and of energetic stellar flares that may drive some of the chemical processing of both solid and gaseous material in the disk. Based on detailed models of the physics of protoplanetary disks, we discuss the required sensitivity, angular resolution and time cadence of programmes aimed at addressing these questions.

For spectral lines, emission from complex and pre-biotic molecules are potentially detectable in protoplanetary disks at the high end of SKA1 frequency range. Given the cold conditions of disk midplanes, organics can be locked into the icy mantles of dust grains and remain undetected. However, cosmic ray induced secondary uv-photons can desorb ice in heavily shielded regions, as recent Herschel measurements of water in cores and protoplanetary disks suggest (Hogerheijde et al. 2011; Caselli et al. 2012; Podio et al. 2013). This process would allow for the release of organic molecules in the gas phase. We discuss model computations of the expected emission within the SKA1 bands from the amino acid Glycine desorbed from icy mantles in disks. We conclude that detection may be possible, albeit not easy with SKA1, paving the way for abundance studies of this important pre-biotic molecule.

2. Grain growth in disks

Grain settling and growth in protoplanetary disks is thought to be the initial step of the formation of the rocky cores of planets (see e.g. Beckwith et al. 2000). In the last decades, the processes of collision and sticking of grains have been studied theoretically and in laboratory experiments (eg. Blum & Wurm 2008), and are used in global disk evolution models to describe the physics of dust evolution (eg. Birnstiel et al. 2012). The recent review of Testi et al. (2014) provides a summary of the status of our theoretical, experimental and observational understanding of the grain growth process in disks. In Figure 1 we show a sketch of a protoplanetary disk with the physical processes related to grain growth and an indication of the regions that can be probed with current and future observing facilities.

The main observational signature for the growth of grains in the disks midplane is the spectral index of the dust opacity coefficient, which can be reliably measured once the thermal structure of the disk is properly modeled and contamination from other sources of continuum emission (e.g. from electrons in winds) is properly taken into account (Testi et al. 2003, 2001). The combination of sensitive millimetre and centimetre observations of the nearby TW Hya disk disentangle emission mechanisms and provide strong evidence for pebble-sized grains (Pascucci et al. 2012; Wilner et al. 2005). Results from recent millimetre wave surveys of the continuum emission from disks have shown that grain growth is a widespread phenomenon, also occurring very early in the lifetime of disks (eg. at the disk formation stage; Miotello et al. 2014) and also, somewhat unexpectedly, in exotic systems (eg. brown dwarf disks; Ricci et al. 2012, 2014). These results, if confirmed, would suggest that the early growth of planetary cores, and perhaps full planets, is a fast process in protoplanetary disks.

PoS(AASKA14)117

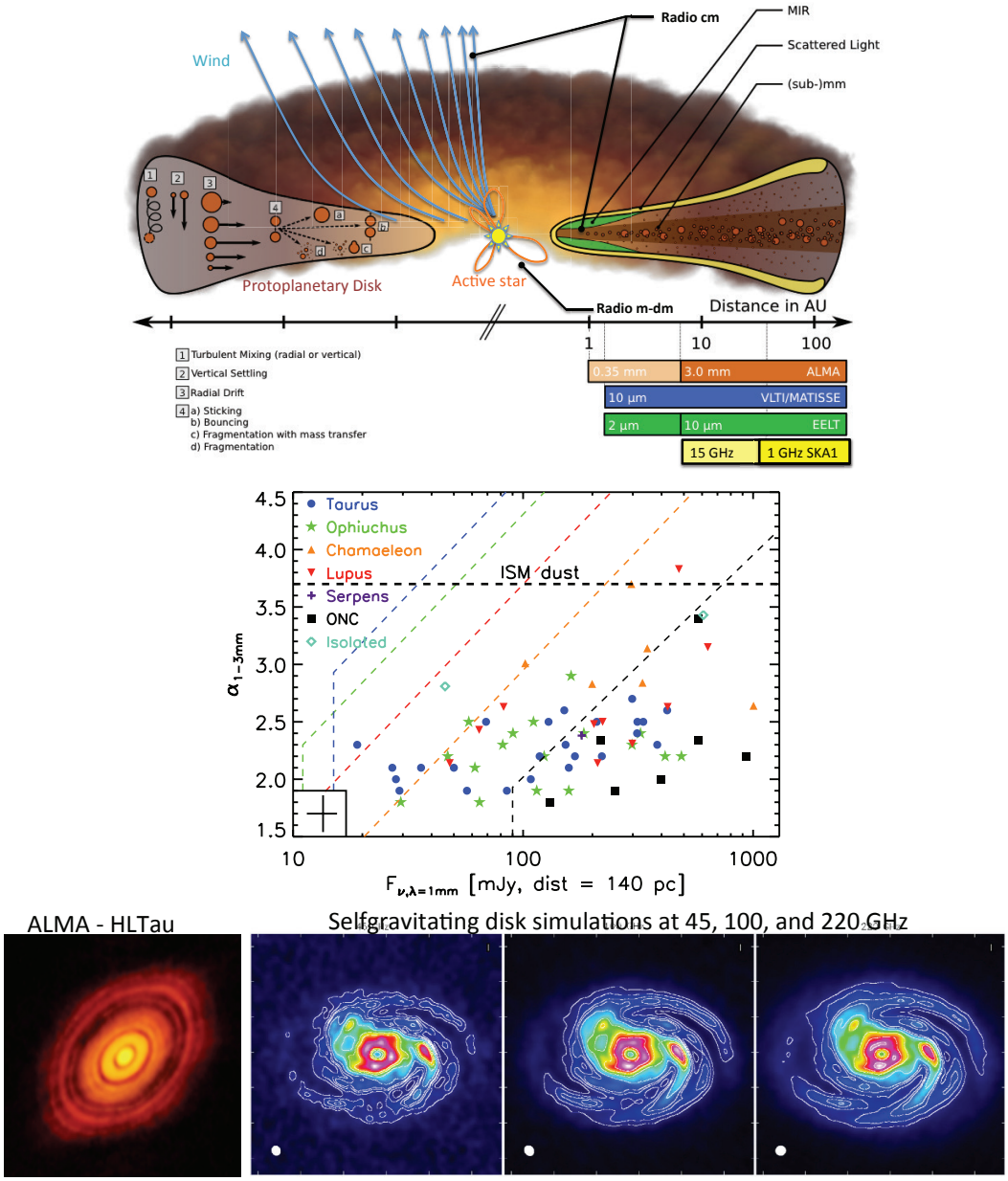

Figure 1: Observing grain growth in disks, from models to observations. Top panel: sketch of a disk-star system, indicated are the main sources of continuum emission in the thermal infrared, submillimetre and radio domains; the physical processes for grain growth in the disk and the scales probed by various facilities for disks in nearby star forming regions are also shown. Middle panel: surveys of the 1 to 3 mm spectral index versus 1 mm flux of disks in nearby star forming regions; small values of the spectral index correspond to grain growth, the value expected for the interstellar medium (ISM) grains is shown; all observations have been scaled to a common distance of 140 pc. Bottom: the leftmost panel is the ALMA-SV dust emission image at 230 GHz of the HL Tau disk, at a spatial resolution of approximately 5 AU, the ring features in the outer disk likely represent dust aimuthal concentrations; the other panels show simulated disk images for an angular resolution of $\sim$0.15 $''$ at 45, 100 and 220 GHz (from left to right), the theoretical disk has been located at a distance of 50 pc from the Sun, corresponding to the closest known protoplanetary disk system (TW Hya). The two top panels have been adapted and modified from Testi et al. (2014), the bottom panels have been adapted from Dipierro et al. (2014) and from `http://www.eso.org/public/news/eso1436/`.

PoS(AASKA14)117

Models have difficulties in explaining these findings, unless some form of grain trapping or localized growth is occurring in the disk (Pinilla et al. 2012). The future observational work will thus be focused on trying to spatially resolve grain growth in disks. Observations at cm-wavelengths play a key role as they allow us to trace solids grown to pebble sizes across the cm-size barriers, this process is expected to be very localized in protoplanetary disks. A key and unique contribution of SKA1 will be the ability to detect and resolve spatially the wind emission from the disk/star, which needs to be carefully accounted for and removed to study the dust properties. Initial results have been and are being obtained combining data from millimetre interferometers (including ALMA) with data from the JVLA at 0.7, 1.3 and 6 cm. Pérez et al. (2012) found convincing evidence for a radial stratification of the dust properties in protoplanetary disks, confirming earlier suggestions (Banzatti et al. 2011; Guilloteau et al. 2011). The angular resolution and surface brightness sensitivity to detect localized growth is just becoming available for the outer disk regions with ALMA. A dramatic demonstration of the power of high angular resolution onservations to study the dust distribution in disks has just been obtained by the ALMA Science Verification observations of HL Tau, shown in Fig. 1, bottom panel. Note that ALMA will not be able to provide the angular resolution to resolve these structures at its longest operating wavelengths, which will instead be made possible with SKA1.

In Figure 1 we show an example of a simulated disk with spiral arms in the gas distribution, in this case caused by gravitational instability. The higher gas densities in the arms provide local pressure maxima that could very effectively trap large dust particles. The simulated ALMA observations show that high angular resolution (of the order or better than $0.1''$ is critical to detect the expected features in these disks (Cossins et al. 2010; Dipierro et al. 2014).

2.1 Dust evolution with SKA1

The main contribution of SKA1 to the study of dust evolution will be to extend with a significant improvement in sensitivity and resolution the work done by JVLA in combination with ALMA. During the early science phase, the first key step will be to produce sensitive multi-frequency surveys of disks in nearby star forming regions at a few arcsecond resolution. Those young star clusters that are inaccessible to the JVLA in particular can be surveyed for the first time in the 1-14 GHz range. Combined with ALMA surveys that are and will be carried out in the coming years, these will allow to separate the dust emission from the contaminating wind emission in the SED and to provide robust statistics of the timescale for grain growth in protoplanetary disks, which is still lacking. This will be an essential milestone to constrain the timescales for the formation of the rocky cores of planets.

With the completed SKA1-MID it will be possible to map the grain growth as a function of radius with a resolution of few AU on selected bright disks in nearby star forming regions. These requirements are well captured in the current version of the SKA1 science requirements (Braun (2014), in particular for the continuum sensitivity near 1 and 12 GHz).

2.2 Dust evolution beyond SKA1

With the full SKA it will be possible to routinely map grain growth at even higher resolution and on wide range of targets. To fully resolve planet formation and probe the physics of grain

PoS(AASKA14)117

trapping and growth, it is necessary to obtain an angular resolution comparable to the disk scale height, which is roughly 10% of the distance from the central star. This implies that within 10 AU, where the relevant planet formation region is occurring, the angular resolution has to be of the order or better than 1 AU. At the distance of the nearby star forming regions this corresponds to 10 mas resolution and the required surface brightness sensitivity will be tens of K in the continuum. These figures will define the key requirements for this science beyond SKA1.

3. Complex organic molecules in disks

Complex organic molecules are produced in the interstellar medium, most efficiently through solid state chemistry channels. The "ices" in dense interiors of molecular clouds represent a location where atoms and molecules are packed close together and partly shielded from the dissociative interstellar radiation field. For the simple organic H_2CO, there are already indications from resolved morphology and low excitation in disks that the predominant formation pathway is hydrogenation of CO ice followed by desorption (Qi et al. 2013). How far the chemistry of complex organic molecules and pre-biotic molecules goes in the interstellar medium is an important area to be understood in order to figure out the complexity of the material that is delivered on the planetary surfaces. There is convincing evidence for the presence of simple amino acids in meteorites and possibly in comets of our own Solar System (Pizzarello et al. 1991; Glavin et al. 2006; Elsila et al. 2009), laboratory experiments have also shown that complex molecules and simple amino acids like Glycine (NH_2CH_2COOH) can form in irradiated interstellar ice analogs (Muñoz Caro et al. 2002; Holtom et al. 2005; Modica & Palumbo 2010).

The recent detection of water vapour in the prestellar core L1544 shows that even in the cold interior of these dense cores, cosmic rays yelding secondary high energy radiation can desorb a measurable quantity of molecules from the ices (Caselli et al. 2012). Jiménez-Serra et al. (2014) have shown that not only water, but also complex pre-biotic molecules (like Glycine) may be detectable if desorbed together with the water molecules (see Figure 2 for the predictions of Glycine emission in the prestellar core L1544). We expect that this result can be extended to the cold midplanes of protoplanetary disks (see Figure 2 bottom panel). The direct detection in the gas phase and measurements of the abundance with respect to water of complex organic molecules would be a significant milestone in studying our cosmic heritage and the ability of ISM and disk chemistry to produce the raw material required for the development of life on exoplanets. As complex organic molecules are easily destroyed in the warm molecular layers of disks, which are exposed to the heating radiation from the star, the best hope to detect and study them is in the cold interior of disks, where they may be desorbed from ices as outlined. In these cool conditions, the rotational spectra of complex molecules is significantly skewed towards low frequencies. As a consequence the detection with ALMA is less easy and limited to the (as of today unfunded) Band 1 and 2 covering the 35-80 GHz range. The high frequency SKA band with its superb sensitivity can play a major role in detecting and studying complex organic molecules.

3.1 Detection of complex organic molecules in disks with SKA1

The requirements to observe complex organic molecules in protoplanetary disks imply that it will be necessary to reach at least $\sim$50 mK sensitivity for narrow lines ($\Delta V \sim 0.2$ km/s) at $\sim 3''$

PoS(AASKA14)117

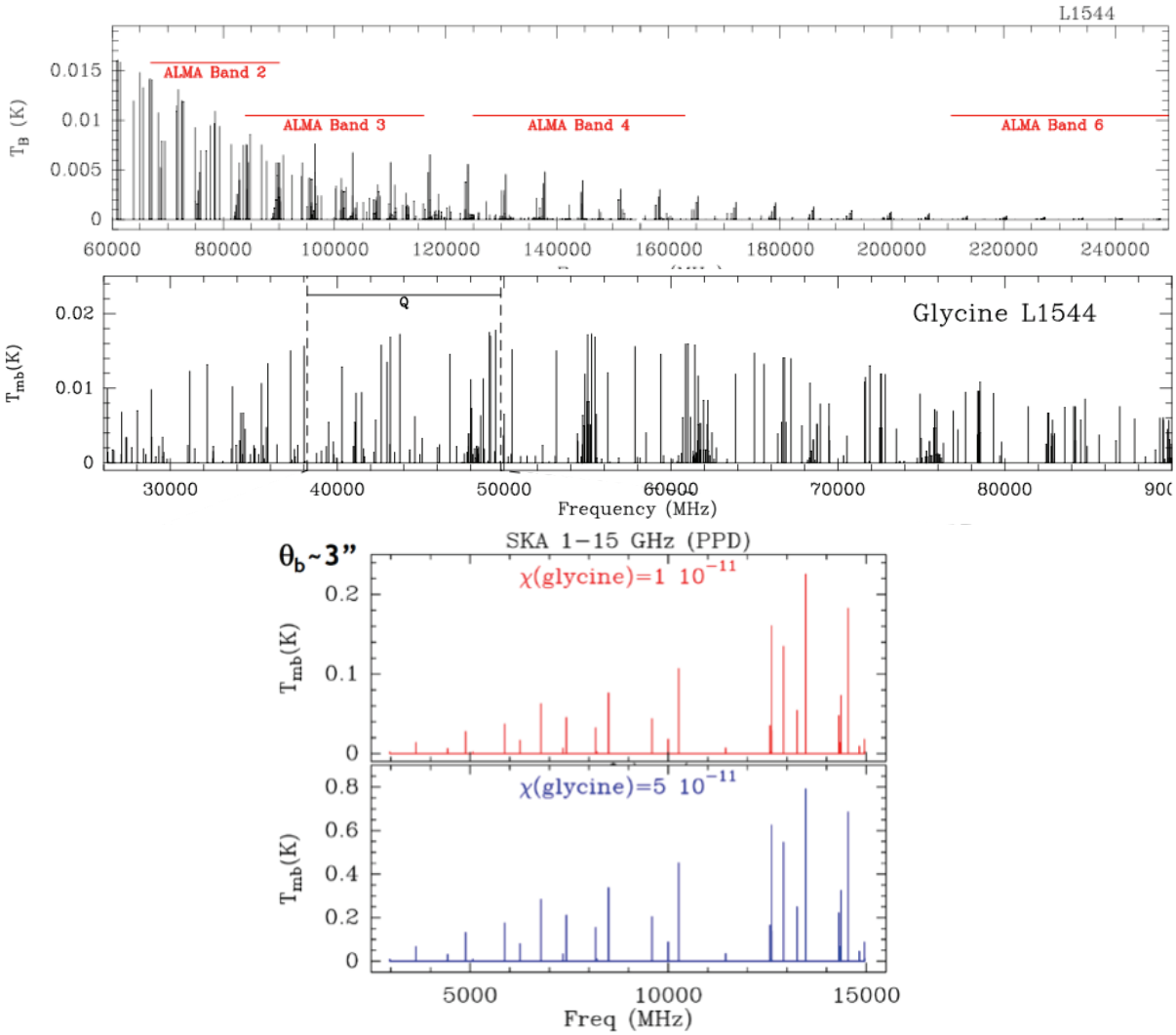

Figure 2: Top and middle panels: predictions for the Glycine rotational spectrum in a cold prestellar core (L1544); the spectrum shows the frequency ranges covered by the low frequency ALMA receivers (top) and the high frequency JVLA bands; the predicted intensities are low and difficult to reach even with these very sensitive facilities (adapted from the models of Jiménez-Serra et al. 2014). Bottom panel: preliminary preditions of Glycine line intensities in the frequency range from 1 through 15 GHz covered by SKA1 for the TW Hya protoplanetary disk with two assumptions on the Glycine gas phase abundance (Jimenez-Serra et al., in preparation).

resolution, corresponding to typical disk sizes in the nearby star forming regions. This requirement is captured in the SKA1 science requirements (Braun 2014) which has been derived for prestellar cores, but can also apply to protoplanetary disks, scaling for the smaller expected size and narrower line. In fact, if the gas phase abundance of Glycine is on the high side of the expectated range, then the detection should not be very demanding and achievable with about 10 h on source. In addition, we remark that the simplistic assumption of local thermodynamic equilibrium for the line excitation, made in the computations, is very simplistic and may not apply to the conditions of these heavy molecules. The detection and analysis of Carbodiimide (HNCNH) in Sgr B2 has

PoS(AASKA14)117

shown that several low frequency lines may be masing, increasing their chances for detection, but significantly complicating the physical modeling and interpretation (McGuire et al. 2012). It is important to note that these computations were made with the (ambitious) goal of detecting Glycine, it is expected that more abundant and less complex organic molecules will be easier to detect; note however that this field is still in its infancy as no complex organic molecule has yet been detected in protoplanetary disks. While ALMA is already tranforming the chemical study of warm and young protostars (eg. Jørgensen et al. 2012; Sakai et al. 2014), it is the lower frequency regime, the one probed by SKA1 with Band 5 or by the as yet unfunded ALMA Band 1 and 2, that will allow us to investigate throughly the chemical complexity of cold protoplanetary disk midplanes. We note that while an SKA1 equipped with Band 5 will allow to detect complex organic (and possibly pre-biotic) molecules in disks in nearby star forming regions, the interpretations of these lines will not be straightforward (see eg. Faure et al. 2014) and significant effort should be spent on laboratory measurements as well as chemical and astrophysical modeling to make the most effective use of the observations. However, SKA1 may not be able to produce resolved images of these faint molecular species, but this will be possible with the full SKA.

3.2 Imaging of complex organic molecules in disks beyond SKA1

To study complex molecule chemistry and the variation of abundance as a function of distance from the central star and across the snowlines, it will be necessary to perform spatially resolved studies. These studies will require a significant improvement of the sensitivity coupled with a good imaging performance. One order of magnitude improvement in sensitivity will be required to be able to image the disks at $1''$ resolution, which will allow to probe the effect of the CO snowline in the nearest disks around relatively massive stars (2-4 $M_{\odot}$). Two orders of magnitude increase will allow to perform a detailed analysis of the chemistry of the disk around solar mass young stellar objects, possibly resolving the inner planet formation regions at $0.3''$ resolution.

4. The temperament of young stars and its effect on disks

Young stellar objects with disks produce high energy radiation in the ultraviolet and X-rays, caused by the accretion of material from the disk to the young star and by the active chromospheres. X-ray variability is thought to originate from flaring powered by reconnection events in the stellar magnetosphere and is known to be very variable in young stellar objects with disks (see e.g. the recent surveys in ONC, Taurus and Ophiuchus star forming regions: Grosso et al. 2005; Güdel et al. 2007; Pillitteri et al. 2010). The high energy radiation from the central star (either from accretion or chromospheric activity) is known to affect disk evolution (Gorti et al. 2009), and is also expected to affect disk gas and solids chemistry (eg. Ábrahám et al. 2009; Banzatti et al. 2012). A systematic study of the effect of this high-energy irradiation variability on the disks is lacking because of the difficulties to set up coordinated X-ray and millimetre/infrared campaigns.

Radio continuum observations in the 1-12 GHz range is an important tool to study the long term effects of stellar radiation on the disk by constraining the photoevaporative winds (Galván-Madrid et al. 2014; Pascucci et al. 2011, 2012), and has also the potential of allowing us to execute coordinated studies for the effects of energetic flares on the disk chemistry. X-ray activity and flaring is also known to be connected with radio flaring, although the sensitivity of existing radio

PoS(AASKA14)117

facilities is limited and only a fraction of the X-ray detected objects are also identified as radio flaring (eg. Forbrich et al. 2011; Forbrich & Wolk 2013).

4.1 The temperament of young stars and its effect on disks with SKA1

To detect and characterize photoevaporative winds in nearby star forming regions, it is necessary to reach μJy sensitivities at 1-10 GHz (Pascucci et al. 2012; Galván-Madrid et al. 2014) at least over the areas of the nearby star forming regions in the Gould Belt (these requirements are well captured in the SKA Level 0 Science Requirements, Braun (2014)). In addition, to perform systematic studies of radio flares and coordinate these studies with complementary observations of the molecular and solid state features with ALMA and/or the ELTs, it will be necessary to reach high sensitivity at low to intermediate frequencies (0.1-1 GHz) and have the ability to immediately trigger pointed followups on the flaring sources. These observations will be possible with SKA1.

4.2 The temperament of young stars and its effect on disks beyond SKA1

One possible important avenue to pursue these studies in the future will be through the resolved spatial and kinematical imaging of the HI radio recombination lines expected in the disk photoevaporative flows (Pascucci et al. 2012). To allow resolved imaging, high sensitivity and imaging performance at $0.1''$ angular resolution and 0.1 km/s spectral resolution are required. For this purpose the full SKA will be needed. The radio recombination line studies could be carried out with a slightly relaxed sensitivity ($\sim$30-100 mK), but with an angular resolution improved by approximately a factor of 100 over SKA1. This will require at least two orders of magnitude improvement in the sensitivity. While millimetre arrays, and especially ALMA, will allow to access the higher frequency, and brighter radio recombination lines, the combination of sensitivity and angular resolution of these facilities may not be adequate for this study.

5. Summary

In this chapter we have illustrated which would potentially be the unique contributions of SKA1 for the study of protoplanetary disks and planet formation. An SKA1 equipped with the high frequency Band 5 and satysfying the current version of the science requirements would provide transformational results in this area, addressing the fundamental questions of the formation of the rocky cores of planets, of the degree of chemical complexity of ices in protoplanetary disks and of the effects of the young stars on the disk physical and chemical evolution. We also outline the limitations of SKA1 and the potential areas to be addressed by a significantly upgraded version of the SKA.

Acknowledgements. This work was partly supported by the Italian Ministero dell´Istruzione, Università e Ricerca through the grant Progetti Premiali 2012 – iALMA (CUP C52I13000140001). Part of this research was carried out at the Jet Propulsion Laboratory, California Institute of Technology, under a contract with the National Aeronautics and Space Administration.

References

Ábrahám, P., Juhász, A., Dullemond, C. P., et al. 2009, Nature, 459, 224

PoS(AASKA14)117

Banzatti, A., Meyer, M. R., Bruderer, S., et al. 2012, ApJ, 745, 90
Banzatti, A., Testi, L., Isella, A., et al. 2011, A&A, 525, A12
Beckwith, S. V. W., Henning, T., & Nakagawa, Y. 2000, Protostars and Planets IV, 533
Beckwith, S. V. W. & Sargent, A. I. 1991, ApJ, 381, 250
Beckwith, S. V. W., Sargent, A. I., Chini, R. S., & Guesten, R. 1990, AJ, 99, 924
Birnstiel, T., Klahr, H., & Ercolano, B. 2012, A&A, 539, A148
Blum, J. & Wurm, G. 2008, ARA&A, 46, 21
Braun, R. 2014, “SKA1 Level 0 Science Requirements", Document number SKA-TEL.SCI-SKO-SRQ-001, SKA Organisation
Caselli, P., Keto, E., Bergin, E. A., et al. 2012, ApJL, 759, L37
Cossins, P., Lodato, G., & Testi, L. 2010, MNRAS, 407, 181
Dipierro, G., Lodato, G., Testi, L., & de Gregorio Monsalvo, I. 2014, MNRAS, 444, 1919
Elsila, J. E., Glavin, D. P., & Dworkin, J. P. 2009, Meteoritics and Planetary Science, 44, 1323
Faure, A., Remijan, A. J., Szalewicz, K., & Wiesenfeld, L. 2014, ApJ, 783, 72
Forbrich, J., Osten, R. A., & Wolk, S. J. 2011, ApJ, 736, 25
Forbrich, J. & Wolk, S. J. 2013, A&A, 551, A56
Galván-Madrid, R., Liu, H. B., Felice Manara, C., et al. 2014, A&A, 570, L9
Glavin, D. P., Dworkin, J. P., Aubrey, A., et al. 2006, Meteoritics and Planetary Science, 41, 889
Gorti, U., Dullemond, C. P., & Hollenbach, D. 2009, ApJ, 705, 1237
Grosso, N., Feigelson, E. D., Getman, K. V., et al. 2005, ApJS, 160, 530
Güdel, M., Briggs, K. R., Arzner, K., et al. 2007, A&A, 468, 353
Guilloteau, S., Dutrey, A., Piétu, V., & Boehler, Y. 2011, A&A, 529, A105
Hogerheijde, M. R., Bergin, E. A., Brinch, C., et al. 2011, Science, 334, 338
Holtom, P. D., Bennett, C. J., Osamura, Y., Mason, N. J., & Kaiser, R. I. 2005, ApJ, 626, 940
Jiménez-Serra, I., Testi, L., Caselli, P., & Viti, S. 2014, ApJL, 787, L33
Jørgensen, J. K., Favre, C., Bisschop, S. E., et al. 2012, ApJL, 757, L4
McGuire, B. A., Loomis, R. A., Charness, C. M., et al. 2012, ApJL, 758, L33
Miotello, A., Testi, L., Lodato, G., et al. 2014, A&A, 567, A32
Modica, P. & Palumbo, M. E. 2010, A&A, 519, A22
Muñoz Caro, G. M., Meierhenrich, U. J., Schutte, W. A., et al. 2002, Nature, 416, 403
O’dell, C. R., Wen, Z., & Hu, X. 1993, ApJ, 410, 696
Pascucci, I., Gorti, U., & Hollenbach, D. 2012, ApJL, 751, L42
Pascucci, I., Sterzik, M., Alexander, R. D., et al. 2011, ApJ, 736, 13
Pérez, L. M., Carpenter, J. M., Chandler, C. J., et al. 2012, ApJL, 760, L17
Pillitteri, I., Sciortino, S., Flaccomio, E., et al. 2010, A&A, 519, A34
Pinilla, P., Birnstiel, T., Ricci, L., et al. 2012, A&A, 538, A114
Pizzarello, S., Krishnamurthy, R. V., Epstein, S., & Cronin, J. R. 1991, GeCoA, 55, 905
Podio, L., Kamp, I., Codella, C., et al. 2013, ApJL, 766, L5
Qi, C., Öberg, K. I., & Wilner, D. J. 2013, ApJ, 765, 34
Ricci, L., Testi, L., Natta, A., Scholz, A., & de Gregorio-Monsalvo, I. 2012, ApJL, 761, L20
Ricci, L., Testi, L., Natta, A., et al. 2014, ApJ, 791, 20
Sakai, N., Sakai, T., Hirota, T., et al. 2014, Nature, 507, 78
Shu, F. H., Adams, F. C., & Lizano, S. 1987, ARA&A, 25, 23

PoS(AASKA14)117

Testi, L., Birnstiel, T., Ricci, L., et al. 2014, Protostars and Planets VI, in press, arxiv:1402.1354
Testi, L., Natta, A., Shepherd, D. S., & Wilner, D. J. 2001, ApJ, 554, 1087
Testi, L., Natta, A., Shepherd, D. S., & Wilner, D. J. 2003, A&A, 403, 323
Williams, J. P. & Cieza, L. A. 2011, ARA&A, 49, 67
Wilner, D. J. 2004, NewAR, 48, 1363
Wilner, D. J., D'Alessio, P., Calvet, N., Claussen, M. J., & Hartmann, L. 2005, ApJL, 626, L109

PoS(AASKA14)117

PROCEEDINGS OF SCIENCE

The impact of the SKA on Galactic Radioastronomy: continuum observations

Grazia Umana*[1], Corrado Trigilio[1], Luciano Cerrigone[2], Riccardo Cesaroni[3], Albert A. Zijlstra[4], Melvin Hoare[5], Kerstin Weis[6], Anthony J. Beasley[7], Dominik Bomans[6], Greg Hallinan[8], Sergio Molinari[9], Russ Taylor[10], Leonardo Testi[11], Mark Thompson[12],

[1]*INAF OACT, Catania, Italy;* [2]*JCentro de Astrobiologia (INTA-CSIC), Madrid, Spain;* [3]*INAF Osservatorio Astrofisico di Arcetri, Firenze Italy;* [4]*Jodrell Bank Centre for Astrophysics, Manchester M13 9PL, UK;* [5]*University of Leeds, Leeds, UK;* [6]*Astronomisches Institut, Ruhr-Universitaet, Bochum, Germany;* [7]*National Radio Astronomy Observatory, Charlottesville, USA;* [8]*Department of Astronomy, California Institute of Technology, Pasadena, CA 91125, USA;* [9]*INAF IAPS, Roma, Italy;* [10] *University of Cape Town and The University of the Western Cape, SA;* [11] *ESO, Karl Schwarzschild str. 2, D-85748 Garching, Germany;* [12]*University of Hertfordshire, UK*

E-mail: Grazia.Umana@oact.inaf.it

The SKA will be a state of the art radiotelescope optimized for both large area surveys as well as for deep pointed observations. In this paper we analyze the impact that the SKA will have on Galactic studies, starting from the immense legacy value of the all-sky survey proposed by the continuum SWG but also presenting some areas of Galactic Science that particularly benefit from SKA observations both surveys and pointed.

The planned all-sky survey will be characterized by unique spatial resolution, sensitivity and survey speed, providing us with a wide-field atlas of the Galactic continuum emission. Synergies with existing, current and planned radio Galactic Plane surveys will be discussed. SKA will give the opportunity to create a sensitive catalog of discrete Galactic radio sources, most of them representing the interaction of stars at various stages of their evolution with the environment: complete census of all stage of HII regions evolution; complete census of late stages of stellar evolution such as PNe and SNRs; detection of stellar winds, thermal jets, Symbiotic systems, Chemically Peculiar and dMe stars, active binary systems in both flaring and quiescent states. Coherent emission events like Cyclotron Maser in the magnetospheres of different classes of stars can be detected. Pointed, deep observations will allow new insights into the physics of the coronae and plasma processes in active stellar systems and single stars, enabling the detection of flaring activity in larger stellar population for a better comprehension of the mechanism of energy release in the atmospheres of stars with different masses and age.

Advancing Astrophysics with the Square Kilometre Array
June 8-13, 2014
Giardini Naxos, Italy

*Speaker.

PoS(AASKA14)118

1. The all-sky SKA1 survey

The proposed SKA1 all sky continuum survey (SASS1: Norris et al. 2015), covering most ($\sim 70\%$) of the Galactic Plane with unprecedented spatial resolution, sensitivity and survey speed at band 2 (650-1670 MHz), will provide us with a sensitive wide-field atlas of Galactic continuum emission. Up to now, existing interferometric radio continuum surveys of the Galactic Plane have been carried out either at high angular resolution, but over a limited survey area, or over wider areas but at low angular resolution. This is the case of MAGPIS (Helfand et al., 2006) and CORNISH surveys (Hoare et al., 2012), covering an area of $\sim$ square degrees at an angular resolution of 1-6 $''$. On the other side, the International Galactic Plane Survey (McClure-Griffiths et al., 2005; Taylor et al., 2003) and the 2nd Epoch Molonglo Galactic Plane Surveys (MGPS-2: Murphy et al., 2007) cover several hundred square degrees at a typical resolution of $\sim$1 arcmin.

In the meantime, two major surveys including or aimed at mapping the Galactic Plane will be carried out by the two SKA precursors, namely: the Evolutionary Map of the Universe (EMU, Norris et al., 2011) a deep ($\sim 10\mu$Jy/beam), almost full sky (75%), $\sim 10''$ angular resolution survey to be carried out at 1.4 GHz with the Australian SKA Pathfinder (ASKAP); and MeerGal (PIs M. Thompson and S. Goedhart) a deep ($\sim 30\mu$Jy/beam) survey of the Milky Way Galaxy (140 square degrees) to be carried out at 14 GHz with MeerKAT at a sub-arcsec ($\sim 0.8''$) angular resolution.

We can anticipate that both surveys will provide us with a new view of the radio Galactic Plane. However, SASS1, due to the increase in sensitivity, angular resolution and survey speed, will bridge the gap between the two types of existing radio surveys of the Galactic Plane and will improve the results from EMU and MeerGAL, detecting and cataloguing objects such as HII regions, supernova remnants (SNRs), planetary nebulae (PNe) and radio stars, down to the μJy level. Most of these sources represent the interaction of stars at various stages of evolution with their environment. The known radio populations of each of these types of objects are limited by a combination of issues including the limited area covered by existing surveys, sensitivity, angular resolution or biases against large scale structures introduced by limited uv coverage snapshot surveys. Moreover, the lessons learnt from EMU will guide the SASS1 design in identifying issues arising from the complex continuum structure associated with the Galactic Plane and from the variable sources in the Galactic Plane.
However, besides the legacy value of SASS1, some areas of Galactic Science will particularly benefit from SKA observations, in particular from those conducted at higher frequencies (band 4 and/or 5) and at higher resolution (sub-arcsec). We will present some among the possible Galactic science goals that can be addressed with the SKA1 and the full SKA. In the following, we assume the SKA1 and SKA performances as reported in the SKA1 Baseline Design (Dewdney et al., 2013) and in the Performance Memo (Braun, 2014).

2. Massive star formation

A straightforward application of SKA will be the study of ionized regions around massive, early-type stars. Thanks to its overwhelming sensitivity and dynamic range SKA will be the ideal instrument to detect and resolve these objects, whose size may vary from 10^3 au, for hypercompact

PoS(AASKA14)118

(HC) HII regions, to 100 pc, for giant HII regions. This is equivalent to span a broad range of ages, as HII regions are known to expand with time, which makes SKA an excellent tool to investigate the evolution of these intriguing objects.

While the most extended (and hence old) stages can be (and have effectively been) studied with the Very Large Array, the youngest sources have been so far quite elusive. The HC HII regions may be as small as $<$0.03 pc, which turns into an angular size $< 1''$ at the typical distances of OB-type stars ($>$1 kpc). Such a small size, combined with the large opacity of the free-free emission in the radio regime, makes it challenging to detect this type of objects and even more to resolve them. The limited information available on the earliest evolution of HII regions is frustrating, as this is considered a crucial step in the formation of a high-mass star (Keto, 2003). The youngest, densest HII regions arise as the star contracts towards its main sequence configuration. As long as accretion at high rates goes on, the protostar may swell up (Hosokawa et al., 2010) and cool down, thus dramatically reducing the ionizing photon output. This implies that the appearance of an HC HII region must correspond to the termination of the main accretion phase. In this context, the morphology of the youngest HIIs tells us also about the distribution of material immediately surrounding the forming massive star in terms of the interaction between infall and outflow.

As a matter of fact, HII regions appear to remain in the most compact phases of their evolution longer than expected on the basis of a simple expansion model, as witnessed by the number of ultracompact HII regions in the Galaxy (Wood & Churchwell, 1989; Mottram et al., 2011). This result implies the existence of some confinement, which could be tightly related to the accretion mechanism itself, as shown by Keto (2002). Alternatively, effects of density gradients and stellar winds may play a role (Arthur & Hoare, 2006) or intrinsic variability driven by changes in the accretion rate (De Pree et al., 2014). Therefore, shedding light on the earliest phases of HII regions might be equivalent to unveiling the process of high-mass star formation.

What is needed to boost our knowledge of (hypercompact) HII regions is both a statistically complete sample and a detailed analysis of selected candidates. Note also that radio observations should be better performed at higher frequencies, as this regime is well suited to actually determine the morphology of the youngest, most compact HII regions. SKA can fulfil all of these requirements, thanks to its superior sensitivity, angular resolution, and frequency coverage. The sensitivity issue is illustrated in Fig. 1, where we show the detection limits of SKA1 and SKA. In our estimate we have assumed a classical (Strömgren) HII region ionized by a zero-age main-sequence star. The figures plot the intensity of an HII region as a function of the Strömgren radius and Lyman continuum of the ionizing star. The curves correspond to the 3σ level attainable with 10 min integration on-source at 9 GHz with $1''$ resolution, for a source distance of 1 kpc (solid line) and 20 kpc (dashed). The HII regions falling above the curve are detectable. One sees that even SKA1 will be sensitive enough to detect HII regions as small as a few 10 au (the size of our Solar system!) around a B2 star or earlier, across the whole Galaxy. The great potential of SKA will permit to perform unbiased surveys of the Galactic plane in a limited amount of time and with great sensitivity, and thus allow a complete census of Galactic hypercompact (besides more extended) HII regions.

Resolving a HC HII region is more challenging. The maximum diameter is $\sim$0.03 pc (Kurtz, 2005) (i.e. $0.6''$ at a distance of, e.g., 10 kpc) and requires a synthesized beam at least $\sim$10 times smaller (i.e. $<0.06''$) to be properly imaged. In Fig. 2 we show a plot analogous to those in Fig. 1, but this time we fix the ratio between the synthesized beam and the source angular diameter to

PoS(AASKA14)118

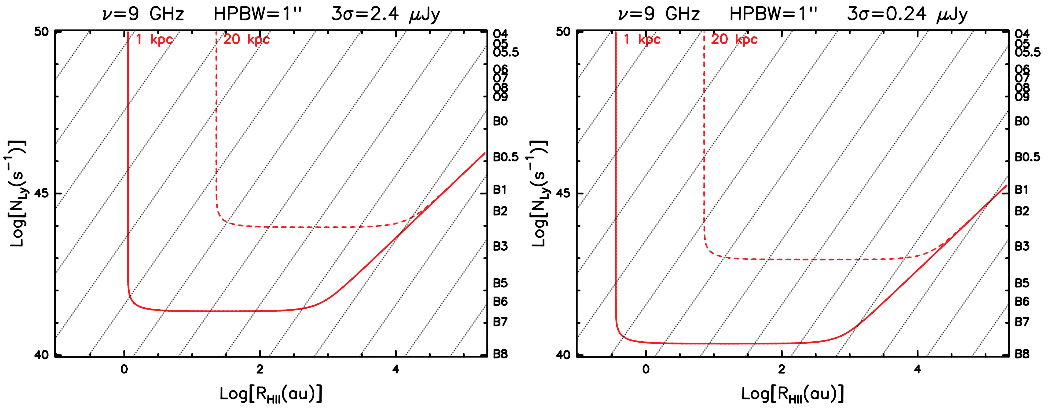

Figure 1: Left: Plot of the peak free-free continuum flux density of an homogenous, isothermal (Strömgren) HII region as a function of the HII region radius and Lyman continuum photon rate of the ionizing star. The calculation has been performed assuming an observing frequency of 9 GHz and an angular resolution of $1''$. The two curves correspond to a 3σ detection level of 2.4 μJy (obtainable in 10 min on-source with SKA1) at a distance of 1 kpc (solid curve) and 20 kpc (dashed). The dotted lines correspond to fixed values of the HII region densities, ranging from 10^{-1} cm^{-3} in the bottom right to 10^{12} cm^{-3} in the top right, in steps of a factor 10. **Right:** Same as left panel, for a detection threshold of 0.24 μJy, attainable with SKA in 10 minute integration on-source.

10. The curves correspond to S/N=10 for 10 min integration on-source, assuming a 1σ RMS of 0.08 μJy for SKA at 9 GHz. Points above the solid blue line have electron densities in excess of 10^6 cm^{-3}, the minimum value for a HC HII region (see Kurtz 2005). We conclude that the SKA will resolve HC HII regions around B1 stars or earlier, all over the Galaxy.

In addition to the sensitivity and angular resolution, SKA will provide us also with a broad instantaneous frequency coverage, thus allowing us to measure the spectral index of the radio emission. Although not sufficient by itself, knowledge of the spectral slope is a crucial piece of information to discriminate between HII regions and thermal jets, and determine the optical depth of the emission. Indeed, radio jets might be confused with faint HII regions and are detectable even at large distances (see Anglada et al. 2015).

3. Late stages of stellar evolution

SKA will also contribute to unveil the so-far missed populations of Planetary Nebulae (PNe) and Supernova remnants (SNRs). Those objects represent the late stages of stellar evolution of low and intermediate mass stars and massive stars, respectively. Details on the potential of SKA on SNRs science can be found in Wang et al. (2015). Low and intermediate mass stars (LIMS: 0.8–8 $M_\odot$) constitute 90% of all stars which have died in the Universe. During their final evolution, these stars eject between 40% and 80% of their total mass, enriched by the products of nucleosynthesis. The ejecta are the source of half the recycled gas in the Galaxy and are major contributors to chemical evolution of the Galaxy. The mass loss also determines the final mass of stellar remnants. The mass-loss process is one the main open problems in stellar astrophysics. Current areas

PoS(AASKA14)118

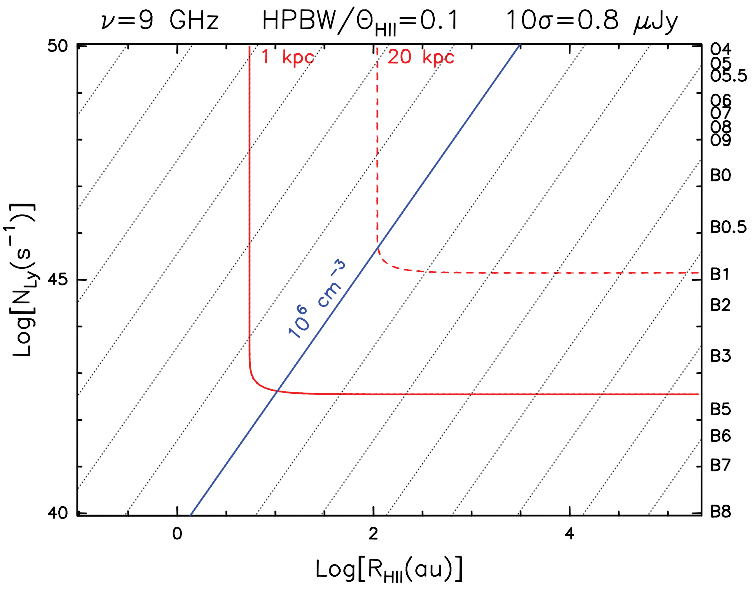

Figure 2: Same as previous figure. The difference is that here we fix the ratio between synthesized beam and source angular diameter diameter to 0.1 and allow for a S/N=10 for an integration of 10 min on-source with SKA (resulting in $1\sigma \simeq 0.08$ μJy). The blue line corresponds to an HII region density of 10^6 cm^{-3}.

of research are: what drives the mass loss, how is it affected by binary interactions and magnetic fields, and whether there is a unique initial-final mass relation.

Planetary nebulae (PNe) are formed when the ejecta are briefly ionized by the stellar remnant; they are known for their often beautiful morphologies. Since they have a rich emission-line spectrum, they can also be used to trace the kinematics of their host galaxies as well as serve as standard candles (e.g. Ciardullo, 2010). Although they trace 90% of all stars, they are short-lived (a few 10^4 yr), hence relatively rare, with a population density $\sim 10^{-6}$ of that of the total stellar population. This is compensated by their high luminosity ($\sim 10^4\,L_\odot$).

PNe are among the most numerous Galactic radio sources detected so far in radio surveys (about 700 in the NVSS). However, our census of this type of stars is far below the number expected from theoretical counts, which, on the other hand, heavily depend on the assumptions on the previous evolution of the stars. If, for example, only binary interaction is required to form a PN, we can expect to observe ∼6600 PNe in our Galaxy, but this number can go up to ∼46000, if binaries are not strictly necessary (Jacoby et al., 2010). The number of detected Galactic PNe is only ∼3000 (Parker et al., 2006).

It is therefore possible that there is a missing population of PNe. The main reason for such a large mismatch between the expected and the observed number of sources is that most PNe are hidden by dust absorption. Among other factors that can hamper PN detections, there are the intrinsic low brightness of the more evolved sources, which numerically dominate the PN luminosity function and are then expected to constitute the main component of volume-limited samples (Parker et al., 2006), the interaction with the ISM, which can disrupt the nebulae and shorten their lives, and the fact that Galactic latitudes beyond ±10 deg have not been adequately surveyed (Jacoby et al., 2010).

PoS(AASKA14)118

The sensitivity of the SKA and its ability to map large areas of the sky quickly will allow us to detect every PN in the Milky Way. If we consider a typical expansion velocity of 10 km s^{-1}, the shell expands in 2×10^4 yr to a distance of about 0.2 pc from the central star. Assuming optically thin emission from an ionised mass of 0.1 $M_\odot$ (n_e $\sim$140 cm^{-3}) filling 2/3 of the shell, we expect a flux density of about 4 $\mu Jy/beam$ at a distance of 61 kpc, over a beam of 0.8″. This means that SKA1 will be able to detect and map evolved PNe not only in the whole Galaxy, but also in the Magellanic Clouds. The number counts, distribution and brightness temperature will test the mass-loss models of LIMS. This survey can be done at frequencies between 1 and 5 GHz, with lower confusion and less effect from optical depth (for the younger nebulae) at the higher frequencies.

Besides evolved PNe, the SKA will allow us to detect more objects in the rapid transition from post-AGB stars to PNe, like CRL 618. This is a critical phase, when the development and expansion of the ionisation front radically changes the physical conditions in the circumstellar environment (Umana et al., 2004; Cerrigone et al., 2008, 2011). This transition lasts for a small fraction of the post-AGB time (which amounts to some 10^3 yr), which makes it challenging to detect stars going through it. Again, the deeper survey obtainable with the SKA will find new transition stars by sampling a larger volume of our Galaxy. In this context, it must be noted that transition objects are often optically thick below 3 GHz, therefore high-frequency receivers will be necessary to characterize the nebulae by observing their optically-thin emission. The flux may increase by 1% per year or more, a variation readily detectable if the survey is repeated over a few years.

Post-AGB stars such as CRL618 commonly show jet-like outflows. The origin and driving is not clear but magnetic-driven models have recently come in vogue (Huarte-Espinosa et al., 2012), strengthened by synchrotron emission from one such jet (Pérez-Sánchez et al., 2013). The SKA can detect synchrotron components to the radio emission through its sensitivity and wide frequency band: this will test the shaping mechanisms operating in PNe. This is best done at 1 GHz.

Finally, the SKA can also measure the mass of the stellar remnants inside the PN. This is done indirectly, through the evolution of the radio flux density. The rate of heating of the central star (temperature increase in K/yr) is a very strong function of the stellar mass. For stars which have not yet reached their maximum temperature, the radio flux is expected to decrease by 0.01-0.1% per year, due to the decrease in number of ionizing photons (hotter stars have fewer photons as each photon carries more energy). The rate of change of the optically thin radio flux yields the stellar mass, to an accuracy of better than 5%. This has so far only been done for NGC 7027 (Zijlstra et al., 2008). The changes during the earlier evolution are faster (Cerrigone et al., 2011) but less deterministic. The SKA survey can detect a 0.1% change for PNe as faint as 10mJy, which brings the Galactic Bulge population in range. A deeper, targeted survey could go further.

These measurements will best be carried out at 4–6 GHz (Zijlstra et al., 1989; Aaquist & Kwok, 1990). One way to achieve the temporal sensitivity is to repeat the Galactic plane area of the SKA survey 5–10 times, which would also improve sensitivity.

4. Stellar Radio emission

4.1 General

Stars emit, in the radio band, a negligible fraction of their total luminosity. In the case of the quiet Sun the ratio between its radio and its bolometric luminosity is less than 10^{-12}. Nevertheless,

PoS(AASKA14)118

in many cases, radio observations are the only way to reveal and study astrophysical phenomena that play a fundamental role in our understanding of stellar evolution. This is the case of stellar magnetic fields, whose topology can be directly mapped via VLBI observations (e.g. Trigilio et al., 1993; Peterson et al., 2010) and its influence on energy amplification and subsequent release in stellar coronae can be investigated via the correlation between radio and X-ray emission and the statistics of stellar flares (Benz & Guedel, 2010, and references therein); of stellar winds, where the detection of thermal radio emission is widely used to determine the mass-loss rate in hot stars (Wright & Barlow, 1975; Panagia & Felli, 1975; Scuderi et al., 1998; Blomme, 2011) and has revealed to be particularly powerful when other diagnostics cannot be used, as in the cases of dust enshrouded objects (Umana et al., 2005)

The improvement of the observational capabilities have lead to the discovery of radio emission in a wide variety of stellar objects from all stages of stellar evolution. Broadly speaking, the brightest stellar radio emission appears to be associated with enhanced stellar mass-loss (winds, nebulae) in the cases of thermal emission (large emitting surface) or to magnetically-induced phenomena, such as stellar flares, for non-thermal emission processes (high brightness temperature). In the following we briefly illustrate some representative examples for each type of stellar radio emitters.

4.1.1 Thermal emitters

Thermal emission (bremsstrahlung emission) is expected from winds associated with massive stars, shells surrounding Novae and jets from symbiotic systems (O'Brien et al. 2015), class 0 pre-main sequence (PMS) stars and classical TTauri (White, 2004).

Massive stars play a fundamental role in the evolution of galaxies. They are among major contributors to the interstellar UV radiation and, via their strong stellar winds, provide enrichment of processed material (gas and dust) and mechanical energy to the interstellar medium. Moreover, mass-loss from massive stars is very important for stellar evolution and understanding the different types of SN explosion.

Typical mass-loss rate for OB stars is of the order of $10^{-6} M_{\odot}/yr$, with wind speeds of $(1-3)\times 10^{3} km/sec$. More evolved massive stars include the classes of Luminous Blue Variables (LBVs) and Wolf-Rayet (WR). Luminous Blue Variables are massive evolved stars in an highly unstable state. Photometric and spectral variablities are as characteristic for that phase as is a highly enhanced mass loss (up to few $10^{-4} M_{\odot}/yr$) in various wind phases in which the wind velocities alternate between slow and fast. WR are further evolved, hotter and more stable massive stars with similar strong mass loss. The strong mass-loss of both object classes lead to extreme obscuration, in some cases, of the stellar surface. The mass-loss rate of massive star winds can be in principle derived from continuum radio observations, which trace the ionized gas through its optically thick free-free emission, providing the distance to the source and the velocity of the wind are known. A stellar wind has a typical spectral signature in the radio related to the radial density gradient of the wind (Panagia & Felli, 1975).

Radio observations have been proven to be more efficient than usual diagnostics for ionized gas, such as H_{α}, because they don't suffer from extinction and are indeed the only way to probe ionized gas in very reddened objects, embedded in dense, dusty circumstellar material. However, while mass-loss rates from radio continuum observations have been routinely obtained from a large

PoS(AASKA14)118

number of objects, quite recently it was realized that canonical mass-loss rates from massive stars need to be revised downwards, mostly because the assumed stellar-wind model does not include the effect of clumping or porosity (Blomme, 2011).

4.1.2 Non-thermal emitters

Much of our knowledge of non-thermal emission from radio stars comes from the study of active stars and binary systems as a large fraction of them have been found to be strong radio sources (Slee et al., 1987; Drake et al., 1989; Umana et al., 1991, 1993, 1998). Both classes of star are characterized by a magnetically heated outer atmosphere and display all the manifestations of solar activity (spots, chromospheric active regions, coronal X-ray emission, flares). In binary systems the observed phenomenology is more extreme than in the solar case because of the forced rotation induced by tidal forces that contributes to generate a more efficient dynamo action. The radio emission arises from the interaction between the stellar magnetic field with mildly relativistic particles (Dulk, 1985, i. e. gyrosynchrotron emission) and is highly variable. Two different regimes are usually observed: quiescent periods, during which a basal flux density of a few mJy is observed, and active periods, characterized by a continuous strong flaring which can last for several days (Umana et al., 1995).

Non-thermal radio emission is also observed in Ultracool dwarf (UCDs). The class of UCDs consists of stellar objects located on the boundary with sub-stellar bodies such as gas giant planets, including fully convective, very low mass M stars (later than M6) and Brown Dwarf (BDs).

The recent discovery of intense radio emission pulses lasting a few minutes from a number of UCDs has changed the conventional way to interpret their coronal emission physics; such objects exhibit very low chromospheric H-alpha and coronal X-ray activity and, consequently, were expected to be radio quiet (McLean et al., 2012, and references therein). This detection has immense implications for our understanding of both stellar magnetic activity and the dynamo mechanism generating magnetic fields in fully convective stars. This manifestation of magnetic activity is a significant departure from the incoherent gyrosynchrotron emission model generally applied to cool stars and bears more resemblance to planetary auroral activity than coronal stellar activity, indicating a possible transition in activity at the end of the main sequence. The radio pulses are thought to be due to highly beamed electron cyclotron maser emission and thus provide an accurate measurement of magnetic field strength at the location of the emission. This has been successfully used to provide the first measurements of magnetic field strengths for L and T dwarfs (Berger et al., 2009; Hallinan et al., 2007; Route & Wolszczan, 2012).

In several UCDs, such coherent emission is periodic, with a period consistent with their respective rotational periods (Berger et al., 2009; Hallinan et al., 2007). The long-term stability of the radio emission also indicates that the magnetic field (and hence the dynamo) is stable over a long timescale. How such fields are created and sustained remains a mystery.

Another example of non-thermal radio emitter is the class of Magnetic Chemically Peculiar stars (CPs). They are B-A main sequence stars characterized by strong dipolar magnetic fields with axis tilted with respect to the rotational one (oblique rotator). There are no convective motions in their stellar envelopes, and the magnetic field is thought to be fossil, remnant of the dynamo fields generated in the pre main-sequence phase.

PoS(AASKA14)118

CPs can show radio continuum emission, variable with the rotational period, but stable in time (Leone & Umana, 1993). The current model assumes that particles of the stellar wind are accelerated in the current sheets at Alfvén radius, and then propagate in a thin magnetospheric layer toward the star, emitting gyrosynchrotron radiation (Trigilio et al., 2004; Leto et al., 2006). Radio observations at 1.4-2 GHz of the CP star CU Vir have revealed the presence of a coherent, highly directive, 100% per cent polarized radio emission component (Trigilio et al., 2000), interpreted as cyclotron maser. In the framework of the radio emission from CP stars, maser amplification can occur in annular rings above the pole, generating auroral radio emission similar to what has been detected in the planets of the solar system, including the Earth (Trigilio et al., 2011).The coherent emission is stable on a time-scale of more than 10 years and has been used as a marker of the rotation of the star, revealing changes of the rotational period (Trigilio et al., 2008). The well known topology of CPs magnetic fields makes this type of object a perfect template for studies of stellar magnetosphere, magnetoactive plasma, particle acceleration, and stellar spin-down.

4.2 Radio stars detection forecast

In the last years, a few hundreds of radio stars have been detected (Guedel, 2002) but nearly all of the detections are the results of targeted observations directed at small samples of stars thought to be likely radio emitters. Therefore, all the detections suffer from a strong selection bias as the targeted observations were aimed at addressing specific problems related to some kind of peculiarities observed in other spectral regimes. This approach has been proven to be quite productive but it is biased against discovering unknown, unexpected, or intrinsically rare objects, preventing a good knowledge of radio stars at the sub-mJy level. In Fig. 3, schematic continuum radio spectra of several classes of radio emitting stars are drawn. Fluxes have been derived assuming a typical radio luminosity (Seaquist, 1993; Umana et al., 1993; Guedel, 2002; Berger et al., 2005; Trigilio et al., 2008), and a typical distance for each different types of radio stars: 10 pc for flare stars and late M-L, 100 pc for active binary systems, 1 kpc for supergiants, OB and WR, 500 pc for CP stars. The flux density of the quiet Sun has been derived from the solar quiescent radio luminosity assuming a distance of 10pc. The spectral and sensitive characteristics of SASS1 and SKA-MID, in both phases SKA1 and SKA, have been also drawn. The sensitivity for SKA1 and SKA is obtained assuming an integration time of 1 hour. For SKA1, we assume that band 2, band 4 and band 5 will be available, while for the full SKA we assume the deployment of all five frequency bands.

Stellar winds and non-thermal radio emission from many active binaries, flare stars and PMS stars will be easily detected, within the considered distances, with an rms sensitivity of $2\,\mu$Jy$\,beam^{-1}$ (SASS1), even during its early phase of deployment. With SKA1 we will be able to detect a quiescent Sun, but only if band 4 or 5 is used.

Another way to see this is to estimate, starting from the typical radio luminosity and assuming a limiting sensitivity, at what distance is possible to detect a star belonging to a particular class of radio emitting object. With the limiting sensitivity detectable flux density of SKA1-MID, for 10 minutes of integration time, all the WR, OB and stars and Symbiotic systems of the Galaxy can be detected, while CP, PMS, RSCVn and Supergiants could be seen up to the distance of the Galactic Center (GC). With the same integration time, SKA-MID will be able to detect almost all the above classes in the Milky Way, and probably in the nearby galaxies, providing sufficient angular resolution ($\leq 0.02''$), M Giant photospheres to the distance of the GC, flare stars and UCDs

PoS(AASKA14)118

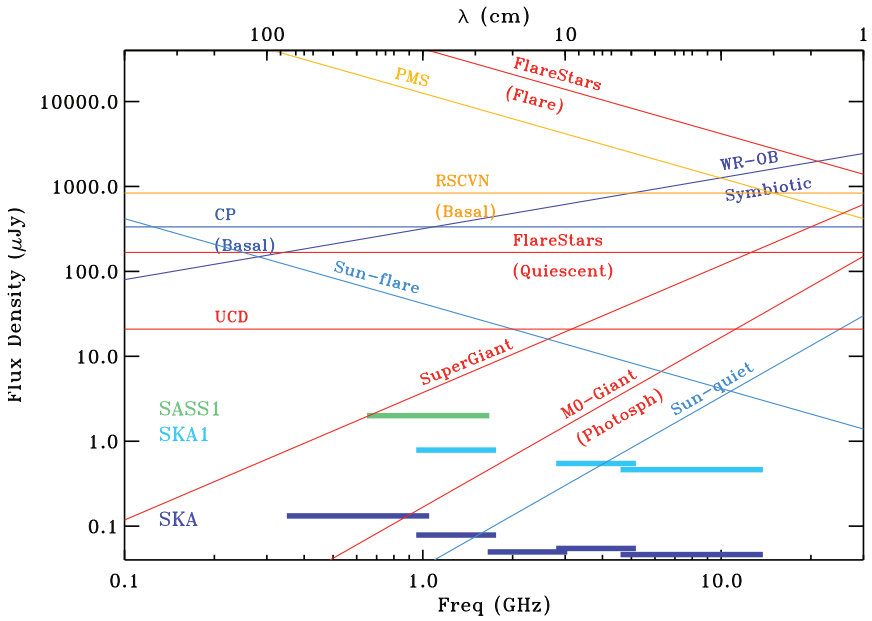

Figure 3: Typical radio spectrum of several classes of radio emitting stars. Fluxes have been derived from the radio luminosity assuming a distance as appropriate for each type of radio stars. Detection limits for SKA1 and SKA have been computed for one hour integration time. See text for explanation.

within several hundreds pc, and "a quiescent Sun analog" up to 50 pc (Fig. 4).
The unique capabilities of SKA will allow to detect many classes of stars over the entire Milky Way. This will produce a real revolution in stellar physics as the radio properties of different stellar populations will be defined, allowing timely comparisons with other stellar parameters, such as age, mass, magnetic fields, chemical composition, and evolutionary stages.
There are some particular areas of stellar radio emission that will particularly benefit from high sensitive and high angular resolution radio observations as those provided by the SKA. These are the study of non-thermal stellar flares in active stars and binary systems, the search for coherent events in different classes of stellar systems and the use of radio observations to derive mass-loss rate in massive stars.
It has not be established yet if the complete set of polarisation measurements (Stokes I, Q, U and V) will be available with both SKA1 and SKA foreseen observations. In particular circular polarisation information on a series of non-thermal radio emitting stars will complete our understanding of particular phenomena such as those related to coherent emission, allowing to immediately point-out coherent radio flares occurring in a particular target. However, most of the scientific goals, as reported in the following, could be reached even if only I, Q and U maps will be available.

4.2.1 Stellar Coronae: the solar-stellar connection:

In the Sun, during flares, beams of fast electrons travel down magnetic fields and release their energy in the chromosphere, where heated plasma expands into coronal magnetic flux tubes. This

PoS(AASKA14)118

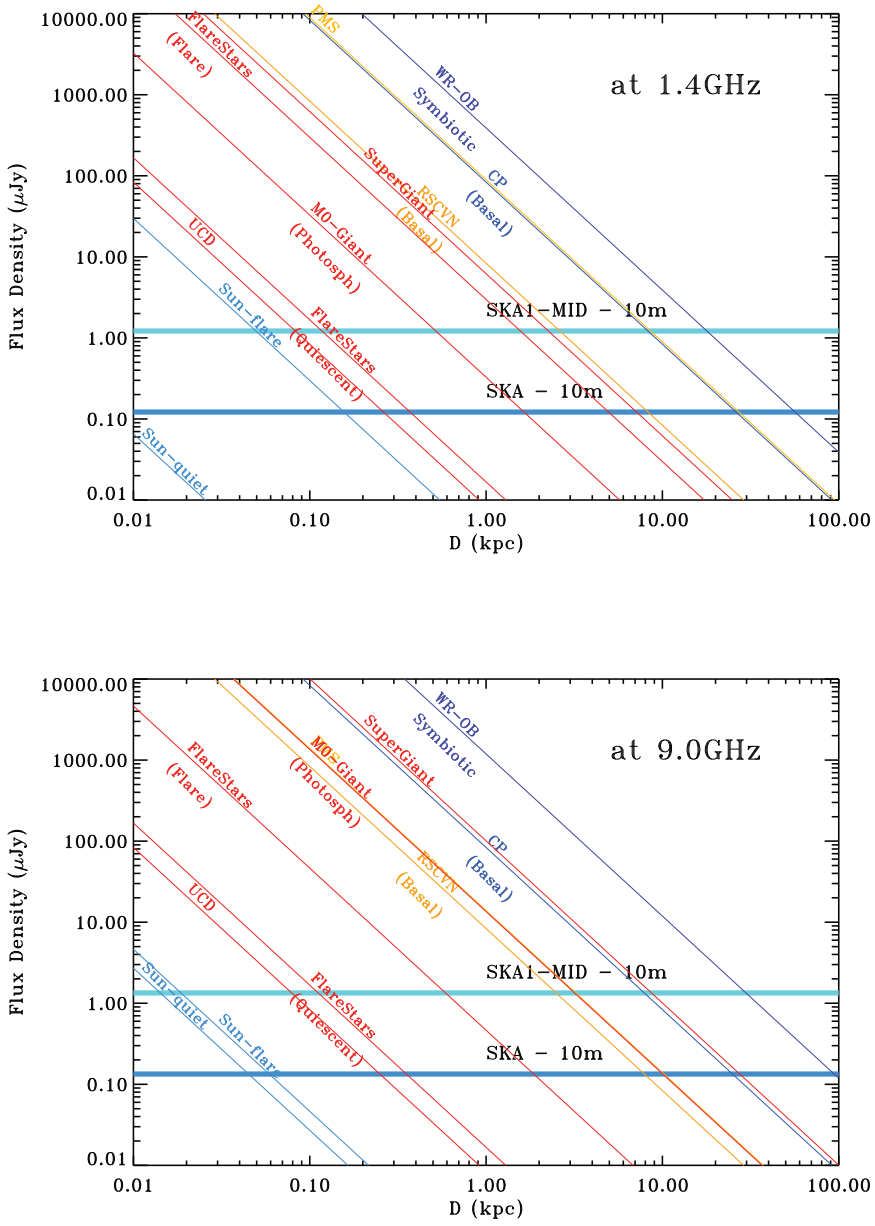

Figure 4: Top panel: Typical distances at which different classes of radio stars can be detected, assuming as limit flux the sensitivity that can be achieved with 10 minutes of integration band with SKA-MID in its band 2, in both SKA phase 1 and 2. **Bottom panel**: Same as top panel but for band 5.

PoS(AASKA14)118

hot plasma then cools radiatively and through conduction. Several attempts to use the solar model as a proxy to understand the energetics and location of flares in active stars have been carried out. Various theoretical mechanisms have been proposed, but more observations are clearly needed.

Until now, all the information on the radio emission from active stars and stellar systems originate from targeted observations of very few, bright, well known objects, usually selected on the basis of the strong magnetic activity displayed in other spectral regions.

Even if limited to a very small sample, we have now some knowledge of their radio emission characteristics (e.g. flare development, spectral and polarisation evolution, emission mechanism, etc). Deep radio measurements, as those that we can perform with SKA, would significantly enlarge the number of active stars and stellar systems, without bias effects, allowing new insights into the physics of objects showing magnetic activity. SKA1 would allow us to detect all the flares stars and active binary systems up to few kpc, while SKA will allow us to detect them over the whole Galaxy (Fig. 4) and thus to increase of two orders of magnitude the number of active stars that can be studied in the radio.

The study of large samples of active stars will provide us with important clues on stellar magnetism and dynamo processes as a function of internal structure of the stars and other physical parameters (mass, age, rotation...). Moreover, a clear understanding of the key parameters that control magnetic activity in different types of stars is very important since it affects habitability of possible orbiting planets.

It will be possible to identify radio coronae across a range of cool type stars. Detailed studies of a large number of stellar coronae will improve our knowledge of energy release in the upper atmospheres of stars of different mass and age. This will also permit to investigate the correlation between radio and X-ray emission and thus study the occurrence of the Neupert effect in stellar coronae (Guedel, 2009).

Systematic, multi-epoch deep surveys will enable the detection of serendipitous flaring activity and will hence permit to derive the typical behaviour (occurrence rate, evolution, etc.) from a statistical study of larger samples. Multi-wavelength type follow-up observing campaigns would allow to study magnetic activity manifestations at different layers of the stellar outer atmosphere and to explore the relationship of electron energization to the long-lived centers of surface activity (photospheric spots), pointing out the existence of possible magnetic cycles also in the radio.

Finally, the unique sensitivity of SKA will allow to follow the development of flares with unprecedented details and time-resolution. A typical, solar-type weak flare (0.1 mJy at 1.3 pc) can be detected in 5 sec with SKA1 (5σ). Such kind of observation will provide new insights in the open question of coronal heating and, in particular, a piece of evidence that the radio quiescent corona is maintained by a series of micro-flares.

4.2.2 Coherent events

There is a growing evidence that stellar radio flares can occur also as narrow band, rapid, intense and highly polarized (up to 100 %) radio bursts, that are observed especially at low frequencies ($<$1.5 GHz). For their extreme characteristics, they have been generally interpreted as result of coherent emission mechanisms. such as the Electron Cyclotron Maser Emission (ECME). Coherent burst emission has been observed in different classes of stellar objects: RS CVns and

PoS(AASKA14)118

Flare stars (Osten & Bastian, 2008; Slee et al., 2008), Ultra Cool dwarfs (Hallinan et al., 2008; Route & Wolszczan, 2012) Chemically Peculiar stars (Trigilio et al., 2008, 2011), all having, as common ingredient, a strong and also, but not necessarily, variable magnetic field and a source of energetic particles. The number of stars where coherent emission has been detected is still limited to few tens, because of the limited sensitivity of the available instruments and the stochastic nature of the events.

Deep radio observations, such those that SKA will provide the best opportunity to determine how common coherent radio emission is from stars, stellar and sub-stellar systems. The detection of coherent emission in a large sample of different types of stars will have immense implications for our understanding of both stellar magnetic activity and the dynamo mechanism generating magnetic fields in fully convective stars and brown dwarfs (Hallinan et al., 2008; Ravi et al., 2011).

Coherent emission observed in binary systems and active stars and in UCD stars shares several characteristics with that observed in CP stars (Trigilio et al., 2000), since both require a large scale magnetosphere, and are similar to the low frequency coherent radio emission observed in the planets with magnetic field of the solar system (Trigilio et al., 2011). To better understand the ECM in the wider context of plasma processes it is necessary to extend radio observations to a larger sample of CP stars. We want to stress here that CP stars provide us with the unique possibility to study plasma processes in stable magnetic structures, whose topologies are quite often well determined by several independent diagnostics (Bychkov et al., 2005), thus overcoming the problem of variability of the magnetic field observed in very active stars such dMe or close binary systems.

The foreseen sensitivity of SKA, just in its first phase, will allow to detect CP stars up to 10 kpc in 10 minute integration time (Fig. 4). Following Renson & Manfroid (2009), we can assume the CP stars are uniformly distributed in space. This would imply that the number of radio detections will increase by about an order of magnitude, giving the opportunity to get a larger statistics of the physical conditions of the magnetospheres to be correlated to the ECM.

If coherent emission is present in many radio active stars, with the same characteristics, it will constitute an excellent diagnostic for star magnetospheres, and a powerful probe of magnetic field topology. In the case of UCDs the study of ECM instability provides the only potential probe into magnetic field strengths for late-M, L and T dwarfs.

More observations of wider samples of active stars are also necessary to establish the percentage of active stars and binary systems that show coherent emission, exploring time-scales of its variability and how this is related to the basic physical parameters of the stars. Follow-ups of the detected sample would allow to point-out any similarities between ECME from single stars and binary systems and thus discriminate between different causes for the population inversion that drives the ECME events (Slee et al., 2008).

The discovery of other radio lighthouses similar to those observed in CU Vir (Trigilio et al., 2008; Ravi et al., 2011) will enable high precision studies of the rotation period, and thus angular momentum evolution, in different classes of stars.

4.2.3 Mass-loss from Massive stars

The recent discovery that the mass-loss rates derived for hot main sequence massive stars need to be revised downwards (Blomme 2011), poses serious questions on the evolution of massive stars.

PoS(AASKA14)118

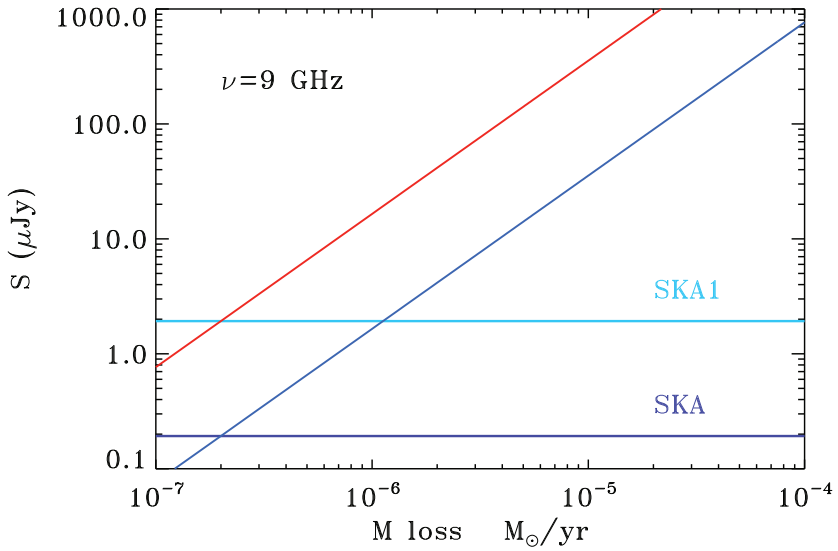

Figure 5: Mass-loss rates detectable at the distance of the Galactic Center (8 kpc) for two values of wind velocities. Sensitivity (rms), for 10 minute integration time for both SKA1 and SKA band 5, has been assumed.

.

An O-type star on the Main Sequence (MS), whose mass may be as large as 150 $M_\odot$, will evolve into a Wolf-Rayet star, with a typical mass not in excess of 30 $M_\odot$, but MS mass-loss rates are insufficient to account for such a huge mass-loss. Severe mass-loss probably occurs through strong stellar winds and/or eruptions during the post-MS evolution. Many luminous classes of stars belong to this phase, hot supergiants (BSGs, B[e]s and LBVs), cool Yellow Hypergiants (YHGs) and red Supergiants (RSGs) stars. The exact evolutionary path leading to a W-R, as a function of the mass and rotation, is however not well constrained, mostly because a crucial piece of information, i.e. mass-loss rates and lifetime and thus the total amount of mass lost during the post-MS is currently incomplete.

LBVs may play a key role in this scenario; as well as being characterized by a strong mass-loss, they can also undergo giant eruptions, in which larger amounts of mass are being ejected. As a consequence of the strong stellar wind and/or the giant eruption, circumstellar nebulae (LBVN) are formed (few $M_\odot$ for the wind scenario, several $M_\odot$ by ejection), which are a few parsec in size and have expansion velocities between 10-200 km/s, in extreme cases several 1000 km/s are detected (Weis, 2011). The nebulae are seen in optical and IR emission lines, radio continuum emission and IR excess emission. The possibility that such spectacular mass-loss events may be metallicity-independent has greatly increased the interest in LBVs, as this can have important implications for the mass-loss and therefore the evolution of Population III stars. Observations of LBV eruption and other variabilities of massive stars in local very low metallicity galaxies already hint at additional physics, which will improve the link from local massive stars to stars at the time of reionization (Bomans & Weis, 2011).

Mass-loss rates from a number of LBVs and LBVs candidates have been recently derived by

PoS(AASKA14)118

radio observation in our own Galaxy (Umana et al., 2005, 2010, 2012) and in the LMC (Agliozzo et al., 2012). Radio observations have also allow to determine the morphology of the ionized fraction of some LBVNs and to quantify the mass of ionized material (Buemi et al., 2010; Umana et al., 2011). When radio maps are combined with detailed mid-IR maps, tracing the dusty component, the presence of multi-epoch mass-loss events have been pointed out and estimates of the total content in mass of LBVNs have been derived (Umana et al., 2012; Agliozzo et al., 2014). Of further interest will be a comparison of the radio data with optical/NIR images of several LBVN. Weis (2011) showed that the morphology of LBVN as deduced from [NII] or H_α images and a kinematic analysis (Weis, 2003, i.e.) is bipolar in about 50% of all nebulae; for galactic LBVNs this rises to 75%. MIR dust nebulae appear to give different results, but are due to another driving mechanism, therefore radio observations are crucial for the understanding of formation and evolution of nebulae, e.g. determining the influence of wind-wind interactions and stellar rotation.

In Fig 5, the mass-loss rates detectable at the distance of the Galactic Center (8 kpc), assuming the SKA1 and SKA sensitivity with a 10 minute integration time, are shown. The red line refers to a wind velocity of $100 km/sec$, while the blue line to $1000 km/sec$. The minimum detectable flux has been calculated for SKA-MID band 5, as it is at higher frequency that we have the highest contribution from the optically thick, thermal stellar wind. Fig. 5 indicates that with the SKA, in both phases, we will reach, in 10 minute integration time, a detection limit sufficient to measure also very small mass-loss rates ($\sim 10^{-7} M_\odot yr^{-1}$) at the distance of the Galactic Center. This would allow studies, similar to those currently conducted on LBVs, to be carried out inside the three massive stellar clusters, located near the Galactic Center (Arches, Quintuplet and the Central Cluster). These young stellar clusters are more massive than any other cluster in the Milky Way and are likely to contain massive stars at all stage of evolution, including pre-main sequence, LBV and W-R, allowing to explore a plethora of stellar winds and associated Nebulae from a stellar population at the same age and, given the unique location, to study as these can be affected by environmental parameters.

References

Aaquist, O. B., & Kwok, S. 1990, A&AS, 84, 229
Agliozzo, C., Umana, G., Trigilio, C., et al. 2012, MNRAS, 426, 181
Agliozzo, C., Noriega-Crespo, A., Umana, G., et al. 2014, MNRAS, 440, 1391
Anglada, G., Rodríguez, L.F., Carrasco-González, C., 2015, "Radio Jets in Young Stellar Objects with the SKA", in proceedings of "Advancing Astrophysics with the Square Kilometre Array", PoS(AASKA14)121
Arthur, S. J., & Hoare, M. G. 2006, ApJS, 165, 283
Benz A.O., Güdel, M., 2010, ARA&A, 48, 241
Berger E., Rutledge R.E., Reid I.N. et al., 2005, ApJ, 627,960
Berger E., Rutledge R.E., Phan-Bao N., et al., 2009, ApJ, 695, 310
Blomme, R. 2011, Bulletin de la Societe Royale des Sciences de Liege, 80, 67
Bychkov, V. D., Bychkova, L. V., & Madej, J. 2005, A&A, 430, 1143
Bomans, D. J., & Weis, K. 2011, IAU Symposium, 272, 265

PoS(AASKA14)118

Braun, R., 2014, "SKA1 Imaging Science Performance", Document number SKA-TEL-SKO-DD-XXX Revision A Draft 2
Buemi, C. S., Umana, G., Trigilio, et al. 2010, ApJ, 721, 1404
Cerrigone, L., Umana, G., Trigilio, C., et al. 2008, MNRAS, 390, 363
Cerrigone, L., Trigilio, C., Umana, G., et al. 2011, MNRAS, 412, 1137
Ciardullo, R. 2010, *PASA*, 27, 149
De Pree, C. G., Peters, T., Mac Low, M.-M., et al. 2014, ApJ, 781, L36
Dewdney, P., Turner, W., Millenaar, R., McCool, R., Lazio, J., Cornwell, T., 2013, "SKA1 System Baseline Design", Document number SKA-TEL-SKO-DD-001 Revision 1
Drake S.A., Simon T., Linsky J.L., 1989, ApJS, 71, 905
Dulk, G. A. 1985, ARA&A, 23, 169
Güdel, M., 2002, ARA&A, 40, 2017
Güdel, M., 2009, LNP, 778, 269
Hallinan G., Bourke S., Lane C., 2007, ApJ, 663, 25
Hallinan G., Antonova A., Doyle J.G. et al., 2008, ApJ, 684, 644
Helfand, D. J., Becker, R. H., White, R. L. et al., 2006, AJ, 131, 2525
Hoare, M. G., Purcell, C. R., Churchwell, E. B., et al. 2012, PASP, 124, 939
Hosokawa, T., Yorke, H. W., & Omukai, K. 2010, ApJ, 721, 478
Huarte-Espinosa, M., Frank, A., Blackman, E. G., et al. 2012, ApJ, 757, 66
Jacoby, G. H., Kronberger, M., Patchick, D., et al. 2010, *PASA*, 27, 156
Keto, E. 2002, ApJ, 580, 980
Keto, E. 2003, ApJ, 599, 1196
Kurtz, S. 2005, Astrochemistry: Recent Successes and Current Challenges, 231, 47
Leone F., Umana G., 1993, A&A, 268, 667
Leto P.,Trigilio C., Buemi C.S. et al., 2006, A&A, 458, 831
McClure-Griffiths, N. M., Dickey, J. M., Gaensler, B. M., et al. 2005, ApJS, 158, 178
McLean M., Berger E., & Reiners A., 2012, ApJ, 746, 23
Mottram, J. C., Hoare, M. G., Davies, B., et al. 2011, ApJ, 730, L33
Murphy, T., Mauch, T., Green, A., et al. 2007, MNRAS, 382, 382
Norris, R. P., Hopkins, A. M., Afonso, J., et al., 2011, PASA, 28, 215
Norris, R. P., Basu, K., Brown, M., et al., 2015, "The SKA Mid-frequency All-sky Continuum Survey: Discovering the unexpected and transforming radio-astronomy" in proceedings of "Advancing Astrophysics with the Square Kilometre Array", PoS(AASKA14)086
O'Brien, T., Rupen, M., Chomiuk, L., et al., 2015, "Thermal radio emission from novae & symbiotics with the Square Kilometre Array" in proceedings of "Advancing Astrophysics with the Square Kilometre Array", PoS(AASKA14)062
Osten R.A., Bastian T.S., 2008, ApJ, 674, 1078
Panagia, N., & Felli, M. 1975, A&A, 39, 1
Parker, Q. A., Acker, A., Frew, D. J., et al. 2006, MNRAS, 373, 79
Pérez-Sánchez, A. F., Vlemmings, W. H. T., Tafoya, D. et al., 2013, MNRAS, 436, L79
Peterson, W. M., Mutel, R. L., Güdel, M. et al., 2010, Nature, 463, 207
Ravi V., Hobbs G., Wickramasinghe D. et al., 2010, MNRAS, 408, 99
Ravi V., Hallinan G., Hobbs G. et al., 2011, ApJ, 735, L2

PoS(AASKA14)118

Renson, P., & Manfroid, J. 2009, A&A, 498, 961
Route, M., & Wolszczan, A. 2012, ApJ, 747, L22
Scuderi, S., Panagia, N., Stanghellini, C. et al., 1998, A&A, 332, 251
Seaquist E.R., 1993, RPPh, 56, 1145
Slee O.B., Nelson G.J., Stewart R.T. et al., 1987, MNRAS, 229, 659
Slee O.B., Willes A.J., Robinson R.D., 2003, PASA, 20, 257
Slee O.B., Wilson W., Ramsay G., 2008, PASA, 25, 94
Taylor, A. R., Gibson, S. J., Peracaula, M., et al. 2003, AJ, 125, 3145
Trigilio, C.,Umana, G., & Migenes, V. 1993, MNRAS, 260, 903
Trigilio C., Leto P., Leone F., Umana G. et al., 2000, A&A, 362, 281
Trigilio C., Leto P., Umana G., Leone F., Buemi C.S., A&A, 2004, 418, 593
Trigilio C., Leto P., Umana G. et al., 2008, MNRAS, 384, 1437
Trigilio C., Leto P., Umana G. et al., 2011, MNRAS, 739, L10
Umana G., Catalano S., Rodonó M., 1991, A&A, 249,217
Umana G., Trigilio C., Tumino M. et al., 1993, A&A, 267, 126
Umana G., Trigilio C., Hjellming R.M. et al., 1995, A&A, 298, 143
Umana G., Trigilio C., Catalano S., 1998, A&A, 329, 1010
Umana, G., Cerrigone, L., Trigilio, C., & Zappalà, R. A. 2004, A&A, 428, 121
Umana, G., Buemi, C. S., Trigilio, C. et al., 2005, A&A, 437, L1
Umana, G., Buemi, C. S.,Trigilio et al., 2010, ApJ, 718, 1036
Umana, G., Buemi, C. S.,Trigilio, C., et al. 2011, ApJ, 739, L11
Umana, G., Ingallinera, A., Trigilio, C., et al. 2012, MNRAS, 427, 2975
Wang, L., Cui, X., Zhu, H., Tian, W., 2015, “Investigations of supernovae and supernova remnants in the era of SKA", in proceedings of "Advancing Astrophysics with the Square Kilometre Array", PoS(AASKA14)064
Weis, K. 2003, A&A, 408, 205
Weis, K. 2011, IAU Symposium, 272, 372
White, S. M. 2004, New Astronomy Reviews, 48, 1319
Wood, D. O. S., & Churchwell, E. 1989, ApJ, 340, 265
Wright, A. E., & Barlow, M. J. 1975, MNRAS, 170, 41
Zijlstra, A. A., Pottasch, S. R., & Bignell, C. 1989, A&AS, 79, 329
Zijlstra, A. A., van Hoof, P. A. M., & Perley, R. A. 2008, ApJ, 681, 1296

PoS(AASKA14)118

PROCEEDINGS OF SCIENCE

Maser Astrometry with VLBI and the SKA

James A. Green[*1], **Huib Jan van Langevelde**[2], **Andreas Brunthaler**[3], **Simon Ellingsen**[4], **Hiroshi Imai**[5], **Wouter Vlemmings**[6], **Mark Reid**[7], **and Anita Richards**[8]

[1] *SKA Organisation* [2] *JIVE/Sterrewacht Leiden* [3] *MPIfR Bonn* [4] *University of Tasmania*
[5] *Kagoshima University* [6] *Chalmers University of Technology* [7] *Harvard-Smithsonian CfA*
[8] *University of Manchester*
E-mail: J.Green@skatelescope.org

We discuss the unique opportunities for maser astrometry with the inclusion of the Square Kilometre Array (SKA) in Very Long Baseline Interferometry (VLBI) networks. The first phase of the SKA will enable observations of hydroxyl and methanol masers, positioning the latter to an accuracy of 5 microarcseconds, and the second phase may allow water maser observations. These observations will provide trigonometric distances with errors as small as 1%. The unrivalled sensitivity of the SKA will enable large-scale surveys and, through joint operations, will turn any VLBI network into a fast astrometry device. Both evolved stars and high mass star formation regions will be accessible throughout the (Southern) Milky Way, completing our understanding of the content, dynamics and history of our Galaxy. Maser velocities and proper motions will be measurable in the Local Group of galaxies and beyond, providing new insights into their kinematics and evolution.

Advancing Astrophysics with the Square Kilometre Array
June 8-13, 2014
Giardini Naxos, Italy

*Speaker.

PoS(AASKA14)119

1. Introduction

Through its sheer collecting area, the Square Kilometre Array (SKA) will have unprecedented sensitivity for spectral lines. The full receiver suite of the first phase of the SKA (SKA1) will include the hydroxyl (OH) ground- and excited-state maser transitions (at 1.612, 1.665, 1.667, 1.720, 4.765, 6.030 and 6.035 GHz), methanol (CH_3OH) maser transitions (at 6.668 and 12.178 GHz), and other rarer maser transitions such as from the formaldehyde (H_2CO) molecule (at 4.8 GHz). The second phase of the SKA (SKA2) has the prospect to allow for studies of water (H_2O) masers (at 22.235 GHz). This frequency coverage, in joint operation with one or more Very Long Baseline Interferometry (VLBI) network(s) (Paragi et al. 2015), will allow revolutionary science to be done in the field of Galactic and extragalactic structure and dynamics during all phases of the SKA.

In this chapter we highlight the VLBI capabilities for maser astrometry of SKA1-MID and SKA1-SUR, combined with existing telescopes in the Southern Hemisphere (the Long Baseline Array, LBA, in Australia, New Zealand and South Africa), Asia (including VLBI networks in Japan, South Korea and China), North America (the Very Long Baseline Array, VLBA) and Europe (the European VLBI Network, EVN). We will assume this will be complemented by further development of the various VLBI arrays, notably in Africa (the African VLBI Network, AVN), and potentially in South America as well. This will be an array with competitive uv-coverage and incredible sensitivity, dominated by the collecting area of the SKA element(s). As the SKA will synthesise a small beam on the sky, for the most efficient observing (and to reach the highest accuracies), it will be necessary to form multiple beams with the SKA to cover both targets and calibrators (position reference sources) within a single beam of the other VLBI telescopes (Paragi et al. 2015).

Maser astrometry yields a direct measurement of the distance and proper motions of individual young and evolved stars, calibrating their astrophysical properties. Moreover, major strides have been made in recent years in our understanding of the Milky Way through maser astrometry (see Reid et al. 2014 and Reid & Honma 2014 for recent compilations and analysis). The developments include: refining parameters of Galactic rotation and the local standard of rest; refining the distance to the Galactic centre; and establishing accurate configurations of the spiral arms. These developments have wide ranging impacts, such as in the testing of general relativity through the effect of gravitational radiation damping binary pulsar systems (where the accuracy of the solar distance and rotation are fundamental, Reid et al. 2014).

The timeline for the first phase of the SKA will overlap with the expected timescale for the results of the *Gaia* mission. The radio astrometry of VLBI with the SKA and the optical astrometry of *Gaia* will be highly complementary, with the former providing distances to the dust enshrouded regions and individual evolved stars, the latter the formed and optically radiant stars. This is particularly true for the inner Galaxy, where *Gaia*'s ability to penetrate the dust is limited.

2. The technique of VLBI maser astrometry

As an introduction to the science enabled by VLBI we briefly outline the technique of maser astrometry: it utilises position monitoring measurements of the maser source relative to an appropriate distant calibrator (background quasar), precisely determining a proper motion and a position

PoS(AASKA14)119

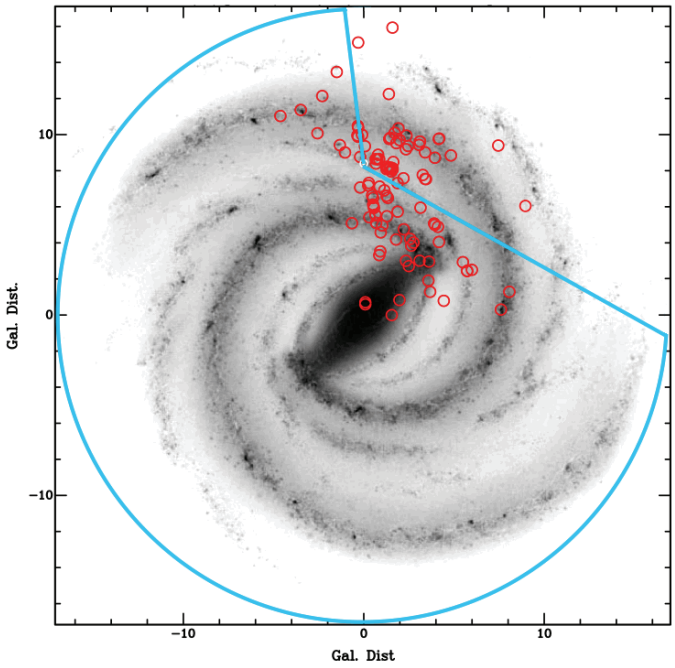

Figure 1: Masers (red circles) with astrometric parallaxes from the BeSSel survey and other observations (Reid et al. 2014), overlaid on the informed artist impression of the Milky Way (R. Hurt: NASA/JPL-Caltech/SSC). The blue lines enclose the regions accessible with Southern Hemisphere SKA-VLBI, in which there are of the order of 1000 known methanol masers.

(through parallax) which gives the distance to the source. Phase-referencing astrometric observations involving a background quasar and a maser source essentially involve measuring the phase delay between the two sources to determine their relative positions. This requires precise calibration of all the factors which contribute to the observed delay, including the station and source coordinates, instrumental and atmospheric delays (see Honma et al. 2008 for an in depth discussion, and Section 5 of this paper for discussion in the context of SKA). The following sections describe the Galactic and extragalactic science achievable through this technique.

3. Aims of astrometric measurements for Galactic science

The crucial scientific goal of maser astrometry with the SKA is obtaining distances to hundreds of sources in the Southern sky, together with a significant increase in Northern sources accessible with the SKA (south of declination 20°), more than doubling those obtained to date. We will simultaneously obtain the full three dimensional kinematics, through the combination of the line-of-sight velocity (from the Doppler shift of the line) and the proper motion. With the deployment of band 5 receivers on SKA1-MID (as defined in Dewdney et al. 2013), the widespread 6.7 and 12.2 GHz methanol masers, proven to be exclusive probes of high mass star formation (Breen et al. 2013), will be studied. Due to their tight association with the spiral arms and molecular gas, they directly trace the spatial structure and dynamics of the Galaxy. To date over 100 maser parallaxes have been measured in the Northern Hemisphere, through the BeSSel project (Brunthaler et al. 2011),

PoS(AASKA14)119

together with observations with the Japanese VLBI Exploration of Radio Astronomy, VERA, network. With Southern Hemisphere VLBI including the SKA, the current results can be improved through several hundred more maser measurements, providing a total sample of $\sim$1000, reaching an order of magnitude better statistics over the current sample. These observations will complement the *Gaia* results, for which close to the Galactic plane, can only penetrate limited distances. Together with radio continuum astrometry, we have the capability to measure the distance to the majority of star forming regions that the Atacama Large Millimeter Array (ALMA) can observe. The precise distances (1% errors for distances of $\sim$2 kpc, rising to 5% for $\sim$10 kpc) will allow the derivation of accurate physical parameters (including linear scale, mass, luminosity) and will offer the opportunity to improve distances to associated objects (including star forming regions, supernova remnants, planetary nebulae). Besides a handle on the dark matter distribution, the formation and evolution of the Galaxy can be studied through its dynamics and the orbital motions of the Magellanic Clouds together with signatures of past and recent mergers (see Section 4).

VLBI capabilities for the hydroxyl and methanol maser lines also enable detailed studies of the gas kinematics and excitation on the scales at which accretion processes in high-mass stars are expected to occur (through the '3-D' velocities provided by the line-of-sight velocities and proper motions). This will complement ALMA observations which have more modest resolution, but are sensitive to thermal excitations.

Together with atomic hydrogen, SKA1-MID and SKA1-SUR will be sensitive to the hydroxyl main and satellite lines at 18cm (each with their respective band 2 receivers, as defined in Dewdney et al. 2013). These lines can be used to trace star forming regions, the circumstellar envelopes of evolved stars and supernova remnants. Compared to previous efforts, the SKA will have the sensitivity to quickly survey the Galaxy (Etoka et al. 2015). However, the moderate resolution of the SKA alone will leave some confusion when comparing with objects at other wavelengths. As such, VLBI baselines that include SKA1-MID and SKA1-SUR will be required. The existing LBA and EVN are both well equipped in this band and the AVN will benefit from this frequency capability.

Astrometry of circumstellar OH masers can yield proper motions and parallaxes of individual AGB stars (Vlemmings & van Langevelde 2007). Compared to methanol masers the method is limited by the poorer resolution and the intrinsically limited brightness of the OH masers. However with the SKA in a VLBI array very many objects within a few kpc should be accessible. The direct measurements of distance are fundamental for quantitatively understanding the physics and chemistry processes associated with these mass-losing stars, calibrating their feedback to the Galactic lifecycle of elements. Measuring distances to highly obscured stars and in highly obscured parts of the Galaxy is again complementary to what *Gaia* will deliver. Radio observations can for example extend determinations of the Period-Luminosity relation for AGB stars to the regime with higher mass-loss by including more extreme objects. When the capabilities of SKA and the VLBI array cover water masers, the higher frequencies will enable us to overcome the effects of scintillation and it will become feasible to sample stellar orbits in the inner Galaxy, in which the dynamic signature of the bar and merging events could be detectable.

In addition to regions of star formation and evolved objects, the satellite line transition at 1720 MHz is found in supernova remnants, and as such is used to probe the interaction with surrounding molecular clouds and examine the processes involved (e.g. Brogan et al. 2013). Maser astrometry

PoS(AASKA14)119

of this transition will demonstrate the three dimensional geometry, provide proper motions for analysis of turbulent and shocked structures, and precisely locate the masers relative to x- and gamma-ray radiation (enabling tests of pre- and post-shocked conditions).

Furthermore, astrometric measurements will complement the study of the large-scale Galactic magnetic field through Zeeman measurements of hydroxyl masers, tying Galactic structure determined through parallax with the fields, and the study of small-scale fields around young massive stellar objects through Zeeman measurements of methanol masers (Robishaw et al. 2015).

3.1 Phased deployment of SKA and expected results

Maser astrometry with VLBI (using 'traditional' phase referencing) represents a field which has the potential for scientific return through utilising antennas in early phase SKA (i.e. in the build up to phase 1, when there are less than 50% of the antennas available). An example would be incorporating SKA1-SUR antennas with the LBA, where even a few dishes will make a measurable difference with the benefit of enhanced east–west baselines. The first science from the Australian SKA Pathfinder (ASKAP) was a VLBI experiment with one ASKAP antenna included in the LBA (Tzioumis et al. 2010).

For the first phase of the SKA, we can expect System Equivalent Flux Densities (SEFDs) of 2.1 Jy at the hydroxyl frequencies and 2.8 Jy at the methanol frequency (Dewdney et al. 2013). There are currently $\sim$1200 known sources of methanol maser emission (Pestalozzi et al. 2005; Green et al. 2009). Of the order of 300–400 of these will be observed from the Northern Hemisphere with existing VLBI networks (e.g. Brunthaler et al. 2011), and we can expect, through $\sim$1500 hrs observing, to detect and obtain 5 microarcsecond parallaxes for $\sim$300 from the Southern Hemisphere with SKA1. This would allow observations of methanol masers with peak flux densities $\geq$0.7 Jy, more than an order of magnitude weaker than can currently be observed with the LBA. SKA1 will also be able to detect several thousand hydroxyl maser sources (Imai 2013) with SKA1-MID and SKA1-SUR combined, although not all of these will be accessible for direct parallax measurements because of the limited resolution at frequencies of $\sim$1.6 GHz.

SKA2, with an expected sensitivity 10 times that of SKA1-MID and with extended baselines, will vastly improve on SKA1, with an expectation of being able to detect the very faintest methanol masers, a further 400-600 sources, bringing the total with parallax measurements to $\sim$1200. It has been suggested that the luminosity of methanol masers increases with age (Ellingsen et al. 2013), and the full SKA will allow direct testing of this hypothesis (as the less luminous masers should be found preferentially towards the leading edge of the spiral arms). Several thousand hydroxyl masers will be detectable with SKA2 (Etoka et al. 2015). Although not covered by the band designations in the current baseline design for SKA1, the dishes of SKA1-MID are able to work at 22 GHz, and SKA2 may be equipped with appropriate receivers. The SKA would then be sensitive to water masers from both evolved stars and young stellar objects. As water masers are intrinsically very bright, the capability to observe these sources has exciting applications, both in Galactic and extragalactic astrometry (see following Sections).

4. Aims of maser astrometry for extragalactic science

The SKA will enable us to significantly develop resolved stellar kinematic studies in other

PoS(AASKA14)119

galaxies, in particular the Local Group of galaxies (the satellite galaxies of the Milky Way and beyond), enabling determination of their rotation, distances and proper motions. The kinematics of these galaxies are quite unique, providing an account of the history of the Milky Way including past and future interactions, insight into exotic events such as star bursts (as found in the Large Magellanic Cloud, e.g. Livanou et al. 2006; Anderson et al. 2014) and the dynamical friction in the galaxies. Hydroxyl, methanol and water masers can be used for this purpose, providing the opportunity for proper motion measurements (for example as described in Dickey et al. 2013).

The two nearest local group galaxies, the Large Magellanic Cloud (LMC) and the Small Magellanic Cloud (SMC), are prominent Southern Hemisphere objects. At distances of ~ 50 kpc and ~ 62 kpc for the LMC and SMC respectively, they are a benchmark for studies of a variety of topics, including stellar populations, the interstellar medium, and the cosmological distance scale. Clearly evident in the radio are signs of interaction between the two individual Clouds (Putman et al. 2003; Brüns et al. 2005), and between the pair and the Milky Way (McClure-Griffiths et al. 2008; Nidever et al. 2008; Besla et al. 2012). The Magellanic Clouds offer the best opportunity to view cosmological processes of hierarchical structure formation in action. Observations of the Magellanic Clouds can be compared with cosmological simulations to determine how interactions may have led to the triggering of star formation (Anderson et al. 2014). Stellar population studies have highlighted several episodes of heightened star formation at defined periods 0.2, 2, and 5 Gyrs ago, raising the question as to how the timing and strength of these episodes may correspond with tidal interactions in the three body system.

The SKA will have the sensitivity to make astrometric observations of significantly more maser sources in the LMC, SMC and other Local Group galaxies than can be achieved with current facilities. These observations will enable more rapid and accurate determination of the proper motions of interstellar masers in these galaxies, and, combined with the line-of-sight component from the Doppler shift of the maser line, will provide full '3-D' velocities. The observed proper motions have three contributions: a component due to the proper motion of the Centre of Mass of the galaxy; a component due to the orbital motion of the maser associated source about the Centre of Mass of the galaxy; a component due to internal motions of the masing gas within the star formation region. The first of these is the critical one for investigations of galaxy interaction, but the uncertainty in its determination depends upon both the precision in the proper motion measurement and the accuracy with which the other two components can be estimated. Observations of a larger number of individual maser regions in each southern local group galaxy will enable more accurate estimates of the proper motion of their centres of mass and also the orbital properties of the maser-associated objects. These results will dramatically improve constraints on the physical processes of galaxy interaction by providing an accurate description of their motion.

Beyond the Magellanic Clouds, current VLBI arrays already have the astrometric accuracy to measure proper motions. However, the sensitivity of current arrays has limited this to only a handful of sources in nearby galaxies (for example M33, M31, and IC 10). The superior sensitivity of the SKA (although in some cases at its northern limit) will allow us not only to detect many more masers within the Local Group, but also in nearby galaxy groups and even the Virgo cluster. This will allow us to understand the flow of galaxies in the local universe.

It is widely believed that the motion of the Milky Way relative to the cosmic microwave background (CMB), which is of the order of 500 km/s, is induced by mass concentrations within

PoS(AASKA14)119

150 Mpc of the local universe, but there is a discrepancy between the direction of the motion and the distribution of visible mass in the local universe (see e.g. Loeb & Narayan 2008 and references therein). This could be caused for example by a significant proper motion of the Milky Way relative to M31 or by a nearby structure in the Zone of Avoidance (behind the plane of the Milky Way). A measurement or a constraint on the proper motion of the Milky Way relative to the Virgo Cluster would be an important experiment to help understand this apparent discrepancy.

4.1 Phased deployment of SKA and expected results

Although the initial phases of SKA1 (with $\leq$50% of the antennas) will be beneficial for Galactic science, capabilities for extragalactic studies will only be enhanced over current capabilities once sensitivities approach those of the full deployment of SKA1 (i.e. SEFDs of 2.1 and 2.8 Jy for the hydroxyl and methanol frequencies respectively). We expect that the GASKAP project (Dickey et al. 2013) will detect around 100 hydroxyl maser in the Magellanic clouds, nearly an order of magnitude increase over the number currently known. VLBI astrometry including SKA1 will enable their proper motions to be measured and significantly improve the accuracy to which the Centre-of-Mass motions are currently known (e.g. Kallivayalil et al. (2013)). The strength of the full SKA will be in allowing kinematic measurements of galaxies beyond the Magellanic Clouds (as described in the previous Section).

5. The requirements for VLBI maser astrometry with the SKA

The general requirements for VLBI with the SKA are detailed in Paragi et al. (2015), but here we highlight specific requirements relevant for astrometric maser measurements, both in the 'traditional' sense of phase referencing and in the 'multi–view' sense of in-beam calibration. The antenna positions must be accurately known (to a precision of a few millimetres) and there must be adequate calibrator sources with precise positions (positional accuracies of $\leq$1 milliarcsecond when used for removing the differential atmospheric delay residual). Once the coordinates (positions) of the masers are determined to an accuracy of a few tens of milliarcseconds, then the correlator will be required to average over a few seconds between outputs. This will cover position offsets of the individual maser spots from the determined source coordinates, taking into account time-average smearing.

There will need to be the ability to determine zenith atmospheric delay contributions from the ionosphere and the troposphere. Traditionally rapid switching between the calibrator and target sources is used to effectively remove the short term atmospheric variations, however, it cannot estimate the delay difference due to the slightly different path through the airmass between the calibrator and target source. There are two components to the atmospheric delay, one due to the ionosphere which is dispersive and dominates at low frequencies and the other due to the troposphere which is non-dispersive and dominates at frequencies above 10 GHz. For SKA1 the ionosphere will be the dominant source of zenith delay uncertainty. Global Positioning Satellite (GPS) observations are routinely used to produce global ionospheric models, which can be used to reduce the impact of ionospheric effects by factors of two to five (Walker & Chatterjee 1999). This technique yields residual zenith ionospheric delays accurate to around 3 cm and it will be important to develop improved techniques, such as utilising continuous GPS observations at the telescope

PoS(AASKA14)119

sites (e.g. Honma et al. 2008), to maximise the improved astrometry the SKA will facilitate. As described in Paragi et al. (2015), VLBI with the SKA will utilise multiple beams for calibration, which will aid the atmospheric calibration with in-beam phase referencing, providing an alternative to the 'traditional' process described above, significantly reducing overheads (which often exceed 50%). The experiments described in Sections 3 and 4 assume this 'multi-view' method of observing. This requires adequate background calibrators (quasars) within the primary beam of the SKA antennas. At 1.6 GHz, based on the predictions of Fomalont et al. (1991) and Condon (2007) we would expect plenty of sources, of the order of 450 sources brighter than 400 μJy, but at 6.7 GHz this will be challenging in the first phase, with only $\sim$5 sources brighter than 100 μJy. The 'multi-view' approach is also heavily dependent on the field of view of the other antennas within the VLBI array – if the array includes antennas with diameters significantly exceeding the 15m of the SKA antennas, the number of available in-beam calibrators may be limited (the increased sensitivity is offset by the decreased field of view). However, a number of developments, such as multi-beam feeds or focal plane arrays for the larger antennas, and different calibration techniques, such as 'boot strapping' and reverse phase referencing, may provide an avenue to overcome these limitations.

For the hydroxyl and methanol observations, scheduling should be optimised to observe maxima in the parallax sinusoid, typically requiring four epochs over a one–to–two year period, for water maser observations more frequent scheduling will be required. However, the availability for VLBI in a sub array will allow appropriate scheduling, possibly concurrently with other observations (sub-arraying will additionally allow different size scales to be probed). From a correlator perspective, VLBI maser astrometry will require wide bandwidths for continuum calibration and narrower bands with high spectral resolution for the target maser emission. For the latter, a few tenths of km s^{-1} or less will be required for Galactic sources (necessary to sufficiently sample the maser spectrum and enable reliable identification of maser emission between epochs), and up to a few tens km s^{-1} for the fainter extra-galactic OH masers. Additionally, it is crucial to obtain a very high dynamic range (or signal-to-noise ratio) in the VLBI data, to achieve a sufficiently high astrometric accuracy for the ground-state hydroxyl transitions at $\sim$1.6–1.7 GHz. In comparison for methanol, a dynamic range of 600-6000:1 is required for the maser source, 60:1 for the continuum calibrator.

6. Conclusions

The SKA offers exciting options to study the dynamics of the Milky Way and nearby galaxies out to the Virgo Cluster. Maser astrometry offers a scientific return across the deployment of the SKA, from early stages through to the full SKA capability. Such studies will have important synergies with *Gaia* and ALMA in unraveling the spiral structure of the inner Galaxy, its dynamics and even its formation history.

References

Anderson, C. N., Meier, D. S., Ott, J., et al. 2014, ApJ, 793, 37
Besla, G., Kallivayalil, N., Hernquist, L., et al. 2012, MNRAS, 421, 2109

PoS(AASKA14)119

Breen, S. L., Ellingsen, S. P., Contreras, Y., & et l. 2013, MNRAS, 435, 524
Brogan, C. L., Goss, W. M., Hunter, T. R., et al. 2013, ApJ, 771, 91
Brüns, C., Kerp, J., Staveley-Smith, L., et al. 2005, A&A, 432, 45
Brunthaler, A., Reid, M. J., Menten, K. M., et al. 2011, Astronomische Nachrichten, 332, 461
Condon, J. J. 2007, in Astronomical Society of the Pacific Conference Series, Vol. 380, Deepest Astronomical Surveys, ed. J. Afonso, H. C. Ferguson, B. Mobasher, & R. Norris, 189
Dewdney, P., Turner, W., Millenaar, R., et al. 2013, "SKA1 System Baseline Design", Document number SKA-TEL-SKO-DD-001 Revision 1
Dickey, J. M., McClure-Griffiths, N., Gibson, S. J., et al. 2013, PASA, 30, 3
Ellingsen, S. P., Breen, S. L., Voronkov, M. A., & Dawson, J. R. 2013, MNRAS, 429, 3501
Etoka, S., Engels, D., et al. 2015, "OH masers in the Milky Way and Local Group galaxies in the SKA era" in proc. *Advancing Astrophysics with the Square Kilometre Array*, PoS(AASKA14)125
Fomalont, E. B., Windhorst, R. A., Kristian, J. A., & Kellerman, K. I. 1991, AJ, 102, 1258
Green, J. A., Caswell, J. L., Fuller, G. A., et al. 2009, MNRAS, 392, 783
Honma, M., Tamura, Y., & Reid, M. J. 2008, PASJ, 60, 951
Imai, H. 2013, Proceedings of the SKA Science Workshop in East Asia
Kallivayalil, N., van der Marel, R. P., Besla, G., Anderson, J., & Alcock, C. 2013, ApJ, 764, 161
Livanou, E., Kontizas, M., Gonidakis, I., et al. 2006, A&A, 451, 431
Loeb, A., & Narayan, R. 2008, MNRAS, 386, 2221
McClure-Griffiths, N. M., Staveley-Smith, L., Lockman, F. J., et al. 2008, ApJL, 673, L143
Nidever, D. L., Majewski, S. R., & Burton, W. B. 2008, ApJ, 679, 432
Paragi, Z., Godfrey, L., Reynolds, C., Dodson, R., et al. 2015, "Very Long Baseline Interferometry with the SKA" in proc. *Advancing Astrophysics with the Square Kilometre Array*, PoS(AASKA14)143
Pestalozzi, M. R., Minier, V., & Booth, R. S. 2005, A&A, 432, 737
Putman, M. E., Staveley-Smith, L., Freeman, K. C., Gibson, B. K., & Barnes, D. G. 2003, ApJ, 586, 170
Reid, M. J., & Honma, M. 2014, ARAA, 52, 339
Reid, M. J., Menten, K. M., Brunthaler, A., et al. 2014, ApJ, 783, 130
Robishaw, T., Green, J., Surcis, G., et al. 2015, "Measuring Magnetic Fields Near and Far with the SKA via the Zeeman Effect" in proc. *Advancing Astrophysics with the Square Kilometre Array*, PoS(AASKA14)110
Tzioumis, A. K., Tingay, S. J., Stansby, B., et al. 2010, AJ, 140, 1506
Vlemmings, W. H. T., & van Langevelde, H. J. 2007, A&A, 472, 547
Walker, C., & Chatterjee, S. 1999, VLBA Scientific Memo

PoS(AASKA14)119

PROCEEDINGS OF SCIENCE

Magnetospheric Radio Emissions from Exoplanets with the SKA

Philippe Zarka[*1], **T. Joseph W. Lazio**[2,3], **Gregg Hallinan**[3], **& "Cradle of Life" WG**

[1]*LESIA, CNRS – Obs. Paris, Meudon, France;* [2]*JPL;* [3]*Caltech, Pasadena, CA, USA*

E-mail: philippe.zarka@obspm.fr

Planetary-scale magnetic fields are a window to a planet's interior and provide shielding of the planet's atmosphere and surface for life. The Earth, Mercury, Ganymede, and the giant planets of the solar system all contain internal dynamo currents that generate planetary-scale magnetic fields. When coupled to energetic (keV) electrons, such as those produced by solar wind-magnetosphere interaction (compression or magnetic reconnection), magnetosphere-ionosphere or magnetosphere-satellite coupling, the polar regions of a planetary magnetic field are the place of intense, coherent, circularly polarized cyclotron radio emissions. These emissions – that may be as intense as solar ones – are produced by all magnetized planets in the solar system in the MHz range, and up to 40 MHz at Jupiter. Detection of similar emissions from exoplanets will provide constraints on the thermal state, composition, and dynamics of their interior – very difficult to determine by other means – as well as an improved understanding of the planetary dynamo process and of the physics of star-planet plasma interactions.

Detailed knowledge of magnetospheric emissions from solar system planets and the discovery of exoplanets motivated both theoretical and observational work on magnetospheric emissions from exoplanets. Scaling laws and theoretical frameworks were built and extrapolated to obtain order-of-magnitude predictions of frequencies and flux densities of exoplanetary radio emissions. The present stage of the theory suggests that radio detection of exoplanets will develop the new field of comparative exo-magnetospheric physics, but also permit to measure exoplanetary parameters such as rotation or orbit inclination. Observational searches started even before the confirmed discovery of the first exoplanet.

We review the scientific return of the detection of exoplanetary radio emissions, the current status of observational searches, and discuss the future promise in the context of SKA, especially SKA1-LOW. To the extent that Jupiter's magnetic field is not exceptionally strong, the current lower frequency limit of 50 MHz implies that SKA1-LOW will likely detect Jovian-mass planets. With the currently planned sensitivity of SKA1-LOW, we estimate that a Jupiter-like planet could be detected to about 10 pc. Within this volume there are ∼200 known stars and ∼35 currently known exoplanets, and this number should increase substantially with coming space missions dedicated to transits and powerful ground-based instruments. The accessible volume will be much increased if scaling laws derived in our solar system can be reliably extrapolated to exoplanetary systems, permitting to measure lower mass planets' dynamos and magnetospheres.

Advancing Astrophysics with the Square Kilometre Array
June 8-13, 2014
Giardini Naxos, Sicily, Italy

[*]Speaker.

PoS(AASKA14)120

1. Introduction

Planets appear to be the most favourable cradle of life in the context of present astrobiology. With the growing number of exoplanets (>1800, cf. *www.exoplanet.eu*) detected by radial velocity or transits, which cover a broad range of sizes, masses and orbital parameters, it is increasingly desirable to determine the physical properties of exoplanetary systems to carry in-depth comparative studies. Topics of interest include magnetospheric dynamics, energetics of star-planet interactions, planetary rotation, planetary dynamos (large-scale planetary magnetic fields play an important role in protecting the planet's surface and atmosphere), etc.

Experience from our solar system planets and theory tell us that the most intense electromagnetic emissions from magnetospheres result from coherent cyclotron radiation, through which keV electrons in strong magnetic fields generate intense, circularly polarized, sporadic emissions in the MHz to tens of MHz range (synchrotron emission is also produced at higher frequencies, but with a much lower intensity). Measuring the dynamic spectra in intensity and (circular) polarization of these cyclotron emissions can give access to the above physical parameters, as well as orbit inclination and the presence of satellites.

In section 2, we summarize our observational and theoretical knowledge of solar system magnetospheres and radio emissions, review the drivers for electron acceleration (star-planet or stellar wind-planet interactions, and magnetosphere-ionosphere or magnetosphere-satellite coupling), and extrapolate them to various exoplanetary conditions. In section 3, we summarize past and ongoing observations. Non detections put a stringent limit on planetary emission above $\sim$150 MHz, and hints of detections remain to be confirmed. In section 4, we examine the prospects for SKA observations, from early science operations through Phase 1 to Phase 2. In section 5, we give a special attention to synergies, both with other SKA observations and with observations at other wavelengths.

2. Background and Motivation

2.1 Solar system magnetospheres and radio emissions

The Earth, Mercury, Ganymede, and the giant planets of the solar system all contain internal dynamo currents that generate planetary-scale magnetic fields. These internal dynamo currents arise from differential rotation, convection, compositional dynamics, or a combination of these in objects' interiors. Interaction of these planetary-scale magnetic fields with the solar wind creates a magnetosphere, a cavity in the wind dominated by the planet's magnetic field. Inside the cavity, charged particles are accelerated to keV-MeV energies by various processes (magnetic reconnection at the boundaries, interaction with embedded moons, waves...).

Accelerated charged particles in a magnetic field generate radio emissions. The most intense ones are produced at high magnetic latitudes (so-called auroral, circumpolar regions) by a non-thermal coherent process well-identified today, that involves keV electrons: the Cyclotron Maser Instability (CMI) (Treumann 2006). This process widely operates at all magnetized planets, which are thus strong radio emitters (Zarka 1998). Emitted frequencies are local cyclotron frequencies met by energetic electrons moving along magnetic field lines. Their range extend from very low values (a few kHz) far from the planet, up to the maximum surface cyclotron frequency (f_{ce} [MHz]

PoS(AASKA14)120

= 2.8 B [G] ; 1 G = 10^{-4} T). For most solar system planets, planetary surface field magnitude is $\leq$1 G, thus emitted frequencies lie below $\sim$2 MHz. They are reflected off by the Earth's ionosphere and thus cannot be detected from the ground. Jupiter, having a stronger dynamo and surface field (up to 14 G), emits CMI radiation up to 40 MHz, which consists of bursts of duration from sub-millisecond to several tens of minutes. These bursts are easily detected by ground-based radiotelescopes.

MeV electrons also produce synchrotron emission in Jupiter's inner magnetosphere (so-called radiation belts) (de Pater 2004). Its spectrum extends over high harmonics of the cyclotron frequencies, up to several GHz. The synchrotron process is a nonthermal incoherent mechanism, much less efficient than the CMI, so that this emission is 10^5 times weaker than the CMI. It is also much more stable in time, showing variations at timescales longer than days/weeks.

2.2 Predictions for radio emissions from exoplanets

Due to the high efficiency of the CMI, Jupiter's auroral radio emissions are extremely intense (brightness temperature $\geq 10^{19}$ K, flux density $\geq 10^7$ Jy at Earth (Zarka 2004)), as intense as solar ones (which are mostly due to plasma radiation), as shown on Figure 1. Considering this favourable planet-star contrast $\sim$1, much larger than in the visible ($\sim 10^{-9}$) or infrared ($\sim 10^{-6}$) ranges, observational searches for low frequency radio emission from exoplanets started even before the confirmed discovery of any exoplanet (Zarka 2011, and references therein). It proved to be a difficult task and no unambiguous detection has been obtained yet (see below). But the discovery of many exoplanets by radial velocities and transit methods has motivated both theoretical and observational work on magnetospheric emissions from exoplanets.

It was soon realized that due to the high brightness of the galactic radio background, Jupiter's decametric CMI emission cannot be detected at stellar distances (several pc) even with the largest existing instruments. The search for more intense planetary emissions followed two complementary directions: (i) establishing empirical scaling laws for radio emissions from solar system planets and extrapolating them to exoplanets, and (ii) identifying the primary engine of planetary radio emissions and the regime of parameters which allow this engine to produce more powerful emissions.

A scaling law was first found to relate the average magnetospheric radio output with the total solar wind power input (dominated by the solar wind ram pressure) on the magnetospheric cross section (Farrell et al. 1999), with a proportionality constant $\sim 10^{-5}$. The specific case of coronal mass ejections (CME) impacting a magnetosphere was also considered (Grießmeier et al. 2007). A second scaling law was found to relate the same radio output with the incident Poynting flux convected by the solar wind on the magnetospheric cross section (Zarka et al. 2001, Grießmeier et al. 2007), with a proportionality constant $\sim$ a few $\times 10^{-3}$, as illustrated in Figure 2. This scaling law was found to apply more generally to any plasma flow-obstacle interaction (contrary to the scaling law based on total power input), including Io-Jupiter and Ganymede-Jupiter interactions, and at least to one documented example of magnetized binary star (the RS CVn system V711τ) (Zarka 2010, and references therein).

The physical mechanisms underlying these scaling laws include magnetospheric compressions by the solar wind or CME and associated shocks, magnetic reconnection between the magnetic

PoS(AASKA14)120

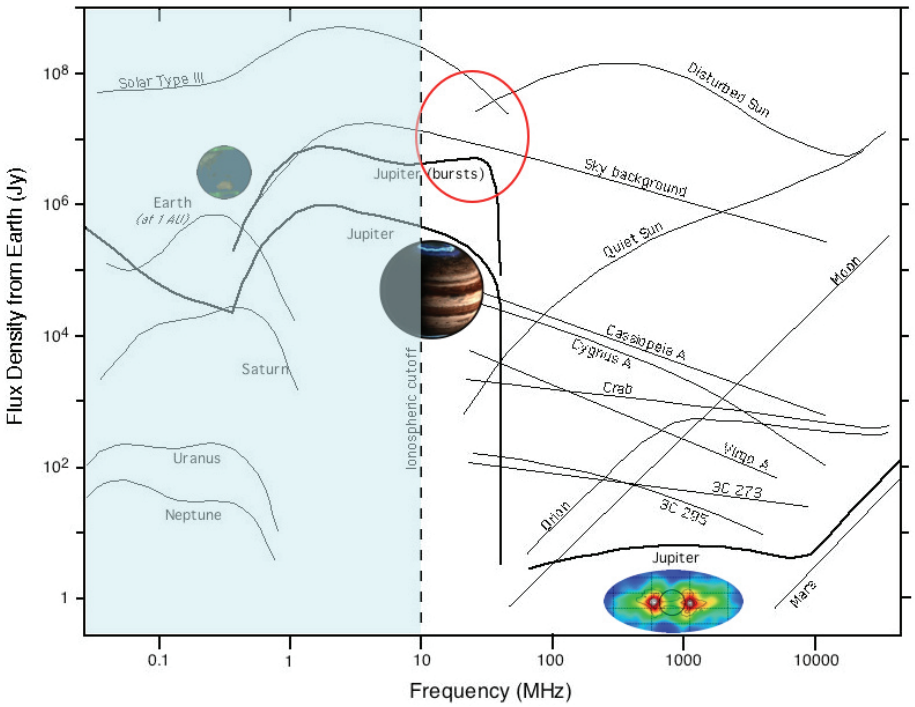

Figure 1: Spectra of astronomical radiosources detected from the Earth's vicinity. Auroral planetary spectra lie below the Earth's ionospheric cutoff, except Jupiter's decametric (CMI, auroral and Io-induced) and metric-decimetric (synchrotron) emissions. Normalized to the same observer distance of 1 AU, Jupiter's spectrum must be upscaled by $\times 20$, Saturn's by $\times 100$, Uranus' by $\times 400$, and Neptune's by $\times 900$, so that all are grouped within 2-3 orders of magnitude.

fields of the flow and of the obstacle, and Alfvén waves produced by the so-called "unipolar inductor" interaction of a conducting non-magnetized body (the moon Io) moving across magnetic field lines (of Jupiter). All these mechanisms lead to the acceleration of electrons that in turn emit radio waves. Jardine & Cameron (2008) proposed direct electron acceleration at the magnetosphere's nose through a runaway mechanism. Nichols (2011) estimated the power dissipated by magnetosphere-ionosphere coupling, independent of the solar wind.

For exoplanets orbiting very close to their parent star, especially hot jupiters, it was found that star-planet magnetic/plasma interactions (SPI – incl. magnetospheric compression, magnetic reconnection, and unipolar inductor) involve a power 10^3 to 10^6 times larger than that of the solar wind-Jupiter interaction (Zarka 2007). In the unipolar inductor case, the star needs to be strongly magnetized (surface field $\geq 10^{1-2}$ G), the exoplanet plays the role of Io and its parent star that of Jupiter. Extrapolating the above scaling laws, their radio output should accordingly be 10^3 to 10^6 times that of Jupiter. Willes & Wu (2005) studied the particular case of terrestrial planets in close orbits around magnetic white dwarf stars, acting as a unipolar inductor, and generating CMI radio emission with large flux densities. These systems could be remnants of main sequence stars with a planet surviving the stellar expansion phase and back in stable orbit.

For exoplanetary magnetospheres governed by internal processes (magnetosphere-ionosphere coupling), it was found that for giant planets orbiting at a few AU from their parent star, the auroral

PoS(AASKA14)120

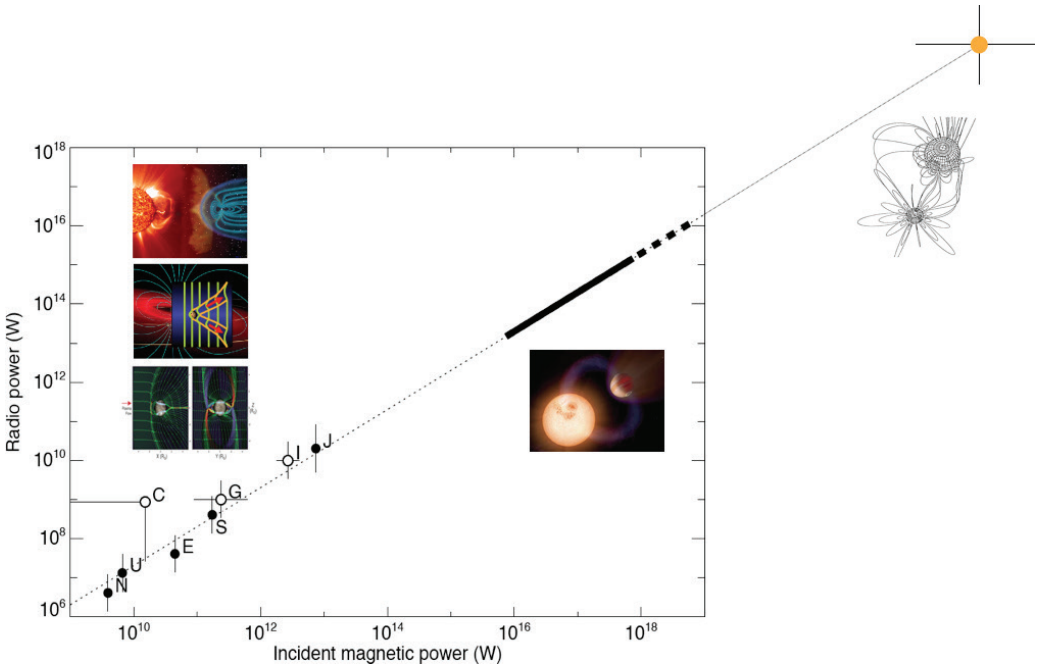

Figure 2: Scaling law relating magnetospheric (Earth, Jupiter, Saturn, Uranus and Neptune) and satellite-induced (Io, Ganymede, Callisto) average radio power to incident Poynting flux of the plasma flow on the obstacle. Dashed line has slope 1, emphasizing the proportionality between ordinates and abscissae, with a coefficient $\sim 2\times10^{-3}$. Note that planetary radio bursts can reach $10\times$ (resp. $100\times$) the average value $\sim$10% (resp. $\sim$1%) of the time. The thick bar extrapolates to hot jupiters the magnetospheric interaction (solid) and satellite-planet electrodynamic interactions (dashed). The orange dot illustrates the case of the RS CVn magnetic binary V711τ discussed in the text. Insets sketch the types of interaction.

radio output may reach 10^4 to 10^5 times that of Jupiter if the star has a strong X-UV output and the planet has a fast rotation (P=1-3 hours).

All theoretical predictions thus suggest that exoplanetary magnetospheric radio emissions much stronger than Jupiter's are likely to exist, and thus be detectable at stellar distances with large enough instruments. Sporadic further amplifications may occur e.g. due to scintillations. CMI radio emission generated within the exoplanet's magnetosphere is likely to be restricted to low frequencies (10's of MHz, depending on the planetary field strength), whereas unipolar inductor driven CMI emission, being excited by the exoplanet in the stellar magnetic field, may reach higher frequencies (100's MHz to a few GHz).

Finally, it must be noted that CMI radiation is strongly circularly/elliptically polarized (synchrotron emission from Jupiter's radiation belts is linearly polarized), and beamed anisotropically so that it is always deeply modulated by the planetary rotation. Conversely, solar/stellar plasma radiation is essentially unpolarized and sporadic. Even in the absence of sufficient angular resolution (known exoplanets orbit at $\ll$1" from their parent star), polarization and temporal modulations should allow to discriminate stellar and exoplanetary radio emissions, as demonstrated by the simulations presented in the next section. Theoretical predictions thus suggest that detection and identification of CMI radio emission from exoplanets is possible, so that it is worth observing. But what do we have to learn through radio emission detection ?

PoS(AASKA14)120

2.3 Motivations for the search for exoplanet's radio emissions

Planetary magnetic fields are a window to a planet's interior, and magnetospheric radio emissions are a probe of planetary magnetic fields. Ground-based detection of Jupiter's decametric radio emission (Burke & Franklin 1955) provided the first proof of existence and the first measurement of the Jovian magnetic field. Its monitoring allowed one to define accurately the rotation of its interior, and to discover the existence of a strong interaction between the moon Io and the Jovian magnetosphere (Bigg 1964). Maps of the synchrotron emission revealed the tilt of the magnetic field relative to the rotation axis ($\sim$10°) (Berge & Gulkis 1976). Magnetospheric radio emissions are thus a unique tool for probing exoplanet's interior structure (composition, thermal state) and dynamics (including the effect of spin-orbit locking for hot jupiters), leading to an improved understanding of the planetary dynamo process.

Each planetary magnetosphere – in our solar system – is a space plasma physics laboratory. In-situ spacecraft exploration and remote electromagnetic (Radio, UV, IR, X) observations permitted to infer their general properties, but also revealed numerous specificities related to the magnetic field amplitude, tilt, distance to Sun, presence of embedded moons and rings, atmospheric composition...

The CMI theory provides a well-understood, quantitative framework for studying magnetospheric radio emissions properties and using them as a diagnostic tool of planetary plasma environments and processes. Recent simulations in that framework (Hess & Zarka 2011) showed that the measurement of the radio dynamic spectrum – in intensity and polarization – of an exoplanetary system, in addition to allowing us to discriminate between stellar and exoplanetary emissions, would bring the following informations (difficult or impossible to determine by other means) about these objects, as illustrated in Figure 3 : in addition to the exoplanet's magnetic field intensity and tilt, one will be able to measure the planetary rotation and revolution periods (effectively testing tidal spin-orbit synchronization), the orbit inclination (resolving the ambiguity on the planet's mass), and identify the primary engine of the electromagnetic output of the system: SPI (magnetospheric compression, stellar wind-magnetosphere magnetic reconnection, or "unipolar inductor" interaction if the exoplanet is weakly magnetized and the star strongly magnetized), or internal magnetospheric processes (magnetosphere-ionosphere or magnetosphere-moon coupling). Temporal modulations different from the planetary rotation and orbital periods could even reveal the presence of moons or the signature of the stellar wind activity.

Similar to the question of solar system formation, which requires comparison of numerous systems to infer general properties, the recent field of comparative magnetospheric physics (which relies on a corpus of 6 very different planetary magnetospheres so far) will considerably expand with the detection of exoplanetary radio emissions, that will permit to explore a large range of parameters (star-planet distance, stellar magnetic field and wind strength, stellar X-UV flux, planetary magnetic field, rotation, orbit inclination...), better understand the diversity of planetary dynamos, study interactions between plasma flows (magnetized or not) and obstacles (magnetized or not) in various regimes, and infer the energy dissipation involved in SPI. Furthermore, the above scaling laws will be confirmed and/or modified or refined, expanding their range of application and their predicting capability.

Existence of a magnetosphere is also an essential ingredient in favour of the possibility to de-

PoS(AASKA14)120

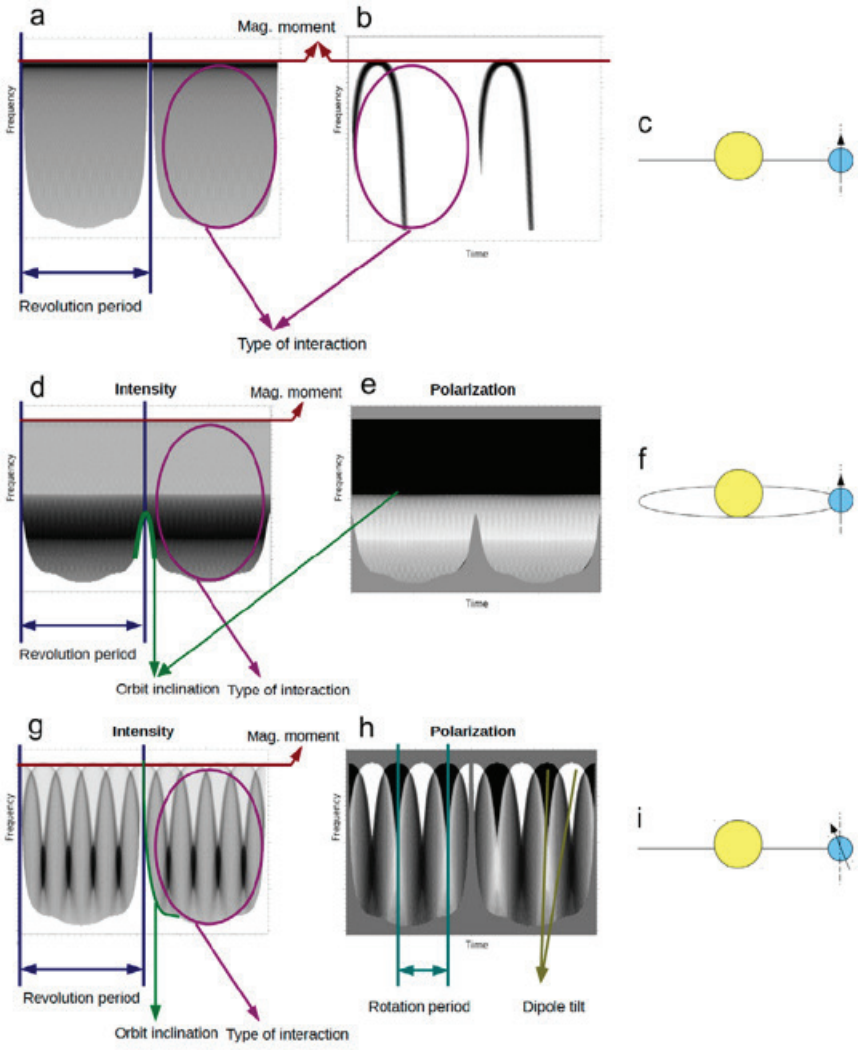

Figure 3: Simulated dynamic spectra in intensity (a,b,d,g) and circular polarization (e,h) and associated parameters of the system that can be determined: (a,b,c) exoplanetary magnetic field aligned with the rotation axis and 0° orbit inclination, for emission (a) of a full exoplanet's auroral oval and (b) an auroral active sector fixed in local time. (d,e,f) aligned exoplanetary magnetic field and 15° orbit inclination, for emission of a full auroral oval. (g,h,i) exoplanetary magnetic field tilted by 15° and 0° orbit inclination, for emission of a full auroral oval. From (Hess & Zarka 2011).

velop life: it ensures shielding of the planet's atmosphere and surface, preventing O_3 destruction by cosmic rays bombardment as well as atmospheric erosion by the stellar wind or CMEs. It also limits its atmospheric escape, as ionized material following dipolar field lines returns to the atmosphere (Grießmeier et al. 2004, 2005). Finally, radio detection may evolve as an independent discovery tool, complementary to radial velocities or transit measurements because it is more adapted to finding planets (giant or terrestrial) around active, magnetic or variable stars.

PoS(AASKA14)120

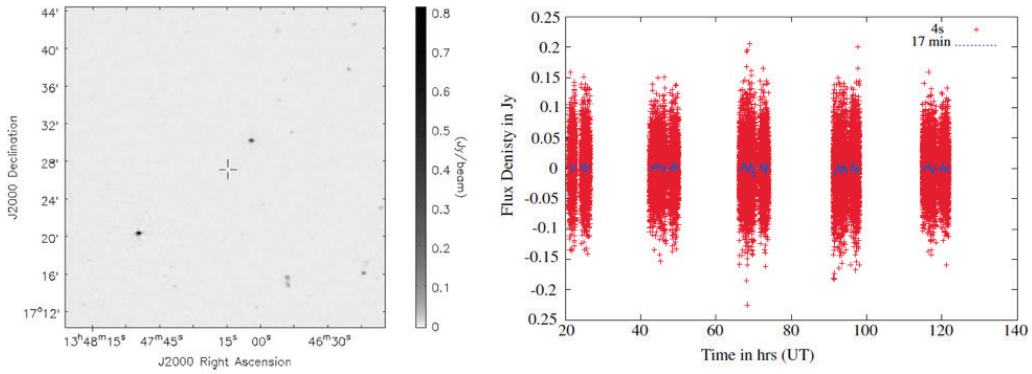

Figure 4: (left) 153 MHz GMRT image of the τ Boo field integrated over 40 hours. The crosshairs indicate the position of the star (and planet). The rms noise in 400 μJy near the position of the undetected planet. (right) Light curves for the right circularly polarized flux at the position of τ Boo over the 40 hours of observation. Time series at time resolution of 4 sec (red) and 17 min (blue) have rms noise of 65 mJy and 4 mJy respectively. No evidence of emission is present at any observed orbital/rotational phase of the planet. From (Hallinan et al. 2013).

3. Past and ongoing observations and results

Most of the searches focussed on known exoplanetary systems discovered by radial velocity or transits measurements. Application of scaling laws to the exoplanet census (e.g. from *exoplanet.eu*) guided target selection (Lazio et al. 2004, Grießmeier et al. 2007, 2011), with promising candidates such as τ Boo, υ And or 55 Cnc. Other selection criteria included the existence of a strong stellar magnetic field, measured by Zeeman-Doppler imaging (as for the transiting planet HD 189733) (Farès et al. 2010), planets with a very elliptical orbit and a periastron very close to the star (HD 80606), or planets for which SPI was tentatively detected via optical measurements (HD 179949, υ And), although the sporadicity of observed signatures makes them not fully convincing (Shkolnik et al. 2008, and references therein).

Observations at the VLA provided no detection of τ Boo at 74 MHz with $\sim$100 mJy sensitivity (Farrell et al. 2003, 2004), or of HD 80606 at 330 MHz and 1465 MHz with resp. 1.7 mJy and 0.048 mJy sensitivities (Lazio & Farrell 2007, Lazio et al., 2010a). Negative results were also obtained with the GMRT at 153, 244 and 614 MHz on HD 189733 (Lecavelier et al. 2009, 2011) with resp. 2.1 mJy, 2 mJy and 0.16 mJy sensitivities, and at 153 MHz on various targets (υ And, ε Eri, HD 128311) (Winterhalter et al. 2006, George & Stevens 2007, 2008). A recent very significant negative result, shown in Figure 4, comes from the deepest 150 MHz observation of τ Boo at GMRT, for 40 h (half of the exoplanet's orbital period) covering all orbital/rotational phases, that provided no detection at $\sim$1 mJy level, setting this flux density level as an upper limit for both quiescent and rotationally modulated radio emission from a hot Jupiter (Hallinan et al. 2013). No detection either was obtained on a dozen targets observed during a few hours each at UTR-2 between $\sim$15 and 30 MHz, specifically looking for pulses shorter than $\sim$1 min., for which statistical data accumulation led to a sensitivity between 100 mJy and 1500 mJy depending on the target (Zarka et al. 1997, Ryabov et al. 2004).

These non detections, summarized in Figure 5, can be due to the absence of significant emis-

PoS(AASKA14)120

sion from these targets (permanent of at observation epochs, due to their intrinsic variability), to magnetic dipole moments of the observed exoplanets too weak to generate a surface magnetic field permitting CMI emission to occur at the observed frequencies ($B_{surface}$ > 26 G at 74 MHz, $B_{surface}$ > 54 G at 150 MHz...), or to the Earth lying outside the beaming pattern of the planet's radio emission at the time of observation (CMI indeed produces narrowly beamed emission at specific angles relative to the magnetic field in the source ; this beaming strongly affects the visibility of the emission as a function of time). In the case of UTR-2, the frequency range matches the decametric emission from Jupiter but the sensitivity was moderate.

More encouraging results were obtained at two occasions with the GMRT: (i) a ∼3.9 mJy emission was detected in 2009 at 153 MHz at <1 FWHM beam distance from the system HAT-P-11 that includes a Neptune-mass transiting exoplanet, and the light curve was consistent with an eclipse when the planet passed behind the star (Figure 6) ; but an equally sensitive observation repeated in 2010 did not detect any significant signal in the radio light curve near the same position, suggesting a variable planetary emission or a false positive (5% probability) in 2009 (Lecavelier et al. 2013). (ii) The first published part of the ongoing GMRT sky survey (TGSS) at 150 MHz encompasses 175 exoplanetary systems; for 4 of them (61 Vir, 1RXS1609, HD 86226, and HD 164509) TGSS radio sources were found coinciding with or located very close to their coordinates, with flux densities of ∼120, 28, 19, and 18 mJy respectively (Sirothia et al. 2014). For the latter two, detection is marginal and should be confirmed by deeper observations. For all four ones, further observations are needed to exclude possible coincidence with a background radio source. The authors do not claim any unambiguous detection, but this may be the top of the iceberg showing up. For the other 171 exoplanetary systems, TGSS non detection provides 3σ upper limits between 8.7 mJy and 136 mJy.

Ongoing targeted searches are carried on (by the authors of this chapter) with UTR-2 and LOFAR, several tens of hours being distributed on a few dozen targets (a few hours per target, and recently 32 hours on 55 Cnc). More extensive observations are carried out with the LWA in the frame of the HJUDE project, aiming at thousands of observing hours distributed on a few targets (incl. τ Boo) (Hartman et al. 2013). UTR-2 has the advantage of a large effective area (∼150000 m^2) and observes at the lowest frequencies accessible from the ground (10-32 MHz), but measures a single linear (EW) polarization and has to deal with a polluted radio spectrum. LOFAR is the largest present radio telescope (interferometer) in the range 30-250 MHz, that may extend down to 10 MHz with reduced sensitivity (van Haarlem et al. 2013). Exoplanet search is conducted in its low band (∼20-80 MHz), in full polarization. HJUDE relies on a relatively small instrument (256 dipoles) in the 10-88 MHz band, but with a large duty cycle (searching for periodic signals at exoplanet's orbital periods) and full polarization measurements. Data analysis is ongoing in all cases.

Systematic searches in survey data will continue in the next releases of the TGSS, and is starting in LOFAR's Multifrequency Snapshot Sky Survey (Heald et al. 2014). The latter is a northern sky survey in the spectral ranges 30-75 MHz (8 × 2 MHz bands, ≤100" resolution, ≤15 mJy/beam) and 120-160 MHz (8 × 2 MHz bands, ≤120" resolution, ≤5 mJy/beam). The high-frequency part is near complete whereas the low-frequency part is ongoing.

We are thus in a situation where efforts intensify, both for targeted observations (still at a modest level with large instruments) and systematic searches in sky surveys (that become available

PoS(AASKA14)120

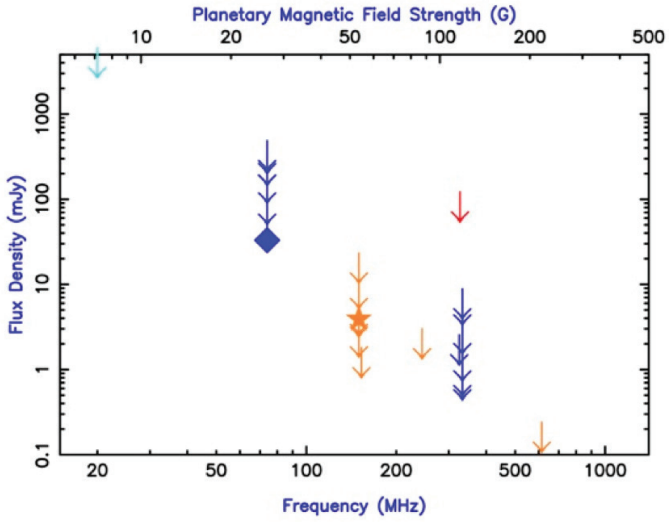

Figure 5: Summary of previous attempts to detect radio emissions from exoplanets. Blue symbols are from the VLA, red from the GBT, orange from the GMRT, and cyan from UTR-2. Arrows are upper limits from various targeted observations. The blue diamond is the statistical upper limit from Lazio et al. (2010b) on the average emission from potential planets in the solar neighbourhood. The orange star is the unconfirmed detection from Lecavelier et al. (2013).

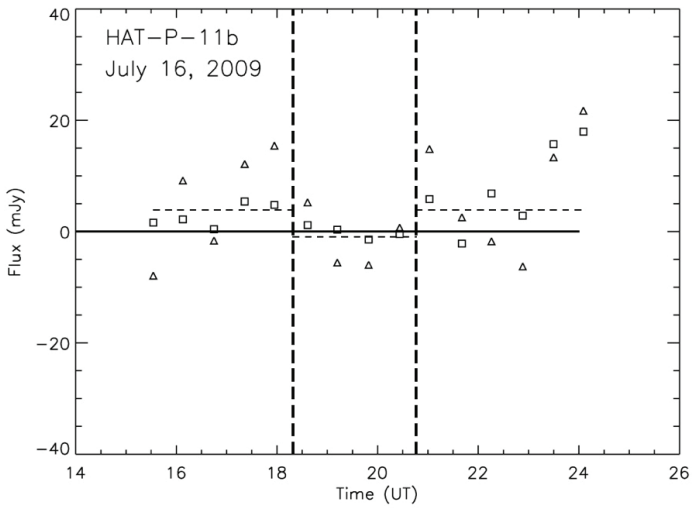

Figure 6: Time series of the 150 MHz flux density measured on July 16, 2009, in the direction of the radio source near HAT-P-11. Measurements have been rebinned to 36 min. Triangles and squares correspond to the right and left circular polarizations. The two vertical – dashed lines indicate the beginning and the end of the planet's eclipse behind the host star. The dashed horizontal lines show the box-shaped eclipse light curve fitted to the data points. From (Lecavelier et al. 2013).

PoS(AASKA14)120

for the first time at low enough frequencies). First hints of detection are encouraging but not yet unambiguous.

4. Science outcome enabled by SKA

The result of past searches suggest that magnetospheric radio emissions much stronger than Jupiter's and at frequencies $\geq$150 MHz are rare. It is thus needed to explore a large sample of targets with highest possible continuum sensitivity, preferably at low frequencies (although unipolar inductor driven CMI emission may reach hundreds of MHz). At the SKA angular resolution ($\sim$11" for SKA1-LOW at 110 MHz, $\sim$1" for SKA1-SUR and SKA1-MID at 0.5-1 GHz), it will generally not be possible to resolve exoplanet-star systems. Once a signal is detected, attributing it to the exoplanet's magnetosphere, to an exoplanet-induced signal into the star's magnetic field, or to exoplanet-independent stellar activity should be relatively easy on the basis of polarization and temporal modulations of the signal (see section 2.3). Thus measurements in circular (V-Stokes) or full polarization (4-Stokes) are required, over long or repeated observations for each target. Such measurements should be wealy affected by confusion, provided that the beam shape remains smooth and stable with time.

Experience from LOFAR, that uses elementary dipole antennas seeing a large fraction of the sky at any time, taught us that imaging will be more powerful than beamformed observations at least at the initial – detection – stage, because it allows to better remove the contribution of sources around the target and to obtain high dynamic range images, reaching a sensitivity of order of the thermal noise. Beamformed observations will be very useful to monitor – at much lower computational cost – the targets detected by imagery. New imaging techniques are also being developed, including predictor/estimator schemes such as Kalman filters (Tasse 2014), or decomposition of the imaging process on the Fourier transform of the observation time, that may considerably improve the efficiency of variable source imaging in the future.

4.1 SKA Phase 1

Jupiter bursts in the 30-40 MHz range can exceed 10^7 Jy at Earth, i.e. 40 μJy at 10 pc range, the average flux density of the emission at hour timescale being about one order of magnitude lower. SKA1-LOW, consisting of some 250000 dipoles in a radio-quiet site (Dewdney et al. 2013), will bring an improvement in sensitivity by a factor $\sim$ 10 to 30 with respect to LOFAR in the range 50-250 MHz. SKA1-LOW will have a sensitivity (1σ) between 70 and 7 μJy across the band 50-350 MHz, with 4 MHz $\times$ 1 hour integration (Figure 7). Confusion noise affecting deep images will be a few times larger in total intensity at the lowest frequencies (dashed line in Fig. 7, computed from (Condon 2005)). Detection of time-variable and/or circularly polarized emission will be less severely affected. Thus, Jupiter-like exoplanets will become detectable for the first time from distances of several parsecs. Even if bursts are intrinsically shorter, statistical accumulation (Ryabov et al. 2004) will permit to reach long integration times without diluting the signal.

Being little dependent on extrapolations of the scaling laws of section 2.2 to high-power ranges for reaching detectable emission levels (we will need emissions $\geq 10^{0-1}\times$ rather than $\geq 10^3\times$ Jupiter), and needing exoplanetary magnetic fields only slightly larger than Jupiter's to emit above 50 MHz, it is highly likely that SKA1-LOW will detect exoplanetary radio signals.

PoS(AASKA14)120

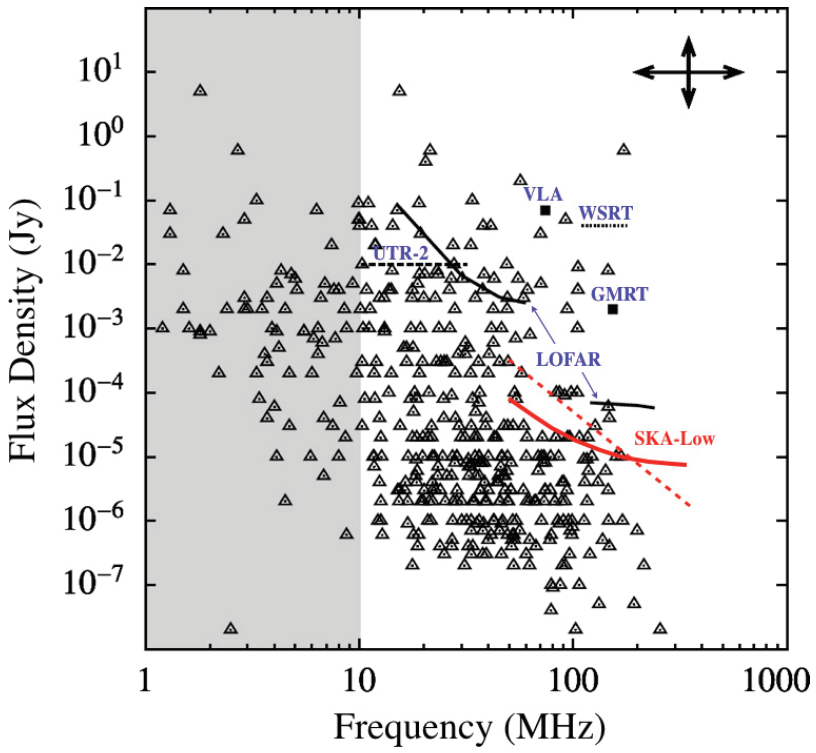

Figure 7: Predicted maximum emission frequency and expected radio flux for known exoplanets (in 2011, indicated by triangle symbols) for a rotation-independent planetary magnetic field and the scaling law of Fig. 2. The approximate sensitivity of several instruments is shown (for 1 h of integration time and a bandwidth of 4 MHz, or an equivalent combination). Confusion limit for SKA1-LOW is indicated by the dashed red line. Frequencies below 10 MHz are not observable from the ground (ionospheric cutoff). Adapted from (Grießmeier et al. 2011).

But it remains correct to assume that exoplanets closer to their parent star, or orbiting stars with large X-UV flux, should emit stronger signals (e.g. 20× larger than Jupiter's for a Jovian-like exoplanet at 1 AU from a solar-type star), and that unipolar inductor SPI do exist for exoplanets orbiting strongly magnetized stars. Thus a systematic search should reveal a large number of radio-emitting exoplanets. These detections will give access to numerous measurements of exoplanetary magnetic fields, rotation periods, orbits inclinations, and SPI regimes and powers. They will open the field of comparative (exo-)planetary magnetospheric physics, may allow to discover moons around exoplanets (generating Io-Jupiter like CMI radiation), and will help to select favourable systems to study further in search for life signatures.

The search strategy should significantly evolve as compared to previous targeted searches. There are ∼400 stars and white and brown dwarfs within 10 pc, out of which ∼200 are known or observable, and ∼35 exoplanets are currently known, and about 2500 known stars within 30 pc, with about 200 currently known planets. It will be possible with SKA to conduct an authoritative survey of all stars (visible from the SKA site) within 10 pc and a large fraction of those within 30 pc, allowing to detect any radio emission ∼ 1 to 10 times stronger than Jupiter's up to a distance of 10 pc, and any emission one order of magnitude stronger up to a distance of 30 pc. In parallel, all known exoplanets should be monitored (>1800 planets are known today within >1100 systems

PoS(AASKA14)120

– *exoplanet.eu*). Further emphasis may be put on systems for which the stellar magnetic field is measured and large, the phase of strongest radio signals being predictable in that case from stellar magnetic field extrapolations (Farès et al. 2010) (and unique information can thus be obtained from the comparison between observational results and predictions). Exoplanet-rich fields of view (e.g. deduced from Kepler observations and the new generation ESO-VLT instruments – see section 5.2) are also targets of particular interest, where it will be possible to search in long observations series any periodic signal matching an exoplanet's rotation or orbital period.

For each target, several observations of several hours each should be performed to account for phase effects (combined to the narrow beaming of CMI emission) or intrinsic variability. Maximum sensitivity is needed at all times, implying the use of the full array, and circular or full-polarization observations. Modest temporal and spectral resolutions are needed for meeting the physical objectives described above, typically δf/f $\simeq 1\%$ (or $\sim$1 MHz spectral channels) and δt $\simeq$ 1 sec to 1 min. Finer resolutions are temporary required for the purpose of RFI mitigation before post-integration. The large number of targets to observe several times requires large duty cycles and large fields of view. In order to increase the SKA1-LOW FoV ($\sim 5 \times 5^{\circ 2}$ at 110 MHz, scaling as λ^2), multi-beam observations are very desirable. As emissions are more likely to occur at low frequencies, restricting the beam bandwidth (e.g. to 50 MHz) can allow to form many beams at little cost on the system capabilities. The availability of as many beams as possible will be a significant advantage for exoplanet search, as for searches or any other transient signals (exoplanetary radio emissions are slow transients).

Finally, all survey-type programs that will be conducted with SKA1-LOW during SKA Phase 1 (e.g. transients searches) should have their data correlated with the exoplanet catalog (*exoplanet.eu*), searching for coincidences (as for the GMRT and LOFAR sky surveys), that may guide follow-on observations. More generally, the search for emission at the coordinates of all known exoplanets should be systematically performed commensally to all SKA1-LOW observations.

4.2 Early science operations of SKA Phase 1

At a fraction $\sim$50% of SKA1-LOW capabilities, SKA1-LOW will already be a powerful instrument to detect radio emissions from exoplanets. There is thus interest to start intensive observations at an early phase of the project, concentrating on the most favourable targets among those listed above, i.e. stars within 5 to 10 pc, known exoplanets for which a large radio flux is predicted (Lazio et al. 2004, Grießmeier et al. 2007, 2011, Nichols 2012), or for which a hint of detection exist (Lecavelier et al. 2013, Sirothia et al. 2014), and known exoplanets orbiting strongly magnetized stars. The commensal searches mentioned in the previous section should be carried on from the beginning of the operations. More generally, advantage should be taken from synergies with observations at other wavelengths, as described in section 5.2 below, from the early phases of the project.

4.3 Science outcome anticipated from SKA Phase 2

The imaging observations in search for exoplanetary signals conducted in Phase 1 will be limited by confusion rather than by thermal noise. Confusion noise will actually be several tens to hundreds of μJy across the SKA1-LOW band ((Condon 2005) and Fig. 7). Extending SKA-LOW to a less compact array configuration, with baselines e.g. up to 200 km as for SKA1-MID,

PoS(AASKA14)120

would reduce the confusion to values close to the thermal noise (and at the same time reduce the thermal noise because of increased collecting area), down to a few μJy in the range 50-350 MHz, making Jupiter-like emission easily detectable at >10 pc range. Increased field of view will improve systematic searches. The higher signal-to-noise ratio with which dynamic spectra of exoplanet's radio emissions will be measured, beyonf the few dB required for mere detection, will enable detailed quantitative interpretation of the observations in the frame of the simulations of (Hess & Zarka 2011) (see section 2.3).

SKA2 will also extend and deepen large surveys started with SKA1. This will make increasingly relevant the systematic search of exoplanetary signals in these surveys by correlation with the exoplanet catalog. Increased angular resolution of the observations (to $\leq$3" at 110 MHz) will make coincidences more robust, less likely to be due to background radio sources. With the development of SKA1-SUR and SKA1-MID, searches for periodic higher frequency unipolar inductor emission such as predicted by Willes & Wu (2004, 2005) should be targeted at known (magnetic) white dwarfs, following a strategy that will depend of the statistics of known white dwarf properties (known magnetic field, angular distribution, distance...). Multi-beam capability will undoubtly be very useful. More synergies will become relevant, with other SKA observations (section 5.1 below), as well as with observations at other wavelengths (section 5.2).

5. Synergies

5.1 Synergies with other SKA observations

Detection of stellar radio flares with SKA will have similar instrumental requirements as exoplanet radio detection (sensitivity, circular polarization, detection of bursts, large duty cycles). For example, SKA1-LOW will be able to detect the brightest solar bursts out to $\geq$10 pc.

But there are also deep physical connections between stellar physics and activity and exoplanet search:

- Stellar flares and mass ejections – such as solar CMEs and associated solar "type II" radio bursts – can excite magnetospheric planetary emissions (and cause atmospheric loss).
- Some stellar flares could actually be induced by an orbiting close-in exoplanet (through unipolar induction or magnetic reconnection).
- There is probably a continuum of physical conditions from brown dwarfs to exoplanets (decreasing rotational period, increasingly cool and neutral atmosphere, transition to large-scale stable magnetic field topologies, with weaker magnetic field magnitude). Circularly polarized periodic bursts have been discovered from the former at GHz frequencies (Hallinan et al. 2007, 2008), with brightness temperatures > 10^{15} K. They have been attributed to CMI emission in kGauss magnetic fields. The duration of the bursts is a few percent of the recurrence period. This justifies the large duty-cycle required for their detection, and similarly for the detection of exoplanetary radio signals. Tracing magnetic fields and radio flux densities from brown dwarfs to planets will bring unique constraints for dynamo theories as well as for radio emission scaling laws.

PoS(AASKA14)120

- Finally, Kepler has shown that lower mass planets are more frequent around M dwarfs (Dressing & Charbonneau 2013), and close-in planets may be located in the habitable zone (although habitability may need to be redefined based on magnetic activity).

Provided that complex time domain voltage data from tied array beams can be exported in parallel with imaging or beamformed spectral observations, sensitive SETI searches could be commensally performed with exoplanetary observations, in spectral ranges little or not explored by past SETI searches (see corresponding chapter).

5.2 Synergies with observations at other wavelengths

As already mentioned above, measurements of stellar magnetic fields by Zeeman-Doppler imaging (with instruments such as CFHT/Espadons and TBL/Narval in visible light, and with CFHT/Spirou in the infrared in the near-future) are a key ingredient to assess SPI whose associated emission will be measured with SKA. Magnetic topology can influence the direction of emission of CMEs and in turn their impact on orbiting exoplanets. Measurements of large magnetic fields will also motivate SKA observations in search for unipolar inductor emissions, whose level can be in principle predicted along the planet's orbit (Farès et al. 2010). UV and X observations by HST, XMM-Newton, Chandra, and in the future by the Athena+ X-ray observatory will characterize stellar outputs and allow to identify best exoplanet candidates for enhanced magnetosphere-ionosphere coupling (Nichols 2011, 2012). Observations of large flares can also motivate specific searches of radio emissions triggered by these flares (in parallel with spectroscopic studies of their impact on exoplanet's atmosphere), as was done successfully to detect Uranus' aurorae (Lamy et al. 2012).

The number of known planets in the solar neighbourhood should increase substantially thanks to the missions PLATO (Planetary Transits and Oscillations of stars) and TESS (Transiting Exoplanet Survey Satellite), whereas Spirou will find Earth-like planets around nearby red dwarfs. The JWST will be able to characterize the atmospheres of these nearby planets, whereas magnetospheric studies with SKA will bring constraints to their habitability. Studies of lower mass planets will also provide insights to different regimes of planetary dynamos. New surveys by the ESO-VLT instruments NGTS (Next-Generation Transit Survey) and ESPRESSO (Echelle SPectrograph for Rocky Exoplanet and Stable Spectroscopic Observations) will likely increase the number of confirmed exoplanets up to several tens per field of view of SKA1-LOW.

Finally, LOFAR will continue to provide observations within part of the SKA1-LOW range in the northern hemisphere, whereas the lower frequency ($\leq$50 MHz and down to 10 MHz) radiotelescopes UTR-2, NenuFAR, OLWA, will perform follow-on observations of SKA1-LOW candidates (in the overlapping part of the sky) or vice-versa.

6. Conclusion

Thanks to our experience of solar system magnetospheres and radio emissions, and extensive theoretical studies, the interpretation frame of exoplanetary radio observations is ready, waiting for the first confirmed detections and measurements of dynamic spectra. Beyond the measurement of several exoplanet's parameters, including the magnetic field (with implications on dynamo theory and habitability) and rotation, radio detections will open the new field of comparative exoplanetary

PoS(AASKA14)120

magnetospheric physics and permit to study flow-obstacle plasma interactions in various speed, density, magnetic field, mass regimes, from hot jupiters to low-mass planets around (M) dwarfs.

Up to now, detecting the signal is the most difficult step. But the characteristics of SKA1-LOW (minimum frequency of 50 MHz, sensitivity of a few to a few 10s μJy, full Stokes measurements) will permit the detection of Jupiter like emission from $\geq$10 pc, independent of any extrapolation of solar system-based scaling laws (provided that Jupiter's magnetic field and radio flux density are not exceptionally high). Actually, scaling laws and theory suggest the existence of much stronger emissions, that will allow us to search much larger volumes of space.

The context of these searches will be favoured by the expected rapid growth in the number of known exoplanets due to new instruments and space missions (PLATO, TESS, JWST, NGTS, EXPRESSO...) that could result in tens of exoplanets per SKA1-LOW field of view. In order to take full advantage of this context, large duty-cycles are needed (repeated, hours-long observations), for which a multi-beam capability will be extremely useful. Observations will include targeted searches, commensal observations, and correlation of surveys to up-to-date exoplanet catalog. Radio flux densities of 1-10$\times$ Jupiter's will be detectable within 10 pc, where all stars should be observed. A large fraction of all stars within 30 pc should also be observed, with a detection threshold one order of magnitude larger. All exoplanets should eventually be the subject of targeted searches, starting with systems with large stellar magnetic field or large X-UV flux.

Such synergies with observations at different wavelengths will be important, but also synergies with other SKA observations, especially concerning the "star-planet connection": a study of the field topology, dynamo, and radio output from dwarfs to planets. Eventually, radio detection may evolve as a discovery tool, e.g. adapted to finding planets (giant or terrestrial) around active, magnetic or variable stars. The realm that remains to explore is huge.

Acknowlegments

Part of this research was carried out at the Jet Propulsion Laboratory, California Institute of Technology, under a contract with the National Aeronautics and Space Administration. PZ thanks L. Lamy for useful comments.

REFERENCES

Berge, G. L. & Gulkis, S. 1976, in Jupiter, T. Gehrels ed., Univ. Arizona Press, 621
Bigg, E. K. 1964, Nature, 203, 1008
Burke, B. F., & Franklin, K. L. 1955, J. Geophys. Res., 60, 213
Condon, J. J. 2005, ASPC 345: From Clark Lake to the LWA, N. E. Kassim et al. eds., 237
de Pater, I. 2004, Planet. Space Sci., 52, 1449
Dewdney, P., Turner, W., Millenaar, R., et al. 2013, SKA1 System Baseline Design, Document number SKA-TEL-SKO-DD-001, Rev. 1
Dressing, C. D., & Charbonneau, D. 2013, Astrophys. J., 767, 95
Farès, R., Donati, J.-F., Moutou, C., et al. 2010, MNRAS, 406, 409
Farrell, W. M., Desch, M. D., & Zarka, P. 1999, J. Geophys. Res., 104, 14025

PoS(AASKA14)120

Farrell, W. M., Desch, M. D., Lazio, T. J., et al. 2003, ASPC 294: Scientific Frontiers in Research on Extrasolar Planets, 151
Farrell, W. M., Lazio, T. J., Desch, M. D., et al. 2004, IAUS 213, Bioastronomy 2002: Life Among the Stars, R. Norris & F. Stootman eds., ASP, 73
George, S. J., & Stevens I. R. 2007, MNRAS, 382, 455
George, S. J., & Stevens, I. R. 2008, MNRAS, 390, 741
Grießmeier, J.-M., Stadelmann, A., Penz, T., et al. 2004, Astron. Astrophys., 425, 753
Grießmeier, J.-M., Stadelmann, A., Motschmann, U., et al. 2005, Astrobiology, 5(5), 587
Grießmeier, J.-M., Zarka, P., & Spreeuw, H. 2007, Astron. Astrophys., 475, 359
Grießmeier, J.-M., Zarka, P., & Girard, J. N. 2011, Radio Science, 46, RS0F09
Jardine, M., & Cameron, A. C. 2008, Astron. Astrophys., 490, 843
Hallinan, G., Bourke, S., Lane, C., et al. 2007, Astrophys. J., 663, L25
Hallinan, G., Antonova, A., Doyle, J. G., et al. 2008, Astrophys. J., 684, 644
Hallinan, G., Sirothia, S. K., Antonova, A., et al. 2013, Astrophys. J., 762, 34
Hartman, J., Hallinan, G., Taylor, G., et al. 2013, LWA Users Meeting, Arlington, VA
Heald, G., & the MSSS team 2014, LOFAR science meeting, Amsterdam, *www.astron.nl/lofarscience2014/*
Hess, S. L. G., & Zarka, P. 2011, Astron. Astrophys., 531, A29
Lamy, L., Prangé, R., Hansen, K. C., et al. 2012, Geophys. Res. Lett., 39, L07105
Lazio, T. J. W., Farrell, W. M., Dietrick, J., et al. 2004, Astrophys. J., 612, 511
Lazio, T. J. W., & Farrell, W. M. 2007, Astrophys. J., 668, 1182
Lazio, T. J. W., Shankland, P. D., Farrell, W. M., et al. 2010a, Astron. J., 140, 1929
Lazio, T. J. W., Carmichael, S., Clark, J., et al. 2010b, Astron. J., 139, 96
Lecavelier des Etangs, A., Sirothia, S. K., Gopal-Krishna, et al. 2009, Astron. Astrophys., 500, L51
Lecavelier des Etangs, A., Sirothia, S. K., Gopal-Krishna, et al. 2011, Astron. Astrophys., 533, A50
Lecavelier des Etangs, A., Sirothia, S. K., Gopal-Krishna, et al. 2013, Astron. Astrophys., 552, A65
Nichols, J. D. 2011, MNRAS, 414, 2125
Nichols, J. D. 2012, MNRAS, 427, L75
Ryabov, V. B., Zarka, P., & Ryabov, B. P. 2004, Planet. Space Sci., 52, 1479
Shkolnik, E., Bohlender, D. A., Walker, G. A. H., et al. 2008, Astrophys. J., 676, 628
Sirothia, S. K., Lecavelier des Etangs, A., Gopal-Krishna, et al. 2014, Astron. Astrophys., 562, A108
Tasse, C. 2014, Astron. Astrophys., 566, A127
Treumann, R. 2006, Astron. Astrophys. Rev, 13, 229
van Haarlem, M. P., & the LOFAR collaboration 2013, Astron. Astrophys., 556, A2
Willes, A. J., & Wu, K. 2004, MNRAS, 348, 285
Willes, A. J., & Wu, K. 2005, Astron. Astrophys., 432, 1091
Winterhalter, D., Kuiper, T., Majid, W., et al. 2006, in Planetary Radio Emissions VI, H. O. Rucker et al. eds., Austrian Acad. Sci. Press, 595
Zarka, P., Queinnec, J., Ryabov, B. P., et al. 1997, in Planetary Radio Emissions IV, H. O. Rucker et al. eds., Austrian Acad. Sci. Press, 51

PoS(AASKA14)120

Zarka, P. 1998, J. Geophys. Res., 103, 20159
Zarka, P., Treumann, R. A., Ryabov, B. P., et al. 2001, Astrophys. Space Sci., 277, 293
Zarka, P. 2004, Planet. Space Sci., 52, 1455
Zarka, P. 2007, Planet. Space Sci., 55, 598
Zarka, P. 2010, in Pathways Towards Habitable Planets, ASPC 430, V. Coudé du Foresto et al. eds., 175
Zarka, P. 2011, in Planetary Radio Emissions VII, H. O. Rucker et al. eds., Austrian Acad. Sci. Press, 287

PoS(AASKA14)120

PROCEEDINGS OF SCIENCE

Radio Jets in Young Stellar Objects with the SKA

Guillem Anglada*
Instituto de Astrofísica de Andalucía, CSIC, Spain
E-mail: guillem@iaa.es

Luis F. Rodríguez
Centro de Radioastronomía y Astrofísica, UNAM, México
E-mail: l.rodriguez@crya.unam.mx

Carlos Carrasco-González
Centro de Radioastronomía y Astrofísica, UNAM, México
E-mail: c.carrasco@crya.unam.mx

Jets and outflows are ubiquitous in the process of formation of stars since accretion is intimately associated with outflow. Free-free radio continuum emission in the centimeter domain is associated with these jets. The emission is weak, and sensitive telescopes are required to detect it.
One of the key problems in the study of outflows is to determine how they are accelerated and collimated. Observations in the cm range are most useful to trace the base of the ionized jets, close to the young central object and its accretion disk, where optical or near-IR images are obscured by the high extinction present. Radio recombination lines in jets (in combination with proper motions) should provide their 3D kinematics at very small scale (near their origin). SKA will be crucial to perform this kind of observations.
Thermal jets are associated with both low and high mass protostars. The ionizing mechanism of these radio jets appears to be related to shocks in the associated outflows, as suggested by the observed correlation between the centimeter luminosity and the outflow momentum rate. From this correlation and that with the bolometric luminosity of the driving star it will be possible to discriminate with SKA between unresolved HII regions and jets, and to infer physical properties of the embedded objects.
Some jets associated with young stellar objects (YSOs) show indications of non-thermal emission (negative spectral indices) in part of their lobes. Linearly polarized synchrotron emission has been found in the jet of HH 80-81, allowing us to measure the direction and intensity of the jet magnetic field, a clue ingredient in determining the collimation and ejection mechanisms. As only a fraction of the emission is polarized, very sensitive observations such as those that will be feasible with SKA are required to perform these studies.
Jets are common in many kinds of astrophysical scenarios. Characterizing radio jets in YSOs, where thermal emission allows us to determine their physical conditions in a reliable way, would be also useful in understanding acceleration and collimation mechanisms in all kinds of astrophysical jets.

Advancing Astrophysics with the Square Kilometre Array
June 8-13, 2014
Giardini Naxos, Italy

*Speaker.

PoS(AASKA14)121

1. Introduction

In the last years it has become clear that collimated outflows are present in young stars across all the stellar spectrum, from O-type protostars to brown dwarfs, suggesting that the disk-jet scenario is valid to describe the formation of stars of all masses.

Outflows associated with young stars frequently exhibit a central weak centimeter emission source (Anglada et al. 1992; Anglada 1995; Rodríguez & Reipurth 1998). In the best studied cases, these sources are resolved angularly at the sub-arcsec scale and found to be elongated in the direction of the large-scale tracers of the outflow (e.g. Rodríguez et al. 1990; Rodríguez 1995, 1996; Anglada 1996), indicating that they trace the region, very close to the exciting star, where the outflow phenomenon originates. The centimeter flux density usually rises slowly with frequency (positive spectral index). Given their morphology and spectrum these sources are usually referred to as "thermal" radio jets. These radio jets have been found during all the stages of the star-formation process, from Class 0 protostars to stars associated with transitional disks, suggesting that outflow and accretion are intimately related (Rodríguez et al. 2014).

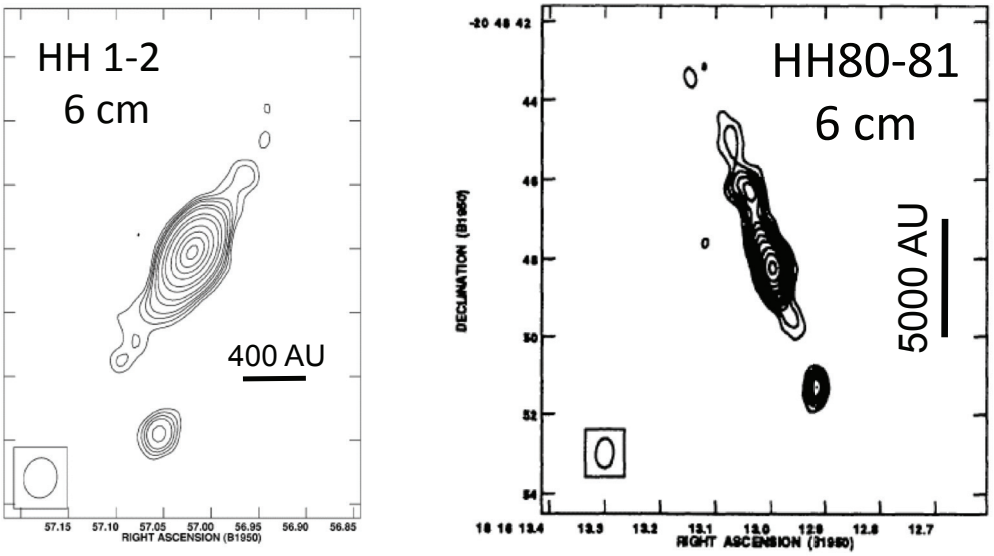

Figure 1: (Left) HH1-2 radio jet, associated with a low-mass object (Rodríguez et al. 2000). (Right) HH80-81 radio jet, associated with a high-mass object (Martí et al. 1993).

With the extraordinary sensitivity of the Jansky VLA, e-MERLIN, and the SKA it is expected that all nearby (a few kpc) young stellar objects (YSOs) known to be associated with outflows, both molecular and/or optical/infrared, will be detectable as centimeter sources (Anglada et al. 2015, in preparation). The topic of radio jets from young stars has been reviewed by Anglada (1996) and Rodríguez (1997; 2011).

2. Properties of Radio Jets

The study of jets associated with young stars at radio wavelengths is important in several aspects. Given the large obscuration present towards the very young stars, the detection of the

PoS(AASKA14)121

radio jet provides so far the best way to obtain their accurate positions. These observations also provide information on the direction and collimation of the gas ejected by the young system in the last few years (see Table 1) that can be compared with the gas in the molecular outflows and optical/infrared HH jets, which traces the ejection over timescales several orders of magnitude larger. This comparison allows us to make evident the changes in the ejection direction, possibly resulting from precession or orbital motions in binary systems (Rodríguez et al. 2008; Masqué et al. 2012).

The radio jets from YSOs can be described using the free-free models of Reynolds (1986). In particular, for a jet of constant temperature, velocity and ionization fraction, these models predict that the flux density increases with frequency as $S_\nu \propto \nu^\alpha$, where $\alpha = 1.3 - 0.7/\varepsilon$, and ε is the index of the power-law dependence of the jet width with distance to its origin. The case of $\varepsilon = 1$ corresponds to a conical (constant opening angle) jet. The angular size of the major axis of the jet decreases with frequency as $\theta_\nu \propto \nu^{-0.7/\varepsilon} = \nu^{\alpha-1.3}$. This behavior in flux density and size can be tested with multi-frequency observations.

With the Reynolds (1986) models it is also possible to determine from the observations the ionized mass loss rate, $\dot{M}_i$, in the jet and the radius at which ionization starts, r_0. The jet velocity, V_j, necessary to determine $\dot{M}_i$ can be estimated from proper motion measurements obtained from multi-epoch observations. In Table 1 we present the parameters of a few selected radio jets. These well-known jets have centimeter flux densities of 1 mJy or more. However, most of the jets associated with low mass stars or even brown dwarfs present centimeter flux densities in the order of tens of μJy (Rodríguez et al. 2015, in preparation) and their detection and study will require of the high sensitivity of SKA.

Table 1: Properties of Selected Angularly Resolved Radio Jets in YSOs

Source	$L_{\rm bol}$ ($L_\odot$)	$M_\star$ ($M_\odot$)	d (kpc)	S_ν (mJy)	α	θ_0 (deg)	Size (AU)	V_j (km s^{-1})	$t_{\rm dyn}$ (yr)	ε	$\dot{M}_i$ ($M_\odot$ yr^{-1})	r_0 (AU)	Refs.
HH 1-2 VLA1	20	$\sim$1	0.4	1	0.3	19	200	270	2	0.7	1×10^{-8}	$\leq$11	1, 2, 3, 4
NGC 2071-IRS3	$\sim$500	4	0.4	3	0.6	40	200	400[a]	3	1	2×10^{-7}	$\leq$18	5, 6, 2, 7
Cep A HW2	1×10^4	15	0.7	10	0.7	14	400	460	3	0.9	5×10^{-7}	$\leq$60	8, 9, 10, 11, 12
HH 80-81	2×10^4	15	1.7	5	0.2	34	1500	1000	7	0.6	1×10^{-6}	$\leq$25	13, 14, 15, 16, 17, 18

[a] Assumed.

References: (1) Fischer et al. 2010; (2) Menten et al. 2007; (3) Rodríguez et al. 1990; (4) Rodríguez et al. 2000; (5) Butner et al. 1990; (6) Carrasco-González et al. 2012a; (7) Torrelles et al. 1998; (8) Hughes et al. 1995; (9) Patel et al. 2005; (10) Dzib et al. 2011; (11) Curiel et al. 2006; (12) Rodríguez et al. 1994; (13) Aspin & Geballe 1992; (14) Fernández-López et al. 2011; (15) Rodríguez et al. 1980; (16) Martí et al. 1995; (17) Martí et al. 1993; (18) Carrasco-González et al. 2012b.

Sensitive, very high angular resolution observations at centimeter wavelengths can trace the base of the jets down to the injection radius, at scales of a few AUs, where the ionized jet is expected to begin. Exploration of this inner region will eventually shed new light on the jet acceleration and collimation mechanisms, helping to distinguish between different theoretical approaches such as the X-wind (Shu et al. 2000) and disk-wind (Königl & Pudritz 2000) models. Shang et al. (2004) use the X-wind model to calculate the expected properties of the centimeter free-free emission of YSO jets. A comparison of detailed modeling results and high quality observations can provide an

PoS(AASKA14)121

accurate description of the jet physical parameters.

Additionally, we note that a good knowledge of the jet properties is indispensable for grain growth studies in protoplanetary disks to separate the dust emission of the disk from the free-free emission of the jet. It is known that even transitional disks present free-free emission in their central regions (Rodríguez et al. 2014).

3. Bolometric Luminosity, Outflow, and Radio Continuum Correlations

Photoionization does not appear to be the ionizing mechanism of radio jets, since in the sources associated with low-luminosity objects, the number of UV photons from the star is clearly insufficient to produce the ionization required to explain the observed radio continuum emission (e.g., Rodríguez et al. 1989; Anglada 1995). The radio luminosity of radio jets ($S_\nu d^2$) is correlated with the bolometric luminosity of the source, $L_{\rm bol}$, and with the momentum rate in the molecular outflow, $\dot{P}$ (Anglada 1995, 1996; see Fig. 2):

$$\left(\frac{S_\nu d^2}{\rm mJy\ kpc^2}\right) = 0.008 \left(\frac{L_{\rm bol}}{L_\odot}\right)^{0.6}, \tag{3.1}$$

$$\left(\frac{S_\nu d^2}{\rm mJy\ kpc^2}\right) = 190 \left(\frac{\dot{P}}{M_\odot\ {\rm yr}^{-1}\ {\rm km\ s}^{-1}}\right)^{0.9}. \tag{3.2}$$

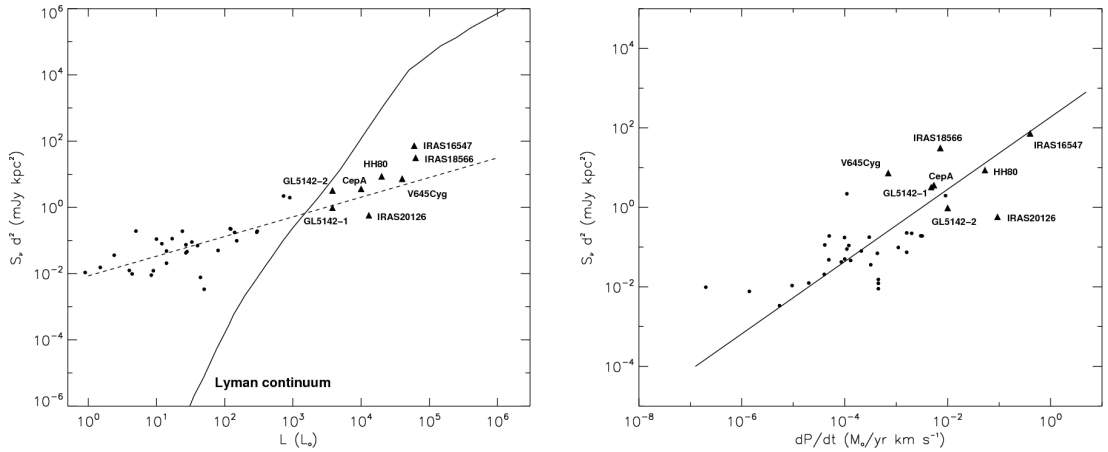

Figure 2: (Left) Radio luminosity versus bolometric luminosity correlation for young stellar objects (dashed line). The solid line (Lyman continuum) represents the radio luminosity expected from photoionization. (Right) Radio luminosity versus outflow momentum rate (solid line). The high luminosity objects are labeled in the figures.

These correlations include young stellar objects with luminosities spanning from 1 to 10^5 $L_\odot$. In particular, these diagrams can be used to discriminate between the thermal radio jets (that should follow these correlations) and HII regions (that should fall close to the Lyman continuum line). Also, detection of radio recombination lines (RRLs, see Sect. 4) in jets could be useful to distinguish between jets and HII regions, since lines are expected to be broader in jets, as noted by Hoare et al. (2007) (see their Fig. 6).

PoS(AASKA14)121

4. Radio Recombination Lines

Radio jets are expected to show RRLs as part of the emission processes of the plasma. RRLs in jets (in combination with proper motions) should provide their 3D kinematics at very small scale (near their origin).

Assuming local thermodynamic equilibrium (LTE) for line and continuum and a standard biconical jet with constant velocity and ionized fraction, the expected line to continuum flux density ratio in the centimeter wavelength regime is given by (Rodríguez et al. 2015, in preparation):

$$\frac{S_L}{S_C} = 0.19 \left(\frac{\nu_L}{\mathrm{GHz}}\right)^{1.1} \left(\frac{T}{10^4\ \mathrm{K}}\right)^{-1.1} \left(\frac{\Delta V}{\mathrm{km\ s^{-1}}}\right)^{-1} (1+Y^+)^{-1}. \quad (4.1)$$

In the above equation, ν_L is the frequency of the line, ΔV the full width at half maximum of the line, and Y^+ is the ionized helium to ionized hydrogen ratio. Since the lines from a jet are expected to be wide, $\Delta V \simeq 100$ km s^{-1}, their detectability will be challenging. For example, at 10 GHz the line-to-continuum ratio is expected to be $\sim$0.02. Thus, for a jet with a continuum flux density of 1 mJy, the peak line flux density will be only $\sim$20 μJy. So far, there are no detections of RRLs in jets at the expected LTE level. Jiménez-Serra et al. (2011) report the detection, at millimeter wavelengths, of broad recombination maser lines toward the jet in Cepheus A HW2 with flux densities about 5 times larger than those expected for LTE. Additional observations are needed to understand the nature of RRLs from jets and start using them as tools to study the outflow kinematics.

5. Non-thermal Emission

As discussed above, jets from YSOs have been long studied at radio wavelengths through their thermal free-free emission which traces the base of the ionized jet, and shows a characteristic positive spectral index. However, in the last two decades, negative spectral indices have been found in some regions of YSO jets (e.g., Rodríguez et al. 1989, 2005; Curiel et al. 1993; Martí et al. 1993; Garay et al. 1996; Wilner et al. 1999; see Fig. 3 left). This negative spectral-index emission is usually found in strong radio knots, that usually appear in pairs, sometimes found moving away from the central protostar at velocities of several hundreds of kilometers per second. Because of these characteristics, it has been proposed that these knots would be tracing strong shocks of the jet against dense material in the surrounding molecular cloud. Their negative spectral indices have been interpreted as indicating non-thermal synchrotron emission from a small population of relativistic particles that would be accelerated in the ensuing strong shocks.

This scenario has been confirmed only very recently, with detection of linearly polarized emission from the HH 80-81 jet (Carrasco-González et al. 2010; see Fig. 3 right). This result provided for the first time conclusive evidence for the presence of synchrotron emission in a YSO jet making it possible the direct measure and study of the properties of the magnetic field strength and morphology. Measuring linear polarization in YSO jets is difficult because it is only a fraction of the total emission. Ultrasensitive radio interferometers, such as the SKA, will allow us to detect and image the magnetic field in a large sample of YSO jets. In combination with the physical parameters (density, temperature, velocity) derived from observations of the thermal component,

PoS(AASKA14)121

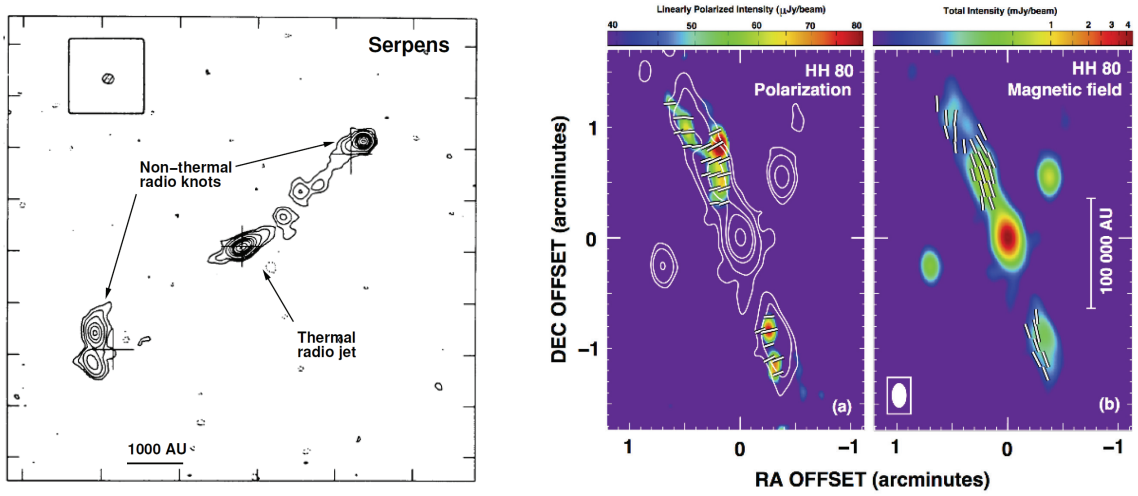

Figure 3: (Left) VLA image at 3.6 cm of the radio jet in Serpens, one of the first YSO jets where synchrotron emission was proposed to arise as a result of strong shocks with the ambient medium. The central source shows a positive spectral index at radio wavelengths, consistent with free-free emission, while the two bright knots at the end of the lobes show negative spectral indices indicative of thermal emission (adapted from Curiel et al. 1993). (Right) VLA images at 6 cm of the HH 80-81 jet showing the first detection of linearly polarized synchrotron emission in a YSO jet. Panel (a) shows in color scale the polarized emission and the polarization direction as white bars. Panel (b) shows the direction of the magnetic field as white bars. The total continuum intensity is shown in contours (a) and in color scale (b) (from Carrasco-González et al. 2010).

the measurement of the magnetic field from the non-thermal component will help in understanding YSO jet acceleration and collimation mechanisms, that appear to be similar for all kinds of astrophysical objects.

6. Expectations for SKA Observations of Radio Jets

The study of radio jets will greatly benefit from the higher frequency bands of SKA. In particular, given the rising spectrum and compact size of the radio jets, we anticipate that most observations of these sources will be carried out in band 5. SKA will allow us to survey the southern hemisphere for radio jets associated with young stars across the mass spectrum, including proto-brown dwarfs. At a distance of 500 pc, a radio jet from a proto-brown dwarf is estimated to have a flux density of 12 μJy at 10 GHz (Palau et al. 2015, in preparation). The SKA1-MID will detect this weak emission at the 10-σ level in only 20 minutes of on-source integration time. Detection of the jets from the most massive protostars (with expected radio luminosities of 10-100 mJy kpc^2, see Fig. 1) will in principle be feasible with at least a similar signal-to-noise ratio across the whole Galaxy. In the "early science" phase of SKA1 the detection of jets from brown dwarfs will reach 300 pc and in the case of massive protostars, it will cover most of the Galaxy.

Observations at different frequencies across band 5 (providing angular resolutions in the 30 to 80 mas range) will determine the variations of the physical parameters along the jet axis and to image the region around the injection radius of the ionized gas in the jet. However, the high angular resolution study of radio jets with SKA1-MID only will be possible for jets of relatively

PoS(AASKA14)121

high flux density (a few tenths of mJy). For weaker jets the full SKA (SKA2) will be required, since the uniform weighting SKA1 sensitivity is expected to be several times worst than for natural weighting (unless the antenna configuration is changed to favor longer baselines). For example, mapping the jet of a proto-brown dwarf is expected to take about 1.5 hours with SKA2, while it would take several hundreds of hours with SKA1.

A search for linear polarization using SKA1-MID will be feasible in the jets with relatively bright non-thermal knots. These knots have characteristic flux densities of about 100 μJy. Assuming a linear polarization degree of 10%, the detection of the Stokes parameters at a signal-to-noise ratio of 10, will require on-source integration times of order 30 minutes (about 2 hours in the "early science" phase of SKA1). With the full SKA (SKA2) it will be possible to search for linear polarization, and even to perform a high angular resolution mapping, in a much more extended sample.

For radio jets with continuum flux densities of order 3 mJy, a peak RRL flux density of 75 μJy is expected (assuming a line width of about 100 km s^{-1}, see formula 4.1). Adopting a velocity resolution comparable to the line width, a 6-σ detection will be achieved with an on-source integration time of 1 hour with SKA1-MID (4 h in the "early science" phase of SKA1). If the emission is resolved spatially or we want better velocity resolution, the on-source time will increase accordingly. On the other hand, many recombination lines will be available in the SKA bands and it will be possible to stack them and improve the detectability (there are 35 RRLs in band 5, improving signal-to-noise ratio by a factor of $\sim$6). This type of observations will reach its full potential with the full SKA (SKA2), when it will be possible to map the radial velocity distribution of the jet and in combination with proper motions obtain the 3D kinematics.

Finally, the high sensitivity and angular resolution of SKA will make it possible to study the equatorial winds, probably driven by radiation pressure acting on the gas on the surface layers of the disk, that have been observed in a number of massive young stars, and to distinguish this kind of sources from jets, as has been done in S140 IRS1 with MERLIN by Hoare (2006).

Acknowledgments

GA acknowledges support from MICINN (Spain) grant AYA2011-30228-C03 (co-funded with FEDER funds) and partial support from Junta de Andalucía (TIC-126). LFR and CC-G acknowledge support from DGAPA, UNAM and CONACyT (Mexico).

REFERENCES

Anglada, G. 1995, RevMexAA Conf. Ser., 1, 67
Anglada, G. 1996, Radio Emission from the Stars and the Sun, ASP Conf. Ser., 93, 3
Anglada, G., Rodríguez, L. F., Cantó, J., Estalella, R., & Torrelles, J. M. 1992, ApJ, 395, 494
Aspin, C., & Geballe, T. R. 1992, A&A, 266, 219
Butner, H. M., Evans, N. J., II, Harvey, P. M., et al. 1990, ApJ, 364, 164
Carrasco-González, C., Galván-Madrid, R., Anglada, G., et al. 2012b, ApJL, 752, L29
Carrasco-González, C., Osorio, M., Anglada, G., et al. 2012a, ApJ, 746, 71
Carrasco-González, C., Rodríguez, L. F., Anglada, G., et al. 2010, Science, 330, 1209

PoS(AASKA14)121

Curiel, S., Ho, P. T. P., Patel, N. A., et al. 2006, ApJ, 638, 878
Curiel, S., Rodríguez, L. F., Moran, J. M., & Cantó, J. 1993, ApJ, 415, 191
Dzib, S., Loinard, L., Rodríguez, L. F., Mioduszewski, A. J., & Torres, R. M. 2011, ApJ, 733, 71
Fernández-López, M., Girart, J. M., Curiel, S., et al. 2011, AJ, 142, 97
Fischer, W. J., Megeath, S. T., Ali, B., et al. 2010, A&A, 518, L122
Garay, G., Ramírez, S., Rodríguez, L. F., Curiel, S., & Torrelles, J. M. 1996, ApJ, 459, 193
Hoare, M. G. 2006, ApJ, 649, 856
Hoare, M. G., Kurtz, S. E., Lizano, S., Keto, E. Hofner, P. 2007, Protostars and Planets V, 181
Hughes, V. A., Cohen, R. J., & Garrington, S. 1995, MNRAS, 272, 469
Jiménez-Serra, I., Martín-Pintado, J., Báez-Rubio, A., Patel, N., & Thum, C. 2011, ApJL, 732, L27
Königl, A., & Pudritz, R. E. 2000, Protostars and Planets IV, 759
Martí, J., Rodríguez, L. F., & Reipurth, B. 1993, ApJ, 416, 208
Martí, J., Rodríguez, L. F., & Reipurth, B. 1995, ApJ, 449, 184
Masqué, J. M., Girart, J. M., Estalella, R., Rodríguez, L. F., & Beltrán, M. T. 2012, ApJL, 758, L10
Menten, K. M., Reid, M. J., Forbrich, J., & Brunthaler, A. 2007, A&A, 474, 515
Patel, N. A., Curiel, S., Sridharan, T. K., et al. 2005, Nature, 437, 109
Reynolds, S. P. 1986, ApJ, 304, 713
Rodríguez, L. F. 1995, RevMexAA Conf. Ser., 1, 1
Rodríguez, L. F. 1996, RevMexAA Conf. Ser., 4, 7
Rodríguez, L. F. 1997, IAU Symposium, 182, 83
Rodríguez, L. F. 2011, IAU Symposium, 275, 367
Rodríguez, L. F., Curiel, S., Moran, J. M., et al. 1989, ApJL, 346, L85
Rodríguez, L. F., Delgado-Arellano, V. G., Gómez, Y., et al. 2000, AJ, 119, 882
Rodríguez, L. F., Garay, G., Brooks, K. J., & Mardones, D. 2005, ApJ, 626, 953
Rodríguez, L. F., Garay, G., Curiel, S., et al. 1994, ApJL, 430, L65
Rodríguez, L. F., Ho, P. T. P., Torrelles, J. M., Curiel, S., & Cantó, J. 1990, ApJ, 352, 645
Rodríguez, L. F., Moran, J. M., Ho, P. T. P., & Gottlieb, E. W. 1980, ApJ, 235, 845
Rodríguez, L. F., Myers, P. C., Cruz-González, I., & Terebey, S. 1989, ApJ, 347, 461
Rodríguez, L. F., Moran, J. M., Franco-Hernández, R., et al. 2008, AJ, 135, 2370
Rodríguez, L. F., & Reipurth, B. 1998, RevMexAA, 34, 13
Rodríguez, L. F., Zapata, L. A., Dzib, S. A., et al. 2014, ApJL, 793, L21
Shang, H., Lizano, S., Glassgold, A., & Shu, F. 2004, ApJL, 612, L69
Shu, F. H., Najita, J. R., Shang, H., & Li, Z.-Y. 2000, Protostars and Planets IV, 789
Torrelles, J. M., Gómez, J. F., Rodríguez, L. F., et al. 1998, ApJ, 505, 756
Wilner, D. J., Reid, M. J., & Menten, K. M. 1999, ApJ, 513, 775

PoS(AASKA14)121

PROCEEDINGS OF SCIENCE

Complex organic molecules in protostellar environments in the SKA era

C. Codella[1], L. Podio*[1], F. Fontani[1], I. Jiménez-Serra[2], P. Caselli[3], C. Ceccarelli[4], M.E. Palumbo[5], A. López-Sepulcre[6,4], M.T. Beltrán[1], B. Lefloch[4], J.R. Brucato[1], S. Viti[7], L. Testi[2,1]

[1] *INAF, Osservatorio Astrofisico di Arcetri, Largo E. Fermi 5, 50125 Firenze (Italy);* [2] *ESO, Karl Schwarzschild srt. 2, 85748 Garching (Germany);* [3] *MPE, Giessenbachstr.1, 85748 Garching (Germany);* [4] *IPAG, UMR 5274, UJF-Grenoble 1/CNRS-INSU, 38041 Grenoble (France);* [5] *INAF, Osservatorio Astrofisico di Catania, via S. Sofia 78, 95123 Catania (Italy);* [6] *Department of Physics, The University of Tokyo, Bunkyo-ku, Tokyo 113-0033, Japan;* [7] *UCL, Gower Street, WC1E 6B London (UK)*

E-mail: codella@arcetri.astro.it

Molecular complexity builds up at each step of the Sun-like star formation process, starting from simple molecules and ending up in large polyatomic species. Complex organic molecules (COMs; such as methyl formate, $HCOOCH_3$, dymethyl ether, CH_3OCH_3, formamide, NH_2CHO, or glycoaldehyde, $HCOCH_2OH$) are formed in all the components of the star formation recipe (e.g. pre-stellar cores, hot-corinos, circumstellar disks, shocks induced by fast jets), due to ice grain mantle sublimation or sputtering as well as gas-phase reactions. Understanding in great detail the involved processes is likely the only way to predict the ultimate molecular complexity reached in the ISM, as the detection of large molecules is increasingly more difficult with the increase of the number of atoms constituting them.

Thanks to the recent spectacular progress of astronomical observations, due to the Herschel (sub-mm and IR), IRAM and SMA (mm and sub-mm), and NRAO (cm) telescopes, an enormous activity is being developed in the field of Astrochemistry, extending from astronomical observatories to chemical laboratories. We are involved in several observational projects providing unbiased spectral surveys (in the 80-300 and 500-2000 GHz ranges) with unprecedented sensitivity of templates of dense cores and protostars. Forests of COM lines have been detected. In this chapter we will focus on the chemistry of both cold prestellar cores and hot shocked regions, (i) reviewing results and open questions provided by mm–FIR observations, and (ii) showing the need of carrying on the observations of COMs at lower frequencies, where SKA will operate. We will also emphasize the importance of analysing the spectra by the light of the experimental studies performed by our team, who is investigating the chemical effects induced by ionising radiation bombarding astrophysically relevant ices.

Advancing Astrophysics with the Square Kilometre Array
June 8-13, 2014
Giardini Naxos, Italy

*Speaker.

PoS(AASKA14)123

1. The molecular complexity in a Sun-like forming system

The formation of Sun-like stars and the chemical complexity of the molecular gas involved in the process are sketched in Fig. 1, following Caselli & Ceccarelli (2012), and here summarised:

1. matter slowly accumulates toward the center of a molecular cloud. The central density increases while the temperature decreases, forming the so-called prestellar cores. Atoms and molecules in the gas phase freeze-out onto the cold surfaces of the dust grains, forming the grain mantles. Hydrogenation of atoms and molecules takes place, forming molecules such as water (H_2O), formaldehyde (H_2CO) and methanol (CH_3OH). In these regions the formation of new molecules in icy mantles is also caused by the effects of UV photons and low-energy cosmic rays. Indeed, the recent detection of CH_3CHO, CH_3OCH_3, CH_3OHO, and CH_2CO in the prestellar core L1689B (Bacmann et al. 2012) shows that COM synthesis has already started at the prestellar stage.

2. The collapse starts, the gravitational energy is converted into radiation and the envelope around the central object warms up. The molecules frozen on the mantles acquire mobility and form new, more complex species. When the temperature reaches about 100 K mantle sublimates, and we have the so called hot corinos ($\leq$ 0.01 pc) phase. Molecules in the mantles are injected in the gas, where they react and form new, more complex, molecules. The abundance of COMs (such as methyl formate, $HCOOCH_3$, or dymethyl ether, CH_3OCH_3) dramatically increases. A classical example is provided by IRAS16293-2422 (e.g. Cazaux et al. 2003; Ceccarelli et al. 2007; Bottinelli et al. 2007), where recently also glycoaldehyde ($HCOCH_2OH$), crucial molecules for the formation of metabolic molecules, has been detected (Jörgensen et al. 2012).

3. Simultaneously to the collapse, a newborn protostar generates a fast and well collimated jet, possibly surrounded by a wider angle wind. In turn, the ejected material drives shocks travelling through the surrounding high-density medium. Shocks heat the gas up to thousands of K and trigger several processes such as endothermic chemical reactions and ice grain mantle sublimation or sputtering. Several molecular species undergo significant enhancements in their abundances. The prototypical chemical rich shock is L1157-B1. Towards this source, not only relatively simple complex molecules, like methanol, have been detected (Bachiller et al. 2001), but also molecules considered hot corinos tracers, like methyl cyanide (CH_3CN), ethanol (C_2H_5OH), formic acid (HCOOH), and $HCOOCH_3$ (Arce et al. 2008). The emission of these species is concentrated in a small (around 1000 AU) region associated with the violent shocks at the head of the outflowing material (Codella et al. 2009). The presence of COMs in molecular outflows strongly suggests that these species were part of the sputtered icy mantles as the time elapsed since the shock is too short for any gas-phase route to build up COMs.

4. The envelope dissipates with time and eventually only a circumstellar disk remains, also called protoplanetary disk. In the hot regions, close to the central forming star, new complex molecules are synthesized by reactions between the species formed in the protostellar phase. In the cold regions of the disk, where the vast majority of matter resides, the molecules

PoS(AASKA14)123

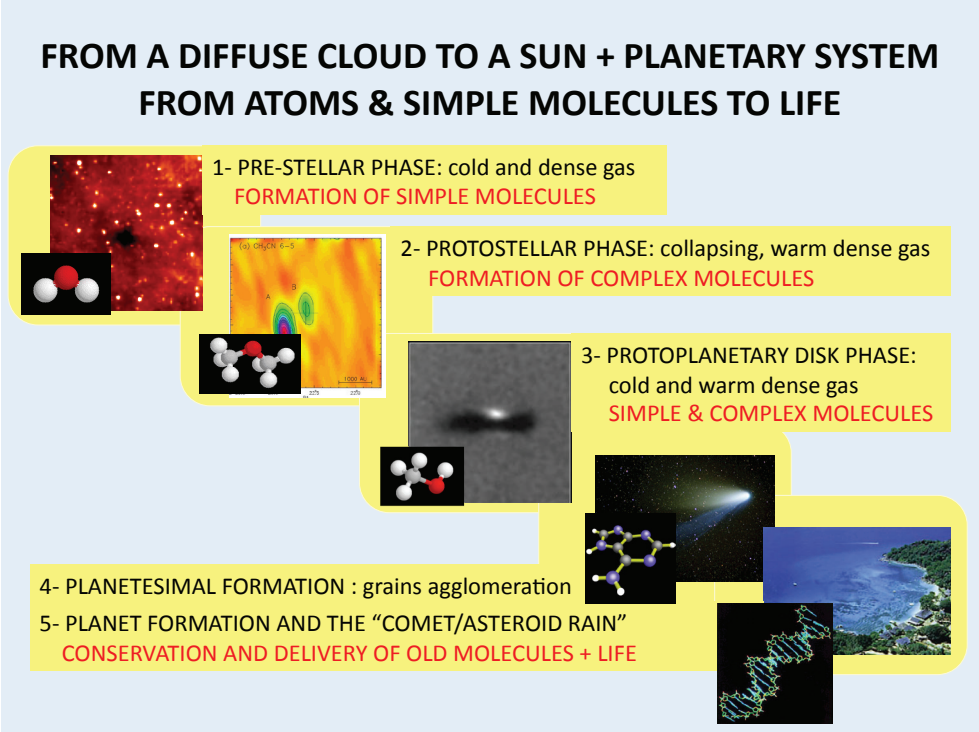

Figure 1: Star formation and chemical complexity (from Caselli & Ceccarelli 2012). The formation of a star and a planetary system, like the Solar System, passes through different phases, marked in the sketch.

formed in the protostellar phase freeze-out onto the grain mantles again. Dust grains then coagulate into larger planetesimals, the bricks of future planets, comets, and asteroids.

In this chapter, we focus on the earliest stages reviewing the importance of COMs in the prestellar cores as well as in the hot shocked regions produced by protostellar jets. Planetary disks will be discussed in a separate chapter (Testi et al. 2014).

2. The lessons provided by mm–FIR unbiased spectral surveys

In the last years several large programs started collecting unbiased spectral surveys with high frequency resolutions and unprecedented sensitivities of different targets considered among the typical laboratories of different stages of the low-mass star forming process (as e.g. prestellar cores, hot-corinos, protostellar shocks, more evolved Class I objects). One of the main goals is indeed the detection of complex and rare molecular species in the interstellar space through emission due to their ro-vibrational transitions. In particular, these efforts have been recently carried out in the 80–300 GHz range using the IRAM 30-m ground based observatory (ASAI: Astrochemical Surveys At IRAM; http://www.oan.es/asai) and between 500 GHz and 2000 GHz using the ESO Herschel Space Observatory (CHESS: Chemical HErschel Surveys of Star forming regions; http://www-laog.obs.ujf-grenoble.fr/heberges/chess/). The collected spectra are very rich in COMs, reflecting

PoS(AASKA14)123

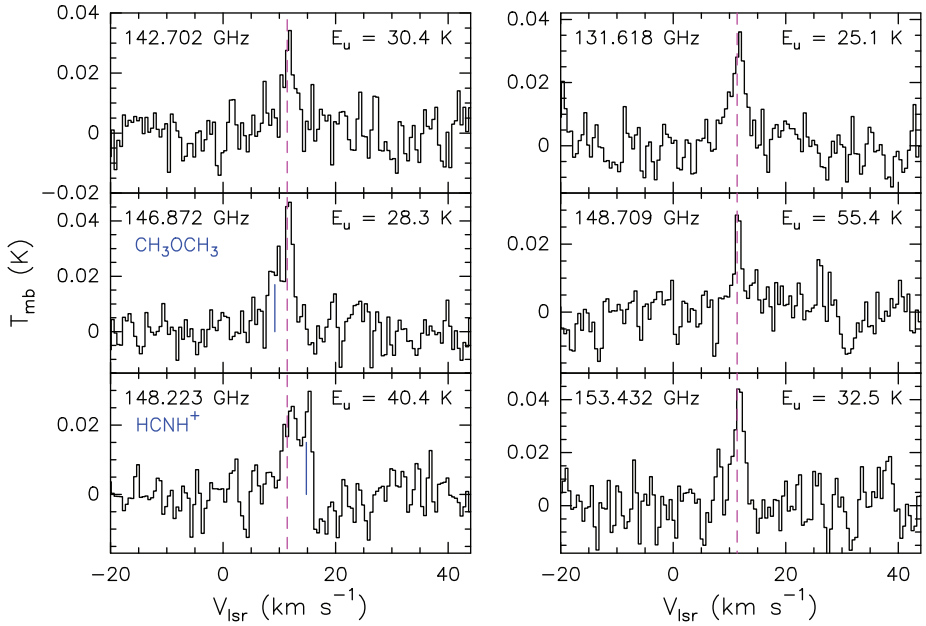

Figure 2: NH_2CHO lines detected at 2 mm in OMC-2 FIR4 with the IRAM 30-m antenna in the ASAI framework (from López-Sepulcre et al. 2014). The magenta dashed lines mark the systemic velocity of OMC-2 FIR4. The blue solid lines mark the position of blended lines.

the chemical complexity of all the components involved in the low-mass star formation, and, in the case of hot-corinos around protostars and jet-driven shocks amazing forest of lines are detected (e.g. Ceccarelli et al. 2010). The analysis of the large number of emission lines due to COMs is still in progress, but the preliminary results are very encouraging: for instance formamide (NH_2CHO), the simplest possible amide and a central molecule in the synthesis of metabolic and genetic molecules, has been revealed towards IRAS16293-2422, NGC1333-IRAS4A, SVS13A, OMC-2 FIR4, CephE, and the L1157-B1 shock (Kahane et al. 2013; Mendoza et al. 2014; López-Sepulcre et al. 2014, see Fig. 2).

A huge effort is carried out also using interferometers to provide high-spatial resolution images. The IRAM Plateau de Bure interferometer (PdBI) large program CALYPSO (Continuum and Lines from Young ProtoStellar Objects; http://irfu.cea.fr/Projects/Calypso) is providing the first sub-arcsecond statistical study, in the 80–300 GHz window, of the inner environments of the low-luminosity Class 0 sources. Also in this case spectacular forests of lines are observed, showing an amazing large number of lines at high excitation due to COMs such as ethylene glycol (*aGa*′–$(CH_2OH)_2$) and NH_2CHO. As an example, Fig. 3 shows the NGC1333–IRAS2A case (Maury et al. 2014): COM emission inside the protostellar envelope has been imaged, finding that it originates from a region of radius 40–100 AU, centered on the protostar. This spatial scale is consistent with the size of the inner envelope where $T_{\rm dust} \geq 100$ K is expected, supporting the hot-corino origin.

In conclusion, the synergy between spectral surveys using single-dishes and interferometric observations is of paramount importance to detect and analyse the COM emission. On the one hand, the unbiased spectral surveys provide the largest possible frequency range, and thus the most complete census of COMs; a multiline approach is also needed to safely identify the emission

PoS(AASKA14)123

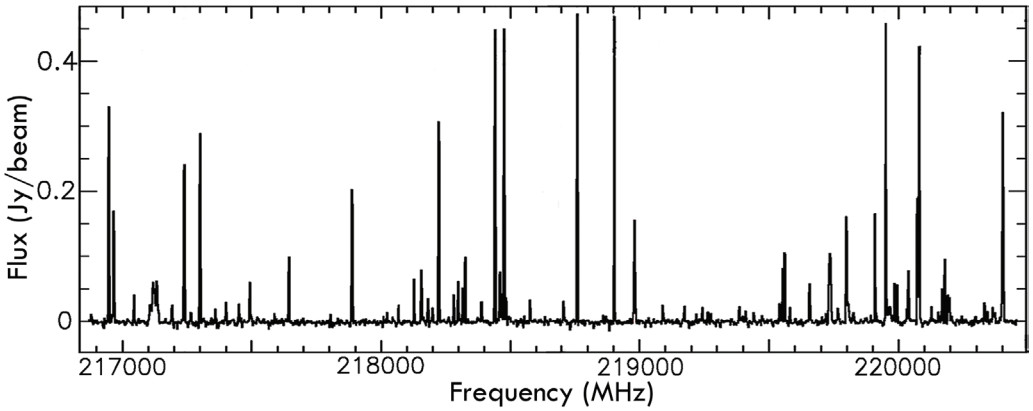

Figure 3: Continuum-subtracted PdBI spectrum around 218.5 GHz, at the position of the IRAS2A protostar (from Maury et al. 2014). Several COMs are detected, as e.g. CH_3OCH_3, CH_3OCHO, aGa'–$(CH_2OH)_2$, and NH_2CHO.

spectrum of complex species. On the other hand, interferometric images provide the size and morphology of the emitting regions, overcome the filling factor limitation of single-dish spectra, and allow one to propely derive physical conditions such as density, temperature, and abundance. In addition, the linewidths of COMs are typically reduced in interferometric observations, which allows a better identification of the molecular lines since it reduces line blending.

3. Cold cases: prestellar cores and very early protostars

3.1 Detectability of aminoacids in Solar-system precursors

The increasing performance of millimeter instrumentation in the past years has opened up the possibility to carry out high-sensitivity molecular line surveys even toward the earliest (and coldest) stages of low-mass star formation. These initial conditions are represented by cold dark cores and in particular, by pre-stellar cores, i.e. dense and cold condensations on the verge of gravitational collapse (central H_2 densities of some 10^4 cm^{-3} and temperatures $\leq$ 10 K; Caselli et al. 1999; Crapsi et al. 2007). These observations have shown that COMs (such as propylene - CH_2CHCH_3 - or acetaldehyde - CH_3CHO) are also present in the cold gas of these cores, unexpectedly revealing a high chemical complexity in these objects (see Marcelino et al. 2007 and Bacmann et al. 2012).

Among these complex organics, amino acids are of high interest in Astrochemistry and Astrobiology because of their role in the synthesis of proteins in living organisms. It is currently believed that their formation may have occurred in the interstellar medium (ISM) since amino acids, including glycine and alanine, have been found in meteorites (Pizzarello et al. 1991; Ehrenfreund et al. 2001; Glavin et al. 2006) and comets (as in Wild 2; Elsila et al 2009). This idea is supported by laboratory experiments which have shown that amino acids precursor are largely produced in UV-photon and ion-irradiated interstellar ice analogs (Munõz-Caro et al. 2002; Bernstein et al. 2002; Holtom et al. 2005). The detection of amino acids in the ISM is however challenging since their partition function is large and therefore, their emission is spread among many transitions. The detection of amino acids in the ISM remains to be reported.

PoS(AASKA14)123

Recently, it has been proposed that pre-stellar cores may be well suited for the detection of amino acids in the ISM (Jiménez-Serra et al. 2014). The gas temperatures in pre-stellar cores are $\leq$ 10 K, which yields a low level of line confusion since the number of molecular transitions excited at these temperatures is small. The linewidths of the molecular line emission in these cores are ≤ 0.5 km s^{-1}, which allows accurate identifications of the observed molecular lines because they suffer less from line blending. In addition, water vapour has recently been found toward the central few thousand AU of one pre-stellar core, L1544, which indicates that a small fraction of the ices ($\sim$ 0.5% of the total water abundance in the mantles) has been released into the gas phase (Caselli et al. 2012). These authors have proposed that water vapour in L1544 is produced by the partial photo-desorption of ices by secondary, cosmic ray induced UV-photons. Since COMs form in the outer layers of the mantles (Cuppen et al. 2009; Taquet et al. 2012), these molecules are also expected to be photo-desorbed together with water in pre-stellar cores, making these objects excellent candidates to test the detectability of amino acids in Solar-system precursors.

Simple radiative transfer calculations of glycine (NH_2CH_2COOH, i.e. the simplest amino acid) towards the L1544 pre-stellar core show that several glycine lines could reach detectable levels (peak line intensities $\geq$ 10 mK) in the frequency range between 60 and 80 GHz (Jiménez Serra et al. 2014). We have extrapolated these results to the frequency range covered by SKA1-MID Bands 4 and 5, where we evaluate whether glycine could be detected with this instrument (see Fig. 4). These calculations assume a solid abundance of glycine in ices of a few 10^{-4} with respect to water, similar to those synthesized in laboratory experiments of UV photon- and ion-irradiated interstellar ice analogs (Munõz-Caro et al. 2002; Bernstein et al. 2002; Holtom et al. 2005). This solid abundance translates into a maximum gas-phase abundance of glycine of $\sim 8\times10^{-11}$ after ice photo-desorption.

In Fig. 4, we report the predicted intensities of glycine for the L1544 core, assuming that the gas-phase abundance of glycine (of $\sim 8\times10^{-11}$) remains constant across the core. The velocity resolution used in the simulations is ~ 0.2 km s^{-1} and the expected linewidth of the glycine emission is ~ 0.3 km s^{-1}. The assumed source size is $\sim$ 12". Figure 4 shows that a few glycine lines could reach detectable levels with S/N ratios $\geq$ 3 in a total of $\sim$ 1000 hrs of integration time in SKA1-MID Band 5. For this integration time, a rms noise level of 50 microJy is indeed expected at a velocity resolution of 0.2 km s^{-1} within a 12"-beam (see the Level 0 Science Requirement SKA1-SCI-19). However, we stress that if the frequency coverage of SKA were extended to higher frequencies (e.g. up to 25 GHz, which would also allow to observe the NH_3(1,1) inversion lines at $\sim$ 23 GHz; see Fig. 4), this detection experiment could be performed in 10 times less time thanks to the presence of 3 times brighter glycine lines around $\sim$ 20 GHz (intensities $\geq$ 0.5 mJy beam^{-1}). In any case, a gas-phase abundance as low as $\sim 8\times10^{-11}$ would be the lowest abundance of glycine that could be detected with this experiment in SKA1-MID Band 5.

It is important to stress that Bands 1 and 2 of ALMA are currently unfunded, and therefore SKA may represent in the future the only instrument that could perform this kind of detection experiment for amino acids. We also note that although glycine shows a collection of transitions at millimetre wavelengths, observations at centimetre wavelengths with SKA1-MID Band 5 (8.8 to 13.8 GHz) are essential to provide reliable identifications of these lines due to the increasing frequency span between transitions at longer wavelengths (preventing line blending and line confusion). In addition, other complex organics such as the precursors of the glycine chemistry, e.g.

PoS(AASKA14)123

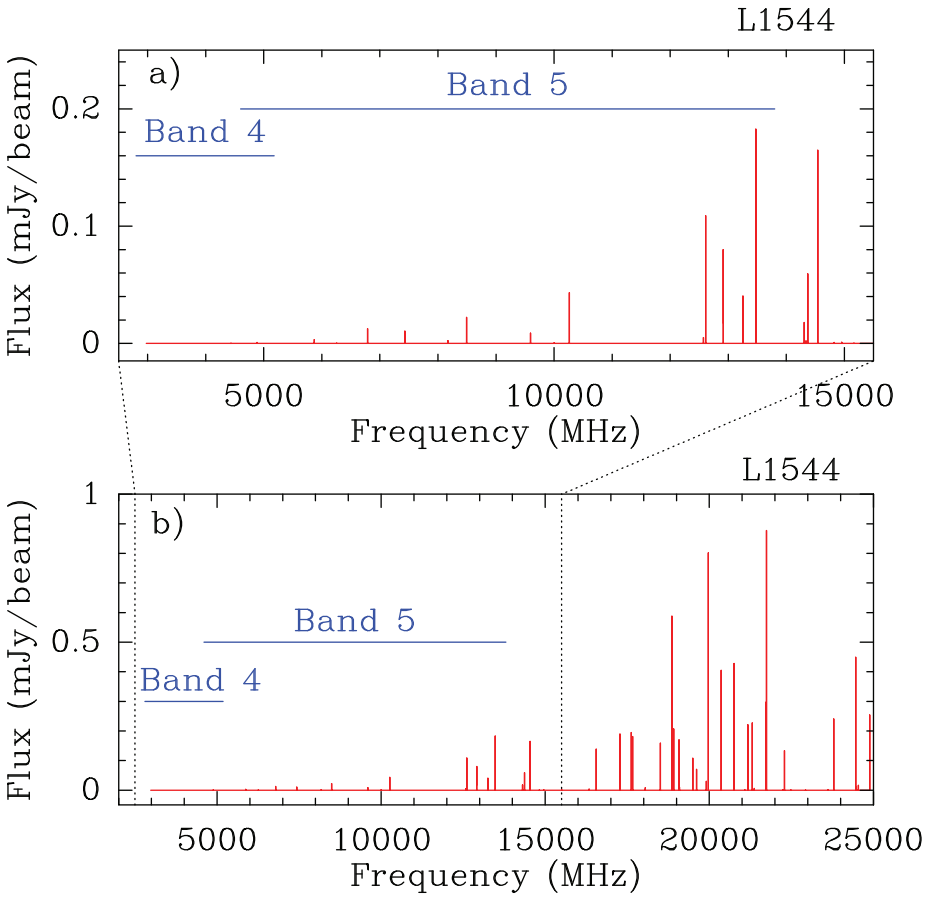

Figure 4: Upper panel: Simulations of the spectrum of glycine (conformer I) obtained for the frequency range between 2.5 GHz and 15.5 GHz, considering the physical structure of the L1544 pre-stellar core (Caselli et al. 2012), a solid glycine abundance of a few 10^{-4} with respect to water in ices, and LTE conditions. Horizontal blue lines indicate the frequency coverage of SKA1-MID Bands 4 and 5. Lower panel: LTE spectrum of glycine predicted for frequencies between 2.5 GHz and 25 GHz. The glycine lines around 20 GHz are factors of ∼3 brighter than those covered by SKA1-MID Band 5, which would allow the detection of this amino acid in 10 times less observing time.

amino acetonitrile or methyl formate, are expected to be factors of ∼100 more abundant than glycine (Belloche et al. 2008, 2013), and therefore they would be easier to detect with SKA1-MID Bands 4 and 5.

The detection of glycine, and of its precursors, in these Solar-system precursors will represent a major milestone in Astrochemistry and Astrobiology, providing a unique opportunity to link the pre-biotic chemistry in the ISM to their subsequent delivery onto planetary systems.

3.2 Deuterated COMs

There are no doubts that one of the most important chemical processes occuring in the cold ($T \leq 20$ K) and dense ($\geq 10^4$ cm^{-3}) pre–stellar cores is the freeze-out of atoms and molecules on the surface of dust grains, where the depletion of both C-bearing and N-bearing molecules is found to be high in low- and high-mass pre–stellar cores (e.g. Caselli et al. 1999, Friesen et al. 2010,

PoS(AASKA14)123

Fontani et al. 2012). Frozen on grain mantles, atoms and molecules can undergo hydrogenation, due to the high mobility of the light H atoms. In particular, from hydrogenation of CO (the most abundant neutral molecule after H_2) one forms sequentially HCO, H_2CO and CH_3OH, which is thus the species that is formed last. Moreover, the low temperature favours the deuteration of the species mentioned, because of the endothermicity of the chemical reactions which replace D atoms into their hydrogenated counterparts. Therefore, as time proceeds, the formation of methanol and its deuterated forms (CH_2DOH, CH_3OD, CHD_2OH, etc.) is boosted, until the energy released by the nascent protostellar object in the form of radiation increases the temperature of its environment, causing the evaporation of the grain mantles and the release of these molecules into the gas. As the temperature increases, the deuterated species are expected to get gradually destroyed due to the higher efficiency of the backward endothermic reactions (Caselli & Ceccarelli 2012). Therefore, high deuterated fractions of methanol, i.e. the ratio between the column density of the species containing D and that of CH_3OH, are expected to be powerful tracers of the short-living evolutionary stage in between the pre-stellar and the protostellar phase, at which the evaporation/sputtering of the grain mantles is efficient, and the warm gas-phase reactions have no time to change significantly the chemical composition of the gas.

Of course, testing these predictions is challenging because the deuterated forms of methanol are supposed to originate faint lines, which, at (sub-)millimeter wavelengths, can be easily overwhelmed by nearby stronger emission lines of lighter and more abundant molecules. Several transitions of CH_2DOH can be observed in the range 1–15 GHz as can be seen in Fig. 5. In this spectral window, the contamination of lines of more abundant molecules is expected to be negligible. The combination of high angular resolution and high sensitivity offered by SKA (see Sect. 7) will be eminently suitable to map these lines, which are expected to arise from very compact regions (sizes ≤ 3", e.g. Peng et al. 2012). As an example, we can estimate the time required to detected some of the lines shown in the synthetic spectrum in Fig. 5. The spectrum includes all transitions of CH_2DOH in the spectroscopic band $\sim 1-15$ GHz, as modeled by GILDAS–Weeds package (Maret et al. 2011) assuming the following parameters: $T_{\rm kin} = 20$ K, $N(CH_2DOH) = 5 \times 10^{15}$ cm^{-2}, source size = 1", line FWHM = 1 km s^{-1}. The column density assumed is a mean source-averaged value measured towards protostellar cores (e.g. Parise et al. 2006; Fontani et al. 2014b). Using the SKA1 Imaging Science Performance document (Braun R., 2014-06-02 version), at a rest frequency of 5 GHz, assuming $T_{\rm sys} = 20$ K, 190 dishes of 15 m, 2 polarisations, a velocity resolution of ~ 1 km s^{-1}, the 1σ rms noise in the spectrum after 50 hrs of integration on source is 0.077 mJy. Figure 5 tells us that several lines have intensity peak well above 3σ. Therefore, this will allow us not only to just detect the presence of the molecule, but also to derive estimates of some important physical parameters (e.g. rotation temperature and column density from the rotation diagrams).

Moreover, other deuterated species of complex molecules (CH_2DCCH, $HDNCH_2CN$, etc.) possess lines in the same frequency range. If detected, these species will put other relevant constraints on chemical models, in an effort to reach a general knowledge of the deuteration mechanism(s) during the earliest phases of the star formation process.

4. Hot protostellar shocks versus hot-corinos

The L1157 region at 250 pc hosts a Class 0 protostar (L1157-mm) driving a spectacular chem-

PoS(AASKA14)123

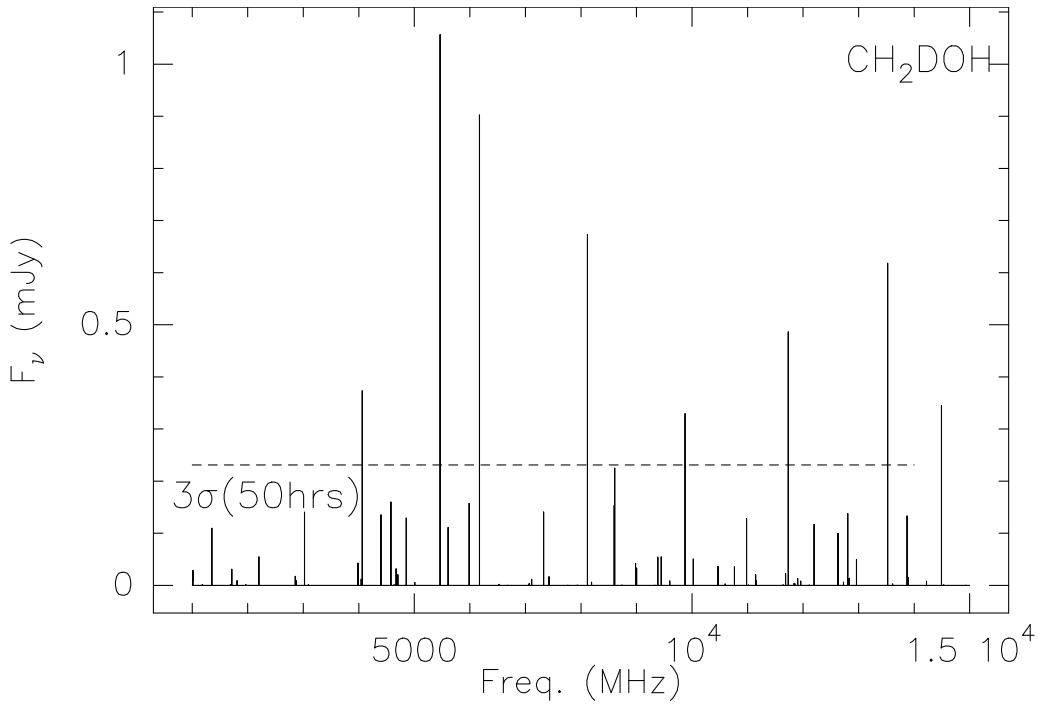

Figure 5: Synthetic spectrum of CH_2DOH modeled for SKA1-MID with GILDAS–Weeds package (Maret et al. 2011) in the range $\sim$ 1–15 GHz, assuming LTE conditions, $T_{\rm kin} = 20$ K, $N(CH_2DOH) = 5 \times 10^{15}$ cm^{-2}, source size = 1", and line FWHM = 1 km s^{-1}. The dashed line represents the expected 3σ level in the spectrum that can be achieved after 50 hours of integration on source (see text for details).

ically rich bipolar outflow (Bachiller et al. 2001). The southern lobe is associated with two cavities seen in the IR H_2 and CO lines (e.g. Neufeld et al. 2009; Gueth et al. 1996), likely created by episodic events in a precessing jet. Located at the apex of the more recent cavity, the bright bow shock called B1 has a kinematical age of 2000 years. The bow shocks, when mapped with the IRAM PdB and VLA interferometers, reveal a clumpy structure, with clumps located at the wall of the cavity (e.g. Tafalla & Bachiller 1995; Codella et al. 2009), and well traced by typical products of both grain mantle sputtering (such as NH_3, CH_3OH, and H_2CO) and refractory core disruption (SiO). Thus, the young L1157-B1 shock offers an exceptional opportunity to investigate in details the chemical composition of the grain ice mantles as well as how the gas phase is chemically enriched after the shock occurrence.

Thanks to PdBI observations (see Fig. 6), three COMs have been so far imaged in L1157-B1: CH_3OH, acetaldehyde (CH_3CHO), and CH_3CN (Benedettini et al. 2007, 2013; Codella et al. 2009, 2014). The CH_3CN image shows a clumpy structure superimposed to the classical B1 arch-like shape, displaying a unique continuous structure tracing the propagation of a large bow shock. In principle, CH_3CN could form on the surface of grains and then injected in the gas phase due to shock sputtering. Alternatively, CH_3CN may belong to the so-called second generation species, i.e. the molecules formed in the warm gas-phase chemically enriched after the mantle release (see e.g. Bottinelli et al. 2007; Bisschop et al. 2008). Both scenarios need an increase of temperature, as in the L1157-B1 case (up to about 10^3 K, Busquet et al. 2013). The CH_3CN-to-CH_3OH ratio is $\simeq 10^{-4}$–10^{-3}, i.e. smaller with respect to those found in hot-corinos (10^{-2}–10^{-1}). This difference

PoS(AASKA14)123

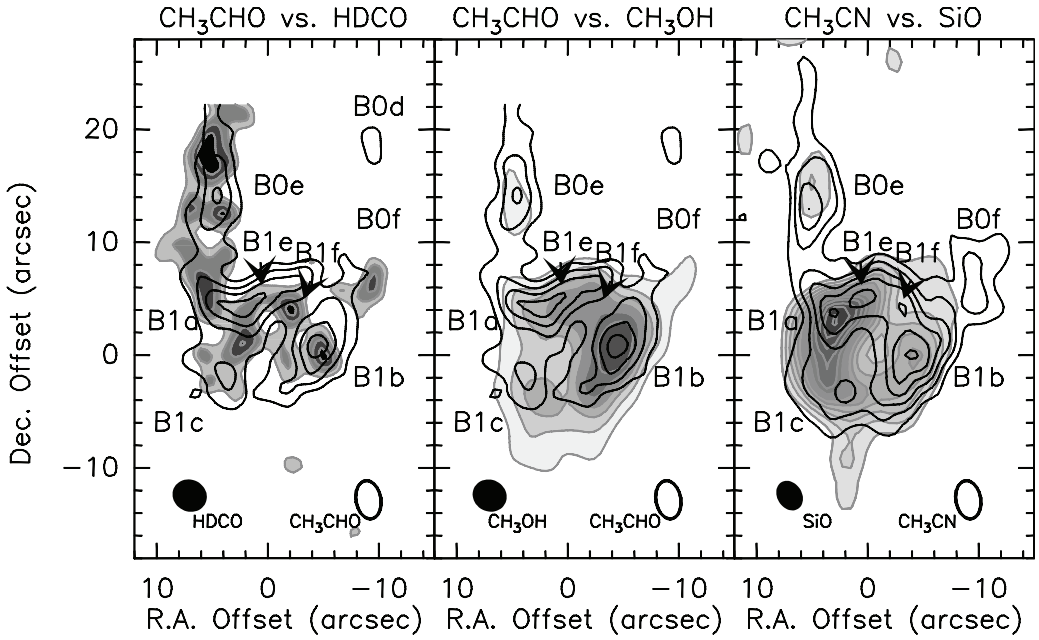

Figure 6: Chemical differentiation in L1157-B1: the maps are centred at $\Delta\alpha$ = +21^o and $\Delta\delta$ = –64^o from the driving protostar L1157-mm. Overlay of the integrated intensity IRAM PdBI map at 2 mm of the $CH_3CHO(7_{0,7}–6_{0,6})$AE (contours, from Codella et al. 2014) on the $HDCO(2_{1,1}–1_{0,1})$ (left panel, from Fontani et al. 2014a) and $CH_3OH(3_K–2_K)$ emission (middle panel; from Benedettini et al. 2013). Righ panel compares the $CH_3CN(8_K–7_K)$ and SiO(2–1) spatial distributions (Gueth et al. 1998, Codella et al. 2009). Labels are for the different L1157-B1 molecular clumps well imaged in the CH_3CN map. The synthesised beams are shown in the bottom part of the panels.

suggests that a significant amount of CH_3CN may form in the gas phase and that in L1157-B1 the CH_3CN abundance has not yet reached its maximum, given the young age of the shock.

Recently, also CH_3CHO has been mapped at PdBI (Codella et al. 2014), and also in this case there is a good agreement with the CH_3OH (and CH_3CN) spatial distribution, confirming COMs are emitting where mantles have been recently sputtered. This is further indicated by the excellent spatial correpondance with HDCO emission (Fontani et al. 2014a) tracing deuterated formaldehyde formed on grains and then injected in the shocked gas. For acetaldehyde, the abundance ratio with respect to methanol is quite high ($\sim 10^{-2}$) and in any case similar to that observed towards a typical hot-corino such as IRAS16293-2422 (Bisschop et al. 2008). These findings support for CH_3CHO either a direct formation on grain mantles or a quick ($\leq$ 2000 yr) formation in a chemically enriched gas phase.

These first results show the importance of studying shocked regions as laboratories where (i) to investigate the COMs formation routes and (ii) to verify whether the study of hot-corinos chemistry can be affected by COM emission arising from shocked envelope material at the base of the inner (unresolved) jet. Interferometric observations are instructive to minimise beam dilution effects. In addition, the multiline approach is needed to carefully sample the excitation conditions and correctly derive the abundances of COMs. In particular, the 1–15 GHz frequency range allows one to well sample low-excitation ($E_u \leq 20$ K) and bright ($S\mu^2 \geq 1$ D^2) emissions due to COMs (see Sect. 7).

PoS(AASKA14)123

5. The SKA case for high-mass star formation

While the detection and study of COMs in low-mass star forming regions has a clear impact on our understaning of the origin of life, we should underline that COMs in massive star forming regions have recently proved to be ideal tracers of the physical conditions of the very central compact core where the massive star forms. In this subsection we therefore briefly make a case for why SKA is the ideal instrument to study COMS in high-mass star forming regions. The earliest stages of the massive star formation are characterised by the occurrence of the so called hot cores, i.e. hot ($\geq$ 100 K), small ($\leq$ 0.1 pc), and massive (up to thousands of solar masses) clumps warmed by the stellar radiation. In fact, the largest body of detections of COMs comes from observations of hot cores. In the standard paradigm, at densities as high as those of hot cores, gases freeze onto the surface of dust grains in the cold quiescent phase of the molecular cloud. This material is processed to greater molecular complexity via a number of possible surface reactions, perhaps catalyzed by UV, cosmic rays or thermal effects, and is subsequently released back into the gas phase as a result of thermal sublimation due to the heating effect of the newly-formed star. The rich chemistry, comprising of species such as ethyl cyanide, glycoaldehyde and its isomers (e.g. Beltrán et al. 2009, Fuente et al. 2014, Calcutt et al. 2014, and references therein), that results from this sublimation, thus potentially provide powerful diagnostics of the physical and chemical history of the very central core where the star is born. Interestingly, and somewhat surprisingly, hot cores differ from hot corinos not only for the larger sizes, but also chemically: when normalized to methanol or formaldehyde, hot cores have typically one order of magnitude less abundant COMs (such as $HCOOCH_3$ or CH_3OCH_3) than hot corinos (e.g. Herbst and van Dishoeck 2009). Such differences are likely due to various factors, such as the composition of the sublimated ices, governed by the past prestellar history. COMs in hot cores are even more of a powerful star formation diagnostics because they are excellent tracers of the very central (often not spatially resolved) part of the core, where the protostar is born; their detection is therefore a confirmation of the high density warm cores and, most importantly, their emission is so compact that they must trace the most central region of the hot core, close to the YSOs. Clearly interferometric observations are essential in order to resolve such small scale structures.

Despite tracing such a small extent of gas, it is found (e.g. Calcutt et al. 2014) that there are significant variations in abundances and abundance ratios across COMs, making these species also excellent tracers of chemical and physical differentiation across the different classes of objects. Of particular interest in the study of COMs are the three isomers of $C_2H_4O_2$, all of which have now been detected in star-forming regions. Acetic acid and glycolaldehyde are particularly interesting due to their significant prebiotic significance, since the former is linked to the formation of ribose and the latter is only an amine group (NH_2) away from glycine, the simplest amino acid. However, so far the identification and characerization of COMs in hot cores have been hampered by the incredibly high number of lines in the sub-millimeter spectra: the latter suffer from strong line confusion due to (i) the richness of the spectrum: the higher the gas density and temperature, the more crowded the spectra will be; (ii) blending due to also the large linewidths, and (iii) uncertainties in the laboratory rest frequencies as well as in the observations. These issues lead, in some cases, to only tentative detections and contribute to the scarcity of observed transitions and number of objects.

PoS(AASKA14)123

The SKA frequency range offers a unique opportunity to identify and study a large number of COMs in high mass star forming regions: the frequency range covered is clear of contamination because the low energy of smaller molecules fall at higher frequencies, hence line confusion is minimized. Interferometric observations are very useful in hot cores since they filter out much of the extended envelope and therefore the linewidths of COMs can be significantly reduced allowing a better identification of the lines. Also, COMs are characerized by the fact that their level population covers many energy levels because of their large partition functions and hence several of their transitions fall in the SKA range from 4 GHz to $\sim$ 25 GHz. As an example, within the 4 GHz limit, there are tens of glycolaldehyde and ethylene glycol transitions covering rotational transitions from J as low as 1 (for ethylene glycol) and 4 (for glycolaldehyde) up to $J = 30$. Clearly, by removing the problem of line confusing and simultaneously observing a large number of transitions for each COM we will be able to accurately derive column densities, and hence, with the aid of state of the art chemical and radiative transfer modelling, determine the physical conditions of the most compact cores in high-mass star forming regions. The combination of all these requirements are only met by the SKA.

6. The need of laboratory experiments

In dense molecular clouds ($n > 10^4$ cm^{-3}) gas phase species condense on silicatic and carbonaceous grains giving rise to icy mantles. These mantles are made of molecules which directly freeze out from the gas phase (such as CO) and molecules which are formed after grain surface reactions (such as H_2O). The presence of icy grain mantles is indirectly deduced from depletion of gas phase species and is observed in the infrared from absorption features attributed to vibrational modes of solid phase molecules superposed to the background stellar spectrum. Ices have been observed in star forming regions (both low- and high-mass young stellar objects) as well as in quiescent dense clouds. It is widely accepted that icy grain mantles are continuously processed by low-energy cosmic rays, electrons, and UV photons.

Ten different molecular species have been firmly identified in interstellar icy grain mantles (e.g. Gibb et al. 2004). In particular, water (H_2O), carbon monoxide (CO), carbon dioxide (CO_2), methanol (CH_3OH), methane (CH_4), carbonyl sulphide (OCS), formaldehyde (H_2CO), formic acid (HCOOH), cyanate ion (OCN^-) and ammonia (NH_3).

Most of the knowledge on the physical and chemical properties of ices is based on the comparison between observations and laboratory experiments performed at low temperature (10-80 K). Laboratory infrared spectra of icy samples show that the profile of absorption bands depends on different parameters such as the other molecules each species is mixed with and the temperature (e.g. Sandford et al. 1988; Ehrenfreund et al. 1999; Palumbo & Baratta 2000; Öberg et al. 2007). The properties of icy samples also depend on processing by fast ions, electrons, and UV photons (e.g. Grim & Greenberg 1987; Palumbo & Strazzulla 1993; Hudson et al. 2001; Strazzulla et al. 2001; Baratta et al. 2002; Bennet et al. 2007; Öberg et al. 2009; Islam et al. 2014). Energetic ions (keV-MeV) passing through molecular solids release energy to the target along the ion track. As a consequence molecular bonds are broken and radicals and molecular fragments recombine giving rise to molecular species not present in the original sample. Furthermore the structure and morphology of the sample is also modified (e.g. Palumbo 2006; Raut et al. 2001). In the case

PoS(AASKA14)123

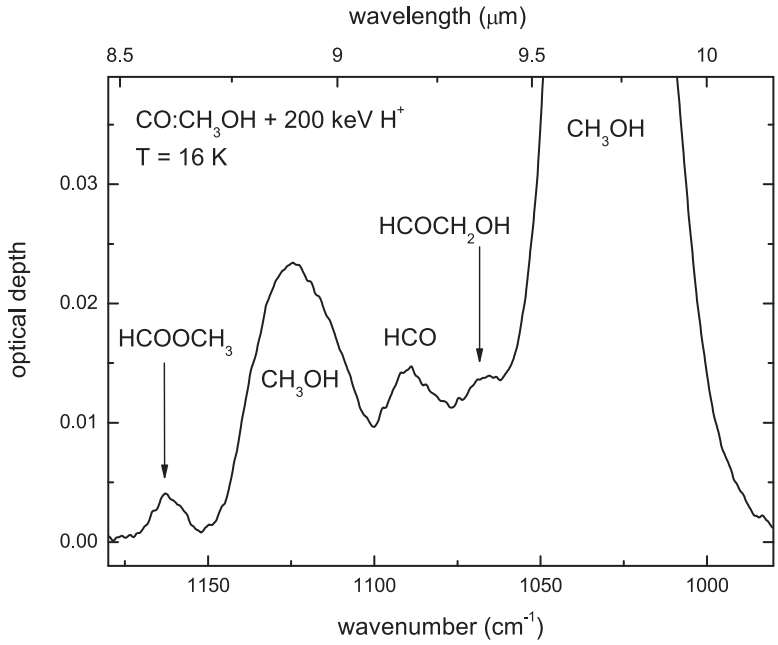

Figure 7: Infrared transmission spectrum (from Modica & Palumbo 2010), in optical depth scale, of a mixture $CO:CH_3OH$ bombarded with 200 keV protons at 16 K. Labels indicate absorption bands due to pristine methanol and bands due to species formed after energetic processing.

of UV photolysis the energy is released to the target material through single photo-dissociation or ionization events per incoming photon. Thus after ion bombardment and UV photolysis the chemical composition and the structure of the sample is modified. Both more volatile and less volatile species are formed and if C-bearing species are present in the original sample a refractory residue is left over after warm-up at room temperature (e.g. Moore et al. 1983; Foti et al. 1984; Palumbo et al. 2004).

In the past 35 years several experiments have been performed to study the effects of ion bombardment and UV photolysis on the chemical composition of icy samples. As an example, laboratory experiments have shown that after energetic processing of methanol the column density of pristine methanol decreases and new bands appear in the infrared spectra indicating the formation of other, also complex, molecules. Species clearly identified are carbon monoxide (CO), carbon dioxide (CO_2), methane (CH_4), formyl radical (HCO), formaldehyde (H_2CO), ethylene glycol ($C_2H_4(OH)_2$), methyl formate ($HCOOCH_3$), and glycolaldehyde ($HCOCH_2OH$) (e.g. Moore et al. 1996; Palumbo et al. 1999, Hudson & Moore 2000; Bennett et al. 2007; Öberg et al. 2009; Modica & Palumbo 2010). Figure 7 shows the infrared spectrum in the 1180-980 cm^{-1} (8.47-10.20 μm) range of a mixture $CO:CH_3OH$ bombarded with 200 keV protons at 16 K (Modica & Palumbo 2010).

Recently, Compagnini et al. (2009) and Puglisi et al. (2014) have shown, by infrared and Raman spectroscopy, that polyynes ($-(C{\equiv}C)_n-$) and polycumulenes ($=(C{=}C)_n=$) are formed after ion

PoS(AASKA14)123

bombardment of acetylene (C_2H_2), ethylene (C_2H_4), ethane (C_2H_6), and benzene (C_6H_6). Jones & Kaiser (2013) have studied the effects of electron irradiation of pure CH_4 by reflectron time-of-flight mass spectrometry and have found that high-molecular-weight hydrocarbons of up to C_{22}, among them alkanes, alkenes and alkynes, are formed. Other experiments (e.g. Kobayashi et al. 1995; Munõz-Caro et al. 2002; Bernstein et al. 2002; Holtom et al. 2005) have shown, by high performance liquid chromatography, that amino acid precursors are present in the residue formed after energetic processing of simple ice mixtures.

Based on these experimental results it has been suggested that icy grain mantles are constituted not only by the molecular species that have been firmly identified but also by other, more complex, molecules which cannot be detected in the solid phase by IR spectroscopy. These species are expected to enrich the gas phase composition after desorption of icy grain mantles (e.g. Palumbo et al. 2008; Modica & Palumbo 2010) and could be incorporated in planetesimals and comets.

Finally, these results support the experimental effort (e.g. Allodi et al. 2013) to use more sensitive techniques to evidence the formation of complex molecules and/or fragments that could be of primary relevance for Astrobiology also to understand which species should be searched for, by ground-based or space-born facilities, in protostellar environments, protoplanetary disks and in the atmospheres of extrasolar planets and moons.

7. Why SKA?

The numerous detections of high-excitation COM lines in the mm-window call for observations at lower wavelengths, where heavy species are expected to emit (JPL, http://spec.jpl.nasa.gov, and CDMS, http://www.astro.uni-koeln.de/cdms). Even more important, the millimeter frequency bands are often so full of lines that it is paradoxically difficult to identify species through a large number of emission lines simply due to confusion. On the other hand, this low frequency band is relatively clear, given that low energy transitions of light molecules fall at much higher frequencies. The completion of the results obtained at mm-wavelengths with spectral surveys in the cm-window will allow one to have the possibility to have, for different species, a large number of transitions, which is needed to reliably detect the largest COMs for which the population is distributed over many energy states, having large partition functions. Figure 8 shows as an example the simulation of the $HCOOCH_3$ and $HCOCH_2OH$ spectrum as expected for SKA1-MID modeled with GILDAS-Weeds (Maret et al. 2011) in the range $\sim 1-15$ GHz, assuming LTE conditions and physical parameters expected in hot-corinos (see e.g. Jörgensen et al. 2012). In particular, if we consider bright lines ($S\mu^2 \geq 1$ D^2) at low excitation ($E_u \leq 20$ K), then the 1-15 GHz band contains a considerable number of COMs transitions. As an example the line densities for bright, low-excitation transitions of methyl formate and glycoaldehyde in the 1–15 GHz range is ~ 1 line/GHz, ten times higher than in the 80–300 GHz spectral window.

An instructive view is given by the NRAO 100-m GBT PRIMOS Legacy Project, which recorded the spectrum from 300 MHz to 46 GHz towards the Sgr B2(N) molecular cloud. The PRIMOS data have resulted in numerous new detections in astrochemistry (e.g. Loomis et al. 2013, and references therein). The COM emission is expected to come from regions at sub-arcsec scale (hot corinos, jets, shocks). SKA1 with band 5 operating at 5-14 GHz will reach $\sim$35 mas resolution. Therefore, the spatial resolutions offered by SKA are fundamental to re-

PoS(AASKA14)123

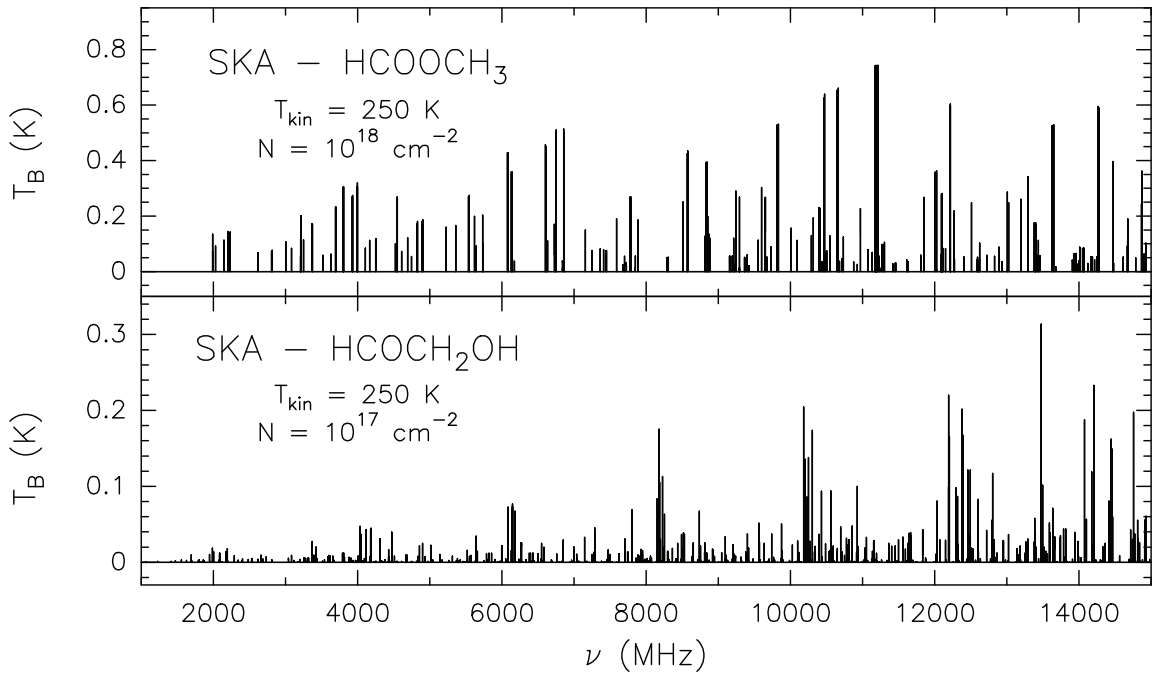

Figure 8: Simulations of the spectrum of $HCOOCH_3$ and $HCOCH_2OH$ as observed by SKA1-MID modeled with GILDAS-Weeds (Maret et al. 2011) in the range $\sim$ 1–15 GHz, assuming LTE conditions and physical parameters expected for methyl formate and glycolaldehyde in hot-corinos (see e.g. Jörgensen et al. 2012): $T_{\rm kin} = 250$ K, $N(HCOOCH_3) = 10^{18}$ cm^{-2}, $N(HCOCH_2OH) = 10^{17}$ cm^{-2}, source size = 1", and line FWHM = 4 km s^{-1}.

solve and image the emitting region. As a comparison, the NRAO VLA interferometer, with 36 km maximum baseline, obtains a synthetisized beam between 130 mas (15 GHz) and 2" (1 GHz) (https://science.nrao.edu/facilities/vla/docs/manuals/oss). In this way, (i) we will have bright line emission, and (ii) we will correctly evaluate COMs' abundances. In addition, the sensitivity achieved by SKA for larger beam sizes will be unbeatable, offering the possibility to detect the emission from glycine and other amino acids in pre-stellar cores, where their emission is expected to be relatively extended (around tens of arcseconds). To conclude, SKA offers a unique combination of spatial resolution and high sensitivity to produce a complete inventory of known interstellar species accessible in the centimeter wavelength range that can be used to put severe constrains on the physical conditions of the emitting gas, as well as on COMs abundances.

This work was partly supported by the Italian Ministero dell'Istruzione, Università e Ricerca (MIUR) through the grant *Progetti Premiali 2012 - iALMA*.

REFERENCES

Allodi, M.A., Baragiola, R.A., Baratta, G.A., et al. 2013, Space Science Reviews 180, 101
Baratta, G.A., Leto, G., Palumbo, M.E. 2002, A&A 384, 343
Bennett, C.J., Chen, S.-H., Sun, B.-J., Chang, A.H.H., Kaiser, R. 2007, ApJ 660, 1588
Arce, H.G., Santiago-García, J., Jörgensen, J.K., Tafalla, M., Bachiller, R. 2008, A&A 681, L21

PoS(AASKA14)123

Bachiller, R., Pérez Gutiérrez, M., Kumar, M.S.N., Tafalla, M. 2001, A&A 372, 899
Bacmann, A., Taquet, V., Faure, A., Kahane, C., Ceccarelli, C. 2012, A&A 541, L12
Belloche, A., Müller, H.S.P., Menten, K.M., Schilke, P., Comito, C. 2013, A&A 559A, 47B
Belloche, A., Menten, K.M., Comito, C., et al. 2008, A&A 482, 179
Beltrán, M.T., Codella, C., Viti, S., Neri, R., Cesaroni, R. 2009, ApJ, L93
Benedettini, M., Viti S., Codella, C., et al. 2007, MNRAS 381, 1127
Benedettini, M., Busquet, B., Lefloch, B., et al. 2012, A&A 539, L3
Bernstein, M.P., Dworkin, J.P., Sandford, S.A., Cooper, G.W., Allamandola, L.J. 2002, Nature 416, 401
Bisschop, S.E., Jörgensen, J.K., Bourke, T.L., Bottinelli, S., van Dishoeck, E.F. 2008, A&A 488, 959
Bottinelli, S., Ceccarelli, C., Williams, J.P., Lefloch, B. 2007, A&A 463, 601
Busquet, B., Lefloch, B., Benedettini, M., et al. 2014, A&A 561, 120
Calcutt H., Viti S., Codella C., et al. 2014, MNRAS, in press
Caselli P., Ceccarelli C., 2012 The Astronomy and Astrophysics Review, 20, 56
Caselli, P., Walmsley, C.M., Tafalla, M., Dore, L., Myers, P.C. 1999, ApJ 523, L165
Caselli, P., Keto, E., Bergin, E.A., et al. 2012, ApJ 759, L37
Caselli, P., Walmsley, C.M., Tafalla, M., Dore, L., Myers, P.C. 1999, ApJL, 523, L165
Cazaux, S., Tielens, A.G.G.M., Ceccarelli C., et al. 2003, ApJ 593, L51
Ceccarelli, C., Caselli, P., Herbst, E., Tielens, A.G.G.M., Caux, E. 2007 Protostars and Planets V, University of Arizona Press, Tucson, 47
Ceccarelli, C., Bacmann, A., Boogert, A., et al. 2010, A&A 521, L22 Protostars and Planets V, University of Arizona Press, Tucson, 197
Codella, C., Benedettini, M., Beltrán, M.T., et al. 2009, A&A 507, L25
Codella, C., Fontani, F., Ceccarelli, C., et al. 2014, ApJL, submitted
Compagnini, G., D'Urso, L., Puglisi, O., Baratta, G. A., Strazzulla, G. 2009, Carbon 47, 1605
Crapsi, A., Caselli, P., Walmsley, C.M., Tafalla, M. 2007, A&A 470, 221
Cuppen, H.M., van Dishoeck, E.F., Herbst, E., Tielens, A.G.G.M. 2009, A&A 508, 275
Ehrenfreund, P., Kerkhof, O., Schutte, W.A. et al. 1999, A&A 350, 240
Ehrenfreund, P., Glavin, D.P., Botta, O., Cooper, G., Bada, J.L. 2001, PNAS 98, 2138
Elsila, J.E., Glavin, D.P., Dworkin, J.P. 2009, M&PS 44, 1323
Fontani, F., Palau, A., Caselli, P., et al. 2011, A&A 529, L11
Fontani, F., Giannetti, A., Beltrán, M.T., et al. 2012, MNRAS 423, 2342
Fontani, F., Codella, C., Ceccarelli, C., Lefloch, B., Viti, S., Benedettini, M. 2014a, ApJ 788, L43
Fontani, F., Busquet, G., Palau, A., et al. 2014b, A&A, in press
Foti, G., Calcagno, L., Sheng, K.L., Strazzulla, G. 1984, Nature 310, 126
Friesen, R.K., Di Francesco, J., Shimajiri, Y., Takakuwa, S. 2010, ApJ 708, 1002
Fuente A., Cernicharo J., Caselli P., et al. 2014, A&A 568, 65
Gibb, E.L., Whittet, D.C.B., Boogert, A.C.A., Tielens, A.G.G.M. 2004, ApJS 151, 35
Glavin, D.P., Dworkin, J.P., Aubrey, A., et al. 2006, M&PS 41, 889
Grim, R.J.A., & Greenberg, J.M. 1987, ApJ 321, L91
Gueth F., Guilloteau S., & Bachiller R. 1996, A&A 307, 891
Gueth F., Guilloteau S., & Bachiller R. 1998, A&A 333, 287

PoS(AASKA14)123

Herbst, E., van Dishoeck, E.F. 2009, ARA&A 47, 427
Holtom, P.D., Bennett, C.J., Osamura, Y., Mason, N.J., Kaiser, R.I. 2005, ApJ 626, 940
Hudson, R.J., & Moore, M.H. 2000, Icarus 145, 661
Hudson, R.L., Moore, M.H., Gerakines, P.A. 2001, ApJ 550, 1140
Islam, F., Baratta, G.A., Palumbo, M.E. 2014, A&A 561, A73
Jiménez-Serra, I., Testi, L., Caselli, P., Viti, S. 2014, ApJ 787, L83
Jones, B.M., & Kaiser R.I. 2013, J. Phys. Chem. Lett. 4, 1965
Jörgensen, J.K., Favre, C. Bisschop, S.E., Bourke, T.L., van Dishoeck, E.F., Schmalzl, M. 2012, ApJ 757, L4
Kahane, C., Ceccarelli C., Faure, A., Caux, E. 2013, ApJ 763, L38
Kobayashi, K., Kasamatsu, T., Kaneko, T., et al. 1995, Adv. Space Res. 16, 21
Kurtz, S., Cesaroni, R., Churchwell, E., Hofner, P., Walmsley, C.M. 2000 Protostars and Planets IV, University of Arizona Press, Tucson, 299
Loomis, R.A., Zaleski, D.P.; Steber, A.L., et al. 2013, ApJ 765, L9
López-Sepulcre, A., Mendoza, E., Lefloch, B., et al. 2014, MNRAS, submitted
Marcelino, N., Cernicharo, J.; Agúndez, M., et al. 2007, ApJ 665, L127
Maret S., Hily-Blant P., Pety J., et al., A&A 526, A47
Maury, A.J., Belloche, A., André, Ph., et al. 2014, A&A 563, L2
Mendoza, E., Lefloch, B., López-Sepulcre, A., et al. 2014, MNRAS 445, 151
Modica, P., Palumbo, M. E., 2010, A&A 519, 22
Moore, M.H., Donn, B., Khanna, R., & A'Hearn, M. 1983, Icarus, 54, 388
Moore, M. H., Ferrante, R. F., Nuth J. A. 1996, Planetary and Space Science, 44, 927
Muñoz Caro, G.M., Meierhenrich, U.J.; Schutte, W.A., et al. 2002, Nature 416, 403
Neufeld, D.A., Nisini, B., Giannini, T., et al. 2009, ApJ 706, 170
Öberg, K.I., Fraser, H.J., Boogert, A.C.A., et al. 2007, A&A, 462, 1187
Öberg, K.I., Garrod, R.T., van Dishoeck, E.F., Linnartz, H., 2009, A&A 504, 891
Palumbo, M.E., & Strazzulla, G. 1993, A&A 269, 568
Palumbo, M.E., Castorina, A.C., Strazzulla, G. 1999, A&A 342, 551
Palumbo, M.E., & Baratta, G.A. 2000, A&A 361, 298
Palumbo, M.E., Ferini, G., Baratta, G.A. 2004, Advances in Space Research 33, 49
Palumbo, M.E. 2006, A&A 453, 903
Palumbo, M.E., Leto, P., Siringo, C., Trigilio, C. 2008, ApJ 685, 1033
Parise, B., Castets, A., Herbst, E., et al. 2004, A&A 416, 159
Parise, B., Ceccarelli, C., Tielens, A.G.G.M., et al. 2006, A&A 453, 949
Peng, T.-C., Despois, D., Brouillet, N., Parise, B., Baudry, A. 2012, A&A 543, 152
Pizzarello, S., Krishnamurthy, R.V., Epstein, S., Cronin, J.R. 1991, GeCoA 55, 905
Puglisi, O., Compagnini, G., D'Urso, L., Baratta, G.A., Palumbo, M.E., Strazzulla, G. 2014, Nucl. Instr. Meth. B. 326, 2
Raut, U., Teolis, B.D., Loeffler, M.J., Vidal, R.A., Famá, M., Baragiola, R.A. 2007, J. Chem. Phys. 126, 244511
Sandford, S.A., Allamandola, L.J., Tielens, A.G.G.M., Valero, G.C. 1988, ApJ 329, 498
Strazzulla, G., Baratta, G.A., Palumbo, M.E. 2001, Spectroch. Acta A 57, 825
Tafalla M., & Bachiller R. 1995, ApJ 443, L37

PoS(AASKA14)123

Taquet, V., Ceccarelli, C., Kahane, C. 2012, A&A 538, 42

Testi, L., Perez, L., Jimenez-Serra, I., et al., 2015, Protoplanetary disks and the dawn of planets with SKA, in proceedings of "Advancing Astrophysics with the Square Kilometre Array", PoS(AASKA14)117

PoS(AASKA14)123

PROCEEDINGS OF SCIENCE

Studies of Anomalous Microwave Emission (AME) with the SKA

Clive Dickinson,[1] **Y. Ali-Haïmoud,**[2] **R. J. Beswick,**[1] **S. Casassus,**[3] **K. Cleary,**[4] **B. T. Draine,**[5] **R. Genova-Santos,**[6] **K. Grainge,**[1] **T. C. Hoang,**[7] **A. Lazarian,**[8] **E. J. Murphy,**[9] **R. Paladini,**[9] **M. W. Peel,**[1] **Y. Perrott,**[10] **J.-A. Rubiño-Martin,**[6] **A. Scaife,**[11] **C. T. Tibbs,**[9] **L. Verstraete,**[12] **M. Vidal,**[1] **R A. Watson,**[1] **N. Ysard**[13]

[1] *Jodrell Bank Centre for Astrophysics, The University of Manchester, UK*
[2] *Institute for Advanced Study, Einstein Drive, Princeton, New Jersey 08540, USA*
[3] *Departamento de Astronomía, Universidad de Chile, Casilla 36-D, Santiago, Chile*
[4] *Cahill Center for Astronomy & Astrophysics, Caltech, Pasadena CA, 91125, USA*
[5] *Princeton University Observatory, Princeton, NJ 08544-1001, USA*
[6] *Instituto de Astrofiśica de Canarias, 38200 La Laguna, Tenerife, Canary Islands, Spain*
[7] *Institut für Theoretische Physik, Lehrstuhl IV: Weltraum- und Astrophysik, Bochum, Germany*
[8] *Department of Astronomy, University of Wisconsin, Madison, WI 53706, USA*
[9] *IPAC, Caltech, Pasadena CA, 91125, USA*
[10] *Astrophysics Group, Cavendish Laboratory, University of Cambridge CB3 0HE, UK*
[11] *School of Physics & Astronomy, University of Southampton, Southampton, SO17 1BJ, UK*
[12] *IAS, CNRS, Université Paris-Sud 11, Orsay, France*
[13] *Department of Physics, PO Box 64, FI-00014 University of Helsinki, Finland,*
E-mail: Clive.Dickinson@manchester.ac.uk

In this chapter, we will outline the scientific motivation for studying Anomalous Microwave Emission (AME) with the SKA. AME is thought to be due to electric dipole radiation from small spinning dust grains, although thermal fluctuations of magnetic dust grains may also contribute. Studies of this mysterious component would shed light on the emission mechanism, which then opens up a new window onto the interstellar medium (ISM). AME is emitted mostly in the frequency range $\sim$ 10–100 GHz, and thus the SKA has the potential of measuring the low frequency side of the AME spectrum, particularly in band 5. Science targets include dense molecular clouds in the Milky Way, as well as extragalactic sources. We also discuss the possibility of detecting rotational line emission from Poly-cyclic Aromatic Hydrocarbons (PAHs), which could be the main carriers of AME. Detecting PAH lines of a given spacing would allow for a definitive identification of specific PAH species.

Advancing Astrophysics with the Square Kilometre Array
June 8-13, 2014
Giardini Naxos, Sicily, Italy

PoS(AASKA14)124

1. Introduction

Anomalous Microwave Emission (AME) is a mysterious component of microwave radiation emitted from the diffuse interstellar medium (ISM), which was first discovered in the late 1990s by sensitive CMB experiments operating at frequencies above 10 GHz (Leitch et al. 1997; Kogut et al. 1996). Since then, it has been detected by numerous experiments operating in the frequency range $\sim$ 10–100 GHz, both in diffuse cirrus at high Galactic latitude (de Oliveira-Costa et al. 1999, 2004; Banday et al. 2003; Finkbeiner 2004; Davies et al. 2006; Gold et al. 2011; Ghosh et al. 2012; Bennett et al. 2012) as well as from individual Galactic clouds (Finkbeiner et al. 2002; Watson et al. 2005; Casassus et al. 2006; Dickinson et al. 2009; Scaife et al. 2009, 2010a; Dickinson et al. 2009, 2010; Vidal et al. 2011; Planck Collaboration et al. 2013). More recently it has been detected from individual star forming regions in a nearby galaxy (Murphy et al. 2010; Scaife et al. 2010b). The intensity is closely correlated with the thermal radiation at mid and far infrared (FIR) wavelengths associated with interstellar dust grains, but thermal dust emission cannot account for the observed microwave excess, which appears to peak at frequencies $\sim$ 20–40 GHz. Other traditional emission mechanisms (e.g., CMB, synchrotron, free-free) also cannot easily explain it.

A number of models have been proposed to explain the AME. The most plausible is electric dipole radiation from ultra-small rapidly spinning dust grains (a.k.a. "spinning dust"; see § 2.1). Low resolution *Planck* data and theoretical modelling of the Perseus and ρ Ophiuchi molecular clouds show, beyond reasonable doubt, that the AME in these regions is indeed due to spinning dust (Planck Collaboration et al. 2011). However, a number of mysteries still remain. The classical picture of spinning dust grains does not appear to fit so well on small angular scales. Even though AME has been detected on arcmin scales (Scaife et al. 2009; Tibbs et al. 2013), the emission appears to be correlated with the strength of the radiation field rather than the column of small grains/PAHs along some sight-lines (Tibbs et al. 2011, 2012). Also, in some objects (such as compact HII regions), the data have failed to detect AME at all (Scaife et al. 2008). The AME could also be due to another mechanism, such as thermal fluctuations in magnetic grains (a.k.a. "magnetic dust"; see § 2.2). Detailed observations of AME will help us understand this mysterious component and, in principle, open up a new window on the ISM, both in the Milky Way and in external galaxies.

In this chapter, we begin by reviewing the two main models for AME (§ 2) and what the predictions are for their radio emission. We also mention the possibility of detecting rotational PAH lines in AME regions. We then discuss potential targets (§ 3.1) and the instrumental requirements (§ 3.2) that would allow the SKA to observe AME and what we could learn from them. We conclude and summarise the outlook for AME observations with the SKA (§ 4).

2. Models for the AME - Brief Overview and Predictions

AME was given its name (Leitch et al. 1997) because it could not easily be explained in terms of conventional physical emission mechanisms - synchrotron, free-free, thermal dust, or CMB emissions. A number of possibilities have been explored, including flat spectrum synchrotron radiation (Bennett et al. 2003; Peel et al. 2012) and hot ($T_e \gtrsim 10^6$ K) free-free emission (Leitch et al. 1997). There are currently two plausible explanations for the AME - electric dipole radiation

PoS(AASKA14)124

from small rapidly spinning dust grains and thermal fluctuations in magnetic dust grains. Although spinning dust is the most widely accepted explanation there is still a possibility that some, or all, of the AME is from magnetic dust. Here we briefly review the theory and predictions. Finally, we also mention the possibility of detecting rotational line emission from PAHs, which has recently been proposed[1] (Ali-Haïmoud 2014).

2.1 Spinning dust

Electric dipole radiation from small spinning dust grains has been predicted for a long time (Erickson 1957). However, it had not received much attention until the late 1990s when several experiments detected excess emission at high frequencies (10–60 GHz). The first detailed theory and predictions were made by Draine & Lazarian (1998), with subsequent minor improvements over recent years (Ali-Haïmoud et al. 2009; Ysard & Verstraete 2010; Hoang et al. 2010, 2011).

The idea is simple - rotating electric dipoles radiate. Interstellar dust grains will naturally possess permanent electric dipoles, μ, due to an uneven distribution of charges, impurities (such as nitrogen in PAHs), or an asymmetric structure; even spherically symmetric grains will have, on average, a residual dipole moment. Also, interstellar dust grains are known to spin at high rates due to a number of excitation mechanisms (photons, collisions, formation of molecules etc). Classically, the power radiated by a dipole rotating at angular velocity ω, with electric dipole component $\mu_\perp$ perpendicular to ω is given by

$$P = \frac{2}{3}\frac{\mu_\perp^2 \omega^4}{c^3} \, . \tag{2.1}$$

This power is emitted at a frequency $\nu = \omega/2\pi$. To calculate the detailed frequency spectrum of spinning dust, one needs to integrate the emission over a distribution of grain sizes, electric dipole moments, and angular velocities. Specifically, the emissivity per H atom is (Ali-Haïmoud et al. 2009):

$$\frac{j_\nu}{n_{\rm H}} = \frac{1}{4\pi}\int_{a_{\rm min}}^{a_{\rm max}} da \frac{1}{n_{\rm H}}\frac{dn_{\rm gr}}{da} 4\pi\omega^2 f_{\rm a}(\omega) 2\pi \frac{2}{3}\frac{\mu_{a\perp}^2 \omega^4}{c^3}, \tag{2.2}$$

where $\omega = 2\pi\nu$, $dn_{\rm gr}/da$ is the grain size distribution, $f_{\rm a}(\omega)$ is the rotational velocity distribution.

It is easy to see that for grains to emit appreciable power at radio frequencies, the grains must spin at a very high rate - at GHz frequencies. Larger grains, due to their larger moments-of-inertia, emit at lower frequencies and with a lower emissivity. At frequencies < 5 GHz, spinning dust is expected to be very weak, and typically swamped by the usual free-free and synchrotron components. The high frequency cut-off is determined by the very smallest grains (VSGs) and PAHs, which are the most emissive and dominate the spectrum, resulting in a peaked spectrum. Fig. 1 shows a theoretically predicted spectrum for specific conditions typical of the Cold Neutral Medium (CNM). It can be seen that most of the emission comes from the very smallest grains.

Although there is still significant debate about the origin of the diffuse high latitude AME observed in CMB experiments (Bennett et al. 2003), there are a few examples of Galactic molecular clouds that are now widely accepted to emit significant amounts of spinning dust at frequencies

[1]Note that the line emission is in addition to continuum emission from spinning dust grains.

PoS(AASKA14)124

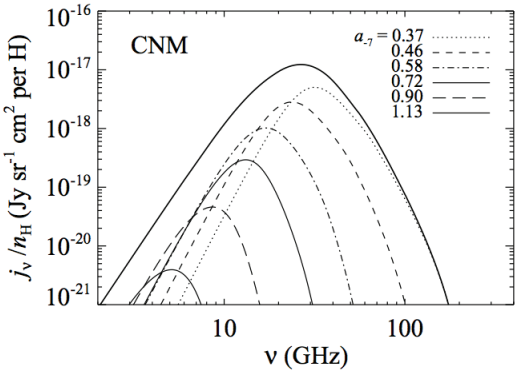

Figure 1: Theoretical spinning dust emissivity for a CNM environment (thick solid line). Contributions from grains of various sizes are shown [$a_7 \equiv a/(10^{-7}$ cm]. This spectrum is typical of spinning dust models, which show a highly peaked spectrum, with a peak frequency ~ 30 GHz, but is very sensitive to the properties of the grain and environment. Reproduced from Ali-Haïmoud et al. (2009).

~ 30 GHz. The best two examples are the Perseus and ρ Ophiuchi molecular clouds; Fig. 2 shows the SED of G160.26–18.62 in the Perseus molecular cloud and the spinning dust residuals including *Planck* data (Planck Collaboration et al. 2011). The spinning dust is modelled by 2 components representing the atomic and molecular phases of the ISM. The analysis not only showed that the spectrum can be well-fitted by spinning dust but also that the physical parameters that define the model are consistent with expectations i.e. the model is physically motivated, or alternatively, that we expect to see spinning dust at this level in this region. In fact, a number of new observations are now suggesting that a significant fraction (tens of percent) of the 30 GHz emission in our Galaxy is due to AME (Planck Collaboration et al. 2014b). This could have significant consequences for astronomical observations of our Galaxy and extragalactic sources[2]

Spinning dust emission is largely unpolarized because the smallest grains that dominate the power do not align efficiently with the magnetic field. At 30 GHz the polarized fraction is expected to be $< 1\,\%$ (Lazarian & Draine 2000; Hoang et al. 2013), consistent with current upper limits (Dickinson et al. 2011; López-Caraballo et al. 2011; Rubiño-Martín et al. 2012). At lower frequencies, where larger grains contribute, the polarization can be significant (few %) but will be difficult to measure due to confusion with synchrotron/free-free emission. Nevertheless, measuring polarization would provide constraints on paramagnetic alignment and resonance relaxation models of small grain alignment (Lazarian & Draine 2000) and, perhaps more importantly, may allow us to distinguish between spinning dust (low polarization) and magnetic dust (§ 2.2) mechanisms (high polarization).

2.2 Magnetic dust

An alternative explanation for AME was proposed by Draine & Lazarian (1999) in terms of thermal fluctuations of the magnetization within individual interstellar grains. Such thermal fluctuations result in magnetic dipole radiation. The predictions of magnetic dust are based on

[2]The study of AME may be of relevance to studying star formation in galaxies via their free-free emission (Beswick 2015; Murphy 2015), since a separation between the synchrotron/free-free/AME components is required above ~ 10 GHz.

PoS(AASKA14)124

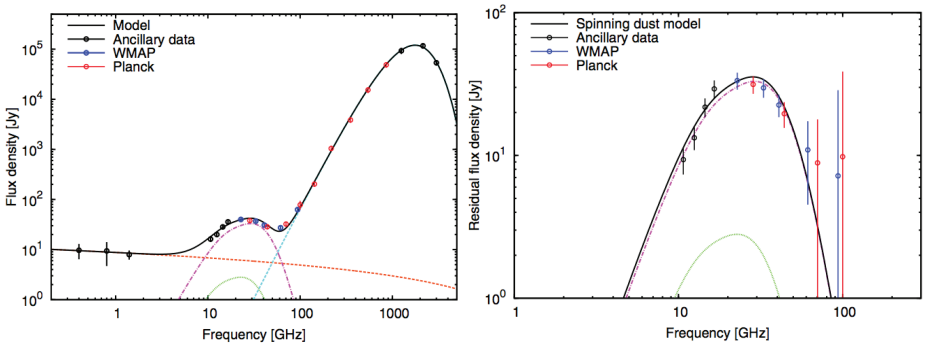

Figure 2: The spectrum of G160.26–18.62 in the Perseus molecular cloud (*left*) and the residual spectrum showing the spinning dust component (*right*). The spectrum is fitted by components of free-free (orange dashed line), CMB (not visible), thermal dust (dashed cyan line) and spinning dust (green dotted and magenta dot-dashed lines for the atomic and molecular phases, respectively), which peaks at ≈ 30 GHz. The spectrum is a remarkably good fit to the data with parameters that are physically motivated. Reproduced from Planck Collaboration et al. (2011).

the magnetic properties of dust using the Gilbert equation (Draine & Hensley 2012) and are quite diverse. Although ordinary paramagnetic grains cannot account for the bulk of the AME, stronger magnetic dipole radiation will result if a fraction of the grain material is ferromagnetic by the inclusion of iron (Fe). Since $\sim 90\,\%$ of the Fe is missing from the gas phase, it must be locked up in solid grains; very little is known about the nature of the Fe-containing material. Again, the predictions depend critically on the form of Fe e.g. as free flyers, inclusions on grains, metallic Fe, magnetite, maghemite etc. (Draine & Hensley 2013).

Magnetic dust has not been definitively detected as of yet. However, a number of hints have been indicated. A study of the sub-mm spectrum of the Small Magellanic Cloud (SMC) has shown that the sub-mm excess can be readily accounted for by magnetic dust (Draine & Hensley 2012). Fig. 3 shows the spectrum of the SMC, fitted with two models including a contribution from magnetic dust. It is worth noting that the magnetic dust does not depend sensitively on the size of grains (unlike for spinning dust) and thus it could emit from anywhere there is dust.

The polarization of magnetic dust is similarly complicated and depends on the form of the magnetic nanoparticles. Most models predict a very high ($\sim 35\,\%$) polarization in the sub-mm, decreasing towards microwave/radio wavelengths. Indeed, a recent analysis of *Planck* polarization data shows a fall in the polarized fraction from 353 GHz to 100 GHz, which may indicate a component of magnetic dust (Planck Collaboration et al. 2014a). This polarization signature is the most clear way to distinguish between magnetic dust and other emission mechanisms such as spinning and thermal dust. Note that the polarization undergoes a reversal at frequencies ~ 3–20 GHz, depending on grain geometry and composition i.e. the emission will go from being aligned with the magnetic field to being perpendicular to it (Draine & Hensley 2012). This would be a smoking gun indication of this process, although confusion from the polarized synchrotron radiation will likely make this difficult.

2.3 Rotational spectroscopy of interstellar PAHs

Carbonaceous dust grains are thought to extend down to the molecular regime at the small

PoS(AASKA14)124

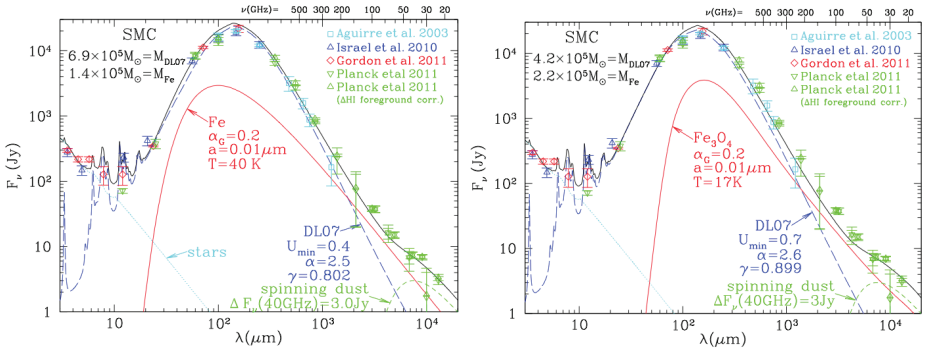

Figure 3: The spectrum of the SMC, fitted with two example models including magnetic dust. The excess emission relative to a simple thermal dust model is observed at frequencies $\sim$ 50–200 GHz. In these fits, a combination of spinning dust (dashed green line) and magnetic dust (red line) can explain most of the excess. The plots show two different example models from metallic Fe at $T = 40$ K (*left*) and magnetite at $T = 17$ K (*right*). Reproduced from Draine & Hensley (2012).

size end, where they take the form of Poly-cyclic Aromatic Hydrocarbons (PAHs) (Tielens 2008). PAHs are widely recognised as the carriers of the near-infrared aromatic features, are abundant in the interstellar medium, and are important actors in its chemical and thermal balance. They are also presumably the emitters of spinning dust radiation. Yet, no specific interstellar PAH has been identified to date, as the near-infrared features are not molecule-specific. Detecting and identifying interstellar PAHs would close any remaining doubt about the nature of the carriers of near-infrared features (Kwok & Zhang 2013) and could lead to a more quantitative understanding of their formation mechanisms.

It was recently suggested that rotational spectroscopy combined with matched filtering techniques could be used to identify interstellar PAHs (Ali-Haïmoud 2014). General PAHs are large asymmetric molecules and have a very complex rotational spectrum, unusable for identification purposes. However, quasi-symmetric PAHs (such as nitrogen-substituted coronene or circumcoronone; Hudgins et al. 2005) have very regular rotational spectra, taking the shape of "combs" of evenly spaced lines with width of order of a MHz[3]. The line separation ranges from a few tens of MHz to a few hundreds of MHz and is highly sensitive to the size of the emitting species; see the table in Fig. 4 for the approximate line spacing of a few representative species.

Structure	Formula	Comb spacing (MHz)	Structure	Formula	Comb spacing (MHz)
	$C_{24}H_{12}$ (coronene)	335		$C_{42}H_{18}$	100
	$C_{37}H_{15}$	140		$C_{54}H_{18}$ (circumcoronene)	67

Figure 4: Approximate line spacing for representative symmetric PAHs, computed assuming a perfectly hexagonal carbon skeleton with a C-C bond length of 1.4 Å and a C-H bond length of 1.1 Å for the peripheral hydrogen atoms.

[3]Each "tooth" of the comb spectrum is really a stack of lines spread across $\sim$ 1 MHz. Observed with a $\sim$ MHz resolution these stacks would appear as lines.

PoS(AASKA14)124

The expected strength of the lines is highly uncertain, as it depends of the fraction of PAHs that are quasi-symmetrical. If of order one percent of PAH molecules are in the form of coronene, for example, we expect a line strength of order a mJy (near the peak of AME, at $\sim$ 10–30 GHz) for a molecular cloud observed with arcmin resolution. The highly regular shape of the spectrum allows for a more efficient search using matched filtering techniques.

3. Observations of AME with the SKA

3.1 Potential targets

AME from spinning and magnetic dust radiation is expected, at some level, from any object containing small dust grains. Therefore, there are potentially a very wide range of objects that could be studied, including molecular clouds, photodissociation regions (PDRs), dense cores, circumstellar disks etc. However, some consideration is needed for the contribution of synchrotron/free-free since the SKA will operate at < 20 GHz where these are significant for many objects. Furthermore, many of these sources are very diffuse with the emission being distributed on scales of arcmin and larger. This will cause difficulties in imaging the large-scale emission (resolving out flux, deconvolution etc.). Nevertheless, ISM structures invariably emit over a wide range of scales and we would need to focus on regions that have a significant column of dust, using ancillary IR/sub-mm data.

One of the best targets would be dense pre-stellar cores. These collapsing dust clouds have typical sizes of $\sim$ 1 arcmin or less, which is well matched to the shorter SKA baselines. Although a large fraction of these are found within large molecular cloud complexes with strong synchrotron/free-free emission, some are less contaminated and have clean lines-of-sight. There is an interesting possibility of using the profile of spinning dust emission as a probe of these clouds. Ysard et al. (2011) have shown that this could in principle be used to study the grain properties and environment within the cloud. In particular, they proposed a scheme to estimate the abundances of the major ions (HII, CII), which would be complementary to direct observations. The emission may also be relatively strong at the centre of dense clouds where the mid-IR PAH emission is weak and could provide a new way to trace grain growth from diffuse to dense media.

Circumstellar disks would also be a good target for AME. Near-IR studies (and more recently results from the Atacama Large Millimeter Array; ALMA) of disks around Herbig Ae/Be stars have demonstrated that a substantial amount of dust mass can be locked up in nanometre-sized particles. Modelling has shown that spinning dust could contribute of order mJy at $\sim$ 20 GHz (Rafikov 2006) and hence at levels comparable to the Rayleigh-Jeans tail of the sub-mm continuum. SKA would provide high resolution imaging of disks and the separation from synchrotron/free-free could be achieved by observing at lower frequencies. Detection of the spinning dust emission would provide important evidence for the existence, properties, and origin of the population of small dust particles in proto-planetary disks, with possible ramifications for planet formation. VSGs are key to the thermal balance of proto-planetary disks, and their detection at radio frequencies would allow a new probe of their distribution, unhindered by the central circumstellar glare that affects the IR observations.

Another obvious target for the high resolution capabilities of SKA, is external galaxies (see also Murphy 2015). Strangely, AME has only been detected in one external galaxy, NGC6946

PoS(AASKA14)124

(Murphy et al. 2010; Scaife et al. 2010b) (and possibly SMC/LMC). In fact, it was only significantly detected in two out of ten star forming regions within the spiral arms of NGC6946. It is possible that AME may only be strongly emitted in a small volume of an entire galaxy, and thus the integrated contribution of AME could be small in general. On the other hand, there have been few detailed measurements at frequencies above a few GHz, thus we may have simply missed it. Another interesting possibility is that high redshift galaxies ($z > 2$), would emit AME at observed frequencies below ~ 10 GHz, which may be more suited to the SKA. The higher star formation rates, and therefore increased dust production at these redshifts, may result in a relatively larger fraction of AME.

For the detection of rotational PAH lines, we would target regions that are known to have column density of PAHs (via IR maps e.g. *Spitzer* 8 μm) but little ionized gas to reduce contamination from radio recombination and other ionic lines. AME-dominated targets would be obvious targets.

3.2 Instrument requirements

AME, whether from spinning or magnetic dust, emits at relatively high radio (microwave) frequencies - at ~ 10 GHz and above. The ideal instrument would cover frequencies of a few GHz up to ~ 300 GHz. However, there is a dearth of observations in the range 10–30 GHz. The SKA would be complementary to sub-mm data (e.g. ALMA and *Planck*) and would provide the crucial low frequency data required to separate synchrotron/free-free/AME.

In SKA1-MID, the highest frequency corresponds to band 5 covering 4.6–13.8 GHz and with a bandwidth of 2.5 GHz in each polarisation (Dewdney et al. 2013). For spinning dust, the focus would be on intensity rather than polarization, while for magnetic dust the polarization would be the main interest. Polarization observations either side of the predicted ~ 15 GHz reversal (e.g. combined with ALMA band 1 30 GHz observations or Very Large Array) would provide a smoking gun detection of magnetic nanoparticles. The full SKA is expected to include the highest frequency band 5 and may go up to 24 GHz, or possibly even a little higher. Clearly this would open up the SKA to studies of AME, both spinning dust and magnetic dust. Assuming a build-out from the central core of SKA1-MID, bright AME targets offer the opportunity for early science with $< 50\,\%$ capability of the full SKA1-MID.

The angular scale coverage is more difficult to define since there is a wide range of potential targets such as prestellar cores, diffuse molecular clouds and extragalactic sources (§ 3.1). An important consideration is the surface brightness sensitivity since the majority of AME detections have been from diffuse regions rather than from compact sources. We therefore require good u, v coverage with many short baselines. For continuum, SKA1-MID is likely to provide sufficient sensitivity for many of our targets, which would be chosen carefully to match the u, v coverage that was available. Utilising the lower bands of SKA (band 3 [1.6–3.1 GHz] and band 4 [2.8–5.2 GHz]), using matched baselines to give equivalent u, v-coverage, could be used to differentiate AME from synchrotron/free-free emissions.

To appreciate the sensitivity and power of the SKA, we make an order-of-magnitude estimate of the integration time required for SKA-MID to detect AME in one of the well-known diffuse molecular clouds. We consider the filamentary structure observed in the Perseus molecular cloud by the Arc Minute Imager (AMI) at 16 GHz and synthesized beam of ≈ 2 arcmin. AME structure was detected on the scale of the beam at a level of ≈ 6 mJy/beam (Tibbs et al. 2013). If we

PoS(AASKA14)124

conservatively assume that the emission is completely smooth (does not have structure on scales smaller than the beam), we can calculate the lower limit to the flux density observed with the 1 km core of SKA-MID, which corresponds to an angular resolution of ~ 3 arcmin, of $\sim 4\,\mu$Jy/beam. For early observations with 50 % early phase 1 SKA, the system equivalent flux density is 3.4 Jy (1.7 Jy for the full array; Dewdney et al. 2013). For a bandwidth of 2.5 GHz, an integration time of 2300 secs (~ 1 hour) is required to achieve a 5σ detection. It is therefore clear that even for diffuse ISM structures, the SKA can potentially be very powerful.

For the rotational lines of PAHs, we require a frequency resolution of ~ 1 MHz or better, which would be easily achievable with 16384 channels over a 5 GHz bandwidth centred at ≈ 20 GHz. The required sensitivity of $\sim \mu$Jy/beam is readily feasible as long as the ISM structures were matched to the SKA baselines, while the stacking analysis can be made to be robust against bandpass and other calibration errors (Ali-Haïmoud 2014).

4. Conclusions and outlook

SKA, operating at frequencies above ~ 10 GHz would provide high resolution (arcsec and better) and high fidelity wide-field imaging of Galactic clouds and similar regions in nearby galaxies. Precise continuum measurements of the frequency spectrum of AME would provide definitive confirmation of the spinning dust model across a wide range of scales. Sensitive and high resolution observations of molecular dust clouds, away from hot ionized gas (which is invariably associated with star forming clouds), would give a clear picture of AME. Combined with higher frequency data (e.g. ALMA band 1 at 30 GHz) we can establish the full spinning dust SED for a variety of targets.

Once spinning dust is confirmed, we can then use this unique tracer of small dust grains as a new probe of the ISM. The spinning dust spectrum and intensity is very sensitive to a number of parameters associated with the ISM, that are otherwise difficult to constrain. Combined with theoretical modelling, it would allow the dust grain size distribution to be measured as well as the density and interstellar radiation field (and possibly other parameters such as the electric dipole moment), which affect the rotational excitation of interstellar grains. Models already exist for cold prestellar cores, which predict specific signatures of spinning dust that can be tested and unique information on the physics of star-forming regions can be gained. Complementary high resolution FIR/sub-mm data (e.g. *Spitzer/Herschel*, ALMA) would provide a complete picture of the ISM, which could be studied on a wide range of scales and environments.

Finally, we outline the possibility of detecting comb-like line emission from PAHs, which would provide definitive identification of specific, free-floating interstellar PAHs.

CD acknowledges support from an ERC Starting (Consolidator) Grant (no 307209).

References

Ali-Haïmoud, Y. 2014, MNRAS, 437, 2728

Ali-Haïmoud, Y., Hirata, C. M., & Dickinson, C. 2009, MNRAS, 395, 1055

Banday, A. J., Dickinson, C., Davies, R. D., Davis, R. J., & Górski, K. M. 2003, MNRAS, 345, 897

PoS(AASKA14)124

Bennett, C. L., Hill, R. S., Hinshaw, G., et al. 2003, ApJS, 148, 97
Bennett, C. L., Larson, D., Weiland, J. L., et al. 2012, accepted in ApJSS, (ArXiv:1212.5225), arXiv:1212.5225
Beswick, R. J., et al. 2015, "SKA studies of nearby galaxies: star-formation, accretion processes and molecular gas across all environments", in Advancing Astrophysics with the Square Kilometre Array, PoS(AASKA14)070
Casassus, S., Cabrera, G. F., Förster, F., et al. 2006, ApJ, 639, 951
Davies, R. D., Dickinson, C., Banday, A. J., et al. 2006, MNRAS, 370, 1125
de Oliveira-Costa, A., Tegmark, M., Davies, R. D., et al. 2004, ApJ, 606, L89
de Oliveira-Costa, A., Tegmark, M., Gutierrez, C. M., et al. 1999, ApJ, 527, L9
Dewdney, P. E., Turner, W., Millenaar, R., et al. 2013, SKA1 System Baseline Design, Tech. Rep. SKA-TEL-SKO-DD-001 Revision 1, SKA Organisation
Dickinson, C., Peel, M., & Vidal, M. 2011, MNRAS, 418, L35
Dickinson, C., Davies, R. D., Allison, J. R., et al. 2009, ApJ, 690, 1585
Dickinson, C., Casassus, S., Davies, R. D., et al. 2010, MNRAS, 407, 2223
Draine, B. T., & Hensley, B. 2012, ApJ, 757, 103
—. 2013, ApJ, 765, 159
Draine, B. T., & Lazarian, A. 1998, ApJ, 508, 157
—. 1999, ApJ, 512, 740
Erickson, W. C. 1957, ApJ, 126, 480
Finkbeiner, D. P. 2004, ApJ, 614, 186
Finkbeiner, D. P., Schlegel, D. J., Frank, C., & Heiles, C. 2002, ApJ, 566, 898
Ghosh, T., Banday, A. J., Jaffe, T., et al. 2012, MNRAS, 422, 3617
Gold, B., Odegard, N., Weiland, J. L., et al. 2011, ApJS, 192, 15
Hoang, T., Draine, B. T., & Lazarian, A. 2010, ApJ, 715, 1462
Hoang, T., Lazarian, A., & Draine, B. T. 2011, ApJ, 741, 87
Hoang, T., Lazarian, A., & Martin, P. G. 2013, ApJ, 779, 152
Hudgins, D. M., Bauschlicher, Jr., C. W., & Allamandola, L. J. 2005, ApJ, 632, 316
Kogut, A., Banday, A. J., Bennett, C. L., et al. 1996, ApJ, 464, L5
Kwok, S., & Zhang, Y. 2013, ApJ, 771, 5
Lazarian, A., & Draine, B. T. 2000, ApJ, 536, L15
Leitch, E. M., Readhead, A. C. S., Pearson, T. J., & Myers, S. T. 1997, ApJ, 486, L23
López-Caraballo, C. H., Rubiño-Martín, J. A., Rebolo, R., & Génova-Santos, R. 2011, ApJ, 729, 25
Murphy, E. J., et al. 2015, "The Astrophysics of Star Formation Across Cosmic Time at >10 GHz with the Square Kilometre Array", in Advancing Astrophysics with the Square Kilometre Array, PoS(AASKA14)085
Murphy, E. J., Helou, G., Condon, J. J., et al. 2010, ApJ, 709, L108
Peel, M. W., Dickinson, C., Davies, R. D., et al. 2012, MNRAS, 424, 2676
Planck Collaboration, Ade, P. A. R., Aghanim, N., et al. 2011, A&A, 536, A20
—. 2013, ArXiv e-prints, arXiv:1309.1357
Planck Collaboration, Ade, P. A. R., Alves, M. I. R., et al. 2014a, submitted to A&A, arXiv:1405.0874

PoS(AASKA14)124

Planck Collaboration, Ade, P. A. R., Aghanim, N., et al. 2014b, Submitted to A&A, arXiv:1406.5093

Rafikov, R. R. 2006, ApJ, 646, 288

Rubiño-Martín, J. A., López-Caraballo, C. H., Génova-Santos, R., & Rebolo, R. 2012, Advances in Astronomy, 2012, doi:10.1155/2012/351836

Scaife, A. M. M., Hurley-Walker, N., Davies, M. L., et al. 2008, MNRAS, 385, 809

Scaife, A. M. M., Hurley-Walker, N., Green, D. A., et al. 2009, MNRAS, 400, 1394

Scaife, A. M. M., Green, D. A., Pooley, G. G., et al. 2010a, MNRAS, 403, L46

Scaife, A. M. M., Nikolic, B., Green, D. A., et al. 2010b, MNRAS, 406, L45

Tibbs, C. T., Scaife, A. M. M., Dickinson, C., et al. 2013, ApJ, 768, 98

Tibbs, C. T., Flagey, N., Paladini, R., et al. 2011, MNRAS, 418, 1889

Tibbs, C. T., Paladini, R., Compiègne, M., et al. 2012, ApJ, 754, 94

Tielens, A. G. G. M. 2008, ARA&A, 46, 289

Vidal, M., Casassus, S., Dickinson, C., et al. 2011, MNRAS, 414, 2424

Watson, R. A., Rebolo, R., Rubiño-Martín, J. A., et al. 2005, ApJ, 624, L89

Ysard, N., Juvela, M., & Verstraete, L. 2011, A&A, 535, A89

Ysard, N., & Verstraete, L. 2010, A&A, 509, A12

PoS(AASKA14)124

PROCEEDINGS OF SCIENCE

OH masers in the Milky Way and Local Group galaxies in the SKA era

Sandra Etoka[*1], **Dieter Engels**[1], **Hiroshi Imai**[2], **Joanne Dawson**[3], **Simon Ellingsen**[4], **Lorant Sjouwerman**[5], **Huib van Langevelde**[6,7]

[1]*Hamburger Sternwarte,* [2]*Kagoshima University,* [3]*Macquarie University,* [4]*University of Tasmania,* [5]*National Radio Astronomy Observatory,* [6]*Joint Institute for VLBI in Europe,* [7]*Sterrewacht Leiden*

E-mail: sandra.etoka@googlemail.com

The intense line emission of OH masers is a perfect tracer of regions where new stars are born as well as of evolved stars, shedding large amounts of processed matter into the interstellar medium. From SKA deep surveys at 18 cm, where the maser lines from the ground-state of the OH molecule arise, we predict the discovery of more than 20000 sources of stellar and interstellar origin throughout the Galaxy. The study of this maser emission has many applications, including the determination of magnetic field strengths from polarisation measurements, studies of stellar kinematics using the precisely determined radial velocities, and distance determinations from VLBI astrometry. A new opportunity to study shocked gas in different galactic environments is expected to arise with the detection of lower luminosity masers. For the first time, larger numbers of OH masers will be detected in Local Group galaxies. New insights are expected in structure formation in galaxies by comparing maser populations in galaxies of different metallicity, as both their properties as well as their numbers depend on it. With the full capabilities of SKA, further maser transitions such as from excited OH and from methanol will be accessible, providing new tools to study the evolution of star-forming regions in particular.

Advancing Astrophysics with the Square Kilometre Array
June 8-13, 2014
Giardini Naxos, Italy

*Speaker.

PoS(AASKA14)125

1. Introduction

In the Milky Way, maser emission is often observed in the circumstellar shells of red giant stars and in the surroundings of young stellar objects (YSOs). These are environments which are cool enough to form molecules and provide sufficient velocity coherence and density, so that the masers are naturally excited. The strongest stellar masers are those of oxygen-bearing molecules like hydroxyl (OH), water (H_2O) and silicon-monoxide (SiO). In addition, methanol (CH_3OH) and to lesser extent, ammonia (NH_3) and formaldehyde (H_2CO) masers are detected close to star-formation regions (SFRs). The major maser transitions accessible with the SKA during Phase 1 will be from OH at frequencies of 1612, 1665 and 1667 MHz in band 2 and 1720 MHz in band 3.

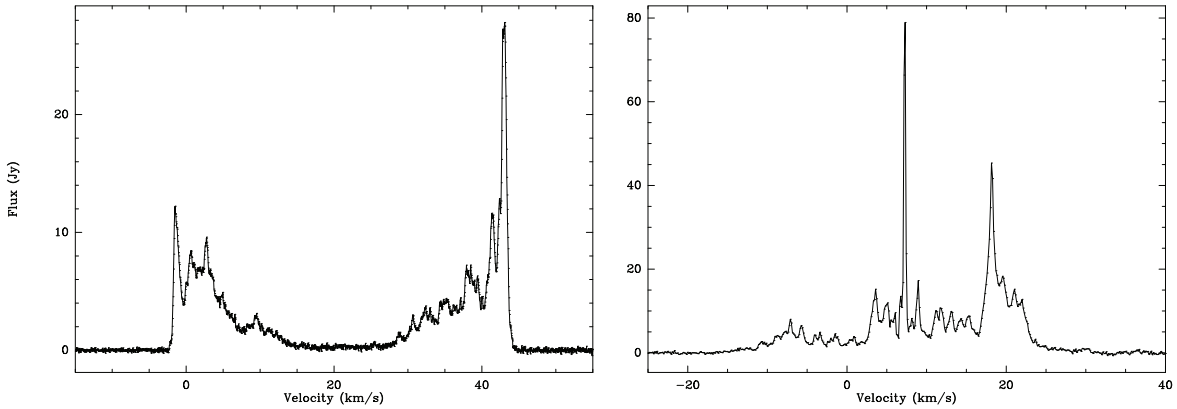

Figure 1: Left: 1612-MHz OH maser of the long-period variable star OH 16.1-0.2 **Right:** 1665-MHz OH maser of the star-forming region Orion KL. Both spectra were taken with the Nançay radiotelescope.

Known OH masers in the Galaxy are typically located in the plane at distances 2-8 kpc. The evolved-star and star-forming-region origin can be differentiated from their spectral shapes and the ratio of intensities between the transitions.

Evolved stars are generally strongest in the 1612-MHz transition and have a spectral shape dominated by two peaks with a separation of 30 ± 10 km s^{-1} (e.g. Fig. 1 left panel). The shape is due to the origin of the masers in an expanding circumstellar shell where the strongest amplification occurs radially. The two strong peaks then come from the front and the back sides of the shell, and the radial velocity of the star and the expansion velocity of the shell can be determined directly from the central velocity of the double-peaked profile and the velocity interval covered by the emission. The evolved-star masers vary in phase with the stellar luminosity variations. Superposed on this are peculiar variations due to flares or intervals of generally low emission levels.

All 4 ground-state lines can be observed towards SFRs, though the main-lines (1665 and 1667 MHz) are the most commonly observed. Typically, SFR maser spectra are composed of narrow spectral components ($\leq$1-2 km s^{-1}) which can spread over a wide range of velocity depending on the complexity of the SFR. The intensity of the individual components can vary by up to four orders of magnitude within the same SFR complex (e.g. Fig. 1 right panel showing the rich 1665-MHz spectrum towards the Orion-KL SFR complex). Often, these spectra show substan-

PoS(AASKA14)125

tial polarisation (including Zeeman pattern signatures) as well as substantial temporal variability (including flares) and periodic behaviours have also even been recorded towards class II 6.7-GHz methanol masers (e.g. Goedhart, Gaylard & van der Walt 2004).

Masers originating from SFRs and supernova remnants (SNRs) are commonly referred to as "interstellar masers". This term shall be used hereafter, bearing in mind that we are focusing here on the evolved-star and SFR populations. The differentiation between SFRs and SNRs will be made to remove any ambiguity when appropriate.

2. SKA survey framework

2.1 Luminosity distributions of galactic OH masers

Currently >2000 stellar (Engels & Bunzel, 2014; hereafter EB14) and several hundred interstellar OH masers are known in the Milky Way. Most were discovered by surveys with single-dish radiotelescopes with typical survey limits of several hundred mJy. The most comprehensive survey for stellar OH masers so far, is the ATCA/VLA OH 1612-MHz survey (Sevenster et al. 2001), covering the Galactic plane at $\mid l \mid \leq 45^\circ$ and $\mid b \mid \leq 3^\circ$. From this survey, we know that the number of detections is still increasing with increasing sensitivity.

A series of surveys for interstellar masers were made by Caswell, Haynes & Goss (1980); Caswell & Haynes (1983a&b and 1987), Caswell (1998) and Caswell, Green & Phillips (2013, 2014). They cover the Galactic plane to within 1 degree, in the range $233^\circ \leq l \leq 60^\circ$, and extend to masers slightly weaker than 1 Jy for the 1980s series of survey and $\sim$0.2 Jy for the more recent series. The ongoing Southern Parkes Large-Area Survey (SPLASH) for OH masers, which has a mean 5-sigma flux limit of 0.3 Jy, has already doubled the number of known masers for the area in common with previous surveys (Dawson et al. 2014).

To estimate the yields of more sensitive surveys, we have constructed distributions of specific OH luminosities $L_\nu = f_{peak} \cdot 4\pi D^2$, with f_{peak} the peak flux density of the strongest feature in the maser spectrum and D the kinematic distance. The distribution of flux densities and specific luminosities for stellar sources, taken from EB14, are shown in the first row of Fig. 2. For the interstellar masers we used the flux densities from the survey of Caswell and collaborators, and calculated specific luminosities using the kinematic distances provided by them. In case of ambiguity we used the distance quoted as 'more likely'. The distributions obtained for the interstellar sources are shown in the second row of Fig. 2.

The flux distributions are peaking at ~ 0.5 Jy (1612 MHz) for stellar and at ~ 4 Jy (1665/67 MHz) for interstellar masers, reflecting the different sensitivities of the contributing surveys. The luminosity distributions peak at 2×10^{15} Watt Hz^{-1} and $\sim 10^{16}$ Watt Hz^{-1} for the two different maser origins. The decrease in number at lower luminosities is very likely due to incompleteness, and this will be probed by future surveys.

2.2 Implications of maser variability on surveys

Due to the variability of the masers, single epoch surveys detect only a fraction of the full population. Detection rates less than 50% are common for targeted surveys toward infrared selected samples of red giants. The missing detections cannot be explained by sensitivity limitations alone,

PoS(AASKA14)125

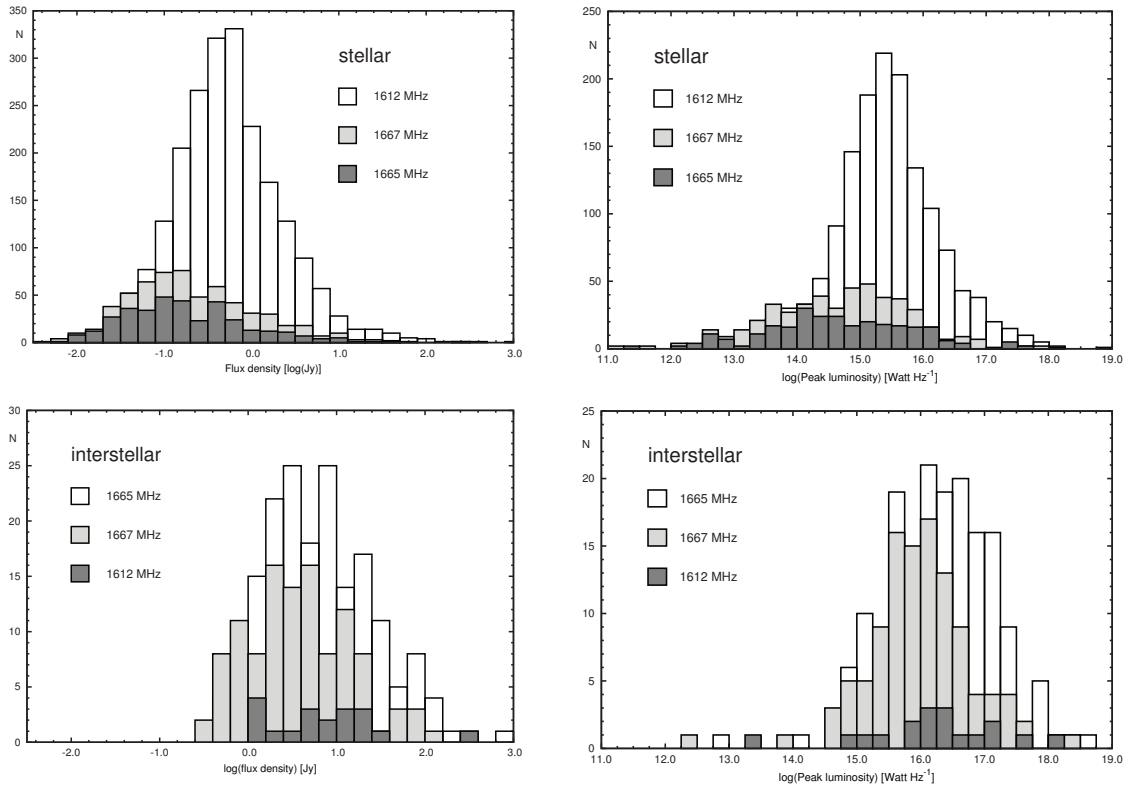

Figure 2: Left panel: Distribution of peak flux densities for stellar masers (top) and for interstellar masers (bottom). Increasing shading denotes the 1612, 1667, 1665 MHz transition for stellar and 1665, 1667, 1612 MHz transition for interstellar masers. **Right panel:** Distribution of corresponding peak luminosities assuming kinematic distances for stellar (top) and interstellar masers (bottom).

but most likely are due to variability on a range of timescales. On timescales of years, the stellar masers vary in response to the luminosity variations of the parent star. Repeated observations usually produce detections for such cases. Part of the O-rich population however are persistently not detected, although 'maser' and 'non-maser' AGB stars show no differences in their optical or infrared properties. The fraction η of 'maser' AGB stars is dependent on infrared colour (e.g. mass-loss rates) and ranges between 10 and 60% for a flux density limit of $\approx$50 mJy (Lewis, 1992).

Either these 'non-maser' stars possess only low-luminosity masers or the distribution of maser sites in their circumstellar shells is not spherically symmetric, so that only those stars are detected in which the OH maser emission is beamed toward Earth. Such issues are also valid for interstellar masers. For stellar masers, the beaming directions may change on timescales related to the crossing time through the shell ($\sim$ 1000 years). Therefore, we predict that the coming OH maser surveys, which will be separated $\sim$ 30 years from the historical ones, are also expected to discover new bright ($\gg$ 1 Jy) masers. The rate of new discoveries in stars not detected previously are a direct test of the timescales on which reconfigurations in the expanding circumstellar shells may occur.

2.3 The Galactic OH maser population

A rough estimate of the yield of future surveys for stellar OH masers can be made for 1612 MHz

PoS(AASKA14)125

using the model of Jackson et al. (2002) for the Galactic distribution of AGB stars. This model is based on the analysis of the Galactic distribution of $\approx$ 10000 IRAS sources with colours appropriate for mass-losing AGB stars. It predicts $\approx$ 200 000 AGB stars in the Milky Way. 1612-MHz OH flux densities can be estimated on the basis of dust mass-loss rates $\dot{M}_{dust}$ (in $M_{\odot}$ yr^{-1}) from the relation $f_{OH} = 3.15 \times 10^{9} \dot{M}_{dust} \, (v_{exp} \, D^{2})^{-1}$ (Zijlstra et al. 1996, taking into account the factor 2 needed for a better fit of the LMC data as predicated by Marshall et al. 2004), where f_{OH} is the peak flux density in Jy, v_{exp} the expansion velocity in km/s, and D the distance in kpc. For a given volume in the Galaxy, the space density of AGB stars was obtained from the Jackson et al. model, and it was assumed that the stars have a fixed IRAS colour distribution. The IRAS colours were converted to $\dot{M}_{dust}$ using the pure silicate models of Groenewegen (2006), which predict infrared colours for a range of gas mass-loss rates for fixed bolometric luminosity $L = 3000 \, L_{\odot}$, $v_{exp} = 10$ km s^{-1}, and a gas-to-dust ratio $\Psi = 200$. From the dust mass-loss rates, OH flux densities were obtained as described above.

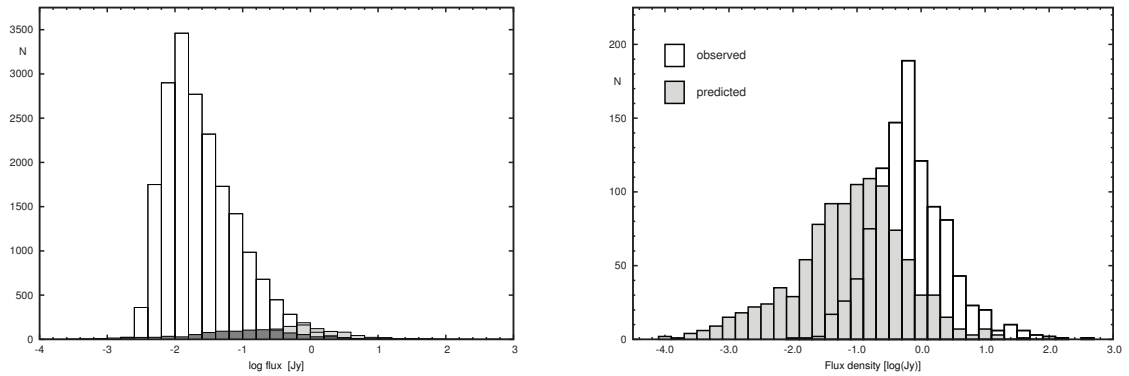

Figure 3: Left panel: Predicted distribution of 1612-MHz stellar OH maser flux densities based on the model of the Galactic distribution of AGB stars of Jackson et al. (2002) and a relation between dust mass-loss rates and OH maser luminosities from Marshall et al. (2004). The shaded distributions are from the right panel. **Right panel:** Observed stellar OH maser population in the front part of the solar Galactic hemisphere (that is up to a distance of $D \cdot cos(l) \leq 8.0$ kpc) and its predicted counterpart in the anti-solar Galactic hemisphere (see Sect. 3.2). The observed population is taken from the EB14 catalogue.

The actual numbers of OH masers predicted depend critically on the distribution of the mass-loss rates (or IR colours) among the AGB star population and also on the fraction η of AGB stars actually showing a maser with the predicted luminosity. The observed IRAS colour distributions are biased towards higher mass-loss rates, because these stars emit most of their energy in the mid-infrared. Corrections have to be estimated therefore for low $\dot{M}_{dust}$. The range of possible $\dot{M}_{dust}$ distributions and the fraction η of OH emitting AGB stars was constrained by the requirement that the model reproduces the results of the survey of Sevenster et al. (2001), e.g. the number of detections down to the survey limit of $\approx$ 150 mJy and the flux distribution.

The result for $\eta = 0.1$ is shown in Fig. 3 (left panel), giving $\approx$ 11 000 stellar OH 1612-MHz maser with $F_{OH} \geq 10$ mJy in the Galactic plane ($\mid b \mid < 3$ deg). This value of η is at the lower end of the range observed by Lewis (1992), but includes also by default 'non-maser' carbon-rich AGB stars in the population. Higher estimates can be created by adopting a steeper colour distribution, demanding $\eta > 0.1$ to reproduce the observed high-luminosity masers. Accordingly, the prediction

PoS(AASKA14)125

of the number of fainter masers will be scaled up.

In addition to the predicted number of stellar masers, an unknown number of interstellar masers will be present in the Galactic plane. Some of these masers will be detected prior to the SKA by surveys such as GASKAP. This survey aims to reach an rms for point sources of 1 mJy in the Galactic plane and of 0.5 mJy in the Magellanic Clouds. However, the angular resolution will only be ∼20 arcsec (Dickey et al. 2013), and thus the masers at the lowest flux limits may not be distinguishable from thermal extended emission. From a simple extrapolation of the number of identified maser sources in the pilot SPLASH region (∼200 sources within an area 10° width in Galactic Longitude), it is expected that at the SPLASH 5-sigma flux limit of 0.3 Jy several thousand maser sources are detectable. The number of interstellar masers detectable down to $F_{OH} \geq 10$ mJy is therefore at least as large as that predicted for the stellar masers, yielding a total number of detectable masers in the Galactic plane of ≥ 20000.

3. The impact of OH maser surveys with SKA1

Adopting the specific luminosity distributions from Fig. 2 as representative for the stellar and interstellar maser luminosity distributions in the Galaxy, sensitivity limits for an SKA survey to detect a major part of these maser populations at different distances can be estimated. Adopting 3×10^{14} Watt Hz^{-1} (at 1612 MHz for stellar and 1665/1667 MHz for interstellar masers) as the lower limit for the maser population to study, and a detection threshold of S/N=10, sensitivity limits $F_{lim} = 4$, 1, and 0.1 mJy are required to probe the population at distances of 8, 16 and 50 kpc respectively. These correspond to the Galactic center, the anti-solar, and the Large Magellanic Cloud distances.

Most of the ground-state OH maser surveys undertaken in the Milky Way have been made with an angular resolution of typically 20 arcsec and GASKAP will deliver a similar resolution. A new SKA1 survey, with a resolving power 20 times that of GASKAP, will allow a direct comparison of the other side of the Galaxy, LMC & SMC stellar and interstellar maser populations at resolution roughly similar to Galactic surveys.

The 3 ground-states lines at 1612, 1665 and 1667 MHz are simultanously covered by Band 2 with SKA1-MID and SKA1-SUR and the 4^{th} OH ground-state line at 1720 MHz can be accessed with Band 3. While SKA1-SUR will offer an unprecedented survey speed, SKA1-MID, with a SEFD 4 times better than SKA1-SUR as well as an increase by a factor of 4 in the power of resolution (0.22 compared to 0.9 arcsec respectively), will be better suited for investigating the structure of the maser emission to the same resolution as e.g. eMERLIN. SKA1-MID Band 5 would offer the ability of accessing the 6-GHz excited-OH maser transitions, as well as the class-II 6.7-GHz methanol maser transition associated exclusively with the formation process of high-mass stars.

In the following sections, OH maser surveys rendered possible with SKA1-MID and SKA1-SUR capabilities are discussed. They are summarised in Table 1.

PoS(AASKA14)125

Table 1: SKA1 maser surveys

SKA1 Survey Name	Sensitivity (mJy)	Int. per[1] pointing (hours)	Coverage	Pointing Nb	Total[1,2] time (hours)	Aim
SUR–All-Sky	4	0.11	21000 deg^2	1300	143	All-Sky shallow survey
SUR–Shallow	1.0	1.75	$-60^\circ \leq l \leq +60^\circ$ $b \leq 4^\circ$	30	52.5	Anti-solar Galactic hemisphere maser pop.
SUR–Deep	0.3	19	$-60^\circ \leq l \leq +60^\circ$ $b \leq 4^\circ$	30	570	Seach for low luminosity pop.
SUR–LMC	0.1	175	11×10 deg^{2,3}	9	1575	LMC survey (3-sigma)
SUR–SMC	0.1	175	5.5×3.5 deg^{2,3}	4	700	SMC survey (3-sigma)
MID–MC	0.05	40		100	4000	LMC+SMC confirmation targeted survey (6-sigma)
MID–GAL	0.05	40	1 deg^2	4	160	Triangulum Survey

1: for a channel width of 5 kHz $\Leftrightarrow$ ∼0.9 km/s; $SEFD_{MID}$=1.7 (cf. Table 1 of SKA–TEL–SKO–DD–001 (Dewdney et al. 2013); corresponding to "combined": 190 antennas + Meerkat); $SEFD_{SUR}$=7.1

2: FOV_{MID}=0.5 deg^2; FOV_{SUR}=18 deg^2

3: from the NED (http://ned.ipac.caltech.edu/)

3.1 OH masers in the anti-solar Galactic hemisphere

To estimate the likely range of flux densities of stellar OH masers in the Milky Way located beyond the Galactic center (hereafter the anti-solar Galactic hemisphere), we used all stellar masers with kinematic distance estimates from EB14 with $D \cdot cos(l) \leq 8.0$ kpc, e.g., the population of stellar masers in the solar Galactic hemisphere. We assumed that the population in the anti-solar Galactic hemisphere is a mirror of the front part population and calculated their flux densities as if observed from the Sun. The result is shown in Fig. 3 (right panel), where the open bins represent the observed population and the shaded bins represent the predicted population in the anti-solar Galactic hemisphere. The bulk of the predicted population has flux densities between 10 and 500 mJy in good agreement with the maximum of the flux density distribution obtained from the prediction presented in Sect. 2.3. This population can be detected in ∼50 hours with SKA1-SUR (cf. SUR-Shallow in Table 1).

3.2 Low-luminosity masers

Surveys of increasing sensitivity in the Galaxy will not only extend the distances out to which masers will be detected, but will also extend the maser luminosity range towards lower levels than before. It is unknown whether the specific luminosities of masers have lower limits. A plausible assumption is that there is no such limit. A good illustration of this issue is the OH flaring Mira population (Etoka & Le Squeren 1997). *o* Ceti is an ideal example amongst these stars, as it shows absence of detectable OH maser emission for decades followed by long-lasting OH flaring events (Etoka et al. 2010a). The mean intensity of the OH flaring emission towards *o* Ceti is ∼2 Jy, corresponding to a luminosity of $\sim 2 \times 10^{12}$ Watt Hz^{-1}, which can be taken as a typical threshold for this type of stellar maser population. The dichotomy 'maser' and 'non-maser' O-rich AGB stars would then vanish with increasingly sensitive surveys. In addition, it seems also plausible that OH maser emission will be discovered in classes of objects, which do not, or rarely possess

PoS(AASKA14)125

high-luminosity masers. One example are Planetary Nebulae (PNe). There are only six sources in which the presence of (1612 MHz) OH maser emission has been confirmed (Uscanga et al. 2012). Another example is the so far unique detection of 1720-MHz maser emission from an evolved star (made towards the post-AGB star OH 9.097-0.392 by Sevenster & Chapman 2001). In post-AGB stars and PNe, the maser emission is probably related to shock-excitation in the interface between a fast post-AGB wind with a remnant slow AGB wind (Etoka et al. 2009). These excitation events might be short-lived, might lead to beamed emission or produce only low-luminosity maser emission. It seems likely, that new sensitive surveys will discover many new masers in stars already evolved away from the AGB, allowing us to study the bipolar outflows emerging in this phase in more detail. Towards SFRs, faint ground-state 1665/1667 MHz OH maser from young stars which will not ionize their environment has been found (e.g. the Turner-Welch object detected in the W3(OH) SFR complex by Argon, Reid & Menten 2003). A ∼140-hours survey over the complete sky accessible by SKA1-SUR (cf. SUR-All-Sky in Table 1) with a flux limit of 4 mJy will probe the presence of a population of low-luminosity masers (e.g. $L_{OH} < 3 \times 10^{14}$ W Hz^{-1}) among evolved stars and SFRs in the solar vicinity, which previous surveys have only investigated for higher luminosity masers. A deeper blind search for such low-luminosity masers in the inner Galactic disk could be achieved within ∼570 hours (cf. SUR-Deep in Table 1).

3.3 Galactic analog OH masers in galaxies of the Local Group

Late-type star evolution and the star formation process may differ in galaxies with other metallicity environments. The extension of the Galactic maser research to galaxies in the Local Group will provide another tool to study these differences. Due to their proximity, the Magellanic Clouds with their low-metallicity environment are the first galaxies to address.

Only a small number of maser sources with luminosities similar to their Galactic analogs are known outside the Milky Way. In the LMC, ten 1612-MHz OH masers with peak-flux densities 17-600 mJy are known in evolved stars (Marshall et al. 2004). These low-metallicity, high-mass LMC stars have contributed significantly to our understanding of the expansion velocities as indicators of metallicity. A few searches for ground-state OH maser of interstellar origin have been made in the 1980's and 1990's. A handful of 1665-MHz maser sources (sometimes accompanied with fainter 1667 MHz) have been detected towards the LMC (Brooks & Whiteoak 1997). A similar number of detections of 1720-MHz maser emission originating from SNRs have also been found towards the LMC (Brogan et al. 2004). Regarding the SMC, to date, OH masers have not been detected. Furthermore, maser emission of evolved-star origin has not been detected so far, and the number of maser sources of SFR origin detected is very low (in total 6 H_2O masers of SFR origin: Scalise & Braz 1982; Breen et al. 2013; also, the systematic survey done by Green et al. (2008) failed to detect any class II 6.7-GHz methanol masers).

With the sensitivities provided by SKA1, the options for maser research in the Magellanic Clouds may dramatically increase. To verify our ideas about Galactic structure evolution, it would be of great importance to compare the populations of stellar masers in the Galaxy with those in other galactic environments. Currently known stellar masers in the LMC were discovered by targeted searches towards luminous and mid-infrared bright sources. Their specific luminosities L_{OH} cover the range $15.50 < \log L_{OH} < 17.50$, which corresponds to the bright tail of the luminosity

PoS(AASKA14)125

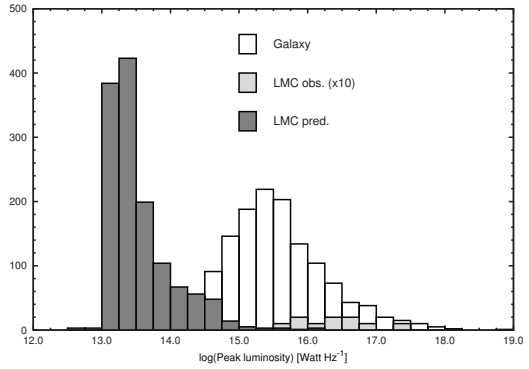

Figure 4: Predicted specific luminosity distribution for 1612-MHz OH masers in the LMC. The prediction is compared to the luminosities of the observed masers in the LMC (numbers are multiplied by 10) and the distribution of known masers in the Galaxy from the EB14 catalogue.

distribution in the Galaxy (cf. Fig. 4). An inventory of evolved stars in the LMC (~ 50 deg^2) and the SMC (~ 30 deg^2) has been provided by the SAGE-Spitzer survey (Meixner et al. 2006, Gordon et al. 2011) in the infrared. In the LMC, depending on the photometric classification according to chemistry, 20000–25000 of them are expected to be oxygen-rich (Riebel et al. 2012). For most stars, the dust mass-loss rates given by Riebel et al. are low ($\dot{M}_{dust} < 5 \times 10^{-10}\ M_{\odot}\ \mathrm{yr}^{-1}$) and their circumstellar shells do not qualify as OH maser hosts. To estimate the OH maser luminosities of the ~ 1300 stars with higher dust mass-loss rates we used the relation from Sect. 2.3 relating $\dot{M}_{dust}$ with 1612-MHz OH maser flux densities f_{OH}. Assuming $v_{exp} = 14$ km s^{-1} and D = 50 kpc, the luminosity distribution shown in Fig. 4 is obtained. The result indicates that most bright masers in the LMC are already known, and the luminosities of the masers to be discovered will be lower than that of the bulk of the known Galactic masers. The reason for this is the classification of almost all stars with high mass-loss rates ("extreme AGB stars") as C-stars by the SAGE-Spitzer survey. The validity of this photometric classification will be directly probed by an OH maser survey of the LMC covering the full AGB population.

As expected, the number of masers in Fig. 4 increases for lower luminosities, following the increase of the number of AGB stars with decreasing mass-loss rates. With a survey limit of 0.1 mJy and S/N=3, ≈ 200 new stellar 1612-MHz OH masers with $L_{OH} > 10^{14}$ Watt Hz^{-1} will be detected. These numbers should be seen as upper limits, if detection rates as in the Galaxy apply. On the other hand, more 1612-MHz OH masers might be found if there are more O-rich AGB stars among the "extreme AGB stars" than expected. Furthermore, since (preferentially main-line) masers are commonly present in the vicinity of Galactic YSOs, they are probably present around their LMC analogs. A mid-IR photometry search for high- and intermediate-mass YSOs in the LMC has been made by Gruendl & Chu (2009) yielding > 1000 sources. The number of OH masers detectable in the LMC with a 0.1 mJy survey limit is therefore well above 200.

The number of O-rich evolved stars qualifying as potential OH maser hosts in the SMC is >2000 (Boyer et al., 2011), about 10% of the LMC. Assuming, that the number of YSOs is also 10% of the corresponding number in the LMC, and allowing for the larger distance (D = 60 kpc), about two dozen new OH masers might be found, adopting the same survey limit as in the LMC. They will be the first ever detected in this galaxy. Both Magellanic Clouds can be surveyed in $\sim$2300 hours for the 0.1 mJy flux limit required (SUR-LMC, SUR-SMC in Table 1). Follow-up observations to improve the spatial resolution and the signal-to-noise ratio of the most interesting new discoveries are foreseen using SKA1-MID, adopting 100 pointings as a figure of merit (MID-

PoS(AASKA14)125

MC in Table 1).

The recent interest in the evolved stellar population and in the mass-loss and age-metallicity relation in the Sagittarius Dwarf Spheroidal (Lagadec et al. 2008 & 2009), located at only 25 kpc midway between the Galaxy and the LMC, has prompted searches for OH masers in this dwarf galaxy. However, the current sensitivity limits are barely sufficient to perform statistical comparisons with evolved stars in the Galaxy and other nearby different metallicity systems. Such studies clearly have to wait for SKA.

Triangulum (M33) is the third largest member of the local group, and with $\delta = 30.6^{\circ}$ is accessible with the SKA. Three H_2O masers are known in this galaxy (Brunthaler et al. 2006), while searches for methanol masers (Goldsmith et al. 2008) and OH masers (Fix & Mutel 1985; Baan, Haschick & Henkel 1992) have to date been unsuccessful. The limiting sensitivity of the OH observations was ≈ 15 mJy (5σ), which sets an upper limit of 1.5×10^{18} Watt Hz^{-1} on the luminosity of potential M33 OH masers, adopting a distance of ≈ 880 kpc. The non-detection of OH masers in previous observations is not surprising, as only a small number of Galactic OH masers have luminosities in excess of this limit. We expect however that the brightest interstellar and the bright stellar OH masers, with $L_{OH} > 5 \times 10^{15}$ Watt Hz^{-1}, among the more than 10 000 AGB stars identified by Cioni et al. (2008) in M33 will be detectable with a survey (MID-GAL in Table 1), having the same sensitivity to that proposed for the LMC+SMC follow-up observations.

The study of OH masers with SKA in galaxies beyond the Local Group will focus on OH megamaser emission. This emission is 10^8 times more luminous than Galactic analog OH masers, and is observed towards luminous and ultra-luminous infrared galaxies. These megamaser-hosting galaxies are either mergers or show evidence of interaction with other galaxies and are associated with a burst of star formation. Hence, megamasers are useful probes of the conditions where star formation is taking place in such galaxies as well as allowing extragalactic magnetic field measurements (McBride, Heiles & Elitzur 2013, Robishaw, Quartaert & Heiles 2008, cf. also Beswick et al. 2015 & Robishaw et al. 2015).

4. Survey applications

4.1 Polarisation & magnetic fields

OH masers, characterised by their spectral narrowness and their high sensitivity to magnetic fields, can be strongly polarised and commonly exhibit Zeeman splitting. Hence, they are a particularly useful tool for polarisation properties studies and retrieving the magnetic field structure and strength of the medium they are probing. They can be used for this purpose towards both evolved-stars (Amiri, Vlemmings & van Langevelde 2011; Etoka & Diamond 2010b) and SFRs (Caswell, Hutawarakorn & Reynolds 2011a,b; Asanok et al. 2010; Wright, Gray & Diamond 2004a,b; Hutawarakorn et al. 2002). Not only can the Zeeman splitting be used to explore the magnetic fields from individual objects, but also as a whole throughout the Milky Way and the galaxies of the Local Group (Green et al. 2012, cf. also Robishaw et al. 2015).

4.2 Stellar kinematics

Similar to SiO masers, a large variety of stellar populations host OH masers: evolved stars in

PoS(AASKA14)125

the Galactic thick disk, bulge, and globular clusters in the halo as well as young stellar clusters in the Galactic thin disk (Deguchi et al. 2004). A large sample of OH masers will reveal the velocity fields of these Galactic components. The high luminosity of the masers together with the radial velocity information provided, allow the study of the stellar kinematics in the various Galactic components (yielding for example evidence for a bar in the Milky Way: Habing et al. 2006). The information on the kinematics, supplemented with the age and metallicity of the stars, will point to common origins and clues for Galactic evolution models. These studies will be greatly enhanced by increasing numbers of southern sources.

4.3 VLBI & astrometry

Among evolved stars, OH/IR stars are sizeable objects of typically 10000 AU when mapped in the ground-state OH (Etoka & Diamond 2004, 2010b), and so are SFR complexes (Cohen et al. 2006). This typical size corresponds to 1.25 arcsec at 8 kpc and 0.2 arcsec at 50 kpc. With an achievable resolution of 0.22 arcsec, SKA-MID will be able to map a good fraction of the OH/IR stars and SFR complexes detected at Galactic-center distances and beyond, as well as the strongest and most extended objects in the LMC. To derive distances, VLBI-Astrometry (Vlemmings & van Langevelde 2007) or the "phase-lag technique" can be used (Engels et al. 2014). Since OH/IR stars can be found in all the Galactic components (cf. the previous subsection 4.2), as opposed to SFRs, and provided that the OH circumstellar shell is extended, the distances of these various components (and hence a better presentation of the galactic structure) can potentially be inferred using this method.

Admittedly, extended OH/IR stars can be significantly resolved out with baselines longer than 1000 km (Imai et al. 2013). Since the resolving power increases with frequency, higher frequency masers (i.e. in Band 5) in VLBI in-beam mode will allow high resolution astrometry and hence distance determinations with the possibility of a 3D mapping of the structure of our Galaxy but also that of the LMC and SMC (cf. Green et al. 2015).

4.4 SNR & the Galactic center circumnuclear Disk

Whereas the 1612-MHz OH masers are predominantly seen in circumstellar environments and the mainline 1665- and 1667-MHz OH masers are signposts for SFRs, the collisionally pumped 1720-MHz OH maser is typically seen as the only OH transition outlining shocked environments. Small shocks, like in the formation of massive stars and in post-AGB outflows are currently difficult to detect and thus limit our understanding of these stellar evolutionary phases. However, the more energetic shocks generated by SNRs plowing into dense (molecular) clouds are readily recognised by bright 1720-MHz maser emission observed at the interaction regions (Claussen et al. 1997, Frail et al. 1996). With more sensitive observations available, less bright masers appear and make it possible to probe shocks in different evolutionary stages of stars. The construction of 3-dimensional velocity models of expanding SNRs and of dynamical structures like the circumnuclear disk in the Galactic center will be possible (Sjouwerman & Pihlstrom 2008).

4.5 Synergy between HI and OH surveys

Recent studies have revealed weak extended HI shells around evolved stars (Libert, Gérard, & Le Bertre 2007). While GASKAP will be able to provide a catalogue of such shells, the SKA

PoS(AASKA14)125

higher angular resolution and sensitivity is needed for the study of these HI shells in greater detail. This will provide extra information on the mass-loss history and on the way stellar matter, enriched in elements produced in the stellar interior, is re-injected into the interstellar medium.

Since SFRs are converging and dispersing points of matter in the interstellar space, combining the OH maser distribution and the map of HI emission will provide a panoramic view of the life-cycle of matter in the Galaxy. GASKAP will pioneer this aspect through simultaneous surveys of OH and HI emission. SKA1 will allow a better correlation between OH masers and HI clumps by resolving the smaller structures of HI directly associated with the OH maser sources.

5. Prospects of research with the full SKA enhanced capabilities

Because of the complex non-linear nature of maser pumping, there is no simple means of inferring the physical conditions from observations from the maser intensity itself. Nonetheless, maser transitions are inverted for a range of physical conditions. Thus, combining various maser species and within the same species different transitions to study SFR regions is quite powerful as a probe of e.g. local density and temperature variations down to a few hundreds of AU (Etoka, Cohen & Gray 2005). Hence the combined information can give us access to the different physical components structure (i.e., outflows or disks) around a given YSO (Etoka, Gray & Fuller 2012).

As mentioned in section 3, Band 2, 3 & 5 will allow access to a wide range of maser transitions. Since different maser transitions have different sensivities, or dependencies on the physical conditions, the presence or absence of the various transitions is expected to change as the star formation region evolves. These relationships can only be determined through statistical population studies of the different maser transitions (e.g. Breen et al. 2010). The ability of the SKA and its pathfinder instruments to make rapid, sensitive surveys of the Galactic Plane will open up new opportunities to undertake such studies on scales which have not previously been possible.

OH masers are already known to be present towards a handful of PPNe-PNe in the Galaxy, but it could be that faint OH masers (e.g., from AGB OH-shell remnants) towards these objects have not been detected in previous surveys due to sensitivity. Similarly, excited OH maser has also been found towards a handful of evolved objects (Desmurs et al. 2010).

The sensitivity and frequency range covered by the full SKA, will allow us to increase the statistics on these “rare events” through a systematic survey, and identify when in the evolutionary stage this occurs and probe for other possible “new classes of masers”.

Acknowledgments

This Chapter is dedicated to the late Jim Caswell, whose review helped to improve the text considerably. His extensive and systematic research on masers in star-forming regions was invaluable to evaluate the prospects of SKA for maser research.

REFERENCES

Amiri N., Vlemmings W. & van Langevelde H.J., 2011, A&A, 532, 149
Argon A., Reid M.J. & Menten K.M., 2003, ApJ, 593, 925

PoS(AASKA14)125

Asanok K., Etoka S., Gray M.D. et al., 2010, MNRAS, 404, 120
Baan W.A., Haschick A. & Henkel C., 1992, AJ, 103,728
Beswick R., et al., 2015, "SKA studies of nearby galaxies: star-formation & accretion processes across all environments", in proceedings of "Advancing Astrophysics with the Square Kilometre Array", PoS(AASKA14)070
Boyer M., et al., 2011, AJ 142, 103
Breen S.L., Ellingsen S.P., Caswell J.L. & Lewis, B.E., 2010, MNRAS, 401, 2219
Breen S.L., Lovell J.E.J., Ellingsen S.P. et al., 2013, MNRAS, 432, 1382
Brogan C.L., Goss W.M., Lazendic J.S. & Green A.J., 2004, ApJ, 128, 700
Brooks K.J. & Whiteoak J.B., 1997, MNRAS, 291, 395
Brunthaler A., Henkel C., de Blok W.J.G. et al., 2006, A&A, 457, 109
Caswell J.L., Haynes R.F. & Goss M.W., 1980, Aust. J. Phys., 33, 639
Caswell J.L. & Haynes R.F. 1983a, Aust. J. Phys., 36, 361
Caswell J.L. & Haynes R.F. 1983b, Aust. J. Phys., 36, 417
Caswell J.L. & Haynes R.F. 1987, Aust. J. Phys., 40, 215
Caswell J.L., 1998, MNRAS, 439, 1680
Caswell J.L., Kramer B.-Hutawarakorn & Reynolds J.E., 2011a, MNRAS, 414, 1914
Caswell J.L., Kramer B.-Hutawarakorn & Reynolds J.E., 2011b, MNRAS, 415, 3872
Caswell J.L., Green J.A. & Phillips C.J., 2013, MNRAS, 431, 1180
Caswell J.L., Green J.A. & Phillips C.J., 2014, MNRAS, 439, 1680
Cioni M.-R.L., Irwin M., Ferguson A.M.N. et al. 2008, A&A, 487, 131
Cohen R.J., Gasiprong N., Meaburn J. & Graham M.F., 2006, MNRAS, 367, 541
Claussen M., et al. 1997, ApJ, 489, 143
Dawson J., et al., 2014, MNRAS, 439, 1596
Deguchi S., Fujii T., Glass, I. et al. 2004, PASJ, 56, 765
Desmurs J.-F., Baudry A., Sivagnanam P., Henkel C., Richards A.M.S.& Bains I., 2010, A&A, 520, A45
Dewdney P., Turner W., Millenaar R., McCool R., Lazio J., Cornwell T., 2013, "SKA1 System Baseline Design", Document number SKA–TEL–SKO–DD–001, Revision 1
Dickey, J., et al. 2013, PASA, 30, 3
Engels D. & Bunzel F., 2014, A&A, *submitted*; Database of Circumstellar Masers v2.4, http://www.hs.uni-hamburg.de/maserdb
Engels D., Etoka S., Gérard E. & Richards A.M.S., 2014, Proc. of the conference "Why galaxies care about AGB stars III", Eds. F.Kerschbaum, J. Hron & B. Wing *(in press)*
Etoka S. & Le Squeren A.M., 1997, A&A, 321, 877
Etoka S. & Diamond P.J., 2004, MNRAS, 348, 34
Etoka S., Cohen R.J. & Gray M.D., 2005, MNRAS, 360, 1162
Etoka S., Zijlstra A., Richards A.M., Matsuura M. & Lagadec E., 2009, ASPC, 404, 311
Etoka S., Gérard E., Richards A. et al., 2010a, evn conf, 6
Etoka S. & Diamond P.J., 2010b, MNRAS 406, 2218
Etoka S., Gray M.D. & Fuller G.A., 2012, MNRAS, 423, 647
Fix J.D. & Mutel R.L, 1985, AJ, 90, 736
Frail D., et al.1996, AJ, 111, 1651

PoS(AASKA14)125

Goedhart S., Gaylard M.J. & van der Walt D.J., 2004, MNRAS, 355, 553
Goldsmith P.F., Pandian J,D. & Deshpande A. A., 2008, ApJ, 680,1132
Gordon K., et al., 2011, AJ, 142, 102
Green J., et al. 2008, MNRAS, 385, 948
Green J.A., McClure-Griffiths N.M., Caswell J.L., Robishaw T.& Harvey-Smith L., 2012, MNRAS, 425, 2530
Green J., et al., 2015, "Maser Astrometry with VLBI and the SKA", in proceedings of "Advancing Astrophysics with the Square Kilometre Array", PoS(AASKA14)119
Groenewegen M., 2006, A&A, 448, 181
Gruendl R.A. & Chu Y.-H.,2009, ApJS, 184, 172
Habing H.J., Sevenster M.N., Messineo M., van de Ven G. & Kuijken K., 2006, A&A, 458, 151
Hutawarakorn B., Cohen R.J. & Brebner G.C., 2002, MNRAS, 330, 349
Imai H., Deguchi S., Nakashima J.-I., Kwok S., & Diamond P.J., 2013, ApJ, 773, 182
Jackson T., Ivezic Z. & Knapp G.R., 2002, MNRAS, 337, 749
Lagadec E., et al. 2008, MNRAS, 383, 399
Lagadec E., et al. 2009, MNRAS 396, 598
Lewis B.M., 1992, ApJ, 396, 251
Libert Y., Gérard E. & Le Bertre T., 2007, MNRAS, 380, 1161
McBride J., Heiles C. & Elitzur M., 2013, ApJ, 774, 35
Marshall J.R., van Loon J.T., Matsuura M. et al., 2004, MNRAS, 355, 1348
Meixner M., et al., 2006, AJ, 132, 2268
Riebel D., Srinivasan S., Sargent B. & Meixner M., 2012, ApJ, 753, 71
Robishaw T., Quartaert E. & Heiles C., 2008, ApJ, 680, 981
Robishaw T., et al., 2015, "Measuring Magnetic Fields Near and Far via the Zeeman Effect", in proceedings of "Advancing Astrophysics with the Square Kilometre Array", PoS(AASKA14)110
Scalise E. Jr. & Braz M.A., 1982, ApJ, 87, 528
Sevenster M.N. & Chapman J.M., 2001, ApJ, 546L, 119
Sevenster M.N., van Langevelde H.J., Moody R.A. et al., 2001, A&A, 366, 481
Sjouwerman L. & Pihlstrom Y., 2008, ApJ, 681, 1287
Uscanga L., Gómez J.F., Suárez O. & Miranda L.F., 2012, A&A, 547, A40
Vlemmings W.H.T. & van Langevelde H.J., 2007, A&A, 472, 547
Wright M.M., Gray M.D. & Diamond P.J., 2004a, MNRAS, 350, 1253
Wright M.M., Gray M.D. & Diamond P.J., 2004b, MNRAS, 350, 1272
Zijlstra A., et al., 1996, MNRAS, 279, 32

PoS(AASKA14)125

PROCEEDINGS OF SCIENCE

The ionised, radical and molecular Milky Way: spectroscopic surveys with the SKA

Mark Thompson[*1], **Henrik Beuther**[2], **Clive Dickinson**[3], **Joseph C. Mottram**[5] **Pamela Klaassen**[5,6] **Adam Ginsburg**[7] **Steve Longmore**[4] **Anthony Remijan**[8], **Karl Menten**[9]

[1] *University of Hertfordshire;* [2] *MPIA Heidelberg;* [3] *University of Manchester;* [4] *Liverpool John Moores University;* [5] *Leiden University;* [6] *UK Astronomy Technology Centre;* [7] *European Southern Observatory;* [8] *National Radio Astronomy Observatory;* [9] *MPIfR Bonn;*
E-mail: m.a.thompson at herts.ac.uk

The bandwith, sensitivity and sheer survey speed of the SKA offers unique potential for deep spectroscopic surveys of the Milky Way. Within the frequency bands available to the SKA lie many transitions that trace the ionised, radical and molecular components of the interstellar medium and which will revolutionise our understanding of many physical processes. In this chapter we describe the impact on our understanding of the Milky Way that can be achieved by spectroscopic SKA surveys, including "out of the box" early science with radio recombination lines, Phase 1 surveys of the molecular ISM using anomalous formaldehyde absorption, and full SKA surveys of ammonia inversion lines.

Advancing Astrophysics with the Square Kilometre Array
June 8-13, 2014
Giardini Naxos, Sicily, Italy

*Speaker.

PoS(AASKA14)126

1. Introduction

Over the last decade there has been a renaissance in multiwavelength surveys of the Milky Way, exploiting new facilities and instrumentation to conduct wide area surveys that are over an order of magnitude deeper and at much higher angular resolution than their predecessors. The combination of this wealth of survey data is beginning to revolutionise our understanding of the complex cycle that relates the interstellar medium (ISM) to star formation. Two factors play a part in the process: firstly the different wavelengths covered by each survey trace (very) different components of the ISM; and secondly the surveys have essentially close to matching angular resolution ($\sim$10–20$''$ over the bulk of their combined wavelength range.

Spectroscopic surveys are a key piece of the puzzle, as they trace the detailed kinematics of the ISM and reveal the complex 3-dimensional structure of the Milky Way, providing the crucial third dimension to continuum surveys. The extra complexity and depth required by spectroscopic surveys means that they are in general one "generation" behind the most recent corresponding continuum surveys. For example, the current state of the art in surveys of the atomic and molecular components of the ISM are the $\sim 1'$ resolution surveys of HI and CO (e.g. the International Galactic Plane Survey, the Galactic Ring Survey & the FCRAO Outer Galaxy Survey). By the time of the SKA these projects are likely to be superseded by higher resolution and more sensitive HI/CO surveys (with JVLA, ASKAP, MeerKAT, JCMT and possibly CCAT) that will match the resolution of the current far-infrared-millimetre wave continuum surveys.

However, there are a number of areas that will *not* be addressed by forthcoming spectroscopic surveys, where the sheer potential of the SKA in mapping faint radio-wavelength lines will play an important role across all the components of the ISM. As one of the principal raisons d'être of the SKA is radio spectroscopy, the compact $\sim$1 km cores of SKA1-MID and SKA1-SUR (leading to the $\sim$ 4 km core of the full SKA) are optimised for brightness temperature sensitivity. Combined with the relatively large FOV of the 15m dishes, this makes the SKA an incredibly powerful facility for wide area spectroscopic surveys of not just HI but all radio-wavelength lines. Within the wavelength ranges available in SKA Bands 1–5 there are many lines that trace multiple components of the ISM, including thousands of radio recombination lines (RRLs), several lines from light hydride radicals (OH and CH), the $^3He^+$ hyperfine line and the two anomalous absorption lines of o-H_2CO. These faint radio phenomena which were all discovered in the 1960s can be deployed as standard tools in the SKA era to study the ionised, radical and molecular components of the ISM in unprecedented detail.

In this chapter we will describe the ISM science that can be achieved with the SKA by mapping (classical) RRLs, hydride radical lines and anomalous absorption formaldehyde lines. These studies have tremendous scope for improving our understanding of a range of processes within the Milky Way, from accretion processes in massive star formation, stellar feedback into the ISM and the origin of the warm diffuse ionised ISM. We refer readers interested in HI, diffuse RRLs and OH masers to the chapters by McClure-Griffiths et al. (2015), Oonk et al. (2015) and Etoka et al. (2015) respectively. We will outline a series of strawman projects that could be accomplished by the SKA in "early science" mode, showing how the expanding capabilities of SKA1-MID and SKA1-SUR naturally lead to enhanced science capabilities. Finally we briefly dwell upon the potential that a fully frequency-capable SKA ($\nu \leq 24$ GHz) has for large area surveys of NH_3.

PoS(AASKA14)126

2. Radio Recombination lines: the kinematics of the ionised ISM

Radio recombination lines (RRLs) arise from atomic transitions between large principal quantum numbers (typically $n \geq 40$), where the small difference between energy levels means that the emitted photons are of radio wavelength. The usual convention to describe the transition $n+m \rightarrow n$ is $n\alpha$, $n\beta$, $n\gamma$... for $m = 1,2,3,\ldots$, hence α transitions (which are the most probable) correspond to a change in the quantum number of one. Despite the intrinsic faintness of their high quantum number transitions RRLs are one of the best tracers of astrophysical plasmas due to their well-understood physics (Gordon & Sorochenko 2002), their immunity to extinction (unlike the Balmer Hα or OIII fine structure lines) and the sheer line density of their spectra (many lines of H, He and C are found close together in frequency). From RRL measurements one can determine many physical properties of the ionised gas, e.g. temperature and electron density (Gordon & Sorochenko 2002; Brocklehurst & Seaton 1972), metallicity (Balser et al. 2001), the hardness of the illuminating UV spectrum (Roshi et al. 2012), and potentially magnetic field strengths from C RRL linewidths (Roshi 2007). By careful selection of various lines it is also possible to use RRLs to trace the kinematics of ionised gas from the extended low density medium to the densest parts of young compact HII regions and planetary nebulae.

The main limitation of current RRL studies is the tradeoff between brightness temperature sensitivity and angular resolution. Single dish studies like SIGGMA on Arecibo (Liu et al. 2013) and HIPASS on Parkes (Alves et al. 2012) offer mK sensitivity and trace electron densities down to $n_e \sim 10\,\mathrm{cm}^{-3}$ but with an angular resolution of several arcminutes. Interferometric surveys like the JVLA THOR survey (Bihr et al. 2013), which is mapping a 52° long strip of the northern Galactic Plane, reach angular resolutions of $10''$ but are only sensitive to ~ 1 K lines which corresponds to $n_e \gtrsim 1000\,\mathrm{cm}^{-3}$ (and moreover, only for the brightest nα lines). Obviously, single-dish apertures such as FAST are more suited to trace the truly extended diffuse medium, but the SKA has the unique potential for high resolution studies of the intermediate density gas ($n_e \sim 100\ \mathrm{cm}^{-3}$) at the interface between HII regions and the diffuse ionised interstellar medium. This would enable the morphology and kinematics of the HII region boundaries to be explored at comparable resolution to HI & CO observations, plus determine the spectrum of the escaping radiation via simultaneous detections of H and He RRLs.

The sheer sensitivity, broadband feeds and highly capable correlator make the SKA an ideal instrument to observe RRLs. The widths of the lines are a few 10s of $\mathrm{km\,s}^{-1}$, so they can be comfortably observed in the continuum mode of the SKA correlator. Coupled with the wide bandwidths and density of RRL spectra, this means that there are literally thousands of RRLs available to be observed in SKA1-MID and SUR Bands 1, 2 & 3 — falling to hundreds of lines in SKA1-MID Band 5. Secondly, for detection experiments the well understood physics governing the line frequencies (essentially the Rydberg equation) implies that the lines can easily be stacked to improve the signal to noise. As the line separations are fixed, adaptive stacking at different input V_{lsr} can be used to retrieve line detections even if the line of sight velocity of the gas is not initially known. The larger instantaneous bandwidths of SKA1-MID over SKA1-SUR make SKA1-MID competitive in mapping speed once line stacking is taken into consideration. Indeed, assuming that half the lines in the passband are free from RFI, a line-to-continuum ratio of 0.02 and channel width of $10\ \mathrm{km\,s}^{-1}$, SKA1-SUR and SKA1-MID have a stacked RRL spectroscopic survey speed for H$n\alpha$

PoS(AASKA14)126

lines that is within a factor 2 of the VLA (not JVLA!) *continuum* survey speed. It will be well within the capability of the Phase 1 SKA to perform spectroscopic RRL surveys that have the same sensitivity to ionised gas that present day surveys, e.g. the VLA Galactic Plane Survey (Stil et al. 2006), achieve in continuum.

Thirdly, the broadband feeds imply the simultaneous detection of multiple *n* and *m* lines from the same atomic species. This enables detailed radiative transfer models to be created that constrain the effects of stimulated emission and departures from LTE. In addition, multiple lines at different *n* values can be used to estimate the pressure broadening effects and determine the velocity and density structure of the ionised gas. Finally, the SKA will also observe RRLs from multiple atomic species, principally Helium and Carbon, as these lines are found within 2 MHz of corresponding H RRLs. Helium lines are typically $\sim$8 percent of the brightness of Hydrogen RRLs, but are valuable tracers of both the metallicity of the ionised gas (e.g. Balser et al. (2001)) and the hardness of the illuminating UV spectrum (Roshi et al. 2012). More than 90% of the observed ^{4}He in the ISM of the Milky Way was produced via primordial nucleosynthesis (Wilson & Rood 1994). Observations of He RRLs at high angular resolution are a unique window into this process, allowing the excitation and total abundance to be properly modelled. Carbon RRLs are produced in the PDRs surrounding HII regions and so these lines are a valuable tracer of the physical conditions in this gas, particularly when combined with observations of the 158 μm CII line (Natta et al. 1994). Their line brightnesses are typically $\sim$30% of H RRLs. The non-thermal linewidths of C RRLs may also allow magnetic field strengths to be measured (Roshi 2007).

3. Anomalous formaldehyde absorption: tracing the volume density of H_2 via silhouettes on the CMB

The lowest two transitions of ortho formaldehyde (at 4.8 and 14.4 GHz) have a curious property, in that collisional excitation of these transitions drives an "anti-inversion" which cools the lines with respect to the CMB temperature. The transitions can then absorb CMB photons and appear in absorption against the CMB. This phenomenon is known as anomalous absorption and was first observed by Palmer et al. (1969) and theoretically explained by Townes & Cheung (1969). Anomalous formaldehyde absorption is an incredibly useful tool for studying molecular clouds. As the illuminating source is isotropic and fills the Universe, anomalous absorption is distance-independent and wholly dependent on the number of absorbing molecules. Moreover, the ratio of the 4.8 and 14.4 GHz lines is highly sensitive to the H_2 *volume density* (Mangum et al. 2008; Ginsburg et al. 2011), making the combination of these transitions an effective molecular densitometer analogous with the molecular thermometer of the 218 GHz para formaldehyde K-doublet. This densitometer is unaffected by the sub-thermal excitation, line trapping or optical depth effects that plague CO observations, allowing the H_2 mass of the absorbing source to be determined within 0.3 dex. So with sufficient sensitivity and angular resolution (to couple the synthesised beam to the absorbing source) one can use anomalous absorption to accurately measure the density and mass of molecular gas clouds from the Milky Way (Ginsburg et al. 2011) to local galaxies (Mangum et al. 2008) and beyond to the high-redshift Universe (Zeiger & Darling 2010; Darling & Zeiger 2012).

However, these absorption lines are faint and narrow, and thus require long integration times to adequately detect. This means that they cannot currently be used in wide area surveys — unlike

PoS(AASKA14)126

the bright CO rotational transitions which have been widely used to map molecular emission in the Milky Way. For example, to detect the absorption lines from Galactic clouds requires a sensitivity of $\sim$0.1 K, which takes at least a full 12-hour track with the VLA (Evans et al. 1987). But with SKA1-MID it will become possible to detect these lines in only 1–2 hours (and minutes with the SKA) making it feasible to survey the Milky Way's molecular clouds at much better angular resolution than existing single-dish CO surveys, and with none of the excitation or optical depth issues that affect CO surveys. In addition to anomalous absorption, a wide area SKA survey will also observe "non-anomalous" absorption against hundreds to thousands of bright continuum sources within and without the Milky Way (e.g. radio galaxies and HII regions). Many of the compact HII regions will have accurately measured trigonometric parallaxes from associated maser sources (see the chapter by Green et al. 2015). This offers the potential to conduct 3D tomography of the molecular ISM by using a network of hundreds of known illuminating sources with well-characterised heliocentric distances.

It must be stressed that the current SKA baseline design for SKA1-MID Band 5 does not cover the 14.4 GHz H_2CO line, but a modest extension to the upper frequency limit of Band 5 from 13.8 GHz to 14.4 GHz would enable the line ratios to be measured and *uniquely* permit molecular gas volume densities to be determined across the Milky Way and beyond.

4. Hydride radicals: thermal OH and CH

Here we discuss thermal emission from the two main hydride radical species in the SKA bands: OH at 1.7 GHz in SKA1-MID band 2 (band 3 in SKA1-SUR) and the 0.7 & 3.3 GHz CH lines in SKA1-MID bands 1 and 4 (band 3 in SKA1-SUR). There are a number of current OH surveys, the single-dish SPLASH in the Southern Hemisphere (Dawson et al. 2014) and the interferometric THOR survey in the Northern Hemisphere (Bihr et al. 2013), with a planned deeper ASKAP survey (GASKAP: Dickey et al. (2013)). Thermal emission from OH is often overlooked in favour of the much brighter non-thermal OH masers (see the Chapter by Etoka et al. 2015)) — nevertheless as OH has a largely constant abundance across diffuse and translucent molecular clouds, has four closely spaced transitions, and is thermalised even at low densities ($n_{\rm crit} \leq 4$ cm^{-3}) this molecule is a useful tracer of the temperature and density of the neutral ISM. Thermal OH may even allow the detection of CO-dark gas hinted at by gamma ray emission (e.g. Abdo et al. 2010), *Herschel* CII observations (Langer et al. 2014) and single-dish OH pencil beam studies (Allen et al. 2012). Again, the SKA will bring the benefit of its brightness temperature sensitivity to the study of thermal OH, reaching and order of magnitude greater sensitivity and spatial resolution over GASKAP.

CH was one of the first molecular radicals detected in the interstellar medium via optical absorption spectroscopy, and is a very good tracer of H_2 column density in UV-dominated regions (Sheffer et al. 2008) and the diffuse ISM (Qin et al. 2010). The 0.7 and 3.3 GHz lines available to the SKA have also been postulated to be a sensitive probe of changes in fundamental constants, although as these lines are subject to non-LTE effects caution must be taken to model the lines carefully, possibly also using higher frequency data from *Herschel* or SOFIA. The SKA enables wide area and sensitive surveys of CH, and in combination with OH and H_2CO anomalous absorp-

PoS(AASKA14)126

tion allows the entire dynamic range of the molecular ISM to be traced from PDRs, to diffuse and dense H_2 clouds.

5. Potential SKA spectroscopic surveys

In this section we describe potential RRL survey projects that the SKA could carry out, paying particular attention to the science outcomes that are enabled by the different components of the SKA and the possibilities for Early Science.

In the following we concentrate on SKA1-MID and -SUR Band 2 and SKA1-MID Band 5, as these offer the greatest potential for studies of the diffuse and dense ionised ISM, hydrides and anomalous formaldehyde absorption, but as mentioned earlier there are many RRLs present in the other SKA bands that could be part of commensal studies. In the following calculations we have assumed the noise and imaging performance values for the Baseline Design of SKA1-MID and SKA1-SUR (Dewdney et al. 2013) given in the SKA1 Imaging Science Performance memo (Braun 2014). We have also conservatively assumed that in SKA1-MID and -SUR Band 2 we will be able to stack 25 RRLs using the 1 GHz bandwidth of SKA1-MID and 12 RRLs using the 500 MHz bandwidth of SKA1-SUR. Thus, in a 1 hour integration SKA1-MID is able to reach an rms flux of 106 μJy per 10 km s^{-1} channel, which translates into a stacked RRL sensitivity for α lines of 21 μJy per 10 km s^{-1} channel. Similarly SKA1-SUR is able to achieve rms fluxes of 430 μJy and 124 μJy per 10 km s^{-1} channel in unstacked and stacked data respectively. Comparing these values to the relative fields-of-view of SKA1-MID and SKA1-SUR, it can be seen that SKA1-MID is highly competitive for RRL mapping over small areas in Band 2 due to its larger instantaneous bandwidth and low SEFD, although SKA1-SUR has a faster mapping speed over areas larger than a single PAF tile.

5.1 Early Science: the structure and kinematics of the most luminous HII regions and their impact on the ISM

The most luminous HII region complexes in the Milky Way have been identified using a combination of WMAP, Spitzer and MSX data by Murray & Rahman (2010). The 18 most luminous of these complexes are responsible for just over half the total Galactic ionising flux, and it is thought to be the UV photons "leaking" from the HII region complexes that are responsible for the diffuse warm ionised medium (e.g. Liu et al. 2013)). This hypothesis is supported by wide area RRL mapping at $\sim$15$'$ resolution (Alves et al. 2012) which finds that the distribution of the diffuse medium is correlated with HII regions. However, constraints on the ionising spectrum from He RRLs are not fully consistent with this hypothesis (Roshi et al. 2012). Thus higher resolution observations of H RRLs and more sensitive observations to detect He RRLs are required. A better theoretical understanding of the interplay between HII region boundaries and the diffuse surrounding medium would also complement further observations, particularly at the smaller physical scales available to the SKA.

The SKA has the unique potential for deep, high resolution studies of the intermediate density gas ($n_e \sim 100$ cm^{-3}) at the interface between HII regions and the diffuse medium. This would enable the morphology and kinematics of the HII region boundaries to be explored at comparable resolution to HI & CO observations, plus determine the spectrum of the escaping radiation via

PoS(AASKA14)126

simultaneous detections of H and He RRLs. Additionally, as the RRLs in SKA1-MID and -SUR Band 2 do not become appreciably pressure broadened until electron densities reach $n_e \simeq 1400$ cm^{-3}, it will also be possible to produce velocity-resolved maps of the electron density (strictly n_e^2) and temperature of the ionised gas within all but the densest parts of the giant HII complexes. A detailed picture of the density distribution and kinematics of HII regions is needed to understand their evolution — in particular the relative role of radiation pressure and stellar winds, which has serious implications for the interpretation of galaxy population synthesis models (Verdolini et al. 2013).

To detect H RRL emission from gas with n_e a few 100 cm^{-3} requires a brightness temperature sensitivity of ~ 0.1 K, integrating over a 30 km s^{-1} line and assuming a 1 pc column (Alves et al. 2012). With Early Science SEFDs of 14.2 Jy for SKA1-SUR and 3.4 Jy for SKA1-MID it is possible to achieve this sensitivity over a 30″ beam on the order of 50 hours and 4 hours integration time respectively. By stacking the He$n\alpha$ and C$n\alpha$ lines it will be possible to achieve a detection to the same (or slightly deeper) gas densities as the (unstacked) Hydrogen lines. By further stacking the Hydrogen lines it is possible to reach densities as low as 50 cm^{-3} in the same integration times. These observations will reveal the full gamut of α, β, γ lines at higher densities, probing deeper into the HII regions and allowing finer velocity and spatial resolution (as the RRL brightness temperatures go as n_e^2) to study the distribution and kinematics of the ionised gas on smaller spatial and velocity scales.

A project to map most of the Murray & Rahman complexes is eminently feasible in SKA Early Science, taking of the order of 200 hours to map the top 10 most luminous complexes (small complexes with MID and larger ones with SUR). These observations can be done "out of the box" at the workhorse SKA1-MID and -SUR Band 2 frequencies without the need to commission spectral zoom modes, effectively demonstrating the potential of the SKA for deeper and wider line surveys.

5.2 SKA Phase 1: Galactic Plane surveys in Bands 2 and 5

With Phase 1 capability it becomes feasible to extend the Early Science Band 2 studies into a much deeper full Galactic Plane Survey for recombination lines. A Band 2 RRL and thermal OH survey of the Galactic Plane can be carried out commensally with the HI survey described in the chapter by McClure-Griffiths et al. (2015) — rendering simultaneous maps of the atomic, ionised and molecular radical ISM in breathtaking detail. If we assume a survey of adjoining 4° wide SKA1-SUR tiles along the Galactic Plane and a nominal dwell time of 50 hours per tile (see McClure-Griffiths et al. 2015) then a survey of the full Galactic Plane visible to SKA would take on the order of $\sim$ 2000 hours. With 50 hours per tile and an SEFD of 7.1 Jy for SKA1-SUR it would be possible to reach electron densities of $\sim$70 cm^{-3} for H lines without line stacking and 40 cm^{-3} with line stacking.

It is worth noting that the stacked RRL spectral datacube would allow H RRL emission to be detected to twice as deep a continuum depth as the 1.4 GHz International Galactic Plane Survey (assuming a line-to-continuum ratio of 0.02). Such a survey would allow the creation of a detailed position-velocity map of the ionised ISM, separating the synchrotron contribution from that of the free-free emission. The RRL Galactic Plane survey will result in two main products: a continuum map from line-free channels (which will have approximately 1.5 μJy rms, assuming a 300 MHz continuum bandwidth) and RRL spectral datacubes for individual and stacked lines. By combining

PoS(AASKA14)126

these two maps the synchrotron contribution to the continuum can be determined (e.g. (Alves et al. 2012)), resulting in a position-velocity map of the free-free emission that matches the resolution of atomic, molecular and dust surveys. In addition to HII regions, many Planetary Nebulae (PNe) would be revealed. PNe have been mainly overlooked in existing RRL surveys due to the limited angular resolution and resulting beam dilution. RRL observations offer a novel means of determining the distance to the Planetary Nebulae via the determination of their expansion rate (e.g. Gomez et al. 1989; Gulyaev 2003)). Multiple RRLs observed simultaneously will be the key to disentangling pressure broadening effects from the observed lines, which is one of the reasons why this approach has not been more commonly used.

The main aim of a Band 5 SKA1-MID survey would be to map the molecular ISM of the Milky Way using anomalous formaldehyde absorption but, as in the Band 2 survey described above, significant additional benefits can also be obtained simultaneously. The 2×2.5 GHz bandwidth in Band 5 allows the simultaneous detection of 75 H$n\alpha$, He$n\alpha$ and C$n\alpha$ RRLs. These lines are not appreciably pressure broadened until $n_e \sim 10^5$ cm^{-3} and so they can be used to study the kinematics of compact HII regions and young dense PNe. As yet unexplained highly turbulent motions are observed towards a number of compact and ultracompact HII regions (Keto et al. 2008), which may be due to trapping of ionised accretion flows (Galván-Madrid et al. 2011) or ionised outflows (Klaassen et al. 2013). The ^{3}He$^+$ hyperfine line also lies within Band 5 at a rest frequency of 8.7 GHz. A large survey of HII regions and PNe in this line would enable constraints to be placed on the primordial abundance of ^{3}He via Big Bang nucleosynthesis (Bania et al. 2007) and perhaps provide a solution to the "^{3}He problem" (Guzman-Ramirez et al. 2013). Moreover, a survey to the depth required to detect anomalous absorption would also result in a very deep 5 GHz continuum survey ($\sim 0.4\ \mu$Jy), which would revolutionise the study of radio stars in the Milky Way (see the chapter by Umana et al. 2015).

The necessary sensitivity for an anomalous absorption survey is ∼0.1–0.2 K rms over a channel width of 0.1 km s^{-1} (required to detect the narrow H_2CO lines. With SKA1-MID it is possible to reach this sensitivity over a 15″ beam in on the order of 1 hour integration time, which implies a roughly 100 deg^2 survey could be achieved in 1000 hours at 4.8 GHz. To enable the H_2 volume density to be determined requires further observations of the 14.4 GHz line and the most efficient way to achieve these would be targeted followups of regions where 4.8 GHz absorption is observed. These observations would also map out the high frequency RRL emission around these regions. These followups would take on the order of 500 hours to complete, leading to a total survey time of ∼1500 hours. Without the followup of the 14.4 GHz H_2CO line, the 4.8 GHz observations can only constrain the H_2CO column density rather than the H_2 volume density , hence the extension of SKA1-MID Band 5 to higher frequency is crucial to add this important capability. This project would lead to the most comprehensive map of the molecular gas in the southern Milky Way to date, with uniform sensitivity to gas from volume densities $n(H_2)$ of $10^{2.5}$–10^6 cm^{-3} and accuracy of ∼0.3 dex.

5.3 The full SKA

With the deployment of the full SKA it will become possible to conduct wide-area maps of RRLs from ionised gas of below 50 cm^{-3}, routinely detecting transitions from $n\alpha$, β and γ transitions from H, He and C. The deployment of frequency bands up to 25 GHz will permit lines

PoS(AASKA14)126

up to H64α to be observed, which extend the gas densities that can be traced up to 10^6 cm^{-3} and allow the study of the bulk of ionised jets and winds from low mass and high mass stars (Hoare 2004). There is particular synergy here with ALMA studies of higher frequency millimetre-wave recombination lines and SKA2 observations of 10–25 GHz lines. Millimetre wave RRLs are more subject to non-LTE effects than microwave lines and the comparison of their velocity resolved spectra can illustrate inflow and outflow within optically thick ultra and hyper-compact HII regions (Peters et al. 2012). Only the SKA will have the surface brightness sensitivity to match ALMA high resolution observations.

In addition, the 24 GHz inversion transitions of ammonia (including both $^{14}NH_3$ and $^{15}NH_3$ isotopologues) will also become available. Using the antennas from the 4 km compact core would permit a deep Galactic Plane survey of ammonia to be carried out at $\sim 2''$ resolution, i.e. comparable to ALMA Bands 6/7 in compact configuration. Ammonia is a molecular thermometer *par excellence*, and there are tremendous synergies between ALMA molecular observations and the accurate kinetic temperatures that would result from wide area SKA surveys. The sensitivity of the full SKA implies that to detect NH_3 lines of a few 0.1 K brightness temperature would take on the order of five minutes per pointing. Although the primary beam at 24 GHz is only 0.08 deg^2, such a short integration time implies a survey speed of ~ 1 deg^2 hr^{-1}, making it feasible to carry out a $2''$ resolution survey of the Galactic Plane in only a few hundred hours.

References

Abdo, A. A., Ackermann, M., Ajello, M., et al. 2010, ApJ, 710, 133

Allen, R. J., Ivette Rodríguez, M., Black, J. H., & Booth, R. S. 2012, AJ, 143, 97

Alves, M. I. R., Davies, R. D., Dickinson, C., et al. 2012, MNRAS, 422, 2429

Balser, D. S., Goss, W. M., & De Pree, C. G. 2001, AJ, 121, 371

Bania, T. M., Rood, R. T., & Balser, D. S. 2007, SSRv, 130, 53

Bihr, S., Beuther, H., Johnston, K., et al. 2013, in Protostars and Planets VI Posters, 50

Braun, R. 2014, "SKA1 Imaging Performance", Document number SKA-TEL-SKO-DD-XXX Revision A Draft 2

Brocklehurst, M., & Seaton, M. J. 1972, MNRAS, 157, 179

Darling, J., & Zeiger, B. 2012, ApJL, 749, L33

Dawson, J. R., Walsh, A. J., Jones, P. A., et al. 2014, MNRAS, 439, 1596

Dewdney, P., Turner, W., Millenaar, R., et al. 2013, “SKA1 System Baseline Design", Document number SKA-TEL-SKO-DD-001 Revision 1

Dickey, J. M., McClure-Griffiths, N., Gibson, S. J., et al. 2013, PASA, 30, 3

Etoka, S., et al. 2015, “OH masers in the Milky Way and Local Group galaxies in the SKA era”, in proceedings of “Advancing Astrophysics with the Square Kilometre Array", PoS(AASKA14)119

Evans, II, N. J., Kutner, M. L., & Mundy, L. G. 1987, ApJ, 323, 145

Galván-Madrid, R., Peters, T., Keto, E. R., et al. 2011, MNRAS, 416, 1033

Ginsburg, A., Darling, J., Battersby, C., Zeiger, B., & Bally, J. 2011, ApJ, 736, 149

Gomez, Y., Rodriguez, L. F., Moran, J. M., & Garay, G. 1989, ApJ, 345, 862

PoS(AASKA14)126

Gordon, M. A., & Sorochenko, R. L., eds. 2002, Astrophysics and Space Science Library, Vol. 282, Radio Recombination Lines. Their Physics and Astronomical Applications

Green, J., et al. 2015, “Maser Astrometry with VLBI and the SKA”, in proceedings of “Advancing Astrophysics with the Square Kilometre Array", PoS(AASKA14)125

Gulyaev, S. 2003, in IAU Symposium, Vol. 209, Planetary Nebulae: Their Evolution and Role in the Universe, ed. S. Kwok, M. Dopita, & R. Sutherland, 533

Guzman-Ramirez, L., Pineda, J. E., Zijlstra, A. A., Stancliffe, R., & Karakas, A. 2013, MNRAS, 432, 793

Hoare, M. G. 2004, New Astronomy Reviews, 48, 1327

Keto, E., Zhang, Q., & Kurtz, S. 2008, ApJ, 672, 423

Klaassen, P. D., Galván-Madrid, R., Peters, T., Longmore, S. N., & Maercker, M. 2013, A&A, 556, A107

Langer, W. D., Velusamy, T., Pineda, J. L., Willacy, K., & Goldsmith, P. F. 2014, A&A, 561, A122

Liu, B., McIntyre, T., Terzian, Y., et al. 2013, AJ, 146, 80

Mangum, J. G., Darling, J., Menten, K. M., & Henkel, C. 2008, ApJ, 673, 832

McClure-Griffiths, N. M., et al. 2015, “Galactic and Magellanic Evolution with the SKA”, in proceedings of “Advancing Astrophysics with the Square Kilometre Array", PoS(AASKA14)130

Murray, N., & Rahman, M. 2010, ApJ, 709, 424

Natta, A., Walmsley, C. M., & Tielens, A. G. G. M. 1994, ApJ, 428, 209

Oonk, R., et al. 2015, “The Physics of the Cold Neutral Medium: Low-frequency Radio Recombination Lines with the Square Kilometre Array”, in proceedings of “Advancing Astrophysics with the Square Kilometre Array", PoS(AASKA14)139

Palmer, P., Zuckerman, B., Buhl, D., & Snyder, L. E. 1969, ApJL, 156, L147

Peters, T., Longmore, S. N., & Dullemond, C. P. 2012, MNRAS, 425, 2352

Qin, S.-L., Schilke, P., Comito, C., et al. 2010, A&A, 521, L14

Roshi, D. A. 2007, ApJL, 658, L41

Roshi, D. A., Plunkett, A., Rosero, V., & Vaddi, S. 2012, ApJ, 749, 49

Sheffer, Y., Rogers, M., Federman, S. R., et al. 2008, ApJ, 687, 1075

Stil, J. M., Taylor, A. R., Dickey, J. M., et al. 2006, AJ, 132, 1158

Townes, C. H., & Cheung, A. C. 1969, ApJL, 157, L103

Umana, G., et al. 2015, “The impact of SKA on Galactic Radioastronomy: continuum observations”, in proceedings of “Advancing Astrophysics with the Square Kilometre Array", PoS(AASKA14)118

Verdolini, S., Yeh, S. C. C., Krumholz, M. R., Matzner, C. D., & Tielens, A. G. G. M. 2013, ApJ, 769, 12

Wilson, T. L., & Rood, R. 1994, ARA&A, 32, 191

Zeiger, B., & Darling, J. 2010, ApJ, 709, 386

PoS(AASKA14)126

PROCEEDINGS OF SCIENCE

Tomography of Galactic star-forming regions and spiral arms with the Square Kilometre Array

Laurent Loinard[1], **Mark Thompson**[2], **Melvin Hoare**[3], **Huib Jan van Langevelde**[4], **Simon Ellingsen**[5], **Andreas Brunthaler**[6], **Jan Forbrich**[7], **Kazi L.J. Rygl**[8], **Luis F. Rodríguez**[1], **Amy J. Mioduszewski**[9], **Rosa M. Torres-López**[10], **Sergio A. Dzib**[6], **Gisela N. Ortiz-León**[1], **Tyler L. Bourke**[11], **James A. Green**[11]

[1]*CRyA-UNAM Morelia* [2]*University of Hertfordshire* [3]*Leeds University* [4]*JIVE/Sterrewacht Leiden* [5]*University of Tasmania* [6]*MPIfR Bonn* [7]*University of Vienna* [8]*ESA-ESTEC Noordwijk* [9]*NRAO Socorro* [10]*Universidad de Guadalajara* [11]*SKA Organisation*
E-mail: l.loinard@crya.unam.mx

Very Long Baseline Interferometry (VLBI) at radio wavelengths can provide astrometry accurate to 10 micro-arcseconds or better (i.e. better than the target GAIA accuracy) without being limited by dust obscuration. This means that unlike GAIA, VLBI can be applied to star-forming regions independently of their internal and line-of-sight extinction. Low-mass young stellar objects (particularly T Tauri stars) are often non-thermal compact radio emitters, ideal for astrometric VLBI radio continuum experiments. Existing observations for nearby regions (e.g. Taurus, Ophiuchus, or Orion) demonstrate that VLBI astrometry of such active T Tauri stars enables the reconstruction of both the regions' 3D structure (through parallax measurements) and their internal kinematics (through proper motions, combined with radial velocities). The extraordinary sensitivity of the SKA telescope will enable similar *tomographic mappings* to be extended to regions located several kpc from Earth, in particular to nearby spiral arm segments. This will have important implications for Galactic science, galactic dynamics and spiral structure theories.

Advancing Astrophysics with the Square Kilometre Array,
June 8-13, 2014
Giardini Naxos, Sicily, Italy

PoS(AASKA14)166

1. Introduction

Very Long Baseline Interferometry at radio frequencies (e.g. Thompson et al. 2007) can readily provide astrometric accuracies of order 10 micro-arcseconds (μas) or better, for compact radio sources of sufficient brightness ($T_b \approx 10^7$ K). This enables the determination of trigonometric parallaxes with an accuracy of a few percent for any source within a few kpc (for instance, a 10 μas astrometric accuracy translates to a 2% parallax accuracy at 2 kpc). Similarly, proper motions can be measured to an accuracy of 0.2 km s^{-1} in one year at a distance of 2 kpc. As a consequence, **radio VLBI measurements have the potential to provide distances accurate to better than a few percent, and tangential velocities accurate to better than a few tenths of a km s^{-1} for any source within a few kpc** (Reid & Honma 2014). The GAIA space mission is expected to deliver similar results, and will do so for many millions of stars (de Bruijne 2012). However, radio VLBI observations have the distinct advantage that they are not affected by dust extinction. Thus, they can be used to complement GAIA for sources that are either deeply embedded within dusty regions, or located behind a large column of line-of-sight dust (or both). Star-forming regions are clearly in this situation, and are therefore prime targets for VLBI astrometric observations.

The astrometric potential of radio VLBI observations can only be realized if the intended targets are detectable. As mentioned earlier, this requires the brightness temperature to be of order 10^7 K (Thompson et al. 2007), and effectively restricts the pool of potential targets to non-thermal emitters.[1] In star-forming regions, there are two classes of sources that meet the brightness criteria: masers and chromospherically active young stars. Masers (hydroxyl, water, methanol, and to a lesser extent silicon monoxide) are commonly found in high-mass star-forming regions (Bartkiewicz & van Langevelde 2012) and can be extremely bright. This makes them ideal tracers to map the distribution of high-mass star-forming regions across the Milky Way (Reid et al. 2014; Green et al. 2015). Chromospherically active young stars, on the other hand, are often radio sources thanks to the gyration of relativistic electrons in their strong surface magnetic fields (Dulk 1985). This results in continuum cyclotron, gyrosynchrotron, or synchrotron emission depending on the energy of the gyrating electrons. This emission is normally confined to regions extending only a few stellar radii around the stars, and therefore remains very compact even in the nearest star-forming regions (4 $R_\odot \equiv 50$ μas at 300 pc). We note that for this mechanism to operate, a strong magnetic field (kGauss) must exist, and this normally requires the dynamo process to operate within the young star. This, in turns, requires the star to be convective, so only **low-mass** young stars are expected non-thermal radio emitters. There are, however, some exceptions to this rule (Loinard et al. 2008; Dzib et al. 2010).

Since masers and magnetically active low-mass young stars can both be used for VLBI astrometric observations, it is useful to consider their relative merits. Masers are typically much brighter and can therefore be detected much farther than magnetically active young stars. On the other hand, active young stars are much more ubiquitous. First, they do exist in regions of low, intermediate, and high-mass star formation, whereas bright, steady masers are largely restricted to high-mass regions. A limited number of masers have been identified in association with low-mass stars but they are typically of lower luminosity (Kalenskii et al. 2010) than those found toward high-mass star formation regions. Second, tens or hundreds of magnetically active low-mass young stars might

[1] For instance, a compact HII region with a brightness temperature of order 10^4 K is undetectable with a VLBI array.

PoS(AASKA14)166

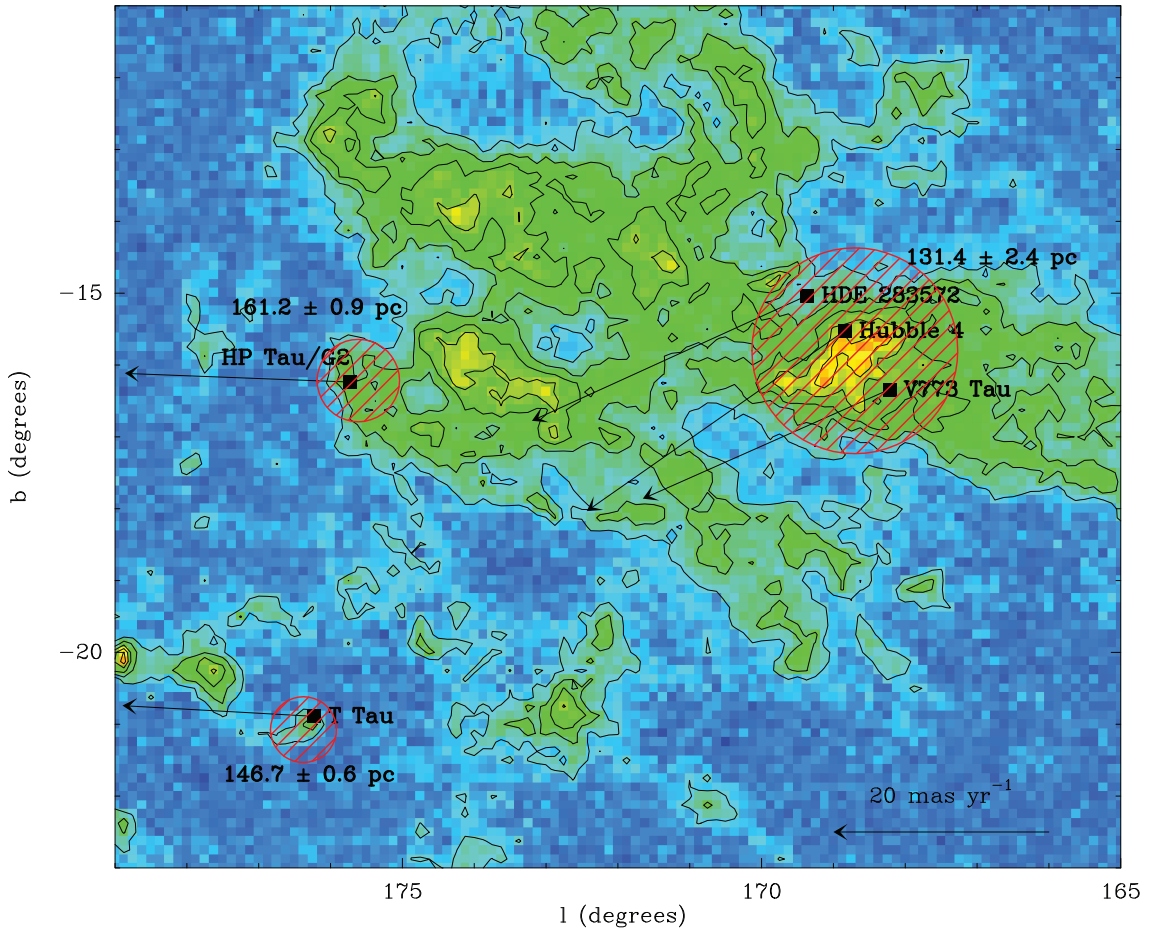

Figure 1: Positions, distances, and proper motions of Hubble 4, HDE 283572, V773 Tau, T Tau, and HP Tau/G2 superposed on the CO(1-0) map of Taurus from Dame et al. (2001). Adapted from Loinard et al. (2007); Torres et al. (2007, 2009, 2012).

be present in a high-mass star-forming region where only a few strong maser spots exist. For instance, only a few maser sources are known in the Orion region (Gaume et al. 1998) where we have recently detected well over 50 magnetically active young stars in moderately deep VLBA observations (M. Kounkel et al., in preparation). A very interesting application of this ubiquity is that distances and proper motions can be measured to stars distributed across a given region, and the three-dimensional structure and kinematics of the region can be reconstructed. This has recently be exemplified in the case of the Taurus star-forming region (Torres et al. 2007, 2009, 2012) thanks to multi-source VLBA observations. As Figure 1 shows, the young stars located to the west of the Taurus regions are at a common distance of 130 pc, and share similar proper motions. Measurements from the literature show that they also have similar radial velocities. The stars to the east and south of the complex, on the other hand, are significantly farther (145-160 pc) and have different proper motions and radial velocities. Although based on a very limited number of targets, this example demonstrates that multi-source VLBI observations enable *tomographic mappings* of individual star-forming regions. In this contribution, we build the case for extending such observations using VLBI with the SKA to regions farther from Earth, and particularly to nearby segments

PoS(AASKA14)166

of spiral arms.

2. Scientific Rationale and synergy with other projects

Thanks to its enormous collecting area, the SKA will provide unprecedented sensitivity for radio continuum observations. As will be shown below, this will enable tomographic mappings with unprecedented accuracy of nearby regions such as Orion in a fairly modest amount of telescope time, even during the SKA1-MID phase. Such detailed reconstruction of the 3D structure and kinematics of individual star-forming regions will provide important tests for models of star-formation and early stellar evolution. For instance, a complete 6D (3 spatial + 3 velocity components) description of the young stellar population in a given cluster could be used to test theoretical models such as those proposed by Hartmann & Burkert (2007) for Orion. Similarly, very accurate HR diagrams made possible by accurate distances could be used to constrain pre-main sequence evolutionary models (see Loinard et al. 2011, for details). It will also be interesting the characterize the magnetospheric activity on young stars (Forbrich et al. 2011) by statistically examining the relation between evolutionary stage, mass, and magnetic activity.

For a full description of the 3D structure of star-forming regions, one has to consider, apart from the young stars and star-forming regions, also the molecular cloud. It impossible to measure parallaxes to extended structures such as clouds, but one can unravel the cloud through its dust content, assuming a ratio between the gas and the dust. The advantage of the dust is that we can measure its optically thin emission in the infrared to sub-millimeter and at the same time that dust will redden the stellar light in the optical and the near-infrared. Stars with accurate distances and stellar types can thus be used as pinpoints to reconstruct the cloud structure by measuring their reddening (for example Knude 2009). As clouds can have extents of several tens of parsecs, the distance accuracies have to be high, better than $\sim$10 pc, to obtain a detailed structure of the cloud.

Imposing a 2% parallax accuracy requirement, GAIA will deliver astrometry of B-G dwarfs out to 3–1 kpc (for B dwarfs) and 850–200 pc (G dwarfs) for visual extinctions of 1 to 10 mag, respectively. Later, but more common spectral types, such as M stars, have their astrometry limited to the very nearby stars only (200–50 pc for A_V of 1-10 magnitudes). Herschel maps show that the nearby low-mass clouds have most of their extent at $A_V < 10$ mag (see e.g., Peretto et al. 2012, Rygl et al. 2013, Kirk et al. 2013). Hence, combining VLBI and GAIA astrometries, we can measure both the low-density and the high-density extent of nearby molecular clouds, and have a complete 3D picture of the stars *and* the cloud, and the kinematics of the young and main sequence stars of stellar complexes. With early type stars (O-A) such studies could be extended out to the nearby segments of spiral arms.

With the full SKA2, VLBI tomographic mappings could be extended to the nearest spiral arm segments at 2–3 kpc (see Section 4.2). Spiral arms are likely to have a width of at least several hundred parsecs (several times the size of a massive star-forming region like Orion), so a parallax accuracy of order 1% at 2.5 kpc would easily reveal the depth of a spiral arm segment. Thus, the tomography proposed here would reveal the inner structure of Galactic spiral arms in unprecedented details, as well as the 3D motions of the young stars along and across the arm. This could be directly compared with the predictions of theoretical models (e.g. Bertin & Lin 1996), and would represent a major contribution to the study of the dynamics of galactic disks in general. It is

PoS(AASKA14)166

important to stress that the level of details that would be achieved through this type of observations could not be obtained in any external galaxy for the foreseeable future, nor in our own Galaxy with GAIA due to a combination of crowding and dust obscuration.

There is a clear synergy between the tomographic mappings proposed here and the maser and pulsar astrometric observations described in Green et al. (2015) and Han et al. (2015).

3. VLBI observations incorporating the SKA and strategies for astrometry

In all that follows, we will assume that the observations are made at a frequency of order 6 GHz, i.e. at the lower frequency end of SKA Band 5. We consider a VLBI array consisting of 70% of the SKA1-MID collecting area phased-up, and a further 10 other stations with characteristics similar to those of an individual SKA1-MID antenna. Assuming a 1 GHz bandwidth (the sum of two orthogonal polarizations; implying a data rate of 4 Gbps per antenna), we obtain an rms per baseline (phased SKA1-MID to single antenna) in the continuum of 220 μJy in 60 seconds and 97 μJy in 5 minutes. We estimate the image sensitivity by dividing the baseline sensitivity by $\sqrt{N_{ant}-1}$ and applying no weighting, since baselines to the phased SKA1-MID are so much more sensitive than those between the rest of the antennas in the array. The corresponding continuum image sensitivities (1σ) for 1 and 5 minutes are 97 and 31 μJy respectively.

A crucial ingredient for accurate astrometric measurements with the SKA is the presence of nearby calibrators, ideally within the primary beam of the SKA antennas, so that with multiple beams from the phased SKA1-MID we can simultaneously observe both the targets and the background quasar. The VLA was used by Fomalont et al. (1991) to characterize the faint source population at 5 GHz and found that N, the number of sources per square arc minute stronger than flux density S (where S is in μJy) is given by

$$N(S) = (23.2 \pm 2.8) S^{-1.18 \pm 0.19}.$$

The fraction of faint 5 GHz sources which are compact on VLBI scales has (to our knowledge) not been measured but it is safe to assume that it is higher than 20% (the fraction of faint source population detected in deep VLA observations at 1.4 GHz that are compact on VLBI angular scales (Garrett 2005)). Taking all this into account, we predict 3 sources in the primary beam stronger than 150 μJy and perhaps one source stronger than 500 μJy.

The astrometry precision for a single epoch VLBI observation is given by

$$\theta_{ast} = \frac{\theta_{beam}}{2 \times \mathrm{SNR} \sqrt{N_{cal}}},$$

where N_{cal} is the number of calibrators. For a maximum baseline length of 8000 km we have a synthesized beam of 1.2 mas (3.1 mas for a 3000 km baseline). To achieve an astrometric accuracy of 5 μas after 4 epochs (which would yield distances accurate to 1% at 2 kpc), we will need a per epoch accuracy of around 10 μas (including systematic components of astrometric calibration). We see from above that we need the product $2 \times \mathrm{SNR} \times \sqrt{Ncal}$ to be approximately 120 if we have an 8000 km baseline length or 310 if the maximum baseline length is shorter. For 150 μJy calibrators we then need an SNR of around 30 (3 in-beam calibrators), which implies on-source time per epoch of 4 hours per source. For a 500 μJy calibrator we need an SNR of around 60 (only 1 in-beam calibrator), which implies an on-source time per epoch of 1 hour.

PoS(AASKA14)166

4. Staged approach to tomographic mappings of star-forming regions with the SKA

4.1 SKA1-MID

It is clear from the previous section that the SKA will have the potential of carrying out detailed tomographic observations of regions of star-formation located at distances of up to several kpc. We propose to realize this potential through a staged approach. In an initial phase, we would focus on a nearby region (e.g. the Orion Nebula Cluster – ONC) to demonstrate the capabilities of VLBI astrometric observations with the SKA1-MID. We would observe at least 200 young stars distributed across the complex (we know from VLA and VLBI observations that this number of non-thermal targets is present within the region). This would require observing about 20 primary fields of view distributed across the region, and ideally the capability of targeting simultaneously 10 to 20 fields within each primary field. With the current SKA1-MID baseline design of four VLBI beams per primary beam, and restricting ourselves to one calibrator and three targets per primary beam, we would need to observe each primary field at least 3 times. Assuming further that we focus on fields where calibrators brighter than 500 μJy exist, we would need 4 (epochs) $\times$ 20 (primary fields) $\times$ 3 passes per field $\times$ 1 hour (per field) = 240 hours. Including a 20% overhead brings the total required time for this project to 300 hours. If the capability of 10 to 20 VLBI beams was implemented in phase 1 this project would take only 100 hrs.

4.2 SKA2

If the observations with SKA1-MID are successful, we would move on to a more ambitious project utilizing the full SKA2. Taking advantage of the order of magnitude improvement in sensitivity, we would be able to carry out similar tomographic observations up to 2-3 kpc, i.e. the distance of the nearest spiral arm segments. For time estimate purposes, we will consider the mapping of a representative portion of a spiral arm segments of length 250 pc, and height 60 pc located at about 2.5 kpc of the Earth. This corresponds to a solid angle of 32,900 square arcminutes, or 180 SKA fields of view. We would, of course, only image the portions of the fields that contain young stellar objects or calibrators, thereby alleviating the computational requirements of the experiments. Assuming again 4 epochs, one hour per epoch, and 20% overheads, we obtain a total of 1,000 hours to obtain a complete tomographic mapping of a nearby spiral arm segment.

5. Conclusions and specific requirements

Thanks to its extraordinary collecting area, the SKA will be the premier instrument for radio frequency astrometry. In this contribution, we make the case for using that capability to obtain tomographic mapping of star-forming regions and spiral arm segments within several kpc of the Earth. This would represent a unique contribution to galactic dynamics, and would have important implications for spiral structure theories.

The general requirements to reach the necessary astrometric accuracy are given in detail in Green et al. (2015) and Paragi (2015). Here we emphasize that to carry out the tomographic observations presented here, at least a few tens of targets would have to be observed in a single primary beam of the SKA1-MID antennas. This would include both young stellar sources (targets)

PoS(AASKA14)166

and background quasars (calibrators). Without this capability, the time needed to carry out the observations would become prohibitive.

References

Bartkiewicz, A., & van Langevelde, H. J. 2012, IAU Symposium, 287, 117

Bertin, G., & Lin, C. C. 1996, Spiral structure in galaxies a density wave theory, Publisher: Cambridge, MA MIT Press, 1996

de Bruijne, J. H. J. 2012, Astrophysics and Space Science, 341, 31

Dame, T. M., Hartmann, D., & Thaddeus, P. 2001, The Astrophysical Journal, 547, 792

Dulk, G. A. 1985, Annual Reviews of Astronomy & Astrophysics, 23, 169

Dzib, S., Loinard, L., Mioduszewski, A. J., et al. 2010, The Astrophysical Journal, 718, 610

Fomalont, E. B., Windhorst, R. A., Kristian, J. A., & Kellerman, K. I. 1991, The Astronomical Journal, 102, 1258

Forbrich, J., Wolk, S. J., Güdel, M., et al. 2011, 16th Cambridge Workshop on Cool Stars, Stellar Systems, and the Sun, 448, 455

Garrett, M. A. 2005, EAS Publications Series, 15, 73

Gaume, R. A., Wilson, T. L., Vrba, F. J., Johnston, K. J., & Schmid-Burgk, J. 1998, The Astrophysical Journal, 493, 940

Green, J., et al. 2015, "Maser Astrometry with VLBI and the SKA", in proceedings of "Advancing Astrophysics with the SKA" PoS(AASKA2014)119

Han, J., et al. 2015, "Three-dimensional Tomography of the Galactic and Extragalactic Magnetoionic Medium with the SKA", in proceedings of "Advancing Astrophysics with the SKA" PoS(AASKA2014)041

Hartmann, L., & Burkert, A. 2007, The Astrophysical Journal, 654, 988

Kalenskii, S. V., Johansson, L. E. B., Bergman, P., et al. 2010, Monthly Notices of the Royal Astronomical Society, 405, 613

Kirk, J. M., Ward-Thompson, D., Palmeirim, P., et al. 2013, Monthly Notices of the Royal Astronomical Society, 432, 1424

Knude, J. 2009, IAU Symposium, 254, 35

Loinard, L., Mioduszewski, A. J., Torres, R. M., et al. 2011, Revista Mexicana de Astronomia y Astrofisica Conference Series, 40, 205

Loinard, L., Torres, R. M., Mioduszewski, A. J., et al. 2007, The Astrophysical Journal, 671, 546

Loinard, L., Torres, R. M., Mioduszewski, A. J., & Rodríguez, L. F. 2008, The Astrophysical Journal, 675, L29

Paragi, Z., et al. 2015, "Very Long Baseline Interferometry with the SKA", in proceedings of "Advancing Astrophysics with the SKA" PoS(AASKA2014)143

Peretto, N., André, P., Könyves, V., et al. 2012, Astronomy & Astrophysics, 541, AA63

Reid, M. J., & Honma, M. 2014, Annual Reviews of Astronomy & Astrophysics, 52, 339

Reid, M. J., Menten, K. M., Brunthaler, A., et al. 2014, The Astrophysical Journal, 783, 130

Rygl, K. L. J., Benedettini, M., Schisano, E., et al. 2013, Astronomy & Astrophysics, 549, LL1

Thompson, A. R., Moran, J. M., & Swenson, G. W. 2007, Interferometry and Synthesis in Radio Astronomy, by A.R. Thomspon, J.M. Moran, and G.W. Swenson. John Wiley & Sons, 2007.

PoS(AASKA14)166

Torres, R. M., Loinard, L., Mioduszewski, A. J., & Rodríguez, L. F. 2007, The Astrophysical Journal, 671, 1813

Torres, R. M., Loinard, L., Mioduszewski, A. J., & Rodríguez, L. F. 2009, The Astrophysical Journal, 698, 242

Torres, R. M., Loinard, L., Mioduszewski, A. J., et al. 2012, The Astrophysical Journal, 747, 18

PoS(AASKA14)166

Fundamental Physics with Pulsars

PROCEEDINGS OF SCIENCE

Pulsar Science with the SKA

Michael Kramer[*1,2], **Ben Stappers**[2]
[1] *MPI für Radioastronomie, Auf dem Hügel 69, 53121 Bonn, Germany*
[2] *Jodrell Bank Centre for Astrophysics, University of Manchester, M13 9PL, UK*
E-mail: mkramer at mpifr.de

The SKA will be transformational for many areas of science, but in particular for the study of neutron stars and their usage as tools for fundamental physics in the form of radio pulsars. Since the last science case for the SKA, numerous and unexpected advances have been made broadening the science goals even further. With the design of SKA Phase 1 being finalised, it is time to confront the new knowledge in this field, with the prospects promised by this exciting new telescope. While technically challenging, we can build our expectations on recent discoveries and technical developments that have reinforced our previous science goals.

Advancing Astrophysics with the Square Kilometre Array
June 8-13, 2014
Giardini Naxos, Sicily, Italy

[*] Speaker.

PoS(AASKA14)036

1. Introduction

Pulsars are a physicist's dream come true. Their study combines a wide range of physics and astrophysics, from the fundamental laws of nature to the structure of the Milky Way. Pulsars, as compact objects of the most extreme matter, store a huge amount of rotational energy, making them massive flywheels and very stable rotators. With a radio beam fixed relative to the surface of this rotating object, which has a strange superfluid superconducting material inside a solid iron crust, it acts like a cosmic lighthouse. On long time-scales, the frequency stability of the lighthouse's beacon rivals atomic clocks on Earth and allows us to test the terrestrial time standards. If the pulsar has a companion, they fall together in the gravitational potential of the Galaxy. By studying the way in which they fall, we can test general relativity and alternative theories of gravity under strong-field conditions in a unique and elegant, simple and clean way by measuring the times-of-arrival (ToA) of the pulses on Earth. These ToAs and the pulse properties are modified by the interstellar medium, in turn allowing us to probe its properties. As we are always looking for even better laboratories, we stare at the sky with our radio telescopes to find new pulsars with ever better sensitivity and instrumentation. Once in a while, we discover something truly unexpected, such as the Fast Radio Bursts (FRB) from cosmological distances. With the Square Kilometre Array (SKA) and its sensitivity, we will not only be able to continue this research but we will take it to a new level. This overview chapter summarises the specialised chapters in the remainder of the book and puts them into perspective of what the community proposed in 2004 in the chapters by Kramer et al. (2004) and Cordes et al. (2004) in the SKA Science Book edited by Carilli & Rawlings (2004).

1.1 The discovery potential of the SKA

Almost all the science presented in the "pulsar chapters" in this book and summarised below was already proposed for the SKA in 2004. However that definitely does not mean that, in the intervening 10 years, this research field has stood still. The very opposite is true. If anything, the rate of discoveries has even increased, largely due to the employment of new instrumentation, providing unprecedented sensitivity and time resolution – all possible due to the recent ability to digitise and process large bandwidths with commodity computing equipment. Far exceeding all of this, the SKA will provide yet another gigantic leap in various areas of instrumentation, giving orders of magnitude improvement in sensitivity, FoV, survey speed and many more. In order to demonstrate this, we summarise the relevant discoveries in Figure 1. The left panel shows the cumulative increase in pulsar discoveries as a function of time, with a number of important discoveries in the last decade. In total, we know of more than 2300 normal pulsars and about 250 millisecond (recycled) pulsars, of which about 80% are in binaries. With the full SKA we can expect more than a 10-fold increase in each of these numbers, a large fraction of which can be already found with Phase I, as described in the census chapter by Keane et al. (2015). These numbers are even somewhat larger than predicted by Kramer et al. (2004) and Cordes et al. (2004) as our knowledge of the populations has increased dramatically. The right panel of Figure 1 puts the expected numbers in relation to the current ones, demonstrating that these new discoveries will lead clearly to excellent science, resulting from the subsequent (needed) follow-up and timing observations, as described in the accompanying chapters.

PoS(AASKA14)036

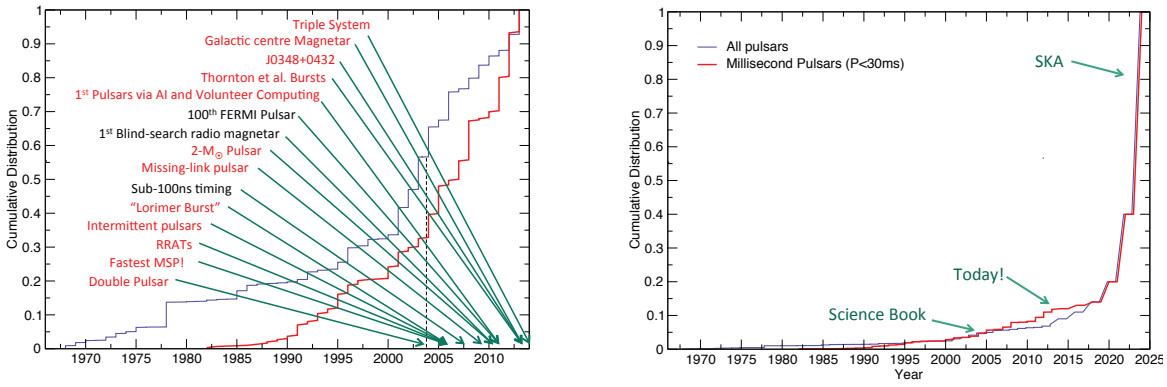

Figure 1: Pulsar-related discoveries as a function of time. The time of the first SKA Science Book is marked and some important (selected) discoveries since are marked. The right panel puts the current numbers into perspective with those expected for the SKA.

2. Science enabled by the discovery & study of pulsars and radio emitting neutron stars with the SKA

The pulsar key science described in the first SKA Science Book had a number of related components, which were summarised under the theme of "Testing Gravity". With pulsars being strongly self-gravitating bodies and precision clocks at the same time, timing observations of binary and isolated millisecond pulsars allow unprecedented strong-field experiments. These include testing general relativity and alternative theories of gravity using binary pulsars and (the yet to be discovered) pulsar-black hole systems as well as the direct detection of gravitational waves using a "Pulsar Timing Array" (PTA) experiment. Given the advances in recent years, prospects are now described in two separate chapters by Shao et al. (2015) and Janssen et al. (2015), respectively. In addition to those, we provide here a summary of the rich and varied science goals for the SKA described in the appropriate chapters:

Chapter 37 — Gravitational wave astronomy with the SKA — Janssen et al. (2015) A Pulsar Timing Array (PTA) is used as a cosmic gravitational wave (GW) detector. As described in the chapter by Janssen et al. (2015), Phase I essentially guarantees the direct detection of a GW signal. This may appear as a stochastic background from binary super-massive black holes in the process of early galaxy evolution, or it may be bright individual source(s) of this kind. Exotic phenomena like cosmic strings may also be expected to produce measurable GW signals, should they exist. The last ten years have seen a much better understanding of the source population, the detection procedures and the use of a PTA for fundamental physics (such as graviton properties, e.g. Lee et al. 2010) or single source localisation capabilities (e.g. Lee et al. 2011), all of which is described in the corresponding chapter.

Chapter 38 — Understanding pulsar magnetospheres with the SKA — Karastergiou et al. (2015) Considerable progress has been made with our understanding of the pulsar emission mechanism in the last decade. However, the wide bandwidth and exceptional sensitivity of the SKA will revolutionise our understanding of radio emission from all types of radio emitting neu-

PoS(AASKA14)036

tron stars. Combined with the excellent high frequency data sets being accumulated by instruments like XMM, Chandra, FERMI, Magic, Veritas and HESS and new data from contemporaneous instruments like CTA, the data from SKA in Phase 1 will allow us to map the magnetosphere with unprecedented detail. With the SKA we will have an even greater range of radio frequencies available and sensitivity to study with more detail a greater number of sources. The high cadence of observing that should be afforded by the wide fields of view, sub-arraying capabilities, multi-beaming and commensal observing modes will revolutionise our understanding of the crucial relationship between the emission and spin properties of large samples of pulsars. The raw sensitivity of both MID and LOW will not only improve our understanding of the magnetospheric phenomena such as nulling and moding in a significantly increased sample of pulsars, it will also reveal in more detail how these manifest in millisecond pulsars. Both of these elements will be crucial in understanding the pulsar emission physics, but also for improving the use of pulsars as precision timing instruments. As we go from Phase 1 to SKA there will be significant improvements in the number of sources that can be studied, due to the large number of new sources and increased sensitivity, and even wider range of frequencies while the improved computing will enable even higher cadence.

Chapter 39 - Understanding the Neutron Star Population with the SKA - Tauris et al. (2015) The census will give a complete overview of the Galactic neutron star population. Not only has the number of neutron stars increased significantly in the last 10 years, but also new types of neutron stars have been discovered, such as Intermittent Pulsars (Kramer et al. 2006) or RRATs (McLaughlin et al. 2006), and unexpected types of binary systems. Also, some magnetars are now detected at radio frequencies, and it is therefore essential that we revisit the birth channels and properties of neutron stars and their evolution. The ingredients needed to understand the complex "zoo" of neutron stars and their inter-relationships is summarised in the chapter by Tauris et al. (2015).

Chapter 40 - A Cosmic Census of Radio Pulsars with the SKA - Keane et al. (2015) To transform and facilitate all of the science discussed here and in this book, it is essential to discover the largest possible fraction of the entire Galactic radio-emitting neutron star population. This is possible with the SKA. Moreover, this population, in itself, will provide an unparalleled opportunity to study the population as a whole and all that can tell us about the star formation and dynamical history of the Milky Way. This chapter presents a comprehensive analysis of the survey approaches and expected yields. We refer here only to selected highlights, noting that in the sample of radio emitting neutron stars we include RRATs and magnetars. In Phase 1 of the SKA, our simulations show that an optimised combination of pulsar search capabilities using both LOW and Bands 1 & 2 of MID can survey the entire sky visible from the SKA sites in a reasonable amount of observing time. Such a survey, with the rebaselined configurations of MID and LOW, would result in a yield of at least 7500 normal pulsars and 1200 millisecond pulsars. This assumes similar integration times on MID and LOW, if there were more time available on LOW a doubling of the integration time could be used to increase this yield by as much as 30%. Full SKA simulations have shown that a combination of a LOW, MID and an Aperture Array instrument working at below a GHz, could increase the total number of radio emitting neutron stars known in the Galaxy to more than 45,000 including more than 5,000 millisecond pulsars. In the majority of the regions of the Galaxy this would constitute the entire radio emitting neutron star population. In the Galactic centre a deep dedicated survey with Band 5 of the first phase of SKA will be sensitive

PoS(AASKA14)036

to normal and millisecond pulsars, with the high frequency mitigating the deleterious effects of the interstellar medium (ISM) and the collecting area compensating for the steep pulsar spectra. With more than 1,000 pulsars predicted to be located with in the central parsec, in Phase 1 we can expect to detect dozens of pulsars in this region of the sky, and the later addition to the SKA of bands 3 & 4 combined with overall improved collecting area, will discover the vast majority of this predicted population.

Chapter 41 - Three-dimensional Tomography of the Galactic and Extragalactic Magnetoionic Medium with the SKA - Han et al. (2015) Another spin-off from the pulsar surveys will be the significant increase in the number of lines-of-sight through the Galaxy where we will be able to measure both the magnetic field properties and the electron column density, see this chapter for a full discussion. In Phase 1 there will already be an order of magnitude increase in the number of sources and the combination of LOW and MID will allow both near and distant sources, including some deep in the centre of the Galaxy, to be studied. The wide bandwidths, high frequency resolution and large number of sources will provide the accurate rotation measures and dispersions measure to generate a 3D tomographic view of the magneto-ionic properties of the Galaxy. With the full SKA revealing almost the entire radio pulsar population in the Galaxy it will allow one to probe the far side and also study the finer detail. Already in Phase 1 we will be able to find pulsars outside of our Galaxy and so study the fields inside those galaxies and also in the intervening medium. However the real renaissance in this area will come with the exceptional sensitivity of the SKA.

Chapter 42 - Testing Gravity with Pulsars in the SKA Era - Shao et al. (2015) New discoveries also lead to new exotic laboratories for fundamental physics, in particular for the study of gravity. Discoveries in recent years have continued to confirm this impression. The unique Double Pulsar system was found unexpectedly (Burgay et al. 2003; Lyne et al. 2004), providing unique and, so far, the best tests of general relativity for strongly-self gravitating bodies (Kramer et al. 2006); the most massive neutron star in a relativistic binary was found and probes a previously untested regime for alternative theories of gravity (Antoniadis et al. 2013); and the SKA observations of a unique discovered triple system (Ransom et al. 2014) promises to enable tests of the Strong Equivalence Principle that will surpass solar system limits.

We expect that among the discoveries are also pulsar-black hole systems. Using pulsars as test masses, we can probe the properties of black holes and measure the mass and the spin, χ. This will lead to precision tests of the "Cosmic Censorship Conjecture", which states that every astrophysical black hole should have an event horizon (cf. Liu et al. 2014). In order to test also the "no-hair" theorem, stating that all black hole properties are uniquely described by the mass and spin (and charge) of the black hole, we would need to also measure the quadrupole moment, Q, of the black hole, which should be identical to the value predicted by the measured combination of mass and spin.

Chapter 43 - Probing the neutron star interior and the Equation of State of cold dense matter with the SKA - Watts et al. (2015) Finding a large population of neutron stars will also yield the extreme objects. The SKA surveys will yield the fastest spinning pulsars, perhaps even sub-ms pulsars should they exist, the most massive pulsars and also of high interest, the lightest neutron stars. All this information will be used to study the equation-of-state (EOS) of super-dense matter. With neutron stars consisting of the densest matter in the observable Universe, we cannot

PoS(AASKA14)036

create the corresponding conditions in terrestrial laboratories, so that pulsar observations, including those of glitches, moment-of-inertia measurements, provide a unique insight into the EOS(s?), as discussed in detailed in the chapter by Watts et al. Combining this insight with X-ray observations will also be extremely valuable as discussed further below.

Chapter 45 - Observing Radio Pulsars in the Galactic Centre with the Square Kilometre Array - Eatough et al. (2015) Measuring the quadrupole moment Q, and hence testing the "no-hair" theorem, for stellar mass black holes is difficult, even with the SKA. It will be much easier using a pulsar in orbit about the super-massive black hole in the centre of our Milky Way. The recipe for how to extract this science using observations of relativistic effects such as frame-dragging was first presented by Wex et al. (1999). This was further studied (Kramer et al. 2004; Liu et al. 2012) and is discussed in much detail in the corresponding chapter by Eatough et al. (2015). The SKA prospects of measuring the mass of SGR A* to a precision of $1M_{\odot}$ (!), its spin χ to 0.1% or better and the quadrupole moment Q to about 1%, even with a normal pulsar orbiting SGR A* is exciting and unprecedented.

Chapter 46 - Pulsar Wind Nebulae in the SKA era - Gelfand et al. As well as making a great step forward in studying pulsars and their environments using their properties in the time domain, the SKA can also make enormous strides by studying the environments of pulsars through imaging. This chapter discusses how the bulk of the rotational energy of pulsars is radiated away in the pulsar wind and the only way to study it is through its interaction with the surrounding interstellar medium or with a binary companion and/or its wind. The SKA, using both the MID and LOW elements, in Phase 1 will already unveil dozens of new pulsar wind nebulae providing vital new insight in to the composition of the wind and the acceleration of leptons up to PeV energies. These interactions will also reveal important details of the ISM, the companion star composition and their winds. When combined with the existing and upcoming data from instruments such as HESS, Veritas, Magic and Fermi and that from instruments such as CTA, this will revolutionise our understanding of pulsar winds and their environments.

Chapter 47 - Pulsars in Globular Clusters with the SKA - Hessels et al. (2015) The sheer number of pulsars and radio emitting neutron stars in globular clusters make them ideal targets for the SKA, especially as the vast majority are best viewed from the Southern Hemisphere. As discussed in this chapter, the excellent sensitivity of both LOW and MID in Phase 1 will already more than triple the number of pulsars known in globular clusters, while the SKA will discover a sample of millisecond pulsars to rival the rest of the Galactic population. Not only does this provide the opportunity to find rare systems for some of the applications discussed above, it provides unique tools to probe the magneto-ionic properties of the clusters, the star formation and dynamical history of these important Galactic building blocks. In the vein of targeted searches both LOW and MID will be excellent instruments for searching for pulsars in sources that are likely to contain neutron stars, either through their high frequency emission, in particular Fermi unidentified sources, or their steep spectrum radio emission. The ability to frequently search these targets will also reveal more of the evolutionarily important transition sources, that mark the birth of radio millisecond pulsars. Already in Phase 1 we will be to find dozens more pulsars in the Magellanic clouds enabling us to sample the pulsar population in completely different environments to our own Galaxy and we will sample the top end of the luminosity function of any pulsars located in other nearby dwarf galaxies. By looking for giant pulse like emission, as exhibited by the Crab pulsar, the reach will extend well

PoS(AASKA14)036

out into the local group galaxies in Phase 1. With the SKA we will not only sample a very large fraction of the pulsars in the Magellanic clouds but will be able to detect significant numbers of pulsars in many of the galaxies in the local group and giant pulse emitters out to the Virgo Cluster.

Chapter 157 - SKA and the next-generation multi-wavelength observatories - Antoniadis et al. (2015) We have already alluded to a few of the synergies between pulsar work with the SKA and other instruments. However there are many more, and these are detailed in this chapter on synergies. These include the synergy with new and next generation gravitational wave detectors where the discovery of an increased number of double-neutron star binaries will enhance our understanding of the binary merger rate, the discovery of thousands of more radio pulsars may unveil some that are sufficiently distorted to emit gravitational waves, provide timing ephemerides for all of these pulsars to search for gravitational waves. There is also the possibility of the PTAs uncovering burst sources of GWs that can be followed up with instruments like LSST, IXO/Athena, Astro-H and of course proposed binary supermassive black holes can be searched for in the PTA data. Combining the astrometric information on binary systems with optical studies of their companions with instruments like LSST, E-ELT and GAIA can provide new insight into the stellar evolution, Galactic dynamics and cooling properties and ages of the stars. Combined X-ray and radio searches can reveal new transition systems which can reveal more about the formation process of millisecond pulsars and studies at both wavelengths can provide important input into our understanding of the neutron star equation of state. In particular, we are looking forward to synergies with Advanced LIGO and other ground (or even space-based) detectors. One one hand, they complement the SKA tests in the strong-gravity regime in a nearly perfect way, while they also allow us to probe similar sources in different evolutionary stages and across the mass scale.

3. Where does the SKA fit?

3.1 The synergy between SKA LOW and MID

It is important to recognise that the combined value of SKA LOW and MID in both Phase 1 and Phase 2 is more than the sum of its parts. This is true for all of the pulsar science discussed in this book, except only for the study of the innermost regions of the Galaxy. The significant increase in computing power to allow the removal of dispersion in the ISM combined with the ultra-wide bandwidths of instruments like LOFAR, MWA and the LWA have highlighted the value of returning to the lowest few octaves of the radio spectrum visible from the Earth for both pulsar searching and detailed pulsar studies. The excellent sensitivity of LOW already in Phase 1 will make it the ideal instrument for performing pulsar searches off the plane, where it is likely to find at least half of the known pulsars beamed in our direction. On the other hand the higher frequencies of MID will allow us to reach deep into the Galactic plane and see through the ISM to find thousands of pulsars there. It is essential though, that for both instruments there are sufficient numbers of tied-array beams available to ensure a sufficiently rapid survey speed with sufficiently long integration times. This will be possible with a minimum of 500 tied-array beams available for LOW and about 1500 beams for MID in Phase 1.

The ability of the SKA to have almost continuous frequency coverage from 50 MHz up to about 15 GHz with continuous up to 1.8 GHz in Phase 1, is of real value for studies of the pulsar

PoS(AASKA14)036

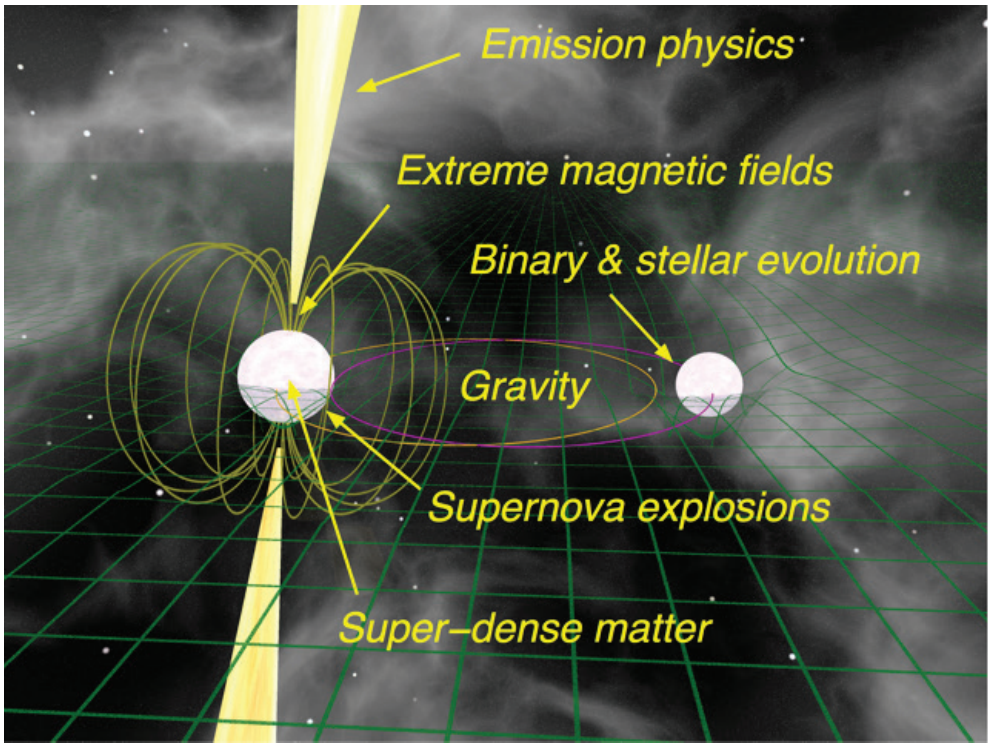

Figure 2: Artistic impression demonstrating the wide range of physics and astrophysics that finds its application when studying pulsars.

emission mechanism and magnetospheres, providing the ability to sufficiently sample the variations in emission properties as a function of frequency. The ability to correct for the influence of the ISM on high precision timing will be essential for all of the gravity studies and this is made possible through measuring the ISM weather through the continuous frequency bands. This is even more important if the highest frequency for pulsar timing in Phase 1 is around 1.8 GHz. Studies of the ISM and the Galactic distribution of electrons and the structure of the magnetic fields also value the combination of frequencies allowing measurements to be made nearby where the effects are best seen at LOW frequencies, and further away using the higher frequency bands. In the case of the pulsar wind nebulae the two instruments provide an ability to trace the energy deposition history and the physics of the pulsar wind.

3.2 Synergies with other SKA science goals

The pulsar surveys and associated observing and processing infrastructure naturally lead to a strong overlap with the fast transients goals (see Chapter 51). It is highly desirable therefore that the infrastructure, including the beamformer, be made available for searching for short duration radio bursts, be they from radio emitting neutron stars or from other radio transients, operate commensally, ideally with all other observations with both SKA MID and LOW, but certainly as frequently as possible. This will increase the yield for both the pulsar and radio emitting neutron star searches but also for the fast transients. As discussed in Chapter 41 and others, pulsars are very useful for the study of the ISM, providing full knowledge about the Milky Way, its constituents and its magnetic

PoS(AASKA14)036

field structure. Synergies will also be present by comparing experimental results in gravity (via pulsars and cosmology) and the detailed characterisation of individual sources. In general, the aim should be to share discoveries with these communities as soon as possible to maximise the science return as rapidly as possible.

3.3 Impact of the SKA

The impact of the pulsar science obtained with the SKA promises to be very significant. Pulsars are among the very few objects that are visible across the whole electromagnetic spectrum and through new, unexplored windows like gravitational wave astronomy. At the same time, the understanding requires the application of theories ranging from quantum mechanics and solid states physics to gravitation and extreme plasma physics. Consequently, the variety of expected results is guaranteed to be relevant for a global community of physicists and astronomers alike. Literally, we can expect that we can mark our understanding of neutron stars, gravity and the Milky Way itself in a time before and after the SKA came online.

Besides this massive scientific impact, the pulsar science with the SKA also has the potential to draw great attention and interest from the general public. Neutron stars and in particular the black holes studied with the pulsars always fascinate the public. The fact that we can visualize pusar data in a unique dynamic way — and make them even audible — will make it easy to advocate the SKA and its science in general.

3.4 Risk and challenges

The technological components of "non-imaging processing" are challenging. This involves the task of beamforming and, due to the high data rates, the required on-line search processing. Data can not be stored but have to be analysed in real time. Imperfect algorithms would require a repeat of the experiment or parts of it. This may be both expensive or even impossible. On the other hand, the discovery rate could be high, consequently.

There are also scientific risks that are more difficult to quantify, as we are conducting discovery science. The biggest risk here is probably the uncertainty in the number of suitable pulsar - black hole systems or of pulsars about Sgr A* to conduct the proposed key science. Nevertheless, we know that extreme binary systems can be found in globular cluster (see Chapter 47) or in the regions of high stellar density in the central Galaxy. Here, the discovery of a rare radio-loud magnetar Eatough et al. (2013) however gives confidence that the expections are warranted (see Chapter 45).

4. Technical requirements of non-imaging processing with the SKA

The key technical requirements of the SKA are beyond the scope of this chapter and so we refer the interested reader to the papers by Smits et al. (2009, 2011) as well as to the detailed technical design from both the Non-Imaging work in the Central Signal Processing and Science Data Processor consortia[1] and also in the associated Chapters in this book. However, we highlight here some of the key requirements on both SKA MID and LOW to achieve the pulsar science goals.

[1] www.skatelescope.org

PoS(AASKA14)036

- It is essential that in Phase 1 of SKA MID and LOW that there be a sufficiently large number of beams (e.g. 1,500 and 500 respectively) to be able to survey the sky sufficiently rapidly and with sufficient sensitivity.
- When searching for the extreme binary systems that are key to the gravity studies it is not possible to trade integration time for sensitivity as the required processing capacity scales as the third power of the integration time. So maximum sensitivity possible in the core regions needs to be maintained.
- Sub-arraying and a significant number of beams capable of undertaking precision timing are required to be able to enable characterisation of the large numbers of pulsars that will be discovered, but also to enable the high cadence observing required to reveal the physics of neutron star interiors and magnetospheres.
- Commensal observing will allow for transformation changes to the observing cadence achievable on the largest possible sample of objects.
- It should be possible to combine as many of the elements as possible, when forming the smaller number of beams to be used for the timing experiments to maximise sensitivity.
- Having as complete as possible frequency coverage across the entire LOW range and the ability to subarray so that that different frequencies can be observed simultaneously will be highly valuable for the physics of the magnetosphere.
- A combination of pulsar timing on both the LOW and MID instruments is required in order to be able to fully characterise and correct for the contribution of the ISM in the high precision pulsar timing experiments.
- It will be necessary to be able to calibrate the polarisation purity of the array to at least -40 dB for high precision timing experiments.

5. Summary

The science summarized in this overview can only give a glimpse of the science promises given by the SKA. With Phase 1 of the telescope being defined, we can safely predict what will be possible. However, the most exciting results will be, of course, obtained by unpredicted, unexpected discoveries and results. We may not be able to imagine what awaits us, but even the "expected" results are strong motivation to make the SKA a reality.

References

Antoniadis K. et al., 2013, Science, 340, 448

Antoniadis, J., Guillemot, L., Possenti, A. et al., 2015, "Multi-wavelength, Multi-Messenger Pulsar Science in the SKA Era", in proc. *Advancing Astrophysics with the Square Kilometre Array*, PoS(AASKA14)157

Burgay M. et al., 2003, Nature, 426, 531

PoS(AASKA14)036

Carilli, C., & Rawlings, S., 2004, eds. “Science with the Square Kilometre Array", NewAR, Vol. 48

Cordes, J. M., Kramer, M., Lazio, T. J. W., Stappers, B. W., Backer, D. C., Johnston, S., 2004, NewAR, 48, 1413

Eatough R. P. et al., 2013, Nature, 501, 391

Eatough, R. P., Lazio, J. T. W., Casanellas, J. et al., 2015, “Observing Radio Pulsars in the Galactic Centre with the Square Kilometre Array”, in proc. *Advancing Astrophysics with the Square Kilometre Array*, PoS(AASKA14)045

Fender, R., Stewart, A., Macquart, J-P. et al., 2015, “Transients with the SKA: the scientific potential, and how to optimise the telescope”, in proc. *Advancing Astrophysics with the Square Kilometre Array*, PoS(AASKA14)051

Gelfand, J. D., Breton, R. P., Ng, C.-Y. et al., 2015, “Pulsar Wind Nebulae in the SKA era”, in proc. *Advancing Astrophysics with the Square Kilometre Array*, PoS(AASKA14)046

Han J. L., van Straten, W., Lazio, T. J. W. et. al., 2015, “Three-dimensional Tomography of the Galactic and Extragalactic Magnetoionic Medium with the SKA”, in proc. *Advancing Astrophysics with the Square Kilometre Array*, PoS(AASKA14)041

Hessels, J. W. T., Possenti, A., Bailes, M. et al., 2015, “Pulsars in Globular Clusters with the SKA”, in proc. *Advancing Astrophysics with the Square Kilometre Array*, PoS(AASKA14)047

Janssen, G. H., Hobbs, G., McLaughlin, M. A. et al., 2015, “Gravitational Wave Astronomy with the SKA”, in proc. *Advancing Astrophysics with the Square Kilometre Array*, PoS(AASKA14)037

Karastergiou, A., Johnston, S., Andersson, N., et al., 2015, “Understanding pulsar magnetospheres with the SKA”, in proc. *Advancing Astrophysics with the Square Kilometre Array*, PoS(AASKA14)038

Keane, E. F., Bhattacharyya, B., Kramer, M., & et al. 2015, “A Cosmic Census of Radio Pulsars with the SKA”, in proc. *Advancing Astrophysics with the Square Kilometre Array*, PoS(AASKA14)040

Kramer M., Backer D. C., Cordes J. M., Lazio T. J. W., Stappers B. W., Johnston S., 2004, NewAR, 48, 993

Kramer M., Lyne A. G., O’Brien J. T., Jordan C. A., Lorimer D. R., 2006, Science, 312, 549

Kramer M. et al., 2006, Science, 314, 97

Lee K., Jenet F. A., Price R. H., Wex N., Kramer M., 2010, ApJ, 722, 1589

Lee K. J., Wex N., Kramer M., Stappers B. W., Bassa C. G., Janssen G. H., Karuppusamy R., Smits R., 2011, MNRAS, 414, 3251

Liu K., Wex N., Kramer M., Cordes J. M., Lazio T. J. W., 2012, ApJ, 747, 1

Liu K., Eatough R. P., Wex N., Kramer M., 2014, MNRAS, 445, 3115

Lyne A. G. et al., 2004, Science, 303, 1153

McLaughlin M. A. et al., 2006, Nature, 439, 817

Ransom S. M. et al., 2014, Nature, 505, 520

Shao, L., Stairs, I. H., Antoniadis, J., & et al., 2015, “Testing Gravity with Pulsars in the SKA Era”, in proc. *Advancing Astrophysics with the Square Kilometre Array*, PoS(AASKA14)042

Smits R., Lorimer D. R., Kramer M., Manchester R., Stappers B., Jin C. J., Nan R. D., Li D., 2009, A&A, 505, 919

PoS(AASKA14)036

Smits R., Tingay T., Wex N., Kramer M., Stappers B., 2011, A&A, 528, 108

Tauris, T. M., Kaspi, V. M. Breton, R. P. et al., 2015, "Understanding the Neutron Star Population with the SKA", in proc. *Advancing Astrophysics with the Square Kilometre Array*, PoS(AASKA14)039

Watts, A. L, Xu, R., Espinoza, C. M. et al. 2015, "Probing the neutron star interior and the Equation of State of cold dense matter with the SKA", in proc. *Advancing Astrophysics with the Square Kilometre Array*, PoS(AASKA14)043

Wex N., Kopeikin S., 1999, ApJ, 513, 388

PoS(AASKA14)036

PROCEEDINGS OF SCIENCE

Gravitational wave astronomy with the SKA

G. H. Janssen[*1], **G. Hobbs**[2], **M. McLaughlin**[3], **C. G. Bassa**[1], **A. T. Deller**[1], **M. Kramer**[4,5], **K. J. Lee**[6,4], **C. M. F. Mingarelli**[4,7,8], **P. A. Rosado**[9,10], **S. Sanidas**[5], **A. Sesana**[11], **L. Shao**[12], **I. H. Stairs**[13], **B. W. Stappers**[5], **J. P. W. Verbiest**[14,4]

[1]*Netherlands Institute for Radio Astronomy (ASTRON), The Netherlands; E-mail:* janssen@astron.nl; [2]*CSIRO Astronomy and Space Science, Australia;* [3]*Department of Physics, West Virginia University, USA;* [4]*Max-Planck-Institut für Radioastronomie, Bonn, Germany;* [5]*University of Manchester, UK;* [6]*Kavli Institute for Astronomy and Astrophysics, Peking University, P.R. China;* [7]*Theoretical Astrophysics, California Institute of Technology, USA;* [8]*School of Physics and Astronomy, University of Birmingham, UK;* [9]*Max-Planck-Institut für Gravitationsphysik, AEI Hanover, Germany;* [10]*Swinburne University of Technology, Australia* [11]*Max-Planck-Institut für Gravitationsphysik, AEI Golm, Germany;* [12]*School of Physics, Peking University, P.R. China;* [13]*University of British Columbia, Canada;* [14]*Universität Bielefeld, Germany*

On a time scale of years to decades, gravitational wave (GW) astronomy will become a reality. Low frequency ($\sim 10^{-9}$ Hz) GWs are detectable through long-term timing observations of the most stable pulsars. Radio observatories worldwide are currently carrying out observing programmes to detect GWs, with data sets being shared through the International Pulsar Timing Array project. One of the most likely sources of low frequency GWs are supermassive black hole binaries (SMBHBs), detectable as a background due to a large number of binaries, or as continuous or burst emission from individual sources. No GW signal has yet been detected, but stringent constraints are already being placed on galaxy evolution models. The SKA will bring this research to fruition.

In this chapter, we describe how timing observations using SKA1 will contribute to detecting GWs, or can confirm a detection if a first signal already has been identified when SKA1 commences observations. We describe how SKA observations will identify the source(s) of a GW signal, search for anisotropies in the background, improve models of galaxy evolution, test theories of gravity, and characterise the early inspiral phase of a SMBHB system.

We describe the impact of the large number of millisecond pulsars to be discovered by the SKA; and the observing cadence, observation durations, and instrumentation required to reach the necessary sensitivity. We describe the noise processes that will influence the achievable precision with the SKA. We assume a long-term timing programme using the SKA1-MID array and consider the implications of modifications to the current design. We describe the possible benefits from observations using SKA1-LOW. Finally, we describe GW detection prospects with SKA1 and SKA2, and end with a description of the expectations of GW astronomy.

Advancing Astrophysics with the Square Kilometre Array
June 8-13, 2014
Giardini Naxos, Italy

[*]Speaker.

PoS(AASKA14)037

1. Introduction

Radio observations of binary pulsars provide irrefutable evidence that gravitational waves (GWs) exist. The impact of their emission on e.g. the orbital period of binary pulsars can be used to test general relativity and other theories of gravity (e.g. Taylor & Weisberg 1982; Kramer et al. 2004; Cordes et al. 2004). The effect of external GWs on pulsar timing (Detweiler 1979) can be used to make a direct detection of low-frequency GWs through the analysis of a large ensemble of pulsars, forming a galactic-scale GW detector: a Pulsar Timing Array (PTA; Hellings & Downs 1983; Romani 1989; Foster & Backer 1990). Global efforts are underway to directly detect low-frequency GWs via PTA experiments.

In this chapter we describe how a PTA project for the SKA will allow the characterisation of GW signals. PTA projects are based on pulsar timing observations in which pulse times of arrival (ToAs) for a sample of pulsars are measured. The ToAs are subsequently compared with predictions for those arrival times based on simple physical models of the pulsars. Any differences between the predicted and measured ToAs are referred to as the "timing residuals" and indicate that a physical phenomenon, not (or incorrectly) included in the model, is affecting the pulse ToAs at a measurable level. Residuals caused by the irregular rotation of a given pulsar, variability in the interstellar medium, or inaccuracies in the timing model parameters are typically different between pulsars. In contrast, GWs passing the Earth will lead to timing residuals whose functional form will depend upon the pulsar-Earth-GW angle. PTA projects therefore differ from more traditional pulsar timing experiments in that they aim to extract common signals present within the timing residuals for multiple pulsars in order to detect GWs and other correlated signals, like fluctuations in global atomic time standards (Hobbs et al. 2012) or unmodelled effects in the Solar system ephemeris that is used to convert pulse ToAs to the Solar system barycentre (Champion et al. 2010).

Long-term observations of millisecond pulsars were carried out at telescopes around the world starting in the 1980s and 1990s, producing data sets that can be usefully added to modern PTA observations (see e.g. Kaspi et al. 1994). Three PTAs are presently in existence. The European Pulsar Timing Array (EPTA; see Kramer & Champion 2013, for a review) uses five radio telescopes in Europe (the 100-m Effelsberg telescope in Germany, the 76-m Lovell telescope at Jodrell Bank in the UK, the 94-m equivalent Nançay telescope in France, the 64-m Sardinia radio telescope in Italy, the 94-m equivalent Westerbork Synthesis Radio Telescope in The Netherlands) and complementary low-frequency (< 250 MHz) observations obtained with LOFAR (van Haarlem et al. 2013; Stappers et al. 2011) for some pulsars. The North American Nanohertz Observatory for Gravitational Waves (NANOGrav; Demorest et al. 2013), uses the 305-m Arecibo and 100-m Green Bank telescopes, and the Parkes Pulsar Timing Array (PPTA; Manchester et al. 2013), uses the 64-m Parkes telescope. All collaborations have well established pulsar timing programmes on at least 20 millisecond pulsars with time baselines of 10 years or more. Regular timing observations for these pulsars are being obtained over a wide range of observing frequencies (300 to 3000 MHz) to mitigate the effects of variations in dispersion. Since 2008, the three PTAs are collaborating as members of the International Pulsar Timing Array (IPTA; Manchester & IPTA 2013). Over the years, all PTAs have increased their sensitivity to GWs through improvements in instrumentation, software, and observing cadence and data span. Furthermore, the EPTA is using interferometric techniques to form the LEAP telescope, a tied-array of the five large European radio telescopes

PoS(AASKA14)037

(Kramer & Stappers 2010; Bassa et al. in prep.). In the near future it is expected that PTA observations will be also carried out using the SKA Pathfinder telescope MeerKAT, and with the Five-hundred-meter Aperture Spherical Telescope (FAST; Hobbs et al. 2014).

There is a broad GW spectrum, rich with information ranging from processes in the early Universe to compact binary coalescences.

Cosmological GW signatures at frequencies of $\sim 10^{-16}$ Hz are targeted by cosmic microwave background (CMB) polarisation experiments such as BICEP2 and Planck (e.g. Ade et al. 2014; Planck Collaboration 2014). Ground-based interferometer GW observatories, like the (advanced) LIGO and Virgo, and a space-based mission, like the proposed eLISA, operate at $\sim$ 1–10^3 Hz and $\sim 10^{-4}$–1 Hz, respectively (see e.g. Pitkin et al. 2011; eLisa Consortium 2013, for overviews). Therefore, PTAs with sensitivities peaking at frequencies of 10^{-9}–10^{-7} Hz represent a unique complementary laboratory to other GW experiments and are able to detect and study unique classes of sources (see Figure 1).

Throughout this chapter we concentrate on the detection and subsequent analysis of GWs. However, the data sets produced for this work will be useful in numerous ways; including studying the interstellar medium, the pulsars themselves, terrestrial time standards, planetary ephemerides, the solar wind, and testing theories of gravity. We first describe the expected sources of GW emission detectable by PTAs (§2) . In §3 we describe how the SKA will enable both GW detection and GW source characterisation. In §4 we highlight various limiting noise processes that need to be accounted for in the detection analyses. In §5 we describe a realistic PTA for the SKA which includes a plausible observing strategy. The effect of a cut in the baseline design is described in §5.4. We describe the future of GW astronomy with the SKA in §6.

2. Sources of gravitational waves

There are numerous GW sources that could lead to detectable signatures in pulsar data sets. Most recent work has concentrated upon searching for a GW background formed by the superposition of a large number of GWs from supermassive black hole binaries (SMBHBs; see e.g. Sesana et al. 2008; Ravi et al. 2012; Ölmez et al. 2010), cosmic strings (e.g. Sanidas et al. 2012) or inflation (e.g. Tong et al. 2014). Various algorithms have been published to constrain such a background or to attempt to detect the background (see e.g. Jenet et al. 2006; Yardley et al. 2011; van Haasteren et al. 2011; Sanidas et al. 2012; Demorest et al. 2013; Shannon et al. 2013). These bounds have assumed that the GW background spectrum is a power law defined by an amplitude A and spectral index α. The stochastic GW backgrounds of the sources probed by PTAs have a range of spectral indices, depending on the details of the theoretical models, with the most widely used values being $\alpha \sim -2/3$ for SMBHBs without environment interactions (Phinney 2001), $\alpha \sim -7/6$ for high emission modes from cosmic string cusps and $\alpha \sim -1$ for slow-roll inflation. Current bounds are beginning to rule out some extreme models for the coalescence rate of SMBHBs and for the tension and loop size of cosmic strings. The most stringent published limit, from PPTA data, on characteristic amplitude due to a stochastic GW background is 2.4×10^{-15} (at a reference frequency of yr^{-1}; Shannon et al. 2013). Figure 1 shows a nominal upper bound at the level we expect to reach with the full IPTA ($h_c \sim 4 \times 10^{-15}$ at 5×10^{-9}Hz, which corresponds to about $h_c \sim 10^{-15}$ at a frequency

PoS(AASKA14)037

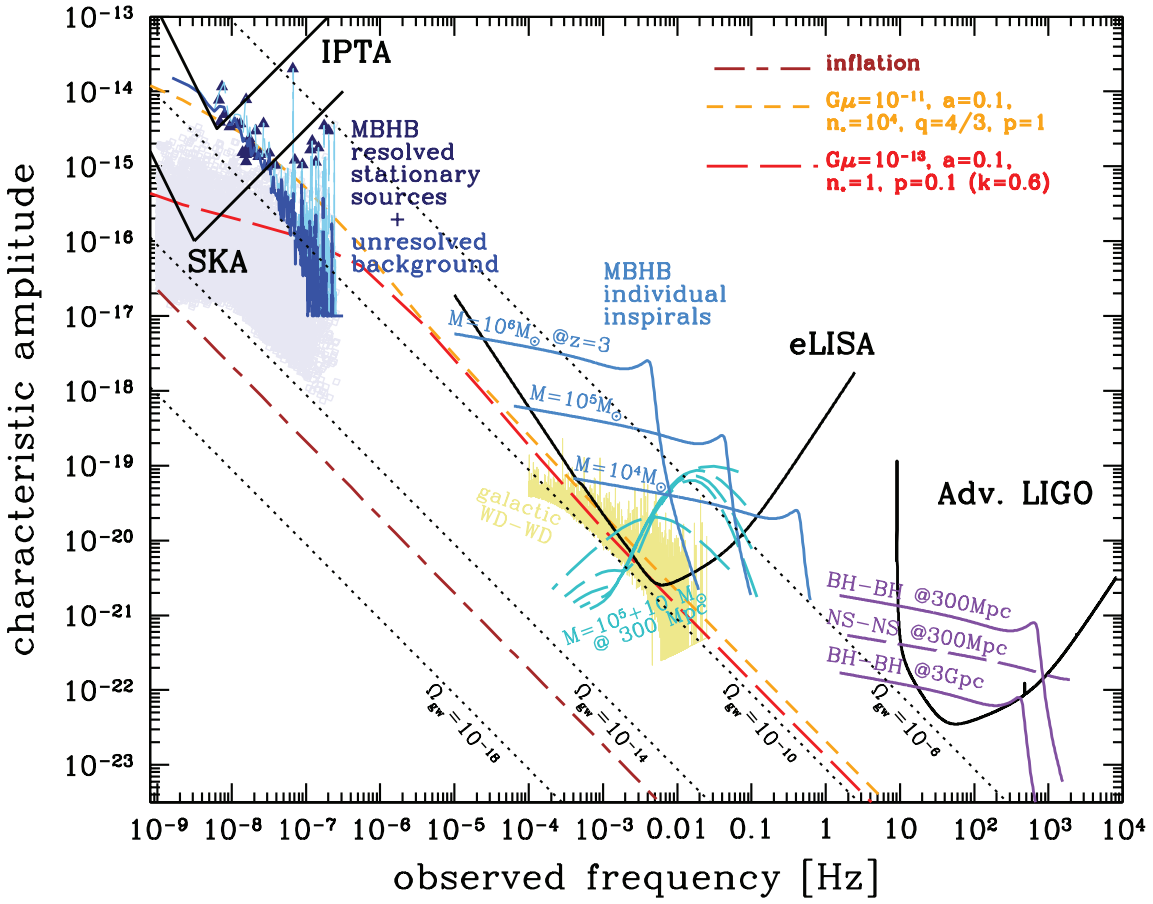

Figure 1: The gravitational wave landscape: characteristic amplitude (h_c), vs frequency. In the nHz frequency range a selected realisation of the expected GW signal from the cosmological population of SMBHBs is shown. Small lavender squares are individual SMBHB contributions to the signal, the dark blue triangles are loud, individually resolvable systems and the blue jagged line is the level of the unresolved background. Nominal sensitivity levels for the IPTA and SKA are also shown. In the mHz frequency range, the eLISA sensitivity curve is shown together with typical circular SMBHB inspirals at z=3 (pale blue), the overall signal from Galactic WD-WD binaries (yellow) and an example of extreme mass ratio inspiral (aquamarine, only the first 5 harmonics are shown). In the kHz range an advanced LIGO curve (based on calculations for a single interferometer) is shown together with selected compact object inspirals (purple). The brown, red and orange lines running through the whole frequency range are expected cosmological backgrounds from standard inflation and selected string models, as labeled in figure. Black dotted lines mark different levels of GW energy density content as a function of frequency ($\Omega_{gw} \propto h_c^2 f^2$).

of yr^{-1} for an extrapolated $f^{-2/3}$ power law) , and the expected levels to be reached by the SKA ($h_c \sim 10^{-16} - 10^{-17}$ at a reference frequency of yr^{-1}).

Pulsar timing can also be used to search for individual sources of GWs: individual SMBHBs that produce a continuous wave. A single (effectively non-evolving) circular binary system of supermassive black holes produces a sinusoidal signal. Various algorithms have recently been developed to search for such waves. These include a frequentist-based approach (Jenet et al. 2004; Yardley et al. 2010) and Bayesian methods (van Haasteren et al. 2009; Lee et al. 2011; Babak &

PoS(AASKA14)037

Sesana 2012; Ellis et al. 2012; Petiteau et al. 2013; Ellis 2013; Arzoumanian et al. 2014). Pulsar timing experiments are sensitive to sources emitting GWs with periods from a few weeks (defined by the average observing cadence in the PTA) to around the total duration of the data set. Using the algorithms mentioned above, bounds have been placed on such GWs in this frequency range. For existing PTAs, GWs with periods of one or half a year are undetectable because of the necessity of fitting for each pulsar's position and parallax during the analysis (this can be improved by using astrometric parameters independently measured through VLBI observations; see §3.4). Figure 1 shows examples of individually detectable SMBHB systems in a selected synthetic realisation of the cosmic SMBHB population using dark-blue triangle symbols. Another source of GWs in the PTA band is caused by the merger of two supermassive black holes; this may lead to a permanent deformation of their surrounding space-time, which can be detectable as a memory event that takes the form of a "glitch" in the timing residuals (van Haasteren & Levin 2010; Cordes & Jenet 2012).

3. Detecting gravitational waves

Direct gravitational wave detection and its subsequent confirmation is likely to be a long process. Currently, searches for GWs with PTAs are setting evermore stringent upper limits on the amplitude of the stochastic GW background. At some time (our predictions suggest that this will be soon), the signatures of the GWs (most likely red noise from a GW background) will become apparent in the timing residuals of the pulsars with the lowest rms timing residuals. At this point the bounds will not improve with time and it will become possible to study the signal, determine its amplitude, frequency (for a continuous wave source) or spectral index (for a background). However, confirmation of the GW nature of the signal will only come when the expected correlation signature for an isotropic stochastic GW background (Hellings & Downs curve; 1983), is found in the timing residuals of many pulsars. Making a highly significant measurement of such correlations requires much longer data sets than is needed for a bound. We therefore consider the following three scenarios for the SKA PTA project: 1) no sign of a GW signal has been seen in the existing PTA data, 2) a red noise signal has been identified, but the data sets are insufficient to "make a detection" and 3) a GW detection has already been made. We conclude this section by highlighting the role of Very Long Baseline Interferometry for improving the SKA's sensitivity to GWs.

3.1 No signal has been seen

With the current limits (e.g. Shannon et al. 2013) starting to constrain the low-redshift SMBHB population, it is likely that, by the time the SKA1 is commissioned, data from existing PTA experiments will already indicate the presence of a GW signal. However, if no such signal is observed then it is likely that either the pulse arrival times have not been measured with sufficient precision, that jitter noise is dominating the data sets, that not enough pulsars are being observed or that timing noise is affecting the detectability of the signal. The SKA can provide significant improvements in all these areas. With its unprecedented sensitivity the SKA should be able to observe a large number of currently unusable millisecond pulsars. The timing precision achievable for many pulsars will be limited by fluctuations in the pulse shape from individual pulses. This "jitter noise" (see §4 for more details) can be mitigated using the SKA by forming sub-arrays, and thereby integrating

PoS(AASKA14)037

for longer on multiple pulsars in parallel. With a much larger number of pulsars, timed with better precision than currently available, it is likely that GW detection can be made with shorter data spans (Rosado, Sesana & Gair in prep.). Having a shorter time span may also mitigate issues relating to timing noise. Moreover, we will be able to combine new data with archival data collected up to SKA operation, so that the crucial time baseline can be extended, albeit with a lower sensitivity.

3.2 Red noise signal has already been identified

If red noise (or a low-frequency signal) has been identified then the SKA data sets can be used in conjunction with the longer existing data sets to improve their sensitivity to GWs. Research is ongoing to make reasonable predictions for GW detection for a specified real (or future) data set. Siemens et al. (2013) made an initial attempt to calculate the scaling of the signal-to-noise of an idealised PTAs as the signal builds up in the array. They demonstrate that the significance of a detection of a GW signal will increase with longer data spans at a different rate for these three different regimes: 1) where the GW signal is weak and the white noise dominates, 2) where the GW signal is strong and 3) an intermediate regime where only the power in the lowest frequencies of the GW background is above the white noise level. A realistic array is likely to be complex and contain some pulsars for which the GW signal is weak compared to other red noise signals in the data, and other pulsars for which the signal will be comparatively strong. Consequently, it is challenging to make analytic predictions for the time to detection for a given array. A full analysis will require an improved understanding of the expected signal strength and the noise processes (such as timing noise and jitter noise), as well as a model-independent characterisation of the statistical properties of the signal.

3.3 GW detection has already been made

If a GW signal has already been detected and published then the SKA would begin the exciting work of studying the properties of the GWs and characterising the GW background and sources (see also §6). For instance an SKA PTA would:

- *Confirm the detection:* When a stochastic GW background has been detected, the signficance of the detection will increase as the quality and durations of data sets increase. SKA data sets would provide dramatically increased sensitivity and could be used to provide a confirmation of the detection, with a shorter timespan of data, different instrumentation, and different sample of millisecond pulsars.

- *Confirm the nature of the GW signal:* The induced residuals from a background of cosmic strings, the inflationary era, and merging supermassive black holes will all have the same characteristic angular signature. Futhermore, they all have red power spectra which will initially be indistinguishable. The SKA should be able to distinguish between the different spectral indices for the various sources. A confirmed GW background from supermassive black hole mergers would provide strong evidence of the existence for a large population of SMBHBs where each binary is separated by less than a parsec, proving another crucial prediction of the hierarchical model of structure formation (Sesana 2013b). Moreover, Mingarelli et al. (2013) show that some level of anisotropy may be present in the stochastic GW

PoS(AASKA14)037

background, and characterisation of the GW energy density at different angular scales carries information on the nature of the GW background. With increasing spatial and frequency resolution, SKA will be also able to identify the loudest astrophysical GW sources, disentangling individual SMBHBs from the overall GW background (e.g. Babak & Sesana 2012; Petiteau et al. 2013)

- *Detect a turn-over in the GW spectrum:* For a background of SMBHBs, the expected simple power-law form for the characteristic strain spectrum is only valid for circular binaries whose evolution is driven solely by GW emission (Sesana 2013a; Ravi et al. 2014). Any spectral turn-over would indicate interactions between the supermassive black holes and their environment (for instance, the effects of stellar scattering the presence of circumbinary discs). Furthermore, the GW spectrum for a background formed from cosmic strings could also have a complicated shape in the region of interest for PTA experiments (Sanidas et al. 2013).

3.4 The role of VLBI

For each pulsar in a PTA, the effect of a gravitational wave can be partially absorbed into parameters in the pulsar timing model, reducing low-frequency sensitivity. It is therefore advantageous to obtain independent measurements of the parameters that can be held fixed in the pulsar timing model. The most common method of providing external information is via Very Long Baseline Interferometry (VLBI), which yields very accurate positions in the International Celestial Reference Frame (ICRF). By repeating such measurements over time, pulsar reference positions, proper motions, parallaxes, and in some cases orbital parameters are obtained (e.g. Deller et al. 2013). In addition to being an independent source of information, unaffected by low-frequency GWs, VLBI astronomy gives higher precision than is possible via timing in almost all cases (see Paragi et al. 2015, for more details). A caveat is that at present transferral from the ICRF to the Solar system barycentric frame reduces the usefulness of the VLBI-derived *reference position* values, as the uncertainty in the frame tie (presently $\sim$milliarcseconds) is orders of magnitude larger than the formal uncertainty (but see however the third point below).

The three main benefits of VLBI information for gravitational wave searches are as follows:

1. The sensitivity is greatly improved to GWs with periods of $\sim$0.5 years and $\sim$1.0 years, due to the GW contribution no longer being absorbed into the fit for parallax and proper motion (plus reference position if transferrable; e.g. Madison et al. 2013).

2. If very accurate distances can be derived for one or more pulsars, such that the remaining uncertainty is a small fraction of a gravitational wavelength, then sensitivity to individual sources can be greatly enhanced. In this case, the contribution to the timing residuals from the gravitational wave at the pulsar (the "pulsar term") can be coherently accounted for (Lee et al. 2011), which is a particular benefit for the pulsars with the highest timing precision. If several such measurements can be made and multiple individual gravitational wave sources can be detected, then it will even be possible to determine the distances of other pulsars in the array to high precision using the gravitational wave fit directly (Lee et al. 2011; Boyle & Pen 2012)

PoS(AASKA14)037

3. By comparing a large sample of VLBI positions and pulsar timing positions, it will be possible to improve the planetary ephemeris used to convert pulsar arrival times to the solar system barycentre, which will lead to improved accuracy for timing-derived pulsar positions (Madison et al. 2013).

4. Limiting noise processes

The raw sensitivity of the SKA will enable ToAs to be determined with much higher precision and will allow a much larger sample of pulsars to be included in PTA experiments. However, even though the ToA timing precision will increase, a limit may exist in timing precision due to various effects like pulse jitter on short time scales, intrinsic pulsar timing noise on longer time scales and interstellar medium effects such as scattering (Cordes & Shannon 2012). In this section we describe the various noise processes that, if uncorrectable, will limit the achievable precision with the SKA.

4.1 Pulse jitter

The phenomenon of "jitter noise" results from intrinsic variability in the shape of individual pulses from a pulsar. This has been shown to be the limiting factor in the achievable timing precision for PSR J0437−4715 (Osłowski et al. 2011), where a floor of the timing precision of ~ 40 ns in a one-hour observation (and worse with shorter observations) is reached, even when using the largest telescopes available. Similar results have been found for PSR J1713+0747 using Arecibo observations (Shannon & Cordes 2012).

Jitter noise is thought to be, at some level, a limiting noise process. However, an improvement of nearly 40% in the rms timing residual for PSR J0437−4715 was achieved by using information from the polarised pulse profile (Osłowski et al. 2013), with the result ultimately limited by variable Faraday rotation in the Earth's ionosphere. Current studies of jitter noise are limited by the sensitivity of available telescopes, with only a handful of millisecond pulsars having detectable single pulses. As telescopes become larger, we will be able to significantly improve our understanding of the jitter phenomenon. This, along with robust calibration of data, could possibly lead to the development of strategies to remove the effects of jitter from SKA data.

If jitter noise is uncorrectable, the SKA holds no advantage for a jitter-dominated pulsar over a less-sensitive telescope. It is, however, likely that the SKA will observe many pulsars that are in the jitter-dominated regime. In order to maximise the scientific output it will therefore be essential to sub-array the telescope, enabling multiple pulsars to be observed simultaneously for long sessions.

4.2 Timing noise

An analysis of timing irregularities for 366 pulsars allowed the first large-scale analysis of timing noise over time-scales of >10 yr (Hobbs et al. 2010). The youngest pulsars were shown to be dominated by the recovery from glitch events (sudden increases in the spin frequency), while the timing irregularities for older pulsars seemed to exhibit quasi-periodic structure. Millisecond pulsars were included in the sample, but the data set used (from the Lovell telescope at Jodrell Bank) did not allow an analysis of timing noise with the precision necessary for PTA-research. The first major assessment of timing noise on the precision timing of millisecond pulsars concluded that

PoS(AASKA14)037

timing noise is present in most millisecond pulsars and will be measurable in many objects when observed over long data spans (Shannon & Cordes 2010).

There is currently no proven method for removing timing noise. Furthermore, the power spectrum of timing noise is red, with most of the power at low frequencies, and for some MSPs can be even steeper than the expected spectrum of the stochastic GW background. Timing noise will therefore provide a stringent limit for long-term timing projects. The SKA will need to either observe pulsars that exhibit small amounts of timing noise, observe a sufficiently large number of pulsars to achieve the science goals before timing noise dominates the residuals, or observe over long enough data spans for the timing noise level to plateau.

For young pulsars, timing noise can be modelled as a process in which the spin-down rate of the pulsar flips between two stable states (Lyne et al. 2010). These variations are accompanied by pulse profile changes as well. This leads to the possibilities that 1) millisecond pulsar timing noise can also be modelled as a two-state process and that 2) the state at a given time can be determined from the pulse shape. If true, it may be possible to completely remove the effect of timing noise.

4.3 Effects from the interstellar medium

The free electron content of the Galaxy affects radio wave propagation in a number of different ways. Most importantly, the presence of these charged particles changes the refractive index of the interstellar medium, and therefore the group velocity of the radio waves. In the context of pulsar timing, this is observed as a dispersion delay that strongly scales with the observing frequency ($\tau_{DM} \propto \nu^{-2}$) and which is characterised by the dispersion measure (DM), defined as the integrated electron density between the pulsar and Earth, in units of $\mathrm{cm}^{-3}\mathrm{pc}$ (Lorimer & Kramer 2005).

This dispersive delay in itself does not affect high-precision pulsar timing experiments, but because pulsars are high-velocity objects (Hobbs et al. 2004), the integrated electron density between Earth and a given pulsar changes slightly as the line of sight samples different regions of the turbulent interstellar medium (ISM) (Brisken et al. 2010). This makes the DM and its associated frequency-dependent delay time-variable, which in turn introduces unmodelled variations in the pulsar timing data. This time variability is the main cause of unmodelled ToA variations in high-precision pulsar timing data (Verbiest et al. 2009); therefore, mitigating this effect is a critical challenge in moving towards gravitational-wave detection (Keith et al. 2013; Lee et al. 2014).

There are essentially three approaches to dealing with this problem; and most likely a combination of approaches will be needed in order to obtain the best results.

Firstly, because the dispersive ISM delay is strongly frequency-dependent, observations with large bandwidths can measure these delays with very high accuracy. Lee et al. (2014) have evaluated the covariance of DM variation and timing precision, where they found that a wider band and better precision is necessary to reduce such covariance. Several pathfinder projects where ultra-broadband receivers simultaneously observe at all frequencies between $\sim$500MHz and $\sim$2 GHz are ongoing, and the efficacy of this approach is being evaluated. This method is unique because the data used for the high-precision timing project are the same data used for DM determination, allowing a simultaneous determination of all parameters at the cost of increased covariance between parameters. The main challenge of this method involves possible corruptions introduced by unmodelled frequency-dependence of the pulse profile and possible frequency-dependent behaviour of pulse phase jitter (see §4.1). In recent work by Liu et al. (2014) and Pennucci et al. (2014)

PoS(AASKA14)037

algorithms have been presented to model the frequency dependence of the pulse profile and improve the timing accuracy of pulsar observations obtained with wide band instruments. However, to accurately asses these problems SKA1 sensitivity is required.

A second approach is, instead of determining the DM values simultaneously across a very wide bandwidth, to use only the very lowest frequencies available ($\sim$100–300 MHz) to determine the DM values independently from the timing data obtained at higher frequencies. This approach puts smaller demands on available observing time and does not require a very high instantaneous bandwidth. One potential problem with this approach, however, is that the lowest observing frequencies may actually sample a different part of the ISM than the higher observing frequencies, because the refractive angles are different for different frequency bands. In practice this effect should be limited for a homogeneous and smooth ISM, but the turbulent ISM can hardly be expected to be smooth and homogeneous. This approach is currently being tested with the LOFAR pathfinder and as yet the inhomogeneities of the ISM do not seem to pose a problem (Hassall et al. 2012).

Finally, with sufficient sensitivity, a large telescope could collect pulsar timing data at high observing frequencies (3 GHz and up). This would strongly diminish the effects of DM variations and thereby avoid the need to correct for variable interstellar delays. The steep spectral index of most pulsars will require a longer integration time at these frequencies, but this may be required to combat the effects of pulse phase jitter. The clear disadvantage of this method, is two-fold: most importantly, without corrections for variable DMs, the red noise spectrum of the DM variations (Armstrong et al. 1995) will bring these variable delays to a level where they do affect the timing and hence gravitational-wave sensitivity. At that point, if no other multi-frequency information is available the data set will no longer be useful, as back-correction for DM variability is not possible. A secondary draw-back is that the spin-off science of studying the hot ionised component of the ISM would become impossible with high-frequency data alone.

A more subtle effect of the ionised interstellar medium is interstellar scattering. This effect is primarily observable through relatively innocuous variations in the pulsar's brightness (scintillation), caused through interference between rays with slightly different path lengths. In a more extreme form, this difference in path length between rays that are scattered off different density inhomogeneities in the ISM actually causes significant amounts of flux to arrive at the telescope with an observable delay. This causes the shape of the pulse profile to display an exponential decay (a so-called "scattering tail"). This scattering degrades timing precision because the scattering tail washes out any fine-scale features of the pulse profile (which are particularly useful in locking down the phase of the observed pulses). More importantly, if the scattering is time-variable (and, again, given the pulsar's high spatial velocity and the turbulent character of the ISM, this is to be expected), then the shape of the pulse profile will vary in time, affecting the timing in an unpredictable manner. Because of the strong dependence of scattering on density inhomogeneities, the scaling of scattering with frequency is less well-defined than for dispersive delays, but scattering strength typically scales even more strongly with frequency ($\propto \nu^{-4.4}$, Bhat et al. 2004), providing another impetus for high-frequency timing observations. While it is impossible to remove scattering exactly as in the case of dispersive delays, one promising technique termed cyclic spectoscopy has been demonstrated to retrieve the intrinsic, unscattered pulse profiles for one highly scattered, bright millisecond pulsar (Demorest 2011; Walker et al. 2013). A wider study is required to assess how broadly this method will be applicable to less scattered and weaker PTA pulsars.

PoS(AASKA14)037

5. A realistic PTA using the SKA

In this section we consider a realistic PTA project carried out using the SKA. We consider the expected number of pulsars, the plausible timing precision achievable, the time span for the experiment, specific issues relating to the SKA design, and the other telescopes available for PTA observations that will be operating at the same time as the SKA1.

5.1 Telescopes observing pulsars in the SKA1 era

While the SKA1 is being commissioned, the existing radio telescopes are expected to continue their PTA observations. Even with the increased sensitivity that the SKA1 provides, combining SKA1 data with the long time baselines of the existing PTAs improves the sensitivity for the detection of gravitational waves. Furthermore, it is essential for long-term pulsar timing experiments that a long overlap period is included between two observing systems in order to characterise the timing offsets between them. Finally, obtaining PTA observations with multiple telescopes provides greater cadence and coverage of observing frequencies.

As the SKA1 is commissioned it is likely that most of the current 100-m class telescopes will still be observing pulsars along with the Five-hundred-meter Aperture Spherical Telescope (FAST) and the Xinjiang Qitai 110m Radio Telescope (QTT) in China. The Giant Metrewave Radio Telescope (GMRT) in India may begin to play a larger role, as its capability to simultaneously observe at 300 and 600 MHz is useful for DM corrections. LOFAR could also be useful for DM montoring of Northern pulsars. The Murchison Widefield Array will complement LOFAR observations in the Southern hemisphere and can be used to monitor effects of the interstellar medium. In addition, the upcoming 100-m class CHIME (Canadian Hydrogen Intensity Mapping Experiment) will make daily observations of Northern-sky pulsars at frequencies between 400 and 800 MHz, providing densely-sampled records of DM and scattering changes toward the relevant MSPs.

At the time that SKA1 is commissioned the ASKAP COAST project is likely to be underway. This project aims to discover new pulsars (many of which may become part of the SKA PTA sample) and to carry out timing observations. The ASKAP sensitivity is relatively low and therefore it is likely that the majority of high precision timing being carried out in the Southern hemisphere at the time will be being obtained with Parkes telescope and the MeerKAT array. The baseline design indicates that the MeerKAT array will be combined as part of the SKA1-MID. However, it will be essential either for the Parkes telescope to provide an overlap period with the SKA1, or for MeerKAT to continue to operate in an overlap mode with the SKA1-MID for at least 1 year.

With the collecting area of FAST and the SKA1-MID, it is likely that most of the currently observed millisecond pulsars will be jitter dominated. An analysis of a PTA for the FAST telescope (Hobbs et al. 2014) showed that 1) long observation times ~ 1 hour per pulsar will still be required to obtain high time-precision observations for most of the currently known pulsars and 2) for pulsars that are jitter dominated there is no advantage (for timing purposes) in using a very large telescope (see also Liu et al. 2012). However, the SKA1-MID has the advantage that sub-arrays can be formed enabling observations of multiple pulsars (at, or close to, the jitter level) simultaneously.

Optimising the observation strategy has been investigated by Lee et al. (2012), where both the single and multiple telescope optimisations were considered under the influence of radiometer, jitter, and red noise. They found that, because of jitter noise, it is preferable to use a smaller telescope

PoS(AASKA14)037

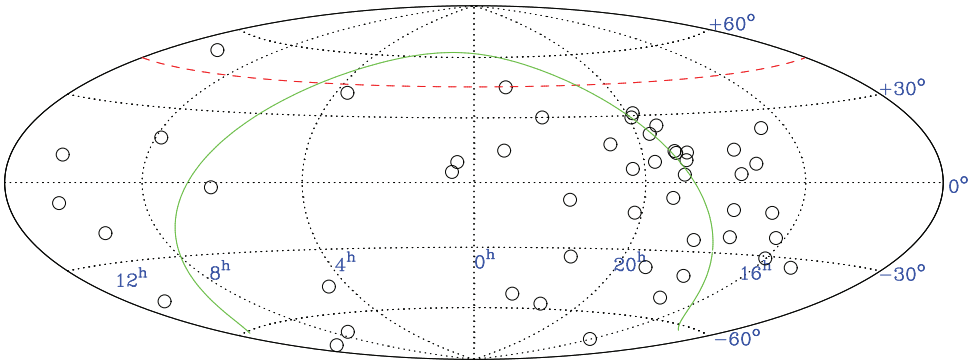

Figure 2: Expected sky coverage of the SKA, overlaid with the positions of the current pulsars being observed as part of the IPTA project (open circles). For an array mainly at latitude -30° the telescope will have an approximate declination range from -90° to $+45^\circ$ (red dashed line). We note that 49 out of the 50 current IPTA pulsars could be observed by the SKA. The green line indicates the Galactic plane.

to observe the brightest pulsars. In this way, for certain bright pulsars, it can be more efficient to split the SKA1-MID (or SKA1-LOW) into sub-arrays or use existing 100-m class telescopes.

5.2 Observing strategy

Current predictions for the detectable GW signal suggest that high cadence observing is important, but ensuring a long baseline of observations over years to decades is essential. A realistic scenario would be to observe a sample of pulsars once per week. In order to obtain the highest possible timing precision it will be necessary to obtain high quality polarisation calibration. This will require dedicated pointing directly at the pulsar. It is unlikely that more than one PTA-quality pulsar will be within the primary beam of the telescope, meaning that multiple tied-array beams will not necessarily be useful for the high precision timing programme, however the remaining beams can be used in parallel for other timing projects. The full sensitivity of the telescope will not be required in cases where the pulsars are dominated by jitter noise. In that case, it is more efficient to sub-array the telescope to observe multiple pulsars simultaneously.

It is likely that around 50 pulsars could be observed during a single 24-hour observing block providing a timing precision of <100 ns. This gives observation times of ~ 15 minutes per pulsar (assuming some nominal setup time for each observation) assuming that each pulsar is observed with two receivers. In order to account for DM and scattering variations it will be necessary to observe at a wide frequency range. Because of the steep radio spectra of pulsars, current PTA observations are limited to frequencies below ~ 3 GHz. With SKA1-MID, PTA observations will be carried out with bands 2, 3 and 4 (0.95 to 1.76 GHz, 1.65 to 3.05 GHz and 2.80 to 5.18 GHz respectively). As discussed in §4.3, lower frequency bands, and SKA1-LOW should be used for tracking variations in dispersion measures.

5.3 Offline data analysis

The data taken for the current PTA projects are generally stored in greatly compressed form, with typical data file sizes for a single pulsar observation currently around $\sim$ 1GB (for a data file containing 64 subintegrations, 1024 frequency channels and 2048 phase bins). These data

PoS(AASKA14)037

sizes have not posed any major challenges for current timing programmes. However, as data rates increase, recording, archiving and processing are all becoming more challenging. With wider bands available it is plausible that the SKA would produce data files of ~ 10 GB for each standard observation. A year of observing 100 pulsars with weekly cadence would lead to ~ 60 TB for each backend instrument. This is not impractical, but it will be necessary to provide copies of these data at the data processing centres. Furthermore, it is likely that new methods for high-precision timing will soon be developed. These could include using bright individual pulses, higher-order moments of the electric field, or dynamic spectra, all of which would require additional processing and the storage of additional products. Some methods, such as cyclic spectroscopy, may even require the storage of all data in raw, baseband form.

The supporting infrastructure that enables multiple copies of the data to be replicated at different sites and enables the processing of that data will need to be planned in detail. Keeping these systems operating and providing data and processing power to the community is non-trivial and will require significant management. Standard processing of the pulsar arrival times requires minimal computing resources. A typical set of 260 observations for a given pulsar spread over five years can easily be processed with the pulsar timing software package TEMPO2 (Hobbs et al. 2006) on a laptop computer. However, with the wide bandwidths available it is likely that a large number of ToAs at different frequencies will be calculated and stored for a single observation. Many of the gravitational wave detection codes (both frequentist and Bayesian based methods) require the analysis of $N_{\rm toa} \times N_{\rm toa}$ matrices and many of the algorithms require $N_{\rm toa}^3$ operations. This can quickly become prohibitive for a large number of ToAs, particularly if it is necessary to also run the detection code on a large number of simulated data sets. It is therefore essential that the data sets can be processed on high performance computers. Much of the pulsar processing software is now being modified to allow the use of Graphics Processing Units (GPUs) where available. GPUs are well suited for dealing with processing large matrices and we therefore recommend that the infrastructure created for the SKA allows the data to be processed both on Central Processing Units (CPUs) and also on GPUs.

5.4 Time to detection

In general, high-precision pulsar timing experiments rely on a sensitive telescope with sufficient frequency coverage to mitigate noise sources. As mentioned in §3, the success of detecting and studying GWs with the SKA depends on the quality of the observations and the number of pulsars in the array. In Figure 3, a comparison is shown between different PTA configurations and the probabilities of detecting a GW background or a continuous GW source. To produce these plots, $\sim 10^5$ simulations of the GW signal from SMBHBs have been analysed (Rosado, Sesana & Gair in prep.). All the models assumed in the production of these simulations are consistent with current electromagnetic observations (Sesana 2013a).

With the SKA as described in the baseline design document, it will have a 50% probability of detecting a GW source (either single or background) after five years. This is a conservative estimate since pre-existing IPTA data sets have not been included in the probability calculations. The PTA project on the SKA would not be significantly affected by a modification to the maximum and minimum baselines available. However, significant changes to the GW-sensitivity of the PTA would occur if a major reduction was made to the telescope sensitivity (e.g. fewer dishes

PoS(AASKA14)037

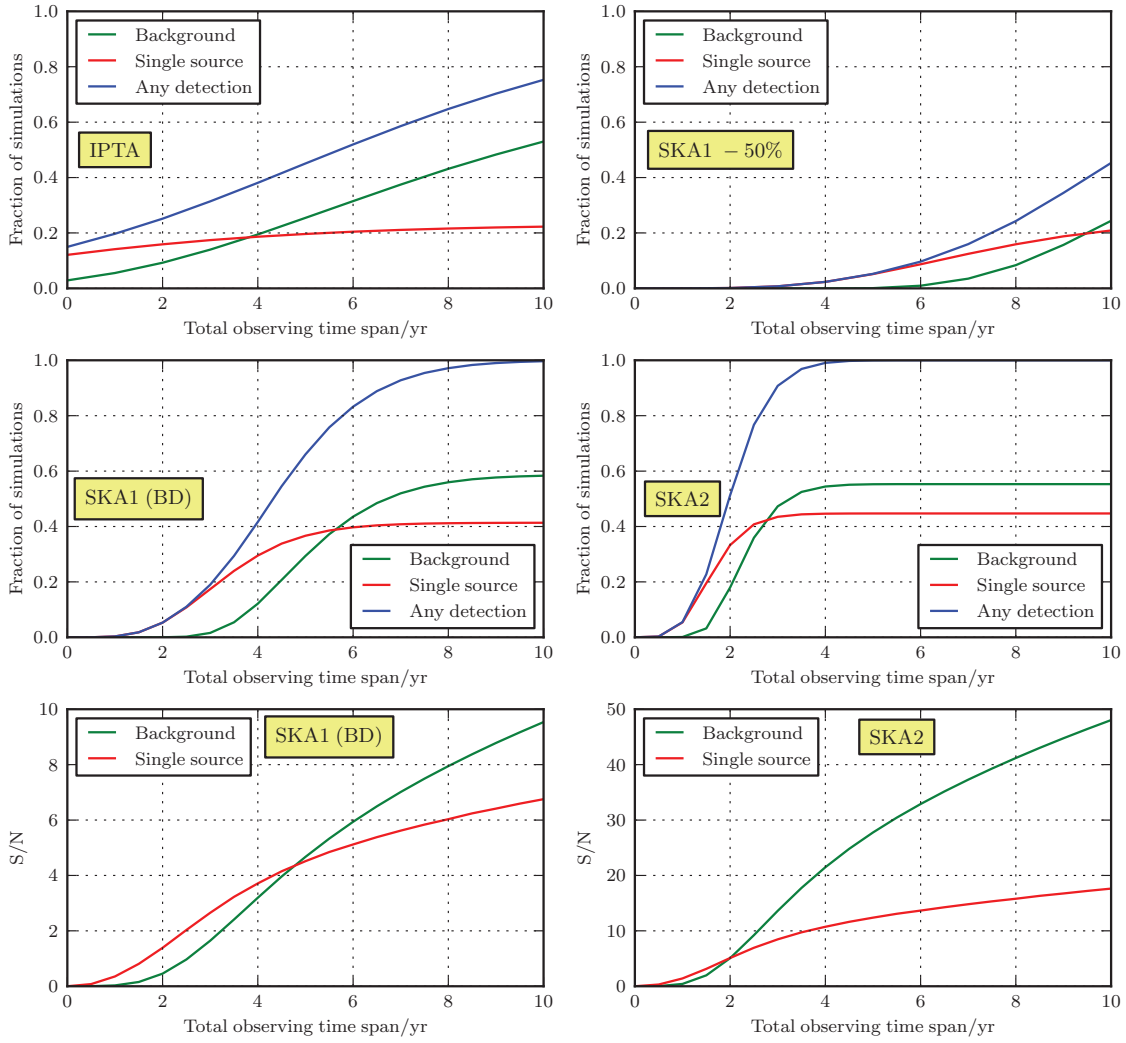

Figure 3: Detection probability for four different PTAs; top left: IPTA; top right: SKA1 at an early science (50%) sensitivity level; middle left: SKA1 as defined in the baseline design document; middle right: SKA2. The top and middle panels show the predictions on the *first* GW detection by different PTAs as a function of time. In the IPTA case, the starting point corresponds to the present day, after 10 years of previous observations. In the SKA cases, the starting points correspond to the beginning of the SKA data-taking, disregarding previous data. The green curve gives the fraction of simulations of the Universe (which can be considered as a probability) in which a stochastic background is detected first. The red curve gives the probability of a single binary being detected first. The blue curve gives the overall probability of detecting any kind of GW signal. We assume that a GW signal is detected when it produces a signal-to-noise ratio (S/N) larger than a certain threshold. The chosen S/N threshold is 4, which may be considered realistic for single binaries, but a bit conservative for a background. A more detailed study can be found in Rosado, Sesana & Gair (in prep.). The S/N of a detection of a single binary and of a background are obtained as described in Sesana & Vecchio (2010) and Siemens et al. (2013), respectively, and are plotted as function of time in the bottom plots for SKA1 and SKA2 PTAs.

PoS(AASKA14)037

or degraded receiver performance), if only a small frequency band was available or without the possibility of sub-arraying the telescope. The main effect of a reduced sensitivity on the SKA1 is a prolonged timescale for all GW detections. For example, in the case that the sensitivity of the SKA1 is reduced by 50%, the overall GW detection probability after five years is reduced to 10%.

6. The future of gravitational wave astronomy

SKA1, or the IPTA using pre-existing telescopes, is likely to make the first direct detection of GWs and will start to probe the properties of those waves. With the increased sensitivity of SKA2, gravitational wave astronomy will become a reality and the detailed properties of GWs can be studied. Unexplored territories of both astronomy and physics will be unveiled for the first time. The foreseeable breakthroughs include:

- *Constraining models for galaxy evolution:* Determining the GW properties (amplitude, spectral index, anisotropy or source distribution) of a GW background from coalescing supermassive black hole systems will lead to an improved understanding of galaxy evolution and black hole growth. With SKA2 it will eventually be possible to study the high end of the SMBHB mass distribution at low redshifts.

- *Source localisation and population:* By decomposing the stochastic GW background on a basis of spherical harmonics (Mingarelli et al. 2013), it is possible to characterise the GW background on any angular scale up to the maximum angular resolution of the PTA. This characterisation of the background can confirm its cosmological origin, but is also completely general. It is therefore possible to use this method to find GW hotspots, which may help to confine sky areas which need to be covered by continuous wave searches. Bayesian search techniques have been recently developed by Taylor & Gair (2013), and are being implemented in anisotropic stochastic GW background searches. A CMB-like search has also been recently proposed by Gair et al. (2014), which can be used to recover the components of an arbitrary background.

- *Testing gravity in the strong-field regime:* Although there is still lack of a consistent framework to quantise the well accepted theory of general relativity, the quantisation for weak GWs was succesfully initialised in the 1960s. There are two basic intrinsic properties for particles: their mass and spin states. In general relativity, the corresponding particles, the gravitons, are zero-mass spin-2 particles. However, other theories of gravity predict up to six polarisation states of GWs. Investigating the polarisation states and constraining the mass of the graviton with a PTA (Lee et al. 2008, 2010; Cordes & Shannon 2012; Chamberlin & Siemens 2012; Lee 2013) will help to understand the intrinsic symmetry of the gravitational interaction and may give valuable inputs for quantising gravity in the strong-field regime, which is one of the key questions of modern theoretical physics. While timing of binary pulsars is providing important insights into the dynamics of gravitation with strongly-gravitating bodies (Shao et al. 2015), PTAs will present an unique opportunity to study gravitation in the radiative regime with GWs.

PoS(AASKA14)037

- *Studying and testing cosmological GWs:* As shown by Sanidas et al. (2012), cosmic strings are predicted to generate a different GW background compared to a background generated by SMBHBs. The properties of a cosmic string-generated GW background are defined by their string linear energy density, the details of the string GW emission mechanism (kinks and cusps), the birth-scale of cosmic string loops, the intercommutation probability (the probability with which two cosmic string segments exchange partners when crossing each other) and possible deviations from the simple scaling evolution (e.g. Sousa & Avelino 2013). By identifying the GW background generated by cosmic strings, we will get access to a unique cosmological lab that will give us access to physics at an energy scale close to the GUT scale. In the case of cosmic superstrings, the expected results are even more profound since we will achieve a measurement of a fundamental string theory parameter for the first time, such as the fundamental string coupling or the compactification/warping scale. By measuring their properties, we will be able to investigate underlying dynamics and make a distinction between cosmic strings and superstrings. Besides the cosmic string stochastic GWB, an SKA PTA project might also be able to detect a stochastic GWB created by several other mechanisms in the early Universe, (e.g. Fenu et al. 2009; Figueroa et al. 2013).

- *GW distance scales:* When a sub-lightyear accuracy for pulsar distances can be achieved with SKA2 (Lee et al. 2011), Galactic dynamics can be investigated. A PTA is a unique type of GW detector working in the short wavelength regime, i.e. many radiation wavelengths separate pulsar pairs from each other and the Earth. This makes the angular resolution of PTA higher ($\delta\theta \simeq \lambda/D \sim 1$ arcmin; Lee et al. 2011) if we know the exact pulsar distance. With SKA1-MID, the pulsar distance will not be measured accurate enough, which prevents us from achieving such high resolution. Nevertheless, anisotropies in a GW background will still result in a different decomposition of the Hellings & Downs curve. When the nature of the anisotropy can be measured (Taylor & Gair 2013), the nature of the population of the GW sources can be studied (Mingarelli et al. 2013). With the SKA2, the pulsar timing parallax will bring the pulsar distance error down to a few light years. Such precise distance information will:
  I) make the PTA signal to single GW sources coherent, allowing perform GW interferometric imaging of the whole sky with angular resolutions of arcminutes (Lee et al. 2011). This will enable the search for electromagnetic counterparts to the GW sources, possibly enabling the follow-ups of GW sources with the traditional astronomical tools which can lead to the study of galaxy mergers (Burke-Spolaor 2013; Rosado & Sesana 2014; Deane et al. 2015).
  II) allow us to measure the mass and spin of a SMBHB and map the non-linear dynamics of the gravitational field (Mingarelli et al. 2012); when the pulsar term can be distinguished from the Earth term, each pulsar term sees a slightly different piece of the evolutionary history of the binary since its orbital period evolves over the light travel time between the Earth and the pulsar. Concatenating these different snapshots of the waveform may allow for the measurement of the mass and spin of the binary, and furthermore, measuring post-Newtonian parameters up to 1.5 order.

- *Probing the inflationary era of the universe:* There are two major methods to probe the inflationary era of the universe with PTA. The first one is to examine relic GWs, which give

PoS(AASKA14)037

constraints on the tensor-to-scalar ratio (Zhao et al. 2013). The second one is to check the effects of structure formation, e.g. primordial black hole population, which give us information on the primordial density fluctuation (Saito & Yokoyama 2009).

7. Conclusions

The first direct detection of GWs in the nano-Hertz regime using PTA observations is expected within a decade. The SKA will play an important role in this, either through making the first detection, or by confirming the detection independently, and providing the sensitivity to characterise continuous sources as well as the stochastic GW background. In general, pulsar timing precision will be greatly enhanced by the unprecedented collecting area and bandwidth of the SKA, and PTA sensitivity will be revolutionised though regular observations of a large number of pulsars. These would include many of the weaker pulsars wich may – through the added sensitivity of the array – for the first time be timed at the precision that is required for PTA work.

In the early stages of the science, even before the SKA PTA achieves a direct GW detection, these data sets will already enable exciting scientific results; for example tests of theories of gravity, studies of binary and millisecond pulsars, searches for irregularities in the terrestrial time standards, and studies of the interstellar medium. While these results are scientifically interesting in their own right, they will also aid the characterisation of the pulsars and the observing system in a way that continuously enhances our sensitivity to GWs. Without a doubt, a PTA is an ideal experiment for the SKA.

References

Ade, P. A. R. et al. (Bicep2 Collaboration) 2014, Physical Review Letters, 112, 241101
Armstrong, J. W., Rickett, B. J., & Spangler, S. R. 1995, ApJ, 443, 209
Arzoumanian, Z., Brazier, A., Burke-Spoloar, S., et al. 2014, ApJ, 794, 141
Babak, S. & Sesana, A. 2012, Phys. Rev. D, 85, 044034
Bhat, N. D. R., Cordes, J. M., Camilo, F., et al. 2004, ApJ, 605, 759
Boyle, L. & Pen, U.-L. 2012, Phys. Rev. D, 86, 124028
Brisken, W. F., Macquart, J.-P., Gao, et al. 2010, ApJ, 708, 232
Burke-Spolaor, S. 2013, Class. Quant Grav., 30, 224013
Chamberlin, S. J. & Siemens, X. 2012, Phys. Rev. D, 85, 082001
Champion, D. J., Hobbs, G. B., Manchester, et al. 2010, ApJ, 720, L201
Cordes, J. M. & Jenet, F. A. 2012, ApJ, 752, 54
Cordes, J. M., Kramer, M., Lazio, T. J. W., et al. 2004, New Astr., 48, 1413
Cordes, J. M. & Shannon, R. M. 2012, ApJ, 750, 89
Deane, R., Paragi, Z., Jarvis, M., et al., 2015, "Multiple supermassive black hole systems: SKA's future leading role", in proc. *Advancing Astrophysics with the Square Kilometre Array*, PoS(AASKA14)151
Deller, A. T., Boyles, J., Lorimer, D. R., et al. 2013, ApJ, 770, 145
Demorest, P. B. 2011, MNRAS, 416, 2821
Demorest, P. B., Ferdman, R. D., Gonzalez, M. E., et al. 2013, ApJ, 762, 94

PoS(AASKA14)037

Detweiler, S. 1979, ApJ, 234, 1100
eLisa Constortium: Seoane, P. A., Aoudia, S., et al. 2013, arXiv:1305.5720
Ellis, J. A. 2013, Class. Quant Grav., 30, 224004
Ellis, J. A., Siemens, X., & Creighton, J. D. E. 2012, ApJ, 756, 175
Fenu, E., Figueroa, D. G., Durrer, R., et al. 2009, Journal of Cosm. and Astro-Particle Phys., 10, 5
Figueroa, D. G., Hindmarsh, M., & Urrestilla, J. 2013, Phys. Rev. Lett., 110, 101302
Foster, R. S. & Backer, D. C. 1990, ApJ, 361, 300
Gair, J. R., Romano, J. D., Taylor, S., & Mingarelli, C. M. F. 2014, Phys. Rev. D, 90, 082001
Hassall, T. E., Stappers, B. W., Hessels, J. W. T., et al. 2012, A&A, 543, A66
Hellings, R. W. & Downs, G. S. 1983, ApJ, 265, L39
Hobbs, G., Coles, W., Manchester, R. N., et al. 2012, MNRAS, 427, 2780
Hobbs, G., Dai, S., Manchester, R. N., et al.2014, arXiv: 1407.0435
Hobbs, G., Lyne, A. G., & Kramer, M. 2010, MNRAS, 402, 1027
Hobbs, G., Lyne, A. G., Kramer, M., et al. 2004, MNRAS, 353, 1311
Hobbs, G. B., Edwards, R. T., & Manchester, R. N. 2006, MNRAS, 369, 655
Jenet, F. A., Hobbs, G. B., van Straten, W., et al. 2006, ApJ, 653, 1571
Jenet, F. A., Lommen, A., Larson, S. L., & Wen, L. 2004, ApJ, 606, 799
Kaspi, V. M., Taylor, J. H., & Ryba, M. 1994, ApJ, 428, 713
Keith, M. J., Coles, W., Shannon, R. M., et al. 2013, MNRAS, 429, 2161
Kramer, M., Backer, D. C., Cordes, J. M., et al. 2004, New Astron. Rev., 48, 993
Kramer, M. & Champion, D. J. 2013, Class. Quant Grav., 30, 224009
Kramer, M. & Stappers, B. 2010, in ISKAF2010 Science Meeting, arXiv: 1009.1938
Lee, K., Jenet, F. A., Price, R. H., et al. 2010, ApJ, 722, 1589
Lee, K. J. 2013, Class. Quant Grav., 30, 224016
Lee, K. J., Bassa, C. G., Janssen, G. H., et al. 2014, MNRAS, 441, 2831
Lee, K. J., Bassa, C. G., Janssen, G. H., et al. 2012, MNRAS, 423, 2642
Lee, K. J., Jenet, F. A., & Price, R. H. 2008, ApJ, 685, 1304
Lee, K. J., Wex, N., Kramer, M., et al. 2011, MNRAS, 414, 3251
Liu, K., Desvignes, G., Cognard, I., et al. 2014, MNRAS, 443, 3752
Liu, K., Keane, E. F., Lee, K. J., et al. 2012, MNRAS, 420, 361
Lorimer, D. R. & Kramer, M. 2005, Handbook of Pulsar Astronomy (Cambridge University Press)
Lyne, A., Hobbs, G., Kramer, M., et al. 2010, Science, 329, 408
Madison, D. R., Chatterjee, S., & Cordes, J. M. 2013, ApJ, 777, 104
Manchester, R. N., Hobbs, G., Bailes, M., et al. 2013, PASA, 30, 17
Manchester, R. N. & IPTA. 2013, Class. Quant Grav., 30, 224010
Mingarelli, C. M. F., Grover, K., Sidery, T., et al. 2012, Phys. Rev. Lett., 109, 081104
Mingarelli, C. M. F., Sidery, T., Mandel, I., & Vecchio, A. 2013, Phys. Rev. D, 88, 062005
Ölmez, S., Mandic, V., & Siemens, X. 2010, Phys. Rev. D, 81, 104028
Osłowski, S., van Straten, W., Demorest, P., & Bailes, M. 2013, MNRAS, 430, 416
Osłowski, S., van Straten, W., Hobbs, G. B., et al. 2011, MNRAS, 418, 1258
Paragi, Z., Godfrey, L., Reynolds, C., et al. 2015, "Very Long Baseline Interferometry with the SKA", in proc. *Advancing Astrophysics with the Square Kilometre Array*, PoS(AASKA14)143
Pennucci, T. T., Demorest, P. B., & Ransom, S. M. 2014, ApJ, 790, 93

PoS(AASKA14)037

Petiteau, A., Babak, S., Sesana, A., & de Araújo, M. 2013, Phys. Rev. D, 87, 064036
Phinney, E. S. 2001, arXiv:astro-ph/0108028
Pitkin, M., Reid, S., Rowan, S., & Hough, J. 2011, Living Reviews in Relativity, 14, 5
Planck Collaboration XXX 2014, arXiv:1409.5738
Ravi, V., Wyithe, J. S. B., Hobbs, G., et al. 2012, ApJ, 761, 84
Ravi, V., Wyithe, J. S. B., Shannon, et al. 2014, MNRAS, 442, 56
Romani, R. W. 1989, in Timing Neutron Stars, ed. H. Ögelman & E. P. J. van den Heuvel, 113–117
Rosado, P. A. & Sesana, A. 2014, MNRAS, 439, 3986
Saito, R. & Yokoyama, J. 2009, Phys. Rev. Lett., 102, 161101
Sanidas, S. A., Battye, R. A., & Stappers, B. W. 2012, Phys. Rev. D, 85, 122003
Sanidas, S. A., Battye, R. A., & Stappers, B. W. 2013, ApJ, 764, 108
Sesana, A. 2013a, Class. Quant Grav., 30, 224014
Sesana, A. 2013b, MNRAS, 433, L1
Sesana, A. & Vecchio, A. 2010, Phys. Rev. D, 81, 104008
Sesana, A., Vecchio, A., & Colacino, C. N. 2008, MNRAS, 390, 192
Shannon, R. M. & Cordes, J. M. 2010, ApJ, 725, 1607
Shannon, R. M. & Cordes, J. M. 2012, ApJ, 761, 64
Shannon, R. M., Ravi, V., Coles, W. A., et al. 2013, Science, 342, 334
Shao, L., Stairs, I. H., Antoniadis, J., et al. 2015, "Testing Gravity with Pulsars in the SKA Era", in proc. *Advancing Astrophysics with the Square Kilometre Array* PoS(AASKA14)042
Siemens, X., Ellis, J., Jenet, F., & Romano, J. D. 2013, Class. Quant Grav., 30, 224015
Sousa, L. & Avelino, P. P. 2013, Phys. Rev. D, 88, 023516
Stappers, B. W., Hessels, J. W. T., Alexov, A., et al. 2011, A&A, 530, A80
Taylor, J. H. & Weisberg, J. M. 1982, ApJ, 253, 908
Taylor, S. R. & Gair, J. R. 2013, Phys. Rev. D, 88, 084001
Tong, M. L., Zhang, Y., Zhao, W., et al. 2014, Class. Quant Grav., 31, 035001
van Haarlem, M. P., Wise, M. W., Gunst, A. W., et al. 2013, A&A, 556, A2
van Haasteren, R. & Levin, Y. 2010, MNRAS, 401, 2372
van Haasteren, R., Levin, Y., Janssen, G. H., et al. 2011, MNRAS, 414, 3117
van Haasteren, R., Levin, Y., McDonald, P., & Lu, T. 2009, MNRAS, 395, 1005
Verbiest, J. P. W., Bailes, M., Coles, W. A., et al. 2009, MNRAS, 400, 951
Walker, M. A., Demorest, P. B., & van Straten, W. 2013, ApJ, 779, 99
Yardley, D. R. B., Coles, W. A., Hobbs, G. B., et al. 2011, MNRAS, 414, 1777
Yardley, D. R. B., Hobbs, G. B., Jenet, F. A., et al. 2010, MNRAS, 407, 669
Zhao, W., Zhang, Y., You, X.-P., & Zhu, Z.-H. 2013, Phys. Rev. D, 87, 124012

PoS(AASKA14)037

PROCEEDINGS OF SCIENCE

Understanding pulsar magnetospheres with the SKA

A. Karastergiou[*1], **S. Johnston**[2], **N. Andersson**[3], **R. Breton**[4], **P. Brook**[1], **C. Gwinn**[5], **N. Lewandowska**[6], **E. Keane**[7], **M. Kramer**[8], **J.-P. Macquart**[9], **M. Serylak**[10], **R. Shannon**[2], **B. Stappers**[11], **J. van Leeuwen**[12], **J. P. W. Verbiest**[13], **P. Weltevrede**[11], **G. Wright**[14,11]

[1] *Oxford Astrophysics, Oxford, UK. E-mail:* aris@astro.ox.ac.uk; [2] *CSIRO Astronomy & Space Science, Australia Telescope National Facility;* [3] *University of Southampton, UK;* [4] *University of Southampton, UK;* [5] *University of California, Santa Barbara, USA;* [6] *University of Würzburg, Germany;* [7] *Swinburne University of Technology, Australia;* [8] *Max-Planck-Institut fuer Radioastronomie, Germany.;* [9] *ICRAR/Curtin Institute of Radio Astronomy, Australia;* [10] *University of the Western Cape, South Africa;* [11] *University of Manchester, UK;* [12] *ASTRON, The Netherlands;* [13] *Universitaet Bielefeld Germany;* [14] *University of Sussex, UK*

The SKA will discover tens of thousands of pulsars and provide unprecedented data quality on these, as well as the currently known population, due to its unrivalled sensitivity. Pulsars are known to be variable on numerous timescales: from nanoseconds to decades, corresponding to events, likely associated with the emission process itself through to discrete stable magnetospheric states. Timescales in between show phenomena such as pulse-to-pulse variations, sub-pulse drifting and nulling in operation, in addition to the relevant orbital, cooling and magnetic field decay timescales. The SKA will allow us to study these effects with higher fidelity than ever before. Moreover, it will be possible to perform these studies down to the individual pulse level for a large sample of millisecond pulsars. With their significantly different magnetic field strength and magnetospheric extent, this will provide important clues to the magnetospheric physics. Polarization profiles of a large number of pulsars, and their evolution over a broad frequency range, will enable us to perform measurements, with unprecedented detail, of the geometry of the emission regions of these systems. In addition to studying the plethora of new sources, we will perform intense targeted studies of already known objects. For example, with the SKA we will get a unique view of the magnetospheres of the two stars in the Double Pulsar System, down to the precision of a single rotation period, over a wide range of frequencies with full polarization information. We will be able to map the magnetospheres of selected sources by performing high sensitivity observations from 50 MHz all the way through to gamma-rays. Furthermore, using scintillation imaging techniques, we will be able to actually resolve pulsar magnetospheric features. With the good sample of radio-emitting magnetars from SKA, we will be able to compare, and identify any magnetospheric differences, between these and the standard pulsar population. As well as finally settling the questions about the pulsar emission mechanism and magnetospheric structure once and for all, we can use this understanding to improve pulsars' usefulness as astrophysical tools.

Advancing Astrophysics with the Square Kilometre Array
June 8-13, 2014
Giardini Naxos, Italy

PoS(AASKA14)038

1. Pulsar magnetospheres and the SKA

Pulsar radio emission is used as a high precision tool in a number of astrophysical experiments. Currently, the most high profile experiments involve tests of gravity through pulsar timing, and the related search for a stochastic gravitational wave background. To take full advantage of the intrinsic rotational stability that characterizes pulsars, it is necessary to model all the effects that perturbe the measured pulse times-of-arrival. Over the past decade, the importance of modelling radio pulse propagation through the interstellar medium has been understood, and improvements are now becoming evident in timing residuals. This has revealed the next level of "timing noise", most likely related to processes that occur near and within the radio emitting magnetosphere. For the first time, it is becoming clear that the lack of understanding of the pulsar radio emission mechanism is presenting obstacles to experiments that use pulsars as tools.

The quest to improve this situation with the SKA, relies on its ability to deliver the following elements:
1. high sensitivity, to observe individual pulses from pulsars at a high signal-to-noise ratio;
2. broadband receivers and backends, to study the frequency dependence of emission phenomena;
3. polarization, to better understand the pulsar geometries, the structure of the pulsar radio beams and the details of emission and propagation in the pulsar magnetosphere.
4. high-cadence monitoring, by observing multiple sources in sub-array mode, to uncover the physics that govern variability on all timescales.

The sole motivation to understand the radio emission mechanism is not to improve timing experiments. A steady stream of science output in areas such as relativistic plasmas in the magnetosphere, variability due to internal or external triggers, pulsar winds and supernova physics has resulted from the study of details of the radio emission mechanism on numerous interesting pulsars. The SKA surveys will deliver a new population of radio pulsars, among which we expect a group of sources that are ideal to address specific aspects of the emission mechanism problem (e.g. pulsars with interpulses for polarimetric studies of pulsar geometry).

In this chapter, we present the state of the art in observations aiming at understanding the magnetospheres of pulsars. We address this topic from three angles:
1. Understanding the three dimensional (3D) structure of the radio emission beam;
2.Understanding how magnetospheres evolve between different classes of pulsars;
3. Unlocking the information in the characteristic observational timescales of pulsar emission.

2. The radio emission beam

Our current understanding of the emission mechanism which operates in the magnetospheres of radio pulsars is limited. Progress can be achieved by determining where in the magnetosphere the radio emission is generated. Understanding where charged particles are accelerated to relativistic energies, would provide a better picture of the global pulsar electrodynamics, an essential element in solving the puzzle of how pulsars operate. In this section it is described how radio observations with the SKA are expected to advance our understanding of the elusive radio emission mechanism by allowing the construction of a 3D map of the pulsar magnetosphere.

*Speaker.

PoS(AASKA14)038

2.1 Pulsar geometry and polarization

Radio polarization measurements allow geometrical properties of the radio beam to be quantified. Basic viewing geometry parameters include the magnetic inclination angle (angle between the magnetic dipole axis and the rotation axis of the neutron star) and the angle between our line-of-sight and the rotation axis. Since the early days of pulsar astronomy, the way the position angle of the linear polarization changes during the rotation of the star (PA-swing) is interpreted with the rotating vector model (Radhakrishnan & Cooke 1969; Komesaroff 1970, RVM), which directly depends on these two angles. Another important parameter of the emission beam, which can be derived using polarization measurements, is the radio emission height: co-rotation of the emitting region causes the PA-swing to be delayed with respect to the pulse profile, the magnitude of the shift being determined by the emission height (Blaskiewicz et al. 1991).

Currently, the viewing geometries have been derived for about a hundred objects (see e.g. Rankin 1990; Gould 1994), while emission heights are determined for only a fraction of those (e.g. Mitra & Rankin 2002; Rankin 1993; Weltevrede & Johnston 2008a). There are a number of complications which limit the precision and the fraction of the total population of pulsars suitable for this kind of analysis. Firstly, emission is only observed for a small interval of the rotation of the star. This limit makes a large range of RVM solutions become degenerate and in virtually all cases the viewing geometry cannot be determined from RVM fitting alone. In order to get unique solutions, additional assumptions are necessary. However, this introduces large and poorly understood systematics. Drawing statistical conclusions about the population as a whole is, therefore, known to be problematic, and emission heights determined in different ways often do not agree (see e.g. Mitra & Li 2004; Weltevrede & Johnston 2008a). Secondly, many pulsars do not have RVM-like PA-swings, showing that our understanding of pulsar polarization is incomplete. This severely limits the sample suitable for studying their viewing geometry. Moreover, because young pulsars are more suitable for this kind of analysis (see e.g. Johnston & Weisberg 2006; Weltevrede & Johnston 2008a) and references therein), the sample is necessarily biased. Thirdly, the above method to determine emission heights requires knowledge about which point in the radio profile corresponds to the closest approach of the line of light to the magnetic axis. Therefore knowledge about how the emission regions are distributed within the beam is crucial.

There is currently only one pulsar for which RVM fitting alone provide us with a unique viewing geometry without making additional assumptions (Kramer & Johnston 2008). This was possible because this pulsar has an interpulse (both magnetic poles are observed, which provides more rotational phase coverage) and it is young (therefore the PA-swing obeys the RVM very precisely). Simply observing currently known pulsars with a greater sensitivity is not expected to be effective, as systematic errors are the problem. The key is to find more of these "ideal case" pulsars, which then can be used to find out which additional assumptions are justified allowing emission geometries to be determined for a larger sample.

The SKA will discover many additional pulsars, including a sufficiently large "clean" sample of pulsars with RVM-like PA-swings to allow statistical studies of the pulsar population. As described above, this will be a biased sample in terms of their location in the P-$\dot{P}$ diagram. By comparing the results of the "clean" sample with the results of a larger sample the poorly understood biases can be investigated in detail. This ultimately will lead to a better understanding in the

PoS(AASKA14)038

physical processes which are currently missing in models, thereby advancing our understanding of the emission mechanism.

As shown for instance by Dyks (2008), non-RVM-like PA-swings can teach us about the deformations of the magnetic field structure due to magnetospheric currents and rotational sweep-back of the magnetic field lines (see e.g. Dyks & Harding 2004). The determination of emission geometries can also be used to determine the way the magnetic inclination angle changes over time (Tauris & Manchester 1998; Weltevrede & Johnston 2008b; Young et al. 2010), which provides information about the torque acting on the pulsar. In addition, propagation effects of the radio waves in the pulsar magnetosphere are expected (e.g. Boyle & Pen 2012). Better understanding will allow the relevant plasma parameters of the emission mechanism to be determined. Good determination of emission geometry is also important for the study of drifting subpulses, as it allows the emission fluctuations observed for our line-of-sight to be related to a changing beam structure over time (see e.g. Deshpande & Rankin 2001; Vivekanand & Joshi 1997).

2.2 Radio emission regions

Despite the limited success at building a theoretical framework for the interpretation of pulsar radio emission, empirical models that attempt classifications of emission characteristics have uncovered observational patterns that any theory should be able to account for. For example, in a series of papers by Rankin and collaborators (Rankin 1983, 1990, 1993), evidence is presented that points to radio emission emanating from sets of active magnetic field lines, forming one, two or more hollow cones of emission. Different heights then correspond to different frequencies, in accordance with the observation that pulse profiles often become narrower towards high frequencies (e.g. Thorsett 1991). In addition to the hollow cones, Rankin's classification included a type of component originating close to the magnetic axis which was labelled core. These often show distinguishing emission properties such as steeper spectra and complicated polarization features.

In contrast, Lyne & Manchester (1988) showed that the two-dimensional organization of radio components of a large population of pulsars is patchy, and although their characteristics broadly match the Rankin classification, there is no strong evidence of two emission mechanisms for core and cone emission. It was also noted that some young pulsars have observable emission from both magnetic poles. This property, coupled with the wide, relatively simple profiles of young pulsars and their polarization characteristics, was used by Johnston & Weisberg (2006) to suggest that radio emission originates from high altitudes in young pulsars compared to the older pulsar population. This idea was expanded further Karastergiou & Johnston (2007) to produce a phenomenological model that statistically explains the complexity of profiles from young and old pulsars (not millisecond pulsars). The main element of this model includes emission from a small number of discrete multiple heights for older pulsars, following ideas presented in Gangadhara & Gupta (2001). Multiple emission heights have implications on geometrical modeling.

Broadband observations, polarization and sensitive single pulse observations are all essential to understanding the detailed 3D location of radio emission regions in pulsar magnetospheres.

2.3 Radio spectra and broadband nature of emission

The radio emission of pulsars is produced by relativistic particles in the circumpulsar plasma. Pulsar spectra must be explained by a model which describes the emission mechanism, in com-

PoS(AASKA14)038

bination with the energy distribution of the particles responsible for the observed emission (e.g. Malofeev & Malov 1980). Therefore, detailed measurements of pulsar spectra provide valuable information about how the radio emission is produced. In addition, understanding the pulsar spectrum in a statistical sense for the pulsar population is crucial for population synthesis to refine models for the parent distribution of pulsars, which gives rise to the observed distribution (Bates et al. 2013).

The spectra of radio pulsars are broadband and resemble (at least to first order) power laws with a relatively steep frequency dependence. Above $\sim$200 MHz the average spectral index was shown by Maron et al. (2000) to be -1.8, with a standard deviation of 0.2 (i.e. pulsars are brighter at lower frequencies), although Bates et al. (2013) suggest a mean spectral index closer to -1.4 with unity standard deviation. The dependence on pulsar parameters, such as P and $\dot{P}$, is weak, but correlations with characteristic age are found (Lorimer et al. 1995). Understanding the way spectra depend on the spin parameters will give insight into how magnetospheric conditions change throughout the $P-\dot{P}$ diagram.

In general, deviations are observed from this first order behavior, one of which is that at lower frequencies, the spectrum often "turns over" (e.g. Sieber 2002, and references therein). It is currently unknown if this is because of a decrease in efficiency of the emission mechanism, or because of an absorption mechanism becoming effective. It is also not known why some pulsars do not have these low-frequency turnovers, but others do. There is a hint that these spectral turnovers do not happen for millisecond pulsars (Kuzmin & Losovsky 2001), suggesting that their magnetospheric conditions are significantly different compared to normal (non-recycled) pulsars. Apart from the lack of a spectral break at low frequencies the spectra of MSPs and slow pulsars are remarkably similar (Kramer et al. 1998). At higher frequencies ($\sim$ 10 GHz or above) spectral breaks are observed, such that the spectrum flattens or even turns up (Wielebinski et al. 1993; Kramer et al. 1997).

A complication in the interpretation of radio spectra is that the observed spectrum is affected by a geometric feature. This feature arises because the beam shape is frequency dependent such that we see different parts of the beam at different frequencies. An understanding of this effect is therefore crucial to infer the intrinsic spectra from those observed.

2.4 The interstellar medium as an interferometer of resolved pulsar magnetospheres

Interstellar scintillation affords the potential to resolve the tiny emission regions of pulsars. By virtue of the compactness of the emission, pulsar radiation is subject to strong interference effects as it propagates through the turbulent plasma of the Interstellar Medium (ISM). However, pulsar magnetospheres have a finite size and, for extended sources, each ray path produces a subimage. The radiation observed at Earth is the result of the interference between many thousands of subimages, or speckles, across the scattering region. Since the scale of the speckle pattern exceeds $\sim$ 10 AU in some cases (e.g Brisken et al. 2010), interstellar scattering offers the prospect of achieving *p*icoarcsecond angular resolution. Scintillation-based tests of the emission size fall into three broad categories according to the manner in which the finite size of the emission region manifests itself on the radiation properties.

An angular displacement in the emission site causes a lateral displacement in the scintillation pattern at Earth. If that displacement is parallel to the direction of motion of the pulsar, and the

PoS(AASKA14)038

turbulence is "frozen", then a lag in time produces precisely the same effect on the scintillation pattern as a change in pulse phase. This technique was applied by Wolszczan & Cordes (1987) during a double imaging event to place an upper limit on the emission size of PSR B1237+25 of 10^6 km, roughly an order of magnitude larger than its light cylinder.

Although the different lines of sight from the source are coherent, the different parts of the subimages are not. For a point source, interference forms a diffraction pattern, a "scintillation pattern", in the observer plane. The intensity varies randomly from zero to many times the average; indeed, zero intensity is the most common value. A resolved source forms a superposition of diffraction patterns from each individual point on the source; these points are not coherent, so that the observed pattern is the incoherent superposition of the patterns from a point source. The effect upon the diffraction pattern depends on the size of the source, with a typical scale of the angular resolution of the scattering region, viewed as a lens, as the size of a source that affects the distribution of intensity significantly. The observed distribution of intensity, or of interferometric visibility, provides a measure of the size of the source. Comparison of the pattern between two widely spaced observatories can provide information on the shape of the source. The technique was used by Gwinn et al. (2012) to measure a size for the emission region of the Vela pulsar of < 100 km to 1000 km, with the smallest size near pulse center and the largest at the beginning and end. A single-dish technique was used by Johnson et al. (2012) to set an upper limit of < 40 km, averaged over the entire pulse. The difference in measured size may reflect the emergence of an additional, "conal" component at the shorter wavelength, the broader pulse, or other factors.

The technique of speckle scintellometry extends the technique that deduces the emission region structure based on the lateral displacement of the scintillation pattern by using holographic techniques to further boost the S/N of the pulsar signal by partially descattering the radiation (Walker et al. 2008). Application of this technique to PSR B0834+06 yields a determination of the astrometric phase shift across the pulse profile equivalent to an angular resolution of 150 picoarcseconds, or 10 km at the distance of the pulsar (Pen et al. 2014).

2.5 Neutron Star Precession

2.5.1 Mapping pulsar beams

The observed pulse profiles show a large variety of shapes produced by a one-dimensional cut through the two-dimensional intensity distribution given by the pulsar beam. In General Relativity, the proper reference frame of a freely falling object suffers a precession with respect to a distant observer, called geodetic precession. In a binary pulsar system, this geodetic precession leads to a relativistic spin-orbit coupling, analogous to spin-orbit coupling in atomic physics. As a consequence, the pulsar spin axis precesses about the total angular momentum vector, changing the relative orientation of the pulsar towards Earth. In such a case, we should expect a change in the radio emission received from the pulsar, as first proposed by Damour & Ruffini (1974) very soon after the discovery of PSR B1913+16. Indeed, as our line-of-sight moves through the emission beam, each profile represents a slightly different cut through the beam structure. By adding measured profiles in the right order, it is possible to reconstruct a real 2-D map of a pulsar beam. One also expects that the polarization will change with time. Currently, such an experiment has been successfully applied to PSRs B1913+16 (Weisberg & Taylor 2002; Clifton & Weisberg 2008;

PoS(AASKA14)038

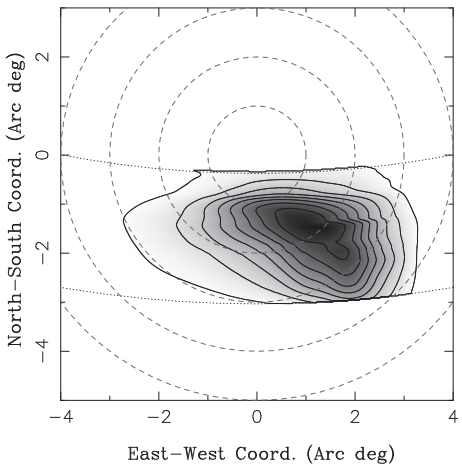

Figure 1: Two-dimensional shape of the emission beam over the traversed region in PSR J1141–6545. The inclination of the magnetic axis is taken to be 160°. The dotted lines show the path traversed by the line of sight; the lower one corresponds to the beginning of the data span and the upper one to the minimum impact parameter reached around MJD 54000. For more details see Manchester et al. (2010).

Kramer 2002), J1141−6545 (Manchester et al. 2010) (see Fig. 1), J1906+0746 (Kasian 2012) and recently J0737−3039B (Perera et al. 2010). The results are so far inconclusive as to whether a systematic pattern exists.

2.5.2 Free precession

Free precession is the most general motion executed by a rotating solid body. Given that neutron stars have elastic crusts (and may contain solid components in their core, according to some nuclear physics models), they can sustain asymmetries which may lead to the system precessing. In order to illustrate the main issues, let us consider the case of PSR B1828–11, which provides the strongest evidence in favour of free precession so far (Stairs et al. 2000). Possible precession solutions for the data, which shows periodicity at both around 500d and 1000d, were first discussed in Jones & Anderson (2001); Link & Epstein (2001). More recently, it has been argued that the observed periodicity does not in fact represent free precession but is a result of state-switching in the magnetosphere (Lyne et al. 2010). However, as argued in Jones (2012), this does not necessarily mean that precession does not play a role in the system.

If we, for the moment, assume that PSR B1828–11 is freely precessing, then Jones & Anderson (2001) argue that the data requires the magnetic dipole to be very nearly orthogonal to the star's deformation axis (associated with the asymmetry that forces the precession). This would lead to an inferred wobble angle in excellent agreement with the value estimated from the amplitude modulation. The data for PSR B1828–11 is at variance with the level of superfluid pinning required to explain the large glitches seen in the Vela pulsar. It also does not allow for the expected pinning of superfluid vortices to magnetic fluxtubes in the star's superconducting core (Link 2003). At the moment we seem to have three options: i) Our understanding of neutron stars superfluidity/superconductivity is not quite right (Link 2003), ii) various instabilities may intervene and affect the fluid motion, thus altering the conclusions (Glampedakis et al. 2008), or iii) we are not

PoS(AASKA14)038

seeing free precession (Lyne et al. 2010).

3. Energetics of pulsar magnetospheres and radio emission

Within the pulsar population, there are particular populations with clear and to some extent interpretable emission characteristics (Tauris et al. 2015). The SKA pulsar surveys will allow for new breakthroughs (Keane et al. 2015) by providing significantly more examples from each of the populations described in the following.

3.1 Young Pulsars

The youngest pulsars, which have the highest spin-down energy loss rates, appear to have different emission properties to the more middle-aged pulsars. In particular, they possess extremely high levels of linear polarization (Johnston & Weisberg 2006; Weltevrede & Johnston 2008a), not generally seen in the older pulsars. Furthermore, the polarization position angles follow the RVM curve to a much greater degree than the old pulsars do; this is particularly important in determining their geometry (see section 2.1). Curiously, it appears as if the orientation of their linear polarization is either parallel to the magnetic field or perpendicular to it (Johnston et al. 2005; Rankin 2007). This can be understood in terms of plasma physics, which predicts orthogonal polarization modes (Manchester et al. 1975). Some evidence suggests that the younger pulsars have 'simpler' profiles to those of the middle-aged pulsars (Karastergiou & Johnston 2007).

The majority of young pulsars are also high-energy emitters. Since the launch of the *Fermi* satellite more than 200 pulsars are now known to be γ-ray emitters (Abdo et al. 2013). The relationship between the γ-ray emission and the radio emission is a critical one to our understanding of the magnetosphere. Much progress has been made in this area in recent times, but results are still inconclusive (see e.g. Watters et al. 2009; Romani & Watters 2010; Pierbattista et al. 2012). This class of pulsars is likely to grow in importance as more high-energy pulsars are detected.

3.2 Magnetars

Magnetars are a class of neutron stars composed of Anomalous X-ray Pulsars (AXPs) and Soft Gamma-ray Repeaters (SGRs). Currently there are 21 magnetars detected with 5 more awaiting confirmation [1]. Originally, SGRs were discovered to have bursting emission in the hard X-ray/soft gamma-ray range (Mazets et al. 1979), while AXPs are steady, X-ray emitting sources with rotational periods exceeding few seconds (Fahlman & Gregory 1981). Subsequent observations of powerful bursts from AXPs (Gavriil et al. 2002), as well as the discovery of persistent X-ray emission and slow rotational periods from SGRs (Kouveliotou et al. 1998) have revealed the common nature of their emission properties (Duncan & Thompson 1992). Magnetars were typically known to share the following properties: very strong magnetic fields exceeding the quantum critical value for electrons ($B \sim 4.4 \times 10^{14}$ G); decay of such fields is believed to create the observable high X-ray and gamma-ray luminosities (Thompson & Duncan 1995; Thompson & Duncan 1996), often visible in bursts; spin periods of $5-12$ s with rapid spin-down on timescales of $10^3 - 10^5$ years; and absence of radio emission.

[1] http://www.physics.mcgill.ca/∼pulsar/magnetar/main.html

PoS(AASKA14)038

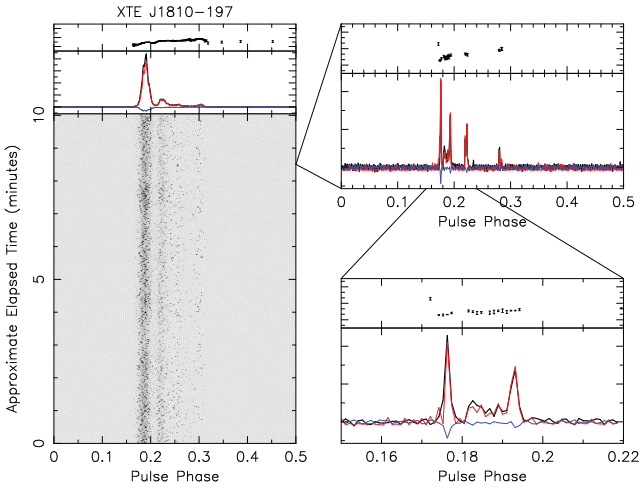

Figure 2: Left: **Pulse stack from an** 8.35 GHz observation with the average profile and position angle swing plotted on top. Total intensity is plotted in black, while linear and circular polarization are plotted in red and blue respectively. **Top right**: Individual single pulse profile with visible narrow and spiky emission. **Bottom right**: Close-up of the pulse plotted above.

Recent discoveries of pulsars with spin periods and inferred dipolar magnetic field strengths typically seen in magnetars (Camilo et al. 2000; McLaughlin et al. 2003) and at which radio emission should not occur, bring magnetars and pulsars closer as a single population. The detection of transient radio emission from XTE J1810–197 and 1E 1547–5408 (Camilo et al. 2006, 2007a), followed by the discovery of PSR J1622–4950, a magnetar first detected in radio (Levin et al. 2010) with subsequent identification of its X-ray counterpart (Anderson et al. 2012), further strengthens this link. Another example is SGR J1745–2900, the only radio emitting magnetar found in the inner parsec of the Galactic Centre (Eatough et al. 2013; Shannon & Johnston 2013). The radio emission from magnetars is highly variable in nature and usually declines in tandem with its higher energy counterparts. Magnetar radio emission typically appears after X-ray outbursts; has a flat spectral index (Lazaridis et al. 2008) which enables detection even of individual pulses at frequencies above 88 GHz (Camilo et al. 2007d); shows pulse profile morphology changing dramatically on timescales of minutes to days (Camilo et al. 2007c,b; Levin et al. 2013); shows polarization similar to the emission properties of normal radio pulsars but with differences which can be explained as propagation effects in a non-dipolar magnetic field (Camilo et al. 2008; Kramer et al. 2007). Fig. 2 shows a typical observation of XTE J1810–197 with the 100-m Effelsberg radio telescope at 8.35 GHz.

The population of radio magnetars is very small at present. As they emit over a wide spectrum of wavelengths (γ-ray, X-ray, optical, near infrared and radio) studies at multiple frequencies are best poised to provide information on these objects. The SKA pulsar surveys will significantly increase the sample of radio emitting magnetars and uncover their relationships with the other populations of radio emitting neutron stars.

3.3 Millisecond Pulsars

Most of our current knowledge of the pulsar emission mechanism and pulsar magnetospheres

PoS(AASKA14)038

is derived from observations of slow pulsars. Only a very limited number of the known millisecond pulsars (MSPs) is bright enough to enable detailed studies of their single-pulse and magnetospheric properties. However, the studies that have been performed so far have shown interesting differences between MSPs and slow pulsars, motivating detailed studies of MSPs at the high sensitivity provided by the SKA.

The first clear difference between MSPs and slow pulsars is that the RVM cannot explain the polarimetry of MSP emission, even though other polarimetric properties (such as polarization degree and the presence of orthogonally polarized modes), do not differ (Yan et al. 2011). Similarly ambiguous results are found in the profile variations as a function of observing frequency: even though the pulse profiles of MSPs vary less strongly (which indicates a far smaller emission region than in the case of slow pulsars), the overall changes are reminiscent of slow pulsars, but shifted to higher frequencies (Kramer et al. 1999). Concerning intensity variations of single pulses, Jenet & Gil (2004) found no variations (other than giant pulses) in PSR B1937+21, while clear pulse-to-pulse modulations were found in PSR J0437-4715 (Jenet & Gil 2004; Osłowski et al. 2014). Edwards & Stappers (2003) discovered giant pulses in several pulsars and possible sub-pulse drifting. For the brightest MSP, PSR J0437-4715, the recent work by Osłowski et al. (2014) rules out drifting sub-pulses.

In summary, a clear picture of the emission properties of MSPs has yet to emerge. The lack in telescope sensitivity has limited this area of research to essentially the two brightest MSPs, which are far from representative of the whole MSP population in many regards. Early indications do show that the emission mechanism for slow pulsars and MSPs must be similar, if not identical. Understanding the emission process in MSPs is an essential element in the continued research of pulsar magnetospheres.

3.4 The double pulsar

The double pulsar PSR J0737−3039A/B is not only a remarkable system in the context of testing gravity theories; it also provides a unique window of opportunity to study pulsar magnetospheres. This binary comprises a rapidly spinning 23-ms pulsar, *A*, in a 2.4-hr orbit with a slowly rotating 2.8-s pulsar, *B*. The fortunate nearly edge-on alignment of the orbit with our sight line is such that pulsar A is eclipsed for ~ 20 s when it passes behind pulsar B. The duration implies a transverse cross-section of a few km at the location of pulsar B from A, thus implying a magnetospheric origin. A high time resolution study by McLaughlin et al. (2004) revealed that the eclipsed signal from A is modulated by the rotation of B during the eclipse, a phenomenon which led Lyutikov & Thompson (2005) to interpret the eclipses as being caused by synchrotron resonance in the closed field lines of pulsar B. The modulation naturally arises from the change in optical depth as the magnetic field geometry changes over the course of B's rotation. Subsequently, Breton et al. (2008) demonstrated the success of this model in a long-term study of the radio eclipses, which led to the direct measurement of relativistic spin precession of pulsar B.

The double pulsar eclipses have two majors implication for the study of pulsar magnetospheres. Firstly, they allow us to directly probe the topology of a pulsar's magnetic field, which has been shown to be primarily dipolar (Breton et al. 2012). Secondly, multi-frequency observations of the eclipse profile can constrain plasma properties such as the density, profile and multiplicity of the plasma. It has been shown that the density profile drops abruptly at a radius well inside the

PoS(AASKA14)038

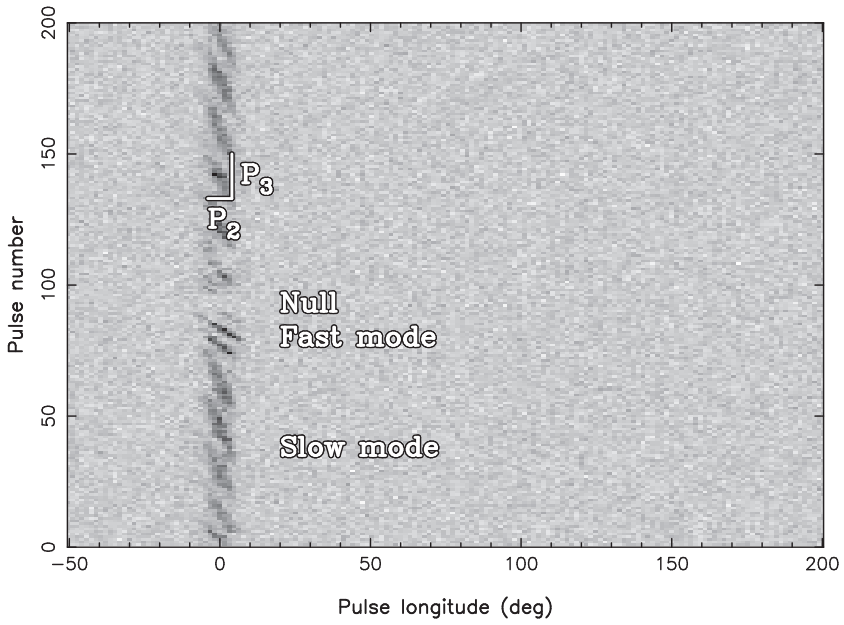

Figure 3: A pulse-stack of successive radio pulses of PSR B1819−22. The radio intensity (darker is brighter) is plotted as function of rotational phase (or longitude) versus pulse numbers. The emission (in the subpulses separated by P_2) appear to "march" in rotational phase from pulse to pulse creating a distinct pattern which repeats itself every P_3 pulses, a phenomenon called "drifting subpulses". In addition this pulsar shows "mode changes", which in this case manifests itself as two distinct drift modes: the slow and fast mode. The pulsar also has a "null" state, i.e. for a few stellar rotations there was no radio emission emitted by the pulsar. This figure shows 1380 MHz data obtained by the Westerbork Synthesis Radio Telescope (Weltevrede et al. 2006).

co-rotation radius (i.e. light cyclinder) and requires a large multiplicity (Breton et al. 2012). SKA1 will allow us to perform a polarization study of the eclipses which will yield an independent test of the eclipse mechanism and geometry of the system (Lyutikov & Thompson 2005). Polarization studies will also allow us to infer the strength of the magnetic field and compare it to predictions from pulsar timing.

4. Timescales in pulsar magnetospheres

While it has been known since the early days of pulsar astronomy that individual pulses are intrinsically variable, over the past decade a number of important observational results have shown that both radio emission and the magnetosphere itself can vary on timescales spanning at least 18 orders of magnitude, from nanoseconds to decades. In the following, we describe the current understanding of radio emission phenomenology on all timescales and how this relates to pulsar timing experiments. It is important that SKA pulsar observation scheduling is determined by our understanding of the timescales of magnetospheric variability, in order to maximize scientific return.

4.1 Short timescale phenomena

Radio pulsars display a myriad of amplitude modulation effects, as seen in Fig. 3. Aver-

PoS(AASKA14)038

aged over many rotations, most pulsars have a reproducible pulse shape, reflective of the long-term stability of their rotation and magnetic fields. However, pulse shape and intensity can vary considerably in sequential rotations of a pulsar. Ordered and stochastic processes affect some pulsars to varying degrees; ordered modulations include sub-pulse drift (gradual phase shift of pulse peak), mode changing (regular changes between two or three distinct pulse shapes), and nulling (cessation of the radio beam). Pulse statistics using full polarimetry (Stinebring et al. 1984a,b; Karastergiou et al. 2002; Mitra et al. 2007) have led to gradual improvement of our understanding of orthogonal mode emission (McKinnon 2003; Edwards & Stappers 2004). Drifting sub-pulses in PSR B0943+10 led Deshpande & Rankin (2001) to champion the 'rotating carousel' model for the circulation of the pulsar beamlets (see e.g. Rankin et al. 2006; Mitra & Rankin 2008). However, it is far from clear if this model can be applied in every case of drifting subpulses and other models have been proposed (e.g. Clemens & Rosen 2004).

It is also of particular interest to understand contributions of pulse-to-pulse variability to precision pulsar timing, referred to as jitter noise. Correcting, or at least accounting for, jitter noise is imperative for optimizing strategies for SKA pulsar timing activities (Shannon et al. 2014). The brightest MSPs at decimetre wavelengths, PSR J0437−4715 and J1713+0747, have been the most extensively studied (Shannon & Cordes 2012; Osłowski et al. 2014). While the emission of these two millisecond pulsars show many similarities to that of slower pulsars, many of the classic single pulse phenomena, such as drifting subpulses or pulse nulling are not observed (Vivekanand et al. 1998).

Pulse nulling, where the radio emission appears to switch off, was one of the first phenomena identified (Backer 1970b), and is the prototypical example of pulsar variability (see review by Biggs 1992). In the "classical" nullers, emission is observed to switch off and on rapidly (few tens of pulses) and some pulsars had a relatively high "off" fraction (Wang et al. 2007). It came as a major surprise when McLaughlin et al. (2006) discovered pulsars, which only produce one pulse of emission every tens of minutes (the so-called RRATs). Several tens of these objects have now been found (McLaughlin et al. 2009). Because their duty cycle is so low, their population could rival that of the normal pulsars (Keane & Kramer 2008).

Kerr et al. (2014) show that several distinct timescales are present in the PSR J1717−4054, which has both long (many hours) and short (few seconds) nulling periods. The broadband nature of pulse nulling was investigated by Bhat et al. (2007). Our knowledge of how these various populations fit together is given by Burke-Spolaor et al. (2012).

Other effects such as intense giant pulses (Staelin & Reifenstein 1968; Comella et al. 1969) or "giant micropulses" (Johnston et al. 2001) occur in some pulsars at a limited phase range. The energy distribution of radio pulses can provide a window into the state of pulsar plasma and the method of emission generation. There exist a great number of viable plasma-state models, a few of which predict pulse energy distributions; the most commonly-proposed predictions are of Gaussian, log-normal, and power-law distributions. Cairns et al. (2001, 2003) and references therein, provide discussion on these models. Energy distributions have now been examined in detail for a number of pulsars (Burke-Spolaor et al. 2012), demonstrating that most pulsars obey log-normal statistics. These analyses have substantially contributed to the hypothesis that genuine "giant pulses" are generated separately from standard pulse generation and are much more rare. Giant pulses appear to have power-law energy distributions, distinct from the otherwise log-normal main pulse

PoS(AASKA14)038

components (Lundgren et al. 1995; Johnston & Romani 2002).

It was giant pulses that led to the discovery of the Crab pulsar (Staelin & Reifenstein 1968). Classical Crab pulsar giant pulses are characterized by their appearance at the same phase range as the high-energy emission (Lundgren et al. 1995), high flux densities (Hankins et al. 2003; Popov & Stappers 2007), and power-law intensity distributions (Argyle & Gower 1972; Lundgren et al. 1995), Since the discovery of the Crab pulsar, other giant pulse emitters have been observed, both in young pulsars (like for instance the Crab twin PSR B0540-69 Johnston & Romani 2003), and in millisecond pulsars (Cognard et al. 1996; Romani & Johnston 2001; Knight et al. 2006). Common aspects between all giant pulse emitting pulsars are currently not known. Giant pulses in the Crab seem to share properties such as their short pulse widths down to 0.4 ns (Hankins et al. 2003; Hankins & Eilek 2007), and high brightness temperatures up to 10^{39} K (Soglasnov et al. 2004), indicating coherent emission mechanisms. In addition to the giant pulses, bright, rare, 'spiky' emission is seen in other pulsars, for example the bursty emission in PSR B0656+14 (Weltevrede et al. 2006), the giant-like pulses from PSRs J1048–5832 and J1709–4429 (Johnston & Romani 2002) and the giant micro-pulses from the Vela pulsar (Johnston et al. 2001).

A number of tests of pulsar models can be performed using the statistics of per-rotation pulsar modulation. Weisberg et al. (1986) first noted differences in modulation between core and conal-type pulse profiles, while Jenet & Gil (2003) derived theoretical predictions for anti-correlations between pulse-to-pulse modulation and four "complexity parameters," corresponding to four pulsar emission models. Their complexity parameters are: $a_1 = 5\dot{P}^{2/6}P^{-9/14}$, for the sparking gap model, $a_2 = (\dot{P}/P^3)^{0.5}$ for the continuous current outflow instabilities, $a_3 = (P\dot{P})^{0.5}$ for surface magneto-hydrodynamic wave instabilities, and $a_4 = (\dot{P}/P^5)^{0.5}$ for outer magnetospheric instabilities. Few observational studies have been done to test these effects, however the Jenet & Gil (2003) study for a small sample of core-type profiles disfavoured the magnetohydrodynamic wave instability model, and the study of $\sim$190 pulsars (Weltevrede et al. 2006, 2007) at 21 and 92 cm indicated that the modulation index is generally higher at lower frequencies, and noted a weak correlation between modulation index and age that is dampened at higher frequency.

The study of single-pulse modulation in a large pulsar sample can also contribute to several practical questions, for instance: how common is giant-pulse emission? Are the prospects of pulsar detection in other galaxies better for single-pulse or Fourier searches? Quantification of pulsars' modulation will also aid in understanding the physical makeup of "rotating radio transients" (McLaughlin et al. 2006), which mostly appear to represent an extreme case of nulling pulsar and may contribute a problematically large contribution to Galactic pulsar populations (Keane & Kramer 2008).

4.2 Long timescale phenomena and pulsar timing

As mentioned above, since the early days of pulsar astronomy, pulsars have been known to change between modes on short (minute to hour) time scales (Backer 1970a) and been extensively studied since. Of particular interest recently is the discovery that PSR B0943+10 changes modes simultaneously in radio and in X-rays (Hermsen et al. 2013). The X-ray state change from a thermal to a non-thermal component is challenging for models of pulsar emission.

The question of pulse profile variation on the very long timescales remains active. Kramer et al. (2006) identified the first of the so-called intermittent pulsars, which was found to quasiperiodically

PoS(AASKA14)038

change between a 10 day radio-bright state and 30-day radio faint state. The timing data from PSR B1931+24 are well fit by a model with two rates of spin-down, one for each emission phase. During the inactive phase, the spin-down rate is -10.8×10^{-15} Hz s^{-1}, but switches to -16.3×10^{-15} Hz s^{-1} when active, an increase of around 50%. Longer periods of quiescence have been detected in PSRs J1841–0500 and J1832+0029 with similar behaviour in the timing of the pulsars (Camilo et al. 2012).

A less extreme version of correlated emission and rotation changes is seen in a small number of pulsars identified by Lyne et al. (2010). Six pulsars are seen to show distinct emission states, identified by long-term pulse-shape changes which are accompanied by correlated changes in spin-down rate. The magnitude of the spin-down rate changes produced is much smaller than is seen in the intermittent pulsars; less than 10% in each case.

The relationship between emission state and rotation rate is explained by changing charged particle currents in the pulsar magnetosphere. A global failure of these currents is thought to be responsible for the inactive phase, creating a dearth of charged particles at the magnetic poles. When the outflowing particles are present and producing radio emission, they also provide an additional torque, resulting in the increased spin-down rate seen during the active phase.

Glitches appear to have at least some effect on the pulse profile (for the latest papers on observed glitches see Espinoza et al. 2011; Yu et al. 2013). For PSR J0742–2822, Keith et al. (2013) found that the degree of correlation was influenced by a glitch occurring midway through the dataset; a strong correlation was found after the glitch, with no correlation before. Glitches have previously been linked to emission changes in radio pulsars and in magnetars (Camilo et al. 2007c; Weltevrede et al. 2011).

A further example of correlated changes in emission and rotation is seen in PSR J0738–4042 (Brook et al. 2014). In 2005, the pulsar exhibited a sudden change in pulse-shape, which had been relatively stable for at least 16 years prior, and occurred simultaneously with a 15% drop in the pulsar's spin-down rate. The changes were attributed to variations in magnetospheric current flow, hypothesised to have been due to an influx of external material, such as an asteroid (Brook et al. 2014; Shannon et al. 2013). Lyne et al. (2013) report on a 20 year dataset of the Crab pulsar which appears to show that the magnetic axis is slowly migrating away from the axis of rotation in contrast to population studies (Tauris & Manchester 1998; Weltevrede & Johnston 2008b) which conclude the opposite.

What is the link between the nanosecond emission, the microstructure and the components in a pulse profile? Why do some pulsars produce giant pulses, while others null? What sets the on and off null durations? How do pulsar profiles change with age and do glitches play a role in this? These questions are fundamental to our understanding of the emission mechanism, and should be addressed by high cadence monitoring of many hundreds of sources in the SKA era. Furthermore, the entire question of pulse profile stability, one of the shibboleths in pulsar astronomy, has been called into question over the past decade. There now appears to be a clear link between rotational instabilities and profile changes, though questions of cause and effects remain unclear. In addition it seems possible that some changes are externally driven while some remain intrinsic to the pulsar itself. Pulse profile stability is crucial to high precision timing and the quest for gravitational waves and therefore understanding profile stability is a key priority for the SKA.

PoS(AASKA14)038

5. Conclusions and early science

The SKA brings high sensitivity over a broad frequency range, ideal for the study of broadband, highly variable, weak sources such as pulsars. In the SKA era, great strides will be made in understanding the location and behaviour of the coherent radio emission from pulsars. In turn, this understanding of pulsar emission will be crucial for the detection and study of gravitational waves, surely to be one of the crowning glories of SKA science.

As demonstrated above, the science enabled by SKA studies of pulsar emission and magnetospheres is impressive. For the first time since the discovery of pulsars, we have the chance to find the "Rosetta stones" of pulsar research that will allow us to infer the fundamental emission properties and their origin as well as the conditions in the magnetosphere. The importance of just a few sources for our understanding has been demonstrated, e.g., by the few known intermittent pulsars and the double-pulsar. The SKA will deliver more of those and other types of radio emitting neutron stars (Tauris et al. 2015; Keane et al. 2015). At the same time, the sheer number of pulsars that the SKA will be able to study in exquisite detail promises to make real advances in solving the decade-old "pulsar problem". This will be aided by observations with other facilities at other wavelengths.

The key in advancing the radio studies will however be the supreme sensitivity of the SKA. Clearly, already SKA1 (LOW and MID) will be superb tools. Eventually, more sensitivity with full SKA will help even more. In terms of early science with SKA1, this hinges on early new pulsar discoveries and the telecsope sensitivity during the early stages. It is difficult to estimate precisely what can be achieved during this phase, as the impact will be different for different sources. Nevertheless, the science proposed here can be addressed as long as the telescope has the characteristics of bandwidth, polarization purity and sensitivity required to study in detail the sources discovered. It is, however, the full SKA-1 that will really enable substantial progress in this area, given the large number of new sources including pulsars that can be studied in detail with full polarization, in single pulses and at regular intervals to understand variability. Given that the SKA will probably be the largest radio telescope built for a while, we should not miss this golden opportunity to solve one of the great mysteries in astrophysics.

Acknowledgements

J-PM acknowledges work supported through the Australian Research Council grant DP140104114.

References

Abdo, A. A., Ajello, M., Allafort, A., & et al. 2013, ApJS, 208, 17
Anderson, G. E., Gaensler, B. M., Slane, P. O., et al. 2012, ApJ, 751, 53
Argyle, E., & Gower, J. F. R. 1972, ApJ, 175, L89
Backer, D. C. 1970a, Nature, 227, 692
—. 1970b, Nature, 228, 42
Bates, S. D., Lorimer, D. R., & Verbiest, J. L. 2013, MNRAS, 431, 1352
Bhat, N. D. R., Gupta, Y., Kramer, M., et al. 2007, A&A, 462, 257

PoS(AASKA14)038

Biggs, J. D. 1992, ApJ, 394, 574
Blaskiewicz, M., Cordes, J. M., & Wasserman, I. 1991, ApJ, 370, 643
Boyle, L., & Pen, U.-L. 2012, Phys. Rev. D, 86, 124028
Breton, R. P., Kaspi, V. M., Kramer, M., et al. 2008, Science, 321, 104
Breton, R. P., Kaspi, V. M., McLaughlin, M. A., et al. 2012, ApJ, 747, 89
Brisken, W. F., Macquart, J.-P., Gao, J. J., et al. 2010, ApJ, 708, 232
Brook, P. R., Karastergiou, A., Buchner, S., et al. 2014, ApJ, 780, L31
Burke-Spolaor, S., Johnston, S., Bailes, M., et al. 2012, MNRAS, 423, 1351
Cairns, I. H., Johnston, S., & Das, P. 2001, ApJ, 563, L65
—. 2003, MNRAS, 343, 512
Camilo, F., Kaspi, V. M., Lyne, A. G., et al. 2000, ApJ, 541, 367
Camilo, F., Ransom, S. M., Chatterjee, S., Johnston, S., & Demorest, P. 2012, ApJ, 746, 63
Camilo, F., Ransom, S. M., Halpern, J. P., & Reynolds, J. 2007a, ApJ, 666, L93
Camilo, F., Ransom, S. M., Halpern, J. P., et al. 2006, Nature, 442, 892
Camilo, F., Reynolds, J., Johnston, S., Halpern, J. P., & Ransom, S. M. 2008, ApJ, 679, 681
Camilo, F., Reynolds, J., Johnston, S., et al. 2007b, ApJ, 659, L37
Camilo, F., Cognard, I., Ransom, S. M., et al. 2007c, ApJ, 663, 497
Camilo, F., Ransom, S. M., Peñalver, J., et al. 2007d, ApJ, 669, 561
Clemens, J. C., & Rosen, R. 2004, ApJ, 609, 340
Clifton, T., & Weisberg, J. M. 2008, ApJ, 679, 687
Cognard, I., Shrauner, J. A., Taylor, J. H., & Thorsett, S. E. 1996, ApJ, 457, 81
Comella, J. M., Craft, H. D., Lovelace, R. V. E., Sutton, J. M., & Tyler, G. L. 1969, Nature, 221, 453
Damour, T., & Ruffini, R. 1974, 279, 971
Deshpande, A. A., & Rankin, J. M. 2001, MNRAS, 322, 438
Duncan, R. C., & Thompson, C. 1992, ApJ, 392, L9
Dyks, J. 2008, MNRAS, 391, 859
Dyks, J., & Harding, A. K. 2004, ApJ, 614, 869
Eatough, R. P., Falcke, H., Karuppusamy, R., et al. 2013, Nature, 501, 391
Edwards, R. T., & Stappers, B. W. 2003, A&A, 407, 273
—. 2004, A&A, 421, 681
Espinoza, C. M., Lyne, A. G., Stappers, B. W., & Kramer, M. 2011, MNRAS, 414, 1679
Fahlman, G. G., & Gregory, P. C. 1981, Nature, 293, 202
Gangadhara, R. T., & Gupta, Y. 2001, ApJ, 555, 31
Gavriil, F. P., Kaspi, V. M., & Woods, P. M. 2002, Nature, 419, 142
Glampedakis, K., Andersson, N., & Jones, D. I. 2008, Physical Review Letters, 100
Gould, D. M. 1994, PhD thesis, The University of Manchester
Gwinn, C. R., Johnson, M. D., Reynolds, J. E., et al. 2012, ApJ, 758, 7
Hankins, T. H., & Eilek, J. A. 2007, ApJ, 670, 693
Hankins, T. H., Kern, J. S., Weatherall, J. C., & Eilek, J. A. 2003, Nature, 422
Hermsen, W., Hessels, J. W. T., Kuiper, L., et al. 2013, Science, 339, 436
Jenet, F. A., & Gil, J. 2003, ApJ, 596, L215
—. 2004, ApJ, 602, L89

PoS(AASKA14)038

Johnson, M. D., Gwinn, C. R., & Demorest, P. 2012, ApJ, 758, 8
Johnston, S., Hobbs, G., Vigeland, S., et al. 2005, MNRAS, 364, 1397
Johnston, S., & Romani, R. 2002, MNRAS, 332, 109
—. 2003, ApJ, 590, L95
Johnston, S., van Straten, W., Kramer, M., & Bailes, M. 2001, ApJ, 549, L101
Johnston, S., & Weisberg, J. M. 2006, MNRAS, 368, 1856
Jones, D. I. 2012, MNRAS, 420, 2325
Jones, D. I., & Anderson, N. 2001, MNRAS, 324, 811
Karastergiou, A., & Johnston, S. 2007, MNRAS, 380, 1678
Karastergiou, A., Kramer, M., Johnston, S., et al. 2002, A&A, 391, 247
Kasian, L. E. 2012, PhD thesis, The University of British Columbia
Keane, E. F., Bhattacharyya, B., Kramer, M., & et al. 2015, "A Cosmic Census of Radio Pulsars with the SKA", in proc. *Advancing Astrophysics with the Square Kilometre Array*, PoS(AASKA14)040
Keane, E. F., & Kramer, M. 2008, MNRAS, 391, 2009
Keith, M. J., Shannon, R. M., & Johnston, S. 2013, MNRAS, 432, 3080
Knight, H. S., Bailes, M., Manchester, R. N., Ord, S. M., & Jacoby, B. A. 2006, ApJ, 640, 941
Komesaroff, M. M. 1970, Nature, 225, 612
Kouveliotou, C., Dieters, S., Strohmayer, T., et al. 1998, Nature, 393, 235
Kramer, M. 2002, in IX Marcel Grossmann Meeting, ed. R. J. V.G. Gurzadyan & R. Ruffini (World Scientific)
Kramer, M., Jessner, A., Doroshenko, O., & Wielebinski, R. 1997, ApJ, 489, 364
Kramer, M., & Johnston, S. 2008, MNRAS, 390, 87
Kramer, M., Lange, C., Lorimer, D. R., et al. 1999, ApJ, 526, 957
Kramer, M., Lyne, A. G., O'Brien, J. T., Jordan, C. A., & Lorimer, D. R. 2006, Science, 312, 549
Kramer, M., Stappers, B. W., Jessner, A., Lyne, A. G., & Jordan, C. A. 2007, MNRAS, 377, 107
Kramer, M., Xilouris, K. M., Lorimer, D. R., et al. 1998, ApJ, 501, 270
Kuzmin, A. D., & Losovsky, B. Y. 2001, A&A, 368, 230
Lazaridis, K., Jessner, A., Kramer, M., et al. 2008, MNRAS, 390, 839
Levin, L., Bailes, M., Bates, S., et al. 2010, ApJ, 721, L33
Levin, L., Bailes, M., Barsdell, B. R., et al. 2013, MNRAS, 434, 1387
Link, B. 2003, Physical Review Letters, 91, 101101
Link, B., & Epstein, R. I. 2001, ApJ, 556, 392
Lorimer, D. R., Yates, J. A., Lyne, A. G., & Gould, D. M. 1995, MNRAS, 273, 411
Lundgren, S. C., Cordes, J. M., Ulmer, M., et al. 1995, ApJ, 453, 433
Lyne, A., Graham-Smith, F., Weltevrede, P., et al. 2013, Science, 342, 598
Lyne, A., Hobbs, G., Kramer, M., Stairs, I., & Stappers, B. 2010, Science, 329, 408
Lyne, A. G., & Manchester, R. N. 1988, MNRAS, 234, 477
Lyutikov, M., & Thompson, C. 2005, ApJ, 634, 1223
Malofeev, V. M., & Malov, I. F. 1980, Sov. Astron., 24, 54
Manchester, R. N., Taylor, J. H., & Huguenin, G. R. 1975, ApJ, 196, 83
Manchester, R. N., Kramer, M., Stairs, I. H., et al. 2010, ApJ, 710, 1694
Maron, O., Kijak, J., Kramer, M., & Wielebinski, R. 2000, A&AS, 147, 195

PoS(AASKA14)038

Mazets, E. P., Golenetskii, S. V., Ilinskii, V. N., Apetkar, R. L., & Guryan, Y. A. 1979, Nature, 282, 587
McKinnon, M. M. 2003, ApJS, 148, 519
McLaughlin, M. A., Stairs, I. H., Kaspi, V. M., et al. 2003, ApJ, 591, L135
McLaughlin, M. A., Lyne, A. G., Lorimer, D. R., et al. 2004, ApJ, 616, L131
—. 2006, Nature, 439, 817
McLaughlin, M. A., Lyne, A. G., Keane, E. F., et al. 2009, MNRAS, 400, 1431
Mitra, D., & Li, X. H. 2004, A&A, 421, 215
Mitra, D., & Rankin, J. M. 2002, ApJ, 577, 322
Mitra, D., & Rankin, J. M. 2008, MNRAS, 385, 606
Mitra, D., Rankin, J. M., & Gupta, Y. 2007, MNRAS, 379, 932
Osłowski, S., van Straten, W., Bailes, M., Jameson, A., & Hobbs, G. 2014, MNRAS, 441, 3148
Pen, U.-L., Macquart, J.-P., Deller, A. T., & Brisken, W. 2014, MNRAS, 440, L36
Perera, B. B. P., McLaughlin, M. A., Kramer, M., et al. 2010, ApJ, 721, 1193
Pierbattista, M., Grenier, I. A., Harding, A. K., & Gonthier, P. L. 2012, A&A, 545, A42
Popov, M. V., & Stappers, B. 2007, A&A, 470, 1003
Radhakrishnan, V., & Cooke, D. J. 1969, Astrophys. Lett., 3, 225
Rankin, J. M. 1983, ApJ, 274, 333
—. 1990, ApJ, 352, 247
—. 1993, ApJ, 405, 285
Rankin, J. M. 2007, ApJ, 664, 443
Rankin, J. M., Ramachandran, R., van Leeuwen, J., & Suleymanova, S. A. 2006, A&A, 455, 215
Romani, R., & Johnston, S. 2001, ApJ, 557, L93
Romani, R. W., & Watters, K. P. 2010, ApJ, 714, 810
Shannon, R. M., & Cordes, J. M. 2012, ApJ, 761, 64
Shannon, R. M., & Johnston, S. 2013, MNRAS, 435, L29
Shannon, R. M., Cordes, J. M., Metcalfe, T. S., et al. 2013, ApJ, 766, 5
Shannon, R. M., Osłowski, S., Dai, S., et al. 2014, MNRAS, 443, 1463
Sieber, W. 2002, in WE-Heraeus Seminar on Neutron Stars, Pulsars, and Supernova Remnants, ed. W. Becker, H. Lesch, & J. Trümper (Garching: Max-Plank-Institut für Extraterrestrische Physik), 171
Soglasnov, V. A., Popov, M. V., Bartel, N., et al. 2004, ApJ, 616, 439
Staelin, D. H., & Reifenstein, III, E. C. 1968, Science, 162, 1481
Stairs, I. H., Lyne, A. G., & Shemar, S. 2000, Nature, 406, 484
Stinebring, D. R., Cordes, J. M., Rankin, J. M., Weisberg, J. M., & Boriakoff, V. 1984a, ApJS, 55, 247
Stinebring, D. R., Cordes, J. M., Weisberg, J. M., Rankin, J. M., & Boriakoff, V. 1984b, ApJS, 55, 279
Tauris, T. M., Kaspi, V. M., Breton, R. P., & et al., 2015, "Understanding the Neutron Star Population with the SKA", in proc. *Advancing Astrophysics with the Square Kilometre Array*, PoS(AASKA14)039
Tauris, T. M., & Manchester, R. N. 1998, MNRAS, 298, 625
Thompson, C., & Duncan, R. C. 1995, MNRAS, 275, 255

PoS(AASKA14)038

Thompson, C., & Duncan, R. C. 1996, ApJ, 473, 322
Thorsett, S. E. 1991, ApJ, 377, 263
Vivekanand, M., Ables, J., & McConnell, D. 1998, ApJ, 501, 823
Vivekanand, M., & Joshi, V. 1997, ApJ, 477, 431
Walker, M. A., Koopmans, L. V. E., Stinebring, D. R., & van Straten, W. 2008, MNRAS, 388, 1214
Wang, N., Manchester, R. N., & Johnston, S. 2007, MNRAS, 377, 1383
Watters, K. P., Romani, R. W., Weltevrede, P., & Johnston, S. 2009, ApJ, 695, 1289
Weisberg, J. M., Armstrong, B. K., Backus, P. R., et al. 1986, AJ, 92, 621
Weisberg, J. M., & Taylor, J. H. 2002, ApJ, 576, 942
Weltevrede, P., Edwards, R. T., & Stappers, B. W. 2006, A&A, 445, 243
Weltevrede, P., & Johnston, S. 2008a, MNRAS, 391, 1210
—. 2008b, MNRAS, 387, 1755
Weltevrede, P., Johnston, S., & Espinoza, C. M. 2011, MNRAS, 411, 1917
Weltevrede, P., Stappers, B. W., & Edwards, R. T. 2007, A&A, 469, 607
Weltevrede, P., Stappers, B. W., Rankin, J. M., & Wright, G. A. E. 2006, ApJ, 645, L149
Wielebinski, R., Jessner, A., Kramer, M., & Gil, J. A. 1993, A&A, 272, L13
Wolszczan, A., & Cordes, J. M. 1987, ApJ, 320, L35
Yan, W. M., Manchester, R. N., van Straten, W., et al. 2011, MNRAS, 414, 2087
Young, M. D. T., Chan, L. S., Burman, R. R., & Blair, D. G. 2010, MNRAS, 402, 1317
Yu, M., Manchester, R. N., Hobbs, G., et al. 2013, MNRAS, 429, 688

PoS(AASKA14)038

PROCEEDINGS OF SCIENCE

Understanding the Neutron Star Population with the SKA

Thomas M. Tauris[1,2], Victoria M. Kaspi*[3], Rene P. Breton[4], Adam T. Deller[5], Evan F. Keane[6,7], Michael Kramer[2], Duncan R. Lorimer[8], Maura A. McLaughlin[8], Andrea Possenti[9], Paul S. Ray[10], Ben W. Stappers[11], Patrick Weltevrede[11]

[1]*Argelander-Institute for Astronomy, University of Bonn, Germany;* [2]*MPIfR, Germany;* [3]*McGill University, Canada;* [4]*University of Southampton, UK;* [5]*ASTRON, The Netherlands;* [6]*Swinburne University of Technology, Australia;* [7]*ARC Centre of Excellence for All-Sky Astrophysics (CAASTRO);* [8]*West Virginia University, USA;* [9]*INAF-Osservatorio Astronomico di Cagliari, Italy;* [10]*Naval Research Laboratory, USA;* [11]*University of Manchester, UK*

E-mail: tauris@astro.uni-bonn.de vkaspi@physics.mcgill.ca

Since their discovery in the late 1960's the population of known neutron stars has grown to $\sim$2500. This sample has yielded many surprises and demonstrated that the observational properties of neutron stars are remarkably diverse. The surveys that will be performed with the SKA will produce a further tenfold increase in the number of Galactic neutron stars known. Moreover, the SKA's broad spectral coverage, sub-arraying and multi-beaming capabilities will allow us to characterise these sources with unprecedented efficiency, in turn enabling a giant leap in the understanding of their properties. We review the neutron star population and outline strategies for studying each of the growing number of diverse classes that are populating the "neutron star zoo". Questions that will be addressed by the much larger statistical samples and vastly improved timing efficiency provided by SKA include: (i) the spin period and spin-down rate distributions (and thus magnetic fields) at birth, and the associated information about the supernovae wherein they are formed; (ii) the radio pulsar–magnetar connection; (iii) the link between normal radio pulsars, intermittent pulsars and rotating radio transients; (iv) the slowest possible spin period for a radio pulsar (revealing the conditions at the pulsar death-line); (v) proper motions of pulsars (revealing supernova kick physics); (vi) the mass distribution of neutron stars; (vii) the fastest possible spin period for a recycled pulsar (constraining magnetosphere-accretion disc interactions, gravitational wave radiation and the equation-of-state); (viii) the origin of high eccentricity millisecond pulsars; (ix) the formation channels for recently identified triple systems; and finally (x) how isolated millisecond pulsars are formed. We can also expect that the first phase of the SKA (SKA1), and in particular the full SKA (SKA2), will break new ground unveiling exotic and heretofore unknown systems that will challenge our current knowledge and theories, thus fostering the development of new research areas. Some possibilities for future landmark discoveries representing significant milestones in the astrophysics of compact objects include: (i) sub-millisecond pulsars; (ii) neutron stars born as millisecond pulsars; (iii) neutron stars with masses below 1.1 or above 2.5 $M_{\odot}$; (iv) neutron star-black hole binaries; and (v) a triple system containing a pair of neutron stars.

Advancing Astrophysics with the Square Kilometre Array
June 8-13, 2014
Giardini Naxos, Italy

*Speaker.

PoS(AASKA14)039

1. Introduction

The recent era of multi-wavelength observations has revealed a greater variety of possibly distinct observational classes of neutron stars (NSs) than ever before. In addition to isolated NSs, these compact objects are found in binaries and even triple stellar systems which demands theoretical research on their origin and evolution, besides enabling precise mass measurements. With emission spanning the entire electromagnetic spectrum and some NSs showing strange transient behaviour and even dramatic high-energy outbursts, such incredible range and diversity was not only unpredicted, but in many ways astonishing given the perhaps naively simple nature of the NS — the last stellar bastion before the total collapse to a black hole. But why do NSs exhibit so much 'hair'? Even within the field there is confusion about the sheer number of different NS class nomenclature. For a recent review on the members of the NS zoo and the possible unification of the various flavours, we refer to Kaspi (2010) and references therein. An overview of the formation and evolution of NSs in binaries is given, for example, in Bhattacharya & van den Heuvel (1991); Tauris & van den Heuvel (2006).

In Figure 1 we have plotted all currently known radio pulsars with measured values of spin period (P) and its time derivative ($\dot{P}$). The differences in P and $\dot{P}$ imply fundamentally different magnetic field strengths and ages for each sub-group of the population. Treating the pulsar as a

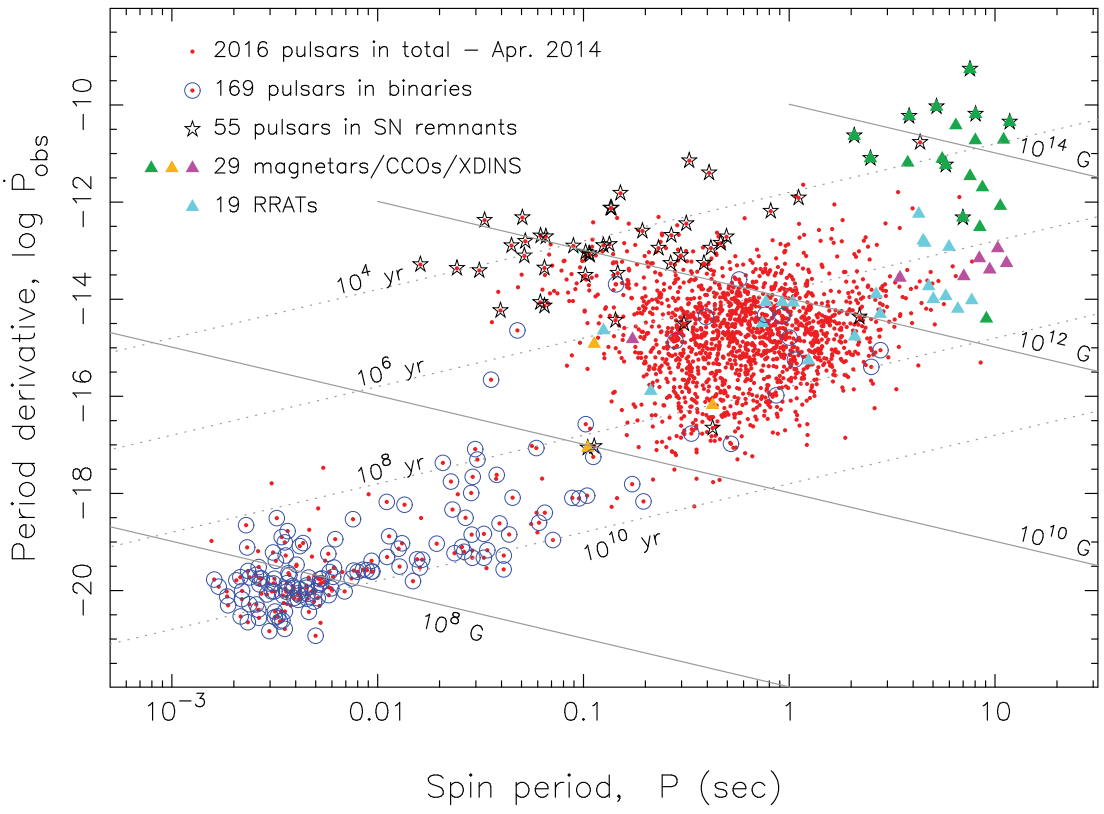

Figure 1: All currently known pulsars with measured P and $\dot{P}$. Data from the ATNF Pulsar Catalogue (Manchester et al. 2005) – April 2014. Lines of constant characteristic age and constant B-field are marked.

PoS(AASKA14)039

rotating magnetic dipole, one may show (e.g. Lorimer & Kramer 2004) that the surface magnetic field strength $B \propto (P\dot{P})^{1/2}$ and define a *characteristic age* $\tau_c = P/(2\dot{P})$. The classic *radio pulsars* (red dots) are concentrated in the region with $P \simeq 0.2-2$ sec and $\dot{P} \simeq 10^{-16}-10^{-13}$. They have magnetic fields of the order $B \simeq 10^{10}-10^{13}$ G and a lifetime as a radio source of a few 10^7 yr. The population plotted in blue circles are binary pulsars and clearly indicate a connection to the rapidly spinning *millisecond pulsars*. The pulsars marked with stars indicate young pulsars observed inside, or near, their gaseous supernova (SN) ejecta remnants. Then there are the "drama queens" of the NS population: the *magnetars* which undergo high-energy bursts and are powered by their huge magnetic energy reservoirs. Also plotted are the mysterious *rotating radio transients* (RRATs), the *isolated X-ray dim NSs* (XDINS) and the *compact central objects* (CCOs). In addition, we briefly discuss other exotic radio pulsars such as the *intermittent pulsars*, the *black widows* and *redbacks*, and pulsars in triple systems.

A main challenge of the past decade was — and continues to be — to find a way to unify this variety into a coherent physical picture. The NS zoo raises essential questions like: What determines whether a NS will be born with, for example, magnetar-like properties or as a Crab-like pulsar? What are the branching ratios for the various varieties, and, given estimates of their lifetimes, how many of each are there in the Galaxy? Can individual NSs evolve from one species to another (and why)? How does a NS interact with a companion star during and near the end of mass transfer (recycling)? And what limits its final spin period? Ultimately such questions are fundamental to understanding the fate of massive stars, close binary evolution and the nature of core-collapse SNe, while simultaneously relating to a wider variety of interesting fundamental physics and astrophysics questions ranging from the physics of matter in ultra-high magnetic fields, to the equation-of-state of ultra-dense matter and details of accretion processes.

In this chapter we address the many faces of NSs with a strong emphasis on radio pulsars and how the SKA will push this research area further to the forefront of modern astrophysics. The structure of the chapter follows the NS population from its very youngest sources, that still bear the imprint of their birth conditions, to the oldest recycled millisecond pulsars, resulting from interactions with a companion star on a Gyr timescale. The bulk of the NSs are somewhere in the middle of their evolutionary journey, so that ultimately detailed population synthesis studies of the full bounty offered by future SKA searches will be key to a complete picture. Whereas the chapter on "A Cosmic Census of Radio Pulsars" (Keane et al. 2015) addresses more technical aspects and emphasizes what sources might be found, this chapter has more specific focus on the consequences of these discoveries and how they would relate to the general population of neutron stars and our understanding thereof.

2. Magnetars

Without doubt the most dramatic and radiatively unpredictable of NSs are the so-called "magnetars," believed to be very young and the most highly magnetized of the population. These objects, of which 26 are currently known (Olausen & Kaspi 2014)[1], have as their hallmark emission bright occasional super-Eddington bursts of X-rays and soft gamma rays. The energy source for these

[1] See online magnetar catalogue at http://www.physics.mcgill.ca/ pulsar/magnetar/main.html

PoS(AASKA14)039

bursts, as well as for the luminous X-ray pulsations observed from many in this class of objects, is believed to be the decay of an intense internal magnetic field, which causes stresses and fractures of the stellar crust (Thompson & Duncan 1995, 1996). These fields are inferred from a variety of different arguments (see, Thompson & Duncan 1996) but arguably most commonly from the spin period and period derivative measured from the X-ray pulsations via the conventional dipole spin-down formula: $B = 3.2 \times 10^{19} \sqrt{P\dot{P}}$ G, often yielding dipolar B-fields $> 10^{14}$ G. Outstanding questions regarding magnetars include the origin of such high magnetic fields (Damour & Taylor 1992), what fraction of the NS population is born as magnetars (Keane & Kramer 2008), and whether there is an evolutionary relationship between magnetars and other NSs, such as high-magnetic-field radio pulsars (see Section 3 below) or isolated NSs (Turolla 2009). Recently, Klus et al. (2014) have suggested that magnetars may populate a group of high-mass X-ray binaries observed in the Small Magellanic Cloud.

Of the 26 known magnetars, only four have been radio-detected thus far (Camilo et al. 2006, 2007a; Levin et al. 2010; Eatough et al. 2013) in spite of sensitive searches of many others (Burgay et al. 2006; Crawford et al. 2007; Lazarus et al. 2012). The four solidly detected magnetars show interesting radio properties. The first radio-detected magnetar, XTE J1810−197 (Camilo et al. 2006), became a bright radio pulsar only after its 2003 X-ray outburst, and showed a remarkably flat radio spectrum, at some point being the brightest known radio pulsar above 20 GHz. Extreme variability as well as a very high degree ($\sim 100\%$) of linear polarization were also observed (Kramer et al. 2007; Camilo et al. 2007b) as well as dramatic pulse profile changes (Camilo et al. 2007c). Meanwhile, the second-detected radio magnetar, 1E 1547.0−5408 (Camilo et al. 2007a), has shown properties quite similar to those of XTE J1810−197. A third radio-loud magnetar, PSR J1622−4950, was discovered (Levin et al. 2010) in apparent X-ray quiescence during a standard survey for radio pulsars, hence making it the first radio-discovered magnetar. It too was characterized by extreme variability, with epochs during which it was undetectable, and a flat or even inverted radio spectrum. Subsequent X-ray observations suggest that it is likely recovering from an earlier X-ray outburst (Anderson et al. 2012), further suggesting that magnetar radio emission is associated with post-outburst events.

Very recently, a fourth radio magnetar, SGR J1745−29, was discovered via its X-ray emission, only $3''$ from the Galactic Centre (Mori et al. 2013). The subsequent radio detection (Eatough et al. 2013; Shannon & Johnston 2013) showed again high linear polarization, and the largest dispersion and rotation measures for any known pulsar. In contrast to the other three radio-detected magnetars, this source appears to be far less radio variable, even as the X-ray emission fades (Kaspi et al. 2014; Lynch & Kaspi 2015). Interestingly, the high Faraday rotation as inferred from radio observations argues for a dynamically significant magnetic field near the central super-massive black hole, relevant to the physics of the accretion flow (Eatough et al. 2013). Importantly, a multi-wavelength pulse profile study (Spitler et al. 2014) shows the pulse is scatter-broadened by an order of magnitude less than was predicted by the in-standard-use Cordes & Lazio (2002) model, a conclusion supported by radio angular broadening measurements (Bower et al. 2014). This is significant for potential SKA pulsar searches of the Galactic Center region (see, Eatough et al. 2015; Keane et al. 2015), as it implies pulsars may be easier to find there than has been previously thought (Chennamangalam & Lorimer 2014), particularly at high radio frequencies such as SKA1-MID band 5, even in spite of the very few detections thus far in relatively high-frequency surveys

PoS(AASKA14)039

(Bates et al. 2011). The radio detections of pulsars within the central parsec of the Galaxy could allow unique dynamical tests that could constrain properties of the central super-massive black hole as well as test theories of gravity (Pfahl & Loeb 2004; Liu et al. 2012; Eatough et al. 2015).

2.1 The contribution of SKA

The SKA will be of great use for the radio study of magnetars. Current upper limits on radio observed, but yet undetected, sources are in the range of 0.01–0.04 mJy for periodic emission and 0.1–10 mJy for single pulses, depending on pulse width (e.g. Lazarus et al. 2012). SKA sensitivities are up to an order of magnitude better than was previously possible, thereby greatly increasing the available phase space for detection at a wide range of frequencies. The detection and/or improved upper limits for additional sources will help determine if the bulk are indeed radio quiet, as might be expected in some models of pulsar emission (Baring & Harding 2001) or due to small beaming angles (Lazarus et al. 2012). The SKA detection of radio emission from a magnetar which previously appeared to have faded beyond observability in the radio band could demonstrate persistent low-level radio emission. A comparison of the radio properties of such a source in radio quiescence with those when it was in outburst may be further constraining of models. Differences in polarization profiles between these two states could prove to be highly effective diagnostics of geometric differences expected in twisted magnetosphere models (Thompson et al. 2002; Beloborodov & Thompson 2007). Regular monitoring of magnetars with SKA-type sensitivities could help determine whether their hallmark bursts are present in the radio band as has been suggested in some burst models (Lyutikov 2002). Furthermore, some authors have suggested fundamental physics experiments with magnetar radio emission, such as axion detection using photon beam splitting (Guendelman & Chelouche 2011), which may be facilitated with more sources detected.

3. High B-Field Radio Pulsars

One question regarding the NS population is what distinguishes magnetars from otherwise apparently conventional radio pulsars which appear, from their P and $\dot{P}$, to have magnetar-strength B-fields. Indeed currently there are 9 known, otherwise conventional radio pulsars, having spin-inferred surface dipolar magnetic field strengths above 4.4×10^{13} G (a somewhat arbitrary limit derived from the so-called "quantum critical field" $B = m^2c^2/\hbar e$), with the highest known being $B = 9.4 \times 10^{13}$ G for PSR J1847−0130. Such fields clearly overlap, and in some cases exceed, those of magnetars, for which the smallest spin-inferred dipolar magnetic field is a paltry $B = 6.1 \times 10^{12}$ G (Rea et al. 2013). Therefore, there is reason to expect potential magnetar-like behavior in high-B radio pulsars. Indeed, PSR J1846−0258 in the SN remnant Kes 73 has shown magnetar-like phenomenology (Gavriil et al. 2008) in the form of a short-lived X-ray outburst simultaneous with a large rotation glitch. Deep X-ray observations of high-B radio pulsars using telescopes like *Chandra* and *XMM-Newton* have also shown strong evidence for enhanced thermal X-ray emission from high-B radio pulsars relative to that seen in lower-B radio pulsars of comparable age (Kaspi & McLaughlin 2005; Zhu et al. 2011; Olausen et al. 2013). This could be understood in terms of magneto-thermal evolution in NSs, in which B-fields decay internally, releasing energy and keeping the NS hot (Aguilera et al. 2008; Perna et al. 2013).

PoS(AASKA14)039

3.1 The contribution of SKA

The discovery of new high-B radio pulsars in surveys with the SKA has the potential to make important progress in this field, primarily because of the paucity of high-B pulsars currently known. With new examples, together with follow-up X-ray observations, particularly with future high-throughput X-ray missions such as *ATHENA*[2], additional data points can be added on NS cooling curves (Olausen et al. 2013). Given the expectations for the numbers of pulsars to be discovered with SKA, and assuming the current ratio of high-B radio pulsars to the rest of the population ($\sim$0.4%) continues to hold, SKA should discover 50–100 new high-B sources for X-ray follow-up.

Moreover, regular monitoring of these high-B radio pulsars for timing purposes is likely to reveal many spin glitches, particularly given how ubiquitous and dramatic such events are in magnetars (Dib et al. 2008; Dib & Kaspi 2014): spin-up and -down glitches have been observed and are generally accompanied by flux enhancements as well as pulse profile changes and bursts. The timely detection of a glitch in a high-B radio pulsar could yield an opportunity for rapid X-ray follow-up observations to search for an X-ray outburst. Indeed, there already exist three examples of high-B radio pulsars exhibiting interesting pulse variability at glitch epochs (Gavriil et al. 2008; Weltevrede et al. 2011; Keith et al. 2013). The discovery of new, young high-B radio pulsars could permit the measurement of more braking indices. The young radio pulsar PSR J1734−3333 has $B = 5 \times 10^{13}$ G, and a braking index of only $n = 0.9 \pm 0.2$ (Espinoza et al. 2011), the lowest yet measured for any radio pulsar and well below the canonical $n = 3$ expected for magnetic dipole radiation in a vacuum. Such a low braking index can be interpreted as resulting from magnetic-field growth, suggesting that magnetars could be descendants of high-B radio pulsars.

4. Central Compact Objects and Neutron Stars in Supernova Remnants

Another group of NSs are the central compact objects (CCOs; see e.g. Pavlov et al. 2002). These are isolated, non-variable point sources associated with supernova remnants (SNRs), seen in thermal X-rays. So far they are without optical or radio counterparts (although the latter are single-dish limits). CCOs have low X-ray luminosities ($\sim 10^{33}$ erg s^{-1}) and do not have associated pulsar wind nebulae, suggesting that these stars are NSs which may not yet be active as pulsars. There are currently eight confirmed CCO sources plus three candidates[3] (Weisskopf et al. 2006; de Luca 2008; Gotthelf et al. 2013) and multi-wavelength observing campaigns have been undertaken to search for more sources in nearby SNRs (Kaplan et al. 2006). For three of the CCOs, the spin characteristics (P and $\dot{P}$) are known (see Figure 1) from X-ray timing observations and indicate surprisingly low magnetic fields ($\sim 10^{10}$ G, now in two cases, e.g. Gotthelf et al. (2013)).

Despite the small number of known CCOs it is possible to estimate a minimum Galactic birth rate of these sources using the ages estimated from the SNR expansion times. This yields $\beta_{\rm CCO} \sim 0.5$ century^{-1} (Gaensler et al. 2000). CCOs are thus a significant contributor to the so-called "NS birthrate problem" (Keane & Kramer 2008): the problem that arises if one assumes all of the various NS manifestations discussed in this chapter are evolutionarily independent. Their cumulative birthrate does not tally with the estimated core-collapse SN rate for the Galaxy and so the

[2]http://www.the-athena-x-ray-observatory.eu/

[3]Some authors also define 1E 161348−5055, the variable X-ray source associated with the RCW 103 SNR as a CCO. However here we follow the definition of Halpern & Gotthelf (2010) and take CCOs as having steady X-ray flux.

PoS(AASKA14)039

various groups must evolve into one another along as yet uncertain evolutionary sequences. Moreover, the spin-inferred magnetic fields of CCOs are so small that their expected lifetimes above the death-line in the P-$\dot{P}$ diagram are tens to hundreds of millions of years; this conflicts strongly with the apparent paucity of sources in this region of the P-$\dot{P}$ diagram, *if* the typical CCO is a radio emitter. CCOs are thus a very important part of the puzzle on NS evolutionary pathways.

4.1 The contribution of SKA

A deep investigation with both SKA1 and SKA2 could determine once and for all whether CCOs are radio emitters. In addition to the CCOs, there are currently 55 pulsars with SNR associations. Figure 1 shows that these sources are predominantly "young" with $\tau_c = 10^{4-5}$ yr, consistent with the short lifetimes of visible SNRs. The "older" sources with SNR associations are either chance superpositions (Bogdanov et al. 2014) or are in fact young, i.e. having been born with a slow birth period causing their characteristic age to be much larger than their true age. The SKA will enable unprecedented deep searches of all of the Galactic SNRs visible in the SKA-sky and will firmly detect all of those showing even minute levels of radio pulsar emission. Timing these pulsars with the SKA will allow measurement of their spin characteristics and thence enable us to "rewind" the spin history of these stars to determine a more realistic birth period distribution for pulsars, a notoriously difficult aspect of pulsar evolution to model (Faucher-Giguère & Kaspi 2006; Noutsos et al. 2013).

5. Rotating Radio Transients

Rotating radio transients (RRATs) are a class of pulsars from which pulses are only sporadically detectable (McLaughlin et al. 2006). The appropriate definition of this class of objects, and indeed whether a definition is even necessary, has been debated (Keane & McLaughlin 2011). Here, we define RRATs as NSs which were originally detectable only through their single pulses and not through a periodicity search (though we exclude the first pulsars discovered before the regular application of periodicity searches). Using this definition, there are roughly 100 known RRATs[4]. Their periods range from 0.125 s to 7.7 s, with a mean of 2.6 s. A fraction ($\sim$20%) of the RRATs do not yet have determined periods due to a small number of detected pulses. These periods show some evidence of being longer than those of other pulsars. It is unclear if longer-period pulsars become sporadic emitters, or if this is a selection effect due to the smaller number of pulses in an observation — and hence, for longer period pulsars, higher likelihood of being more detectable in a single-pulse search.

Measuring period derivatives for RRATs often requires much more observing time than for normal pulsars due to their sporadic emission. Therefore, only $\sim$25% of the RRATs have measured period derivatives (cf. Figure 1). These do not appear to be significantly different than the period derivatives of other pulsars, but due to the longer periods, the inferred surface dipole magnetic fields of the RRATs are possibly higher than for other pulsars, with a mean of 3×10^{12} G.

When the discovery of the RRATs was first announced (McLaughlin et al. 2006), it was believed that they were a new class of radio-emitting NSs. Under this assumption, their sporadic

[4]See the online catalogue of RRATs at http://astro.phys.wvu.edu/rratalog

PoS(AASKA14)039

properties imply that for each detected RRAT, there are many more undetected objects, leading one to infer a very large population of these sources, and hence NSs, in the Galaxy (McLaughlin et al. 2006). This issue was further explored and Keane et al. (2010) found that, assuming that the RRATs form a population distinct to other NSs, the total inferred number of Galactic NSs is discrepant with Galactic SN rate estimates. One solution to this problem is if RRATs are a part of the same population as other pulsars.

This assumption seems reasonable, given the similarity between the properties of RRATs and other pulsars, and the apparent continuum in intermittency bridging these two (perhaps not distinct) populations. Studies of the single pulses of RRATs indicate that their brightness temperatures are no greater than the single-pulse brightness temperatures for other pulsars. In addition, the pulse shapes and widths of RRAT pulses are similar to those of other long-period pulsars. Furthermore, some RRATs were initially detectable only through their single pulses, but with observations at a lower frequency or with a more sensitive telescope, they are detectable through periodicity searches like normal pulsars. It is therefore plausible to assume that RRATs are simply pulsars which sit on the tail end of a continuous intermittency spectrum and are not part of any special population.

6. Intermittent Pulsars

While there has been progress in the theoretical understanding of the magnetospheric processes in pulsars (e.g. Contopoulos et al. 1999; Spitkovsky 2006), some of the most important experimental insight comes from the study of a class of NSs called *intermittent pulsars*. The archetype of this relatively recently discovered class is radio pulsar B1931+24 (Kramer et al. 2006a; Young et al. 2013), which is only active for a few days between periods of roughly a month during which the pulsar is not detectable. The fact that pulsars are able to switch on and off is something that has been known for a long time and is often observed at much shorter timescales, in which case it is known as *nulling* (e.g. Backer 1970; Wang et al. 2007). The exciting result for the intermittent pulsars is that these sudden switches are accompanied by changes in the spin-down rate of the NS rotation, suggestive of significant changes in the torque generated by magnetospheric currents. For PSR B1931+24 the spin-down was shown to be 50% larger when the radio emission of the pulsar is in the *on-state* compared to the *off-state* (Kramer et al. 2006a), explaining at the same time the seemingly noisy timing behaviour for this source (see Figure 2).

Besides PSR B1931+24, there are only two other intermittent pulsars known which change their spin-down rate. For PSR J1832+0029 (Lorimer et al. 2012) the spin-down rate changes by a factor of 1.8, while for PSR J1841–0500 (Camilo et al. 2012) the spin-down rate changes by a factor of 2.5. All three intermittent pulsars appear to be part of the bulk of the pulsars in the P-$\dot{P}$ diagram. At first, it may seem somewhat surprising that radio emission is linked to the spin-down rate of pulsars. The amount of energy in the radio emission is tiny in comparison to the total loss rate of the rotational energy of the NS (i.e. $\dot{E}$), so one could expect the radio emission to be an indicator of higher order effects rather than fundamental processes within the pulsar magnetosphere. Nevertheless, the radio emission appears to be a tracer of powerful currents in the magnetosphere.

The behavior of intermittent pulsars can be explained by a relatively simple two-state magnetospheric model (Kramer et al. 2006a; Li et al. 2012). In one of the states the open field line region is filled with a co-rotating plasma which as a consequence should have the Goldreich–Julian den-

PoS(AASKA14)039

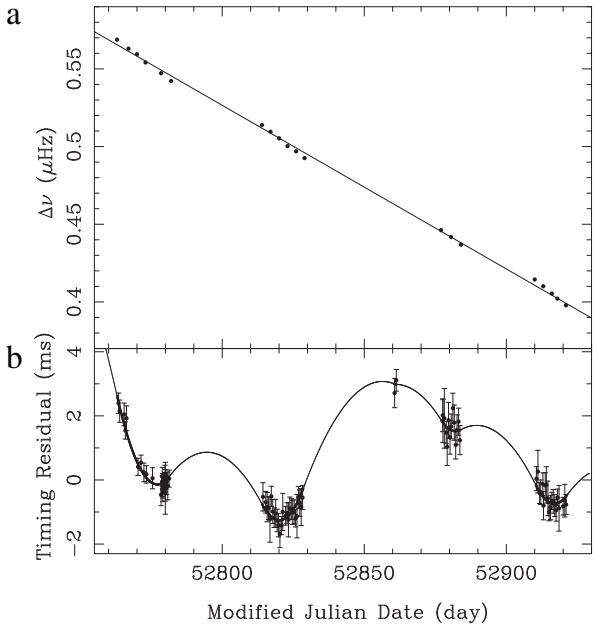

Figure 2: Changes in the spin-rate of PSR B1931+24 (upper panel) when 'on' (radio bright). The rotational frequency is clearly decreasing faster (i.e. the gradient is steeper) in the 'on'-state compared to the average spin-down rate (indicated by the solid line), implying that the pulsar is spinning down slower in the 'off' (radio quiet) state. Taking the switch between two different slow-down rates into account, the apparent noisy timing behaviour can be explained perfectly (lower panel). Figure from Kramer et al. (2006a).

sity (Goldreich & Julian 1969). This magnetospheric state can in good approximation be described by a force-free magnetospheric solution (Spitkovsky 2006). This plasma is generated by the same mechanism which produces the radio emission observed during the on-state. When this mechanism switches off both the radio emission and plasma production ceases, resulting in the open field line region to get depleted from plasma. This vacuum state will have a different spin-down rate by a factor which depends on the magnetic inclination angle (Li et al. 2012), which can explain the range (1.8–2.5) in observed factors by which the spin-down rate is changing.

An alternative model has been suggested (Timokhin 2010) in which the switching between stable magnetospheric states causes different geometries or/and different distributions of currents which can explain the persistent "nulling" during the off-states. Furthermore, it has become clear that there are more subtle ways in which the radio emission and spin-down rate are linked. There are a number of objects which show pulse profile changes concurrent with changes in the spin-down rate (Lyne et al. 2010). This has led to the suggestion that all the so-called timing-noise (deviations from a simple spin-down model) could be ascribed to switches between magnetospheric states. These more subtle changes in the emission result in more subtle changes in spin-down, which can be less than 1%. One should note, however, that most of these state changes (e.g. the so-called "moding") happens on time-scales of minutes to hours and are therefore too fast to measure (and, hence, separate) correlated changes in spin-down rate (Young et al. 2012).

PoS(AASKA14)039

6.1 The contribution of SKA

The SKA can help in several ways to make progress in our understanding of the pulsar magnetosphere using intermittent pulsars (see also Karastergiou et al. 2015). Firstly, we will progress by discovering more intermittent pulsars. This will lead to additional measurements of the changes in the spin-down rate between the on- and the off-state for many more sources, thus understanding better the magnetospheric state changes. For this it will be important, however, that repeated passes are performed over given search areas. The time between these passes should vary from hours and days to weeks and months, similar to the range of time scales observed for both intermittent and nulling pulsars (as well as RRATs, see Section 5). Indeed, an important question which the SKA will help to address is what the difference (if any) is between intermittent pulsars and nulling pulsars, as the main difference appears to be the duration of the off-state.

It is important to note that the large sensitivity of the SKA will not necessarily mean that we can detect much smaller changes in the spin-down rate or changes which are shorter in duration. However, the high sensitivity of the SKA can put better (important) limits on the presence of radio emission during the off-state. It is easy to confuse nulls with very weak emission, as has been shown for instance for PSR B0826–34 (Esamdin et al. 2005). The presence of very weak emission during the off-state of intermittent pulsars would show that there are at least some currents present in the pulsar magnetosphere at all times. Additionally, the multi-beaming capability of the SKA will allow a dense monitoring of the known intermittent (and other) pulsars. The much larger possible cadence will allow us to determine the exact switch times between the states more accurately. This is important for two reasons: i) we can probe the plasma conditions much better by constraining the currents present in the magnetospheres and correlate the results to other properties of pulsars, and ii) we can potentially use the information to correct for timing noise in non-recycled pulsars, hence, opening up the possibility to use them also for high precision experiments such as gravitational wave detection (Lyne et al. 2010).

7. Isolated Pulsar Evolution on the P-$\dot{P}$ Diagram

A common approach to understand the distribution of pulsars in the P-$\dot{P}$ diagram (Figure 1) is to take a prescription for the spin evolution of NSs (often a simple magnetic dipole model) and evolve pulsars forward from some birth distributions in P and B in time to find the present-day distribution. Ideally, after accounting for observational selection effects (Emmering & Chevalier 1989), this distribution would be statistically indistinguishable from the one that is observed. The major challenge facing all these studies is to decouple various competing and covariant effects that shape this distribution. Assuming that radiation beaming (Tauris & Manchester 1998) and the selection effect modelling process (Faucher-Giguère & Kaspi 2006) are reasonably well understood, the main factors involved are discussed in turn below. A less model dependent approach is to compute the flux or "current" of pulsars through the P-$\dot{P}$ diagram by taking into account detection biases (Phinney & Blandford 1981; Vivekanand & Narayan 1981; Narayan 1987). Recently, Lee et al. (2012) have attempted to categorize sub-populations within the distribution using Gaussian mixture models. The main factors for shaping the pulsar distribution are:

PoS(AASKA14)039

- **Neutron star birth parameters.** While the overall consensus on the distribution of B-fields seems to favour a single-component log-normal distribution, much debate has taken place over the form of the period distribution. The view put forward by early studies (e.g. Lyne et al. 1985) which favoured a model in which all pulsars were born spinning rapidly was challenged by the idea of an "injection" of pulsars into the population with birth periods of around 0.5 s (Vivekanand & Narayan 1981; Narayan 1987; Narayan & Ostriker 1990). Current studies (Faucher-Giguère & Kaspi 2006; Ridley & Lorimer 2010) favour a broad normal distribution with a mean of 0.3 s and standard deviation of 0.5 s. Independent constraints on the initial period distribution from pulsar–SN remnant pairs (Popov & Turolla 2012) suggest a mean and standard deviation of 0.1 s.

- **Magnetic field strength evolution.** Solving the differential equation $B \propto (P\dot{P})^{1/2}$ to obtain the evolution of P and $\dot{P}$ with time in the magnetic dipole model is most readily achieved assuming that B is constant. Such models provide good matches to the P-$\dot{P}$ distribution (Bhattacharya et al. 1992; Faucher-Giguère & Kaspi 2006). However, models which invoke a very modestly decaying magnetic field (Popov et al. 2010) are also consistent with the data. Earlier theoretical work (Tauris & Konar 2001) also reached similar conclusions.

- **Magnetic inclination evolution.** Within the frame of a rotating magnetic dipole in a vacuum, the torque acting on the spinning NS is proportional to $B^2 \sin^2\alpha$, where α is the angle between the spin and magnetic axes. This relationship implies that magnetic field decay mentioned in the previous item can also be mimicked by a decay in the inclination angle, α. Several independent studies (Tauris & Manchester 1998; Weltevrede & Johnston 2008; Young et al. 2010) conclude that α decays with time. An outstanding issue (Ridley & Lorimer 2010) is how this decay translates to a change in the braking torque on the pulsar. While Tauris & Konar (2001) suggest that a decay in the braking torque is required by the P-$\dot{P}$ distribution, as Ridley & Lorimer (2010) demonstrate, Monte Carlo simulations assuming magnetic alignment cannot satisfactorily explain the observed sample.

- **Non-standard magnetic dipole evolution.** One possible solution to the alignment issue discussed above is to evolve the pulse period according to a different spin-down law. A revised model has been proposed (Contopoulos & Spitkovsky 2006) with different evolutionary tracks which allow for a constant magnetic field and alignment. Detailed Monte Carlo models (Ridley & Lorimer 2010) have, however, so far not been able to reproduce the P-$\dot{P}$ diagram using this framework.

- **Luminosity "law" and evolution.** In the absence of a well developed theoretical framework for understanding the radio emission of pulsars, the luminosity L is often calculated from a power-law expression of the form $L \propto P^{\alpha}\dot{P}^{\beta}$. This approach has been adopted by numerous studies (e.g. Lyne et al. 1985; Stollman 1987; Narayan & Ostriker 1990; Faucher-Giguère & Kaspi 2006), with quite different values for the exponents α and β. It is noteworthy (Lorimer et al. 1993) that the adopted values for α and β significantly impact the conclusions regarding population parameters. For example, combinations which favour high luminosity with short periods generally support injection into the population (Narayan 1987). Recent work

PoS(AASKA14)039

by Bates et al. (2014) find $\alpha \simeq -1.4$ and $\beta \simeq 0.5$ which is very similar to the relationship found for the gamma-ray pulsar population (Perera et al. 2013). This combination of parameters leads inexorably to the conclusion that the radio luminosity decays significantly with time. Expressions which describe these trends are provided by Bates et al. (2014) and make predictions for large-scale surveys, such as the SKA.

- **Death-lines and valleys.** The dearth of pulsars in the lower right-hand side of the P-$\dot{P}$ diagram has long been associated with a physical limit on radio emission; for a review see Chen & Ruderman (1993). As such, death-lines (or valleys) are frequently included in pulsar population syntheses. Very recently, a reasonable reproduction of the P-$\dot{P}$ diagram has been carried out without the adoption of a death-line, or any luminosity law (Szary et al. 2014). Instead, the study invoked an inverse correlation between radio efficiency and age. This approach appears to argue against any dependence of radio luminosity with P and $\dot{P}$.

- **Braking indices.** Additional measurements of the braking indices of pulsars (Livingstone et al. 2007) would help to pin down the directionality in the flow of pulsars in the diagram. Indeed, some of the braking indices measured so far for young pulsars are not consistent with the locations of older pulsars and hint at the idea that some radio pulsars may evolve into magnetars (Espinoza et al. 2011). As noted by earlier authors (e.g. Tauris & Konar 2001), a change in the braking index is required throughout the lifetime of a pulsar. This implication has yet to be fully addressed by population studies.

It is evident from the preceding discussion that many uncertainties remain in our understanding of the P-$\dot{P}$ diagram. The larger sample of pulsars provided by SKA surveys will undoubtedly help to clarify many of these issues, including the shape and the faint-end of the pulsar luminosity function. While many authors (e.g. Lyne et al. 1985; Lorimer et al. 1993) adopt power-law models of pulsars luminosities, recent work (Faucher-Giguère & Kaspi 2006; Ridley & Lorimer 2010; Bates et al. 2014) suggests that the parent population is more log-normal in nature.

8. Millisecond and Binary Pulsar Surveys with SKA

The large total collecting area, wide range of frequencies, and rapid survey speed available with SKA1 will revolutionize our understanding of the MSP population in the Milky Way. Currently, there are $\sim$300 MSPs (defined here as $P < 30$ ms) known in the Galaxy, including those associated with globular clusters (see the chapter by Hessels et al. 2015). Their distribution on the sky and in the Galaxy is shown in Figure 3. The primary SKA project that will drive our understanding of the MSP population is the SKA1-MID pulsar survey, which will cover 36,000 sq. deg. of sky. This is only possible with the large collecting area and very fast survey speed of SKA1-MID. Surveys at high latitude may reveal new bright, stable pulsars that will contribute to pulsar timing array projects, and will fill out our understanding of the low end of the MSP luminosity function (< 0.1 mJy kpc^2 at 1400 MHz). In the plane SKA will explore a larger volume of the Galaxy than ever before to find rare systems and constrain the Galactic population of MSPs (see Section 9). The SKA1-MID pulsar survey, as defined in the SKA1 System Baseline Design is of similar sensitivity to the ongoing PALFA survey being done with the Arecibo Telescope, with flux

PoS(AASKA14)039

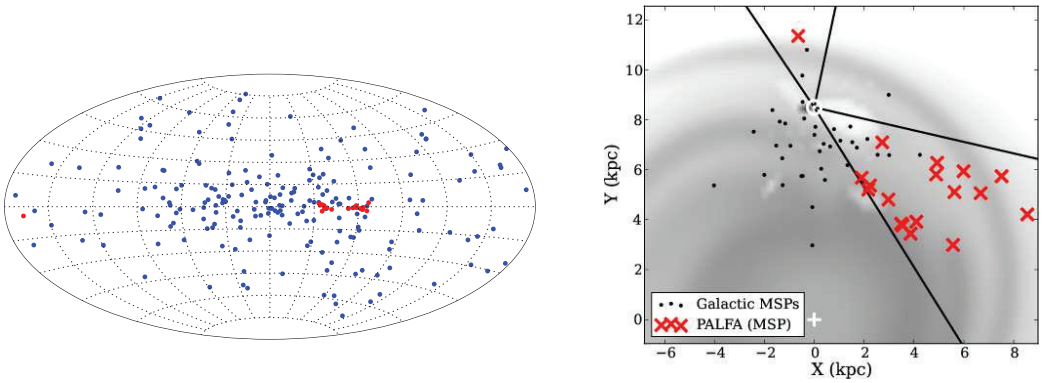

Figure 3: Left: Locations of the 216 known MSPs outside of globular clusters. Discoveries from the PALFA survey at Arecibo are shown in red. Right: Top down view of the galaxy with MSP locations marked. Again, red symbols denote PALFA MSPs (reproduced from Lazarus 2013), which are systematically more distant than the previously known population. The solid lines show the portion of the plane visible from Arecibo. SKA1 will expand that to cover nearly the entire Galaxy.

limits in the neighborhood of 40 μJy. The big difference is that the SKA1-MID survey extends that sensitivity over the full visible sky, while PALFA is constrained to narrow strips of the Galactic plane visible from Arecibo (see Figure 3).

These very deep surveys are sensitive to pulsars at large dispersion measure, because of the relatively high observing frequencies, and thus probe a much larger volume of the Galaxy than previous large-area surveys. For directions in the plane, the volume sampled increases as the square of the distance probed. Figure 3 shows that PALFA is seeing a much more distant population than other surveys. SKA1-MID will expand this over nearly all of the plane, particularly towards the Galactic Bulge, where large numbers of low-mass X-ray binaries (the progenitor systems for MSPs) are known to reside. This will help constrain the total number of MSPs in the Galaxy and their density as a function of galactocentric radius, which is important for population modeling.

From an evolutionary point of view, many of the most interesting pulsars are found in tight relativistic orbits, allowing the measurement of post-Keplerian parameters. This implies that the pulsar will be accelerated for most of its orbit, requiring either short integration time with high sensitivity or sophisticated acceleration processing. Compensating for a sensitivity loss of about 10% (with respect to the baseline design) with increased observing time results in a doubling of the processing requirements to find the same relativistic binary pulsars. Hence, conducting pulsar searches with SKA1-LOW and its exceptional collecting area is a promising method for finding binary pulsars away from the Galactic plane. Indeed, our simulations show that a combined SKA1-MID and SKA1-LOW survey targeting regions on and off the Galactic plane respectively finds approximately 20% more pulsars than can be found with SKA1-MID alone (Kramer & Stappers 2014; Keane et al. 2015). Binary pulsar masses (Section 11) can only be determined if regular timing observations can be done. Though some sources may be bright enough to follow-up with other radio telescopes, it is likely that most sources will require the SKA. Sub-arraying can help alleviate the observing load for sources that are easily detectable with a fraction of the collecting area. It may also be advantageous in some cases to run pulsar timing experiments in parallel with imaging observations to boost the observing efficiency.

PoS(AASKA14)039

When SKA2 is realized, the additional sensitivity will enable considerably more breakthrough science in this field. SKA will not only provide further sources to characterize the MSP and binary pulsar population (in particular via a high frequency survey in the Galactic bulge and central region), also the detection of giant pulses in extra-galactic MSPs (e.g. in M31 and IC 10) may be realistic.

9. Pulsar Recycling and Formation of Exotic Binaries and Triples

Radio pulsars have been discovered in binary systems with a variety of companions: white dwarfs (WDs), NSs, main sequence stars, and even planets. The vast majority of these systems contain an MSP with a helium WD companion. Based on stellar evolution theory, it is expected that pulsars could also be found with a helium star or a black hole companion. These systems have not yet been discovered but it is likely that the SKA will reveal such pulsars. There is a growing number of systems where the companion star is being ablated by the pulsar wind, the so-called *black widows* and *redbacks* (Roberts 2013). This is evidenced by the radio signal from the pulsar being eclipsed for some fraction of the orbit (Fruchter et al. 1988; Stappers et al. 1996; Archibald et al. 2009). These companions are low-mass semi-degenerate stars with a mass between $0.02 - 0.3\ M_\odot$ (Roberts 2013; Breton et al. 2013). Whereas some studies clearly indicate that the two populations of black widows and redbacks are distinct (Chen et al. 2013) others argue in favour of a continuous evolutionary link (Benvenuto et al. 2014). This question is important to settle; as well as the long standing issue about whether they are the progenitors of the isolated MSPs (Ruderman et al. 1989; Possenti 2013; Deloye & Bildsten 2003).

In recent years, a few binary pulsars with peculiar properties have been discovered and which indicate a hierarchical triple system origin — e.g. PSR J1903+0327 (Champion et al. 2008; Freire et al. 2011; Portegies Zwart et al. 2011). In 2013, two puzzling MSPs were discovered in eccentric binaries: PSR J2234+06 (Deneva et al. 2013) and PSR J1946+3417 (Barr et al. 2013). These two systems might also have a triple origin. However, their eccentricities and orbital periods have led to the suggestion of an alternative hypothesis of direct MSP formation via a rotationally delayed accretion-induced collapse of a massive WD (Freire & Tauris 2014). Whereas the origin of these systems remains unclear, a triple system MSP with two WD companions (PSR J0337+1715) was announced earlier this year by Ransom et al. (2014). This amazing system must have survived at least 3 phases of mass transfer and one SN explosion and challenges current knowledge of multiple stellar system evolution (Tauris & van den Heuvel 2014). To understand the underlying physics it is therefore important to find more of these exotic systems.

Surveys with SKA1-MID (including a coverage of the Magellanic Clouds) will indeed find many more rare systems. It is likely that SKA1 will increase the population of known pulsars and MSPs by at least a factor of 5 and thus greatly increase the number of systems which can be used to study the evolution of pulsars that are in, or have been members of, multi-stellar systems.

MSPs obtain their rapid spin (and weak B-field) via a long phase of accretion of matter from a companion star in a low-mass X-ray binary (LMXB; Backer et al. 1982; Alpar et al. 1982; Radhakrishnan & Srinivasan 1982; Bhattacharya & van den Heuvel 1991; Tauris et al. 2012). This is evidenced by the high incidence of binaries found among these fast spinning pulsars (see Figure 1). This model was beautifully confirmed by the discovery of the first millisecond X-ray pulsar in the

PoS(AASKA14)039

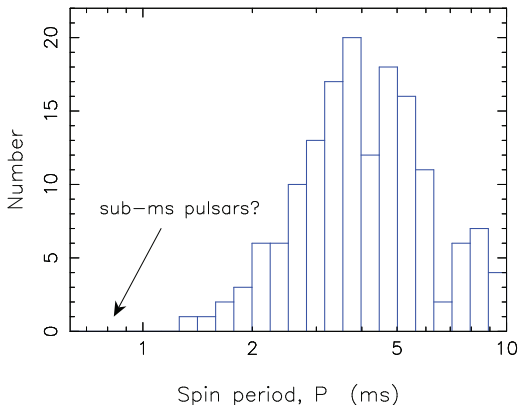

Figure 4: The observed spin period distribution of MSPs. Data taken from the ATNF Pulsar Catalogue (Manchester et al. 2005) – version 1.49, April 2014. The discovery of sub-ms MSPs with the SKA would have a huge scientific impact.

LMXB system SAX 1808.4–3658 (Wijnands & van der Klis 1998), and more recently by the detection of the so-called transitional MSPs which undergo changes between accretion and rotational powered states (Archibald et al. 2009; Papitto et al. 2013). Many details of the recycling process, however, remain unclear. Some of the most important issues (e.g. Tauris et al. 2012, and references therein) are: the accretion-induced decay of the surface magnetic field; the maximum possible spin rate of an MSP; the Roche-lobe decoupling phase; the accretion torque reversals and the spin-up line; and the progenitors of the isolated MSPs.

There is empirical evidence that the surface magnetic field strength of NSs decays as a consequence of accretion, but the exact reason for this process is not well understood (Bhattacharya 2002). Nor is it known what dictates the fastest possible spin rate of a radio MSP. In Figure 4 we have shown the spin period distribution of radio MSPs. Does the equation-of-state (EoS) for dense nuclear matter allow for the existence of sub-ms pulsars? Or is the current spin frequency limit, slightly above 700 Hz (Hessels et al. 2006), set by the onset of gravitational wave (GW) emission during accretion (Chakrabarty et al. 2003), or subsequent r-mode instabilities? Alternatively, the spin-up torque might saturate due to magnetosphere–disc conditions, thus preventing sub-ms MSPs to form. In addition, it has been demonstrated (Tauris 2012) that during the final stage of mass transfer, MSPs may lose up to 50% of their rotational energy when the donor star decouples from its Roche lobe.

9.1 The contribution of SKA

As described in detail elsewhere in this book, the large scale surveys performed with SKA1 will lead to a significant increase in the number of catalogued MSPs. That will also include several new exotic (and therefore intrinsically rare, possibly unprecedented) objects, suitable to directly address some of the key-questions reported above: i.e. the discovery of even a single MSP spinning at a period well below 1 ms would provide strong constraints on the NS structure and the EoS of dense nuclear matter. In the context of evolutionary studies, it will be particularly interesting to use SKA1-MID for performing a deep search for pulsars at a higher frequency (between 2 and 3 GHz)

PoS(AASKA14)039

than ever for an all-sky survey. In fact, at those frequencies, the absorbing/eclipsing effects of the plasma released by the companion star are significantly reduced with respect to what happens at the lower frequencies typically used in all the past large scale surveys. That could finally unveil the radio signal from several ultra close-orbit binary pulsars in the last phases of their recycling, i.e. the transitional MSPs which are among the most precious systems for investigating the still unanswered issues discussed in this section.

SKA2 will then provide an extremely large population of recycled pulsars, eventually enabling a statistically sound comparison between the properties of the various classes of binary and isolated MSPs, thus firmly establishing relationships and evolutionary connections. Similarly, it has been shown in several works (e.g. Possenti et al. 1999; Tauris et al. 2012, and references therein) that the availability of a large population of MSPs (maybe including still unknown MSPs with surface B-fields below 10^7 G, or MSPs with relatively high B-fields) would constrain the physical processes during the last stages of accretion. This includes new knowledge on the evolutionary phases experienced by a pulsar close to the spin-up line and/or the occurrence of GW emission from the accreting NS, as well as the radio emission mechanism in old NSs (i.e. the death-line for low B-field pulsars).

10. Double Neutron Star and Neutron Star/Black Hole Systems

In 1974 a new class of radio pulsars was discovered with the detection of the first double NS system (Hulse & Taylor 1975). Today we know a dozen double NS systems. The formation and evolution of such relativistic binaries (tight systems with massive compact stars) is a key topic in modern astrophysics with many applications to fundamental physics in general. In particular, double NS systems are important for: pre-SN binary evolution and explosion physics, measurements of NS masses, testing theories of gravity, and their mergers are prime candidates for detection of high-frequency gravitational waves with LIGO/VIRGO within the next few years.

Double NS binaries are important for both stellar astrophysics and SN explosion modelling since their observed orbital characteristics represent a fossil relic of the last (second) SN explosion. Hence, from observations of double NS binaries we can place constraints on both the pre-SN conditions and the explosion mechanism itself. Many of the systems have rather small eccentricities and small masses of the last (second) formed NS. This is indeed expected if these SNe were either caused by electron capture SNe (Podsiadlowski et al. 2004) and/or a result of pre-SN ultra-stripping of the collapsing star (Tauris et al. 2013a). However, also higher birth masses of NSs are expected from stellar evolution (Tauris et al. 2011) and the many new double NS binaries anticipated to be discovered by the SKA will finally probe the full distribution of NS birth masses in these systems (see Section 11). The SKA is very likely to discover more double pulsar systems like PSR J0737−3039A/B. From observations (Breton et al. 2008, 2012) and modelling (Lyutikov & Thompson 2005) of interactions, via eclipse light curves, between the emission beam of one pulsar with the magnetosphere of its companion pulsar, detailed knowledge can be obtained with respect to the magnetospheric structure (see also Karastergiou et al. 2015), the plasma properties, and relativistic precession of pulsars.

With the many new pulsar discoveries to be expected with the SKA there is realistic hope that they will also include a few long-sought-after NS–black hole (NS–BH) binaries. NS–BH binaries

PoS(AASKA14)039

have the potential to revolutionize gravity tests (Kramer et al. 2006b; Wex 2014; Shao et al. 2015) and will also bring new insight to the final stages of massive stellar evolution and SNe.

Understanding the NS–NS and NS–BH populations is important since their merger events are prime candidate sources for the upcoming detection of high-frequency gravitational waves with LIGO/VIRGO. The event rate of detections is expected to be of the order 0.1–10 per week (Voss & Tauris 2003; Abadie et al. 2010) and this rate should match the observed distributions of orbital separations and eccentricities among Galactic NS–NS and NS–BH sources. The LIGO/VIRGO detection rate is based on the Galactic merger rate of NS–NS and NS–BH systems which is of the order a few Myr^{-1}. However, this number is highly uncertain due to the many complex factors involved in computing the formation rate of these systems (e.g. Voss & Tauris 2003).

11. Neutron Star Masses

The masses of NSs play a vital role in a number of aspects pertaining to their structure, formation and evolution. So far, all pulsar mass measurements rely on one form or another of dynamical proxies offered by binary systems. The starting point is pulsar timing, which provides a very accurate determination of the mass function of the system and links the orbital inclination to the two masses. Supplementing it with two additional constraints therefore breaks the degeneracy. This can be achieved in various ways: i) Relativistic binaries — usually double NS systems — allow for the measurement of post-Keplerian parameters (such as the Shapiro delay and the periastron advance) that each yield an extra constraint, see Shao et al. (2015); ii) Binaries containing an optically bright companion may provide its projected radial velocity via spectroscopy, a companion mass determination (e.g. via the atmosphere modelling of WDs, van Kerkwijk et al. 2005), or a measure of the mass ratio and orbital inclination via light curve modelling (e.g. Breton et al. 2013).

Since any given EoS (see e.g. the chapter by Watts et al. 2015) sets a maximum mass stability limit, hunting for massive pulsars can provide an efficient way of constraining its nature. With a significant sample of NS masses, however, one can statistically constrain their EoS. Current observational evidence (Demorest et al. 2010; Antoniadis et al. 2013) disfavours a "soft" EoS, which cannot reach much beyond the measured $2\,M_\odot$.

Pulsar masses are also fundamental tracers of their formation and subsequent evolution via accretion. The birth mass of a NS relates to its formation and reflects the SN physics (Tauris et al. 2011; Ferdman et al. 2013, 2014). Hence the presence of multiple modes in the birth mass distribution will probe their formation channels (i.e. iron core-collapse SNe and electron capture SNe). The mass distribution of NS–NS and NS–WD binaries was recently analysed (Kiziltan et al. 2013) and it was concluded that they peak at $1.33\,M_\odot$ and $1.55\,M_\odot$, respectively, with the first having a nearly symmetrical spread of $0.12\,M_\odot$ (1-σ) while the other one being skewed towards higher masses. This arises from the fact that the observed pulsar masses are convoluted by the evolutionary history of the binary system in which they lie. For instance, pulsars with low-mass WD companions have gone through a long-lasting LMXB phase which has likely increased their mass anywhere from $\sim 0.1 - 0.5\,\mathrm{M}_\odot$ (see the previous Section 9 on pulsar recycling). Double NS binaries, on the other hand, should reflect the birth mass more closely since the first-born NS only accretes $< 0.01\,M_\odot$ during/following a common-envelope evolution (Tauris et al. 2012) while the

PoS(AASKA14)039

second NS should have accreted none. Comparing the masses from the two sub-populations might therefore provide a powerful probe for mass transfer in binaries.

11.1 The contribution of SKA

SKA1 is expected to increase the number of known pulsar binaries by more than a factor of five, which should therefore grow the NS mass sample size by a similar factor. This naive assumption is certainly justified for relativistic NS–NS binaries since their mass measurements rely on radio timing only, while in other binaries they suffer the caveat that they require optical data as well. Projects such as the Thirty-Meter Telescope and the European Extremely Large Telescope will provide a ten-fold increase in sensitivity, thus enabling to push down the luminosity function of the probed systems to sustain the growth of mass measurements in these systems as well.

Given a factor of ten increase in the mass sample with SKA2, how well can we expect to determine the minimum and maximum mass range of NSs? Based on the distribution of Kiziltan et al. (2013), i.e. a normal distribution $\mathcal{N}(\mu = 1.33\,M_\odot, \sigma = 0.12\,M_\odot)$, the probability of finding a mass below the putative 1.08 $M_\odot$ lower limit is 1.86%, which implies that a 200-NS masses sample from NS–NS systems would have a 97.7% chance of containing such a low-mass NS (should they exist). If a low-mass limit cutoff exists, it will as well manifest as a skewness in the distribution, which would lack data at the low end. Regarding the upper mass limit, we turn toward NS–WD systems. Here, for simplicity, we assume that they have the same underlying birth-mass distribution as the NS–NS systems (i.e. $\mathcal{N}(\mu = 1.33, \sigma = 0.12)$), and have then accreted some arbitrary mass that we model using a gamma distribution with a scale parameter 0.15 and a shape parameter 2.0. Based on this we infer the probability of finding a mass above 2.4 $M_\odot$ is 0.42%, thus corresponding to 47% odds of having a NS above that limit in a sample of 150 (should such a NS exist). From the distribution of NS masses and eccentricities it is even possible to place limits on the gravitational binding energy of NSs (Podsiadlowski et al. 2005), released via neutrinos during the SN event. Thus future SKA observations can also via this method help to narrow down the EoS of dense nuclear matter (see the chapter by Watts et al. 2015).

12. Neutron Star Kicks and Velocities

Soon after the discovery of pulsars, it was recognized that their average space velocity greatly exceeds that of their progenitor stars (Gunn & Ostriker 1970). At the present time, with proper motions measured for hundreds of pulsars via timing or VLBI, it is clear that most radio pulsars receive a large kick ($\sim$400 km s^{-1}) during their formation event (Hobbs et al. 2005). However, a number of plausible processes remain for the exact physical mechanism responsible for imparting this kick during the SN (Lai et al. 2001; Janka 2012). Many pulsars are observed in globular clusters which have small escape velocities of $\lesssim 40\,\mathrm{km\,s^{-1}}$. Theoretical studies of electron capture SNe and the accretion-induced collapse (AIC) of massive WDs provide a plausible NS formation mechanism which predicts a low kick velocity (Podsiadlowski et al. 2004; Schwab et al. 2010; Tauris et al. 2013b). In addition, there is the interesting question of a possible alignment at birth between the pulsar velocity vector and its spin axis, as suggested by recent observational evidence and modelling (Noutsos et al. 2013).

PoS(AASKA14)039

In order to differentiate between the competing models for NS birth kicks, reliable velocity estimates are needed for a larger fraction of the known pulsar population. The fact that the radial component of velocity is inaccessible for pulsars in all but a very few cases sharpens the need for a large sample of objects. As of early 2014, transverse velocity estimates are available for around 270 pulsars[5], but most of these are of low precision, either because of the proper motion measurement itself or (more commonly) uncertainties in the pulsar distance provided from the pulsar dispersion measure and the NE2001 model of the Galactic electron density distribution (Cordes & Lazio 2002; Deller et al. 2009, 2011). In order to improve the reliability and size of the pulsar velocity distribution sample, three things are needed: i) Additional proper motion measurements, via timing or high resolution astrometry; ii) Accurate, model-independent distance measurements for a larger fraction of the objects with proper motion measurements (again via timing and - more commonly - high resolution astrometry); and iii) A better model of the Galactic electron density distribution, allowing more reliable model-dependent distance estimates for the remaining pulsars.

12.1 The contribution of SKA

With its phenomenal sensitivity, SKA will be able to measure proper motions and parallax distances for radio pulsars via the current approaches (high precision timing and high resolution astrometric observations) but with greatly improved accuracy, and for a much larger number of systems (Smits et al. 2011). For recycled pulsars with very stable rotation properties, SKA will be able to measure proper motion and often parallax via timing. In many cases, this will come as a byproduct of programs undertaken for other purposes, as described earlier in this chapter. The remaining pulsars can be addressed via astrometry. With the moderate baselines of SKA1-MID ($\sim$100 km) it will be possible to measure positions accurate to several milli-arcseconds in a single observation for all but the faintest pulsars. This will be sufficient to measure a proper motion for the majority of pulsars if several observations are made over a multi-year period.

However, to obtain the parallax measurements necessary to anchor the distance scale, much higher angular resolution will be needed. This can be achieved using a phased SKA1-MID and SKA1-SUR as part of a wider intercontinental VLBI network.

The biggest impact of SKA2 for pulsar velocity studies is the extension of baselines to SKA1-MID. With a resolution of a few tens of milli-arcseconds or better at GHz frequencies, coupled with 10$\times$ higher sensitivity than SKA1-MID, SKA2 will be able to perform ultra-precision astrometry on the majority of the entire radio pulsar population visible from the site. In terms of providing the accurate velocity and distance information needed to characterise the pulsar population, SKA2 as currently envisaged encompasses all of the required capabilities.

13. A brief summary of the impact of early phase SKA1 (50% SKA1)

We end this chapter with a brief summary of the outlooks for early deployment of SKA1 and its expected impact on pulsar science (see also Kramer & Stappers 2014).

Early deployment of SKA1 at 50% sensitivity would not provide access to the faintest pulsars of the population. Simulations for SKA1 by Keane et al. (2015) predict detection of $\sim$ 10000 normal pulsars and $\sim$ 1500 MSPs, whereas for early phase SKA1 (50% SKA1) the expected numbers

[5]http://www.atnf.csiro.au/people/pulsar/psrcat/

PoS(AASKA14)039

are roughly 6000 and 750, respectively (keeping the integration time the same). To partly compensate for the sensitivity loss one could, for example, double the integration time. In that case the predicted number of detections are about 7500 normal pulsars and 950 MSPs. However, an increase in integration time would also largely increase the required amount of data processing given that the latter scales with the integration time cubed. An additional handicap for discovering the fast spinning MSPs (as well as double NS and NS–BH binaries) would be the increase in Doppler-smearing of the radio pulses using longer integration times, given that many MSPs are being highly accelerated in tight binaries.

The expected sensitivity limit for the SKA1-MID survey can be compared with, for example, the HTRU survey (Keith et al. 2010) ongoing at the Parkes Radio Telescope and the Arecibo PALFA survey (Cordes et al. 2006). Whereas the sensitivity for SKA1 50% would only be about half the sensitivity of the Arecibo PALFA survey (which, on the other hand, has a very limited sky coverage), it would still be significantly better than the HTRU survey by a factor of 2–6, depending on the Galactic latitude. Another comparison can be made to the complete 64 dishes MeerKAT Radio Telescope. MeerKAT will be operational in 2017 and will later become an integrated part of SKA1-MID. Early deployment of SKA1 at 50% would still have a sensitivity about two times better than that of MeerKAT.

For the measurement of NS kicks and velocities, early-phase observations with SKA1 at 50% sensitivity would be unable to access the faintest pulsars, limiting the maximum number of accurate transverse velocity measurements that could be made (whether by timing with SKA1-MID, imaging with SKA1-MID, or imaging with SKA1-VLBI). The pool of remaining targets still represents a factor-of-many increase over the current state of affairs, and in any case is likely larger than the observing time available in early-phase SKA1.

As pointed out elsewhere, the SKA1 is not only a simple stepping stone towards SKA2. Due to limitations in processing power, it is unlikely that the full area of the completed SKA can be utilized for a blind, large-scale survey for some time to come. SKA1 with a highly concentrated core represents a significant fraction of collecting area usable for surveys with SKA2. Although the outcome will depend on the number of dishes, the bandwidth and the central frequency of a given survey (or a composite survey covered by SKA1-LOW and SKA1-MID), the total number of beams, and the computer power available, significant achievements can even be made in finding MSPs and binary pulsars during early deployment pulsar searching at the 50% SKA level.

References

Abadie, J., Abbott, B. P., Abbott, R., et al. 2010, Classical and Quantum Gravity, 27, 173001
Aguilera, D. N., Pons, J. A., & Miralles, J. A. 2008, A&A, 486, 255
Alpar, M. A., Cheng, A. F., Ruderman, M. A., & Shaham, J. 1982, Nature, 300, 728
Anderson, G. E., Gaensler, B. M., Slane, P. O., et al. 2012, ApJ, 751, 53
Antoniadis, J., Freire, P. C. C., Wex, N., et al. 2013, Science, 340, 448
Archibald, A. M., Stairs, I. H., Ransom, S. M., et al. 2009, Science, 324, 1411
Backer, D. C. 1970, Nature, 228, 42
Backer, D. C., Kulkarni, S. R., Heiles, C., Davis, M. M., & Goss, W. M. 1982, Nature, 300, 615
Baring, M. G., & Harding, A. K. 2001, ApJ, 547, 929

PoS(AASKA14)039

Barr, E. D., Champion, D. J., Kramer, M., et al. 2013, MNRAS, 435, 2234
Bates, S. D., Lorimer, D. R., Rane, A., & Swiggum, J. 2014, MNRAS, 439, 2893
Bates, S. D., Johnston, S., Lorimer, D. R., et al. 2011, MNRAS, 411, 1575
Beloborodov, A. M., & Thompson, C. 2007, ApJ, 657, 967
Benvenuto, O. G., De Vito, M. A., & Horvath, J. E. 2014, ApJ, 786, L7
Bhattacharya, D. 2002, Journal of Astrophysics and Astronomy, 23, 67
Bhattacharya, D., & van den Heuvel, E. P. J. 1991, Physics Reports, 203, 1
Bhattacharya, D., Wijers, R. A. M. J., Hartman, J. W., & Verbunt, F. 1992, A&A, 254, 198
Bogdanov, S., Ng, C.-Y., & Kaspi, V. M. 2014, ApJ, 792, L36
Bower, G. C., Deller, A., Demorest, P., et al. 2014, ApJ, 780, L2
Breton, R. P., Kaspi, V. M., Kramer, M., et al. 2008, Science, 321, 104
Breton, R. P., Kaspi, V. M., McLaughlin, M. A., et al. 2012, ApJ, 747, 89
Breton, R. P., van Kerkwijk, M. H., Roberts, M. S. E., et al. 2013, ApJ, 769, 108
Burgay, M., Rea, N., Israel, G. L., et al. 2006, MNRAS, 372, 410
Camilo, F., Ransom, S. M., Chatterjee, S., Johnston, S., & Demorest, P. 2012, ApJ, 746, 63
Camilo, F., Ransom, S. M., Halpern, J. P., & Reynolds, J. 2007a, ApJ, 666, L93
Camilo, F., Ransom, S. M., Halpern, J. P., et al. 2006, Nature, 442, 892
Camilo, F., Reynolds, J., Johnston, S., et al. 2007b, ApJ, 659, L37
Camilo, F., Cognard, I., Ransom, S. M., et al. 2007c, ApJ, 663, 497
Chakrabarty, D., Morgan, E. H., Muno, M. P., et al. 2003, Nature, 424, 42
Champion, D. J., Ransom, S. M., Lazarus, P., & et al. 2008, Science, 320, 1309
Chen, H.-L., Chen, X., Tauris, T. M., & Han, Z. 2013, ApJ, 775, 27
Chen, K., & Ruderman, M. 1993, ApJ, 402, 264
Chennamangalam, J., & Lorimer, D. R. 2014, MNRAS, 440, L86
Contopoulos, I., Kazanas, D., & Fendt, C. 1999, ApJ, 511, 351
Contopoulos, I., & Spitkovsky, A. 2006, ApJ, 643, 1139
Cordes, J. M., & Lazio, T. J. W. 2002, ArXiv: astro-ph/0207156, astro-ph/0207156
Cordes, J. M., Freire, P. C. C., Lorimer, D. R., et al. 2006, ApJ, 637, 446
Crawford, F., Hessels, J. W. T., & Kaspi, V. M. 2007, ApJ, 662, 1183
Damour, T., & Taylor, J. H. 1992, Phys. Rev. D, 45, 1840
de Luca, A. 2008, in American Institute of Physics Conference Series, Vol. 983, 40 Years of Pulsars: Millisecond Pulsars, Magnetars and More, ed. C. Bassa, Z. Wang, A. Cumming, & V. M. Kaspi, 311–319
Deller, A. T., Tingay, S. J., Bailes, M., & Reynolds, J. E. 2009, ApJ, 701, 1243
Deller, A. T., Brisken, W. F., Chatterjee, S., et al. 2011, in 20th Meeting of the European VLBI Group for Geodesy and Astronomy, held in Bonn, Germany, March 29-30, 2011, Eds: W. Alef, S. Bernhart, and A. Nothnagel, Institut für Geodäsie und Geoinformation, Rheinischen Friedrich-Wilhelms-Universität Bonn, p. 178-182, ed. W. Alef, S. Bernhart, & A. Nothnagel, 178–182
Deloye, C. J., & Bildsten, L. 2003, ApJ, 598, 1217
Demorest, P. B., Pennucci, T., Ransom, S. M., Roberts, M. S. E., & Hessels, J. W. T. 2010, Nature, 467, 1081
Deneva, J. S., Stovall, K., McLaughlin, M. A., et al. 2013, ApJ, 775, 51

PoS(AASKA14)039

Dib, R., & Kaspi, V. M. 2014, ApJ, 784, 37
Dib, R., Kaspi, V. M., & Gavriil, F. P. 2008, ApJ, 673, 1044
Eatough, R. P., Lazio, T. J. W., Casanellas, J., & et al., 2015, "Observing Radio Pulsars in the Galactic Centre with the Square Kilometre Array", in proc. *Advancing Astrophysics with the Square Kilometre Array*, PoS(AASKA14)045
Eatough, R. P., Falcke, H., Karuppusamy, R., et al. 2013, Nature, 501, 391
Emmering, R. T., & Chevalier, R. A. 1989, ApJ, 345, 931
Esamdin, A., Lyne, A. G., Graham-Smith, F., et al. 2005, MNRAS, 356, 59
Espinoza, C. M., Lyne, A. G., Kramer, M., Manchester, R. N., & Kaspi, V. M. 2011, ApJ, 741, L13
Faucher-Giguère, C.-A., & Kaspi, V. M. 2006, ApJ, 643, 332
Ferdman, R. D., Stairs, I. H., Kramer, M., et al. 2013, ApJ, 767, 85
—. 2014, MNRAS, 443, 2183
Freire, P. C. C., & Tauris, T. M. 2014, MNRAS, 438, L86
Freire, P. C. C., Bassa, C. G., Wex, N., et al. 2011, MNRAS, 412, 2763
Fruchter, A. S., Stinebring, D. R., & Taylor, J. H. 1988, Nature, 333, 237
Gaensler, B. M., Bock, D. C.-J., & Stappers, B. W. 2000, ApJ, 537, L35
Gavriil, F. P., Gonzalez, M. E., Gotthelf, E. V., et al. 2008, Science, 319, 1802
Goldreich, P., & Julian, W. H. 1969, ApJ, 157, 869
Gotthelf, E. V., Halpern, J. P., & Alford, J. 2013, ApJ, 765, 58
Guendelman, E. I., & Chelouche, D. 2011, International Journal of Modern Physics E, 20, 100
Gunn, J. E., & Ostriker, J. P. 1970, ApJ, 160, 979
Halpern, J. P., & Gotthelf, E. V. 2010, ApJ, 709, 436
Hessels, J. W. T., Possenti, A., Bailes, M., & et al., 2015, "Pulsars in Globular Clusters with the SKA", in proc. *Advancing Astrophysics with the Square Kilometre Array*, PoS(AASKA14)047
Hessels, J. W. T., Ransom, S. M., Stairs, I. H., et al. 2006, Science, 311, 1901
Hobbs, G., Lorimer, D. R., Lyne, A. G., & Kramer, M. 2005, MNRAS, 360, 974
Hulse, R. A., & Taylor, J. H. 1975, ApJ, 195, L51
Janka, H.-T. 2012, Annual Review of Nuclear and Particle Science, 62, 407
Kaplan, D. L., Gaensler, B. M., Kulkarni, S. R., & Slane, P. O. 2006, ApJS, 163, 344
Karastergiou, A., Johnston, S., Andersson, N., & et al. 2015, "Understanding pulsar magnetospheres with the SKA", in proc. *Advancing Astrophysics with the Square Kilometre Array*, PoS(AASKA14)038
Kaspi, V. M. 2010, Proceedings of the National Academy of Science, 107, 7147
Kaspi, V. M., & McLaughlin, M. A. 2005, ApJ, 618, L41
Kaspi, V. M., Archibald, R. F., Bhalerao, V., et al. 2014, ApJ, 786, 84
Keane, E. F., Bhattacharyya, B., Kramer, M., & et al. 2015, "A Cosmic Census of Radio Pulsars with the SKA", in proc. *Advancing Astrophysics with the Square Kilometre Array*, PoS(AASKA14)040
Keane, E. F., & Kramer, M. 2008, MNRAS, 391, 2009
Keane, E. F., Ludovici, D. A., Eatough, R. P., et al. 2010, MNRAS, 401, 1057
Keane, E. F., & McLaughlin, M. A. 2011, Bulletin of the Astronomical Society of India, 39, 333
Keith, M. J., Shannon, R. M., & Johnston, S. 2013, MNRAS, 432, 3080
Keith, M. J., Jameson, A., van Straten, W., et al. 2010, MNRAS, 409, 619

PoS(AASKA14)039

Kiziltan, B., Kottas, A., De Yoreo, M., & Thorsett, S. E. 2013, ApJ, 778, 66
Klus, H., Ho, W. C. G., Coe, M. J., Corbet, R. H. D., & Townsend, L. J. 2014, MNRAS, 437, 3863
Kramer, M., Lyne, A. G., O'Brien, J. T., Jordan, C. A., & Lorimer, D. R. 2006a, Science, 312, 549
Kramer, M., & Stappers, B. W. 2014, SKA Pulsar Science Assessment Workshop report (available at https://indico.skatelescope.org/conferenceDisplay.py?confId=260)
Kramer, M., Stappers, B. W., Jessner, A., Lyne, A. G., & Jordan, C. A. 2007, MNRAS, 377, 107
Kramer, M., Stairs, I. H., Manchester, R. N., et al. 2006b, Science, 314, 97
Lai, D., Chernoff, D. F., & Cordes, J. M. 2001, ApJ, 549, 1111
Lazarus, P. 2013, in IAU Symposium, Vol. 291, IAU Symposium, ed. J. van Leeuwen, 35–40
Lazarus, P., Kaspi, V. M., Champion, D. J., Hessels, J. W. T., & Dib, R. 2012, ApJ, 744, 97
Lee, K. J., Guillemot, L., Yue, Y. L., Kramer, M., & Champion, D. J. 2012, MNRAS, 424, 2832
Levin, L., Bailes, M., Bates, S., et al. 2010, ApJ, 721, L33
Li, J., Spitkovsky, A., & Tchekhovskoy, A. 2012, ApJ, 746, 60
Liu, K., Wex, N., Kramer, M., Cordes, J. M., & Lazio, T. J. W. 2012, ApJ, 747, 1
Livingstone, M. A., Kaspi, V. M., Gavriil, F. P., et al. 2007, Ap&SS, 308, 317
Lorimer, D. R., Bailes, M., Dewey, R. J., & Harrison, P. A. 1993, MNRAS, 263, 403
Lorimer, D. R., & Kramer, M. 2004, Handbook of Pulsar Astronomy, Cambridge University Press
Lorimer, D. R., Lyne, A. G., McLaughlin, M. A., et al. 2012, ApJ, 758, 141
Lynch, R. S., & Kaspi, V. M. 2015, in preparation
Lyne, A., Hobbs, G., Kramer, M., Stairs, I., & Stappers, B. 2010, Science, 329, 408
Lyne, A. G., Manchester, R. N., & Taylor, J. H. 1985, MNRAS, 213, 613
Lyutikov, M. 2002, ApJ, 580, L65
Lyutikov, M., & Thompson, C. 2005, ApJ, 634, 1223
Manchester, R. N., Hobbs, G. B., Teoh, A., & Hobbs, M. 2005, AJ, 129, 1993
McLaughlin, M. A., Lyne, A. G., Lorimer, D. R., et al. 2006, Nature, 439, 817
Mori, K., Gotthelf, E. V., Zhang, S., et al. 2013, ApJ, 770, L23
Narayan, R. 1987, ApJ, 319, 162
Narayan, R., & Ostriker, J. P. 1990, ApJ, 352, 222
Noutsos, A., Schnitzeler, D. H. F. M., Keane, E. F., Kramer, M., & Johnston, S. 2013, MNRAS, 430, 2281
Olausen, S. A., & Kaspi, V. M. 2014, ApJS, 212, 6
Olausen, S. A., Zhu, W. W., Vogel, J. K., et al. 2013, ApJ, 764, 1
Papitto, A., Ferrigno, C., Bozzo, E., et al. 2013, Nature, 501, 517
Pavlov, G. G., Sanwal, D., Garmire, G. P., & Zavlin, V. E. 2002, in Astronomical Society of the Pacific Conference Series, Vol. 271, Neutron Stars in Supernova Remnants, ed. P. O. Slane & B. M. Gaensler, 247
Perera, B. B. P., McLaughlin, M. A., Cordes, J. M., et al. 2013, ApJ, 776, 61
Perna, R., Viganò, D., Pons, J. A., & Rea, N. 2013, MNRAS, 434, 2362
Pfahl, E., & Loeb, A. 2004, ApJ, 615, 253
Phinney, E. S., & Blandford, R. D. 1981, MNRAS, 194, 137
Podsiadlowski, P., Dewi, J. D. M., Lesaffre, P., et al. 2005, MNRAS, 361, 1243
Podsiadlowski, P., Langer, N., Poelarends, A. J. T., et al. 2004, ApJ, 612, 1044
Popov, S. B., Pons, J. A., Miralles, J. A., Boldin, P. A., & Posselt, B. 2010, MNRAS, 401, 2675

PoS(AASKA14)039

Popov, S. B., & Turolla, R. 2012, Ap&SS, 341, 457
Portegies Zwart, S., van den Heuvel, E. P. J., van Leeuwen, J., & Nelemans, G. 2011, ApJ, 734, 55
Possenti, A. 2013, in IAU Symposium, Vol. 291, IAU Symposium, ed. J. van Leeuwen, 121–126
Possenti, A., Colpi, M., Geppert, U., Burderi, L., & D'Amico, N. 1999, ApJS, 125, 463
Radhakrishnan, V., & Srinivasan, G. 1982, Current Science, 51, 1096
Ransom, S. M., Stairs, I. H., Archibald, A. M., et al. 2014, Nature, 505, 520
Rea, N., Israel, G. L., Pons, J. A., et al. 2013, ApJ, 770, 65
Ridley, J. P., & Lorimer, D. R. 2010, MNRAS, 404, 1081
Roberts, M. S. E. 2013, in IAU Symposium, Vol. 291, IAU Symposium, ed. J. van Leeuwen, 127–132
Ruderman, M., Shaham, J., & Tavani, M. 1989, ApJ, 336, 507
Schwab, J., Podsiadlowski, P., & Rappaport, S. 2010, ApJ, 719, 722
Shannon, R. M., & Johnston, S. 2013, MNRAS, 435, L29
Shao, L., Stairs, I. H., Antoniadis, J., & et al., 2015, "Testing Gravity with Pulsars in the SKA Era", in proc. *Advancing Astrophysics with the Square Kilometre Array*, PoS(AASKA14)042
Smits, R., Tingay, S. J., Wex, N., Kramer, M., & Stappers, B. 2011, A&A, 528, A108
Spitkovsky, A. 2006, ApJ, 648, L51
Spitler, L. G., Lee, K. J., Eatough, R. P., et al. 2014, ApJ, 780, L3
Stappers, B. W., Bailes, M., Lyne, A. G., et al. 1996, ApJ, 465, L119
Stollman, G. M. 1987, A&A, 171, 152
Szary, A., Zhang, B., Melikidze, G. I., Gil, J., & Xu, R.-X. 2014, ApJ, 784, 59
Tauris, T. M. 2012, Science, 335, 561
Tauris, T. M., & Konar, S. 2001, A&A, 376, 543
Tauris, T. M., Langer, N., & Kramer, M. 2011, MNRAS, 416, 2130
—. 2012, MNRAS, 425, 1601
Tauris, T. M., Langer, N., Moriya, T. J., et al. 2013a, ApJ, 778, L23
Tauris, T. M., & Manchester, R. N. 1998, MNRAS, 298, 625
Tauris, T. M., Sanyal, D., Yoon, S.-C., & Langer, N. 2013b, A&A, 558, A39
Tauris, T. M., & van den Heuvel, E. P. J. 2006, Formation and evolution of compact stellar X-ray sources (Cambridge University Press), 623–665
—. 2014, ApJ, 781, L13
Thompson, C., & Duncan, R. C. 1995, MNRAS, 275, 255
—. 1996, ApJ, 473, 322
Thompson, C., Lyutikov, M., & Kulkarni, S. R. 2002, ApJ, 574, 332
Timokhin, A. N. 2010, MNRAS, 408, L41
Turolla, R. 2009, in Astrophysics and Space Science Library, Vol. 357, Astrophysics and Space Science Library, ed. W. Becker, 141
van Kerkwijk, M. H., Bassa, C. G., Jacoby, B. A., & Jonker, P. G. 2005, in Astronomical Society of the Pacific Conference Series, Vol. 328, Binary Radio Pulsars, ed. F. A. Rasio & I. H. Stairs, 357–+
Vivekanand, M., & Narayan, R. 1981, Journal of Astrophysics and Astronomy, 2, 315
Voss, R., & Tauris, T. M. 2003, MNRAS, 342, 1169
Wang, N., Manchester, R. N., & Johnston, S. 2007, MNRAS, 377, 1383

PoS(AASKA14)039

Watts, A., Xu, R., Espinoza, C., & et al. 2015, "Probing the neutron star interior and the Equation of State of cold dense matter with the SKA", in proc. *Advancing Astrophysics with the Square Kilometre Array*, PoS(AASKA14)043
Weisskopf, M. C., Swartz, D. A., Carramiñana, A., et al. 2006, ApJ, 652, 387
Weltevrede, P., & Johnston, S. 2008, MNRAS, 387, 1755
Weltevrede, P., Johnston, S., & Espinoza, C. M. 2011, MNRAS, 411, 1917
Wex, N. 2014, ArXiv: 1402.5594
Wijnands, R., & van der Klis, M. 1998, Nature, 394, 344
Young, M. D. T., Chan, L. S., Burman, R. R., & Blair, D. G. 2010, MNRAS, 402, 1317
Young, N. J., Stappers, B. W., Lyne, A. G., et al. 2013, MNRAS, 429, 2569
Young, N. J., Stappers, B. W., Weltevrede, P., Lyne, A. G., & Kramer, M. 2012, MNRAS, 427, 114
Zhu, W. W., Kaspi, V. M., McLaughlin, M. A., et al. 2011, ApJ, 734, 44

PoS(AASKA14)039

PROCEEDINGS OF SCIENCE

A Cosmic Census of Radio Pulsars with the SKA

E. F. Keane[*1,2,3], **B. Bhattacharyya**[4,5], **M. Kramer**[6,4], **B. W. Stappers**[4], **S. D. Bates**[7], **M. Burgay**[8], **S. Chatterjee**[9], **D. J. Champion**[6], **R. P. Eatough**[6], **J. W. T. Hessels**[10,11], **G. Janssen**[10], **K. J. Lee**[12,6], **J. van Leeuwen**[10,11], **J. Margueron**[13], **M. Oertel**[14], **A. Possenti**[8], **S. Ransom**[15], **G. Theureau**[16] **& P. Torne**[6]

[1] *Swinburne University of Technology, Australia;* [2] *ARC Centre of Excellence for All-Sky Astrophysics (CAASTRO);* [3] *E-mail:* ekeane@swin.edu.au; [4] *University of Manchester, UK;* [5] *E-mail:* bhaswati.bhattacharyya@manchester.ac.uk; [6] *MPIfR Germany;* [7] *NRAO Green Bank, USA;* [8] *INAF-Osservatorio Astronomico di Cagliari, Italy;* [9] *Cornell University, USA;* [10] *Netherlands Institute for Radio Astronomy (ASTRON), The Netherlands;* [11] *University of Amsterdam, The Netherlands;* [12] *Peking University, P.R.China;* [13] *Institut de Physique Nucléaire de Lyon, CNRS, France;* [14] *Paris Observatory, France;* [15] *NRAO Charlottesville, USA;* [16] *CNRS-Université d'Orléans, France.*

The SKA will make ground breaking discoveries in pulsar science. The wide field-of-view, high sensitivity, multi-beaming and sub-arraying capabilities, coupled with advanced pulsar search backends, will result in the discovery of a large population of pulsars and new, high-quality data on select sources from the known pulsar population. This chapter outlines surveys for new pulsars, as well as the necessary follow-up timing observations, which will enable all of the SKA's headline pulsar science goals (tests of General Relativity with pulsar binary systems, investigating black hole theorems with pulsar-black hole binaries, and direct detection of gravitational waves in a pulsar timing array). SKA Milky Way surveys at multiple frequencies will increase the number of known pulsars by more than an order of magnitude. SKA2 will potentially find all of the Galactic radio-emitting pulsars in the SKA sky which are beamed in our direction. This will give a clear picture of the birth properties of pulsars and of the gravitational potential, magnetic field structure and interstellar matter content of the Galaxy. Targeted searches will enable detection of the most exotic systems, such as the $\sim$ 1000 pulsars we infer to be closely orbiting Sgr A*, the supermassive black hole in the Galactic Centre. In addition to Galactic pulsars, the SKA will detect pulsars from local group galaxies, which can be used as probes of the local intergalactic medium. All of the discoveries will require regular re-observations for a few months in order to derive their spin characteristics and establish the particular science questions they can be used to address. For efficiency, live searches will be performed, using sub-arraying and dynamic scheduling to time pulsars as soon as they are discovered, while simultaneously continuing survey observations. The large projected number of discoveries suggests that we will uncover currently unknown rare systems that can be exploited to push the boundaries of our understanding of astrophysics and provide tools for testing physics, as has been done by the pulsar community in the past.

Advancing Astrophysics with the Square Kilometre Array
June 8-13, 2014
Giardini Naxos, Italy

[*] Speaker.

PoS(AASKA14)040

1. Introduction

The SKA will be a discovery machine. Apart from delivering transformational science based on the expected huge increase in pulsar timing precision, the SKA's high sensitivity, wide field of view (FoV), and frequency coverage will allow us to explore the variable radio sky in an unprecedented way. This will lead to the discovery of previously unknown types of sources and enable us to probe a wide range of explosive and dynamic events. Eventually, it will lead to a full census of detectable radio pulsars in the Milky Way and beyond. Among the new sources will be fast, spin-stable millisecond pulsars (MSPs) whose period distribution reflects the equation of state of nuclear matter and some of which will serve as detectors of nano-Hz gravitational waves (GWs). Relativistic binary pulsars, particularly those with orbital periods of a few hours or less, will allow strong-field tests of General Relativity and other theories of gravity. The discovered pulsars will also be superb probes for an enhanced understanding of the Milky Way, its structure and its constituents, including magnetic fields, the free electron distribution etc. Other applications across a wide range of physics and astrophysics topics are described in the accompanying chapters.

The first step toward these unique achievements will be enabled by Phase I of the SKA (referred to as SKA1 hereafter). Apart from being a transformational telescope in its own right, the first science phase of this unique telescope will set the scene for the experiments to be conducted with the full array. However, it is important to realize that for searching, SKA1 is not only a simple stepping stone towards SKA2. Due to limitations in processing power, it is unlikely that the full area of the completed SKA can be utilized for a blind, large-scale survey for some time to come. Hence, SKA1, with a highly concentrated core, represents a significant fraction of the collecting area usable for surveys with SKA2, and substantial achievements can be made in pulsar searching in the early science phase.

When considering the specifications for SKA1, we point out that, in general, a loss in sensitivity (i.e. collecting area) cannot be simply compensated by longer integration times. In the best case, a reduction in collecting area that can be phased up coherently may require a significant increase in computing power (both for beam-forming, and processing). These costs are typically prohibitive, e.g. as illustrated by Figure 1 a 30% loss in raw sensitivity, if compensated for by doubling the observing time, results in a ten-fold increase in computation in order to find *the same pulsars*. Rephrased, this shows that as SKA1 approaches the optimal combination of dishes in the core region, pulsar searching becomes ever more efficient. In the worst case, a loss in sensitivity means a degradation in the science that is possible.

1.1 Pulsar Searching Basics

The pulsar signal is periodic with known periods covering nearly four orders of magnitude, i.e. 1 ms to 10 s. The pulse duty cycle ranges, typically, from less than one degree in rotational phase to the full pulse period. Hence, the discovery of pulsars requires a search of the radio sky in dispersion measure, pulse period and pulse duty cycle. For binary pulsars, a search for acceleration is also required. The standard search technique is consequently computationally expensive and it involves the Fourier-transform of correspondingly prepared time-series where the search in duty cycle uses a technique known as *harmonic summing*. Apart from these data processing requirements, forming beams for a sufficiently large FoV to enable reasonable survey speed, is computationally

PoS(AASKA14)040

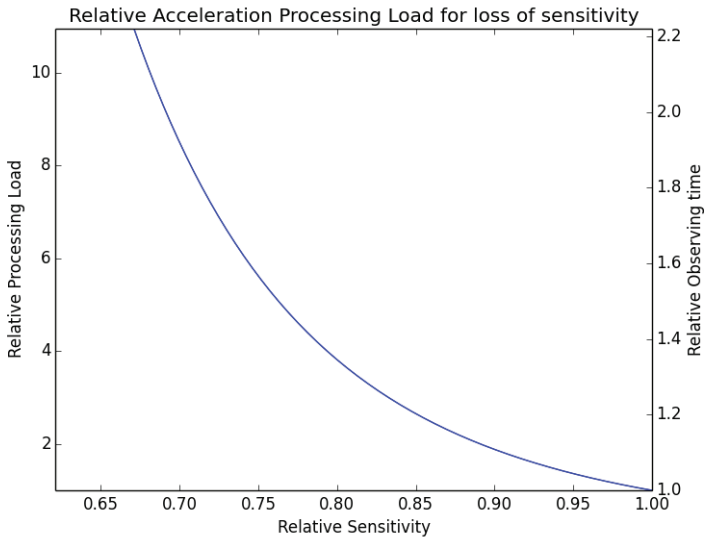

Figure 1: The 'cost', in terms of the increased observing time and (most significantly) computer processing required to find accelerated binary systems, in the event of a reduction in sensitivity.

challenging in the signal processing chain, in particular if the array configuration is not sufficiently compact. In order to ease the computational requirements, we have explored different observing strategies for the search for pulsars, depending on sky (i.e. Galactic) location, frequency (and hence receiver technology), and observing modes.

1.2 Acceleration searches

Arguably, the most interesting systems to be found will be highly accelerated. The SKA promises an advance over existing telescopes in the particular ability to allow for short integration times due to its large sensitivity. That means that only a small fraction of the orbit is sampled, so that the pulse frequency may not change significantly due to varying Doppler shifts. In contrast, reduced sensitivities imply longer integration times, which mean more Doppler-smearing that needs to be compensated for (if possible at all) by computational means. In the best case, one can assume constant acceleration. Even in the simplest acceleration search, the computing power needed scales with the cube of the observing time. In other words, a 10%-reduction in sensitivity implies a required increase in computing efforts by a factor of two in order to find the same systems (see Figure 1). In practice, the penalty is much higher, for two reasons. Firstly, the previous assumption of constant acceleration will be wrong for the most compact systems when the integration time becomes a significant fraction of the orbital period (depending also on the unknown eccentricity of the system). Secondly, even if antennae at longer baselines could be included coherently in effective collecting area, it would require an increased amount of beam forming.

The impact on the population so-lost is difficult to quantify as the result depends not only on the (unknown) luminosity of the sources, but also on the orbital parameters. Population syntheses are used to infer information (see § 3), but we can be certain that there are more compact orbits than the Double Pulsar ($P_b = 147$ min) or the shortest pulsar binaries known ($P_b = 92$ min). It

PoS(AASKA14)040

is notable that the Double Pulsar was not detected in the regular pointings of the Parkes Multi-beam Pulsar Survey ($t_{\rm int} = 35$ min) because of Doppler-smearing. Only in the 10-times shorter integrations of the "PH"-survey, was it finally discovered. It is conceivable that most of the strong (mildly-accelerated) sources are discovered with the currently available sensitivity and computer resources. This would imply that the remaining sources are either relatively weak or very highly accelerated. In other words a loss in SKA sensitivity (the largest that we can ever expect to achieve) would suggest a certain (and final) blindness to the most exciting systems.

SKA radio pulsar surveys will produce a large volume of prospective candidates, the majority of which will be forms of noise. Typically, such large numbers of candidates need to be visually inspected in order to determine if they are real pulsars. This process can be labour intensive and delay the candidate confirmation. In order to process pulsar searching candidates in a real time fashion, computer software to perform candidate ranking or classifying is demanded. At present, software using machine learning (Eatough et al. 2010; Lyon et al. 2013; Zhu et al. 2014) or statistical classifiers (Lee et al. 2013; Morello et al. 2014) can increase the identification rate by a factor of about 50 to 1000. This will significantly improve the efficiency of pulsar searches with SKA1 and SKA2, allowing for fast identification and confirmation of the candidates.

1.3 Structure of this Chapter

The remainder of this chapter is structured as follows: In § 2.1 we describe the large parameter space probed in pulsar searches. Surveys with SKA-LOW and SKA-MID are described in § 2.2 and § 2.3, respectively. § 3 describes the results of population syntheses, and the results of simulations of the survey yields, and evaluates different search strategies. In addition to the 'blind' surveys we describe targeted searches in § 4. We review, in § 5, the wide range of anticipated discoveries and their scientific importance. Finally, in § 6 we discuss the important issue of the follow-up timing strategies of the newly discovered pulsars which are needed to maximize the scientific yield.

2. Pulsar searches with the SKA

2.1 Parameter-space for search

As described above, and elsewhere in this book, one of the key aims of the SKA, in both Phase 1 and with SKA2, is to discover as many pulsars as possible. The pulsars of interest for the different astrophysical goals may be located anywhere within, or even beyond, our Galaxy and so it is necessary to perform a "blind" survey of the entire sky visible from the sites in Australia and South Africa. To survey this area efficiently we need to achieve the maximum possible survey speed and this requires excellent sensitivity combined with a wide-FoV (Smits et al. 2009). The high time resolution required to discover pulsars means that it is not effective to search for them in the images that are the traditional data product of interferometers like the SKA. Instead we have to form the coherent sum of as many dishes/stations as possible to give us the required sensitivity. However, as the dishes are sparsely distributed, the FoV shrinks as we add more dishes to improve our sensitivity. This can be overcome by forming more beams, but that comes with a computing cost associated with forming and processing those beams. Depending on the exact configuration of the all-sky pulsar survey to be undertaken with SKA1 between 1500 and 2200 tied-array beams are

PoS(AASKA14)040

required for SKA1-MID and 500 tied-array beams are required for SKA1-LOW. With SKA2 at least 10,000 beams will be required, which will allow more dishes to be included in the array, improving sensitivity, but while also increasing the FoV (this increased 'survey speed' also allowing longer integrations).

The radio emission from pulsars is dispersed, before it arrives at Earth, by the free electrons along the line of sight to the pulsar. This causes a frequency-dependent delay which needs to be removed in order to recover the pulsed signal. Unfortunately, the degree of dispersion cannot be predicted and so a search over a range of so-called dispersion measures is required. The maximum dispersion measure is of course highly dependent on where the pulsar is located, and with the majority of pulsars located in the Galactic plane, where the dispersion can reach its highest values, it is necessary to search over a wide range of dispersion measures. This is very important for the SKA where the sensitivity is high enough to allow us to discover the most distant sources. With SKA1 it is proposed that the search be possible out to dispersion measures of 3000 DM units; with the proposed search parameters — $|\mathrm{acc}| < 350$ m/s/s, 2048 beams and harmonic folding — the computaional requirement is at least 7 Petaflop/s. However, with SKA2 and/or higher frequency observations it should be possible to search out to dispersion measures of 10,000 DM units and beyond.

To search for the systems critical to the key gravity studies, such as the pulsar-black hole (PSR-BH) and double neutron star (DNS) systems, requires that one is able to at least partially correct the modulation of the pulse frequency caused by its motion in the binary — usually via acceleration searches. The orbital acceleration that might be observed in compact PSR-BH binaries could be an order of magnitude larger than that seen in the most relativistic DNS systems (see § 5.1). For the proposed integration time of SKA1 (10 min, see § 2.3) the aim is to search for accelerations > 1000 m/s/s; indeed using fluctuation frequency domain methods this will be readily achievable for spin periods greater than > 16 ms (Lorimer & Kramer 2005). In highly eccentric PSR-BH systems, the acceleration can be larger by factors of a few near periastron. While at the moment acceleration searches (in both the time and frequency domain) over such ranges and with uniform spin frequency sensitivity are computationally prohibitive, for SKA this should be the goal.

2.2 An all-sky pulsar survey with SKA-LOW

All-sky pulsar searches are often most efficiently done using low radio observing frequencies ($100 - 600$ MHz). Such surveys benefit from the typically steep spectra of pulsars ($S \propto \nu^{-1.6}$; Bates et al. 2013), as well as the naturally larger FoV of the telescope (FoV scales as ν^{-2} for a fixed aperture size or baseline length). Interstellar propagation effects, most notably dispersive delay, multi-path propagation due to scattering, and sky temperature, are the main limitations at low frequencies. Dispersive delay, which scales as ν^{-2}, is a correctable effect however, as long as the channel bandwidth is sufficiently narrow that intra-channel smearing of the pulse is minimal compared with the sampling time. Scattering, which scales as $\sim \nu^{-4}$, is not practically correctable in a blind survey and is a major limitation for finding distant pulsars in the Galactic plane, especially at short rotational periods. Sky temperature scales as $\nu^{-2.6}$, but is only ~ 35 K (at 400 MHz) for high Galactic latitudes. For these reasons low-frequency pulsar surveys are the preferred option for Galactic latitudes beyond $|b| \approx 5$ degrees.

PoS(AASKA14)040

Of the ~ 2300 known pulsars: there are 766 pulsars with $|b| > 5$ degrees; of the 172 Galactic Fields MSPs (P < 30 ms): 113, i.e. *two thirds* are at $|b| > 5$ degrees (Manchester et al. 2005). Furthermore, population synthesis of the entire Galactic pulsar population indicates that if SKA1-LOW and SKA1-MID are used in a complementary way to survey the entire SKA-visible sky, then the maximum yield of pulsar discoveries can be achieved (assuming a constant on-sky survey time) if SKA1-LOW surveys at Galactic latitude $|b| > 5$ degrees and SKA1-MID surveys the Galactic plane.

There are currently three major, ongoing low-frequency pulsar surveys: (i) the Arecibo 327-MHz Drift Survey[1], operating from $300-350$ MHz; (ii) the Green Bank Northern Celestial Cap Survey[2], which in a certain sense is a continuation of the Green Bank Drift-Scan Survey[3] as well as the GBT350 Galactic Plane survey, and is operating from $300-400$ MHz; and (iii) the LOFAR Tied-Array All-Sky Survey[4], which is operating from $119-151$ MHz and is very similar in approach to how SKA-LOW will survey for pulsars and fast transients. Together, these low-frequency GBT, Arecibo and LOFAR surveys have discovered 176 pulsars in the last decade. The GBT surveys have used scan lengths of ~ 2 minutes and reached a minimum flux density $S^{350}_{\rm min} \approx 1$ mJy. Each pointing covers 0.25 sq. degrees. The Arecibo survey provides only 40-s in-beam time, and reaches $S^{350}_{\rm min} \approx 0.5$ mJy. Each pointing covers 0.05 sq. degrees. LOFAR's much larger FoV — which is enabled by the use of 219 simultaneous tied-array beams to cover 9 sq. degrees of sky — allows 1-hr integrations, which reach $S^{150}_{\rm min} \approx 1$ mJy.

SKA1-LOW will provide an enormous leap in sensitivity and survey efficiency compared with these ongoing surveys. An all-sky survey using just the 600-m (radius) core of SKA1-LOW along with 10-min dwell time and 500 tied-array beams will reach $S^{350}_{\rm min} \approx 0.05$ mJy (ten times deeper than any ongoing survey) and will cover ~ 1 sq. degrees per pointing. We also note that the instantaneous sensitivity of the 600-m SKA1-LOW core at 350 MHz will be a factor of a few greater than Arecibo. Instantaneous sensitivity is the important factor for detecting weak individual pulses, like those from the intermittent radio pulsars and the fast radio bursts (see the Chapter on "Fast Transients at Cosmological Distances", Macquart et al. 2015, for a discussion of this).

We emphasize that a cosmic census of radio-emitting neutron stars requires the complementarity provided by SKA-LOW and SKA-MID (here, to clarify, we are referring to both SKA1 and SKA2). For the reasons outlined above (primarily scattering and $T_{\rm sky}$), SKA-MID will be the main tool for discovering distant pulsars in the Galactic plane, whereas SKA-LOW can both go deeper and survey faster at higher Galactic latitudes. Together, these two surveys will characterize the spectra and distribution of Galactic radio pulsars in beautiful detail. They will both discover exotic individual systems which can be used to test theories of dense matter and gravity. For example the GBT Drift-Scan survey found PSR J0337+1715, a unique millisecond pulsar in a stellar triple system, which promises a very strong constraint on deviations from the Strong Equivalence Principle of General Relativity (Ransom et al. 2014).

[1] http://www.naic.edu/ deneva/drift-search/

[2] http://arcc.phys.utb.edu/gbncc/

[3] http://astro.phys.wvu.edu/GBTdrift350/

[4] http://www.astron.nl/lotaas/

PoS(AASKA14)040

2.3 Composite survey with SKA1-LOW and SKA1-MID

To consider the usefulness of surveying with SKA1-LOW, we first compare the number and type of pulsars it will find with those found by SKA1-MID. We have shown with the help of simulations (see the next section for details) that all-sky surveys with SKA1-MID find a larger number of normal pulsars and MSPs than SKA1-LOW. However, with SKA1-LOW we will find many additional pulsars to those found with SKA1-MID, thereby the two greatly complement each other. While young pulsars (ages of $10^3 - 10^7$ yr) are strongly confined to their birth places in the Galactic plane (though sources at $\lesssim 1$ kpc will still appear to be isotropic), the much older MSPs (ages of $\gtrsim 10^8$ yr) will appear across the sky. This means that an all-sky pulsar survey is critical for finding the best pulsar clocks for use in direct GW detection and other fundamental physics experiments. Conversely, a deep Galactic plane search is needed to find the DNS binaries or the PSR-BH binaries that will provide the most stringent tests of General Relativity.

To carry out a large area survey with SKA1-LOW would require that a beamformer and a pulsar search backend be built. In the present scenario we have considered that we would use the collecting area of SKA1-LOW out to a radius of 700 m to include a total of 500 stations. Although this is a larger radius than used for SKA1-MID the significantly lower observing frequency means that the beam size is about 7 times larger for SKA1-LOW and so to achieve the same survey speed fewer beams would be required. We consider here a scenario where we preserve the total number of beams defined in the baseline design for the SKA1-MID beamformer of about 2048 beams and we split them across both telescopes with SKA1-LOW having 500 beams and SKA1-MID having 1500 beams. As the pulsar survey processing cost scales approximately linearly with the number of beams this transferring of the beams from SKA1-MID to SKA1-LOW is almost cost neutral. We also note that in this scenario the decrease in the area to be surveyed with SKA1-MID would allow for a smaller tied-array beam size. If one changes the integration times for SKA1-LOW to (say) 1800 s and SKA1-MID to 2600 s respectively, the relative yield will be different from the results obtained with a fixed integration time of 600 s for both telescopes. This optimization can be performed later, when further results from the ongoing surveys with Parkes, LOFAR and the GBT are available, enabling an informed judgment. It is clear, however, that SKA1-LOW should be equipped with searching capabilities.

3. Simulations

3.1 SKA1 Simulations

To determine how to achieve the maximal possible number of pulsar discoveries with SKA1 we have performed a number of simulations which take into account all of the potentially available resources. We then consider how this might project forward to SKA2. Our simulations presented here are based on the *PSRPOP.py* code (Bates et al. 2014) but are consistent with those obtained with the code used in van Leeuwen & Stappers (2010) for LOFAR. The simulations only considered SKA1-LOW and SKA1-MID, as large area surveys with SKA1-SUR require integration times that are too long to achieve useful sensitivity and, therefore, require presently unachievable computational requirements to reveal the desired binary systems.

PoS(AASKA14)040

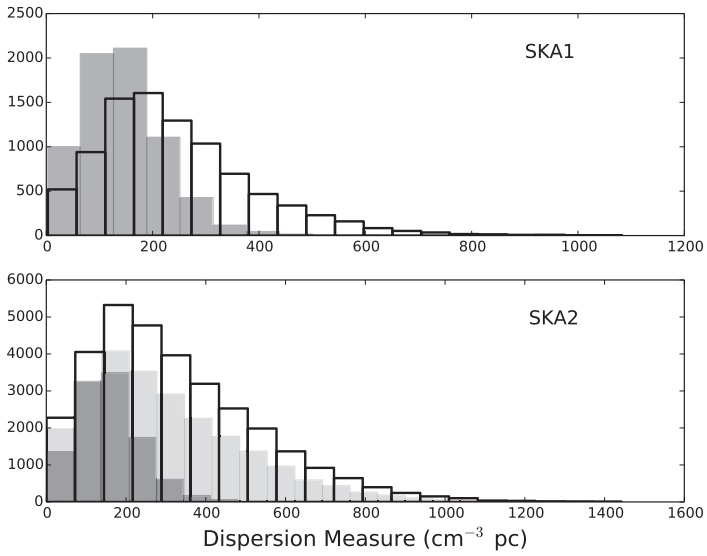

Figure 2: Histograms showing the pulsar search performance of the LOW and MID telescopes in both phases of the SKA. In SKA Phase 1 one can see how LOW (Dark bars) performs better at low dispersion measures due to the raw sensitivity but MID (clear bars) reaches deeper into the Galaxy. With the full SKA we consider two options for MID(DISH) of a five- and ten-fold improvement in sensitivity, light grey and clear bars respectively and also an improved LOW (dark bars). As with SKA1, LOW finds a different set of pulsars compared to MID.

We first considered the optimal frequency for pulsar searching with SKA1-LOW by performing simulations across the entire expected available band from $100-450$ MHz assuming sensitivity parameters as described in the baseline design. We find that, for a 100-MHz bandwidth, the optimum central frequency is 250 MHz, where this is a compromise between pulsar spectral index, sky temperature and effective collecting area of the log-dipole antennas. Multiple simulations were then performed for all-sky surveys with SKA1-LOW and SKA1-MID assuming a fixed integration time of 600 s per pointing as described in the baseline design. These show that SKA1-MID would detect about 9000 normal pulsars and about 1400 MSPs while the numbers for SKA1-LOW are about 7000 normal pulsars and about 900 MSPs. It appears, therefore, that SKA1-LOW is less competitive, but it is important to remember that SKA1-LOW sees a smaller fraction of the sky and if one looks at the number of pulsars discovered as a function of dispersion measure, that SKA1-LOW finds more pulsars at low dispersion measure. This clearly shows that the lower frequencies observed with SKA1-LOW mean that the dispersion smearing and the scattering in the ISM along lines of sight to and through the Galactic plane reduce the number of pulsars that can be detected there, while the superior collecting area of SKA1-LOW means that it is able to find more pulsars nearby.

The results of these simulations indicate that a composite survey, where the complementary regions are covered by the two telescopes, provides the best combination to maximise the number of pulsars that can be found with SKA1. We therefore performed composite survey simulations which used both telescopes to survey different regions to maximise the pulsar yield and we found that an optimal survey strategy would be to search with SKA1-MID up to Galactic latitudes of about ± 10 degrees and the region of the sky in the North where SKA1-LOW cannot reach. SKA1-LOW would then be used to survey the rest of the sky down to a Galactic latitude of ± 5 degrees. The reason for the overlap in this region is two-fold: firstly it allows effective cross-calibration

PoS(AASKA14)040

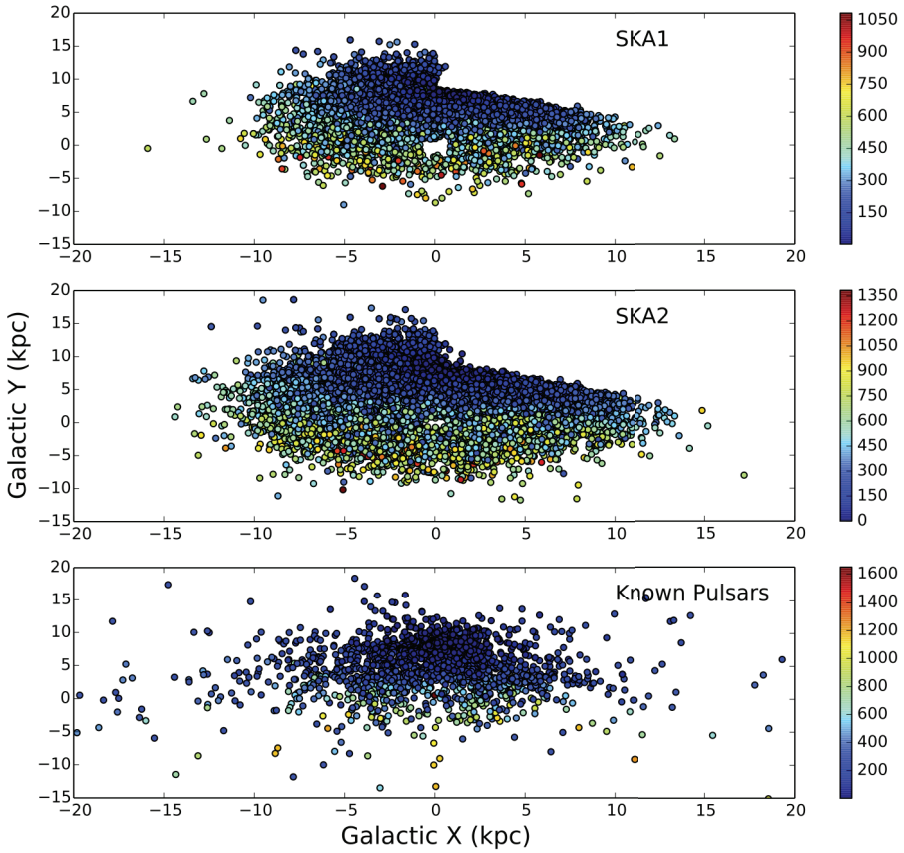

Figure 3: The number of pulsars expected to be found with the SKA and their approximate distribution throughout the Galaxy, projected onto the Galactic plane, compared to the known pulsar distribution. The colour coding indicates the approximate range of dispersion measures of the simulated pulsars that will be discovered. We note the dramatic increase in the number of pulsars discovered in each phase of the SKA, including a much greater sampling of the Galaxy.

of the two surveys, to ensure that the relative sensitivities are understood as required for effective modeling of the population; and secondly because, as we can see from the MSP simulations, it is apparent that in this region of the sky the two telescopes are finding different sources, SKA1-LOW faint nearby objects and SKA1-MID further away objects. This will, therefore, maximize the return on MSPs, the key target of the survey. In this scenario we find that we can detect a total of about 10,000 normal pulsars and as many as 1500 MSPs.

This highlights the importance of having the beam former and pulsar search capabilities available for SKA1-LOW in both phases of the SKA. It also offers up the possibility of an ever-higher pulsar yield, as with the survey being split across both telescopes, the same survey can be achieved in the same time with longer integration times, further enhancing our sensitivity, with the proviso of the highly accelerated binary systems.

We have also examined the yield of a preliminary survey with an early phase SKA1, defined as 50% the sensitivity of SKA1. For the same integration times as above, a composite survey would detect about 6000 normal pulsars and as many as 700 MSPs. As expected, doubling the integration time to increase the sensitivity results in a higher yield of 7500 normal pulsars and 950 MSPs, but

PoS(AASKA14)040

at a much higher, and impractical, processing cost (a factor of $\gtrsim 10$ times increase), as per Figure 1.

3.2 Full SKA Simulations

We have carried out simulations for the number of pulsars that will be found with SKA2 in both the LOW and MID (DISH) configurations. In the case of LOW we have assumed that there is a four-fold sensitivity increase and that all of that increase can also be applied to the pulsar search application, when compared to SKA1. In the case of MID-DISH the nominal improvement in sensitivity is expected to be about an order of magnitude. However, depending on how those dishes are distributed and the amount of compute resource that is available it may not be possible to utilise all of that increase for pulsar searches. Therefore we consider here two options: the full ten-fold increase can be used and a five-fold increase in sensitivity. With SKA-LOW we find a total of 11,000 pulsars including about 1500 MSPs, while SKA-MID(DISH) will find between 24,000 and 30,000 pulsars, of which between 2400 and 3000 will be MSPs depending on the exact improvement in sensitivity. In some regions of the sky *this corresponds to detecting the entire population of pulsars that are beamed in our direction*. As with SKA1, LOW and MID are highly complementary with LOW finding the nearby pulsars and MID probing deep into the Galaxy.

Simulations of pulsar surveys with a mid-frequency aperture array centered at 750 MHz with 500 MHz of bandwidth show that such a system would likely be complementary to the LOW and MID surveys already considered. The survey would detect around 27,000 normal pulsars, around 6000 of which would not be detected in either the LOW or MID surveys, and 3000 MSPs, 800 of which would be unique discoveries. Further analysis will be required on computational costs and scientific returns to see how the survey will be distributed over the three antenna types when more detailed specifications are available.

4. Targeted Searches

Targeted searches allow for longer integration times and hence better sensitivity than wide-area surveys. This enables characterisation of specific environments in ways unattainable otherwise, and can elucidate evolutionary links between different types of neutron stars and their progenitors.

4.1 Galactic Centre Pulsars

The Galactic Centre (GC) is a region of intense interest as pulsars discovered here are excellent tools for measurements of the magnetised ISM in this extreme environment, and could act as unrivaled probes of the space-time surrounding our nearest supermassive black hole candidate, Sgr A* (Liu et al. 2012). Despite strong evidence for a large neutron star population in the GC, e.g. $\gtrsim 1000$ in the central pc around Sgr A* (Wharton et al. 2012; Chennamangalam et al. 2014), and multi-frequency searches for pulsars, the number of detections remains low with just 6 active radio pulsars within $15'$ (36 pc) of Sgr A*. This has primarily been explained by extreme scattering of radio waves caused by inhomogeneities in the ionised component of the GC ISM (Cordes & Lazio 1997; Lazio et al. 1998). Scattering, which causes temporal broadening of pulses, and a corresponding reduction in pulse signal-to-noise ratio (S/N), can only be mitigated by observing at higher frequencies. Unfortunately, the steep radio spectra of pulsars typically prohibits detection above 2 GHz. Finding the optimum balance between the effects of pulse scattering in the GC and

PoS(AASKA14)040

the intrinsic luminosity of pulsars has been an on-going problem. It is therefore clear that the large increase in sensitivity offered by the proposed collecting areas of SKA1 and the complete SKA will greatly help searches in the GC.

The recent detection of an X-ray and radio loud magnetar just 3" (~ 0.1 pc) from Sgr A* has both raised hopes for the possibility of more pulsars in this region, and allowed measurements of the level of pulse scattering, $\tau_{\rm scatt}$, in this direction (Kennea et al 2013; Mori et al. 2013; Eatough et al. 2013; Shannon & Johnston 2013; Spitler et al. 2014; Tauris et al. 2015). While the exact nature of scattering toward the GC remains uncertain, these recent measurements suggest that normal slow and some recycled pulsars might be observable in the GC with SKA1-MID bands 3 and 4 ($\tau_{\rm scatt} \sim 50$ ms and 7 ms respectively), whereas MSPs will require band 5 ($\tau_{\rm scatt} \sim 4$ ms to 60 µs at the bottom and top of band 5 respectively). For a more detailed discussion of the prospects for GC pulsar searches and fundamental physics to be performed therewith we refer the reader to the chapter on observing radio pulsars in the Galactic Centre (Eatough et al. 2015).

4.2 Extragalactic

Pulsars beyond the disk of the Milky Way are currently known only in globular clusters and in the Magellanic Clouds, owing to their intrinsic faintness. While single, non-repeating bursts of apparent extragalactic origin have recently been detected (Lorimer et al. 2007; Keane et al. 2012; Thornton et al. 2013; Spitler et al. 2014), their astrophysical source remains unclear. For repetitive, pulsar-like bursts, only much weaker candidates were found. With the SKA, galaxies in the local group are within reach using periodicity searches while giant pulses like those seen from the Crab pulsar can be detected from galaxies out to well beyond a Mpc. *What is the importance of detecting pulsars in other Galaxies?* The pulsars likely to be detected will be young with high luminosities that can be correlated with catalogs of supernova remnants. This will yield estimates of the star-formation rate and the branching ratio for supernovae to form spin-driven pulsars as opposed to magnetars and black holes. Extragalactic pulsars will also provide information about the magnetoionic media along the line of sight through determination of the dispersion, scattering and rotation measures. Unambiguous study of the intergalactic medium in the local group requires removal of contributions to these measures from the foreground gas in the Galaxy and gas in the host galaxy. The more pulsars detected in a galaxy, the more robust this removal will be. Extragalactic pulsars can be found through blind surveys for both periodic sources and individual giant pulses. Additional successes will follow from targeted surveys of individual supernova remnants in the nearest galaxies. In §2.1 we discussed the requirements on sensitivity and FoV. The SKA2-MID sensitivity will be applied to targeted searches of, for instance, supernova remnants in nearby galaxies. However, blind surveys over wider fields such as whole galaxies, will only use the core array.

Giant pulses from the Crab pulsar serve as a useful prototype for estimating detection of strong pulses from nearby galaxies. The strongest pulse observed at 0.43 GHz in one hour has $S/N_{\rm max} = 10^4$, even with the system noise dominated by the Crab Nebula. For objects in other galaxies, the system noise is dominated by non-nebular contributions, implying that the S/N in this case would have increased by a factor of about 300. We can estimate the maximum distance of detection at a

PoS(AASKA14)040

specified signal-to-noise ratio, $(S/N)_{\rm det}$ as:

$$D_{\rm max} = \frac{1.6\,{\rm Mpc}}{\sqrt{(S/N)_{\rm det}/5}} \left(\frac{f_{\rm core}\, S_{\rm SKA-MID}}{S_{\rm Arecibo}} \right)^{1/2} = \frac{1.6\,{\rm Mpc}}{\sqrt{(S/N)_{\rm det}/5}} \left(\frac{0.4 \times 1630\,{\rm m^2/K}}{1150\,{\rm m^2/K}} \right)^{1/2} \quad (4.1)$$

where $S_{\rm SKA-MID}$ and $S_{\rm Arecibo}$ are the ratios of effective area over system temperature for SKA-MID and Arecibo, respectively (Table 1 in SKA-TEL-SKO-DD-001); and $f_{\rm core}$ is the SKA collecting area that can be used for a giant pulse survey. For $f_{\rm core} = 0.4$, $A_{\rm SKA}/A_{\rm Arecibo} \approx 1$, the standard one-per-hour pulse seen at Arecibo could be detected out to ≈ 1.2 Mpc.

In conclusion, SKA will enable not only the discovery of most, if not all, pulsars in the Milky Way which are beamed towards Earth, but also allows present-day-survey sensitivities to pulsars in the closest galaxies. With the single-pulse search techniques, it should be possible to detect giant pulses from pulsars as distant as the Virgo Cluster. Studies of the significant numbers of extragalactic pulsars expected to be detectable by the SKA would allow measurements of the *intergalactic*, as opposed to the interstellar, medium.

4.3 Globular Clusters & High Energy Targets

Targeted searches of globular clusters with SKA1-LOW and SKA1-MID will utilise the vastly improved sensitivity to discover many new exotic systems. Pulsars in globular clusters are subject to a much higher rate of encounters which enables systems to form which would be impossible in the lower density environment of the Milky Way. For a detailed discussion of globular cluster search strategies, and the scienctific applications of these systems, we refer the reader to the chapter on Globular Clusters (Hessels et al. 2015).

Similarly, targeted searches of unidentified sources found by high-energy telescopes (such as the LAT on Fermi) will be employed, as has been done with great success in recent years (Ray et al. 2011). These discoveries are mainly highly energetic young pulsars, and millisecond pulsars, both isolated and in binary systems. The first group of energetic pulsars is opening a new window to the pulsars' radio and high-energy emission mechanisms. The second group, of older neutron stars, is increasing our ability to study neutron star evolution and is adding numbers to the important population of MSPs, that are also required to build a Galaxy-size gravitational wave detector based on these objects (see section 5.2). The SKA will be able to probe high-energy sources that are still unidentified with greater sensitivity, and more generally it will be able to search for unknown radio pulsars in any sources found by telescopes operating across the spectrum. Particularly for very high energy targets the wide FoV of the SKA is also a great advantage. Since in many cases the exact location of the small neutron star within the high-energy emitting region is unknown, current large single-dish telescopes, with their small beams, need to do several pointings in order to overcome these positional uncertainties in the surveys. More on the possibility of finding new pulsars in sources discovered at different wavelengths or in completely different regimes (e.g. gravitational waves and neutrinos) is described in the chapters on multi-messenger pulsar science and on the neutron star population (Antoniadis et al. 2015; Tauris et al. 2015).

PoS(AASKA14)040

5. Expected discoveries and their importance

5.1 Pulsar-Black Hole Binaries and other binaries for GR tests

Since early in the conception of the SKA, the detection and study of highly relativistic binary pulsar systems has been one of the Key Science goals (Kramer et al. 2004). Such systems have provided the first strong evidence for the existence of GWs with the double neutron star PSR B1913+16 (Taylor et al. 1979), the most precise tests of Einstein's theory of General Relativity (GR) with the double pulsar PSRs J0737–3039A/B (Kramer et al. 2006), and the best tests of alternative gravity theories with, for example, PSR J0348+0432 (Antoniadis et al. 2013). However, in the collection of these remarkable "gravity labs" the most prized system has so far eluded detection: a pulsar - black hole binary (hereafter PSR-BH). The study of a PSR-BH will allow not only precision tests of GR, but should, for the first time, allow the properties of the BH to be measured in a model independent fashion.

The Science prospects from discovery of a PSR-BH system: A PSR-BH system will allow us to probe BH properties, as well providing stringent tests of theories of gravity in general. If the "No-hair theorem" holds, we expect that BHs are remarkably simple objects described by mass and spin (and perhaps charge) only. Once the mass and spin are known, other properties like the quadrupole moment are pre-determined, so that by measuring all quantities at the same time the no-hair theorem can be tested. For the same reason, we do not expect a BH to carry a "scalar charge", in contrast to other compact objects like neutron stars where this is possible. The existence, or not, of a scalar charge results in vastly different behaviours in the orbital motion of a system involving a BH, when predictions of GR are compared with alternatives like tensor-scalar theories. Indeed, it can be argued that a PSR-BH is probably the best foreseeable probe for testing alternative theories of gravity (Damour & Esposito-Farèse 1996). Moreover, measuring relativistic spin-orbit coupling and frame dragging, will allow us to determine the spin of the BH with high precision. While the mass of the BH can be determined with high precision, the (unitless) spin parameter should be measured to be smaller than unity, in order for an event horizon to exist — a fact that can, with the SKA, be easily tested (Kramer et al. 2004). Measuring the effects of classical spin-orbit coupling will also provide the quadrupole moment of the BH, which can then be compared to the predictions based on the mass and the spin. Whether we will be able to measure the spin and quadrupole moment depends also on the mass of the BH. While Liu et al. (2012) have shown that it will be difficult to measure the qudrupole moment for stellar-sized BHs, the BH in the centre of the Milky Way is an ideal target to attempt this experiment (see e.g. Eatough et al. 2015).

The search strategy: Naturally, these exceptional gravity tests will first require the detection of a PSR-BH. As outlined above, a composite survey with SKA-LOW and -MID is proposed to find all pulsars beaming towards us, with significant inroads being made already with SKA1. However, it is fair to say that a PSR-BH might be the most challenging of all the systems in the "pulsar zoo" to detect. In Figure 4 the effectiveness of acceleration searches in the detection of a simulated PSR-BH is shown. Panels (a) and (b) show contours of 30%, 60% and 90% signal recovery at the orbital phase at which the integration has started[5]. For longer integration times (Panel (a), $\sim 6\%$ of the

[5]Here "signal recovery" is given by the S/N achieved in an acceleration search, normalised by the S/N for an equivalent search of the same pulsar, but with no orbital motion.

PoS(AASKA14)040

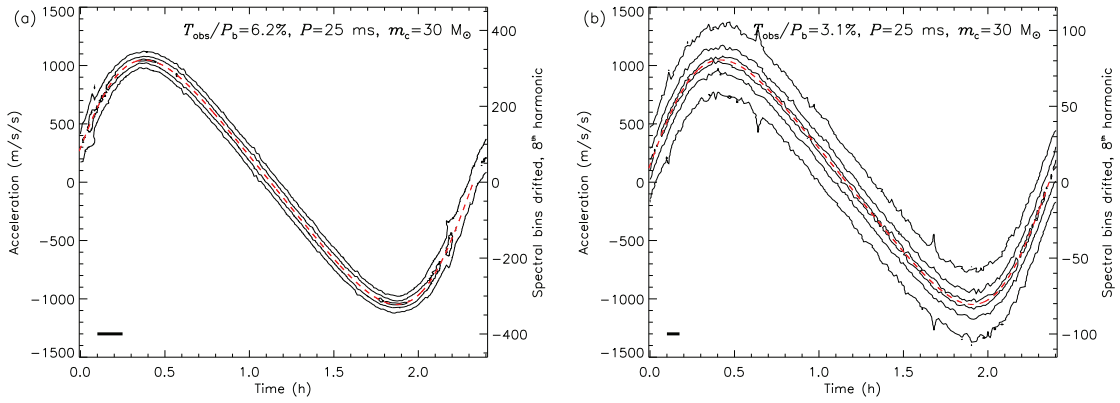

Figure 4: The effectiveness of acceleration searches in the detection of a simulated PSR-BH system. While such a system would be ideal for gravity tests, its detection through blind searches would be extremely challenging. Here we represent a "worst-case scenario", where the pulsar has a short spin period of 25 ms; expected in systems that have formed via exchange interactions in dense stellar environments, or where the pulsar is the first-born object. The black hole mass is at the high end of what is expected for stellar mass black holes (30 $M_\odot$), and the orbital period is small ($P_b = 2.4$ hr) and has low eccentricity ($e = 0.1$). To worsen matters the system is viewed edge-on, where the deleterious effects of line-of-sight motion are strongest. Contours mark the 30%, 60% and 90% pulsar signal recovery levels for constant acceleration searches of data integrations which are $\sim 6\%$ and $\sim 3\%$ of the orbital period (panels (a) and (b) respectively). Because a survey observation can start at any phase in the orbit, the starting point of the acceleration search has been incremented in steps of 50 s across the entire orbit. The thick black line shows the integration length analyzed. The red dashed line shows the true acceleration value at the mid-point of integration (Liu et al. in prep).

orbital period) full pulsar signal recovery levels are only achieved at a minority of orbital phases where the acceleration is varying least. By reducing the integration time, the amount by which the signal is smeared out (due to higher order effects) in the frequency domain is reduced. Panel (b) shows acceleration searches on integrations with half the duration ($\sim 3\%$ of orbital period). Although the raw sensitivity would be reduced by a factor of $\sqrt{2}$, the recovery level is now $> 90\%$ over the majority of the orbit. From sensitivity considerations the 60% contours in Panel (a) are approximately equivalent to the 90% contours in Panel (b), however there is uneven sensitivity coverage across the entire orbit at 60% levels in Panel (a). The increased instantaneous sensitivity, and therefore reduced integration time, offered by the SKA will undoubtedly improve the chances of detecting a PSR-BH.

Searches with SKA1 and SKA2 are expected to be performed in real-time (or pseudo real-time) because of data storage constraints. In searches for PSR-BH systems, where extreme levels of orbital acceleration might be observed (see Figure 4 where the line of sight acceleration can be greater than 1000 $\mathrm{m\,s^{-2}}$), even one-dimensional acceleration searches constitute an extreme data processing task. The degree of computational requirements of time-domain pulsar acceleration search algorithms has a strong dependence on the integration time ($\propto T^3$). As shown in Figure 4, acceleration analyses of half length integrations can result in an equivalent sensitivity to extreme PSR-BH as in longer integrations, but with 8 times less computational expense. Of course, it is only because of the superb sensitivity of the SKA that integration times will be able to be kept to a minimum. In addition, the reduced integration length also implies that more computational effort can be spent searching a wider parameter space.

PoS(AASKA14)040

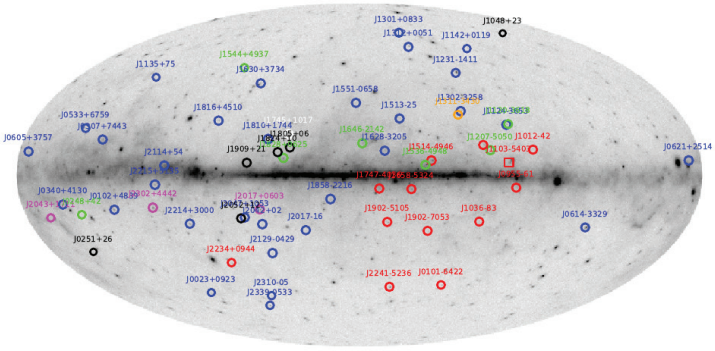

Figure 5: The initial ∼60 newly discovered radio MSPs detected via pointed radio searches towards *Fermi* associated γ-ray sources. The nearly isotropic distribution of the relatively nearby (∼1−3 kpc) systems is obvious. The colours indicate the discovery telescope: blue is the GBT, red is Parkes, black is Arecibo, green is the GMRT, magenta is Nançay, and white is Effelsberg. SKA surveys should find *thousands* of new MSPs, perhaps 5−10% of which will be suitable for high-precision timing work. Searches, especially with SKA1, of pulsar-like *Fermi* associated sources for new MSPs will provide excellent early-science opportunities for the SKA. Figure courtesy Paul Ray, NRL.

5.2 MSPs for PTAs and GW searches

Millisecond pulsars live $10^2 - 10^3$ times longer than ∼1-sec pulsars and have substantially larger scale heights in the Galaxy. For these reasons, the majority of the ∼200 currently known Galactic MSPs are *local* objects within ∼1−2 kpc from the Sun, and as such, are distributed nearly isotropically on the sky (see Figure 5). Recent population studies (Grégoire & Knödlseder 2013; Lorimer 2013; Levin et al. 2013) suggest that the Galaxy holds about 30,000 detectable MSPs in total, thousands of which will be within reach of SKA pulsar surveys. The MSPs are undoubtedly some of the most difficult pulsars to detect, due to their rapid spin rates (demanding fast sampling and high frequency resolution) and their typical binary nature. However, their high rotational stability and related timing precision makes these searches eminently worthwhile, as they can be used for some of our most important physics experiments, such as the direct detection of nano-Hz-frequency GWs (Manchester 2013).

Pulsar timing arrays require the very best MSPs, which are selected based on their flux density, the shapes of their radio pulses (narrow features are better), their timing stability (unknown until measured), and their distribution across the sky (a nearly isotropic distribution is close to ideal for the detection of a stochastic GW background). SKA all-sky surveys will find thousands of new MSPs, but only a relatively small fraction — perhaps 5−10% — will be of sufficient quality to include in an SKA-based PTA (e.g. Figure 6). Finding these rare pulsars is crucial as recent work has shown that GW sensitivities are *directly* proportional to the number of 'good' pulsars being timed (Siemens et al. 2013). In addition, these ultra-stable MSPs will provide spectacular 'secondary' science such as high-precision pulsar masses which will constrain the Equation of State of nuclear matter (Demorest et al 2010).

5.3 Testing the neutron star equation of state

Together with precise mass determinations in binary systems (see e.g. Demorest et al 2010; Antoniadis et al. 2013), pulsar spin rates are among the most accurately known observables which

PoS(AASKA14)040

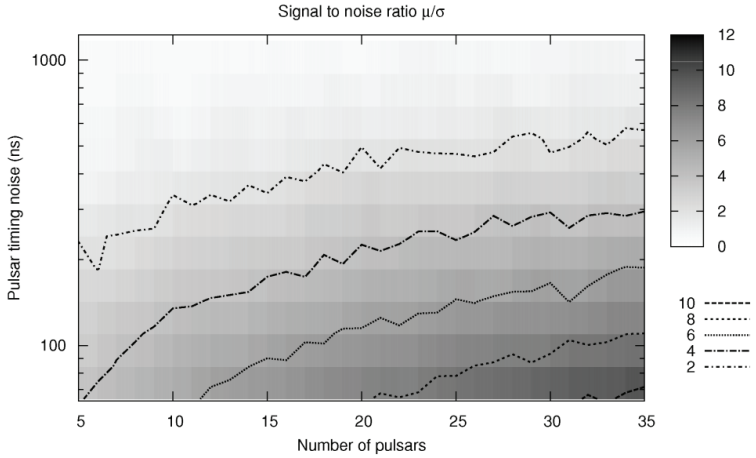

Figure 6: Density plot (grey scale) and contours of the signal-to-noise ratio for GW detection for different realisations of pulsar timing residuals, as a function of pulsar timing noise and the number of pulsars timed. Here, we have assumed 100 data points per pulsars, approximately evenly distributed over a period of 7.5 years and a simulated GW background with amplitude of 10^{15} yr$^{1/2}$ (van Haasteren et al. 2009).

could constrain the neutron star EoS. Pulsars can only be spun up to a limiting period, $P_{\rm sh}$, below which the star, due to centrifugal forces, becomes unstable to *mass shedding* at its equator. The binary MSP J1748−2446ad (Hessels et al. 2006), is the neutron star with the shortest known rotational period, $P_{\rm min} = 1.396$ ms[6], implying that the radius, if it were a canonical 1.4 $M_\odot$ neutron star, should be smaller than ~ 15 km (Hessels et al. 2006). Irrespective of the proposed EoSs, the period $P_{\rm min}$ of J1748−2446ad must be longer than $P_{\rm sh}$. The value of $P_{\rm sh}$ strongly depends on the EoS (Phinney & Kulkarni 1994; Stergioulas & Friedman 1995), with the observed $P_{\rm min}$ very close to the mass-shedding limit for the most 'stiff' EoSs (see Figure 7). However, the re-acceleration of a neutron star with an initial mass of 1.4 $M_\odot$ could in principle proceed down to limiting spin periods as fast as 0.6 ms for most 'soft' EoSs (Cook et al. 1994). As a consequence, even the discovery of one sub-ms pulsar, with a rotational frequency well above 1 kHz, would lead to the rejection of a wide class of EoSs and provide crucial information about the behaviour of matter at supra-nuclear densities.

Although few recent pulsar surveys could have detected sub-millisecond radio pulsations, a strong bias exists against detecting fast spinning MSPs as a result of the observed preference of these neutron stars to be hosted in eclipsing binaries (9 cases out of a total of 11 binary MSPs with $P < 2$ ms, including PSR J1748−2446ad). In these systems matter released by the companion engulfs the system and obscures the radio pulsations for a large fraction of the orbital period and, occasionally, for the entire orbit, particularly at lower radio frequencies. Also, a pulsar like J1748−2446ad is too faint (about 80 μJy at 1.95 GHz) to be detectable by most of the past and/or ongoing large scale surveys. Most of these difficulties will be overcome, or strongly mitigated, by a deep all-sky survey at a frequency of about 2 GHz with SKA1-MID. Provided sub-ms pulsars exist, and they mostly reside in eclipsing binaries, this experiment will provide an unprecedented opportunity to uncover these objects.

[6]An 0.89-ms period for the X-ray source XTE J1739−285 (Kaaret et al. 2007) still awaits confirmation.

PoS(AASKA14)040

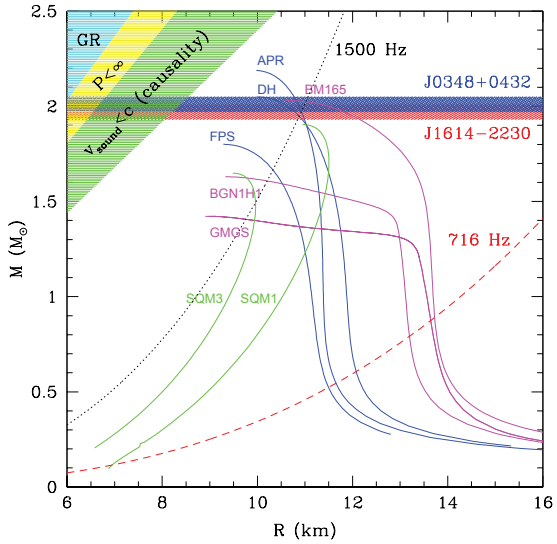

Figure 7: Different equations of state are shown, with regions in the neutron star mass versus radius parameter space which are ruled out or as yet allowed highlighted. Figure adapted from Demorest et al (2010). For further details we refer the reader to the chapter on probing the NS interior and the cold dense matter equation of state (Watts et al. 2015).

6. Importance of follow-up timing and strategies

When new pulsars are discovered their rotational, astrometric and binary properties (in case of a companion), need to be determined in order to be able to acquire a stable timing model that can be used to predict the arrival times of the pulses. It is this which enables the many high precision measurements possible using pulsars. The first approximation of a timing model requires very regular observations, starting from daily monitoring to gradually increased spacing between observations. In order to separate the position of the pulsar from the basic spin parameters, at least half a year of timing is necessary (although positional determination using VLBI methods, where possible, can remove this requirement). Pulsars in binary orbits need a high-cadence sampling of the binary orbit to measure the first-order binary parameters. In case of relativistic binaries, the post-Keplerian parameters can usually only be measured after multiple years of timing.

For all pulsars, multi-band monitoring is required to mitigate ISM effects on the signal. In general, lower frequencies are better for measuring dispersion measure variations and scattering delays, and therefore we expect most pulsars will require monitoring at the lower bands of SKA-MID. In addition, SKA-LOW can also be used for follow-up timing for the relatively brighter and/or more nearby pulsars. However, in some cases higher frequencies (around 3 GHz) will be essential to get a better coverage of binary orbits. As described above, the fastest-spinning pulsars are likely to be found in eclipsing binaries. Due to the fact that the effect on the higher-frequency part of the signal is smaller, the pulses can be detected for a larger fraction of the orbit at those frequencies and makes determining and monitoring the binary parameters possible or easier.

We aim for regular follow-up for all known and newly discovered pulsars visible in the SKA sky. Even the slow pulsars need to be covered in the SKA timing programme on a regular basis. The 45-year timing programme at Jodrell Bank, where up to 800 pulsars have been observed, has

PoS(AASKA14)040

led to unexpected results on various timescales for all kinds of pulsars (Lyne et al. 2010; Espinoza et al. 2011; Lyne et al. 2013) showing that different types of pulsars require different strategies in their follow-up and long-term timing observations.

Pulsars that show timing noise or rotational irregularities: These are typically young pulsars, or high-magnetic field pulsars that show timing irregularities, mode changes on various timescales or glitches. The required cadence for observing depends on the relevant variability time scales and varies from once a week to once a month. Many pulsars exhibit glitches, sudden (probably instantaneous) increases in the rotation rate of a pulsar that happen on different timescales and on an irregular basis (Espinoza et al. 2011). They are thought to be the result of changes in the interior of the neutron star where angular momentum is transferred from the interior to the crust. Therefore closely monitoring the recovery in the spin parameters of the pulsar after a glitch can provide us with information of the glitch mechanism itself, and the equation-of-state inside the neutron star (for more details see Watts et al. 2015). *Intermittent and mode-changing pulsars:* these sources show differences in spin-down rates on various timescales (Kramer et al. 2006; Lyne et al. 2010). An observing cadence matching the time scale of the variability is required. *Rotational RAdio Transients (RRATs):* These are neutron stars that only emit detectable single pulses (McLaughlin et al. 2006; Keane & McLaughlin 2011) on a very irregular basis and therefore require more integrated observing time and/or a higher cadence per source to get to a stable timing solution.

Binary MSPs: observations at least once a month, and occasional high-cadence (or full-orbit, when orbital periods are less than about a day) orbital sampling are required to measure the orbital parameters. GR tests need both dense orbital coverage to measure the binary parameters accurately, as well as a long-term timing programme to detect and monitor secular changes in binary orbits and astrometric parameters, and to disentangle those. *Exotic binary MSPs:* the SKA promises to uncover many exotic systems, e.g. when PSR-BH systems are found we might expect that the post-Keplerian effects on the orbit could become more complex than in the currently known systems that are used for GR tests. Second, or higher order, post-Newtonian effects would then become important requiring long-term and high-cadence observations. In this scenario it is necessary to obtain a high-cadence coverage of the PSR-BH binary orbit (or full-orbit observations, depending on the orbital period) as well as daily monitoring of the system to ensure coherence is maintained. It is likely that other exotic systems like triple systems will be found, especially in globular cluster searches, as multi-body systems are more likely to be found there. It has been shown (Ransom et al. 2014) that daily monitoring is required to maintain coherence for those systems.

PTA pulsars: one of the main goals of long-term timing is to directly detect low-frequency GWs using a pulsar timing array. A set of stable MSPs is used as a Galaxy-scale GW detector which depends on having long-term timing observations for pulsars distributed across the sky. There are different classes of GWs which may each require a slightly different observing strategy (for more information, see the chapter on "Gravitational wave astronomy with the SKA", Janssen et al. 2015). Overall, given the large number of MSPs that the SKA will discover (see above), for GW work the requirements are: (1) observe as many MSPs as possible on a regular basis with multi-frequency coverage; and (2) identify the most stable pulsars by long-term monitoring and determining the red-noise contamination in their timing residuals. As most PTA pulsars are in binaries, they have the same requirements as those listed above for the binary pulsars.

Follow-up pulsar timing also supports multi-wavelength observations by providing precise

PoS(AASKA14)040

ephemerides. Over a hundred pulsars are now known to emit pulses in the X−ray and/or γ−ray regimes. To fold their photons correctly, in many cases the γ−ray and sometimes X−ray communities are dependent on up-to-date timing ephemerides based on radio observations. Also, multi-wavelength counterpart observations can be used to independently constrain distances, and study the pulsar emission mechanism. Thus the short-term follow-up timing of all newly discovered sources requires a short-spacing campaign to make an initial coherent timing solution. Depending on the parameters and the complexity of the source (timing irregularities, binary parameters, etc) the longer-term timing cadence can be expected to be somewhere between daily and monthly, with full-orbit campaigns on a regular basis for the most important or complex systems.

In this chapter, we have demonstrated that significant achievements can be made in pulsar searching in the early science phase of SKA1 with a highly concentrated core. In contrast, in order to achieve the highest precision in pulsar timing, the gain in using SKA2 is enormous when compared to timing observations enabled with SKA1. It is this gain in timing precision for selected KSP objects which will ultimately require the sensitivity of SKA2.

References

Antoniadis, I., Freire, P. C. C., Wex, N., et al., 2013 Science, 340, 448
Bates, S. D., Lorimer, D. R., Verbiest, J. P. W. 2013, MNRAS, 431, 1352
Bates, S. D., Lorimer, D. R., Rane, A. & Swiggum, J., 2014, MNRAS, 439, 2893
Chennamangalam, J, Lorimer, D. R., 2014, MNRAS, 440, L86-L90
Cordes, J. M., & Lazio, J. T. W. 1997, ApJ, 475, 557
Cook, G. B., Shapiro, S. L. & Teukolsky, S. A. 1994, ApJ, 424, 823
Damour, T. & Esposito-Farèse, G., 1996, PhysRevD, 54, 1474
Demorest, P.B., Pennucci, T., Ransom, S.M., Roberts, M.S.E. & Hessels, J.W.T., 2010, Nature, 467, 1081
Eatough, R. P., Molkenthin, N., Kramer, M. et al., 2010, MNRAS, 407, 2443
Eatough, R. P., Falcke, H., Karuppusamy, R. et al. 2013, Nature, 501, 391E
Eatough, R. P., Lazio, J. T. W., Casanellas, J. et al., 2015, "Observing Radio Pulsars in the Galactic Centre with the Square Kilometre Array", in proc. *Advancing Astrophysics with the Square Kilometre Array*, PoS(AASKA14)045
Espinoza, C. M., Lyne A. G., Stappers, B. W. & Kramer, M., 2011, MNRAS, 414, 1679
Grégoire T & Knödlseder J., 2013, A&A, 554, A62
Antoniadis. J, Guillemot, L., Possenti, A., et al., 2015, "Multi-wavelength, Multi-Messenger Pulsar Science in the SKA Era", in proc. *Advancing Astrophysics with the Square Kilometre Array*, PoS(AASKA14)157
van Haasteren, R., Levin, Y., McDonald, P. & Lu, T., 2009, MNRAS, 395, 1005
Hessels, J. W. T., Ransom, S. M., Stairs, I. H. et al., 2006, Science, 311, 1901 730, L36
Hessels, J. W. T., Possenti, A., Bailes, M. et al., 2015, "Pulsars in Globular Clusters with the SKA", in proc. *Advancing Astrophysics with the Square Kilometre Array*, PoS(AASKA14)047

PoS(AASKA14)040

Janssen, G. H., Hobbs, G., McLaughlin, M. A. et al., 2015, "Gravitational Wave Astronomy with the SKA", in proc. *Advancing Astrophysics with the Square Kilometre Array*, PoS(AASKA14)037
Kaaret, P., Prieskorn, Z., in 't Zand, J. J. et al., 2007, ApJ, 657, L97
Kennea, J. A., Burrows, D. N., Kouveliotou, C. et al., 2013, ApJ, 770L, 24
Keane, E. F. & McLaughlin, M. A., 2011, BASI, 39, 333
Keane, E.F., Stappers, B.W., Kramer, M. & Lyne, A.G., 2012, MNRAS, 425, L71
Kramer, M., Backer, D. C., Cordes, J. M. et al., 2004, New Astronomy Reviews, 48, 993
Kramer, M., Stairs, I. H., Manchester, R. N. et al., 2006, Science, 314, 97
Lee, K. J., Stovall, K., Jenet, F. A. et al., 2013, MNRAS, 433, 688
Lazio, T. J. W. & Cordes, J. M., 1998, ApJ, 505, 715
van Leeuwen, J. & Stappers, B. W., 2010, A&A, 509, 7
Levin, L., Bailes, M., Barsdell, B. R. et al. 2013, MNRAS, 434, 1387
Liu, K., Wex, N., Kramer, M. & Cordes, J. M., 2012, ApJ, L747, 1
Lorimer, D. R. & Kramer, M., 2005, Handbook of Pulsar Astronomy, CUP.
Lorimer, D. R., 2013, IAU, 291, 237
Lorimer, D.R., Bailes, M., McLaughlin, M.A., Narkevic, D.J. & Crawford, F. 2007, Science, 318
Lyon, R., Brooke, J. M., Knowles, J. D. & Stappers, B. W., 2013, IEEE International Conference on Systems, Man, and Cybernetics.
Lyne, A. G., Hobbs, G., Kramer, M. & Stairs I. H., 2010, Science, 329, 408
Lyne, A. G., Graham-Smith, F., Weltevrede, P. et al., 2013, Science, 342, 598
Mori, K., Gotthelf, E. V., Zhang, S. et al., 2013, ApJ, 770L, 23M
Manchester, R.N., Hobbs, G.B., Teoh, A. & Hobbs, M. 2005, VRODC, 7245
Manchester R. N., IPTA, 2013, CQG 30: 224010
Macquart, J.-P., Keane, E. F., Grainge, K. et al. 2015, "Fast Transients at Cosmological Distances with the SKA", in proc. *Advancing Astrophysics with the Square Kilometre Array*, PoS(AASKA14)055
McLaughlin M. A., Lyne, A. G., Lorimer, D. R. et al., 2006, Nature, 439, 817
Morello, V., Barr, E. D., Bailes, M. et al., 2014, MNRAS, 443, 1651
Phinney, E. S., & Kulkarni, S. R. 1994, ARAA, 32, 591
Ray, P. S., Abdo, A. A., Parent, D. et al. 2011, Fermi Symposium proceedings - eConf C110509
Ransom, S. M., Stairs, I. H., Archibald, A. M. et al. 2014, Nature, 505, 520.
Siemens X., Ellis J., Jenet F. & Romano J. D. 2013, CQG 30: 224015.
Shannon, R. M. & Johnston, S., MNRAS, 2013, 435L, 29
Smits, R., Kramer, M. & Stappers, B. W., 2009, A&A, 493, 1161
Spitler, L. G., Lee, K. J., Eatough, R. P. et al. 2014, ApJ, 780L, 3
Stergioulas, N., & Friedman, J. 1995, ApJ, 444, 306
Tauris, T. M., Kaspi, V. M. Breton, R. P. et al., 2015, "Understanding the Neutron Star Population with the SKA", in proc. *Advancing Astrophysics with the Square Kilometre Array*, PoS(AASKA14)039
Taylor, J. H., Fowler, L. A. & McCulloch, P. M., 1979, Nature, 277, 437
Thornton, D., Stappers, B., Bailes, M. et al. 2013, Science, 341
Watts, A. L, Xu, R., Espinoza, C. M. et al. 2015, "Probing the neutron star interior and the Equation

PoS(AASKA14)040

of State of cold dense matter with the SKA", in proc. *Advancing Astrophysics with the Square Kilometre Array*, PoS(AASKA14)043
Wharton, R. S., Chatterjee, S., Cordes, J. M., Deneva, J. S. & Lazio, T. J. W., 2012, ApJ, 753, 108
Zhu, X.-J., Hobbs, G., Wen, L. et al., 2014, ApJ, 781, 117

PoS(AASKA14)040

PROCEEDINGS OF SCIENCE

Three-dimensional Tomography of the Galactic and Extragalactic Magnetoionic Medium with the SKA

J. L. Han[*1], **W. van Straten**[2], **T. J. W. Lazio**[3], **A. Deller**[4], **C. Sobey**[4], **J. Xu**[1], **D. Schnitzeler**[5], **H. Imai**[6], **S. Chatterjee**[7], **J.-P. Macquart**[8], **M. Kramer**[5], **J. Cordes**[7]

[1]*National Astronomical Observatories, Chinese Academy of Sciences, Beijing 100012, China;* [2]*Swinburne University of Technology, Australia;* [3]*Jet Propulsion Laboratory, California Institute of Technology, USA;* [4]*ASTRON, The Netherlands;* [5]*MPIfR, Germany;* [6]*Kagoshima University, Japan;* [7]*Cornell University, USA;* [8]*Curtin University, Australia.*

E-mail: hjl@bao.ac.cn

The magneto-ionic structures of the interstellar medium of the Milky Way and the intergalactic medium are still poorly understood, especially at distances larger than a few kiloparsecs from the Sun. The three-dimensional (3D) structure of the Galactic magnetic field and electron density distribution may be probed through observations of radio pulsars, primarily owing to their compact nature, high velocities, and highly-polarized short-duration radio pulses. Phase 1 of the SKA, i.e. SKA1, will increase the known pulsar population by an order of magnitude, and the full SKA, i.e. SKA2, will discover pulsars in the most distant regions of our Galaxy. SKA1-VLBI will produce model-independent distances to a large number of pulsars, and wide-band polarization observations by SKA1-LOW and SKA1-MID will yield high precision dispersion measure, scattering measure, and rotation measure estimates along thousands of lines of sight. When combined, these observations will enable detailed tomography of the large-scale magneto-ionic structure of both the Galactic disk and the Galactic halo. Turbulence in the interstellar medium can be studied through the variations of these observables and the dynamic spectra of pulsar flux densities. SKA1-LOW and SKA1-MID will monitor interstellar weather and produce sensitive dynamic and secondary spectra of pulsar scintillation, which can be used to make speckle images of the ISM, study turbulence on scales between $\sim 10^8$ and 10^{13} m, and probe pulsar emission regions on scales down to $\sim$10 km. In addition, extragalactic pulsars or fast radio bursts to be discovered by SKA1 and SKA2 can be used to probe the electron density distribution and magnetic fields in the intergalactic medium beyond the Milky Way.

Advancing Astrophysics with the Square Kilometre Array
8-13 June 2014
Giardini Naxos, Italy

[*]Speaker.

PoS(AASKA14)041

1. Introduction

Our Milky Way consists of the Galactic disk, which has a few spiral arms, the extended Galactic halo, the Galactic bulge, and a central bar. However, a detailed picture of the Milky Way is not yet clear. Spiral structures have been observed only in the closest half of our Milky Way, and the pitch angles of only a few arm segments have been determined (see Hou & Han 2014). Embedded in these large-scale structures, the interstellar medium (ISM) consists of diffuse neutral hydrogen (H I) gas and H I clouds, higher density regions of molecular clouds, diffuse ionized gas (H II) and extended or compact H II regions. In turn, the ISM is permeated by magnetic fields, and the magnetized interstellar plasma is known as the magnetoionic medium. Although the magnetoionic medium occupies a significant fraction (~ 0.2) of the volume of the ISM, we have only limited knowledge of its distribution in the disk and halo. A considerable amount of energy is required to keep the ISM ionized, roughly 15–20% of the luminosity of all O/B stars in the Galaxy. Accordingly, ionized gas traces the energy input into the ISM, which is dominated by supernova remnants and the stellar winds of bright young stars. Therefore, in the Galactic disk, more ionized gas and more disturbed small-scale structures are expected to be associated with the spiral arms (as opposed to the interarm regions). However, the origin of hot gas in the Galactic halo, where very few hot stars exist, is not clear.

Magnetic fields are ubiquitous throughout the Universe. The magnetic fields in our Galaxy play a crucial role in numerous astrophysical processes: they affect the propagation of cosmic rays, impact the evolution of molecular clouds and star formation, and facilitate the transport of heat, angular momentum and energy. Measurements of the magnetic structure of the Milky Way are sparse, especially at distances greater than several kiloparsecs from the Sun and on length scales shorter than tens of parsecs. Zeeman splitting measurements probe the in situ magnetic fields of small-scale star formation regions, which are evidently related to the large scale structure of the Galactic magnetic field (Han & Zhang 2007; see also Green et al. 2015 and Robishaw et al. 2015 in this volume).

Faraday rotation measurements probe the integrated magnetic field along the line of sight to pulsars and extragalactic radio sources. Because pulsars are distributed throughout the Milky Way, their compact nature and short-duration, highly-polarized radio pulses make them ideal probes of the three-dimensional structure of the diffuse magnetoionic medium in our Galaxy. Extraction of the common contribution to Faraday rotation measures of extragalactic radio sources yields the total Faraday rotation due to the Galactic magnetoionic medium (Xu & Han 2014a,b; Haverkorn et al. 2015 in this volume).

To date, 2300 pulsars have been discovered using single dish telescopes (see the updated catalog of Manchester et al. 2005). Most of the known pulsars are in the Galactic disk, and about 20% of them are in the Galactic halo (see Figure 1). The distribution of pulsars at low Galactic latitudes occupies about half of the Galactic disk; at high latitudes, the distribution is limited to about 4 kpc from the Sun. A large spatial volume of the Milky Way is left for future pulsar discovery by the next generation of radio telescopes with extremely high sensitivity, such as FAST (Nan et al. 2011), LOFAR (Coenen et al. 2014) and the SKA (Keane et al. 2015).

According to the current SKA1 Baseline Design (Dewdney et al. 2013), Phase 1 of the SKA will consist of three arrays: a low-frequency array (SKA1-LOW), a mid-frequency array (SKA1-

PoS(AASKA14)041

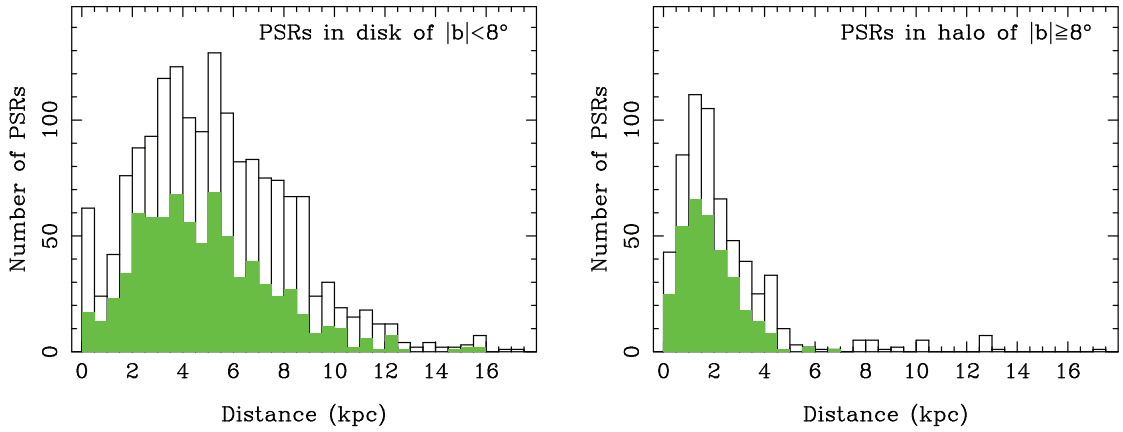

Figure 1: Distance distribution of known pulsars in the Galactic disk ($|b| < 8°$) and in the Galactic halo $|b| \geq 8°$. The green histograms correspond to pulsars with available RMs.

MID), and a wide-field survey array (SKA1-SUR). SKA1-LOW will be able to observe the $-67° <$ Dec $< 13°$ sky in the frequency range of 50-350 MHz. The core array with a maximum baseline of 50 km will have a resolution of $11''$, and its collecting area of 800,000 m^2 will reach a flux density limit of 2μJy hr$^{-1/2}$. In 10-min integrations, the 600 m core array can reach 0.05 mJy. It is predicted that SKA1-LOW will find about 7,000 normal pulsars and about 900 millisecond pulsars (Keane et al. 2015), mostly in the closest half of the Galactic halo. SKA1-MID will operate in 5 different frequency bands; of relevance to this study are the three bands that overlap with those of SKA1-SUR: band-1: 350–1,050 MHz (MID) or 350–900 MHz (SUR); band-2: 950–1,760 MHz (MID) or 650–1,670 MHz (SUR); and band-3: 1,650–3,050 MHz (MID) or 1,500–4,000 MHz (SUR). Band-1 will be used to survey the halo pulsars at high Galactic latitudes, band-2 will be used at mid latitudes and to reach pulsars in the furthest reaches of the Galactic disk, and band-3 will be used at very low latitudes (e.g. $|b| < 10°$). According to simulations, SKA1-MID will find about 9,000 normal pulsars and about 1400 millisecond pulsars (see Fig. 3 of Keane et al. 2015) distributed in about $2/3$ of the Galactic disk and reaching 5 kpc farther than the Galactic center. With approximately 50% of the sensitivity of SKA1, the early phase SKA1 will discover only 1/4 or 1/3 of the above predicted numbers of pulsars (assuming that similar surveys are done). SKA2-LOW is expected to discover 11,000 pulsars, including 1500 millisecond pulsars, and SKA2-MID will find 24,000 – 30,000 pulsars, of which 2,400 – 3,000 will be millisecond pulsars. The most distant pulsars will be about 10 kpc beyond the Galactic center in the other half of the disk.

The large numbers of pulsars discovered by SKA1 and SKA2 can be used to constrain the structure of the magnetoionic medium with unprecedented detail. Using pulsar dispersion measure (DM) and scattering measure (SM) estimates, combined with parallax distance estimates, we will construct the three-dimensional electron density distribution of the Milky Way, especially the poorly-explored region around the Galactic center and in the halo, as discussed in Section 2. Furthermore, the small-scale structure of the magnetoionic medium will be illuminated by high quality scintillation data and the dynamic spectra of many bright pulsars. Pulsar Faraday rotation measure (RM) estimates, combined with pulsar DM estimates, will be used to reveal the detailed three-dimensional structure of the Galactic magnetic field, as shown in Section 3. In fact, the high

PoS(AASKA14)041

sensitivity of SKA1 and SKA2 should also enable the discovery of a large number of pulsars in nearby galaxies, which opens the window for the study of the intergalactic medium (IGM), as discussed in Section 4. The conclusions of this chapter are presented in Section 5.

2. SKA1 for electron density distribution

A better understanding of the electron-density distribution is crucial for estimating distances to large numbers of distant pulsars and deriving the magnetic field from Faraday rotation measurements (see Sect. 3). The ionized gas in the ISM is not uniformly distributed. In the Galactic disk, high density clumps are associated with H II regions and bright stars, such that the distribution of higher density ionized gas follows the spiral arms. There are also many voids that are associated with bubbles or superbubbles. The ionized gas can be directly imaged by Hα surveys (Finkbeiner 2003), but its distribution throughout the Galactic disk is difficult to ascertain owing to our location near the edge of the Galactic disk. Measurements of ionized gas in the Galactic halo and in the area around the Galactic center are limited.

2.1 Pulsar distances and the electron density distribution

The dispersion measure (DM) of a pulsar is the integral of the free electron density between the pulsar and us, $\mathrm{D}M = \int_{\mathrm{us}}^{\mathrm{PSR}} n_e\, dl$. The DMs of a large number of widely distributed pulsars can be used to construct a model of the electron density distribution, as long as the distances to these pulsars can be independently measured. However, pulsar distances are difficult to measure. Available methods include 1) measuring annual parallax using Very Long Baseline Interferometry (VLBI) astrometry, pulsar timing, or even by direct multi-epoch high resolution optical images; 2) establishing an association between a pulsar and a supernova remnant (SNR) that has an estimated distance; 3) observing HI absorption and deriving the kinematic distance with the Galactic rotation curve. Only with an accurate distance can a pulsar dispersion measure be converted to an average electron density along the line of sight, and a large number of such sight-lines (of different length and in different directions) are necessary to construct a suitably detailed model of the ionized ISM of the Milky Way.

Currently, the most widely used model for the electron density distribution in the Milky Way is the NE2001 model (Cordes and Lazio 2002; see the yellow background in Fig. 3), which has received over 800 citations and is an essential reference model for Galactic studies. At the time it was constructed, distance estimates were available for $\sim$100 pulsars: 19 via parallax (13 via VLBI, 5 via timing and 1 via optical imaging), 74 via HI absorption, 8 via SNR associations, 16 via globular cluster associations, and 8 pulsars in the Magellanic clouds.

In order to improve our understanding of the ionized ISM, it is crucial to accurately estimate the distance to as many pulsars as possible. Since NE2001 was finalized, a wealth of new information on pulsar distances has been obtained, with the number of measured parallaxes[1] increasing five-fold. In particular, the number of precise measurements made with Very Long Baseline Interferometry has exploded, predominantly due to careful work with the Very Long Baseline Array (Brisken et al. 2002; Chatterjee et al. 2009; Deller et al. 2011). Using pulsars at known distances,

[1] see e.g. http://www.astro.cornell.edu/research/parallax/

PoS(AASKA14)041

which come from either parallax measurements or by association with Galactic globular clusters or the Magellanic Clouds, Gaensler et al. (2008) found that the ionized thick disk in the Milky Way could have a scale height of $1.8^{+0.1}_{-0.2}$ kpc, which is almost a factor of two larger than the scale height used in NE2001 and its predecessor, the TC93 model by Taylor & Cordes (1993). By also including other model components from TC93 and NE2001 when fitting for the scale height of the thick disk, Schnitzeler (2012) subsequently showed that the difference in scale height is probably not so large. These results demonstrate that measuring geometric parallaxes for a large sample of pulsars has the potential to considerably change our understanding of the structure of the ionized Milky Way. A revised "NE2014" model incorporating the latest distance and scattering constraints would already form a considerable advance in our knowledge of the ionized ISM.

However, despite the recent advances in VLBI precision (where parallax errors of 0.02 mas and better are now attainable; see e.g. Deller et al. 2013), most pulsars with a geometric distance measurement are still in the local Galactic neighbourhood; the existing VLBI and timing parallaxes span 6.4 to 0.2 mas, and the median of 64 distances measured by parallax is just $\sim$0.9 kpc. To make a truly Galactic-scale model, many new constraints at larger distances are required.

Fortunately, in addition to discovering many new pulsars, the SKA will also excel in the measurement of their distances. Precision timing of millisecond pulsars with SKA1 will yield a significant number of timing parallax distances widely distributed across the Galaxy (Keane et al. 2015). The exact number will depend on the observing time allocated to pulsar timing programs, but observations for pulsar timing arrays (Janssen et al. 2015 in this volume) will ensure a moderately sized sample.

SKA1-VLBI observations (in which SKA1-mid and SKA1-survey are used as sensitive phased-array elements in a VLBI array; Paragi et al. 2015) will provide even greater parallax precision, capable of measuring distances across the Galaxy. This technique will also be more widely applicable because all radio pulsars can be targeted, not only millisecond pulsars. Observing time will likely limit the number of sources for which VLBI parallaxes can be obtained with SKA1, but it will remain possible to obtain a sample of sources that cover a representative region of the Galaxy. Both timing and VLBI parallaxes will be possible with early-phase SKA1 at 50% sensitivity, although in each case they will be unable to access the faintest members of the population.

With SKA2, the situation improves further. The increase in collecting area will make even higher precision timing parallaxes possible for fainter sources; for imaging observations, the addition of several thousand km baselines to the SKA will make VLBI-style observations possible with SKA2 alone. Smits et al. (2011) estimated that of order 10,000 pulsar distances could be measured by SKA2, with the majority obtained via imaging observations.

2.2 Wide-band observations of pulsar scattering

The emission region of pulsars is very small (less than a few hundred kilometers), such that pulsars are effectively point radio sources (with angular sizes of nanoarcseconds). When pulsed radio emission from a point source passes through the inhomogeneous interstellar plasma, two manifestations of multi-path propagation effects can be observed: pulse broadening in the time domain and a scattering disk in the image domain. With the SKA, the inhomogeneous interstellar plasma will produce observable effects on lines of sight to thousands of pulsars. These effects will be most significant in the SKA1-LOW band, and combination with the wide frequency range in the

PoS(AASKA14)041

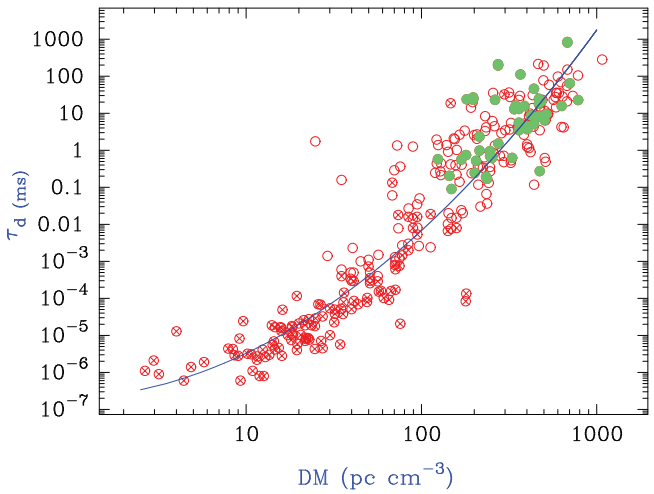

Figure 2: The time scales of pulse broadening are related to pulsar DM, in addition to the frequency dependence $\nu^{-\alpha}$ (see Bhat et al. 2004 for details: the filled dots denote measurements from multifrequency profiles presented in that paper, crossed circles denote measurements based on pulsar decorrelation bandwidths, and open circles denote previous measurements in the literature. The line is the best fit of equation 2.1 to the data).

two lower bands of SKA1-MID and SKA1-SUR will enable the unprecedented use of interstellar scattering to study the properties of the intervening medium.

To date, pulse broadening has been measured at several frequencies for only about 150 pulsars (e.g. Löhmer et al. 2001, 2004; Bhat et al. 2004; Lewandowski et al. 2013). For nearby pulsars (within a few kpc) the pulse broadening time scale varies with radio frequency as $\tau \sim \nu^{-\alpha}$, where $\alpha \sim 4.4$, which is consistent with a Kolmogorov spectrum of electron density fluctuations. For distant pulsars, the α values deviate from a single thin screen model. Because ISM irregularities are associated with spiral arms, the most distant pulsars with sight-lines passing through several spiral arms should exhibit very different scattering behaviour that is not as simple as the Kolmogorov spectrum (Lewandowski et al. 2013). The time scale of pulse broadening is related to the pulsar DM by

$$\log \tau \simeq a + b(\log \mathrm{DM}) + c(\log \mathrm{DM})^2 - \alpha \log \nu \qquad (2.1)$$

(see Fig.2 of Bhat et al. 2004) with $a = -6.46$, $b = 0.154$ and $c = 1.07$. The estimated value of $\alpha = 3.86 \pm 0.16$ is significantly lower than the value of 4.4 that is appropriate for a Kolmogorov medium. However, the dispersion of τ estimates spans one or two orders of magnitude in Fig. 2. Some pulsars with high DMs do not show strong scattering as expected, such as PSR B2002+31 (Lyne 1971) and the Galactic center pulsar PSR J1745−2900 (Spitler et al. 2014b). This probably indicates a predominantly uniform medium along these lines of sight. It is possible that the interstellar plasmas in the Galactic halo and near the Galactic center have fewer irregularities and are more uniformly distributed than in the disk.

The scattering disks of only a few pulsars have been observed to date (e.g. Lazio 2004). The angular diameter of the disk depends on radio frequency as $\theta \sim \nu^{-\beta}$, where $\beta = -2.2$ for an electron density distribution described by a Kolmogorov spectrum. Note that angular broadening measurements often indicate $\beta \sim 2.0$ (e.g. at the Galactic Centre) and decorrelation bandwidths

PoS(AASKA14)041

often scale as ν^{-4}, both of which indicate that the diffractive scale probed by pulsar observations is within the inner scale of the turbulent cascade in the ISM. SKA-VLBI (Paragi et al. 2015) will provide the sensitivity, wide frequency coverage, high resolution, and high dynamic range required to overcome the technical challenges associated with observations of angular broadening.

Scattering in the ISM operates as an interferometer whose maximum baseline is of order the size of the scattering disk, up to tens of AU (e.g. Pen & Levin 2014; Pen et al. 2014). Pulsar longitude-resolved SKA-VLBI observations at low frequencies can constrain source structure on nanoarcsecond scales, which will enable us to image pulsar magnetospheres on scales down to $\sim$10 km; for more details, see Karastergiou et al. (2015) in this volume.

2.3 Wide-band observations of pulsar scintillation

Owing to the inhomogeneity of the ISM and the high relative velocities of neutron stars, pulsars exhibit flux density modulations as a function of radio frequency and time, known as scintillation. To characterize the diffractive scintillation, dynamic scintillation spectra are analyzed using a two-dimensional autocorrelation function to obtain the temporal and spectral scales of decorrelation, which are related to the diameter of scattering disk. Small-scale structures in the ISM cause rapid intensity variations (diffractive scintillation) and large-scale density structures cause slow refractive scintillation.

Very high sensitivity is required to observe the dynamic spectrum of a pulsar, which must be detectable in a narrow band in a short integration time. Accordingly, dynamic spectra have been observed for only the brightest pulsars (e.g. Gupta et al. 1994). Owing primarily to the high velocities of pulsars, the differences between dynamic spectra observed at different epochs probe the irregularities of the ISM on scales ranging of $\sim 10^8$ to 10^{13} m.

Dynamic spectra with high signal-to-noise ratio (S/N) can be further analyzed via the two-dimensional Fourier transformation to yield the power spectrum of the dynamic spectrum, known as the secondary spectrum. Secondary spectra typically exhibit power concentrated in parabolic arcs, and each point on this arc arises from interference between points in the scattered image of the source. The parabolic shape arises from differential Doppler shift and differential delay between points in the scattered image, which vary linearly and quadratically, respectively, with scattering angle (e.g. Cordes et al. 2006). Features in the secondary spectra also vary as a function of radio frequency and observing epoch, see e.g. figures 1, 2 and 3 in Cordes et al. (2006) and figure 1 of Stinebring (2006). Multiple parabolic arcs are likely produced by multiple scattering screens along the line of sight.

The best observations of secondary spectra have been carried out at Arecibo (e.g. Cordes et al. 2006). Using the core array of SKA1-LOW and SKA1-MID, high S/N dynamic and secondary scintillation spectra can be obtained for many pulsars in a wide-range of low frequencies; these can be used to study both the static and dynamic structure of the ISM.

2.4 Interstellar weather

The large collecting area and large fractional bandwidth at low frequencies of SKA-LOW combined with bands 1 and 2 of SKA-MID or SKA-SUR (including SKA1 and the early phase of SKA1) will provide very accurate DM and RM estimates for thousands of known and newly

PoS(AASKA14)041

discovered pulsars. Owing to the λ^2 dependence of dispersive and refractive effects in the ISM, DM and RM estimates are best made at lower frequencies using wider bandwidths, as long as the pulse profile is not adversely affected by scattering.

Monitoring DM variations over time probes the structure of the ionized gas on length scales of the order of 10^8 – 10^{13} m. The time scale for DM variations depends on the velocity of the pulsar and the characteristic size of clouds or filaments of ionized gas along the line of sight. Increased sensitivity enables the detection of DM variations on short time intervals due to small-scale clouds. By monitoring short-term DM variations along large numbers of pulsar lines of sight, SKA1 will probe the physical processes acting within the interstellar plasma that generate or maintain sub-AU density fluctuations.

Monitoring long-term DM variations reveals large clumps of ionized gas drifting across the lines of sight. Such observations have been made at Parkes using timing array pulsars over several years (You et al. 2007; Keith et al. 2013) and a sample of 168 young pulsars over 6 years (Petroff et al. 2013). DM and RM variations of pulsars near the ecliptic plane can also be used to study the solar wind (You et al. 2012). Note, however, that correcting ionospheric Faraday rotation is essential for such experiments (e.g. Sotomayor-Beltran et al. 2013).

3. Interstellar magnetic fields

Pulsars are ideal probes of interstellar magnetic fields for the following four reasons: 1) owing to the high degree of linear polarization of pulsar signals, the RM is easily measured; 2) intrinsic Faraday rotation in the pulsar magnetosphere is negligible, such that the observed Faraday rotation is completely due to the interstellar magnetoionic medium (after correcting for ionospheric Faraday rotation); 3) the pulsar DM provides the integrated free electron column density, allowing the line-of-sight magnetic field to be decoupled (Eq. 3.1); and 4) there are a large number of pulsars distributed throughout the Galaxy in both the disk and the halo, facilitating a three-dimensional picture of the Galactic electron density and magnetic field. For a pulsar at distance D (in pc), the RM is given by $\mathrm{RM} = 0.810 \int_0^D n_e \mathbf{B} \cdot d\mathbf{l}$, (in rad m^{-2}). With the pulsar dispersion measure, $\mathrm{DM} = \int_0^D n_e\, dl$, (in pc cm^{-3}), we obtain a direct estimate of the magnetic field strength parallel to the line of sight, $\langle B_{||} \rangle$ in μG, weighted by the local free electron density:

$$\langle B_{||} \rangle = \frac{\int_0^D n_e \mathbf{B} \cdot d\mathbf{l}}{\int_0^D n_e\, dl} = 1.232\, \frac{\mathrm{RM}}{\mathrm{DM}}. \tag{3.1}$$

When RM and DM data are available for multiple pulsars along similar lines of sight, e.g. one pulsar at D_0 and one at D_1, the variation of DM and RM with distance can be used to derive the field direction and field strength in the region between D_0 and D_1,

$$\langle B_{||} \rangle_{D_1 - D_0} = 1.232 \frac{\Delta\mathrm{RM}}{\Delta\mathrm{DM}}, \tag{3.2}$$

where $\langle B_{||} \rangle_{D_1 - D_0}$ is the mean line-of-sight field component, $\Delta\mathrm{RM} = \mathrm{RM}_{D_1} - \mathrm{RM}_{D_0}$ and $\Delta\mathrm{DM} = \mathrm{DM}_{D_1} - \mathrm{DM}_{D_0}$. This derived field strength is not dependent on the electron density model, though the pulsar distances may have to be estimated from the electron density model if they have not been independently measured (e.g. by VLBI or pulsar timing).

PoS(AASKA14)041

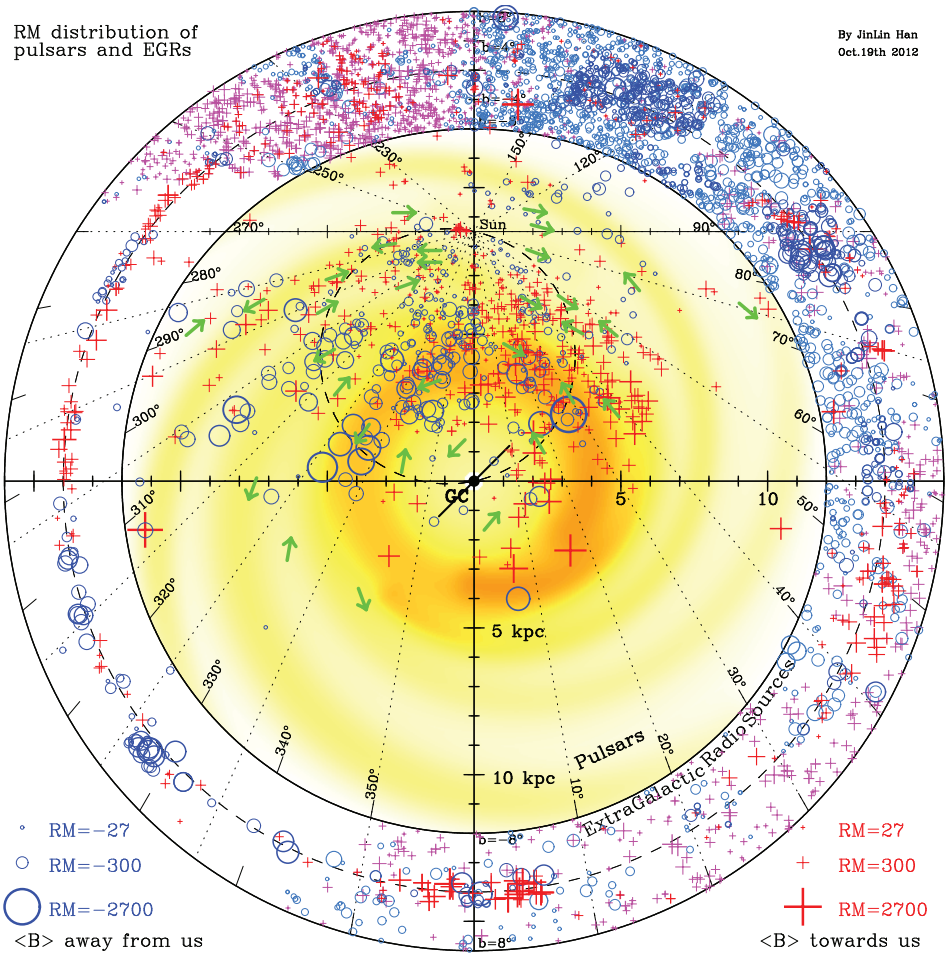

Figure 3: The RM distribution of 736 pulsars located within $|b| < 8^\circ$ projected onto the Galactic plane. The background shows the approximate locations of spiral arms used in the NE2001 electron density model (Cordes & Lazio 2002). RMs of extragalactic radio sources (Xu & Han 2014b) located within $|b| < 8^\circ$ are displayed in the outer ring according to their l and b, with the same convention of RM symbols and limits. The derived large-scale structure of magnetic fields in the Galactic disk are indicated by arrows. See Han (2013) for details.

There are currently over 2,300 pulsars that have been discovered, and only 30% of these have published RM values. The RMs in the Galactic disk have been used to reveal the magnetic field structure in the closest half of the disk (Han et al. 2006). Over large scales, the magnetic fields follow the spiral arms; however, many field reversals are also observed (see Fig.3). It is clear that pulsar RM data are scarce in many regions of the closest half of the disk; there are only a few pulsar RM estimates in the most distant regions of the Galaxy. The distribution of RMs of extragalactic radio sources behind the Galactic disk (see Fig.3) can be used to derive the field structures beyond pulsars, and also can constrain the disk-field model (e.g. Sun et al. 2008).

The detailed structure of magnetic fields in the Galactic disk will be revealed by SKA1, which will discover several thousand pulsars in the closest half of the disk and measure their DMs and RMs, and SKA2, which will discover at least ten thousand pulsars in the most distant half of the disk (see Keane et al. 2015). Full-polarization observations of the newly discovered pulsars using

PoS(AASKA14)041

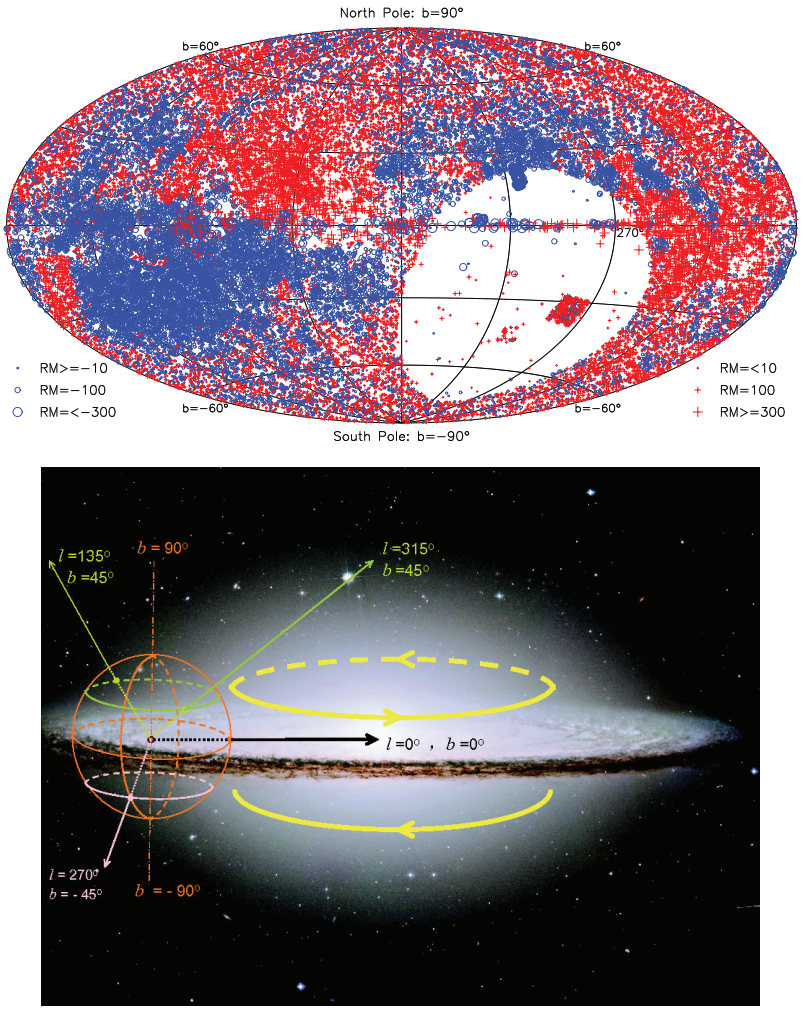

Figure 4: The sky distribution of RMs of extragalactic radio sources (*top*) and the Galactic coordinates and the azimuthal magnetic fields in the Galactic halo (*bottom*), see Han et al. (1997, 1999) and Xu & Han (2014b). Currently, pulsar data are available only ~ 3 kpc from the Sun (see Fig.1). RMs of several thousand distant pulsars to be discovered by the SKA at the high latitudes are ultimate data to reveal the large-scale field structure in the Galactic halo.

SKA1-LOW (50 –350 MHz), and band 1 of SKA1-MID (350 –850 MHz) and SKA1-SUR (650–1,150 MHz) with high spectral resolution (up to 256,000 frequency channels in each band) will determine RMs with unprecedented precision (~ 0.1 rad m^{-2}) and constrain the detailed structure of the Galactic magnetoionic medium. Note, however, that such RM precision is only achievable if the ionospheric contribution is accurately corrected.

SKA1 and SKA2 will also complement the pulsar RM data by increasing the density of extragalactic radio sources with RM estimates. Some constraints on the large-scale structure of the Galactic magnetic field have been derived from the RMs of extragalactic radio sources, namely the striking antisymmetry in the inner Galaxy and the large-scale toroidal magnetic fields in the Galactic halo with reversed directions above and below the Galactic plane (see Fig.4). These structures were originally proposed by Han et al. (1997, 1999) and later modeled by other authors (e.g. Prouza

PoS(AASKA14)041

& Šmída 2003, Sun et al. 2008, Ferriére & Terral 2014). However, the detailed properties of the halo magnetic field (e.g. the variation of field strength with radius and height) are not yet well constrained. Thousands of distant pulsars in the Galactic halo will be discovered by the SKA and their RMs will reveal the large-scale magnetic field structure in the Galactic halo.

In addition to the large-scale structure of the Galactic magnetic field, a variety of experiments probe small-scale structures in the interstellar magnetoionic medium. For example, compared to foreground pulsars along similar lines of sight, pulsars behind H II regions have significantly different Faraday rotation measures (e.g. Mitra et al. 2003). Evidence of similar small-scale fields associated with H II regions, supernova remnants and filaments has also been found in the RMs of extragalactic radio sources (e.g. Harvey-Smith et al. 2011; Sun et al. 2011; Savage et al. 2013). Such regions may be explored in greater detail by exploiting the increased density of extragalactic radio sources detected by SKA2, SKA1, and the early phase of SKA1.

Clearly, interstellar magnetic fields exist over a broad range of spatial scales, from large Galactic scales to very small dissipative scales. Determination of the magnetic energy spectrum offers a solid observational test for dynamo and other theories of Galactic magnetic field origin. The magnetic energy spectrum is currently constrained for only a small range of wavenumbers in relatively few regions. Magnetic fields on small spatial scales should follow the the Kolmogorov spectrum. Minter & Spangler (1996) found that structure functions of rotation measure and emission measure were consistent with a Kolmogorov spectrum of three-dimensional turbulence in magnetic fields up to 4 pc, but with two-dimensional turbulence between 4 pc and 80 pc. Using pulsar RMs in a large region of the Galactic disk, Han et al. (2004) obtained a power law distribution of magnetic field fluctuations described by $E_B(k) = C\ (k/\mathrm{kpc}^{-1})^{-0.37\pm0.10}$ over spatial scales from $1/k = 0.5$ kpc to 15 kpc. An apparent turn over in the spectrum between 0.5 kpc and 80 pc is not yet clear (Han 2009). In combination with the RM spectra of intervening polarised sources, the dense grid of pulsars discovered with the SKA will probe the energy spectrum at least down to 100 pc scales.

4. The extragalactic magnetoionic medium

In addition to significantly improving our understanding of the physics of the ISM in the Milky Way, the SKA will reveal the electron density distribution and magnetic field structure in nearby galaxies and the IGM. First, it will measure the DMs and RMs of extragalactic pulsars (especially their giant pulses) and single pulses of extragalactic origin, such as the Fast Radio Bursts (FRBs; Lorimer et al. 2007; Thornton et al. 2013, Spitler et al. 2014); see Macquart et al. (2015) in this volume for more details. Second, the SKA will yield high resolution observations of megamaser Zeeman splitting in nearby galaxies (e.g. Robishaw et al. 2008; McBridge & Heiles 2013); for more details, see Robishaw et al. (2015) in this volume. Third, the SKA will observe the polarization of all radio sources in the sky over a wide band, yielding high precision RMs of a large number of distant radio sources shining through galaxies, clusters of galaxies and cosmic web in the nearby universe; see Heald et al. (2015), Johnston-Hollitt et al. (2015) and Beck et al. (2015) in this volume.

The high sensitivity, wide field of view, and wide bandwidth of SKA1 and SKA2 will yield a large sample of pulsars in nearby galaxies such as M31 and M33 (see Keane et al. 2015, this volume). At present, DMs of extragalactic objects have been estimated for only a handful of

PoS(AASKA14)041

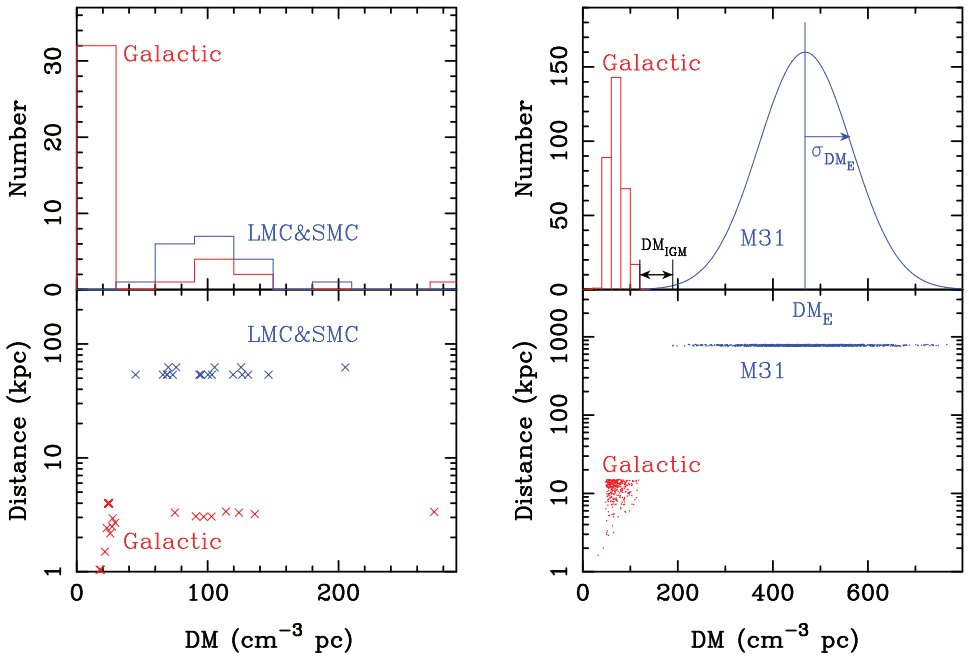

Figure 5: DM distributions of extragalactic pulsars (blue) and Galactic pulsars (red) within a 10° radius around the host galaxy. Current data for pulsars in the large and small Magellanic Clouds are compared with Milky Way pulsars *on the left* and simulated data for pulsars in M31 are compared with simulated Milky Way pulsars *on the right*. Currently a small sample of pulsars in the Magellanic Clouds and a small sample of foreground Galactic pulsars around the clouds are not enough to deduce the intergalactic DM (or RM). However, the SKA will discover a much larger sample of Galactic and extragalactic pulsars (e.g. in M31) for this purpose. The DM range of extragalactic pulsars depends on the inclination angle of the host galaxy disk.

pulsars in the Magellanic Clouds (Manchester et al. 2006) and a few FRBs (Thornton et al. 2013). Scattering has been detected and studied for only four FRBs (e.g. Thornton et al. 2013); the RM of an FRB is yet to be observed.

Two key steps are needed to derive intergalactic DM and RM estimates from observations of extragalactic pulsars or pulses: 1) subtraction of the foreground DM or RM contribution from our Milky Way; and 2) constraining the local contribution from the host galaxy. Both steps require a large sample of pulsars. Estimating the foreground column density of electrons in the Milky Way requires a large sample of Galactic pulsars in the region of sky immediately around the direction of the host galaxy. To estimate the Galactic foreground contribution to the measured Faraday rotation also requires a large number of extragalactic radio sources around the direction of the host galaxy. SKA1 will observe a large number of extragalactic RMs as part of the cosmic magnetism project (e.g. Johnston-Hollitt et al. 2015); the average RM of background radio sources, $\langle \mathrm{RM_{BGS}} \rangle$, in the direction of a host galaxy represents the foreground contribution of the Milky Way to the estimated RM of an extragalactic pulsar or pulse (e.g. see Xu & Han 2014b).

For an individual extragalactic pulsar or pulse, it is difficult to estimate the dispersion and Faraday rotation contributed by the host galaxy. When a large sample of pulsars are discovered in a host galaxy, the minimum DM of these pulsars, $\min(\mathrm{DM_{extraPSRs}})$, can be used as the upper limit of $\mathrm{DM_{IGM}}$ plus the Galactic DM foreground, $\max(\mathrm{DM_{GalacPSRs}})$, as shown in Fig. 5. When

PoS(AASKA14)041

averaged over a sample of extragalactic pulsars in the same host galaxy, the mean RM contributed by the host is likely to approach zero. Therefore, to probe the electron density and magnetic field of the IGM, we can estimate $\mathrm{DM_{IGM}} = \min(\mathrm{DM_{extraPSRs}}) - \max(\mathrm{DM_{GalacPSRs}})$ and $\mathrm{RM_{IGM}} = \langle \mathrm{RM_{extraPSRs}} \rangle - \langle \mathrm{RM_{BGS}} \rangle$.

In addition to observing extragalactic pulsars and pulses, the SKA will be able to reveal extragalactic magnetism in a nearby galaxy by observing the RMs of either a large number of radio sources behind the galaxy or diffuse emission from the galaxy (see Heald et al. 2015). On the other hand, when a large sample of RMs of quasars or other objects with known redshifts are available (e.g. Johnston-Hollitt et al. 2015), the residual RMs (i.e. the values after subtracting the foreground RM from the observed RM values) can be used to explore the magnetoionic medium in the cosmic web and intervening clouds (see Xu & Han 2014a). The distribution and statistics of residual RMs can reveal weak magnetic fields and their evolution over cosmological distances much greater than most detectable extragalactic pulsars.

5. Conclusions

Pulsars are the best probes of the interstellar magnetoionic medium in the Milky Way. By measuring dispersion toward a large number of pulsars and their distances, we can construct a detailed electron density distribution model. Scattering measurements derived from either the extended tails of pulsar profiles at low frequencies or from pulsar dynamic spectra will reveal the dynamics of small-scale structures in the ionized ISM. Faraday rotation probes the large and small scale structure of interstellar magnetic fields. Following the discussion in previous sections, we conclude the following:

- SKA1: Beginning with the early phase of SKA1, wide-band polarimetry with SKA1-LOW and SKA1-MID will provides a much better understanding of the structure of the interstellar medium. The DMs of several thousand newly discovered pulsars spread across the Milky Way will dramatically improve the electron density model, especially once independent and precise distances can be estimated for a substantial fraction of pulsars using both SKA1 pulsar timing and SKA1-VLBI. The distribution of pulsar RMs can be used to map out magnetic field structures in high detail.

- SKA2: By performing a complete census of those pulsars in our Galaxy that are visible in the southern hemisphere, and in concert with large telescopes in the northern hemisphere, SKA2 will complete the model of electron density distribution and magnetic field structure in *the entire Milky Way*,

- Intergalactic medium: SKA1 and SKA2 can be used to discover a large number of pulsars in nearby galaxies. By observing the DMs and RMs of a large sample of extragalactic pulsars and subtracting the Galactic foreground and host galaxy contributions, we will have the unique chance to detect the baryonic content and magnetic field of the intergalactic medium. The high sensitivity of the SKA is essential to this purpose. In addition, the statistics of RMs of a large number of extragalactic radio sources can reveal the weak magnetic fields in the cosmic web and other intervening galaxies.

PoS(AASKA14)041

Acknowledgments

JinLin Han is supported by the National Natural Science Foundation (No.11473034) and by the Strategic Priority Research Program "The Emergence of Cosmological Structures" of the Chinese Academy of Sciences, Grant No. XDB09010200. The research of Joseph Lazio was performed at the Jet Propulsion Laboratory, California Institute of Technology, under a contract with the National Aeronautics and Space Administration.

PoS(AASKA14)041

REFERENCES

Beck, R., Bomans, D., Colafrancesco, S. et al., 2015, "Structure, dynamical impact and origin of magnetic fields in nearby galaxies in the SKA era", in proc. *Advancing Astrophysics with the Square Kilometre Array*, PoS(AASKA14)094

Bhat, N. D. Ramesh, Cordes, J. M., Camilo, F., et al. 2004, ApJ, 605, 759

Brisken, W. F., Benson, J. M., Goss, W. M., & Thorsett, S. E. 2002, ApJ, 571, 906

Chatterjee, S., Brisken, W. F., Vlemmings, W. H. T., et al. 2009, ApJ, 698, 250

Coenen, T., van Leeuwen, J., Hessels, J. W. T., et al. 2014, A&A, 570, 60

Cordes, J. M., Lazio, T. J. W. 2002, preprint (arXiv:astro-ph/0207156)

Cordes, J. M., Rickett, B. J., Stinebring, D. R., Coles, W. A. 2006, ApJ, 637, 346

Deller, A. T., Boyles, J., Lorimer, D. R. et al., 2013, ApJ, 770, 145.

Deller, A. T., Brisken, W. F., Chatterjee, S., et al. 2011, 20th Meeting of EVGA, (Bonn, Germany, March 29-30, 2011), Eds: W. Alef, S. Bernhart, and A. Nothnagel, p. 178-182

Dewdney, P., Turner, W., Millenaar, R., McCool, R., Lazio, J., Cornwell, T., 2013, "SKA1 System Baseline Design", Document number SKA-TEL-SKO-DD-001 Revision 1

Ferriére, K., Terral, P. 2014, A&A 561, 100

Finkbeiner, D. P., 2003, ApJS, 146, 407.

Gaensler, B. M., Madsen, G. J., Chatterjee, S. & Mao, S. A. 2008, PASA, 25, 184

Green, J., van Langevelde, H. J., Brunthaler, A., et al., 2015, "Maser astrometry with VLBI and the SKA", in proc. *Advancing Astrophysics with the Square Kilometre Array*, PoS(AASKA14)119

Gupta, P., Rickett, B. J., Lyne, A. 1994, MNRAS, 269, 1035

Han, J. L., 2009, "Magnetic structure of our Galaxy: A review of observations", in proceedings of "Cosmic Magnetic Fields: From Planets, to Stars and Galaxies", IAU Symp. 259, 455

Han, J. L., 2013, "Pulsars as excellent probes for the magnetic structure in our Milky Way", in proceedings of "Neutron Stars and Pulsars: Challenges and Opportunities after 80 years", IAU Symp. 291, 223

Han, J. L., Ferriere, K., Manchester, R. N. 2004, ApJ, 610, 820.

Han, J. L., Manchester, R. N., Berkhuijsen, E. M., Beck, R. 1997, A&A 322, 98

Han, J. L., Manchester, R. N., Lyne, A. G., Qiao, G. J., van Straten, W. 2006, ApJ, 642, 868.

Han, J. L., Manchester, Qiao, G. J. 1999, MNRAS, 306, 371.

Han, J. L., Zhang, J. S. 2007, A&A, 464, 609

Harvey-Smith, L., Madsen, G. J., Gaensler, B. M. 2011, ApJ, 736, 83

Haverkorn, M., Akahori, T., Carretti, E., et al., 2015, "Measuring magnetism in the Milky Way with the Square Kilometre Array", in proc. *Advancing Astrophysics with the Square Kilometre Array*, PoS(AASKA14)096

Heald, G., Beck, R., de Blok, W. J. G., et al., 2015, "Magnetic field tomography in nearby galaxies with the Square Kilometre Array", in proc. *Advancing Astrophysics with the Square Kilometre Array*, PoS(AASKA14)106

Hou, L. G., Han, J. L., 2014, A&A, 569, A125

Janssen, G. H., Hobbs, G., McLaughlin, M. et al., 2015, "Gravitational wave astronomy with the SKA", in proc. *Advancing Astrophysics with the Square Kilometre Array*, PoS(AASKA14)037

Johnston-Hollitt M., 2015, "Using SKA Rotation Measures to Reveal the Mysteries of the Magnetised Universe", in proc. *Advancing Astrophysics with the Square Kilometre Array*, PoS(AASKA14)092

Karastergiou, A., Johnston, S., Andersson, N., et al. 2015, "Understanding pulsar magnetospheres with the SKA", in proc. *Advancing Astrophysics with the Square Kilometre Array*, PoS(AASKA14)038

Keane, E. F., Bhattacharyya, B., Kramer, M., et al. 2015, "A Cosmic Census of Radio Pulsars with the SKA", in proc. *Advancing Astrophysics with the Square Kilometre Array*, PoS(AASKA14)040

Keith, M. J., et al. 2013, MNRAS, 429, 2161

Lazio, T. J. W., 2004, ApJ, 613, 1023

Lewandowski, W., Dembska, M., Kijak, J., Kowalinska, M., 2013, MNRAS, 434, 69

Löhmer, O., Kramer, M., Mitra, D., Lorimer, D. R., Lyne, A. G. 2001, ApJ, 562, L157

Löhmer, O., Mitra, D., Gupta, Y., Kramer, M., Ahuja, A. 2004, A&A, 425, 569

Lorimer, D. R., Bailes, M., McLaughlin, M. A., et al. 2007, Science, 318, 777

Lyne, A. G., 1971, in Proceedings of IAU Symp. 46, p.182

Manchester, R. N., Fan, G., Lyne, A. G., et al. 2006, ApJ, 649, 235

Macquart J.-P., Keane, E. F., Grainge, K., et al. 2015, "Fast transients at cosmological distances", in proc. *Advancing Astrophysics with the Square Kilometre Array*, PoS(AASKA14)055

Manchester, R. N., Hobbs, G. B., Teoh, A., Hobbs, M., 2005, AJ, 129, 1993

McBride, J., Heiles, C., 2013, ApJ, 763, 8

Minter, A. H., Spangler, S. R., 1996, ApJ, 458, 194

Mitra, D., Wielebinski, R., Kramer, M., Jessner, A. 2003, A&A, 398, 993

Nan, R., Li, D., Jin, C., et al., 2011, International Journal of Modern Physics D, 20, 989

Paragi, Z., Godfrey, L., Reynolds, C. et al, 2015, "Very Long Baseline Interferometry with the SKA", in proc. *Advancing Astrophysics with the Square Kilometre Array*, PoS(AASKA14)143

Pen, U.-L., Levin, Y., 2014, MNRAS 442, 3338

Pen, U.-L., Macquart, J.-P., Deller, A. T., Brisken W., 2014, MNRAS, 440, L36

Petroff, E., Keith, M. J., Johnston, S., van Straten, W., Shannon, R. M. 2013, MNRAS, 435, 1610

Prouza, M., Šmída, R. 2003, A&A, 410, 1

Robishaw, T., Green, J. A., Surcis, G., et al., 2015, "Measuring Magnetic Fields Near and Far with the SKA via the Zeeman Effect", in proc. *Advancing Astrophysics with the Square Kilometre Array*, PoS(AASKA14)110

Robishaw, T., Quataert, E., Heiles, C., 2008, ApJ, 680, 981

PoS(AASKA14)041

Savage, A. H., Spangler, S. R., & Fischer, P. D. 2013, ApJ, 765, 42
Schnitzeler, D. H. F. M 2012, MNRAS, 427, 664
Smits, R., Tingay, S. J., Wex, N., Kramer, M., Stappers, B. 2011, A&A, 528, 108
Sotomayor-Beltran, C., Sobey, C., Hessels, J. W. T., et al. 2013, A&A, 552, A58
Spitler, L. G., Cordes, J. M., Hessels, J. W. T., Lorimer, D. R., et al. 2014a, ApJ, 790, 101
Spitler, L. G., Lee, K. J., Eatough, R. P., et al. 2014b, ApJ, 780, L3
Stinebring, D. R., 2006, ChJAS, Vol.6, Issue S2, 204
Sun, X. H., Reich, W., Waelkens, A., Enßlin, T. A. 2008, A&A 477, 573
Sun, X. H., Reich, W., Wang, C., Han, J. L., Reich, P. 2011, A&A 535, A64
Taylor, J. H., Cordes, J. M., 1993, ApJ, 411, 674
Thornton, D., Stappers, B., Bailes, M., et al. 2013, Science, 341, 53
Xu, J., Han, J. L, 2014a, MNRAS, 442, 3329
Xu, J., Han, J. L, 2014b, RAA, 14, 942
You, X. P., Hobbs, G., Coles, W. A., et al. 2007, MNRAS, 378, 493
You, X. P., Coles, W. A., Hobbs, G., Manchester, R. N. 2012, MNRAS, 422, 1160

PoS(AASKA14)041

PROCEEDINGS OF SCIENCE

Testing Gravity with Pulsars in the SKA Era

Lijing Shao[*1], **Ingrid H. Stairs**[2], **John Antoniadis**[3], **Adam T. Deller**[4], **Paulo C. C. Freire**[3], **Jason W. T. Hessels**[4,5], **Gemma H. Janssen**[4], **Michael Kramer**[3,6], **Jutta Kunz**[7], **Claus Lämmerzahl**[8], **Volker Perlick**[8], **Andrea Possenti**[9], **Scott Ransom**[10], **Benjamin W. Stappers**[6], **Willem van Straten**[11]

[1] *School of Physics, Peking University, Beijing 100871, China*
[2] *Department of Physics and Astronomy, University of British Columbia, 6224 Agricultural Rd., Vancouver, BC V6T 1Z1, Canada*
[3] *Max-Planck-Institut für Radioastronomie, Auf dem Hügel 69, D-53121 Bonn, Germany*
[4] *ASTRON, The Netherlands Institute for Radio Astronomy, 7990 AA Dwingeloo, The Netherlands*
[5] *Anton Pannekoek Institute for Astronomy, University of Amsterdam, Science Park 904, 1098 XH Amsterdam, The Netherlands*
[6] *Jodrell Bank Centre for Astrophysics, The University of Manchester, M13 9PL, United Kingdom*
[7] *University of Oldenburg, Department of Physics, 26111 Oldenburg, Germany*
[8] *University of Bremen, ZARM, 28359 Bremen, Germany*
[9] *INAF-Osservatorio Astronomico di Cagliari, via della Scienza 5, 09047 Selargius (CA), Italy*
[10] *National Radio Astronomy Observatory, 520 Edgemont Road, Charlottesville, VA 22903, USA*
[11] *Centre for Astrophysics and Supercomputing and ARC Centre for All-Sky Astrophysics (CAASTRO), Swinburne University of Technology, PO Box 218 Hawthorn, VIC 3122, Australia*

E-mails: lshao@pku.edu.cn (LS); stairs@astro.ubc.ca (IHS)

The Square Kilometre Array (SKA) will use pulsars to enable precise measurements of strong gravity effects in pulsar systems, which yield tests of gravitational theories that cannot be carried out anywhere else. The Galactic census of pulsars will discover dozens of relativistic pulsar systems, possibly including pulsar – black hole binaries which can be used to test the "cosmic censorship conjecture" and the "no-hair theorem". Also, the SKA's remarkable sensitivity will vastly improve the timing precision of millisecond pulsars, allowing probes of potential deviations from general relativity (GR). Aspects of gravitation to be explored include tests of strong equivalence principles, gravitational dipole radiation, extra field components of gravitation, gravitomagnetism, and spacetime symmetries.

Advancing Astrophysics with the Square Kilometre Array
June 8-13, 2014
Giardini Naxos, Italy

[*] Speaker.

PoS(AASKA14)042

1. Introduction

In November 1915, Albert Einstein published the final paper that completed his theory of gravity and spacetime now known as general relativity (GR), changing our view of gravity and spacetime for ever. During its first fifty years, GR was considered a theoretical tour-de-force but one with meager observational evidence. Only in the 1960s did technology usher in the remarkable field of experimental gravity (Misner et al. 1973; Will 1993). Over the subsequent fifty years, GR has passed all experimental tests in laboratories, in the Solar System and in various stellar systems, particularly in binary pulsars (Will 2014). Astrophysical observations using radio bands have played one of the most important parts in the history of testing GR, with the ability to make precise measurements and probe into the vicinity of compact bodies, namely black holes (BHs) and neutron stars (NSs). Particularly, radio timing of binary pulsars has precisely probed the gravitational properties of NSs and, for the first time, tested the radiative properties of gravity, demonstrating that gravitational waves exist and that compact binaries lose energy from their emission at the rates predicted by GR (Hulse & Taylor 1975; Taylor et al. 1979; Kramer et al. 2006; Weisberg et al. 2010; Freire et al. 2012b; Antoniadis et al. 2013). This confirmation and precise characterisation of the radiative properties of gravity is not only critical from the point of view of our understanding of fundamental physics and many aspects of astrophysics, but it will also open, via gravitational wave detectors, a whole new window on the Universe. The Square Kilometre Array (SKA), as the most powerful member of the next generation of radio telescopes, will allow much more precise radio timing of pulsars and will discover dozens of rare relativistic binary systems. For this reason it will play a unique role in many areas of experimental gravity.

Despite its success over the last century, GR still faces great challenges on the research frontiers of modern physics. First, it is known to be incomplete, since it fails at the centre of BHs. Second, as a non-renormalisable field theory, it appears to be incompatible with quantum principles. Reconciling gravity with quantum mechanics stands out as one of the great challenges of fundamental physics today. Furthermore, concepts like dark matter and dark energy pose additional challenges for our understanding of gravity, and modifications of gravity theories have been proposed to explain these phenomena (Capozziello & de Laurentis 2011), like the Tensor-Vector-Scalar (TeVeS) theory, which was advanced to explain dark matter (Bekenstein 2004).

The important thing to us is that pulsar timing can be used to test some of these theories. Pulsar timing uses large radio telescopes to record the times of arrival (TOAs) of pulsed signals, produced by the rotation of the pulsar. These TOAs depend on the rotational and astrometric parameters of the pulsar, dispersion in the interstellar medium that the signals traverse, and the motion of the radio telescope in the Solar System. If the pulsar is in a binary, the TOAs also depend on the orbital dynamics of the binary, which are determined by the underlying gravitational theory (Weisberg & Taylor 1981; Damour & Taylor 1992; Edwards et al. 2006). Some theories of gravity, like a family of TeVeS-like theories introduced in Freire et al. (2012b), result in orbital dynamics that is sufficiently different from GR to be detected in the timing of some binary pulsars. Therefore, precise timing measurements of these binary pulsars can constrain, or altogether rule out, some of these gravity theories.

For example, in the Jordan-Fierz-Brans-Dicke theory (Jordan 1959; Fierz 1956; Brans & Dicke 1961), gravity is mediated by a scalar field, φ, in addition to the canonical metric field, $g_{\mu\nu}$. The

PoS(AASKA14)042

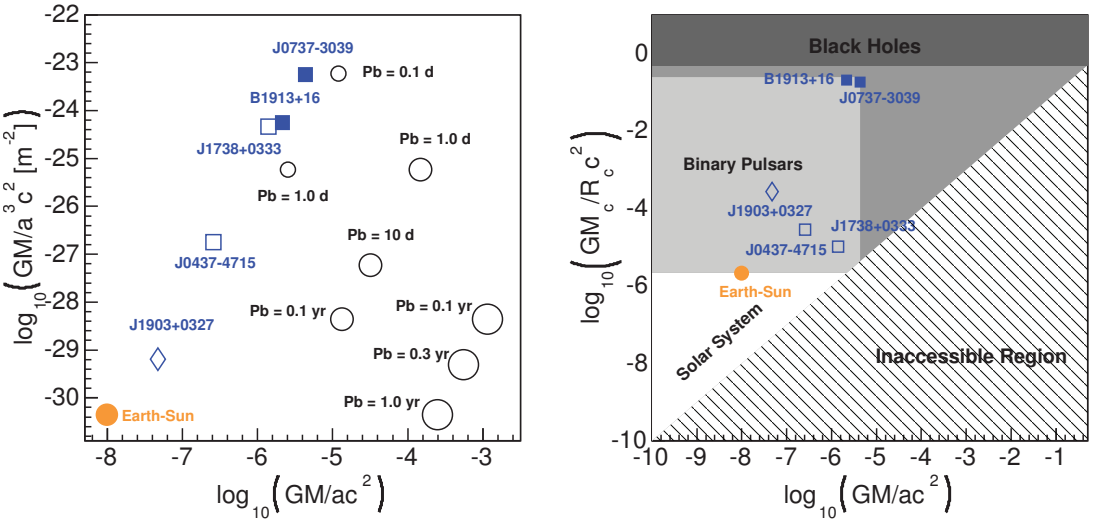

Figure 1: *Left:* Parameter space for quantifying the strength of a gravitational field (Psaltis 2008). The horizontal axis measures the gravitational potential and the vertical axis measures the spacetime curvature of an orbit with a semimajor axis, a, and a total mass, M (here G is the gravitational constant, and c is the light speed). Solid and empty squares are known neutron star – neutron star (NS-NS) and neutron star – white dwarf (NS-WD) binaries, respectively. The diamond is a known neutron star – main sequence star binary. Circles from large to small are pulsar – Sgr A* BH, pulsar – 5000 $M_\odot$ BH, and pulsar – 10 $M_\odot$ BH binaries with their assumed orbital periods aside. *Right:* The compactness of the gravitating companion star versus the compactness of the orbit; M_c and R_c are the mass and the radius of the companion star, respectively (Kramer et al. 2004).

variation of φ in spacetime introduces observable effects in gravitational experiments, like the time-variation of the local gravitational constant G and the existence of gravitational dipole radiation in a binary. In a more general class of scalar-tensor theories (Damour & Esposito-Farèse 1993, 1996), the coupling strength of the scalar field φ to matter depends on the field itself φ as $\alpha_0 + \varphi\beta_0$, where α_0 and β_0 fully characterise the theory. Within some of the (α_0, β_0) space, non-perturbative effects, called "spontaneous scalarisation", may happen in compact bodies like NSs (Damour & Esposito-Farèse 1993), which can influence the orbital dynamics of a binary system dramatically. Similar effects are also possible within an extended family of TeVeS-like theories (Freire et al. 2012b). With their ability to probe strong-field effects, binary pulsars are ideal laboratories with which to study these alternative gravitational theories. With the non-detection of gravitational dipole radiation from radio pulsar timing, binary pulsars have already severely constrained the parameter spaces of these theories and provided the most stringent tests of the strong-field[1] and radiative properties of gravity (Freire et al. 2012b; Antoniadis et al. 2013; Stairs 2003; Wex 2014).

[1] Compared to the coalescence of two compact objects (that will be the main source for ground-based gravitational wave detectors), two components of a binary pulsar are well separated, that might be prejudicially termed as "weak field". However, as shown by explicit calculations, "strong-field effects" associated with strongly self-gravitating NSs could have significant effects on the binary orbital dynamics (Damour & Esposito-Farèse 1993).

PoS(AASKA14)042

1.1 The role of the Square Kilometre Array

The Square Kilometre Array will have a major impact on radio astronomy. The SKA Phase 1 (SKA1) will feature roughly half of its total collecting area within a dense core, in the cases of SKA1-LOW and SKA1-MID. By synthesising a coherent sum of these elements, it will be possible to deeply search for new relativistic binary pulsars, over the whole sky, and to subsequently time them with great precision using the full SKA1-MID array (*i.e.* including the longer baselines). The SKA Phase 2 (SKA2) will provide another major leap in sensitivity, and thus also in timing precision. Both phases of the SKA will significantly advance experimental tests of gravitational theories to a new level (Kramer et al. 2004).

This will happen through two avenues. On the one hand, SKA1-MID and SKA2 will strongly improve the quality of the observations of the most interesting binaries currently known (*e.g.*, PSR J0737−3039 (Burgay et al. 2003; Lyne et al. 2004; Kramer et al. 2006)) and triple systems (*e.g.*, PSR J0337+1715 (Ransom et al. 2014)), in turn dramatically improving the quality of the existing tests and enabling proposed new tests. Compared with the current status quo, SKA1-MID will improve the timing precision for southern pulsars by about an order of magnitude, and SKA2 will improve it by up to two orders of magnitude. Different pulsars will gain different improvements in precision, depending on their sky locations, pulse characteristics, timing stabilities, and so on.

For precision pulsar timing, raw sensitivity is one of the most important factors. High cadence may also be needed for some experiments, in which case sub-arraying will be needed. Typically, TOAs for a particular pulsar are collected every few weeks, though in come cases a much higher cadence is necessary, *e.g.* to focus on orbital conjunction in order to measure the Shapiro delay. Sub-arraying can also help if many sources need to be timed, and if reduced sensitivity is acceptable. Though SKA1-MID will provide the highest-precision TOAs, regular measurements with SKA1-LOW may also be needed to track the time-variable interstellar propagation effects that also influence the TOAs. In all cases, coherently dedispersing the data is essential for achieving the maximum timing precision and accuracy. Such timing observations can already begin in an early phase of SKA1 (say, with 50% of the collecting area available), though they will naturally obtain less precise TOAs than with the complete array. For some sources 50% sensitivity will be sufficient, while for others certain relativistic effects may only become clearly detectable once the full array is in place.

The SKA will also *discover* new relativistic systems with which to carry out similar and completely novel tests. With a larger field of view and high sensitivity, the SKA is more efficient in finding new pulsars. The larger sensitivity of the SKA means that a shorter integration time is needed to achieve the required signal to noise ratio. Consequently, in an "acceleration search" with an assumed constant orbital acceleration (Lorimer & Kramer 2004), the smearing due to varying acceleration in an actual binary will be reduced, making the SKA much more effective than current telescopes at finding relativistic binaries. Simulations show that the SKA1 can discover a total of about 10,000 normal pulsars and perhaps as many as 1,800 millisecond pulsars (MSPs), with SKA1-LOW surveying the sky with the Galactic latitude $|b| \geq 5^\circ$, and SKA1-MID surveying the sky with the Galactic latitude $|b| \leq 10^\circ$ (Keane et al. 2015). The SKA2 will discover even more pulsars, and it is possible that among them there will be pulsar – black hole (PSR-BH) binaries

PoS(AASKA14)042

(Kramer et al. 2004; Keane et al. 2015). The discovery of even a single tight PSR-BH system will open a new era of studying BH physics with great precision, including possible tests of the "cosmic censorship conjecture" and the "no-hair theorem" (Damour & Esposito-Farèse 1998; Wex & Kopeikin 1999; Kramer et al. 2004; Liu 2012; Liu et al. 2012). Figure 1 shows the vast unprobed regions in the gravity sector that can be probed with different kinds of PSR-BH systems.

2. Relativistic Binaries

Pulsar timing takes advantage of the tremendous rotational stability of pulsars, allowing us to treat them as free-falling clocks. As a pulsar is monitored over months and years, an ephemeris is calculated which accounts for every rotation of the pulsar and can be used to predict future pulse TOAs. A pulsar ephemeris always incorporates the spin frequency and generally at least one spin derivative accounting for rotational energy loss, plus astrometric parameters. Binary pulsar orbits require a further translation of reference frame, accomplished for most binary systems by the five Keplerian parameters describing an eccentric Keplerian orbit. In order to account for relativistic effects beyond a Keplerian orbit, a set of theory-independent "post-Keplerian" (PK) parameters are introduced (Damour & Deruelle 1986; Damour & Taylor 1992) (see Table 1 for an incomplete collection of the most important PK parameters). In practice, PK parameters could be contaminated by astrophysical effects other than relativistic effects due to gravity. For example, the observed orbital decay parameter, $\dot{P}_b$, has "kinematic" contributions, which result from the proper motion of the system and the difference of Galactic accelerations between that system and the Solar System Barycentre. Here unless otherwise stated, we assume that non-gravitational contributions are properly corrected or demonstrably negligible in effect. If so, in the case of two well-separated masses with negligible spin contributions, the PK parameters are functions of the well-measured Keplerian parameters, the component masses, the equation of state (EOS) of stellar matters, and the parameters describing the gravitational theory (Damour & Taylor 1992) (in GR, the internal constitution of the star is irrelevant to a high "post-Newtonian" (PN) order, only the total masses matter — this is the "effacement" property to be discussed in section 3).

Measuring two PK parameters, we can use a specific theory of gravity to determine the component masses of the system; these are important to study stellar evolution theories and, in some cases, to constrain EOS (Watts et al. 2015). If more PK parameters are measured, then the theory can be tested by a self-consistent argument — using the masses derived in the first stage one should be able to predict the subsequent PK measurements. Another way of viewing this is the so-called "mass-mass diagram" (see Figure 2 for a GR-based example for PSR J0737−3039 (Kramer et al. 2006; Breton et al. 2008)). For a gravitational theory to pass the test(s), all curves in the diagram should intersect in some region, *i.e.*, the theory must be able to describe the component masses in a self-consistent way (Taylor & Weisberg 1982).

The current state-of-the-art binary in this area is the Double Pulsar (PSR J0737−3039A/B) (Burgay et al. 2003; Lyne et al. 2004), which enables five tests of GR. Figure 2 shows its mass-mass diagram, where seven curves corresponding to seven mass constraints intersect at one point (Kramer et al. 2006; Breton et al. 2008; Kramer & Wex 2009), indicating that GR provides a self-consistent description of all of its timing measurements. The Double Pulsar resides in the southern sky and will be an important target for the SKA. The timing precision of the SKA will enable tests

PoS(AASKA14)042

Table 1: The most important PK parameters that could be used in pulsar timing of binaries (Damour & Deruelle 1986; Damour & Taylor 1992; Wex & Kopeikin 1999; Lorimer & Kramer 2004; Edwards et al. 2006). In practice, for a specific binary pulsar, only some PK parameters are measured, depending on the characteristics of the pulsar timing experiment.

Parameter	
$\dot{\omega}$	time derivative of the longitude of periastron ω
γ	amplitude of the Einstein delay
$\dot{P}_b$	time derivative of the orbital period P_b
r	range of the Shapiro delay
s	shape of the Shapiro delay
$\Omega_{\rm SO}$	precession rate of the pulsar spin
δ_θ	mismatch in eccentricities (see text)
$\dot{e}$	time derivative of the orbital eccentricity e
$\dot{x}$	time derivative of the projected semimajor axis of the pulsar orbit x
$\ddot{\omega}$	second time derivative of the longitude of periastron
$\ddot{x}$	second time derivative of the projected semimajor axis of the pulsar orbit

of relativistic effects beyond their first-order PN approximations (Kramer & Wex 2009). Measuring higher-order PN effects is important since it allows the investigation of the effects from pulsar spin (Barker & O'Connell 1975; Damour & Schaefer 1988; Kramer & Wex 2009). The fractional effects due to the next PN order[2] on the advance rate of periastron, namely $\dot{\omega}^{\rm 2PN}/\dot{\omega}^{\rm 1PN}$, and on the orbital decay, namely $\dot{P}_b^{\rm 3.5PN}/\dot{P}_b^{\rm 2.5PN}$, are both at the order of $\mathscr{O}(10^{-5})$. Simulations showed that by obtaining a timing variance below $\sim 5\,\mu$s for the Double Pulsar we will reach the precision required to detect higher-order effects (Kramer & Wex 2009); this is very likely with SKA1-MID, scaling from current observations. The SKA2 will have sub-μs timing precision for the Double Pulsar (assuming its pulse profile shape can still be well modelled), raising the prospect of highly precise measurements of these higher-order parameters.

Besides the orbital dynamics of two point masses, spin contributions may play an important role in the observations of pulsar binaries (Barker & O'Connell 1975). Due to the curvature of the spacetime produced by the companion star, the rotation axis of a freely falling object (here the pulsar) suffers a precession with respect to a distant observer; this effect is known as "geodetic precession". Because of it, over time different emitting regions of the magnetosphere will be visible from the Earth, thus causing a secular change in the observed pulse profile. This effect has been observed in some tight binary pulsars, for example, in PSRs B1913+16 (Weisberg et al. 1989; Kramer 1998), B1534+12 (Stairs et al. 2004; Fonseca et al. 2014), J1141−6545 (Manchester et al. 2010), J1906+0746 (Lorimer et al. 2006) and J0737−3039B (Perera et al. 2010). For PSRs B1534+12 and J0737−3039B we even have direct measurements of the precession rates, which match the GR predictions (Stairs et al. 2004; Fonseca et al. 2014; Breton et al. 2008). The SKA1-MID will have comparable sensitivity to the Arecibo telescope, meaning that significant improvement in pre-

[2]Effects due to the PN orders are those that are suppressed by the ratio of the orbital velocity, v, to the light speed, c, compared with those due to Newtonian gravity (Will 2014). It is denoted as "nPN" if the suppression factor is $\mathscr{O}(v^{2n}/c^{2n})$.

PoS(AASKA14)042

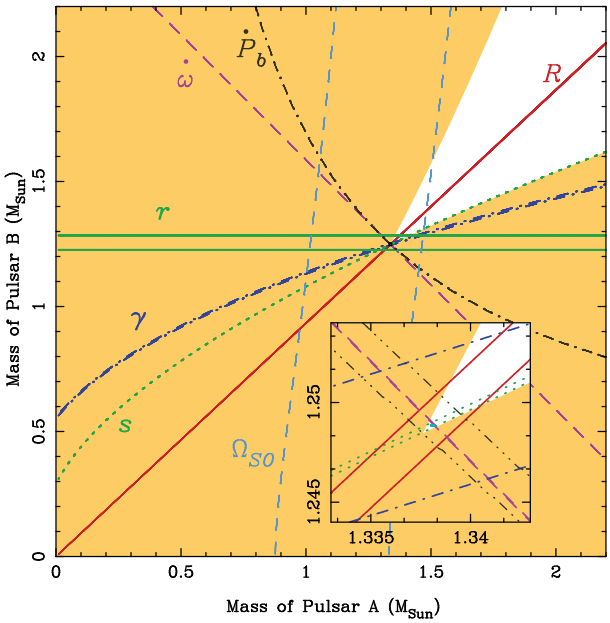

Figure 2: The mass-mass diagram of PSR J0737−3039A/B, also known as the Double Pulsar (Kramer et al. 2006; Breton et al. 2008) (Kramer et al., in prep.). In the figure the underlying gravitational theory is assumed to be GR. Shaded regions are forbidden by the individual mass functions because the sine of the orbital inclination must be ≤ 1. The inset is an expanded view of the region of principal interest, where the intersection of seven curves at one point within measurement uncertainties proves the existence and uniqueness of a solution. For more details, see Kramer et al. (2006) and Breton et al. (2008).

cession measurements of the pulsars that are in the Arecibo sky will await the SKA2. However, precessing pulsars not visible to the Arecibo telescope will be prime targets for SKA1-MID. For example, in the Double Pulsar, the precession rate of the B pulsar can be measured by modelling the orientation of its magnetosphere as it causes "flickering" eclipses of pulsar A (Breton et al. 2008). The rapidly changing eclipse-period flux density will be much better measured by both phases of the SKA, leading to a more stringent test of the precession rate's agreement with GR.

Since in GR the total angular momentum must be conserved up to 2PN order, a change in the direction of the pulsar spin must be compensated by a change in the direction of the orbital angular momentum, contributing a variation to the projected semimajor axis of the orbit ($\dot{x} \neq 0$). This spin-orbit coupling is also known as the Lense-Thirring effect or frame-dragging effect, and it is a small effect that is numerically at 2PN order for slowly rotating neutron stars, whose measurement requires a high timing precision (Damour & Schaefer 1988). However, measuring it is important since it offers the potential to measure the moment of inertia of the pulsar (Damour & Schaefer 1988; O'Connell 2004), of great interest for the EOS of cold dense nuclear matter (Watts et al. 2015).

For the Double Pulsar, the recycled pulsar (pulsar A) dominates the contribution to the Lense-Thirring precession, because it is a faster rotator. The effect on $\dot{x}$ will be almost impossible to

PoS(AASKA14)042

measure, not only because in this case there is a close alignment of the orbital angular momentum and the spin of pulsar A (Ferdman et al. 2013), but also because the system is viewed almost edge-on (Kramer et al. 2006). However, the SKA Galactic census will discover many NS-NS systems (scaling from the current population, we expect 100 from the SKA1 and 180 from the SKA2 (Keane et al. 2015)), and there may well be binaries that will enable the direct measurement of $\dot{x}$. In order to achieve the goal, a tight binary with good timing precision is needed. In addition, the misalignment angle between the pulsar spin and the orbital norm should be reasonably large, *i.e.*, geodetic precession should be observable. This requires a relatively large "supernova kick velocity" for the second-formed compact object — in other words, an iron-core-collapse supernova, instead of an electron-capture supernova as likely happened in the Double Pulsar (Ferdman et al. 2013). In such misaligned binaries, the frame dragging introduces nonlinear evolution in time in the longitude of periastron and its projected semimajor axis; thus one might be able to extract $\ddot{\omega}$ and $\ddot{x}$ from radio timing. This would impose useful constraints on the system's geometry (Wex & Kopeikin 1999).

The Lense-Thirring effect also contributes to $\dot{\omega}$ with a magnitude comparable to that of $\dot{\omega}^{\rm 2PN}$ (Damour & Schaefer 1988; Kramer & Wex 2009). For the Double Pulsar, this can in principle be extracted from the advance rate of periastron. To do this we must determine the component masses very precisely using two other precise PK parameters. One of them (the shape of Shapiro delay, s) already possesses the required precision (Kramer et al. in prep.). For the other one, $\dot{P}_b$, the orbital decay due to the emission of GW waves, we will need to estimate the distance to the pulsar carefully, in order to estimate precisely the kinematic corrections to it. This can only be done with the timing precision provided by the SKA. Again, if this Lense-Thirring contribution to $\dot{\omega}$ can be estimated precisely, we will then be able to estimate the moment of inertia of pulsar A with similar precision. Because this measurement will be done for a pulsar with an exquisitely well-determined mass, it will be a very important constraint on the EOS for dense matter (Lattimer & Schutz 2005; Kramer & Wex 2009; Watts et al. 2015).

The SKA will also confirm general-relativistic orbital deformation for the first time. Damour & Deruelle (1986) used three different eccentricities to describe the timing of a pulsar. Two parameters were introduced in the pulsar timing formula, namely δ_θ and δ_r, where the former is in principle an observable (Damour & Taylor 1992). However, it only adds a tiny periodic variance to the TOAs and the signal has a strong correlation with the Einstein delay that is caused by the transverse Doppler effect and the gravitational redshift, its amplitude is $e^2/\sqrt{1-e^2}$ in binaries of mass ratio near unity, where e is the eccentricity of the orbit. Therefore, we will need highly eccentric orbits to "amplify" the effect, and highly relativistic orbits with large periastron advance rate to break the degeneracy with the Einstein delay. The SKA is likely to find such a system in the southern sky and time it with high precision. We simulate TOAs with orbital parameters similar to that of PSR B1913+16 (Hulse & Taylor 1975; Weisberg et al. 2010) with the `TEMPO` software[3]. It is assumed that 60 TOAs with a precision $\sim 1\,\mu$s are obtained per month with the SKA1. After 10 years of observation, the δ_θ parameter can be determined to a precision $\sim 10\%$. A more eccentric (or a more relativistic) binary can achieve a better test. These results support earlier simulations done with the Double Pulsar (Kramer & Wex 2009).

[3]http://tempo.sourceforge.net

PoS(AASKA14)042

Where parameters in the timing model can be measured to high precision by other means, they can be restricted to an allowed range in the timing fit. This can lead to significantly reduced uncertainties for the remaining parameters in the presence of covariances. The most common source of external information is the estimation of position, proper motion and annual parallax using Very Long Baseline Interferometry (VLBI). The use of VLBI can improve gravitational tests when applied to pulsar binaries. For instance, astrometric information provided by VLBI was used to calculate the kinematic contamination of the measured orbital period derivative of the Double Pulsar, improving the potential accuracy of tests of gravitational radiation to the 0.01% level (Deller et al. 2009). In a second example, the previously unmeasured Shapiro delay for PSR J2222−0137 was precisely ascertained after the position, proper motion, and parallax were fixed using VLBI information (Deller et al. 2013). Since VLBI measures motions on the plane of the sky, it has different "blind spots" with respect to pulsar timing; VLBI has no "blind spots" to parallax at the ecliptic pole and proper motion in the ecliptic plane. With current VLBI instruments, precisions of 10 micro-arcseconds for parallax and 10 micro-arcseconds per year for proper motion can be reached (Deller et al. 2013). The SKA1 will allow a similar leap in VLBI precision as it will provide in the timing precision, and so VLBI using the SKA1 will be able to deliver better results for parallax and proper motion than timing in most cases for nearby pulsars (Paragi et al. 2015). These measurements will be very important to subtract the Shklovskii contribution (which usually dominates the error budget), and the differential Galactic rotation, and vertical acceleration in the Galactic potential (which also depend on relatively well-constrained Galactic models), thus measure the intrinsic orbital period change to high precision.

3. Gravitational Dipole Radiation and Equivalence-Principle Tests

One of the characteristics of GR is the property of "effacement" (Damour 1987). It states that the finite extents of two bodies in a binary are largely irrelevant to their orbital dynamics as long as they are well separated. Effacement is deeply rooted in the strong equivalence principle (SEP) (Will 1993). However, in alternative theories of gravity, the SEP is generally violated, and the strong gravitational fields associated with a NS may have measurable impact on the orbital dynamics of the binary and the trajectory of light propagation (Will 1993; Damour & Esposito-Farèse 1992, 1993). Figure 1 shows various binary systems, with the gravitational field strength characterised by the compactness and curvature of the orbit and the compactness of the companion star.

3.1 Gravitational dipole radiation and time-variation of the gravitational constant

A possible violation of the SEP could be identified by the occurrence of gravitational dipole radiation. The dipole radiation is at lower PN order than the canonical quadrupole radiation predicted by GR, thus in principle it can dominate over the quadrupole mode (Damour & Esposito-Farèse 1992, 1993; Will 1993, 2014). It carries away the gravitational energy of the orbit more rapidly than that in GR, collapsing the binary more quickly, and modifying the waveform of gravitational radiation that can be detected by future ground-based GW detectors. The leading change in the orbital period of a binary is given by the dipolar contribution with a form $\dot{P}_b^{\rm dipole} \propto (\alpha_1 - \alpha_2)^2$, where α_i $(i = 1, 2)$ is the effective coupling strength between body i and the fields associated with

PoS(AASKA14)042

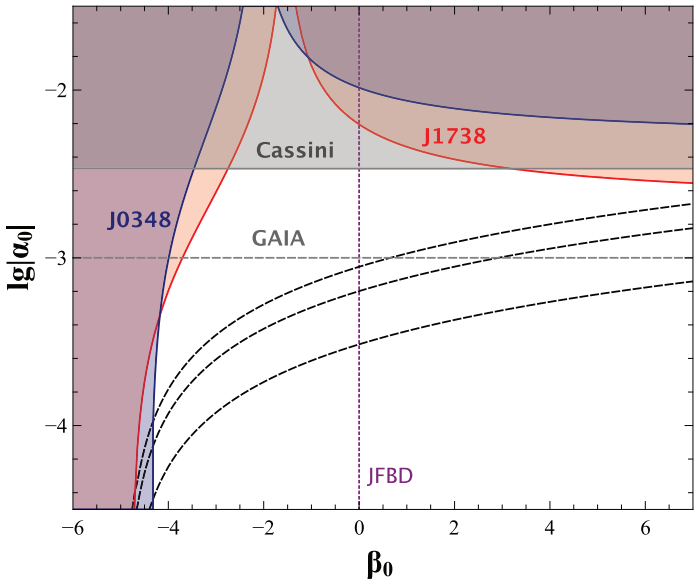

Figure 3: Constraints on the parameter space of scalar-tensor theories (figure courtesy of N. Wex). Coloured regions are excluded by current Solar System and pulsar experiments: Cassini spacecraft (Bertotti et al. 2003), PSR J1738+0333 (Freire et al. 2012b), and PSR J0348+0432 (Antoniadis et al. 2013). The EOS is chosen as MPA1. Black dashed lines are based on simulations for a MSP-BH system with $(M_{\rm BH}, M_{\rm MSP}) = (10\,M_\odot, 1.4\,M_\odot)$, $P_b = 5$ d, and $e = 0.8$; the constraints from top to bottom are based on: 10 years with a 100-m class radio telescope, 5 years with the FAST telescope, and 5 years with the SKA (Liu et al. 2014). The vertical dashed purple line "JFBD" indicates the Jordan-Fierz-Brans-Dicke gravity. The horizontal dashed grey line "GAIA" indicates the limit expected from near-future Solar-System experiments, foremost from the astrometric satellite GAIA.

the dipole moment. In the best-studied gravitational theory of this type, the scalar-tensor theory (Damour & Esposito-Farèse 1992; Will 1993), we generally have $\alpha_{\rm NS} \neq \alpha_{\rm WD}$ in a NS-WD binary (see the right panel of Figure 1). Therefore, NS-WD binaries are the ideal laboratories for testing these theories and, if they are correct, searching for the existence of gravitational dipole radiation, which if detected would falsify GR.

In these NS-WD binaries, the combined radio observation of the pulsar and optical observation of the WD can give rise to precise measurements of two component masses (Antoniadis et al. 2012, 2013; Wex 2014). The mass measurements can be used to predict the amount of gravitational radiation within a specific theory, and this in turn is confronted with the radio timing observation of the orbital decay caused by gravitational damping. As mentioned, the dipolar radiation can in principle be dominant over the quadrupolar radiation, therefore, agreement between the observed $\dot{P}_b$ and the quadrupole formula in GR stringently constrains the dipolar radiation contribution, as in the cases of PSRs J1738+0333 (Freire et al. 2012b) and J0348+0432 (Antoniadis et al. 2013).

In Figure 3, the constraints from those two binaries are plotted in the α_0-β_0 parameter space mentioned in section 1. The best constraint from the Cassini spacecraft in the Solar System is also plotted. The limits from two binary pulsars stringently constrain the parameter space of scalar-tensor theories, especially when the β_0 parameter is negative. The reason for this is that, as showed by Damour & Esposito-Farèse (1993), in this region NSs develop non-perturbative strong-field

PoS(AASKA14)042

effects like "spontaneous scalarisation" that are absent in the weak-field experiments in the Solar System; such effects would cause a very large increase in the emission of dipolar gravitational waves. The more massive the pulsar the less negative β_0 has to be for the spontaneous scalarisation to appear. For this reason, the timing of PSR J0348+0432, a two-solar-mass NS in a relativistic orbit where the orbital decay has been measured with some precision, introduces uniquely stringent constraints on the allowed range of β_0 (Antoniadis et al. 2013).

In Jordan-Fierz-Brans-Dicke theory and (from a broader viewpoint) in the generic scalar-tensor theories, the scalar field plays the role of local gravitational constant, implying that the latter may vary with space and time (Damour & Esposito-Farèse 1992; Will 1993). The possible time-variation in the gravitational constant contributes to the decay of a binary orbit (Damour et al. 1988; Wex 2014). The extra contribution can be constrained by the measurement of $\dot{P}_b$ for binary pulsars by assuming a null contribution from the dipole radiation. In general, however, a varying gravitational constant is accompanied by the dipole radiation (Lazaridis et al. 2009). With more than one binary pulsar, one can also conduct a joint constraint simultaneously on both the dipole radiation and the time-variation in the gravitational constant, utilising the fact that these two effects have different dependence on the orbital period of the binary (Lazaridis et al. 2009). The latest constraint from pulsars on the time-variation of the gravitational constant (Freire et al. 2012b), which relies on VLBI (Deller et al. 2008) and timing (Verbiest et al. 2008) of PSR J0437−4715 and J1738+0333, is already comparable to the best constraint from the Solar System experiments (Will 2014). Moreover, pulsar tests are sensitive to strong-field effects on $\dot{G}$ (Wex 2014).

These examples already show how important proper subtraction of the contributions from Galactic acceleration and the Shklovskii effect is, and how crucial VLBI is for reducing uncertainties in distances and proper motions. Furthermore, in the near future a more accurate understanding of the Galactic potential will also be available (*e.g.*, by the GAIA satellite[4]), further improving the estimates of the kinematic corrections of $\dot{P}_b$.

The next generation of 30-m class optical telescopes, for examples, the Thirty Meter Telescope (TMT)[5], the Giant Magellan Telescope (GMT)[6], and the European Extremely Large Telescope (E-ELT)[7], may also significantly advance the optical observations of WDs, improving their mass and distance estimates; which will soon limit the precision of some of the current gravity tests (Freire et al. 2012b).

In short, in the SKA era, pulsar observations will improve significantly and maintain their unique importance in testing alternative theories of gravity, but will benefit extensively from inputting other techniques like VLBI and optical observation. They will be crucial for tests of some extended gravitational theories that incorporate dark matter and dark energy as gravitational effects.

If any relativistic PSR-BH binaries are discovered, they will also be promising test beds for gravitational dipolar radiation because the no-hair theorem also applies to scalar-tensor theories of gravity; this implies that BHs have no scalar charge[8]. A consequence of this is that any radiative

[4]http://sci.esa.int/gaia/

[5]http://www.tmt.org/

[6]http://www.gmto.org/

[7]http://www.eelt.org.uk/

[8]However, see Herdeiro & Radu (2014) for "Kerr BHs" with scalar hair after a complex, massive scalar field, minimally coupled to GR, is included (Herdeiro & Radu 2014).

PoS(AASKA14)042

test that constrains $(\alpha_{\rm NS} - \alpha_{\rm BH})$ will therefore constrain $\alpha_{\rm NS}$ directly (Damour & Esposito-Farèse 1998). The constraints from simulations of a hypothetical PSR-BH system ($M_{\rm BH} = 10\,{\rm M}_\odot$, $P_b = 5$ day and $e = 0.8$) are depicted as dashed lines in Figure 3 (Liu et al. 2014). Five years of weekly observations with the SKA will constrain $|\alpha_0|$ down to the order of $\mathscr{O}(10^{-4})$ (Liu 2012; Wex et al. 2013), improving upon the expected constraint from the GAIA satellite. Worthy to note that, unlike NS-WD binaries, these tests with PSR-BH binaries will also constrain the parameter space with $\beta_0 \sim -1$.

3.2 Equivalence-principle violation and its effects on orbital dynamics

A possible violation of the SEP has also been investigated by tracing the orbital dynamics of small-eccentricity NS-WD binaries (Damour & Schaefer 1991). The differential free fall rates of the NS and the WD in the potential of the Milky Way will induce a characteristic time evolution of the orbital eccentricity vector (Damour & Schaefer 1991). The SEP violation tends to polarise the Laplace-Runge-Lenz vector of the orbit towards the direction of the Galactic acceleration. By using statistical studies on the eccentricity distribution of NS-WD binaries with a probabilistic assumption (Wex 2000), the dimensionless SEP violation parameter (the Nordtvedt parameter), η, was constrained to a comparable magnitude to that from the tests in the Solar System (Stairs et al. 2005; Gonzalez et al. 2011; Will 2014). A direct test of SEP with binary pulsars that uses the time-variations in orbital parameters was also developed (Freire et al. 2012a). It does not rely on statistical or probabilistic assumptions.

The recently discovered triple system, PSR J0337+1715 (Ransom et al. 2014), provides an opportunity to improve the SEP test by many orders of magnitude (Freire et al. 2012a). In this system, an outer WD orbits an inner NS-WD binary in less than one year. Usually, in the tests of SEP violation, the Galactic acceleration exerted on the binary is of the order $\mathscr{O}(10^{-10}\,{\rm m\,s^{-2}})$, which is the force that would "polarise" the inner orbit in the case of SEP violation. In PSR J0337+1715, the outer WD provides a "polarising" acceleration that is more than one million times larger than the Galactic acceleration on the inner pair. As a rough estimate, we use the acceleration in Eq. (4) of Damour & Schaefer (1991), by replacing the relativistic rate of advance of periastron for the inner binary with the *orbital* angular velocity of the outer orbit (also see Eq. (8.18) in Will (1993)). Based on the current measurement precision of the orbital eccentricities in the triple system, a possible upper limit of the SEP violation parameter is estimated, $|\Delta| \lesssim 4 \times 10^{-7}$, which is 10^4 times better than the current pulsar constraint (N. Wex, private communication). Due to this pulsar's detectability with the Arecibo telescope, observations with SKA1-MID will mostly improve the SEP-violation test via the accumulation of more data[9], but the SKA2 will improve the timing precision by a factor of ten, which should improve the test by a corresponding factor.

It was estimated in Ransom et al. (2014) that there could be $\lesssim 100$ such systems with MSPs residing in the Galaxy. Since the SKA will discover almost all visible pulsars in the Galaxy (Keane et al. 2015), it is likely that it will discover other triple systems like PSR J0337+1715, and it is possible that the SKA might even discover a triple system consisting of an inner NS-WD close binary and where the outer star is another NS. Such a system could be (again) many orders of

[9] In principle, SKA1-MID is better due to less radio frequency interference (RFI), and much wider bands than that of the Arecibo telescope.

PoS(AASKA14)042

magnitude more sensitive to SEP violation effects than PSR J0337+1715. The reason is that the SEP violation effects are proportional to $(\alpha_1^{\rm inner} - \alpha_2^{\rm inner}) \cdot \alpha_3^{\rm outer}$ (Freire et al. 2012a), where $\alpha_{1,2}^{\rm inner}$ are the couplings of the inner bodies to the scalar field and $\alpha_3^{\rm outer}$ is the coupling of the outer body to the scalar field. If the outer body is a WD, then $\alpha_3^{\rm outer} \simeq \alpha_0$ (α_0 is coupling in the weak field), but if it is a NS, then $\alpha_3^{\rm outer}$ could, according to some alternative theories of gravity, be many orders of magnitude larger than α_0. For such theories, the predicted SEP violation effects would be roughly "$\alpha_{\rm NS}/\alpha_0$" times larger than their prediction for PSR J0337+1715, therefore making the system much more sensitive to the SEP violation predicted in these theories. The non-detection of SEP violation in such a system would provide a stringent constraint on alternative theories of gravity that predict such SEP violation.

3.3 Local Lorentz invariance and local position invariance of gravity

Besides the universality of the free fall, the other two aspects of the Einstein equivalence principle (Will 2014), namely local Lorentz invariance (LLI) and local position invariance (LPI) of gravity, can also be tested with pulsar timing experiments. Scenarios with LLI violation have recently raised great interests in the gravitational community, for examples, in the Einstein-æther theory and the Hořava-Lifshitz theory. Two generic frameworks for testing deviations from GR are the parametrised post-Newtonian (PPN) formalism (Will 1993, 2014) and the standard-model extension (SME) (Bailey & Kostelecký 2006), both of which contain parameters for LLI violation.

Generically, violation of LLI and LPI leads to modifications of the orbital dynamics of binary pulsars and the spin evolution of solitary pulsars in characteristic ways (Damour & Esposito-Farèse 1992; Bailey & Kostelecký 2006; Wex & Kramer 2007; Shao & Wex 2012; Shao et al. 2013; Shao 2014; Shao & Wex 2013). The LLI-violating modifications of the orbital dynamics of a binary pulsar introduce time-variations in the orbital eccentricity and orbital inclination, plus an extra contribution to the periastron advance rate, thus resulting in changes in the PK parameters, $\dot{e}$, $\dot{x}$, and $\dot{\omega}$ (Damour & Esposito-Farèse 1992; Bailey & Kostelecký 2006; Shao & Wex 2012; Shao 2014). The violation of LLI also leads to spin precession of a solitary pulsar with respect to a fixed direction[10] (Shao et al. 2013; Shao 2014), while the violation of LPI leads to spin precession of a solitary pulsar around its "absolute" acceleration towards the Galactic centre (Shao & Wex 2013). They both change our view on the emission region of a pulsar, and result in characteristic changes versus time in the pulse profiles. Interestingly, modifications of the orbital dynamics and spin evolution are related and controlled by one set of parameters in both PPN and SME frameworks. These modifications can be jointly constrained and cross-checked. The current best constraints on the LLI of gravity and LPI of gravity are from pulsar experiments (Stairs et al. 2005; Shao & Wex 2012; Shao et al. 2013; Shao & Wex 2013; Shao 2014). It was shown that these constraints are proportional to the timing precision of binary pulsars. With the SKA, tests will be improved dramatically with better sensitivities. Simulations show that, if the signal to noise ratio of pulse profiles improves by a factor of 10 with the SKA, then the limits on Lorentz-violating parameters improve the same factor over the current best ones with solely 10-year observations (say, from 2020 to 2030). The acquisition of one stable profile biweekly is assumed for two MSPs in Shao et al.

[10] If there exists a preferred frame, the fixed direction will be the direction of the "absolute" velocity of the binary with respect to this preferred frame.

PoS(AASKA14)042

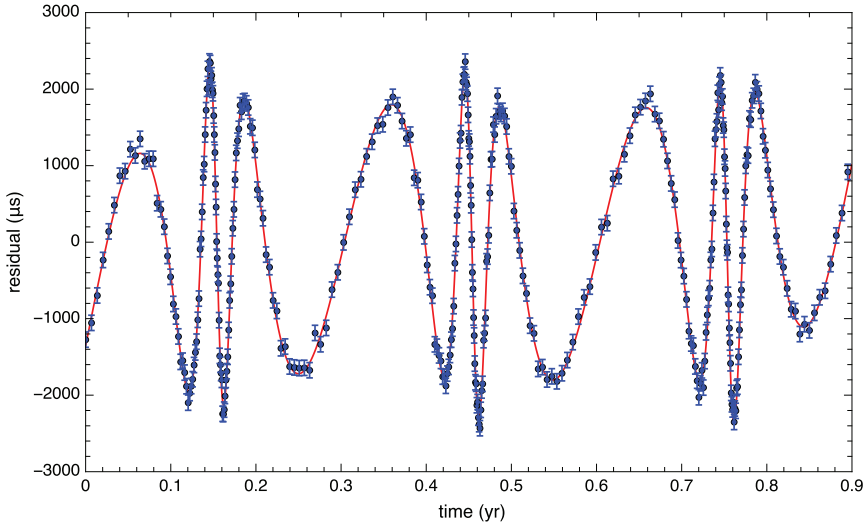

Figure 4: Characteristic pulsar timing residuals caused by the quadrupole moment of Sgr A* BH from simulated TOAs for three orbital phases (Liu et al. 2012) (figure courtesy of N. Wex). The orbital period is assumed to be $P_b = 0.3$ yr and the eccentricity $e = 0.5$. The red line is the fitted model.

(2013). If these SKA observations are properly combined with the 20-year pre-SKA observations (say, from 2000 to 2020), the improvement will be a factor of ~ 50. In addition, new stable MSPs from the Galactic census will be very helpful in breaking the degeneracies of parameters in the test, due to the vectorial and/or tensorial field condensations in the spacetime with such violations (Shao 2014).

4. Pulsar – Black Hole Binaries

BHs are predicted to be the ultimate outcome of massive stars in the theory of GR. Evidence for the existence of BHs in various astrophysical environments has accumulated during the past few decades, and is now rather robust (Narayan & McClintock 2013). However, such observations are still indirect, and no high-precision tests of BHs are yet possible. Testing BH physics is a fantastic and intriguing goal in the fields of astronomy and physics. The goal of precision tests of properties of BHs will be achieved with the SKA (Kramer et al. 2004).

The combination of the sensitivity and the large field of view of the SKA will inevitably multiply the number of pulsars by tens to hundreds, making detection of rare objects like PSR-BH binaries possible. The shorter integration time in pulsar search (say, a 10-min integration as proposed) will be beneficial to discoveries of extremely relativistic binaries. A relativistic PSR-BH system in a clean environment represents a "holy grail" of pulsar astronomy. A vast unexplored parameter space in terms of gravitational potential, spacetime curvature and object compactness will then become accessible (see Figure 1). Pulsar – stellar-mass BH binaries, pulsar – intermediate-mass BH binaries, and pulsars orbiting the Sgr A* BH probe different new regimes of gravity where no other gravity experiments are yet able to be performed with precision tests (Wex & Kopeikin 1999; Pfahl & Loeb 2004). The pulsar – stellar-mass BH binary may naturally come from a primary binary composed of a $> 20\,M_\odot$ massive star and another $> 8\,M_\odot$ star, where the former ends

PoS(AASKA14)042

up as a BH and the latter ends up as a NS. The pulsar – intermediate-mass BH binaries may exist in the centre of some globular clusters (Clausen et al. 2014; Hessels et al. 2015). Given the dense environment in the Galactic centre, there may be numerous NSs orbiting the Sgr A* BH, some of which may be detected as radio pulsars (Pfahl & Loeb 2004). However, no pulsars close enough to Sgr A* BH for gravity tests have been detected yet. Recently, a magnetar was detected through X-ray (Mori et al. 2013; Kennea et al. 2013) and radio (Eatough et al. 2013) observations, however, it is not close enough to the Sgr A* BH for precision tests of gravity (Eatough et al. 2013, 2015). Because of scattering by the interstellar medium, in general we will need the SKA2 to detect these pulsars in the Galactic centre (Wharton et al. 2012; Wex et al. 2013; Eatough et al. 2015), although this will depend on which bands are included in SKA1-MID, for example, the inclusion of Band 5 will greatly enhance the prospects for doing this. For detecting the other two types of PSR-BH binaries, the SKA1 will start to contribute significantly.

In the case of relativistic PSR-BH binaries, the prominent effects from gravitation will, on one hand, reinforce better measurements of existing tests such as the Shapiro delay and the gravitational wave damping, and on the other hand, enable completely new tests of the "cosmic censorship conjecture" and the "no-hair theorem" (Damour & Esposito-Farèse 1998; Wex & Kopeikin 1999; Liu et al. 2012, 2014). The "cosmic censorship conjecture" states that for a realistic BH, there always exists an event horizon which prevents us from looking into its central singularity, thus preserving classical predictability in a spacetime. It imposes a maximum spin, $S_{\rm max} = GM^2/c$, on a rotating BH with a given mass M. The dimensionless spin of a BH, $\chi \equiv cS/GM^2$, should always satisfy the constraint $\chi \leq 1$ (Misner et al. 1973). In alternative gravitational theories, this bound may be slightly violated, as in the Einstein-Gauss-Bonnet theory, where, besides the Einstein-Hilbert term, the Gauss-Bonnet topological term is included in the Lagrangian of gravity (Kleihaus et al. 2011). The "no-hair theorem" states the uniqueness of a Kerr BH after it settles down. It relates the higher-order moments of a BH exclusively to its mass and spin. For example, if the "no-hair theorem" is valid, the dimensionless quadrupole of a BH, $q \equiv c^4 Q/G^2M^3$ where Q is the quadrupole moment of BH, should satisfy $q = -\chi^2$ (Misner et al. 1973). If a complex, massive scalar field, minimally coupled to GR, is introduced, then the "no-hair theorem" could be violated (Herdeiro & Radu 2014).

For a relativistic PSR – Sgr A* BH system, the pulsar can be treated as a test particle in the first-order approximation (Hackmann & Lämmerzahl 2008, 2012). The strategy of performing the tests of the "cosmic censorship conjecture" and the "no-hair theorem" was investigated in Liu et al. (2012). First of all, as usual in pulsar timing, we can estimate the mass of the Sgr A* BH through the measurement of the periastron advance rate. After that, a better mass determination and the geometry information can be obtained with the detection of the Shapiro delay and the Einstein delay. With the help of the frame-dragging effects (see section 2), the spin-orbit coupling then allows an initial extraction of an upper limit of the spin magnitude of the Sgr A* BH. Thus an initial test of the "cosmic censorship conjecture" becomes available by looking at the magnitude of χ. This may enable us to look into the bizarre possibility of Sgr A* BH being a boson star (Kleihaus et al. 2012). With a better determination of the Sgr A* BH mass, the separation of the impact on the periastron advance from the BH spin is made plausible. This further determines the 3-dimensional spin of the BH with magnitude and direction. An extraction of the periodic effects of the quadrupole from timing residuals will then allow a quantitative test of the "no-hair theorem".

PoS(AASKA14)042

The timing residual from the quadrupole of Sgr A* BH has a characteristic shape, as illustrated in Figure 4 for a hypothetical system with an orbital period $P_b \simeq 0.3$ yr and an eccentricity $e \simeq 0.5$ (Liu et al. 2012). According to simulations for an orbit with a period of several months, the spin and the quadrupole can be measured with precisions of $\sim 0.1\%$ and $\sim 1\%$ respectively after five years of observations with the SKA. Therefore, the test of the "no-hair theorem" can be performed at the $\sim 1\%$ level by then (Liu et al. 2012).

Similarly, in the cases of stellar-mass BH and intermediate-mass BH binaries, the spin information of the BH can be extracted with the help of frame dragging as well if the orbit is tight enough (Wex & Kopeikin 1999). For the stellar-mass BH companion, a relativistic binary can provide much better constraints on the scalar-tensor theories than the tests with gravitational waves from inspiralling binaries (Damour & Esposito-Farèse 1998). These constraints will also be an order of magnitude better than the expected near-future constraint from the GAIA satellite when β_0 is negative or small; see Figure 3 for results from a simulated PSR-BH system (Liu et al. 2014).

5. Conclusion and Outlook

By the 2020s, radio astronomy will undergo a revolution brought by the onset of the SKA1. Its pulsar survey will deliver a large population of pulsars, among which there will be ~ 1800 MSPs. The most stable ones of them will be used to perform a number of precision gravity tests. The improvement in the sensitivity of the timing precision allows us a closer look at many aspects of the foundation of gravity. In the era of the SKA, the existing tests will be pushed to new extremes, and completely new tests will also be made possible with systems including NS-NS binaries, NS-WD binaries and NS-BH binaries. Advances from the theoretical side will also contribute to the area of experimental gravity with novel tests. It is indeed a virtue of nature that pulsar binaries of different types are equipped with different characteristics to perform different tests with. For example, the NS-NS systems provide extremely precise tests of GR, in particular periodic, non-dissipative effects in orbital dynamics (*e.g.* with the Einstein delay and general-relativistic orbital deformation), while the NS-WD and NS-BH systems are suitable to study the dissipative radiative property of gravity in the presence of asymmetry in gravitational binding energy (*e.g.* tests of the gravitational dipole radiation and the constancy of the gravitational constant). Furthermore, PSR-BH binaries will be useful to test the BH physics (*e.g.* the "cosmic censorship conjecture" and the "no-hair" theorem). Tests of gravitational theories from many facets in the era of the SKA will profoundly advance our understandings of fundamental physics.

The output of gravity tests with pulsars has two possibilities. In the first possibility, GR is falsified. This will certainly provide an important hint for our further understanding of the fundamental interaction, gravity, and the nature of spacetime. In the second possibility, GR is confirmed to new precision with flying colours. This will further reinforce our confidence in using GR as a tool to investigate other phenomena, for example, using GR effects to make mass measurements of binary pulsars, helping to deepen our understandings of non-perturbative QCD effects (Watts et al. 2015). It also casts experimental constraints on constructing new gravitational theories in relevant areas, for example, to explain the nature of dark matter and dark energy. In both cases, tests of gravitational theories with great precision will provide important clues to reconcile GR and quantum principles.

PoS(AASKA14)042

As a final remark, with the better timing capability and new discoveries of stable pulsars from the SKA, the pulsar timing array (PTA) projects will leap towards a new era as well. Complementary to the strong-field tests discussed here, PTAs make tests of gravitational theories with gravitational waves in the radiative regime available (Janssen et al. 2015).

Acknowledgement

We thank Norbert Wex for kindly providing figures and carefully reading the manuscript.

References

Antoniadis, J., Freire, P. C. C., Wex, N., et al. 2013, Science, 340, 448
Antoniadis, J., van Kerkwijk, M. H., Koester, D., et al. 2012, MNRAS, 423, 3316
Bailey, Q. G. & Kostelecký, V. A. 2006, Phys. Rev. D, 74, 045001
Barker, B. M. & O'Connell, R. F. 1975, Phys. Rev. D, 12, 329
Bekenstein, J. D. 2004, Phys. Rev. D, 70, 083509
Bertotti, B., Iess, L., & Tortora, P. 2003, Nature, 425, 374
Brans, C. & Dicke, R. H. 1961, Physical Review, 124, 925
Breton, R. P., Kaspi, V. M., Kramer, M., et al. 2008, Science, 321, 104
Burgay, M., D'Amico, N., Possenti, A., et al. 2003, Nature, 426, 531
Capozziello, S. & de Laurentis, M. 2011, Phys. Rep., 509, 167
Clausen, D., Sigurdsson, S., & Chernoff, D. F. 2014, MNRAS, 442, 207
Damour, T. 1987, The problem of motion in Newtonian and Einsteinian gravity., ed. S. W. Hawking & W. Israel, 128–198
Damour, T. & Deruelle, N. 1986, Ann. Inst. Henri Poincaré Phys. Théor., 44, 263
Damour, T. & Esposito-Farèse, G. 1992, Classical and Quantum Gravity, 9, 2093
—. 1992, Phys. Rev. D, 46, 4128
—. 1993, Physical Review Letters, 70, 2220
—. 1996, Phys. Rev. D, 54, 1474
—. 1998, Phys. Rev. D, 58, 042001
Damour, T., Gibbons, G. W., & Taylor, J. H. 1988, Physical Review Letters, 61, 1151
Damour, T. & Schaefer, G. 1991, Physical Review Letters, 66, 2549
—. 1988, Nuovo Cimento B, 101, 127
Damour, T. & Taylor, J. H. 1992, Phys. Rev. D, 45, 1840
Deller, A. T., Bailes, M., & Tingay, S. J. 2009, Science, 323, 1327
Deller, A. T., Boyles, J., Lorimer, D. R., et al. 2013, ApJ, 770, 145
Deller, A. T., Verbiest, J. P. W., Tingay, S. J., & Bailes, M. 2008, ApJL, 685, L67
Eatough, R. P., Falcke, H., Karuppusamy, R., et al. 2013, Nature, 501, 391
Eatough, R. P., Lazio, T. J. W., Casanellas, J., et al., 2015, "Observing Radio Pulsars in the Galactic Centre with the Square Kilometre Array", in proc. *Advancing Astrophysics with the Square Kilometre Array*, PoS(AASKA14)045
Edwards, R. T., Hobbs, G. B., & Manchester, R. N. 2006, MNRAS, 372, 1549
Ferdman, R. D., Stairs, I. H., Kramer, M., et al. 2013, ApJ, 767, 85

PoS(AASKA14)042

Fierz, M. 1956, Helv. Phys. Acta, 29, 128
Fonseca, E., Stairs, I. H., & Thorsett, S. E. 2014, ApJ, 787, 82
Freire, P. C. C., Kramer, M., & Wex, N. 2012a, Classical and Quantum Gravity, 29, 184007
Freire, P. C. C., Wex, N., Esposito-Farèse, G., et al. 2012b, MNRAS, 423, 3328
Gonzalez, M. E., Stairs, I. H., Ferdman, R. D., et al. 2011, ApJ, 743, 102
Hackmann, E. & Lämmerzahl, C. 2008, Physical Review Letters, 100, 171101
—. 2012, Phys. Rev. D, 85, 044049
Herdeiro, C. A. R. & Radu, E. 2014, Physical Review Letters, 112, 221101
Hessels, J. W. T., Possenti, A., Bailes, M., et al., 2015, "Pulsars in Globular Clusters with the SKA", in proc. *Advancing Astrophysics with the Square Kilometre Array*, PoS(AASKA14)047
Hulse, R. A. & Taylor, J. H. 1975, ApJL, 195, L51
Janssen, G. H., Hobbs, G., McLaughlin, M., et al., 2015, "Gravitational wave astronomy with the SKA", in proc. *Advancing Astrophysics with the Square Kilometre Array*, PoS(AASKA14)037
Jordan, P. 1959, Zeitschrift fur Physik, 157, 112
Keane, E. F., Bhattacharyya, B., Kramer, M., et al., 2015, "A Cosmic Census of Radio Pulsars with the SKA", in proc. *Advancing Astrophysics with the Square Kilometre Array*, PoS(AASKA14)040
Kennea, J. A., Burrows, D. N., Kouveliotou, C., et al. 2013, ApJL, 770, L24
Kleihaus, B., Kunz, J., & Radu, E. 2011, Physical Review Letters, 106, 151104
Kleihaus, B., Kunz, J., & Schneider, S. 2012, Phys. Rev. D, 85, 024045
Kramer, M. 1998, ApJ, 509, 856
Kramer, M., Backer, D. C., Cordes, J. M., et al. 2004, New Astron. Rev., 48, 993
Kramer, M., Stairs, I. H., Manchester, R. N., et al. 2006, Science, 314, 97
Kramer, M. & Wex, N. 2009, Classical and Quantum Gravity, 26, 073001
Lattimer, J. M. & Schutz, B. F. 2005, ApJ, 629, 979
Lazaridis, K., Wex, N., Jessner, A., et al. 2009, MNRAS, 400, 805
Liu, K. 2012, PhD thesis (The University of Manchester)
Liu, K., Eatough, R. P., Wex, N., & Kramer, M. 2014, MNRAS, 445, 3115
Liu, K., Wex, N., Kramer, M., Cordes, J. M., & Lazio, T. J. W. 2012, ApJ, 747, 1
Lorimer, D. R. & Kramer, M. 2004, Handbook of Pulsar Astronomy (Cambridge University Press)
Lorimer, D. R., Stairs, I. H., Freire, P. C. C., et al. 2006, ApJ, 640, 428
Lyne, A. G., Burgay, M., Kramer, M., et al. 2004, Science, 303, 1153
Manchester, R. N., Kramer, M., Stairs, I. H., et al. 2010, ApJ, 710, 1694
Misner, C. W., Thorne, K. S., & Wheeler, J. A. 1973, Gravitation (San Francisco: W. H. Freeman and Company)
Mori, K., Gotthelf, E. V., Zhang, S., et al. 2013, ApJL, 770, L23
Narayan, R. & McClintock, J. E. 2013, ArXiv e-prints, arXiv:1312.6698
O'Connell, R. F. 2004, Physical Review Letters, 93, 081103
Paragi, Z., Godfrey, L., Reynolds, C., et al., 2015, "Very Long Baseline Interferometry with the SKA", in proc. *Advancing Astrophysics with the Square Kilometre Array*, PoS(AASKA14)143
Perera, B. B. P., McLaughlin, M. A., Kramer, M., et al. 2010, ApJ, 721, 1193
Pfahl, E. & Loeb, A. 2004, ApJ, 615, 253
Psaltis, D. 2008, Living Reviews in Relativity, 11, 9

PoS(AASKA14)042

Ransom, S. M., Stairs, I. H., Archibald, A. M., et al. 2014, Nature, 505, 520
Shao, L. 2014, Physical Review Letters, 112, 111103
Shao, L., Caballero, R. N., Kramer, M., et al. 2013, Classical and Quantum Gravity, 30, 165019
Shao, L. & Wex, N. 2012, Classical and Quantum Gravity, 29, 215018
—. 2013, Classical and Quantum Gravity, 30, 165020
Stairs, I. H. 2003, Living Reviews in Relativity, 6, 5
Stairs, I. H., Faulkner, A. J., Lyne, A. G., et al. 2005, ApJ, 632, 1060
Stairs, I. H., Thorsett, S. E., & Arzoumanian, Z. 2004, Physical Review Letters, 93, 141101
Taylor, J. H., Fowler, L. A., & McCulloch, P. M. 1979, Nature, 277, 437
Taylor, J. H. & Weisberg, J. M. 1982, ApJ, 253, 908
Verbiest, J. P. W., Bailes, M., van Straten, W., et al. 2008, ApJ, 679, 675
Watts, A. L., Xu, R., Espinoza, C., et al., 2015, "Probing the neutron star interior and the Equation of State of cold dense matter with the SKA", in proc. *Advancing Astrophysics with the Square Kilometre Array*, PoS(AASKA14)043
Weisberg, J. M., Nice, D. J., & Taylor, J. H. 2010, ApJ, 722, 1030
Weisberg, J. M., Romani, R. W., & Taylor, J. H. 1989, ApJ, 347, 1030
Weisberg, J. M. & Taylor, J. H. 1981, General Relativity and Gravitation, 13, 1
Wex, N. 2000, in Astronomical Society of the Pacific Conference Series, Vol. 202, IAU Colloq. 177: Pulsar Astronomy – 2000 and Beyond, ed. M. Kramer, N. Wex, & R. Wielebinski, 113
—. 2014, ArXiv e-prints, arXiv:1402.5594
Wex, N. & Kopeikin, S. M. 1999, ApJ, 514, 388
Wex, N. & Kramer, M. 2007, MNRAS, 380, 455
Wex, N., Liu, K., Eatough, R. P., et al. 2013, in IAU Symposium, Vol. 291, IAU Symposium, ed. J. van Leeuwen, 171–176
Wharton, R. S., Chatterjee, S., Cordes, J. M., Deneva, J. S., & Lazio, T. J. W. 2012, ApJ, 753, 108
Will, C. M. 1993, Theory and Experiment in Gravitational Physics (Cambridge University Press)
—. 2014, Living Reviews in Relativity, 17, 4

PoS(AASKA14)042

PROCEEDINGS OF SCIENCE

Probing the neutron star interior and the Equation of State of cold dense matter with the SKA

Anna Watts[*1], **Renxin Xu**[2], **Cristóbal Espinoza**[3], **Nils Andersson**[4], **John Antoniadis**[5], **Danai Antonopoulou**[1], **Sarah Buchner**[7], **Shi Dai**[8], **Paul Demorest**[9], **Paulo Freire**[6], **Jason Hessels**[1,10], **Jérôme Margueron**[11], **Micaela Oertel**[12], **Alessandro Patruno**[13,10], **Andrea Possenti**[14], **Scott Ransom**[9], **Ingrid Stairs**[15], **Ben Stappers**[16]

[1] *University of Amsterdam;* [2] *KIAA Peking University;* [3] *PUC, Chile;* [4] *University of Southampton;* [5] *University of Toronto* [6] *Max Planck Institute for Radio Astronomy;* [7] *HRAO, University of Witwatersrand;* [8] *ATNF;* [9] *NRAO Charlottesville;* [10] *ASTRON;* [11] *IPNL, CNRS/IN2P3, Université Lyon;* [12] *LUTH, CNRS, Observatoire de Paris, Université Paris Diderot;* [13] *Leiden University;* [14] *INAF-Osservatorio Astronomico di Cagliari;* [15] *University of British Columbia;* [16] *University of Manchester.*

E-mail: A.L.Watts@uva.nl

With an average density higher than the nuclear density, neutron stars (NS) provide a unique test-ground for nuclear physics, quantum chromodynamics (QCD), and nuclear superfluidity. Determination of the fundamental interactions that govern matter under such extreme conditions is one of the major unsolved problems of modern physics, and – since it is impossible to replicate these conditions on Earth – a major scientific motivation for SKA. The most stringent observational constraints come from measurements of NS bulk properties: each model for the microscopic behaviour of matter predicts a specific density-pressure relation (its 'Equation of state', EOS). This generates a unique mass-radius relation which predicts a characteristic radius for a large range of masses and a maximum mass above which NS collapse to black holes. It also uniquely predicts other bulk quantities, like maximum spin frequency and moment of inertia. The SKA, in Phase 2 and particularly in Phase 2 will, thanks to the exquisite timing precision enabled by its raw sensitivity, and surveys that dramatically increase the number of sources: 1) Provide many more precise NS mass measurements (high mass NS measurements are particularly important for ruling out EOS models); 2) Allow the measurement of the NS moment of inertia in highly relativistic binaries such as the Double Pulsar; 3) Greatly increase the number of fast-spinning NS, with the potential discovery of spin frequencies above those allowed by some EOS models; 4) Improve our knowledge of new classes of binary pulsars such as black widows and redbacks (which may be massive as a class) through sensitive broad-band radio observations; and 5) Improve our understanding of dense matter superfluidity and the state of matter in the interior through the study of rotational glitches, provided that an ad-hoc campaign is developed.

Advancing Astrophysics with the Square Kilometer Array
June 8-13, 2014
Giardini Naxos, Italy

[*] Speaker.

PoS(AASKA14)043

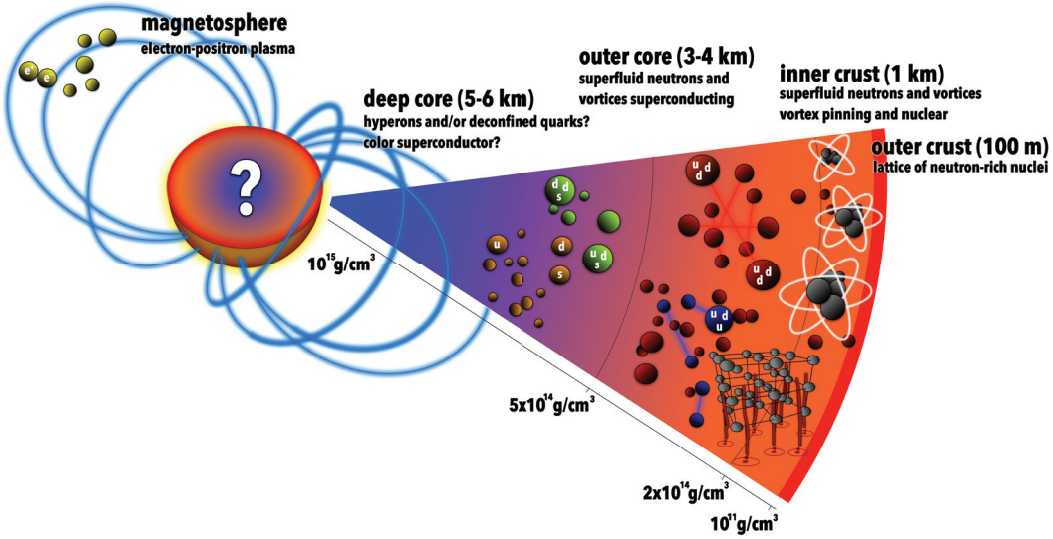

Figure 1: Schematic structure of a NS. The outer layer is a solid ionic crust supported by electron degeneracy pressure. Neutrons begin to leak out of nuclei at densities $\sim 4 \times 10^{11}$ g/cm^3 (the neutron drip line, which separates inner and outer crust), where neutron degeneracy also starts to play a role. At densities $\sim 2 \times 10^{14}$ g/cm^3, the crust-core boundary, nuclei dissolve completely. In the core, densities may reach up to ten times the nuclear saturation density $\rho_{\rm sat} = 2.8 \times 10^{14}$ g/cm^3 (the density in normal atomic nuclei).

1. Introduction

Neutron stars (NS) are the densest objects in the Universe. Composition evolves from ions embedded in a sea of degenerate electrons (and eventually neutrons) in the solid crust, through the crust-core transition where nuclei dissolve to form neutron-rich nucleonic matter, to the supranuclear densities of the core, where theory suggests the presence of exotic non-nucleonic matter (Figure 1). The nature of matter in such extreme conditions is one of the great unsolved problems in modern science, making NS unparalleled laboratories for nuclear physics and quantum chromodynamics (QCD). NS also host super-strong internal magnetic fields, and share the rich phenomenology of low-temperature physics. Although born in the hot furnace of a supernova collapse, NS cool rapidly to temperatures far below the relevant Fermi temperature. When matter cools there are two options: it can freeze to form a solid, or become superfluid (or superconducting if there are free charge carriers involved). NS are expected to exhibit both these phases. The outer kilometre or so of the star forms a solid crustal lattice of increasingly neutron-rich nuclei, while the star's core hosts a neutron superfluid coupled to a proton superconductor and a free gas of electrons (as required to make the conglomerate charge neutral). The free neutrons permeating the crustal lattice in the inner crust are also expected to be superfluid.

The most fundamental macroscopic diagnostic of dense matter interactions is the pressure-density-temperature relation of bulk matter, the equation of state (EOS). The EOS can be used to infer key aspects of the microphysics, such as the nature of the three-nucleon interaction or the presence of free quarks at high densities. Determining the EOS of supranuclear density matter is therefore of major importance to fundamental physics. However it is also critical to astrophysics, to understand not only NS but also NS/NS and NS/Black Hole (BH) mergers, prime sources of grav-

PoS(AASKA14)043

itational waves and the likely engines of short gamma-ray bursts (Bauswein et al. 2012; Lackey et al. 2012). The EOS affects merger dynamics, BH formation timescales, the precise gravitational wave and neutrino signals, any associated mass loss and r-process nucleosynthesis, and the attendant gamma-ray bursts and optical flashes (Metzger et al. 2010; Hotokezaka et al. 2011). The cold EOS probed with NS, and the way it joins up with the hot EOS that determines explosion conditions (Janka et al. 2007), are also vital to understanding the late stages of core collapse supernovae, including their gravitational wave signal.

1.1 Unknowns in dense matter physics

The properties of NS, like those of atomic nuclei, depend crucially on the interactions between protons and neutrons (nucleons), which are a starting point for ab-initio calculations of the nuclear many-body problem. While two-body interactions are well constrained by experiment, three- and more-body forces are a frontier in nuclear physics. At low energies, effective field theories based on QCD symmetries provide a systematic expansion of nuclear forces, which predict two- and more-nucleon interactions. There are also complementary efforts using lattice approaches to nuclear forces to provide few-body nucleon-nucleon and more generally baryon-baryon interactions, but this approach is still affected by large uncertainties. Some of the predictions of these models can be tested against current nuclear data; where data are not yet available, predictions are based on the consistency of the approach. The appearance of shell closure in neutron-rich isotopes, as well as the position of the neutron drip-line is found to be very sensitive to the three-body forces. Exotic neutron-rich nuclei, the focus of present and upcoming laboratory experiments, also provide interesting constraints on effective interactions for many-body systems.

NS observations, by contrast, challenge many-nucleon interactions at extremes of density, neutron richness, and baryonic content. Astrophysical inputs are essential to make progress (Figure 2), although extracting information from the data is harder than for lab experiments. Current approximate models all have major uncertainties, both at high density and for neutron-rich matter (Wiringa et al. 1995; Pieper et al. 2001; Stone & Reinhard 2007; Hebeler & Schwenk 2010; Steiner & Gandolfi 2012). Although experimental information on matter near the nuclear saturation density is plentiful, there are only a few experimental constraints at high densities and/or for neutron-rich matter (Tsang et al. 2009; Kortelainen et al. 2010; Roca-Maza et al. 2011; Piekarewicz et al. 2012). NS thus provide a unique environment to test models.

At the very highest densities reached in NS cores, we also expect transitions to non-nucleonic states of matter (Glendenning 2000). Some of the most exciting possibilities involve strange quarks: unlike heavy ion collision experiments, which always produce very short-lived and hot, dense states, the stable gravitationally confined environment of a NS permits slow-acting weak interactions that can form matter with a high net strangeness. Possibilities include the formation of hyperons (strange baryons), free quarks (forming a hybrid star), or color-superconducting states (Alford et al. 2008). It is even possible that the entire star converts into a lower energy self-bound state consisting of up, down and strange quarks, known as a strange quark star (Witten 1984; Weber 2005), possibly in a solid state (Xu 2003). Other states that have been hypothesized include Bose-Einstein condensates of mesons (pions or kaons, the latter containing a strange quark) and Δ baryons (resonant states). The densities at which such phases would appear, and the degree to which they might co-exist with other phases, are highly uncertain.

PoS(AASKA14)043

In principle, all these phases are governed by the strong force. First principle calculations of the interactions for many-body QCD systems are however presently unfeasible due to the fermion sign problem. Because fermion wave functions change sign upon exchange of particles, computing the expected energy of a system involves the addition of a large number of terms with alternating signs. This is especially problematic at high density, and it is at present impossible to obtain direct predictions for strongly interacting quark matter. Instead one has to resort to phenomenological models. This is particularly true for hadronic many-body systems, since a single hadron is already a complex many-body QCD system. Here, the different models are all based on hadronic interactions. For the non-nucleonic degrees of freedom such as hyperons, experimental information is scarce and uncertainties even larger than for purely nuclear systems. Lattice approaches and effective field theory expansion could help in the future to improve the starting point of ab-initio hadronic many-body calculations with these degrees of freedom. Planned laboratory experiments on hypernuclei (nuclei containing at least one hyperon) will also give additional constraints.

Figure 2 compares the parameter space that can be accessed within the laboratory to that explored with NS. While the two are complementary, it is obvious that NS provide a truly unique exploration space. In addition to the high densities, the gravitational confinement in NS renders them sufficiently long-lived such that weak beta equilibrium is achieved and as far as the EOS is concerned, NS can be considered as cold. Thus, neither the neutron rich ground state of beta equilibrated ultra-dense nuclear matter nor the exotic non-nucleonic states of matter described in the previous paragraph can be reached in the laboratory.

1.2 Unknowns in dense matter superfluidity

The presence of superfluid components has significant effects on the star's long term evolution and dynamics. Superfluidity suppresses the nuclear reactions that lead to cooling, but also leads to new neutrino emission channels. The suggestion of rapid cooling of the young NS in the Cassiopeia A supernova remnant (Page et al. 2011; Shternin et al. 2011) has stimulated a detailed discussion of the impact on superfluid parameters. If confirmed, such a fast cooling epoch would constrain the critical temperature at which the neutrons in the core become superfluid. At the same time, the effect requires the onset of proton superconductivity to have taken place much earlier. In pulsar timing, superfluidity is thought to be associated with the observed restlessness, ranging from the enigmatic glitches seen in young pulsars to the timing noise that appears to be generic in all systems. A superfluid rotates by forming an array of quantised vortices (Figure 1). The motion of these tiny tornadoes determines the star's spindown behaviour, e.g. whether it proceeds smoothly or in an erratic fashion.

Key issues involve the friction experienced by the vortices and whether or not they are pinned to some other component in the system. Current models suggest that the most important source of friction is electron scattering off of magnetic fields associated with the vortices (Alpar et al. 1984; Mendell 1991; Andersson et al. 2006). The outcome depends to a large extent on the so-called entrainment. This is a non-dissipative effect that determines the dynamical effective mass of the particles involved, effectively encoding how mobile the superfluid component is. In the core of the star, the entrainment arises due to the strong interaction (Alpar et al. 1984; Borumand et al. 1996), while in the inner crust it is due to Bragg scattering off of the nuclear lattice (Chamel 2006). The interaction between magnetised vortices and the much more plentiful fluxtubes associated with the

PoS(AASKA14)043

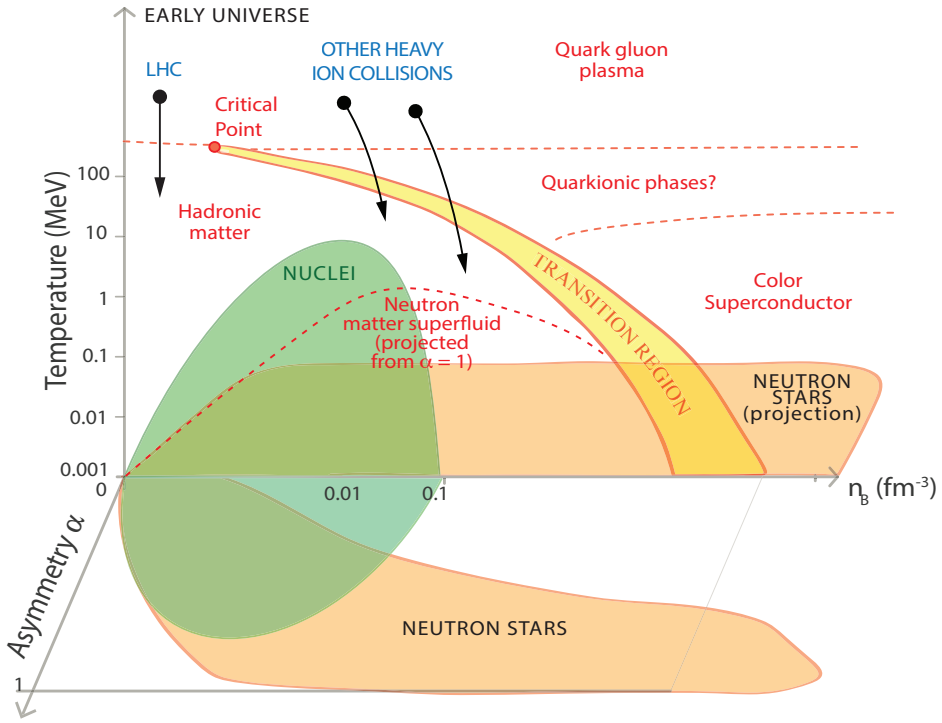

Figure 2: The parameter space and the states of matter accessed by NS, as compared to laboratory experiments on Earth. The figure shows temperature T against baryon number density n_B against asymmetry $\alpha = 1 - 2Y_q$, where Y_q is the hadronic charge fraction (in general number of protons/number of baryons). $\alpha = 0$ for matter with equal numbers of neutrons and protons, and $\alpha = 1$ for pure neutron matter. Green region: Isolated nuclei up to $\alpha \approx 0.3$, above this one would find a mix of nuclei and light particles.

proton superconductor (e.g. the star's bulk magnetic field) may also be dissipative (Link 2003). In some regimes it may even cause pinning, which would link the star's spin evolution to changes in the magnetic field. In the star's crust, vortices are expect to pin to (or between) the lattice nuclei. As outlined below, precision timing provides a unique probe of the parameters associated with these phenomena, going far beyond the current constraint on the critical temperature from cooling data and the ballpark superfluid moment of inertia from glitch observations.

In the absence of friction and pinning, the neutron superfluid would be more or less decoupled from the charged components in the star. This would have a major effect on the moment of inertia associated with the spindown, and could in fact lead to a complicated evolution of the braking index as the star cools and the superfluid region grows (Ho & Andersson 2012). On the other hand, vortex pinning is a key requirement for the "cartoon-level" explanation for glitches, where a pinned component builds up an angular momentum reservoir as the system evolves. The stored angular momentum is then released in some large scale unpinning event and the pulsar is seen to spin up. The relaxation that follows should be determined by vortex friction (Sidery et al. 2010) and the mechanism that repins the vortices to return the system to the point where it may glitch again. This is a very complicated story, and there has been precious little progress in our

PoS(AASKA14)043

theoretical understanding of the glitch phenomenon since the first observations at the end of the 1960s. However, a well-designed SKA campaign could change the situation dramatically. At the same time a concerted effort is, obviously, required on the theory side. Finally, superfluidity is also expected to have impact on possible free precession. Significant vortex pinning would, in fact, prevent slow precession (Jones & Andersson 2001; Link 2003). Instead, one would expect the precession period to be similar to the rotation period. Higher quality data may allow us to constrain — or even rule out — this possibility.

2. Methodology

2.1 Connecting observables to physics using pulsar timing

The relativistic equations of stellar structure[1] relate the EOS of dense matter, which depends on the microphysics of composition and the strong force, to macroscopic observables including the mass M and radius R of the NS. Figure 3 illustrates the relationship between the EOS and the M-R relation for different models: there is a unique map between the two (Lindblom 1992). Constraints on or measurements of M and/or R therefore limit EOS models, and hence the interior composition of NS. Ideally, we would like to use the SKA to measure M and R for many NS in order to trace out the EOS in the M-R diagram. Unfortunately, direct measurements of R in the radio are likely impossible, and even indirect measurements through estimates of the moment of inertia are, as discussed later in this chapter, incredibly difficult. However measuring *masses* is something that radio observations of pulsars, via high-precision timing measurements, can do exceedingly well, and the SKA will be a fantastic tool for this purpose.

Pulsar timing is the process of unambiguously accounting for every rotation of a NS over extended time periods (as long as decades, currently), and it provides astonishingly precise measurements of the pulsar's spin, astrometric, and (if appropriate) orbital parameters, including how each of these changes with time (Lorimer 2008). For "recycled" pulsars, most of which are in binary systems, the five Keplerian orbital parameters (orbital period P_b, projected semi-major axis $x \equiv a_1 \sin i/c$ (where i is the orbital inclination and c is the speed of light), eccentricity e, time of periastron passage T_o, and the argument of periapsis ω) are measured with typically $4-12$ significant figures, making them essentially perfectly known.

For some binary pulsars, one or more of the "post-Keplerian" (PK) timing parameters may be measurable (Shao et al. 2015). These observables (the precession of the argument of periapsis $\dot{\omega}$, the orbital period decay $\dot{P}_b$, the combination of time dilation and gravitational redshift γ, and the Shapiro delay "range" r and "shape" s) can be expressed in the framework of general relativity (GR) as functions of only physical constants (e.g. solar mass in time units $T_\odot \equiv GM_\odot/c^3 \sim 5\,\mu$s), the extremely well-measured Keplerian parameters, and the masses of the pulsar m_p and the companion star m_c. Since m_p and m_c are the only two unknowns, if two PK observables are measured, the two equations can be used to solve for m_p and m_c. Tests of GR come from measurements of additional PK parameters.

[1] The Tolman-Oppenheimer-Volkoff equations (the equation of mass continuity, force balance, and the EOS P = P(ρ) where ρ is the total density and P the pressure), modified to take into account rotation. The EOS should also include temperature: but for NS, we are so far below Fermi temperature that this can be neglected in computing bulk structure.

PoS(AASKA14)043

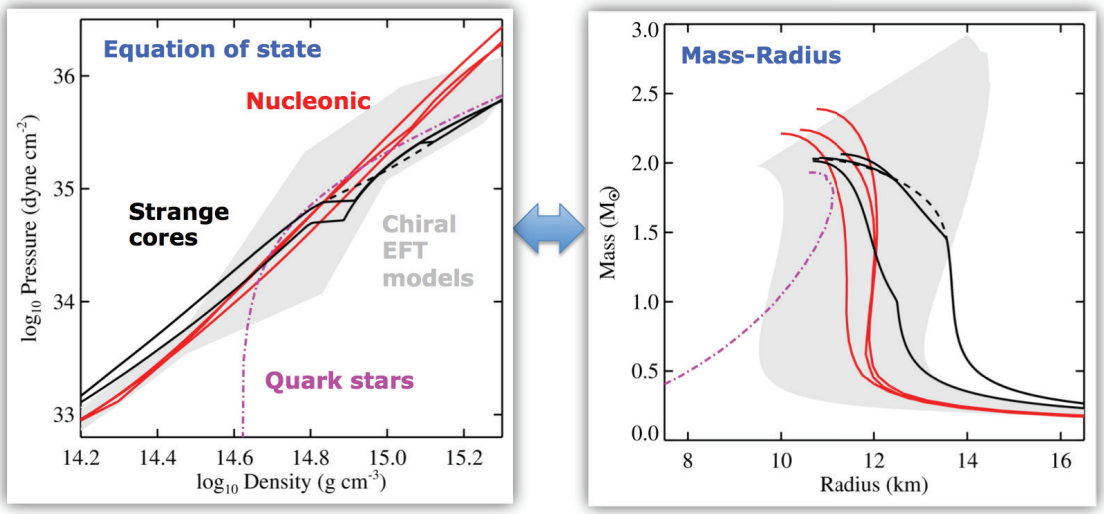

Figure 3: The link between uncertainty in fundamental nuclear physics, the EOS, and the NS M-R relation. The figure shows the pressure density relation (left) and the corresponding mass-radius relation (right) for different EOS models. Grey band: range of nucleonic EOS based on chiral effective field theory (Hebeler et al. 2013). Black solid: Hybrid EOS from Zdunik & Haensel (2013). Black dashed: Nucleon + hyperon core EOS from Bednarek et al. (2012). The other EOS are from Lattimer & Prakash (2001): Red (nucleonic); Magenta (quark stars). All models shown are compatible with the existence of 2 $M_\odot$ NS: discovery of a higher mass star would rule out the softer EOS with the lowest maximum masses.

Unfortunately, only a small fraction of binary pulsars have timing precisions, orbital parameters, or companions which allow the measurement of PK parameters. To measure $\dot{\omega}$, for instance, which by itself provides the total system mass $m_p + m_c$ and is exactly the same effect as Mercury's precession of perihelion, we need pulsars in eccentric enough orbits so that we can trace ω precisely. Most millisecond pulsars (MSPs) in the Galactic disk have extremely circular orbits and so even though their orbital parameters are measured to extraordinary precision, $\dot{\omega}$ cannot be. However, globular clusters contain many eccentric MSPs (Ransom 2008; Hessels et al. 2015) and there is evidence for a population of them in the Galactic disk as well (Champion et al. 2008; Barr et al. 2013), providing opportunities for new discoveries of eccentric systems by the SKA.

Detection of orbital period decay $\dot{P}_b$, due to the emission of gravitational radiation, demands compact systems such as the original Hulse-Taylor binary (Weisberg et al. 2010). These double NS (DNS) systems (Kramer et al. 2006; Fonseca et al. 2014) tend to be in highly eccentric orbits, which allows measurement of $\dot{\omega}$, and after enough precession has occured, γ (the requirement for measurable precession makes γ effectively impossible to measure in systems with near-circular orbits, even if they are compact and relativistic). Several compact NS—white dwarf (WD) systems have been discovered recently which allow measurement of $\dot{P}_b$ (Bhat et al. 2008; Freire et al. 2012; Antoniadis et al. 2013), implying that the SKA should find many more such systems.

The final PK parameters of interest are those making up the Shapiro delay, which is a relativistic propagation delay, typically of the order of μs, caused as the pulses travel through the gravitational potential of the companion star. The amplitude of this effect depends sensitively on the inclination angle and requires nearly edge on viewing and high timing precision to become

PoS(AASKA14)043

measurable. With huge improvements in timing precision over the last decade, as well as the discovery of many new MSPs, the number of Shapiro delay measurements has increased substantially, and that number should increase tremendously with the SKA. The first high-precision $2M_\odot$ NS was measured with this technique (Demorest et al. 2010), and that single number has provided exceptionally strong constraints on the EOS (Hebeler et al. 2013).

For non-binary slowly-spinning pulsars it is impossible to measure orbital or PK parameters, yet rapid-cadence (daily or every few days) timing observations can detect the timing "glitches" which young pulsars often exhibit (Section 3.4). These virtually instantaneous increases in the pulsar's spin rate and (sometimes) spin-down rate, and the subsequent relaxation process, probe the superfluid interiors of NS.

2.2 Importance of large surveys to sample populations

Surveys continue to be a major driver for pulsar science and its applications. By increasing the known population, we increase the number of outlier systems whose exceptional properties make them powerful physics laboratories, e.g.(Kramer et al. 2006; Ransom et al. 2014). Consider the fact that there are 2300 known radio pulsars (Manchester et al. 2005) out of an estimated total Galactic population of a few tens of thousand sources beaming towards the Earth (Keane et al. 2015). Of these known sources, fewer than 10% are in binary (or trinary) systems, a pre-requisite for precision mass measurement through either Shapiro delay or a combination of PK orbital parameters and constraints from spectroscopic modeling of the optical companion star. Unfortunately, but unsurprisingly, only a handful of systems have extreme properties that push the envelope in terms of constraining the EOS. There are only 10 radio pulsars with rotational periods less than 2ms, and only 2 NS with precision mass measurements of $M_{\rm NS} \gtrsim 2$ M$_\odot$ (Demorest et al. 2010; Antoniadis et al. 2013). Pushing to faster spin rates, which can constrain the maximum NS radius, and higher masses will require both a significant increase in the known population (a doubling or tripling) as well as careful follow-up and precision timing of the most promising discoveries.

In addition to strong constraints on the EOS from maximum masses, a much larger sample will also provide precision mass measurements across the known distribution $M_{\rm NS} \sim (1.2-2)M_\odot$ (lower mass limit from Janssen et al. (2008); Ferdman et al. (2014)). Mapping the NS mass distribution (Tauris et al. 2015) is important for understanding the *astro*physics of NS formation in core-collapse supernovae (EOS dependent) and subsequent 'recycling' in a binary system (Alpar et al. 1982). The lowest mass NS are also potentially extremely interesting. If these systems are formed by electron capture supernovae (Kitaura et al. 2006; Ferdman et al. 2014), this could place a tight constraint on the EOS in terms of the relation between gravitational and baryonic mass (Podsiadlowski et al. 2005). This idea is, however, subject to uncertainties in both the astrophysical setup (such as the progenitors), and on the nuclear physics side with respect to the nuclear reactions during the SN and the EOS used for the extraction of the masses.

SKA1-MID and SKA1-LOW will conduct both wide-field and targeted pulsar surveys. It is expected that an all-sky survey will discover ~ 10000 pulsars (Keane et al. 2015), of which ~ 1800 will be MSPs and ~ 100 DNS. Though impossible to predict precisely, $\sim 10\%$ of these should be well-suited for EOS constraints. SKA1 will also do deep targeted searches of unidentified *Fermi* γ-ray sources (Keane et al. 2015) and the Galactic globular cluster systems (Hessels et al. 2015). These searches will discover primarily MSPs, some of which will also be EOS laboratories. The

PoS(AASKA14)043

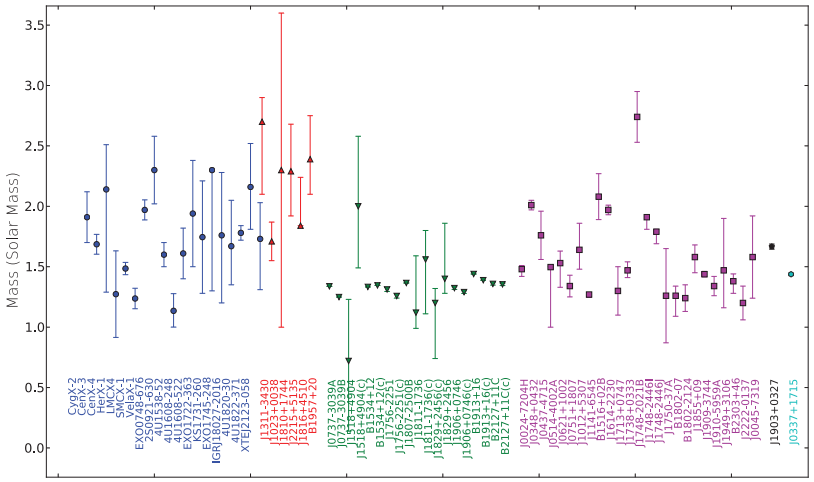

Figure 4: Current NS mass measurements, 68% confidence intervals (http://jantoniadis.wordpress.com/research/ns-masses/ for original references). Blue -LMXBs; Red - Eclipsing MSPs; Green - DNS; Magenta - NS-WD binaries; Black - MSP-Main Sequence binaries; Cyan - Triple Pulsar. Though some sources may have higher masses than PSRs J1614-2230 and J0348+0432, there are large systematic uncertainties on these measurements or other reasons why they are not as direct or reliable a measurement.

current spin record holder resides in the globular cluster Terzan 5 (Hessels et al. 2006). A significant fraction of the MSPs found in targeted searches will be in eclipsing binaries ('black widows' and 'redbacks' (Roberts 2011)), which, although more difficult to detect and time precisely, may harbour the most massive NS created by nature (van Kerkwijk et al. 2011; Romani et al. 2012) because they have accreted significant mass from their companion and/or were formed more massive.

3. State of the art (observations and theory)

3.1 State of the art: masses

A measurement of a NS mass, even without a simultaneous measurement of R, constrains the EOS if it exceeds the maximum mass predicted by a given model (Figure 3). Figure 4 shows current NS mass measurements. The two most constraining systems are PSRs J1614−2230 (Demorest et al. 2010) and J0348+0432 (Antoniadis et al. 2013), with masses of 1.97 ± 0.04 and $2.01 \pm 0.03\,M_\odot$ respectively. PSR J1614−2230 is a 3.1 ms MSP orbiting an intermediate-mass WD every 8.7 days. The system has a very high inclination (89.17°) resulting in a strong Shapiro delay signal. PSR J0348+0432 is a 39 ms pulsar in a relativistic, 2.46 h orbit with a low-mass WD. For this binary the PK parameters cannot be measured and the masses have been measured through phase-resolved optical spectroscopy of the bright WD companion.

Current knowledge of hadronic physics suggests it is nearly impossible for matter to be purely nucleonic at the expected massive NS core densities of (7-10) $\rho_{\rm sat}$. No matter what the precise composition, all alternative possibilities add additional degrees of freedom. The immediate effect is

PoS(AASKA14)043

a softening of the EOS, lowering the maximum mass, unless the interaction of the new constituents provides the necessary repulsion to counter-balance the strong gravitational force. While $2M_\odot$ NS do not directly exclude any components in the NS interior they do, however, put very stringent constraints on the respective interactions. In particular, they have triggered intensive discussions on the "hyperon puzzle": ab-initio many-body calculations predict the appearance of hyperons at 2-3 $\rho_{\rm sat}$ but the maximum masses of such models do not exceed $\sim 1.7\ M_\odot$. Proposed solutions include a very early transition to quark matter, additional repulsion in the ab-initio calculations via two- or more-body hyperonic forces and the appearance of other new particles such as Δ-baryons.

Evidence for even more massive NS has been reported for eclipsing binary pulsars with low-mass companions (van Kerkwijk et al. 2011; Romani et al. 2012). Based on optical observations of the companions, these systems seem to host NS with $M \sim 2.4M_\odot$, well above the predictions of many EOS models. However, there are fairly large systematic uncertainties associated with lightcurve modeling (which mostly impact the determination of inclination), rendering these measurements so far unreliable for EOS constraints. A significant improvement of these measurements will most likely require synergy of sensitive radio and optical observations with next-generation observatories such as SKA and E-ELT (Antoniadis et al. 2015).

3.2 State of the art: moments of inertia

Moment of inertia I is a function of M and R, so yields R if M is known independently. Current constraints on I are very approximate, and are based mostly on γ-ray flux measurements. PSR J1614$-$2230 is an especially interesting case, since its mass is well known. This pulsar was among the first MSPs detected in γ-rays (Abdo et al. 2009). Assume that the spin down luminosity $\dot{E} = 4\pi^2 I\dot{P}/P^3$ (Lorimer & Kramer 2005). Since the measured γ-ray luminosity must be $< 100\%$ of $\dot{E}$, this yields a lower limit on I. If the distance to PSR J1614$-$2230 is given by the free-electron model of the Galaxy (Cordes & Lazio 2002), this yields $I > 10^{45}\,{\rm g\,cm^2}$ (not very constraining). Distance estimates, which fix the γ-ray luminosity, are however uncertain. The distance is also necessary to evaluate kinematic contributions (which may be large) to $\dot{P}$. Detailed knowledge and modelling of the emission geometry is also necessary to estimate the real luminosity of the pulsar: the estimate above assumes isotropic emission, which is not appropriate since in this case there would be no pulsations. One advantage of this method, however, is that such lower limits on I will eventually be available for a variety of other pulsars (Guillemot et al. 2012) with a variety of masses, something that might improve its stringency.

3.3 State of the art: spin rates

During recycling, a bare non-magnetic NS could easily attain very rapid spin after accreting only $\sim 0.1M_\odot$ (Cook et al. 1994; Burderi et al. 1999)[2] . Irrespective of the proposed EOS, the spin frequency f must be lower than the Keplerian frequency f_K above which a NS, due to centrifugal forces, becomes unstable to mass shedding at its equator. To a very good approximation $f_K = C(M/M_\odot)^{1/2}(R/10{\rm km})^{-3/2}$ (Haensel et al. 2009). where M is the (gravitational) mass of the Keplerian configuration and R denotes the (circumferential) radius of the non-rotating configuration of the same gravitational mass. C is 1.08 kHz for NS and 1.12 kHz for strange stars (Haensel

[2]Although there are limiting mechanisms that might halt spin up, see Patruno & Watts (2012) for a review.

PoS(AASKA14)043

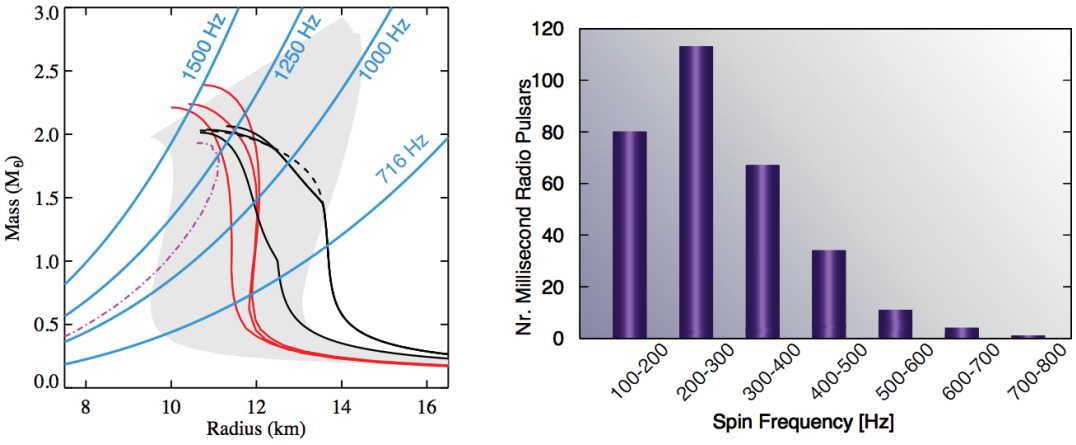

Figure 5: Left: Constraints arising from different spin rate measurements. NS of a given spin rate must lie to the left of the relevant limiting line in the M-R plane (shown in blue for various spins). EOS models as in Figure 3. The current record holder, which spins at 716 Hz (Hessels et al. 2006) is not constraining, but given a high enough spin individual EOS can be ruled out. Between 1 kHz and 1.25 kHz, for example, individual EOS in the grey band of nucleonic EOS would be excluded. Right: The spin distribution of radio MSPs with a spin frequency > 100 Hz. The spin distribution of the smaller sample of accreting NS is similar (Patruno & Watts 2012; Watts 2012).

et al. 2009), obtained from fits to general relativistic calculations of rotating stars. Since we require $f < f_K$, this results in a constraint on the radius:

$$R < 10\, C^{2/3} \left[\frac{M}{M_\odot}\right]^{1/3} \left[\frac{f}{1\ \mathrm{kHz}}\right]^{-2/3} \ \mathrm{km} \tag{3.1}$$

The more compact the star is, the higher the supported rotation rate can be, and the tighter the constraint on the EOS. Figure 5 shows the spin distribution of the known radio pulsars. The binary MSP J1748−2446ad (Hessels et al. 2006) is the NS with the shortest known rotational period, $P_{min} = 1.396$ ms, corresponding to a spin frequency of 716 Hz (the most rapidly rotating accretion-powered NS rotates at 619 Hz (Hartman et al. 2003)). The resulting constraint is shown in Figure 5: the radius of a non-rotating 1.4 $M_\odot$ star would have to be smaller than 15 km. This is not particularly constraining for current models: rotation rates faster than a millisecond are required to rule out EOS.

3.4 State of the art: glitches

The majority of the glitches known today have been detected in the data of long monitoring programs (at Jodrell Bank, Parkes and Urumqi; (Yuan et al. 2010b; Espinoza et al. 2011; Yu et al. 2013)). This is because glitches are inferred from observations before and after the glitch epoch. The most minimal characterisation of a glitch is the measurement of the step in spin frequency ($\Delta\nu$). However, many glitches also induce a change in spin-down rate ($\Delta\dot{\nu}$) and a process of relaxation towards the pre-glitch rotational values, with timescales that can go up to a few hundred days. Constraints and information on the glitch mechanism and the rotational dynamics of the neutron

PoS(AASKA14)043

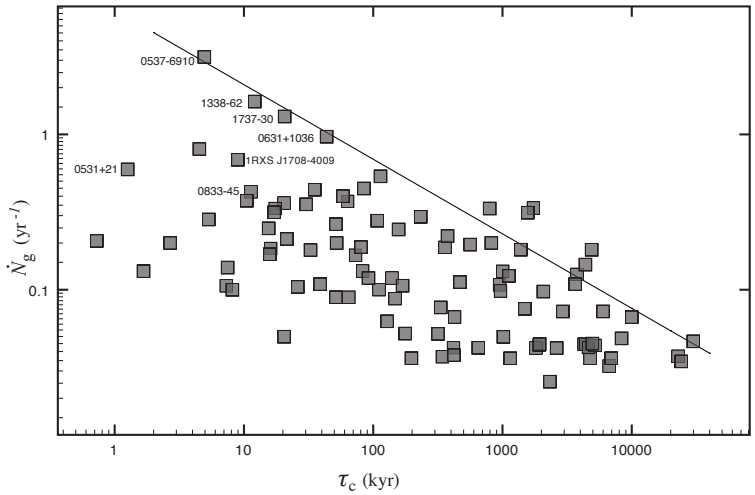

Figure 6: Number of glitches per year for most pulsars known to have glitched and observed for more than 3 yr (by 2010, from Espinoza et al. (2011)). The straight line is a linear fit to the maximum value of $\dot{N}_g$ in each half-decade of characteristic age τ_c.

superfluid can be obtained if we can detect and characterise many (if not all) glitches in several sources, precisely. Our ability to do this depends directly on the cadence of the observations, as well as on the accuracy of the TOAs. At the moment we know of $\sim$ 440 glitches in $\sim$150 pulsars. Glitch activity is concentrated in young objects ($\tau_c < 100$ kyr) and there is an almost linear correlation with spin-down rate, i.e. the faster a pulsar spins down, the higher its glitch activity (Lyne et al. 2000; Espinoza et al. 2011). The occurrence of glitches is in general not periodic and most pulsars exhibit less than one glitch every 2 years. This shows the importance of monitoring a large number of pulsars over a long time (Figure 6) using sub-arraying to observe multiple sources at higher cadence when possible.

The size of the largest glitches has already constrained the amount and location of the participating superfluid (Andersson et al. 2012; Chamel 2013; Piekarewicz et al. 2014). The detection of small glitches and the lower end of the $\Delta\nu$ distribution are however highly uncertain. Below certain sizes detection is compromised and there is confusion with phenomena like timing noise and disperson measure (DM) variations. A study of the glitch activity of the Crab pulsar has shown that the number of glitches decreases significantly below $\Delta\nu = 0.05\,\mu$Hz, implying a rather large minimum glitch size (Espinoza et al. 2014) which can in principle constrain the trigger mechanism. However, the minimum size found for the Crab glitches is larger than many glitches detected in other pulsars. In-depth studies of other pulsars will be important to assess the universality of the existence of a lower cut-off and to reach a better comprehension of the glitch trigger mechanism. To accomplish this it is necessary to have observations sensitive to very small glitches: the Crab pulsar glitch study was enabled by the high cadence (one observation per day) and high precision of the data.

Glitch recoveries provide information on the dynamics of the internal superfluid and its interaction with the other NS constituents. The Vela pulsar is the prototype source showing glitch recoveries, which are also observed in many other young pulsars. During the relaxation process the

PoS(AASKA14)043

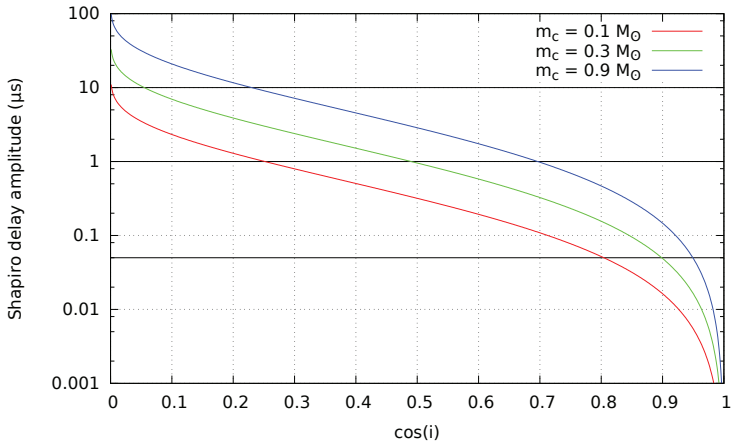

Figure 7: Observable Shapiro delay amplitude – i.e., the portion of the signal that is not covariant with other orbital parameters – as a function of inclination i and binary companion mass. Assuming orientations have uniform $\cos i$, at timing precision of $\sim$50 ns, $\gtrsim$80% of NS-WD binary systems with $m_c \geq 0.1$ M$_\odot$ should show detectable Shapiro delay.

spin-down rate slowly decays from the rather large (very negative) value induced by the glitch. It takes years for it to again reach pre-glitch levels and in many cases the process will be interrupted by a new glitch. PSR B2334+61 exhibited one of the largest glitches known to date, followed by a standard recovery process. Nonetheless, significant oscillations were reported in post-glitch timing residuals (Yuan et al. 2010a). To date no post-glitch oscillations have been detected in other pulsars. This could be related to the size of the glitch but could also just be an observational bias against detecting similar effects in lower sensitivity data taken at lower observing cadence..

Other pulsars have shown peculiar glitch recoveries, like the RRAT PSR J1819−1458 and the radio pulsar PSR J1119−6127 (Lyne et al. 2009; Weltevrede et al. 2011). In these two cases the spin-down rate over relaxed and reached values significantly smaller than the pre-glitch levels. Pulse shape variations were detected in a couple of observations following the glitch in PSR J1119−6127 but the rather low cadence available (month^{-1}) prevented a more detailed study. The unique recoveries were attributed to the large dipole fields of the two pulsars, though no physical mechanism was proposed. The analysis of glitch recoveries can tell us about differences between the regions responsible for the rotational relaxation, for instance whether there is pinning in the outer core or not. These studies would benefit from higher cadence and more precise observations.

4. Expectations from SKA

4.1 Improvements in mass measurements

The SKA is expected to improve on the number of measured NS masses in two ways. First, the dramatic increase in the number of known radio pulsars will yield more exotic systems in which masses can be determined (e.g. via measurable Shapiro delay). We might expect these to comprise roughly the same fraction of the total population as is observed now, or $\sim$1–2%. Even so, this effect alone would increase the number of total mass measurements by a factor $\sim$ 10. The second way that the SKA will improve mass measurements is through the improved timing precision that will

PoS(AASKA14)043

be achievable with the massive increase in telescope sensitivity. This will improve the uncertainty on already-measured masses. It also has potential to increase the *fraction* of systems in which masses can be measured, boosting the total numbers even further. Detection of Shapiro delay in significant fractions of the NS-WD population may become possible (Figure 7).

In contrast to many of the other relativistic timing parameters, Shapiro delay is not heavily dependent on special environmental or evolutionary history. The effect applies to all binary systems, is insensitive to contamination by non-relativistic effects, and its detectability mainly depends on random geometrical orientation – at high inclinations, the radio pulses we receive must travel close to the companion star, resulting in a much larger time delay[3]. Furthermore at low inclinations, the effect becomes highly covariant with the Keplerian orbital parameters, which reduces its observable amplitude even further (Freire & Wex 2010). Nevertheless, if high enough timing precision can be achieved, the effect can be detected even in fairly low-inclination systems. This is illustrated in Figure 7, which shows the observable (non-covariant) Shapiro delay amplitude versus $\cos i$. At $\sim$50 ns timing precision, Shapiro delay is potentially detectable at inclinations as low as $\sim 40^\circ$ – this includes $\sim$80% of all binary systems assuming random orientations (uniformly distributed in $\cos i$). The SKA is expected to achieve sufficient timing precision, and discover enough new binary systems, that we might expect at least a factor of five more Shapiro delay based mass measurements.

4.2 Improvements in moment of inertia measurements

The SKA opens up the possibility of a precise measurement of moment of inertia I for one pulsar for which the mass is already precisely known, the Double Pulsar PSR J0737−3039A. There are three routes by which pulsar timing measurements can lead to a measurement of I (Kramer & Wex 2009). A highly relativistic system such as the Double Pulsar (Burgay et al. 2003; Lyne et al. 2004) is required in order for the effects of I on the pulsar timing to be discernable. The first measurable effect is expected to be a contribution comparable in size to the 2PN-level correction to the advance of periastron, $\dot{\omega}$. This would produce an offset between the measured value of $\dot{\omega}$ and that expected by taking the other measured PK timing parameters and combining them for a (1PN) prediction. In practice, this will require very precise measurement of at least two other PK parameters which produce largely orthogonal curves in the mass-mass plane. For the Double Pulsar, the parameters best suited to this prediction will be the sine of the orbital inclination angle, s, and the rate of decay of the orbital period, $\dot{P}_{\rm b}$. Simulations assuming 5 μs timing precision predict a 10% measurement of I in 20 years (Kramer & Wex 2009). Timing with SKA1 should do even better than this. An important point is that the corrections to $\dot{P}_{\rm b}$ for the relative acceleration of the Solar System and the pulsar system must be known to high accuracy in order for this method to work. These corrections require precise measurements of the pulsar's proper motion and distance, things that should be easily achieved for the Double Pulsar with the timing and VLBI capabalities of SKA1. A further issue is the need for a reliable model of the Galactic potential; as the Double Pulsar is close to the Plane, this should not pose an insurmountable problem in this particular case, and models will also be improved on the necessary timescale by the results of the GAIA satellite.

[3]Note however that detectability of a Shapiro delay would be adversely affected if the inclination were so high that the system was in fact eclipsing.

PoS(AASKA14)043

The second method involves determining non-linear time evolution of the longitude of periastron, if the spin of the (recycled) pulsar is inclined with respect to the system's angular momentum. This should allow the measurement of the projection of the pulsar's spin vector on the orbital plane, leading to I via a precession-determined estimate of the spin-orbit misalignment angle δ. The third technique relies on measuring two time derivatives of the projected semi-major axis of the pulsar's orbit, x, once again leading to an estimate of $I\sin\delta$, although this effect would need to be separated from aberration-induced changes in projection of the orbit (Damour & Schäfer 1988; Wex & Kopeikin 1999; Damour & Taylor 1991). For the Double Pulsar these last two techniques are not promising, as the spin-orbit misalignment angle for the recycled pulsar is known to be small (Ferdman et al. 2013) and furthermore the orbit happens to be nearly edge-on to the line of sight, making the changes in projection tiny. The small misalignment angle is likely the result of a fairly symmetric, low-mass-loss explosion in the second supernova in the system (Podsiadlowski et al. 2004), but there are other DNS systems that are known to be significantly misaligned (Kramer 1998; Weisberg & Taylor 2002; Fonseca et al. 2014). The SKA (1,2) is expected to discover (100,180) DNS systems, and it is reasonable to hope that favourable geometries, and indeed even more relativistic orbits will be found in some of them.

4.3 Improvements to spin measurements

In the more than three decades since the discovery of the first MSP B1937+21 ($P = 1.56$ ms) (Backer et al. 1982), only one object, PSR J1748−2446ad ($P = 1.39$ ms) (Hessels et al. 2006) has been found that spins faster. Until a few years ago, the sometimes prohibitive computational costs of a large survey sensitive to very rapidly rotating objects lent support to the hypothesis that there might have been an observational bias limiting the number of known MSPs with spin period close to that of the record holders or below. However, the improvement of the computational capabilities implemented in modern pulsar search experiments made them nominally able to pick up ultra-fast radio pulsations and several new binary MSPs with spin periods below 2 ms have been discovered in recent years. An additional contribution to the increment of this population of rapidly spinning NS came from the targeted radio searches towards γ-ray unidentified sources selected from the *Fermi* catalogues.

Interestingly, in 9 cases (over a total of 11 binary MSPs having $P < 2$ ms), including the spin record-holder PSR J1748−2446ad, the most rapidly rotating pulsars appear to be hosted in eclipsing systems: binaries in which the matter from the companion obscures the radio pulsations for a large fraction of or perhaps even the entire orbit. This suggests that although there may be no observational bias against discovering the most rapidly rotating systems, they be nonetheless be hidden by obscuration from the companion star. However, the eclipses in these systems appear to be strongly frequency dependent, with the eclipses being significantly longer at frequencies at a GHz and below. It is also interesting to note that many pulsars in eclipsing systems were discovered in a 2 GHz survey of globular clusters with the GBT.

Due to the very large numbers of beams needed to cover the sky and accounting for the long dwell time needed to reach the required sensitivity (a pulsar like J1748−2446ad has a flux density of only ~ 80 μJy at 2 GHz) a deep all-sky survey at 2 GHz is not feasible with the current generation of radio telescopes. The beam-forming capabilities (allowing simultaneous search of tens or hundreds of sky positions), and the higher instantaneous sensitivity of SKA1-MID (reach-

PoS(AASKA14)043

ing ~ 10 μJy sensitivity in a relatively short integration time) will give the first opportunity for a deep all-sky survey at 2 GHz[4]. Provided the sub-millisecond pulsars exist and are mostly hidden in eclipsing binaries, this experiment would be the best designed ever in the radio band with the aim of uncovering at least the brightest objects in this category. A similar later experiment performed with SKA2 will be finally sensitive even to sub-millisecond pulsars in a portion of the Galaxy well beyond the volume probed by the *Fermi* γ-ray satellite.

Even if SKA1-MID and SKA2 do not find sub-millisecond pulsars, SKA1-MID will certainly discover at least few MSPs spinning faster than PSR J1748−2446ad, while SKA2 will deliver a full census of the population of the of the nearby, thus unaffected by scattering and dispersion delays, ultra rapidly spinning MSPs. Likely, the accurate timing observations possible with SKA will also lead to a measurement of the pulsar mass (via relativistic effects) for at least a sub-group of the objects. It will then be possible to exploit the large sample of rapidly spinning sources in order to derive statistically sound results. Population analysis (Possenti et al. 1999; Chakrabarty 2008; Ho et al. 2011; Papitto et al. 2014) may constrain not only the EOS, but will also elucidate other fundamental physical processes related to the final stage of the recycling that may depend on the EOS e.g.: *(i)* the role of the emission of gravitational wave radiation (r-modes or accretion induced quadrupole moments (Bildsten 1998; Bondarescu & Wasserman 2013)) in halting the pulsar spin up; *(ii)* the physical process provoking the decay of the surface magnetic field in the MSPs; *(iii)* the relative importance of the radio ejection (Burderi et al. 2001) and of the Roche-lobe decoupling phase (Tauris 2012) in shaping the spin distribution of the MSPs (see also Kiziltan & Thorsett (2010)).

The impact of a NS rotating at over ~ 1.1 kHz would be substantial, and 1.5 kHz would be revolutionary: no current models can sustain such a fast spin. A hypothetically observed frequency of 1.4 kHz, for example, would constrain the radius of a 1.4 $M_\odot$ NS to less than 9.5 km (Figure 5). In general higher frequencies favour additional non-nucleonic degrees of freedom, since they give more compact stars. Simultaneous measurement of high mass and high spin would be particularly constraining (Haensel et al. 2008). While massive NS require repulsion among their constituents at high density, fast rotation requires the interaction not to be too repulsive to counter-balance the centrifugal force.

4.4 Improvements in glitch sampling

The detection of glitches and the characterisation of their recoveries rely strongly on the constant monitoring of a sample of pulsars. The observing capabilities which are currently offered by the radio observatories that monitor young pulsars are sufficient for the detection of medium to large glitches. The detection of small glitches and the study of the lower end of the glitch size distribution are, however hard to attain with the current observing programs. SKA glitch studies should focus on monitoring a selected group of pulsars and should be able to provide the complete glitch sample for the observed sources during the observing campaign. Besides uncovering the lower end of the size distribution, this will allow the study of waiting time (inter-glitch time intervals) distributions, which can also shed light on the glitch mechanism.

[4]If observing time does not permit a full survey, one would instead focus on pointed observations of GCs, *Fermi* sources, and quiescent LMXBs to find the fastest spinning pulsars.

PoS(AASKA14)043

There are two main factors limiting the detection of glitches (Espinoza et al. 2014): *1)* How often pulsars are observed, and *2)* σ_ϕ, the larger of the dispersion of the timing residuals in a given time-interval (10-15 observations) and the average uncertainty of the TOAs. Compared to the current observing setups the SKA will offer superior sensitivity, hence we assume that σ_ϕ will never be dominated by TOA uncertainties. Unmodelled rotational irregularities and observing cadence will likely be the main limiting factors in glitch detection. Among the known effects that can increase the dispersion of the timing residuals are DM variations and timing noise. DM variations will be corrected via regular multi-frequency observations (highlighting the need for SKA1-LOW), necessary to achieve high precision timing, and therefore should not affect glitch detection. Timing noise, on the other hand, still needs to be well understood in order to correct the data for its effects. The detection of small glitches (for a given pulsar) will therefore be dependent on the intrinsic levels of timing noise and its characteristic timescales in combination with the observing cadence.

The nominal cadence of SKA observations for new pulsars is 1 observation per 2 weeks, for at least a year. In addition, timing campaigns for pulsars should last at least 10 years. Although this might seems appropriate, with one observation every two weeks the SKA might not be able to improve substantially the statistics of small glitches already accomplished by some of the current programs, nor to sample satisfactorily post-glitch recoveries. Glitch studies need a higher cadence and a longer campaign over a fixed set of pulsars. More frequent SKA observations are planned for a sub-sample of interesting MSPs, but these are expected to glitch at an average rate lower than 1 glitch per millennium (Espinoza et al. 2011). More complete monitoring of a larger sample of pulsars may be achievable using SKA1-LOW, which, with the wider field of view and sufficiently large numbers of tied-array beams, should facilitate daily observations of large numbers of sources.

Glitch detectability limits also depend on the size of the spin-down rate steps, improving for smaller steps. Known glitches have $|\Delta\dot{\nu}|$ values in the range 10^{-3} to 10^{4} ($\times 10^{-15}$ Hz s^{-1}). The two-weeks cadence strongly limits the detection of glitches with $|\Delta\dot{\nu}| > 1 \times 10^{-15}$ Hz s^{-1}. For instance, some of the Crab pulsar glitches could not be unambiguously detected, as demonstrated in Figure 8. The bias in glitch detection is clear from the left hand side plot, being dominated by σ_ϕ at low $|\Delta\dot{\nu}|$ values. For some pulsars σ_ϕ is driven by timing noise, but for others is driven by TOA precision. The right hand side plot shows the increased parameter space that SKA observations could achieve with daily observations and a timing precision of at least 5×10^{-5} rotations (equivalent to 5×10^{3} ns, for a period of 0.1 s). The SKA could easily achieve this precision for many pulsars, but the level of timing noise present in a given time-interval (10-15 TOAs) could be higher.

The number of pulsars monitored for glitches need not be large (20–30 objects) and should include those that hav e already been monitored for years (to track long-term glitch history), which are bright for SKA standards. Precision can thus be traded for higher cadence. The Aperture Array systems should allow an optimum combination of sensitivity, field-of-view and number of beams to yield exceptional cadence on a very large number of sources. With one *short* ($\sim$ 2 mins[5]) observation per day giving a TOA precision of at least 5×10^{-5} rotations, over years and for a sample of pulsars, we can explore fully the glitch size distribution and track the recoveries of all detected glitches. SKA will thus yield the ideal sample to probe the glitch mechanism.

[5]Assuming $A_{eff}/T_{sys} = 1000\,\mathrm{m^2\,K^{-1}}$ (SKA 1) and for a duty cycle of 10%, average flux 0.5 mJy and a bandwidth of 500 MHz, 2 mins. of observation gives 2×10^{-5} s precision (for P=0.1 s)

PoS(AASKA14)043

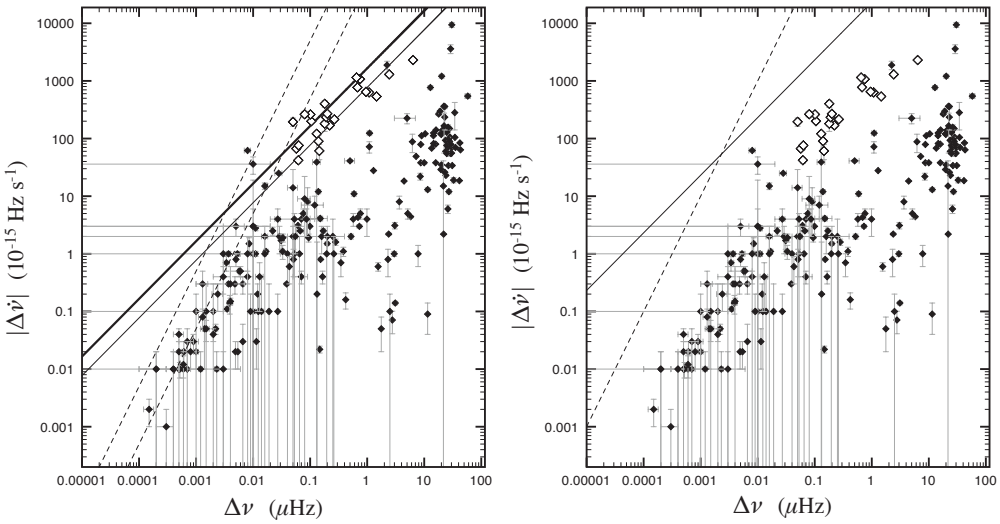

Figure 8: 245 glitches in the $|\Delta\dot{\nu}|$–$\Delta\nu$ plane (Espinoza et al. 2011). Open diamonds: Crab pulsar glitches. *Left*: Detectability limits for observing cadences of 14 days (solid thick line) and 30 days (solid line). The segmented lines are for σ_ϕ equal to 0.01 (rightmost) and 0.001 (leftmost) rotations, which are values commonly reached today. *Right*: Same as *Left* but for a cadence of 1 day and TOA precision of 5×10^{-5} rotations.

5. Summary

The nature of the strong interaction is fundamental to understanding the behaviour of systems from nuclei to neutron stars, and remains a serious challenge to physicists even though it is mathematically well-defined. SKA1, and ultimately the full SKA, will progressively give us the opportunity to explore the nature of matter, the strong force and superfluidity under the extreme conditions that prevail inside NS, via precise measurement of pulsar masses and moments of inertia, the discovery of rapidly-spinning and new types of pulsars, and high cadence observations to detect pulsar glitches.

References

Abdo, A.A., Ackermann, M., Ajello, M., et al. 2009, Science, 325, 848

Alford, M. G., Schmitt, A., Rajagopal, K., & Schäfer, T., 2008, Rev. Mod. Phys., 80, 1455

Alpar, M.A., Cheng, A.F., Ruderman, M.A., & Shaham, J., 1982, Nature, 200, 728

Alpar, M. A., Langer, S. A., & Sauls, J. A., 1984, Ap. J, 282, 533

Andersson, N., Sidery, T., & Comer, G. L., 2006, MNRAS, 368, 162

Andersson, N., Glampedakis, K., Ho, W.C.G., & Espinoza, C.M. 2012, Phys. Rev. Lett., 109, 241103

Antoniadis, I., Freire, P.C.C., Wex, N., et al. 2013, Science, 340, 448

Antoniadis I., Guillemot, I., Possenti, A., et al., 2015, "Multi-wavelength, multi-messenger pulsar science in the SKA Era", in proc. *Advancing Astrophysics with the Square Kilometre Array*, Pos(AASKA14)157

PoS(AASKA14)043

Backer, D. C., Kulkarni, S. R., Heiles, C., Davis, M. M., & Goss, W. M., 1982, Nature, 300, 615
Barr, E.D., Champion, D.J., Kramer, M. et al. 2013, MNRAS, 435, 2234
Bauswein, A., Janka, H.-T., Hebeler, K., & Schwenk, A., 2012, Phys. Rev. D, 86, 063001
Bednarek, I., Haensel, P., Zdunik, J.L., Bejger, M., & Mańka R., 2012, A&A, 543, 157
Bhat, N.D.R., Bailes, M., & Verbiest, J.P.W., 2008, Phys Rev D, 12, 124017
Bildsten, L. 1998, ApJ, 501, L89
Bondarescu, R., & Wasserman, I., 2013, ApJ, 778, 13
Borumand, M., Joynt, R., & Kluzniak, W., 1996, Phys. Rev. C, 54, 2745
Burderi, L., Possenti, A., Colpi, M. Di Salvo, T., & D'Amico, N. 1999, ApJ, 519, 285
Burderi, L., Possenti, A., D'Antona, F. et al. 2001, ApJ, 560, L71
Burgay, M., D'Amico, N., Possenti, A. et al., 2003, Nature, 426, 531
Chakrabarty, D., 2008, AIP Conf. Proc., 1068, 67
Chamel, N., 2006, Nucl. Phys. A, 773, 263
Chamel, N. 2013, Phys. Rev. Lett., 110, 011101
Champion, D.J., Ransom, S.M., Lazarus, P. et al., 2008, Science, 320, 1309
Cook, G.B., Shapiro, S.L., & Teukolsky, S.A. 1994, ApJ, 424, 823
Cordes, J.M., & Lazio, T.J.W. 2002, arXiv:astro-ph/0207156
Damour, T., & Schäfer, G., 1988, Nuovo Cim., 101, 127
Damour, T., & Taylor, J.H., 1991, Phys Rev D, 45, 1840
Demorest, P.B., Pennucci, T., Ransom, S.M. et al., 2010, Nature, 467, 1081
Espinoza, C.M., Antonopoulou, D., Stappers, B.W., Watts, A., & Lyne, A.G., 2014, MNRAS, 440, 2755
Espinoza, C.M., Lyne, A.G., Stappers, B.W., & Kramer, M. 2011, MNRAS, 414, 1679
Ferdman, R.D., Stairs, I.H., Kramer, M. et al., 2013, ApJ, 767, 85
Ferdman, R.D., Stairs, I.H., Kramer, M. et al., 2014, MNRAS, 443, 2183
Fonseca, E., Stairs, I.H., & Thorsett, S.E., 2014, ApJ, 787, 82
Freire, P.C.C., & Wex, N., 2010, MNRAS, 409, 199
Freire, P.C.C., Wex, N., Esposito-Farèse, G. et al. 2012, MNRAS, 423, 3328
Glendenning, N., 2000, *Compact Stars*, Springer-Verlag, New York
Guillemot, L., Freire, P.C.C., Cognard, I., et al. 2012, MNRAS, 422, 1294
Haensel, P., Zdunik, J.L., & Bejger, M., 2008, New AR., 51, 785
Haensel, P., Zdunik, J.L., Bejger, M., & Lattimer, J.M., 2009, A&A, 502, 605
Hartman, J.M., Chakrabarty, D., Galloway, D.K. et al., 2003, BAAS 35, 865.
Hebeler, K., & Schwenk, A., 2010, Phys. Rev. C., 82, 014314
Hebeler, K., Lattimer, J.M., Pethick, C.J., & Schwenk, A., 2013, ApJ, 773, 11
Hessels, J.W.T., Ransom S.M., Stairs, I.H. et al., 2006, Science, 311, 1901
Hessels, J.W.T., Possenti, A., Bailes, M. et al., 2015, "Pulsars in Globular Clusters with the SKA", in proc. *Advancing Astrophysics with the Square Kilometre Array*, PoS(AASKA14)047
Ho, W.C.G., Maccarone, T.J., & Andersson, N. 2011, ApJ, 730, L36
Ho, W.C.G., & Andersson, N. 2012, Nature Physics, 8, 787-789
Hotokezaka, K., Kyutoku, K., Okawa, H., Shibata, M., & Kiuchi, K., 2011, Phys Rev D, 83, 124008
Janka, H.T., Langanke, K., Marek, A., Martínez-Pinedo, G., & Müller, B., 2007, Phys. Reports,

PoS(AASKA14)043

442, 38
Janssen, G.H., Stappers, B.W., Kramer, M. et al., 2008, A&A, 490, 753
Jones, D. I., & Andersson, N., 2001, MNRAS, 324, 811
Keane, E.F., Bhattacharyya, B., Kramer, M., et al., 2015, "A cosmic census of radio pulsars with the SKA", in proc. *Advancing Astrophysics with the Square Kilometre Array*, PoS(AASKA14)040
Kitaura, F.S., Janka, H.-T., & Hillebrandt, W., 2006, A&A, 450, 345
Kiziltan, B., & Thorsett, S.E., 2010, ApJ, 715, 335
Kortelainen, M., Lesinski, T., Moré, J. et al., 2010, Phys Rev C, 82, 024313
Kramer, M., 1998, ApJ, 509, 856
Kramer, M., Stairs, I.H., Manchester, R.N. et al., 2006, Science, 314, 97
Kramer, M., & Wex, N., 2009, Classical and Quantum Gravity, 26, 7
Lackey, B.D., Kyutoku, K., Shibata, M., Brady, P.R., Friedman, J.L., 2012, Phys. Rev. D., 85, 044061
Lattimer, J.M., & Prakash, M., 2001, ApJ, 550, 426
Lindblom, L., 1992, ApJ, 398, 569
Link, B., 2003, Phys. Rev. Lett., 91, 101101
Lorimer, D.R., 2008, Living Reviews in Relativity, 11, 8
Lorimer, D.R., & Kramer, M., 2005, *Handbook of pulsar astronomy*, Cambridge University Press
Lyne, A.G., Shemar, S.L., & Graham-Smith, F., 2000, MNRAS, 315, 534
Lyne, A. G., Burgay, M., Kramer, M. et al., 2004, Science, 303, 1153
Lyne, A.G., McLaughlin, M.A., Keane, E.F. et al. 2009, MNRAS, 400, 1439
Manchester, R.N., Hobbs, G.B., Teoh, A., & Hobbs, M., 2005, AJ, 129, 1993
Mendell, G., 1991, ApJ, 380, 530
Metzger, B.D., Martínez-Pinedo, G., Darbha, S. et al., 2010, MNRAS, 406, 2650
Page, D., Prakash, M., Lattimer, J.M., & Steiner, A.W., 2011, Phys. Rev. Lett., 106, 081101
Papitto, A., Torres, D.F., Rea, N. & Tauris, T.M., 2014, A&A, 566, 64
Patruno A., & Watts A.L., 2012, arXiv:1206.2727
Piekarewicz, J., Agrawal, B.K., Colò, G. et al., 2012, Phys Rev C, 85, 041302
Piekarewicz, J., Fattoyev, F.J., & Horowitz, C.J. 2014, Phys. Rev. C, 90, 015803
Pieper, S.C., Pandharipande, V.R., Wiringa, R.B., & Carlson, J., 2001, Phys Rev C, 64, 014001
Podsiadlowski, P., Langer, N., Poelarends, A.J.T. et al., 2004, ApJ, 612, 104
Podsiadlowski, P., Dewi, J.D.M., Lesaffre, P. et al., 2005, MNRAS, 361, 1243
Possenti, A., Colpi, M., Geppert, U., Burderi, L., & D'Amico, N. 1999, ApJS, 125, 463
Ransom, S.M., 2008, *Pulsars in globular clusters*, IAU Symposium 246, 291, Vesperini E. et al. eds.
Ransom, S.M., Stairs, I.H., Archibald, A.M. et al., 2014, Nature, 505, 520
Roberts, M.S.E. 2011, *New black widows and redbacks in the Galactic field*, AIP Conf. Ser. 1357, 127
Roca-Maza, X., Centelles, M., Viñas, X., & Warda, M., 2011, Phys Rev Lett, 106, 252501
Romani, R.W., Filippenko, A.V., Silverman, J.M. et al., 2012, ApJ, 760, L36
Shao, L., Stairs, I. H., Antoniadis, J., et al., 2015, "Testing Gravity with Pulsars in the SKA Era", in proc. *Advancing Astrophysics with the Square Kilometre Array*, PoS(AASKA14)042
Shternin, P.S., Yakovlev, D.G., Heinke, C.O., Ho W.C.G., & Patnaude, D.J., 2011, MNRAS, 412,

PoS(AASKA14)043

L108
Sidery, T., Passamonti, A., & Andersson, N., 2010, MNRAS, 405, 1061
Steiner, A.W., & Gandolfi, S., 2012, Phys. Rev. Lett., 108, 081102
Stone, J.R., & Reinhard, P.G., 2007, Prog. Part. Nuc. Phys., 58, 587
Tauris, T.M. 2012, Science, 335, 561
Tauris, T.M., Kaspi, V.M., Breton, R.P., et al., 2015, "Understanding the neutron star population with the SKA", in proc. *Advancing Astrophysics with the Square Kilometre Array*, PoS(AASKA14)039
Tsang, M.B., Stone, J.R., Camera, F. et al., 2009, Phys Rev C, 86, 015803
van Kerkwijk, M.H., Breton, R.P., & Kulkarni, S.R., 2011, ApJ, 728, 95
Watts, A.L., 2012, Ann. Rev. Astron. Astrophys., 50, 609
Weltevrede, P., Johnston, S., & Espinoza, C.M., 2011, MNRAS, 411, 1917
Weber, F., 2005, Prog. Nuc. Part. Phys., 54, 193
Weisberg, J.M., & Taylor, J.H., 2002, ApJ, 576, 942
Weisberg, J.M., Nice, D.J., & Taylor, J.H., 2010, ApJ, 722, 1030
Wex, N., & Kopeikin, S., 1999, ApJ, 513, 388
Wiringa, R.B., Stoks, V.G.J., & Schiavilla, R., 1995, Phys. Rev C, 51, 38
Witten, E., 1984, Phys Rev D, 30, 272
Xu, R.X., 2003, ApJ, 596, L59
Yu, M., Manchester, R.N., Hobbs, G. et al., 2013, MNRAS, 429, 688
Yuan, J.P., Manchester, R.N., Wang, N. et al., 2010a, ApJ, 719, L111
Yuan, J.P., Wang, N., Manchester, R.N., & Liu, Z.Y., 2010b, MNRAS, 404, 289
Zdunik, J.L.,& Haensel, P., 2013, A&A, 551, 61

PoS(AASKA14)043

PROCEEDINGS OF SCIENCE

Observing Radio Pulsars in the Galactic Centre with the Square Kilometre Array

R. P. Eatough[*1,2], **T. J. W. Lazio**[3,4], **J. Casanellas**[5], **S. Chatterjee**[6], **J. M. Cordes**[6], **P. B. Demorest**[7], **M. Kramer**[1,8], **K. J. Lee**[9,1], **K. Liu**[1,10], **S. M. Ransom**[7], **N. Wex**[1]

[1]*Max-Planck-Institut für Radioastronomie, Bonn, 53121, Germany;* [2]*E-mail:* reatough@mpifr-bonn.mpg.de*;* [3]*Jet Propulsion Laboratory, California Institute of Technology, M/S 138-308, 4800 Oak Grove Dr, Pasadena, CA 91109, USA;* [4]*E-mail:* joseph.lazio@jpl.nasa.gov*;* [5]*Max Planck Institute for Gravitational Physics (Albert Einstein Institute), Science Park Potsdam-Golm, Am Mühlenberg 1, D-14476, Germany;* [6]*Department of Astronomy and Space Sciences, Cornell University, Ithaca, NY 14853, USA;* [7]*National Radio Astronomy Observatory, 520 Edgemont Road, Charlottesville, Virginia 22903-2475, USA;* [8]*Jodrell Bank Centre for Astrophysics, Alan Turing Building, University of Manchester, Manchester, M13 9PL, UK;* [9]*Kavli institute for Astronomy and Astrophysics, Peking University, Beijing 100871, P. R. China,;* [10]*Station de radioastronomie de Nançay, Observatoire de Paris, CNRS/INSU, Université d'Orléans, F-18330 Nançay, France.*

The discovery and timing of radio pulsars within the Galactic centre is a fundamental aspect of the SKA Science Case, responding to the topic of "*Strong Field Tests of Gravity with Pulsars and Black Holes*" (Kramer et al. 2004; Cordes et al. 2004). Pulsars have in many ways proven to be excellent tools for testing the General theory of Relativity and alternative gravity theories (see Wex (2014) for a recent review). Timing a pulsar in orbit around a companion, provides a unique way of probing the relativistic dynamics and spacetime of such a system. The strictest tests of gravity, in strong field conditions, are expected to come from a pulsar orbiting a black hole. In this sense, a pulsar in a close orbit ($P_{\rm orb} < 1$ yr) around our nearest supermassive black hole candidate, Sagittarius A* - at a distance of $\simeq 8.3$ kpc in the Galactic centre (Gillessen et al. 2009a) - would be the ideal tool. Given the size of the orbit and the relativistic effects associated with it, even a slowly spinning pulsar would allow the black hole spacetime to be explored in great detail (Liu et al. 2012). For example, measurement of the frame dragging caused by the rotation of the supermassive black hole, would allow a test of the "cosmic censorship conjecture." The "no-hair theorem" can be tested by measuring the quadrupole moment of the black hole. These are two of the prime examples for the fundamental studies of gravity one could do with a pulsar around Sagittarius A*. As will be shown here, SKA1-MID and ultimately the SKA will provide the opportunity to begin to find and time the pulsars in this extreme environment.

Advancing Astrophysics with the Square Kilometre Array
June 8-13, 2014
Giardini Naxos, Italy

[*]Speaker.

PoS(AASKA14)045

1. Background

A combination of radio and infrared (IR) astrometric observations has established the presence of a dark mass in the Galactic centre (GC), whose properties are most consistent with being a supermassive black hole (BH) (Eckart & Genzel 1996; Ghez et al. 1998; Reid & Brunthaler 2004; Ghez et al. 2008; Gillessen et al. 2009a,b). Known by its radio nomenclature of Sagittarius A* (Sgr A*), current estimates are that the mass of this BH is $4.30 \pm 0.20_{(\mathrm{stat})} \pm 0.30_{(\mathrm{sys})} \times 10^6$ $\mathrm{M}_\odot$ (Gillessen et al. 2009a). Monitoring the orbits of the closest stars S0-2 (Schödel et al. 2002) and S0-102 (Meyer et al. 2012) could provide constraints on the extent to which their orbits are perturbed which in turn would constrain the enclosed mass, which could be stars, dark matter, or both (Sabha et al. 2012; Gillessen et al. 2009b). Current work with the Keck Telescope, the VLT and with the VLT interferometer (VLTI) and proposed work with extremely large telescopes (ELTs; e.g. the European ELT and the GSMT) will lead to IR astrometric precisions of 0.5 mas with single apertures and 10 μas with the VLTI and the GRAVITY instrument (Weinberg et al. 2005; Eisenhauer et al. 2011). These resolutions allow orbital perturbations of 4.15 and 0.08 au, respectively, to be measured that will arise from General Relativity (GR) and from Newtonian effects caused by other stars and dark matter. It is expected that source confusion in IR surveys with ELTs will limit the sample of stars to those with orbits larger than about 200 to 300 au; ~ 100 stars with semi-major axes $\lesssim 3000$ au for a 30-m ELT (Weinberg et al. 2005).

The discovery and timing of radio pulsars orbiting Sgr A*, and within the central stellar cluster, will provide a powerful means to test GR, as well as probe the dark matter content and magnetoionic medium within the nucleus of our Galaxy. An SKA radio pulsar program can yield much more precise localizations on objects arbitrarily close to the innermost stable circular orbit (ISCO, radius $\gtrsim 0.1$ au, depending on the spin of the Sgr A* BH). Confusion limits do not apply to the time-varying signals of pulsars. In comparison with the best forecasted precisions of IR astrometry and Doppler measurements, pulsar timing has the potential of increasing the testing and diagnostic precision by *at least three orders of magnitude*. Pulsars offer this prospect because timing precisions correspond to spatial localizations (from *ranging*) smaller than a light second (0.2 μas) compared to the localizations expected from the best proposed IR interferometry, of no better than 10 μas (0.1 au).

2. The pulsar population in the GC

Several lines of argument suggest that not only is there a large neutron star (NS) population in the GC but that many NSs should be active radio pulsars. Figure 1 (left panel) shows schematically the contents of the GC as determined both empirically and from theoretical arguments about galaxy formation. Ghez et al. (2008) and Gillessen et al. (2009b) show that the stellar cluster around Sgr A* consists mainly of early-type stars, whose short lifetimes ($\sim 10^7$ yr) means that either massive star formation in the region is ongoing or that there has been a starburst of order 6 Myr ago, although the presence of young, massive stars in a region where tidal forces should inhibit star formation present a conundrum: "the paradox of youth" - (Ghez et al. 2003). Nonetheless, stars with masses of 10–20 $\mathrm{M}_\odot$ are NS progenitors, and the presence of a population of young massive stars near Sgr A* suggests that there must exist a numerous NS population as well. The time scales

PoS(AASKA14)045

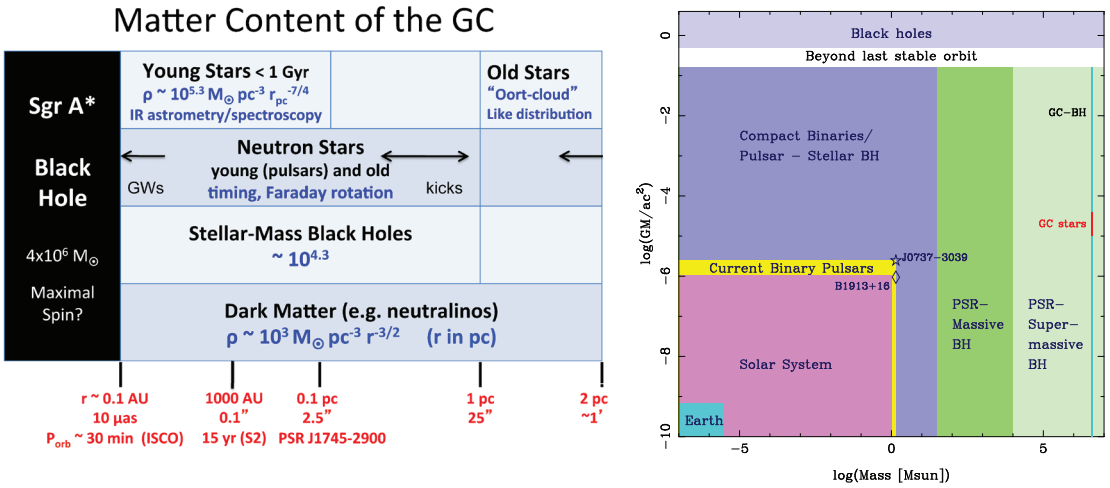

Figure 1: (*Left*) Schematic view of the matter content of the GC. Young stars (e.g., S0-2) are known to approach as close as $0.1''$ (1000 AU) to Sgr A*. The combination of young, hot stars in the GC and mass segregation suggests that there are likely to be compact stellar remnants (NSs and BHs) at least within 1000 au, and potentially much closer. Finally, there could also be dark matter particles. The SKA, operating at frequencies near 10 GHz, will search for NS, in the form of active radio pulsars, as close as possible to Sgr A*. (*Right*) Depth of gravitational potential (GM/ac^2) probed by an orbit of semi-major axis a as a function of the mass of the binary system M. The regions probed by solar system tests and known pulsars in binary systems are indicated, with the double neutron star systems PSR B1913+16 and PSR J0737−3039 shown explicitly. The vertical cyan line indicates the mass of Sgr A* (GC-BH). The red line segment shows the region probed by the S stars in the GC. It is clear that substantially deeper gravitational potentials (larger GM/ac^2) remains to be probed, and would be accessible to radio pulsar observations (Kramer et al. 2004).

also work out for many of these NSs to be active radio pulsars: radio emission of canonical 10^{12} G objects lasts for ~ 10 Myr, the time scale for spindown to lengthen spin periods past the "death line" of a few seconds.

Estimates of the supernova rate within 100 pc of Sgr A* based on the number of young stars in the region and on the heating of X-ray gas range from 10^{-3} yr^{-1} to 10^{-2} yr^{-1} and are consistent, after accounting for the fraction of supernovae that produce pulsars, with the number of point radio sources in the region that could be pulsars (Lazio & Cordes 2008). Such agreement is coarse but suggestive that there are of order 10^3 to 10^4 active pulsars in the region, of which about 200 to 2000 (20%) would be beamed toward the Earth. More recently, and by combining results from the GC radio point source counts described above, the detected GC pulsar population at that time, non-detections in high-frequency pulsar surveys of the inner parsec, radio and gamma-ray measurements of diffuse emission, infra-red observations of massive stellar GC populations, pulsar wind nebulae candidates, and the supernova rates from X-ray data, Wharton et al. (2012) estimate that $\sim 10^3$ active radio pulsars in the inner parsec should be beamed toward Earth.

Pulsars in the GC, like other stellar populations, will orbit the central BH Sgr A* mostly as isolated objects but some will be in binaries with companions of all types: main-sequence and post-main-sequence stars, white dwarfs, NSs, or even BHs (Faucher-Giguère & Loeb 2011). A population of "recycled" pulsars (i.e., NSs spun up to millisecond periods by accretion) is also expected because the stellar density in the GC is large enough so that tidal capture and exchange

PoS(AASKA14)045

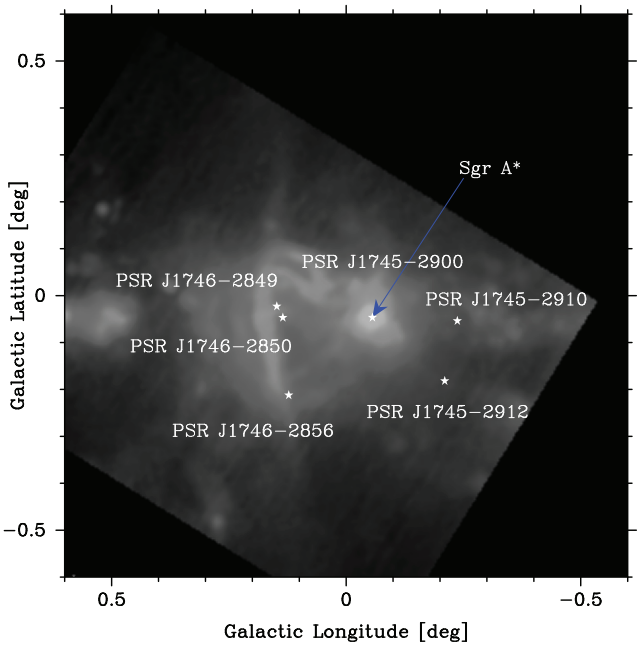

Figure 2: The positions of detected radio pulsars in the central 0.5° toward the GC overlaid on a 10.55 GHz continuum map made with the Effelsberg telescope (Seiradakis et al. 1989). Assuming a GC distance of 8.3 kpc, 0.5°corresponds to a projected distance of $\sim$ 70 pc. Even PSR J1745−2900, which overlaps the position of Sgr A* on this scale ($\sim 3'' \equiv 0.1$ pc offset), is too distant for gravity tests. Figure courtesy of B. Klein.

reactions should occur as they do in globular clusters. Voss & Gilfanov (2007) show that tidal capture of NSs by low-mass main-sequence stars is the dominant mechanism for forming binary NS in approximately the central $1'$ of M31 and these can produce millisecond pulsars (MSPs) via long-term accretion. Along with similarly captured stellar-mass BHs, accreting objects in the central part of M31 can account for the excess number of point X-ray sources in the inner bulge of M31. The same processes should occur in the GC over a similar-sized region (0.1–0.2 kpc) (Muno et al. 2005).

Arguably the strongest evidence for a significant NS population in the central parsec now comes from the recent detection of a radio loud magnetar - PSR J1745−2900, an inherently rare class of pulsar, just $\sim 3''$(0.1 pc) from Sgr A* (Kennea et al. 2013; Mori et al. 2013; Eatough et al. 2013a; Shannon & Johnston 2013). Along with the five pulsars previously discovered in proximity to Sgr A* (at $10'-15'$- see Figure 2 (Johnston et al. 2006; Deneva et al. 2009)) these objects cannot be explained as part of a Galactic disk population because the number of foreground pulsars expected in the pulsar surveys to date is much less than one. Consequently, the question of the GC pulsar population has been recently revisited by a number of authors (Chennamangalam & Lorimer 2014; Zhang et al. 2014; Dexter & O'Leary 2014). As will be described in Section 3, it is pulsars in compact orbits ($P_{\rm orb} < 1$ yr - corresponding to a semi-major axis of $\sim$ 160 au) around the BH that will enable the most precise tests of GR. Recent simulations suggest that up $\sim$ 200 pulsars could orbit within 4000 au of the BH, the closest of which could have a semi-major axis of $\sim$ 120 au (Zhang et al. 2014). It is only through observations with the SKA that the full GC pulsar

PoS(AASKA14)045

population (whatever its size) will be detected.

Certain dark matter models predict that dark matter particles can efficiently accumulate inside compact objects such as NS, eventually causing them to collapse into a BH. The GC pulsar population, as detected by the SKA, can thus also be used to place stringent constraints on dark matter models, with older pulsars and MSPs being the most constraining (Bramante & Linden 2014).

3. Testing gravity with GC pulsars

With their large moments of inertia and fast spin rates, radio pulsars are excellent clocks. The clocklike property of pulsars orbiting Sgr A* will provide unique probes of the spacetime, plasma and dark matter around the massive central BH and are a powerful probe of GR (Paczynski & Trimble 1979; Wex et al. 1996; Pfahl & Loeb 2004) itself. As we show below, GR and other perturbations of GC pulsars are large enough so that even rather "noisy" pulsars, relative to typical precision timing requirements, will do the job.

Pulse times-of-arrival (TOAs) from an orbiting pulsar can be described in terms of the standard Keplerian parameters and in a model-independent parameterized post-Newtonian (PPN) formalism. Any deviations from the PPN values expected from GR would provide strong evidence of a post-GR theory of gravity. The most recent illustration of this method of testing theories of gravity is from the double pulsar PSR J0737−3039A/B, for which the measured PPN parameters indicate agreement with GR at better than the 1% level (Kramer & Stairs 2008). However, PSR J0737−3039A/B still represents a relatively weak field case. Consider the depth of the gravitational potential to be GM/ac^2, for a total system mass M and semi-major axis a, with G and c being the usual physical constants. The current population of binary pulsars probes only to $GM/ac^2 \lesssim 10^{-5.5}$. By contrast, a pulsar with an orbit comparable to the star S0-2 (≈ 15 yr) would probe to $GM/ac^2 \sim 10^{-4.5}$; pulsars with shorter orbital periods could probe to even larger values of GM/ac^2 (Figure 1). Star-star interactions of course can cause perturbations that make GR tests more difficult.

For a pulsar in a close orbit ($P_{\rm orb} < 1$ yr) around Sgr A* one expects to see a number of relativistic effects, like time dilation, Shapiro delay and relativistic peri-center precession, all of them with a magnitude, that as we mention above, does not even require a particularly high timing precision to measure them with excellent accuracy (Liu et al. 2012). The time dilation, for instance, is expected to be of order 10 to 20 minutes. Consequently, soon after the discovery relativistic effects will be well measured, give the mass of Sgr A* with high precision, and allow for the first gravity tests. After a few orbits, one will be able to separate the Lense-Thirring drag from the orbital motion and measure the spin of the BH with a fractional precision of 10^{-2} to 10^{-3} (Liu et al. 2012). A first test is to see if the dimensionless spin-parameter does not exceed one, as expected for a Kerr BH in GR (cosmic censorship conjecture - see Liu et al. (2012)). The quadrupole moment of Sgr A* leads to a characteristic signature in the timing residuals, directly related to the quadrupolar structure of its potential (Figure 3). By this, the effect of the quadrupole can uniquely be identified in the motion of the pulsar, and its magnitude can be measured with good to very good precision, allowing for a test of the no-hair theorem due to the unique relation of mass, spin and quadrupole for a Kerr solution (Wex & Kopeikin 1999; Liu et al. 2012). Figure 4 illustrates some of the relativistic effects that could be determined from measuring pulse TOAs of

PoS(AASKA14)045

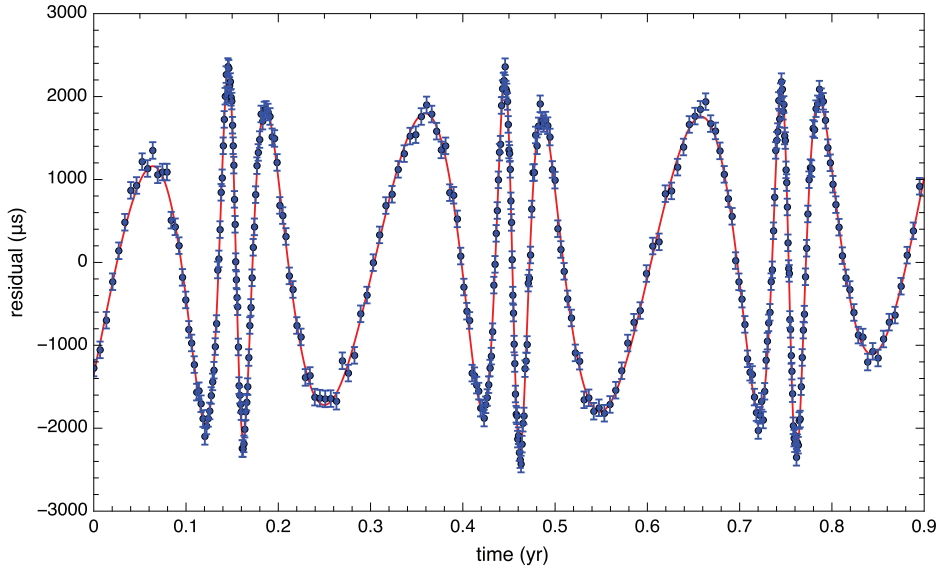

Figure 3: Characteristic pulsar timing residuals caused by the quadrupole moment of the Sgr A* BH in simulated times-of-arrival (TOAs) over three orbital cycles (Liu et al. 2012). The orbital period is assumed to be $P_{\rm orb} = 0.3\,{\rm yr}$ and the eccentricity $e = 0.5$. The red line is the fitted pulsar timing model.

a pulsar orbiting Sgr A* in extremely short orbits ($P_{\rm orb} < 100$ hr). For instance, measurement of the relativistic apsidal advance, the second order Doppler shift, and the Shapiro delay (not shown) yield redundant constraints on the individual masses in the system as well as provide precision tests of GR. The Shapiro delay is detectable for elliptical orbits even when the orbit is face on. Geodetic precession of the spin axis will cause secular or periodic changes in measured pulse shapes if there is misalignment of the spin and orbital angular momenta, and secular orbital decay from gravitational radiation will be measurable for the more compact orbits ($P_{\rm orb} \lesssim 10$ hr). Moreover, as Figure 4 demonstrates, only for these shortest orbital periods will the orbital decay time become so small that we will have little likelihood of detecting any such pulsar. Perhaps the most notable aspect of GC pulsars is that orbital perturbations are large enough so that even canonical (10^{12} G) pulsars with long periods ($\gtrsim 0.5$ s), which ordinarily are considered to be noisy clocks, are suitable for making timing measurements. This means that *any* pulsar found in the GC is useful for the SKA pulsar program.

While many effects contribute to imprecision of TOAs (Cordes & Shannon 2010), the dominant ones for GC pulsars with canonical periods will be intrinsic spin noise (Hobbs et al. 2010; Shannon & Cordes 2010) and the large pulse widths that result from scattering broadening. With a conservative goal of about 1 s timing "precision" (in quotes because detection of gravitational waves with millisecond pulsars requires < 100 ns precision - Janssen et al. (2015)), many GR effects and orbital perturbations from stellar encounters can be measured one to two orders of magnitude better than the best IR interferometric measurements. The RMS spin noise for most objects will be below the 1 s target and the timing error from the pulsar width W is $\delta t \sim W/({\rm S/N})$, where S/N is the peak signal to noise ratio of the pulse. For widths $W < 1$ s, it is reasonable to expect $\delta t \sim 0.01$ to 0.1 s, providing even more precise orbital measurements.

At present, all these considerations rest on the assumption that the environment around Sgr

PoS(AASKA14)045

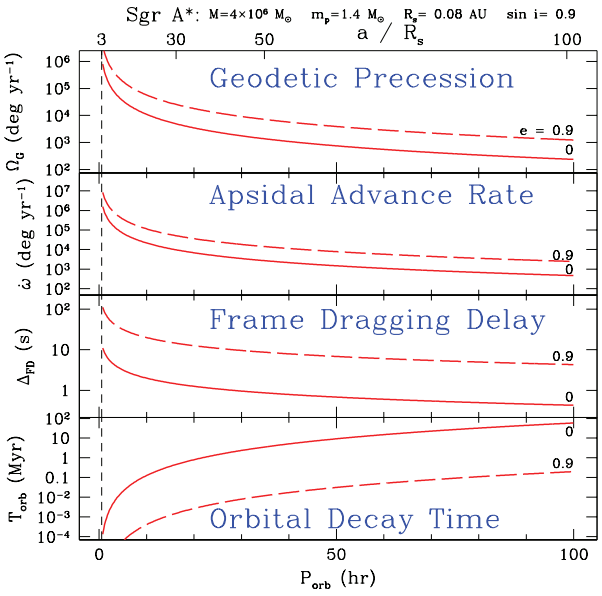

Figure 4: Relativistic effects that could be determined from measuring pulse TOAs from a pulsar closely orbiting Sgr A*. The *bottom* axis shows the orbital period, and the *top* axis shows the semi-major axis of the orbit, in units of the Schwarzschild radius of Sgr A*. All of the effects shown, except for frame dragging, have been detected in timing observations of binary pulsars. In all panels, the solid line indicates a circular orbit ($e = 0$) while the dashed line indicates a highly eccentric orbit ($e = 0.9$). For reference, the apsidal advance rates of PSR J0737−3039, B1913+16, and Mercury are *too small* to be plotted ($\dot{\omega} < 20\,\mathrm{deg\,yr^{-1}}$).

A* is sufficiently clean, i.e. external perturbations on the pulsar motion are negligible. As shown in Figure 1 the matter content of the GC consists not only of Sgr A* , but early-type, late-type and evolved stars, dark matter, and magnetized plasma all of which will cause many perturbations that can be detected in pulsar TOAs. By measuring the Newtonian precession of elliptical orbits, estimation of the smoothly distributed mass, including both stars and dark matter, will be possible (Weinberg et al. 2005). In addition, strong constraints can be made on the density of stars from two-body perturbations of pulsar orbits (Weinberg et al. 2005; Merritt et al. 2010). To model potential external perturbations to TOAs, and see how they can be accounted for, or how much they degrade our capability to test GR, is subject to current research.

Chromatic effects from intervening magnetized plasmas are discussed in the next section; these effects are strongly frequency dependent and can be removed (after extracting all valuable scientific information on the properties of the GC interstellar medium) through appropriate multi-frequency measurements.

4. Chromatic radio propagation effects

Individual pulsar TOAs will show the well known dispersion and multipath delays caused by the integrated electron column density (the dispersion measure, DM) and by scattering from small-scale ($\lesssim$ 1 au) density irregularities, characterized by the scattering measure (SM). Polarization measurements of pulse profiles will show Faraday rotation from which the rotation measure (RM) can be determined, thus constraining the integrated magnetic field.

Chromatic perturbations from magnetized plasma along the line of sight include the differential *dispersion delay* across a narrow bandwidth $\Delta\nu$ (in MHz), $\Delta t(\nu) = 8.3\,\mu\mathrm{s\,DM}\Delta\nu/\nu^3$, where ν is the observing frequency (in GHz) and DM is the *dispersion measure* (in pc cm^{-3}), which is the electron column density, $\mathrm{DM} \equiv \int dl\, n_e$. Such delays are removed from multi-frequency data both

PoS(AASKA14)045

as part of the survey analysis (typically by the use of *filterbanks*) and also, with greater precision, during timing measurements.

Towards the GC, a more important factor is pulse broadening from scattering caused by fluctuations in electron density δn_e that extend down to scales of a few hundred kilometers and have a roughly Kolmogorov wavenumber spectrum (Armstrong et al. 1995). For the strong scattering towards Sgr A*, first identified by angular diameter measurements of OH/IR masers and background AGNs, the pulse broadening has a time scale $\tau_s \propto D\nu^{\sim -4}$SM, where D is the pulsar distance and the scattering measure SM is the line of sight integral of C_n^2, the coefficient of the wavenumber spectrum for δn_e (Cordes & Lazio 2003). Unlike dispersion, which is easily removed to maximize the S/N of a pulse, the deleterious effect of scatter broadening cannot be corrected for when many "scintles[1]" are summed across the observing bandwidth, as they will be for GC pulsars.

Magnetized plasma Faraday rotates the linear polarization by an angle ν^{-2}RM and is routinely measured for most pulsars using full Stokes parameter pulse shape measurements. In the GC this effect was demonstrated by measurements of the pulse polarization of the recently discovered magnetar, PSR J1745−2900, that revealed the second largest RM known in the Galaxy (the largest being that of Sgr A* itself) (Eatough et al. 2013a; Shannon & Johnston 2013). From X-ray observations of the hot gas phase that Sgr A* is accreting from (and which the magnetar is likely located in) a simple density profile was used to place limits on the strength of the magnetic field in this region; a value which can affect the dynamics of the accretion process onto the supermassive BH (Eatough et al. 2013a).

Once found, pulsars in the GC will therefore provide individual values of all three measures (DM, SM, and RM) for different lines of sight into the GC. Though not measured directly, the emission measure EM (the integral of n_e^2) can be related to DM and SM so as to constrain the "outer scale" of the wavenumber spectrum of δn_e (Cordes & Lazio 2002). The EM, while large toward Sgr A* , does not cause significant free-free absorption that would prohibit detection of pulsars as is clear since Sgr A* is seen through optically thin plasma down to at least 1 GHz.

5. Finding and timing pulsars in the GC with the SKA

5.1 Past searches and updates on GC scattering

Despite predictions that a large number of radio loud pulsars should be present in the GC (see Section 2.), at the time of writing just six are known within 0.5° (Figure 2). It has been understood that the deficit in GC pulsars could be primarily explained by extreme scattering of radio waves in the GC (Cordes & Lazio 1997; Lazio & Cordes 1998; Cordes & Lazio 2002, 2003). As mentioned in Section 4. scattering, which causes temporal broadening of pulses and a corresponding reduction in pulse S/N, has a strong frequency dependence ($\propto \nu^{\sim -4}$). A clear mitigation strategy for dealing with pulse broadening due to scattering is to observe at frequencies much higher than typically used for pulsar searching. The significant constraint on this mitigation strategy is that typical pulsars have power-law spectra ($S_\nu \propto \nu^\alpha$), usually with very steep spectra indices ($\langle\alpha\rangle \simeq -1.7$) so their

[1]Scintles are the constructive interference patches seen in the frequency-time plane for nearby pulsars. The scattering towards Sgr A* is strong enough to prohibit measurement of individual scintles because they are narrower than typical frequency channel widths even at higher radio frequencies e.g. 14 GHz.

PoS(AASKA14)045

flux densities decline rapidly with increasing frequency (Kramer et al. 1998). Fortunately, there is a subset of pulsars with relatively flat spectra. For example, of 293 pulsars with derived spectral indices in the ATNF catalog[2] (Manchester et al. 2005), approximately 40 (or 14%) have $\alpha > -1$. Moreover, a small number of pulsars have been detected at frequencies as high as 90 GHz (Kramer et al. 1997; Morris et al. 1997). With such pulsars in mind, surveys of the GC at progressively higher radio frequencies have been performed (Klein et al. 2004; Johnston et al. 2006; Deneva et al. 2009; Deneva 2010; Macquart et al. 2010; Bates et al. 2011; Eatough et al. 2013b; Siemion et al. 2013) and resulted in the detection of five of the six pulsars displayed in Figure 2 (Johnston et al. 2006; Deneva et al. 2009); albeit at lower frequencies $\lesssim 3$ GHz.

The sixth known GC pulsar, PSR J1745−2900, was first identified at X-ray wavelengths (Kennea et al. 2013; Mori et al. 2013) before detection in the radio (Eatough et al. 2013a; Shannon & Johnston 2013). Recent measurements of the pulse broadening in this pulsar indicate the degree of scattering toward the GC is less than previously predicted (Spitler et al. 2014). In addition, measurements with the Very Long Baseline Array (VLBA) of the angular scatter broadening show that it has an angular size equivalent to Sgr A* itself. This suggests that PSR J1745−2900 and Sgr A* are behind the same scattering region. This fact coupled with the smaller pulse broadening time indicate that the scattering region (if modelled as a single thin screen of material) could be distant from the GC (Bower et al. 2014). However, the authors note that the paucity of GC pulsars still indicates that regions of intense scattering might exist in the GC. These regions could be of a more complex structure than in the simple picture described above (Spitler et al. 2014). Therefore high observing frequencies ($\gtrsim 9$ GHz) might still be necessary to detect GC pulsars.

In the following section we use the latest information about GC scattering to re-investigate the prospects for GC pulsar searches with the SKA.

5.2 Prospects for GC pulsar searches with the SKA

Our top goal is to find and then time radio pulsars within the central parsec ($30''$ radius), with the highest priority placed upon pulsars as close as possible to Sgr A* . A secondary goal is to conduct a more complete census of the larger region ($\sim 30'$) in order to understand better the overall GC NS population. While the pulse broadening time due to scattering appears to be less than previously predicted, the effect is still large enough to necessitate pulsar searches of the GC at higher frequencies. In Figure 5 we show the detection sensitivity of pulsar periodicity searches of the GC performed with SKA1-MID and utilizing three of the proposed frequency bands outlined in (Dewdney et al. 2013). The figure shows the radio "pseudo luminosity" at 1.4 GHz (given by $L_{\rm p} = S_{1400}D^2$, where S_{1400} and D are the period-averaged flux density at 1.4 GHz and the distance respectively) versus the spin period. The dots are the actual values for known pulsars in the current (May 2014) ATNF catalog (Manchester et al. 2005). The curves plotted for each frequency band are derived from estimations of the minimum detectable flux density, $S_{\rm min}$, given by the radiometer equation as applied to pulsar observations,

$$S_{\rm min} = \beta \frac{\mathrm{S/N_{min}} T_{\rm sys}}{G\sqrt{N_{\rm pol}\,\Delta\nu\,T_{\rm obs}}} \sqrt{\frac{W_{\rm eff}}{P - W_{\rm eff}}}, \tag{5.1}$$

[2]http://www.atnf.csiro.au/people/pulsar/psrcat/

PoS(AASKA14)045

where β is a digitization factor, S/N_{min} is the detection threshold, T_{sys} is the system temperature, G is the telescope gain (in units of KJy^{-1}), N_{pol} is the number of polarization channels summed, $\Delta\nu$ is the bandwidth, T_{obs} is the observation time, P is the pulsar spin period and W_{eff} is the effective pulse width. Certain parameters have fairly standard values, namely, $\beta \approx 1$, $N_{pol} = 2$, and $S/N_{min} \approx 10$. The effective pulse width is given by the vector sum of the intrinsic pulse width and any unaccounted for pulse broadening effects in the following:

$$W_{eff} = \sqrt{(W_{50}^2 + \tau_{samp}^2 + \tau_{DM}^2 + \tau_s^2)} \tag{5.2}$$

where W_{50} is the intrinsic pulse width at half the pulse height (here assumed to be $0.05P$), τ_{samp} is the data sampling interval, τ_{DM} is the intra-channel dispersion broadening (in a filterbank) and τ_s is the scatter broadening. The curves, which mark the minimum detectable pulsar spin period and luminosity, are plotted for pulsars at the distance of the GC and take into account the effects of scatter broadening, based on measurements of τ_s from PSR J1745−2900 (Spitler et al. 2014), and assume a typical spectral index of $\alpha = -1.7$, thereby allowing the limits to be scaled to the equivalent sensitivity at 1.4 GHz. Further details of the numbers used in defining these curves are given in the caption to Figure 5.

If the scattering toward PSR J1745−2900 is representative of the inner GC as a whole Figure 5 shows that the common pulsars, with spin periods around 0.5 s, might be detectable at frequencies as low as 2.4 GHz (Band 3) with SKA1-MID. For mildly recycled pulsars, with spin periods from a few milliseconds to a few tens of milliseconds, 4 GHz (Band 4) observations would be needed. Frequencies up to at least 9 GHz (Band 5) might be required to detect the longer lived MSPs in the GC. As well as the possibility of detecting MSPs, GC pulsar surveys at higher frequencies offer the additional benefit of reduced background sky temperatures, improving sensitivity.

For comparison with current facilities a line for a 9 GHz GC search with the Green Bank Telescope (GBT) has also been marked. The fact that a large fraction of the known pulsar population is already above this line might be of cause for concern for the prospects for finding more GC pulsars, however, (Chennamangalam & Lorimer 2014) note that current non-detections from past GC surveys cannot yet rule out a large GC pulsar population which still need deeper surveys to be detected. SKA1-MID and the SKA are needed to address this problem.

Our search methodology consists of both *periodicity searches*, including correction for orbital motion, and *searches for transient sources*, because some pulsars are more easily detectable in single-pulse detection algorithms than in Fourier searches. In addition, the potential for discovering new classes of objects is maximized by searching for individual bursts.

Periodicity Searches: Periodicity searches are a standard tool for searching for pulsars and have been used for many years, in many directions, not limited to the GC. These algorithms include standard de-dispersion to remove dispersion delays, orbital demodulation, Fourier analysis of the resulting time series, and identification of signals above threshold, which requires classification as interference, instrumental contamination, or pulsars. For the GC, the most important aspect of algorithmic development concerns orbital demodulation, as it is for the shortest orbital period pulsars that the maximum GR effects can be measured. The simplest orbital demodulation is an acceleration search, which removes a parabolic signature

PoS(AASKA14)045

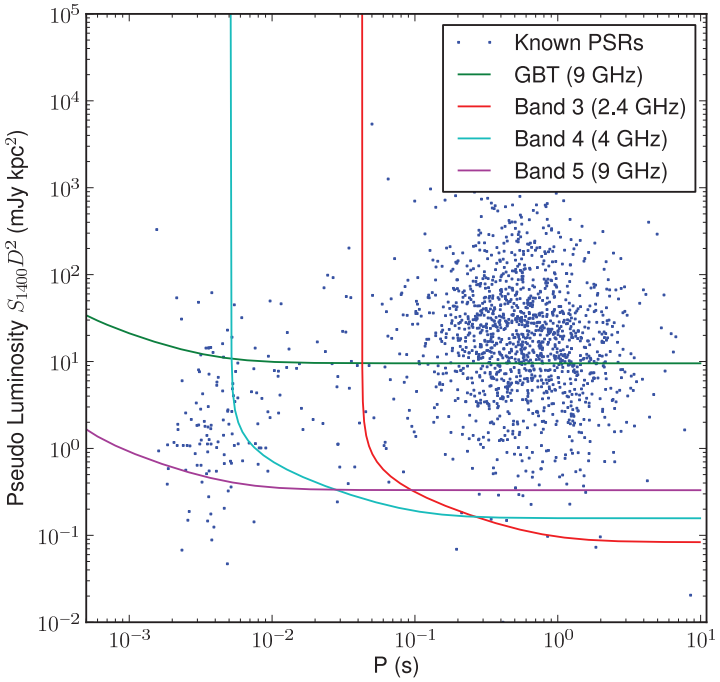

Figure 5: Detectability of pulsars in the GC via a periodicity search of a 6 hr integration with the GBT at 9 GHz and SKA1-MID at three of the proposed frequency bands. Points denote the period-averaged "pseudo luminosity" at 1.4 GHz ($L = S_{1400}D^2$) versus spin period for known pulsars in the ATNF catalog (Manchester et al. 2005). The curves show sensitivity limits derived from the minimum detectable flux density (Equation 5.1). Pulsars are detectable if they are *above* a given curve. We have used a GC distance of 8.3 kpc; a S/N = 10 detection threshold; a bandwidth $\Delta\nu = 0.8$ GHz for the GBT, and bandwidths $\Delta\nu = 1.4$, 2.4 and 9.2 GHz for SKA1-MID Bands 3, 4 and 5 respectively (Dewdney et al. 2013); a system temperature, neglecting the effects background sky temperature, of $T_{\rm sys}$ =27 K; and a spectral index of $\alpha = -1.7$, while recognizing that some objects have flatter and some steeper spectra. Pulse broadening, τ_s, values in the direction of Sgr A* are provided by measurements from the GG magnetar PSR J1745−2900 (Spitler et al. 2014). The curves will move lower for pulsars having spectra less steep than $\nu^{-1.7}$. The curves will also move lower if multiple integrations are combined (e.g., through incoherent combination of power spectra (Eatough et al. 2013b)). On the other hand, if for example the sensitivity of the core of SKA1-MID that is used for the pulsar search is reduced, by making the collecting area two thirds of the proposed size, the curves will move upward by an amount of log(1.5).

as an approximation to a Keplerian orbit. This approach works for data sets that have a duration which is a small fraction of the orbital period (Ransom et al. 2003).

Transient Searches: For compact orbits around Sgr A* , such as those < 100 hr shown in Figure 4, the large GR effects that make such pulsars extremely attractive targets will also make them more difficult to detect. Fast geodetic precession, for example, may mimic an orbital period over a 6 hr observation time and may be detectable at the output of an acceleration search. However, precession of the pulsar beam will make objects intermittent because the beam will precess out of our line of sight for a sizable fraction of the precession period. This

PoS(AASKA14)045

effect has been seen in several of the NS-NS binaries, including the Hulse-Taylor pulsar (Kramer 1998). Consequently, single epoch search observations may be inadequate to find such sources. Moreover, some pulsars emit "giant" pulses, with strengths that are 1000× the mean pulse intensity (Hankins & Rickett 1975; Hankins et al. 2003; Cognard et al. 1996; Johnston & Romani 2003). In the case of the Crab pulsar, some giant pulses outshine the entire Crab Nebula (Hankins & Rickett 1975), corresponding to brightness temperatures of order 10^{31} K; (Hankins et al. 2003) observed "nano-giant" pulses having durations of only 2 ns and implied brightness temperatures of 10^{38} K, by far the most luminous emission from any astronomical object.

Once GC pulsars are found with the SKA, our approach will be similar to that already used by e.g. (Deneva et al. 2009), namely they will be timed over short and moderate time periods to characterize their spin properties and any orbital motion. Each will be observed at multiple frequencies to find the optimal band for timing precision, which depends on period, pulse width, flux density and spectral index, and on the exact level of scattering. Depending on the object, we will then embark on a long-term timing campaign for measuring GR effects and probing the GC environment, with a cadence determined by the orbital period around Sgr A* and on any stellar orbital motion.

References

Armstrong, J. W., Rickett, B. J., & Spangler, S. R. 1995, ApJ, 443, 209
Bates, S. D., Johnston, S., Lorimer, D. R., et al., 2011, MNRAS, 411, 1575B
Bower, G. C., Deller, A., Demorest, P., et al., 2014, ApJ, 780L, 2B
Bramante, J. & Linden, T., 2014, Physical Review Letters, 113, 191301
Chennamangalam, J. & Lorimer, D. R., 2014, MNRAS, 440, L86
Cognard, I., Shrauner, J. A., Taylor, J. H., & Thorsett, S. E. 1996, ApJ, 457, L81
Cordes, J. M., & Lazio, T. J. W. 1997, ApJ, 475, 557
Cordes, J. M., & Lazio, T. J. W. 2002, arXiv:astro-ph/0207156
Cordes, J. M., & Lazio, T. J. W. 2003, arXiv:astro-ph/0301598
Cordes, J. M., Kramer, M., Lazio, T. J. W., et al., 2004, New Astronomy Reviews, 48, 1413
Cordes, J. M. & Shannon, R. M., 2010, ArXiv e-prints, arXiv:1010.3785
Deneva, J. S., 2010, PhD thesis, Cornell University
Deneva, J. S., Cordes, J. M., & Lazio, T. J. W., 2009, ApJ, 702, L177
Dewdney, P. E., Turner, W., Millenaar, R., et al., 2013, "SKA1 System Baseline Design", SKA-TEL-SKO-DD-001 Revision 1
Dexter, J. & O'Leary, R. M. 2014, ApJ, 783, L7
Eatough, R. P., Falcke, H., Karuppusamy, R., et al. 2013a, Nature, 501, 391
Eatough, R. P., Kramer, M., Klein, B., et al. 2013b, IAU Symposium, 291, 382E
Eckart, A. & Genzel, R. 1996, Nature, 383, 415
Eisenhauer, F., Perrin, G., Brandner, W., et al. 2011, The Messenger, 143, 16
Faucher-Giguère, C.-A, Loeb, A. 2011, MNRAS, 415, 3951
Ghez, A. M., Klein, B. L., Morris, M., & Becklin, E. E. 1998, ApJ, 509, 678

PoS(AASKA14)045

Ghez, A. M., Duchêne, G., Matthews, K., et al. 2003, ApJ, 586, L127
Ghez, A. M., Salim, S., Weinberg, N. N., et al. 2008, ApJ, 689, 1044
Gillessen, S., Eisenhauer, F., Fritz, T. K., et al. 2009a, ApJ, 707, L114
Gillessen, S., Eisenhauer, F., Trippe, S., et al. 2009b, ApJ, 692, 1075
Hankins, T. H., Kern, J. S., Weatherall, J. C., et al. 2003, Nature, 422, 141
Hankins, T. H. & Rickett, B. J. 1975, Methods in Computational Physics. Volume 14 - Radio astronomy, 14, 55
Hobbs, G., Lyne, A. G., & Kramer, M. 2010, MNRAS, 402, 1027
Janssen G. H., Hobbs G., McLaughlin M., et al. 2015, "Gravitational wave astronomy with the SKA," in proc. *Advancing Astrophysics with the Square Kilometre Array*, PoS(AASKA14)037
Johnston, S., Kramer, M., Lorimer, D. R., et al. 2006, MNRAS, 373, L6
Johnston, S. & Romani, R. W. 2003, ApJ, 590, L95
Kennea, J. A., Burrows, D. N., Kouveliotou, C., et al. 2013, ApJ, 770, L24
Klein, B., Kramer, M., Müller, P., et al. 2004, IAU Symposium, 218, 133K
Kramer, M., Xilouris, K. M., Jessner, A., et al. 1997, A&A, 322, 846
Kramer, M. 1998, ApJ, 509, 856
Kramer, M., Xilouris, K. M., Lorimer, D. R., et al. 1998, ApJ, 501, 270
Kramer, M., Backer, D. C., Cordes, J. M., et al. 2004, New Astronomy Reviews, 48, 993
Kramer, M., & Stairs, I. H. 2008, ARA&A, 46, 541
Lazio, T. J. W., & Cordes, J. M. 2008, ApJS, 174, 481
Lazio, T. J. W., & Cordes, J. M. 1998, ApJS, 118, 201
Liu, K., Wex, N., Kramer, M., et al. 2012, ApJ, 747, 1
Macquart, J.-P., Kanekar, N., Frail, D. A., & Ransom, S. M. 2010, ApJ, 715, 939M
Manchester, R. N., Hobbs, G. B., Teoh, A. & Hobbs, M. 2005, AJ, 129, 1993
Merritt, D., Alexander, T., Mikkola, S., & Will, C. M. 2010, Physical Review D, 81, 062002
Meyer, L., Ghez, A. M., Schödel, R., et al. 2012, Science, 338, 84
Mori, K., Gotthelf, E. V., Zhang, S., et al. 2013, 770, L23
Morris, D., Kramer, M., Thum, C., et al. 1997, A&A, 322, L17
Muno, M. P., Pfahl, E., Baganoff, F. K., et al. 2005, ApJ, 622, L113
Paczynski, B., & Trimble, V. 1979, The Large-Scale Characteristics of the Galaxy, ed. W. B. Burton (Dordrecht: Reidel) p. 401
Pfahl, E., & Loeb, A. 2004, ApJ, 615, 253
Ransom, S. M., Cordes, J. M., Eikenberry, S. S. 2003, ApJ, 589, 911
Reid, M. J., & Brunthaler, A. 2004, ApJ, 616, 872
Sabha, N., Eckart, A., Merritt, D., et al. 2012, A&A, 545, A70
Schödel, R., Ott, T., Genzel, R., et al. 2002, Nature, 419, 694
Seiradakis, J. H., Reich, W., Wielebinski, R., Lasenby, A. N., & Yusef-Zadeh, F. 1989, A&AS, 81, 291S
Shannon, R. M. & Cordes, J. M. 2010, ArXiv e-prints, arXiv:1010.4794
Shannon, R. M. & Johnston, S. 2013, MNRAS, 435, L29
Siemion, A., Bailes, M., Bower, G. 2013, IAU Symposium, 291, 57S
Spitler, L. G., Lee, K. J., Eatough, R. P., et al. 2014, ApJ, 780L, 3S
Voss, R & Gilfanov, M. 2007, MNRAS, 380, 1685

PoS(AASKA14)045

Wang, Y., Creighton, T., Price, R. H., & Jenet, F. A. 2009, ApJ, 705, 1252
Weinberg, N. N., Milosavljevic, M., & Ghez, A. M. 2005, ApJ, 622, 878
Wex, N. & Kopeikin, S. 1999, ApJ, 513, 388
Wex N., 2014, Brumberg Festschrift, arXiv:1402.5594
Wex, N., Gil, J., & Sendyk, M. 1996, A&A, 311, 746
Wharton, R. S., Chatterjee, S., Cordes, J. M., Deneva, J. S., Lazio, T. J. W. 2012, ApJ, 753, 108
Zhang, F., Lu, Y., & Yu, Q. 2014, ApJ, 784, 106

PoS(AASKA14)045

PROCEEDINGS OF SCIENCE

Pulsar Wind Nebulae in the SKA era

J. D. Gelfand[*ab], **R. P. Breton**[cf], **C.-Y. Ng**[d], **J. W. T. Hessels**[e], **B. Stappers**[f], **M. S. E. Roberts**[a], **A. Possenti**[g]

[a] *New York University Abu Dhabi, PO Box 129188, Abu Dhabi, United Arab Emirates; E-mail:* joseph.gelfand@nyu.edu, mallory.roberts@nyu.edu

[b] *Center for Cosmology and Particle Physics, New York University, Meyer Hall of Physics, 4 Washington Place, New York, NY 10003*

[c] *School of Physics and Astronomy, University of Southampton, Southampton, United Kingdom; E-mail:* rene.breton@manchester.ac.uk

[d] *Department of Physics, The University of Hong Kong, Pokfulam Road, Hong Kong; E-mail:* ncy@bohr.physics.hku.hk

[e] *ASTRON, Postbus 2, 7990 AA Dwingeloo, The Netherlands / University of Amsterdam; E-mail:* hessels@astron.nl

[f] *The School of Physics and Astronomy, The University of Manchester, Manchester, United Kingdom; E-mail:* ben.stappers@manchester.ac.uk

[g] *Astronomical Observatory of Cagliari, Selargius, Italy; E-mail:* possenti@oa-cagliari.inaf.it

Neutron stars lose the bulk of their rotational energy in the form of a pulsar wind: an ultra-relativistic outflow of predominantly electrons and positrons. This pulsar wind significantly impacts the environment and possible binary companion of the neutron star, and studying the resultant pulsar wind nebulae is critical for understanding the formation of neutron stars and millisecond pulsars, the physics of the neutron star magnetosphere, the acceleration of leptons up to PeV energies, and how these particles impact the interstellar medium. With the SKA1 and the SKA2, it could be possible to study literally hundreds of PWNe in detail, critical for understanding the many open questions in the topics listed above.

Advancing Astrophysics with the Square Kilometre Array
June 8-13, 2014
Giardini Naxos, Italy

*Speaker.

PoS(AASKA14)046

1. Introduction

Roughly every 100 years, a neutron star is born in the Milky Way (e.g., Faucher-Giguère & Kaspi 2006). The rotational energy of a neutron star powers a highly relativistic, magnetized outflow called a "pulsar wind" (e.g., Goldreich & Julian 1969), which creates a "pulsar wind nebula" (PWN) as it expands into its surroundings. The properties of the PWN depend on how this wind is generated inside the neutron star's magnetosphere, how PeV and higher energy particles are generated inside this outflow, and the wind's interaction with its surroundings.

This is true for neutron stars young and old, isolated and in binaries. When the neutron star is young ($\lesssim 10^4 - 10^5$ years old), it is still inside the supernova remnant (SNR) created by the progenitor explosion, and the expansion of the PWN inside the SNR creates a "composite SNR" (Helfand & Becker 1987). As described in §2, not only do such systems allow us to study the generation and properties of the pulsar wind for the most energetic neutron stars, they can be used to determine the neutron star's initial spin period and the mass and initial kinetic energy of the supernova ejecta – important quantities for understanding how neutron stars are formed in these explosions. As described in §3, in binary systems the PWN is produced by the interaction between the neutron star's pulsar wind and its companion. By studying such PWNe, one can measure the properties of the pulsar wind under very different conditions than in composite SNRs and gain valuable insight into the last stages of the formation of millisecond pulsars (MSPs). Last, but not least, as described in §4, older neutron stars moving supersonically through the interstellar medium (ISM) also produce PWNe. Studying these PWNe is important for understanding the magnetic field structure of the pulsar, and how it interacts with its surroundings.

Therefore, PWNe play an important role in many areas of astrophysics – from the explosion mechanism of core-collapse supernovae to the physics of magnetized plasmas to the acceleration of particles in many different physical conditions. As described in §5, the significant improvements in collecting area and observing capabilities promised by the SKA1 and SKA 2 has the potential to revolutionize this field by increasing the number of well-studied PWNe by $\sim 10 - 100\times$, allowing for the statistical studies needed to answer the above questions.

2. Composite Supernova Remnants

When the pulsar wind leaves the neutron star magnetosphere, it is thought to be a primarily equatorial outflow comprised of regions of alternating magnetic field polarity whose energy is mainly in the form of magnetic fields (e.g., Bogovalov 1999). The confinement of the pulsar wind by the surrounding medium creates a "termination shock," where the "cold" pulsar wind is converted to a "hot" outflow (e.g., Kennel & Coroniti 1984). The PWN is then formed by the expansion of the shocked, now particle dominated, pulsar wind into the surrounding medium. The significant fraction of Galactic TeV γ-ray sources associated with PWNe ($\sim 40\%$; Wakely & Horan 2008) requires that these objects produce extremely high energy particles. While observations support this general picture, many basic questions remain unanswered: How is the pulsar wind generated in the magnetosphere? What is responsible for converting the pulsar wind from a magnetically dominated to a particle dominated outflow? How are particles accelerated in these objects?

PoS(AASKA14)046

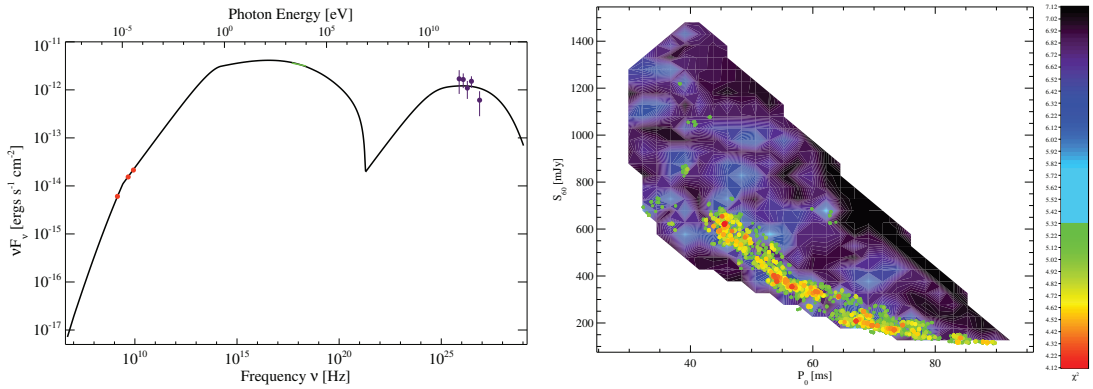

Figure 1: *Left*: Broadband SED of PWN G54.1+0.3 overlaid with the best fit model SED. *Right*: The model-predicted 60 MHz flux density S_{60} of G54.1+0.3 as a function of the initial spin period P_0 of the central pulsar. The color bar indicates the χ^2 of the model fit to the observed data, with red (lower χ^2) indicating a better fit (Gelfand et al. submitted).

Answering these questions requires studying, in detail, the PWNe produced by the youngest, and most energetic, neutron stars. Understanding how particles are created in the neutron star's magnetosphere requires measuring the total number of particles produced by a pulsar over its lifetime. This is possible only for pulsars whose PWN is detected at both radio and γ-ray energies (e.g., de Jager 2007; Gelfand et al. submitted). Currently, only ~ 10 pulsars meet these criteria (e.g., Roberts 2004), with the SKA and the Cerenkov Telescope Array (CTA), this number could increase by a factor of $\sim 5-10\times$ (§5). Ions in the pulsar wind can explain both the high acceleration efficiency of PWNe (e.g., Amato & Arons 2006) and the detection of variable "wisps" near the termination shock of several PWNe (e.g., Spitkovsky & Arons 2004), as can magnetic reconnection in the pulsar wind before (e.g., Kirk & Skjæraasen 2003), at (e.g., Lyubarsky 2003), or after the termination shock (e.g., Porth et al. 2013). Distinguishing between these models requires sensitive measurements of a PWN's radio polarization structure and spectrum (e.g., Olmi et al. 2014). Currently, this is possible for maybe a handful of PWNe – too few to draw any strong conclusions. With the SKA, it should be possible for dozens (§5).

As mentioned in §1, when a neutron star is young and most energetic, it is likely inside the SNR produced by the progenitor explosion. In this case, the evolution of a PWN is sensitive to the initial spin period of the central neutron star as well as the mass and initial kinetic energy of the supernova ejecta (e.g., Chevalier 2005; Gelfand et al. 2009). This can be done using models for the evolution of a PWN inside a SNR (Figure 1, e.g., Gelfand et al. submitted), but requires measuring the current spin-down luminosity and characteristic age of the central neutron star, the radio, X-ray, and γ-ray spectrum of the PWN, and the radius of the surrounding SNR. Currently, only ~ 10 composite SNRs meet this criteria (e.g., Bucciantini et al. 2011; Torres et al. 2014), since only $\sim 50\%$ of all PWNe are associated with a pulsar (e.g., Roberts 2004), $< 50\%$ of these are associated with a SNR, and many of the remaining PWNe detected at γ-ray energies (e.g., Ferrand & Safi-Harb 2012) are undetected in the radio. Even worse, a precise estimate of the initial spin-period requires measuring the braking index of the central pulsar (e.g., Gelfand et al. 2014), currently accomplished for < 5 sources. As described in §5, the SKA could increase this number by $\sim 5-10\times$, enabling one to directly test different models for the formation of neutron stars in

PoS(AASKA14)046

core-collapse supernovae (e.g., Watts & Andersson 2002; Blondin & Mezzacappa 2007).

Lastly, as mentioned above, PWNe dominate the luminous TeV γ-ray population of the Milky Way (Carrigan et al. 2013), with TeV PWNe typically associated with pulsars whose characteristic ages are $t_{\rm ch} \lesssim 10^5$ years (Wakely & Horan 2008). Therefore, the majority of these pulsars, and PWNe, will be inside the SNR of their progenitor explosion even if this SNR is not detected. With the SKA1 and SKA2, we will determine if this is true for the considerable number of currently unidentified Milky Way TeV sources, by discovering a coincident "young" radio pulsar, diffuse, flat spectrum radio emission characteristic of a PWN, and/or a surrounding steep-spectrum shell suggestive of a SNR. Additionally, the SKA1 and SKA2 will discover PWNe around energetic pulsars whose radio beams do *not* point towards the Earth. For all these objects, the flux densities measured by SKA1-LOW will allow us to estimate their initial periods even if pulsed emission is not detected.

3. Neutron Star Binaries

If a neutron star is in a binary system, the highly relativistic "pulsar wind" powered by its rotational energy will interact with its companion. The interaction between the neutron star's pulsar wind and its stellar companion leads to an intrabinary shock which possibly accelerates particles to high energies (e.g., Bogdanov et al. 2011), filling the system with plasma. Evidence for plasma production in pulsar binaries has been observed from high-mass X-ray binaries (e.g., Moldón et al. 2014) to "black widow" and "redback" systems (e.g., Roberts et al. 2014), where the pulsar wind actually ablates material from the companion star (Figure 2, e.g., Fruchter et al. 1988). Studying the intrabinary plasma probes the pulsar wind much closer to the neutron star magnetosphere (Pétri & Dubus 2011) than the systems described in §2, where extremely different conditions may prevail. In fact, analysis of one binary pulsar system suggests the wind is strongly magnetized in this regime (Bogdanov et al. 2011), while the study of the PWNe described in §2 require a weakly magnetized wind further from the neutron star. If correct, this places strong constraints on models for magnetic reconnection in the pulsar wind (§2), the currently leading theory for particle acceleration in these systems (e.g. Kirk & Skjæraasen 2003).

Typically, such studies require detecting orbitally-modulated non-thermal X-ray emission from the binary (e.g., Bogdanov et al. 2011), not achievable with a radio telescope like the SKA. However, as described in §5, the collecting area of the SKA2 could increase by $> 10\times$ the number of binary pulsars – providing much needed targets for these X-ray studies. Additionally, inhomogeneities and/or free-free absorption in the cloud of plasma generated at the intrabinary shock is believed to be responsible for the "eclipses" in the pulsed radio emission (Fig. 2) observed from ~ 50 binaries pulsars (Roberts 2013; Freire 2013). By simultaneously measuring the pulsed and unpulsed continuum radio flux of these systems, it is possible to determine the density, geometry, and filling factor of this plasma as well as the structure of its magnetic field – especially if there are simultaneous or contemporaneous γ-ray observations. With the SKA1 and SKA2, we expect to make such measurements for ~ 300 eclipsing binaries (§5), allowing one to determine how the properties of the plasma produced in this interaction depend on the characteristics of the neutron star and binary system (e.g., neutron star spin-down luminosity, binary separation, companion mass and radius).

PoS(AASKA14)046

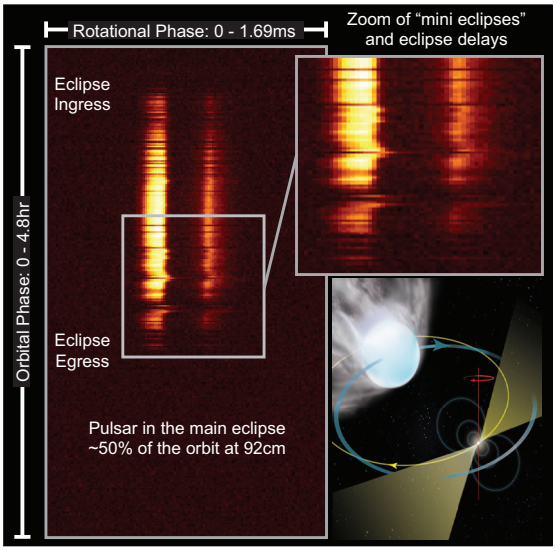

Figure 2: Eclipses in the pulsed radio emission from PSR J1023+0038 (Hessels, priv. comm.) as well as an artist's impression of the cloud of plasma resulting from the ablation of its low-mass companion by its pulsar wind (Bill Saxton, NRAO).

Lastly, the recent discovery of several millisecond pulsars (MSPs) / low mass X-ray binaries (LMXBs) transitioning between an "accretion"-dominated phase where no radio pulsations are detected and a MSP phase which shows no evidence for accretion (e.g., Archibald et al. 2009; Bassa et al. 2014; Papitto et al. 2013; Stappers et al. 2014) promises important insight into the formation of MSPs as well as understanding accretion onto magnetized neutron stars. Since studies of intermittent pulsars strongly suggest that the emission of radio pulses is connected to their loss of rotational energy (e.g., Young et al. 2013; Li et al. 2014), the physical mechanism responsible for generating a pulsar wind likely plays an important role in this transition. Only by studying the radio and higher energy (X-ray, γ-ray) properties of such systems will it be possible to understand the interplay between accretion and a neutron star's magnetosphere. As described in §5, the potential multi-beam and high-frequency capabilities of the SKA are critical for understanding the physics of these transitions which may comprise the final stage in the formation of a MSP (though some systems might be stuck transitioning back-and-forth to a LMXB state).

4. Isolated Pulsars in the Interstellar Medium

The pulsar winds of isolated, older neutron stars will also significantly impact their surrounding. In this case, the pulsar wind is confined by the ram pressure created by the neutron star's supersonic motion. The morphology (e.g., Vigelius et al. 2007) and the magnetic field structure (e.g., Bucciantini et al. 2005) of such PWNe are sensitive to the density structure of the ISM, the speed and direction of the neutron star's spatial velocity, and the geometry of its pulsar wind. Additionally, X-ray observations suggest such PWNe efficiently inject high-energy particles into the surrounding ISM, often in directions misaligned with the neutron star's proper motion (e.g., Bandiera (2008); De Luca et al. (2013); Marelli et al. (2013); Pavan et al. (2014)).

Understanding the structure of these pulsar winds, and how high energy particles escape the PWN, requires mapping the polarized radio emission for a range of neutron star and ISM properties. Currently, this is possible for $\lesssim 5-10$ systems, but even this small sample shows significant diversity in their magnetic field structure – for example, the "Frying Pan" (G315.9−0.0) PWN has

PoS(AASKA14)046

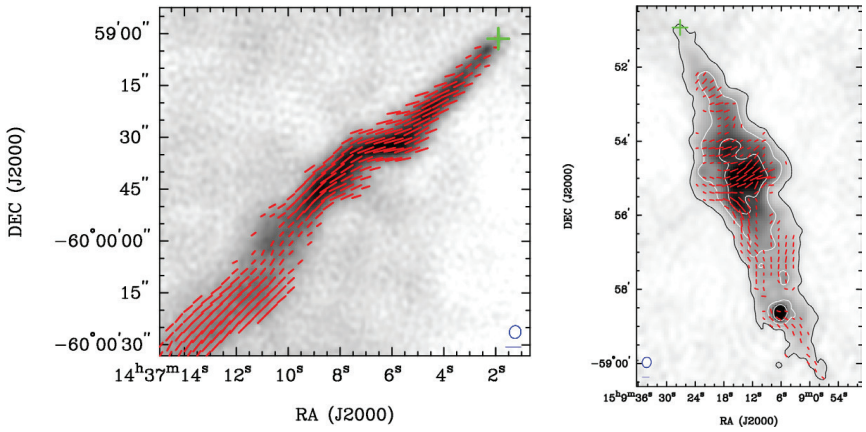

Figure 3: The radio nebulae G315.9−0.0 (*left*; Ng et al. 2012) and G319.9−0.7 (*right*; Ng et al. 2010. The location of the associated pulsars are indicated by the green crosses, while the polarization $\vec{B}$-vector is shown by the red lines.

a magnetic field aligned with the pulsar's proper motion (Ng et al. 2012), while the magnetic field of G319.9−0.7 has a helical structure Ng et al. (2010) (Figure 3) – suggesting a dependence on the flow conditions, pulsar speed, and/or misalignment between the pulsar rotation axis and proper motion. Understanding the relationship between these different physical parameters requires measuring the magnetic field structure of many more PWN which, as described in §5, will become possible with the SKA.

5. Requirements for SKA1 and SKA2

Thanks to the considerable improvement in sensitivity promised by the SKA1 and the SKA2, these instruments should be capable of measuring the radio morphology, spectrum, and polarization properties of ~ 100 PWNe – a significant improvement over the ~ 10 for which such measurements exist, and increase the number of eclipsing binary pulsars from ~ 50 to ~ 300. Such sample sizes are needed to determine how a neutron star's spin-down luminosity, age, and environment affects the evolution of its PWN. Additionally, the SKA1 and especially SKA2 will be able to measure properties of a PWN never before possible. These studies depend less on the collecting area of the SKA1, and therefore are more immune to a 50% reduction of its capabilities, but on the configuration and capabilities of its telescopes as described below:

Discover pulsars: Currently, $\sim 40-50\%$ of PWN candidates are unassociated with a pulsar in any waveband (Roberts 2004), problematic for the analyses discussed in §2 and §4. While beaming explains some of the missing pulsars, for many PWNe it likely results from the limitations of current observatories. The large collecting area of the SKA1-LOW should increase the number of pulsars detected in nearby PWN, but the high dispersion measure (DM) and scattering timescales expected for pulsars on the far side of the Milky Way require that the SKA1-MID also be able to detect pulsars.

Monitor a PWN's pulsed and unpulsed radio emission: Monitoring the timing properties of young, isolated pulsars is needed to measure their braking indices which, as described in §2, is critical for estimating their initial spin period. For eclipsing binary pulsars, monitoring the pulsed

PoS(AASKA14)046

emission allows one to detect changes in the orbital phase and length of radio eclipses changes, and monitoring the pulsed emission of MSP/LMXB is critical for determining if the pulsed radio emission disappears before or after the resumption of accretion onto the neutron star (§3). Both the SKA1-LOW and SKA1-MID require these capabilities since the possible presence of dense plasma in these systems will result in frequency dependent behavior. Additionally, observations of young PWNe every few months are required to measure the variability of "wisps" near the termination shock, critical for determining if ions are present in the pulsar wind (§2). Since these wisps are only a few arcseconds in size (e.g., Bietenholz et al. 2004), this is best done with the higher frequencies of SKA1-MID.

Conduct pulsar gating and VLBI observations: While all pulsars are believed to generate a PWN, radio PWNe are detected around $< 10\%$ of young, energetic pulsars. One possibility is that the radio PWN is masked in continuum observations by the pulsar's pulsed emission. With pulsar gating, it is possible to image the region when the pulsar is "off", making it possible to detect faint radio PWNe (Gaensler et al. 1998). This is particularly important for SKA1-LOW, due to its lower angular resolution and increased brightness of the pulsar relative to the PWN. Pulsar gating of eclipsing binary pulsars allows simultaneous measurements of its pulsed and unpulsed flux, critical for determining the eclipsing mechanism (§3), and significantly improves measurements of a pulsar's parallax and proper motion in VLBI observations – important for measuring the initial spin periods of young pulsars in composite SNRs (e.g., Gelfand et al. submitted) and interpreting the morphology of "bow shock" PWNe (§4).

Observe PWNe across a broad range of frequencies: The broadband radio spectrum of a PWN inside a SNR is expected to have numerous features (e.g., Gelfand et al. 2009). The minimum particle energy injected at the termination shock will result in a "break" at low ($\nu \lesssim 1$ GHz) frequencies, and measuring its flux density below this break is critical for estimating the initial spin period of the central neutron star (e.g., Gelfand et al. submitted; Figure 1). Ions in the pulsar wind and/or magnetic reconnection downstream of the termination shock (§2) is expected to lead to broad "bumps" in the spectrum at higher frequencies ($\nu \gtrsim 10$ GHz; Olmi et al. 2014). Continuous frequency coverage between the different SKA1 and SKA2 observing bands would improve measurements of curvature in the PWN's radio spectrum.

Detect emission on large angular scales: The non-detection of many TeV PWNe at radio wavelengths (e.g., Ferrand & Safi-Harb 2012) and SNRs around young pulsars / PWNe (e.g., Roberts 2004) likely results from the large angular size ($\sim 30' - \lesssim 1^\circ$) and low radio surface brightness of these objects. Current radio interferometers do not have the short baselines needed to detect emission on these angular scales, and single-dish telescopes do not have the sensitivity needed to detect this emission over the Galactic background. While SKA1-LOW and SKA1-MID will have the needed sensitivity, a dense core is required to detect emission on the needed angular scales.instantaneous SKA1-LOW single beam

Measure the polarization properties of PWNe: Last, but not least, mapping the magnetic field structure of young (§2) and old (§4) PWNe requires spatially resolved measurements of their polarized intensity and direction at multiple frequencies to both correct for foreground Faraday rotation

PoS(AASKA14)046

and detect changes in its rotation measure (e.g., Ng et al. 2010). Furthermore, measuring changes in the DM during the "eclipse" of a binary pulsar (e.g., Archibald et al. 2013) are important for measuring the density and magnetic field structure of the intervening plasma (§3). These observations require high polarization purity of both SKA1-LOW and SKA1-MID, and sensitivity to polarized emission over a small bandwidth or at higher ($\nu > 1$ GHz) frequencies to avoid bandwidth depolarization, especially for SKA1-MID. Furthermore, since a PWN's radio emission can be highly linearly polarized, an all-sky polarization survey with the SKA1-SUR could identify new PWNe, particularly around older, isolated pulsars.

ACKNOWLEDGMENTS: CYN is supported by a ECS grant under HKU 709713P. J.W.T.H. acknowledges funding from an NWO Vidi fellowship and ERC Starting Grant "DRAGNET" (337062).

References

Amato, E. & Arons, J. 2006, ApJ, 653, 325
Archibald, A. M. et al.. 2013, ArXiv e-prints: 1311.5161
—. 2009, Science, 324, 1411
Bandiera, R. 2008, A&A, 490, L3
Bassa, C. G. et al.. 2014, MNRAS, 441, 1825
Bietenholz, M. F. et al.. 2004, ApJ, 615, 794
Blondin, J. M. & Mezzacappa, A. 2007, Nature, 445, 58
Bogdanov, S. et al.. 2011, ApJ, 742, 97
Bogovalov, S. V. 1999, A&A, 349, 1017
Bucciantini, N. et al.. 2005, A&A, 434, 189
—. 2011, MNRAS, 410, 381
Carrigan, S. et al.. 2013, ArXiv e-prints: 1307.4690
Chevalier, R. A. 2005, ApJ, 619, 839
de Jager, O. C. 2007, ApJ, 658, 1177
De Luca, A. et al.. 2013, ApJ, 765, L19
Faucher-Giguère, C.-A. & Kaspi, V. M. 2006, ApJ, 643, 332
Ferrand, G. & Safi-Harb, S. 2012, Advances in Space Research, 49, 1313
Freire, P. 2013, http://www.naic.edu/ pfreire/GCpsr.html
Fruchter, A. S. et al.. 1988, Nature, 333, 237
Gaensler, B. M. et al.. 1998, MmSAI, 69, 813
Gelfand, J. D. et al.. 2014, Astronomische Nachrichten, 335, 318
—. submitted, ApJ
—. 2009, ApJ, 703, 2051
Goldreich, P. & Julian, W. H. 1969, ApJ, 157, 869
Helfand, D. J. & Becker, R. H. 1987, ApJ, 314, 203
Kennel, C. F. & Coroniti, F. V. 1984, ApJ, 283, 694
Kirk, J. G. & Skjæraasen, O. 2003, ApJ, 591, 366
Li, L. et al.. 2014, ApJ, 788, 16
Lyubarsky, Y. E. 2003, MNRAS, 345, 153
Marelli, M. et al.. 2013, ApJ, 765, 36

PoS(AASKA14)046

Moldón, J. et al.. 2014, International Journal of Modern Physics Conference Series, 28, 60173
Ng, C.-Y. et al.. 2012, ApJ, 746, 105
—. 2010, ApJ, 712, 596
Olmi, B. et al.. 2014, MNRAS, 438, 1518
Papitto, A. et al.. 2013, Nature, 501, 517
Pavan, L. et al.. 2014, A&A, 562, A122
Pétri, J. & Dubus, G. 2011, MNRAS, 417, 532
Porth, O. et al.. 2013, MNRAS, 431, L48
Roberts, M. S. E. 2004, http://www.physics.mcgill.ca/ pulsar/pwncat.html
Roberts, M. S. E. 2013, in IAU Symposium, Vol. 291, IAU Symposium, ed. J. van Leeuwen, 127–132
Roberts, M. S. E. et al.. 2014, Astronomische Nachrichten, 335, 313
Spitkovsky, A. & Arons, J. 2004, ApJ, 603, 669
Stappers, B. W. et al.. 2014, ApJ, 790, 39
Torres, D. F. et al.. 2014, Journal of High Energy Astrophysics, 1, 31
Vigelius, M. et al.. 2007, MNRAS, 374, 793
Wakely, S. P. & Horan, D. 2008, International Cosmic Ray Conference, 3, 1341
Watts, A. L. & Andersson, N. 2002, MNRAS, 333, 943
Young, N. J. et al.. 2013, MNRAS, 429, 2569

PoS(AASKA14)046

PROCEEDINGS OF SCIENCE

Pulsars in Globular Clusters with the SKA

J. W. T. Hessels[*ab], **A. Possenti**[c], **M. Bailes**[de], **C. G. Bassa**[a], **P. C. C. Freire**[f], **D. R. Lorimer**[g], **R. Lynch**[h], **S. M. Ransom**[i] **& I. H. Stairs**[j]

[a] *ASTRON, the Netherlands Institute for Radio Astronomy, Postbus 2, 7990 AA, Dwingeloo, The Netherlands; E-mail:* hessels@astron.nl

[b] *Anton Pannekoek Institute for Astronomy, University of Amsterdam, Science Park 904, 1098 XH Amsterdam, The Netherlands*

[c] *INAF-Osservatorio Astronomico di Cagliari, Via della Scienza 5, I-09047 Selargius, Italy*

[d] *Centre for Astrophysics and Supercomputing, Swinburne University of Technology, PO Box 218, VIC 3122, Australia*

[e] *ARC Centre of Excellence for All-Sky Astrophysics (CAASTRO)*

[f] *Max-Planck-Institut für Radioastronomie, auf dem Hügel 69, 53121, Bonn, Germany*

[g] *Dept. of Physics and Astronomy, West Virginia University, Morgantown, WV 26506, USA*

[h] *Dept. of Physics, McGill University, 3600 University Street, Montreal, QC H3A 2T8, Canada*

[i] *National Radio Astronomy Observatory, 520 Edgemont Road, Charlottesville, VA 22901, USA*

[j] *Dept. of Physics and Astronomy, University of British Columbia, 6224 Agricultural Road, Vancouver, BC V6T 1Z1, Canada*

Globular clusters are highly efficient radio pulsar factories. These pulsars can be used as precision probes of the clusters' structure, gas content, magnetic field, and formation history; some of them are also highly interesting in their own right because they probe exotic stellar evolution scenarios as well as the physics of dense matter, accretion, and gravity. Deep searches with SKA1-MID and SKA1-LOW will plausibly double to triple the known population. Such searches will only require one to a few tied-array beams, and can be done during early commissioning of the telescope — before an all-sky pulsar survey using hundreds to thousands of tied-array beams is feasible. With SKA2 it will be possible to observe most of the active radio pulsars within a large fraction of the Galactic globular clusters, an estimated population of $600-3700$ observable pulsars (those beamed towards us). This rivals the total population of millisecond pulsars that can be found in the Galactic field; fully characterizing it will provide the best-possible physical laboratories as well as a rich dynamical history of the Galactic globular cluster system.

Advancing Astrophysics with the Square Kilometre Array
June 8-13, 2014
Giardini Naxos, Italy

*Speaker.

PoS(AASKA14)047

1. Introduction: The Science of Globular Cluster Pulsars

Compared with the Galactic field, globular clusters (GCs) contain large numbers of millisecond pulsars (MSPs) per unit stellar mass — for recent reviews see: Camilo & Rasio (2005); Ransom (2008); Freire (2013). The stellar densities in the cores of GCs are orders-of-magnitude larger than in the Galactic plane; these conditions create a unique environment for stellar collisions and interactions (e.g. Sigurdsson & Phinney 1993, 1995). As a result, neutron stars can swap in new companion stars and form exotic binary (and trinary) systems (e.g. Thorsett et al. 1999; Sigurdsson et al. 2003), in which the neutron star is often spun-up to become an MSP through a period of mass and angular momentum transfer (Alpar et al. 1982; Radhakrishnan & Srinivasan 1982). Furthermore, GCs have half-light radii of only a few arc-minutes or less, making them easy targets for directed searches. Deep searches of the Galactic GC system have thus far discovered 144 pulsars in 28 clusters[1]. This includes many remarkable systems, e.g.: the fastest-spinning neutron star known (Hessels et al. 2006), potentially the most massive neutron star known (Freire et al. 2008a,b), a double neutron star system (Prince et al. 1991), a triple system with a white dwarf and Jupiter-mass companion (Thorsett et al. 1999; Sigurdsson et al. 2003), as well as many highly eccentric binaries (Ransom et al. 2005; Freire et al. 2004, 2008a; Lynch et al. 2012) and systems with 'odd' orbits or stellar companions (Lyne et al. 1993; D'Amico et al. 2001).

Population simulations, based on the results of deep pulsar searches in the past decade, show that the Galactic GC system harbors many more pulsars still to be discovered (Bagchi et al. 2011; Chennamangalam et al. 2013; Turk & Lorimer 2013). In particular, once extrapolated to the total sample of 157 known GCs in the Milky Way, the most recent study (Turk & Lorimer 2013) predicts a population range of potentially observable pulsars (i.e. those beamed towards us) between $600 - 3700$ (95% confidence level). The distribution of this population among the various known sub-classes of pulsars (isolated, binaries, trinaries, eclipsing, etc.) has not been carefully explored (though see Verbunt & Freire 2014). Nonetheless, past experience indicates that any significant growth in the known population inevitably leads to the discovery of some exotic and rare new kinds of pulsar systems (e.g. the pulsar triple system PSR J0337+1715; Ransom et al. 2014). In this respect, pulsars in GCs are of special interest because the peculiar environment of the core of a GC provides the conditions for producing systems that are unlike anything that can be easily formed in the Galactic field (e.g. Freire et al. 2004), thus opening the possibility of detecting 'Holy Grail' systems, like the first-ever MSP + black hole binary or even an MSP + MSP binary. The known GC pulsars, and those that the SKA will discover, can be studied very efficiently, because they are all located close to each other on the sky. For example, a single observation using no more than a half dozen tied-array beams could time all 34 known pulsars in Terzan 5.

The science of GC pulsars falls into two main themes:

i) Individual systems that can be used for investigations in fundamental physics, like the equation-of-state of neutron-rich matter at super-nuclear densities and/or tests of gravitational theories (Ransom et al. 2005; Freire et al. 2008a,b; Demorest et al. 2010; Kramer et al. 2006) — see also other relevant chapters in these proceedings (Keane et al. 2015; Shao et al. 2015;

[1] See http://www.naic.edu/∼pfreire/GCpsr.html for an up to date catalog.

PoS(AASKA14)047

Watts et al. 2015). Such systems can also provide novel insights for understanding stellar evolution and accretion physics (Archibald et al. 2009; Papitto et al. 2013; Bassa et al. 2014; Stappers et al. 2014). Although these science cases can also be addressed using pulsars in the Galactic field, the radically different environment of a GC favors the formation of exotic objects, the peculiar parameters of which may be even better suited for certain applications or constraining physical models.

Ultra-Fast Rotators: GCs harbor some of the fastest-spinning neutron stars known, including the 716-Hz record holder in Terzan 5 (Hessels et al. 2006). Though such sources are rare (Hessels et al. 2007), doubling or tripling the known population provides great prospects for pushing towards even faster rotation rates — perhaps even a *sub*-millisecond pulsar, which could strongly constrain the maximum neutron star radius and hence the equation-of-state (Hessels et al. 2006; Lattimer & Prakash 2001). Unlike in the Galactic field, an MSP in a GC can *in principle* experience multiple episodes of recycling (due to dynamical encounters) and hence could be more effectively spun up to its limiting rotational period (as well as growing in mass). This remains to be shown directly, however.

Neutron Star Masses: Many (at least 23) highly eccentric ($e > 0.01$) pulsar binary systems exist in GCs. For these, the neutron star mass can be constrained with the help of periastron precession (e.g. Freire et al. 2008a). In the Galactic field, MSP orbits are almost exclusively extremely circular ($e < 10^{-4}$), and prohibit such measurements in most cases. Besides the obvious implications of the highest-mass sources for constraining the neutron star equation-of-state (Antoniadis et al. 2013; Demorest et al. 2010), mapping the full MSP mass distribution is an important probe of their formation in supernovae, and their later 'recycling' through accretion. Once enough NS masses have been measured, the maximum NS mass should become apparent.

Evolution and Accretion: Some individual systems also pose interesting evolutionary puzzles, which touch on accretion physics, accretion-induced collapse, and stellar exchanges. For example, a handful of slow, apparently young pulsars are also known in GCs (Lyne et al. 1996; Boyles et al. 2011), providing interesting cases for exploring alternatives to the typical core-collapse supernova channel for forming neutron stars. The first MSP with a bloated main-sequence companion was found in a GC (D'Amico et al. 2001). This is now the prototype for a known population of a dozen such sources, some of which are seen to switch between radio MSP and low-mass X-ray binaries in quiescence and/or outburst (Archibald et al. 2009; Papitto et al. 2013; Bassa et al. 2014; Stappers et al. 2014). In fact, there are now 21 eclipsing pulsars (so-called 'black widows' and 'redbacks') in GCs, meaning that there are excellent prospects for studying more such transitions in the future.

Multi-wavelength Studies: Deep multi-wavelength observations of GCs in X-rays (primarily using *Chandra*; see e.g. Grindlay et al. 2001; Pooley et al. 2002; Grindlay et al. 2002; Heinke et al. 2003a,b, 2005, 2006; Bogdanov et al. 2006; Elsner et al. 2008; Bogdanov et al. 2011), γ-rays (primarily using *Fermi*; see e.g. Freire et al. 2011), and optical (primarily using *HST*; see e.g. Edmonds et al. 2001; Bassa et al. 2003, 2004; Pallanca et al. 2010, 2013, 2014) provide complementary information on either the pulsar's magnetospheric emission, intra-binary emission (perhaps from a shock), or the companion itself. The next generation of extremely large telescopes (ELTs) may provide large numbers of radial velocities for constraining the mass ratios of the stellar components, as in Cocozza et al. (2006). Conversely, identifying high-energy GC sources as radio pulsars helps better understand the zoo of objects that can be created (e.g. cataclysmic variables, low-mass X-ray

PoS(AASKA14)047

binaries, etc.) and hence the stellar evolution history of the cluster itself (Heggie & Giersz 2008). For GC pulsars we have an independent measure of the distance (and often the reddening), which can allow stronger constraints on several pulsar+companion quantities measured in optical, X-rays or γ-rays. The *Fermi* satellite is revealing γ-ray emission from several GCs (e.g. Abdo et al. 2010). Comparing the total γ-ray emission with the number and properties of the known radio MSPs in the largest possible sample of GCs will be a new tool for investigating the as yet poorly understood high-energy emission mechanisms of the MSPs (e.g. Harding et al. 2005), as well as constraining the MSP radio beaming factor (i.e. the fraction of the sky swept by the MSP radio beam). *Fermi* is not only detecting several GCs, but has started detecting individual pulsars, like PSR B1820−30A (Freire et al. 2011) and PSR B1821−24A (Johnson et al. 2013).

ii) Using the cumulative population of pulsars to probe the structure, proper motion, dynamical status, magnetic field, and gas content of the cluster itself (Phinney 1993; Meylan & Heggie 1997; Pooley et al. 2003). Pulsar-determined quantities can constrain the still largely obscure GC evolution, as well as its relation with the history of the Galaxy. For example, the pulsar-abundant cluster Terzan 5 contains at least two stellar populations of differing ages, and is possibly the pristine remnant of a building block of the Galactic bulge (Ferraro et al. 2009). The same advances in computing that will allow the creation of the SKA will also allow advances in numerical simulations of GCs. Simulations of the stellar and dynamical evolution of stars in a GC will predict the observable population of neutron stars in each cluster, and this can be directly tested against observations. Neutron stars, as some of the heaviest objects in GCs, play a vital role by acting as an energy reservoir to counter the gravitational collapse through the formation and disruption of binaries. The SKA will provide a census by looking for those neutron stars seen as pulsars, and their spin and binary properties will give important clues to the dynamical state of the cluster (e.g. Verbunt & Freire 2014).

Cluster Potential: Acceleration in the cluster potential affects the pulsars' spin derivatives and binary orbital period derivatives, which can be used to probe the cluster potential in a very direct and unique way, possibly revealing the presence of an intermediate mass black hole at the core. Strong constraints can also be set on the inner mass-to-light ratio by finding a very centrally located pulsar (D'Amico et al. 2002). Thus far, there is no certified intermediate-mass black hole (IMBH) known to exist, anywhere in the Universe. Finding such an object would lead to a wealth of studies to understand its formation and characteristics, e.g. testing if the velocity dispersion of nearby stars in the GC is related to the black hole mass, as is seen in galaxies over a few orders-of-magnitude in mass. The discovery of an MSP orbiting an IMBH would give a unique chance to directly measure the black hole spin (Liu et al. 2014, see also Liu 2012, PhD, U. of Manchester).

Proper Motion: The ensemble of pulsar proper motions, measured through pulsar timing, can be used to determine the cluster's proper motion and hence to infer its orbit in the Galactic gravitational potential (to some extent optical studies already measure GC proper motions, although not very precisely; though this will change with GAIA). While radio can provide accurate proper motion, optical instruments (especially 30-meter-class telescopes) can provide accurate radial motion. The combination produces a 3D velocity vector for the GC. When this is done for a sizable number of GCs, it will be possible to constrain the Galaxy's gravitational potential well. For nearby

PoS(AASKA14)047

clusters, there is also the chance to detect the peculiar motions of the MSPs within each cluster. If they are in binary systems, then also the optical radial motion and hence the 3D motion of the population of binary MSPs in a GC can be determined. Again this will be a handle for constraining the GC potential well, especially in the core, where the relatively massive MSPs (compared to the mean stellar mass) typically reside.

Intra-cluster Medium: Differential dispersion and rotation measures (DMs and RMs) between the detected pulsars can be used as highly sensitive, unique probes of the intra-cluster ionized medium and magnetic field (Freire et al. 2001b). This can teach us about the stellar winds of old stars releasing plasma in the cluster and/or the interactions between this plasma and the winds of MSPs and hot stars. Furthermore, the existence of this plasma, together with sensitive X-ray limits on accretion luminosity from a central source, can be used to place an upper limit on the mass of a possible central black hole. As to the putative magnetic fields in GCs, these will be an additional ingredient in attacking the difficult problem of justifying the occurrence of large-scale magnetic fields in the Universe.

Interaction History: The types of pulsars that are found — e.g. their spin-period distribution, locations in the cluster, and the fraction of binary versus isolated pulsars — can vary quite drastically from cluster to cluster, and encodes information about the dynamical history of the GC (Verbunt & Freire 2014). Here we will learn about the still largely unknown stages of a GC's evolution, with particular emphasis on the process leading to core-collapse. There are indications that the situation is quite different with respect to what was believed until recently; for the relevant theory and observations see Fregeau (2008) and Pooley (2010), respectively.

There are 157 known Galactic GCs (Harris 1996)[2], most of which have now been searched for pulsars. Since the earliest handful of GC pulsar discoveries (Lyne et al. 1987, 1988; Manchester et al. 1990; Anderson et al. 1990; Manchester et al. 1991; Kulkarni et al. 1991), the known population has exploded in the last decade. This has been thanks to a number of large surveys with Parkes (e.g. Camilo et al. 2000; Ransom et al. 2001; Possenti et al. 2003), Arecibo (e.g. Hessels et al. 2007), and the Green Bank Telescope (GBT; e.g. Ransom et al. 2004, 2005). All of these surveys greatly benefitted from new, wide-band pulsar data recorders that provided big leaps in time and frequency resolution, critical for identifying the fastest rotating pulsars. The first major crops of GC pulsars were in M15 (Anderson 1993) and 47 Tuc (Manchester et al. 1990, 1991; Camilo et al. 2000; Freire et al. 2003, 2001a). Deep synthesis imaging underlined the potential for discovery (Fruchter & Goss 2000). For example, deep imaging of Terzan 5 (Fruchter & Goss 2000) spawned great interest in that cluster, which later resulted in a record 34 known MSPs being found (Ransom et al. 2005; Hessels et al. 2006). The discovery rate has recently fallen off, as we have reached the limits of what the current generation of large single dishes can do. As we now discuss, SKA1 can provide the next boom in GC pulsar discoveries, and this can be achieved in the very early days of the telescope, even with a subset of the total collecting area.

2. Observing Pulsars in Globular Clusters with SKA1

The search sample: SKA1 will provide unprecedented sensitivity for targeted GC searches

[2]Last revision from December 2010 available at http://physwww.mcmaster.ca/∼harris/mwgc.dat.

PoS(AASKA14)047

in the southern skies, which is fortunately also where the majority of the most massive, densest, and hence most pulsar-rich GCs can be found, i.e. in the Galactic bulge. Compared with the greater observing and processing challenge of an all-sky search, which will require the formation of hundreds to thousands of tied-array beams, deep targeted searches of these limited fields-of-views will provide early commissioning science by quickly finding dozens, and eventually a few hundred pulsars in these clusters (once sufficient collecting area is in place, even if only 50% of the total, and at least a basic tied-array mode is available; we also note that even an incoherent sum of > 50 dishes would already provide higher sensitivity for those clusters that are currently only visible to Parkes). Follow-up timing observations will also be facilitated by the small required field-of-view. We know that we are currently only sampling the tip of the pulsar luminosity distribution in these predominantly distant ($\gtrsim 4$ kpc) stellar systems. In fact, recent investigations (Bagchi et al. 2011; Chennamangalam et al. 2013) confirmed that the luminosities (defined as $L_\nu = Sd^2$, where S is the observed flux density at central frequency ν in MHz, and d is the GC distance) of the pulsars observed in a GC can be reproduced as the bright tail of either a log-normal distribution — with parameters compatible with the luminosity functions (LFs) inferred for the pulsars in the Galactic field — or a power-law distribution with index ~ -1 (in agreement with earlier results by McConnell et al. 2004; Hessels et al. 2007), with the former functional form providing a slightly better match to the available data. For both the assumed LFs, in a large range of not too weak luminosities (typically above 0.5 mJy kpc^2), the flux density distribution follows dlogN/dlogS$\sim 0.5-1$ for any given cluster. That implies that a large increase in sensitivity will automatically bring many new sources within the reach of detection and will also provide higher-precision studies of the (mostly very faint, $S_{1400} \sim 20\,\mu$Jy) sources that are currently known. This will also enable, e.g., more mass measurements and equation-of-state constraints using already known sources. As we outline below, SKA1 can plausibly increase the known population of 144 pulsars by a factor of two to three and, most importantly, excellent laboratories for studying dense matter physics and gravity will be discovered. In some cases, it may be possible to detect all the active radio pulsars in a given cluster, providing a unique view of the star formation history and interactions over the cluster's lifetime. In most cases, however, the SKA2 will be needed to reach the full observable sample.

Based on population synthesis simulations (Turk & Lorimer 2013), a conservative total of $600-3700$ detectable (i.e. beamed towards us) pulsars in the Galactic GC system can be inferred. This rivals the total expected population of MSPs in the Galactic field, estimated at a few tens of thousands of sources (Faucher-Giguère & Kaspi 2006; Lorimer 2008). Importantly, while Galactic field pulsars are spread across the full 41,000 sq. degrees of the celestial sphere, the total area required to search all known Galactic GCs combined constitutes only ~ 1 sq. degree! Of the 157 known Galactic GCs, there are 154/152 GCs visible to SKA1-MID/SKA1-LOW for at least 2 hrs, assuming elevation limits of 15/30 deg, respectively. For 8-hr integrations, there are still 141/113 clusters available for SKA1-MID/SKA1-LOW, respectively. Of these, 28 have at least one known pulsar, and hence the DM to the cluster is also known (a fact that makes searching significantly easier).

MSPs are in general weak radio sources (phase-averaged flux densities of $S_{1400} \lesssim 1$ mJy), and GCs are typically at $\gtrsim 4$ kpc. Raw sensitivity and long dwell time is thus crucial for finding the weakest cluster pulsars, though long dwell time also adds complications, as we discuss below. The

PoS(AASKA14)047

weakest known GC pulsars have $S_{1400} \lesssim 10\,\mu$Jy and were discovered in multi-hour integrations using the GBT and Arecibo with several hundred MHz of bandwidth at 1.4 or 2 GHz. This sets the bar that SKA1 must surpass.

Searching for binaries: Greater instantaneous sensitivity is not only important for finding weaker sources, but also because more than two-thirds of the known sources are in a binary system. Orbital motion smears the pulsar signal over multiple Fourier bins, and can make such sources undetectable unless this is corrected for (Ransom 2001). For this reason, it is likely that the intrinsic fraction of binary MSPs in clusters is larger than the observed fraction. Typically, binary pulsars are discovered using an 'acceleration search', which approximates the Doppler shift of the signal as a constant drift in the frequency domain (Ransom 2001). This approach is relatively computationally efficient; full searches of all Keplerian orbital parameters (even in the case of a circular orbit, where only three orbital parameters are needed) are currently not tractable for general use. Acceleration searches are only valid when the integration time of the full observation, $T_{\rm obs}$, is less than 10% of the orbital period, $P_{\rm orb}$. In other words, one cannot necessarily gain sensitivity to binary pulsar systems simply by integrating for a longer time (though some analytical techniques do exist; see Ransom 2001). The shortest known orbital period of a GC pulsar is $P_{\rm orb} = 1.5$ hr. Such a system can thus be found in a linear acceleration search of a 10-min data set. In the following, we therefore use 10 min as a fiducial integration time for searches for binary pulsars in compact orbits, while we use 2 hr as an appropriate integration time for longer-period binaries or isolated pulsars. The assumption of a constant acceleration is useful even for eccentric systems, although searches over a 'jerk' parameter may be helpful (Bagchi et al. 2013). With the constant-acceleration assumption, highly eccentric systems are in fact more easily detectable at most orbital phases than low-eccentricity systems[3].

Propagation effects: As in all pulsar surveys, interstellar propagation effects can strongly limit detectability, especially at the shortest spin periods, where residual smearing in time due to uncorrected dispersive or scattering delay can broaden the pulse in time to the point where it is no longer detectable. Many of the densest, most massive GCs known are located in the Galactic bulge. The line-of-sight DM is often large ($\gtrsim 200\,{\rm pc\,cm^{-3}}$), as is the expected scattering. To mitigate these effects, one can observe at higher radio frequency. Taking the competing effect of the typically steep spectra of pulsars ($S \propto \nu^{-\alpha}$, where $1 < \alpha < 3$; Maron et al. 2000; Bates et al. 2013) into account, it turns out that the $1.4-2.0$ GHz band is well suited for searching GCs with DMs greater than $\sim 100\,{\rm pc\,cm^{-3}}$. Roughly 100 of the SKA-visible clusters have expected DM$> 100\,{\rm pc\,cm^{-3}}$ (according to the NE2001 model of Cordes & Lazio 2002), and are excellent targets for SKA1-MID, which provides the maximum instantaneous sensitivity in the $1.4-2.0$ GHz band. For the remaining ~ 60 SKA-visible clusters with lower expected DMs, SKA1-LOW (and/or SKA1-MID at 800 MHz in some cases) presents an exciting opportunity, as we outline below.

Array configuration: GC pulsar searches require the SKA's tied-array observing mode because the data must be recorded with at least $\sim 50\,\mu$s time resolution. Maximum possible sensitivity can be achieved if the data are coherently dedispersed at the average cluster DM (in the case of GCs with known pulsars) or at least at a few trial DMs for clusters with no known sources. In practice, this will likely require the VLBI-like ability to record raw voltages from the tied-array. An important consideration is the sky area that must be covered for such searches. The known

[3] See Madsen 2013, MSc, UBC; https://circle.ubc.ca/handle/2429/44897

PoS(AASKA14)047

Galactic GCs typically have core radii of a few arc-seconds to one or two arc-minutes and half-light radii of $\sim 0.5-3$ arc-minutes (Harris 1996). GC pulsars congregate to a large extent towards the cluster core, and almost all of the known GC pulsars are within one arc-minute of the cluster's optical center-of-light. The 400-m (radius) core of SKA1-MID will provide a tied-array beam with FWHM of 0.9 arc-minute at 2 GHz, meaning that only a single beam will be needed to detect and discover the majority of the GC pulsars using this setup. In order to catch the minority of pulsars further from the core, which are still very interesting for understanding the dynamical history of the cluster, a more than sufficient coverage can be achieved with hexagonally packed grids of 7 or 13 beams. For the 600-m (radius) core of SKA1-LOW, a single 3 arc-minute tied-array beam at 350 MHz will be sufficient. Thus, searching for GC pulsars is an excellent early science and commissioning project, which will naturally lead the way to an all-sky pulsar survey requiring hundreds to thousands of tied-array beams. More ambitious searches using a larger fraction of the SKA1-MID/LOW antennas will be more challenging. For example, to double the instantaneous sensitivity provided by SKA1-MID requires going to a radius of 4000 m from the array center, and thus 100 times more beams to cover the same area of sky. This approach is likely more interesting for follow-up than for initial searches. For example, once new pulsars are found and sufficiently well localized, the further timing observations that are needed to extract the science (e.g. precision astrometry, orbital elements, proper motion, post-Keplerian effects, etc.) can be done by using one narrow, *full-array* tied-array beam on each source.

Achievable sensitivity: The 400-m (radius) core of SKA1-MID, operating from $1.4-2.0$ GHz can achieve an rms noise of 4.0/1.2 μJy for 10-min/2-hr integrations. Using a digital beam-former and back-end similar to those sketched in the SKA Baseline Design (i.e. capable of keeping the smearing effects of interstellar dispersion smaller than the adopted sampling time of 50 μs for all DMs $< 1000\,\mathrm{pc\,cm^{-3}}$), that rms noise translates into a limiting sensitivity (at $\mathrm{S/N} = 8$) of $\sim 12/4$ μJy for a recycled pulsar spinning at a ~ 1 ms period and having an intrinsic pulse duty cycle of 10%. Those sensitivity limits halve for the GCs where 8hr-long tracks with SKA1-MID are possible (this fortunately includes some of the most promising targets)[4]. SKA1-MID can reach a factor of ~ 3 deeper than the state-of-the-art searches performed using the GBT and the GUPPI back-end (DuPlain et al. 2008). Only 32 clusters within declination, δ, of $-2\,\mathrm{deg} < \delta < +38\,\mathrm{deg}$ are visible to Arecibo. For most of the 30 clusters south of $\delta = -40\,\mathrm{deg}$ the best limits have been reached by Parkes; SKA1-MID can go ~ 11 times deeper in these cases. The 600-m (radius) core of SKA1-LOW, operating from $250-450$ MHz, can achieve $\sim 100/30$ μJy sensitivity for 10-min/2-hr integrations (depending on the line-of-sight; for clusters in the Galactic bulge, T_{sky} will be significant). For comparison, the all-sky GBNCC survey at 350 MHz achieves ~ 1 mJy sensitivity (Stovall et al. 2014).

Available discovery space: Figure 1 illustrates the discovery space that is open to SKA1-MID for these kind of pulsar searches (a similar analysis can be made for SKA1-LOW). We define the quantity Γ_{LF} to represent the growth of the probed area of the pulsar luminosity function (LF) of a given GC. This assumes a survey performed with SKA1-MID at 1700 MHz central frequency,

[4]It is important to note that longer integrations do not necessarily improve sensitivity to binary pulsars because only a coherent search of the possible orbital parameters can fully recover the Doppler-smeared signal. Nonetheless, by the time that the SKA is operational, it may be possible to use more advanced binary search techniques than those typically used at present.

PoS(AASKA14)047

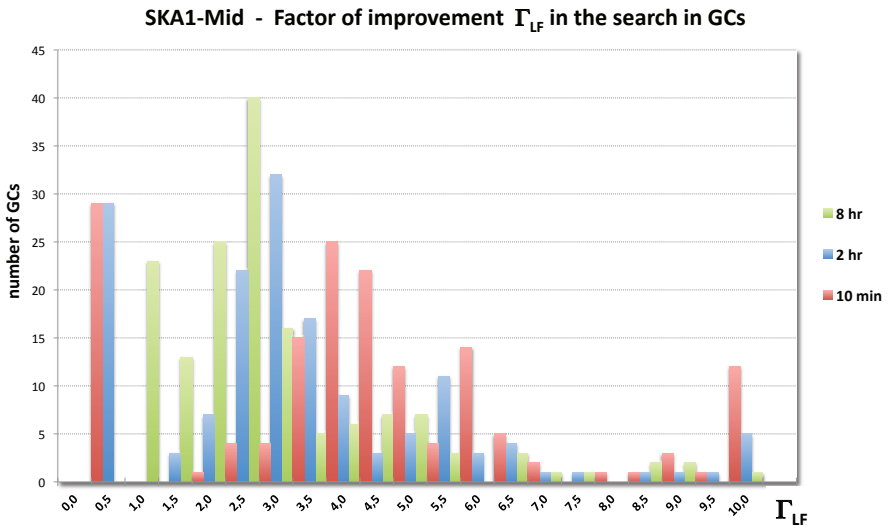

Figure 1: A histogram of the distribution of Γ_{LF}, which represents the growth of the probed area of the pulsar luminosity function, for all GCs visible to the SKA. Here we assume use of SKA1-MID in 10-min, 2-hr, and 8-hr observations, compared to state-of-the-art observations with Arecibo, GBT, and Parkes. See text for further details.

with 600 MHz bandwidth and other survey parameters like those in the SKA Baseline Design. In particular, the histogram of Fig.1 is obtained by comparing the sensitivity of this SKA1-MID survey with that of the best possible GC searches already carried out or still ongoing. For each cluster, we assume that the best-possible search can be conducted by either Arecibo, Parkes, or GBT, depending on the declination of the cluster (Arecibo is the best telescope for all clusters within $-2\,\mathrm{deg} < \delta < +38\,\mathrm{deg}$, Parkes is the best telescope for all clusters $\delta \lesssim -40\,\mathrm{deg}$, and the GBT is the best available for $\delta \gtrsim -40\,\mathrm{deg}$ and outside the Arecibo declination range). For the purpose of comparison, all flux density limits have been scaled to 1400 MHz using a pulsar spectral index $\alpha = -1.7$. We also assume, for simplicity, that the back-ends used in these various surveys are equally as good at minimizing the effects of dispersion. Finally, also the effects of scattering in the ISM have been assumed to be the same at the central frequencies of SKA1-MID and at the reference frequencies of the other telescopes ($\sim$ 1400 MHz for Parkes and Arecibo, and $\sim$ 2000 MHz for GBT). Using these assumptions, and an effective pulsar duty cycle of 25% (which is a typical for millisecond pulsars), we calculated survey flux density limits. The next step in producing Fig. 1 was to feed the calculated sensitivity limits to a log-normal pulsar LF with mean (in units of mJy kpc^2 expressed in a logarithmic base-10 scale) of -1.1 and dispersion 0.9, which is known to reproduce the observed data (Bagchi et al. 2011; Chennamangalam et al. 2013).

We considered the distributions of Γ_{LF} for 3 hypothetical surveys looking at each GC for 10 min, 2 hr, and 8 hr (color-coded in red, blue and green), respectively. It is evident that, for most GCs, SKA1-MID provides up to a factor 5 improvement in probing the LF. The average Γ_{LF} over

PoS(AASKA14)047

the entire population is between 3 and 4[5]. The higher average Γ_{LF} for shorter integration times is due to the shape of the log-normal LF, which is steeper at higher luminosity. In other words, a given increment in sensitivity produces higher values of Γ_{LF} when only the brightest part of the LF is sampled, which typically occurs for short pointings. This effect also largely explains the second peak at $\Gamma_{LF} \sim 10$, which results from the ~ 10 very distant GCs that are visible from Parkes. The increment in sensitivity of SKA1-MID with respect to Parkes is large and, moreover, if a pulsar should be discovered in those GCs by a shallow survey, its luminosity will have to be very high and thus Γ_{LF} is correspondingly very high. Finally, Fig.1 shows that also for the ~ 30 targets in the visibility range of Arecibo (appearing at Γ_{LF} between 0.5 and 1.0 for the case of short or intermediate-duration pointings), SKA1-MID can go deeper when using 8-hr integrations (Arecibo can typically track sources for only $1-3$ hrs).

We note that a direct extrapolation from Γ_{LF} to the expected number of pulsar discoveries in each GC is impossible for the majority of clusters, where there is currently no known pulsar. Such predictions are also uncertain for the GCs with known pulsars, because various effects (e.g. scintillation, fraction of binaries, Doppler smearing of the pulsar signal) can bias any simple relation between Γ_{LF} and the number of known pulsars. Nonetheless, despite all these caveats, the number of pulsars resulting from the direct multiplication of Γ_{LF} with the number of already known objects is compatible with the results of sophisticated statistical analyses (e.g. Bagchi et al. 2011; Chennamangalam et al. 2013) applied to some of the most populated GCs. These predict that the number of potentially observable pulsars should be (within 95% credible intervals) $82-259$ in Terzan 5, $48-137$ in 47 Tuc, and $48-191$ in M28. In summary, Γ_{LF} can be only taken as a figure-of-merit for the capabilities of SKA1-MID in the search for GC pulsars and is mostly useful for comparison with the current state-of-the-art Arecibo, GBT, and Parkes searches. In this respect, we note that a downgrade of SKA1-MID by a factor 50% in sensitivity would significantly reduce the effectiveness of the search for pulsars in GCs. In such a situation, it would be difficult to go significantly deeper than previous GBT searches, and impossible to go deeper than Arecibo. Thus, with a 50% reduction in SKA1-MID sensitivity, a significant sensitivity improvement would be limited to the GCs visible only from Parkes, i.e 1/5 of the total sample.

3. Observing Pulsars in Globular Clusters with SKA2

The great promise of SKA2 is illustrated in Fig. 2, where we show the distribution of the 'completeness percentages' of a GC survey. For example, 50% completeness indicates the capability of probing half of the total area defined by the LF of a given GC — i.e. half of the area under the curve is probed. Even with 8-hr integrations, SKA1-MID cannot see all the potential pulsars in a given GC, whereas SKA2 may detect the majority or even all the active radio pulsars in a large sample of some tens of GCs — enabling detailed comparisons of their evolutions and structures, as well as an unbiased determination of the shape and cut-off of the LF of the millisecond pulsar population. We also note that, when SKA2 will be operational, SKA1-MID will have likely detected at least one pulsar in most GCs, which will provide the possibility for SKA2 to speed up the search

[5]Power-law LFs (with index between -1.0 and -0.7, and cut-off luminosity in the confidence range $0.1-0.5\,\mathrm{mJy\,kpc^2}$) were also explored. Although the shape of the histogram distribution of Γ_{LF} is different with respect to the adoption of a log-normal function, the average value of Γ_{LF} over the whole GC population is similar.

PoS(AASKA14)047

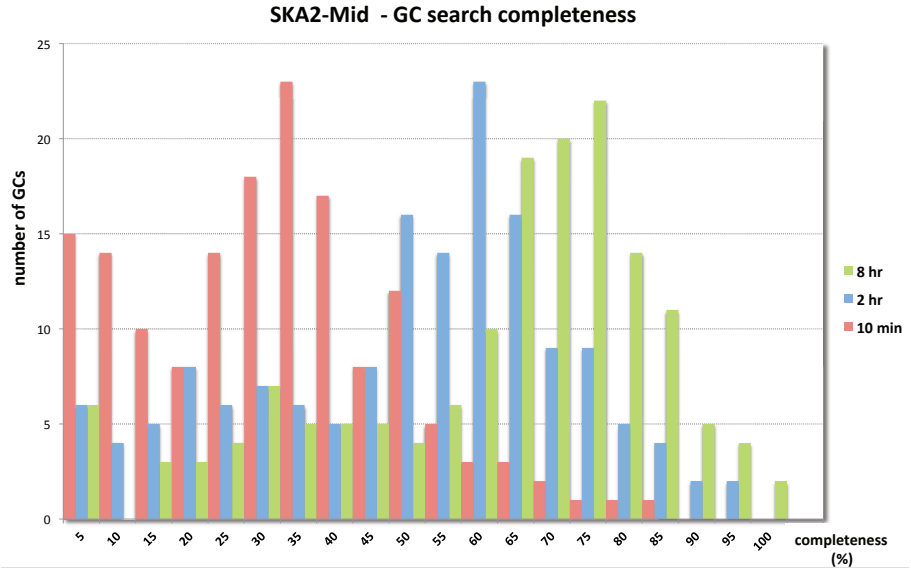

Figure 2: A histogram of the percentage completeness factors for GC pulsar searches with SKA2 (at 1700 MHz), using 10-min, 2-hr, and 8-hr observations. See text for further details.

for additional pulsars (and significantly reduce its computational cost) by using an already known approximate value of the DM.

4. Conclusions

Once constructed, SKA1-MID and SKA1-LOW will be the premier search machines for pulsars in GCs. Their raw sensitivity will surpass that of the GBT by a factor of about 3 and 4, respectively, which opens a large discovery space for faint sources outside of the Arecibo declination range. Though the uncertainties are large, we estimate that a doubling or tripling of the known pulsar population is possible. In other words, anywhere from $100-300$ pulsars can be found in a full census of ~ 150 GCs using 10-min integrations and only one tied-array beam synthesized from the SKA Core. This offers a great opportunity for early SKA pulsar science, even before all the collecting area is in place. A doubling or tripling of the known GC pulsar population means finding more exceptional pulsar systems for testing strong gravity, dense matter, and more. For example, only 3 of the known GC pulsars (all in Terzan 5) have spin rates greater than 500 Hz. A doubling or tripling of the known population gives good prospects for breaking the current 716-Hz rotation record held by Ter5ad. Besides the study of individual pulsar 'jewels' the ensemble of detected pulsars provide a unique probe of the dynamics and evolution. While SKA1 can significantly push such studies forward, SKA2 can bring us within a factor of a few of finding all the detectable (beamed towards us) pulsars in Galactic GC system, a population that has been estimated at $600-3700$, and which is comparable to the total detectable Galactic field population.

PoS(AASKA14)047

Acknowledgements

J.W.T.H. acknowledges funding from an NWO Vidi fellowship and ERC Starting Grant "DRAGNET" (337062).

References

Abdo, A. A. et al. 2010, A&A, 524, A75
Alpar, M. A. et al. 1982, Nature, 300, 728
Anderson, S. B. 1993, PhD thesis, California Institute of Technology, Pasadena.
Anderson, S. B. et al. 1990, Nature, 346, 42
Antoniadis, J. et al. 2013, Science, 340, 448
Archibald, A. M. et al. 2009, Science, 324, 1411
Bagchi, M. et al. 2011, MNRAS, 418, 477
—. 2013, MNRAS, 432, 1303
Bassa, C. et al. 2004, ApJ, 609, 755
Bassa, C. G. et al. 2014, MNRAS, 441, 1825
—. 2003, A&A, 409, L31
Bates, S. D. et al. 2013, MNRAS, 431, 1352
Bogdanov, S. et al. 2006, ApJ, 646, 1104
—. 2011, ApJ, 730, 81
Boyles, J. et al. 2011, ApJ, 742, 51
Camilo, F. et al. 2000, ApJ, 535, 975
Camilo, F. & Rasio, F. A. 2005, in Astronomical Society of the Pacific Conference Series, Vol. 328, Binary Radio Pulsars, ed. F. A. Rasio & I. H. Stairs, 147
Chennamangalam, J. et al. 2013, MNRAS, 431, 874
Cocozza, G. et al. 2006, ApJL, 641, L129
Cordes, J. M. & Lazio, T. J. W. 2002, ArXiv Astrophysics e-prints
D'Amico, N. et al. 2002, ApJL, 570, L89
—. 2001, ApJL, 561, L89
Demorest, P. B. et al. 2010, Nature, 467, 1081
DuPlain, R. et al. 2008, in Society of Photo-Optical Instrumentation Engineers (SPIE) Conference Series, Vol. 7019, Society of Photo-Optical Instrumentation Engineers (SPIE) Conference Series
Edmonds, P. D. et al. 2001, ApJL, 557, L57
Elsner, R. F. et al. 2008, ApJ, 687, 1019
Faucher-Giguère, C.-A. & Kaspi, V. M. 2006, ApJ, 643, 332
Ferraro, F. R. et al. 2009, Nature, 462, 483
Fregeau, J. M. 2008, ApJL, 673, L25
Freire, P. C. et al. 2003, MNRAS, 340, 1359
—. 2001a, MNRAS, 326, 901
—. 2004, ApJL, 606, L53
—. 2001b, ApJL, 557, L105
Freire, P. C. C. 2013, in IAU Symposium, Vol. 291, IAU Symposium, ed. J. van Leeuwen, 243–250

PoS(AASKA14)047

Freire, P. C. C. et al. 2011, Science, 334, 1107
—. 2008a, ApJ, 675, 670
—. 2008b, ApJ, 679, 1433
Fruchter, A. S. & Goss, W. M. 2000, ApJ, 536, 865
Grindlay, J. E. et al. 2002, ApJ, 581, 470
—. 2001, ApJL, 563, L53
Harding, A. K. et al. 2005, ApJ, 622, 531
Harris, W. E. 1996, AJ, 112, 1487
Heggie, D. C. & Giersz, M. 2008, MNRAS, 389, 1858
Heinke, C. O. et al. 2003a, ApJ, 590, 809
—. 2005, ApJ, 625, 796
—. 2003b, ApJ, 598, 516
—. 2006, ApJ, 651, 1098
Hessels, J. W. T. et al. 2006, Science, 311, 1901
—. 2007, ApJ, 670, 363
Johnson, T. J. et al. 2013, ApJ, 778, 106
Keane, E. F., Bhattacharyya, B., Kramer, M., et al, 2015, "A Cosmic Census of Radio Pulsars with the SKA", in proc. *Advancing Astrophysics with the Square Kilometre Array*, PoS(AASKA14)040
Kramer, M. et al. 2006, Science, 314, 97
Kulkarni, S. R. et al. 1991, Nature, 349, 47
Lattimer, J. M. & Prakash, M. 2001, ApJ, 550, 426
Liu, K. et al. 2014, MNRAS, 445, 3115
Lorimer, D. R. 2008, Living Reviews in Relativity, 11, 8
Lynch, R. S. et al. 2012, ApJ, 745, 109
Lyne, A. G. et al. 1988, Nature, 332, 45
—. 1993, Nature, 361, 47
—. 1987, Nature, 328, 399
—. 1996, ApJL, 460, L41
Manchester, R. N. et al. 1990, Nature, 345, 598
—. 1991, Nature, 352, 219
Maron, O. et al. 2000, A&AS, 147, 195
McConnell, D. et al. 2004, MNRAS, 348, 1409
Meylan, G. & Heggie, D. C. 1997, A&ARv, 8, 1
Pallanca, C. et al. 2013, ApJ, 773, 122
—. 2010, ApJ, 725, 1165
—. 2014, ApJ, 795, 29
Papitto, A. et al. 2013, Nature, 501, 517
Phinney, E. S. 1993, in Astronomical Society of the Pacific Conference Series, Vol. 50, Structure and Dynamics of Globular Clusters, ed. S. G. Djorgovski & G. Meylan, 141
Pooley, D. 2010, Proceedings of the National Academy of Science, 107, 7164
Pooley, D. et al. 2003, ApJL, 591, L131
—. 2002, ApJ, 573, 184

PoS(AASKA14)047

Possenti, A. et al. 2003, ApJ, 599, 475
Prince, T. A. et al. 1991, ApJL, 374, L41
Radhakrishnan, V. & Srinivasan, G. 1982, Current Science, 51, 1096
Ransom, S. M. 2001, PhD thesis, Harvard University
Ransom, S. M. 2008, in IAU Symposium, Vol. 246, IAU Symposium, ed. E. Vesperini, M. Giersz, & A. Sills, 291–300
Ransom, S. M. et al. 2001, ApJL, 546, L25
—. 2005, Science, 307, 892
—. 2014, Nature, 505, 520
—. 2004, ApJ, 604, 328
Shao, L., Stairs, I., Antoniadis, J., et al, 2015, "Testing Gravity with Pulsars in the SKA Era", in proc. *Advancing Astrophysics with the Square Kilometre Array*, PoS(AASKA14)042
Sigurdsson, S. & Phinney, E. S. 1993, ApJ, 415, 631
—. 1995, ApJS, 99, 609
Sigurdsson, S. et al. 2003, Science, 301, 193
Stappers, B. W. et al. 2014, ApJ, 790, 39
Stovall, K. et al. 2014, ApJ, 791, 67
Thorsett, S. E. et al. 1999, ApJ, 523, 763
Turk, P. J. & Lorimer, D. R. 2013, MNRAS, 436, 3720
Verbunt, F. & Freire, P. C. C. 2014, A&A, 561, A11
Watts, A. L., Xu, R., Espinoza, C. M. E., et al, 2015, "Probing the neutron star interior and the Equation of State of cold dense matter with the SKA", in proc. *Advancing Astrophysics with the Square Kilometre Array*, PoS(AASKA14)043

PoS(AASKA14)047

Magnetism

PROCEEDINGS OF SCIENCE

Using SKA Rotation Measures to Reveal the Mysteries of the Magnetised Universe

Melanie Johnston-Hollitt[*1], Federica Govoni[2], Rainer Beck[3], Siamak Dehghan[1], Luke Pratley[1], Takuya Akahori[4,5], George Heald[6], Ivan Agudo[7], Annalisa Bonafede[8], Ettore Carretti[2,9], Tracy Clarke[10], Sergio Colafrancesco[11], Torsten Enßlin[12], Luigina Feretti[13], Bryan Gaensler[14], Marijke Haverkorn[15,16], Sui Ann Mao[3], Niels Oppermann[17], Lawrence Rudnick[18], Anna Scaife[19], Dominic Schnitzeler[3], Jeroen Stil[20], A. Russ Taylor[21,22], and Valentina Vacca[12]

[1]*School of Chemical and Physical Sciences, Victoria University of Wellington, P.O. Box 600, Wellington 6140;* [2]*INAF - Osservatorio Astronomico di Cagliari,Italy;* [3]*Max-Planck-Institut für Radioastronomie, Bonn, Germany;* [4]*Graduate School of Science and Engineering, Kagoshima University, Japan;* [5]*SKA Organization, Cheshire, UK;* [6]*ASTRON, Dwingeloo, The Netherlands;* [7]*Instituto de Astrofisica de Andalucia-CSIC, Granada, Spain* [8]*Hamburger Sternwarte, Universität Hamburg, Germany;* [9]*CSIRO Astronomy and Space Science, Australia;* [10]*Naval Research Laboratory, USA;* [11]*School of Physics, University of the Witwatersrand, South Africa;* [12]*Max Planck Institute for Astrophysics, Garching, Germany;* [13]*INAF Istituto di Radioastronomia, Bologna, Italy;* [14]*Dunlap Institute, University of Toronto, Canada;* [15]*Radboud University, the Netherlands;* [16]*Leiden University, the Netherlands;* [17]*Canadian Institute for Theoretical Astrophysics, University of Toronto, Canada;* [18]*Institute for Astrophysics University of Minnesota, USA;* [19]*The University of Manchester, UK;* [20]*The University of Calgary, Calgary, Canada;* [21]*University of Cape Town, South Africa;* [22]*University of the Western Cape, South Africa*

E-mail: Melanie.Johnston-Hollitt at vuw.ac.nz

We know that magnetic fields are pervasive across all scales in the Universe and over all of cosmic time and yet our understanding of many of the properties of magnetic fields is still limited. We do not yet know when, where or how the first magnetic fields in the Universe were formed, nor do we fully understand their role in fundamental processes such as galaxy formation or cosmic ray acceleration or how they influence the evolution of astrophysical objects. The greatest challenge to addressing these issues has been a lack of deep, broad bandwidth polarimetric data over large areas of the sky. The Square Kilometre Array will radically improve this situation via an all-sky polarisation survey that delivers both high quality polarisation imaging in combination with observations of 7-14 million extragalactic rotation measures. Here we summarise how this survey will improve our understanding of a range of astrophysical phenomena on scales from individual Galactic objects to the cosmic web.

Advancing Astrophysics with the Square Kilometre Array
June 8-13, 2014
Giardini Naxos, Sicily, Italy

[*]Speaker.

PoS(AASKA14)092

1. Magnetism Science

Magnetism science can be considered on a variety of scales and the origin and evolution of magnetic fields in the Universe is one of the great outstanding mysteries of modern astrophysics. We do not yet know how magnetic fields first arose in the Universe, nor if these fields formed via a top down or bottom up process. Although we are aware that magnetic fields manifest in a range of astrophysical objects, over vastly differing physical scales from the Mpc-scale halos in galaxy clusters to sub-pc scale jet features in radio galaxies, we are still speculating as to how those fields are important in the ongoing life-cycles of these objects. Additionally, understanding magnetic fields and their associated signatures in radiation fields is of crucial importance for experiments to detect and characterise the Epoch of Reionisation, and for models of inflation theory using B-mode polarisation of the cosmic microwave background radiation. The detailed properties of cosmic magnetic fields are fundamental to resolving the enduring mystery of the origin of ultra-high energy cosmic rays, and the Square Kilometre Array (SKA) will provide this information. Finally, wide-area surveys have the potential to unveil the magnetic field of the cosmic web itself.

Although there are several methods for observing magnetic fields in other parts of the electromagnetic spectrum (e.g. optical polarisation, IR polarisation, observations of synchrotron emission in the optical and X-ray) or indirectly inferring the presence of magnetic fields (e.g. observations of magnetic Kelvin-Helmholtz or Parker instabilities (Vikhlinin et al. 2001) or Zeeman splitting (Robishaw et al. 2015)), all of these methods are limited in both their accuracy and range. Fortunately, observations in the radio are able to detect and characterise magnetic fields to high precision across much of the history of the Universe.

Historically, however, it has been difficult to undertake detailed studies of the magnetic fields of large numbers of objects due to limits in sensitivity, resolution and difficulties with polarisation calibration of the current generation of radio telescopes. Additionally, understanding the complex nature of polarised signals was difficult prior to the advent of techniques to allow us to probe Faraday spectra generated by rotation measure synthesis and to statistically disentangle effects of the line-of-sight foregrounds. With the current generation of new or upgraded instruments, along with better analysis techniques and improvements in computer modelling, we are starting to see an increase in the type and quantity of polarisation science that can be undertaken. Polarisation surveys on current instruments such as the Polarisation Sky Survey of the Universe's Magnetism (POSSUM) (Gaensler et al. 2010) on ASKAP (Hotan et al. 2014), the polarisation analysis of the GaLactic and Extragalactic All-sky MWA (GLEAM) survey (Wayth et al. 2015) on the MWA (Tingay et al. 2013) and the Multifrequency Snapshot Sky Survey (MSSS) (Heald et al., in prep.) on LOFAR (van Haarlem et al. 2013) as well as smaller experiments on such instruments (Bernardi et al. 2013; Jelić et al. 2014) will lay the foundations for an unprecedented period of magnetism science. The first phase of the SKA will take this work one step further providing instruments with high sensitivity, large bandwidths and good sky coverage, moving us into the *"Era of Precision Magnetism Science"*.

In order to exploit the vast potential of the SKA for magnetism science, the greatest priority for the magnetism community is a polarisation survey of the entire observable sky that provides both the polarisation properties of objects and the associated rotation measures. In fact, the goal of conducting an all-sky polarimetric survey on the Square Kilometre Array has been a mainstay

PoS(AASKA14)092

for cosmic magnetism science for over a decade (Gaensler et al. 2004; Feretti & Johnston-Hollitt 2004). The resultant rotation measure (RM) grid continues to provide a compelling observational target to understand both the polarised sources themselves, and as a means to statistically probe numerous important extended foreground sources including the Milky Way, Magellanic Clouds, clusters of galaxies, the lobes of giant radio galaxies, external galaxies and perhaps even the elusive warm-hot intergalactic medium (WHIM). A suitably dense RM grid will provide information along the entire line of sight which, combined with improved statistical techniques, will allow us to answer such outstanding science questions as:

- What is the mechanism to generate and sustain magnetic fields in the Milky Way, Magellanic Clouds and other nearby galaxies?
- How do magnetic fields influence galaxy formation and evolution?
- How do magnetic fields manifest in HII regions, supernova remnants, planetary nebulae and high velocity clouds in the Milky Way?
- Over what scales and at what strengths are magnetic fields generated in galaxy clusters and how does this correlate with cluster dynamical state?
- What is the large-scale structure of the magnetised Universe and can we statistically detect the magnetic fields in the cosmic web?
- What is the evolution of magnetic fields in intervening galaxies and clusters over cosmic time?

Here we will explore the science to be derived from a polarisation survey and the associated RM grid on the Phase 1 SKA and discuss the survey parameters needed to achieve characterisation of the most scientifically interesting objects.

2. Polarisation Science

In this section we will summarise the polarisation science priorities that have been identified for the SKA. We have grouped the topics in terms of the physical scale:

- Large scales ($\sim$Mpc): galaxy clusters and the cosmic web,
- Intermediate scales ($\leq$kpc): the Milky Way and nearby galaxies, and
- Small scales (kpc to pc): pulsars, masers, supernova remnants, high velocity clouds, shells and bubbles in the Milky Way and other galaxies.

2.1 Galaxy Clusters and the Cosmic Web

We know there are magnetic fields permeating galaxy clusters on Mpc-scales via the presence of diffuse synchrotron emission seen as either central radio halos or peripheral radio relics, and via the statistical increase in rotation measures seen through cluster lines of sight (Hennessy et al.

PoS(AASKA14)092

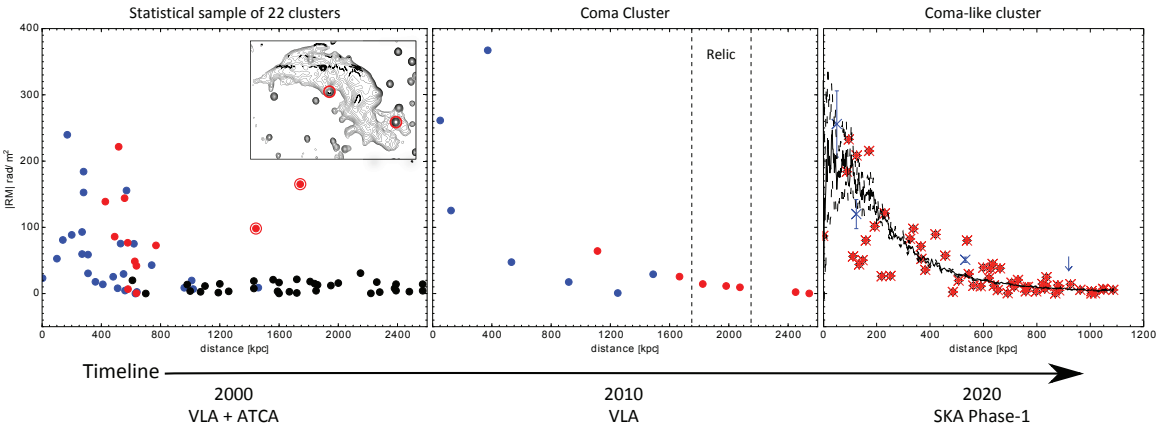

Figure 1: Statistical observations of RMs through galaxy clusters; left panel - observations of 22 clusters with 1-2 RMs per cluster, blue and black points are from Clarke et al. (2001) and red points are from Johnston-Hollitt & Ekers (2004). The plot includes the first observations through a radio relic showing an enhanced RM denoted by the two circled red points on the plot and in the inset showing their location in the relic (Johnston-Hollitt 2004); middle panel - observations of RMs through a single cluster, Coma (Bonafede et al. 2010, 2013) the region of the Coma relic is shown by dashed lines; right panel - predicted number of RMs through a Coma-like cluster as seen with the SKA in Phase 1 (Bonafede et al. 2015). The arrow at the bottom indicates the improvements to this type of work over time going from having only a statistical sample over many clusters 15 years ago to over 10 RMs per cluster in 2010 to finally several tens of RMs per cluster in the SKA era. Note the Galactic RM contribution has been estimated and removed in data presented in the left and middle panel using the latest results from Oppermann et al. (2012).

1989; Kim et al. 1991; Clarke et al. 2001; Johnston-Hollitt 2003; Johnston-Hollitt & Ekers 2004; Bonafede et al. 2013). However, to date, we lack detailed information on the extent or filling factors of the magnetic fields and their relationship to or influence on the dynamical state of the cluster. The SKA has long been thought to be an excellent tool for improving our understanding of clusters using statistical RMs (Feretti & Johnston-Hollitt 2004), and more recently it has been shown to allow the observation of polarised filaments in cluster halos across a range of redshifts (Govoni et al. 2013, 2015).

Progress in our understanding of cluster magnetic fields has been hampered by lack of detail regarding the contributions from foregrounds (both intrinsic and extrinsic), poor sampling of background sources for RM measurements (a result of lack of sensitivity) and poorly sampled polarisation data leading to incorrect RM fits (the result of lack of bandwidth). Progress to statistically sample cluster magnetic fields via the use of RMs of background sources has been slow but steady. We have moved from having to amass statistical values over a number of clusters in which there are only 1-2 measurements per cluster (Clarke et al. 2001; Johnston-Hollitt & Ekers 2004) to being able to easily detect several sources in an individual cluster (Bonafede et al. 2013). Predictions for SKA1 show we will have several tens to a few hundreds of background sources to probe clusters up to a redshift of 0.1[1]. Additionally, we will be able to conduct statistical studies with 1-2 RMs per

[1]Assuming a 1 Mpc radius and extrapolating the current polarised source counts to 4 μJy (Rudnick & Owen 2014; Hales et al. 2014; Stil et al. 2014) gives 60-115 RMs per cluster at z=0.05 and 15-30 at z=0.1, very large, nearby clusters like A3266 would have 180-360 background RMs.

PoS(AASKA14)092

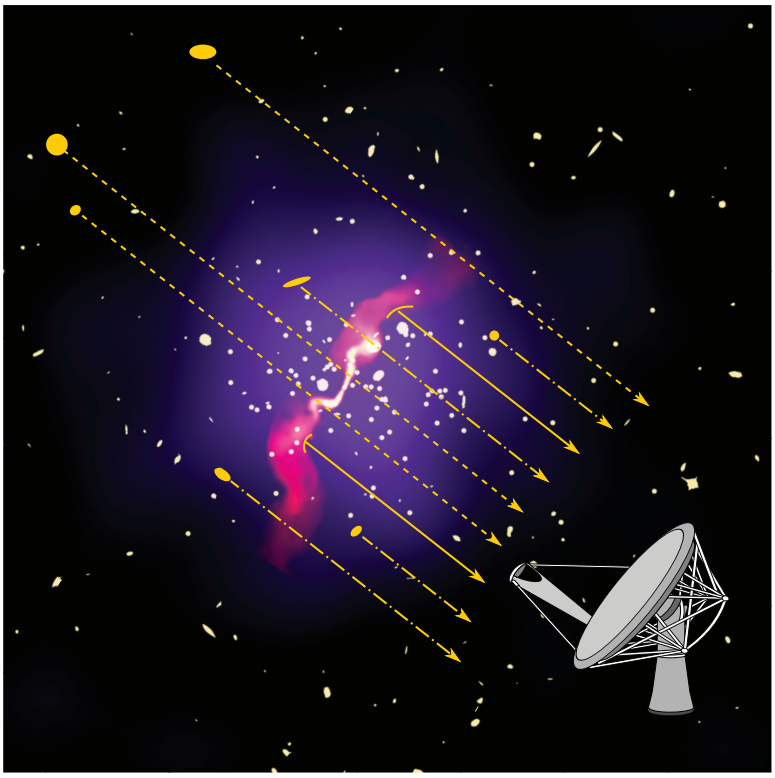

Figure 2: Schematic of a nearby galaxy cluster showing X-ray emission in purple, an extended radio source in pink, and unresolved radio sources in white if unpolarised and gold if polarised. Different path lengths to polarised sources are marked including unresolved background radio galaxies (dashed lines), unresolved embedded sources (dot-dashed lines) and extended embedded sources such as large tailed radio galaxies, the lobes of which are polarised and can be used as screen to examine the cluster magnetic field (solid lines). The wealth of sources located at different locations within the ICM will allow the first Faraday tomography of the magnetic field in galaxy clusters.

cluster out to a redshift of 0.5, this is important to understand the way magnetic fields grow in the intracluster medium (ICM). The vast increase in the number of RMs available in the outskirts of clusters will also allow measurements through magnetic fields in the cluster relics that are thought to be generated by shocks. Observations have shown relics to have highly aligned magnetic fields running perpendicular to the direction of shock propagation. To date only observations through the NW relic in A3667 have shown an increase in RM (Johnston-Hollitt 2004), but simulations predict such enhancements will be readily detectable, particularly with SKA2 (Bonafede et al. 2015). Observations of relic RMs combined with RMs of sources seen in projection through relics will greatly assist in disentangling the shock geometry and allow the first statistical samples of the magnetic fields in shocks to be constructed. Figure 1 provides a schematic to illustrate the improvement in background RMs seen through cluster magnetic fields commencing in 2000 and going through to the expected SKA levels in 2020. By allowing detailed measurements of the magnetic field strength and distribution of individual galaxy clusters, the door is opened to examine changes in the magnetic field as a function of other cluster properties such as X-ray luminosity/mass, dynamical state and importantly will allow us to determine the radial profile of the field and its connection to the gas density.

PoS(AASKA14)092

For nearby galaxy clusters ($z \leq 0.1$) we will have sufficient sources in both the background and embedded within the ICM to perform Faraday tomography of the magnetic field of the cluster. In particular, we will have a host of background sources, embedded point sources and embedded extended sources such as tailed radio galaxies with which to probe different path lengths through the ICM (see Figure 2). The use of embedded cluster sources to probe the magnetic field has already occurred in a few isolated examples (Guidetti et al. 2008; Pizzo et al. 2011; Pratley et al. 2013), but to date we have been unable to undertake the detailed tomographic studies the SKA will allow. In fact, not only will the SKA allow Faraday tomography of the field via the use of a large number of sources as probes to the cluster RM, the resolved structures in some tailed radio galaxies such as the so-called 'corkscrew' radio galaxies could potentially provide information on the magnetic field in clusters over very small scales (Johnston-Hollitt et al. 2015a,b).

Moving away from statistical studies, the SKA will also allow detailed mapping of the magnetic fields associated with cluster relics and potentially even halos which are expected to be detected in large numbers (Cassano et al. 2015). Whilst we have seen polarised filamentary structure in only two cluster halos (Govoni et al. 2005; Bonafede et al. 2009), we expect the SKA, and in particular SKA2, to have sufficient sensitivity to image such structures (Govoni et al. 2013, 2015), potentially at a range of redshifts[2]. This provides the exciting possibility to measure the evolution of central cluster fields as a function of time, examining variables such as changing strength, degree of order, turbulence scales and power spectra. Magnetic fields in galaxy clusters are thought to be turbulent and thus will produce characteristic Faraday depth spectra observable with sufficiently high resolution in Faraday depth space, using the SKA an examination of clusters will thus be able to disentangle different spectral templates attacking questions about field geometries, in particular questions surrounding the existence of asymmetry and vertical components to the field.

Looking on the largest scales, one of the most exciting challenges for the SKA is to discover and characterize the WHIM in the cosmic web, which is the last, major unproven piece predicted by standard inflationary cosmology. Since it is likely that the intergalactic magnetic field (IGMF) permeates the WHIM in the cosmic web (Ryu et al. 2012), in the coming decades the SKA will be the most promising facility to discover and characterize such fields. Direct imaging of the cosmic web has been shown to finally be a possibility with SKA1 (Vazza et al. 2015; Giovannini et al. 2015) and it will also be possible to measure the dispersion measure (DM) of the WHIM via fast radio bursts (Macquart et al. 2015), however, we also expect to detect the statistical RM signal (Taylor et al. 2015). Previous attempts to detect the statistical RM have been difficult due to foreground contamination (Schnitzeler 2010; Xu & Han 2014), but the dense RM grid obtained with the SKA dramatically improves the ability to account for intervening foregrounds and the broad bandwidths of the telescope provide an opportunity to select sources passing through the WHIM (Akahori et al. 2014b) based on Faraday depolarisation and Faraday tomography (Gaensler et al. 2015). The detection of the IGMF and the resultant comparison with theoretical predictions (Akahori et al. 2014a) will be a breakthrough in our understanding of the way in which magnetic fields assemble on large-scales in the Universe.

[2]The ability to detect polarised emission in filaments is a function of the resolution and sensitivity, for SKA1 we expect to be able to see polarisation from only the most luminous radio halos ($L_{1.4} \geq 3 \times 10^{25}$ W/Hz), while SKA2 will be able to achieve similar results for intermediate brightness halos ($L_{1.4} \geq 2 \times 10^{24}$ W/Hz) see Govoni et al. (2015) for further details.

PoS(AASKA14)092

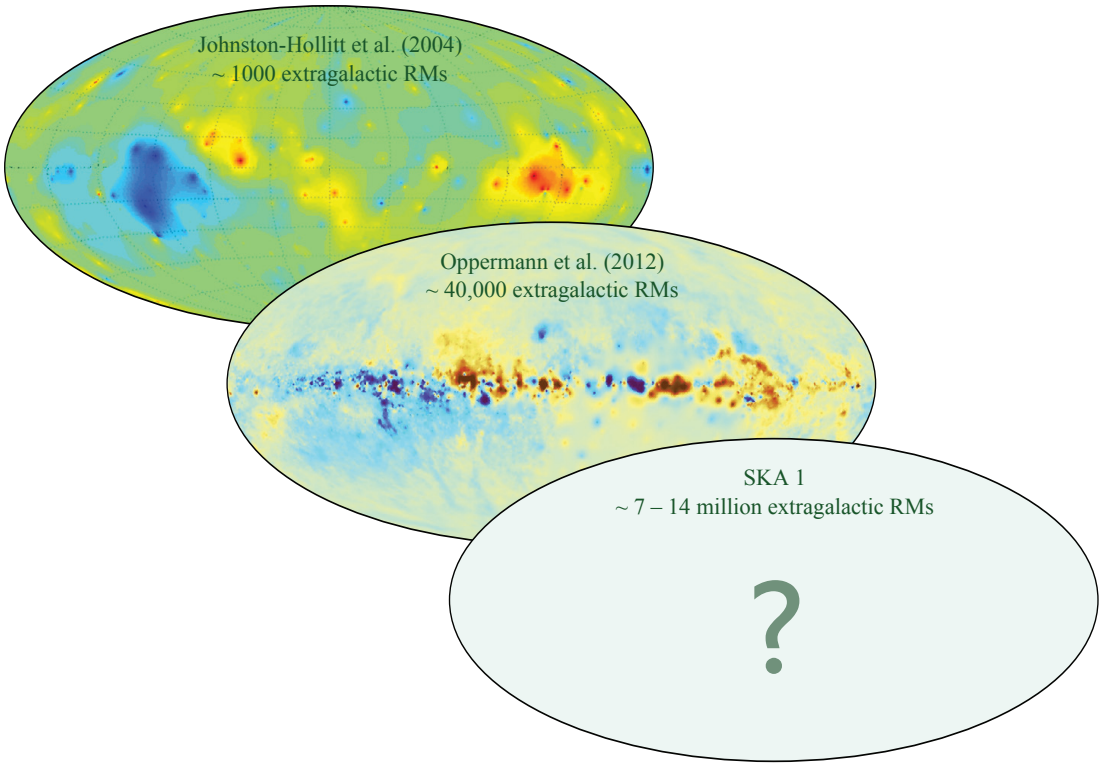

Figure 3: Top projection: The RM sky in Galactic coordinates as interpolated from ∼1000 extragalactic RMs over a decade ago (Johnston-Hollitt 2003; Johnston-Hollitt et al. 2004). Middle projection: The RM Sky as determined from more sophisticated signal processing methods for ∼40,000 extragalactic RMs (Oppermann et al. 2012, 2015). Note that the large-scale features of the field are largely unchanged between the top and middle panel, but the small scale information regarding the magnetic field of the Milky Way is greatly improved with a higher density of RMs. The bottom panel denotes that an all sky RM survey on SKA phase 1 with a sensitivity of 4 μJy/beam at 2" resolution should provide 7-14 million extragalactic RMs with which to probe the RM sky. Red colour scales denote positive RMs and magnetic fields coming out of the plane of the sky, whilst blue colours denote negative RMs and fields going into the plane of the sky.

For further information see the following chapters in the 2015 SKA Science Case: Bonafede et al. (2015); Cassano et al. (2015); Gaensler et al. (2015); Giovannini et al. (2015); Govoni et al. (2015); Johnston-Hollitt et al. (2015a); Macquart et al. (2015); Taylor et al. (2015); Vacca et al. (2015); Vazza et al. (2015).

2.2 Magnetic Field of the Milky Way

Mapping the magnetic field of the Milky Way has been steadily improving over the last decade. The use of extragalactic background sources, embedded pulsars and observations of the diffuse synchrotron emission in polarisation surveys (Reich et al. 2004; Haverkorn et al. 2006; Stutz et al. 2014) have all played important roles in examining the large-scale magnetic field of our Galaxy (Stil et al. 2011; Oppermann et al. 2012). Such work continues to reveal surprising and previously unknown features such as giant magnetised outflows (Carretti et al. 2013), and has permitted mapping of the magnetic field in a range of discrete Galactic objects (McClure-Griffiths et al. 2010;

PoS(AASKA14)092

Harvey-Smith et al. 2011; Purcell et al. 2015) and given the first information on the Mach number of Galactic turbulence (Hill et al. 2008; Gaensler et al. 2011). Despite these advances, many questions as to the exact field configuration remain, including controversy surrounding the direction of the large-scale regular field in the spiral arms, details of the field in the Galactic centre and information on the power spectrum of the turbulent field. The SKA will resolve many of these questions and allow the first reconstruction of the 3D field via detailed Faraday tomography using external and embedded sources.

The leap forward that SKA will provide in our attempts to reconstruct the magnetic field of the Milky Way cannot be overstated. In the last decade, we have moved from initial attempts to reconstruct the large-scale field using only $\sim$1000 RMs gathered from inhomogeneous observations combined with relatively simple interpolation (Johnston-Hollitt et al. 2004) to having access to $\sim$40,000 RMs (Taylor et al. 2009) and advanced statistical techniques (Oppermann et al. 2012, 2015). Improving the sampling rate by a factor of 40 to the level of 1 source per square degree has facilitated a tremendous leap forward for Galactic magnetism (see Figure 3), the phase 1 SKA will further improve the sampling rate by over two orders of magnitude, providing an astounding 7-14 million discrete RMs at a sampling rate of approximately 230 to 450 sources per square degree. Additionally, SKA1 is expected to increase the number of Galactic pulsars by a factor of 5 (Keane et al. 2015) taking the total to roughly 10,000. Parallax measurements will provide accurate distances to a large number of pulsars distributed through the Galaxy (Smits et al. 2011; Keane et al. 2015; Janssen et al. 2015). As with observations of nearby galaxy clusters, combining the rotation measure information from extragalactic background sources and embedded pulsars at precisely known locations will allow an unprecedented 3D reconstruction of the magnetic field of the Milky Way and will resolve uncertainties around field reversals in the spiral arms and complexity in the field configuration in the Galactic Centre as well as provide detailed constraints on the power spectrum of the Galactic magnetic field (Haverkorn et al. 2015; Han et al. 2015).

For further information see the following chapters in the 2015 SKA Science Case: Haverkorn et al. (2015); Han et al. (2015).

2.3 Magnetic Fields on kpc to pc star forming scales

As noted above, the currently available extragalactic RMs have a density of roughly 1 source per square degree which has been sufficient to obtain information on the magnetic fields in a host of Galactic objects including supernova remnants, HII regions, high velocity clouds, star forming regions and shells and bubbles in the Milky Way. As we move to sampling at a rate of approximately 230 to 450 sources per square degree we have the opportunity to probe a huge number of discrete Galactic objects on kpc to pc scales in both the Milky Way and the Magellanic Clouds (see Haverkorn et al. (2015) for further details). Theoretical models suggest that magnetic fields play a vital role in the evolution of dense molecular clouds and the associated star formation within them, this is supported by the extraordinarily close radio–IR correlation observed locally within galaxies (Tabatabaei et al. 2013). The generation of small-scale magnetic fields by supernova-induced turbulence is one possible scenario to explain this correlation, or it may be that a more fundamental relation exists between magnetic fields and molecular gas. Investigating these relations both within the Milky Way and nearby galaxies is crucial to understanding the role of magnetic fields in the structure formation of the molecular interstellar medium (ISM), and in particular, the formation of

PoS(AASKA14)092

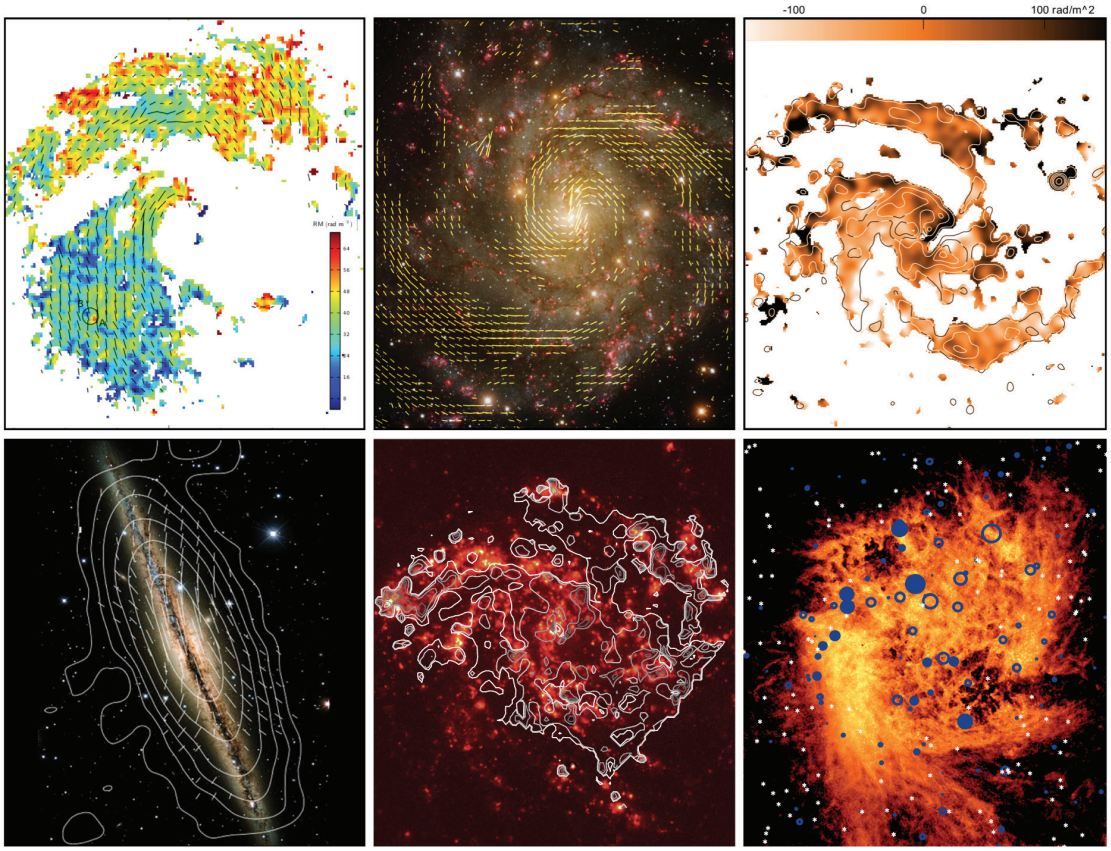

Figure 4: Examples of information that the proposed polarisation survey will provide on the magnetic field of nearby galaxies using different techniques. *Top left:* Rotation measure values overlaid with polarisation vectors for NGC 6946 (Heald 2012). *Top middle:* Magnetic field lines from synchrotron polarisation observations overlaid on an optical image of IC342 (Beck 2015b). *Top right:* rotation measures associated with NGC 6946 (Beck 2007). *Bottom left:* Total radio emission and magnetic field vectors of the edge-on galaxy NGC 891 overlaid on the optical image from CFHT (Krause 2009). *Bottom middle:* Contours of the strength of Faraday dispersion for NGC 6946 overlaid on Hα emission (Williams et al. in prep). *Bottom right:* Extragalactic rotation measures seen in projection through the Large Magellanic Cloud (Gaensler et al. 2005). Note the colour scales of some images have been altered from the original to better highlight features.

giant molecular clouds that are the cradles of massive star formation. Observations of the *in-situ* synchrotron radiation emitted by dense molecular clouds is also a possibility with SKA (Dickinson et al. 2015) and imaging the polarised emission from such clouds will provide constraints on the internal magnetic fields and their distribution in these clouds, which will be crucial to addressing questions regarding the effect of magnetic fields in star formation.

For further information see the following chapters in the 2015 SKA Science Case: Dickinson et al. (2015); Haverkorn et al. (2015).

2.4 Magnetic Fields in Nearby Galaxies

Ordered magnetic fields of spiral shape are observed in all spiral galaxies and even in flocculent galaxies without a spiral pattern in the gas (Beck 2015a). Ordered magnetic fields are generally

PoS(AASKA14)092

strongest in the regions between the material spiral arms, in some cases forming "magnetic arms" with exceptionally high degrees of polarisation (Beck & Hoernes 1996). Although models of large-scale (mean-field) dynamos can basically explain these phenomena (Chamandy et al. 2015; Moss et al. 2015), the physics of galactic dynamos is still far from being understood. Present-day MHD models (including dynamo action) can achieve resolutions of the physically relevant scale of turbulence of a few tens of pc within kpc-size boxes of the ISM (Gent et al. 2013). Global MHD models including gravitational instabilities like bars and spiral arms, and MHD models of galaxy evolution are still to come.

In contrast with simplistic models, real galaxies have complex field patterns that can be described by a power spectrum of Fourier modes imprinted in Faraday rotation measures. Field reversals, density waves, bars and mergers also leave specific signatures in the power spectrum which SKA will be sensitive to. Field reversals between spiral arms on scales of several kpc, like that observed in the Milky Way, have not been detected in external galaxies so far. Such reversals could be present as relics from the early epoch of galaxy evolution, or triggered by a major merger. The number and extent of field reversals may provide new insight into the history of galaxies. RM data with high spatial resolution (less than about 100 pc) are required for a systematic investigation of these phenomena.

The formation of spiral arms is another area where the role of magnetic fields is an open question. Density waves including magnetic fields have two modes of propagation (Lou & Fan 1998). In the fast MHD mode, magnetic field waves that are in-phase with the gas waves may stabilize spiral arms. The out-of-phase magnetic fields of slow MHD waves may become unstable and develop into Parker loops which can be observed via azimuthally periodic variations in Faraday rotation measures (Beck 2015b).

High-resolution polarisation images of nearby galaxies are needed to study and understand the physics of large- and intermediate-scale interstellar magnetic fields, supplementing observations of local small-scale magnetic fields in the Milky Way. There are three basic techniques that we can employ to explore the magnetic field in nearby galaxies.

The first and most straightforward approach is direct imaging of the polarised synchrotron emission emitted by a galaxy to reveal the features in the large-scale ordered fields in the plane of the sky, preferably at high frequencies (above 3 GHz) where the angular resolution is highest and the effects of Faraday rotation and depolarisation are sufficiently small to observe the field's intrinsic orientation and degree of order.

A complementary approach at somewhat lower frequencies is to investigate the polarised emission and its variation across a wide frequency band. The resulting Faraday rotation measure and frequency-dependent depolarisation can be used to examine the detailed internal structure of the magnetoionic medium, both across the galaxy and along the line-of-sight via Faraday tomography (Heald et al. 2015). Details that can be studied include the coherence length of the line-of sight magnetic field, the large-scale three-dimensional magnetic field structure including the vertical structure of magnetic fields and the properties and dynamical impact of magnetic fields in the disk-halo interface of star forming galaxies. To achieve excellent resolution in Faraday depth, we require a wide coverage in λ^2, i.e. wide frequency coverage in a lower frequency band (such as proposed for the polarimetric sky survey).

Finally, as with the Milky Way, we can use the RMs of polarised background galaxies to obtain

PoS(AASKA14)092

information about the magnetic field in the foreground galaxy, averaged along the line-of-sight (the "RM grid" approach). Because this method does not depend on the occurrence of synchrotron-emitting cosmic-ray electrons (CREs) in the foreground galaxy, it can also be exploited to detect and study magnetic fields in the outer regions of galaxies where CREs cannot reach, providing comprehensive information about the extent to which magnetic fields are expelled by outflows at these large radii.

Figure 4 provides examples of each technique. These methods are highly complementary and provide us with the unique opportunity to better understand the magnetic field in a range of galaxies. SKA will permit observations of nearby galaxies using these techniques at kpc resolution out to a redshift of at least 0.025, providing a comprehensive sample of all galaxy field geometries in the local volume.

For further information see the following chapters in the 2015 SKA Science Case: Beck et al. (2015); Heald et al. (2015).

2.5 Magnetic Fields in Active Galactic Nuclei and the Faint Polarised Sky

The lobes and jets of Active Galactic Nuclei (AGN) are rich laboratories to investigate a range of phenomena associated with magnetised plasmas. The polarisation survey on SKA1 will image and provide RMs for a vast number of AGN across cosmic time allowing a diverse set of studies including direct imaging of the magnetised lobes and jets of nearby galaxies, examination of the rotation measure structure (Guidetti et al. 2008, 2012; O'Sullivan et al. 2013) and depolarisation characteristics (Fomalont et al. 1989) across such lobes, use of the lobes themselves as Faraday screens to investigate their local environment, and use of background galaxies to probe structure within the lobes (Feain et al. 2009). Maps such as the spectacular image of Fornax A shown in Figure 5, which shows the rich depolarisation structure evident across the radio lobes, will be possible for all nearby radio galaxies. Such data allow exploration of structure within the lobes themselves and detection of local depolarising screens (e.g. the 'ant' in the western lobe of Fornax). A census of such emission as a function of cosmic time will provide constrains on the environment surrounding these sources (Gaensler et al. 2015; Taylor et al. 2015).

The SKA will enable observations an order of magnitude deeper than current instruments and the observations will be carried out over a large enough area of the sky to provide a statistical overview of the magnetic properties of the faint radio source population. Deep imaging with SKA1 will probe the polarised properties of normal galaxies to high redshifts allowing us to monitor their evolution of these properties over cosmic time and to investigate when magnetic fields in galaxies first emerged and how quickly they were amplified. A deep survey capable of probing star forming galaxies over a wide range of redshifts will capture the population in different stages of evolution. In particular, we will observe galaxies as they convert gas to stars, a process which is believed to be strongly tied to their magnetic properties.

Additionally, examining the polarisation properties of active galaxies over cosmic time provides a powerful tool to constrain jet magneto hydrodynamic and emission models. Deep SKA surveys will thus present the first opportunity to address the longstanding problem of the composition of AGN jets, and their plasma acceleration using large, well designed samples. With such a survey we will be in the ideal position to finally understand the effect of increasing fractional polarisation with decreasing flux density/observational frequency, an effect that suggests there must

PoS(AASKA14)092

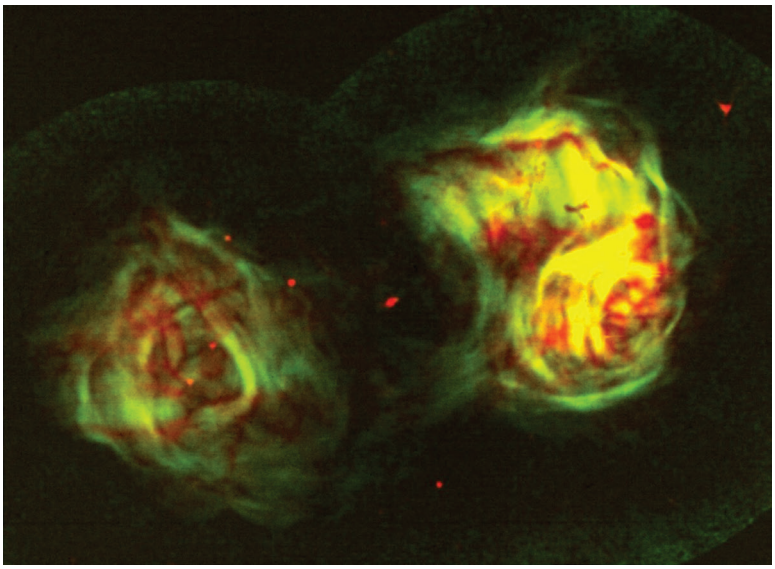

Figure 5: Fornax A shown here in a hue-intensity plot in which flux is represented by intensity and fractional polarisation is represented as hue with regions of high depolarisation appearing red. The depolarisation structures presented here result from a range of phenomena including internal depolarisation in the lobes, depolarisation due to foreground gas (e.g. the 'ant' in the western lobe) or intervening galaxies and instrumental beam depolarisation (Fomalont et al. 1989). SKA1 will routinely produce information across the resolved lobes of radio galaxies.

be either changes in the internal source field structure or their Faraday screens, likely related to the immediate environment of the galaxy. Furthermore, deep SKA surveys will probe the AGN population to redshifts of up to 10, capturing these sources at a time when the interstellar and intergalactic media were considerably denser than the present day. Observing these frustrated sources as they attempt to break out of their host galaxies provides an exciting and potentially unique opportunity to probe not only the magnetic fields, but also the surrounding intergalactic medium (Gaensler et al. 2015; Taylor et al. 2015).

Finally, although we will get the first hints of the magnetic field in the cosmic web through the wide-field polarisation survey, the challenging nature of detecting such faint RMs will be most appropriately ameliorated via a deep survey at high Galactic latitudes, away from galaxy clusters (Taylor et al. 2015).

Even with the sensitivity and depth of the SKA there will be a significant population of objects for which no polarisation signal is detected. Recent work on the faint polarised source population has shown that information can still be obtained on the polarisation properties of these faint sources via stacking analysis (Stil et al. 2014). In the context of the SKA stacking provides an extension to the results of deep surveys, particularly regarding understanding the fractional polarisation as a function of redshift and as a means to investigate the polarisation luminosity function (Stil & Keller 2015).

For further information see the following chapters in the 2015 SKA Science Case: Agudo et al. (2015); Gaensler et al. (2015); Laing (2015); Peng et al. (2015); Stil & Keller (2015); Taylor et al. (2015).

PoS(AASKA14)092

2.6 Other Magnetism Science

Although the wide-area polarisation survey and the associated RM grid experiment cover a great deal of magnetism science, there are other important magnetism topics which are worth elaborating on here. Studies of the Zeeman effect in both emission and absorption towards atomic and molecular clouds in the Milky Way with SKA1 will provide information on the magnetic field in the warm and cold, neutral components of the Galaxy while Zeeman observations of OH masers provide information on large-scale galactic fields (Robishaw et al. 2015). Thus all Zeeman observations will be highly complementary to the extensive Faraday rotation measure observations. Looking forward to SKA2 such work could potentially be extended to nearby galaxies and in particular observations of megamasers are expected to extend out to $z = 1$.

Finally, one intriguing possibility is to use the SKA to probe the nature of dark matter in cosmic structures, from dwarf galaxies to galaxy clusters. Under the assumption that dark matter annihilation produces an observable component to the synchrotron emission detected in cluster and galaxy halos on top of that generated from cosmic rays and star formation, we should detect low-level polarised emission associated with these structures. This is especially the case for (sub-)structures with low star formation activity or cosmic ray density. Studying the magnetic fields in clusters and galaxies is therefore crucial to disentangling the dark matter particle density from the magnetic energy density that is contributing to the predicted annihilation-induced synchrotron emission. The RM grid experiment will be unique in these respects being able to provide simultaneous measurements of the magnetic field while putting constraints on the putative annihilation-generated radio halo emission (Colafrancesco et al. 2015).

For further information see the following chapters in the 2015 SKA Science Case: Colafrancesco et al. (2015); Robishaw et al. (2015).

3. Polarisation Surveys

In order to capitalise on the immense opportunity the SKA provides for magnetism science it is vital that a polarisation survey over the entire accessible sky at 950-1760 MHz (the so-called SKA1-MID band 2) is undertaken down to a sensitivity of 4 μJy/beam. This survey must provide not only full polarisation imaging at 2" resolution, but also deliver the RM catalogue of the expected 7-14 million discrete extragalactic sources, or provide sufficiently calibrated data for these RMs to be determined in post-processing. Such a survey will be a powerful legacy dataset with which to undertake an extensive range of high impact science including the RM grid experiment, imaging of the magnetic field of all nearby galaxies within 100 Mpc radius, detailed mapping of the magnetic field structure in cluster relics and possibly halos, and finally the survey will probe the magnetic field in a range of astrophysical objects from the jets and lobes of radio galaxies to supernova remnants. This survey will thus advance a great deal of progress in a broad range of science cases and is the highest science priority of the SKA magnetism community. We estimate that the survey will require 2.5 years of observing time (inclusive of calibration overheads) on the SKA1-MID instrument in South Africa. This will produce a legacy survey of vast scientific potential, not only for magnetism, but for a host of high-priority continuum science (see Prandoni & Seymour (2015) for further details). The polarisation survey is well suited to be undertaken in a commensal

PoS(AASKA14)092

mode with the survey proposed by the SKA Continuum working group and with the Galactic HI absorption grid experiment. Additionally, there is strong synergy between the observations of nearby galaxies that will be undertaken as a matter of course in the wide-area polarisation and continuum survey, and the spectral line observations of nearby galaxies that will also be performed by the HI group. Comparisons of the polarisation, continuum and HI data for nearby galaxies is pertinent to understanding the physical connections between gas, star formation, and magnetic fields.

Additionally, we propose a series of smaller, deeper surveys to examine the polarisation properties in the very faint galaxy population and to allow an expansion of the accessible range over which we can probe the evolution of magnetism in different classes of objects. The first of these surveys would be a high Galactic latitude survey of order 10 square degrees from 950-1760 MHz. Ideally such a survey would reach a depth of 75 nJy/beam at 2" resolution and would allow the first statistically significant investigation of the faint polarised sky (see Section 2.5 for further details). The definition of other deep survey areas will be the subject of future discussions. Finally, we note that all continuum observations on the SKA will provide useful polarisation information and we would encourage the SKA to provide full polarisation products, including RMs for all observations.

Looking forward to SKA2 we will have even greater sensitivity, resolution and potentially larger bandwidths, all of which will allow another leap forward for magnetism science. We will continue to enhance the density of sources on the RM grid, sampling at least 40 million radio sources allowing an even finer level of detail with which to resolve magnetic fields in a diverse range of objects. The higher spatial resolution will take us into a resolution regime which is currently only accessible with VLBI, but unlike present day VLBI will not be restricted to bright, compact objects. This will be an almost unimaginable change in radio astronomy allowing for unprecedented imaging of jets of AGN, magnetic fields in nearby galaxies, and detection and imaging of the polarised component of radio halos out to redshifts close to 2 when the first clusters were formed. Additionally, we will delve deeper into the history of the Universe in our quest to resolve the overarching questions of where, when and how magnetic fields arose in the Universe.

4. Summary

Future wide-area radio surveys via instruments such as SKA1 will provide very sensitive and yet observationally affordable ways to explore a wide range of science goals, including those associated with the detection and characterisation of magnetic fields over a range of scales. The planned polarisation survey on SKA1 and its associated RM grid will give transformational science for almost every class of astronomical object. With this survey we will undertake a complete census of magnetic properties in normal galaxies and AGN as a function of cosmic time, probe the detailed physics of magnetised plasmas in both the jets of AGN and the cores of galaxy clusters, and measure RM enhancements in shock-driven relics out to a redshift of 0.5. We will conduct Faraday tomography on the magnetic fields in clusters, nearby galaxies and the Milky Way in astounding detail placing limits on the extent, turbulence and radial profile of these fields. Additionally, we will undertake the first analysis of the evolution of magnetic fields in a host of objects and determine their connection to other physical parameters. We will elucidate properties of the medium surrounding AGN potentially to redshift 10 and unveil the first polarisation spectral energy distribu-

PoS(AASKA14)092

tions. Furthermore, the phase 1 SKA will place tight constraints on the magneto-ionic turbulence in our Galaxy, nearby galaxies and perhaps even make the first detection of the magnetic component of the cosmic web itself.

In conclusion, the SKA's sensitivity, bandwidths and field of view will provide a transformational capability with which to explore magnetic fields. The immensely rich polarimetric data provided by the SKA will allow us to finally address fundamental questions relating to the original, evolution and influence of cosmic magnetic fields on all scales in the Universe, and will mark the start of the *"Era of Precision Magnetism Science"*.

References

Agudo, I., Boettcher, M., Falcke, H., et al. 2015, 'Studies of Relativistic Jets in Active Galactic Nuclei with SKA' in proc. *Advancing Astrophysics with the Square Kilometre Array*, PoS(AASKA14)093, arXiv:1501.00420

Akahori, T., Gaensler, B. M., & Ryu, D. 2014a, ApJ, 790, 123

Akahori, T., Kumazaki, K., Takahashi, K., & Ryu, D. 2014b, Publications of the Astronomical Society of Japan, 66, 65

Beck, R. 2007, A&A, 470, 539

Beck, R. 2015a, in Astrophysics and Space Science Library, Vol. 407, Astrophysics and Space Science Library, ed. A. Lazarian, E. M. de Gouveia Dal Pino, & C. Melioli, 507

—. 2015b, ArXiv e-prints, astro-ph/1502.05439, arXiv:1502.05439

Beck, R., & Hoernes, P. 1996, Nature, 379, 47

Beck, R., Bomans, D., Colafrancesco, S., et al. 2015, 'Structure, dynamical impact and origin of magnetic fields in nearby galaxies in the SKA era' in proc. *Advancing Astrophysics with the Square Kilometre Array*, PoS(AASKA14)094, arXiv:1501.00385

Bernardi, G., Greenhill, L. J., Mitchell, D. A., et al. 2013, ApJ, 771, 105

Bonafede, A., Feretti, L., Murgia, M., et al. 2010, A&A, 513, A30

Bonafede, A., Vazza, F., Brüggen, M., et al. 2013, MNRAS, 433, 3208

Bonafede, A., Feretti, L., Giovannini, G., et al. 2009, A&A, 503, 707

Bonafede, A., Vazza, F., Brüggen, M., et al. 2015, 'Unravelling the origin of large-scale magnetic fields in galaxy clusters and beyond through Faraday Rotation Measures with the SKA' in proc. *Advancing Astrophysics with the Square Kilometre Array*, PoS(AASKA14)095, arXiv:1501.00321

Carretti, E., Crocker, R. M., Staveley-Smith, L., et al. 2013, Nature, 493, 66

Cassano, R., Bernardi, G., Brunetti, G., et al. 2015, 'Cluster Radio Halos at the crossroads between astrophysics and cosmology in the SKA era' in proc. *Advancing Astrophysics with the Square Kilometre Array*, PoS(AASKA14)073, arXiv:1412.5940

Chamandy, L., Shukurov, A., & Subramanian, K. 2015, MNRAS, 446, L6

Clarke, T. E., Kronberg, P. P., & Böhringer, H. 2001, ApJL, 547, L111

Colafrancesco, S., Regis, M., Marchegiani, P., et al. 2015, 'Probing the nature of Dark Matter with the SKA' in proc. *Advancing Astrophysics with the Square Kilometre Array*, PoS(AASKA14)100, arXiv:1502.03738

PoS(AASKA14)092

Dickinson, C., Beck, R., Crocker, R., et al. 2015, 'SKA studies of in-situ synchrotron radiation from molecular clouds' in proc. *Advancing Astrophysics with the Square Kilometre Array*, PoS(AASKA14)102, arXiv:1501.00804

Feain, I. J., Ekers, R. D., Murphy, T., et al. 2009, ApJ, 707, 114

Feretti, L., & Johnston-Hollitt, M. 2004, New Astronomy Reviews, 48, 1145

Fomalont, E. B., Ebneter, K. A., van Breugel, W. J. M., & Ekers, R. D. 1989, ApJL, 346, L17

Gaensler, B. M., Beck, R., & Feretti, L. 2004, New Astronomy Reviews, 48, 1003

Gaensler, B. M., Haverkorn, M., Staveley-Smith, L., et al. 2005, Science, 307, 1610

Gaensler, B. M., Landecker, T. L., Taylor, A. R., & POSSUM Collaboration. 2010, in Bulletin of the American Astronomical Society, Vol. 42, American Astronomical Society Meeting Abstracts no. 215, 470.13

Gaensler, B. M., Haverkorn, M., Burkhart, B., et al. 2011, Nature, 478, 214

Gaensler, B. M., Agudo, I., Akahori, T., et al. 2015, 'Broadband Polarimetry with the Square Kilometre Array: A Unique Astrophysical Probe' in proc. *Advancing Astrophysics with the Square Kilometre Array*, PoS(AASKA14)103, arXiv:1501.00626

Gent, F. A., Shukurov, A., Sarson, G. R., Fletcher, A., & Mantere, M. J. 2013, MNRAS, 430, L40

Giovannini, G., Bonafede, A., Brown, S., et al. 2015, 'Mega-parsec scale magnetic fields in low density regions in the SKA era: filaments connecting galaxy clusters and groups' in proc. *Advancing Astrophysics with the Square Kilometre Array*, PoS(AASKA14)104, arXiv:1501.01023

Govoni, F., Murgia, M., Feretti, L., et al. 2005, A&A, 430, L5

Govoni, F., Murgia, M., Xu, H., et al. 2013, A&A, 554, A102

—. 2015, 'Cluster magnetic fields through the study of polarized radio halos in the SKA era' in proc. *Advancing Astrophysics with the Square Kilometre Array*, PoS(AASKA14)105, arXiv:1501.00389

Guidetti, D., Laing, R. A., Croston, J. H., Bridle, A. H., & Parma, P. 2012, MNRAS, 423, 1335

Guidetti, D., Murgia, M., Govoni, F., et al. 2008, A&A, 483, 699

Hales, C. A., Norris, R. P., Gaensler, B. M., et al. 2014, MNRAS, 441, 2555

Han, J. L., van Straten, W., Lazio, T. J. W., et al. 2015, 'Three-dimensional Tomography of the Galactic and Extragalactic Magnetoionic Medium with the SKA' in proc. *Advancing Astrophysics with the Square Kilometre Array*, PoS(AASKA14)041, arXiv:1412.8749

Harvey-Smith, L., Madsen, G. J., & Gaensler, B. M. 2011, ApJ, 736, 83

Haverkorn, M., Gaensler, B. M., McClure-Griffiths, N. M., Dickey, J. M., & Green, A. J. 2006, ApJS, 167, 230

Haverkorn, M., Akahori, T., Carretti, E., et al. 2015, 'Measuring magnetism in the Milky Way with the Square Kilometre Array' in proc. *Advancing Astrophysics with the Square Kilometre Array*, PoS(AASKA14)096, arXiv:1501.00416

Heald, G., Beck, R., de Blok, W. J. G., et al. 2015, 'Magnetic Field Tomography in Nearby Galaxies with the Square Kilometre Array' in proc. *Advancing Astrophysics with the Square Kilometre Array*, PoS(AASKA14)106, arXiv:1501.00408

Heald, G. H. 2012, ApJL, 754, L35

Hennessy, G. S., Owen, F. N., & Eilek, J. A. 1989, ApJ, 347, 144

Hill, A. S., Benjamin, R. A., Kowal, G., et al. 2008, ApJ, 686, 363

Hotan, A. W., Bunton, J. D., Harvey-Smith, L., et al. 2014, Publications of the Astronomical

PoS(AASKA14)092

Society of Australia, 31, 41

Janssen, G. H., Hobbs, G., McLaughlin, M., et al. 2015, 'Stacking for Cosmic Magnetism with SKA Surveys' in proc. *Advancing Astrophysics with the Square Kilometre Array*, PoS(AASKA14)037, arXiv:1501.00127

Jelić, V., de Bruyn, A. G., Mevius, M., et al. 2014, A&A, 568, A101

Johnston-Hollitt, M. 2003, PhD thesis, University of Adelaide

Johnston-Hollitt, M. 2004, in The Riddle of Cooling Flows in Galaxies and Clusters of galaxies, ed. T. Reiprich, J. Kempner, & N. Soker, 51

Johnston-Hollitt, M., Dehghan, S., & Pratley, L. 2015a, 'Using Tailed Radio Galaxies to Probe the Environment and Magnetic Field of Galaxy Clusters in the SKA Era' in proc. *Advancing Astrophysics with the Square Kilometre Array*, PoS(AASKA14)101, arXiv:1501.00761

Johnston-Hollitt, M., Dehghan, S., & Pratley, L. 2015b, in IAU Symposium, Vol. 313, IAU Symposium, ed. F. Massaro, C. C. Cheung, E. Lopez, & A. Siemiginowska, 321–326

Johnston-Hollitt, M., & Ekers, R. D. 2004, ArXiv Astrophysics e-prints, astro-ph/0411045, astro-ph/0411045

Johnston-Hollitt, M., Hollitt, C. P., & Ekers, R. D. 2004, in The Magnetized Interstellar Medium, ed. B. Uyaniker, W. Reich, & R. Wielebinski, 13–18

Keane, E. F., Bhattacharyya, B., Kramer, M., et al. 2015, 'Giant radio galaxies as probes of the ambient WHIM in the era of the SKA' in proc. *Advancing Astrophysics with the Square Kilometre Array*, PoS(AASKA14)040, arXiv:1501.00056

Kim, K.-T., Tribble, P. C., & Kronberg, P. P. 1991, ApJ, 379, 80

Krause, M. 2009, in Revista Mexicana de Astronomia y Astrofisica, vol. 27, Vol. 36, Revista Mexicana de Astronomia y Astrofisica Conference Series, 25–29

Laing, R. A. 2015, 'Kinematics and Dynamics of kiloparsec-scale Jets in Radio Galaxies with SKA' in proc. *Advancing Astrophysics with the Square Kilometre Array*, PoS(AASKA14)107, arXiv:1501.00452

Lou, Y.-Q., & Fan, Z. 1998, ApJ, 493, 102

Macquart, J.-P., Keane, E., Grainge, K., et al. 2015, 'Fast Transients at Cosmological Distances with the SKA' in proc. *Advancing Astrophysics with the Square Kilometre Array*, PoS(AASKA14)055, arXiv:1501.07535

McClure-Griffiths, N. M., Madsen, G. J., Gaensler, B. M., McConnell, D., & Schnitzeler, D. H. F. M. 2010, ApJ, 725, 275

Moss, D., Stepanov, R., Krause, M., Beck, R., & Sokoloff, D. 2015, ArXiv e-prints, astro-ph/1504.07824, arXiv:1504.07824

Oppermann, N., Junklewitz, H., Robbers, G., et al. 2012, A&A, 542, A93

Oppermann, N., Junklewitz, H., Greiner, M., et al. 2015, A&A, 575, A118

O'Sullivan, S. P., Feain, I. J., McClure-Griffiths, N. M., et al. 2013, ApJ, 764, 162

Peng, B., Chen, R.-R., & Strom, R. 2015, 'Giant radio galaxies as probes of the ambient WHIM in the era of the SKA' in proc. *Advancing Astrophysics with the Square Kilometre Array*, PoS(AASKA14)109, arXiv:1501.00407

Pizzo, R. F., de Bruyn, A. G., Bernardi, G., & Brentjens, M. A. 2011, A&A, 525, A104

Prandoni, I., & Seymour, N. 2015, 'Revealing the Physics and Evolution of Galaxies and Galaxy Clusters with SKA Continuum Surveys' in proc. *Advancing Astrophysics with the Square Kilo-*

PoS(AASKA14)092

metre Array, PoS(AASKA14)067, arXiv:1412.6512
Pratley, L., Johnston-Hollitt, M., Dehghan, S., & Sun, M. 2013, MNRAS, 432, 243
Purcell, C. R., Gaensler, B. M., Sun, X. H., et al. 2015, ApJ, 804, 22
Reich, W., Fürst, E., Reich, P., et al. 2004, in The Magnetized Interstellar Medium, ed. B. Uyaniker, W. Reich, & R. Wielebinski, 45–50
Robishaw, T., Green, J. A., Surcis, G., et al. 2015, 'Measuring Magnetic Fields Near and Far with the SKA via the Zeeman Effect' in proc. *Advancing Astrophysics with the Square Kilometre Array*, PoS(AASKA14)110, arXiv:1503.01779
Rudnick, L., & Owen, F. N. 2014, ApJ, 785, 45
Ryu, D., Schleicher, D. R. G., Treumann, R. A., Tsagas, C. G., & Widrow, L. M. 2012, Space Science Reviews, 166, 1
Schnitzeler, D. H. F. M. 2010, MNRAS, 409, L99
Smits, R., Tingay, S. J., Wex, N., Kramer, M., & Stappers, B. 2011, A&A, 528, A108
Stil, J. M., & Keller, B. W. 2015, 'Stacking for Cosmic Magnetism with SKA Surveys' in proc. *Advancing Astrophysics with the Square Kilometre Array*, PoS(AASKA14)112, arXiv:1501.00390
Stil, J. M., Keller, B. W., George, S. J., & Taylor, A. R. 2014, ApJ, 787, 99
Stil, J. M., Taylor, A. R., & Sunstrum, C. 2011, ApJ, 726, 4
Stutz, R. A., Rosolowsky, E. W., Kothes, R., & Landecker, T. L. 2014, ApJ, 787, 34
Tabatabaei, F. S., Schinnerer, E., Murphy, E. J., et al. 2013, A&A, 552, A19
Taylor, A. R., Stil, J. M., & Sunstrum, C. 2009, ApJ, 702, 1230
Taylor, A. R., Agudo, I., Akahori, T., et al. 2015, 'SKA Deep Polarization and Cosmic Magnetism' in proc. *Advancing Astrophysics with the Square Kilometre Array*, PoS(AASKA14)113, arXiv:1501.02298
Tingay, S. J., Goeke, R., Bowman, J. D., et al. 2013, Publications of the Astronomical Society of Australia, 30, 7
Vacca, V., Oppermann, N., Ensslin, T., et al. 2015, 'Statistical methods for the analysis of rotation measure grids in large scale structures in the SKA era' in proc. *Advancing Astrophysics with the Square Kilometre Array*, PoS(AASKA14)114, arXiv:1501.00415
van Haarlem, M. P., Wise, M. W., Gunst, A. W., et al. 2013, A&A, 556, A2
Vazza, F., Ferrari, C., Bonafede, A., et al. 2015, 'Filaments of the radio cosmic web: opportunities and challenges for SKA' in proc. *Advancing Astrophysics with the Square Kilometre Array*, PoS(AASKA14)097, arXiv:1501.00315
Vikhlinin, A., Markevitch, M., & Murray, S. S. 2001, ApJ, 551, 160
Wayth, R. B., Lenc, E., Bell, M., et al. 2015, Publications of the Astronomical Society of Australia, in press, arXiv:1505.06041
Xu, J., & Han, J. L. 2014, MNRAS, 442, 3329

PoS(AASKA14)092

PROCEEDINGS OF SCIENCE

Studies of Relativistic Jets in Active Galactic Nuclei with SKA

Iván Agudo[*1,†], **Markus Böttcher**[2], **Heino Falcke**[3], **Markos Georganopoulos**[4], **Gabriele Ghisellini**[5], **Gabriele Giovannini**[6], **Marcello Giroletti**[7], **Jose L. Gómez**[8], **Leonid Gurvits**[1,9], **Robert Laing**[10], **Matthew Lister**[11], **Jose-María Martí**[12], **Eileen T. Meyer**[13], **Yosuke Mizuno**[14], **Shane O'Sullivan**[15], **Paolo Padovani**[10], **Zsolt Paragi**[1], **Manel Perucho**[12], **Dominik Schleicher**[16], **Łukasz Stawarz**[17], **Nektarios Vlahakis**[18], **and John Wardle**[19]

[1]*Joint Institute for VLBI in Europe;* [2]*North-West University;* [3]*Radboud University Nijmegen;* [4]*University of Maryland;* [5]*INAF - Osservatorio Astronomico di Brera;* [6]*Università di Bologna;* [7]*INAF - Istituto di Radioastronomia;* [8]*Instituto de Astrofísica de Andalucía - CSIC;* [9]*Delf University of Technology;* [10]*European Southern Observatory;* [11]*Purdue University;* [12]*Universitat de València;* [13]*Space Telescope Science Institute;* [14]*National Tsing-Hua University;* [15]*The University of Sydney;* [16]*Georg-August-Universität Göttingen;* [17]*Institute of Space and Astronautical Science –JAXA;* [18]*University of Athens;* [19]*Brandeis University*
E-mail: agudo@jive.nl

Relativistic jets in active galactic nuclei (AGN) are among the most powerful astrophysical objects discovered to date. Indeed, jetted AGN studies have been considered a prominent science case for SKA, and were included in several different chapters of the previous SKA Science Book (Carilli & Rawlings 2004). Most of the fundamental questions about the physics of relativistic jets still remain unanswered, and await high-sensitivity radio instruments such as SKA to solve them. These questions will be addressed specially through analysis of the massive data sets arising from the deep, all-sky surveys (both total and polarimetric flux) from SKA1. Wide-field very-long-baseline-interferometric survey observations involving SKA1 will serve as a unique tool for distinguishing between extragalactic relativistic jets and star forming galaxies via brightness temperature measurements. Subsequent SKA1 studies of relativistic jets at different resolutions will allow for unprecedented cosmological studies of AGN jets up to the epoch of re-ionization, enabling detailed characterization of the jet composition, magnetic field, particle populations, and plasma properties on all scales. SKA will enable us to study the dependence of jet power and star formation on other properties of the AGN system. SKA1 will enable such studies for large samples of jets, while VLBI observations involving SKA1 will provide the sensitivity for pc-scale imaging, and SKA2 (with its extraordinary sensitivity and dynamic range) will allow us for the first time to resolve and model the weakest radio structures in the most powerful radio-loud AGN.

Advancing Astrophysics with the Square Kilometre Array
June 8-13, 2014
Giardini Naxos, Italy

[*]Speaker.
[†]On behalf of the SKA Cosmic Magnetism Working Group

PoS(AASKA14)093

1. Introduction

Relativistic jets in AGN are among the most powerful astrophysical objects so far discovered. Their relativistic nature causes them to emit abundant and extremely time-variable radiation in all spectral ranges from radio wavelengths to gamma-rays, whereas bulk relativistic motion leads to strong Doppler boosting effects, making them detectable at extreme cosmological distances. In AGN, relativistic plasma jets are thought to be formed as the result of accretion onto super-massive black-holes (SMBH) in the presence of rotating accretion disks and co-rotating magnetic fields. The study of the details involved in the jet formation process, which are still largely unknown, makes AGN jets a powerful tool to probe the environment of objects in extremely compact matter-states, and the physics of high-energy plasmas and their magnetic fields.

During recent years, a drastic improvement in our understanding of relativistic jets has been enabled by advances in supercomputing facilities for state-of-the-art numerical simulations, as well as deep, high-resolution radio, optical-IR and X-ray imaging and the advent of comprehensive monitoring programs covering most accessible spectral ranges from radio to gamma-rays. However, most of the fundamental questions about the physics of relativistic jets still remain unanswered, and await high sensitivity radio instruments such as SKA to solve them. These questions include: a) why are jets produced efficiently only in some systems, and what is the relation between jet power and the properties of the black hole and accretion system? b) what influence do magnetic fields have on jet formation, collimation, and maintenance up to distances > 100 kpc? c) what is the actual plasma composition at different jet scales and how does it evolve down the jet? d) how does the particle acceleration mechanism make the jet an efficient emitter on scales exceeding the size of the host galaxy? and d) how does the feedback between the jet and the (inter-)galactic medium influence the evolution of galaxies and clusters, and how do AGN jets and their central black holes evolve on cosmological time scales up to $z \sim 10$?

These questions will perhaps be addressed first by analysis of the massive data sets arising from deep all-sky surveys with SKA1, including both total and polarimetric flux. In particular, SKA1 studies of relativistic jets at different resolutions will allow, for the first time: i) studies (including imaging) of AGN jets throughout cosmic time, back to the epoch of re-ionization; ii) robust jet composition studies through unparalleled circular polarization (CP) sensitivity/purity; iii) an understanding of the origin of intrinsic differences in jet power in AGN via imaging of thousands of radio-weak AGN; iv) a characterization of the three-dimensional distributions of flow parameters such as velocity, proper emissivity, and magnetic field structure (through total flux and polarization imaging), that lead to estimates of key physical quantities such as mass and energy fluxes and entrainment rates; v) a probe of the magnetoionic environments of the jets (perhaps including their confining fields) through deep full Stokes (and Faraday rotation measure) imaging at all scales along and across a large number of objects; and vi) an understanding of the interplay between the jet and the ambient medium, both in the local universe and along cosmic time up to $z \sim 10$.

In § 2–10, we describe the current status of the main research areas involving jetted AGN, and the requirements necessary for SKA1 to advance in these fields. In § 11 and 12 we summarize the general need for future jetted AGN studies with SKA1, and we discuss the prospects for the SKA1 early science phase, as well as for SKA2 on AGN jet investigations.

PoS(AASKA14)093

2. Jet Formation, Collimation, and Evolution

Models proposed to explain the origin of relativistic jets in AGN involve accretion, in the form of a disk, of interstellar mass and gas from tidally disrupted stars onto a supermassive black hole. There is a general agreement that magnetic fields play a crucial role in this process. In the models of magnetically driven outflows, poloidal magnetic fields anchored at the base of the accretion disk generate a toroidal component and a subsequent poloidal electromagnetic flux of energy (Poynting flux) that accelerates the magnetospheric plasma along the poloidal magnetic field lines (see Blandford & Payne 1982; Li et al. 1992, and Fig. 1 for illustration). Energy can also be extracted from rotating black holes with similar efficiencies by the Blandford & Znajek (1977) mechanism. The strength of the magnetic field on the event horizon can be estimated to be of the order of thousands of Gauss. How this magnetic field is built up from the disk magnetic field is the subject of current research (Tchekhovskoy et al. 2011; McKinney et al. 2012).

Since in any version of a magnetic central engine the accretion disk is magnetized, we expect a wind to be driven from its surface (close to the black hole) with a power comparable to the Blandford-Znajek power. If the mass loading of disk winds (mainly formed by electron-proton plasma) were too high to produce ultrarelativistic terminal speeds, both mechanisms would need to operate at the same time, producing stratified jets in both composition (outer electron-proton wind, inner electron-positron jet) and speed. On the other hand, the Blandford-Znajek mechanism does not provide any collimation. Hence the central engine must provide an additional ingredient to confine the outflow until it reaches the superfast magnetosonic regime. Multi-wavelength full-polarization (4-Stokes) studies with SKA1 at all resolutions, down to the milli-arcsecond (mas) scale with SKA1-VLBI (Paragi et al. 2015), including CP observations with precision up to $\sim$ 0.01 %, are ideal to test the above mentioned jet/disc-wind scenario, and therefore of the role of such winds in the collimation of jets (see § 4). Furthermore, full-polarization measurements would allow us to determine the fraction of electron-positron pairs, the shape of the low energy distribution of the relativistic emitting particles and the presence of a dynamically dominant proton component, helping to constrain the initial magnetization of the wind, a very important parameter in the magnetic theory of AGN jets determining the asymptotic speed of the flow.

Theoretical and observational considerations suggest that jets must remain Poynting dominated along the acceleration phase. The success of magnetic acceleration (Vlahakis & Königl 2004) has been confirmed in time-dependent numerical simulations (Komissarov et al. 2007). In the case of parabolic jets, the acceleration continues until the jet becomes particle-dominated, at sub-parsec scales (hundreds to thousands of black hole gravitational radii). To stablish the exact location of the site of this conversion and its possible observational signature, in particular its position in relation to the radio core, is a subject of current active research for multi-spectral-range observational campaigns where high-frequency polarimetric single-dish and VLBI observations are key ingredients. With its superb sensitivity, SKA1-MID in Band 5 (both as a VLBI station or not) will allow these kinds of studies for a large number of sources seen from the southern hemisphere, where a growing number of panchromatic facilities are expected to operate with SKA. These studies are particularly interesting for nearby sources such as Centaurus A and M 87, where the highest linear resolutions will be achieved to resolve the jets both across and along their axis, from the regions close to the SMBH to those where the Poynting flux converts to particle dominated plasma.

PoS(AASKA14)093

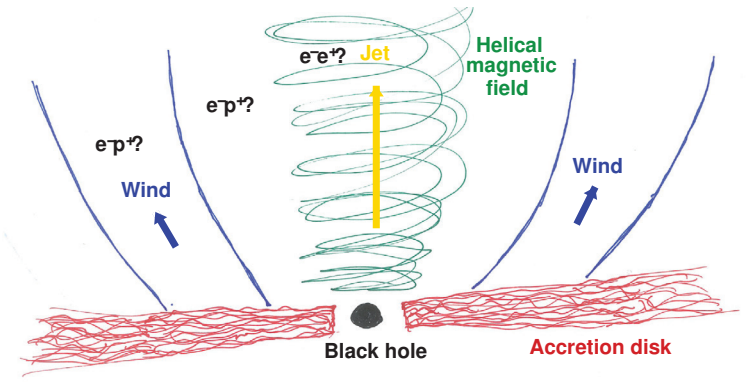

Figure 1: Conceptual illustration of the jet formation and collimation scenario described in § 2.

3. Particle Acceleration in Jets

The ambiguity of the location where Poynting-flux dominated outflows are converted into kinetic dominated jets reflects a general lack of understanding of the particle acceleration processes which are responsible for maintaining power-law distributions of radiating ultra-relativistic electrons over decades of length scales along the jet. These scales range from the sub-pc to pc scale, where the high-energy emission from blazars is likely produced, to the kpc scale where the jets terminate. In the case of low plasma magnetization, diffusive acceleration taking place at the fronts of strong hydrodynamical shocks (see e.g., Summerlin & Baring 2012, and references therein) could be considered as the most efficient way of energizing jet particles, leading naturally to the formation of power-law spectra. In the case of a high magnetization, on the other hand, relativistic magnetic reconnection (e.g. Sironi & Spitkovsky 2014) and stochastic interactions of particles with magnetic turbulence (Stawarz & Petrosian 2008, and references therein) are expected to play a major role. Although the relativistic nature of AGN jets constitutes a difficulty in this context (the aforementioned particle acceleration processes are well understood only in a non-relativistic regime), the slope and normalization of the resulting non-thermal particle spectra depend strongly on the underlying physical conditions in all of these three cases. This offers the opportunity to exploit high-quality observational data to determine the underlying non-thermal particle distributions, which can be used to constrain the acceleration processes at work.

Good-quality radio data provided by SKA1 has the potential to reveal the spectral shapes of freshly accelerated jet electrons. In the case of the extended arcsecond-scale jets and jet cocoons (lobes), such studies are expected to be free of any absorption effects even at low frequencies ($< 1-2$ GHz). The superior SKA1 sensitivity in full polarimetric mode (at $\gtrsim 1$ GHz), combined with simultaneous SKA1-VLBI observations, will enable spatially resolved spectral studies of the radio emission of the innermost regions of AGN jets out to large redshifts, ($z \sim 5-10$). Additional constraints on the acceleration sites of the highest-energy electrons and their radiation environment, based on co-ordinated multi-wavelength observations at high radio frequencies (see previous section), will be facilitated by the location of the SKA1-MID in South Africa, in close vicinity to world-class optical (SALT) and very-high-energy γ-ray (H.E.S.S. and possibly CTA-South) observatories, in combination with satellite-based X-ray and γ-ray (Fermi) observations.

PoS(AASKA14)093

4. Jet Composition through Circular Polarization Studies

Circular polarization observations (Stokes V) of relativistic jets enable us to measure quantities that are not accessible by observation of the first three Stokes parameters (I, Q, U, representing total intensity and linear polarization, LP). These include direct measurement of the magnetic field strength, as well as the vector-ordered part of the magnetic field, and hence the true magnetic flux carried by the jet (a conserved quantity that should be equal to the magnetic flux at the central engine). CP will also enable measurements of the composition of the jet (i.e. the e^+-p^+ ratio) and the low-energy cut-off of the relativistic electron energy distribution (see Homan et al. 2009, where all these physical quantities were estimated for the quasar 3C 279). These quantities are fundamental to understanding the physical properties of relativistic jets and in particular how they are launched (see § 1 and 2, and Fig. 1), and also for calculating the energy carried by the jet and hence for studying AGN feedback. These have long been open questions in AGN physics.

CP is difficult to study in AGN because it is typically weak ($\sim$0.1–1% of Stokes I) and highly variable. The high sensitivity and large instantaneous bandwidths of the SKA1 make it the ideal instrument for measuring CP (and its frequency dependence up to Band 5 of SKA1-MID), as long as the SKA retains excellent polarization purity at all frequencies. As very few circularly polarized AGN are currently known (< 100), a large-area CP-sensitive SKA1 survey across all SKA1 bands from 1 to 20 GHz will revolutionize this field of study (see O'Sullivan et al. 2013, for an example of what can be achieved with broadband CP observations). After finding the CP-brighter sources, SKA1-VLBI is required for follow-up observations to resolve the CP emission region and extract the key jet physical parameters (power, composition, magnetic flux).

CP measurements are unique in their ability to provide a direct measurement of the jet magnetic field strength, if the field vector ordering can be determined. One situation where there must be a vector-ordered field is if the jet carries an electric current, as in several of the electromagnetic mechanisms for launching jets. Indeed, when combined with LP and Faraday rotation measurements, several fundamental properties of the jet can be measured using CP. For example, when a transverse CP gradient and an RM gradient are both detected, they should have the same sign, each confirming the other, allowing direct measurement of the strength of the toroidal component of the magnetic field and hence the magnitude of the jet current, as well as the low energy cutoff of the electron energy distribution (from the RM-CP ratio). Since we are trying to detect very small fractional polarizations, our detected sources will be bright in Stokes I. Thus, as long as SKA1 receivers have excellent polarization purity (~ 0.1 % and ~ 0.01 % for LP and CP, respectively), then even a shallow large-area early-science survey will dramatically improve our knowledge of CP in AGN jets. Sources detected in CP could then be followed up with SKA-VLBI to produce groundbreaking advances in our knowledge of magnetic fields and particle populations in jets.

5. From the Most Powerful to the Weakest Jets

5.1 The Radio-loud/Radio-quiet AGN Issue

AGN come mainly in two classes: radio-loud (RL) AGN, emitting most of their energy over the entire electromagnetic spectrum non-thermally through powerful relativistic jets, and radio-quiet (RQ) AGN, whose multi-wavelength emission is dominated by thermal emission, directly

PoS(AASKA14)093

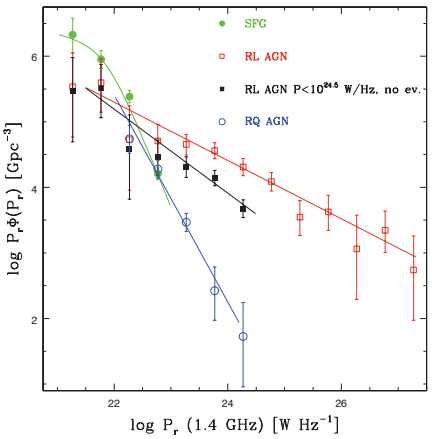

Figure 2: Local 1.4 GHz differential luminosity functions for star forming galaxies and AGNs measured from the *Chandra* Deep Field South VLA survey. Reproduced from Padovani et al. (2011).

or indirectly related to the accretion disk[1]. The mechanism responsible for radio emission in RQ AGN has been a matter of debate for the past fifty years. Alternatives have included a scaled down version of the RL AGN mechanism (e.g., Ulvestad et al. 2005), star formation (Sopp & Alexander 1991), and many others. Very recent results on the evolution and luminosity function of very faint radio sources, based on the Chandra Deep Field South samples including a few hundred sources down to $\sim 6-10$ μJy rms, suggest close ties between star formation and radio emission in RQ AGN, at least at $z \sim 1.5-2$ (Padovani et al. 2011, Fig. 2, and Padovani et al. in prep.). This is further confirmed by the comparison of the star formation rates derived from the far-IR and radio luminosities, assuming that all the radio emission is due to star formation. For RQ AGN and star forming galaxies the two star formation rate estimates are fully consistent, while for RL AGN the agreement is poor due to the large contribution of the relativistic jet to their radio luminosity (Bonzini et al., submitted). SKA will contribute in two different ways to examine this problem, i) by using the data from the full-polarimetric commensal wide and deep surveys that are being planned for SKA1 in Band 3, which will provide larger samples of RQ and RL AGN covering a wide range of redshifts and powers, and ii) by carrying out polarimetric, wide-field SKA1-VLBI survey follow-up observations in Bands 3 and 5 of the brighter sources ($\gtrsim 50\,\mu$Jy) to distinguish between jet and star formation emission (see § 10).

5.2 Jet Power Along the Radio-loud Classification

The more powerful radio-loud AGN jets are traditionally divided into Fanaroff-Riley classes FRI and FRII, with the latter having highly collimated jets that terminate in a bright hotspot, indicative of high-Mach number, relativistic flows (Fanaroff & Riley 1974). Since the pioneering work of Rawlings & Saunders (1991) on radio-loud AGN, that showed that the jet power correlated with the narrow line luminosity, we have reached the firm conclusion that the jet power correlates with the accretion rate. The present large sample of spectroscopically observed radio–loud objects (SDSS), and blazars detected in the γ–ray band reinforced this conclusion (Sbarrato et al. 2012a), and led to

[1] See Bonzini et al. (2013) for a recent definition of radio-quiet and radio-loud AGN

PoS(AASKA14)093

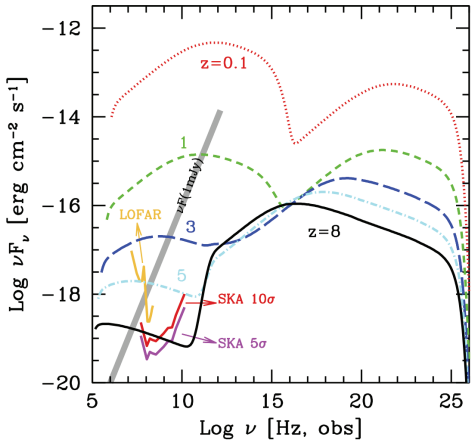

Figure 3: Spectral energy distribution of a typical radio loud quasar at different redshifts as seen in the observer's frame. As redshift increases, the radio spectrum gets progressively more dimmed both because of the larger distance to the source and because of inverse Compton cooling of the particle population responsible for the radio emission. The red and pink continuous lines mark the 10σ and 5σ limits of SKA1 (LOW and MID), respectively, for 30 min integration time, whereas the thick grey line correspons to $F(\nu) = 1\,mJy$. Reproduced from Ghisellini et al. (2014).

the idea that low power radio–loud AGN are associated with radiatively inefficient disks, emitting a small amount of ionizing photons, thus explaining why the broad emission lines are so intrinsically weak in these objects (Sbarrato et al. 2012b). Of course, black hole mass and black hole spin are also thought to play key roles (e.g., Blandford & Znajek 1977; McNamara et al. 2011) by controlling the accretion rate, whereas the external environment also has a strong influence on jet luminosity, as witnessed by 'hybrid' AGN, which exhibit FR I and FR II morphology jets on either side of the active nucleus (Gopal-Krishna & Wiita 2000).

The weaker flavor of radio-loud AGN have a synchrotron emission peaking in the far–UV and X–ray bands, and are radio–weak (but not radio–quiet). To study them at moderate redshifts ($z > 0.4$), it is crucial to measure the IR and optical cosmic background and to constrain the cosmic magnetic field. The large and deep commensal surveys planned for SKA1 will be an extremely useful tool to help studying weak radio AGN associated with TeV emitters observed with CTA (see Giroletti et al. 2015), and to provide a better characterization of the large scale properties of the cosmic magnetic field (Johnston-Hollitt et al. 2015). Moreover, a significant fraction of Seyfert galaxies have radio structures on scales of ~ 1 kpc consistent with weak jets being decelerated by the host galaxy's ISM (Gallimore et al. 2006). High-sensitivity, high-resolution full polarimetric studies with SKA1 and SKA1-VLBI have the potential for imaging many of these sources, to shed new light on the long standing problem of radio-loud/radio-quiet AGN through high resolution imaging of nearby sources.

On the opposite power end, powerful jets are associated with high rates of accretion (Ghisellini et al. 2010). The most powerful objects are therefore those jets associated with high accretion and large SMBH masses. Exploiting the relativistically enhanced jet emission, high power blazars can

PoS(AASKA14)093

be an important tool to explore the far Universe, to find the youngest and most active SMBH, that can constrain (and possibly challenge) current ideas of black hole formation, growth, and feedback (see e.g., Volonteri et al. 2011). For each detected blazar, there must be hundreds of similar sources whose jet is pointing elsewhere. It is this that makes the search for high–redshift blazars with large SMBH masses rewarding. To this task, deep SKA1 surveys at Band 3 or lower frequencies will be crucial. Not only because fluxes weakens with distance, but because, at high z, the cosmic background radiation (CMB, whose energy density $\propto (1+z)^4$), makes the relativistic electrons emit more through the inverse Compton scattering than through the synchrotron process. As a result, the fluxes of powerful blazar jets could be very weak at radio wavelengths (see Ghisellini et al. 2014, and Fig. 3), but still detectable for the SKA1 below 3 GHz for reasonably short integrations ($\sim$ 30 min) up to redshifts $z \sim 8$ and perhaps larger. Deep follow-up Band 3 SKA1-VLBI observations of the first AGN detected will enable studies of the jet morphologies at very high redshifts, and therefore their dense environments. This is also required to discover how the CMB modifies the appearance of radio lobes at high–z. SKA1 can therefore revise the fraction of radio-loud to radio-quiet AGNs at all redshifts, with a strong impact not only on the radio–loud luminosity function and evolution, but, in general, on the feedback on the host galaxy (through the so called radio-mode).

6. Detailed Estimates of Fundamental Jet Parameters

Deep, multifrequency, transverse-resolved radio observations are crucial to the estimation of flow variables in jets. This section concentrates on two topics that are fundamental to jet formation and propagation: velocity fields and magnetic-field topology. One powerful observational technique exploits the intrinsic symmetry of relativistic jet formation. The observed differences between approaching and receding jets are then dominated by the effects of relativistic aberration (Aloy et al. 2000), so by fitting parametrized models to images of both jets in Stokes I, Q and U, it is possible to derive the jet inclination and the three-dimensional variations of velocity, rest-frame emissivity and magnetic-field ordering (Laing & Bridle 2014). A second technique, which can use the same observations, is to analyse the wavelength dependence of linear polarization (and hence internal and external Faraday rotation) across the observing band using RM synthesis. These methods can be used on any scale, given adequate sensitivity and angular resolution. Structural changes on pc scales on timescales of days–years can be monitored, allowing direct measurement of proper motions and the variability of polarization and Faraday rotation structures.

6.1 Velocity Field

Low-luminosity (FR I) jets have been shown to decelerate on kpc scales, developing transverse velocity gradients indicative of boundary-layer entrainment (see Laing & Bridle 2014; Laing 2015). Further progress requires modeling of large samples, to average over intrinsic asymmetries, to explore the dependence of deceleration on jet power and environment and to assess the relative importance of mass injection by stars and boundary-layer entrainment. Resolutions in the range 0.1 – 0.5 arcsec and rms noise levels of 0.1 – 0.5 μJy/beam at GHz frequencies are needed to observe a sufficiently large number of sources ($\sim$ 300) with SKA1-MID, Bands 3 – 5.

The velocity fields of the narrower kpc-scale jets in powerful sources are much less well determined. Here, a key question is whether they have the very fast ($\Gamma \approx 5-10$) spines needed to gen-

PoS(AASKA14)093

erate X-ray emission by inverse Compton scattering of CMB photons as well as slower boundary layers. To answer this question, much better resolution and sensitivity are needed ($\approx$0.01 arcsec, $\approx$10 nJy/beam and dynamic range $> 10^7$:1; SKA2 Band 4 and 5). See Laing (2015) for a more detailed use case.

The increased sensitivity of SKA1-VLBI would in principle allow the technique to be extended to pc scales. Stratification in the total and linearly polarized emission across the jet width are expected in case the synchrotron emitting jet is threaded by a helical magnetic field (Laing 1981; Aloy et al. 2000). In this case, variations in the velocity field can be estimated by searching for changes in the emission stratification along the jet. Such variations have been observed in the jet of 3C 273 – for which there is evidence for the existence of a helical magnetic field (Asada et al. 2008) – by combining data from 48 epochs spanning 14 years of VLBA observations at 15 GHz (see Gómez et al. 2012, and Fig. 4). A similar jet behavior was already observed with 5 GHz VLBI by Lobanov et al. (2001). A change in the side of the jet that is brighter suggests an acceleration of the emitting plasma, in agreement with the observed acceleration of the pattern velocity associated with superluminal components (Jorstad et al. 2005; Lister et al. 2009). The unprecedented sensitivity of SKA1-VLBI will allow us to extend these studies to statistically significant samples of AGN jets.

For sources in which both jets are visible it is also possible to estimate the flow speed on scales where the pattern speeds of moving components can also be measured. If pattern speeds can be measured for components emitted simultaneously in the approaching and receding jets (as can be done for some microquasar jets), then additional constraints can be derived. M 87 is a particularly important target, as the hypothesis of gradual MHD acceleration on scales $\gg R_{\rm Schwarzschild}$ can be tested (see e.g. Asada et al. 2014) . Note, however, that the maximum baseline and observing frequency both need to be high enough to ensure transverse resolution of the jets and removal of any associated Faraday rotation (Kovalev et al. 2007), which makes polarimetric VLBI involving SKA1-MID up to Band 5 the ideal option.

If the velocity field, geometry and external environment of a jet are well characterized, then it is possible to apply conservation laws to derive the fluxes of energy, mass and momentum and the variation of entrainment rate with distance from the AGN (Laing & Bridle 2002).

6.2 Magnetic Field Topology

Most models of jet formation require a vector-ordered (toroidal or helical) field, but this has proved to be difficult to confirm observationally. The alternative of a random field made anisotropic by compression (e.g. shocks) or shear often provides at least as good a fit to observations of linear polarization. There are two key diagnostics. Firstly, a helical field with a significant poloidal component shows characteristic asymmetries in its transverse intensity and polarization emission profiles (Aloy et al. 2000). Secondly, if thermal matter is present within the jet volume, then systematic transverse Faraday rotation gradients are expected (Laing 1981; Broderick & McKinney 2010). Both diagnostics are complicated by effects such as jet bending and foreground Faraday rotation. The best-observed cases on pc scales, 3C 120 (Gómez et al. 2011) and 3C 273 (Asada et al. 2008) suggest a slow foreground screen and jet-related Faraday rotation, respectively. Deep and transverse-resolved observations of the pc-scale emission from a large sample of straight jets are needed, to answer the following questions: Are Faraday rotation gradients preferentially orthogonal to the jet? Does RM synthesis evidence the mixing of thermal and emitting plasma? What are the

PoS(AASKA14)093

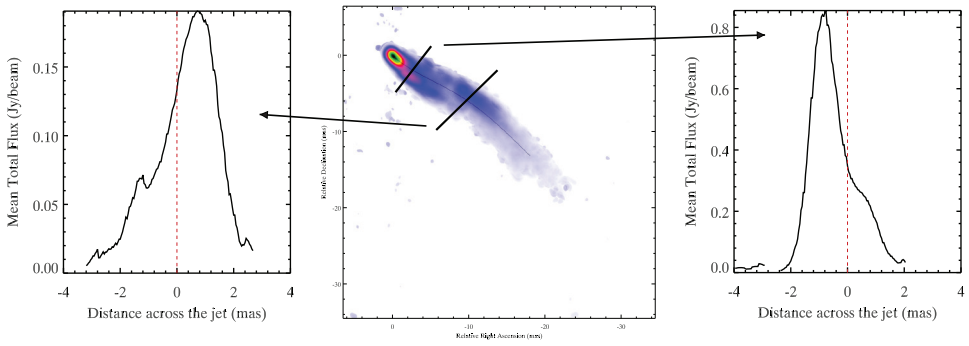

Figure 4: Mean total intensity map of 3C 273 obtained by combining 48 epochs spanning 14 years of VLBA observations at 15 GHz (including data from the MOJAVE program Lister et al. 2013). Left and right panels show slices at 3.1 and 14 mas from the core. A black line extending from the core indicates the jet ridge-line.

relative senses of gradients in the approaching and receding jets? Are transverse emission profiles consistent with the observed rotation? These questions require SKA1-VLBI on Band 5.

The dominant field component on kpc scales in FR I jets is toroidal, but it is unclear whether it is a vector-ordered remnant of the original confining field. If so, systematic and symmetrical gradients in Faraday rotation across the jets are expected. Isolating these from confusing effects of Faraday rotation by the IGM should be feasible for large samples of jets in sparse environments.

7. Understanding Jet Emission at Sub-pc and Multi-kpc Scales

Relativistic jets in AGN carry enormous amounts of kinetic energy out from the central black hole into the kpc-scale galaxy and intercluster medium. Most of the energy dissipation in powerful blazars is through the emission of GeV photons via inverse Compton scattering. However, we lack a clear understanding of where this dissipation takes place. Is it very near to the black hole engine (sub-pc scale) or much further out, beyond the regions dominated by broad-line emitting clouds and the obscuring torus of the unified model? As these scales can differ by orders of magnitude, the answer gives important clues for constraining jet formation and collimation models.

The dominant view during the *EGRET* era in the 1990's was that the gamma-ray emission is taking place within the sub-pc scale broad line region (Sikora et al. 1994). However, recent multi-wavelength monitoring of a few bright sources from radio to the *Fermi* GeV band, strongly suggests that in at least some cases, the emission takes place at distances of *several pc* from the central engine. The key evidence for this is VLBI observations showing that (some) major γ-ray flares take place at the same time with the ejection of superluminal components from the radio core, located several pc downstream of the central engine (e.g. Marscher et al. 2010), or even co-spatial with VLBI components downstream of the core (e.g. Agudo et al. 2011).

The SKA1-MID observational setup will have suitable features to monitor a substantial number of jets with the ideal sensitivity in total intensity and polarization, angular resolution, and time cadence: in particular Band 5 receivers in VLBI mode (Paragi et al. 2015) will provide $\sim$ milliarcsecond resolution, which corresponds to $\sim$ parsec scales for a broad redshift range. The polarization capabilities will be particularly relevant: current work suggest that polarized features can help

PoS(AASKA14)093

in the identification and tracking of jet components and in the characterization of the magnetic field evolution in relativistic jets. Only a massive project based on SKA data, perhaps employing similar observing methods and external multi-spectral range infrastructures as other transient objects (see Fender et al. 2015), will allow us to put these indications on firm grounds.

On much larger (kpc) scales, *Chandra* showed that knots in the jets of powerful quasars are strong X-ray emitters, with the X-ray emission being a separate spectral component from the radio-IR-optical one (first seen in PKS 0637-752, Schwartz et al. 2000; Chartas et al. 2000). The standard interpretation is that the X-rays are from inverse Compton scattering, assuming that the radio emitting electron distribution extends down to electron Lorentz factors $\gamma \sim 10-100$ and that the jets are highly relativistic at kpc scales (bulk Lorentz factors $\Gamma \sim 10-20$, Tavecchio et al. 2000; Celotti et al. 2001). This mechanism requires a jet power comparable to or higher than the Eddington luminosity and jets that are very well aligned to the line of sight and have lengths sometimes exceeding 1 Mpc. An alternative interpretation is that the X-ray emission is synchrotron coming from a second population of electrons (for a review see Harris & Krawczynski 2006). This does not require highly relativistic speeds or extremely powerful jets, but it does require that in situ particle acceleration reaches electron energies of at least ~ 30 TeV.

We are faced, therefore with the choice of fast and powerful jets or slow and multi-TeV particle accelerator jets. Recently, it was shown through *Fermi* observations that in the case of the archetypical quasar 3C 273 the inverse Compton model is ruled out (Meyer & Georganopoulos 2014), favoring synchrotron from a second electron population as the X-ray emission mechanism (see also Cara et al. 2013, for the case of PKS 1136−135 studied through optical/UV polarimetry). Multi-wavelength observations of 3C 273 hint at the two electron populations not being co-spatial (Jester et al. 2005). Understanding if this is indeed the case is imperative for understanding the physical conditions in the knots of these powerful jets, and high-dynamic-range deep radio-images from SKA1-MID (Bands 1–5) at resolutions up to 0.1 arcseconds (and SKA-LOW) are essential for mapping the spectral energy distribution of the extended jet as it extends out into the IGM.

8. Feedback Between AGN Jets and their External Medium

In the last few decades, observations of clusters of galaxies in the X-ray range revealed a lack of cool gas in the centres of many galaxies, contrary to expectations (see e.g. Fabian 2012, and references therein). This fact has not only important implications regarding the star formation rates in the galaxy and the growth of the central black hole (e.g. Cattaneo et al. 2009), but also regarding cold dark matter (CDM) models (Benson et al. 2003). The most accepted heating mechanisms proposed to stop the cooling flows are related to galactic activity or shocks produced during the merging of clusters. Among the former, the observed anti-correlation between the radio lobes formed by jets and the X-ray emission from the cluster gas suggests that the buoyancy of the under-dense cavities formed by the lobes could generate displacement work on the ambient gas, and could be responsible for the heating. Moreover, significant levels of metallicity have been recently detected at considerable distances from the active galaxy, which is possible only if an outflow has dragged those metals, produced from stars in the galaxy (e.g. Werner et al. 2011).

Recent observations have shown that the lobes are surrounded by shocks with low Mach numbers ($M \simeq 1-2$) in powerful sources, i.e., they have not reached the buoyancy stage. This would

PoS(AASKA14)093

imply faster evolution (pressure driven) and, accordingly, larger jet powers than estimated. Shocks may be extremely important and efficient in the heating process of the galactic and cluster gas because they can displace large amounts of gas from the host galaxy, quenching or triggering star formation (e.g. Perucho et al. 2014, and references therein). The discrepancy between CDM models, which predict a power law distribution of dark matter halos around galaxies, and the luminosity function of bright galaxies, which declines exponentially, could be also related to the feedback process (Benson et al. 2003). Recent semi-analytical work taking into account AGN feedback, reproduces the bright end of the luminosity function (e.g. Somerville et al. 2008).

It is clear that the dynamical impact of AGN jets within their host galaxies and environment can be very important to their evolution. The way in which the galactic activity relates to heating and cooling flows, or affects the evolution of the host galaxy, by changing the star formation rates and the growth of the central black hole, represents a fundamental problem in Astrophysics and Cosmology. Old populations of particles in the radio lobes formed by jets will certainly provide deep insight into the interaction between radio-jets and their environments. These particles emit at low radio frequencies and make SKA1-MID and SKA1-SUR (Bands 1 – 3), as well as SKA1-LOW, ideal instruments to detect them, and study how AGN jet activity impacts the evolution of the host galaxy and intra-cluster medium via the injection of particles and energy through relativistic jets (**?**). Angular resolutions on the order of the arcsecond (~ 10 arcseconds for SKA1-LOW), and sensitivities of the order of the μJy/beam in wide band continuum mode will be needed for these studies. The polarimetric capabilities of SKA will be relevant to study the influence of magnetic fields on the interplay of large scale-jets with their environment.

9. AGN Jets Along Cosmic Time

9.1 The First AGN and their Supermassive Black Holes

While AGN are common in the present-day Universe and SMBH with masses larger than 10^9 $M_\odot$ were still reported at $z > 6$ (e.g. Fan et al. 2006), it is natural to ask when the first AGN and their supermassive black holes started to form. In a seminal discussion by Rees (1978), a number of potential pathways, including single stars, stellar clusters and the direct collapse of very massive gas clouds have been considered. While the first stars are expected to have typical masses ranging from a few 10 $M_\odot$ to a few 100 $M_\odot$, the formation of stellar mass black holes from primordial stars seems only possible between $30-120$ $M_\odot$ and $180-1000$ $M_\odot$ (Heger et al. 2001). At least under the assumption of Eddington accretion, it therefore seems difficult that such stars could reach 10^9 $M_\odot$ by $z \sim 6-7$ (e.g. Shapiro 2005).

More massive black hole seeds could be formed from the collapse of dense stellar clusters. Such clusters could form via dust-induced fragmentation in low-metallicity gas, with their collapse leading to characteristic black hole masses of a few times 1000 $M_\odot$ (Devecchi et al. 2012). The first simulations exploring the formation of massive black holes from the direct collapse of massive gas clouds have shown that strong radiation backgrounds are required to prevent the fragmentation into low-mass objects (Bromm & Loeb 2003). Theoretical suggestions indicated that masses of $10^4 - 10^5$ $M_\odot$ could be reached from the low-angular momentum material in the first massive halos at $z \sim 10-15$. Numerical simulations indeed indicate the formation of massive self-gravitating

PoS(AASKA14)093

disks in their centers, with high accretion rates of ~ 1 $M_\odot$ yr^{-1}. The high accretion rates imply the formation of very massive protostars with cool atmospheres and weak radiative feedback, leading to a typical mass scale of 10^5 $M_\odot$ (Schleicher et al. 2013).

These massive black holes are expected to lead to the formation of the first high-redshift quasars, which may contribute to the epoch of reionization. The pathways to observationally probe this population with SKA were outlined by Falcke et al. (2004). The compact radio cores of quasars with black hole masses of 10^7 $M_\odot$ should be visible even at $z > 10$. Due to the dense environments in the first galaxies, Falcke et al. (2004) predict that the black hole jet can potentially not break out from the galaxy, therefore leading to the formation of GHz-Peaked-Spectrum (GPS) sources (see also Taylor et al. 2015; Afonso et al. 2015). Early-Universe GPS sources are expected to be detected at low frequencies (100 – 600 MHz) at sensitivities of 100 μJy and better. This makes wide bandwidth surveys on SKA1-LOW, and SKA1-MID/-SUR at Band 1, the best suited options for the detection of these sources. Also, HI spectroscopy via the 21 cm line, potentially allows for the detection of hundreds to thousands of bright QSOs via their HII regions at $z \sim 8-10$; see Wyithe et al. (2015) for an extended discussion. Later, SKA1-VLBI involving SKA-MID and SKA-SUR at the lowest practical frequencies (i.e. L Band, to maximize UV coverage with additional existing VLBI stations) are probably the right selection to confirm the compact nature of the GPS sources down to scales smaller than a few tens of milliarcsecond.

9.2 Cosmological Studies of Radio-loud AGN. From $z \sim 0-10$

Radio observations are the best-suited means to probe the evolution of radio jets in SMBH over cosmic time, as obscuration has a very low effect and largely unbiased surveys can thus be pursued (Falcke et al. 2004). The latter allows cosmological studies of black hole growth over a large range of black hole masses and cosmological redshifts. The NRAO VLA Sky Survey (NVSS, Condon et al. 1998) has detected 1.8 million sources in total intensity, with 14% of them showing a clear polarization signal of at least 3σ (the majority of these being radio-loud AGN). While typical source counts have been restricted to flux density sensitivities of $\sim 10\mu$Jy in total intensity (e.g. Windhorst 2003), bright sources above 100 mJy typically correspond to the radio-loud FRII sources, while a gradual transition towards FRI sources occurs around 30 mJy. At ~ 1 mJy, an increasing fraction of radio sources is dominated by star formation rather than an active galactic nucleus (see § 5.1), even though a contribution from a radio-quiet AGN may still be present.

An analysis of the polarization data of NVSS shows that the fractional polarization increases with decreasing flux density (Mesa 2002). This trend has been confirmed in subsequent studies and surveys (see Banfield et al. 2011, and references therein), including data from the Dominion Radio Astrophysical Observatory Deep Field polarization study and radio polarimetry of the ELAIS N1 Field. This intriguing anti-correlation clearly suggests a change in the magnetic field structure of the observed sources, even though the physical origin of this behaviour is not yet understood. To investigate the potential origin of the polarization, Shi et al. (2010) studied a sample of highly polarized objects. In their sample, sources with more than 30% polarization were contained in elliptical galaxies with 1.4 GHz luminosities in the range of $10^{23} - 10^{24}$ W Hz^{-1}. As they reported no dependence on optical morphology, redshift, linear size and radio power, the high polarization seems likely a result of intrinsic properties of the source (see also Stil et al. 2014).

PoS(AASKA14)093

The deep total flux and polarimetric surveys that are being suggested by the SKA Magnetism and Continuum Science Working Groups for AGN at SKA1-MID and SKA1-SUR, mainly on Bands 2 and 3 (Taylor et al. 2015; Johnston-Hollitt et al. 2015; Prandoni et al. 2015; Smolcic et al. 2015), will allow further investigations regarding the total and polarized synchrotron emission of AGN. While a measurement of the spectra help to disentangle the contributions of AGN and star formation and provide information about the AGN environment, the measurement of the polarized fractions allows to further investigate the anti-correlation between radio flux and polarization fraction, and to potentially relate it to the power of the central engine, reflected in the jet. Whereas previous studies have found no explicit redshift dependence in the observed correlation up to $z \sim 3$, the far deeper SKA1 surveys are expected to probe radio fluxes to $z \sim 10$ where correlations with redshift cannot be ruled out.

On a second stage, deep follow-up SKA1-VLBI surveys of AGN will have the capability to image much smaller scales to investigate the origin of the I-p anti-correlation in terms of cancellation of orthogonal polarized regions on bright sources. These VLBI surveys will also allow us for studies of the brighter spatially resolved jets on cosmological scales, which will certainly help to provide information on the environments (through VLBI morphological studies). At L band, a 5 min-long VLBI observation including SKA1-MID will achieve a 5σ level of 25 μJy. This can allow to observe $\sim$ 1000 sources in less than 100 hours of observation. The value of these VLBI surveys will be much enhanced by synergies with deep optical surveys such as SDSS (York et al. 2000), and LSST (Bacon et al. 2015).

10. Identifying AGN Populations from SKA1 Surveys

Two main processes contribute to the extragalactic continuum radio emission at intermediate radio frequencies (i.e. 1.4 to 5 GHz): the non-thermal emission associated with relativistic electrons powered by AGN and a combination of free-free and synchrotron emission from the star formation activity in galaxies. The bright radio sky is dominated by the emission driven by radio-loud AGN where the presence of compact or slightly resolved radio cores on milliarcsecond–scale are the best indicators of the AGN activity. At faint flux densities ($< 0.5 - 1$ mJy) the contribution from star-forming galaxies to the radio source population becomes increasingly important (e.g. Seymour et al. 2008; Padovani et al. 2011, and Fig. 2). Moreover, recent work has confirmed that at 10–100 micro-Jy levels, the radio-quiet AGN are not radio-silent (e.g. Bonzini et al. 2012).

Linear polarization and spectral index information from the massive surveys on SKA1-MID and SKA1-SUR described above will be a useful tool to disentangle AGN jet emission from that of star-forming galaxies, thus providing a first selection of AGN candidates from large SKA commensal surveys. Clearly, the optical data and photometric redshifts measured by the Large Synoptic Survey Telescope (LSST) will be an invaluable complement for any kind of SKA survey involving extragalactic sources, e.g. Bacon et al. (2015), and specifically for all those studies interested in radio emitting objects at all ranges of redshift. In particular, the optical photometric data from LSST will also be extremely useful in discriminating between the AGN and star forming galaxy populations. A definitive probe of the presence of AGN radio loud activity will be the detection of high brightness temperature from embedded radio-AGN cores in the host galaxies through

PoS(AASKA14)093

ultra-high-resolution (milliarcsecond or sub-milliarcsecond scale) SKA1-VLBI wide-field-of-view observations, see Paragi et al. (2015).

Adding to the present High Sensitive Array (HSA), the SKA1-MID and/or SKA1-SUR as a phased array, will obtain an angular resolution better than 5 milliarcseconds at L Band, which corresponds to 10 – 40 pc in the redshift range 0.1 to 5. This high angular resolution will be coupled with the exceptional sensitivity provided by the SKA1. One hour of observation with the HSA + SKA1-MID at L Band at a recording rate of 4096 Mb/s will allow to reach 0.75 μJy/beam (0.84 μJy/beam without Arecibo). For less demanding sensitivities, similar VLBI observation will achieve a sensitivity of $\sim 5\,\mu$Jy/beam in 5 min integrations. This high sensitivity – high angular resolution will allow not only identifying starburst galaxies, and resolving and mapping the region of star-formation, but also imaging jets at parsec scales in the inner region of AGN up to high z.

11. Studies of Relativistic Jets in AGN with SKA1: A Summary

Previous sections outline a variety of relevant science cases for cutting-edge studies of relativistic jets in AGN that can be performed with SKA1. In particular, the superb sensitivity of SKA1 will allow us to detect massive samples of AGN from commensal full-polarization all-sky and deep surveys performed at both SKA1-MID and SKA1-SUR at frequencies between ~ 1 and 3 GHz (Taylor et al. 2015; Johnston-Hollitt et al. 2015; Prandoni et al. 2015; Smolcic et al. 2015). Identification of AGN in these surveys may be performed in different and complementary ways by using classification arguments based on linear polarization, spectral index, optical photometry, and brightness temperature measurements. Linear polarization and spectral index information will be available from SKA commensal surveys. Optical photometric and redshift data from the LSST will be of invaluable help, whereas the highly-constraining brightness-temperature information will be provided by follow up wide-field VLBI observations involving SKA1, ideally including both the phased SKA1-MID and SKA1-SUR at L-band, where UV coverage can be optimized by including a large number of non-SKA VLBI stations. The wide field requirement needs multiple (≥ 4) beam formers for the SKA1-MID and SKA1-SUR cores, see Paragi et al. (2015). These cores will dominate the sensitivity of the entire VLBI array, and can therefore reliably detect high brightness temperatures from AGN at a few 10 μJy level or better.

The data from the above-mentioned full-polarimetric surveys at SKA1-MID and SKA1-SUR will be of almost inestimable value for essentially all AGN science cases described in this chapter, specially for radio-loud/radio-weak, and massive cosmological statistical-studies. Investigations of the feedback between large scale AGN jets and their intergalactic medium, and those for the search of the first GPS-like radio AGN and black holes, will also benefit from these enormous survey datasets, as well as from lower frequency all-sky programs at SKA-LOW.

The non-isotropic character of radio AGN, together with the fact that some of the most pressing open questions about AGN are related to their innermost (pc and sub-pc) jet regions, makes ultra-high angular resolution VLBI observations an essential ingredient of next-generation studies. In particular, jet formation, collimation, and acceleration studies will only be complete with the aid of additional super-sensitive full-polarization VLBI observations at multiple observing frequencies up to ~ 15 GHz, which will only be possible with SKA1-MID on Band 5 and lower. These observations are also mandatory for detailed studies of the velocity field and magnetic field properties of

PoS(AASKA14)093

the innermost AGN jet regions, as well as for research on the high energy emission site and emission mechanism in combination with other multi-spectral range facilities operating simultaneously in the southern hemisphere.

Characterizing the jet composition and magnetic field, and measuring the low-energy cut-off of the relativistic electron energy distribution through circular polarization analysis requires not only multi-frequency (up to Band 5) SKA1-MID, and SKA1-VLBI observations to map the different regions of the AGN, but also –and even more importantly– requires high precision circular and linear polarization measurements up to $\sim 0.01\%$, and $\sim 0.1\,\%$, respectively, that can be achieved with linear feeds as planned for SKA1-MID. Great attention must be paid at design time to ensure optimum performance in all four Stokes parameters so that the scientific potential of SKA can be realized in these areas.

12. Considerations for SKA1 Early Science and SKA2

A reduction by $\sim 50\,\%$ in sensitivity during the early-science stage of SKA1 will not dramatically affect most of the science use cases presented here as long as SKA1 receivers retain adequate polarization purity as described above. In particular, the proposed research on jet formation, collimation and acceleration; jet composition, precise characterization of jet parameters and jet emission properties; jet feedback; and the identification of AGN populations from early-science SKA surveys will provide excellent science outcomes even with a large reduction in sensitivity while waiting for the complete SKA1 to be finished.

The requirements for detailed imaging studies of FRII radio galaxies outlined in § 6, i.e. ~ 0.01 arcsec resolution, ~ 10 nJy/beam, and $> 10^7 : 1$ dynamic range at bands 4 and 5 of SKA1-MID, will only be achieved by SKA2. Certainly, the ability of SKA-MID to achieve frequencies up to 24 GHz at the stage of the SKA2 will greatly boost ultra-high-resolution VLBI studies to probe the innermost jet regions of nearby sources, where the jet is still being collimated and accelerated.

During the final stage of SKA, the possibility of SKA2-MID observations including a number of very large ($\gtrsim 1000$ km) baselines employing a homogeneous array of SKA stations would open a new era of extremely high-dynamic-range VLBI observations with the SKA alone (Garrett 1999). These high dynamic-range observations would allow imaging of an unprecedented number of jet-counterjet systems, and their transverse structure, which will certainly allow for extremely high precision estimates of the actual physical conditions at the innermost regions of jets, close to their formation and collimation sites. Of paramount importance for these SKA2-VLBI observations is the availability of quasi-scaled arrays over as wide a range of frequencies as possible to avoid changing resolution with frequency, which is crucial to eliminate resolution biases on the relevant polarization studies described in § 2, 3, 4, and 6.

References

Afonso, J., et al. 2015, "Identifying the first generation of radio powerful AGN in the Universe with the SKA" in proc. *Advancing Astrophysics with the SKA*, PoS(AASKA14)071

Agudo, I., et al. 2011, ApJ, 726, L13

Aloy, M. A., et al. 2000, ApJ, 528, L88

Asada K., et al. 2008, ApJ, 675, 79

PoS(AASKA14)093

Asada K., et al. 2014, ApJ, 781, L2
Bacon, D., et al. 2015, "Synergy between the Large Synoptic Survey Telescope and the Square Kilometre Array" in proc. *Advancing Astrophysics with the SKA*, PoS(AASKA14)145
Banfield, J. K. et al. 2011, ApJ, 733, 69
Benson, A.J., et al., 2003, ApJ, 599, 38
Blandford, R. D. & Znajek, R. L., 1977, MNRAS, 179, 433
Blandford, R. D. & Payne, D. G., 1982, MNRAS, 199, 883
Bonzini et al. 2012, ApJS 203, 15
Bonzini et al. 2013, MNRAS 203, 15
Broderick, A. E., & McKinney, J. C., 2010, ApJ, 725, 750
Bromm, V. & Loeb, A. 2003, ApJ, 596, 34
Cara, M., et al. 2013, ApJ, 773, 186
Carilli, C. L., & Rawlings, S. 2004, New Astronomy Reviews, 48, 979
Cattaneo, A., et al., 2009, Nature, 460, 213
Celotti, A., Ghisellini, G., & Chiaberge, M. 2001, MNRAS, 321, L1
Chartas, G., et al. 2000, ApJ, 542, 655
Condon, J. J., et al. 1998, AJ, 115, 1693
Devecchi et al. 2012, MNRAS, 421, 1465
York, D. G. et al. 2000, AJ, 120, 1579
Fabian, A.C., 2012, ARA&A, 50, 455
Falcke, H., Körding, E. & Nagar, N. M. 2004, New Astronomy Reviews, 48, 1157
Fan et al. 2006, AJ, 131, 1203
Fanaroff, B. L., & Riley, J. M. 1974, MNRAS, 167, 31P
Fender, R., et al. 2015, "The Transient Universe with the Square Kilometre Array", in proc. *Advancing Astrophysics with the SKA*, PoS(AASKA14)051
Finke, J. D., Razzaque, S., & Dermer, C. D., 2010, ApJ, 712, 238
Gallimore, J. F., et al. 2006, AJ, 132, 546
Garrett, M. A. 1999, in proc. "Perspectives on Radio Astronomy: Science with Large Antenna Arrays", 139
Ghisellini G., et al., 2010, MNRAS, 405, 387
Ghisellini G., et al. 2014, MNRAS, 438, 2694
Giroletti, M., et al. 2015, "The connection between radio and high energy emission in black hole powered systems in the SKA era", in proc. *Advancing Astrophysics with the SKA*, PoS(AASKA14)153
Gómez, J. L., et al. 2011, ApJ, 733, 11
Gómez, J. L., et al. 2012, International Journal of Modern Physics, 8, 265
Gopal-Krishna, & Wiita, P. J. 2000, A&A, 363, 507
Harris, D. E., & Krawczynski, H. 2006, ARAA, 44, 463
Heger et al. 2001, NuPhA, 688, 197
Homan, D., et al. 2009, ApJ, 696, 328
Jester, S., et al. 2005, A&A, 431, 477
Johnston-Hollitt, M., et al. 2015, "Using SKA Rotation Measures to Reveal the Mysteries of the Magnetised Universe", in proc. *Advancing Astrophysics with the SKA*, PoS(AASKA14)092
Jorstad, S. G., et al., 2005, AJ, 130, 1418
Komissarov, S. S., et al. 2007, MNRAS, 380, 51
Kovalev Y.Y., et al. 2007, ApJ, 668, L27
Laing R.A., 1981, ApJ, 248, 87
Laing, R. A. & Bridle, A. H., 2002, MNRAS, 336, 1161
Laing, R. A. 2015, "Kinematics and Dynamics of kiloparsec-scale Jets in Radio Galaxies with SKA", in proc. *Advancing Astrophysics with the SKA*, PoS(AASKA14)107

PoS(AASKA14)093

Laing, R. A. & Bridle, A. H., 2014, MNRAS, 437, 3405
Li, Z.-Y., Chiueh, T. & Begelman, M. C., 1992, ApJ, 394, 459
Lister, M. L., et al., 2009, AJ, 138, 1874
Lister M.L., et al., 2013, AJ, 146, 120
Lobanov, A. P. & Zensus, J. A. 2001, Science, 294, 5540
Marscher, A. P., et al. 2010, ApJ, 710, L126
McNamara, B. R., Rohanizadegan, M., & Nulsen, P. E. J. 2011, ApJ, 727, 39
McKinney, J.C., Tchekhovskoy, A. and Blandford, R.D., 2012, MNRAS, 423, 3083
Mesa, D. 2002, A&A, 396, 463
Meyer, E. T., & Georganopoulos, M. 2014, ApJ, 780, L27
O'Sullivan S., et al. 2013, MNRAS, 435,311
Padovani, P., et al. 2011, ApJ, 740, 20
Paragi, Z., et al. 2015, "Very Long Baseline Interferometry with the SKA", in proc. *Advancing Astrophysics with the SKA*, PoS(AASKA14)143
Perucho, M., et al., 2014, submitted.
Prandoni, E., et al. 2015, "Revealing the Physics and Evolution of Galaxies and Galaxy Clusters with SKA Continuum Surveys", in proc. *Advancing Astrophysics with the SKA*, PoS(AASKA14)067
Rawlings S. & Saunders R., 1991, Nature, 349, 138
Rees, M. J. 1978, Phys. Scr., 17, 193
Sbarrato T., et al. 2012a, MNRAS, 421, 1764
Sbarrato T., et al. 2012b, MNRAS, 426, L91
Schleicher, D.R.G. et al. 2013, A&A, 558, 59
Seymour et al. 2008, MNRAS 386, 1695
Shapiro, S. 2005, ApJ, 620, 59
Shi, H. et al. 2010, MNRAS, 409., 821
Sikora, M., Begelman, M. C., & Rees, M. J. 1994, ApJ, 421, 153
Sironi, L., & Spitkovsky, A. 2014, ApJL, 783, L21
Smolcic, V., et al. 2015, "Exploring AGN Activity over Cosmic Time with the SKA", in proc. *Advancing Astrophysics with the SKA*, PoS(AASKA14)069
Somerville, R.S., et al., 2008, MNRAS, 391, 481
Sopp, H.M., & Alexander, P. 1991, MNRAS, 251, 14P
Stawarz, Ł., & Petrosian, V. 2008, ApJ, 681, 1725
Stil, J. M. et al. 2014, ApJ, 787, 99
Summerlin, E. J., & Baring, M. G., 2012, ApJ, 745, 63
Schwartz, D. A., et al. 2000, ApJ, 540, L69
Tavecchio, F., et al. 2000, ApJ, 544, L23
Taylor, R., et al. 2015, "SKA Deep Polarization and Cosmic Magnetism", in proc. *Advancing Astrophysics with the SKA*, PoS(AASKA14)113
Tchekhovskoy, A., Narayan, R., & McKinney, J.C. 2011, MNRAS, 418, L79
Ulvestad, J.S., Antonucci, R.R.J., & Barvainis, R. 2005, ApJ, 621, 123
Vlahakis, N. & Königl, A., 2004, ApJ, 605, 656
Volonteri M., et al., 2011, MNRAS, 416, 216
Werner, N., et al., 2011, MNRAS, 415, 3369
Windhorst, R. A. 2003, New Astronomy Reviews, 47, 357
Wyithe, S., et al. 2015, "Imaging HII Regions from Galaxies and Quasars During Reionisation with SKA", in proc. *Advancing Astrophysics with the SKA*, PoS(AASKA14)015

PoS(AASKA14)093

PROCEEDINGS OF SCIENCE

Structure, dynamical impact and origin of magnetic fields in nearby galaxies in the SKA era

Rainer Beck[*1] [†], **Dominik Bomans**[2], **Sergio Colafrancesco**[3], **Ralf-Jürgen Dettmar**[2], **Katia Ferrière**[4], **Andrew Fletcher**[5], **George Heald**[6], **Volker Heesen**[7], **Cathy Horellou**[8], **Marita Krause**[1], **Yu-Qing Lou**[9], **Sui Ann Mao**[1], **Rosita Paladino**[10], **Eva Schinnerer**[11], **Dmitry Sokoloff**[12], **Jeroen Stil**[13] **and Fatemeh Tabatabaei**[11]

[1] *Max-Planck-Institut für Radioastronomie, Auf dem Hügel 69, 53121 Bonn, Germany*
[2] *Astron. Inst. der Ruhr-Universität Bochum, Universitätsstr. 150, 44780 Bochum, Germany*
[3] *School of Physics, University of the Witwatersrand, South Africa*
[4] *IRAP, Univ. de Toulouse, CNRS, 9 avenue du Colonel Roche, 31028 Toulouse Cedex 4, France*
[5] *School of Mathematics & Statistics, Newcastle University, Newcastle upon Tyne, NE1 7RU, UK*
[6] *ASTRON, Postbus 2, 7990 AA Dwingeloo, The Netherlands*
[7] *School of Physics and Astronomy, University of Southampton, Southampton SO17 1BJ, UK*
[8] *Chalmers University of Technology, Onsala Space Observatory, 439 92 Onsala, Sweden*
[9] *Dept. of Physics and Tsinghua Center for Astrophys., Tsinghua Univ., Beijing, 100084, China*
[10] *INAF-IRA, via Gobetti 101, 40129 Bologna, Italy*
[11] *Max-Planck-Institut für Astronomie, Königstuhl 17, 69117 Heidelberg, Germany*
[12] *Moscow State University, Moscow, 119991, Russia*
[13] *The University of Calgary, Calgary, AB T2N 1N4, Canada*
E-mail: rbeck@mpifr-bonn.mpg.de

Magnetic fields are an important ingredient of the interstellar medium (ISM). Besides their importance for star formation, they govern the transport of cosmic rays, relevant to the launch and regulation of galactic outflows and winds, which in turn are pivotal in shaping the structure of halo magnetic fields. Mapping the small-scale structure of interstellar magnetic fields in many nearby galaxies is crucial to understand the interaction between gas and magnetic fields, in particular how gas flows are affected. Elucidation of the magnetic role in, e.g., triggering star formation, forming and stabilising spiral arms, driving outflows, gas heating by reconnection and magnetising the intergalactic medium has the potential to revolutionise our physical picture of the ISM and galaxy evolution in general. Radio polarisation observations in the very nearest galaxies at high frequencies (≥ 3 GHz) and with high spatial resolution ($\leq 5''$) hold the key here. The galaxy survey with SKA1 that we propose will also be a major step to understand the galactic dynamo, which is important for models of galaxy evolution and for astrophysical magnetohydrodynamics in general. Field amplification by turbulent gas motions, which is crucial for efficient dynamo action, has been investigated so far only in simulations, while compelling evidence of turbulent fields from observations is still lacking.

Advancing Astrophysics with the Square Kilometre Array,
June 8-13, 2014
Giardini Naxos, Sicily, Italy

[*] Speaker.
[†] On behalf of the SKA Cosmic Magnetism Working Group

PoS(AASKA14)094

1. Introduction

Magnetic fields are a major agent in the ISM and control the density and distribution of cosmic rays (CRs). CRs accelerated in supernova remnants can provide the pressure to drive galactic outflows and buoyant loops of magnetic fields via the Parker instability. Outflows from starburst galaxies in the early Universe may have magnetised the intergalactic medium. Ultra-high-energy CRs (UHECRs) are deflected by regular fields and scattered by turbulent fields, so that the structure and the extent of the fields in the disk and halo are necessary parameters for propagation models.

Most of what we know about interstellar magnetic fields comes through the detection of radio waves. The intensity of *synchrotron emission* is a measure of the number density of cosmic-ray electrons (CREs) and of the strength of the component of the total magnetic field in the sky plane. Linearly polarised synchrotron emission emerges from ordered fields in the plane of the sky, which can be *regular (coherent) fields*, with a constant direction over scales of several kpc, or *anisotropic turbulent (or tangled) fields*, reversing their direction on small scales.

High-resolution polarisation images are needed to understand the physics of interstellar magnetic fields. Observations in the Milky Way are hard to interpret because the structures on a range of different scales contribute to the emission and the distances are difficult to determine. In nearby galaxies the sensitivity of present-day radio telescopes is insufficient at high spatial resolution. Here we propose a polarisation survey of nearby galaxies with SKA1 at high frequencies.

2. Magnetic fields in the ISM of galaxies

Coupling between magnetic fields and gas

One of the most fundamental correlations in extragalactic astronomy is the one between the non-thermal radio continuum and the thermal infrared (IR) luminosities of galaxies (Bell 2003). It is almost linear, holds in all star-forming galaxies, is invariant for more than seven orders of magnitude in luminosity (Beswick et al. 2015) and does not evolve between redshifts of zero and about three (Murphy 2009). Hence, radio continuum emission may be regarded as an excellent tracer of star formation at all epochs, but the role of magnetic fields still needs to be understood.

In an optically thick ("calorimeter") model, the linearity of the global correlation is attributed to young massive stars, as the common source of IR and radio emission. In an "equipartition" model (Niklas & Beck 1997), a tight but slightly nonlinear correlation is obtained for a coupling between magnetic fields and total gas density. Assuming that the radio–IR correlation is due to the amplification of turbulent magnetic fields in star-forming regions, Schleicher & Beck (2013) modelled the evolution of the radio–IR correlation with redshift. Since the global correlation holds for starburst galaxies as well as for low-surface-brightness galaxies, Bell (2003) and Lacki et al. (2010) suggested that the correlation is due to a conspiracy of several factors.

Remarkably, the radio–IR correlation also holds locally within galaxies, which can be explained by the magnetic field–gas coupling (Tabatabaei et al. 2013a). To date, observations in a few nearby galaxies show that (1) the exponent of the local correlation is significantly smaller than that of the global correlation, probably due to CRE diffusion (Berkhuijsen et al. 2013), (2) the local correlation holds not only in star-forming regions but also in interarm regions and outskirts with low star formation rates per surface area (Tabatabaei et al. 2013a), (3) the slope of the local

PoS(AASKA14)094

correlation varies from region to region (Dumas et al. 2011, Basu et al. 2012), and (4) the local correlation breaks down below a certain scale that may be interpreted as the diffusion length of CREs (Tabatabaei et al. 2013b). High-resolution radio continuum observations in nearby galaxies are required to assess the models.

The ratio of IR/radio intensities is a measure of current turbulent field amplification in star forming regions (Tabatabaei et al. 2013b). It is not constant across a galaxy's disk but changes with both the surface density of the star formation rate and the magnetic field strength (Murphy et al. 2008, Heesen et al. 2014). Sensitive and high-resolution SKA observations of nearby galaxies will shed light on the amplification of turbulent magnetic fields in different environments.

The correlation between the non-thermal radio continuum and the molecular gas (traced via its CO line emission), observed with 60 pc resolution in the spiral galaxy M51 (Schinnerer et al. 2013), is tighter than the correlation between radio and IR emission, but even less well understood. Much of the molecular gas in the spiral arms of M51 is not directly associated with ongoing massive star formation, implying that star formation cannot be the sole cause for the radio–CO relation. Two scenarios are consistent with the M51 data: (1) increased synchrotron emission from secondary CREs produced in the interaction of the CRs with the dense molecular material (e.g. Murgia et al. 2005) or (2) enhanced radio emission due to a coupling between the gas density and total magnetic field strength (e.g. Niklas & Beck 1997), in connection with fast diffusion of CREs along the ordered magnetic fields of the spiral arms. The proposed SKA1 survey of nearby galaxies with improved resolution in conjunction with high-quality data on molecular gas disks from the Atacama Large Millimeter/Submillimeter Array (ALMA) can provide the necessary information to test which of the proposed origins for this correlation is indeed true. Such observations of the magnetic field properties can be combined with exquisite knowledge of the multiple phases of the molecular gas disk (probed via different molecular lines). Understanding the relation between magnetic fields and molecular gas is critical, as magnetic fields are expected to play a major role in the structure formation of the molecular ISM, and in particular the formation of giant molecular clouds that are the cradles of massive star formation (e.g. Federrath & Klessen 2013).

Magnetic fields and gas dynamics

Magneto-hydrodynamic (MHD) calculations in 2-D indicate that perturbations in the gravitational potential can excite slow and fast MHD density waves in thin galactic disks (Lou & Fan 1998) that may explain the spiral field patterns in galaxies like NGC6946 and M51. Fast MHD density waves are expected to be important for enhancing MHD winds emerging from spiral arms (Lou & Wu 2005). The role of slow MHD density waves is still unclear because they may become unstable in thick galaxy disks and develop into Parker loops. Gaseous spiral arms are smoother and better defined when strong magnetic fields are included because instabilities are suppressed (Dobbs & Price 2008). Global MHD modelling gives evidence that galaxy evolution is modified by magnetic fields (Pakmor & Springel 2013). With the advent of SKA1, the interaction between density perturbations and magnetic fields can be investigated in detail with help of the kinematic data of neutral and ionised gas.

In galaxies with massive bars the magnetic field is aligned with the gas flow and is strong enough to affect the flow. As the gas rotates faster than the bar pattern of a galaxy, a shock occurs in the cold gas and the total magnetic field, which is observable as a ridge of strong radio continuum

PoS(AASKA14)094

emission (Fig. 1 left). The warm diffuse gas has a larger sound speed and hence is only slightly compressed. The ordered magnetic field is coupled to the diffuse gas. The polarisation pattern in barred galaxies and around central bars of spiral galaxies (Fig. 2) can be used as a tracer of shearing gas flows in the plane of the sky and hence complements kinematic data of radial velocities, but no detailed comparison can be performed with the sensitivity of present-day telescopes.

The central regions of barred galaxies are often sites of ongoing intense star formation and strong magnetic fields that can affect gas flows, with NGC1097 as a prominent example (Fig. 1 left). The ordered field in the ring has a spiral pattern and extends towards the active nucleus. The orientation of the innermost spiral field agrees with that of the spiral dust filaments visible in optical images. Magnetic stress in the circumnuclear ring due to the strong total magnetic fields (50–100 μG) or fast MHD density waves can drive gas inflow at a rate of several solar masses per year, which is sufficient to fuel the activity of the nucleus (Lou et al. 2001, Beck et al. 2005). The infall rate is expected to be related to the field strength and structure, which can be tested with SKA1 in a sample of barred galaxies.

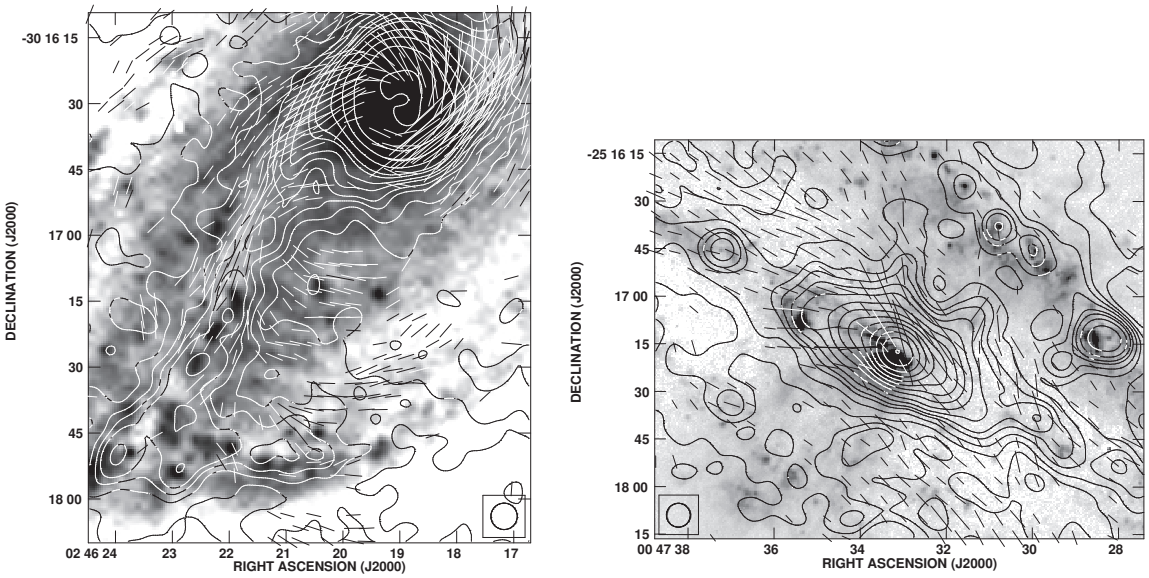

Figure 1: Examples for high-resolution polarisation observations. *Left:* Total intensity (contours) and *B*-vectors of the southern bar of NGC1097, observed at 4.86 GHz at 6″ resolution with the VLA (from Beck et al. (2005)), overlaid onto an optical image. *Right:* Total intensity (contours) and *B*-vectors of the central starburst region of NGC253, observed at 8.46 GHz at 7.5″ resolution with the VLA (from Heesen et al. (2011)), overlaid onto an Hα image.

Ordered fields and field reversals

Ordered fields, observed by polarised radio emission, are not spatially correlated with spiral arms seen in the optical and IR (see example in Fig. 2). They are modified by large-scale dynamical effects like galaxy rotation and density waves, as observed in M51 (Fletcher et al. 2011). Ordered fields can be strongest in shear or compression regions, caused by gas flows (as observed in barred galaxies, see Fig. 1 left), in regions with little star formation by enhanced mean-field dynamo action, or in regions with moderately strong outflows by allowing for more efficient mean-field dy-

PoS(AASKA14)094

namo action (see Sect. 4). Ordered fields are generally strongest in the regions *between* the optical spiral arms, in some cases forming *magnetic arms* with exceptionally high degrees of polarisation (up to 50%), e.g. in NGC6946 (Beck 2007), NGC2997 (Han et al. 1999), M83 (Beck & Wielebinski 2013) and IC342 (Krause 1993; Fig. 2). Proposed explanations are slow MHD density waves (Lou & Fan 1998), shear in a spiral gas flow (Otmianowska-Mazur et al. 2002) or suppression of large-scale dynamo action in the spiral arms (Moss et al. 2013, Chamandy et al. 2015).

Shearing and compressing gas flows make turbulent fields anisotropic, so that the field direction reverses on the correlation scale of turbulence (see below), while dynamo action generates uni-directional regular fields. As polarisation "vectors" are ambiguous by 180°, Faraday rotation measures (RMs) are the only way to distinguish these two types of ordered fields.

Large-scale field reversals at certain distances from the center of a galaxy, like that observed in the Milky Way (Van Eck et al. 2011, Han et al. 2015), have not been detected in external galaxies so far, in spite of many RM data with sufficiently high resolution. A satisfying explanation is still lacking. The reversals may be due to propagating dynamo waves (Ferrière & Schmitt 2000), relics from the early epoch where the field pattern was chaotic (see Sect. 4) or field distortions triggered by a major merger (Moss et al. 2014). The search for reversals in external galaxies, and to measure their number and scale, needs RM data with high spatial resolution of less than 100 pc.

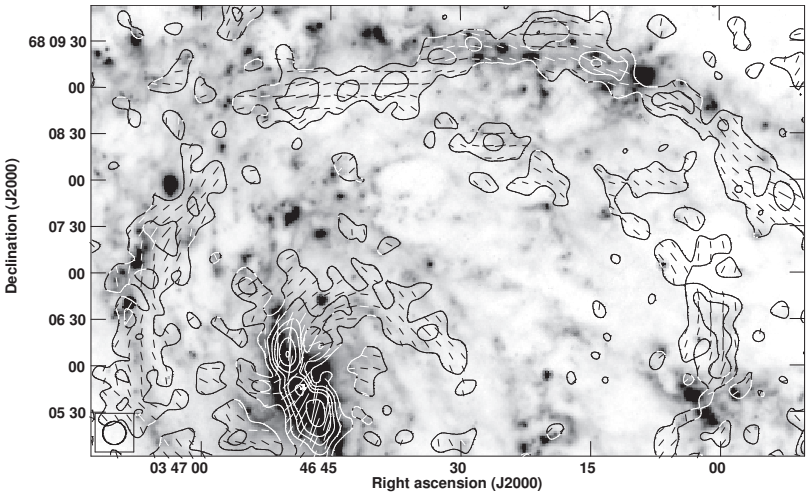

Figure 2: Polarised intensity (contours) and *B*-vectors of IC342, observed at 4.86 GHz at 15″ resolution with the VLA (from Beck (2015)), overlaid onto an 8μm IR image from the SPITZER telescope. Ordered fields can be traced around the central bar, along the inner edges of the eastern and northern spiral arms, and in the interarm region in the northwest.

Properties of turbulent magnetic fields

Turbulent magnetic fields have their origin in the turbulent state of the ISM. The power law of turbulence of the ionised gas in the Milky Way is of Kolmogorov type and spans to a largest scale of at least a few pc (Chepurnov & Lazarian 2010). To understand the origin and role of turbulent fields, they should be described using measures derived from the theory of turbulence. Such fundamental properties are currently unconstrained by observations, apart from a few estimates.

PoS(AASKA14)094

Structure functions of RMs in the Milky Way indicate that the correlation scale (the largest scale of the power law of turbulence) is about 20 pc in spiral arms and about 100 pc in interarm regions (Haverkorn et al. 2006). Faraday depolarisation in nearby galaxies can be explained by a turbulent medium with a correlation scale of about 50 pc (Beck 2007, Fletcher et al. 2011), but the spatial resolution of present-day observations is insufficient to probe such scales directly.

The method for deriving correlation scales from the scatter in the observed polarisation angles at high radio frequencies (where Faraday rotation angles are small) enables measurement of the degree of anisotropy in magnetic field fluctuations (Houde et al. 2013). The application of this technique is currently limited to a few bright patches of polarisation seen at the highest possible resolution in M51, where the correlation lengths parallel and perpendicular to the local ordered field are about 100 pc and 50 pc, which may lead to anisotropic propagation of CREs (see below).

Polarisation observations with SKA with high spatial resolution (i.e. 1–100 pc) and at high frequencies (to avoid Faraday depolarisation) will allow the measurement and mapping of standard quantities, such as the correlation scale and degree of anisotropy and the power spectrum of the turbulent field. It will then be possible to address the origin and role of the turbulent field, for example, in the accumulation of gas clouds from the diffuse ISM, and to determine the sonic type of turbulence from polarisation gradients (Burkhart et al. 2012).

Helical fields

Magnetic helicity is a promising concept in the description of astrophysical magnetic fields. A significant fraction of magnetic fields in the ISM may be helical, but firm observational evidence is still lacking. The reversing RM sign across the outflow cone of NGC253 indicates a large-scale helical field (Heesen et al. 2011). Polarised emission and RMs in the northern radio arm of the galaxy IC342 reveal a helically twisted field (Fig. 2). Simulations of galactic dynamos (see Sect. 4) predict the formation of bi-helical magnetic fields of opposite helicity on large and small scales (Brandenburg 2015). Such fields leave an observational signature in the spectral energy distribution of the polarised signal. A suitable sign of helicity can compensate Faraday depolarisation.

High-resolution polarimetric observations with SKA1 will be very useful to probe the topology of galactic magnetic fields and place constraints on their helicity (Horellou & Fletcher 2014). According to dynamo theory (Sect. 4), the toroidal field should have the same direction above and below the midplane, while the magnetic helicities would change sign about the equatorial plane. For edge-on galaxies, enhanced polarisation can be expected in two opposite quadrants (Brandenburg & Stepanov 2014). Large-scale helical fields in galaxies may also be revealed by investigating the correlation between polarisation angles and RMs (Oppermann et al. 2011).

Magnetic effects on the propagation of cosmic-ray electrons

The degree of order of the magnetic field plays an important role in the propagation of CREs, both in models of the streaming instability (Kulsrud 2005) and in diffusion models (Chuvilgin & Ptuskin 1993). A higher field ordering helps CREs to propagate over larger distances along the field, resulting in a larger propagation length. This is in agreement with the observations in a sample of nearby galaxies, where the smallest scale of the synchrotron–IR cross-correlation increases with field order (Tabatabaei et al. 2013b). With future high-resolution SKA1 data, cross-correlation for different regions of a galaxy will allow us to measure the CRE propagation length as a function of

PoS(AASKA14)094

environmental conditions, in particular of the magnetic fields.

Irregular and dwarf galaxies

The Large and the Small Magellanic Clouds are the closest irregular galaxies at distances of 50 kpc and 60 kpc, respectively, interacting with the Milky Way and each other. A study based on RM grids and thus on line-of-sight magnetic field components suggests that both galaxies host large-scale coherent fields, indicating that a large-scale dynamo also works under the less favourable conditions of slow ordered rotation (Mao et al. 2008). High spatial resolution (about 1 pc!), high-frequency SKA1 observations as proposed here can overcome beam and Faraday depolarisation, allowing one to detect diffuse polarised emission from the main body of the Magellanic Clouds. We can test with unprecedented resolution how well the polarised filaments and their ordered field align with various tidal features in the Magellanic system (the so called Pan-Magellanic magnetic field hypothesis). The proposed observations of the Magellanic Clouds will also allow us to construct the structure function of the complex polarised emission (Sun et al. 2014) to understand the turbulence cascade and dissipation.

With their low rotational speed dwarf galaxies are even less favourable places for the amplification of magnetic fields. Still, several low-mass galaxies (besides the Magellanic Clouds) show a significant large-scale ordered field in some regions, like e.g. IC10 (Chyży et al. 2003). Models of a CR-driven dynamo (Siejkowski et al. 2014) and MHD simulations (Dubois & Teyssier 2010) imply that dwarf galaxies can amplify fields and transport them away in galactic outflows and winds. Still, many details are unexplored, like the effects of magnetic fields early in the formation of the galactic outflow and their role in collimating the outflowing gas.

Due to their low potential well, low-mass galaxies are prone to outflows and galactic winds driven by star formation. The magnetised nature of these large-scale outflows (Chyży et al. 2000, Kepley et al. 2010) is especially noteworthy, since dwarf irregular galaxies are the best local proxies for high-redshift galaxies and even proto-galaxies and a prime candidate for the source of the magnetisation of the intergalactic medium (Bertone et al. 2006). An important observation is that all dwarf galaxies with detected ordered magnetic fields are star-bursting and/or subject to gravitational interaction or gas infall. This may be an observational selection effect but may also hint at the importance of enhanced turbulence in these galaxies.

SKA1 observations of a sample of local dwarf galaxies exploring the effects of burst age, burst strength, mass and interaction properties will shed light on the mechanisms governing the amplification and dispersion of magnetic fields in such galaxies. These observations will also provide critical data for the effects of magnetic fields during galaxy formation and early evolution.

Early-type and elliptical galaxies

Spiral galaxies of type Sa and S0 as well as elliptical galaxies without an active nucleus have very little star formation and hence hardly produce CREs that could emit synchrotron emission. Large-scale regular magnetic fields may exist in differentially rotating early-type galaxies without star formation, because turbulence in the ISM can also be generated by the magneto-rotational instability (MRI). Elliptical galaxies may host turbulent fields generated by the small-scale dynamo. Detection with SKA1 via RM grids needs a sufficiently large number of background sources and hence deep observations of galaxies with large angular sizes.

PoS(AASKA14)094

3. Magnetic fields in galaxy halos

Outflows

Galaxies are not isolated entities, but they can exhibit both accretion and outflow of the gas that fuels star formation. Galactic wind or outflow models can reproduce the available multi-frequency observations only if CRs and magnetic fields help to activate the wind at their base in galactic bulges (Everett et al. 2008). Although CRs were neglected in most earlier galactic wind models, their energy density is in fact comparable to the respective values of energy densities for thermal gas, magnetic fields and turbulent motions. This energy is concentrated in protons and heavy nuclei, while CREs contribute only $\sim 1\%$. Compared with thermal gas, CR protons do not cool efficiently while CREs cool dominantly through inverse Compton scattering (ICS) and synchrotron emission. The combined pressure gradients of gas, CRs and MHD waves are able to drive a galactic wind even in cases of moderate star formation, like in our own Galaxy (Breitschwerdt et al. 1991). A necessary condition is that there is a dynamical coupling between the plasma and the CRs.

If the population of CREs consists of secondary particles of hadronic origin, the γ–ray emission from galaxy winds or outflows is dominated by hadronic emission mechanisms with a typical pion bump originating from $\pi^0 \rightarrow \gamma\gamma$ decay that dominates the GeV energy range, while secondary electrons produce GeV–TeV ICS emission and relativistic bremsstrahlung. In a leptonic-origin model for CREs, ICS emission from primary CREs dominates in the GeV–TeV range.

Therefore, the radio emission must retain the imprints of either hadronic (secondary CREs) or leptonic (primary CREs) produced synchrotron emission with specific spectral shapes and radio polarisation features. The correlation between radio (continuum and polarisation) and γ–ray (GeV–TeV) emission could provide valuable information on the CR origin and propagation and on the magnetic field that confines these particles in the galaxy winds and halos produced by outflows (see Sect. 5). In addition, polarisation from primary CREs is expected to be higher, because secondary CREs are produced in a more isotropic environment.

The distribution of the multi-temperature plasma and of the non-thermal (relativistic) plasma in the winds provides a sea of particles available to produce ICS of the CMB photons pervading all of the Universe and therefore an associated Sunyaev-Zeldovich effect (SZE) with specific spatial and spectral characteristics that are related to the complex plasma distribution in the winds (Colafrancesco et al. 2003). The combination of radio synchrotron emission from CREs (detected with SKA) and the SZE in the same wind/outflow region as produced by the same CREs that up-scatter the CMB photons (detectable with mm and submm telescopes) can be used to obtain a direct estimate of the overall magnetic field energy density $U_{\rm B}$ in the wind or outflow region by measuring the ratio of integrated flux densities $F_{\rm sync}/F_{\rm ICS} \propto U_{\rm B}/U_{\rm CMB}$. While edge-on galaxies are optimal targets (e.g. NGC253), galaxies with disks seen at intermediate inclination angles are also suitable.

Outflow velocities

CRs (the most pervasive of the ISM components) can easily leave the disk either by diffusion and streaming along magnetic field lines or by convective transport in a galactic outflow or wind. Indeed, many edge-on galaxies do clearly exhibit signatures of extra-planar emission and hence the presence of radio halos surrounding them (Krause 2014). Gravitational interaction with a companion galaxy may affect the outflow (Mora & Krause 2013).

PoS(AASKA14)094

Vertical profiles of the radio continuum emission can be well described by a two-component exponential distribution (e.g. Dumke & Krause 1998, Mora & Krause 2013), where the two scale heights describe the thin and the thick disks; the latter can be attributed to the radio halo. As the energy densities of the magnetic field and the stellar background radiation are higher in the inner parts of a galaxy, the CRE lifetimes and hence the scale heights should have a minimum at small galacto-centric radii. This is indeed observed in a few galaxies (Krause 2014). The most striking example is NGC 253, which displays a dumbbell-shaped halo. The linear dependence between scale height and CRE lifetime in its northeastern halo is a signature of a wind with a cosmic-ray bulk speed of 300 ± 30 km s^{-1} (Heesen et al. 2009a), which is similar to the escape velocity in this galaxy. Measuring the velocity of outflows and its variation with height above the plane from the vertical profiles of radio emission needs high-resolution data of a sample of edge-on galaxies.

On a spatial scale of a few tens of parsec, accessible to SKA1, we expect that the disk–halo interface will be resolved into many individual features, among them non-thermal super-bubbles, which are crucial to drive a galactic outflow by supernova feed-back.

X-shaped fields

The large-scale magnetic field in nearby spiral galaxies is not only confined to the galactic disk. Polarisation observations of spiral galaxies seen edge-on show a projected plane-parallel magnetic field in the disk and an X-shaped field structure of similar field strength in the halo (Heesen et al. 2009b, Soida et al. 2011, Krause 2014). According to mean-field $\alpha - \Omega$ dynamo models (see Sect. 4), the regular disk field is accompanied by a poloidal magnetic field component reaching into the halo, which, however, is far too weak to explain the observed X-shaped field. Some similarity to the observed field patterns is achieved if the effects of a galactic wind are included (Gressel et al. 2008, Hanasz et al. 2009). The X-shaped field may also be a superposition of plane-parallel and vertical fields composed of field loops stretched by outflows. Frequent field reversals between adjacent field loops may lead to turbulent reconnection and heating of the halo gas.

Faraday RMs are the adequate tool to test observationally whether the halo field is regular (large $|RM|$) or composed of loops (small $|RM|$), but reliable measurements in galaxy halos are still missing. Making use of the high resolution and sensitivity of SKA1 will settle this issue.

4. Tests of magnetic field models with SKA1 observations

Mean-field dynamo models of galactic magnetic fields

The best developed paradigm to amplify and sustain magnetic fields in the ISM of galaxies is the dynamo (Beck et al. 1996, Brandenburg 2015). A turbulent (small-scale) dynamo in proto-galaxies can amplify weak seed fields to several μG strength (corresponding to the energy level of turbulence) within less than 10^8 yr (Schleicher et al. 2010, Beck et al. 2012). After formation of a gas disk, the small-scale dynamo can continuously supply turbulent fields to the ISM (Moss et al. 2012). To explain the generation of large-scale fields in galaxies, the theory of mean-field $\alpha - \Omega$ dynamo has been developed. It is based on differential rotation (Ω–effect) and helical turbulence (α–effect), presumably driven by supernova explosions (Ferrière & Schmitt 2000, Gent et al. 2013), and predicts that within a few 10^9 yr turbulent fields of a few μG strength are organised into large-scale patterns of regular fields (Arshakian et al. 2009). Field reversals from the early

PoS(AASKA14)094

epochs can survive until today (Shukurov 2005, Moss et al. 2012) and may explain the large-scale field reversal(s) detected in the Milky Way (Van Eck et al. 2011).

The mean-field $\alpha - \Omega$ dynamo generates large-scale magnetic helicity with a non-zero mean in each hemisphere. As the total magnetic helicity is a conserved quantity, the dynamo is quenched by the small-scale fields with opposite helicity unless these are removed from the system (Shukurov et al. 2006). Galactic outflows (see Sect. 3) are essential for efficient $\alpha - \Omega$ dynamo action.

Mean-field $\alpha - \Omega$ dynamo models predict a regular field with a simple axisymmetric pattern, whereas regular fields in real galaxies have complicated patterns that may be described by several Fourier modes (Fletcher 2011). High-resolution observations with SKA1 will allow us to measure the power spectrum (or structure function) of regular fields, from the turbulence scale up to the largest scale the dynamo was able to generate within the galaxy's lifetime. Signature of a fully developed regular field is a peak in the power spectrum at the scale of the whole galaxy (Moss et al. 2012, Gent et al. 2013). Field reversals, density waves, bars and mergers leave specific imprints in the power spectrum.

Connection between magnetic fields, galaxy properties and dynamo action

Mean-field dynamo models depend on observable properties of galaxies. The rotation curve determines the strength of the shear that generates an azimuthal field from the radial field, while the star formation rate governs the frequency of supernova explosions driving the α–effect by which a radial field is generated from the azimuthal field. Gas density and turbulent velocity determine the energy density of turbulence which provides an upper limit on the energy density of the magnetic field. The timescale for large-scale field ordering can be longer than the galaxy age (Arshakian et al. 2009). The stage of development of a field pattern also carries information about the history of a galaxy, e.g. the time and strength of the last major merger (Moss et al. 2014).

Determining the relationships between these well-defined galactic properties and the strength and structure of dynamo-generated magnetic fields will provide a significant step forward in both our understanding of cosmic magnetism and the application of this knowledge to problems in wider astrophysics and cosmology. For example, knowing how turbulent and regular field strengths scale with star formation rate and gas density will immediately allow the inclusion of magnetic fields in analytic and semi-analytic models of galaxy evolution.

Identifying the precise form of the connection between magnetic and other galactic properties is not straightforward because the parameters can combine to produce non-trivial scalings. This difficulty will fortuitously provide another significant result though. Different physical mechanisms have been proposed to provide the non-linearity which is required to saturate the field growth, or allow it to reach a quasi steady state. Examples of the saturation mechanisms are: the back-reaction of the Lorentz force on the turbulent motions when it becomes comparable to the driving forces of turbulence; outflows of hot gas carrying small-scale magnetic fields out of the disk in order to preserve the balance of magnetic helicity. These non-linear saturation mechanisms depend differently on galactic parameters such as star formation rate and gas density (Van Eck et al. 2014). Thus, determining the fundamental scaling relations between the observed magnetic fields and the other galactic parameters will also allow us to identify the saturation mechanism for the dynamo.

Understanding the non-linear behaviour of galactic dynamos will be of major importance for the wider field of cosmic magnetism, because virtually all astronomical objects are magnetised by

PoS(AASKA14)094

dynamo action. Galaxies are special though: They are the only objects where the dynamo-active region is transparent and can be directly observed.

The main problem in carrying out this work now is the lack of suitable magnetic field observations for a reasonable number of galaxies. What is required is a set of data obtained with the same instrument, with the same spatial resolution in each galaxy, the same sensitivity and analysed using the same methods to obtain a reliable catalogue of comparable magnetic field strengths, rotational and vertical field symmetries, and pitch angles.

Origin of small-scale magnetic fields in galaxies

Aside from the regular component, galactic magnetic fields have a small-scale, fluctuating component. The turbulent mirror-asymmetric motions perform twisting and folding of magnetic loops stretched by differential rotation. The same turbulent motions tangle the regular magnetic fields and produce small-scale magnetic fields from the large-scale ones.

Dynamo theory suggests another process: the turbulent dynamo, where stretching, twisting and folding of magnetic loops are produced by random motions. Hence, the total magnetic field $B_{\rm tot}$ can be presented as a sum of the regular field $B_{\rm reg}$, the component $B_{\rm tan}$ produced by tangling of $B_{\rm reg}$ and a component $B_{\rm tur}$ generated by the turbulent dynamo. An equipartition argument suggests that $B_{\rm tan}$ and $B_{\rm tur}$ should be comparable. Sunspot statistics demonstrated that $B_{\rm tur}$ is negligible with respect to $B_{\rm tan}$ on the solar surface (Stenflo 2012).

This issue is of fundamental importance for cosmic MHD: Without a turbulent dynamo the seed field in proto-galaxies would be much weaker and the generation of large-scale fields would take much longer. Hence, it is important to search for turbulent fields in galaxies, where the regime of dynamo action is fully accessible. The magnetic field component $B_{\rm tur}$ can be separated from $B_{\rm tan}$ by high-resolution observations with SKA1. Firstly, the field $B_{\rm tan}$ can be generated only in regions where $B_{\rm reg}$ exists. If somewhere $B_{\rm reg}$ vanishes, $B_{\rm tan}$ decays rapidly and is expected to be small. Observational tests require a resolution of the order of the turbulent scale, 10–100 pc, in order to resolve the vicinity of the point at which $B_{\rm reg}$ vanishes. Secondly, the spatial spectrum of $B_{\rm tan}$ is expected to extend from the scale of the regular magnetic field, at several kpc, down to smaller scales. The spectral slope may also be modified, but no model predictions are available. In contrast, the spectrum of $B_{\rm tur}$ extends from the largest scale of interstellar turbulence, at about 100 pc, down to about 10 pc and possibly lower. If both components contribute to the resulting spectrum of small-scale magnetic fields, a spectral distinction is possible by high-resolution observations.

5. Synergy with observations in other spectral ranges

Dust

The infrared space observatories SPITZER and HERSCHEL have mapped the emission of the dust continuum and also provided exquisite maps of the major ISM cooling lines for several tens of nearby galaxies (e.g. Kennicutt et al. 2011). In addition, the advent of new bolometer cameras for existing millimeter single dishes such as APEX and JCMT, as well as planned ones such as CCAT (or LMT), will allow for high angular resolution imaging of the cold dust component at wavelengths long-ward of about 200 μm with the possibility of polarisation measurements.

PoS(AASKA14)094

Molecular gas

Millimeter and submm observatories (JCMT, APEX, ALMA, PLANCK) have the capacity to map both the flat-spectrum, high-frequency radio emitting regions and the extended halos around normal and starburst galaxies. Future observatories with improved angular resolution and sensitivity (e.g., the ground-based SPT, ACT telescopes and especially the large Millimetron space mission with a sensitivity matching that of SKA1) can provide a great deal of synergy with the SKA1 and SKA2 studies of nearby and moderately distant galaxies.

ALMA is going to revolutionise our understanding of the molecular ISM in local galaxies via high angular resolution observations of the multiple phases present in the molecular gas and the gas kinematics. During its early science phase ALMA has already begun to map the distribution and kinematics of the bulk of the molecular gas in the central regions of a few nearby galaxies. With the full array operational it will be possible to extend such studies not only to more targets probing a wide range in galactic disk properties (quiescent – star forming; flocculent – barred/spiral arms; gas-rich – gas-poor) but also to probe the denser molecular gas that is more closely linked to the actual formation of stars. In addition, polarisation measurements of continuum emission arising from dust and of line emission will become possible (Paladino et al. 2015).

Neutral gas

SKA1 observations of the neutral ISM in nearby galaxies (de Blok et al. 2015) will provide exquisite probes of the properties of cold gas on both small and large scales. In addition to the morphology of the neutral ISM, HI observations also provide highly detailed information about the kinematics. HI line widths can be used to probe small-scale gas motions and draw connections to the turbulent magnetic field structure. Neutral hydrogen can also be traced out to tremendous distances from sites of star formation, yielding large-scale kinematic information including rotation, shear and radial motions. These will provide crucial insight into the influence of dynamics on the local orientation and degree of ordering of the magnetic field in arms, interarm regions and bars, and on dynamo action. HI is also a highly useful probe of the connection between galaxies and their environment, including tidal interactions, mergers and gas inflow and outflow. The excellent column density sensitivity afforded by SKA1 will illuminate the connection between large-scale magnetic field properties and gas conditions, local dynamics and environmental effects.

Ionised gas

The origin of the warm (or diffuse) component of the ISM in spiral galaxies can be traced back to star formation regions, even though substantial parts of this gas are found at large distances from star forming sites. This can be explained by the porosity of the ISM and by large-scale flows caused by the energy input from young stellar populations. Both these explanations depend on the contribution from magnetic fields and CRs to the total pressure of the ISM, since these constituents may contribute about 2/3 of the energy density. To explain the observed temperature structure of the ionised gas, an additional, so far unidentified, heating source is required.

CRs coupled to the ionised gas via magnetic fields could cause this additional heating (Wiener et al. 2013). The new high-sensitivity tunable filter instruments and wide-field integral-field spectrographs (e.g. MUSE) at 4–8 m-sized telescopes will provide more sensitive observations of diagnostic lines and the kinematics for the halo faint gas. These optical/NIR data sets together with

PoS(AASKA14)094

SKA observations at high angular resolution will address the open questions.

X-rays and γ-rays

The relativistic electrons that produce radio synchrotron emission also produce X-ray/gamma-ray emission through bremsstrahlung and ICS. In principle, if the high-energy emission could be used to determine the relativistic-electron density, then the magnetic field strength could be directly inferred from the radio synchrotron data, without having to appeal to the equipartition assumption. In practice, though, X-ray/gamma-ray telescopes lack the required resolution and sensitivity and the high-energy X-ray emission from relativistic electrons is hard to separate from other emission components (π^0 decay, thermal emission and point sources). Halos of edge-on galaxies are preferable targets because their X-ray emission is mostly thermal. On the other hand, it should be possible to infer the un-normalized relativistic-electron spectrum from the measured radio spectral index and use it as a constraint to interpret the high-energy data. This synergy between both spectral ranges would work best outside the 100 MeV–30 GeV range, which is largely dominated by π^0 decay.

On the low-energy side, the most promising telescope could be the Nuclear Spectroscopic Telescope Array (NuSTAR), which was launched in June of 2012, covers the energy band 3–79 keV and has an angular resolution of $18''$. In this energy band, inverse Compton dominates the diffuse interstellar emission from spiral galaxies, but thermal emission is probably dominant both in elliptical galaxies, where the gas temperature is higher ($\approx 10^7$ K) while the density of relativistic electrons is generally very low, and in galaxy clusters, where the gas temperature can be even higher ($\approx 10^8$ K). The main difficulty with the NuSTAR energy range is contamination by point sources – a difficulty which could possibly be alleviated in galaxies with high star formation rates. In this perspective, the starburst galaxy NGC253 will be one of our primary targets.

On the high-energy side, the most appropriate telescope would certainly be the Cherenkov Telescope Array (CTA), which is expected to become operational around 2020. It covers the energy band from a few 10 GeV to about 100 TeV and has an angular resolution $\gtrsim 1'$. A big advantage of the CTA energy range is that the measured emission is most likely dominated by ICS, with little contamination from point sources up to at least 1 TeV. Note, however, that the background photons that can be up-scattered to TeV or sub-TeV energies with GeV electrons (those responsible for the radio synchrotron emission measured by SKA) need to be higher-energy photons.

The recent upgrade of the High Energy Stereoscopic System (HESS) telescope and its enhanced sensitivity to lower energies will provide a useful exploration of a few nearby galaxies in the sub-TeV range that can create interesting synergies with the SKA precursors.

6. Project description

Sample selection

With SKA1, we wish to observe a large-enough sample of star-forming galaxies that are sufficiently nearby to achieve a high spatial resolution. A distance limit of 20 Mpc and declinations of $\leq 15^\circ$ define our preliminary sample:

– Spiral galaxies (moderately inclined): M33[1], NGC300, 628, 1566, 1808, 2997, Circinus

[1] High declination but included due to its proximity.

PoS(AASKA14)094

– Edge-on galaxies: M104, NGC55, 253, 3628, 4666, 4945
– Barred galaxies: M83, NGC1097, 1313, 1365, 1502, 1672, 2442
– Irregular galaxies: LMC, SMC
– Dwarf galaxies: NGC1140, 1705, 5253, IC4662
– Non-active elliptical galaxies: NGC1404, 4697.

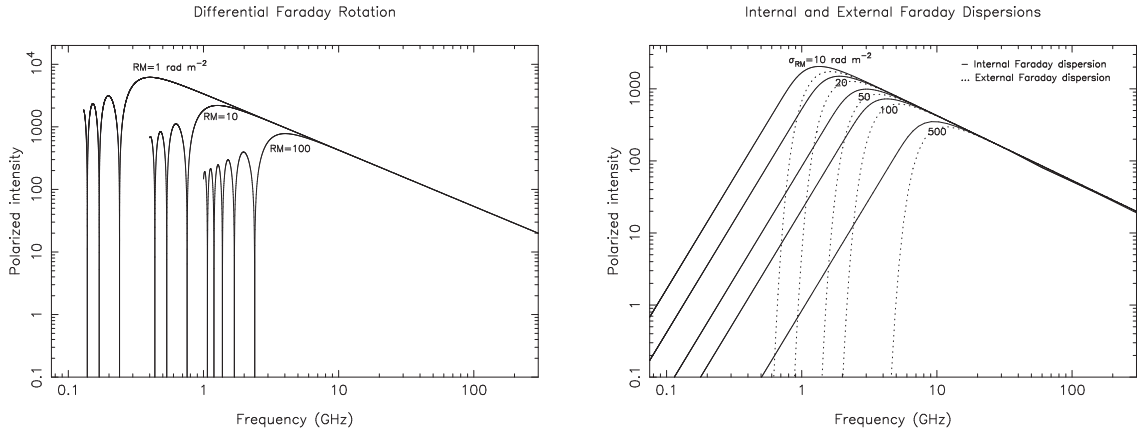

Figure 3: Spectra of polarized intensity (in arbitrary units) for a synchrotron source with spectral index $\alpha = -0.9$ (visible as a straight line at high frequencies), affected by different depolarisation effects. *Left:* depolarisation by differential Faraday rotation at different levels of Faraday rotation measure $|RM|$; *right:* depolarisation by internal (solid line) and external (dashed line) Faraday dispersion at different levels of RM dispersion $\sigma_{\rm RM}$. The distributions of CREs, thermal electrons, regular magnetic field and turbulent magnetic field are assumed to be symmetric. The regular magnetic field is assumed to have a constant direction throughout the source (from Arshakian & Beck 2011).

Frequency selection

We are aiming at:
– Highest angular resolution achievable with sufficiently large signal-to-noise ratios, to detect small-scale field structures and field reversals,
– maximum polarised intensity, which requires a low level of Faraday depolarisation and hence high frequencies,
– high-precision measurements of intrinsic polarisation angles with help of RM Synthesis, which requires a moderate Faraday rotation angle and hence high frequencies (because the error in intrinsic angle increases with the Faraday rotation angle).

SKA1-MID Band 4 (2.8–5.18 GHz) fulfils our requirements: $|RM| = 50 - 200\,\mathrm{rad/m^2}$ and RM dispersions of $\sigma_{\rm RM} = 30 - 200\,\mathrm{rad/m^2}$ are expected in the disks, spiral arms and inner halos of galaxies (Arshakian & Beck 2011). The maximum polarised intensity is expected in the range 3–7 GHz (Fig. 3) and a maximum rotation angle of about $\pm 60^\circ$ at 4 GHz. We will be able to measure regions with mixed emission and Faraday rotation with $|RM| \leq 500\,\mathrm{rad/m^2}$ (corresponding to extended structures in Faraday spectra of up to about $1000\,\mathrm{rad/m^2}$ width), allowing us to detect emission regions with strong regular magnetic fields and high electron density and to determine the intrinsic polarisation angles.

SKA1-MID Band 3 (1.65–3.05 GHz) is less suited because the emission from galaxies with

PoS(AASKA14)094

strong magnetic fields is affected by Faraday depolarisation. SKA1-MID Band 5 (4.6–13.8 GHz) is best suited to detect maximum polarisation in regions with strong magnetic fields, like the central regions and star-forming complexes of galaxies, but less suited for the general ISM and halos where the synchrotron emission is fainter.

Angular resolution
With about $5''$ resolution we can resolve spatial scales of about 1 pc in the LMC/SMC, 20 pc in M33, 100 pc in M83, NGC55 and NGC253, sufficient to reach our goals, and a few 100 pc in the more distant galaxies of our sample, which is still sufficient to reach most of our goals.

Sensitivity
With the planned System Equivalent Flux Density (SEFD) of 2.3 Jy and the bandwidth of 2.38 GHz of SKA1-MID Band 4 (Dewdney et al. 2013), we expect an rms noise of 0.2 μJy/beam within a 12 h integration time. This is sufficient to detect emission from a magnetic field of about 9 μG with $5''$ resolution, assuming an extent along the line of sight of 100 pc, a synchrotron spectral index of -0.8 and energy equipartition between the energy densities of magnetic fields and CRs, or 16 μG with 10 pc extent. As we aim to measure extended emission with highest sensitivity, excellent *uv* coverage within $\leq$5 km baselines is requested.

Science with a 50% early-phase SKA1
With 50% sensitivity for SKA1-MID baselines of $\leq$5 km, an early science programme on the nearest galaxies (LMC, SMC, M33, M83, NGC55, NGC253) is of high scientific value, observing with a somewhat larger beam ($7'' - 10''$).

Perspectives for SKA2
The $\simeq$10x increased sensitivity of SKA2-MID compared to SKA1-MID will allow us to increase the angular resolution by a factor of about three or to increase the sample of galaxies to about three times larger distances. We will also consider to increase our frequency coverage towards higher frequencies, to get better access to galactic regions with strong magnetic fields. The decision will be based on the results from SKA1.

Synergies with other SKA1 projects
The resolution in Faraday space (given by the half-power width of the RM Spread Function) for SKA1-MID Band 4 is about 400 rad/m^2, so that only the average Faraday depth can be measured and multiple components cannot be resolved. 3-D Faraday tomography should be done at lower frequencies (Heald et al. 2015) and perfectly complements this project. SKA1 observations of HI emission in nearby galaxies (de Blok et al. 2015) and in particular in the Magellanic Clouds (McClure-Griffith et al. 2015) will provide data on the properties and dynamics of neutral gas. The Milky Way's magnetic field will be studied with help of the RM grid and Faraday tomography (Haverkorn et al. 2015). The Zeeman effect will allow us to measure magnetic field strengths in star-forming regions of nearby external galaxies (Robishaw et al. 2015). We will get access to evolving magnetic fields in distant galaxies by deep-field observations (Taylor et al. 2015) and by RMs against background sources (Gaensler et al. 2015).

PoS(AASKA14)094

REFERENCES

Arshakian, T.G., Beck, R., Krause, M., & Sokoloff, D. 2009, A&A, 494, 21
Arshakian, T.G., & Beck, R. 2011, MNRAS, 418, 2336
Basu, A., Roy, S., & Mitra, D. 2012, ApJ, 756:141
Beck, A.M., Lesch, H., Dolag, K., et al. 2012, MNRAS, 422, 2152
Beck, R., Brandenburg, A., Moss, D., Shukurov, A., & Sokoloff, D. 1996, ARAA, 34, 155
Beck, R., Fletcher, A., Shukurov, A., et al. 2005, A&A, 444, 739
Beck, R. 2007, A&A, 470, 539
Beck, R., & Wielebinski, R. 2013, in *Planets, Stars and Stellar Systems*, Vol. 5, eds. T.D. Oswalt & G. Gilmore, Springer, Dordrecht, 641
Beck, R. 2015, A&A, submitted
Bell, E.F. 2003, ApJ, 586, 794
Berkhuijsen, E.M., Beck, R., & Tabatabaei, F.S. 2013, MNRAS, 435, 1598
Bertone, S., Vogt, C., & Enßlin, T. 2006, MNRAS, 370, 319
Beswick, R.J., Brinks, E., Pérez-Torres, M.A., et al. 2015, "SKA studies of nearby galaxies: star-formation, accretion processes and molecular gas across all environments" in proc. *Advancing Astrophysics with the Square Kilometre Array*, PoS(AASKA14)070
Brandenburg, A. 2015, in *Magnetic Fields in Diffuse Media*, eds. A. Lazarian et al., Springer, Berlin, 529
Brandenburg, A., & Stepanov, R. 2014, ApJ, 786, 91
Breitschwerdt, D., McKenzie, J.F., & Völk, H.J. 1991, A&A, 245, 79
Burkhart, B., Lazarian, A., & Gaensler, B.M. 2012, ApJ, 749:145
Chamandy, L., Shukurov, A., & Subramanian, K. 2015, MNRAS, 446, L6
Chepurnov, A., & Lazarian, A. 2010, ApJ, 710, 853
Chuvilgin, L.G., & Ptuskin, V.S. 1993, A&A, 279, 278
Chyży, K.T., Beck, R., Kohle, S., Klein, U., & Urbanik, M. 2000, A&A, 355, 128
Chyży, K.T., Knapik, J., Bomans, D.J., et al. 2003, A&A, 405, 513
Colafrancesco, S., Marchegiani, P., & Palladino, E. 2003, A&A, 397, 27
de Blok, E., Fraternali, F., Heald, G.H., et al. 2015, in *Advancing Astrophysics with the Square Kilometre Array*, PoS(AASKA14)129
Dewdney, P., Turner, W., Millenaar, R., et al. 2013, *SKA1 System Baseline Design*, Document number SKA-TEL-SKO-DD-001 Revision 1
Dobbs, C.L., & Price, D.J. 2008, MNRAS, 383, 497
Dubois, Y., & Teyssier, R. 2010, A&A, 523, A72
Dumas, G., Schinnerer, E., Tabatabaei, F.S., et al. 2011, AJ, 141:41
Dumke, M., & Krause, M. 1998, in *The Local Bubble and Beyond*, eds. D. Breitschwerdt et al., Springer, Berlin, 555
Everett, J.E., Zweibel, E.G., Benjamin, R.A., et al. 2008, ApJ, 674, 258
Federrath, C., & Klessen, R.S. 2013, ApJ, 763, 51
Ferrière, K., & Schmitt, D. 2000, A&A, 358, 125
Fletcher, A. 2011, in *The dynamic interstellar medium*, eds. R. Kothes et al., ASP Conf. Ser., 438, 197

PoS(AASKA14)094

Fletcher, A., Beck, R., Shukurov, A., Berkhuijsen, E.M., & Horellou, C. 2011, MNRAS, 412, 2396
Gaensler, B.M., Agudo, I., Akahori, T., et al. 2015, "Broadband Polarimetry with the Square Kilometre Array: A Unique Astrophysical Probe" in proc. *Advancing Astrophysics with the Square Kilometre Array*, PoS(AASKA14)103
Gent, F.A., Shukurov, A., Sarson, G.R., Fletcher, A., & Mantere, M.J. 2013, MNRAS, 430, L40
Gressel, O., Elstner, D., Ziegler, U., & Rüdiger, G. 2008, A&A, 486, L35
Han, J.L., Beck, R., Ehle, M., Haynes, R.F., & Wielebinski, R. 1999, A&A, 348, 405
Han, J.L., van Straten, W., Lazio, T.J.W., et al. 2015, "Three-dimensional Tomography of the Galactic and Extragalactic Magnetoionic Medium with the SKA" in proc. *Advancing Astrophysics with the Square Kilometre Array*, PoS(AASKA14)041
Hanasz, M., Wóltański, D., Kowalik, K. 2009, ApJ, 706, L155
Haverkorn, M., Gaensler, B.M., Brown, J.C., et al. 2006, ApJ, 637, L33
Haverkorn, M., Akahori, T., Carretti, E., et al. 2015, "Measuring magnetism in the Milky Way with the Square Kilometre Array" in proc. *Advancing Astrophysics with the Square Kilometre Array*, PoS(AASKA14)96
Heald, G., Beck, R., de Blok, E., et al. 2015, "Magnetic Field Tomography in Nearby Galaxies with the Square Kilometre Array" in proc. *Advancing Astrophysics with the Square Kilometre Array*, PoS(AASKA14)106
Heesen, V., Beck, R., Krause, M., & Dettmar, R.-J. 2009a, A&A, 494, 563
Heesen, V., Krause, M., Beck, R., & Dettmar, R.-J. 2009b, A&A, 506, 1123
Heesen, V., Beck, R., Krause, M., & Dettmar, R.-J. 2011, A&A, 535, A79
Heesen, V., Brinks, E., Leroy, A.K., et al. 2014, AJ, 147, 103
Horellou, C., & Fletcher, A. 2014, MNRAS, 441, 2049
Houde, M., Fletcher, A., Beck, R., et al. 2013, ApJ, 766:49
Kennicutt, R.C., Calzetti, D., Aniano, G., et al. 2011, PASP, 123, 1327
Kepley, A.A., Mühle, S., Everett, J., et al. 2010, ApJ, 712, 536
Krause, M. 1993, in: *The Cosmic Dynamo*, eds. F. Krause et al., Reidel, Dordrecht, 305
Krause, M. 2014, arXiv:1401.1317
Kulsrud, R.M. 2005, *Plasma Physics for Astrophysics*, Princeton University Press
Lacki, B.C., Thompson, T.A., & Quataert, E. 2010, ApJ, 717, 1
Lou, Y.-Q., & Fan, Z. 1998, ApJ, 493, 102
Lou, Y.-Q., Yuan, C., Fan, Z., & Leon, S. 2001, ApJ, 553, L35
Lou, Y.-Q., & Wu, Y. 2005, MNRAS, 364, 475
Mao, S.A., Gaensler, B.M., Stanimirović, S., et al. 2008, ApJ, 688, 1029
McClure-Griffith, N., Stanimirović, S., Murray, C.E., et al. 2015, "Galactic and Magellanic Evolution with the SKA" in proc. *Advancing Astrophysics with the Square Kilometre Array*, PoS(AASKA14)130
Mora, S.C., & Krause, M. 2013, A&A, 560, A42
Moss, D., Stepanov, R., Arshakian, T.G., et al. 2012, A&A, 537, A68
Moss, D., Beck, R., Sokoloff, D., et al. 2013, A&A, 556, A147
Moss, D., Sokoloff, D., Beck, R., & Krause, M. 2014, A&A, 566, A40
Murgia, M., Helfer, T.T., Ekers, R., et al. 2005, A&A, 437, 389
Murphy, E.J., Helou, G., Kenney, J.D.P., Armus, L., & Braun, R. 2008, ApJ, 678, 828

PoS(AASKA14)094

Murphy, E.J. 2009, ApJ, 706, 482
Niklas, S., & Beck, R. 1997, A&A, 320, 54
Oppermann, N., Junklewitz, H., Robbers, G., & Enßlin, T.A. 2011, A&A, 530, A89
Otmianowska-Mazur, K., Elstner, D., Soida, M., & Urbanik, M. 2002, A&A, 384, 48
Pakmor, R., & Springel, V. 2013, MNRAS, 432, 176
Paladino, R., Brand, J., Orrú, E., et al. 2015, "Synergies between SKA and ALMA: observations of Nearby Galaxies" in proc. *Advancing Astrophysics with the Square Kilometre Array*, PoS(AASKA14)156
Robishaw, T., Green, J.A., Surcis, G., et al. 2015, "Measuring Magnetic Fields Near and Far with the SKA via the Zeeman Effect" in proc. *Advancing Astrophysics with the Square Kilometre Array*, PoS(AASKA14)110
Schinnerer, E., Meidt, S.E., Pety, J., et al. 2013, ApJ, 779:42
Schleicher, D.R.G., Banerjee, R., Sur, S., et al. 2010, A&A, 522, A115
Schleicher, D.R.G., & Beck, R. 2013, A&A, 556, A142
Shukurov, A. 2005, in *Cosmic Magnetic Fields*, eds. R. Wielebinski & R. Beck, Springer, Berlin, 113
Shukurov, A., Sokoloff, D., Subramanian, K., & Brandenburg, A. 2006, A&A, 448, L33
Siejkowski, H., Otmianowska-Mazur, K., Soida, M., Bomans, D. J., & Hanasz, M. 2014, A&A, 562, A136
Soida, M., Krause, M., Dettmar, R.-J., & Urbanik, M. 2011, A&A, 531, A127
Stenflo, J.O. 2012, A&A, 547, A93
Sun, X.H., Gaensler, B.M., Carretti, E., et al. 2014, MNRAS, 437, 2936
Tabatabaei, F.S., Schinnerer, E., Murphy, E.J., et al. 2013a, A&A, 552, A19
Tabatabaei, F.S., Berkhuijsen, E.M., Frick, P., Beck, R., & Schinnerer, E. 2013b, A&A, 557, A129
Taylor, A.R., Agudo, I., Akahori, T., et al. 2015, "SKA Deep Polarization and Cosmic Magnetism" in proc. *Advancing Astrophysics with the Square Kilometre Array*, PoS(AASKA14)113
Van Eck, C.L., Brown, J.C., Stil, J.M., et al. 2011, ApJ, 728:97
Van Eck, C.L., et al. 2014, ApJ, arXiv:1411.1386
Wiener, J., Zweibel, E.G., & Oh, S.P. 2013, ApJ, 767, 87

PoS(AASKA14)094

PROCEEDINGS OF SCIENCE

Unravelling the origin of large-scale magnetic fields in galaxy clusters and beyond through Faraday Rotation Measures with the SKA

Annalisa Bonafede[*1] [†]**Franco Vazza**[1], **Marcus Brüggen**[1], **Takuya Akahori**[2], **Ettore Carretti**[3], **Sergio Colafrancesco**[4], **Luigina Feretti**[5], **Chiara Ferrari**[6], **Gabriele Giovannini**[7], **Federica Govoni**[8], **Melanie Johnston-Hollitt**[9], **Matteo Murgia**[8], **Lawrence Rudnick**[10], **Anna Scaife**[11], **and Valentina Vacca**[12]

[1]*Hamburger Sternwarte, Universität Hamburg, Gojenbergsweg 112, 21029, Hamburg, Germany.* [2]*Sydney Institute for Astronomy, School of Physics A28, University of Sydney, NSW 2006 Australia.* [3]*CSIRO Astronomy and Space Science, PO Box 76 Epping NSW 1710 Australia.* [4]*University of the Witwatersrand, 1 Jan Smuts Avenue, Braamfontein 2000, Johannesburg 2000, South Africa.* [5]*INAF Istituto di Radioastronomia, Via P. Gobetti, 101 40129 Bologna, Italy.* [6]*Laboratoire Lagrange, UMR 7293, Observatoire de la côte d'Azur, Boulevard de l'Observatoire, 06300 Nice, France.* [7]*Dipartimento di Fisica e Astronomia, Viale Berti Pichat 6/2, Bologna University, Italy.* [8]*INAF-Osservatorio Astronomico di Cagliari, Via della Scienza 5, 09047 Selargius (CA), Italy.* [9]*Victoria University of Wellington, PO Box 600, Wellington, 6140, New Zeland.* [10]*Institute for Astrophysics University of Minnesota, 116 Church St. SE Minneapolis, MN 55455, USA.* [11]*University of Southampton, University Rd, Southampton SO17 1BJ, UK.* [12]*Max Planck Institute for Astrophysics, Karl-Schwarzschild-Strasse 1, 85748 Garching bei München, Germany.*

E-mail: annalisa.bonafede@hs.uni-hamburg.de

We investigate the possibility for the SKA to detect and study the magnetic fields in galaxy clusters and in the less dense environments surrounding them using Faraday Rotation Measures. To this end, we produce 3-dimensional magnetic field models for galaxy clusters of different masses and in different stages of their evolution, and derive mock rotation measure observations of background radiogalaxies. According to our results, already in phase I, we will be able to infer the magnetic field properties in galaxy clusters as a function of the cluster mass, down to 10^{13} solar-masses. Moreover, using cosmological simulations to model the gas density, we have computed the expected rotation measure through shock-fronts that occur in the intra-cluster medium during cluster mergers. The enhancement in the rotation measure due to the density jump will permit to constraint the magnetic field strength and structure after the shock passage. SKA observations of polarised sources located behind galaxy clusters will answer several questions about the magnetic field strength and structure in galaxy clusters, and its evolution with cosmic time.

Advancing Astrophysics with the Square Kilometre Array
June 8-13, 2014
Giardini Naxos, Italy

[*]Speaker.
[†]On behalf of the SKA magnetism working group.

PoS(AASKA14)095

1. Introduction

Magnetic fields are ubiquitous in the Universe but their origin is unknown. On large scales, magnetic fields are the hardest to explain because the usually invoked dynamo mechanism does not have the time to amplify the field on the largest scales starting from a weak initial seed. In addition, the magnetic fields in galaxy clusters are poorly constrained from an observational point of view, and it is unclear whether they are formed from primordial seeds - amplified during the process of structure formation - or are formed from magnetic fields injected by AGN or galactic outflows. The presence of magnetic field in galaxy clusters can be probed by diffuse radio sources associated with clusters (see contribution by Johnston-Hollitt et al., Govoni et al., Ferrari et al.), and by Faraday rotation measures (RM) of embedded and background polarised sources (see e.g. Govoni & Feretti 2004 for a review). In the last decade, there have been revolutionary improvements in modelling the magnetic field in galaxy clusters, based partly on observations and partly on numerical simulations (e.g. Bonafede et al. 2011a, Brüggen 2013, Dolag et al. 2008, Govoni et al. 2006, Vacca et al. 2012). Much of what is known about the magnetic field in galaxy clusters comes from sensitive polarised observations. The observed polarisation angle ϕ_{obs} of a synchrotron-emitting source observed in the background of a galaxy cluster is rotated with respect to the intrinsic polarisation angle by a quantity called Faraday Rotation Measure, defined as $RM = \int_{cluster} n_e(l) B_{//}(l) dl$, where n_e is the thermal gas density in the intra-cluster medium (ICM), and $B_{//}$ is the magnetic field component along the line-of-sight. Recent studies have given us important clues to elucidate the evolution of the magnetic fields in galaxy clusters. However, because of the limits of current instruments, further improvements will be hard to achieve. A primary limiting factor is the sensitivity of present facilities, that limits the feasibility of such studies to a few nearby clusters where a sufficient number of background and embedded polarised sources can be detected. A secondary limiting factor is the small field-of-view of the instruments, which require multiple pointings and, hence, an enormous observing time to survey the entire cluster. In this work, we analyse the capabilities of the SKA in studying the properties of magnetic fields in the ICM through a dense RM sampling of sources detected in the background of these objects. Using different approaches, we have produced mock RM observations of galaxy clusters and of the regions around them. In Sec. 2 we outline the method used to produce the RM mock observations, and in Sec. 3 we apply this method to clusters of different masses, magnetic field strengths and dynamical status. In Sec. 4 we make use of cosmological simulations to explore the SKA capabilities in detecting the RM amplification expected in shocked regions. We assume here that SKA1-SUR will be populated in band 1 (350-900 MHz) and band 2 (650 -1670 MHz). This is motivated by the range of RM that we need to sample. Results do not change if SKA1-MID in used instead of SKA1-SUR. We assume that within each band the frequency channel width will be 1 MHz. We discuss in Sec. 5 how our predictions change in view of the progressive development of the SKA.

2. Mock RM observations

In order to predict the capabilities of the SKA in studying the magnetic fields on the large scales, we have produced mock RM observations of single radiogalaxies detected through the ICM. We have used an approach similar to the one described in Murgia et al. (2004) and Bonafede et al.

PoS(AASKA14)095

Table 1: Parameters for the gas and the magnetic field in galaxy cluster simulations

Model	Gas	M	B_0	Λ_{min}	Λ_{max}	η	n_0	r_c	β
		$M_\odot$	μG	kpc	kpc		cm^{-3}	kpc	
BM15_3.9	βModel	10^{15}	3.9	3	34	0.4	3.44×10^{-3}	290	0.75
BM15_4.7	βModel	10^{15}	4.7	3	34	0.5	3.44×10^{-3}	290	0.75
BM15_5.5	βModel	10^{15}	5.5	3	34	0.7	3.44×10^{-3}	290	0.75
BM14_1	βModel	10^{14}	1	3	17	0.5	3.44×10^{-3}	134	0.75
BM14_3	βModel	10^{14}	3	3	17	0.5	3.44×10^{-3}	134	0.75
BM14_5	βModel	10^{14}	5	3	17	0.5	3.44×10^{-3}	134	0.75
BM13_1	βModel	10^{13}	1	3	17	0.5	3.44×10^{-3}	62	0.75
BM13_3	βModel	10^{13}	3	3	17	0.5	3.44×10^{-3}	62	0.75
BM13_5	βModel	10^{13}	5	3	17	0.5	3.44×10^{-3}	62	0.75
E1_4	Enzo sim	1.12×10^{15}	4	34	115	0.5			
E2_4	Enzo sim	1.12×10^{15}	4	34	115	0.5			
E14_4	Enzo sim	10^{15}	4	34	115	0.5			

(2010), that consists of modelling the gas distribution inside the galaxy cluster and the magnetic field in a separate 3-dimensional box. We define Λ as the spatial scale in the real space, and the magnetic field power spectrum as $P_B(\Lambda) \propto \Lambda^n$ within the range $\Lambda_{min} \leq \Lambda \leq \Lambda_{max}$. We adopt here $n = 11/3$, corresponding to a Kolmogoorv scaling. The magnetic field is initially defined in the vector-potential domain. Through an appropriate choice of the vector potential components, we obtain a magnetic field with Gaussian components, divergence-free, and isotropically oriented throughout the box. The magnetic field is then normalised within the core radius to a given value B_0, and is scaled according to $B \propto B_0\,(n_e/n_0)^\eta$, n_0 being the cluster central gas density as defined in the β-model. The free parameters of our magnetic field model are B_0, Λ_{min}, Λ_{max}, and η. For every realisation of the magnetic field and of the gas density profile (see Tab. 1), we have integrated the RM equation to derive the Faraday RM throughout the cluster. Extrapolating from the deep survey in the GOODS-N field, and following the sensitivity listed in the SKA science memo, the SKA1-SUR is expected to detect 315 polarised sources per square degree at 1.4 GHz with 1 μJy detection threshold and 1.6 arcsec resolution (Rudnick & Owen 2014). Assuming this number, we have computed the expected RM for every polarised background source, whose position is randomly extracted within a circle of given aperture radius, which is chosen depending on the mass of the simulated cluster in order to trace the signal up to the distance where the cluster gives a substantial contribution. This approach has the great advantage of using background objects only, and hence it minimises the possible local ICM contribution due to the interaction of cluster radio-galaxies with their environment. The magnetic field simulations are performed with the *MiRo'* code (see Bonafede et al. 2013 for further details).

3. Magnetic field in galaxy clusters

In the following, we assume two distributions for the gas: (i) a β-model profile Cavaliere & Fusco-Femiano (1976) and (ii) the gas distribution obtained by a set of cosmological simulations

PoS(AASKA14)095

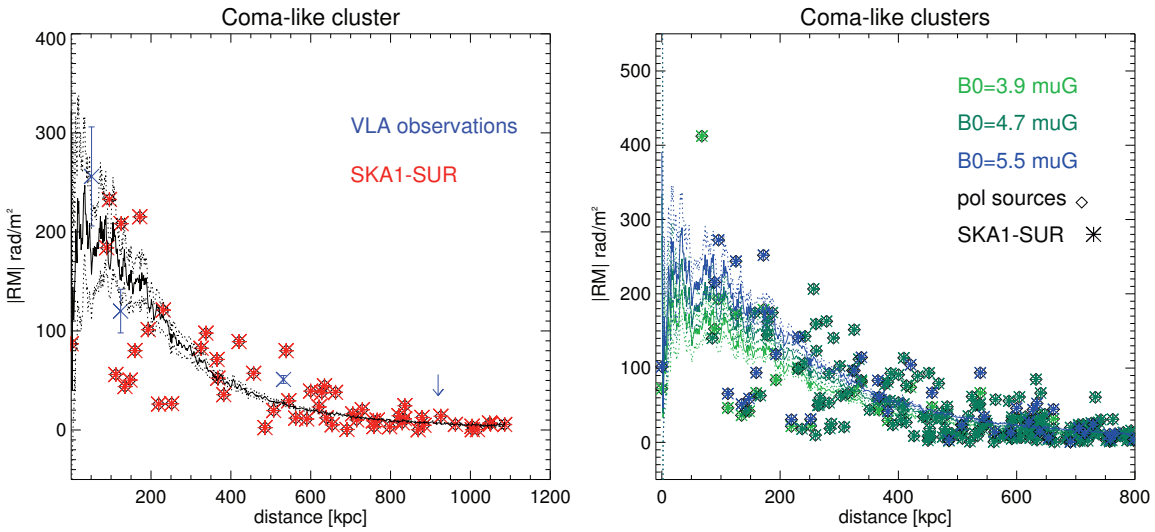

Figure 1: SKA1-SUR predictions for the RM for Coma-like clusters. Left panel: Average profile of the RM (continuous line) and 5σ dispersion (dotted lines) obtained for the BM15_4.7 model. Diamonds represent the sources that the SKA1-SUR will detect in the background of the cluster. Red asterisks mark the sources whose RM is in the range to be detected by the SKA1-SUR. Blue points refer to the observations presented in Bonafede et al. (2010). Right Panel: lines and symbols are like in the left panel, shown in different colours for three different models as indicated in the inset.

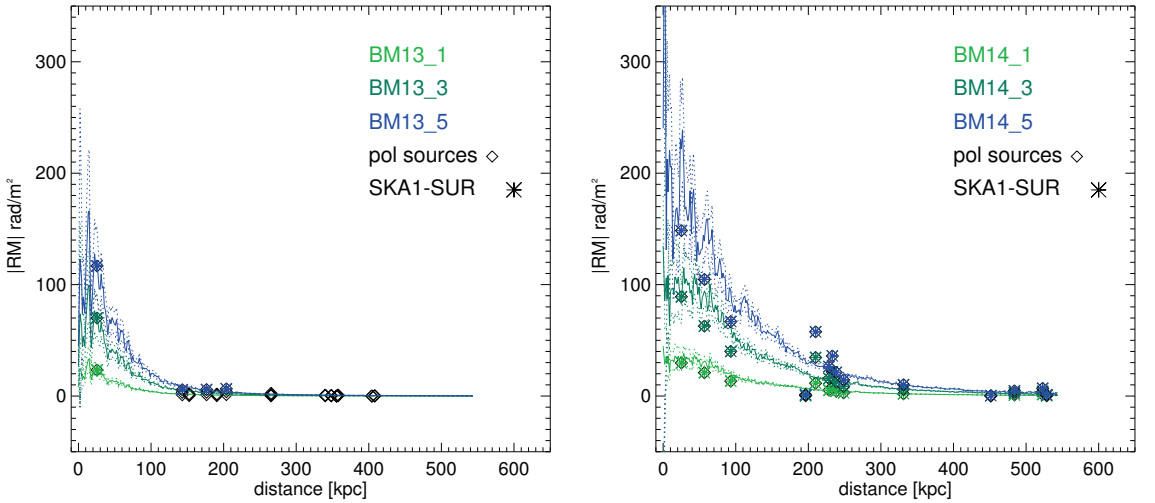

Figure 2: SKA1-SUR predictions for clusters with $M = 10^{13} M_{\odot}$ (left panel), and $M = 10^{14} M_{\odot}$ (right panel). Lines and symbols are like in Figure 1.

by Vazza et al. (2010).

3.1 β-model profiles

Our β-model clusters are meant to illustrate the big step forward allowed by the SKA in studying the magnetic field properties of galaxy clusters, compared to what has been achieved today with pointed observations of individual radiogalaxies.

The magnetic field in the Coma cluster is among the best constrained, and as such, it is a good starting point to investigate the capabilities of the SKA compared to the present facilities.

We have considered a cluster gas density profile that follows the β-model (Cavaliere & Fusco-

PoS(AASKA14)095

Femiano 1976) derived for the Coma cluster by Briel et al. (2001) (models BM15 in Table 1). For Λ_{min}, Λ_{max}, we have adopted the parameters that give the best fit to the Coma cluster magnetic field profile, and we have simulated the different values of B_0 and η that give the best agreement with the observations at 68% confidence level Bonafede et al. (2010). We have investigated the imprint that different values of B_0 and η leave on the RM profile, to see if SKA1-SUR observations will be able to distinguish among these models. In Fig. 1 the RM profile obtained with SKA1-SUR observations is shown for the model BM15_4.7, a "Coma-like" cluster. The results by Bonafede et al. (2010), obtained with VLA pointed observations, are overplotted. SKA1-SUR will allow one to detect the RM from ~ 50 sources in the background of the "Coma-like" clusters. Thanks to the SKA1-SUR field-of-view and sensitivity, similar results for a single cluster will be achieved with a single pointing.
In Fig. 1, we also show the RMs obtained by the SKA1-SUR for the different values of B_0 and η that fit the VLA observations within the 68% confidence level. The resolution in RM of the SKA1-SUR will enable us, in principle, to distinguish among these models, although a more accurate evaluation of the errors needs to be done to definitively assess this point.
Another aim of these β-model clusters is to show how the SKA will be able to recover the magnetic field profiles in relaxed systems depending on their mass and on the actual magnetic field strength at the cluster centre. So far, the magnetic field in galaxy clusters has been mainly analysed in massive and nearby systems. One of the reasons for this, is the number of sources that are needed in the background or inside the cluster to perform a proper analysis. To investigate how the SKA1-SUR will be able to constrain the magnetic field properties in clusters with different masses, we have rescaled the β-model of the Coma cluster in a self-similar way, for clusters with 10^{13} and 10^{14} $M_{\odot}$, keeping the same values for Λ_{min}, and Λ_{max}, and changing the value of B_0, as specified in Table 1 (cluster models BM14 and BM13). In Fig. 2 the predicted number of RM throughout clusters with different masses are shown, together with the RM profile derived from the RM simulation. From these figures we can conclude that the sources relevant to establish the magnetic field properties are those within few hundred kpc from the cluster centre. At larger distances ($\geq$ 300 kpc and 400 kpc for M13 and M14 models, respectively), the signal vanishes because of the lower gas density and magnetic field strength. Using only background sources has the advantage of avoiding a possible local RM enhancement. However, the information at the cluster centre, possibly provided by the radio-emitting central source, will be likely missing. Nonetheless, the SKA will be the first instrument which provides a good sampling of the RM in the background of smaller-mass clusters.

3.2 Cosmological simulations

Although the β-model is often a good representation of the gas density profile in the ICM, high-resolution X-ray observations have shown that the ICM is much more complex and difficult to characterise analytically (see e.g. Borgani & Kravtsov 2009, Ebeling et al. 2007, Ettori et al. 2013). Indeed, cosmological simulations of galaxy clusters show that the matter is continuously accreting onto the cluster, generating turbulence, shock waves, and bulk motions in the ICM, which leave a clear imprint in the gas density distribution. In order to investigate the capabilities of the SKA in more complex and realistic environments, we have repeated the procedure outlined above (Sec. 2) starting from the gas density distribution obtained by cosmological simulations. The sample of clusters by Vazza et al. (2010) consist of 20 clusters, re-simulated with an Adaptive

PoS(AASKA14)095

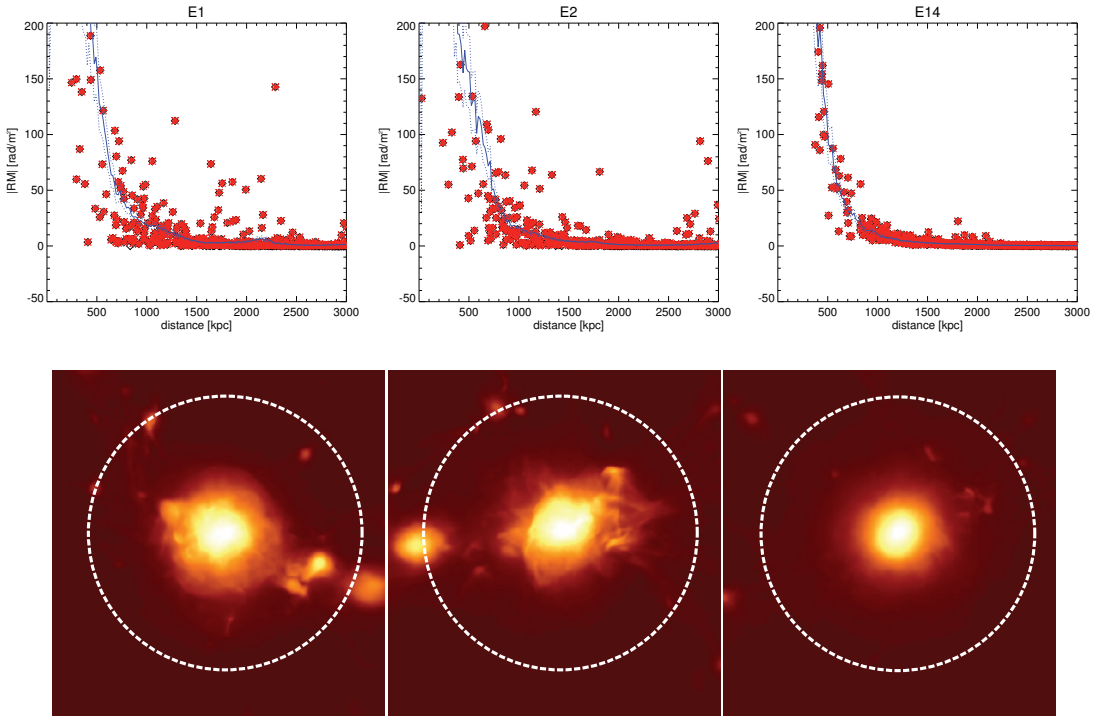

Figure 3: Top panel: RM profiles for the simulated clusters E1 (left), E2 (centre), and E14 (left). The y-axis goes up to 200 rad/m^2 in order to highlight the differences among the different clusters. The blue continuous line represents the radial average of the RM profile, the dotted lines refer to the 5σ dispersion. Red asterisks mark the sources detected by the SKA1-SUR. Bottom panel: X-ray projected luminosity for the clusters shown above. The white dashed-circle is centred on the cluster X-ray peak and has a radius of ~ 1 virial radius.

Mesh refinement method optimised to have a high resolution in the outskirts of the clusters. The authors have classified the clusters as relaxed (RE), merging (ME), and post major-merger (MM). Hence, we can investigate the SKA1-SUR capabilities to recover the magnetic field properties in clusters that are in different phases of their evolution. In this work, we focus on three different clusters, namely E1, E2 and E14, classified as MM, ME, and RE, respectively. The simulations have a resolution of 25 kpc h^{-1}. We have resampled the gas density distribution within the virial radius with a bigger grid, reaching a final resolution of 12 kpc h^{-1}. Ideally, one would need a factor 10 better resolution to match the SKA1-SUR resolution at 1.4 GHz, but this cannot be obtained yet, because of computing power limitations. Since the deviations from the β-model profile occur on scales larger than the resolution achieved here, we can still make useful forecasts for the SKA in detecting magnetic fields in different dynamical environments. The magnetic field is attached to the gas as explained in Sec. 2. We have fixed the parameters B_0, Λ_{max}, Λ_{min}, and η (see Table 1) and we have investigated the different trends of the RM in the different clusters. We have to note that the main limitation of our approach is the use of a magnetic field model, which does not evolve with the cluster. Hence, one can expect to detect only the main differences in the RM behaviour among the clusters. In Fig. 3, the X-ray luminosity of the clusters (from Vazza et al. 2010) together with the RM profiles are shown. From the RM mock observation, we have randomly extracted a number of sources that the SKA1-SUR will detect within one virial radius from the peak of the cluster

PoS(AASKA14)095

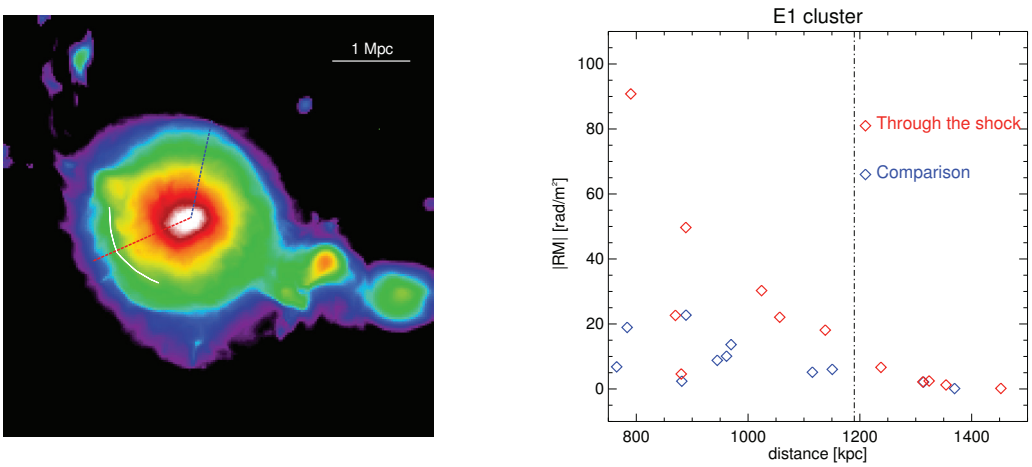

Figure 4: Left panel: Colors display the X-ray luminosity of E1 in the [0.2-5] keV energy range (Vazza et al. 2010). The red and blue dashed lines indicate the two directions considered to extract the RM sources, through a detected shock wave (red) and through a comparison region (blue). Right panel: RM of background sources extracted around the 2 directions shown in the left panel. The dotted-dashed line indicates the approximative position of the shock front.

X-ray emission. In all profiles, a decrease of the RM signal occurs at $\sim$ 1 Mpc (approximatively r_{500}) from the cluster centre. This decrease is more gradual for the clusters E1 and E2 with respect to the E14, which is relaxed. The main differences among E1, E2, and E14 arise at a distance of 500-3000 kpc, and are due to the presence of other clusters or sub-groups in the cases of E1 and E2, and to the almost empty environment which surrounds the relaxed cluster E14.

4. Beyond galaxy clusters: magnetic fields and shock waves

The use of cosmological simulations allows us to derive forecasts for the SKA in yet unexplored environments, such as the outskirts of galaxy clusters and intergalactic filaments (see Vazza et al, this contribution). The merger between massive galaxy clusters leads to the formation of shock waves that travel through the ICM. Shock waves are supposed to be the origin of the so called radio-relic, a class of synchrotron sources that are characterised by a low surface brightness, a steep radio spectrum, and a relatively strong polarisation (for details about radio relics we refer the reader to the reviews by Brüggen et al. 2011 and Feretti et al. 2012). Although the origin of radio relics is not well understood yet, if it understood that they are connected to shock waves. Hence, one expects to detect an enhancement of the RM signal due to the boost in the gas density and in the magnetic field by the shock. Such an enhancement has beed detected so far only for the relic in Abell 3667 (Johnston-Hollitt 2004), while Bonafede et al. (2013) have not found such a clear effect in the case of Coma. The simulations by Vazza et al. (2010) have been generated with a refining method optimised to detect the velocity and temperature jumps in the ICM. Here we focus of the cluster E1, where a shock front has been identified SE of the cluster centre. Using the RM mock observation (model E1_4), we have traced the RM profile in two regions: one across the shock front, and the other in a region where no shock has been detected. As done in the previous Sec., we have randomly extracted a number of sources that the SKA1-SUR will detect in polarisation. In Fig. 4 the two profiles are shown. Although the number of sources does not allow

PoS(AASKA14)095

one to trace a profile and, possibly, detect a jump at the position of the shock front, a significant enhancement of the RM in the shocked region with respect to the comparison region is detected. Our magnetic field simulations would predict a magnetic field strength of $\sim 1\ \mu$G at the position of the shock front, which in fair agreement with the magnetic field strength derived through different methods for radio relics (Feretti et al. 2012). A limitation of our approach is that the magnetic field is attached to the gas a posteriori, and is modelled with a simple recipe, so that the magnetic field compression and amplification expected at the shock position are not included in our mock observations. Including these effects is tricky from a theoretical point of view, since the mechanism through which the different magnetic field components are amplified and ordered on large-scale is not known yet. As a result of this limitation, the enhancement that we obtain has to be regarded as a lower limit to the effective RM enhancement that one would obtain once the compression and amplification of the shock are properly included. Remarkably, the values of the RM that we obtain match with the ones reported by Johnston-Hollitt (2004).

5. Conclusions

We have explored the capabilities of the SKA in studying the properties of magnetic fields inside and around galaxy clusters. Our predictions indicate that the SKA1-SUR will be able to recover tiny differences in the magnetic field properties of the ICM, which are far beyond the capabilities of the present instruments. Thanks to the SKA 1-SUR sensitivity and resolution, we expect to detect hundreds of sources in the background of massive galaxy clusters, and to trace the RM enhancement due to the presence of merging shock waves.The results expected by the SKA in its “early-science" phase depend on the number counts of polarised sources detectable at a sensitivity which is ∼50% of the SKA1-SUR. The reduced number of polarised sources will not allow us yet to detect a sufficient number of RM sources behind small mass clusters ($M \sim 10^{13} M_{\odot}$), and to detect a net enhancement through shocked regions on the ICM. Nonetheless, the results achieved here for massive galaxy clusters will be reachable already in the “early-science" phase, though with lower precision. The SKA2 will have a sensitivity ten times better than the SKA1, and a field of view corresponding to 20 times the one of the SKA1. Although a precise forecast for the number counts of polarised sources is not available yet, even in the most pessimistic case, that the number counts of polarised sources will be the same, the SKA2 will allow to obtain the results presented here in a shorter observing time.

Acknowledgements

A.B. F.V and M.B acknowledge support from the grant FOR1254 from the Deutsche Forschungsgemeinschaft. F.V. acknowledges computational resources under the CINECA-INAF 2008-2010 agreement, and the usage of computational resources on the JUROPA cluster at the at the Juelich Supercomputing Centre (project no. 5963). MJ-H acknowledges support from the Marsden Fund.

References

Bonafede, A., Feretti, L., Murgia, M., et al. 2010, A & A, 513, A30

PoS(AASKA14)095

Bonafede, A., Govoni, F., Feretti, L., et al. 2011a, A & A, 530, A24+
Bonafede, A., Vazza, F., Brüggen, M., et al. 2013, MNRAS, 433, 3208
Borgani, S., & Kravtsov, A. 2009, ArXiv e-prints, arXiv:0906.4370
Briel, U. G., Henry, J. P., Lumb, D. H., et al. 2001, A & A, 365, L60
Brüggen, M. 2013, MNRAS, arXiv:1308.5230
Brüggen, M., Bykov, A., Ryu, D., & Röttgering, H. 2011, Science & Space Review, 138
Cavaliere, A., & Fusco-Femiano, R. 1976, A & A, 49, 137
Dolag, K., Bykov, A. M., & Diaferio, A. 2008, Space Science Reviews, 134, 311
Ebeling, H., Barrett, E., Donovan, D., et al. 2007, ApJL, 661, L33
Ettori, S., Donnarumma, A., Pointecouteau, E., et al. 2013, Science & Space Review, 177, 119
Feretti, L., Giovannini, G., Govoni, F., & Murgia, M. 2012, AAR, arXiv:astro-ph/12051919
Govoni, F., & Feretti, L. 2004, International Journal of Modern Physics D, 13, 1549
Govoni, F., Murgia, M., Feretti, L., et al. 2006, A & A, 460, 425
Johnston-Hollitt, M. 2004, in The Riddle of Cooling Flows in Galaxies and Clusters of galaxies, ed. T. Reiprich, J. Kempner, & N. Soker, 51
Murgia, M., Govoni, F., Feretti, L., et al. 2004, A & A, 424, 429
Rudnick, L., & Owen, F. N. 2014, ApJ, 785, 45
Vacca, V., Murgia, M., Govoni, F., et al. 2012, A & A, 540, A38
Vazza, F., Brunetti, G., Gheller, C., & Brunino, R. 2010, New Astronomy, 15, 695

PoS(AASKA14)095

PROCEEDINGS OF SCIENCE

Measuring magnetism in the Milky Way with the Square Kilometre Array

Marijke Haverkorn[1,2]*, Takuya Akahori[3], Ettore Carretti[4], Katia Ferrière[5], Peter Frick[6], Bryan Gaensler[3,7], George Heald[8], Melanie Johnston-Hollitt[9], David Jones[1], Tom Landecker[10], Sui Ann Mao†[11], Aris Noutsos[11], Niels Oppermann[12], Wolfgang Reich[11], Timothy Robishaw[10], Anna Scaife[13], Dominic Schnitzeler[11], Rodion Stepanov[6,14], Xiaohui Sun[3], and Russ Taylor[15,16]

[1]*Radboud University;* [2]*Leiden University;* [3]*The University of Sydney;* [4]*CSIRO Astronomy and Space Science;* [5]*IRAP, Université de Toulouse, CNRS;* [6]*Institute of Continuous Media Mechanics ;* [7]*ARC Centre of Excellence for All-Sky Astrophysics (CAASTRO);* [8]*Netherlands Institute for Radio Astronomy (ASTRON);* [9]*Victoria University of Wellington;* [10]*Dominion Radio Astrophysical Observatory;* [11]*Max-Planck-Institut für Radioastronomie;* [12]*CITA;* [13]*University of Southampton;* [14]*Perm National Research Polytechnic University;*[15]*University of Cape Town;*[16]*University of the Western Cape*
*E-mail:*m.haverkorn@astro.ru.nl

Magnetic fields in the Milky Way are present on a wide variety of sizes and strengths, influencing many processes in the Galactic ecosystem such as star formation, gas dynamics, jets, and evolution of supernova remnants or pulsar wind nebulae. Observation methods are complex and indirect; the most used of these are a grid of rotation measures of unresolved polarized extragalactic sources, and broadband polarimetry of diffuse emission. Current studies of magnetic fields in the Milky Way reveal a global spiral magnetic field with a significant turbulent component; the limited sample of magnetic field measurements in discrete objects such as supernova remnants and HII regions shows a wide variety is field configurations; a few detections of magnetic fields in Young Stellar Object jets have been published; and the magnetic field structure in the Galactic Center is still under debate.

The SKA will unravel the 3D structure and configurations of magnetic fields in the Milky Way on sub-parsec to galaxy scales, including field structure in the Galactic Center. The global configuration of the Milky Way disk magnetic field, probed through pulsar RMs, will resolve controversy about reversals in the Galactic plane. Characteristics of interstellar turbulence can be determined from the grid of background RMs. We expect to learn to understand magnetic field structures in protostellar jets, supernova remnants, and other discrete sources, due to the vast increase in sample sizes possible with the SKA. This knowledge of magnetic fields in the Milky Way will not only be crucial in understanding of the evolution and interaction of Galactic structures, but will also help to define and remove Galactic foregrounds for a multitude of extragalactic and cosmological studies.

Advancing Astrophysics with the Square Kilometre Array
June 8-13, 2014
Giardini Naxos, Italy

*On behalf of the SKA Cosmic Magnetism Working Group
†Speaker.

PoS(AASKA14)096

1. Introduction

In the past years, cosmic magnetism science has transformed from a niche to a fast growing and exciting field of research. This is largely due to improvements in computational power, and enhanced observational capabilities. The latter led to the presence of extensive new data sets like the Canadian (Landecker et al. 2010) and Southern (Haverkorn et al. 2006a) Galactic Plane Surveys, the Effelsberg 1.4 GHz Medium Latitude Survey (EMLS, Reich et al. 2004), the Urumqi 6 cm survey (Sun et al. 2007), and the S-band Polarization All-Sky Survey (S-PASS) (Carretti et al. 2015); and ongoing surveys like GALFACTS (Taylor & Salter 2010) or GMIMS (Wolleben et al. 2009). Unraveling the structure and strength of magnetic fields in the Universe is such a complex and involved system, however, that much is still under debate or plainly unknown.

Studies of magnetic fields in galaxies are at the center of many open questions regarding cosmic magnetism. Current galactic magnetic fields may originate in the primordial universe, possibly from magnetizing topological defects, from early stellar magnetic fields (Widrow 2002) or from magnetic fields in the cosmic web (Sofue et al 2010). Seed fields may also be generated in protogalaxies by e.g. the Biermann mechanism in the first supernova remnants (Hanayama et al. 2005), the Weibel instability (Lazar et al. 2009), or from plasma fluctuations (Schlickeiser & Felten 2013). Magnetic fields in the intracluster and intergalactic medium may have originated from outflows of galaxies (Donnert et al. 2009). On smaller scales, galactic magnetic fields interact with supernova remnants, and help shape fields in star formation regions (Fish et al. 2003; Green et al. 2012).

The Milky Way is an ideal testbed for many galactic magnetic field studies due to its proximity. We have the most detailed observations and understanding of the multi-phase interstellar environment in the Milky Way to help interpret magnetic field studies. In particular, for magnetic fields in discrete objects and on smaller scales ($\lesssim 1$ pc), the Milky Way is the best location where these can be studied in detail (although parsec-scales become accessible in the Magellanic Clouds as well, see Beck et al (2015)). The global configuration of the magnetic field and characterization of magnetic fields in the gaseous halo is difficult to determine from our location within the Milky Way, and is more easily studied in other (face-on) spiral galaxies. However, the Milky Way provides the opportunity of studying large-scale reversals in this global configuration of the field in unique detail.

In addition, the Milky Way is a significant foreground for a wide variety of extragalactic studies. The magnetic fields in the Milky Way disk and halo provide a characteristic radio-polarimetric pattern, which needs to be understood to enable study of e.g. the Epoch of Reionization, inflation theory through the Cosmic Microwave Background B-mode polarization, or magnetization of the cosmic web. Also, knowledge of the structure of the Galactic magnetic field is imperative to trace back Ultra-High Energy Cosmic Rays to their sources, and to understand the multi-phase, multi-component interstellar medium (ISM).

In the Square Kilometre Array (SKA) Science Case written in 2004, Beck & Gaensler (2004) described SKA observations with magnetic fields in the Milky Way and nearby galaxies, and stated the importance of an *all-sky Rotation Measure (RM) Grid* of compact extragalactic radio sources. In the updated SKA Science Case for magnetic fields in the Milky Way presented in this chapter, we re-emphasize the importance of the RM Grid, but in addition explain the necessity of broadband

PoS(AASKA14)096

polarimetry of diffuse synchrotron emission, enabling Faraday Tomography through RM synthesis (Brentjens & de Bruyn 2005).

Section 2 details the current status of research in magnetic fields in the Milky Way, from the global configuration and turbulent fields, to fields in discrete objects and in the Galactic Center. In Section 3, we describe the Galactic magnetism studies that will become possible with the SKA. Subsection 3.1 details the two methods used, viz. the RM Grid and Faraday Tomography, whereas in the next three subsections we present the possibilities with SKA in phase 1 Early Science, SKA in phase 1 and SKA in phase 2. .

2. Magnetic Fields in the Milky Way

Galactic magnetic fields are amplified and maintained by magnetic dynamo action, through conversion of energy from e.g. differential rotation, turbulence and/or cosmic rays into magnetic energy. Regular fields may be amplified by mean-field, alpha-omega dynamos, which are extensively studied both analytically and numerically. Various dynamo modes may exist, resulting in characteristic configurations of the global galactic field. Specific dynamo modes may indicate the influence of an external disturber or of a bar (Ferrière 2007). In galactic disks, the dynamo mode most easily excited is axisymmetric and has even parity with respect to the midplane (i.e., the horizontal field component has the same direction on either side of the midplane, while the vertical component changes sign across the midplane (e.g., Ruzmaikin et al. 1988)). The field is dominated by its toroidal component, which together with the radial component, forms an axisymmetric spiral pattern. Rarely observed bisymmetric fields in galactic halos could be relics of the initial intergalactic magnetic field (as suggested by Fletcher et al. (2011) for the halo of M 51). As opposed to flat disks, dynamos in spherical objects – such as galactic halos – are expected to favor the axisymmetric mode with odd vertical parity, in which the magnetic field crosses the midplane continuously at right angles and the horizontal component reverses direction across the midplane[1].

In the disk and halo system of the Milky Way, this would result in mixed-parity modes (Sokoloff & Shukurov 1990). Although Moss & Sokoloff (2008) find that in a disk-halo system, usually the stronger dynamo enslaves the other, resulting in either an even-parity or an odd-parity magnetic configuration, mixed-parity modes can be obtained if a moderate Galactic wind is included (Moss et al. 2010). The geometry and parity of the halo magnetic field hold the key to its origin. For instance, an X-shaped field would probably indicate the existence of a large-scale Galactic wind. Moreover, even parity of this X-shaped field would suggest a wind originating near the Galactic plane and advecting the dynamo field of the disk into the halo, while odd parity would suggest a wind blowing from the base of the halo and stretching out the (normally dipole-like) dynamo field of the halo into an X shape (Ferrière & Terral 2014).

Current observations show a picture generally consistent with dynamo models, albeit so rough that it is impossible yet to determine how exactly the Galactic magnetic field is maintained. It is now well-established that the large-scale magnetic field in the Milky Way disk is generally aligned with the spiral arms and has a strength of about 3 μG (see the review by Haverkorn (2014)). However, there is still considerable debate over a few basic properties of the large-scale field, including

[1]Note that the even-parity poloidal field is also said to be quadrupolar, and the odd-parity poloidal field is also named dipolar, although it generally differs from a pure quadrupole and dipole, respectively.

PoS(AASKA14)096

its azimuthal structure (i.e., whether it is axisymmetric, bisymmetric, or neither as concluded by Men et al. (2008)), and the number and location of large-scale reversals in the field direction. Most recent models based on multiple observational tracers favor an axisymmetric spiral structure with a single reversal just inside the Solar circle (Brown et al. 2007; Sun et al. 2008; Van Eck et al. 2011; Jansson & Farrar 2012). However, some of the models based on only pulsar data conclude that multiple reversals must exist (Han et al. 2006; Nota & Katgert 2010). In principle, large-scale field reversals can be produced by dynamos when the rotational velocity has a large vertical gradient (Ferrière & Schmitt 2000), or be a result of early injection of small-scale fields (Hanasz et al. 2009; Moss et al. 2012) or of magneto-rotational instability (Machida et al. 2013). Much of the controversy about the presence of large-scale field reversals in the Milky Way is fueled by the lack of detection of field reversals in external galaxies, with the exception of M 81 which appears to host a bisymmetric field (see Beck et al (2015) for a detailed discussion).

Recent Galactic magnetic field models seem to confirm the mixed parity dynamo modes in disk and halo (Frick et al. 2001; Sun et al. 2008; Jansson & Farrar 2012). This also would explain the apparent contradiction between the observed "butterfly pattern" of rotation measures in the inner Galaxy, indicating a reversal of the azimuthal field component across the Galactic plane (Simard-Normandin & Kronberg 1980) and local measurements of field direction indicating no reversal of this component across the galactic plane (Frick et al. 2001). The first would be associated with the halo field, whereas the second reflects the disk field. However, characterizing the global halo field structure is made difficult by the contamination of local structures. As an example, the Faraday rotation pattern of extragalactic sources recognized as a large-scale dipolar field in previous studies is strongly influenced by a local magnetized bubble (Wolleben et al. 2010; Sun & Reich 2010). Several forms of the halo magnetic field geometry have been proposed in the literature, including a purely azimuthal double-toroidal component (e.g., Sun & Reich (2010)), a spiral component (e.g., Mao et al. (2012)) and an out-of-plane X-shaped component (e.g., Jansson & Farrar (2012)) as observed in external edge-on spiral galaxies and as modeled by Ferrière & Terral (2014). Vertical field components are expected in the Milky Way, by analogy to nearby spirals (Beck et al 2015). However, the vertical component of the field at the Galactocentric radius of the Sun is observed to be small (Mao et al. 2010). This suggests that the Milky Way's vertical field components are concentrated towards the inner Galaxy, as modeled in e.g. Jansson & Farrar (2012).

The observations on which these magnetic field models are based consist of RM Grids of extragalactic sources and pulsars, and/or diffuse synchrotron emission. The models are hampered by low density of polarized sources, uncertain distance estimates of pulsars, and contamination by foreground structures such as supernova remnants (e.g. the radio loops). A good example of this is the wavelet analysis of pulsar data to determine the large-scale structure of the Galactic magnetic field (Frick et al. 2001), which shows good results in the Solar neighborhood, but cannot determine the global field structure due to insufficient data points (Stepanov et al. 2002). This is illustrated in the left plot of Figure 1, which shows a wavelet transform of a test function representing Galactic electron density obtained from an irregular grid of pulsar data (Stepanov et al. 2002). The plot demonstrates the method's unique capability to trace out magnetic spiral arms, but also that this is currently only possible in the Solar vicinity.

PoS(AASKA14)096

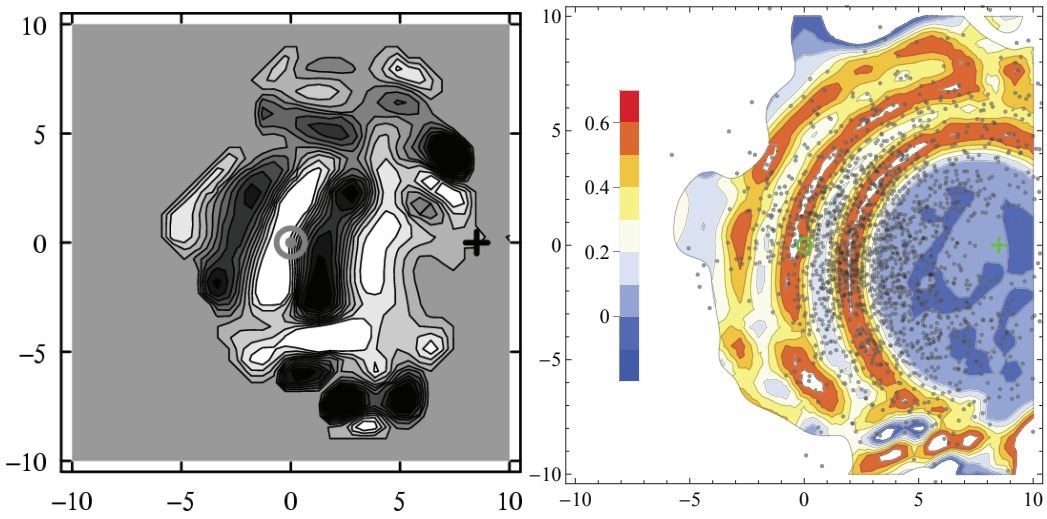

Figure 1: Wavelet transforms of a test function containing a Galactic electron density model, retrieved from pulsar RMs. The Galactic Center is marked with a cross and the Sun is at the center of the frames. The axes are in kpc, and in uniformly grey/white regions, data is too sparse. Left: current situation, using 323 pulsars with known RMs (Stepanov et al. 2002) and a two-arm model. Right: the same with a simulated pulsar data set of 2000 pulsars to be expected with SKA1, fitting well to a three-arm model.

2.1 Galactic turbulence

Both ionized and neutral phases of the Galactic ISM are turbulent, usually displaying a Kolmogorov-like power spectrum in density across a wide range of length scales (Elmegreen & Scalo 2004; Armstrong et al. 1995). Determining the power spectrum of the magnetic field is much more difficult: reliable estimates only exist for related quantities like RM. Observed spectral indices[2] of RM are generally much flatter than Kolmogorov (Haverkorn et al. 2008).

Besides the spectral index, magnetohydrodynamic (MHD) turbulence can be characterized by several fundamental parameters including scales of energy injection and dissipation, the rms Mach number of flow speed, intermittency, and the plasma beta (the pressure ratio of the gas to the magnetic field). The search for such characteristics is important to understand the dynamical and thermal states of the ISM. In addition, numerical modeling of turbulence is essential to understand the physics behind the observations of turbulence parameters. E.g., modeling revealed that known turbulent structures are not enough to explain observed structure functions[3] (SFs) of RM toward high Galactic latitudes (Akahori et al. 2013). A possible cause of the discrepancy would be magnetic fields emerging from the disk to the halo due to the magneto-rotational and Parker instabilities (Machida et al. 2013).

The Mach number of interstellar turbulence can be determined through polarization data, by way of the gradient of the polarization vector (Gaensler et al 2011). Application of this method

[2]Usually, power in RM fluctuations is measured by structure functions (as explained below rather than power spectra, the slope of which is directly related to power spectral index.

[3]The structure function of order n, of a quantity f as a function of scale $\delta\mathbf{x}$ is defined as $\mathrm{SF}_f(\delta\mathbf{x}) = \langle |f(\mathbf{x}) - f(\mathbf{x}+\delta\mathbf{x})|^n \rangle_\mathbf{x}$, where $\langle\rangle_\mathbf{x}$ denotes averaging over all positions x. The second-order structure function ($n = 2$) is most used and usually meant when just "structure function" is used.

PoS(AASKA14)096

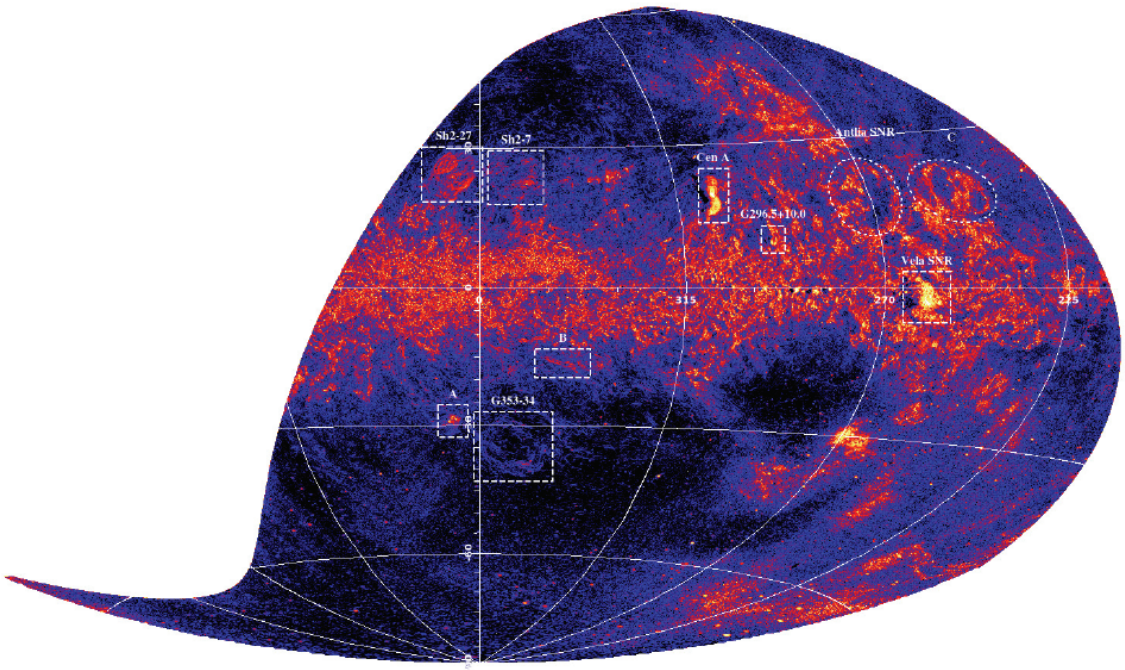

Figure 2: Gradient of the polarization vector over the entire southern sky (Iacobelli et al. 2014). Analysis of the probability distribution function of the polarization gradient shows that interstellar turbulence is transonic in the regions studied.

on a small test region, combined with simulations (Burkhart et al. 2012), reveals that interstellar turbulence is transonic with $M \lesssim 2$. Iacobelli et al. (2014) showed that this Mach number value is roughly consistent over the entire (Southern) sky, as can be derived from the polarization gradient shown in Figure 2.

Measured maximum scales of fluctuations in the magneto-ionized medium are likely to be connected to the scale of energy injection in the interstellar gas. Energetics imply that the main energy sources likely to drive interstellar turbulence are supernova remnants. Early observational studies using correlation functions corroborated this, concluding that the outer scale of turbulence must be $O(100)$ pc (Lazaryan & Shutenkov 1990). Usually, these maximum scales are probed by second-order SFs of RM, to be obtained from measurements of RM Grids. However, recent observations indicate maximum scales of fluctuations smaller than ~ 10 pc (in spiral arms only, Haverkorn et al. 2008), of a few parsecs from anisotropies in TeV cosmic ray nuclei (Malkov et al. 2010), and similar from analysis of synchrotron fluctuations (Iacobelli et al. 2013). These small scales do not necessarily indicate the maximum scale of turbulence, but only show that larger-scale fluctuations in the magneto-ionic medium are not observed. Turbulence may still be present on scales up to $\sim$100 pc, but this structure may be masked by small discrete sources (Haverkorn et al. 2006b), strong small-scale fluctuations in electron density, dominating shock waves in spiral arms, etc. The SF at higher Galactic latitudes has a flatter slope in $> 1^\circ$ scales (Stil et al. 2011). These authors claim that the steep slope of SFs at low latitude could be affected by the local turbulent ISM.

PoS(AASKA14)096

Some evidence exists that interstellar turbulence in dense gas is intermittent, i.e. contains regions with intense turbulence and regions with no turbulence, giving long tails in the distribution of the observable such as density or velocity (Elmegreen & Scalo 2004). This can be detected using higher order SFs. However, in the diffuse ionized gas, current SFs contain far too few sources to be able to construct meaningful higher order SFs.

2.2 Magnetic fields in discrete objects

Star forming regions The launching mechanism for jets in general has been proposed to be universal (e.g. Livio (2011)), crossing orders of magnitude in terms of source energetics and environmental conditions. However, our observational understanding of jets in Young Stellar Objects (YSOs) is almost diametrically opposed to that of their higher energy analogues such as AGN, GRBs and X-ray binaries. While characteristic quantities such as density, temperature and ionization fraction can be well constrained for YSOs from (primarily) line emission data, the strength and orientation of the magnetic field in these systems is still very poorly known (Ray 2009). Observational evidence for these magnetic fields is generally indirect and model dependent: jet rotation, cushioning effects on jet shocks, etc. Although non-thermal radio emission can provide a direct measure of magnetic field strength and configuration, measurements of these properties are very rare (Ray et al. 1997; Carrasco-González et al. 2010; Ainsworth et al. 2014). This is because the associated non-thermal emission is faint ($\sim \mu$Jy), and because radio studies of star forming regions are predominantly total intensity, cm-wave experiments focusing on thermal radio emission from ionized gas.

In spite of this, the role of the magnetic field in jet launching is expected to be inextricably linked to the active accretion of the central object from its gaseous disk and surrounding molecular cloud, through which Galactic magnetic field lines are known to be threaded and where the influence of the magnetized jet may provide turbulent support against collapse. The centrifugal acceleration of material along these field lines is widely accepted to be closely connected to the launching of YSO jets through MHD processes, as well as the collimation of those jets through a "winding-up" of the magnetic field lines anchored in the rotating disk leading to the creation of hoop stresses in the resulting helical field configuration (Blandford & Payne 1982; Ferreira et al. 2006). Furthermore, the magnetic fields in these systems are crucial not only for understanding the star formation process but, through the acceleration of relativistic particles in jet shocks, also act as cosmic-ray factories, contributing to the GeV excess in the Galaxy (Orlando & Strong 2013).[4]

Supernova remnants Magnetic fields in supernova remnants (SNRs) can be enhanced to mG strengths. Magnetic field strengths in young SNRs are generally radially directed, whereas old SNRs have mostly tangential fields, although turbulent fields play a significant role (for a review see Reynolds et al. (2012)). Apart from the importance of magnetic fields for the evolution of SNRs themselves, these fields are crucial for acceleration of Galactic cosmic rays (Blasi 2013). SNRs are also believed to be the main drivers of interstellar turbulence.

There is some evidence from both observations (Gaensler 1998; Uyaniker et al. 2002; Kothes & Brown 2009) and numerical simulations (Stil et al. 2009) that magnetic fields in SNRs carry

[4]For SKA measurements of magnetic fields in molecular and cold gas, linked to the early phases of star formation, we refer the reader to Robishaw et al. (2015).

PoS(AASKA14)096

the signature of larger-scale Galactic magnetic fields which they are expanding in. Similarly, in some SNRs, there is evidence for toroidal fields, interpreted as the product of the stellar wind of the progenitor, swept up by the blast wave (Uyaniker et al. 2002; Harvey-Smith et al. 2010). Some massive stars exhibit non-thermal radio emission, so magnetic fields must occasionally be present in the winds. Nevertheless, de la Chevrotière et al. (2014) failed to find optical evidence of magnetic fields in 11 WR stars (by searching for circular polarization). Only a large sample of SNR magnetic fields will shed light on the relationship between magnetic fields in SNRs and stellar and/or Galactic magnetic fields.

Measurements of magnetic fields in Pulsar Wind Nebulae (PWNe) are scarce and biased towards young, bright PWNe. However, an intriguing example of the importance of observing PWN magnetic fields is given by Kothes et al. (2008), who showed that the older PWN DA 495 has a dipole-like field, giving an estimate of the spin axis of the putative pulsar. The PWN magnetic field configuration is best studied through depolarization and Faraday tomography of the PWN emission itself, but probing through RMs of background sources can contribute. For more discussion on PWN science with the SKA, see Gelfand et al. (2015).

For a discussion on other SNR science with the SKA, see Wang (2015).

HII Regions Typical magnetic field strengths in HII regions are a few to about 12 μG (Sun et al. 2007; Gao et al. 2010; Harvey-Smith et al. 2011), obtained from observations of the Faraday rotation of background Galactic synchrotron emission. Magnetic field measurements in HII regions over a large range of densities should be obtained to understand the dynamic role that magnetic fields play. This can be done using a dense RM Grid. Strömgren spheres tend to be so dense and so turbulent that they are Faraday thick at 1 GHz, so that emission from the objects themselves can only be probed at higher frequencies, where the regions become Faraday thin.

Magnetic fields in HII regions also seem to retain knowledge about larger-scale Galactic magnetic fields (Han & Zhang 2007; Harvey-Smith et al. 2011). In particular, this should be true of Planetary nebulae (PNe), which do not have an intrinsic magnetic field. However, some have recently been shown to have a polarization signature (Ransom et al. 2008, 2010). Therefore, mapping out magnetic field directions in PNe gives an independent probe of the large-scale field. Extensive catalogues exist of PNe, down to arcsecond size objects. Measurements of the Faraday rotation in the ionized shell can be coupled with optical observations which can supply data on the distance, the size of the ionized region, and the electron density. This can lead to the determination of unambiguous magnetic field values all over the Galaxy.

Faraday screens Faraday screens are structures observed through their polarization properties (Gray et al. 1998; Haverkorn et al. 2003; Wolleben & Reich 2004), which are difficult to identify as physical Galactic objects from turbulent structures. These objects are invisible or at best very faint in the continuum, but visible in polarized emission and RM. Some of them can be described as magnetic bubbles with strong regular fields and low thermal electron density, when their magnetic pressure exceeds thermal pressure. At 4.8 GHz, Faraday screens with high RMs of the order of 200 rad m^{-2} were identified in the Galactic plane in polarized emission (Sun et al. 2007; Gao et al. 2010), whereas lower-frequency data reveal screens of a few to a few tens of rad m^{-2}. Many more Faraday screens are expected to have lower RMs, but these are easily be masked by small-scale

PoS(AASKA14)096

polarization from the magnetized turbulent ISM. Some of them may be linked to faded PWNe or old HII regions leaving expanding magnetic bubbles (Iacobelli et al. 2013), but in general their nature and origin are still enigmatic.

2.3 The Galactic Center

The Galactic Center (GC) is important – aside from its intrinsic interest – because it is, by definition, the closest example of a galactic nucleus that we possess. It has a complex magnetic field structure in interaction with the gas and relativistic particles close to the GC (see Ferrière (2009) for a review). The GC magnetic field is most likely a result of dynamo action, either a local dynamo or the dynamo maintaining the Galactic magnetic field, which may require a central galactic wind to stabilize (Moss et al. 2010). Crocker et al. (2011) showed evidence that a GC wind is indeed present. Therefore, measuring and understanding magnetic fields in the GC is also a key component in understanding Galactic magnetic fields.

Large uncertainties still exist about the field strength. Estimates are $\sim (6-22)\ \mu$G (minimum energy), $\gtrsim (50-120)\ \mu$G (synchrotron spectral break, Crocker et al. (2010, 2013)) or ~ 1 mG (pressure balance) in the general intercloud medium. Measurements of the RM and dispersion measure (DM) of the magnetar J1745-2900 indicate that the magnetic field at $\sim$ 0.1 pc from Sgr A* could be as high several mG (Eatough et al. 2013). Zeeman measurements and submm polarimetry in dense clouds show field strengths of 0.1 mG to a few mG (e.g., Killeen et al. 1992; Crutcher et al. 1996; Chuss et al. 2003).

The configuration and structure of the GC magnetic field are also significantly unclear. Novak et al. (2003) and Law et al. (2011) used a RM Grid to obtain a magnetic field geometry organized on ~ 300 pc scales, centered some 50 pc west of the dynamical center of the Galaxy. They interpret polarization in radio synchrotron filaments as a poloidal (vertical) field in the diffuse ISM. This is in conflict with the findings of Roy et al. (2005, 2008), who obtained results – based on an RM Grid of 64 background sources – consistent with a bi-symmetric spiral magnetic field in the Galaxy or with a field oriented along the central bar of the Galaxy, with a field strength of $\sim 20\ \mu$G.

Unanswered questions also remain about how the recently-discovered Fermi Bubbles are related to the central regions of our Galaxy: are they the result of electron-dominated processes (Su et al. 2010) from close to the $\sim 4.1 \times 10^6\ M_\odot$ black hole at the center, or are they formed by proton dominated objects (Crocker & Aharonian 2011) arising from the stellar activity in the central ~ 200 pc? Evidence for the latter seems to have emerged from polarized radio counterparts to the Fermi bubbles detected in the S-PASS survey (Carretti et al. 2013). The magnetic field structure is a critical part to the resolution of this question, since the field structure is likely intimately tied to both the maintenance of the dynamo and the formation of Bubble-like structures in galaxies through the establishment of winds.

3. Galactic Magnetism Science with the Square Kilometre Array

3.1 Methods

Although the Galactic Science described in this chapter is very diverse, the science goals can be reached using two main observational strategies, viz. the RM Grid and Faraday tomography with

PoS(AASKA14)096

broadband polarimetric observations of diffuse Galactic radio emission. We describe these methods in this Section, and then explain how we can reach our science goals with these observations in the SKA1 phase, SKA1 Early Science and in SKA2.

3.1.1 The RM Grid

The *RM Grid* as described in the 2004 SKA Science Case (Beck & Gaensler 2004) continues to be the highest priority for the Cosmic Magnetism Working Group (see Johnston-Hollitt et al. (2015)). The RM Grid possible with SKA1 is based on the summary of the Cosmic Magnetism Science Working Group Assessment Workshop (Govoni et al. 2014). These observations focus on a relatively shallow spectro-polarimetric survey at ~ 1 GHz over a broad frequency coverage, enabling a vastly improved RM Grid. Currently, about 40,000 extragalactic background sources with measured RMs are available in the RM Grid, mostly based on Taylor et al. (2009). A SKA1-SUR Band 2 survey with 2μJy sensitivity (4 hours per pointing with 500 MHz bandwidth) may provide RM Grids of 300-1000 sources/deg^2, i.e. an improvement of $2-3$ orders of magnitude to the current status.

Pulsar RM surveys also offer a vast improvement in data quality. Smits et al. (2011a) estimate that SKA1-LOW will provide $9,000-10,000$ new pulsar detections, including their RMs, whereas SKA1-MID will discover about $12,000-13,000$. Recent estimates predict that 30,000 new pulsars will be discovered with the SKA, 50% of which will already be found with SKA1 (Kramer & Stappers 2015). These pulsar measurements become exceptionally valuable for modeling the Galactic magnetic field when reliable distance estimates are available. For this goal, the step to SKA2 will be crucial: in SKA2, timing parallaxes should allow distance measurements with an accuracy of about 5% up to a maximum distance of 30 kpc, which means throughout the Milky Way (Smits et al. 2011b). See Han et al. (2015) for more detailed discussion of the use of pulsars to investigate the magneto-ionic medium of the Milky Way.

3.1.2 Faraday tomography

In the past few years, Faraday tomography[5] has started to provide new views into the structure of the Galactic magnetic field, albeit still incomplete and puzzling. The few studies available for various sightlines all find that the path length is filled with a small number of discrete synchrotron emission regions, interspersed with Faraday-rotating screens (Schnitzeler et al. 2007; Brentjens 2011; de Bruyn & Pizzo 2014; Jelić et al. 2014). This hints at the complexity of the magnetic field structure, but is at least partially due to the insensitivity of current observations to Faraday-thick structures.

The greatest leap in knowledge about Galactic magnetism may well lie in the opportunities that Faraday tomography will give. Long wavelengths are required for a high maximum detectable Faraday thickness of $\Delta\phi_{\rm max} = \pi/\lambda^2_{min}$, while broad frequency coverage provides a high Faraday depth resolution $\delta\phi = 2\sqrt{3}/\Delta\lambda^2$ (Brentjens & de Bruyn 2005). Typical Faraday depths in the tomography studies above are a few to a few tens of rad m^{-2}, while objects like SNRs or PWNe show Faraday depths up to a few hundred rad m^{-2}. Therefore, a Faraday tomography survey

[5]For an extended explanation, see Heald et al. (2015).

PoS(AASKA14)096

needs high Faraday depth resolution and capability to observe Faraday thick structures (up to $\sim$ 100 rad m^2), necessitating broad frequency coverage at relatively low frequencies (< 1 GHz).

The broad frequency coverage needed for Faraday tomography is a key aspect for the broadband polarimetry project described by Gaensler et al. (2015). Even though their science goals focus on Faraday tomography of extragalactic radio sources themselves, the data can be taken commensally for the two projects. The parameters needed for their survey match well with the Galactic science goals described here.

3.2 Prospects for SKA1-Early Science

For the SKA1 Early Science phase, we intend to use the results from a combined all-sky polarimetric survey with SKA1-SUR Band 2 with the ASKAP-POSSUM survey (Gaensler et al. 2010) as proposed by Gaensler et al. (2015). These combined data would have continuous frequency coverage from 700 MHz to 1500 MHz, which translates into a maximum detectable Faraday thickness $\Delta\phi_{\rm max} \approx 80$ rad m^{-2} and a Faraday depth resolution $\delta\phi = 24$ rad m^{-2}.

For studies of the ordered and random components of the Galactic magnetic field, the Faraday depth resolution of this Early Science survey is too low, although analysis techniques like QU-fitting (O'Sullivan et al. 2012) can increase the Faraday depth resolution significantly.

However, this survey is well suited to study discrete objects like SNRs, which have higher observed RMs. In research on SNRs and other discrete objects, the SKA Pathfinders will already make big advances, given their ability to image SNRs at the other side of the Galaxy ($10''$ resolution at a distance of 15 kpc gives a physical resolution of 1 pc). This will allow some sense of magnetic field strength in these objects.

However, the proposed combined SKA1 Early Science polarimetric survey will be able to *map* magnetic field strengths in SNRs. This will increase the number of SNRs with known magnetic field structure by orders of magnitude, finally making statistical studies of SNR magnetic fields possible. Faraday depths within a SNR have been found to vary by $100 - 200$ rad m^{-2} (Uyaniker et al. 2002; Harvey-Smith et al. 2010). If these Faraday thick components are uniform, this survey will not be able to detect them. However, the Faraday depth maps show ample small-scale structure, making it plausible that a large part of the Faraday depth can be detected. Any missing large-scale Faraday depth may be estimated from the RM Grid. Assuming that we want to probe such a SNR in 10 Faraday depth slices, the proposed survey's sensitivity of ~ 7 μJy bm^{-1} at a resolution of $10''$ will increase the number of SNRs for which we have magnetic field measurements from a few to a few hundred[6].

3.3 Prospects for SKA1

With the increased sensitivity of SKA1 with respect to the Early Science phase, weaker magnetic fields will become visible, such as the interstellar magnetic fields in the Galactic plane and halo, using both broadband polarimetry of diffuse emission and Faraday tomography. Again we suggest to commensally use the proposed Broadband Polarimetry Survey for SKA1 (Gaensler et

[6]Compare to current capabilities of e.g. the Canadian Galactic Plane Survey SNR catalog (Kothes et al. 2006), where 24 SNRs were detected in polarization (single channel) at 1420 MHz, over 110° of the outer Galactic plane, with a sensitivity of $\sim$ 5mJy bm^{-1}.

PoS(AASKA14)096

al. 2015), which will have full frequency coverage over a range of $650-1750$ MHz at $1''$ resolution (ten times the resolution at Early Science) over the whole sky down to a sensitivity of $\sim 5\ \mu$Jy bm^{-1}. The high resolution and sensitivity can be used to unveil the non-thermal emission in star forming regions, and probe SNRs and HII regions to larger distances.

However, detailed mapping of the interstellar magnetic field will need coverage at lower frequencies to obtain sufficient Faraday depth resolution. Assuming that Band 1 will be available for SKA1-SUR, an all-sky survey in the $350-650$ MHz range to complement the SKA1-Early Science survey is needed to provide a Faraday depth resolution of $\delta\phi = 5$ rad m^{-2}. As detailed in Figure 7 in Braun (2013), a $10''$-resolution all-sky survey down to $\sim 7.6\ \mu$Jy bm^{-1} across $350-650$ MHz would imply 2 full years of observing time. Therefore, obtaining these low frequencies down to the sensitivity of the proposed SKA1-SUR Band 2 survey would be better as a SKA2 project (see below).

Galactic magnetic fields In order to assess the possibilities of observing Galactic turbulent magnetic fields with SKA, simulations of high-resolution SKA observations were made of total intensity and polarized Galactic emission in various directions of the sky within the SKADS program (Sun & Reich 2009). Based on realistic Galactic 3D-models of the distribution of thermal electrons, cosmic-ray electrons, and magnetic fields (Sun et al. 2008), $1.6''$ resolution maps at 1.4 GHz for total and polarized intensities and RMs were calculated, similar to the proposed survey above. The extent of diffuse structures depends on the outer scale of the assumed Kolmogorov spectrum for the turbulent magnetic field, the length of the line-of-sight through the Galaxy and also the regular magnetic field. These studies show that even at high latitudes, Galactic total and polarized emission is highly structured at arcsec resolution and must be separated from sensitive SKA maps of extended extragalactic objects in an appropriate way.

Studies of magneto-ionized turbulence through SFs will benefit greatly from a tight RM Grid as provided by SKA1. A grid with 1000 sources per square degree could unveil the second-order SF down to arcmin scales. The survey capability allows us to make the first detailed all-sky map of the energy injection scale, in order to reveal the origins of driving forces. Moreover, a large number of sources with small RM errors (e.g. < 1 rad/m^2) allows us to derive higher-order SFs. Higher-order SFs provide further valuable information of turbulence, e.g. the trend of SF slopes to higher order depends on the characteristics of turbulence.

SKA1 pulsar studies will detect many more pulsars, including more DM measurements and reliable distances. The right hand plot in figure 1 shows the wavelet transform result of a test function representing electron density is obtained using a simulated pulsar data set of 2000 pulsars expected to be detected by SKA1 (R. Smits, priv. comm.). It is obvious from this plot that this method promises major progress in the unraveling of the large-scale structure of the Galactic magnetic field.

Supernova remnants With SKA1, the RM Grid will provide one source every few arcminutes. This means that we will be able to roughly probe the magnetic field of virtually every SNR in the Galaxy using the grid. Faraday tomography with SKA1-LOW/SKA1-SUR Band 1 will delineate magnetic fields in the SNR shell in 3D in pointed observations of individual target sources. Statistical samples of magnetic field structure in HII regions, PWNe, Planetary Nebulae can be built

PoS(AASKA14)096

up with these data. Also, SKA1-LOW will enable a full magnetic field survey of nearby SNRs, but not until the enhanced sensitivity of SKA2 will we be able to probe magnetic fields in SNRs throughout the Milky Way in this way.

Star forming regions The high resolution of the SKA1 survey mentioned above can be used to unveil the non-thermal emission in star forming regions, reconciling the wider Galactic magnetic field with MHD models of star formation, protostellar accretion, disk coupling and jet launching. Emission is likely to be present at ~ 50 μJy at 1000 MHz, with a spectral index of -1 (Ainsworth et al. 2014), i.e. a 10σ detection. SKA1-MID can be used for follow-up to obtain the spectrum. Using the SKA1-MID sensitivity of 63 μJy hr$^{-1/2}$ over a 100 kHz band, a spectrum with a 3σ detection at 1 GHz over 10 MHz channels can be obtained in 30 mins per source. To date, two YSO jets have been detected in pointed observations (Ray et al. 1997; Carrasco-González et al. 2010), making it impossible to estimate reliable detection rates at the moment. We assume that we will be able to inspect the nearest star formation regions in total intensity with SKA1. Even a detection of a handful of YSO jets will make a large impact on the source sample.

Galactic Center The dense SKA1 RM Grid will allow unprecedented modeling of the structure and strength of the magnetic field in the GC, resolving the tension in the findings described in Section 2.3. In particular, detection of 15,000 new pulsars with measured RMs will allow us to understand the overall structure of the GC magnetic field (i.e., is it toroidal? Poloidal?) in a comprehensive manner, and how this connects to the overall Galactic magnetic field structure. Higher-order SFs will become possible due to the high source density in the SKA RM Grid, which will enable determination of hereto elusive properties of interstellar turbulence such as intermittency. The RM Grid will identify Faraday screens and clarify their role in the ISM and hopefully also their origin.

3.4 Prospects for SKA2

A tenfold increase in sensitivity of SKA2 at frequencies from 350 MHz to 24 GHz will allow extension of the all-sky broadband polarimetric survey at high sensitivity down to lower frequencies. This will make a Faraday tomography all-sky map of magnetized turbulence possible, allowing not only to fully characterize these Galactic magnetic fields, but also to describe in detail polarized foregrounds for various cosmological research areas such as the Epoch of Reionization. Also, this increase in sensitivity for SKA2 will enable larger samples of YSO's, making statistical studies possible, and detection of linear polarization, adding information on the orientation and ordering of the field. Finally, Faraday tomography for SNRs throughout the Milky Way can be done, giving a complete sample of 3D magnetic field structure in SNRs throughout the Milky Way.

For the RM Grid, SKA2 will provide us with accurate distances for just about any detectable pulsar in the Milky Way. The large increase of reliable pulsar RMs and distances will finally allow resolution of the issue of number and location of large-scale reversals in the Milky Way, thanks to the accurate parallax distances measured throughout a major part of the Galaxy. Wavelet analysis as in Stepanov et al. (2002) will be possible (a) for the entire Galaxy, and (b) down to scales of about 100 pc, which is comparable to some current estimates of the turbulence injection scale.

Additionally, the SKA2 phase will also allow a high angular and λ^2-space resolution observation of non-thermal radio filaments in the GC such as the Radio Arc, which possesses RMs of

PoS(AASKA14)096

$\sim -3 \times 10^3$ rad m^2 (Yusef-Zadeh et al. 1987) – some of the highest known in our Galaxy – which will allow a detailed modeling of their origin, as well as discovery of numerous others at lower surface brightness.

References

Ainsworth, R. E., Scaife, A. M. M., Ray, T. P., et al. 2014, ApJL, 792, 18
Akahori T., Ryu D., Kim J., & Gaensler B. M. 2013, ApJ, 767, 150
Armstrong, J. W., Rickett, B. J., & Spangler, S. R. 1995, ApJ, 443, 209
Arzoumanian, Z., Safi-Harb, S., Landecker, T. L., Kothes, R., & Camilo, F. 2008, ApJ, 687, 505
Arzoumanian, Z., Gotthelf, E. V., Ransom, S. M., et al. 2011, ApJ, 739, 39
Beck, R., & Gaensler, B. M. 2004, NAR, 48, 1289
Beck, R., Bomans, D., Colafrancesco, S., et al. 2015, "Structure, dynamical impact and origin of magnetic fields in nearby galaxies in the SKA era" in proc. *Advancing Astrophysics with the Square Kilometre Array*, PoS(AASKA15)094
Blandford & Payne, 1982, MNRAS, 199, 883
Blasi, P. 2013, A&AR, 21, 70
Braun, R. "SKA1 Imaging Science Performance", Document number SKA-TEL-SKO-DD-XXX Revision A Draft 2
Brentjens, M. A., & de Bruyn, A. G. 2005, A&A, 441, 1217
Brentjens, M. A. 2011, A&A, 526, A9
Brown, J. C., Haverkorn, M., Gaensler, B. M., et al. 2007, ApJ, 663, 258
Burkhart, B., Lazarian, A., & Gaensler, B. M. 2012, ApJ, 749, 145
Carrasco-González, C., Rodríguez, L. F., Anglada, G., et al. 2010, Science 330, 1209
Carretti, E., Crocker, R. M., Staveley-Smith, L., et al. 2013, Nat, 493, 66
Carretti, E. et al, in preparation
Chevalier, R. A. 2000, ApJL, 539, L45
Chuss, D. T., Davidson, J. A., Dotson, J. L., et al. 2003, ApJ, 599, 1116
Donnert, J., Dolag, K., Lesch, H., et al. 2009, MNRAS, 392, 1008
Crocker, R. M., 2013, ASSP, 34, 397
Crocker, R. M., & Aharonian, F., 2011, Physical Review Letters, 106, 101102
Crocker, R. M., Jones, D. I., Aharonian, F., et al. 2011, MNRAS, 413, 763
Crocker, R. M., Jones, D. I., Melia, F., et al., 2010, Nature, 463, 65
Crutcher, R. M., Roberts, D. A., Mehringer, D. M., et al. 1996, ApJL, 462, L79
De Bruyn, A.G., Pizzo, R., 2014 A&A, in press
de la Chevrotière, A., St-Louis, N., Moffat, A. F. J., & the MiMeS Collaboration 2014, ApJ, 781, 73
Eatough, R. P., Falcke, H., Karuppusamy, R., et al. 2013, Nat, 501, 391
Elmegreen, B. G., & Scalo, J. 2004, ARA&A, 42, 211
Ferreira, J., Dougados, C., & Cabrit, S. 2006, A&A, 453, 785
Ferrière, K., & Schmitt, D. 2000, A&A, 358, 125
Ferrière, K. 2007, EAS Publications Series, 23, 3
Ferrière, K. 2009, A&A, 505, 1183

PoS(AASKA14)096

Ferrière, K., & Terral, P. 2014, A&A, 561, A100
Fish, V. L., Reid, M. J., Argon, A. L., et al. 2003, ApJ, 596, 328
Fletcher, A., Beck, R., Shukurov, A., et al. 2011, MNRAS, 412, 2396
Frick, P., Stepanov, R., Shukurov, A., et al. 2001, MNRAS, 325, 649
Gaensler, B. M. 1998, ApJ, 493, 781
Gaensler, B. M., Landecker, T. L., Taylor, A. R., & POSSUM Collaboration 2010, Bulletin of the American Astronomical Society, 42, #470.13
Gaensler, B. M., Haverkorn, M., Burkhart, B., et al. 2011, Nature, 478, 214
Gaensler. B., Agudo, I., Akahori, T. et al. 2015, "Broadband Polarimetry with the Square Kilometre Array: A Unique Astrophysical Probe" in proc. *Advancing Astrophysics with the Square Kilometre Array*, PoS(AASKA15)103
Gelfand, J., Breton, R., Ng, C. U. et al. 2015, "Pulsar Wind Nebulae in the SKA era" in proc. *Advancing Astrophysics with the Square Kilometre Array*, PoS(AASKA15)046
Gao, X. Y., Reich, W., Han, J. L., et al. 2010, A&A, 515, A64
Govoni, F., Johnston-Hollitt, M., Agudo, I., et al., 2014, Cosmic Magnetism Science in the SKA1 Era, summary of the Cosmic Magnetism Assessment Workshop
Gray, A. D., Landecker, T. L., Dewdney, P. E., et al. 1998, Nat, 393, 660
Green, J. A., McClure-Griffiths, N. M., Caswell, J. L., et al. 2012, MNRAS, 425, 2530
Han, J.L., Van Straten, W., Lazio, T.J.W. et al., 2015, "Three-dimensional Tomography of the Galactic and Extragalactic Magnetoionic Medium with the SKA" in proc. *Advancing Astrophysics with the Square Kilometre Array*, PoS(AASKA15)041
Han, J. L., Manchester, R. N., Lyne, A. G., et al. 2006, ApJ, 642, 868
Han, J. L., & Zhang, J. S. 2007, A&A, 464, 609
Hanasz, M., Wóltański, D., & Kowalik, K. 2009, ApJL, 706, L155
Hanayama, H., Takahashi, K., Kotake, K., et al. 2005, ApJ, 633, 941
Harvey-Smith, L., Gaensler, B. M., Kothes, R., et al. 2010, ApJ, 712, 1157
Harvey-Smith, L., Madsen, G. J., & Gaensler, B. M. 2011, ApJ, 736, 83
Haverkorn, M., Katgert, P., & de Bruyn, A. G. 2003, A&A, 404, 233
Haverkorn, M., Gaensler, B. M., McClure-Griffiths, N. M., et al. 2006, ApJS, 167, 230
Haverkorn, M., Gaensler, B. M., Brown, J. C., et al. 2006, ApJL, 637, L33
Haverkorn, M., Brown, J. C., Gaensler, B. M., et al. 2008, ApJ, 680, 362
Haverkorn, M., 2014, in “Magnetic Fields in Diffuse Media”, eds E. Gouveia dal Pino and A. Lazarian, Springer, arXiv:1406.0283
Heald, G., Beck, R., de Blok, E., et al., 2015, "Magnetic Field Tomography in Nearby Galaxies with the Square Kilometre Array" in proc. *Advancing Astrophysics with the Square Kilometre Array*, PoS(AASKA15)106
Iacobelli, M., Haverkorn, M., & Katgert, P. 2013, A&A, 549, A56
Iacobelli, M., Burkhart, B., Haverkorn, M., et al. 2014, A&A, 566, 5
Jansson, R., & Farrar, G. R. 2012, ApJ, 757, 14
Jelić, V., de Bruyn, A. G., Mevius, M., et al. 2014 A&A, 568, 101
Johnston-Hollitt, M., et al., 2015, "Using SKA Rotation Measures to Reveal the Mysteries of the Magnetised Universe" in proc. *Advancing Astrophysics with the Square Kilometre Array*, PoS(AASKA15)092

PoS(AASKA14)096

Jones, D. I., Crocker, R., M., Reich, W., et al., 2012, ApJ, 747, 12.
Killeen, N. E. B., Lo, K. Y., et al. 1992, ApJ, 385, 585
Kothes, R., & Brown, J.-A. 2009, IAU Symposium, 259, 75
Kothes, R., Fedotov, K., Foster, T. J., et al. 2006, A&A, 457, 1081
Kothes, R., Landecker, T. L., Reich, W., et al. 2008, ApJ, 687, 516
Kramer, M. & Stappers, B., 2015, "An overview of pulsar science with the SKA" in proc. *Advancing Astrophysics with the Square Kilometre Array*, PoS(AASKA15)036
Landecker, T. L., Reich, W., Reid, R. ., et al. 2010, A&A, 520, A80
Law, C. J., Brentjens, M. A. & Novak, G., 2011 ApJ, 731, 36
Lazar, M., Schlickeiser, R., Wielebinski, R., & Poedts, S. 2009, ApJ, 693, 1133
Lazaryan, A. L., & Shutenkov, V. P. 1990, Soviet Astronomy Letters, 16, 297
Livio, 2011, American Institute of Physics Conference Series, J. E. McEnery, J. L. Racusin, N. Gehrels, eds. (2011), 1358, 329
Machida, M., Nakamura, K., Kudo, T., et al. 2013, ApJ, 764, 81
Malkov M. A., Diamond P. H., Drury L., et al. 2010, ApJ 721, 750
Mao, S. A., Gaensler, B. M., Haverkorn, M., et al. 2010, ApJ, 714, 1170
Mao, S. A., McClure-Griffiths, N. M., Gaensler, B. M., et al. 2012, ApJ, 755, 21
Men, H., Ferrière, K., & Han, J. L. 2008, A&A, 486, 819
Moss, D., & Sokoloff, D. 2008, A&A, 487, 197
Moss, D., Sokoloff, D., Beck, R., et al. 2010, A&A, 512, A61
Moss, D., Stepanov, R., Arshakian, T. G., et al. 2012, A&A, 537, A68
Nota, T., & Katgert, P. 2010, A&A, 513, A65
Novak, G., Chuss, D. T., Renbarger, T., et al. 2003, ApJL, 583, L83
Oppermann, N., Junklewitz, H., Robbers, G., et al. 2012, A&A, 542, A93
Orlando & Strong, 2013, Nuclear Physics B Proceedings Supplements 239, 64
O'Sullivan, S. P., Brown, S., Robishaw, T., et al. 2012, MNRAS, 421, 3300
Pacini, F., & Salvati, M. 1973, ApJ, 186, 249
Ransom, R. R., Uyaniker, B., Kothes, R., et al. 2008, ApJ, 684, 1009
Ransom, R. R., Kothes, R., Wolleben, M., et al. 2010, ApJ, 724, 946
Ray, 2009, Revista Mexicana de Astronomia y Astrofisica Conference Series, 36, 179
Ray, T. P., Muxlow, T. W. B., Axon, D. J., et al. 1997, Nature 385, 415
Reich, W., Fürst, E., Reich, P., et al. 2004, The Magnetized Interstellar Medium, 45
Reynolds, S. P., Gaensler, B. M., & Bocchino, F. 2012, SSR, 166, 231
Robishaw, T., Green, J., Surcis, G., et al. 2015, "Measuring Magnetic Fields Near and Far with the SKA via the Zeeman Effect" in proc. *Advancing Astrophysics with the Square Kilometre Array*, PoS(AASKA15)110
Roy, S., Pramesh Rao, A., & Subrahmanyan, R., 2005, MNRAS, 360, 1305.
Roy, S., Pramesh Rao, A., & Subrahmanyan, R., 2008, A&A, 478, 435.
Ruzmaikin, A., Sokolov, D., & Shukurov, A. 1988, Nat, 336, 341
Schlickeiser, R., & Felten, T. 2013, ApJ, 778, 39
Schnitzeler, D. H. F. M., Katgert, P., & de Bruyn, A. G. 2007, A&A, 471, L21
Schnitzeler, D. H. F. M. 2010, MNRAS, 409, L99
Simard-Normandin, M., & Kronberg, P. P. 1980, ApJ, 242, 74

PoS(AASKA14)096

Smits, R., Stappers, B., Kramer, M., Karastergiou, A. 2011a, “Pulsar Survey with SKA Phase I”, Document number WP2-040.030.010-TD-003
Smits, R., Tingay, S. J., Wex, et al. 2011b, A&A, 528, 108
Sofue, Y., Machida, M., & Kudoh, T. 2010, PASJ, 62, 1191
Sokoloff, D.D., Shukurov, A. 1990, Nat, 347, 51
Stil, J., Wityk, N., Ouyed, R., et al. 2009, ApJ, 701, 330
Stil, J. M., Taylor, A. R., & Sunstrum, C. 2011, ApJ, 726, 4
Stepanov, R., Frick, P., Shukurov, A., et al. 2002, A&A, 391, 361
Su, M., Slatyer, T., & Finkbeiner, D., 2010, ApJ, 724, 1044
Sun, X. H., Han, J. L., Reich, W., et al. 2007, A&A, 463, 993
Sun, X. H., Reich, W., Waelkens, A., et al. 2008, A&A, 477, 573
Sun, X. H., & Reich, W. 2009, A&A, 507, 1087
Sun, X.-H., & Reich, W. 2010, Research in Astronomy and Astrophysics, 10, 1287
Taylor, A. R., Stil, J. M., & Sunstrum, C. 2009, ApJ, 702, 1230
Taylor, A. R., & Salter, C. J. 2010, Astronomical Society of the Pacific Conference Series, 438, 402
Uyaniker, B., Kothes, R., & Brunt, C. M. 2002, ApJ, 565, 1022
Van Eck, C. L., Brown, J. C., Stil, J. M., et al. 2011, ApJ, 728, 97
Wang, L., XiaoHong, C., Hui, Z., et al., 2015, "Investigations of supernovae and supernova remnants in the era of SKA" in proc. *Advancing Astrophysics with the Square Kilometre Array*, PoS(AASKA15)064
Widrow, L. M. 2002, Reviews of Modern Physics, 74, 775
Wolleben, M., & Reich, W. 2004, A&A, 427, 537
Wolleben, M., Landecker, T. L., Carretti, E., et al. 2009, IAU Symposium, 259, 89
Wolleben, M., Fletcher, A., Landecker, T. L., et al. 2010, ApJL, 724, L48
Yusef-Zadeh, F., & Morris, M., 1987, ApJ, 322, 721.

PoS(AASKA14)096

PROCEEDINGS OF SCIENCE

Filaments of the radio cosmic web: opportunities and challenges for SKA

Franco Vazza[*1,2], **Chiara Ferrari**[3], **Annalisa Bonafede**[1], **Marcus Brüggen**[1], **Claudio Gheller**[4], **Robert Braun**[5], **Shea Brown**[6]

[1]*Hamburg University (Hamburg Observatory), Gojenbergsweg 112, 21029, Germany;* [2]*INAF, Istitutio di Radioastronomia, via Gobetti 101, 40131, Bologna, Italy;* [3]*Observatoire de la Côte d'Azur, Boulevard de l'Observatoire, B.P. 4229, 06304 Nice, France;* [4]*CSCS, Via Trevano 131, CH-6900 Lugano, Switzerland;* [5]*SKA Organisation, Jodrell Bank Observatory, Macclesfield, Cheshire SK11 9DL, UK;* [6]*Department of Physics and Astronomy, University of Iowa, 203 Van Allen Hall, Iowa City, USA*

E-mail: franco.vazza@hs.uni-hamburg.de

Abstract The detection of the diffuse gas component of the cosmic web remains a formidable challenge. In this work we study synchrotron emission from the cosmic web with simulated SKA1 observations, which can represent an fundamental probe of the warm-hot intergalactic medium. We investigate radio emission originated by relativistic electrons accelerated by shocks surrounding cosmic filaments, assuming diffusive shock acceleration and as a function of the (unknown) large-scale magnetic fields. The detection of the brightest parts of large ($>$ 10Mpc) filaments of the cosmic web should be within reach of the SKA1-LOW, if the magnetic field is at the level of a $\sim$ 10 percent equipartition with the thermal gas, corresponding to $\sim 0.1 \mu G$ for the most massive filaments in simulations. In the course of a 2-years survey with SKA1-LOW, this will enable a first detection of the "tip of the iceberg" of the radio cosmic web, and allow for the use of the SKA as a powerful tool to study the origin of cosmic magnetism in large-scale structures. On the other hand, the SKA1-MID and SKA1-SUR seem less suited for this science case at low redshift ($z \leq 0.4$), owing to the missing short baselines and the consequent lack of signal from the large-scale brightness fluctuations associated with the filaments. In this case only very long exposures ($\sim$ 1000 hr) may enable the detection of $\sim 1-2$ filament for field of view in the SKA1-SUR.

Advancing Astrophysics with the Square Kilometre Array
June 8-13, 2014
Giardini Naxos, Italy

[*]Speaker.

PoS(AASKA14)097

1. Introduction

The Large-Scale Structure in the Universe comprises a complex network of filaments connecting virialized structures and separated by voids. *Mildly nonlinear* structures such as sheets and filaments should contain a wealth of information on the emergence of cosmic structures as individually recognizable objects (e.g. galaxy groups and galaxy clusters). The observational detection of the *warm-hot intergalactic medium* associated with filaments is still challenging, and only a few works claimed a detection in X-rays (e.g. Richter et al. 2008), or more recently with the Sunyaev Zeldovich effect (Planck Collaboration et al. 2013). In the radio waveband, a few cases of radio emission at the possible crossroad of cosmic filaments have been reported (Bagchi et al. 2002; Kronberg et al. 2007; Pizzo et al. 2008; Giovannini et al. 2010; Farnsworth et al. 2013; Giovannini et al. 2015). However, such sources are likely to trace merger shocks in a filamentary environment, rather than *stationary accretion shocks* surrounding filaments. Numerical simulations suggest that filaments are surrounded by nearly stationary accretion shocks ($M \geq 10$), where the baryonic gas is shock-heated for the first time (Ryu et al. 2003; Vazza et al. 2011), and the detection of these shocks would confirm a critical piece of the warm-hot intergalactic medium (WHIM) paradigm (e.g. Davé et al. 2001). The expectations on the magnetic fields are more uncertain and lie in the range of $\sim 1\mathrm{nG} - 0.1\mu\mathrm{G}$, depending on numerical resolution of the cosmological simulation and as well as on the assumed seeding scenario (e.g. Dolag et al. 2008; Ryu et al. 2008; Donnert et al. 2009; Vazza et al. 2014a). Provided that diffusive shock acceleration (see below) and large enough magnetic fields are present in filaments, the SKA could make the first detection of the cosmic web in the radio window (Keshet et al. 2004; Brown 2011; Araya-Melo et al. 2012).

2. Simulated emission

In Vazza et al. (2014b) we produced large cosmological simulations with grid code ENZO (Bryan et al. 2014), designed to study the dynamic properties of cosmic rays (CR) accelerated by cosmological shock waves. Here we mostly focus on a very large filament in our simulated volume, about ~ 20Mpc in length and connecting two galaxy clusters (Fig.1). Given the size of this object, it gives us a first gross estimate of the chances of detecting filaments with the SKA1. Our forecasts of radio emission include two mechanisms: a) primary electron emission from relativistic electrons accelerated at shocks, assuming efficient diffusive shock acceleration (DSA, same model as in Hoeft & Brüggen 2007, Eq. 32); b) secondary electron emission from the relativistic electrons continuously injected by hadronic collisions in the filament volume (Dolag & Enßlin 2000), which are a by-product of our simulations (Vazza et al. 2014b). In general, the contribution from secondary electrons is everywhere negligible, i.e. only a few percent of the primary emission.
The two main unknowns here are the electron acceleration efficiency at shocks (ξ_e) and the magnetic field within the filament (B); a discussion on these assumptions is given in Sec.4. The emitted radio power per frequency, ν, scales as $I_\nu \propto S \cdot n \cdot \xi_e \cdot \nu^{-\delta/2} \cdot T^{3/2} \frac{B^{1+\delta/2}}{(B^2_{\rm CMB}+B^2)}$ (where n and T are the post-shock density/temperature, S is the shock surface, and δ is the slope of the CR-electrons energy spectrum). We can expect cosmic filaments to be a sensitive probe of cosmic magnetic fields, since for shocks in filaments (where $\delta \approx 2$ and $B \ll B_{\rm CMB}$) the previous formula reduces to $I_\nu \propto \xi_e \cdot B^2$. In the following we assume $\xi_e = 10^{-4}$ and *uniform* values of $B = 0.01 - 0.3\mu G$ within

PoS(AASKA14)097

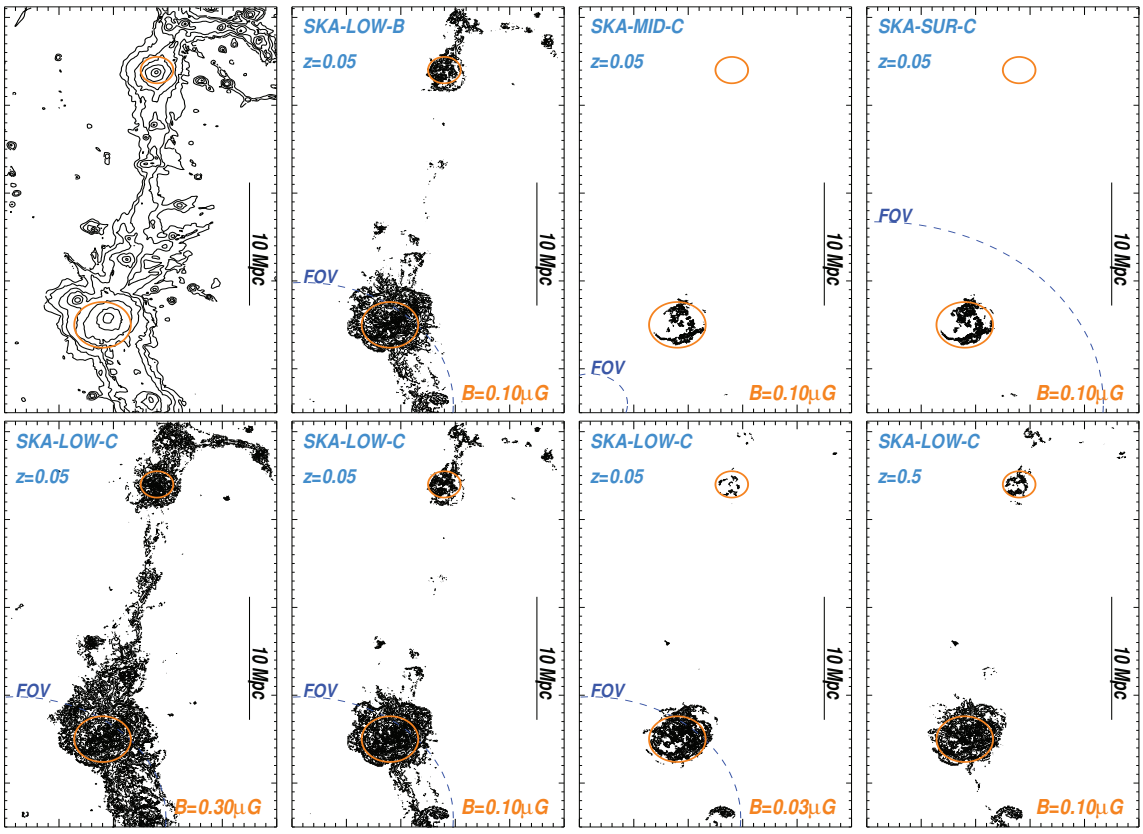

Figure 1: First panel: project gas pressure map for a massive simulated filaments . Other panels: mock radio observations with SKA1-LOW, SKA1-MID and SKA1-SUR. The top panels shows the result for $z = 0.05$ and $B = 0.1\mu G$. The lower panels are taken for the SKA1-LOW-C configuration (2 years survey at 300 MHz and shows the result for different magnetic field strengths ($B = 0.3$, 0.1 and $0.03\mu G$) or redshift ($z = 0.05$ or $z = 0.5$). The additional blue circles represent the field of view of each array (not shown if larger than the image), while the red circles show the virial radius of galaxy clusters in the image. The contours ($log_{10}[\mathrm{Jy/arcsec^2}]$) start from 3 times the nominal surface brightness (confusion) threshold for each array.

the filament volume, and compute the detectable emission by SKA1-LOW (at two frequencies), SKA1-MID and SKA1-SUR. For each array we considered different possible strategies, including long 1000 hr exposures, 2-years surveys and the adoption point source subtraction at high resolution ($\sim$ 1"), followed by tapering on point-source subtracted data (at $\sim$ 10") to have a reduced resolution (Table 1), since spatial-scale smoothing of the point-source subtracted data could significantly increase the signal-to-noise of the diffuse emission, though the power of identifying individual shock-structures would be lost (Brown 2011). For the SKA1-LOW observations we considered two possible central frequencies (110 and 300 MHz) and computed the confusion noise assuming a spectral index of -0.7, at full resolution. In the case of SKA1-MID and SKA1-SUR, we produced forecasts for a 1000 hr exposure or a 2 years survey. In all images we started from the full emission map obtained from the cosmological simulation, and then selected the specific frequency, field of view (FOV), resolution and sensitivity expected for each observation strategy, based on the SKA1

PoS(AASKA14)097

Table 1: Parameters for the investigated SKA1 arrays and imaging strategies, based on the SKA1 Baseline Design and on the SKA Phase 1 Performance Memo. For the tapering cases, we considered a point source subtraction at ~ 1", followed by tapering on point-source subtracted data at ~ 10". The sensitivities are expressed both as a function of the beam (1) and of the sky area (2); in the case of SKA1-LOW the sensitivity is set by the confusion noise, as in SKA Phase 1 Performance Memo by assuming a spectral index of -0.7.. For the SKA1-SUR and SKA1-MID we have considered a 30 percent fractional bandwidth for a 2 years all-sky survey, while for the SKA1-LOW we have considered an all-sky survey down to confusion noise, estimated from the rms confusion brightness at 1.4 GHz (Condon, private communication), with a confusion noise assumed as above.

array	configuration/strategy	frequency [MHz]	beam size [arcsec]	field of view [degrees^2]	min. baseline [m]	sensitivity 1 [μJy/beam]	sensitivity 2 [μJy/arcsec^2]
SKA-LOW-A	full.res+conf., survey	110	6	8	45	5.5	0.134
SKA-LOW-B	full.res+conf,1000 hr	300	3	8	45	0.5	0.0490
SKA-LOW-C	full.res+conf., 2 years	300	10	8	45	9	0.0794
SKA-MID-A	1000hr	1400	0.5	0.49	15	0.09	0.317
SKA-MID-B	2 years	1400	0.5	0.49	15	5.8	20.475
SKA-MID-C	1000 hr+tapering	1400	10	0.49	15	0.14	0.001
SKA-MID-D	2 years+tapering	1400	10	0.49	15	8.8	0.077
SKA-SUR-A	1000hr	1200	1.0	18	15	0.4	0.353
SKA-SUR-B	2years	1200	1.0	18	15	3.8	3.353
SKA-SUR-C	1000hr+tapering	1200	10	18	15	0.5	0.004
SKA-SUR-D	2years+tapering	1200	10	18	15	4.9	0.043

Baseline Design of March 2013 and on the SKA Phase 1 Performance Memo. In addition, we FFT-transformed all images and removed spatial frequencies smaller than the minimum baseline of each configuration, in the Fourier domain, so that the structures with a too large angular scale compared to the chosen array are removed. In all cases, we implicitly assume a perfect removal of the Milky Way foreground.

3. Results

Figure 1 shows a representative set of mock observations with various array configurations of the SKA Phase 1. The top panels, show the performances of the arrays in "deep exposure" mode (1000 hr), for a redshift $z = 0.05$ and assuming $B = 0.1\ \mu G$ [1]. The SKA1-LOW-B array should detect at least a significant portion of the filament at 3σ, and trace some of the brightest emission knots connecting the two clusters in the field, as well as the big filamentary accretion southwards of the most massive cluster, reaching out to ~ 5 Mpc from the virial cluster volume. Instead, with the SKA1-MID and SKA1-SUR arrays the detection of the filament will be impossible even with a 1000 hr pointed observation, because of the smaller sensitivity and the lack of short baselines (at least the central frequencies of 1.4 and 1.2 GHz assumed here). The situation gets even worse by considering the shallower sensitivity reached in the 2-year survey. However, even with the SKA1-LOW the extended emission from the filament connecting the two clusters would be barely

[1] We remark that in this test we are only concerned with the possible emission from the WHIM from the filament, and that this emission model is likely overestimating the radio emission within cluster (e.g. radio relic emission), because of the assumed *constant* electron acceleration efficiency and magnetic fields.

PoS(AASKA14)097

detectable in its entire extent only for a higher magnetic field, e.g. $B = 0.3\mu G$. A non-detection of such structures at low redshift with the SKA1-LOW, would place robust upper-limits on the value of the intergalactic magnetic fields, of the order of $\leq 0.03\mu G$, giving us important cluse on the efficiency of magnetic field amplifications in the WHIM. At larger redshifts ($z \geq 0.1$), the cosmological dimming makes the detection impossible, and also the removal of the contribution from single radio galaxies becomes challenging.

In order to better quantify the detectability of the simulated filament in the different arrays and using different possible imaging strategies, we selected a smaller region inside the main filament (see the map in Fig.2), well outside the surrounding clusters outskirts, in order not to be contaminated by cluster accretion shocks. We computed the total area of the source region above the 3σ surface brightness level, as well as the ratio between the detectable flux and the total one from the same region, as shown in Fig.2, for $B = 0.3\mu G$ or $B = 0.1\mu G$.

If $B = 0.1\mu G$ the SKA1-LOW is the only one giving any chance of detection. Using the planned array configuration for the Phase 1 of SKA1-LOW our forecast is that $\sim 30-60$ percent of the total flux from the filament would be detectable, if most of this emission came from the brightest and densest gas knots within the filament rather than from the diffuse WHIM. With the deep exposure of SKA1-LOW at 300 MHz (case B) the percentage of detectable flux approaches to ~ 60 percent, while the detectable surface goes to ~ 5 percent of the total.

Based on the same computations, we can esimate that an increase in sensitivity of a factor $\times 3-5$ will enable a clear detection of the full emission from such filament, up to several Mpc from the cluster centre, as well as the detection of the brightest emission spots from the filament at $z = 0.5$. This will be feasible in the Phase 2 of the SKA1-LOW, since the planned $\times 20$ increase of the maximum angular resolution (down to ~ 0.15“) in the $50-350$ MHz range will lead to a great decrease of the confusion noise.

On the other hand, in the case of SKA-MID and SKA-SUR even in Phase 2 the lack of short baseline would make it impossible to detect the bulk of synchrotron emission from the largest scales in filaments at the central frequencies we studied here.

4. Discussion

The forecast of radio emission from the diluted gas of cosmic filaments strongly depends on the combined value of $\xi_e \cdot B^2$, both of which uncertain.

- *The electron acceleration efficiency*. The qualitative similarity to strong shocks in supernova remnants suggests that for the acceleration efficiency of electrons at strong shock $\xi_e \approx 10^{-4}$ can be assumed (e.g. Edmon et al. 2011). However, the extrapolation of the DSA to the plasma condition of filaments is uncertain, since a too weak degree magnetisation would inhibit the formation of the magnetic field irregularities responsible for efficient particle scattering. Recent hybrid simulations of collisionless shocks suggest that this mechanism can still operate in presence of very low magnetisation, owing to the fast development of micro-instabilities at parallel shocks (Caprioli & Spitkovsky 2014). In general, *any* detection of radio emission associated to filament shocks will inform us that DSA (or some modified version of the theory) can operate down to this low density regime ($n \leq 10^{-5}\mathrm{cm}^{-3}$), carrying

PoS(AASKA14)097

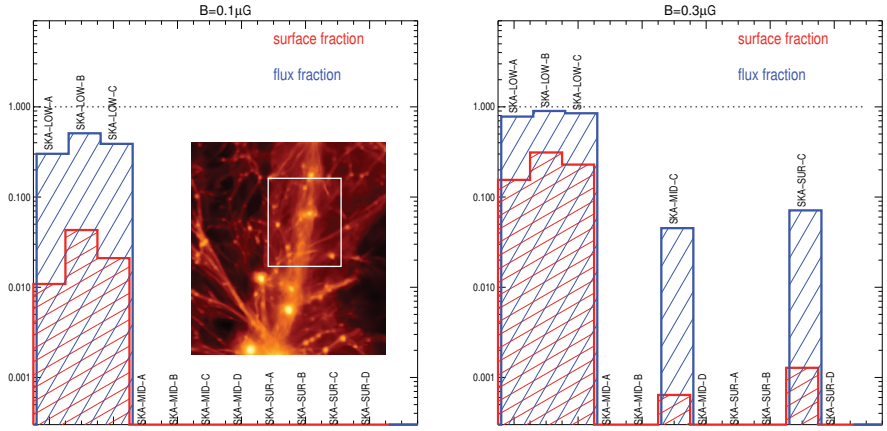

Figure 2: Fraction of the detectable area (red) and flux (blue) from the simulated filament, for $B = 0.1\mu G$ (left) and $B = 0.3\mu G$ (right). For a "detection" we considered a signal $\geq 3\sigma$, considering the sensitivites of Table 2. The inset shows the projected gas density of our filament and the selected white area used to compute the fraction of detectable radio flux.

an important theoretical information.

- *The magnetic field.* The expectations of MHD cosmological simulations lie in the range of $\sim 0.001 - 0.1\mu G$ in filaments, depending on the numerical resolution and on the seeding scenarios. In the case of the giant filament analysed in this work, a value of $B = 0.1\mu G$ correspond to a magnetic energy density at the level of ~ 10 percent of the gas energy, which seems very hardly achievable by small-scale amplification of primordial seed fields alone (Brüggen et al. 2005; Ryu et al. 2008; Vazza et al. 2014a). However, many additional astrophysical seeding scenarios of magnetic fields might add to the cosmological seed field (e.g. Donnert et al. 2009). Any detection of coherent emission on $\geq 1 - 10$ Mpc scales in filaments will rule out the scenario in which the magnetisation of filaments is driven by low-redshift seeding of magnetic fields by galactic activity, owing to the difficulty of covering such large scales with outflows or diffusion. At the same time, the detection of synchrotron from filaments at high redshift will give us important clues on the efficiency of turbulent amplification of magnetic fields over cosmological epochs.

Some insight can also be gained from the fact that no spectacular large-scale filament has been detected so far by LOFAR Cycle 0 observations. The present non-detection can be used to adjust our forecasts for SKA1. Following this conservative approach, we simulated the LOFAR LBA and HBA observations considering $\approx 8\ \mu J/\mathrm{arcsec}^2$ ($\approx 1.7\ \mu J/\mathrm{arcsec}^2$), as achieved in the current LOFAR-LBA (HBA) observations of nearby clusters, and a 23×16 arcsec^2 (6×6arcsec^2) beam [2]. In order *not* to be detected with present LOFAR Cycle 0 observations, $B \leq 0.1\ \mu G$, and we therefore assume this conservative value for the maximum magnetic field in giant filaments, provided that DSA is at work in these environments. As we have seen, even in this case the SKA1-LOW can

[2]https://www.astron.nl/radio-observatory/astronomers/array-configurations/.

PoS(AASKA14)097

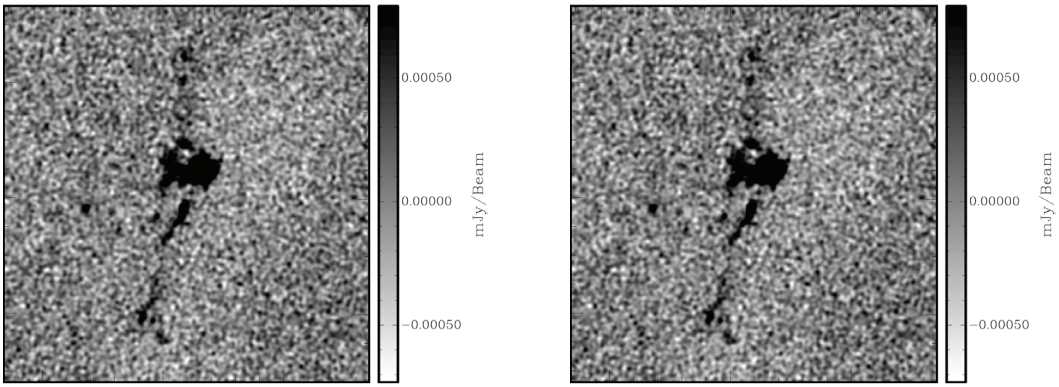

Figure 3: Mock observations ofa ≈ 5 degree area within the filament. (as in the white selection of Fig.2, assuming a distance of $z = 0.02$), using the SKA simulator: 2000 hr pointing (left) and 60 hours pointing (right) at 140 MHz with the SKA1-LOW (see text for more details).

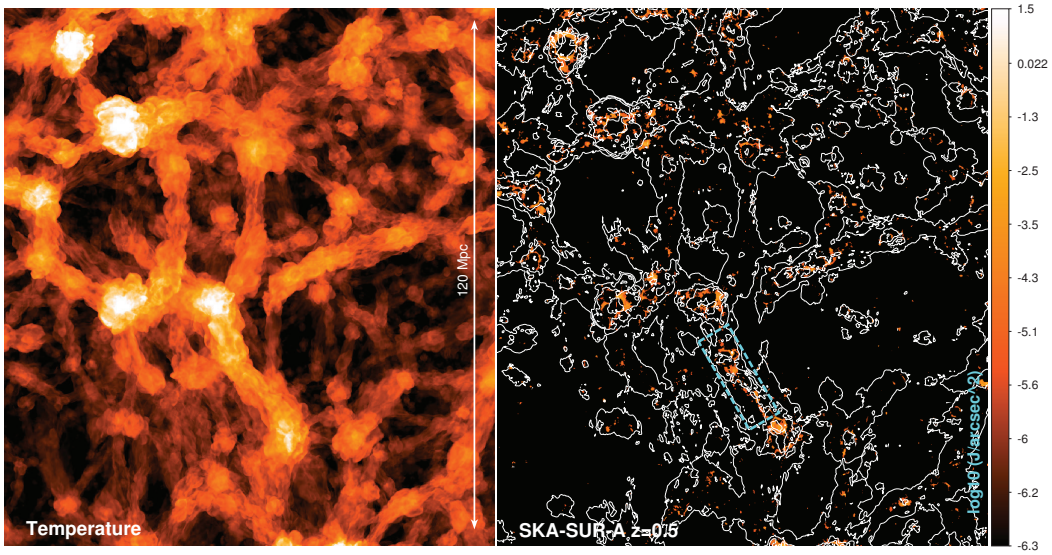

Figure 4: Left panel: projected gas temperature of a large cosmological volume at $z = 0.5$. Right panel: detectable emission by SKA1-SUR-A, using a 1000 hr exposure. The emission coming from inside the virial radius of all simulated clusters has been blanked out. The rectangular selection highlight a giant filament whose detection appears within reach.

still detect a significant portion of the filament emission for $z \leq 0.1$.

5. Conclusions

The detection of large cosmic filaments in radio at low redshift seems to be within reach by the SKA1-LOW, provided that the massive filaments are magnetised at the level of $B \sim 0.1$ μG ($\sim 1-10$ percent of equipartition with the thermal gas energy) and that DSA is at work in the

PoS(AASKA14)097

tenous WHIM environment. The SKA1-LOW is always favoured because of its better sensitivity and sampling of short baselines compared to SKA1-MID and SKA1-SUR. In particular, the SKA1-LOW should be able to detect a significant portion of filament emission at low redshifts ($z \leq 0.1$), while for a better imaging of their full extent or for their detection up to $z = 0.5$ (or for lower magnetic fields) its sensitivity should be improved by a factor $\sim 3-5$. This can be achieved during the Phase 2 of SKA-LOW, thanks to the planned increased in the maximum angular resolution, which will enable to beat the confusion noise. On the other hand, our tests show that for most of cosmic filaments in the nearby ($z \leq 0.1$) Universe a detection with SKA1-MID or SKA1-SUR is made impossible by the lack of short baselines, for which even Phase 2 will not be beneficial.

This work represents just a first step towards the realistic modelling of radio imaging of the cosmic web with the SKA1 and the SKA2. Our schematic procedure of removing the missing baselines in the the Fourier plane is a very crude estimate of the actual UV coverage, and the effect of noise, confusion, finite bandwith etc. are not yet properly accounted for. In order to fill this gap, we produced a first set of simulated observations of our models with the most updated version of the simulated SKA performance [3]. In Figure 3 we present single pointing images at 140 MHz of a ≈ 5 degree field of view centred on the faint filament region at $z = 0.02$ selected in Fig.2, for the $B = 0.1$ μG case. For the central image we used a 2000 hours of integration to achieve ≈ 220 nJy/beam with 30 percent fractional bandwidth, while for the right image we simulated a 60 hour integration, achieving ≈ 1.3 μJy/beam (in both cases using a 300 arcsec beam). The trends we recover with the use of the sophisticated tool provided by the SKA simulator overall agree with our previous estimates: while in a shallow survey mode only the brightest density peaks inside the filament can be marginally detected, the deep integration is able to pinpoint also the faint elongated structure of the filament, thereby suggesting its large-scale orientation and the presence of accretion shocks along several Mpc.

Future deep exposures will also enhance the statistical chance of detecting even more massive filaments in large areas of the sky, not only with the SKA1-LOW if the targets are distant enough to have a sufficient baseline sampling even at higher frequencies. Figure 4 shows a test where we used a large simulated volume of $(150^3 \mathrm{Mpc}^3)$ (using 1024^3 cells) and simulated the detectable emission using a long 1000 hr exposure with SKA1-SUR (SKA1-SUR-A in Tab.1) and assuming a redshift of $z = 0.5$. In this case, we attached a magnetic field to the simulation by assuming an average 5 percent equipartition with the thermal energy within each cell. The field of view in the image approximately corresponds to 3 fields of view of the SKA1 survey Band1 (≈ 18 square degrees). Most of the detectable radio emission by the SKA1-SUR will originate from the cluster outskirts, yet in a few cases also the "tip of the iceberg" of radio emission coming from very big filaments should be detectable, like in the case of the hot filament within the rectangle in Fig.4. Our tests suggest that the redshift range $0.4 \leq z \leq 0.5$ is the best to have some chance of detection with the SKA1- SURVEY PAF Band1, while at $z < 0.4$ and $z > 0.5$ the emission will be filtered-out and suppressed by cosmological dimming, respectively. Based on a crude extrapolation of our data, we expect a detection of $\sim 1-2$ filaments of such giant filaments for every FOVs of SKA1-SUR, using ~ 1000 hr of exposure. Deep exposures in *polarisation* should maximise the chance of detecting these rare structures, since they are expected to be highly polarised owing to their

[3] http://astronomers.skatelescope.org/wp-content/uploads/2014/06/SKA1_Science

PoS(AASKA14)097

strong Mach numbers. Polarised observations are not dynamical-range limited, and warrant that the thermal noise will be reached independently of the presence of strong source within the field of view, thereby increasing the chances of imaging such low-surface brightness structures in the cosmic web.

Acknowledgements

The computations described in this work were performed using the *ENZO* code (http://enzo-project.org). We acknowledge PRACE for awarding us access to CURIE-Genci based in France at Bruyeres-le-Chatel. The support of the TGC Hotline from the Centre CEA-DAM Ile de France to the technical work is gratefully acknowledged. We also acknowledge CSCS-ETH for the use of the Cray XC30 Piz Daint. F.V., M.B. and A.B. acknowledge support from the grant FOR1254 from the Deutsche Forschungsgemeinschaft. We thank the "Tiger Team" of SKA-LOW and J. Condon for useful scientific discussion, and we gratefully acknowledge the assistance by the SKA Office to produce simulated SKA observations.

References

Araya-Melo, P. A., Aragón-Calvo, M. A., Brüggen, M., & Hoeft, M. 2012, MNRAS, 423, 2325
Bagchi, J., Enßlin, T. A., Miniati, F., et al. 2002, New Astronomy, 7, 249
Brown, S. D. 2011, Journal of Astrophysics and Astronomy, 32, 577
Brüggen, M., Ruszkowski, M., Simionescu, A., Hoeft, M., & Dalla Vecchia, C. 2005, ApJL, 631, L21
Bryan, G. L., Norman, M. L., O'Shea, B. W., et al. 2014, ApJS, 211, 19
Caprioli, D., & Spitkovsky, A. 2014, ApJ, 783, 91
Davé, R., Cen, R., Ostriker, J. P., et al. 2001, ApJ, 552, 473
Dolag, K., Bykov, A. M., & Diaferio, A. 2008, Science & Space Review, 134, 311
Dolag, K., & Enßlin, T. A. 2000, A & A, 362, 151
Donnert, J., Dolag, K., Lesch, H., & Müller, E. 2009, MNRAS, 392, 1008
Edmon, P. P., Kang, H., Jones, T. W., & Ma, R. 2011, MNRAS, 414, 3521
Farnsworth, D., Rudnick, L., Brown, S., & Brunetti, G. 2013, ApJ, 779, 189
Giovannini, G., Bonafede, A., Feretti, L., Govoni, F., & Murgia, M. 2010, A & A, 511, L5
Giovannini, G., Bonafede, A., Brown, S., et al. 2015, "Mega-parsec scale magnetic fields in low density regions in the SKA era: filaments connecting galaxy clusters and groups" in proc. *Advancing Astrophysics with the Square Kilometre Array*, PoS(AASKA14)104
Hoeft, M., & Brüggen, M. 2007, MNRAS, 375, 77
Keshet, U., Waxman, E., & Loeb, A. 2004, ApJ, 617, 281
Kronberg, P. P., Kothes, R., Salter, C. J., & Perillat, P. 2007, ApJ, 659, 267
Pizzo, R. F., de Bruyn, A. G., Feretti, L., & Govoni, F. 2008, A & A, 481, L91
Planck Collaboration, Ade, P. A. R., Aghanim, N., et al. 2013, A & A, 550, A134
Richter, P., Paerels, F. B. S., & Kaastra, J. S. 2008, Science & Space Review, 134, 25
Ryu, D., Kang, H., Cho, J., & Das, S. 2008, Science, 320, 909
Ryu, D., Kang, H., Hallman, E., & Jones, T. W. 2003, ApJ, 593, 599

PoS(AASKA14)097

Vazza, F., Brüggen, M., Gheller, C., & Wang, P. 2014a, MNRAS, 445, 3706
Vazza, F., Dolag, K., Ryu, D., et al. 2011, MNRAS, 418, 960
Vazza, F., Gheller, C., & Brüggen, M. 2014b, MNRAS, 439, 2662

PoS(AASKA14)097

PROCEEDINGS OF SCIENCE

Probing the nature of Dark Matter with the SKA

Sergio Colafrancesco[*1], **Marco Regis**[2], **Paolo Marchegiani**[1], **Geoff Beck**[1], **Rainer Beck**[3], **Hannes Zechlin**[2], **Andrei Lobanov**[3], **and Dieter Horns**[4]

[1] *School of Physics, University of the Witwatersrand, Johannesburg, South Africa*
[2] *Dipartimento di Fisica, Università degli Studi di Torino and INFN-Sezione di Torino, via P. Giuria, 1, 10125 Torino, Italy*
[3] *Max-Planck-Institut für Radioastronomie, Auf dem Hügel 69, 53121 Bonn, Germany*
[4] *Institut für Experimentalphysik, Universität Hamburg, Luruper Chaussee 149, 22761 Hamburg, Germany*

E-mail: sergio.colafrancesco@wits.ac.za

Dark Matter (DM) is a fundamental ingredient of our Universe and of structure formation, and yet its nature is elusive to astrophysical probes. Information on the nature and physical properties of the WIMP (neutralino) DM (the leading candidate for a cosmologically relevant DM) can be obtained by studying the astrophysical signals of their annihilation/decay. Among the various e.m. signals, secondary electrons produced by neutralino annihilation generate synchrotron emission in the magnetized atmosphere of galaxy clusters and galaxies which could be observed as a diffuse radio emission (halo or haze) centered on the DM halo. A deep search for DM radio emission with SKA in local dwarf galaxies, galaxy regions with low star formation and galaxy clusters (with offset DM-baryonic distribution, like e.g. the Bullet cluster) can be very effective in constraining the neutralino mass, composition and annihilation cross-section. For the case of a dwarf galaxy, like e.g. Draco, the constraints on the DM annihilation cross-section obtainable with SKA1-MID will be at least a factor $\sim 10^3$ more stringent than the limits obtained by Fermi-LAT in the γ-rays. These limits scale with the value of the B field, and the SKA will have the capability to determine simultaneously both the magnetic field in the DM-dominated structures and the DM particle properties. The optimal frequency band for detecting the DM-induced radio emission is around ~ 1 GHz, with the SKA1-MID Band 1 and 4 important to probe the synchrotron spectral curvature at low-ν (sensitive to DM composition) and at high-ν (sensitive to DM mass).

Advancing Astrophysics with the Square Kilometre Array,
June 8-13, 2014
Giardini Naxos, Sicily, Italy

[*] Speaker.

PoS(AASKA14)100

1. Unveiling the nature of Dark Matter

The Square Kilometre Array (SKA) is the most ambitious radio telescope ever planned, and it is a unique multi-disciplinary experiment. Even though the SKA, in its original conception, has been dedicated to constrain the fundamental physics aspects on dark energy, gravitation and magnetism, much more scientific investigation could be done with its configuration: the exploration of the nature of Dark Matter is one of the most important additional scientific themes.

Among the viable competitors for having a cosmologically relevant DM species, the leading candidate is the lightest particle of the minimal supersymmetric extension of the Standard Model (MSSM, Jungman et al. 1996), plausibly the neutralino χ, with a mass M_χ in the range between a few GeV to several TeV. Information on the nature and physical properties of the neutralino DM can be obtained by studying the astrophysical signals of their interaction/annihilation in the halos of cosmic structures. These signals (see Colafrancesco et al. 2006, 2007 for details) involve, in the case of a χ DM, emission along a wide range of frequencies, from radio to γ-rays (see Fig. 1 for a DM spectral energy distribution (SED) in a typical dwarf galaxy).

Neutral pions produced in $\chi\chi$ annihilation decay promptly in $\pi^0 \to \gamma\gamma$ and generate most of the continuum photon spectrum at energies $E \gtrsim 1$ GeV. Secondary electrons are produced through various prompt generation mechanisms and by the decay of charged pions, $\pi^\pm \to \mu^\pm + \nu_\mu(\bar{\nu}_\mu)$, with $\mu^\pm \to e^\pm + \bar{\nu}_\mu(\nu_\mu) + \nu_e(\bar{\nu}_e)$. The different composition of the $\chi\chi$ annihilation final state will in general affect the form of the electron spectrum. The time evolution of the secondary electron spectrum is described by the transport equation:

$$\frac{\partial n_e}{\partial t} = \nabla\left[D\nabla n_e\right] + \frac{\partial}{\partial E}\left[b_e(E) n_e\right] + Q_e(E,r)\,, \tag{1.1}$$

where $Q_e(E,r)$ is the $e^\pm$ source spectrum, $n_e(E,r)$ is the $e^\pm$ equilibrium spectrum (at each fixed time) and $b_e \equiv -dE/dt$ is the $e^\pm$ energy loss per unit time, $b_e = b_{ICS} + b_{synch} + b_{brem} + b_{Coul}$ (see Colafrancesco et al. 2006 for details). The diffusion coefficient D in eq.(1.1) sets the amount of spatial diffusion for the secondary electrons: it turns out that diffusion can be neglected in galaxy clusters while it is relevant on galactic and sub-galactic scales (see discussion in Colafrancesco et al. 2006, 2007). Under the assumption that the population of high-energy $e^\pm$ can be described by a quasi-stationary ($\partial n_e/\partial t \approx 0$) transport equation, the secondary electron spectrum $n_e(E,r)$ reaches its equilibrium configuration mainly due to synchrotron and ICS losses at energies $E \gtrsim 150$ MeV and due to Coulomb losses at lower energies. Secondary electrons eventually produce radiation by synchrotron emission in the magnetized atmosphere of cosmic structures, bremsstrahlung with ambient protons and ions, and ICS of CMB (and other background) photons (and hence an SZ effect, Colafrancesco 2004). These secondary particles also heat the ambient gas by Coulomb collisions.

A large amount of efforts have been put in the search for DM indirect signals at γ-ray energies looking predominantly for two key spectral features: the $\pi^0 \to \gamma\gamma$ decay spectral bump , and the direct $\chi\chi \to \gamma\gamma$ annihilation line emission, with results that are not conclusive yet (e.g., Daylan et al. 2014, Weniger 2012, Doro et al. 2014). The non-detection of signals related to DM annihilation/decay from various astrophysical targets (including observations of dwarf spheroidal galaxies, the Galactic Center, galaxy clusters, the diffuse gamma-ray background emission) is interpreted in terms of constraints on the (self-)annihilation cross-section (or decay time) of the DM

PoS(AASKA14)100

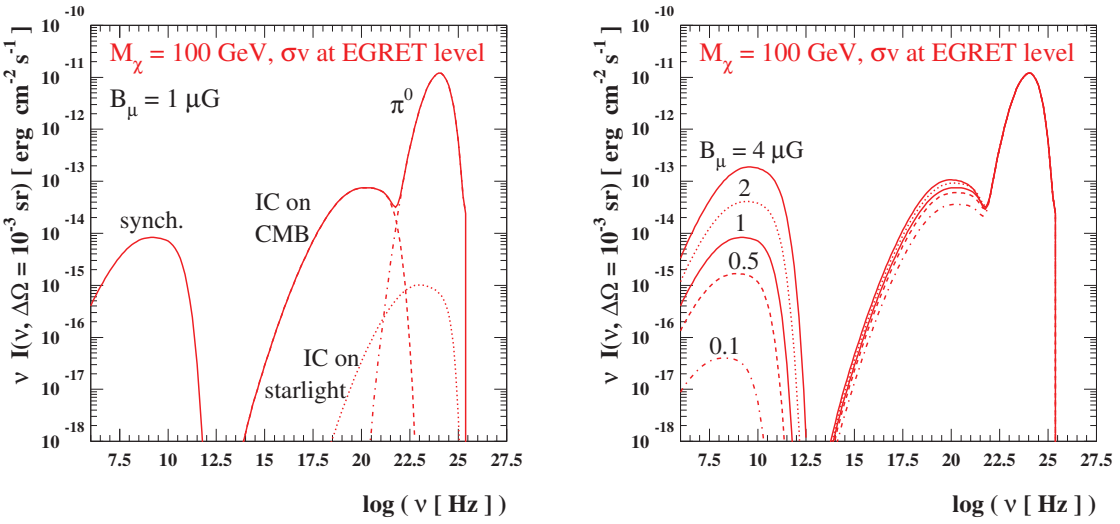

Figure 1: Left. The Draco dSph multi-wavelength spectrum for a 100 GeV WIMP annihilating into $b\bar{b}$. Right. The effect of varying the magnetic field strength on the Draco multi-wavelength spectrum for a 100 GeV WIMP annihilating into $b\bar{b}$. The WIMP pair annihilation rate has been tuned as to give a γ-ray signal at the level of the EGRET measured flux upper limit (from Colafrancesco et al. 2007).

particle candidate. Assuming, for instance, a canonical WIMP of $M_\chi = 100\,\mathrm{GeV}$ annihilating to b-quarks, stacked observations of dwarf spheroidal galaxies with Fermi-LAT put a constraint of $\langle \sigma V \rangle < 2 \times 10^{-25}\,\mathrm{cm}^3\,\mathrm{s}^{-1}$ (95% c.l.) on the thermally-averaged self-annihilation cross-section of DM particles (Ackerman et al. 2014). Hopes of discovering annihilating WIMPs in γ-rays are relegated to Fermi-LAT successors and the forthcoming CTA experiment (Doro et al. 2013).
There are, however, also good hopes to obtain relevant information on the nature of DM from radio observations of DM halos on large scales, i.e. from dwarf galaxies to clusters of galaxies.

2. Radio emission signals from Dark Matter annihilation

Observations of radio halos produced by DM annihilations are, in principle, very effective in constraining the neutralino mass and composition (see, e.g., Colafrancesco and Mele 2001, Colafrancesco et al. 2006, 2007), under the hypothesis that DM annihilation provides an observable contribution to the radio-halo flux.

The wide range of frequencies probed by the SKA and the variety of achievable observational targets (and in turn of magnetic fields) will allow testing the non-thermal electron spectrum from about 1 GeV to few hundreds of GeV, that is the most relevant range in the WIMP search. Figure 2 displays the predicted spectral differences between various annihilation channels and WIMP masses: note that these differences manifest mainly in low-ν slope variation for differing annihilation channels and in the high-ν spectral flattening/steepening for larger/smaller masses. The SKA sensitivity curves for SKA1-LOW and SKA1-MID are taken from Dewdney et al. (2012).
The surface brigthness produced by DM-induced synchrotron emission is heavily affected by dif-

PoS(AASKA14)100

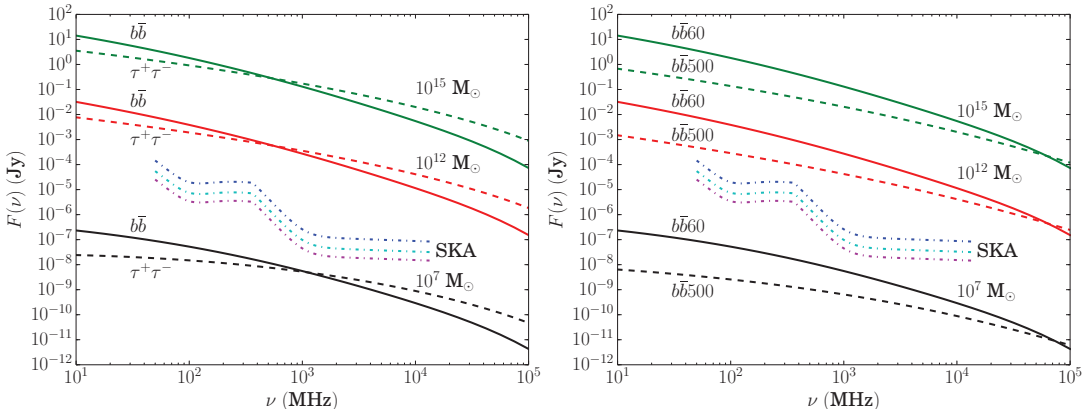

Figure 2: Flux densities for dwarf galaxies ($M = 10^7$ M$_\odot$), galaxies ($M = 10^{12}$ M$_\odot$), and galaxy clusters ($M = 10^{15}$ M$_\odot$). The halo profile is NFW, $\langle B \rangle = 5$ μG, and the annihilation cross section is fixed to the value $\langle \sigma V \rangle \approx 3 \times 10^{-27}$ cm ^{3} s^{-1}. Black lines are for dwarf galaxies, red lines for galaxies and green for clusters. Left: WIMP mass is 60 GeV, solid lines are for composition $b\bar{b}$ and dashed lines for $\tau^+\tau^-$. Right: Composition is $b\bar{b}$, solid lines are for WIMP mass 60 GeV and dashed lines for 500 GeV. Dash-dotted lines are SKA sensitivity limits for integration times of 30, 240 and 1000 hours (Dewdney et al. 2012). The flux is calculated within the virial radius (from Colafrancesco et al. 2014).

fusion in small scale structures, e.g., dwarf and standard galaxies, while it is less important in large structures, e.g., galaxy clusters (see Colafrancesco et al. 2006-2007 for a detailed discussion).

Polarization from DM-induced radio emission is expected at very low fractional levels due to the fact that DM spatial and velocity distribution is nearly homogeneous and that DM annihilation is mediated by secondary particle production. Therefore, a low polarization level of detectable radio signals in the directions of DM halos would be consistent with the DM origin of such radio emission. Residual high-polarization signals could be hence attributed to astrophysical sources in the direction or within the DM halos, and one could use these signals to infer properties of the magnetic field in these structures (see R. Beck et al. 2015, and F. Govoni et al. 2015).

2.1 Cosmological evolution of Dark Matter radio emission

Figure 3 displays the evolution of radio emission from DM halos of mass 10^7 M$_\odot$, 10^{12} M$_\odot$, and 10^{15} M$_\odot$ for a constant magnetic field of 5 μG, in accordance with arguments made in Colafrancesco et al. (2014). The annihilation channel is $b\bar{b}$, the mass of the neutralino is 60 GeV and a DM annihilation cross-section $\langle \sigma V \rangle = 3 \times 10^{-27}$ cm ^{3} s^{-1} was adopted. Emission from dwarf galaxy halos ($M \approx 10^7$ M$_\odot$) is just below the SKA detection threshold for this value of $\langle \sigma V \rangle$ but would be visible at redshift $z \leq 0.01$ for the assumed DM annihilation cross-section. This justify the search of DM-induced radio signals mainly in dwarf galaxies of the local environment, at distances $\lesssim 3$ Mpc ($z \lesssim 0.0007$). Emission from galactic DM halos ($M \approx 10^{12}$ M$_\odot$) are detectable by SKA out to $z \approx 0.8$ even with the reference value of $\langle \sigma V \rangle$, and can provide a non-detection upper-bound on $\langle \sigma V \rangle$ an order of magnitude below the assumed value even at such high redshifts. Emission form galaxy cluster halos can provide similar constraints but out to higher redshifts $z \lesssim 3$. These objects thus offer the option of deep-field observations that can scan a larger fraction of the DM parameter space than the best current data.

PoS(AASKA14)100

Figure 3 also shows that the effect of diffusion are far less significant when observing higher-z objects, again simplifying the modelling and analysis of the SKA observations.

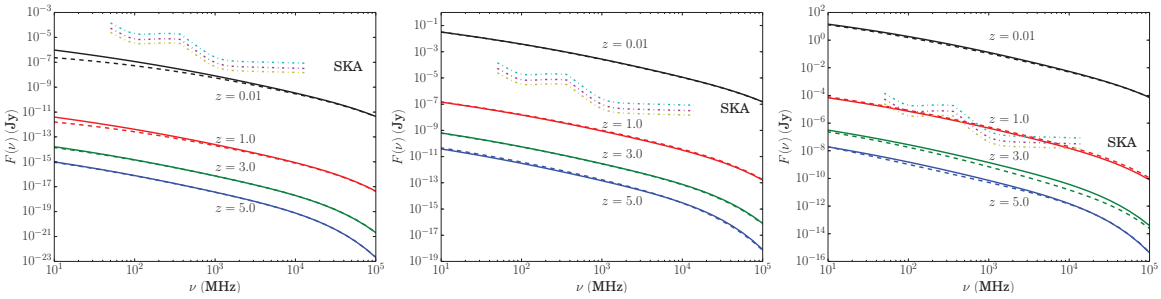

Figure 3: Flux densities for various DM halos within the virial radius. Left: dwarf spheroidal galaxies ($M = 10^7$ M$_\odot$); mid panel: galactic halos ($M = 10^{12}$ M$_\odot$); right panel: galaxy clusters ($M = 10^{15}$ M$_\odot$). We assume a NFW halo profile, $\langle \sigma V \rangle = 3 \times 10^{-27}$ cm ^{3} s^{-1} and $\langle B \rangle = 5$ μG. WIMP mass is 60 GeV and the composition is $b\bar{b}$. Solid lines are without diffusion, and dotted are with diffusion. The SKA sensitivity limits (dash-dotted lines, Dewdney et al. 2012) are shown for integration times of 30, 240 and 1000 hours, respectively (from Colafrancesco et al. 2014).

2.2 Optimal DM laboratories

In order to identify the optimal DM laboratories for radio observations we scan a parameter space extending from dwarf galaxies to galaxy clusters over a wide redshifts range $z \approx 0-5$. The choice to examine the halos of both large and small structures is crucial, as dwarf spheroidal galaxies are well known to be highly DM dominated but produce faint emissions, while larger structures, but not immaculate test-beds for DM emissions, provide substantially stronger fluxes. This indicates that a survey of DM halos with different mass is essential to identify the best detection prospects for future radio telescopes like the SKA.

Figure 4 shows the redshift-mass exclusion plot obtained by using the SKA sensitivity bound for SKA1 LOW and SKA1 MID (at 1 GHz in Band 1). For each DM halo we obtain the DM halo mass and redshift combination that produce the minimal SKA-detectable fluxes. DM-dominated objects lying above the black and green curves cannot be detected with the SKA1 at the given confidence threshold for $\langle \sigma V \rangle = 3 \times 10^{-27}$ cm^3 s^{-1}. Objects below a curve are visible to SKA1, and the further below the curve they lie the greater the region of the cross-section parameter space we can explore through the observation of the object. For reference, the yellow dash-dotted line displays the curve given for $\langle \sigma V \rangle = 3 \times 10^{-30}$ cm^3 s^{-1} and 1σ confidence level. A few representative know objects (irrespective of their location in the sky) with good estimates of the DM mass are plotted in the $M_{DM} - z$ plane for the sake of illustration of the DM search potential with the SKA.

Dwarf galaxies, given their extreme proximity, provide an excellent test-bed for DM radio probes, granting access to a parameter space that extends even below the value $\langle \sigma V \rangle = 3 \times 10^{-30}$ cm^3 s^{-1}. Additionally their large mass-to-light ratios and absence of strong star formation and diffuse non-thermal emission make them very clean sources for radio DM searches.

Galaxies can be probed to significantly larger redshifts than the dwarf galaxies due to their larger DM mass, and those located in the redshift range $0.5 \lesssim z \lesssim 1.0$ provide stronger constraints. However, an optimized DM search should be confined to galaxies with little background radio noise,

PoS(AASKA14)100

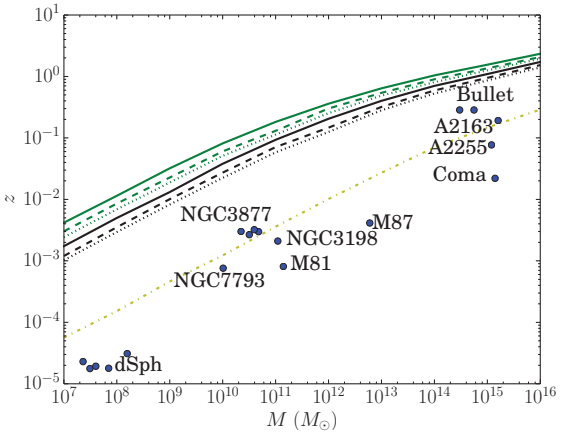

Figure 4: Exclusion plot in redshift versus halo mass based on projected SKA (at 1 GHz in Band 1) sensitivity data for the reference value of $\langle\sigma V\rangle = 3\times10^{-27}$ cm ^{3} s^{-1} with 30 hour integration time (black lines) and 1000 hour integration time (green lines). $\langle B\rangle = 5\ \mu$G was adopted. Solid lines are the 1σ sensitivity exclusion, dashed lines that of 2σ and dotted lines correspond to 3σ. The yellow dash-dotted line corresponds to 30 hours of integration and 1σ confidence with $\langle\sigma V\rangle = 3\times10^{-30}$ cm^3 s^{-1}. An annihilation channel $b\bar{b}$ is assumed with a neutralino mass of 60 GeV. Representative objects with known DM mass are shown for illustrative purposes of DM radio signal detection. The dSph group contains the galaxies: Draco, Sculptor, Fornax, Carina and Sextans. Unlabelled Galaxies are: NGC3917, NGC3949 and NGC4010. For very local objects the redshift is estimated from the average distance data. From Colafrancesco et al. 2014.

making low star-formation-rate galaxies good candidates. High-z galaxies come also with the advantage of observing more primitive structures with fewer sources of baryonic radio emission.
Clusters of galaxies provide extremely good candidates in cases, such as the Bullet cluster, where the dark and baryonic matter are spatially separated. Our recent analysis of the ATCA observation of the Bullet cluster (Colafrancesco and Marchegiani 2014) indicates that deeper radio observations (possible with the SKA) will be able indeed to separate the DM-induced signal from the CR-induced one and hence have the possibly to investigate the nature of DM particles using the technique here proposed. More in general, the large predicted radio fluxes due to DM annihilation in clusters indicate that DM-induced radio emission can be observed in radio out to large redshifts $z \approx 2$, again with the advantage of fewer sources of baryonic radio emission.

2.3 Disentangling magnetic fields and Dark Matter

Studying the magnetic properties of DM halos are crucial to disentangle the DM particle density from the magnetic field energy density contributing to the expected synchrotron radio emission from DM annihilation. The SKA is the most promising experiment to determine the magnetic field structure in extragalactic sources (see Johnston-Hollitt et al. 2015), and will have the potential of measuring RMs toward a large number of sources allowing a detailed description of the strength, structure, and spatial distribution of magnetic fields in dSph galaxies, galaxies (see Beck et al. 2015) and galaxy clusters (see Govoni et al. 2015). We stress that these measurements of the magnetic field can be obtained by the SKA simultaneously, for the first time, with the constraints on DM nature from the expected radio emission.

PoS(AASKA14)100

3. The impact of SKA on the search for the DM nature

Deep observations of radio emission in DM halos are not yet available, and this limits the capabilities of the current radio experiments to set relevant constraints on DM models. We have already explored a project (Regis et al. 2014a,b,c) dedicated to the WIMP search making use of radio interferometers, that could be considered as a pilot experiment for the next generation high-sensitivity and high-resolution radio telescope arrays like the SKA. For the particle DM search we are interested in, the use of multiple array detectors having synthesized beams of $\sim$ arcmin size has a number of advantages with respect to single-dish observations. First, the large collecting area allows for an increase in the sensitivity over that a single-dish telescope. The best beam choice for the detection of a diffuse emission requires a large synthesized beam (in order to maximize the integrated flux), but still smaller than the source itself to be able to resolve it. A good angular resolution is also crucial in order to distinguish between a possible non-thermal astrophysical emission and the DM-induced signal, which clearly becomes very hard if the DM halo is not well-resolved. The possibility of simultaneously detecting small scale sources with the long-baselines of the array allows one to overcome the confusion limit. In the case of arcmin beams, the confusion level can be easily reached with observations lasting for few tens of minutes, even by current telescopes. A source subtraction is thus a mandatory and crucial step of the analysis. Finally, single dish telescopes face the additional complication related to Galactic foreground contaminations, which are instead subdominant for the angular scales typically probed by telescope arrays at GHz frequency.

The limits derived from ATCA observations of 6 dSphs (Regis et al. 2014c) on the WIMP annihilation/decay rate as a function of the mass for different final states of annihilation/decay are already comparable to the best limits obtained with γ-ray observations and are much more constraining than what obtained in the X-ray band or with previous radio observations (Spekkens et al. 2013, Natarayan et al. 2013). In this context, the SKA will have the possibility to explore DM models with cross-section values well below the DM relic abundance one (see Fig.6 in Regis et al. 2014c). The SKA1-MID Band 1 (350 -1050 MHz) will probably be the most promising frequency range for the majority of WIMP models. The full SKA-2 phase will bring another factor $\sim 10\times$ increase in sensitivity and an extended frequency range up to at least 25 GHz. Typical values of the SKA sensitivity ($A_{eff}/T_{sys} = 2 \times 10^4$ m^2/K) and bandwidth (300 MHz at GHz frequency) provide rms flux values of ≈ 30 nJy for 10 hours of integration time. This is about a 10^3 factor of gain in sensitivity with respect to the most recent ATCA observations (Regis et al. 2014a). A further improvement by a factor of 2-3 can be confidently foreseen due to the larger number of accessible dSph satellites from the southern hemisphere. The SKA will also have the unique advantage to be able to determine the dSph magnetic field (via FR measurements and possibly also polarization), provided its strength is around the μG level (as expected from star formation rate arguments, Regis et al. 2014c). This will make the predictions for the expected DM signal much more robust and obtainable with a single experimental configuration. The prospects of detection/constraints of the WIMP particle properties with the SKA will therefore progressively close in on the full parameter space, even in a pessimistic sensitivity case, and up to $\sim$ TeV WIMP masses, irrespective of astrophysical assumptions.

The SKA will also allow to investigate the possibility that point-sources detected in the proximity of the dSph optical center might be associated to the emission from a DM cuspy profile.

PoS(AASKA14)100

This possibility is likely only in the "loss at injection" scenario, while spatial diffusion should in any case flatten the $e^{\pm}$ distribution, making the source extended rather than point-like. The investigation of these sources with the SKA will deserve particular attention, since we have already found that the WIMP scenario can fit the point-like emission with annihilation rates consistent with existing bounds (Regis et al. 2014c).

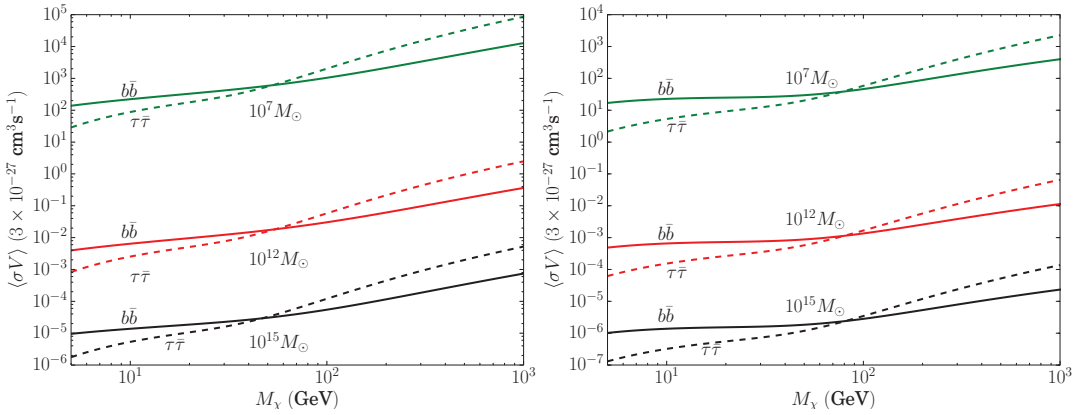

Figure 5: The $\langle\sigma V\rangle$ upper limits from 30 hour of SKA integration time for $z = 0.01$ at 300 MHz (top) and 1 GHz (bottom) as the neutralino mass M_χ is varied with annihilation channel $b\bar{b}$ in solid lines and $\tau\bar{\tau}$ in dashed lines. A value $\langle B\rangle = 5\ \mu$G was adopted. Black lines correspond to halos with mass 10^{15} $M_\odot$, red lines to 10^{12} $M_\odot$ and green lines to 10^7 $M_\odot$ (from Colafrancesco et al. 2014).

The SKA1-MID Band 1 (350-1050 MHz) to Band 4 (2.8-5.18 GHz) are important to probe the DM-induced synchrotron spectral curvature at low-ν (sensitive to DM composition) and at high-ν (sensitive to DM particle mass), and the implementation of Band 5 (4.6-13.8 GHz) will bring further potential to assess the DM-induced radio spectrum. As we can see from Fig.3, the best frequency range to detect these radio emissions is around 1 GHz. So, the upper frequency regions of SKA1-MID Band 1 provides the strongest spectral candidate for probing the cross-section parameter space due to an optimal combination of the SKA sensitivity within this band and the relatively strong fluxes at these frequencies. This frequency band will also allow for an optimal description of the magnetic field (see Johnston-Hollitt et al. 2015).

There are two main caveats in the forecasts for DM detection in the radio frequency band. The first stems from the fact that, for an extended radio emission,the confusion issue becomes stronger and stronger as one tries to probe fainter and fainter fluxes. Thus, the source subtraction procedure becomes crucial and this can affect the estimated sensitivities. The impact of this effect on the actual sensitivity is hardly predictable at the present time, especially for the SKA, since it will depend on the properties of the detected sources, the efficiency of deconvolution algorithms, and the accuracy of the telescope beam shape.

The second caveat is that by bringing down the observational threshold, one can possibly start to probe the very low levels of possible non-thermal emission associated to the tiny rate of star formation in dSph, or in galaxies and galaxy clusters. The DM contribution should be then disentangled from such astrophysical background. The superior angular resolution of the SKA will allow for the precise mapping of emissions, putatively either DM or baryonically induced, and will enable their correlation with the stellar or DM profiles (obtained via optical and/or kinematic measurements).

PoS(AASKA14)100

Early DM science can be done with a small sample of local dSphs, a small sample of nearby galaxies with good DM density profile reconstruction, and the Bullet cluster, observing with a somewhat larger beam ($\approx 7'' - 10''$). These objects have been already studied in radio with similar objectives (e.g., DM limits) and therefore provide the best science cases to prove the capabilities of the SKA1 for the study of the nature of DM with radio observations. The implementation of the SKA1-MID Band 5 (4.6-13.8 GHz) will increase the ability to detect the expected high-frequency spectral curvature of DM-induced radio emissions, and the ability to place constraints on the DM cross-section and to differentiate between different annihilation channel spectra. The $10\times$ increased sensitivity of SKA2 compared to SKA1-MID will allow us to increase the angular resolution by a factor ≈ 20 or to increase the sensitivity of SKA2 to DM-induced radio signals by a factor ≈ 10. The possibility to extend the frequency coverage of the SKA in its Phase-2 realization up to ~ 25 GHz, will allow to detect the expected high-ν spectral cut-off of DM-induced radio emissions, and then set accurate constraints to the DM particle mass.

4. Conclusion

The SKA has the potential to unveil the elusive nature of Dark Matter. Its ability to resolve the intrinsic degeneracy (between magnetic field properties and particle distribution) of the synchrotron emission expected from secondary particles produced in DM annihilation (decay) will allow such a discovery to be unbiased and limited only by the sensitivity to the DM particle mass and annihilation cross-section (decay rate). The unprecedented sensitivity of the SKA to the DM fundamental properties will bring this instrument in a leading position for unveiling the nature of the dark sector of the universe.

The information provided by the SKA can be complemented with analogous studies in other spectral bands, which will be able to prove the ICS signal of DM-produced secondary electrons (spanning from μwaves to hard X-rays and γ-rays) and the distinctive presence of the $\pi^0 \to \gamma\gamma$ emission bump in the γ-rays (see Fig. 1). The next decade will offer excellent multi-frequency opportunities in this respect with the advent of Millimetron, the largest space-borne single-dish mm. astronomy satellite operating in the $10^2 - 10^3$ GHz range (optimal to prove the DM-induced SZ effect), the Astro-H mission operating in the hard X-rays frequency range (with the highest expected sensitivity to probe the high-energy tail of the DM-induced ICS emission), and the CTA with unprecedent sensitivity in the energy range between a few tens GeV to hundreds TeV.

REFERENCES

Ackermann, M., et al., 2014, Phys. Rev. D, 89, 042001

Beck, R., Bomans, D., Colafrancesco, S., et al. 2015, "Structure, dynamical impact and origin of magnetic fields in nearby galaxies in the SKA era" in proc. *Advancing Astrophysics with the Square Kilometre Array*, PoS(AASKA14)094

Borriello, E. et al. 2010, ApJ, 709, L32

Burns, J.O. *et al.*., 1995, ApJ, 446,583

Colafrancesco, S., 2004, A&A, 422, L23

PoS(AASKA14)100

Colafrancesco, S. 2010, invited lecture at the 4th Gamow International Conference on Astrophysics & Cosmology After Gamow (9th Gamow Summer School), AIPC, 1206, 5C
Colafrancesco, S. & Mele, B. 2001, ApJ, 562, 24
Colafrancesco, S., Profumo, S. and Ullio, P. 2006, A&A, 455, 21
Colafrancesco, S., Profumo, S. and Ullio, P. 2007, PhRvD, 75, 3513
Colafrancesco, S. et al. 2011, A&A, 527, 80
Colafrancesco, S., and Marchegiani, P, 2014, A&A, 562L, 2C
Colafrancesco, S., Marchegiani, P. and Beck, G., 2015, JCAP, 02, 032C
Daylan, T. et al., 2014, [arXiv:1402.6703]
Deiss, B.M., Reich, W., Lesch, H. & Wielebinski, R. 1997, A&A, 321, 55
Dewdney, P., Turner, W., Millenaar, R., McCool, R., Lazio, J., Cornwell, T., 2013, "SKA1 System Baseline Design", Document number SKA-TEL-SKO-DD-001 Revision 1
Doro, M., 2014, Nuclear Instruments and Methods in Physics Research A,742, 99
Doro, M., et al., 2013, Astroparticle Physics, 43, 189
Govoni, F., Murgia, M., Feretti, L., et al., 2006, A&A, 460, 425
Govoni, F. Murgia, M., Xu, H., et al. 2015, "Cluster magnetic fields through the study of polarized radio halos in the SKA era" in proc. *Advancing Astrophysics with the Square Kilometre Array*, PoS(AASKA14)105
Johnston-Hollitt, M. et al. 2015, "Using SKA Rotation Measures to Reveal the Mysteries of the Magnetised Universe" in proc. *Advancing Astrophysics with the Square Kilometre Array*, PoS(AASKA14)092
Jungman, G., Kamionkowki, M. & Griest, K. 1996, Phys.rep, 267, 195
Moran, E.C. et al. 2014, [arXiv:1408.4451]
Natarajan, A. et al., 2013, Phys. Rev. D 88 083535
Planck Collaboration, 2011, A&A, 536, A7
Regis, M.; Richter, L.; Colafrancesco, S.; Massardi, M.; de Blok, W. J. G.; Profumo, S.; Orford, N. 2014a, [arXiv:1407.5479]
Regis, M.; Richter, L.; Colafrancesco, S.; et al., 2014b, JCAP, 10, 016R
Regis, M.; Colafrancesco, S.; Profumo, S.; de Blok, W. J. G.; Massardi, M.; Richter, L. 2014c, JCAP, 10, 016R
Spekkens, K., Mason, B.S., Aguirre, J.E. and Nhan, B., 2013, ApJ, 773, 61
Weniger, C., 2012, JCAP, 1208, 007

PoS(AASKA14)100

PROCEEDINGS OF SCIENCE

Using Tailed Radio Galaxies to Probe the Environment and Magnetic Field of Galaxy Clusters in the SKA Era

Melanie Johnston-Hollitt[1]*, **Siamak Dehghan**[1], **and Luke Pratley**[1]

[1] *School of Chemical and Physical Sciences, Victoria University of Wellington, P.O. Box 600, Wellington 6140*

E-mail: melanie.johnston-hollitt at vuw.ac.nz

The morphology of tailed radio galaxies is an invaluable source of environmental information, in which a history of the past interactions in the intra-cluster medium, such as complex galaxy motions and cluster merger shocks, are preserved. In recent years, the use of tailed radio galaxies as environmental probes has gained momentum as a method for galaxy cluster detection, examining the dynamics of individual clusters, measuring the density and velocity flows in the intra-cluster medium, and for probing cluster magnetic fields. To date instrumental limitations in terms of resolution and sensitivity have confined this research to the local ($z < 0.7$) Universe. The advent of SKA1 surveys however will allow detection of roughly 1,000,000 tailed radio galaxies and their associated galaxy clusters out to redshifts of 2 or more. This is in fact ten times more than the current number of known clusters in the Universe. Additionally between 50,000 and 100,000 tailed radio galaxies will be sufficiently polarized to allow characterization of the magnetic field of their parent cluster. Such a substantial sample of tailed galaxies will provide an invaluable tool not only for detecting clusters, but also for characterizing their intra-cluster medium, magnetic fields and dynamical state as a function of cosmic time. In this chapter we present an analysis of the usability of tailed radio galaxies as tracers of dense environments extrapolated from existing deep radio surveys.

Advancing Astrophysics with the Square Kilometre Array
June 8-13, 2014
Giardini Naxos, Sicily, Italy

*on behalf of the SKA Cosmic Magnetism Working Group

PoS(AASKA14)101

1. Introduction

It is well known that matter in the Universe is concentrated in a complicated system of twisted filaments of galaxies in the 'cosmic web'. At the intersection of these enormous filaments, galaxy clusters are formed and evolve. Understanding how these massive systems are created and evolve is crucial to our perception of the large-scale structure of the Universe. In recent years various techniques and advanced instruments have been established or enhanced to detect and characterize filaments, groups, and clusters. These methods are predominantly undertaken in parts of the spectrum other than the radio, and include X-ray (Henry et al. 1982) and Sunyaev-Zeldovich (Sunyaev & Zeldovich 1980) detections, and statistical data analysis and clustering examinations of spectroscopic and photometric redshift surveys (Huchra & Geller 1982; Dehghan & Johnston-Hollitt 2014). However, recent radio wavelength studies of groups and clusters have shown that some types of extended radio sources trace high-density regions of the Universe, and moreover, they provide valuable information on properties of large-scale structures of the Universe. This use of radio sources to probe large-scale structure and understand environmental conditions is set to increase in the Square Kilometre Array (SKA) era (Norris et al. 2013; Cassano et al. 2015; Ferrari et al. 2015; Gitti et al. 2015; Norris et al. 2015).

In this context, the community's attention has recently focused on a class of radio galaxies known as Bent-Tailed sources (BTs) as probes to both locate high density environments (Blanton et al. 2001; Mao et al. 2010; Wing & Blanton 2011) and to study the conditions in these regions (Pfrommer & Jones 2011), including their local magnetic field (Eilek & Owen 2002; Pratley et al. 2013). BTs as a class include radio galaxies with asymmetric radio structure in which lobes or plumes are not lined up with the galaxy itself. A subdivision of such sources with a morphology demonstrating that the jets are bent back through large angles are known as Head-Tail (HT) or Narrow-Angle-Tail (NAT) radio galaxies. HTs, which are almost exclusively found in the vicinity of galaxy clusters, are classified as Fanaroff-Riley class I radio sources (Fanaroff & Riley 1974). The curved radio structure of HTs is believed to be induced by ram pressure due to the relative movement of the host galaxy within the Intra-Cluster Medium (ICM; Gunn & Gott 1972). However, Cowie & McKee (1975) suggested buoyancy forces due to density perturbations in the ICM as an alternative mechanism responsible for the curvature formation in HTs and other BT radio sources. The coexistence of BTs and clusters in the local $(z \leq 0.1)$ Universe, is at a rate of 1-2 per cluster (Mao et al. 2009), and there is growing evidence that such associations carry on as far as redshift 2, at the limits of cluster detection (Dehghan et al. 2014). Thus, the correlation between BTs and galaxy clusters provides a powerful tool to locate the high density regions of the Universe, and additionally, investigate the physical characteristics of rich environments.

The SKA and its precursors will detect BTs in large quantities enabling a range of science goals to be met. Here we review the science that can be derived from BTs and discuss their expected detection numbers with SKA surveys.

2. Detecting Tailed Radio Galaxies in the SKA Era

A series of tiered surveys with increasing sensitivity over smaller and smaller areas are planned to be undertaken with the Square Kilometre Array during phase 1 (SKA1; Norris et al. 2013, 2015).

PoS(AASKA14)101

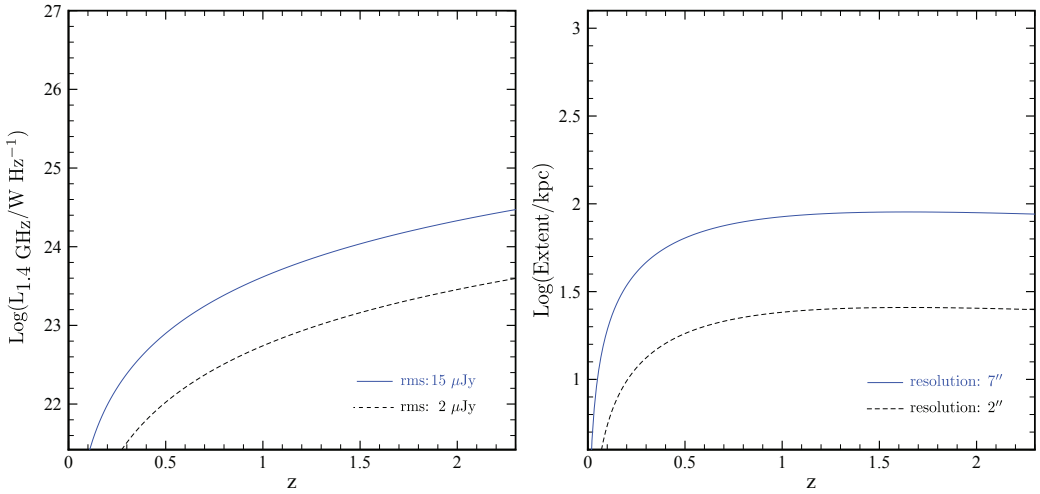

Figure 1: Left panel: The blue line and black dashed lines represent the 6 sigma source detection limit of the ATLAS and SKA1 surveys with the average sensitivity of 15 and 2 μJy, respectively. Right panel: The blue line and black dashed line represent the detection limit of the sources with an extent of 1.5 beams in ATLAS and SKA1 surveys at 7 & 2 arcsec resolution, respectively.

This approach, known as a 'wedding cake' survey strategy, will commence with an 'all-sky' survey (31,000 deg^2) from 1-2 GHz with 2$''$ resolution and 2 μJy sensitivity. Such a survey can be expected to detect numerous BT galaxies and therefore their associated clusters.

In order to assess the number of BT sources likely to be detected with SKA surveys, we can look to detection rates in deep surveys of SKA-level sensitivity carried out on smaller areas. Dehghan et al. (2014) performed a comprehensive radio source investigation in the 4 deg^{2}area of the Australia Telescope Large Area Survey of the Chandra Deep Field-South (ATLAS-CDFS) field, in order to evaluate the ability of SKA1 surveys to identify BT radio sources. The ATLAS-CDFS which has been observed with the Australia Telescope Compact Array at 1.4 GHz (Norris et al. 2006; T. M. O. Franzen et al., in preparation), has about 17$''$ $\times$ 7$''$ resolution and a depth of 15 μJy/beam. In addition, the ATLAS-CDFS image is partially covered by a 2$''$ resolution 1.4 GHz Very Large Array (VLA) image of the Extended CDFS (ECDFS) with an rms noise down to 10 μJy/beam (Miller et al. 2013) which is well matched to the resolution and sensitivity of the planned SKA1 surveys (Norris et al. 2014). It is worthwhile to note that while the expected capabilities of the SKA1 all-sky survey are similar in resolution to the VLA-ECDFS image, the SKA1 survey will be marginally more sensitive (see Figure 1). As Figure 1 demonstrates the SKA1 surveys will detect BT sources of lower power and smaller physical extent then are currently accessible with present wide-field surveys.

Out of a total of $\sim$ 3000 radio sources in the field, Dehghan et al. (2014) found 56 extended and diffuse radio sources, consisting of 45 BTs, a radio relic candidate, and several complex diffuse sources which could not be unambiguously categorized. Based on extrapolating from these detections, forthcoming all-sky 1.4 GHz continuum surveys with a resolution and sensitivity comparable to the ATLAS survey undertaken on pathfinder instruments such as the EMU survey (Norris et al. 2011) on ASKAP, will identify over 590,000 extended and diffuse low-surface-brightness radio sources, including at least 470,000 BT radio galaxies and the SKA1 level surveys will double this

PoS(AASKA14)101

number to of order $\sim$ 1 million BT sources. Statistical studies of such large samples of tailed radio sources will boost our understanding of the evolutionary origins of BTs and the mutual dependency between these intriguing radio sources and their habitat.

The postulated association between BT radio sources and rich environments suggests that the SKA1 will detect more than 1 million clusters and groups, which is more than twenty times the number of clusters identified at present. This, in fact, surpasses the number of clusters expected to be found with future X-ray telescopes such as eROSITA (Merloni et al. 2012) making SKA a powerful new tool for cluster detection. Additionally, assuming that these clusters and groups are found by both eROSITA and SKA1 surveys, there will be an exceptional opportunity to investigate the multi-wavelength characteristics of high-density regions of the Universe up to a redshift of 2.

3. Tailed Radio Galaxies as Environmental Probes

BT radio galaxies represent a wide range of morphologies that are believed to be primarily generated by environmental effects (Burns 1998). Two significant mechanisms are ram pressure and buoyancy forces induced on lobes of tailed radio galaxies. These forces are believed to be created by either relative motion of the host galaxy with respect to the ICM, or considerable deviations in the density of the medium. In particular, radio galaxies falling into a cluster's gravitational well, or sources within a turbulent weather system of clusters in a merger process, are thought to develop curved lobes and jets. On more local scales, the structure of jets in BTs may be notably altered by gravitational influences of satellite and nearby galaxies via bound and unbound orbital motions, near-miss passes, and precession of the accretion disk and jets. As a result BTs have been used with increasing success to probe conditions in their local environment. For example the particular morphology of tailed radio galaxies, if well resolved, can be used to investigate the dynamical state of their parent clusters such as in Perseus (Pfrommer & Jones 2011), A3135 (Pratley et al. 2013) and A3266 (Dehghan 2014; Miller et al., in preparation) where evidence for shocks, cluster winds and the merger direction, respectively, were all provided by the BT galaxies. BTs have also successfully been used to measure the density and velocity flows in the intra-cluster medium (Freeland et al. 2008; Douglass et al. 2011), and for measuring cluster magnetic fields which will be discussed in the next section. Crucially though, all such studies have been undertaken only on individual objects and the wealth of information to be gain from undertaking statistical studies of this type have yet to be realised, though recent steps in this direction have commenced with existing surveys such as FIRST (Wing & Blanton 2011).

An illustration of the wealth of information to be obtained by BTs is presented in Pratley et al. (2013) where a simple mechanical model was developed that simulates the most common observed BT shapes, including V-, M-, S-, and X-shaped radio galaxies, based on likely movement of the host galaxy under different environmental effects. This was then applied to simulate a peculiar tailed radio galaxy in the Abell 3135 galaxy cluster (see Figure 2). This study was able to disentangle various effects at work and showed that a cluster wind combined with both orbital and precessional motions must be present in order to create the observed morphology of this BT radio source. This simple, yet powerful framework applied to a statistical sample of BTs in clusters could elucidate such questions as:

- how often do we find cluster winds and how strong are they?

PoS(AASKA14)101

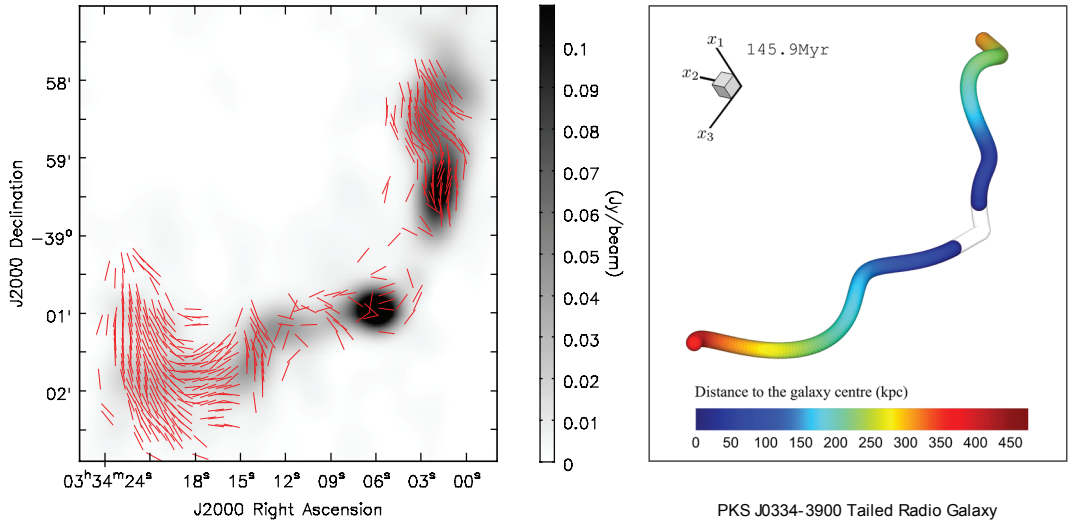

Figure 2: Left panel: Red segments represent the direction of the magnetic component of the polarized emission overlaid on the 1.4 GHz intensity image of the tailed radio galaxy PKS J0334-3900 at the centre of Abell 3135. Right panel: The simulated radio structure of the BT shown in the left panel. For further information see Pratley et al. (2013).

- Do BTs always require a companion galaxy and does this account for their association with clusters and dense groups?
- How often do AGN in BTs precess and can this explain X-shaped radio galaxies alone without having to require black hole - black hole collisions?

The latter question having important implications for recent predictions of the rate of black hole in-spirals and hence generation of gravitational waves expected to be found with next generation detectors such as Advanced LIGO and LISA.

3.1 Using tailed radio galaxies to constrain cluster magnetic fields

While the morphology of tailed radio galaxies provides a probe of the cluster weather, their linearly polarized synchrotron emission provides a probe of the cluster magnetic field. The polarized emission from the jets of the tailed radio galaxy (see Figure 2 for an example) passes through the intra-cluster medium and magnetic field, causing the linear polarization angle to rotate due to Faraday rotation. Knowing the path length (distance) over which the Faraday rotation occurs and the electron density of the intra-cluster medium (available from X-ray observations), it is possible to constrain the strength of the intra-cluster magnetic field.

Cluster magnetic fields are not well understood because they are difficult to measure, however, they are believed to play an important role in the cluster environment. While several authors have focused on the way cluster magnetic fields can be studied in the radio, including the 2004 SKA Science Case chapter by Feretti & Johnston-Hollitt (2004), such works tend to concentrate on the detection of diffuse cluster emission such as relics or statistical studies of background galaxies to probe the intra-cluster magnetic fields. Whilst such techniques remain popular and are the subject of several chapters in the new SKA Science Case (Govoni et al. 2015; Bonafede et al. 2015),

PoS(AASKA14)101

observations of tailed radio galaxies in the last two decades have demonstrated that resolved BTs have a valuable role in constraining the coherence length of magnetic fields in clusters on smaller scales than other methods, e.g. Coma (Feretti et al. 1995; Bonafede et al. 2010), A119 (Feretti et al. 1999; Murgia et al. 2004), A2382 (Guidetti et al. 2008) and 3C129 (Taylor et al. 2001).

In one of the first works to utilise resolved BTs, Eilek & Owen (2002) argued that the Faraday rotation across the tailed radio galaxies in A400 and A2634 is due to the Faraday screen of the intra-cluster medium and its magnetic field, rather than a skin of the radio source. They went on to show that the galaxy clusters have magnetic fields ordered on the scale $\sim 10-20$ kpc, and the geometry of the rotation measure appears to be determined by the intra-cluster medium with magnetic field strengths estimated to be $\sim$1-2 μG. Similarly, Johnston-Hollitt (2003) argued that the coherence length of BTs resolved in A3667 was of order of $10-20$ kpc. Furthermore, Vogt & Enßlin (2003) used the Faraday screen in the foreground of tailed radio galaxies in A400, A2634 and Hydra to measure the power spectrum of the intra-cluster magnetic fields finding a range of magnetic field autocorrelation lengths on small scales. Govoni et al. (2006) investigated using simulations of magnetic fields in A2255 to reproduce the Faraday screens observed from BTs, thus constraining the magnetic field structure. Following the method of Rotation Measure Synthesis (Brentjens & de Bruyn 2005), Pizzo et al. (2011) first explored the use of BTs as resolved screens at different depths within A2255 using the polarization properties as a tool to unveil the position of the radio sources within the cluster. In the study of Pratley et al. (2013), the morphology of a tailed radio galaxy is used to estimate the distance at which Faraday rotation occurs within the cluster A3135. Whereas in Pizzo et al. (2011) the location of the resolved BTs within A2255 along the line of site was not precisely known, in Pratley et al. (2013) there was a wealth of multiwavelength data to understand the location of the BT jets within the cluster. As mentioned above, the BT was modelled so as to constrain several parameters required to generate the observed morphology, including detailed modelling of the jet locations/projection. From this model, it was possible to estimate the distance between the two jets of the radio galaxy along the line of sight. The difference in average Faraday rotation of each jet could then be explained by the separation of the jets along the line of slight, allowing one to estimate the magnetic field over the separation (160 kpc) giving an estimate of the field over small scales within the cluster.

As with the improved statistics SKA1 is expected to yield for the use of extragalactic background source rotation measures (Johnston-Hollitt et al. 2015; Bonafede et al. 2015), the use of resolved tailed radio galaxies as probes of the magnetic fields in clusters will increase by several orders of magnitude. While detailed modelling is required to determine the expected number of sources with sufficient polarized emission for such studies, we may make a back of the envelope estimate by extrapolating from current surveys. This would suggest that approximately 5 to 10 per cent of the 1 million BTs to be detected with SKA1 should have sufficient polarization detected for such studies, giving between 50,000 and 100,000 resolved BTs in clusters for use as probes of the cluster magnetic field. Combined with the other sources of the expected 40 million extragalactic polarized sources detected as part of the RM survey experiment, the BTs embedded within clusters will form a powerful complementary dataset to disentangle cluster magnetic fields and perform tomographic mapping of magnetic fields in galaxy clusters. This will be analogous to the science case for combining background extragalactic RMs with pulsars and diffuse polarization to probe the magnetic field of the Milky Way, and is set to drastically improve our knowledge of the extent

PoS(AASKA14)101

of cluster magnetic fields and their structure on small scales. Importantly, with such a large sample we will be able to probe the evolution of cluster magnetic fields as a function of time, potentially evaluating how the field geometry and strength change, this will give vital clues to understand both the evolution and origin of magnetic fields in the Universe.

4. Impact of SKA Design

Successful searches for BT galaxies require both sensitivity and resolution. Looking forward to SKA2 we can expect to detect even greater numbers of BTs, potentially at even higher redshifts, signalling the first significant movement of objects in dense atmospheres, potentially in the very earliest of clusters.

Potential changes of design to the SKA that might affect the use of BT galaxies to detect and probe the environment of galaxy clusters include both a loss of resolution, which would reduce the redshift range over which such sources can be reliably detected if their physical sizes are small, and a loss of sensitivity which would reduce the chances of detecting faint tailed sources.

Recent studies have shown that BT sources can be as small as $\sim$50 kpc (Dehghan et al. 2014), which if located in a very distant cluster would require at least 1" resolution to unambiguously detect. The impact of sensitivity to this type of science can best be illustrated through the number of BTs detected in the original ATLAS-CDFS field (Mao et al. 2010; Dehghan et al. 2011) as compared to those found in the 3rd data release (Dehghan et al. 2014) in which the resolution was identical, but the sensitivity doubled, increasing the number of BTs by a factor of 5. This suggests that using, say, only of 50% of the currently planned number of antennas would reduce the total number of BTs detected to 200,000 in terms of sensitivity alone. If the reduction also resulted in a decrease in baseline length, this number will reduce even further due to an inability to resolve sources. Of the detected sources with such an array, only 10,000 - 20,000 would then be suitable for polarimetric studies of cluster magnetic fields. These numbers are still large and thus, so long as the resolution were not substantially compromised, a full sky survey with a 50% SKA1 could still advance this type of science considerably.

5. Summary

Future all-sky radio continuum surveys via instruments such as SKA1 will provide more sensitive and yet observationally affordable data to explore a wide range of science goals including those associated with the detection and characterisation of the environment of up to 1 million galaxy clusters using BT galaxies. Combining these data with that of future X-ray missions will provide an exceptional dataset to investigate the dynamical history of galaxy clusters. In addition, between 50,000 and 100,000 detected BTs will be resolved and of sufficient polarization to be used as probes of cluster magnetic fields. Combined with background polarized sources from the RM Survey, the embedded cluster BTs will allow the first tomographic view of cluster magnetic fields as a function of cosmic time. From this we may finally answer questions about the origin and evolution of cluster magnetic fields and how they influence cluster dynamics.

PoS(AASKA14)101

References

Blanton, E. L., Gregg, M. D., Helfand, D. J., Becker, R. H., & Leighly, K. M. 2001, AJ, 121, 2915

Bonafede, A., Feretti, L., Murgia, M., et al. 2010, A&A, 513, A30

Bonafede, A., Vazza, F., Brüggen, M., et al. 2015, "Unravelling the origin of large-scale magnetic fields in galaxy clusters and beyond through Faraday Rotation Measures with the SKA" in proc. *Advancing Astrophysics with the Square Kilometer Array*, PoS(AASKA14)095

Brentjens, M. A. & de Bruyn, A. G. 2005, A&A, 441, 1217

Burns, J. O. 1998, Science, 280, 400

Cassano, R., Bernardi, G., Brunetti, G., et al. 2015, "Cluster Radio Halos at the crossroads between astrophysics and cosmology in the SKA era" in proc. *Advancing Astrophysics with the Square Kilometer Array*, PoS(AASKA14)073

Cowie, L. L. & McKee, C. F. 1975, A&A, 43, 337

Dehghan, S. 2014, PhD thesis, Victoria University of Wellington

Dehghan, S. & Johnston-Hollitt, M. 2014, AJ, 147, 52

Dehghan, S., Johnston-Hollitt, M., Franzen, T. M. O., et al. 2014, AJ, 148, 75

Dehghan, S., Johnston-Hollitt, M., Mao, M., et al. 2011, Journal of Astrophysics and Astronomy, 32, 491

Douglass, E. M., Blanton, E. L., Clarke, T. E., Randall, S. W., & Wing, J. D. 2011, ApJ, 743, 199

Eilek, J. A. & Owen, F. N. 2002, ApJ, 567, 202

Fanaroff, B. L. & Riley, J. M. 1974, MNRAS, 167, 31P

Feretti, L., Dallacasa, D., Giovannini, G., et al. 1995, A&A, 302, 680

Feretti, L., Dallacasa, D., Govoni, F., et al. 1999, A&A, 344, 472

Feretti, L. & Johnston-Hollitt, M. 2004, New Astronomy Reviews, 48, 1145

Ferrari, C., Debbech, A., Smirnov, O., et al. 2015, "Non-thermal emission from galaxy clusters: feasibility study with SKA1" in proc. *Advancing Astrophysics with the Square Kilometer Array*, PoS(AASKA14)075

Freeland, E., Cardoso, R. F., & Wilcots, E. 2008, ApJ, 685, 858

Gitti, M., Tozzi, P., Brunetti, G., et al. 2015, "The SKA view of cool-core clusters: evolution of radio mini-halos and AGN feedback" in proc. *Advancing Astrophysics with the Square Kilometer Array*, PoS(AASKA14)076

Govoni, F., Murgia, M., Feretti, L., et al. 2006, A&A, 460, 425

Govoni, F., Murgia, M., Xu, H., et al. 2015, "Cluster magnetic fields through the study of polarized radio halos in the SKA era" in proc. *Advancing Astrophysics with the Square Kilometer Array*, PoS(AASKA14)105

Guidetti, D., Murgia, M., Govoni, F., et al. 2008, A&A, 483, 699

Gunn, J. E. & Gott, III, J. R. 1972, ApJ, 176, 1

Henry, J. P., Briel, U., Gunn, J. E., & Soltan, A. 1982, ApJ, 262, 1

Huchra, J. P. & Geller, M. J. 1982, ApJ, 257, 423

Johnston-Hollitt et al. 2015, "Using SKA Rotation Measures to Reveal the Mysteries of the Magnetised Universe" in proc. *Advancing Astrophysics with the Square Kilometer Array*, PoS(AASKA14)092

Johnston-Hollitt, M. 2003, PhD thesis, University of Adelaide

PoS(AASKA14)101

Mao, M. Y., Johnston-Hollitt, M., Stevens, J. B., & Wotherspoon, S. J. 2009, MNRAS, 392, 1070
Mao, M. Y., Sharp, R., Saikia, D. J., et al. 2010, MNRAS, 406, 2578
Merloni, A., Predehl, P., Becker, W., et al. 2012, ArXiv e-prints
Miller, N. A., Bonzini, M., Fomalont, E. B., et al. 2013, ApJS, 205, 13
Murgia, M., Govoni, F., Feretti, L., et al. 2004, A&A, 424, 429
Norris, R. P., Afonso, J., Appleton, P. N., et al. 2006, AJ, 132, 2409
Norris, R. P., Afonso, J., Bacon, D., et al. 2013, PASA, 30, 20
Norris, R. P., Basu, K., Brown, M., et al. 2015, "The SKA Mid-frequency All-sky Continuum Survey: Discovering the unexpected and transforming radio-astronomy" in proc. *Advancing Astrophysics with the Square Kilometer Array*, PoS(AASKA14)086
Norris, R. P., Hopkins, A. M., Afonso, J., et al. 2011, PASA, 28, 215
Pfrommer, C. & Jones, T. W. 2011, ApJ, 730, 22
Pizzo, R. F., de Bruyn, A. G., Bernardi, G., & Brentjens, M. A. 2011, A&A, 525, A104
Pratley, L., Johnston-Hollitt, M., Dehghan, S., & Sun, M. 2013, MNRAS, 432, 243
Sunyaev, R. A. & Zeldovich, I. B. 1980, ARAA, 18, 537
Taylor, G. B., Govoni, F., Allen, S. W., & Fabian, A. C. 2001, MNRAS, 326, 2
Vogt, C. & Enßlin, T. A. 2003, A&A, 412, 373
Wing, J. D. & Blanton, E. L. 2011, AJ, 141, 88

PoS(AASKA14)101

PROCEEDINGS OF SCIENCE

SKA studies of *in-situ* synchrotron radiation from molecular clouds

Clive Dickinson,[1]* **R. Beck,**[2] **R. Crocker**[3] **R. M. Crutcher,**[4] **R. D. Davies,**[1] **K. Ferriere,**[5] **G. Fuller,**[1] **T. Jaffe,**[5] **D. I. Jones,**[6] **J. P. Leahy,**[1] **E. J. Murphy,**[7] **M. W. Peel,**[1] **E. Orlando,**[8] **T. Porter,**[8] **R. J. Protheroe,**[9] **T. Robishaw,**[10] **A. W. Strong,**[11] **R. A. Watson,**[1] **and F. Yusef-Zadeh**[12]

[1]*Jodrell Bank Centre for Astrophysics, The University of Manchester, UK*
[2]*MPIfR, Bonn, Germany*
[3]*Australian National University, Canberra, Australia*
[4]*Department of Astronomy, University of Illinois, USA*
[5]*IRAP, Université de Toulouse, CNRS, Toulouse, France*
[6]*Department of Astrophysics, Radboud University, Nijmegen, The Netherlands*
[7]*IPAC, Caltech, MC 220-6, Pasadena CA, 91125, USA*
[8]*Kavli Institute, Stanford University, Stanford, CA 94305, USA*
[9]*Dept of Physics, University of Adelaide, South Australia 5005, Australia*
[10]*DRAO, Penticton, BC, V2A 6J9, Canada*
[11]*MPE, Garching, Germany*
[12]*Department of Physics and Astronomy/CIERA, Northwestern University, Evanston, IL., USA*

Observations of the properties of dense molecular clouds are critical in understanding the process of star-formation. One of the most important, but least understood, is the role of the magnetic fields. We discuss the possibility of using high-resolution, high-sensitivity radio observations with the SKA to measure for the first time the *in-situ* synchrotron radiation from these molecular clouds. If the cosmic-ray (CR) particles penetrate clouds as expected, then we can measure the B-field strength directly using radio data. So far, this signature has never been detected from the collapsing clouds themselves and would be a unique probe of the magnetic field. Dense cores are typically ~ 0.05 pc in size, corresponding to $\sim$arcsec at $\sim$kpc distances, and flux density estimates are $\sim$ mJy at 1 GHz. The SKA should be able to readily detect directly, for the first time, along lines-of-sight that are not contaminated by thermal emission or complex foreground/background synchrotron emission. Polarised synchrotron may also be detectable providing additional information about the regular/turbulent fields.

Advancing Astrophysics with the Square Kilometre Array
June 8-13, 2014
Giardini Naxos, Sicily, Italy

*E-mail: Clive.Dickinson@manchester.ac.uk

PoS(AASKA14)102

1. Introduction

Star formation is one of the key processes in the Universe and is of fundamental importance to astrophysics (McKee & Ostriker 2007). We still do not have a full understanding of star formation and, in particular, on the role that magnetic fields play (Crutcher 2012; Li et al. 2014). Cosmic Rays (CRs) are the main ionising and heating agent in dense, starless, molecular cloud cores (Padovani & Galli 2013). The role of magnetic fields has been debated for decades, but due to a lack of precise measurements it has still not been conclusively settled. There are two major classes of star-formation theories: i) strong field models where the B-field controls the molecular cloud, with ambipolar diffusion driving the formation and collapse of dense cores, and ii) weak-field models where turbulent flows trigger star formation. Although B-fields are at least comparable in strength to the turbulent pressure in the ISM, there is no definitive evidence for B-fields dominating gravity or for ambipolar-diffusion-driven star formation (Crutcher 2012).

It is very difficult to measure the detailed properties of dense molecular clouds, and perhaps the most difficult property is the magnetic field - its strength and geometry. The most common method is via Zeeman splitting of radio-frequency HI, OH, and CN lines or masers, which typically gives only the magnetic field strength along the line-of-sight, $B_{\rm los}$ (Crutcher 2012)[1]. Other methods are also difficult, which include using measurements of optical and near-infrared polarisation (extinction along the line-of-sight) and sub-mm polarised thermal dust emission (difficult from the ground) (Poidevin et al. 2013).

An alternative method of probing the magnetic field is via synchrotron radiation (Brown & Marscher 1977; Marscher & Brown 1978; Orlando & Strong 2013), which has rarely been mentioned in the literature in relation to molecular clouds. Synchrotron radiation is produced primarily by relativistic CR electrons when decelerated by magnetic fields. The intensity of synchrotron radiation depends only on the number and energy spectrum of CR electrons and the magnetic field strength perpendicular to the line-of-sight. We know the measured energy spectrum of CRs (Ackermann et al. 2012), at least on average at energies of relevance to radio synchrotron emission ($\sim$GeV), and we know that the CR density varies slowly throughout the Galaxy and can penetrate dense molecular clouds at these energies and above (Brown & Marscher 1977; Marscher & Brown 1978; Umebayashi & Nakano 1981).[2] In molecular clouds, the magnetic field strength is much larger than in the ambient interstellar medium (Crutcher 1999). Therefore, in principle, the synchrotron intensity should give a detectable signature, which could be used as a probe of the magnetic field. This is a direct way of measuring the total magnetic field strength, including the irregular (turbulent) component, which most other indicators (Zeeman, optical polarisation) are not directly sensitive to, since they measure the regular (Zeeman) or ordered (optical polarisation) field.[3] Polarised synchrotron emission could provide additional information, including the ordered

[1] It is possible to get the total B-field strength when complete line splitting is observed, which is possible with masers (Crutcher 1999); see also Robishaw et al. (2015).

[2] There have been claims that GeV CRs cannot fully penetrate the densest clouds, thus suppressing the CR diffusion coefficient (Jones et al. 2008; Protheroe et al. 2008; Jones et al. 2011).

[3] Other indirect measures of the random component exist, such as the Chandrasekhar-Fermi method, which uses the dispersion of the measured polarisation angles to probe the magnetic field in the plane of the sky (Chandrasekhar & Fermi 1953; Watson et al. 2001; Crutcher et al. 2004). See also Hildebrand et al. (2009) and references therein for further extensions.

PoS(AASKA14)102

versus anisotropic random component and projected angle of the magnetic field on the sky.

It is therefore somewhat surprising that very little attention has been given to using synchrotron as a probe of molecular clouds. Jones et al. (2008) observed two nearby (3–4 kpc) dense cold starless cores (G333.125–0.562 and IRAS15596–5301) with the Australian Telescope Compact Array (ATCA) at 1384 and 2368 MHz, to try to detect secondary leptons.[4] They found upper limits of ~ 0.5 mJy/beam and constrained the B-field strength to $B < 500\,\mu$G. However, this is still compatible with the scaling of $|B|$ and $n_{\rm H}$ - more sensitivity is required. Protheroe et al. (2008); Jones et al. (2011) only found upper limits from Sgr B2 after subtraction of the dominant thermal emission. The only possible candidate so far is from the G0.13–0.13 molecular cloud detection, which was detected at 74 MHz, with an associated CO hotspot (Yusef-Zadeh et al. 2013). However, a displacement between the radio position and molecular core suggests it could be from a different region of space.

These non-detections can be partly understood due to the relatively weak (typically mJy or less) signal that is expected to come from *in-situ* synchrotron emission inside the cloud itself. This is due to the fact that on large scales ($\sim$ 1–10 pc), the magnetic fields in clouds appear to be relatively weak ($\sim 10\,\mu$G) while strong fields are on scales much smaller than this (~ 0.05 pc) resulting in a weak flux signal. Also, most of the collapsing clouds ("cores") are located at low latitudes where there is significant confusion from background synchrotron and free-free emission. Nevertheless, high resolution and high sensitivity observations could allow molecular clouds to be mapped in some sight-lines. This may also shed light on CR penetration into the densest clouds, which sometimes appear as a radio dark cloud (RDC) (Yusef-Zadeh 2012). Note that recent high-resolution 5/20 GHz JVLA observations of the Galactic centre cloud G0.216+0.016 have detected compact (< 2.2 arcsec, or sub-pc) non-thermal sources, which may be the signature of in-situ synchrotron radiation from secondary CR electrons (Jones 2014).

In this chapter we briefly review the physics of synchrotron radiation and magnetic fields, and the relation that appears to exist between them in molecular clouds. We then give the prospects of detecting this signature in molecular clouds with the SKA.

2. Synchrotron radiation

Synchrotron radiation is emitted primarily by relativistic cosmic-ray electrons spiralling in the Galactic magnetic field. It is this radiation that often dominates the radio sky at frequencies below a few GHz. The theory of synchrotron radiation is well understood. For a power-law distribution of electron energies,

$$N(E)dE = N_0 E^{-\gamma} dE \ , \tag{2.1}$$

the emissivity, j_ν, of synchrotron radiation is given by

$$j_\nu \propto N_0 B^{(\gamma+1)/2} \nu^{(1-\gamma)/2} \ , \tag{2.2}$$

[4] In this article we focus on primary CR electrons, although the conversion into secondary leptons could be significant in some clouds (Dogel' & Sharov 1990; Protheroe et al. 2008). Observations with the SKA could also provide useful constraints on secondaries.

PoS(AASKA14)102

where B is the magnetic field strength, N_0 is the number density of electrons, γ is the power-law index of electron energies, and ν is the observing frequency. Highly relativistic (GeV and above) CR electrons are expected to penetrate dense clouds freely (Umebayashi & Nakano 1981). If the electron energy spectrum is a power-law with slope $-\gamma$ then the observed synchrotron radio emission spectrum is also a power-law with slope $\alpha = (1-\gamma)/2$ (flux density $S \propto \nu^{\alpha}$). The cosmic ray energy distribution at energies of order GeV can be approximated by a power-law with slope $\gamma \approx +2.5$–3.0 (Ackermann et al. 2012), which corresponds to a synchrotron index $\alpha \approx -0.8$. This is indeed the typical spectral index observed at GHz frequencies (Reich & Reich 1988; Platania et al. 1998).

It can also be seen that the emissivity scales as $B^{(\gamma+1)/2}$, which means it goes as approximately B^2. This is of relevance to molecular cloud collapse, since the magnetic field is expected to be significantly amplified during collapse, and thus could give a detectable signal from *in-situ* synchrotron radiation.

3. Magnetic fields in collapsing clouds

The role that magnetic fields play in the processes of molecular cloud and star formation has been debated for decades. Theoretical studies suggest that magnetic fields play an important if not crucial role in the evolution of interstellar clouds and the formation of stars. In summary, magnetic fields provide magnetic support against cloud collapse. There are various models of star formation and the details of the magnetic field are always important. For example, the core of a cloud can become unstable due to ambipolar diffusion, collapsing to form stars, while the envelope can remain in place. The connection between the core and the surrounding envelope by magnetic field lines can transfer angular momentum outward and make it possible for stars to form. Other star formation models have the dissipation of magnetised turbulence as a controlling factor in star formation. Measuring the magnetic field is a key observation that allows us to infer i) whether supersonic motions are Alfvenic, and ii) the relative importance of the gravitational, kinetic and magnetic densities in dense clouds (Crutcher 1999). These observables thus allow us to test star formation models such as ambipolar diffusion and turbulence (Crutcher 2012; Lazarian et al. 2012).

Detailed measurements of the magnetic field strength and alignment are difficult. However, in recent years, direct measurements of the magnetic field strength have been made. Most notable are Zeeman splitting data (Crutcher 1999; Crutcher et al. 2010) and also sub-mm thermal dust emission (Poidevin et al. 2013). Detailed studies of Zeeman splitting from a sample of molecular clouds indicate that the thermal-to-magnetic pressure $\beta_p \approx 0.04$, implying that magnetic fields are important. Moreover, the measurements showed that magnetic field strengths scale with gas densities as $B \propto n^{\kappa} \approx 0.5$—$0.7$, as shown in Fig. 1. This is close to the theoretical value $\kappa = 0.47$ predicted by models of ambipolar diffusion (Fiedler & Mouschovias 1993). The latest value appears to be $\kappa = 0.65$ (Crutcher 2012) but there is considerable scatter in the measurement (Fig. 1); our best-fitting value applied to detections above 3σ is $\kappa = 0.54 \pm 0.05$, although there could be biases when neglecting non-detections (Crutcher et al. 2010). The large scatter may be related to the fact that Zeeman splitting is only sensitive to the regular (ordered and directional) magnetic field component along the line-of-sight; the B–$n_{\rm H}$ relation may be different for turbulent fields. Furthermore, this trend only occurs above some density $n_0 \sim 300\,{\rm cm}^{-3}$, although this has still to

PoS(AASKA14)102

be determined precisely. Clearly more data, and complementary probes of the magnetic field, are needed to make progress in this area.

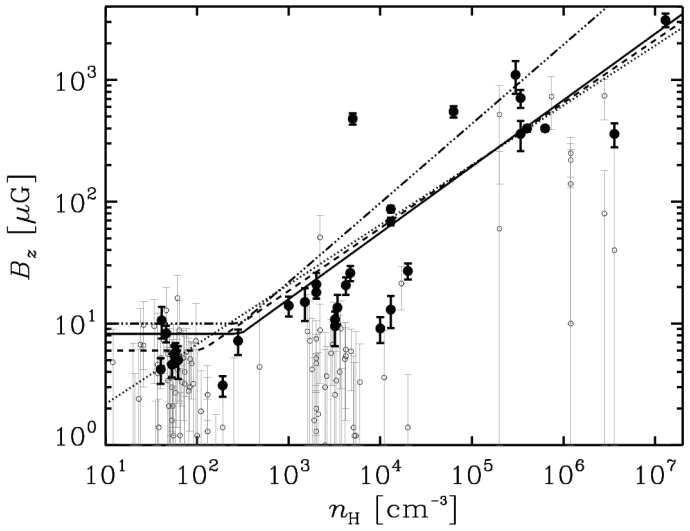

Figure 1: Zeeman splitting measurements of the magnetic field of a number of molecular clouds, plotted against the volume density of molecular gas. Significant ($> 3\sigma$) detections are shown as black filled circles (data taken from Crutcher et al. 2010). There is considerable scatter, yielding various slopes (see overplotted lines) depending on the exact model being fitted. The power-law slope between B_z and density $n_{\rm H}$ is in the range $\kappa \approx 0.5$–0.7. Our best fit (solid line) for detections greater than 3σ significance yields $\kappa = 0.54 \pm 0.05$ above $n_{\rm H} = 300\,{\rm cm}^{-3}$. Preliminary figure reproduced from a forthcoming publication (Strong et al. 2015).

4. Predictions for synchrotron radiation from collapsing clouds

Given that the synchrotron emissivity scales as $\sim B^2$ and B scales as $\sim n_{\rm H}^{0.6}$, it is logical that it should also scale roughly as the volume density i.e. $j_\nu \propto n_{\rm H}$. From this, one might expect low frequency maps such as the Haslam et al. 408 MHz map (Haslam et al. 1982) to be bright around giant molecular clouds (GMCs) and for molecular clouds to be very bright in high resolution observations (e.g. VLA, ATCA). We will now use the observed scaling relation of B with $n_{\rm H}$ to estimate the flux density expected for typical molecular clouds.

We assume that the ambient CR electrons pervade molecular clouds unimpeded and a power-law distribution of CR electron energies with slope γ and a power-law slope between density $n_{\rm H}$ and B-field strength B above a value $n_0 = 300\,{\rm cm}^{-3}$. Using the CR flux model of Strong et al. (2011), the predicted brightness temperature (in mK) at 408 MHz can be be approximated by (Strong et al. 2015):

$$\left(\frac{T_{\rm pred}}{\rm mK}\right) = 2.8 \times 10^3 \left(\frac{N_{\rm H}}{10^{23}\,{\rm cm}^{-2}}\right) \left(\frac{n_{\rm H}}{300\,{\rm cm}^{-3}}\right)^{\kappa(\gamma+1)/2-1}, \qquad (4.1)$$

where $N_{\rm H}$ is the column density (cm^{-2}) and $n_{\rm H}$ the volume density (cm^{-3}). This corresponds to a predicted integrated flux density (in mJy) at 1 GHz, for a source subtending a solid angle $\Omega_{\rm src}$,

PoS(AASKA14)102

Table 1: Molecular cloud data from Crutcher (1999) with estimates of predicted integrated synchrotron flux density $S_{\rm GHz}$ (mJy) at 1 GHz based on the statistical B–$n_{\rm H}$ scaling law (equation 4.2) with $\kappa = 0.6$. The flux density has been scaled to 1 GHz assuming a spectral index $\alpha = -0.8$ ($\gamma = 2.6$). The brightness temperature $T_{\rm GHz}$ is what would be observed with a 51 arcmin beam.

Name	B_z	$n_{\rm H_2}$	R	D	θ	$T_{\rm GHz}$	$S_{\rm GHz}$
	[μG]	[cm^{-3}]	[pc]	[kpc]	[arcsec]	[mK]	[mJy]
W3 OH	3100	6.31×10^6	0.02	2.0	4.0	0.06	0.05
DR21 OH1	710	2.00×10^6	0.05	1.8	11.2	0.30	0.27
Sgr B2	480	2.51×10^3	22.0	7.9	1149	1200	1000
M17 SW	450	3.16×10^4	1.0	1.8	236	31	27.0
W3 (main)	400	3.16×10^5	0.12	2.0	24.3	0.49	0.43
S106	400	2.00×10^5	0.07	0.6	48.1	0.74	0.65
DR21 OH2	360	1.00×10^6	0.05	1.8	11.2	0.14	0.13
OMC-1	360	7.94×10^5	0.05	0.4	50.3	2.3	2.0
NGC2024	87	1.00×10^5	0.2	0.4	196	14.6	13.0
W40	14	5.01×10^2	0.05	0.6	34.4	0.04	0.03
ρ Oph 1	10	1.58×10^4	0.03	0.1	91.7	0.14	0.13

$$\left(\frac{S_{\rm pred}}{\rm mJy}\right) = 6.6 \times 10^6 \left(\frac{\Omega_{\rm src}}{\rm sr}\right) \left(\frac{N_{\rm H}}{10^{23}\,{\rm cm}^{-2}}\right) \left(\frac{n_{\rm H}}{300\,{\rm cm}^{-3}}\right)^{\kappa(\gamma+1)/2-1} . \qquad (4.2)$$

Table 1 lists some example molecular clouds, using data from Crutcher (1999), with predicted flux densities at 1 GHz. We have used the $B - n_{\rm H}$ relation above with $\kappa = 0.6$, assume a synchrotron frequency spectral index $\alpha = 1.0$ ($\gamma = +3.0$), and $\Omega_{\rm src} = \pi/4 \times \theta^2$. Dense molecular clouds have typical densities of 10^5–10^6 cm^{-3} in H_2 and linear sizes of ~ 0.05 pc. This gives column densities of $\sim 10^{23}$ cm^{-2}. For typical distances of a ~kpc, this corresponds to angular sizes of ~ 10 arcsec. It can be seen that many of these sources have predicted flux densities of ~mJy. It is interesting to see that a few sources have much larger predicted flux densities (e.g. Sgr B2 at about 1 Jy). However, one has to be careful since these are due to the large physical size assumed (22 pc for Sgr B2). In practice, the collapsing clouds tend to be very small, often clustered, in a parent cloud that is much larger. The magnetic field measured in the densest regions is unlikely to apply to the entire cloud. Thus it is easy to over-estimate the flux density in this way and this appears to be why dense molecular clouds are not bright in low resolution radio surveys such as the Haslam et al. (1982) 408 MHz map. On the other hand, additional synchrotron from secondary leptons could boost the synchrotron level (Protheroe et al. 2008).

Therefore, the predicted flux densities should only be considered order-of-magnitude estimates at this point since the precise values depend very sensitively on the choice of κ and n_0 and on the observed input parameters. Furthermore, the huge scatter about this relation observed in Fig. 1 already indicates that either the measurements are not representative of the mean field, or, the simple $B - n_{\rm H}$ relationship does not hold. New observations will be crucial for testing this hypothesis.

PoS(AASKA14)102

5. Prospects for the SKA

The high sensitivity and high resolution of the SKA should finally provide the first definitive detection of *in-situ* synchrotron radiation from molecular clouds themselves. The dense cores inside clouds are typically 0.05 pc in size, corresponding to ~ 1 arcsec at a distance of $\sim$kpc. This is well matched to the core of SKA1-MID, which provides good u,v coverage (and therefore good surface brightness sensitivity) up to ~ 5 arcsec. Estimated flux densities are of order mJy for typical dense molecular clouds at GHz frequencies (see Table 1), which is approximately the depth to which current observations have been targeted (e.g. Jones et al. 2008). Optimal frequencies are in the range of a few hundred MHz (band 1–2 of SKA1-MID) to ~ 2 GHz (band 3 of SKA1-MID). The very lowest frequencies ($\lesssim 300$ MHz) will be affected by synchrotron and free-free self-absorption. Above a few GHz, the steep spectrum ($\alpha \approx -0.8$) means the signal will be very weak and more susceptible to free-free contamination, which has a flatter spectral index ($\alpha \approx -0.1$ in the optically thin regime). The SKA is therefore the ideal instrument for studying this, yet untapped, area of radio astronomy.

Multi-frequency (matched u,v coverage) continuum mapping will be important to verify that the emission is non-thermal. In principle, optically thin thermal emission could be removed using radio recombination lines, which could be detected using the wide-band spectral capability of the SKA. Mapping the polarisation of the synchrotron radiation provides further information on the magnetic field, such as the orientation and orderliness. The polarisation fraction could be up to $\approx 75\,\%$ for a ordered field with no depolarisation. However, in practice the observed level will be lower, making this a more difficult measurement to make. Lower frequencies (bands 1/2) will also likely be affected by Faraday depolarisation along the line-of-sight.

Diffuse clouds (e.g., Heiles 1997; Myers et al. 1995) will often not be bound structures, have modest magnetic fields and an in-situ synchrotron signal will not be obvious due to confusion from nearby objects. Given their large size (arcmin to several degrees) and diffuse nature, they will not provide the cleanest signal and are not well-suited to SKA baselines. More well-defined clouds such as CO/sub-mm catalogues of molecular clouds (e.g., Roman-Duval et al. 2010; Planck Collaboration et al. 2011) provide lists of hundreds of clouds but, due to the relatively low angular resolution, they are relatively large in size (5–20 pc) and may not contain the densest clouds of interest here. Proto-stellar outflows may also emit appreciable synchrotron radiation (Sokoloski et al. 2008) which will need to be carefully mapped. Nevertheless, with the large field-of-view of the SKA, it should be possible to find useful areas (Galactic plane and molecular clouds, particularly at high Galactic latitude where cleaner sight-lines should exist) to survey to look for the signature of *in-situ* synchrotron emission.

The best targets will be the most compact and dense clouds, where the magnetic fields are likely to be highest, and the signal will be the cleanest. Examples such as those in Table 1, with angular sizes of $\sim$arcsec are ideal for the SKA. An example would be the ring of dense molecular cores in the W40 complex, where upper limits of $\sim$mJy exist but require deeper observations (Pirogov et al. 2013). The long baselines of SKA will in fact allow us to resolve the emission inside a dense cloud opening up the potential of studying the magnetic field structure within the cloud. Surveying a number of clouds in this way is likely to directly shed light on models of star formation through the alignment of the magnetic field. They should ideally have as little or no

PoS(AASKA14)102

free-free emission from ionised gas or nearby supernova remnants (SNRs).[5] In many cases, such surveys could piggy-back on other SKA surveys of the Galaxy.

The high density and quiescent nature of infrared dark clouds (e.g., Peretto & Fuller 2009), together with high resolution column density images available, will make them interesting targets for SKA observations to probe the magnetic field at early stages of formation. A good example would be the massive star-forming cores within the infrared dark cloud SDC335.579-0.272 (Peretto et al. 2013).

6. Conclusions and outlook

Observations of the properties of dense molecular clouds are critical in understanding the process of star-formation. One of the most important, but least understood, is the role of the magnetic fields. We propose to use high resolution, high sensitivity radio observations with the SKA to measure the *in-situ* synchrotron radiation from these molecular clouds, complementing other methods such as Zeeman splitting (Robishaw et al. 2015). If the CR particles penetrate as expected, then we can measure the B-field strength directly using radio data (the CR flux is relatively smooth and varies slowly throughout the Galaxy with a scale-height of ≈ 1 kpc; Orlando & Strong 2013; Stepanov et al. 2014). If they cannot, then the ability of the SKA to pick up extended, low surface-brightness emission may allow us to search for synchrotron emission from the outer regions of such clouds. Collapsing cores are typically arcsec in size and flux density estimates are $\sim$ mJy at 1 GHz and thus should be readily detectable by the SKA. The large field-of-view will allow many lines-of-sight to be investigated for a given molecular cloud. Multiple frequencies and radio recombination lines will allow separation from free-free emission while polarised data opens up the possibility of mapping the field geometry within collapsing clouds.

CD acknowledges support from an ERC Starting (Consolidator) Grant (no. 307209).

References

Ackermann, M., Ajello, M., Allafort, A., et al. 2012, Physical Review Letters, 108, 011103
Brown, R. L., & Marscher, A. P. 1977, ApJ, 212, 659
Chandrasekhar, S., & Fermi, E. 1953, ApJ, 118, 113
Crutcher, R. M. 1999, ApJ, 520, 706
—. 2012, ARA&A, 50, 29
Crutcher, R. M., Nutter, D. J., Ward-Thompson, D., & Kirk, J. M. 2004, ApJ, 600, 279
Crutcher, R. M., Wandelt, B., Heiles, C., Falgarone, E., & Troland, T. H. 2010, ApJ, 725, 466
Dogel', V. A., & Sharov, G. S. 1990, A&A, 229, 259
Fiedler, R. A., & Mouschovias, T. C. 1993, ApJ, 415, 680
Haslam, C. G. T., Salter, C. J., Stoffel, H., & Wilson, W. E. 1982, A&AS, 47, 1
Heiles, C. 1997, ApJS, 111, 245
Hildebrand, R. H., Kirby, L., Dotson, J. L., Houde, M., & Vaillancourt, J. E. 2009, ApJ, 696, 567

[5] There is a class of SNRs that interact with molecular clouds and they generally show OH masers at the site of the interaction. These sources could be interesting targets for future observations since CRs interact with the cold gas and should produce synchrotron emission (Wardle & Yusef-Zadeh 2002).

PoS(AASKA14)102

Jones, D. I. 2014, ApJ, 792, L14
Jones, D. I., Crocker, R. M., Ott, J., Protheroe, R. J., & Ekers, R. D. 2011, AJ, 141, 82
Jones, D. I., Protheroe, R. J., & Crocker, R. M. 2008, PASA, 25, 161
Lazarian, A., Esquivel, A., & Crutcher, R. 2012, ApJ, 757, 154
Li, H.-b., Goodman, A., Sridharan, T. K., et al. 2014, ArXiv e-prints, arXiv:1404.2024
Marscher, A. P., & Brown, R. L. 1978, ApJ, 221, 588
McKee, C. F., & Ostriker, E. C. 2007, ARA&A, 45, 565
Myers, P. C., Goodman, A. A., Gusten, R., & Heiles, C. 1995, ApJ, 442, 177
Orlando, E., & Strong, A. 2013, MNRAS, 436, 2127
Padovani, M., & Galli, D. 2013, in Advances in Solid State Physics, Vol. 34, Cosmic Rays in Star-Forming Environments, ed. D. F. Torres & O. Reimer, 61
Peretto, N., & Fuller, G. A. 2009, A&A, 505, 405
Peretto, N., Fuller, G. A., Duarte-Cabral, A., et al. 2013, A&A, 555, A112
Pirogov, L., Ojha, D. K., Thomasson, M., Wu, Y.-F., & Zinchenko, I. 2013, MNRAS, 436, 3186
Planck Collaboration, Ade, P. A. R., Aghanim, N., et al. 2011, A&A, 536, A23
Platania, P., Bensadoun, M., Bersanelli, M., et al. 1998, ApJ, 505, 473
Poidevin, F., Falceta-Gonçalves, D., Kowal, G., de Gouveia Dal Pino, E., & Mário Magalhães, A. 2013, ApJ, 777, 112
Protheroe, R. J., Ott, J., Ekers, R. D., Jones, D. I., & Crocker, R. M. 2008, MNRAS, 390, 683
Reich, P., & Reich, W. 1988, A&AS, 74, 7
Robishaw, T., Green, J., Surcis, G., et al. 2015, in "Measuring Magnetic Fields Near and Far with the SKA via the Zeeman Effect" in proc. *Advancing Astrophysics with the Square Kilometre Array*, PoS(AASKA14)110
Roman-Duval, J., Jackson, J. M., Heyer, M., Rathborne, J., & Simon, R. 2010, ApJ, 723, 492
Sokoloski, J. L., Rupen, M. P., & Mioduszewski, A. J. 2008, ApJ, 685, L137
Stepanov, R., Shukurov, A., Fletcher, A., et al. 2014, MNRAS, 437, 2201
Strong, A. W., Dickinson, C., , Murphy, E. J., & et. al. 2015, In preparation
Strong, A. W., Orlando, E., & Jaffe, T. R. 2011, A&A, 534, A54
Umebayashi, T., & Nakano, T. 1981, PASJ, 33, 617
Wardle, M., & Yusef-Zadeh, F. 2002, Science, 296, 2350
Watson, W. D., Wiebe, D. S., & Crutcher, R. M. 2001, ApJ, 549, 377
Yusef-Zadeh, F. 2012, ApJ, 759, L11
Yusef-Zadeh, F., Wardle, M., Lis, D., et al. 2013, Journal of Physical Chemistry A, 117, 9404

PoS(AASKA14)102

PROCEEDINGS OF SCIENCE

Broadband Polarimetry with the Square Kilometre Array: A Unique Astrophysical Probe

B. M. Gaensler[*†‡1,2], **Iván Agudo**[3], **Takuya Akahori**[1,4], **Julie Banfield**[5,6], **Rainer Beck**[7], **Ettore Carretti**[5], **Jamie Farnes**[1,2], **Marijke Haverkorn**[8], **George Heald**[9], **David Jones**[8], **Thomas Landecker**[10], **Sui Ann Mao**[7], **Ray Norris**[5,2], **Shane O'Sullivan**[1,2,11], **Lawrence Rudnick**[12], **Dominic Schnitzeler**[7], **Nicholas Seymour**[5,13], **and Xiaohui Sun**[1]

[1]*The University of Sydney;* [2]*ARC Centre of Excellence for All-sky Astrophysics (CAASTRO);* [3]*JIVE;* [4]*Kagoshima University;* [5]*CSIRO;* [6]*ANU;* [7]*MPIfR;* [8]*Radboud Universe Nijmegen;* [9]*ASTRON;* [10]*DRAO;* [11]*UNAM;* [12]*University of Minnesota;* [13]*ICRAR – Curtin University*

E-mail: bryan.gaensler@sydney.edu.au

Faraday rotation of polarised background sources is a unique probe of astrophysical magnetic fields in a diverse range of foreground objects. However, to understand the properties of the polarised sources themselves and of depolarising phenomena along the line of sight, we need to complement Faraday rotation data with polarisation observations over very broad bandwidths. Just as it is impossible to properly image a complex source with limited *u-v* coverage, we can only meaningfully understand the magneto-ionic properties of polarised sources if we have excellent coverage in λ^2-space. We here propose a set of broadband polarisation surveys with both SKA1 and SKA2, which will provide a singular set of scientific insights on the ways in which galaxies and their environments have evolved over cosmic time.

Advancing Astrophysics with the Square Kilometre Array
June 8-13, 2014
Giardini Naxos, Italy

[*]Speaker.
[†]On behalf of the SKA Cosmic Magnetism Working Group
[‡]Present address: Dunlap Institute for Astronomy and Astrophysics, The University of Toronto

PoS(AASKA14)103

1. Introduction

Faraday rotation is a superb probe of astrophysical magnetic fields at all redshifts. This point was made strongly in the 2004 Square Kilometre Array (SKA) Science Case, in which Beck & Gaensler (2004) proposed a 1.4-GHz polarisation survey with the SKA covering 10 000 deg^2, resulting in a closely spaced "Faraday rotation measure grid" of active galactic nuclei (AGN). As discussed by Gaensler et al. (2004), this rotation measure (RM) grid could then be used to study the detailed magneto-ionic properties of the Milky Way, nearby galaxies, distant galaxies and galaxy clusters, with the ultimate goal of distinguishing between different origins for magnetism throughout the Universe. "Cosmic Magnetism" was correspondingly designated one of the five Key Science Projects for the SKA (Gaensler 2004; Carilli & Rawlings 2004).

A decade later, the relevance and importance of the RM grid have only increased (see Taylor et al. 2007, 2009; Stepanov et al. 2008; Krause et al. 2009; Grant et al. 2010; Hammond et al. 2014; Oppermann et al. 2012, 2014; Hales et al. 2014a; Rudnick & Owen 2014; Stil et al. 2014; Akahori et al. 2014). Specifically, the RM grid remains a powerful tool for probing foreground magnetic fields, i.e., cases where the polarised emitting region and Faraday rotating medium are distinct and well separated, and where the combined statistical properties of a large number of sightlines can be used to extract the global magneto-ionic properties of intervening material (Johnston-Hollitt et al. 2015).

1.1 Beyond The Rotation Measure Grid

For cases in which the polarised emission and Faraday rotation occur in the same source, or in which we are studying the polarisation properties of a single sightline rather than the large ensemble probed by the RM grid, our understanding of polarisation and Faraday rotation has substantially deepened and matured over the last ten years. For example, Beck & Gaensler (2004) assumed that around 50% of polarised AGN would suffer from internal depolarisation, which would manifest itself as a non-linear dependence of polarisation position angle, θ on λ^2 (where λ is the observing wavelength). However, we now realise that even quite simple scenarios (e.g., a source consisting of two spatially unresolved polarised components, each with different RMs) can produce an apparent linear relationship between θ and λ^2, but corresponding to a spurious value of RM; only when one considers the fractional polarisation, $\Pi \equiv \sqrt{(Q^2+U^2)}/I$, as a function of λ^2 does the observer realise that something is amiss (Farnsworth et al. 2011). In such cases, and also in sources for which there is no linear dependence of θ on λ^2, we also now better appreciate the various ways in which $q \equiv Q/I$, $u \equiv U/I$ and Π, all as a function of λ^2, can provide detailed information on magnetic fields, ionised gas and turbulence (Bell et al. 2011; Farnsworth et al. 2011; Beck et al. 2012; Bernet et al. 2012; Farnes et al. 2014a; Brandenburg & Stepanov 2014; Horellou & Fletcher 2014). Furthermore, it is now clear that over a fractional bandwidth of 25% as assumed by Beck & Gaensler (2004), there are considerable degeneracies as to the nature of the observed Faraday rotation (Law et al. 2011; O'Sullivan et al. 2012). Finally, while Beck & Gaensler (2004) proposed that fitting θ vs λ^2 or applying RM synthesis Brentjens & de Bruyn (2005) should be sufficient to extract Faraday rotation in most cases, we now realise that a measurement of RM and its error for a polarised source is an extremely complex problem that as yet has no optimal solution (e.g.,

PoS(AASKA14)103

Farnsworth et al. 2011; Hales et al. 2012; Macquart et al. 2012; Andrecut et al. 2012; Ideguchi et al. 2014; Kumazaki et al. 2014; Sun et al. 2014).

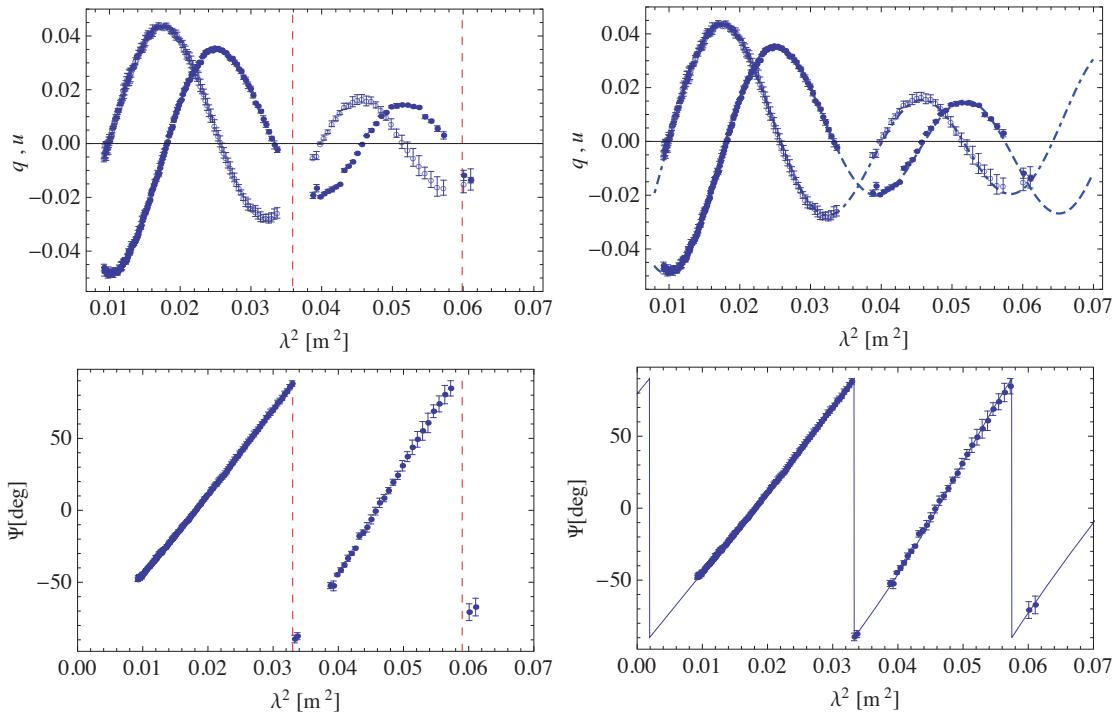

Figure 1: Polarisation data for PKS B1610–771 over the frequency range 1.1 to 3.1 GHz (adapted from Figure 12 of O'Sullivan et al. 2012). Top panel: q (open circles) and u (filled circles) vs λ^2. On the left-hand side, the vertical red lines show the range in λ^2 corresponding to an observation of bandwidth 350 MHz centred on 1.4 GHz; on the right-hand side, the data are fit over the full bandwidth to a model containing two RM components. Bottom row: as for the top row, but showing polarisation angle vs λ^2.

Some of these issues are exemplified in Figure 1, which shows an observation by O'Sullivan et al. (2012) of the bright polarised quasar PKS B1610–771 over the frequency range 1.1 to 3.1 GHz. Three features of note are apparent from these data:

1. The plot of polarisation angle vs λ^2 deviates from a purely linear dependence;
2. The plots of q and u vs λ^2 do not show sinusoids of constant amplitude, and Π is not constant as a function of λ^2;
3. If observed over a relatively narrow bandwidth, none of these behaviours would be apparent.

For example, Beck & Gaensler (2004) consider a representative SKA survey with a bandwidth of 350 MHz centred on 1.4 GHz, corresponding to the vertical red lines in the left column of Figure 1. With such observations, a user would infer a single foreground RM value of +135 rad m^{-2}, would not realise that this value was likely in error, and would have no capacity to identify or understand this source's potentially interesting properties. In contrast, consider the right column of

PoS(AASKA14)103

Figure 1, which shows the same data but now fit with a simple model consisting of two spatially resolved components with different RMs. This shows an excellent match to the data, and allowed O'Sullivan et al. (2012) to infer that this source most likely contains two polarised knots with RMs[1] of +107 rad m^{-2} and +79 rad m^{-2}.

1.2 Broadband Polarimetry with the SKA

Beyond the simple example described in §1.1, there are a whole range of complex behaviours that can only be identified and distinguished if radio polarisation data are recorded over sufficient bandwidth and at high angular resolution and sensitivity. Just as it is impossible to properly image a complex source with limited *u*-*v* coverage, we can only meaningfully understand the magneto-ionic properties of the polarised sources themselves if we have excellent coverage in λ^2-space.

In this Chapter, we highlight the unique new physical insights provided by SKA polarisation surveys over a wide contiguous frequency range. It is important to emphasise that these broadband experiments complement the RM grid, rather than supersede it. The purpose of the RM grid is to study magnetic fields in extended foreground sources such as the Milky Way and the intergalactic medium (IGM).[2] In contrast, broadband data either provide detailed information on *individual* sightlines, or can better probe the *intrinsic* properties of the polarised emitters and their environments. The RM grid primarily probes Faraday rotation, while the broadband studies proposed here primarily probe depolarisation. More fundamentally, broadband polarimetry transcends the study solely of magnetic fields, and instead becomes a highly sensitive tool for addressing a much broader set of issues. In the sections below, we demonstrate that wide-area wide-band polarimetric surveys with the SKA will provide us with powerful new data sets aimed at addressing the following questions:

- What is the relationship between supermassive black holes and their environments? (§2)
- What are the physical properties of absorbing systems? (§3)
- How have galaxies evolved over cosmic time? (§4)

As will be explained below, §2 and §4 focus on polarisation as a probe of the polarised sources themselves and of their immediate environments, while §3 considers the use of background sources to study the effects of Faraday rotation and depolarisation in intervening objects along the line of sight. In §5 we quantify the expected science outcomes for SKA1 and note the relevant observing specifications. In §6, we consider an early science program for SKA1 once it reaches 50% sensitivity. In §7, we anticipate the possible science outcomes that can be pursued with SKA2.

2. What is the Relationship Between Supermassive Black Holes and Their Environments?

All massive galaxies host supermassive black holes (SMBHs). Relativistic outflows from these SMBHs deposit enormous amounts of mechanical energy into their surroundings, pollute the IGM

[1] Note that RM = +135 rad m^{-2} (as would be inferred from observations over a narrow bandwidth) is not even in the range bracketed by these two values.

[2] Sources such as that shown in Figure 1 do not invalidate the RM-grid approach, because only $\lesssim 25\%$ of polarised sources are expected to show behaviour that deviates from the idealised "Faraday thin" case (Law et al. 2011). In addition, the wideband data described here will allow us to explicitly exclude such sources from the RM grid.

PoS(AASKA14)103

with metals and magnetic fields, and regulate star-formation and feedback. A key issue underpinning all these considerations is the extent to which thermal gas from the host galaxy and its surroundings interacts with and is entrained by these outflows. Such entrainment can decelerate the AGN's relativistic jets, suppress star formation, regulate the growth of the central SMBH, and control the acceleration efficiency of ultra-high-energy cosmic rays

Detailed polarimetric studies of individual sources have begun to reveal some of the complex ways in which radio lobes from AGN can interact with their environments — for some sources we see thermal sheaths draped over the radio lobes (e.g., Guidetti et al. 2012), in others we observe compression and mixing of the surrounding thermal gas (e.g., Guidetti et al. 2011), and at least in one case we appear to detect thermal gas *inside* the lobes (O'Sullivan et al. 2013).

However, for the broader population we lack meaningful sample sizes, spatially resolved spectropolarimetry, and a surrounding RM grid to correct for foreground Galactic Faraday rotation. With the SKA, we have the capacity to comprehensively explore the distribution of thermal gas in and around radio lobes from AGN. By simultaneously measuring polarised fractions, Faraday rotation and synchrotron intensity across a broad bandwidth, with the high angular resolution needed to spatially resolve lobes and distinguish them from cores and host galaxies, and in conjunction with information on foreground and background Faraday rotation as supplied by the RM grid, we can provide a comprehensive view of entrainment, outflows, ionised gas and magnetic fields in radio galaxies, covering a wide range of host galaxies, jet powers, environments and redshifts.

3. What Are The Physical Properties of Absorbing Systems?

A fundamental limitation in radio astronomy is the difficulty in studying normal (star-forming) galaxies at large distances. While the SKA will provide the enhanced sensitivity needed to see such sources out to higher redshifts than currently possible, a powerful alternative approach is to study otherwise invisible populations in projection against bright background sources. For the SKA this is typified by surveys for H I absorption toward distant AGN, which will allow an unbiased study of the evolution of normal galaxies over a huge range of cosmic time (Kanekar & Briggs 2004; Morganti et al. 2015).

Polarimetry and Faraday rotation provide an equivalent probe of unseen intervenors, but for ionised rather than neutral gas. Specifically, the detailed magneto-ionic properties of normal galaxies can be studied out to high redshift by determining RMs and polarised fractions as a function of redshift, and by cross-correlating this information with Mg II spectroscopy and deep optical imaging (Kronberg et al. 2008; Bernet et al. 2012, 2013; Farnes et al. 2014b). Through this technique, we can potentially measure the amplitude of turbulence in galactic disks and halos, the amplification time scales and coherence lengths of galactic dynamos, and the covering fraction and spatial extent of intervening systems, all as a function of redshift. However, a number of technical limitations currently prevent any meaningful progress in these areas. To advance this topic, we require:

- Broad bandwidths, with which we can break the degeneracy between different types of Faraday rotation and depolarisation along the line of sight;
- High sensitivity and survey speed, through which we can accumulate a meaningful sample of sources that have both radio polarisation and optical spectroscopy data;

PoS(AASKA14)103

- High angular resolution, with which we can isolate the same sightlines in radio polarisation as are probed by the corresponding optical spectra.

The SKA fulfills all these criteria. When combined with H I absorption surveys (which perhaps can be performed commensally) plus data from next-generation optical and infrared facilities such as 4MOST, WFIRST, LSST and Euclid, we can obtain a complete view of the gas, turbulence, magnetisation and spatial extents of ordinary galaxies over a wide range of redshifts.

4. How Have Galaxies Evolved Over Cosmic Time?

The experiment described in §2 is one of many measurements in which we wish to study the intrinsic properties of radio sources, and to determine how radio galaxies and their associated SMBHs and host galaxies have evolved as a function of redshift. However, any comparison of such sources at different redshifts will be meaningless unless the observed properties are first corrected into the frame of reference in which the emission or Faraday rotation occurs. Usually this requires the application of a "K-correction" (e.g., Hogg et al. 2012), in which the data are shifted to a higher frequency than that with which they were observed. For many applications, the K-correction is simply a direct extrapolation of the source's observed flux using the redshift and spectral index. However, for polarimetry the situation is more complex. Polarisation from AGN as a function of wavelength can show a wide variety of behaviours: some sources depolarise, others "repolarise", and others show oscillatory or other behaviour, as shown in Figure 2. These phenomena are further compounded when a polarised source is spatially unresolved, and contains multiple components with different spectral indices and different polarised fractions.

Thus to determine the polarisation properties of a source in its rest frame, one must directly observe the emitted and subsequently redshifted radiation — extrapolation to frequencies outside the observing band is generally not possible. Such studies require near-continuous polarisation data observed or interpolated across a wide range of frequencies. The wide band is needed both to compare sources over a range of redshifts at a single fixed emitting wavelength, and to characterise the polarisation spectral energy distributions (SEDs) of individual sources. Farnes et al. (2014a) have presented the first large catalogue of polarisation SEDs suitable for comparison of objects at different redshifts in a common rest frame, consisting of 951 sources with multiple polarisation measurements over the frequency range 0.4–100 GHz (see examples in Fig. 2). While the frequency range covered is very large, the sampling is sparse and inconsistent, the individual data points come from different surveys taken at different epochs with different telescopes and differing angular resolutions, and the overall sample size is small.

Using the SKA, broadband polarimetry can provide a very large sample of polarisation SEDs, suitable for robust and accurate rest-frame corrections for many different types of sources over a wide range of redshifts.[3] This will enable a diverse set of powerful experiments with which we can study the polarisation properties of radio galaxies and AGN as a function of redshift. In addition,

[3]Note that two sources at different redshifts will have different effective spacings of adjacent frequency channels in their rest frames. This will mean that a large RM seen at one redshift might not be detectable at another redshift, as per Equation (63) of Brentjens & de Bruyn (2005). However, in practice the expected channel widths for the SKA will be sufficiently narrow that all physically plausible values of RM will be detectable at all redshifts.

PoS(AASKA14)103

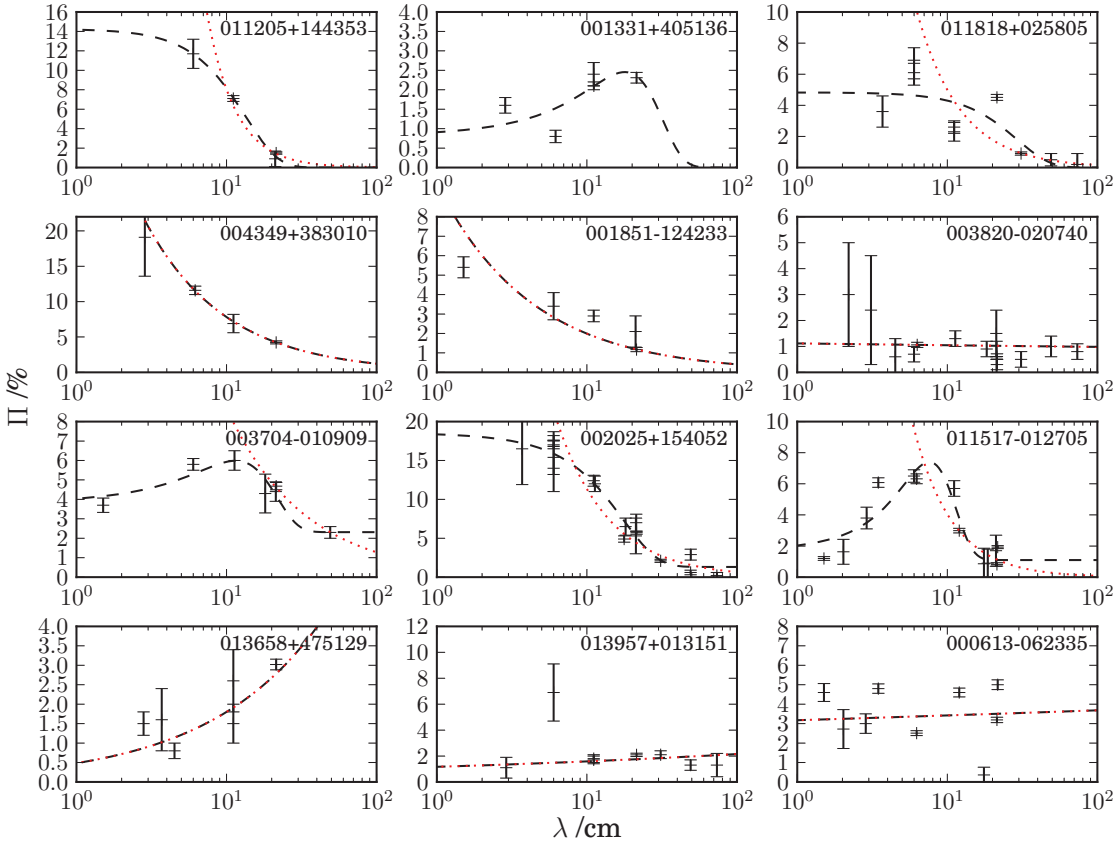

Figure 2: Π vs λ for 12 sources, reproduced from Farnes et al. (2014a) by permission of the AAS. The best-fit polarisation SED chosen from four simple models is shown as a black dashed line: the top row shows sources whose best-fitting polarisation SED has a Gaussian profile, the second row shows depolarising sources, the third row shows SEDs modelled by a Gaussian with a constant term and the last row shows repolarising sources. The red dotted line shows the best-fit power law for Π vs λ. The quality of the fits decreases from left to right.

the SKA will simultaneously obtain total intensity SEDs for an even larger number of sources, which will facilitate detailed studies of spectral indices, spectral curvature and spectral turnover.

5. Science Outcomes for SKA1

The experiments proposed above all require sensitive high-resolution polarisation observations of a large sample of sources over a broad bandwidth. Both SKA1-MID and SKA1-SUR meet these basic specifications. For the RM grid experiment, two additional requirements were all-sky coverage (to fully probe the magnetic field of different parts of the Milky Way) and a very dense sampling of polarised sources (to provide multiple closely spaced sightlines through extended foreground sources). The first of these considerations is not relevant for our purposes, and the second is of reduced importance. Instead, our main drivers are to optimise the frequency coverage and to maximise the number of sources detected. A full consideration of all survey specifications is

PoS(AASKA14)103

beyond the scope of this Chapter, but as for other proposed polarisation and continuum surveys, consideration needs to be given to the requirements on dynamic range, flux calibration (both relative and absolute), $u-v$ coverage, mosaicing strategy and wide-field polarisation purity.

5.1 Choice of Observing Frequency

Arshakian & Beck (2011) have considered the optimum observing frequency, $\nu_{\rm opt}$, for the study of magnetic fields. They define $\nu_{\rm opt}$ as the frequency at which the polarised intensity is a maximum, while requiring a broad bandwidth around this frequency to distinguish between different Faraday and depolarisation effects. Within a given source or intervenor population, at a redshift z and for a standard deviation $\sigma_{\rm RM}$ in RM or Faraday depth (in the frame of the Faraday rotating medium), we have that $\nu_{\rm opt} \propto \sigma_{\rm RM}^{1/2}\,(1+z)^{-1}$. For the case of entrained thermal gas in and around the lobes of radio galaxies as considered in §2, we adopt $\sigma_{\rm RM} \sim 3-6$ rad m^{-2} (O'Sullivan et al. 2013), for which we infer $\nu_{\rm opt} \approx 900-1300\,(1+z)^{-1}$ MHz. For intervening galaxies along the line of sight as discussed in §3, we adopt the "faint galaxy halo" case of Arshakian & Beck (2011), for which $|{\rm RM}| \approx \sigma_{\rm RM} \approx 8$ rad m^{-2} and $\nu_{\rm opt} \approx 1200-1500\,(1+z)^{-1}$ MHz. Finally, for corrections for redshift as proposed in §4, we wish to maximise the redshift range over which sources within a given population can be compared. To achieve this, we must observe over as broad a band as possible, encompassing the optimal frequency $\nu_{\rm opt}$. SKA1-MID Band 2 (950–1760 MHz) and SKA1-SUR Band 2 (650–1670 MHz) both provide the required frequency coverage. SKA1-SUR is preferred because it extends down to lower frequencies than SKA1-MID: in λ^2-space, the coverage of Band 2 is 2.5 times larger for SKA1-SUR than for SKA1-MID. The wavelength coverage of SKA1-MID could be extended by additionally observing with SKA1-MID Band 1 (350–1050 MHz), but the total observing time required would be larger than for SKA1-SUR, despite the larger instantaneous bandwidth for SKA1-MID.

In subsequent discussion, we consider a broadband continuum polarisation survey using SKA1-SUR 2 (650–1670 MHz).[4] This optimises the study of radio lobes (§2) for emitting sources in the redshift range $z \lesssim 0.4-1$ and for intervenors (§3) in the range $z \lesssim 0.8-1.3$, while allowing corrections into a common rest frame (§4) for a population covering the redshift range $\Delta z \approx 1.6(1+z_{\rm min})$ for a minimum redshift $z_{\rm min}$. Thus all three topics can be simultaneously pursued for sources or intervenors in the redshift range $0 < z < 1$.

5.2 Choice of Angular Resolution

The experiments described above require angular resolution sufficiently high to spatially resolve the polarised emission from radio lobes (§2), to match polarisation information to the locations of optical spectra (§3), and to resolve the polarised emission into multiple components (§4). Angular resolutions of $\sim 10''$ to $\sim 1'$, while suitable for the RM grid, cannot address the questions envisaged here.

Our knowledge of polarised morphologies for the faint radio sky is limited. The two deepest polarimetric observations are those of Hales et al. (2014a,b) and Rudnick & Owen (2014). Hales et al. (2014a,b) presented observations at $10''$ resolution, covering the frequency range 1.3–1.5 GHz to a sensitivity of $\approx 30\mu$Jy beam^{-1}. Rudnick & Owen (2014) have reported observations at $1\farcs6$

[4] We note that a possible shift of SKA1-SUR Band 2 to 560–1430 MHz is currently under consideration.

PoS(AASKA14)103

resolution, covering the frequency range 1.3–1.9 GHz to a sensitivity of ≈ 2.4 μJy beam^{-1}. At $10''$ resolution, 36% of polarised sources show extended structure or multiple components in polarised intensity (Hales et al. 2014a), while at $1\farcs6$ resolution, 69% of polarised sources show spatial extent in polarisation[5] (Rudnick & Owen 2014). Thus arcsecond-level (or better) resolution is desired, so as to maximise the number of extended polarised sources detected. This choice also provides the angular resolution needed to compare sources to optical data, and avoids confusion in total intensity even for relatively long integrations. In summary, the angular resolution of the full SKA1-SUR array ($1''$ at 1.4 GHz) is a good match to our requirements.

5.3 Survey Specifications

We first consider the science requirements to study the interaction of radio lobes with thermal gas (§2). To fully investigate this phenomenon, we need a sample large enough to group such sources into 10 redshift bins, 10 luminosity bins and 10 morphological categories (see §6.2.2 of Hales et al. 2014b), with 100 sources in each of these 1000 subsets. We thus aim to observe a total of 10^5 polarised, extended, radio galaxies. Assuming that $\sim 70\%$ of polarised sources are spatially extended at arcsec-resolution (Rudnick & Owen 2014) and that $\sim 20\%$ of sources show complex Faraday depth spectra that might be the signature of interactions with thermal gas, we must observe 7×10^5 polarised sources to obtain our required data set, or a sky density of ~ 23 sources/deg^2 for a survey covering 30 000 deg^2. This sky density is reached for a peak polarised intensity (at 1.4 GHz and at $1\farcs6$ resolution) of ≈ 0.1 mJy beam^{-1} (Rudnick & Owen 2014). The signal-to-noise ratio required for analyses such as that shown in Figure 1 is a topic under active investigation (Sun et al. 2014), but preliminary results suggest that a 20σ detection is sufficient. We therefore require an rms sensitivity of 5 μJy beam^{-1} over the entire bandpass (650–1670 MHz). To cover this bandpass with a 500-MHz instantaneous bandwidth, we require two passes over the sky: a survey at 900 MHz with a 55% fractional bandwidth, and a survey at 1420 MHz with a 35% fractional bandwidth. For a typical source spectral index $\alpha = -0.7$, this requires an rms of 8.5 μJy beam^{-1} at 900 MHz, and 6.2 μJy beam^{-1} at 1420 MHz. Figure 9 of Braun (2014) presents the sensitivity reached by SKA1-SUR as a function of frequency and resolution, assuming a 30% fractional bandwidth and 10 hours per pointing. Scaling from these numbers at $1''$, we require 4.4 and 1.3 hrs per pointing at 900 and 1420 MHz respectively. For ≈ 1700 pointings over 30 000 deg^2, the total survey time is around 10 000 hours. We note that the 1420-MHz component of this survey will simultaneously provide the data needed for observations of an RM grid (Johnston-Hollitt et al. 2015).

For the case of intervenors along the line of sight (§3), we motivate our survey on the results of Farnes et al. (2014b), who were able to show a difference in the radio polarisation properties of quasars with and without foreground Mg II absorbers at 3.5σ significance, using $\sim$140 quasars of which $\sim$40% have one or more Mg II absorbing systems along the line of sight. For SKA1, we aim to double this sample size in subcategories divided into 10 bins of redshift, 5 bins for absorber equivalent-width, and 5 bins of intervenor impact parameter, for a total of 50 000 quasar sightlines. Estimating that quasars are $\sim 10\%$ of the radio source population at the relevant flux levels in total intensity, we therefore require $\sim 7 \times 10^5$ polarised sources in total, or again a sky

[5] Almost all these extended polarised sources fall in the redshift range $z \sim 0.3 - 1$, matching the redshift range covered by SKA1-SUR Band 2 as discussed in §5.1 above

PoS(AASKA14)103

density of 23 sources/deg^2 over 30 000 deg^2. The required rms can be achieved by the same survey as described above. Note that we assume that all 70 000 radio-loud quasars will have associated optical spectroscopy from future surveys, which is reasonable given that the required sky density of such spectra ($\lesssim$2 sources/deg^2) is well below that already available in the northern hemisphere through SDSS ($\gtrsim$ 10 quasar spectra per deg^2).

The total yield of the proposed survey will be 7×10^5 polarised sources detected at $\geq$20-σ significance, corresponding to total intensity fluxes $\gtrsim 5-10$ mJy. We will be able to make use of $\sim$75% of radio galaxies at these flux levels (Wilman et al. 2008) if we seek to apply rest-frame corrections for redshifts $0.5 \lesssim z \lesssim 3$ (see §5.1).

6. An Early Science Program for SKA1

A valuable early science program on broadband polarimetry can be pursued once SKA1 reaches 50% of its full sensitivity. At this stage, SKA1-SUR will consist of 36 12-metre dishes and 24 15-metre dishes, and will have $\sim$5 times the survey speed of ASKAP. One of the survey programs intended for ASKAP is the Polarisation Sky Survey of the Universe's Magnetism (POSSUM; Gaensler et al. 2010), which will image 30 000 deg^2 of the polarised sky to a sensitivity of ~ 10 μJy beam^{-1} at 10$''$ resolution and over the frequency range 1.2–1.5 GHz. Early science for SKA1 could consist of a survey with similar sky coverage, angular resolution and sensitivity to that planned for POSSUM, but covering the frequency range 700–1200 MHz. This would require 2–3 months of observing time with the first 50% of SKA1-SUR. The two data sets would then be combined to provide 700–1500 MHz observations at $\approx$7 μJy beam^{-1} sensitivity at 10$''$ resolution.

While such a data set would not have the high angular resolution and large frequency coverage offered by the full set of broadband observations described in §5, it would provide vital input into the design and approach of these subsequent programs. For example, for studying the interaction of radio lobes with their environments (§2), the proposed early science program would identify $\sim 10^4$ polarised radio lobes that would be spatially resolved at $\approx 10''$ resolution and that would show signatures of thermal entrainment. This is 10% of the full sample size envisaged in §5.3, which would allow us to identify and study the most prominent cases, and to develop the algorithms and models needed to interpret the larger data sets to follow.

7. Considerations for SKA2

The increased sensitivity of SKA2 will obviously allow measurements of effects due to much smaller magnetic field strengths and electron densities in a much larger sample of sources. However, the key point for polarimetry experiments with SKA2 is the increase in the available frequency range, i.e., wide-field survey capability covering 350–1500 MHz. This will allow an extension of the studies described in §5.1 out to redshifts $z \sim 3-4$, corresponding to lookback times when we expect substantial evolution in magnetic field geometry and dynamo activity (Arshakian et al. 2009). Over the next 5 years, new results on the polarised sky from POSSUM, WODAN and the JVLA will greatly advance our understanding of all the issues discussed throughout this Chapter, and will help fully define the goals and expected outcomes for SKA2.

PoS(AASKA14)103

8. Summary and Conclusions

We have described a new polarimetric landscape in which a wide range of Faraday effects have now been identified, each of which provides a unique probe of fundamental properties of galaxies. Over relatively narrow fractional bandwidths ($\lesssim 30\%$), these effects are either undetectable or highly degenerate. However, by using sensitive spectropolarimetric surveys over broad bandwidths, we can reveal the mechanisms by which supermassive black holes couple to their environments, can measure the properties of ordinary galaxies over a large range in redshift, and can understand how different radio source populations have evolved over the Universe's history. Using SKA1-SUR over its full Band 2 frequency range (650–1670 MHz), we can detect polarised emission from the tens of thousands of sources needed to address all these experiments out to redshifts beyond $z \sim 1$. With SKA2, the increased sensitivity and broader frequency coverage will allow us to extend these observations to redshifts $z \sim 3-4$, allowing us to couple existing studies of galaxy evolution and star-formation history to as yet unaddressed questions of how turbulence, ionisation fraction, entrainment efficiency and magnetic field properties have all evolved over cosmic time.

Acknowledgments

B.M.G. acknowledges the support of the Australian Research Council (ARC) through an Australian Laureate Fellowship (FL100100114), and through the ARC Centre of Excellence for All-sky Astrophysics (CE110001020). We thank the referee for a constructive review of the original manuscript.

References

Akahori, T., Gaensler, B. M., & Ryu, D. 2014, ApJ, 790, 123
Andrecut, M., Stil, J. M., & Taylor, A. R. 2012, AJ, 143, 33
Arshakian, T. G. & Beck, R. 2011, MNRAS, 418, 2336
Arshakian, T. G., Beck, R., Krause, M., & Sokoloff, D. 2009, A&A, 494, 21
Beck, R., Frick, P., Stepanov, R., & Sokoloff, D. 2012, A&A, 543, A113
Beck, R. & Gaensler, B. M. 2004, New Astron. Rev., 48, 1289
Bell, M. R., Junklewitz, H., & Enßlin, T. A. 2011, A&A, 535, A85
Bernet, M. L., Miniati, F., & Lilly, S. J. 2012, ApJ, 761, 144
—. 2013, ApJ, 772, L28
Brandenburg, A. & Stepanov, R. 2014, ApJ, 786, 91
Braun, R. 2014, SKA1 Level 0 Science Requirements
Brentjens, M. A. & de Bruyn, A. G. 2005, A&A, 441, 1217
Carilli, C. & Rawlings, S. 2004, New Astron. Rev., 48, 979
Farnes, J. S., Gaensler, B. M., & Carretti, E. 2014a, ApJS, 212, 15
Farnes, J. S., O'Sullivan, S. P., Corrigan, M. E., & Gaensler, B. M. 2014b, ApJ, 795, 63
Farnsworth, D., Rudnick, L., & Brown, S. 2011, AJ, 141, 191
Gaensler, B. M. 2004, Key Science Projects for the SKA (SKA Memo Series, No. 44)
Gaensler, B. M., Beck, R., & Feretti, L. 2004, New Astron. Rev., 48, 1003

PoS(AASKA14)103

Gaensler, B. M., Landecker, T. L., & Taylor, A. R. 2010, BAAS, 42, 470.13
Grant, J. K. et al. 2010, ApJ, 714, 1689
Guidetti, D., Laing, R. A., Bridle, A. H., Parma, P., & Gregorini, L. 2011, MNRAS, 413, 2525
Guidetti, D., Laing, R. A., Croston, J. H., Bridle, A. H., & Parma, P. 2012, MNRAS, 423, 1335
Hales, C. A., Gaensler, B. M., Norris, R. P., & Middelberg, E. 2012, MNRAS, 424, 2160
Hales, C. A., Norris, R. P., Gaensler, B. M., & Middelberg, E. 2014a, MNRAS, 440, 3113
Hales, C. A. et al. 2014b, MNRAS, 441, 2555
Hammond, A. M., Robishaw, T., & Gaensler, B. M. 2014, ApJS, submitted
Hogg, D. W., Baldry, I. K., Blanton, M. R., & Eisenstein, D. J. 2012, arXiv:astro-ph/0210394
Horellou, C. & Fletcher, A. 2014, MNRAS, 441, 2049
Ideguchi, S., Takahashi, K., Akahori, T., Kumazaki, K., & Ryu, D. 2014, PASJ, 66, 5
Johnston-Hollitt, M. et al. 2015, "Using SKA Rotation Measures to Reveal the Mysteries of the Magnetised Universe" in proc. *Advancing Astrophysics with the Square Kilometre Array*, PoS(AASKA14)092
Kanekar, N. & Briggs, F. H. 2004, New Astron. Rev., 48, 1259
Krause, M. et al. 2009, MNRAS, 400, 646
Kronberg, P. P. et al. 2008, ApJ, 676, 70
Kumazaki, K., Akahori, T., Ideguchi, S., Kurayama, T., & Takahashi, K. 2014, PASJ, 66, 617
Law, C. J. et al. 2011, ApJ, 728, 57
Macquart, J.-P., Ekers, R. D., Feain, I., & Johnston-Hollitt, M. 2012, ApJ, 750, 139
Morganti, R., Sadler, E. M., & Curran, S. J. 2015, "Cool Outflows and HI absorbers with SKA" in proc. *Advancing Astrophysics with the Square Kilometre Array*, PoS(AASKA14)134
Oppermann, N. et al. 2014, A&A, submitted (arXiv:1404.3701)
—. 2012, A&A, 542, A93
O'Sullivan, S. P. et al. 2012, MNRAS, 421, 3300
—. 2013, ApJ, 764, 162
Rudnick, L. & Owen, F. N. 2014, ApJ, 785, 45
Stepanov, R., Arshakian, T. G., Beck, R., Frick, P., & Krause, M. 2008, A&A, 480, 45
Stil, J. M., Keller, B. W., George, S. J., & Taylor, A. R. 2014, ApJ, 787, 99
Sun, X. et al. 2014, AJ, 149, 60
Taylor, A. R. et al. 2007, ApJ, 666, 201
Taylor, A. R., Stil, J. M., & Sunstrum, C. 2009, ApJ, 702, 1230
Wilman, R. J. et al. 2008, MNRAS, 388, 1335

PoS(AASKA14)103

PROCEEDINGS OF SCIENCE

Mega-parsec scale magnetic fields in low density regions in the SKA era: filaments connecting galaxy clusters and groups

Gabriele Giovannini[1,2], Annalisa Bonafede[3], Shea Brown[4], Luigina Feretti[1], Chiara Ferrari[5], Myriam Gitti[1,2], Federica Govoni[6], Matteo Murgia[6], and Valentina Vacca[7]

[1]*Istituto di Radioastronomia/INAF (BO), I;* [2]*Dipartimento di Fisica e Astronomia, Bologna University, I;* [3]*Hamburger Sternwarte, Universitat, D;* [4]*Iowa University, USA;* [5]*Lagrange Laboratory, OCA, F;* [6]*Osservatorio Astronomico di Cagliari/INAF, I;* [7]*Max Planck Institute for Astrophysics, D.*

E-mail: ggiovann@ira.inaf.it

The presence of magnetic fields in galaxy clusters has been well established in recent years, and their importance for the understanding of the physical processes at work in the Intra Cluster Medium has been recognized. Halo and relic sources have been detected in several tens clusters. A strong correlation is present between the halo and relic radio power and the X-ray luminosity. Since cluster X-Ray luminosity and mass are related, the correlation between the radio power and X-ray luminosity could derive from a physical dependence of the radio power on the cluster mass, therefore the cluster mass could be a crucial parameter in the formation of these sources. The goal of this project is to investigate the existence of non-thermal structures beyond the Mpc scale, and associated with lower density regions with respect to clusters of galaxies: galaxy filaments connecting rich clusters. We present a piece of evidence of diffuse radio emission in intergalactic filaments. Moreover, we present and discuss the detection of radio emission in galaxy groups and in faint X-Ray clusters, to analyze non-thermal properties in low density regions with physical conditions similar to galaxy filaments. We discuss how SKA1 observations will allow the investigation of this topic and the study of the presence of diffuse radio sources in low density regions. This will be a fundamental step to understand the origin and properties of cosmological magnetic fields.

Advancing Astrophysics with the Square Kilometre Array
June 8-13, 2014
Giardini Naxos, Sicily, Italy

PoS(AASKA14)104

1. Introduction

Magnetism is one of the four fundamental forces and plays an important role in the formation and evolution of objects as large as clusters of galaxies and as small as stars. In spite of the significance of magnetic fields in astrophysics and cosmology, their origin and properties remain poorly understood. Observational evidences derived primarily during the last decade (see e.g. the recent review by Feretti et al. 2012) show that extended magnetic fields within the Intra Cluster Medium (ICM) are common in galaxy clusters:
– for $\sim$ 70 clusters deep radio observations have established the presence of synchrotron extended sources (halos and relics) that are not associated with individual galaxies, but with the ICM as a whole. The observed radio features imply the existence of μG magnetic fields on scales $\sim$ 1 Mpc;
– Faraday-rotation measures of polarized radio sources both within and behind clusters represent independent probes of the strength of intracluster magnetic fields. Studies on both statistical samples and individual clusters (see e.g. Bonafede et al. 2013; Vacca et al. 2012) yield consistent values of 1–5 μG, in cluster central regions.

In addition, evidence has been found for the existence of magnetic fields on even larger scales and in environments of lower density, although in many cases the physical nature of the corresponding structures remains ambiguous.

Here we will present the observational evidence of non-thermal emission in galaxy filaments, poor clusters and low mass regions. These data can improve our knowledge on the origin of cosmological (Mpc scale) magnetic fields. Finally, we will discuss how important the SKA will be for the investigation of this subject.

2. Beyond Galaxy Clusters

The most convincing evidence of radio emission from a genuine filament was presented by Bagchi et al. (2002), who found radio emission coincident with the filament of galaxies ZwCl 2341.1+0000 (see Boschin et al. 2013, for a recent discussion). VLA observations of this field (Giovannini et al. 2010) confirmed the presence of large-scale diffuse emission extending over an area of $\sim$3 Mpc in size. The surface brightness in the faint external regions is $\sim 5 \times 10^{-5}$ mJy/arcsec^2 at 1.4 GHz. The structure is polarized on average at about 10% level.

An additional case of diffuse radio emission possibly associated with a large-scale filament is the Southern component of 0809+39 (Brown & Rudnick 2009). Its origin is uncertain, though its coincidence with a filament of galaxies at z $\sim$ 0.04 suggests that it could be either synchrotron emission from filamentary large-scale structure or old emission from an extinct radio galaxy.

A complex radio emission has also been recently found in the A3411-A3412 structure (Giovannini et al. 2013, Fig. 1). ROSAT X-ray data show a diffuse thermal emission from A3411 and a more compact emission coincident with A3412. The A3411 emission towards A3412 shows a multiple structure with a few sub-components suggesting the presence of an active merger. Optical data confirm the existence of sub-structures and show an extended filament to the SE of A3412, aligned with the A3411 – A3412 system.

The radio image shows a halo source in A3411 and an extended structure in between A3411–A3412 and in the region of the SE filament (see Fig. 1 and Giovannini et al. 2013). The morphology

PoS(AASKA14)104

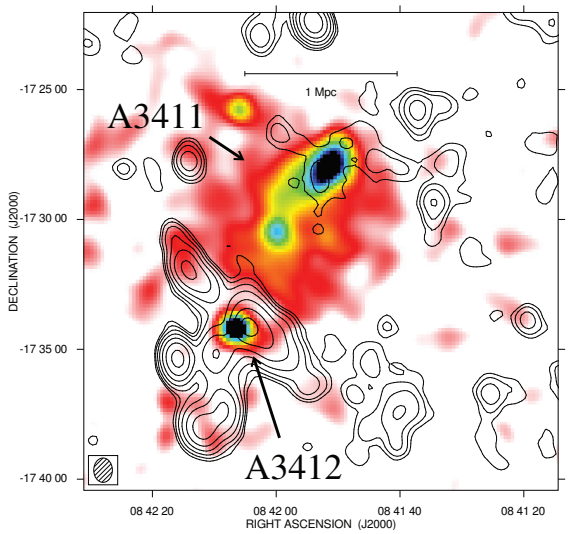

Figure 1: Radio X-ray overlay of the A3411 – A3412 region. Contours show the flux density at 1.4 GHz, half power beam width (HPBW) = 56.3" x 43.1". Contours are from 0.12 mJy/beam with a step of 0.12 mJy/beam. In colour the X-ray image from ROSAT data. Note the extended emission aligned with the A3411–A3412 filament. For more details, see Giovannini et al. (2013).

and properties of the diffuse radio emission could be explained by electron acceleration and magnetic field amplification originated from accretion shocks combined with turbulence in the thermal gas due to the merger between A3411 and A3412 clusters and the SE filament. In particular the diffuse source SE to A3412, oriented along the giant filament could be powered by accretion shocks as material falls onto the filament, as it was suggested by Brown & Rudnick (2011) for the relic of the Coma cluster.

The number of diffuse synchrotron sources connected to galaxy filaments is presently quite low. This is consistent with the relatively high surface brightness limit of present radio surveys (e.g. NVSS) and with the expected low magnetic-field intensity in these regions (e.g. 10 nano-Gauss on the volume average for filaments, Ryu et al. 2008). We could speculate that in the few cases where radio emission has been detected from galaxy filaments, peculiar conditions of merging activity among local sub-groups are able to amplify the magnetic fields and accelerate relativistic particles (see e.g. Boschin et al. 2013 for ZwCl 2341.1+0000 and Vazza et al. 2015).

On a smaller scale, bridges of diffuse radio emission have been found in a few clusters connecting radio halos and peripheral relics (Feretti et al. 2012). These structures may trace the presence of synchrotron emission in filaments of merging material into the main cluster. The prototype is the bridge of radio emission connecting the halo Coma-C with the peripheral relic 1253+275 (Kim et al. 1989). This extended low brightness structure was detected in WSRT data and confirmed by low resolution single dish observations. The surface brightness at 90 cm is lower than $\sim 10^{-4}$ mJy/arcsec^2. Assuming a spectral index of 1.5, a brightness of $\sim 2 \times 10^{-5}$mJy/arcsec^2 at 1.4 GHz is derived. At present, we do not know in detail its morphology and properties because of a too low signal to noise ratio in interferometric data and a too low angular resolution in single dish images. This structure is visible also in X-ray images. Its origin is unknown, but we note that it is in the same direction of the bridge of galaxies connecting Coma to A1367 and forming the super-cluster

PoS(AASKA14)104

structure. A large scale magnetic field is present in the Coma cluster peripheral regions (Bonafede et al. 2010, 2013), but the bridge properties are quite different from those of the central halo and of the relic source. Turbulence in the ICM could be invoked as the origin of the radio emission, but this is problematic because turbulence is not efficient in accelerating particles in low density regions, and a connection to shocks is not clear. Similar features have been found in A2255 and A2744 (Feretti et al. 2012).

3. Poor clusters and low density regions

Since cluster X-Ray luminosity and mass are correlated, the correlation between radio power and X-ray luminosity in radio halos could reflect a dependence of the radio power on the cluster mass. This correlation could indicate that the cluster mass is a crucial parameter in the formation of radio halos and relics. Since it is likely that massive clusters are the result of several major mergers, we can conclude that the cluster total mass and past plus present mergers are the necessary ingredients for the formation and evolution of diffuse radio sources, in agreement with the result that not all clusters with recent mergers show a radio halo or a relic source.

This scenario is presently supported by many observational and theroretical results and it is also in agreement with numerical simulations (see e.g. Brunetti & Lazarian 2011, Vazza et al. 2010, Cassano et al. 2010). However, Brown & Rudnick (2009, 2011), and Giovannini e al. (2009, 2011) have shown the presence of diffuse radio sources in a few clusters with low X-ray luminosity, therefore low mass. Since low-mass clusters and groups are often found in filaments connecting rich galaxy clusters and forming a super–cluster structure, it is important to increase our knowledge of these sources.

The best known case is the poor group of galaxies 0217+70, where an extended central radio halo and double peripheral relic radio sources are present (Brown et al. 2011). Further cases are the radio halo in A523 and in A1213 (Giovannini et al. 2009).

We present in Fig. 2-Left the plot of the total radio power and X-ray luminosity for radio halos as shown in Feretti et al. (2012), where X-ray underluminous clusters are indicated by their name. These halos are overluminous in radio by at least an order of magnitude with respect to the expectation of the radio power – X-ray luminosity correlation. This new population of diffuse radio halos emission opens up the possibility of probing the correlation between low-mass cluster mergers and non-thermal cluster properties (particle acceleration and diffuse magnetic fields) with upcoming deep radio continuum surveys.

4. Two peculiar structures: 0917+75 and A399-A401

The radio source 0917+75 (Fig. 3) is an elongated diffuse emission studied by Dewdney et al. (1991); Harris et al. (1993), and Giovannini & Feretti (2000). It is located in a region away from rich clusters, the nearest one being A786 (z = 0.124) at $\sim$ 4 Mpc. This distance is approximately twice the A786 virial radius, too large for the radio emission being the result of present or past interaction with the cluster. In this region, a few galaxy clusters at the same redshift are present (A787, A762, A748, A765), which belong to the Rood Group of clusters of galaxies N. 27. Their very large distance from the source favours the hypothesis that the diffuse radio structure is related

PoS(AASKA14)104

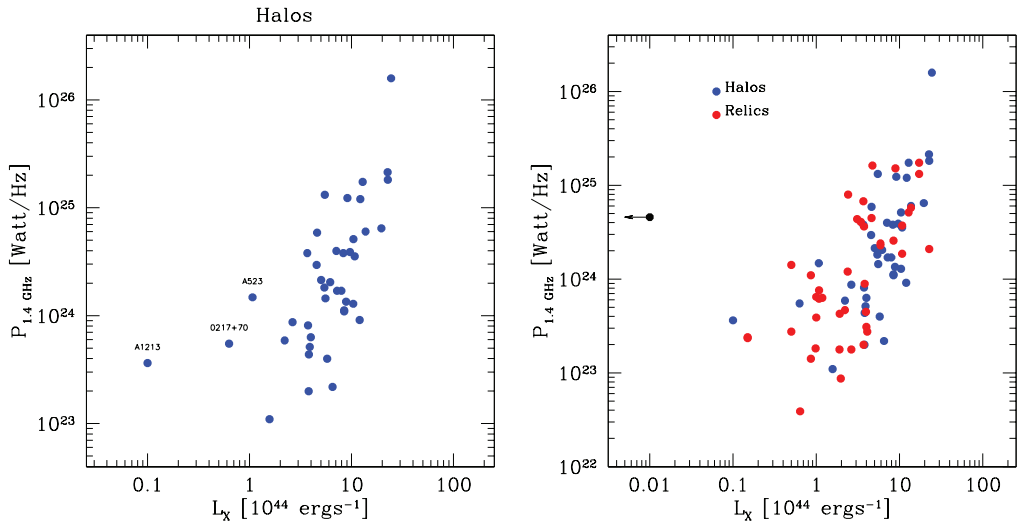

Figure 2: Left: monochromatic radio power of radio halos at 1.4 GHz versus the cluster X-ray luminosity between 0.1 and 2.5 keV for merging clusters with radio halos. Underluminous X-ray clusters are named (from Feretti et al. 2012). Right: monochromatic radio power of radio halos (blue) and relics (red) at 1.4 GHz versus the cluster X-ray luminosity between 0.1 and 2.5 keV for merging clusters (data are from Feretti et al. 2012). The peculiar source 0917+75 is shown in black.

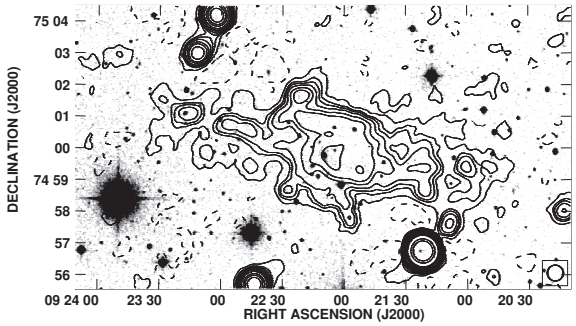

Figure 3: Isocontour image of the diffuse source 0917+75 at 1.4 GHz and HPBW = 20". Contour levels are: -0.2 0.2 0.5 0.7 1 1.5 2 3 5 7 10 30 50 mJy/beam, overimposed on the optical image from the DPSS.

to a galaxy group or to the supercluster structure. Dewdney et al. (1991) noted that a group of galaxies with an apparent magnitude similar to that of galaxies in A786 is present in the region of the diffuse radio emission and obtained the redshift of the two brightest galaxies (0.1241 and 0.1259) confirming the association. Girardi et al. (in progress) studied the distribution of galaxies of the surrounding large scale structure using the SuperCOSMOS Sky Survey. The distribution of the photometric members of the supercluster shows the close clusters as clear overdensities, while several faint galaxies are present in the 0917+75 region, around the two brightest galaxies observed by Dewdney et al. (1991), confirming the presence of a group or a filament. The total spectral index is complex as discussed by Harris et al. (1993), showing an average value between 150 MHz and 1.5 GHz of ~ 1.5, with a possible high frequency steepening. The source is polarized at a 25% level at 1.4 GHz in the brightest inner region (Giovannini et al., in preparation), unexpectedly high for a radio halo.

PoS(AASKA14)104

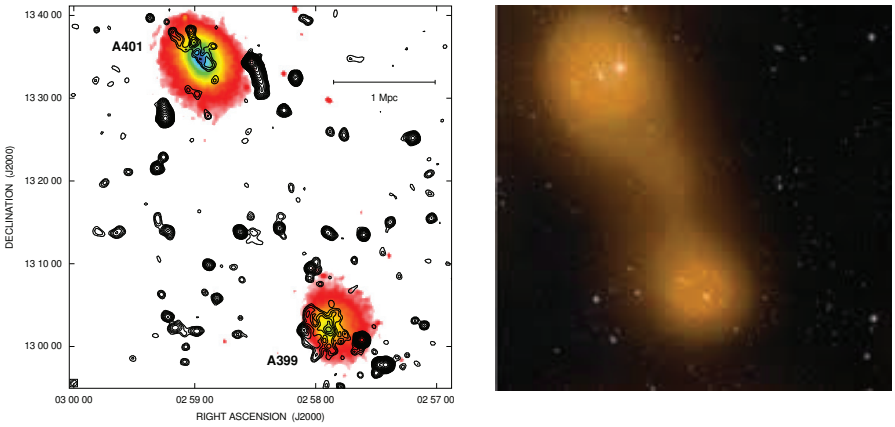

Figure 4: Left: Total intensity radio contours at 1.4 GHz of the system A399–A401 (Murgia et al. 2010), overlaid on the XMM X-ray image. Right: Sunyaev-Zeldovich emission (Planck collaboration 2013) showing a bridge of hot gas connecting A399–A401.

The main peculiarity of this source is the lack of X-ray emission (see Fig. 2-Right). This is unexpected in comparison with other Mpc scale diffuse cluster radio sources (halos or relics), where the radio power is correlated to the X-ray luminosity. X-ray upper limits obtained with the XMM–Newton observatory, impose upper limits on the X-ray flux due to inverse Compton scattering of photons from the cosmic microwave background by relativistic electrons in the diffuse source and imply that the local magnetic field has to be > 0.81 μGauss (three sigma level, Chen et al. 2008). This makes this source quite unique. We suggest that this source could be an inherent feature of the filamentary structure of the Rood 27 supercluster, even if the measured magnetic field lower limit is higher than expected in filamentary structures according to numerical simulations (see e.g. Ryu et al. 2008). Alternatively it could be the remnant of a died radio galaxy. If confirmed it will suggest that AGN activity is important to spread seeds of relativistic particles and magnetic fields in filaments on a scale as large as ~ 2 Mpc.

A399 and A401 is a pair of galaxy clusters separated in projection by an angular distance of 36', corresponding to a linear separation of 3 Mpc. It represents the first example of a double radio halo in the close pair of galaxy clusters (Murgia et al. 2010, Fig. 4). The discovery of this double halo is exceptional, owing to the rarity of halo radio sources in general, and given that X-ray data (e.g. Sakelliou & Ponman 2004, Fujita et al. 2008), seem to suggest that the two clusters are still in a pre-merger state. The existence of these radio halos leads naturally to the question as to whether faint radio emission related to weaker magnetic fields could be present in the intergalactic medium between the two clusters, namely on the scale of galaxy filaments. This question is supported by new Planck satellite data that revealed a Sunyaev–Zeldovich (SZ) signal between A399 and A401 (Planck Collaboration, 2013). The intercluster SZ signal is compatible with a scenario where the intercluster region is populated with a mixture of material from the clusters and the intergalactic medium, indicating the presence of a bridge of matter connecting the two systems. It may be an evidence that the region is witnessing the process of a large–scale structure formation, where cosmic shocks originated by complex merger events are able to amplify magnetic fields and accelerate synchrotron electrons.

PoS(AASKA14)104

5. The Future

To improve our knowledge on the origin and properties of Mpc scale magnetic fields we need a comprehensive view of the radio emission on very large scales, to complement the information obtained from the well known halos and relics present in high X-ray luminous merging clusters:

1) non-thermal emission in larger structures, going from radio halos in clusters to the radio bridges connecting clusters to galaxy filaments and superclusters;

2) non-thermal emission from galaxy clusters with low mass and low X-ray luminosity, often present in supercluster structures connecting rich clusters.

From the surface brightness in the few galaxy filaments discussed above, we can estimate the needs of the expected new observations with SKA1 for a deeper understanding of large scale magnetic fields. The two prototypes of these sources are considered to be ZwCl2341.1+0000 and the bridge in the Coma cluster. In ZwCl2341.1+0000, the surface brightness in fainter diffuse regions is of the order of 0.05 μJy/arcsec^2 at 1.4 GHz. The bridge of radio emission connecting the Coma-C radio halo with the Coma relic source 1253+275 has been detected only at 327 MHz (Giovannini et al. 1990) and its surface brightness $\sim$ 0.02 μJy/arcsec^2 at 1.4 GHz, assuming a spectral index of 1.5 between 327 and 1415 MHz. From these data we estimate that a sensitivity of $\sim 10^{-2}$ μJy/arcsec^2 at 1.4 GHz are needed. In addition, high angular resolution is necessary to avoid confusion limited images. The required compromise between high surface brightness sensitivity and high resolution is best achieved with SKA1-MID (with respect to SKA1-SUR). Comparing Key System Performance Factors for SKA1-MID Array (Table 6 and 7 in Dewdney et al. 2013), with the confusion level estimated by Condon et al. (2012), the best choice would be to observe in Band 2 with the maximum available bandwidth (0.8 GHz) and an angular resolution of $3''$. The minimum detectable flux density in a 2 hour observation should be $\sim$ 0.08 μJy/beam, at the same level of the noise-free confusion limit = 0.08 μJy at this angular resolution. Since the regions with the lowest surface brightness (assuming the conservative hypothesis of uniform distribution) in our sources are at a level of 0.5 – 0.2 μJy/beam, suggested observations should be able to detect likely at 2.5–6 sigma level these kind of radio structures in all covered sky.

To investigate the chance to detect faint halos, we used the synthetic radio halos generated by Xu et al. (2012), under the assumption that the initial magnetic fields are injected into the ICM by AGN at high redshift. Assuming energy equipartition between magnetic fields and non-thermal electrons, Xu et al. compared the global properties of the mock radio halos with the real ones (see Fig. 5). The synthetic radio halos agree with the observed correlations between the radio power versus the cluster X-ray luminosity and between the radio power versus the radio halo size. Out of 16 simulated clusters, eight present a radio halo detectable by present radio telescopes (e.g. JVLA) under the hypothesis of equipartition condition. The eight simulated clusters whose radio emission is below the detection threshold will need deeper radio observations. Using upper limit on total radio power $P_{1.4GHz}$ for the undetected radio halos, assuming a putative size as derived from the total radio power versus the largest linear size correlation, and an average surface brightness of the diffuse emission uniform over the putative halo size, the undetected clusters should host at z = 0.2 radio halos with a 1.4 GHz surface brightness $\sim$ 0.3 μJy/beam, assuming a 3" HPBW. Therefore, also in this case, SKA1-MID observations in 2 hours should be able to detect at 4 sigma level these faint radio halos up to at least z = 0.2 (see Fig. 5).

PoS(AASKA14)104

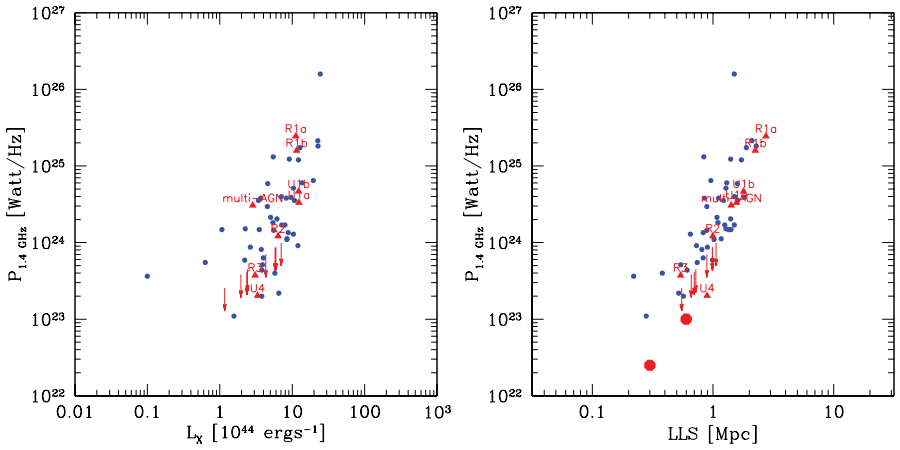

Figure 5: Left: Radio power of radio halos at 1.4 GHz versus the cluster X-ray luminosity in the 0.1–2.4 keV band. Right: radio power of halos at 1.4 GHz versus their largest angular size (LLS). Blue dots are observed clusters, red triangles are simulated clusters, while arrows indicate upper limits on the radio power of simulated clusters (from Xu et al. 2013). Red circles on the Right panel are radio halos detectable at 4 sigma level with SKA1-MID Band 2 at z = 0.2, as discussed in the text.

A caveat is that the angular size of radio emission connected to galaxy filaments is unknown. Moreover, low power sources are best detected at low redshift because of higher flux density, but they could show a large angular size. We note that the bridge of emission in the Coma cluster, as well as the Coma-C radio halo, are not detected by JVLA at 1.4 GHz, not because of sensitivity limit, but because of missing short spacings (the JVLA shortest baseline is $\sim$ 40 meters). To study this kind of structures at this frequency, SKA1-MID should have baselines shorter than 20 m. Observations at low frequencies (SKA1-MID in Band-1, e.g. 700 MHz, and SKA1-LOW) are very suitable to detect this diffuse, steep spectrum radio emission. However, a resolution of a few arcsec is required to avoid confusion limit problems. With a maximun baseline of 100 km, a HPBW $\leq$ 5" is reached down to 150 MHz, thus allowing these observations. The SKA1-LOW requested sensitivity is $\sim$ 10 μJy/beam.

At higher frequencies (i.e. SKA1-MID, Band 3 or 4), these sources are not detected because of missing short spacings, therefore a combination with single-dish data is necessary.

In conclusion, with these observing specifications we expect to be able to estimate the magnetic field strength and radial profile both from synchrotron emission and from Faraday Rotation measure of diffuse and discrete sources within or behind clusters.

Moreover, the large bandwidth will allow to study with a single observation the spectral index distribution of diffuse sources to derive the origin and properties of relativistic particles and acceleration mechanism. Comparison with X-ray images will permit to individuate reacceleration regions and the presence of shocks in the intra-cluster medium.

PoS(AASKA14)104

References

Bagchi, J., Enßlin, T. A., Miniati, F., et al., 2002, New Astronomy, 7, 249
Bonafede, A., Feretti, L., Murgia, M., et al.: A&A 513, 30
Bonafede, A., Vazza, F., Brüggen, M., et al.: 2013 MNRAS 433, 3208
Boschin, W., Girardi, M., Barrena, R.: 2013 MNRAS 434, 772
Brown, S. & Rudnick, L.: 2009 AJ 137, 3158
Brown, S. & Rudnick, L.: 2011 MNRAS 412, 2
Brown, S., Duesterhoeft, J., Rudnick, 2011, ApJ 727, L25
Brunetti, G. & Lazarian, A.: 2011 MNRAS 412, 817
Cassano, R., Ettori, S., Giacintucci, S., et al.,: 2010 ApJ, 721, 82
Chen, C.M.H., Harris, D.E., Harrison, F.A., et al., 2008 MNRAS 383, 1259
Condon, J.J., Cotton, W.D., Fomalont, E.B., et al. 2012 ApJ 758, 23
Dewdney, P.E., Costain, C.H., McHardy, I., et al. 1991 ApJS 76, 1055
Dewdney, P.E., Turner, W., Millenaar, R., et al. 2013 SKA1 System Baseline Design SKA-TEL-SKO-DD-001
Feretti, L., Giovannini, G., Govoni, F., Murgia, M.: 2012, Astron. & Astrophys. Rev. 20, 54
Fujita, Y., Tawa, N., Hayashida, K., et al.: 2008 PASJ 60, 343
Giovannini, G., & Feretti, L.: 2000 New Astronomy, 5, 335
Giovannini, G., Kim, K. T., Kronberg, P. P., Venturi, T.: 1990 IAUS 140, Edrs. R. Beck, P.P. Kronberg, R. Wielebinski p.492
Giovannini, G., Bonafede, A., Feretti, L., et al.: 2009 A&A, 507, 1257
Giovannini, G., Bonafede, A., Feretti, L., et al., 2010 A&A, 511, L5
Giovannini, G., Feretti, L., Girardi, M., et al.: 2011 A&A, 530, 5
Giovannini, G., Vacca, V., Girardi, M., Feretti, L., et al. 2013 MNRAS 435, 518
Harris, D. E., Stern, C. P., Willis, A. G., et al.: 1993 AJ, 105, 769
Kim, K.-T., Kronberg, P. P., Giovannini, G., et al., Nature, 341, 720 (1989)
Murgia, M., Govoni, F., Feretti, L., Giovannini, G.: 2010 A&A 509, 86
Ryu, D., Kang, H., Cho, J., Das, S.: 2008 Science 320, 909
Sakelliou, I., & Ponman, T. 2004 MNRAS 351, 1439
Planck collaboration VIII, 2013 A&A 550, 134
Vacca, V., Murgia, M., Govoni, F., Feretti, L., et al. 2012 A&A 540, 38
Vazza F., Brunetti, G., Gheller, C., Brunino, R.: 2010 NewA 15, 695
Vazza F., Ferrari C., Bonafede A., et al.: 2015 "Filaments of the radio cosmic web: opportunities and challenges for SKA", in proc. *Advancing Astrophysics with the Square Kilometer Array*, PoS(AASKA14)097
Xu, H., Govoni, F., Murgia, M., et al.: 2012 ApJ 759, 40

PoS(AASKA14)104

PROCEEDINGS OF SCIENCE

Cluster magnetic fields through the study of polarized radio halos in the SKA era

Federica Govoni[*1†], **Matteo Murgia**[1], **Hao Xu**[2], **Hui Li**[3], **Michael Norman**[2], **Luigina Feretti**[4], **Gabriele Giovannini**[4,5], **Valentina Vacca**[6], **Gianni Bernardi**[7,8], **Annalisa Bonafede**[9], **Gianfranco Brunetti**[4], **Ettore Carretti**[10], **Sergio Colafrancesco**[11], **Julius Donnert**[4], **Chiara Ferrari**[12], **Myriam Gitti**[4,5], **Luigi Iapichino**[13,14], **Melanie Johnston-Hollitt**[15], **Roberto Pizzo**[16], **and Lawrence Rudnick**[17]

[1]*INAF - Osservatorio Astronomico di Cagliari, Italy;* [2]*University of California at San Diego, CA, USA;* [3]*LANL Los Alamos, NM, USA;* [4]*INAF - Istituto di Radioastronomia Bologna, Italy;* [5]*Dipartimento di Fisica e Astronomia, Universitá degli Studi di Bologna,Italy;* [6]*MPA, Garching, Germany;* [7]*SKA SA, Cape Town, South Africa;* [8]*Department of Physics and Electronics, Rhodes University, Grahamstown, South Africa;* [9]*University of Hamburg, Germany;* [10]*CSIRO, Australia;* [11]*University of the Witwatersrand, SA;* [12]*Observatoire de Nice, France;* [13]*Leibniz-Rechenzentrum, Garching, Germany;* [14]*Universität Heidelberg, ZAH/ITA, Germany* [15]*Victoria University of Wellington, NZ;* [16]*ASTRON, The Netherland;* [17]*Minnesota Institute for Astrophysics, University of Minnesota, USA*

E-mail: fgovoni at oa-cagliari.inaf.it

Galaxy clusters are unique laboratories to investigate turbulent fluid motions and large scale magnetic fields. Synchrotron radio halos at the center of merging galaxy clusters provide the most spectacular and direct evidence of the presence of relativistic particles and magnetic fields associated with the intracluster medium. The study of polarized emission from radio halos is extremely important to constrain the properties of intracluster magnetic fields and the physics of the acceleration and transport of the relativistic particles. However, detecting this polarized signal is a very hard task with the current radio facilities. We use cosmological magneto-hydrodynamical simulations to predict the expected polarized surface brightness of radio halos at 1.4 GHz. We compare these expectations with the sensitivity and the resolution reachable with the SKA1. This allows us to evaluate the potential for studying intracluster magnetic fields in the surveys planned for SKA1.

Advancing Astrophysics with the Square Kilometre Array
June 8-13, 2014
Giardini Naxos, Italy

[*]Speaker.
[†]On behalf of the SKA Cosmic Magnetism Working Group

PoS(AASKA14)105

1. Introduction

An unambiguous proof of the existence of μG magnetic fields spread in the intracluster medium is confirmed by radio observations (Carilli & Taylor 2002, Govoni & Feretti 2004). Information on intracluster magnetic fields can be obtained, in conjunction with X-ray observations of the hot gas, through the analysis of the rotation measure (RM) of radio galaxies lying in the background or embedded within the magnetized intracluster medium (Bonafede et al. 2015). Dedicated software tools and approaches based on a Fourier domain formulation have been developed to constrain the magnetic field power spectrum parameters on the basis of the rotation measure images (Enßlin & Vogt 2003, Murgia et al., 2004, Laing et al. 2008, Kuchar & Enßlin 2011). Typically, rotation measure images of cluster radio galaxies permit investigating the fluctuations of the intracluster magnetic field below a spatial scale of about 50-100 kpc. This does not, however, reach the Mpc scales of radio halos (Ferrari et al.2015, Cassano et al. 2015), which are large-scale diffuse synchrotron sources, located at the center of merging galaxy clusters. They have no optical counterpart and no obvious connection to cluster galaxies, and are therefore associated with the intracluster medium (Feretti et al. 2012).

The study of intracluster magnetic fields is one of the key science themes for the SKA Cosmic Magnetism program. The capability of SKA1 to perform spectro-polarimetric observations with high polarization purity, angular resolution, and sensitivity will permit us to dramatically improve our knowledge of the incidence, strength, and morphology of large-scale magnetic fields in the Universe. An All-Sky Polarization Survey at $\simeq$1 GHz (Johnston-Hollitt et al. 2015), will have the potential of measuring the RM toward a large number of sources (Krause et al. 2009, Bogdanović et al. 2011) permitting derivation of a detailed description of the strength, structure, and radial decrease of cluster magnetic fields. At the same time, this survey will give the opportunity to investigate the total intensity and polarized emission of radio halos at an unprecedent sensitivity and resolution, permitting a detailed investigation of the magnetic field power spectrum in galaxy clusters. The possibility of obtaining both rotation measure and polarized halo emission in the same observation is fundamental to accurately determining the magnetic field spectrum over a large range of spatial scales (Govoni et al. 2006).

Cosmological simulations have been playing an important part in studying the intracluster magnetic field evolution of galaxy clusters (e.g. Dolag et al. 2002, Brüggen et al. 2005, Dubois & Teyssier 2008, Ryu et al. 2008, Donnert et al. 2009, Xu et al. 2009, Dolag & Stasyszyn 2009, Bonafede et al. 2011, Iapichino & Brüggen 2012). Although the existence of cluster-wide magnetic fields is now well-established, their origin, which is ultimately important for understanding the evolution of the intracluster medium during the course of cluster formation, is still unclear (Widrow 2002). Magneto-hydrodynamical simulations of cluster formation have been performed with different initial magnetic fields; these have included random or uniform fields originating at high redshifts, or from the outflows of normal galaxies, or from active galaxies. The cluster magnetic fields of all these simulations are roughly in agreement at low redshifts. They predict μG level magnetic field strengths in the cluster centers and a decrease of the magnetic field strength with radius in the outer regions, in agreement with the observations. Cosmological magneto-hydrodynamical simulations are required at this stage of the project to explore the potential of the SKA1 for investigating intracluster magnetic fields, especially the possibility of detecting polarized radio halo emission.

PoS(AASKA14)105

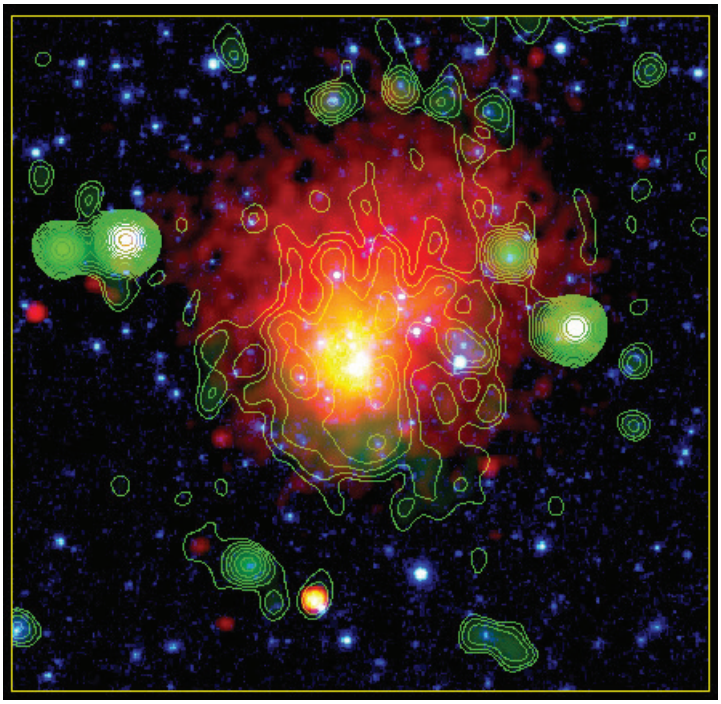

Figure 1: Galaxy cluster A665 at different wavelengths: optical (blue), X-ray (red), and radio (green contours). The radio image, showing an extended diffuse radio halo at the cluster center, has been obtained with the VLA at 1.4 GHz (Vacca et al. 2010).

This chapter will introduce such simulations and their applications.

2. Radio halo studies to investigate cluster magnetic fields

Sensitive radio observations have revealed diffuse emission from the central regions of some merging galaxy clusters. These radio sources, extending over volumes of $\sim$1 Mpc^3 are called radio halos. They are diffuse, low-surface-brightness ($\simeq 1\mu$Jy arcsec^{-2} at 1.4 GHz) and steep-spectrum[1] ($\alpha > 1$) synchrotron sources with no obvious optical counterparts.

The brightness fluctuations of radio halos are closely related to the intracluster magnetic field structure and to the spatial distribution of the emitting relativistic particles (Tribble 1991). Therefore, information on the cluster magnetic fields can be derived from detailed radio halo images. Vacca et al. (2010) presented a study of the magnetic field power spectrum in the galaxy cluster A665, which contains a Mpc-scale radio halo (see Fig. 1). Under the assumption that the magnetic field energy density is in equipartition with that of the relativistic electrons and that these electrons have a power-law energy distribution, their modeling has proven successful in reproducing the observed total intensity fluctuations. The magnetic field model that best reproduces the observations in A665 is characterized by a central strength B_0 =1.3μG, with a magnetic energy density decreasing in proportion to the thermal gas density determined from the intracluster X-ray emission.

[1] $S(\nu) \propto \nu^{-\alpha}$ structures, with α=spectral index.

PoS(AASKA14)105

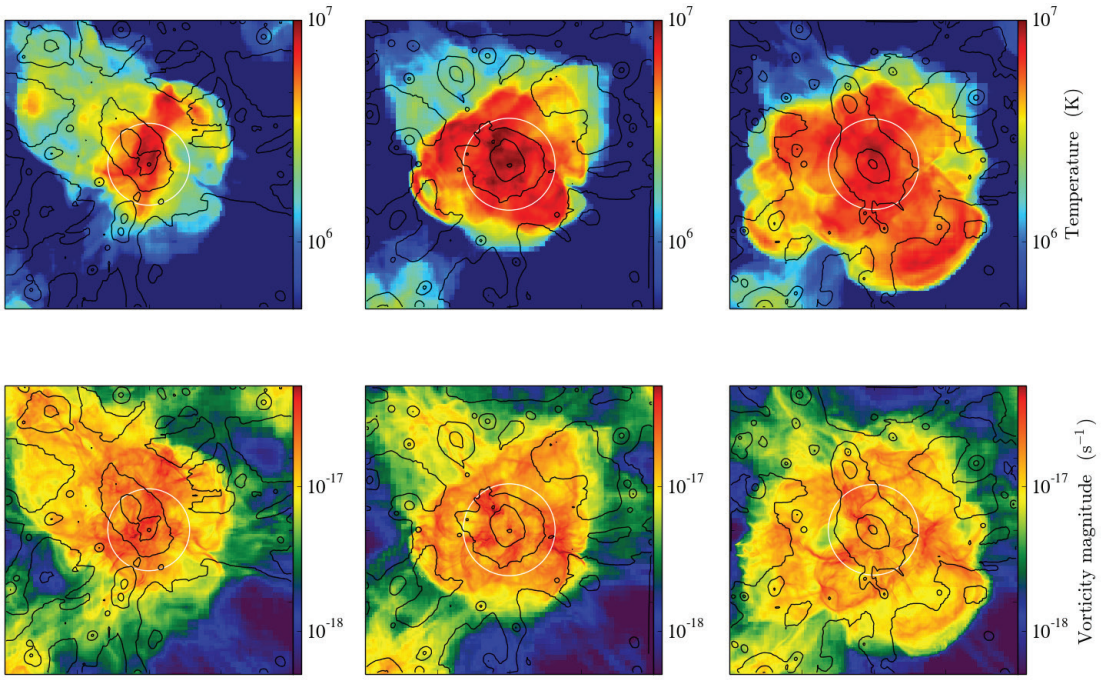

Figure 2: Series of projections (20 Mpc on a side, depth of 20 Mpc) showing gas temperature (upper row) and vorticity magnitude (magnitude of the velocity curl, $|\nabla \times \mathbf{v}|$, lower row) during a cluster major merger (Iapichino 2014). Three different times are shown, namely pre-merger phase (left, $z = 0.43$), post-merger phase (center, $z = 0.15$) and later phase (right, $z = 0$). The region within one virial radius from the cluster centre is enclosed in the white circle. The plots are centered on a massive cluster ($M = 1.3 \times 10^{15}\ M_{\odot}, R_{vir} =$ 3.1 Mpc at $z = 0$).

Assuming a Kolmogorov magnetic field power spectrum, the outer scale of the magnetic field is $\Lambda_{max} \sim$450 kpc.

Interesting morphological similarities between radio and X-ray images have been found in a number of clusters hosting a radio halo (e.g. Govoni et al. 2004). This similarity is generally valid for giant and regular halos. However, more irregular and asymmetric halos have been found in the literature. In these halos, the radio emission may show significant displacement from the X-ray emission. We investigated the statistics of the offset between the radio halo and the X-ray peak of the cluster emission. We found that halos can be quite asymmetric with respect to the X-ray gas distribution, and this becomes more relevant when halos of smaller size are considered (Feretti et al. 2012, Govoni et al. 2012). A possible explanation for this behavior can be attributed to the cluster magnetic field power spectrum. Indeed, on the basis of their magnetic field modeling, Vacca et al. (2010) found that if the outer scale of the magnetic field fluctuations is close to the observing beam, the halo appears smooth and rounded. Increasing the magnetic field correlation length results in a heavily distorted radio halo morphology and in a significant offset of the radio halo peak from the cluster center. Cluster merger events are expected to release a significant amount of energy into the intracluster medium. This energy is injected on large spatial scales, and then turbulent cascades may transport energy to smaller scales. This process is expected to affect the micro-physics of the

PoS(AASKA14)105

intracluster medium : particle transport and acceleration, heating of the intracluster medium, and magnetic field amplification (e.g. Roettiger et al. 1999, Ricker & Sarazin 2001, Dolag et al. 2005, Vazza et al. 2009, Vazza et al. 2011, Xu et al. 2010, Xu et al. 2011, Donnert et al. 2013, Brunetti & Jones 2014). We thus expect a different morphology in the radio halo structure between young and old mergers. Young and smaller systems should have a magnetic field correlation length larger than in the more extended, and dynamical older, radio halos (Govoni et al. 2012). Initially the magnetic field is indeed stirred by the gas-dynamics on scales that are larger than that in dynamically older systems. In addition, both particle acceleration and diffusion/transport depend on turbulent properties (Brunetti & Jones 2014) and a smoother spatial distribution of particles is generally expected in the case of old radio halos. In this framework of energy cascades, smaller halos may have a more distorted morphology if they are young systems in which the energy is still on large scales. They would have a magnetic field correlation length larger than in the more extended, and dynamical older, radio halos. This could be tested by comparing SKA1 observations with the dynamical state of the clusters, as seen in the optical and X-ray bands.

The turbulent dynamo is a widely accepted mechanism for amplifying the magnetic field in the intracluster medium to values well above the level predicted by adiabatic compression. This process is likely to also be important in the cluster outskirts (around and beyond 0.5 R_{vir}), where simulations predict a pressure support by turbulent motions of the order of 10–30 per cent of the total pressure on scales of a few times 100 kpc (Vazza et al. 2011). Interestingly, recent hydrodynamical simulations (Iapichino 2014, Miniati 2014) show that a major merger event can stir the gas and drive turbulent flow even beyond the cluster virial radius. This could persist up to a few Gyr after the merger, thus providing an important mechanism for amplifying magnetic fields not only in cluster cores, but also in the outer regions (see Fig. 2).

2.1 Polarized intensity of radio halos

The detection of polarized emission from radio halos would be extremely important to investigate the magnetic field power spectrum in galaxy clusters and to find merger shocks in the intracluster medium not visible in the X-ray images. Murgia et al. (2004) simulated 3D magnetic fields in galaxy clusters with a single power-law power spectrum of the magnetic field fluctuations $|B_k|^2 \propto k^{-n}$. They investigated how different magnetic field power spectra affect the shape and the polarization properties of radio halos. Models with $n > 3$ and Λ_{max} >100 kpc result in magnetic fields whose energy is larger on the large spatial scales, thus giving rise to possible filamentary and polarized radio halos. Models with $n < 2$, instead, having most of the magnetic field energy on small spatial scales, will give rise to halos with a more regular morphology, and very little polarization.

Typically, radio halos are found to be unpolarized when observed with current radio facilities. But, in agreement with the expectations of Murgia et al. (2004), filaments of polarized emission associated with a radio halo have been detected (see Fig. 3) in A2255 (Govoni et al. 2005) and MACS J0717.5+3745 (Bonafede et al. 2009). The radio halo in MACS J0717+3745 is one of the most powerful radio halos observed so far, with a mean fractional polarization of $\simeq$5 % at 1.4 GHz. The detection of polarized emission indicates that the magnetic field power spectrum in the cluster should be steeper than $n = 3$, and that its maximum scale Λ_{max} should be >100 kpc. On the basis of the interpretation by Govoni et al. (2005), in A2255 a single power law cannot account for the

PoS(AASKA14)105

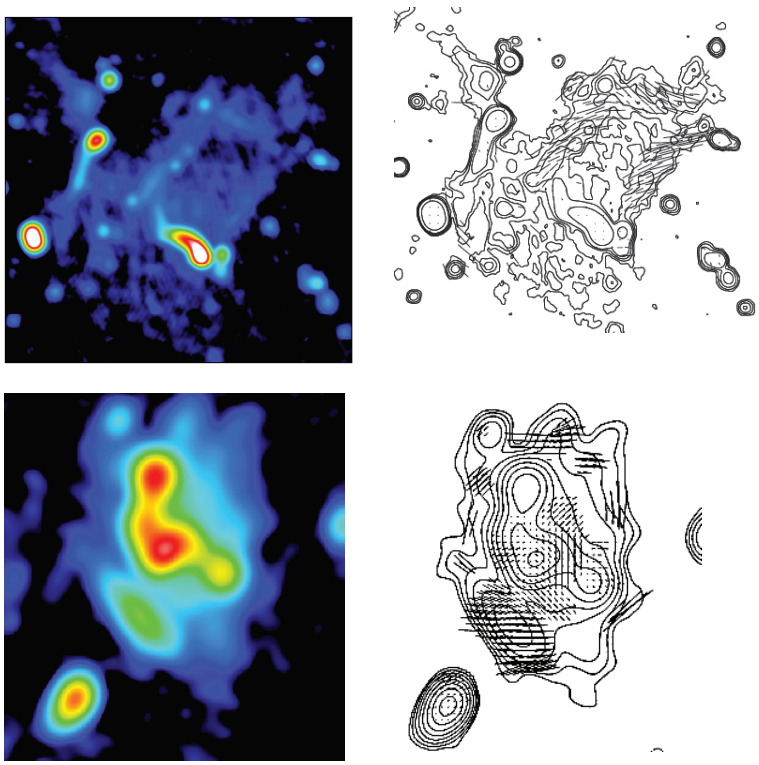

Figure 3: Total intensity and polarization vectors of the radio halos in which a polarized signal has been detected up to now. Top: A2255 (Govoni et al. 2005). Bottom: MACS J0717.5+3745 (Bonafede et al. 2009).

observed polarization. A power spectrum with spectral index $n = 2$ at the cluster center and $n = 4$ at the cluster periphery is needed to produce the observed polarized emission. To explain the highly polarized structures observed in the radio halo it is necessary that most of the magnetic field energy density is on large scales at the cluster periphery. Pizzo et al. (2011) confirmed that the polarized filaments are located at the outskirts of the cluster, but in their interpretation such polarization is not associated with the radio halo emission.

There are several reasons why halo polarization is usually not detected. The orientation of the magnetic field likely changes many times during the path through the cluster. Faraday rotation along the line of sight will suppress the net polarization, due to multiple field reversals along each path. Further depolarization is likely within each beam (beam-depolarization) if the beam size is larger than the angular scale of coherent magnetic field regions.

Recently, Govoni et al. (2013) using cosmological magneto-hydrodynamical simulations showed that radio halos are intrinsically polarized at full-resolution. The fractional polarization at the cluster center is $\simeq 15-35\%$ with values varying from cluster to cluster and increasing with the distance from the cluster center. However, the polarized signal is undetectable if observed with the comparatively shallow sensitivity and low resolution of current radio interferometers.

A high level of intrinsic polarization is also qualitatively in agreement with the early post-merger phase in major mergers, when merger shocks are launched in the cluster's innermost region.

PoS(AASKA14)105

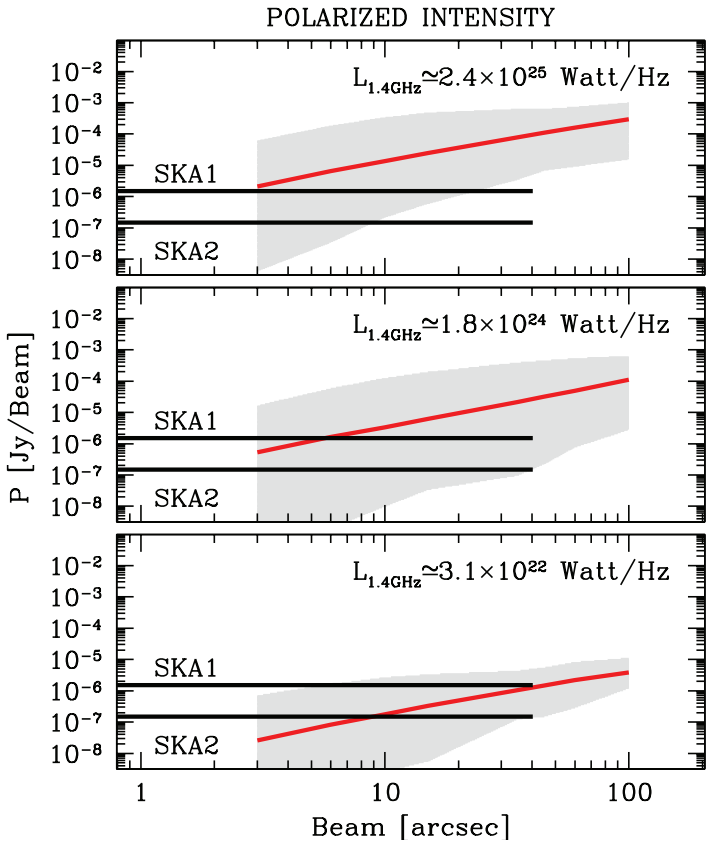

Figure 4: Polarized intensity surface brightness at 1.4GHz as a function of the beam size (3″-100″) for three mock radio halos of different luminosities (Govoni et al. 2013), obtained by using cosmological magneto-hydrodynamical simulations by Xu et al. (2012). The solid red line shows the average brightness, while the shaded region shows the maximum and minimum brightness fluctuations. The simulated surface brightness is compared with a typical sensitivity expected for SKA1 ($\sigma \simeq 1\mu$Jy/beam) and SKA2 ($\sigma \simeq 0.1\mu$Jy/beam). The sensitivity refers to the 3-σ limit.

Simulations of major mergers (e.g. Iapichino 2014, Miniati 2014), suggest that, in this early phase, the flow in the core is dominated by the shock propagation, rather than by turbulent stirring. Targeted studies are needed to determine the duration of this transition in comparison with the radio halo lifetime, and the resulting level of polarization.

3. Magneto-hydrodynamical simulations

In preparation for SKA, several next-generation radio telescopes and upgrades are being constructed around the world. Among them, APERTIF, ASKAP, LOFAR, Meerkat, and the Jansky VLA all offer the chance to explore the polarization properties of cluster diffuse emission. Deep polarization sky surveys are being planned for many of these telescopes. The WODAN survey (Westerbork Observations of the Deep APERTIF Northern-Sky; Röttgering et al., 2011) will use APERTIF to explore at 1.4 GHz the northern sky. This survey will provide a spatial resolution of $\simeq$15″ and a sensitivity of about 10μJy/beam. A similar performance will be reached in the

PoS(AASKA14)105

southern sky with ASKAP through the polarization survey POSSUM (POlarization Sky Survey of the Universe's Magnetism; Gaensler et al. 2010). These resolution and sensitivity values are very promising for detection of the polarized emission of the most powerful ($L_{1.4GHz} \simeq 2.4 \times 10^{25}$ Watt/Hz) radio halos, while halos of intermediate luminosity ($L_{1.4GHz} \simeq 1.8 \times 10^{24}$ Watt/Hz) will still be hardly detectable (Govoni et al. 2013) at this phase.

The high sensitivity and large bandwidths provided by SKA1-MID and SKA1-SUR can be used to exploit the rotation measure synthesis technique and to extract polarized emission at different Faraday depths (Burn 1966, Brentjens & de Bruyn 2005). Pizzo et al. (2011) showed that this technique is very effective in studying the polarized emission of both the discrete sources and the diffuse emission in a comprehensive way. However, alternative techniques like the Faraday synthesis (Bell & Enßlin 2012), modeling of the fractional Q and U as a function of λ^2 (Farnsworth et al. 2011), and stacking radio polarization (Stil & Keller 2015) are also under investigation as ways to best use the capabilities of the SKA and its precursors. We analyzed (Govoni et al. 2013) how the polarization of radio halos will appear at 1.4 GHz, when observed with a bandwidth of 1GHz. In Fig. 4, we present the expected polarized emission of three mock radio halos (characterized by different radio luminosities) as a function of the angular resolution, obtained by applying the rotation measure synthesis. We tentatively represent the 3-σ limit expected with SKA1 ($\sigma \simeq 1\mu$Jy/beam) and SKA2 ($\sigma \simeq 0.1\mu$Jy/beam), by assuming that the confusion limit is negligible in polarization. Fig. 4 shows that at the sensitivity reachable with the SKA1 it will be possible to detect, at high-resolution ($\simeq$5-10$''$), polarized emission in radio halos of high and intermediate luminosity. For fainter halos, ($L_{1.4GHz} \simeq 3.1 \times 10^{22}$ Watt/Hz), the detection of the polarized emission at high resolution is very difficult even for SKA2. Our simulations are based on equipartition between relativistic electrons and magnetic fields and assume that relativistic particles have a power law energy distribution. Simulations including models for acceleration/transport will further shed light on this topic.

4. Conclusions

The detection of polarized signal from radio halos is a very hard task with current radio facilities. Therefore, this is an interesting science case for SKA1. The detection of polarized emission from radio halos may be the key for investigating the magnetic field power spectrum in galaxy clusters and to find merger shocks in the intracluster medium not visible in X-ray images. Indeed, merger shocks with Mach numbers $M \simeq 1-2$, do not produce enough heating to be visible in X-ray images. But, through amplification by compression, they may be detectable in polarization (even before they are seen in total intensity) when observed with SKA1. It is likely that thanks to SKA1 we will be able to detect the polarized emission in a large number of radio halos, obtaining a clearer picture of the power spectrum of the magnetic field fluctuations over the entire volume of the cluster.

PoS(AASKA14)105

REFERENCES

Bell, M. R., & Enßlin, T. A., 2012, A&A, 540, A80
Bogdanović, T., Reynolds, C. S., Massey, R., 2011, ApJ, 731, 7
Bonafede, A., Feretti, L, Giovannini, G., et al., 2009, A&A, 503, 707
Bonafede, A., Dolag, K., Stasyszyn, F., Murante, G., & Borgani, S. 2011, MNRAS, 418, 2234
Bonafede, A., Vazza, F., Brüggen, M., et al., 2015, "Unravelling the origin of large-scale magnetic fields in galaxy clusters and beyond through Faraday Rotation Measures with the SKA" in proc. *Advancing Astrophysics with the Square Kilometre Array*, PoS(AASKA14)095
Brentjens, M.A., de Bruyn, A.G., 2005, A&A, 441, 1217
Brüggen, M., Ruszkowski, M., Simionescu, A., Hoeft, M., Dalla Vecchia, C., 2005, ApJ, 631, L21
Brunetti, G., & Jones, T.W., 2014, International Journal of Modern Physics D, 23, 30007
Burn, B.J., 1966, MNRAS, 133, 67
Carilli, C. L., & Taylor, G. B. 2002, Annual Review of Astronomy and Astrophysics, 40, 319
Cassano, R., Bernardi, G., Brunetti, G., et al., 2015, "Cluster Radio Halos at the crossroads between astrophysics and cosmology in the SKA era" in proc. *Advancing Astrophysics with the Square Kilometre Array*, PoS(AASKA14)073
Dolag, K., Bartelmann, M., Lesch, H., 2002, A&A, 387, 383
Dolag, K., Vazza, F., Brunetti, G., & Tormen, G., 2005, MNRAS, 364, 753
Dolag, K., & Stasyszyn, F. 2009, MNRAS, 398, 1678
Donnert, J., Dolag, K., Lesch, H., Müller, E. 2009, MNRAS, 392, 1008
Donnert, J., Dolag, K., Brunetti, G., Cassano, R., 2013, MNRAS, 429, 3564
Dubois, Y., & Teyssier, R., 2008, A&A, 482, L13
Enßlin T.A., & Vogt C., 2003, A&A, 401, 835
Farnsworth, D., Rudnick, L., Brown, S., 2011, AJ, 141, 191
Feretti, L., Giovannini, G., Govoni, F., & Murgia, M. 2012, The Astronomy and Astrophysics Review, 20, 54
Ferrari, C., Dabbech, A., Smirnov, O., et al., 2015, "Non-thermal emission from galaxy clusters: feasibility study with SKA" in proc. *Advancing Astrophysics with the Square Kilometre Array*, PoS(AASKA14)075
Gaensler, B.M., Landecker, T.L., Taylor, A.R., & POSSUM Collaboration, 2010, Bulletin of the American Astronomical Society, 42, #470.13
Govoni, F., Markevitch, M., Vikhlinin, A., et al. 2004, ApJ, 605, 695
Govoni, F., & Feretti, L. 2004, International Journal of Modern Physics D, 13, 1549
Govoni, F., Murgia, M., Feretti, L., et al., 2005, A&A, 430, L5
Govoni, F., Murgia, M., Feretti, L., et al., 2006, A&A, 460, 425
Govoni, F., Ferrari, C., Feretti, L., et al. 2012, A&A, 545, A74
Govoni, F., Murgia, M., Xu, H., et al., 2013, A&A, 554, A102
Iapichino, L., & Brüggen, M. 2012, MNRAS, 423, 2781
Iapichino, 2014, private communication
Johnston-Hollitt, M., et al., 2015, "Using SKA Rotation Measures to Reveal the Mysteries of the Magnetised Universe" in proc. *Advancing Astrophysics with the Square Kilometre Array*, PoS(AASKA14)092

PoS(AASKA14)105

Krause, M., Alexander, P., Bolton, R., et al., 2009, MNRAS, 400, 646
Kuchar, P., & Enßlin, T.A., 2011, A&A 529, A13
Laing, R.A., Bridle, A.H., Parma, P., Murgia, M., 2008, MNRAS, 391, 521
Miniati, F. 2014, ApJ, 782, 21
Murgia M., Govoni F., Feretti L., et al., 2004, A&A, 424, 429
Pizzo, R.F., de Bruyn, A.G., Bernardi, G., Brentjens, M.A., 2011, A&A, 525, A104
Ricker, P.M., & Sarazin, C.L., 2001, ApJ, 561, 621
Roettiger, K., Stone, J.M., Burns, J.O., 1999, ApJ, 518, 594
Röttgering, H., Afonso, J., Barthel, P., et al., 2011, Journal of Astrophysics and Astronomy, 32, 557
Ryu, D., Kang, H., Cho, J., Das, S., 2008, Science, 320, 909
Stil, J.M., Keller, B.W., 2015, "Stacking for Cosmic Magnetism with SKA Surveys" in proc. *Advancing Astrophysics with the Square Kilometre Array*, PoS(AASKA14)112
Tribble, P.C., 1991, MNRAS, 253, 147
Vacca, V., Murgia, M., Govoni, F., et al., 2010, A&A, 514, A71
Vazza, F., Brunetti, G., Kritsuk, A., et al., 2009, A&A, 504, 33
Vazza, F., Brunetti, G., Gheller, C., Brunino, R., Brüggen, M., 2011, A&A, 529, A17
Widrow, L. M. 2002, Reviews of Modern Physics, 74, 775
Xu, H., Li, H., Collins, D.C., Li, S., Norman, M.L., 2009, ApJ, 698, L14
Xu, H., Li, H., Collins, D.C., Li, S., Norman, M.L., 2010, ApJ, 725, 2152
Xu, H., Li, H., Collins, D.C., Li, S., Norman, M.L., 2011, ApJ, 739, 77
Xu, H., Govoni, F., Murgia, M., et al. 2012, ApJ, 759, 40

PoS(AASKA14)105

PROCEEDINGS OF SCIENCE

Magnetic Field Tomography in Nearby Galaxies with the Square Kilometre Array

George Heald[*1,2†], **Rainer Beck**[3], **W. J. G. de Blok**[1,4,2], **Ralf-Jürgen Dettmar**[5], **Andrew Fletcher**[6], **Bryan Gaensler**[7], **Marijke Haverkorn**[8,9], **Volker Heesen**[10], **Cathy Horellou**[11], **Marita Krause**[3], **Sui Ann Mao**[3], **Niels Oppermann**[12], **Anna Scaife**[10], **Dmitry Sokoloff**[13], **Jeroen Stil**[14], **Fatemeh Tabatabaei**[15], **Keitaro Takahashi**[16], **Russ Taylor**[14,4] **and Anna Williams**[17]

[1]*ASTRON, Postbus 2, 7990 AA Dwingeloo, the Netherlands;* [2]*Kapteyn Astronomical Institute, PO Box 800, 9700 AV Groningen, the Netherlands;* [3]*Max-Planck-Institut für Radioastronomie, Auf dem Hügel 69, 53121 Bonn, Germany;* [4]*University of Cape Town, Private Bag X3, Rondebosch 7701, South Africa;* [5]*Ruhr-Universität Bochum, Universitaetsstrasse 150, 44780, Bochum, Germany;* [6]*School of Mathematics and Statistics, Newcastle University, Newcastle upon Tyne NE1 7RU, UK;* [7]*The University of Sydney, Sydney, NSW 2006, Australia;* [8]*Department of Astrophysics/IMAPP, Radboud University Nijmegen, P.O. Box 9010, 6500 GL Nijmegen, The Netherlands;* [9]*Leiden Observatory, Leiden University, P.O. Box 9513, 2300 RA Leiden, The Netherlands;* [10]*School of Physics and Astronomy, University of Southampton, Southampton SO17 1BJ, UK;* [11]*Chalmers University of Technology, Onsala Space Observatory, 43992, Onsala, Sweden;* [12]*Canadian Institute for Theoretical Astrophysics, University of Toronto, 60 St. George Street, Toronto ON, M5S 3H8, Canada;* [13]*Department of Physics, Moscow University, 119992 Moscow, Russia;* [14]*The University of Calgary, Calgary, AB T2N 1N4, Canada;* [15]*Max-Planck-Institut für Astronomie, Königstuhl 17, 69117 Heidelberg, Germany;* [16]*Kumamoto University, 2-39-1 Kurokami, Kumamoto 860-8555, Japan;* [17]*Department of Astronomy, University of Wisconsin-Madison, Madison, WI, USA*

E-mail: heald@astron.nl

Magnetic fields play an important role in shaping the structure and evolution of the interstellar medium (ISM) of galaxies, but the details of this relationship remain unclear. With SKA1, the 3D structure of galactic magnetic fields and its connection to star formation will be revealed. A highly sensitive probe of the internal structure of the magnetoionized ISM is the partial depolarization of synchrotron radiation from inside the volume. Different configurations of magnetic field and ionized gas within the resolution element of the telescope lead to frequency-dependent changes in the observed degree of polarization. The results of spectro-polarimetric observations are tied to physical structure in the ISM through comparison with detailed modeling, supplemented with the use of new analysis techniques that are being actively developed and studied within the community such as Rotation Measure Synthesis. The SKA will enable this field to come into its own and begin the study of the detailed structure of the magnetized ISM in a sample of nearby galaxies, thanks to its extraordinary wideband capabilities coupled with the combination of excellent surface brightness sensitivity and angular resolution.

Advancing Astrophysics with the Square Kilometre Array
June 8-13, 2014
Giardini Naxos, Sicily, Italy

PoS(AASKA14)106

1. Overview and Techniques

A key issue to be addressed with the SKA is the three-dimensional structure of magnetic fields in galaxies. One of the most powerful tools for studying these structures is the Faraday rotation of polarized synchrotron radiation. Faraday rotation, caused by the birefringence of magnetoionized plasma, rotates the plane of linear polarization by an angle proportional to λ^2, where the constant of proportionality is called the rotation measure (RM). In the simplest cases the RM is equal to the "Faraday depth", the integral of the thermal electron density weighted line-of-sight magnetic field. Modern radio spectropolarimetry typically makes use of the so-called RM Synthesis (Brentjens & de Bruyn 2005) technique to combine broadband, multi-channel observations into Faraday depth spectra, which encode the polarized emission visible as a function of the Faraday depth. The benefits of the RM Synthesis technique are discussed elsewhere (e.g. Heald 2009) but include sensitivity to faint Faraday-rotated polarized emission, along with the related ability to recover – at least partially – polarized emission originating at a range of Faraday depths within the line of sight (LOS) cylinder. Such LOS are typically called "Faraday thick" because their Faraday depth spectra show broad profiles. They are probed by frequencies between approximately 500 MHz and 2 GHz.

RM Synthesis is based on a Fourier transform of the observed complex linear polarization $P(\lambda^2) = Q(\lambda^2) + iU(\lambda^2)$ from the λ^2 domain into the Faraday depth (ϕ) dimension, where Q and U are the linear Stokes parameters. Since the λ^2 coverage of any given observation is incomplete, there is a sampling function called the RM Spread Function (RMSF) in the Faraday domain. The RMSF can be deconvolved from the Faraday spectrum through the use of an algorithm called `RMCLEAN` (Heald, Braun & Edmonds 2009), but it has been recognized (e.g. Farnsworth, Rudnick & Brown 2011) that the technique has some drawbacks. It is usually complemented by fitting in the (Q,U) domain (e.g. O'Sullivan et al. 2012), which requires *a priori* knowledge or assumptions about the physical nature of the emitting region(s), but can lead to a more stable signal reconstruction than deconvolution. In this chapter we assume that data analysis techniques will make use of a suitable combination of RM Synthesis, deconvolution, and guided fitting to recover physical parameters from polarization observations.

SKA observations in Band 4 (Beck et al., this volume) will provide exquisite sensitivity to the small scale structure of magnetic fields in the disks of galaxies and the relation to other morphological information such as the gas distribution. Such observations are rather sensitive because the radiation has suffered very little depolarization, which is caused by structure in the gas and magnetic field distributions on scales smaller than the resolution element of the telescope. Internal depolarization is ubiquitous in galaxies, causes a strongly frequency-dependent modulation of the polarization degree, and carries a great deal of information about the physical conditions of the ISM. With the SKA we can make use of lower frequency observations to provide a new dimension of information that is highly complementary to the higher frequency approach, gaining new insight into the small scale structure of the ISM through detailed modeling of the depolarization. This can then be compared with the small-scale structure of the gaseous component.

*Speaker.

†on behalf of the SKA Cosmic Magnetism Working Group

PoS(AASKA14)106

In this contribution we seek to outline the applicability of this observing setup and analysis approach to gaining leverage on the structure of the ISM in galaxies. While the focus is on spiral galaxies, we note that other objects can be studied in this way, e.g. AGN and intracluster media.

With SKA1, Faraday tomography can be performed in nearby galaxies with excellent spatial resolution (e.g. ~ 34 pc for M 83) and with suitable surface brightness sensitivity. Even in the 50%-sensitivity "early science" phase, SKA1 will provide excellent prospects for this project. The SKA will open the door to the study of these phenomena in even finer detail in the nearest targets and will allow study of the evolution of magnetic field structures in galaxies.

2. Scientific goals

2.1 Small-scale 3D gas and magnetic field structures

Polarization and depolarization are two sides of the same coin. Long considered as a nuisance to observers, especially at long wavelengths where it usually becomes more severe and affects prospects of detection, depolarization has been traditionally more appreciated by theorists who recognized its potential as a powerful probe of the magneto-ionic medium (Burn 1966; Sokoloff et al. 1998). The SKA, with its high sensitivity and broad bandwidth compared to all existing instruments, opens up the possibility to exploit this potential, and learn about both the small-scale and the large-scale structure of the magnetic field in galaxies, and about their interactions with the populations of electrons, thermal and non-thermal (cosmic ray electrons).

The various depolarization mechanisms acting in galaxies are well understood. Most of them have to do with Faraday rotation (differential Faraday rotation, internal or external Faraday dispersion) and are thus wavelength-dependent and related to the thermal component of the gas and the magnetic field component along the line of sight. Depolarization can also be produced within the observing beam, for example by a tangled magnetic field (in which case the observed degree of polarization is wavelength-independent) or due to the averaging of several sources (in which case it could be wavelength-dependent). The signature of random but anisotropic magnetic fields can also be predicted.

For a number of reasons, observations in SKA band 2 ($\nu = 650 - 1670$ MHz or $\lambda = 18 - 46$ cm for SKA1-SUR, or $\nu = 950 - 1760$ MHz for SKA1-MID; see Table 1) are ideal. First, the typically steep synchrotron spectral index ($\alpha \gtrsim 0.7$, for $S_\nu \propto \nu^{-\alpha}$) from the ISM in galaxies means that the continuum emission is strong at these moderate radio frequencies. Moreover the frequency range covered in Band 2 is well-suited to measure the variations of the fractional polarization, for the typical ISM properties in spirals. In a mixed synchrotron-emitting and Faraday-rotating medium, differential Faraday rotation results in a decrease of the fractional polarization with λ^2, as illustrated in Figure 1. The broader the Faraday dispersion function (which describes the intrinsic polarized emission as a function of Faraday depth), the faster the decrease. For LOS with narrow distributions of Faraday depth, there is little depolarization across the band as shown for example by Arshakian & Beck (2011). The variations are shown for top-hat ("Burn slab") models of different widths (10 rad m^{-2}, solid line, and 30 rad m^{-2}, dashed line). A Gaussian model with a dispersion of 30 rad m^{-2} is also shown (dotted line). Faraday dispersion by a random field will accentuate this decrease (Sokoloff et al. 1998). In some magnetic field configurations, such as for helical fields

PoS(AASKA14)106

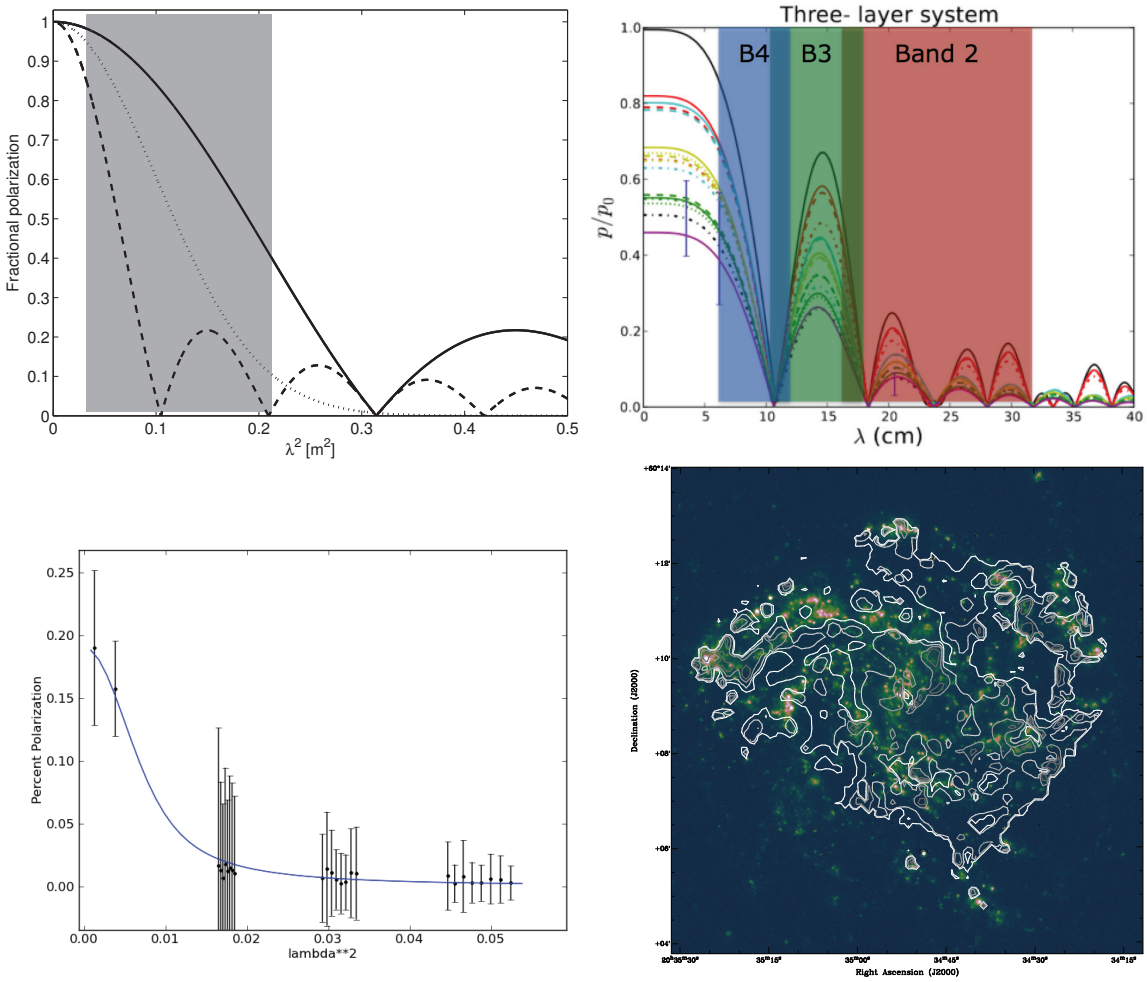

Figure 1: *Top left*: simple models of Faraday dispersion, using a Burn slab (thick line and dashed line) or a Gaussian distribution (dotted line). For the Burn slab the thicker distribution of Faraday depth corresponds to the dashed line and therefore to stronger depolarization across the bandwidth of interest (gray shaded region). *Top right*: Various depolarization models reproduced from Shneider et al. (2014) and overlaid with colored regions indicating the approximate wavelength coverage of the various SKA1-MID bands. *Bottom left*: Faraday dispersion measured in a particular region of the NE interarm region in NGC 6946 (Williams et al. in prep). Measurements of the polarized fraction were made at 3,6,13,18, and 22 cm and fitted with a Gaussian model. *Bottom right*: Strength of Faraday dispersion within NGC 6946, determined by fits like the one in the bottom left panel and presented as contours overlaid on the Hα image from Ferguson et al. (1998) (Hα image on a log stretch). Increased turbulent depolarization tends to be associated with H II regions.

along the line of sight, the degree of polarization may actually increase with wavelength (Sokoloff et al. 1998; Brandenburg & Stepanov 2014; Horellou & Fletcher 2014).

As early examples of Faraday tomography in the pre-SKA era, recent sparsely sampled multi-frequency polarimetric observations of a small number of nearby galaxies are now providing new insight into the ordered and random magnetic fields in the ISM. For example, a combined observation of NGC 6946 using the Westerbork Synthesis Radio Telescope (WSRT) at $\lambda = 13$ cm, 18 cm, and 22 cm, together with 3.5 cm and 6.2 cm data (from Beck 2007), is being used to model the de-

PoS(AASKA14)106

polarization (Williams et al. in prep, see Figure 1), probe new Faraday depths with RM Synthesis, and recover detailed estimates of the magnetic field structure across the entire galaxy. Assuming typical ISM properties and a simple configuration of a large-scale magnetic field along the line of sight and turbulent magnetic cells of equal size and uniform distribution, the Burn slab model (Burn 1966; Sokoloff et al. 1998) can also be utilized to begin to tease out the coherence length of the large-scale line of sight magnetic field and correlation lengths of line of sight random magnetic fields. Applying this rather simple model to all of the various ISM environments in NGC 6946 is a stepping stone toward robustly estimating small scale magnetic field properties and relating those to other ISM tracers. Comparing these results to observations that trace other ISM properties, including star formation and H I line-width profiles, illuminates the roles played by both large- and small-scale magnetic fields in various dynamical processes within galaxies. More sophisticated and detailed models of the 3D magnetic structure (such as those presented by Shneider et al. 2014) are a natural next step and indicate the sort of modeling that can be applied to large samples of galaxies observed with contiguous frequency coverage and excellent sensitivity. This new kind of investigation can be extended with the transformational capabilities of the SKA.

2.2 Connection to properties of the ISM and star formation

The ISM of galactic disks is highly turbulent and the recovery of its intrinsic polarised emission requires observations at high frequencies to avoid Faraday depolarisation (Beck et al., this volume). The Faraday depth spectra of turbulent fields contain many components that can be separated with very high resolution in real and in Faraday space (Frick et al. 2011). The added value provided by the approach advocated in this chapter is the ability to also investigate field structures in the outer disks and halos of galaxies, where turbulence is reduced and polarised emission still significant. Observations of the same sample of galaxies at both high and moderate frequencies address complementary scientific goals and together probe the full galactic volume, on scales ranging from the smallest structure in the ISM to the galaxy as a whole. Are the small scale structures in the disk and halo the same, or are the turbulent properties decoupled?

2.3 Large-scale field structures

Depolarization has been crucial to understand the large-scale magnetic field structure in a sample of nearby galaxies (Heald, Braun & Edmonds 2009; Braun, Heald & Beck 2010). Due to the substantial depolarization in the midplane of star-forming galaxies (e.g. Braun et al. 2007; Vollmer et al. 2013, in the WSRT-SINGS survey and in the Virgo cluster, respectively), only the front layer of the ISM is visible in polarization as could be expected from internal Faraday dispersion (Sokoloff et al. 1998). This depolarization, together with a common large-scale magnetic field topology, leads to a clear and consistent pattern within the sample: an azimuthal variation in fractional polarization exhibiting a minimum at the kinematically receding major axis, together with an azimuthal variation in the rotation measure. These characteristic patterns can be explained with a simple model for the large-scale magnetic field consisting of an axisymmetric trailing spiral together with a quadupolar configuration. Such configurations are predicted by e.g. the $\alpha - \Omega$ dynamo. The minimum in polarized intensity at the receding major axis vanishes when the same galaxies are observed at higher frequencies, where depolarization is reduced and the backside of the galaxy is visible. Additionally, faint polarized emission from the backside of the galaxy was

PoS(AASKA14)106

also recovered at lower frequency in some galaxies (Braun, Heald & Beck 2010), having been substantially depolarized and with an additional dispersion term due to the intervening turbulent ISM.

The SKA will have the capability to move beyond the recognition of this observational effect, and exploit the same physical properties of the magnetized ISM in galaxies to perform a more detailed form of Faraday tomography. When observing at higher frequency, the polarized synchrotron radiation originates from a somewhat greater depth in the ISM due to the frequency-dependent character of the depolarization. Making use of the variation in polarization and RM patterns, together with the field orientation, will lead to a more complete and accurate 3D picture of the large-scale magnetic field in galaxies and permit a more detailed model than the simplistic quadrupolar topology used by Braun, Heald & Beck (2010).

Very weakly polarized emission can be identified statistically in the output of RM Synthesis using the technique introduced by Gießübel et al. (2013). The same strategy can be exploited with the SKA to study still weaker magnetic fields in the halos and outer disks of galaxies.

2.4 Vertical field structures

The structure of regular magnetic fields in the galactic plane has been obtained for a dozen or so different galaxies. The most important of these properties, in that they allow direct comparisons to be made with galactic dynamo theories, are the magnetic field pitch angles and rotational symmetry. The vertical distribution of both regular and random magnetic fields is much more poorly explored, even though these are also closely related to diverse dynamo theory predictions, as well as to other important aspects of galactic astrophysics such as gas flows across the disk-halo boundary. Measurements of how magnetic fields change as a function of height above the galactic plane has been difficult in the past due to the coarse resolution available in both spatial scales and in Faraday depth.

Important questions that will be resolved through study of the depolarization in galaxies with Band 2 of SKA1 include the following. What are the origins of halo magnetic fields: transport from a dynamo active disk, in-situ generation (e.g., Moss et al. 2010), or a primordial leftover from galaxy formation? Are random magnetic fields transported into the halo, providing a route by which a disk dynamo can be saturated, and if so is this transport part of a self-limiting cycle involving the dynamo and outflows or just a fortuitous coincidence? Does a galactic wind/fountain transport magnetic fields out of the galaxy disk (as observed by Heald 2012, based on an RM signature corresponding to a superbubble in NGC 6946) and if so, are helical fields ejected into the halo (Heesen et al. 2011)? How does the magnetic energy density compare to the thermal energy density in outflows? Does magnetic reconnection contribute to gas heating in galaxy halos? How uniform are regular disk fields as a function of height above the galactic plane: in face-on galaxies are we measuring the mid-plane properties or an emission-weighted average and is the field structure the same through all 1 kpc of the disk thickness or not?

Faraday tomographic observations of a sample of disk galaxies, with a range of inclination angles, will allow us to establish, for the first time, three essential aspects of galactic magnetic fields that are key to firmly identifying their origin: (i) How the regular magnetic field structure changes with height above the disk, in particular do the components of the field have even or odd

PoS(AASKA14)106

symmetry with respect to the mid-plane? (ii) What happens at the disk-halo boundary? Are small-scale and/or regular magnetic fields transported into the halo? (iii) Do the ordered fields in the disk and halo have similar or different patterns, and are X-shaped halos common? These field properties are all closely related to the state of the interstellar medium, in particular the buoyancy of hot gas, magnetic fields and cosmic rays driving vertical flows across the disk-halo boundary. The ability to resolve features at least on scales of 100 pc to 1 kpc is required to relate structures in the magnetic field to those in the gaseous distribution, such as H I holes that have typical sizes smaller than 2 kpc (e.g., Bagetakos et al. 2011). Moreover, typical correlation scales of magnetized structures in the ISM range from tens of pc to 1 kpc (e.g., Gaensler et al. 2005; Fletcher et al. 2011; Houde et al. 2013; Mao et al. 2014). Variations in the polarised intensity as a function of both Faraday depth and location in the plane of the sky will be compared and fit to the patterns expected from models with different symmetry properties in their magnetic field, in order to separate properties that are common in all galaxies from properties that are specific to individual galaxies.

3. Synergy with other ISM observations

A key aspect of the study of the Faraday thickness within galaxies is the connection between the magnetoionized structure implied by the depolarization spectra, and the gas phase properties determined from complementary observations. An important observable to relate to the Faraday structure of the ISM is the properties of the neutral gas traced by H I.

Studies of the warm and cold H I in other galaxies were already attempted by Young & Lo (1996, 1997) and Young et al. (2003) who analyzed H I emission velocity profiles of seven nearby dwarf galaxies. By fitting these profiles with Gaussian components, they found evidence for a broad component with a velocity dispersion ranging from about 8 to 13 $\mathrm{km\,s^{-1}}$ as well as a much narrower component with a velocity dispersion ranging from 3 to 5 $\mathrm{km\,s^{-1}}$. The authors associated the narrow component with the CNM and the broad component with the WNM phases of the ISM. A similar study by de Blok & Walter (2006) of the Local Group dwarf galaxy NGC 6822 also found narrow and broad H I components with mean velocity dispersions of 4 $\mathrm{km\,s^{-1}}$ and 8 $\mathrm{km\,s^{-1}}$, respectively. They found that the narrow component is usually located near star-forming regions, whereas the broad component tends to be found along every line of sight. Ianjamasimanana et al. (2012) and Stilp et al. (2013) used stacking of velocity profiles to determine the fractions of cold and warm H I. The key limitation of these studies was angular resolution, and the improved capabilities of the SKA should enable these studies to be repeated for individual profiles, rather than stacked ones. Faraday tomography will provide complementary information about the relevant coherence scales and degree of randomness in the ISM.

4. Prospects with SKA

As has been discussed elsewhere (e.g. Gaensler et al., this volume) the key technical aspect for polarization studies is the total λ^2 coverage. Here we assume that SKA1 Band 2 can be used in its entirety (Band 2 having been selected for the reasons outlined in § 2).

In order to resolve small-scale structures in the disk and reduce beam (frequency-independent) depolarization, high angular resolution is required. For this frequency range and assuming SKA1-

PoS(AASKA14)106

Parameter	SKA1-MID	SKA1-SUR
Lowest frequency (MHz)	950	650
Highest frequency (MHz)	1760	1670
RM resolution $\Delta\phi = 2\sqrt{3}/\Delta\lambda^2$ (rad m^{-2})	51.4	19.2
Maximum RM scale $\pi/\lambda^2_{\rm min}$ (rad m^{-2})	97.4	97.4
Maximum RM[a] (rad m^{-2})	5216	2443

Table 1: Parameters of interest in SKA1 Band 2 polarization observations.

[a]Assuming 1 MHz channel width; far higher RMs can be reached by forming individual polarization images with narrower bandwidth.

MID, $\nu_{\rm min} = 950$ MHz. The current array configuration (Braun 2013; Dewdney 2013) gives a 0.3 arcsec nominal resolution for a 200 km baseline length in SKA1-MID. However, such an extended configuration will not provide sufficient surface brightness sensitivity to reliably image the diffuse polarization in nearby galaxies. In order to match the surface brightness sensitivity obtained with existing instruments (e.g. $10\,\mu$Jy beam^{-1} with $15''$ resolution; Braun, Heald & Beck 2010), with 100h of SKA1 observing time, an angular resolution of $1.5''$ is feasible. This is a dramatic step forward – a factor of 10 reduction in synthesized beam size compared to existing instruments enables the study of magnetic field structures on ≈ 34 pc scales in the typical nearby grand-design galaxy M 83 ($D = 4.61$ Mpc; Saha et al. 2006), sufficient to probe down to the correlation scale of the magnetic field structure – but implies that only baselines out to ≈ 40 km will usefully contribute to the observation. This is reflected in the sensitivity calculations in this chapter. In practice, for these calculations we excluded the outer 30 antennas in SKA1-MID, and the outer 18 antennas in SKA1-SUR. The MeerKAT and ASKAP arrays are assumed to remain in place and contribute to the sensitivities.

For proper analysis of the frequency-dependent depolarization in galaxies, the same angular resolution has to be considered at all frequencies. For this reason we have further adjusted the sensitivity calculation to reflect the fact that the outer antennas are effectively lost for the high-frequency end of the band. For both SKA1-MID and SKA1-SUR the effect is approximated by discarding the outer 10 antennas for the upper half of the frequency band, taking the SEFD values from the Science Performance document (Braun 2013), and calculating image noise values with the formula provided in § 7.1 in that document.

4.1 SKA Phase I

Using the full available bandwidth, the broadband sensitivity from SKA1-MID band 2 after a deep 100h integration is estimated to be approximately $0.1\,\mu$Jy beam^{-1} (approximately 10 times more sensitive for an observation of fixed duration than the Jansky VLA at L-band), or about $1\,\mu$Jy beam^{-1} for a relatively shallow 1h observation. For SKA1-SUR, the same sensitivities are approximately 0.4 and $4\,\mu$Jy beam^{-1}. The large sensitivity discrepancy is of obvious importance for single-field pointings that we consider for the study of individual galaxies; for a few galaxies with large angular size ($\gtrsim 1^\circ$), multiple SKA1-MID pointings will be required, offsetting some of the benefit of the higher sensitivity provided by SKA1-MID. It should also be noted that in terms of RM precision, the larger bandwidth of SKA1-SUR does not necessarily provide a better

PoS(AASKA14)106

observing capability, since the increased sensitivity of SKA1-MID compared to SKA1-SUR for a given observing time more than compensates for the larger λ^2 coverage of SKA1-SUR ($\Delta\phi_{\rm eff} \approx \Delta\phi/[2 \times S/N]$ by analogy to the astrometric precision in the image plane; Fomalont 1999). In this case, the net improvement in effective RM precision is such that SKA1-MID has $\approx 54\%$ better RM precision that SKA1-SUR, for the same on-source integration time. On the other hand, a narrower RMSF is always preferable to properly reconstruct closely spaced features in Faraday depth spectra (features more closely spaced than the FWHM of the main lobe of the RMSF cannot be reliably interpreted; e.g., Farnsworth, Rudnick & Brown 2011; Sun et al. 2014). The use of SKA1-SUR may be preferable where recovery of complex Faraday depth spectra is judged to be more important than sheer RM precision.

SKA1-MID will be able to robustly study diffuse polarization at 100 pc resolution in galaxies out to 14 Mpc, and at 1 kpc resolution to $z \approx 0.04$. The detailed study of magnetic field structures will be possible through shallow observations of hundreds of galaxies (so that similarities and peculiarities across the galaxy population can be investigated). Deeper polarization observations, ideally performed together with deep H I observations, will enable an exquisite view of the connection between magnetism and ISM structure in tens of individual galaxies.

4.2 SKA Phase I in its early stages

During the "early science" period when each array has half of its final collecting area, excellent surface brightness sensitivity can still be achieved. Here we assume that the relative distribution of collecting area within the array configurations is held fixed, but the number of stations is halved. In that case the broadband sensitivity for a 100h observation in SKA1-MID is $160\,\mu$Jy beam^{-1}, or $580\,\mu$Jy beam^{-1} for SKA1-SUR (both in Band 2 and using the entire bandwidth in each case).

4.3 SKA2

For SKA2, the sensitivity to extended emission is far superior to current capabilities. Assuming ten times the sensitivity of SKA1-MID and using the same considerations as above, a 100h broadband integration would provide a sensitivity of 18 nJy beam^{-1} at the full angular resolution, assuming a 50% sensitivity loss because of visibility weighting. SKA2 will enable Faraday tomography on 10 pc scales in nearby galaxies like M 83, with the same surface brightness sensitivity as existing facilities. Galaxies within 50 Mpc can be studied at 100 pc resolution. SKA2 will allow the extension of this study to substantially larger distances, permitting large samples and even opening the door to the tomographic study of the evolution of the 3D magnetic field structure in galaxies out to $z \approx 0.125$, where structures on scales of ≈ 1 kpc can be resolved.

5. Concluding Remarks

Depolarization is an essential tool with which to study the three-dimensional structure of the magnetized ISM in galaxies. Both large- and small-scale magnetic structures will be revealed in exquisite detail by the SKA, even in its early incarnations. Detailed and sophisticated analysis techniques will be required to make the most of the transformational capabilities of the SKA. The SKA will provide a huge step forward in studying galactic magnetism: SKA1 represents an order of magnitude improvement in angular resolution for polarization studies of galaxies in the local

PoS(AASKA14)106

Universe and an extension to a much larger volume than is feasible today, while SKA2 will extend the same study to a cosmologically interesting volume and illuminate the evolution of magnetic field structure in galaxies.

References

Arshakian, T. G. and Beck, R. 2011, MNRAS, 418, 2336
Bagetakos, I., Brinks, E., Walter, F. et al. 2011, AJ, 141, 23
Beck, R. 2007, A&A, 470, 539
de Blok, W. J. G. and Walter, F. 2006, AJ, 131, 363
Brandenburg, A. and Stepanov, R. 2014, ApJ, 786, 91
Braun, R., Oosterloo, T. A., Morganti, R., Klein, U., and Beck, R. 2007, A&A, 461, 455
Braun, R., Heald, G., and Beck, R. 2010, A&A, 514, 42
Braun, R., "SKA1 Imaging Science Performance", Document number SKA-TEL-SKO-DD-XXX Revision A Draft 2
Brentjens, M. A. and de Bruyn, A. G. 2005, A&A, 441, 1217
Burn, B. J. 1966, MNRAS, 133, 67
Dewdney, P., Turner, W., Millenaar, R. et al. 2013, "SKA1 System Baseline Design", Document number SKA-TEL-SKO-DD-001 Revision 1
Farnsworth, D., Rudnick, L., and Brown, S. 2011, AJ, 141, 191
Fomalont, E. B. 1999, ASPC, 180, 301
Frick, P., Sokoloff, D., Stepanov, R., and Beck, R. 2011, MNRAS, 414, 2540
Ferguson, A. M. N., Gallagher, J. S., and Wyse, R. F. G. 1998, AJ, 116, 673
Fletcher, A., Beck, R., Shukurov, A., Berkhuijsen, E. M., and Horellou, C. 2011, MNRAS, 412, 2396
Gaensler, B. M., Haverkorn, M., Staveley-Smith, L. et al.2005, Science, 307, 1610
Gießübel, R., Heald, G., Beck, R., and Arshakian, T. G. 2013, A&A, 559, 27
Heald, G. 2009, IAUS, 259, 591
Heald, G., Braun, R., and Edmonds, R. 2009, A&A, 503, 409
Heald, G. H. 2012, ApJ, 754, L35
Heesen, V., Beck, R., Krause, M., and Dettmar, R.-J. 2011, A&A, 535, 79
Horellou, C. and Fletcher, A. 2014, MNRAS, 441, 2049
Houde, M., Fletcher, A., Beck, R. et al.2013, ApJ, 766, 49
Ianjamasimanana, R., de Blok, W. J. G., Walter, F., and Heald, G. H. 2012, AJ, 144, 96
Mao, S. A., Zweibel, E., Fletcher, A., Ott, J., and Tabatabaei, F. 2015, ApJ, 800, 92
Moss, D., Sokoloff, D., Beck, R., and Krause, M. 2010, A&A, 512, 61
O'Sullivan, S. P., Brown, S., Robishaw, T. et al. 2012, MNRAS, 421, 3300
Saha, A., Thim, F., Tammann, G. A., Reindl, B., and Sandage, A. 2006, ApJS, 165, 108
Shneider, C., Haverkorn, M., Fletcher, A., and Shukurov, A. 2014, A&A, 567, 82
Sokoloff, D. D., Bykov, A. A., Shukurov, A. et al. 1998, MNRAS, 299, 189
Stilp, A. M., Dalcanton, J. J., Warren, S. R. et al. 2013, ApJ, 765, 136
Sun, X. H., Rudnick, L., Akahori, T. et al. 2015, AJ, 149, 60
Vollmer, B., Soida, M., Beck, R. et al. 2013, A&A, 553, 116

PoS(AASKA14)106

Williams, A. et al. 2015, ApJ, in prep
Young, L. M. and Lo, K. Y. 1996, ApJ, 462, 203
Young, L. M. and Lo, K. Y. 1997, ApJ, 490, 710
Young, L. M., van Zee, L., Lo, K. Y., Dohm-Palmer, R. C., and Beierle, M. E. 2003, ApJ, 592, 111

PoS(AASKA14)106

PROCEEDINGS OF SCIENCE

Kinematics and Dynamics of kiloparsec-scale Jets in Radio Galaxies with SKA

R.A. Laing
ESO, Karl-Schwarzschild-Straße 2, D-85748 Garching-bei-München, Germany
E-mail: rlaing@eso.org

We explore the use of SKA to deduce the physical parameters of kiloparsec-scale jet flows in radio galaxies. Jets in Active Galactic Nuclei are relativistic where they are first formed, but their speeds and compositions change as they propagate. It has long been known that kiloparsec-scale jets in radio galaxies can be divided into two flavours: strong (found in powerful sources, narrow and terminating in compact hot-spots) and weak (found in low-luminosity sources, geometrically flaring, unable to form hot-spots and terminating in diffuse lobes or tails). We have developed methods to model AGN jets as intrinsically symmetrical, relativistic flows by fitting to deep, well-resolved radio images in Stokes I, Q and U. This has yielded a wealth of information about the brightest few weak-flavour jets. Our first key objective is to observe large samples of weak and transition jets at 0.1 – 0.5 arcsec resolution with SKA1-MID. This would allow us to see how jet propagation depends on power and environment and to quantify the energy and momentum input into the IGM. We will require typical noise levels of 1μJy/beam, and may be able to exploit survey imaging in some cases. Our second, more challenging, application is to determine the velocity fields in strong-flavour jets. Do they have very fast ($\Gamma \approx 5-10$) spines? Is there evidence for magnetic confinement by a toroidal field? What are their energy fluxes? This is a major imaging challenge for SKA2: we need resolution better than 0.05 arcsec, ideally in the 1 – 10 GHz frequency range, with rms noise levels $\approx$10 nJy/beam and extremely high dynamic range, imaging fidelity and polarization purity.

Advancing Astrophysics with the Square Kilometre Array,
June 9-13, 2014
Giardini Naxos, Sicily, Italy

PoS(AASKA14)107

R.A. Laing

1. Introduction

Jets from active galactic nuclei (AGN) are important in many areas of astrophysics: they extract energy from supermassive black holes, produce the most energetic photons (and perhaps cosmic rays) we observe, act as conveyors of ultrarelativistic particles and magnetic fields from the parsec-scale environments of AGN to the multi-kiloparsec scales of extended radio galaxies and quasars, and supply copious amounts of energy to their surroundings, thereby preventing cooling and profoundly affecting the evolution of massive galaxies and clusters.

An overview of the study of AGN jets with SKA is given by Agudo et al. (2015). This paper covers one aspect – the physics of jets on kpc scales – in more detail, emphasising a number of key topics (cf. Blandford 2008), as follows.

1. What are the velocity fields? Why do some jets expand rapidly, increase in brightness and decelerate while others remain fast and collimated? How does this relate to the origin of the Fanaroff-Riley classes (Fanaroff & Riley 1974)?
2. How does jet composition change with distance from the AGN? What are the typical mass fluxes and entrainment rates?
3. What is the magnetic-field topology on kpc scales – ordered or disordered?
4. How is jet propagation determined by the external environment (density, pressure, temperature, magnetization)?
5. How are jets confined: by external gas pressure, magnetic fields, some other mechanism or not at all?
6. Where and by what process are relativistic particles accelerated?
7. What are the jet energy and momentum fluxes?
8. What effects do the jets have on their surrounding IGM/ICM? Do they lead to shocks and heating? What effect do they have on external magnetic fields and hence on thermal transport?

It has long been known that AGN radio jets divide into strong and weak 'flavours' (Bridle 1984). Strong-flavour jets are usually one-sided ($>$4:1) and well-collimated over their whole lengths and often terminate in compact hot spots. Weak-flavour jets are initially asymmetric, but tend to symmetrize far from the nucleus. They also 'flare' with increasing distance from the AGN in two distinct senses: *geometrically* (a significant increase in apparent spreading rate) and *in brightness* (an increase in apparent intensity, often following an initial 'gap', or extended region in which the radio emission is weak or undetectable). The qualitative picture is that both jet flavours are initially relativistic, but weak-flavour jets decelerate to subrelativistic speeds on kpc scales, while strong-flavour jets remain highly relativistic until they reach the outer parts of the sources.

PoS(AASKA14)107

Thus far, we have derived quantitative models only for a small number of *weak-flavour jets* using deep VLA observations. *Strong-flavour jets* are harder to study as they are narrower than weak-flavour jets (thus harder to resolve) and their counter-jets are faint and difficult to isolate from surrounding lobe emission. After outlining the modelling methods and associated imaging requirements (Section 2), we therefore consider in turn the use of SKA1-MID to observe large samples of weak-flavour jets (Section 3) and SKA2 to model strong-flavour jets for the first time with our methods (Section 4).

2. Measuring the flow parameters of jets

Although numerical (GRMHD) simulations of jet formation have made considerable progress recently (e.g. McKinney et al. 2013), the problem of simulating the propagation of a very light, relativistic, magnetized jet in three dimensions is computationally prohibitive, with poorly known initial conditions: no simulation can yet hope to follow a jet all the way from its formation on scales comparable with the gravitational radius of the central black hole to the kiloparsec scales which SKA can best resolve. A more empirical approach to estimation of jet flow parameters is therefore needed.

One powerful method is based on the realization that kpc-scale jets are both significantly relativistic and intrinsically symmetrical, in the specific sense that *apparent asymmetries due to relativistic aberration are much larger than any intrinsic asymmetries*. Jets emit (often highly) polarized synchrotron radiation. With the assumptions that the flows are (on average) axisymmetric, intrinsically symmetrical and stationary, the observed brightness distributions in Stokes I, Q and U can be modelled to fit for geometry, velocity field, intrinsic emissivity variation and three-dimensional magnetic field configuration. The method was first described in Laing & Bridle (2002a); a comprehensive overview is given by Laing & Bridle (2014). The key to the method is to determine the velocity and inclination angle independently by comparing emission from the main and counter-jets in *both total intensity and linear polarization*. The observed polarizations in the approaching and receding jets are not the same because they are effectively observed at different angles to the line of sight in the rest frame, θ'. For antiparallel jets at angle θ to the line of sight in the observed frame,

$$\sin\theta'_{\rm j} = [\Gamma(1-\beta\cos\theta)]^{-1}\sin\theta$$
$$\sin\theta'_{\rm cj} = [\Gamma(1+\beta\cos\theta)]^{-1}\sin\theta$$

where subscripts j and cj refer to the approaching and receding jets, β is the flow velocity in units of c and Γ is the bulk Lorentz factor. β and θ cannot be determined independently from images of total intensity alone: the use of linear polarization is crucial.

This method has proved to be very successful in modelling the jet flows in bright, nearby (FR I) radio galaxies, as we describe in Section 3. Given the derived velocity fields (and the assumption of pressure equilibrium with the surroundings on large scales), we can also use the laws of conservation of mass, momentum and energy to estimate the energy and mass fluxes and the run of entrainment rate along the jets (Laing & Bridle 2002b). The magnetic-field topology is not completely determined, however. The models show that longitudinal and toroidal components dominate

PoS(AASKA14)107

(at small and large distances, respectively). The observed symmetry of the transverse profiles of I and Q tells us that the field structure is not a simple 'grand design' helix on these scales (Laing et al. 2003), but leaves open the question of whether the toroidal component is vector-ordered. If it is, there should be systematic gradients in Faraday rotation across the jets (we know that thermal electrons must be entrained even if they are not present near the AGN). Such searches have so far been frustrated by large fluctuations in foreground Faraday rotation.

The observational requirements for this technique are images of both jets with good fidelity, at least 5 and preferably >10 beams across their widths and noise levels low enough to detect 10% polarization at 4σ everywhere. It must also be possible to correct the effects of Faraday rotation (and depolarization) to high accuracy.

These methods have so far managed to provide answers to many of the questions posed in Section 1, but only for a small number of carefully selected sources. We have been restricted to jets which are bright and easily resolved. Thus we sample a limited (intermediate) range of luminosity, and can only model jets with large opening angles. We know very little about more powerful, highly-collimated jets, intrinsically weak sources or the systematic dependences of jet physics on power and environment. To do better, we need much large samples of low-luminosity sources (high sensitivity at moderate resolution) and an instrument capable of much higher resolution and very high sensitivity for the powerful sources. We explore these applications in the following two sections.

3. Decelerating jets: SKA1-MID

3.1 Current results

Our current results on decelerating, FR I jets are summarised in Laing & Bridle (2014), and an example is shown in Fig. 1. All of the jets first increase in opening angle and then recollimate to form conical flows at a fiducial distance r_0 (the *flaring region*) in the range 2 – 35 kpc from the AGN. At $\approx 0.1 r_0$, the jets brighten abruptly at the onset of a high-emissivity region and we find an outflow speed of $\approx 0.8c$, with a uniform transverse profile. Jet deceleration first becomes detectable at $\approx 0.2 r_0$ and the outflow often becomes slower at its edges than it is on-axis. Deceleration continues until $\approx 0.6 r_0$, after which the outflow speed is usually constant. The dominant magnetic-field component is longitudinal close to the AGN and toroidal after recollimation, but the field evolution is initially much slower than predicted by flux-freezing. In the flaring region, acceleration of ultrarelativistic particles is required to counterbalance the effects of adiabatic losses and account for observed X-ray synchrotron emission, but the brightness evolution of the outer jets is consistent with adiabatic losses alone. These results are best interpreted as effects of the interaction between the jets and their surroundings. The initial increase in brightness occurs in a rapidly falling external pressure gradient in a hot, dense, kpc-scale corona around the AGN. We interpret the high-emissivity region as the base of a transonic 'spine' and suggest that a subsonic shear layer starts to penetrate the flow there. Most of the resulting entrainment must occur before the jets start to recollimate.

3.2 SKA1-MID observations

While the basic process of jet deceleration in twin-jet sources has become clearer, there are still

PoS(AASKA14)107

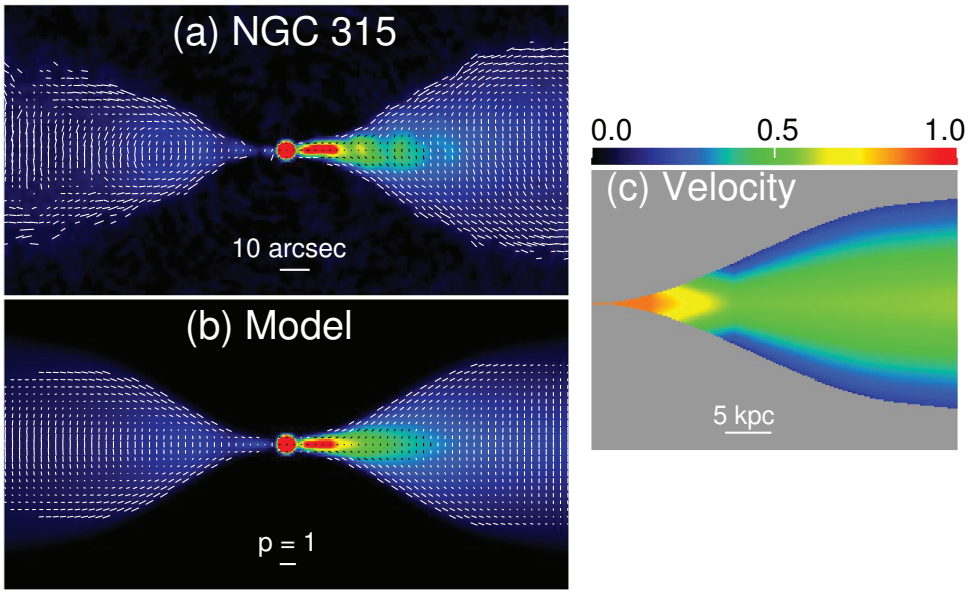

Figure 1: Observations and models of the nearby radio galaxy NGC 315 (Laing & Bridle 2014). (a) Vectors with magnitudes proportional to the degree of polarization, p, and directions along the apparent magnetic field superposed on a false-colour plot of total intensity. (b) Model fit corresponding to (a). (c) The derived velocity field, in units of c.

many unanswered questions. Almost all of the sources we have modelled so far have luminosities close to $P \approx 10^{24.5}$ WHz^{-1} at 1.4 GHz. The next set of questions includes the following.

1. How does the characteristic recollimation scale r_0 vary with luminosity (jet power) and external pressure? Can we develop a way of predicting a priori which jets will decelerate and the form of their outer structures?

2. What are the distributions of energy and mass flux? How do these depend on black hole mass, accretion rate and ISM/IGM properties? Do they correlate with estimates from the size and pressure of jet-blown 'cavities' in the IGM/ICM? Can we infer the energy and momentum input integrated over the source population for comparison with galaxy formation models?

3. What causes jet emission to 'turn on' at the flaring point, $\approx 0.1 r_0$?

4. How important is stellar mass input in decelerating the weakest jets (it can be differentiated from boundary-layer entrainment because no slow boundary layer is formed)?

5. Can we decide unequivocally whether the toroidal field component is vector ordered and, if so, does it contribute to jet collimation on kpc scales? [To do this, we will need to measure Faraday rotation for a sample of sources selected to have low foreground contamination.]

6. How important are intrinsic and environmental asymmetries? This cannot be assessed for an individual object, but relativistic and environmental asymmetries are expected to be uncorrelated, so we can separate their effects statistically for a sufficiently large sample.

PoS(AASKA14)107

In order to answer these questions with any statistical significance, we will need to increase the number of modelled sources from 10 to at least a few hundred and to identify sub-samples with different luminosities and environments. Our long VLA observations typically reach rms noise levels between 5 and 10μJy/beam at angular resolutions between 0.25 and 2.5 arcsec (The upgraded Karl G. Jansky VLA is allowing us to go up to a factor of 5 deeper, but only with long multi-configuration observations in special cases). For an integral source count $N(>S) \propto S^{-1.5}$ (appropriate for these nearby sources), we would need to increase the sensitivity by a factor of 10 from the flux densities alone (i.e. an rms noise level of $0.5-1.0\mu$Jy/beam). Detailed trade-offs depend on source brightness, size and environment. For example: the need to measure low Faraday rotations argues for lower frequencies, but we cannot tolerate a significant variation of rotation across the observing beam; there are systematic variations of jet size (and therefore required resolution) with luminosity, and so on. Band 3 is therefore preferred for the measurement of low Faraday depths; Band 5 for jet modelling. These observations would also probe the magnetoionic environments of the radio galaxies in great detail (Laing et al. 2008; Guidetti et al. 2011).

An initial estimate is that we would need ≈300 observations (mostly pointed, but perhaps also obtained from surveys) with high image fidelity, resolution ≈0.25 arcsec and rms noise level $\lesssim 1\,\mu$Jy/beam in SKA1-MID, Band 5. For the combined SKA1-MID array (Dewdney et al. 2013, Table 9) and allowing for a factor of 2 increase in noise from weighting (Braun 2013), this would give an average of $\gtrsim 50$ min on-source time per observation, or $\gtrsim 240$ hr in total. The observations would still be feasible in an Early Science phase, but longer integrations (by factors $\gtrsim 4$) or correspondingly smaller sample sizes would be required.

4. Fast, powerful jets: SKA2

The strong-flavour jets found in powerful radio galaxies and quasars, particularly those associated with FR II sources, are far harder to study, as they are narrow and (in the case of counter-jets) also very faint (e.g. Fig. 2).

We aim to distinguish between two hypotheses: (a) strong jets are only mildly relativistic ($\beta \approx 0.5-0.7$; $\Gamma \approx 1.2-1.4$) as inferred naively from the statistics of their integrated sidedness ratios (Wardle & Aaron 1997; Mullin & Hardcastle 2009) or (b) they have a two-component velocity structure, with a much faster ($\beta > 0.95$) spine surrounded by a slower shear layer that dominates the emission except in very end-on cases. Case (b) has long been suspected (Bridle et al. 1994), but never proved: arguments in favour include the following.

1. High pattern speeds are inferred from VLBI proper-motion measurements for pc-scale jets in flat-spectrum quasars (the end-on counterparts of sources like 3C 334; Lister et al. 2013). If these are representative of the bulk motion, then flow Lorentz factors up to $\Gamma \approx 40$ are required. Deceleration of such powerful jets to mildly relativistic speeds on kpc scales cannot occur without disruption.

2. If the X-rays observed in the extended jets associated with core-dominated sources are generated by inverse Compton scattering of cosmic microwave background photons by relativistic electrons in the jet, then the bulk Lorentz factors must be large ($\Gamma \gtrsim 10$) and the jets must be close to the line of sight (Tavecchio et al. 2000; Celotti et al. 2001). Note, however, that

PoS(AASKA14)107

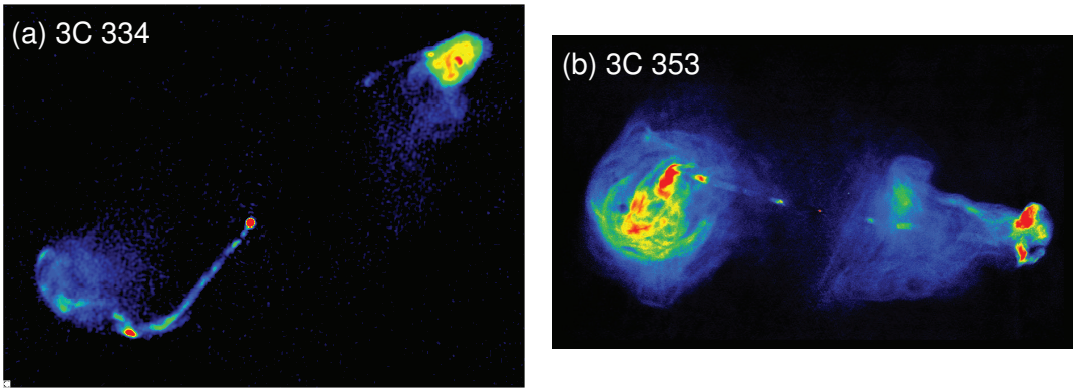

Figure 2: VLA images of (a) the powerful quasar 3C 334 (Bridle et al. 1994) and (b) the radio galaxy 3C 353 (Swain et al. 1998). Note the very narrow strong-flavour jets. 3C 334 is thought to be at $\lesssim 40^\circ$ to the line of sight and shows a pronounced jet/counter-jet asymmetry (the counter-jet is only visible at large distances from the AGN). In contrast, 3C 353 is close to the plane of the sky and both jets are visible, but its asymmetries are dominated by the environment.

there are arguments against this interpretation of the X-ray emission, at least in some sources (Hardcastle 2006; Meyer & Georganopoulos 2013).

3. The jet/counter-jet ratio and observations of apparent superluminal speeds in the jet of M 87 both indicate $\Gamma \gtrsim 6$ over at least part of its length (Asada et al. 2014).

There are a number of transition cases between weak and strong-flavour jets which do not appear to decelerate significantly but which have counter-jets that can now be imaged with the VLA. The best example is NGC 6251 (Fig 3), for which observations are under way.

Modelling of true strong-flavour jets such as those found in luminous quasars is a far more challenging prospect, even for SKA2. Counter-jets can currently only be imaged with something approaching adequate s/n in sources such as 3C 353 (Fig. 2, Swain et al. 1998) which are very close to the plane of the sky (in which case our modelling technique does not work). We really need to image both jets in powerful sources which are reasonably inclined. As an example, if the straight part of the counter-jet in 3C 334 (Fig. 2) has $I \approx 10\mu$Jy/beam at 5 GHz with a beam of 0.35 arcsec (just below the current limit) and a width of 0.2 – 0.6 arcsec, we would need a resolution of $\approx$0.05 arcsec, and an rms noise level of $\lesssim 10$ nJy to be able to image and model the counter-jet in linear polarization. In turn, this requires a dynamic range of $\gtrsim 10^7 : 1$ (peak:rms). Both requirements could be relaxed if adequate resolution could be obtained at a lower frequency.

5. Summary

We have outlined some of the ways in which SKA could contribute to the study of large-scale jets in radio galaxies. Extension of current work on low and intermediate luminosity sources to large samples is feasible for SKA1-MID. The case of powerful jets is an interesting challenge for SKA2.

PoS(AASKA14)107

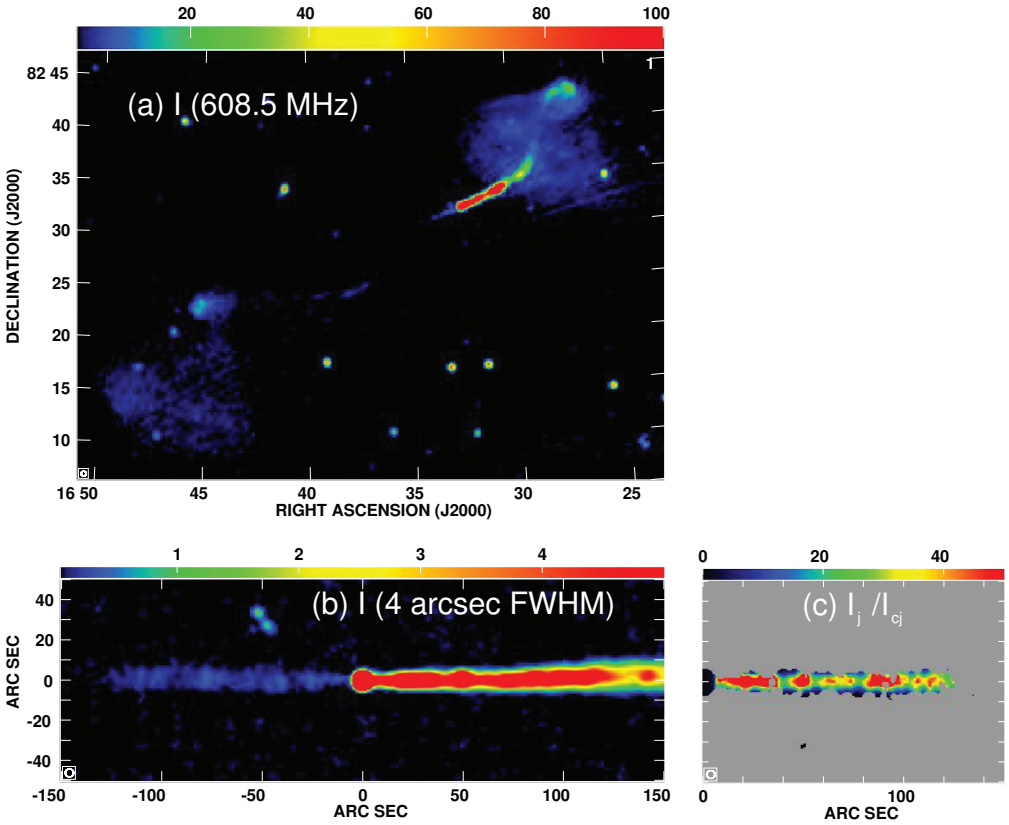

Figure 3: Images of NGC 6251. (a) Overall structure (WSRT, 609 MHz, from Mack et al., 1997). (b) Rotated image of the jets at 1665 MHz, 4 arcsec FWHM from archival VLA data. (c) Sidedness ratio $R = I_{\rm j}/I_{\rm cj}$, derived from (b) and blanked (grey) where $I < 3\sigma$ in either jet. The jets in this source represent a transition between weak and strong flavours: they flare, but still maintain a large side-to-side ratio. The sidedness ratio image in panel (c) strongly suggests a substantial velocity gradient across the jets.

References

Agudo, I., Böttcher, M., Falcke, H., et al. 2015, "Studies of Relativistic Jets in Active Galactic Nuclei with SKA", in proc. *Advancing Astrophysics with the Square Kilometre Array*, PoS(AASKA14)093

Asada K., Nakamura M., Do, A., Nagai H., & Inoue, M. 2014, ApJ, 781, L2

Blandford R. D. 2008, in Extragalactic Jets: Theory and Observation from Radio to Gamma Ray, ASP Conference Series, 386, 3

Braun, R., "SKA1 Imaging Science Performance", Document number SKA-TEL-SKO-DD-XXX Revision A Draft 2

Bridle A. H. 1984, AJ, 89, 979

Bridle A. H., Hough D. H., Lonsdale C. J. Burns J. O., & Laing R. A. 1994, AJ, 108, 766

Celotti A., Ghisellini G., & Chiaberge M. 2001, MNRAS, 321, L1

Dewdney, P., Turner, W., Millenaar, R., McCool, R., Lazio, J., Cornwell, T. 2013, "SKA1 System Baseline Design", Document number SKA-TEL-SKO-DD-001 Revision 1

Fanaroff B. L., & Riley J. M. 1974, MNRAS, 167, 31P

PoS(AASKA14)107

Guidetti D., Laing R. A., Bridle A. H., Parma P., & Gregorini L. 2011, MNRAS, 413, 2525
Hardcastle M. J. 2006, MNRAS, 366, 1465
Laing R. A., & Bridle A. H. 2002a, MNRAS, 336, 328
Laing R. A., & Bridle A. H. 2002b, MNRAS, 336, 1161
Laing R. A., & Bridle A. H. 2014, MNRAS, 437, 3405
Laing R. A., Bridle A. H., Parma P., & Murgia M. 2008, MNRAS, 391, 521
Laing R. A., Canvin J. R., & Bridle A. H. 2003, AN, 327, 523
Lister M. L., Aller M. F., Aller H. D., et al. 2013, AJ, 146, 120
Mack, K.-H., Klein, U., O'Dea, C. P., Willis, A. G. 1997, A&AS, 123, 423
McKinney J. C., Tchekhovskoy A., & Blandford R. D. 2013, Science, 339, 49
Meyer, E. T., & Georganopoulos M. 2014, ApJ, 780, L27
Mullin L. M., & Hardcastle M. J. 2009, MNRAS, 398, 1989
Tavecchio F., Maraschi L., Sambruna R. M., & Urry C. M. 2000, ApJ, 544, L23
Swain M.R., Bridle A.H., & Baum, S.A., 1998 ApJ, 507, L29
Wardle J.F.C., & Aaron S.E., 1997 MNRAS, 286, 425

PoS(AASKA14)107

PROCEEDINGS OF SCIENCE

Giant radio galaxies as probes of ambient WHIM in the era of the SKA

Bo Peng[1,2], **Ru-Rong Chen**[1], **and Richard Strom**[1,3]
[1]NAOC; [2]JLRAT; [3]ASTRON
E-mail: pb@bao.ac.cn

The missing baryons are usually thought to reside in galaxy filaments as warm-hot intergalactic medium (WHIM). From previous studies, giant radio galaxies are usually associated with galaxy groups, which normally trace the WHIM. We propose observations with the powerful SKA1 to make a census of giant radio galaxies in the southern hemisphere, which will probe the ambient WHIM. The radio galaxies discovered will also be investigated to search for dying radio sources. With the highly improved sensitivity and resolution of SKA1, more than 6,000 giant radio sources will be discovered within 250 hours.

Advancing Astrophysics with the Square Kilometre Array,
June 8-13, 2014
Giardini Naxos, Sicily, Italy

PoS(AASKA14)109

1. The WHIM

Baryonic matter - protons, neutrons, and electrons - belongs to a class of massive elementary particles which make up the atoms of all materials on Earth and in the stars. From the Big Bang theory and the results of WMAP, baryonic matter contributes no more than 5 percent of the cosmos, though it remains not completely accounted for. From a census of the observable baryonic density in the current Universe (e.g. Shull, Smith & Danforth (2012)), all the stars, dust and gas within galaxies constitute less than 50 percent of baryons predicted by the theory. By analyzing light from distant quasars, the number of baryons in cosmic history can be counted. Its amount has remained constant even going back to 10 billion years ago. Quantifying the missing baryons is essential to obtaining a complete picture of galaxy formation and evolution. The missing baryons are generally thought to reside between galaxies, as warm-hot intergalactic medium (WHIM) with temperatures of $10^5 - 10^7$ K. Material in the WHIM is highly ionized and can only be observed at far-ultraviolet or low-energy X-ray wavelengths. This diffuse plasma is a common prediction in the Λ cold dark matter (ΛCDM) cosmologies (e.g. Davé et al. (2010)). However, because its density is relatively low, the detection remains a challenge (Davé et al. 2001; Dietrich et al. 2012; Werner et al. 2008).

2. Giant radio galaxies (GRGs)

Giant radio galaxies (GRGs) (linear size >0.7 Mpc, h = 0.71) are a quite unique category, as they are the biggest objects in the sky with large radio structures. It is generally believed that their radio lobes are powered by beams of relativistic particles and magnetic fields from an active nucleus. Radio structures of many known GRGs are asymmetric over their mega-parsec extents (Lara et al. 2001; Machalski, Jamrozy & Zola 2001; Saripalli et al. 2005; Schoenmakers et al. 2000; Strom et al. 2013) (see Figure 1). As the radio lobes expand, they interact with the ambient medium and can act as tracers of this barely detectable material. The large extent of GRGs provides a good opportunity to investigate the ambient gas.

3. Radio galaxies and cosmology

By 1950, several compact radio sources had been associated with distant galaxies (Bolton, Stanley & Slee 1949; Ryle, Smith & Elsmore 1950), and with the identification of the very strong radio source Cygnus A (Baade & Minkowski 1954; Smith 1951) with a $z = 0.056$ galaxy, the potential of radio sources for probing the Universe became apparent. This expectation was confirmed when 3C 295 was shown to be associated with a $z = 0.461$ galaxy (Minkowski 1960). Simultaneously, radio source structure was found to be double lobed (Jennison & Das Gupta 1953), with sizes ranging from parsecs to hundreds of kilo-parsecs.

Much effort went into identifying (and measuring the redshifts of) radio sources from reliable catalogues, especially 3C. High resolution radio maps (made by the One Mile Telescope, Westerbork and the VLA) tied down the radio source structures. The angular size measured could be translated into linear dimensions. Inverse Compton scattering of the radio emitting high-energy electrons becomes increasingly important at greater redshift. This effect could "snuff out" radio sources at high z (Miley 1968) before they could attain the dimensions found among the largest radio galaxies in the local Universe.

PoS(AASKA14)109

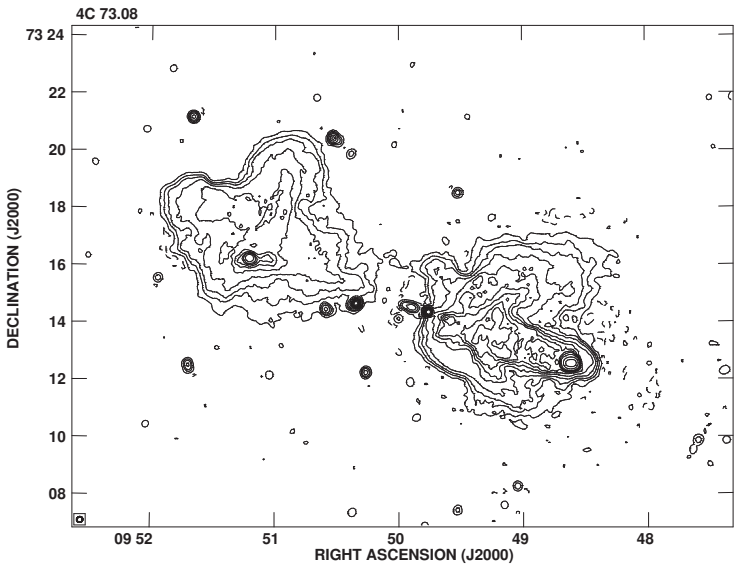

Figure 1: WSRT map at 21 cm wavelength of the radio galaxy 4C 73.08. The brighter western lobe is more compact than its eastern counterpart. A similar effect is seen in NGC 6251 (Figure.2).

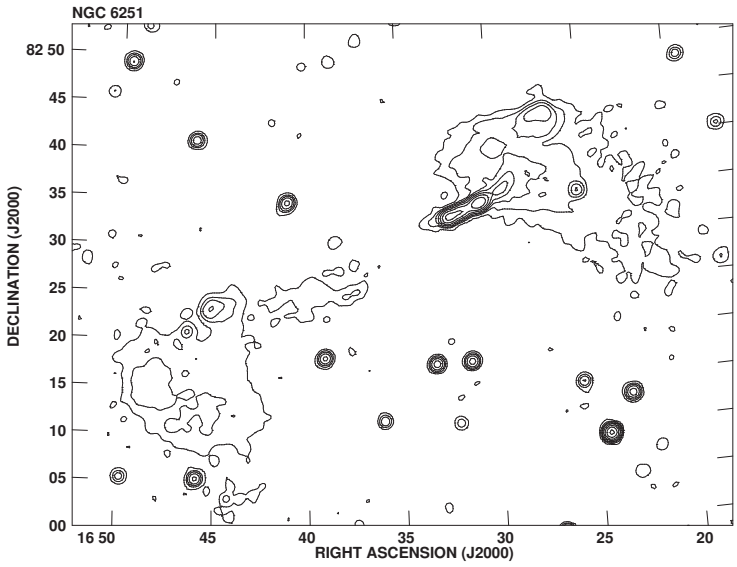

Figure 2: WSRT map made at 92 cm wavelength of the radio galaxy NGC 6251. Like all of the GRGs, it is srongly polarized at long wavelengths. Note how unequal the distances between the ends of the two lobes and the host are.

PoS(AASKA14)109

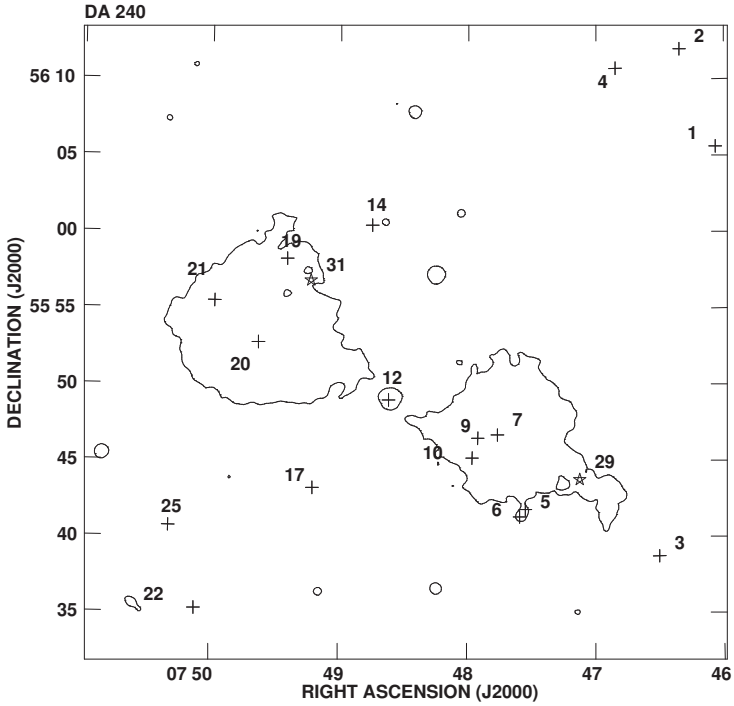

Figure 3: WSRT map made at 49 cm wavelength of the radio galaxy DA 240. Galaxies which are members of the DA 240 group have their positions indicated by symbols.

4. Tracing the WHIM with GRGs

As was clear from early WSRT observations of DA 240, 3C 236 and NGC 6251 (Figure 2), giant radio galaxies are strongly polarized at 608 MHz (Willis, Strom & Wilson 1974). The implied low ambient densities were at least qualitatively consistent with the large linear sizes of the radio components. A definitive study of five GRGs carried out by Mack et al. (1997) mapped their linear polarization at wavelengths from 92 to 2.8 cm. All of the sources were found to be polarized in many places at the longest wavelengths, indicating an internal rotation measure of $\sim$ 1 rad m^{-2}. The implied densities within the lobes depend upon the magnetic field strength. For equipartition field strengths of typically 1 μG, the particle densities are of order 10^{-5} cm^{-3}. In a more general consideration of densities associated with GRGs, Mack et al. (1998) conclude that the IGM with which the radio components interact has a density of 1 - 4$\times$ 10^{-5} cm^{-3}.

Several recent studies have explored the use of GRGs for probing the WHIM. In both the cases of Subrahmanyan et al. (2008), and Safouris et al. (2009), sensitive radio continuum images of two GRGs were used to relate their morphology to the ambient medium on the Mpc scale. They made spectroscopic observations to investigate galaxy distribution within a 2° field surrounding the radio galaxy hosts. Both studies showed clear correspondence between the giant synchrotron lobes and the surrounding galaxy distributions. Such a correspondence was also found in a series of papers (Chen et al. 2011b, 2012a,b). They found the existence of a galaxy group around each giant radio galaxy (NGC 6251, NGC 315 and 4C 73.08) through optical spectroscopic observations. However,

PoS(AASKA14)109

in the case of DA 240 (Chen et al. 2011a; Peng et al. 2004), the relatively symmetrical lobes coincide with a galaxy group. The group members evenly reside along the major axis of the lobes while the isolated host galaxy lies in the middle (Figure 3). The expected X-ray luminosities are much higher than the observed values, which suggests that the matter density within the lobes is quite low. A similar conclusion was obtained by Malarechi et al. (2013). In the investigation of a sample of 12 GRGs, they derived lobe energy densities from the radio observations via equipartition arguments. The inferred pressures in the lobes of the giant radio sources, which range from 1.1×10^{-15} to 2.0×10^{-14} Pa, are lower than inferred from X-ray observations of dense filaments. This demonstrates the potential of using GRGs to study the WHIM gas within which their lobes evolve and interact.

5. Prospects with SKA1

A significant fraction of known giant radio galaxies were identified from the surveys of the WSRT and VLA: WENSS, NVSS and FIRST. The SKA1_SUR will be equipped with 96 dishes in Western Australia, including 36 dishes of ASKAP (latitude is about 27°S). At L band, it will have a high survey speed figure of merit (FoM) of about 156 times greater than the VLA, and 1.5 times better sensitivity as well as a 1.6 to 49 times higher angular resolution (Table 1). If it carries out a survey similar to the NVSS, with integration times of 10 minutes and a bandwidth of 500 MHz at L band, the noise level should achieve 9.1 μJy/beam. Since the GRGs usually have intermediate power between 10^{25} and 10^{26} W/Hz at 1.4 GHz, if the *SNR* is presumed (based on experience) to be 150 (Machalski, Jamrozy & Zola 2001; Schoenmakers et al. 2000), the luminosity distance will be 7825 Mpc ($z\sim 1.2$). Since the minimum elevation angle is about 15 degree (similar to the ASKAP), SKA1_SUR can observe the sky up to $+48^\circ$ (more than 80 percent of the whole sky). If the Galactic latitude is set to be $|b|>12.5^\circ$ to avoid the confusion of the Milky Way, the sky coverage will then be reduced to about 27,000 deg^2. Adopting a number density of 10^{-7} Mpc^{-3} (Saripalli et al. 2005), the SKA1_SUR is expected to detect about 12,000 GRGs in a total observing time of about 250 hours (formula listed in the Appendix). Even at an early phase (50% capability), SKA1_SUR will still be able to detect about 6,000 GRGs, which can be identified with counterparts obtained from optical surveys, such as SDSS, 2dF, and the planned LSST. The GRG sample will then increase by more than an order of magnitude.

At the same time, the SKA1_MID will be equipped with 254 dishes in South Africa, including 64 dishes from MeerKAT. Compared with the VLA, this will provide 6.2 times better sensitivity and 74 times higher survey speed. Moreover, the angular resolution will be 6.4 to 200 times better. After GRG candidates have been obtained from the SKA1_SUR, SKA1_MID can be used for a deeper investigation, especially for low surface brightness lobes, which is important for their use as cosmological probes. If the SKA2_MID could be equipped with PAFs, the survey speed with SKA2_MID would be greatly increased, and this will make the SKA2_MID quite a powerful instrument for discovering more of these faint, extended radio sources at higher redshift.

Furthermore, since the frequency ν of radio synchrotron emission is proportional to the square of the electrons' energy E and the ambient magnetic field B ($\nu\sim E^2B$), which is expected to be low and weak in the diffuse radio lobes of GRGs, detection of new radio structures in GRGs is likely from observations using the SKA1 low frequency array. There may even be discovery of new ones

PoS(AASKA14)109

Table 1: Summary of system sensitivity, survey speed and angular resolution of SKA1, VLA, WSRT at L band, and LOFAR at low frequency (extracted from Dewdney et al. (2013)).

		JVLA	WSRT	SKA1_MID	SKA1_SUR	LOFAR	SKA1_LOW
A_{sys}/T_{sys}	m^2/K	265	124	1630	391	61	1000
Survey Speed FoM	$deg^2m^4K^{-2}$	1.76E4	3.84E3	1.3E6	2.75E6	5.21E4	2.7E7
Resolution	arcsec	1.4 - 44	16	0.22	0.9	5	11
FoV	deg^2	0.25	0.25	0.49	18	14	27
Bandwidth	MHz	1000	160	250	500	4	250

(like the discovery of GRG UGC 09555 with LOFAR). The low frequency array of SKA1 will be equipped with 250,000 antennas in Western Australia, with 16 times higher sensitivity and 520 times quicker survey speed compared with LOFAR.

Recently, Luo & Sadler (2010) modelled the evolution of FRI and II radio sources, finding that the latter evolve with decreasing monochromatic radio power, while the power of the former increases with age. The final stage for both sees rapidly declining emission as the radio source fades away, the lobes receiving little or no energy from the host nucleus or jets. As the lobes decline, their radio spectra will steepen, so a dying radio galaxy should have lobes with a steep radio spectrum and no jets or nuclear component. Finding candidates for this GRG phase will be well-suited to the SKA1 capability at low frequencies.

With the highly improved system sensitivity, survey speed and angular resolution of SKA1, there should be more than one order of magnitude increase in the number of GRGs from about 140 at present (a small fraction of which have redshifts greater than 0.5 (Komverg & Pashchenko 2009)). With their ability to trace the ambient IGM, more GRGs will help illuminate the distribution and physical state of the WHIM and identify whether it can explain the missing baryon problem. And with more details on high-z GRGs, being able to compare them with low redshift sources will help to clarify how giant radio galaxies evolve, and especially how their environments affect their radio structures, and whether there are significant differences in group size, composition, morphology, etc., with cosmic epoch.

At low redshifts, SKA1 with its excellent sensitivity and angular resolution will be able to investigate GRG groups in unprecedented detail. In several groups (like DA 240, Chen et al. (2011a); Peng et al. (2004); and 4C 73.08, Chen et al. (2012b); Strom et al. (2013)) we find that a large fraction of the companion galaxies are weak radio sources. The SKA1 sensitivity will enable us to explore the weak radio emissions of companion galaxies further. In addition, a number of the group galaxies appear to be spiral galaxies. 21 cm HI observations of them are likely to turn up a number of detections. One can use the HI data to estimate the amount of mass present, and study the group kinematics.

6. Conclusions

Our goal with SKA1 is to carry out a large-scale survey to search for giant radio galaxies. The survey should be unbiased and complete down to a well-defined brightness or flux density, over a specified sky area. The GRGs found will be used to trace out the WHIM, while we also hope

PoS(AASKA14)109

to detect candidate dying RGs, objects of low surface brightness with little evidence for compact features (jets, nuclear components), but with a steep radio spectrum. The high-z GRGs will be used to investigate how giant radio sources evolve. Some of the relatively nearby groups (like that surrounding DA 240) appear to have several spiral companions. We plan to observe them in the 21 cm HI line to study the motion and masses of GRG group members.

Among the questions we hope to answer, we note the following: Can one use the GRGs to detect the WHIM? And if so, can we pinpoint the missing baryons? Can one use GRGs and their surrounding companions to trace the distribution and physical state of the WHIM? Finally, are there enough high-z giant radio galaxies to investigate how radio galaxies evolve?

Acknowledgements

This work was partially supported by the Chinese Ministry of Science and Technology under the State Key Development Program for Basic Research, Grant Nos. 2013CB837900 and 2012CB821800, the Projects of International Cooperation and Exchange, NSFC, Grant No. 112611-40641, the key research program of the Chinese Academy of Sciences (CAS), Grant No. KJZD-EW-T01, and the Open Project Program of the Key Laboratory of Radio Astronomy. RGS wishes to thank the Chinese Academy of Sciences for the award of a visiting professorship, when most of this research was done.

References

Baade, W. & Minkowski, R., 1954, ApJ, 119, 215
Bolton, J., Stanley, G., & Slee, O., 1949, Nature, 164, 101
Burns, J., 1998, Sci, 280, 400
Chen, R., Peng, B., Strom, R., Wei, J., & Zhao, Y., 2011a, A&A, 529, A5
Chen, R., Peng, B., Strom, R., & Wei, J., 2011b, MNRAS, 412, 2433
Chen, R., Peng, B., Strom, R., & Wei, J., 2012a, MNRAS, 420, 2715
Chen, R., Peng, B., Strom, R., & Wei, J., 2012b, MNRAS, 422, 3004
de Zotti, G., Massardi, M., Negrello, M., & Wall, J., 2010, A&ARv, 18, 1
Davé, R., Cen, R., Ostriker, J., Bryan, G., Hernquist, L. et al., 2001, ApJ, 552, 473
Davé, R., Oppenheimer, B., Katz, N., Kollmeier, J., & Weinberg, D., 2010, MNRAS, 408, 2051
Dewdney, P., Turner, W., Millenaar, R., MacCool, R., Lazio, J., Cornwell, T., 2013, "SKA1 System Baseline Design", Document number SKA-TEL-SKO-DD-001 Revision 1
Dietrich, J., Werner, N., Clowe, D., Finoguenov, A., Kitching, T. et al., 2012, Nat, 487, 202
Jennison, R. & Das Gupta, M., 1953, Nat, 172, 996
Komberg, B. & Pashchenko, I., 2009, ARep, 52, 1086
Lara, L., Cotton, W., Feretti, L., Giovannini, G., Marcaide, J. et al., 2001, A&A, 370, 409
Luo, Q. & Sadler, E. M., 2010, ApJ, 713, 398
Mack, K., Klein, U., O' Dea, C. P., & Willis, A. G. 1997, A&A, 123, 423
Mack, K., Klein, U., O' Dea, P., Willis, G., & Saripalli, L. 1998, A&A, 329, 431
McCarthy, P., van Breugel, W. & Kapahi, V., 1991, ApJ, 371, 478
Machalski, J., Jamrozy, M., Zola, S., 2001, A&A, 371, 445

PoS(AASKA14)109

Malarecki, J., Staveley-Smith, L., Saripalli, L., Subrahmanyan, R., Jones, D. et al., 2013, MNRAS, 432, 200
Miley, G., 1968, Nat, 218, 933
Minkowski, R., 1960, ApJ, 132, 908
Peng, B., Strom, R., Wei, J., & Zhao, Y., 2004, A&A, 415, 487
Ryle, M., Smith, F., & Elsmore, B., 1950, MNRAS, 110, 508
Safouris, V., Subrahmanyan, R., Bicknell, G., & Saripalli, L., 2009, MNRAS,393, 2
Saripalli, L., Hunstead, R., Subrahmanyan, R., & Boyce, E., 2005, AJ, 130,896
Schoenmakers, A., Mack, K.-H, de Bruyn, A., Rottgering, H., Klein, U., & van der Laan, H., 2000, A&AS, 146, 293
Schoenmakers, A., de Bruyn, A., Röttgering, H. & van der Laan, H. 2001, A&A, 374, 861
Shull, J., Smith, B. & Danforth, C., 2012, ApJ, 759, 23
Smith, F., 1951, Nat, 168, 555
Strom, R., Chen, R., Yang, J., & Peng, B., 2013, MNRAS, 430, 2090
Subrahmanyan, R., Saripalli, L., Safouris, V., & Hunstead, R., 2008, ApJ,677, 63
Werner, N., Finoguenov, A., Kaastra, J., Simionescu, A., Dietrich, J. et al., 2008, A&A, 482, L29
Willis, A.G., Strom, R.G. & Wilson, A.S., 1974, Nat, 250, 625

Appendix

A. Formula used to estimate the number of GRGs for SKA_SUR

Number of giant radio galaxies:

$$N = \rho \times V_{\rm co} \tag{A.1}$$

Number density: $\rho = 10^{-7}$ (Mpc^{-3})
Comoving volume: (Mpc^3)

$$V_{\rm co} = \frac{1}{3} A_{\rm sky} D_{\rm co}^3 \tag{A.2}$$

Sky coverage: (deg^2)

$$A_{\rm sky} = \Delta RA \times \Delta\sin(Dec) - \Delta l \times \Delta\sin(b) \tag{A.3}$$

Comoving distance: (Mpc)

$$D_{\rm co} = \frac{D_L}{1+z} \tag{A.4}$$

Redshift z: (www.icosmos.co.uk)
Luminosity distance: (Mpc)

$$D_L = \sqrt{\frac{L_\nu}{4\pi S_{\rm obs}}} \tag{A.5}$$

Luminosity at frequency of ν: L_ν, $10^{25} - 10^{26}$ W/Hz at 1.4 GHz
Flux density observed with telescope: (Jy)

$$S_{\rm obs} = SNR \times \sigma \tag{A.6}$$

Sigma to noise: $SNR > 150$
Noise level with two polarizations: (Jy/beam)

$$\sigma = \frac{S_{\rm sys}}{\sqrt{2B\tau}} \tag{A.7}$$

PoS(AASKA14)109

System equivalent flux density:

$$S_{\rm sys} = \frac{2k_{\rm b}T_{\rm sys}}{A_{\rm eff}} \tag{A.8}$$

Boltzman constant: $k_{\rm b} = 1.38 \times 10^{-23}$ J/K
For SKA1_SUR, sensitivity specification: $\frac{A_{\rm eff}}{T_{\rm sys}} = 391$ m^{2}K^{-1}; bandwidth: $B = 500$ MHz
Integrated time: $\tau = 10$ minutes with NVSS observing model

B. Estimate of the total observing time

$$t = \frac{\tau A_{\rm sky}}{FoV} \tag{B.1}$$

For SKA1_SUR, field of view: $FoV = 18$ (deg^2); integrated time: $\tau = 10$ minutes with NVSS observing model; sky coverage: $A_{\rm sky}$ (equation A.3)

PoS(AASKA14)109

PROCEEDINGS OF SCIENCE

Measuring Magnetic Fields Near and Far with the SKA via the Zeeman Effect

Timothy Robishaw[*1,†], **James A. Green**[2], **Gabriele Surcis**[3], **Wouter Vlemmings**[4], **A. M. S. Richards**[5], **Sandra Etoka**[6], **Tyler L. Bourke**[2], **Vincent Fish**[7], **Malcolm Gray**[5], **Hiroshi Imai**[8], **Busaba Kramer**[9], **James McBride**[10], **Emmanuel Momjian**[11], **Anuj Sarma**[12], **and Albert Zijlstra**[5]

[1]*National Research Council Canada;* [2]*SKA Organization;* [3]*Joint Institute for VLBI in Europe;* [4]*Chalmers University of Technology* [5]*Jodrell Bank Centre for Astrophysics;* [6]*Hamburger Sternwarte;* [7]*MIT Haystack Observatory;* [8]*Kagoshima University;* [9]*Max Planck Institute for Radio Astronomy;* [10]*University of California at Berkeley;* [11]*National Radio Astronomy Observatory;* [12]*DePaul University;*
E-mail: tim.robishaw@nrc-cnrc.gc.ca

The measurement of Zeeman splitting in spectral lines—both in emission and absorption—can provide direct estimates of the magnetic field strength and direction in atomic and molecular clouds, both in our own Milky Way and in external galaxies. This method will probe the magnetic field in the warm and cold neutral components of the interstellar medium, providing a complement to the extensive SKA Faraday studies planning to probe the field in the ionized components.

Advancing Astrophysics with the Square Kilometre Array
June 8-13, 2014
Giardini Naxos, Sicily, Italy

[*]Speaker.
[†]On behalf of the SKA Cosmic Magnetism Working Group.

PoS(AASKA14)110

1. Introduction

The Zeeman effect leaves its fingerprint on the circular polarization of a spectral line. A magnetic field threading the gas where a spectral line for certain atomic and molecular transitions is emitted or absorbed will cause the two senses of circular polarization to split apart in frequency. The amplitude of the splitting between the two components is directly proportional to the strength of the magnetic field and a constant that depends on the atomic or molecular transition:

$$\Delta\nu[\mathrm{Hz}] = bB_{\mathrm{los}}[\mu\mathrm{G}](1+z)^{-1}\,, \tag{1.1}$$

where b is the Zeeman coefficient of the transition being observed and is measured in Hz μG^{-1}, B_{los} is the line-of-sight magnetic field measured in microgauss, and z is the redshift of the source. Tables of all known Zeeman coefficients can be found in Heiles et al. (1993) and Robishaw (2008).

The amplitude of the effect measured in the Stokes V spectrum (defined as IEEE right-hand minus left-hand circular polarization) towards sources in the Galactic interstellar medium (ISM) is generally very weak compared to the total intensity of the line measured in the Stokes I spectrum because the splitting is usually very small compared to the width of the line. However, some Galactic maser emission lines can be so narrow that the two circularly polarized components appear completely split; in this case, the splitting is proportional to the total field strength rather than the line-of-sight field (Crutcher et al. 1993).

In this chapter we discuss the potential for using the SKA to measure the Zeeman effect in various targets of interest in increasing order of distance.

1.1 Assumptions in This Chapter

The document "SKA1 Imaging Science Performance" (Braun 2014) provides parametrizations for sensitivity in spectral line and continuum modes that are the basis for the performance estimates in this chapter. In particular we utilize their Figure 5, which shows the spectral line sensitivity distribution for a single deep pointing with channel width of 30 km s^{-1} and an integration time of 1000 h. The L-band 1–2 GHz range shows that for beam widths between $0.3''$ and $300''$, we would measure a maximum rms of 12 μJy, with a minimum rms of 4 μJy at $10''$.

2. Molecular Clouds and Star Forming Regions in the Milky Way

The role of magnetic fields during the formation of high-mass stars ($M > 8M_{\odot}$) is still a matter of debate, even in the face of many recent investigations, both theoretical and observational (Seifried et al. 2012; Surcis et al. 2013). Recent magnetohydrodynamical simulations show that the collimation of outflows and the formation of accretion discs strongly depend on the strength of magnetic fields (Seifried et al. 2012). In addition, simulations show that magnetic fields also prevent fragmentation, reduce angular momentum, and determine the size of H II regions (Peters et al. 2011; Hennebelle et al. 2011; Seifried et al. 2012). The simulations take into account only relative values of magnetic field strengths obtained considering ratios of magnetic energy with other types of energies (e.g., gravitational energy). Therefore, no real values of magnetic field strengths are currently used in the theoretical calculations. To provide observational measurements

PoS(AASKA14)110

of magnetic field strengths close to the massive young stellar objects (YSOs) is of great importance. The best probes of magnetic fields at small scales close to YSOs are masers, in particular the Class II methanol maser transition at 6.7 GHz and 22 GHz water masers (Vlemmings et al. 2006a; Surcis et al. 2011, 2013, 2014). Methanol masers, which are the most numerous high-mass star formation (HMSF) maser species, are playing a crucial role in determining the magnetic field morphology (Vlemmings et al. 2010; Surcis et al. 2012, 2013). Moreover, Vlemmings et al. (2006b, 2011) showed that at arcsecond resolution, methanol masers also display significant circular polarization. In fact, 70% of their total Effelsberg+Parkes flux-limited (>50 Jy) sample (51 sources) show circularly polarized emission. This has also been confirmed at milliarcsecond scale via interferometric observations for a smaller number of sources (Surcis et al. 2012, 2013). However, the exact proportionality between the measured Zeeman-splitting of the methanol maser emission and the magnetic field strength is still under investigation by a team of theoretical chemists and astrophysicists and the final results will be published in 2015. Current instrumentation limits the maser magnetic field studies to up to only two dozen sources, for which only a few lines of sight can be probed. To properly compare with models and simulations, one would need several tens of field measurements on the individual maser features of each source. Additionally, to properly sample different evolutionary stages, a total of up to 100 sources needs to be observed in detail. Unfortunately, our ability to increase this sample is completely limited by the currently available instruments, which allow us to measure the very weak circular polarization signal (usually of the order 0.3%-0.5%) only towards methanol maser sources with flux exceeding 25 Jy in a reasonable observation time. Fortunately, the upcoming SKA1-MID will allow us to investigate a much larger sample of sources. A 30 min integration time at a resolution of 0.1 km s^{-1}—necessary to detect the splitting—will produce an rms of 9 mJy at 6.7 GHz. This means that we could make 5σ detections down to a circular polarization fraction of at least 0.3% towards methanol masers with flux >15 Jy. Therefore with SKA1-MID we could easily measure the magnetic field strength in hundreds of HMSF regions and consequently enlarge the investigated area of the Milky Way.

The SKA will be invaluable in the study of Galactic masers, such as very high-resolution follow-up of catalogues like the Methanol (and OH) Multibeam Survey (Green et al. 2009). Multiple transitions provide a chronometer with thousand-year resolution for HMSF concentrated in the Galactic plane (Ellingsen 2007; Breen et al. 2010). Southern hemisphere centimeter-wave studies with resolutions of a few hundred milliarcseconds or better are needed to complement ALMA and to map magnetic field structures. At the other end of stellar evolution, we do not really understand the precise mechanisms whereby cool red giants, AGB stars and supergiants lose mass, nor how almost-spherical stars give rise to asymmetric PNe and SNR. The SKA and ALMA will not only map the kinematics and magnetic fields at high resolution with masers, but, for the first time, relate these to thermal lines and dust emission with high precision.

Evolved OH/IR stars commonly exhibit OH maser emission that probes the outer part of their circumstellar envelopes (CSEs) where ordered magnetic fields of a few milligauss are detectable (Etoka & Diamond 2010, 2004). Such observations can trace fields even at the proto-planetary-nebula stage (Etoka et al. 2009). Though they start their lives as spherically symmetric objects, a large fraction of planetary nebulae are asymmetrical objects. Although the change of symmetry might be linked primarily to binarity, the organized magnetic fields detected at the distance where OH masers operate in the CSEs seem to indicate the possible role of magnetism in this morpholog-

PoS(AASKA14)110

ical development. It is anticipated that thousands of such objects can be detected throughout the Galaxy down to a flux limit of 4 mJy with SKA1-SUR in ∼140 hours (Etoka et al. 2015).

3. The Magnetic Field Structure of the Milky Way

3.1 H I Absorptions Lines against Background Continuum Sources

The magnetic field in the cold neutral medium (CNM) can be probed via the absorption of continuum emission from compact sources at 21 cm. This method was successfully used by Heiles & Troland (2004, 2005) at the Arecibo telescope to make an uprecedented survey of the CNM towards 41 radio-loud sources; 20 magnetic field components were detected throughout the Milky Way. The limiting sensitivity of their survey was 3 mJy. For a $10''$ beam and 0.5 km s^{-1} channels, SKA1-MID would achieve this sensitivity in 75 minutes. Therefore, a census of the CNM fields throughout the southern sky should be readily achievable. It should be noted that FAST will certainly make great advances in this endeavour in the northern sky before SKA is online. However, it should be said that single-dish H I absorption spectra are produced by subtracting an off-position spectrum and are therefore inherently inaccurate; the possibility also arises that polarized sidelobes can contaminate Stokes V spectra for weak sources when using this method. These problems are mitigated by interferometric measurements.

3.2 H I Self-Absorption

An intriguing group of targets includes positions that show 21-cm self-absorption (Li & Goldsmith 2003, the "self" prefix distinguishing this case from that of absorption against a background continuum source). Dozens of clouds throughout the Perseus/Taurus molecular complex show H I absorption at velocities for which OH and CO emission is seen. McClure-Griffiths et al. (2006) detected H I self-absorption throughout the Riegel-Crutcher cloud, an 8°-by-8° region at the Galactic Center showing an incredible network of long, cold filaments. When the method of Chandrasekhar & Fermi (1953) is used to investigate stellar polarization measurements along these filaments, magnetic fields in excess of 30 μG are inferred. The H I absorption profile has a height of 100 K and a width of 3.5 km s^{-1}. A 30 μG field produces a Stokes V profile with peak-to-peak extent only 1.6% of the line height, or 1.6 K. This can be fitted if observed with a sensitivity of 0.3 K. The width of the filaments is between $2'$–$5'$, so an integration time of 2 hours per pointing would be required if observed by SKA1-MID with a $120''$ beam. The map would require hundreds of pointings, meaning this is best left for SKA2 when the sensitivity will increase tenfold and the field of view will increase twentyfold.

3.3 Diffuse 21-cm Emission

Diffuse 21-cm emission is seen in every direction in the sky. This fact, combined with the strong splitting coefficient for the 21-cm line, makes H I emission an enticing target for Zeeman studies. This line of work was pursued successfully using single dishes for decades before being abandoned in the mid-1990s (Heiles & Troland 1982; Heiles 1988, 1989, 1996, 1997; Troland & Heiles 1982a,b; Verschuur 1989; Goodman & Heiles 1994; Myers et al. 1995). Reliable measurements require a careful accounting of instrumental circular polarization contributions from polarized sidelobes of the telescope.

PoS(AASKA14)110

As far as we know, nobody has successfully used an interferometer to measure 21-cm Zeeman splitting in diffuse emission. This scenario maintains at the VLA because its circular polarization response contains a severe squint induced by placement of the *L*-band feed far off the symmetry axis of each dish. This is not impossible to model, measure, and account for, but it is a major undertaking. The SKA dishes will be designed such that the secondary and feed alignment satisfy the "Mizigutch criterion" (Mizugutch et al. 1976), which should minimize cross polarization and, therefore, the Stokes *V* squint. If the circularly polarized beam can be characterized for the SKA, then we presume that the instrumental contribution to a Stokes *V* measurement can be modeled and accounted for. (Indeed, Agudo et al. 2015 require circular polarization precision of 0.01% to measure relativistic jet properties.) The many polarization projects that will be undertaken with the SKA guarantee that a thorough accounting of the polarizaton properties of the array will be made, thus enhancing the possibility that the SKA might be the first interferometer to study the Zeeman effect in diffuse 21-cm emission.

3.4 OH Masers Tracing the Galactic Magnetic Field

Davies (1974) found the amazing result that the magnetic field measured in OH masers seemingly traces the large-scale field that the masers are embedded in. VLBI observations of OH masers at the highest resolutions have demonstrated that maser Zeeman splitting shows field directions and magnitudes which are largely coherent (e.g. Fish et al. 2003; Vlemmings & van Langevelde 2007). The splitting is often replicated in the lower resolution single-dish studies (Fish et al. 2005; Szymczak & Gérard 2009). Following the work of Davies (1974), several authors have investigated the concept of maser Zeeman splitting tracing the Galactic magnetic field (e.g. Reid & Silverstein 1990; Fish et al. 2003; Han & Zhang 2007), finding fields consistent across kiloparsec scales. These studies were conducted mostly with samples of masers collated from a range of heterogeneous observations; the largest set of systematic observations were those of Fish et al. (2003), but these were limited to only 40 star-forming regions, all visible from the northern hemisphere, and with only a few masers per spiral arm. Despite these limitations, there is an implication that the magnetic fields traced by the masers are tied to the large-scale Galactic magnetic fields, such as those traced by rotation measures (e.g. Han et al. 2006; Brown et al. 2007; Van Eck et al. 2011).

The 'MAGMO' survey (Green et al. 2014) was launched at the Australia Telescope Compact Array (ATCA) in order to potentially map out the magnetic field in the Galactic plane by searching for Zeeman splitting in OH masers. MAGMO observations achieved a sensitivity of 50 mJy in 30 min of ATCA observing with an $8''$ beam, and consisted of targeted follow-up of positions where 6.7 GHz methanol masers were detected. This species of maser is an exclusive tracer of HMSF (Minier et al. 2003; Pestalozzi et al. 2005; Xu et al. 2008; Breen et al. 2013) and as such traces the key structural features of the Galaxy—the spiral arms, 3-kpc arms and bar interaction. The combination of structure and magnetic field information can be a very powerful tool for understanding the dynamics and evolution of the Milky Way.

The logical extension of the MAGMO project would be a blind gridded survey for OH masers in the Galactic plane using SKA1-MID. A survey covering $-2^\circ < b < +2^\circ$ and $190^\circ < l < 60^\circ$ would subtend 920 sq deg, providing a sensitivity of 3.7 mJy in one month of observing at the 18 cm OH transitions with 0.1 km s^{-1} resolution and a $10''$ beam. The scale height for HMSF is well known and this latitude range will capture the vast majority of star forming sources (>95%).

PoS(AASKA14)110

A blind survey to lower sensitivities than achieved by the targeted MAGMO study will bring about a larger detection rate towards regions of HMSF and will increase the number of Zeeman detections. This will markedly improve statistics, both within individual regions, and within Galactic structures such as individual spiral arms. The increased number of measurements will allow for a comparison of maser field directions with those probed via Faraday rotation of polarized continuum sources through nearby sightlines that contain a magnetoionic medium, which will in turn be vastly improved in the SKA era through all-sky polarimetric surveys (Johnston-Hollitt 2015).

An SKA-MAGMO study will explore whether the additional sensitivity that the SKA affords will result in a larger detection rate towards regions of HMSF or a larger number of sources per HMSF site. With the extra sensitivity we would expect an increase in the number of Zeeman pairs/triplets, which will provide more measurements to compare with Faraday rotation measures, decreasing the statistical error. The additional measurements will allow exploration of whether there is any relation to magnetic field strength for much weaker sources, also exploring the proportion of Zeeman pairs compared to Zeeman triplets for weaker sources. The SKA-MAGMO study would further enhance our understanding of the dynamics and evolution of our Galaxy through association with precise positions of HMSF regions (Green et al. 2015).

4. Zeeman Splitting in External Galaxies

Masers have the highest luminosity per unit frequency of any radio source, so it is natural to use Zeeman splitting in these beacons to measure magnetic fields in distant galaxies. Luckily, as we saw above in discussing the MAGMO project, OH has a very large Zeeman coefficient and is therefore a sensitive tracer of magnetic fields. We discuss the possibilities of using OH masers and megamasers as extragalactic magnetometers.

4.1 OH Masers in Nearby Galaxies

SKA2 could be used to survey the local group galaxies for OH maser emission and Zeeman splitting. If detected, the field structure inferred would be of great interest when comparing to MAGMO results in our own Galaxy because our Galactic study will be confined only to the plane.

Brooks & Whiteoak (1997) detected OH masers in the LMC, needing a sensitivity of $\sim$40 mJy to obtain a 5σ detection in Stokes I. For a beam of $10''$ and a channel resolution of 0.1 km s^{-1}, the SKA1-MID would require less than a minute to detect Zeeman splitting in such a source. A survey of the OH maser emission in the LMC and SMC is therefore of great interest: any field structure detected in the OH maser distribution could be compared directly with the fields already mapped in the SMC and LMC via Faraday rotation (Mao et al. 2008; Gaensler et al. 2005).

OH masers have yet to be detected in M31. Willett (2011) conducted a search using the VLA and found nothing above a 5σ 10 mJy limit concluding that an order of magnitude increase in sensitivity would be required to probe the OH masers. This would require 10 hours of SKA1-MID integration time with a velocity resolution of 1 km s^{-1}.

M82 is the canonical starburst galaxy, located at a distance of 3.5 Mpc. Argo et al. (2010) used 61 hours of VLA observing with a $1''$ beam to show that OH masers (actually, "kilomasers") are seen throughout M82 with line widths of $\sim$10 km s^{-1} and fluxes as weak as 2 mJy. For a 5σ detection of all the Stokes I features in M82, we'd require 7 hours of SKA1-MID observing time

PoS(AASKA14)110

with 1 km s^{-1} channels. However, unlike in the Milky Way, the OH maser lines in M82 are broad enough that they are only partially split even for large fields of 3 mG. The peak-to-peak amplitude of the Zeeman feature in Stokes V will be 50% of the line height for a splitting induced by a 3 mG field. For the weakest detected OH maser, we can fit a Zeeman profile easily to a sensitivity limit of 0.3 mJy. So to detect Zeeman splitting in all observed maser features using SKA1-MID would require 13 hours of integration. This would allow for a complete mapping of the field as traced by OH masers in M82.

4.2 Megamasers

Megamasers have been detected in hundreds of galaxies at $z \sim 0.1$, and, with the aid of lensing, as far away as $z = 2.6$ (Castangia et al. 2011). Intrinsically compact both spatially (detectable down to micro-arcsec scales) and spectrally (sub-km s^{-1}), they provide the best directly mappable tracers of high-resolution structure in the inner few hundred parsecs of active galaxies. The early stages of the SKA are suited to studies of the larger-scale OH masers (rest frequency 1.67 GHz) associated with nuclear starbursts and Seyfert galaxies. The position of individual maser spots can be measured with an accuracy proportional to (beam size)/(signal-to-noise). For example, at a redshift of order 0.05, MERLIN (resolution 120 mas) could resolve 10-parsec details in Markarian 231 and 273 (Richards et al. 2005; Yates et al. 2000) showing warped discs and orbiting mass densities of 300–900 M$_\odot$ pc^{-3}.

The most exciting use of OH megamasers (OHMs) has been the measurement of *in situ* magnetic fields in 15 external galaxies by Robishaw et al. (2008) and McBride & Heiles (2013), who used the high spectral resolution of Arecibo to separate multiple Zeeman components and compared these with VLBI and MERLIN total-intensity lower-resolution spectra extracted from spatially-discrete regions. The inferred magnetic field strengths of 0.5–80 mG provide an energy density comparable to the hydrostatic gas pressure in the masing regions, likely to be active star formation sites. The results from OHMs also suggest that magnetic fields are dynamically important throughout the central starburst region, whereas weaker magnetic fields are inferred from radio synchrotron measurements assuming equipartition. The OHM-derived estimates are consistent with the linearity of the far-infrared–radio correlation (McBride et al. 2014).

The total OHM velocity span can exceed 1000 km s^{-1} but typical Zeeman splitting detections have been associated with lines that have velocity widths $<$20 km s^{-1} and flux densities $>$3 mJy. The Arecibo detections required an rms flux density of 3 mJy in 0.5 km s^{-1} channels. SKA1-MID will be able to survey all southern galaxies for OHM Zeeman splitting; a 1$''$ beam at 1.6 GHz will reach 1 mJy sensitivity in 2 hours with 0.5 km s^{-1} channels, sufficient to detect analogues of the sources in the Arecibo sky. If all SKA-visible Arecibo targets were searched with this threefold improvement in sensitivity, we could expect to double the number of galaxies with Zeeman detections in 2 days of observing with SKA1-MID. The southern sky has not been thoroughly searched for OHMs; blind 21-cm surveys with the SKA are bound to catalog the southern OHM population. Deep follow-up observations of the southern OHM galaxies will yield at least another doubling of the number of Zeeman-detected galaxies; sampling the 100 brightest OHMs would require 200 hours of SKA1-MID time. The most distant Zeeman detections occurred in OHMs at $z \sim 0.2$. The sensitivity increase afforded by SKA2 will allow Zeeman splitting to be probed in OHMs out

PoS(AASKA14)110

past $z = 1$, allowing these beacons to become invaluable tools for studying galactic magnetic fields through cosmic time.

Previous OHM studies have relied on literature VLBI imaging, but this adds uncertainty as the intervals between observations are comparable to the variability timescales of compact masing clouds. SKA2 will reach the same 1 mJy rms per 120 mas beam in the same time in 25 km s^{-1} channels, allowing comparison between simultaneous high spectral- and high spatial-resolution results. SKA2 will extend its reach to more highly redshifted OH masers and possibly to 22 GHz water masers, which trace material orbiting black holes and jet-ISM interactions on sub-pc scales. However, the splitting coefficient for H_2O is 1000 times weaker than that for OH such that Zeeman splitting in water megamasers has thus far eluded detection (Modjaz et al. 2005).

4.3 H I Absorption in Damped Lyα Absorbers

Damped Lyα absorbing systems (DLAs) are a class of quasar absorber in which hydrogen remains mostly neutral. The neutral gas content of the Universe is dominated up to redshift 5 by DLAs and the H I layers producing the absorption are considered to be the progenitors of modern galaxies. DLAs are perhaps the best and only sample of an interstellar medium in the high-redshift Universe (Wolfe et al. 2005). As such, the possibility of measuring Zeeman splitting in the 21 cm line absorption in these systems would allow us to test the importance of the role of magnetic fields in galaxy formation and evolution and constrain dynamo models for the generation and amplification of magnetic fields in the early Universe. Wolfe et al. (2011, 2008) describe Green Bank Telescope observations of a DLA at $z = 0.692$ towards 3C 286. No Zeeman signature was detected in the Stokes V spectrum at 839.40 MHz down to a field limit of 17 μG. It would take SKA1-MID 90 min to probe down to 5 μG field strengths in this DLA with 1.5 km s^{-1} channels. The ability to probe such systems to lower sensitivities and therefore lower limiting magnetic fields is tantalizing. Because of the large redshifts of these systems, all observations would be carried out in bands 1 and 2. These DLAs are viable targets for all phases of SKA deployment.

5. Conclusions

Measurement of the Zeeman effect is sensitivity limited. Our ability to use this method to probe magnetic fields in the Milky Way and beyond is completely dependent on the development of telescopes with better sensitivity than is currently achievable by the world's largest observatories. The SKA will make significant improvements in our pursuit of measuring Zeeman splitting in spectral lines, both in emission and absorption. These measurements will provide direct estimates of and upper limits to the magnetic field strength and direction in atomic and molecular clouds, both in our own Milky Way and in external galaxies. This method will probe the magnetic field in the warm and cold neutral components of the interstellar medium, providing a complement to the extensive SKA Faraday studies planning to probe the field in the ionized components.

The early phase SKA1 is estimated to yield a 50% reduction in sensitivity, resulting in a quadrupling of the the required integration times calculated here. Of the possible SKA1 experiments described, only the OH megamaser survey would be prohibitively long and require the full deployment of SKA1.

PoS(AASKA14)110

References

Agudo, I., Böttcher, M., Falcke, H., et al. 2015, "Studies of Relativistic Jets in Active Galactic Nuclei with SKA", in proc. *Advancing Astrophysics with the Square Kilometre Array*, PoS(AASKA14)093

Argo, M. K., Pedlar, A., Beswick, R. J., Muxlow, T. W. B., & Fenech, D. M. 2010, MNRAS, 402, 2703

Braun, R. 2014, "SKA1 Imaging Science Performance", Document SKA-TEL-SKO-DD-XXX Rev. A Draft 5

Breen, S. L., Ellingsen, S. P., Caswell, J. L., & Lewis, B. E. 2010, MNRAS, 401, 2219

Breen, S. L., Ellingsen, S. P., Contreras, Y., et al. 2013, MNRAS, 435, 524

Brooks, K. J., & Whiteoak, J. B. 1997, MNRAS, 291, 395

Brown, J. C., Haverkorn, M., Gaensler, B. M., et al. 2007, ApJ, 663, 258

Castangia, P., Impellizzeri, C. M. V., McKean, J. P., et al. 2011, A&A, 529, A150

Chandrasekhar, S., & Fermi, E. 1953, ApJ, 118, 113

Crutcher, R. M., Troland, T. H., Goodman, A. A., et al. 1993, ApJ, 407, 175

Davies, R. D. 1974, in IAU Symp. 60, Galactic Radio Astronomy, ed. F. J. Kerr & S. C. Simonson (Dordrecht: Reidel), 275

Ellingsen, S. P. 2007, MNRAS, 377, 571

Etoka, S., & Diamond, P. 2004, MNRAS, 348, 34

Etoka, S., & Diamond, P. J. 2010, MNRAS, 406, 2218

Etoka, S., Engels, D., Imai, H., et al. 2015, "OH masers in the Milky Way and Local Group galaxies in the SKA era", in proc. *Advancing Astrophysics with the Square Kilometre Array*, PoS(AASKA14)125

Etoka, S., Zijlstra, A., Richards, A. M., Matsuura, M., & Lagadec, E. 2009, in Astronomical Society of the Pacific Conference Series 404, The Eighth Pacific Rim Conference on Stellar Astrophysics: A Tribute to Kam-Ching Leung, ed. B. Soonthornthum, S. Komonjinda, K. S. Cheng, & K. C. Leung (San Francisco: ASP), 311

Fish, V. L., Reid, M. J., Argon, A. L., & Menten, K. M. 2003, ApJ, 596, 328

Fish, V. L., Reid, M. J., Argon, A. L., & Zheng, X.-W. 2005, ApJS, 160, 220

Gaensler, B. M., Haverkorn, M., Staveley-Smith, L., et al. 2005, Science, 307, 1610

Goodman, A. A., & Heiles, C. 1994, ApJ, 424, 208

Green, J. A., Caswell, J. L., Fuller, G. A., et al. 2009, MNRAS, 392, 783

Green, J. A., Gray, M. D., Robishaw, T., Caswell, J. L., & McClure-Griffiths, N. M. 2014, MNRAS, 440, 2988

Green, J. A., van Langevelde, H. J., Brunthaler, A., et al. 2015, "Maser Astrometry with the SKA", in proc. *Advancing Astrophysics with the Square Kilometre Array*, PoS(AASKA14)119

Han, J. L., Manchester, R. N., Lyne, A. G., Qiao, G. J., & van Straten, W. 2006, ApJ, 642, 868

Han, J. L., & Zhang, J. S. 2007, A&A, 464, 609

Heiles, C. 1988, ApJ, 324, 321

———. 1989, ApJ, 336, 808

———. 1996, ApJ, 466, 224

———. 1997, ApJS, 111, 245

PoS(AASKA14)110

Heiles, C., Goodman, A. A., McKee, C. F., & Zweibel, E. G. 1993, in Protostars and Planets III, ed. E. H. Levy & J. I. Lunine (Tucson: Univ. Arizona Press), 279
Heiles, C., & Troland, T. H. 1982, ApJ, 260, L23
———. 2004, ApJS, 151, 271
———. 2005, ApJ, 624, 773
Hennebelle, P., Commerçon, B., Joos, M., et al. 2011, A&A, 528, A72
Johnston-Hollitt, M. 2015, "Using SKA Rotation Measures to Reveal the Mysteries of the Magnetised Universe", in proc. *Advancing Astrophysics with the Square Kilometre Array*, PoS(AASKA14)092
Li, D., & Goldsmith, P. F. 2003, ApJ, 585, 823
Mao, S. A., Gaensler, B. M., Stanimirović, S., et al. 2008, ApJ, 688, 1029
McBride, J., & Heiles, C. 2013, ApJ, 763, 8
McBride, J., Quataert, E., Heiles, C., & Bauermeister, A. 2014, ApJ, 780, 182
McClure-Griffiths, N. M., Dickey, J. M., Gaensler, B. M., Green, A. J., & Haverkorn, M. 2006, ApJ, 652, 1339
Minier, V., Ellingsen, S. P., Norris, R. P., & Booth, R. S. 2003, A&A, 403, 1095
Mizugutch, Y., Akagawa, M., & Yokoi, H. 1976, ISA Proceedings, 2
Modjaz, M., Moran, J. M., Kondratko, P. T., & Greenhill, L. J. 2005, ApJ, 626, 104
Myers, P. C., Goodman, A. A., Gusten, R., & Heiles, C. 1995, ApJ, 442, 177
Pestalozzi, M. R., Minier, V., & Booth, R. S. 2005, A&A, 432, 737
Peters, T., Banerjee, R., Klessen, R. S., & Mac Low, M.-M. 2011, ApJ, 729, 72
Reid, M. J., & Silverstein, E. M. 1990, ApJ, 361, 483
Richards, A. M. S., Knapen, J. H., Yates, J. A., et al. 2005, MNRAS, 364, 353
Robishaw, T. 2008, Ph.D. thesis, University of California at Berkeley
Robishaw, T., Quataert, E., & Heiles, C. 2008, ApJ, 680, 981
Seifried, D., Banerjee, R., Pudritz, R. E., & Klessen, R. S. 2012, MNRAS, 423, L40
Surcis, G., Vlemmings, W. H. T., Curiel, S., et al. 2011, A&A, 527, A48
Surcis, G., Vlemmings, W. H. T., van Langevelde, H. J., et al. 2014, A&A, 565, L8
Surcis, G., Vlemmings, W. H. T., van Langevelde, H. J., & Hutawarakorn Kramer, B. 2012, A&A, 541, A47
Surcis, G., Vlemmings, W. H. T., van Langevelde, H. J., Hutawarakorn Kramer, B., & Quiroga-Nuñez, L. H. 2013, A&A, 556, A73
Szymczak, M., & Gérard, E. 2009, A&A, 494, 117
Troland, T. H., & Heiles, C. 1982a, ApJ, 252, 179
———. 1982b, ApJ, 260, L19
Van Eck, C. L., Brown, J. C., Stil, J. M., et al. 2011, ApJ, 728, 97
Verschuur, G. L. 1989, ApJ, 339, 163
Vlemmings, W. H. T., Diamond, P. J., van Langevelde, H. J., & Torrelles, J. M. 2006a, A&A, 448, 597
Vlemmings, W. H. T., Harvey-Smith, L., & Cohen, R. J. 2006b, MNRAS, 371, L26
Vlemmings, W. H. T., Surcis, G., Torstensson, K. J. E., & van Langevelde, H. J. 2010, MNRAS, 404, 134
Vlemmings, W. H. T., Torres, R. M., & Dodson, R. 2011, A&A, 529, A95

PoS(AASKA14)110

Vlemmings, W. H. T., & van Langevelde, H. J. 2007, A&A, 472, 547
Willett, K. W. 2011, Ph.D. thesis, PhD Thesis, University of Colorado, 2011
Wolfe, A. M., Gawiser, E., & Prochaska, J. X. 2005, ARA&A, 43, 861
Wolfe, A. M., Jorgenson, R. A., Robishaw, T., Heiles, C., & Prochaska, J. X. 2008, Nature, 455, 638
———. 2011, ApJ, 733, 24
Xu, Y., Li, J. J., Hachisuka, K., et al. 2008, A&A, 485, 729
Yates, J. A., Richards, A. M. S., Wright, M. M., et al. 2000, MNRAS, 317, 28

PoS(AASKA14)110

PROCEEDINGS OF SCIENCE

Stacking for Cosmic Magnetism with SKA surveys

Jeroen M. Stil[*†]
Department of Physics & Astronomy, The University of Calgary
E-mail: jstil@ucalgary.ca

Ben W. Keller
Department of Physics & Astronomy, MacMaster University
E-mail: kellerbw@mcmaster.ca

Stacking polarized radio emission in SKA surveys provides statistical data on large samples that is not accessible otherwise due to limitations set by a combination of sensitivity, source statistics, and frequency averaging. Polarization is a special case because one obvious source of stacking targets is the Stokes I source catalog, possibly in combination with external catalogs, for example an SKA HI survey or a non-radio survey. We point out the significance of stacking polarization of subsamples selected by additional observable parameters. Applications of stacking polarization include but are not limited to obtaining in a statistical sense polarization information to the detection limit in total intensity, investigating depolarization as a function of cosmic time at consistent source-frame wavelengths, magnetic field properties in objects with a low radio luminosity such as dwarf and low-surface-brightness galaxies, and investigating potential correlations of observable parameters with the average magnetic field direction in a sample. We also point out the potential use of stacking in validating the polarization calibration of a survey. While stacking is flexible in terms of survey definition, we discuss optimal survey parameters for the science experiments presented, as well as computing and archiving requirements.

Advancing Astrophysics with the Square Kilometre Array
June 8-13, 2014
Giardini Naxos, Italy

[*]Speaker.
[†]On behalf of the SKA Cosmic Magnetism Working Group

PoS(AASKA14)112

1. Why Stack Polarization?

One of the areas of strength for SKA on the evolution of galaxies and their magnetic fields is in the analysis of very large samples over a wide range of redshift. Stacking is a statistical analysis of the emission of a sources that are too faint to be detected individually in the survey, whose position is known from another survey. Stacking provides a flux density representative for a carefully selected sample of sources. The astrophysical interpretation depends on the selection criteria of the input catalog. A particularly useful application is to compare subsamples distinguished by an observable parameter, e.g. inclination, flux at another wavelength, galaxy type, or spectral index.

Stacking radio polarization Stil et al. (2014) offers three significant benefits. The first is that it allows investigation of the polarization of radio sources to the detection limit in total intensity, even though the polarized signal is usually only a few percent of the total flux density. The second is that application of stacking polarization as a function of flux density allows a uniform investigation of the polarization of radio sources without applying a detection threshold in polarized intensity. The third benefit of stacking polarization is that it provides an opportunity to study polarization of sources as a function of frequency with high sensitivity without the need to average over all observed frequencies. Faraday rotation and depolarization are highly dependent on wavelength at the source.

Figure 1 illustrates some of these advantages from stacking the NVSS survey (Condon et al. (1998)). The left panel in Figure 1 shows fractional polarization versus flux density for all NVSS sources. Each data point in this figure represents a stacking experiment and a sequence of Monte-Carlo realizations of the stack to correct for polarization bias and determine the error bars. A direct investigation of sources with detectable polarized flux limits this analysis to sources with $S_{1.4} \gtrsim$ 80 mJy (Mesa et al. (2002),Tucci et al. (2004)). While deep surveys can detect polarization in fainter sources, detecting the gradual change in fractional polarization in Figure 1 requires sample sizes for which current deep fields are too small. The noise in the median image of the faintest bin is 1 μJy, sufficient to detect polarization in the faintest sources in the NVSS catalog witout concern for confusion.

Splitting up the sample also by spectral index reveals how the dependence of polarization on flux density is mainly due to sources with intermediate spectral index (Figure 1, right). A difference between bright flat and steep spectrum sources was reported by Mesa et al. (2002); Tucci et al. (2004), but the trends in Figure 1 can only be studied through stacking at this time. Does the trend for for sources with intermediate spectral index continue at lower flux density, and what does it mean? This example illustrates how subdivision of the input catalog - in this case by spectral index - provided additional information by revealing a correlation with an observable parameter. The flux density limit in the right panel of Figure 1 is set by uncertainty in the spectral index used to define the subsamples. One should lso be careful when constructing the subsamples. For example, we subdivided the sample at the modal spectral index -0.75 so that noise broadening of the spectral index distribution of faint sources does not affect the number of steep-spectrum sources in the intermediate spectral index range.

This example illustrates an important point about polarization stacking: significant gains can be made using only the Stokes I source catalog as the input catalog. Such experiments would not suffer from confusion or source blending, and the interpretation of the stacked polarization is

PoS(AASKA14)112

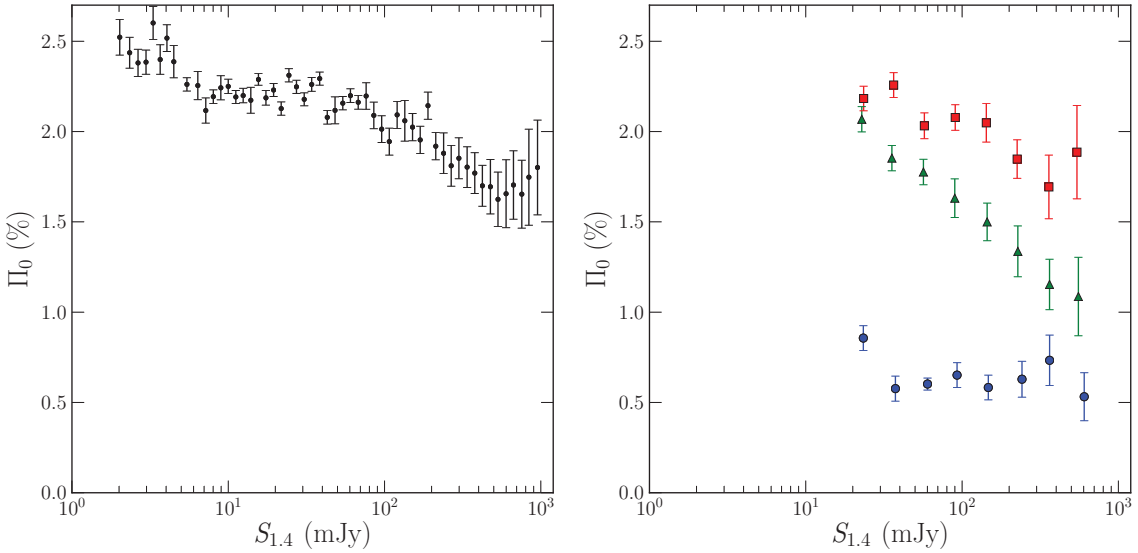

Figure 1: Fractional polarization of radio sources at 1.4 GHz as a function of flux density from stacking NVSS Condon et al. (1998) polarized intensity. Left: results from Stil et al. (2014) using all NVSS sources. Right: preliminary results stacking sources as a function of spectral index in the area of overlap between the WENSS (325 MHz) (Rengelink et al. (1997)) and the NVSS (1400 MHz). Blue circles: $\alpha > -0.3$, green triangles: $-0.75 < \alpha < -0.3$, red squares: $\alpha < -0.75$. The flux density range is limited on the high end because of the samples are smaller, and on the low end by the quality of the spectral indices of flat spectrum sources.

straightforward by subdividing the sample in ranges of total flux density. If additional information is available, possibly only for some part of the survey area, it becomes possible to do additional stacking experiments that provide further insight in the physics of the polarized emission by revealing correlations with observable parameters.

2. Stacking Applications for Cosmic Magnetism

We do not aim to give an exhaustive description of all possible stacking experiments that can be done with an SKA polarization survey. The few applications mentioned here serve to illustrate how this analysis can advance science with the SKA, supplementing other techniques.

2.1 Fractional polarization as a function of redshift

Faraday Synthesis averages the polarization across the a wide frequency range to optimize sensitivity and resolution in Faraday depth. Faraday rotation and depolarization in a source at redshift z occur at the sourceframe wavelength $\lambda_{\rm src} = \lambda_{\rm obs}/(1+z)$. For observations related to the evolution of cosmic magnetism it is preferable to compare for example depolarization in similar sources at the same $\lambda_{\rm src}$, or equivalent wavelength range in the source frame. If not, interpretation of the results will be model dependent. For Faraday Synthesis, the ability to track the same range in $\lambda^2_{\rm src}$ as a function of redshift requires a trade-off with sensitivity, or an additional survey at longer wavelength targeting high-redshift objects.

PoS(AASKA14)112

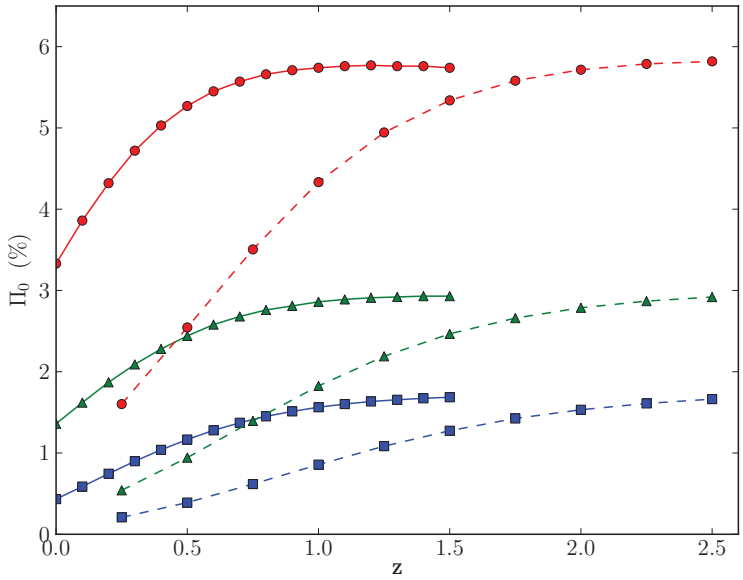

Figure 2: Fractional polarization derived from the peak of the Faraday depth spectrum from Faraday synthesis of models of the integrated polarization of galaxies in SKA-SUR band 3 (1.5 - 4.0 GHz; continuous curve) and SKA-MID band 2 (0.95 - 1.76 GHz; dashed curve). Galaxy models were evaluated for inclination 60°, and ratio of random to regular magnetic field strength 2.0 (red circles), 3.0 (green triangles), and 4.0 (blue squares).

Figure 2 shows fractional polarization from Faraday Synthesis of models of unresolved galaxies from **?** in two bands: SKA-SUR band 3 and SKA-MID band 2. It is expected that star forming galaxies make up a majority of the faint radio source population observable with the SKA, but the discussion that follows holds qualitatively for any segment that is affected by depolarization local to the source. Figure 2 shows that the observed polarization increases significantly for same galaxy as a function of redshift as the observed frequency band shifts to shorter wavelengths in the source frame. Qualitatively, one would expect a passively evolving disk galaxy over time to deplete its interstellar medium and decrease its star formation rate per unit mass. We expect that the mean electron density is higher and that the magnetic field is more tangled in a high-redshift analogue of the Milky Way. The effect of galaxy evolution is therefore that depolarization at the same $\lambda_{\rm src}$ is stronger at higher redshift, a trend opposite to the one observed in Figure 2. As a consequence, interpretation of such data will be model dependent.

Stacking polarization averaged over narrow ranges of $\lambda_{\rm obs}$ (1 or more channels) for samples of galaxies as a function of redshift will allow us to derive fractional polarization as a function of $\lambda_{\rm em}$ to the extent allowed by the frequency range of the survey. SKA-SUR band 3 for lower redshifts and SKA-MID band 2 for higher redshifts (and higher sensitivity) are well positioned for this experiment. While Faraday synthesis of these galaxies provides a band-averaged fractional polarization, stacking will benefit from less depolarization at the short-wavelength end. The sample would necessarily require indentification of optical counterparts with redshifts, as well as a criterium to reject galaxies with an AGN, for example through the infrared-radio correlation. It will require sample sizes of 10^5 per stack to derive the median polarization to the detection limit in total

PoS(AASKA14)112

intensity. In practice, the analysis will be limited by the size of the optical target catalogue, also because separating galaxies by inclination is important.

Stacking samples with known redshifts allows us to use the broad-band capability of the SKA to explore depolarization in a way that supplements information from Faraday Synthesis. This analysis requires cubes of Stokes I, Q, and U to be archived. In Section 3 we address the question what level of channel averaging can be done without compromising the analysis.

2.2 Probing deeper into the luminosity function

There are various reasons to investigate the polarization properties of less luminous AGN in comparison with higher luminosity AGN. The FRI/FRII morphological distinction is related to luminosity (**?**). Since part of the radio emission of these sources is beamed, polarization may also be related to (isotropic) luminosity through the orientation of the source axis. An important reason to probe the polarization of starforming galaxies with a lower radio luminosity is to probe the degree of ordering in magnetic fields in galaxy disks as a function of specific star formation rate and dynamics. These are important parameters in dynamo theory through the amount of shear and injection of turbulent energy through stellar feedback (see the chapter on nearby galaxies by R. Beck for a discussion).

Polarization of low-surface brightness galaxies and dwarf galaxies that are faint in the continuum extends our investigation of galactic magnetic fields into a different part of parameter space in terms of dynamics and star formation. Using an HI selected sample that includes subselection on the ratio of HI mass to stellar mass, shape of the line profile (dynamics, shear) and inclination we can address the question whether magnetic fields in quiescent galaxies with a low surface brightness are different from those in high-surface brightness galaxies with strong continuum emission. An HI selected sample has complete redshift information by definition, although this work is limited in redshift by the depth of the HI survey. The advantage of stacking polarization in this case is to probe magnetic field structure in objects with a low radio luminosity that have different properties that affect the galactic dynamo.

2.3 Stacking Stokes Q and U

At first sight it may not appear useful to consider Stokes Q and U individually for stacking. However, if a potential predictor for polarization angle can be identified, its correlation with polarization angle can be tested by stacking samples based on the value of the predictor, or rotated by a parallactic angle based on the predictor before stacking. A simple significance test can be constructed by randomizing the orientation of the sample. If the sample is also stacked in polarized intensity, then the median Q and U may be compared with the median polarization of the sample in order to model the degree of corelation with polarization angle. Possible predictors include optical polarization angle, optical minor axis for disk galaxies, or orientation of the jet.

If a predictor for polarization angle is identified, one can stack the sample as a function of frequency, to investigate if the predictor for polarization angle is equally valid at longer wavelengths. If the sample is generally Faraday thin at the highest frequencies, but experiences significant and diverse Faraday rotation at lower frequencies, this should be observable as the median stacked Q and U converge to zero as frequency decreases. Combining this with the behavioour of the median

PoS(AASKA14)112

fractional polarization in the same frequency range provides an interesting test for models of Faraday rotation in the sample. As before, extending this analysis to the faintest sources detectable in total intensity should be straightforward, depending on the availability of a predictor. Variation of resolution across the band should be considered. It can be avoided by integrating Q and U over the same aperture before stacking.

2.4 Stacking in relation to commissioning and data verification

Stacking requires a sound understanding of the data, including the statistics of the noise and systematics. A statistical analysis may reveal subtle features of the data that are difficult to identify otherwise. Examples are preferred polarization angles in the NVSS survey (Battye et al. (2008)), the effect of clean bias in stacking quasars in the FIRST survey (White et al. (2007)), and bandwidth depolarization in the NVSS (Stil & Taylor (2007)).

Direction-dependent quality control for polarization calibration is challenging because of the limited smber of bright polarized sources. A stacking analysis of samples selected by their position in the field (the nearest beam or PAF element in a mosaic tile) can be used as part of the verification of polarization purity of a commissioning survey.

3. Optimal surveys for stacking experiments

Most surveys can be considered for stacking experiments. There are good reasons to stack wide surveys and deep fields. Wide surveys tend to be more effective because of the much larger number of target sources. However, deep surveys target areas of the sky for that are also covered by other deep surveys, allowing for a more sophisticated sample selection. Stacking a narrow deep survey may not provide a better measurement of the median polarization of a sample if the sample size is too small. Including sources near the edge of a survey where the noise is higher may be counter-productive. Sample size and noise are included in Monte-Carlo simulations that correct for polarization bias and estimate error bars. We do not anticipate stacking experiments on images that include zero-spacing data, but note that there may be applications for stacking positions in objects that are much larger than the beam.

Confusion is the most significant factor in deciding the suitability of a survey for a particular stacking experiment. For example, it is not possible to investigate the polarization of SDSS quasars by stacking the NVSS survey, because the density of the targets is so high that one is forced to stack well below the confusion limit of the NVSS. While confusion is a problem stacking total intensity, it is prohibitive for stacking polarization because of blending of sources with different polarization angle.

Higher angular resolution results in a lower tolerance for position errors in the input catalog, and some targets may be resolved. Targets selected from an X-ray or UV catalog have substantial position errors due to limited photon statistics, and the X-ray emission may be offset from the radio position. All of these complicate the interpretation of the stacking result as a representative flux density for the sample. These issues can be mitigated by integrating Stokes I, Q, and U over an aperture centered on the target position by the stacking software.

Channel averaging before stacking can increase the sensitivity before stacking and reduce the footprint of the stacking analysis in terms of data access. Channel averaging is the same as Faraday

PoS(AASKA14)112

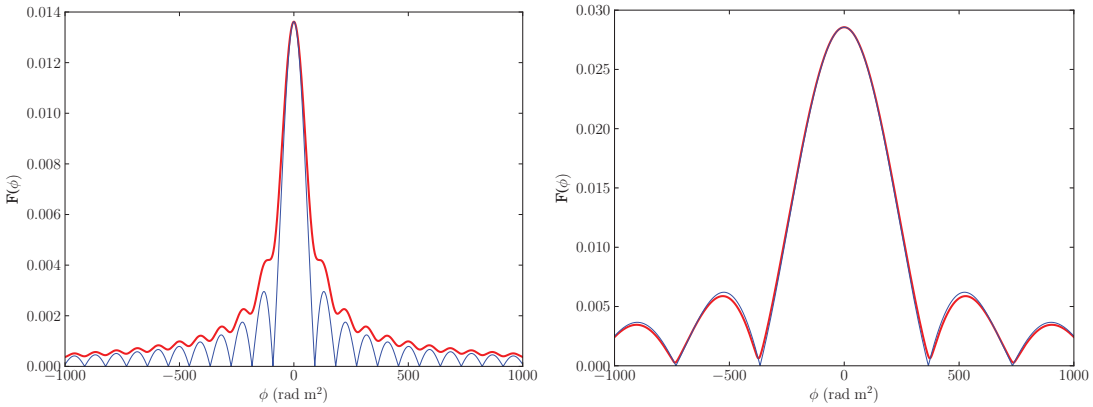

Figure 3: Model Faraday depth spectra (red) and associated RMTF (blue) of the same galaxy at two different redshifts, observed in SKA-SUR band 3. Left: $z = 0$, right: $z = 1$. At low redshift, the Faraday depth spectrum is clearly resolved, revealing Faraday rotation of diffuse emission in the disk. If the same galaxy at $z = 1$ is observed in the same frequency band, the resolution in Faraday depth is much reduced, allowing stacking of Faraday depth spectra.

synthesis under the assumption that Faraday rotation is negligible over the frequency range that is averaged. The question how much channel averaging can be done before stacking is therefore analogous to that of alignment errors in stacking: as long as the errors remain significantly smaller than the resolution of the survey, their effect is small. Potential issues with Faraday thick sources are no different from issues encountered when stacking HI line profiles of galaxies. If some of the targets experience significant Faraday rotation over the frequency range that is averaged, then these sources will appear depolarized after channel averaging Q and U. The difference between stacking channel averaged polarized intensity and channel averaged Q/U can be used as a test to decide if this is significant.

The resolution in Faraday depth in an object at redshift z using only data from wavelength $\lambda_{\rm obs,1}$ to $\lambda_{\rm obs,2}$ is (Brentjens & De Bruyn (2005))

$$\Delta\phi_z = \frac{2\sqrt{3}}{\lambda^2_{\rm obs,2} - \lambda^2_{\rm obs,1}}(1+z)^2, \tag{3.1}$$

Figure 3 illustrates the effect of redshift on the Faraday depth spectrum of the identical objects observed in the same frequency range. For averaging channels one should always consider at least the Galactic foreground at $z = 0$ and the range of Faraday depths in the sample. At high Galactic latitude the foreground rotation may be estimated and removed with accuracy of a few rad m^{-2}. Compression of the λ^2 range and shift to shorter wavelength allows for a greater tolerance for the unknown Faraday depth of the same if a lower limit for the redshift of the sample is available. For a given uncertainty in Faraday depth of both foreground and the sample, Equation 3.1 can be inverted to derive the wavelength range that can be averaged for stacking polarization.

PoS(AASKA14)112

4. Archive and Computing Resources

4.1 Stacking Computational Resources

Generally, polarization stacking is computationally efficient, and amenable to parallelized implementation. The primary direct cost for median stacking is the selection of median values for each pixel. For stacked images m pixels across, this naturally means m^2 selections must be performed. Modern selection algorithms, such as *quickselect*, as used by Stil et al. (2014), have linear scaling to the number of sources in the average case. Thus, for a stack of N sources with $m \times m$ images, the computational complexity is $\mathcal{O}\ (m^2 N)$, with the same spatial complexity (quickselect can be sorted in-place). However, the simple task of generating median values from a generated stack is not the only cost associated with stacking analysis. For example, if one wishes to use oversampled source alignment prior to generating a stack, each of N images must be interpolated to a higher resolution. This task can be accomplished in parallel, with each stacked image oversampled independently.

4.2 Bias Correction Computational Costs

As Stil et al. (2014) showed, bias correction for a polarized intensity stack is non-trivial. With Monte-Carlo realizations, a significant amount of CPU time is required to generate an estimate for the true stacked polarization. For a typical NVSS stack, roughly 5 CPU hours (on an AMD Opteron 2218 CPU) was required. However, little time has been spent optimizing our Monte-Carlo method, and this number can likely be reduced by an order of magnitude or more. Beyond this, the reduction for a large number of stacks containing many sources is extremely amenable to parallelization. A parallel implementation should be capable of scaling to many hundreds to thousands of CPUs.

4.3 Storage and Archive Requirements

While stacking can be used to push well beyond the sensitivity of a survey, a significant new application of this technique to wide-band radio data is to the statistics of samples as a function of frequency. These are not limited to stacking polarization (e.g. Stil et al. 2014). These applications depend on archiving image cubes, as the band-averaged images do not contain the necessary information, although some compromise can be made regarding averaging piecewise over channels. Stacking polarization invariable requires stacking total intensity in the same frequency range.

Working from existing survey images, stacking analysis requires negligible additional storage resources. With double-precision pixel values, each $m \times m$ stacked image requires a meagre $16m^2$ bytes per stacked sample. Stacking analysis on-the-fly (a stacking survey) offers the opportunity to greatly reduce the storage costs associated with storing massive amounts of survey data. By discarding data once a stack has been generated, the storage needed for generating a stack of N sources can be reduced by a factor of N. For large stacks, this can mean a reduction in storage requirements by many orders of magnitude.

References

Battye, R. A., Browne, I. W. A., & Jackson, N. 2009, MNRAS, 2008, 385, 274

PoS(AASKA14)112

Brentjens, M. A., & De Bruyn, A. G. 2005, A&A 441, 1217

Condon, J. J., Cotton, W. D., Greisen, E. W., Yin, Q. F., Perley, R. A., Taylor, G. B., & Broderick, J. J. 1998, AJ, 115, 1693

Mesa, D., Baccigalupi, C., De Zotti, G., Gregorini, L., Mack, K.-H.,Vigotti, M. & Klein, U. 2002, A&A 396, 463

Rengelink, R. B., Tang, Y., De Bruyn, A. G., Miley, G. K., Bremer, M. N., Röttgering H. J. A., & Bremer, M. A. R. 1997, A&AS, 124, 259

Stil, J. M., & Taylor, A. R. 2007, ApJ, 663, L21

Stil, J. M., Keller, B. W., George, S. J. & Taylor, A. R. 2014, ApJ, 787, 99

Tucci, M., Martínez-González, E., Toffolatti, L., González-Nuevo, J., & De Zotti, G. 2004, MNRAS, 349, 1267

White, R. L., Helfand, D. J., Becker, R. H., Glikman, E. & De Vries, W. 2007, ApJ, 654, 99

PoS(AASKA14)112

PROCEEDINGS OF SCIENCE

SKA Deep Polarization and Cosmic Magnetism

A.R. Taylor[*a,b], **Ivan Agudo**[c], **Takuya Akahori**[d], **Rainer Beck**[e], **Bryan Gaensler**[f], **George Heald**[g], **Melanie Johnston-Hollitt**[h], **Mathieu Langer**[i], **Lawrence Rudnick**[j], **Dongsu Ryu**[k], **Anna Scaife**[l], **Dominik Schleicher**[m], **and Jeroen Stil**[n]

[a] *University of Cape Town, E-mail:* russ@ast.uct.ac.ca
[b] *University of the Western Cape, E-mail:* russ@ast.uct.ac.ca
[c] *Joint Institute for VLBI in Europe, E-mail:* agudo@jive.nl
[d] *University of Sydney, E-mail:* akahori@physics.usyd.edu.au
[e] *Max-Planck-Institut für Radioastronomy, E-mail:* rbeck@mpifr-bonn.mpg.de
[f] *University of Sydney, E-mail:* bryan.gaensler@sydney.edu.au
[g] *ASTRON, E-mail:* heald@astron.nl
[h] *Victoria University of Wellington, E-mail:* Melanie.Johnstron-Hollitt@vuw.ac.nz
[i] *Université Paris-Sud, E-mail:* mathieu.langer@ias.u-psud.fr
[j] *University of Minnesota E-mail:* larry@unm.edu
[k] *UNIST, E-mail:* ryu@sirius.unist.ac.kr
[l] *University of Southampton, E-mail:* A.scaife@soton.ac.uk
[m] *Institut für Astrophysik Göttingen, E-mail:* dschleic@astro.physik.uni-goettingen.de
[n] *University of Calgary, E-mail:* jstil@ucalgary.ca

Deep surveys with the SKA1-MID array offer for the first time the opportunity to systematically explore the polarization properties of the microJy source population. Our knowledge of the polarized sky approaching these levels is still very limited. In total intensity the population will be dominated by star-forming and normal galaxies to intermediate redshifts ($z \sim 1-2$), and low-luminosity AGN to high redshift. The polarized emission from these objects is a powerful probe of their intrinsic magnetic fields and of their magnetic environments. For redshift of order 1 and above the broad bandwidth of the mid-bands span the Faraday thick and thin regimes allowing study of the intrinsic polarization properties of these objects as well as depolarization from embedded and foreground plasmas. The deep field polarization images will provide Rotation Measures data with very high solid angle density allowing a sensitive statistical analysis of the angular variation of RM on critical arc-minute scales from a magnetic component of Large Scale Structure of the Universe.

Advancing Astrophysics with the Square Kilometre Array
June 8-13, 2014
Giardini Naxos, Italy

*Speaker.

PoS(AASKA14)113

1. Introduction

The implementation of broad bandwidths and new correlator capacities on the Jansky Very Large Array (JVLA) and the Giant Meterwave Radio Telescope (GMRT) are opening up polarization imaging of the radio sky at mid-frequencies to μJy sensitivities (Rudnick & Owen 2014, Taylor et al. 2014). However, the survey speeds of these instruments limit the amount of sky that can be imaged at these sensitivities in a reasonable time to a square degree or less, thus current studies of the polarized radio source population at these flux densities suffer from low number statistics. The MeerKAT SKA precursor continuum surveys will extend imaging at these sensitivities to larger areas (35 sq deg. to rms of 1.5 μJy), albeit with lower angular resolution. At 75 nJy rms and arc second resolution SKA1-MID can take a step in sensitivity of over an order magnitude compared to the present state-of-the-art and planned precursor projects, and will survey a large enough area of sky to provide a statistical overview of the magnetic properties of source populations over cosmic time.

Current studies hint at what the SKA1 deep polarized sky will reveal. Figure 1 shows at left a compilation of cumulative number counts of polarised sources at 1.4 GHz down to 15 μJy from recent deep imaging projects. The plot demonstrates significant variation of results from different observers, likely due to both low number statistics and sensitivity to angular resolution. A slight flattening of the cumulative counts is suggested (Rudnick & Owen 2014). This may reflect either a smaller overall number of polarized sources, perhaps arising from a decreasing fraction of Active Galactic Nuclei (AGN), and/or an on-average smaller fractional polarization for fainter sources. The latter is consistent with integrated polarization properties of disk galaxies in which internal depolarization effects from thermal plasma decreases the fractional polarization at frequencies below a few GHz (Stil et al. 2009, Heald et al. 2015). Faint polarized counts are thus expected to be frequency dependent and broad-band data are required to unravel the underlying astrophysics. The right hand of Figure 1 shows polarized source counts at 5 GHz down to 5 μJy (Taylor et al. 2014). The rising blue dashed line shows the predicted polarized counts for disk galaxies based on the polarization properties of nearby galaxies (Stil et al. 2009). Deep imaging with SKA1 at GHz frequencies will probe the polarized properties of galaxies to high redshift.

2. Emergence and Evolution of Magnetic Fields in Galaxies

Through its ability to detect polarization of sources at high redshift, a deep survey is the cornerstone for investigation of the evolution of cosmic magnetic fields as it allows us to compare similar objects over the largest possible range in redshift, and place observations of local samples (e.g. Beck et al. 2015) in an evolutionary context. For disk galaxies, this range is $z \gtrsim 2.5$, and for AGN and starbursts it reaches out to $z \gtrsim 7$, into the epoch of reionization. Over this period, galaxies formed and evolved, converting most of their gas into stars. The evolution of plasma and magnetic fields in galaxies is therefore closely related to the evolution of the cosmic star formation rate, and tied to the intergalactic medium through accretion, galactic winds, tidal and ram stripping, and AGN activity.

With the SKA1 we can study magnetic fields over cosmic time through polarization of synchrotron emission in the source, Faraday rotation and depolarization, and Zeeman splitting. These

PoS(AASKA14)113

typically require much higher sensitivity than detection of the source in total intensity. In the case of Faraday rotation and Zeeman splitting, chance alignment with a source in the background will allow detection of magnetic fields in sources that cannot be detected by their own emission. Since the background source must be at higher redshift, a deep field is more suitable to detect polarized background sources for high-redshift objects.

A majority of radio sources fainter than 100 μJy will be star-forming galaxies. The most luminous of these will be Ultra-luminous Infrared Galaxies (ULIRGs) and galaxy mergers. More common are relatively quiescent disk galaxies with a star formation rate that declines gradually by an order of magnitude from redshift 2 to the present. Deep surveys at other wavelengths are important to classify objects, and to measure the plasma density necessary to derive the magnetic field strength from Faraday rotation. In turn, a deep radio survey is required to detect polarization in high-redshift galaxies detected in infrared and optical surveys.

For star forming galaxies, evolution of the magnetic field is closely related to evolution of the galaxy itself. While μG strength magnetic fields with kpc scales should have formed in galaxy disks by z = 3, field ordering on the scale of a galaxy may have taken until z = 0.5, depending on galaxy mass (Arshakian et al. 2009). Competing with this, galaxy interactions and continuous feedback by supernovae and stellar winds that enhance the turbulent component of the magnetic field, and may drive outflows that transport plasma and magnetic field from the disk into the halo. Since these processes scale with the global star formation rate, significant evolution is expected between z = 2 and the present. Also, the density of Faraday rotating plasma will gradually decrease over time as galaxies transform a significant fraction of their gaseous mass into stars, implying a gradual evolution in Faraday depth. Figure 2 shows the predicted redshift distribution of galaxies with polarized flux density more than 10σ in an SKA1-MID band 2 & 3 survey with sensitivity 75 nJy. These simulations are based on models by Stil et al. (2009) for spiral galaxies at redshift

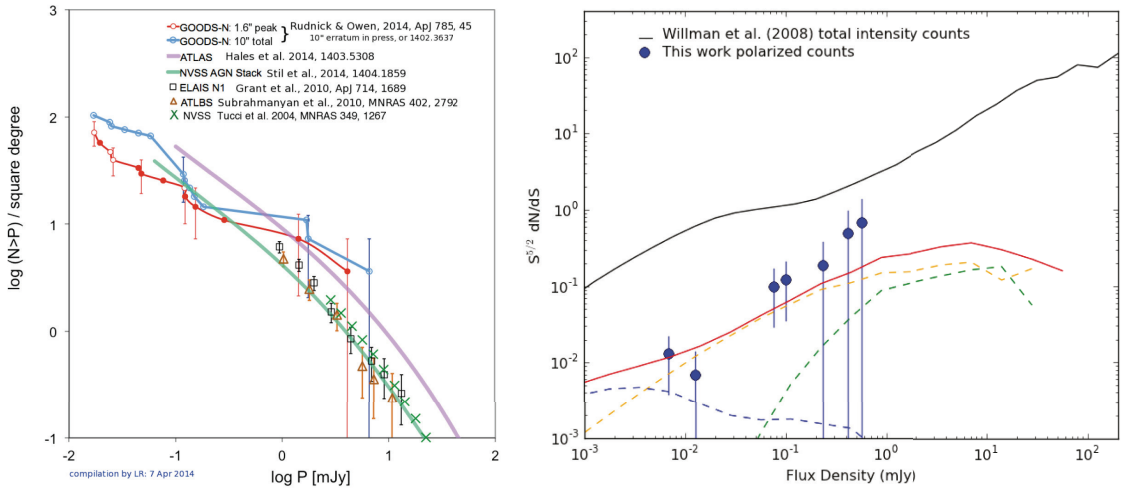

Figure 1: Left: Compilation of cumulative polarized source counts down at 1.4 GHz to $\sim 15\,\mu$Jy from recent studies. Right: Differential polarized source counts at 5 GHz down to 5 μJy compared to predicted polarized counts of AGN (green and orange dashed lines) and disk galaxies (blue dashed line) [**?**].

PoS(AASKA14)113

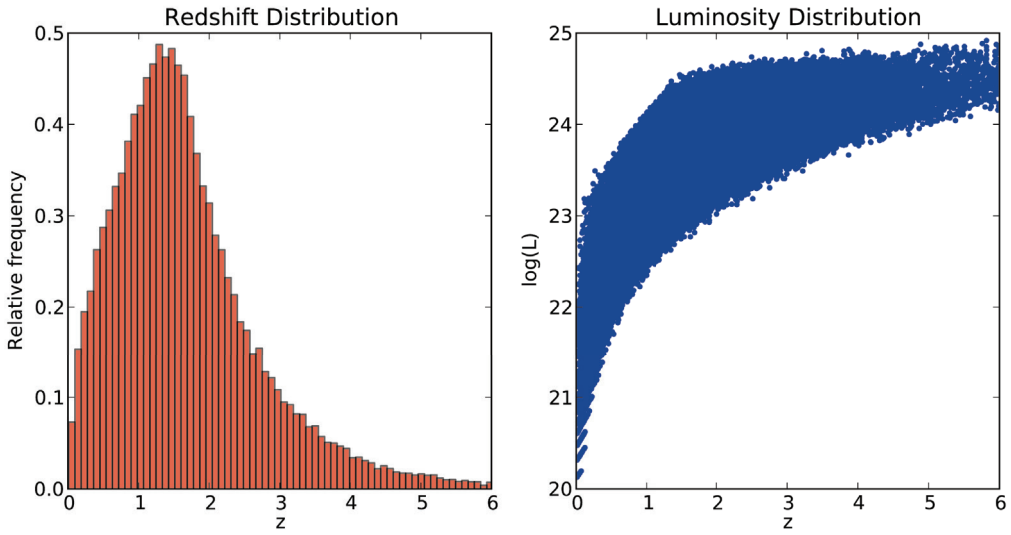

Figure 2: Left: Redshift distribution of normal star-forming galaxies with polarization properties of local disk galaxies that will have polarized flux density greater than 10σ in the proposed SKA1 deep polarization field. Right: redshift versus radio luminosity of the same galaxies, showing that the galaxies probed are in the bright tail of the radio luminosity function and have significant luminosity evolution.

0, applied to normal star forming galaxies in the SKADS S3 simulation of Wilman et al. (2008). We expect to detect $\sim$5000 galaxies per square degree above 10σ. A 10 square degree survey would thus provide probes of the presence of ordered magnetic fields in of order 50,000 galaxies out to redshift > 4. The luminosity- redshift diagram for these galaxies shows that many will have experienced significant luminosity evolution to redshift 0. SKA1-MID is well-positioned to distinguish polarization properties of the more luminous regular star forming galaxies from those of their local (present day) counterparts. Zeeman splitting of HI absorption and Faraday rotation by systems in the line of sight to distant AGN will allow us to investigate magnetic fields in galaxies with radio emission below the detection limit of this survey.

Extreme starbursts in ULIRGS are environments that are very rare in the local universe. Little is known about magnetic fields in these objects. The dense interstellar medium suggests that any polarized emission related to star formation or an embedded AGN will be subject to very strong Faraday rotation. These objects may also have extended synchrotron halos associated with a galactic wind, or extended magnetic fields associated with tidal tails. These magnetic fields exist at the boundary of galactic and intergalactic space and may serve as seed fields for a more wide-spread intergalactic magnetic field.

3. Magnetic Properties of AGN over Cosmic Time

Active galactic nuclei are powered by supermassive black holes that accrete matter and are capable of forming pairs of relativistic jets that can extend up to distances far larger than the size of the host galaxy. The fact that jets in AGN are formed from magnetic systems, and that the magnetic field participating in their formation is partially dragged all along the jets, make polariza-

PoS(AASKA14)113

tion observations of their synchrotron emission a powerful tool to test magneto-hydrodynamic and emission models. However, polarization studies of the radio AGN phenomenon have been limited by the lack of polarization purity, sensitivity, bandwidth and spectral resolution to make adequate studies of magnetic fields in AGN jets and their environments for massive samples of sources. A deep full-polarimetric SKA1-MID survey on Bands 2 and 3 reaching a sensitivity of 75 nJy/beam will have the ability to attack the long standing problem of the composition of AGN jets (i.e. the electron-proton content), and their plasma acceleration from large samples suited for statistical studies for the first time, see Agudo et al. (2015). For that, it is essential to have available a circular polarization purity at least ~ 0.01 %, since AGN typically show circular polarization moduli in the range $0.1 - 1$ % at centimetre radio wavelengths.

The first large scale investigations on the polarization of AGN sources have been based on the NRAO VLA Sky Survey (NVSS) (Condon et al. 1998), which has detected 1.8 million extragalactic sources in total intensity. From these, 14% show a clear polarization signal of at least 3σ, and the majority of polarized extragalactic sources in the NVSS are AGN. Bright sources above 100 mJy correspond to the radio-loud FRII sources (Fanaroff & Riley 1974), and a gradual transition towards FRI sources occurs around 30 mJy. Around a flux density of 1 mJy, the contribution from star-forming galaxies becomes more relevant. So far, typical deep imaging projects have been restricted to flux density sensitivities of $\sim 10\mu$J in total intensity (Hopkins et al. 2003). While no dependence of polarization properties on redshifts out to $z \sim 3$ has been found, it is very interesting that surveys, including the NVSS, and the Dominion Radio Astrophysical Observatory Deep ELAIS N1 Field indicate an increase in fractional polarization with decreasing flux density (Mesa et al. 2002, Taylor et al. 2007). This anti-correlation suggests either a) a change in the magnetic field structure of the observed sources or b) a change of the properties their Faraday screen, perhaps related to the close intergalactic environment of the sources. Different solutions for this anti-correlation have been suggested, reflecting either a change in the population (Mesa et al. 2002), a change in the fraction of radio-quiet AGN or the FRII-FRI transition. From detailed studies of samples with high polarization, no strong dependence on optical morphology, redshift, linear size or radio power has been found (Shi et al. 2010), while a stacking analysis confirmed that the observed correlation continues toward very low flux densities in the NVSS (Stil et al. 2014). SKA1-MID will provide the means to take a major next step in this research, i.e. a deep polarimetric survey of the AGN populations up to the highest achievable sensitivities.

The superb sensitivity of SKA1 opens a new window to study the AGN phenomenon and its surrounding medium, from a cosmological perspective, back to the epoch of reionization, including the potential appearance of radio galaxies near or above $z \sim 10$, at a time where the densities in the Universe were considerably enhanced by a factor of $\sim 10^3$. Due to the enhanced densities in the interstellar and intergalactic medium, it becomes more difficult for jets to break out from their host galaxy (Falcke et al. 2004). Such systems known as GHz-Peaked-Spectrum (GPS) sources have been observed in the local Universe, corresponding to environments that are either very dense or where the jet is very young (ODea 1998). Due to the characteristic evolution of angular scales and observed frequency with redshift, the population of high-z GPS sources will likely be shifted towards lower frequencies, but will show sizes compared to those of their local counterparts (Falcke et al. 2004). The latter peak their radio spectrum at ~ 1 GHz, hence making a deep SKA1-MID total intensity survey between 1 and 3 GHz less suited for searches of high-z GPS

PoS(AASKA14)113

than a parallel SKA1-LOW deep survey. In contrast, a deep and wide band survey at frequencies > 1 GHz, where the sources are expected to be a factor of ~ 10 fainter than in the SKA1-LOW bands, avoids strong Faraday depolarization by the dense environments in which the first AGN are expected to be embedded, and therefore perhaps allowing the detection of their linear polarization. A deep-polarimetric and wide-band SKA1-MID survey in Bands 2 and 3 hence opens the exciting possibility not only to probe the magnetic fields in the first AGN jets, but also their immediate dense intergalactic medium at $z \sim 10$.

4. Detecting Magnetic Fields in the Cosmic Web

The SKA1 deep polarization survey will provide the supremely-dense RM grid of polarization probes of the intergalactic medium required to detect and measure the properties of magnetic fields embedded in the large scale structure of the universe. The LCDM cosmology predicts the cosmic web of galaxy clusters and filaments. While clusters contain hot plasma of T $> 10^7$ K, filaments are filled with plasma of 10^7 K $>$ T $> 10^5$ K which is referred to as the Warm Hot Intergalactic Medium (WHIM). The plasmas are expected to be magnetized; diverse processes for seed magnetic fields have been suggested, and the seed fields can be further amplified through compression and turbulent dynamo as well as leakage of galactic media during the hierarchical structure formation in the Universe. See Ryu et al. (2012) and Widraw et al. (2012) for reviews.

The Intergalactic Magnetic Field (IGMF) in the cosmic web plays important roles in various astrophysical phenomena. For instance, the IGMF imprints its own existence on the cosmic microwave background, deflects the trajectory of cosmic-rays through the cosmic web, and it affects the thermal and dynamical evolutions of galaxy clusters. In addition, the IGMF may have provided seed fields of galaxies and influenced the origin and nature of magnetic fields in spiral galaxies.

RM has been the main tool for studies of the IGMF. It has revealed $B \sim 1 - 0$ μG in clusters. Detection of magnetic fields in filaments is challenged due to the expected very low value of RM. Cosmological simulations suggest the IGMF in filaments may have $B \sim 1 - 100$ nG (Ryu et al. 2008). With the IGMF, the rms value of RM, $\mathrm{RM_{rms}}$, through a single filament would be ~ 1 rad m^{-2} (Figure 3 left, (Akahori & Ryu 2010)), while $\mathrm{RM_{rms}}$ through a number of filaments up to z $\sim$ a few would reach several rad m^{-2} (Figure 3 middle, (Akahori & Ryu 2011)). Interestingly, such RM is comparable to the estimate of extragalactic contribution to the observed RM of $6 - 15$ rad m^{-2} (Schnitzeler 2010, Hammond et al. 2012).

Simulations predict that the IGMF in filaments would induce RM with a flat second-order structure function (SF) of $\sim$100 rad^2 m^{-4} for angular separation of r $\gtrsim 0.1^\circ$ (Figure 3 right). Toward high galactic latitudes where the Galactic contribution is minimum, the Galactic magnetic field, on the other hand, should produce substantially smaller and steeper SF in angular scale (Akahori et al. 2013). Observed SFs toward high latitude, while poorly sampled, are consistent with a flat SF on the smallest scales (Mao et al. 2010, Stil et al. 2011), suggesting a contribution from the IGMF on scales below 1°.

Directions toward high Galactic latitude and toward outside of galaxy clusters should be chosen for deep-field surveys to detect the RM of the IGMF in cosmic filaments. The RM due to the Galactic magnetic field could be substantially reduced with spatial filtering to remove the large scale variance (Akahori et al. 2014). Simulations have shown that a RM data set with a sky den-

PoS(AASKA14)113

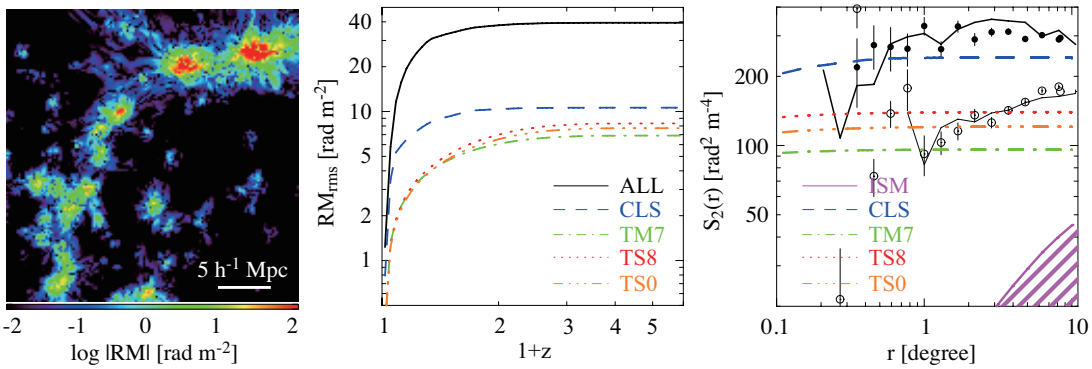

Figure 3: Left: The RM map of the local universe of a 100 h^{-1}Mpc depth (Akahori & Ryu 2010). Middle: The rms value of RM integrated up to $z = 5$ (Akahori & Ryu 2011). Results with different methods for cluster subtractions are shown as different colors. Right: Second-order structure functions of RM. Black circles (Mao et al. 2010) and lines (Stil. et al. 2011) are observed ones for ~ 900 deg^2 fields-of-view toward North (filled, thick) and South (open, thin) Galactic poles. The purple area indicates possible amplitudes for the Milky Way RM toward the poles (Akahori et al. 2013).

sity of several 100 to 1000 per square degree and with RM precision of $\sim$1 rad m^{-2} is required to accurately reconstruction the structure function of RM variance due to the IGMF in the cosmic web (Akahori et al. 2014). An SKA1-MID deep polarization survey to below 100 nJy with band 2 & 3 would yield formal errors in RM of 1 rad m^{-2} for sources with polarized flux density greater than 1.3 μJy. At this polarized flux density the source density will approach the required 1000 per square degree (see Figure 1). A significant fraction of this population will be galaxies. The alignment of polarization position angle with optical minor axis seen in local disk galaxies (Stil et al. 2009) offers the possibility to also use polarization and optical alignments of galaxies as another powerful probe of weak Faraday Rotation from large scale structure.

5. Technical Summary

The Cosmic Magnetism Deep Fields are intended to be observed commensally with the continuum survey deep fields using SKA1-MID over a frequency range of 950 − 3050 MHz (Band 2 & 3). Band 3 will sample the regime where internal Faraday depolarization effects are negligible and alignment of polarization and geometric properties of the galaxy are preserved. Band 2 samples the depolarization regime and allows measurement of internal Faraday processes from galaxy structure (Heald et al. 2015). The significant depolarization in band 2 for nearby galaxies will be substantially reduced at z >1. Emission from galaxies in SKA1-MID Band 1 will suffer very significant depolarization for the red shifts available to SKA1. SKA1 Band 1 and 2 frequency coverage will provide formal precision better than RM of 1 rad m^{-2} down to polarized intensity of 1 μJy beam^{-1}. Integration times sufficient for a sensitivity of 75 nJy beam^{-1} are required per field at a resolution of 1 arcsec. At this resolution the continuum (monochromatic) rms noise for SKA1-MID is expected to be twice (three times) that of the naturally weighted visibility data for Band 2, given current array configuration projections.

Star-forming galaxies with partly ordered regular fields are expected to have Faraday depth of

PoS(AASKA14)113

~ 50 rad m^{-2} at $z \sim 0.5$. Large-scale field reversals may exist in those epochs and lead to several Faraday Depth components with different signs, so that a resolution of 50 rad m^{-2} is required, Band 2 & 3 combine to provide Faraday depth resolution of 31 rad m^{-2}

The majority of galaxies are expected of exhibit integrated polarized fraction of order 1 to a few percent, so linear polarization purity of 0.1% across the field of view is required. Circular polarization purity of 0.01% would allow circular polarization to be studied for the fist time in a vast number of AGN.

Imaging of an area of the order 10 square degrees is required to provide statistical sampling of magnetic fields in galaxies and AGN and for sampling of large-scale structure for detection of the cosmic magnetic web. We expect a several tens of thousands of objects detected in polarization for study of the evolution of intrinsic magnetic fields with cosmic time. The dense grid of thousands of sources per square degree will probe the "foreground" cosmic magnetic web.

Both continuum and spectral imaging will be required in full polarization for these data with a coarse spectral resolution of $\Delta\nu$ = 1 MHz. Processing of the polarization deep fields will require some additions to a standard imaging pipeline. Channelized polarization products will need to be formed in full Stokes with high dynamic range per channel. To avoid contamination from bright sources in the fields a dynamic range requirement of 10^6 (10^5) in total intensity (polarization) is required for continuum imaging and 10^4 (10^3) per channel for spectral data. To achieve this dynamic range, full Stokes A-projection will be required in addition to standard W-projection. Direction-dependent calibration will be necessary, followed by multifrequency synthesis.

These fully calibrated polarization data can then be transformed from frequency into Faraday dispersion cubes. Standard RM-synthesis would utilize the channelized QU image cube (Brentjens & de Bruyn 2005). However to achieve full dynamic range in the Faraday dispersion cube images from the broad bandwidth will require multi-frequency synthesis techniques to be adapted to Stokes Q, U data. Integration of multi-frequency synthesis and Faraday dispersion imaging would require Faraday de-dispersion to operate on the visibilities prior to imaging and deconvolution.

REFERENCES

Agudo, I. et al. 2015, "Studies of Relativistic Jets in Active Galactic Nuclei with SKA" in proc. *Advancing Astrophysics with the SKA*, PoS(AASKA14)093

Akahori T., & Ryu D. 2010, ApJ, 723, 476

Akahori T., & Ryu D. 2011, ApJ, 738, 134

Akahori T., Ryu D., Kim J., & Gaensler B. M. 2013, ApJ, 767, 150

Akahori T., Gaensler, B. M., & Ryu, D., 2014, ApJ, 790. 123

Arshakian, T. G., Beck, R., Krause, M., & Sokoloff, D. 2009, AA, 494, 21

Beck, R. et al. 2015, "Structure, dynamical impact and origin of magnetic fields in nearby galaxies in the SKA era" in proc. *Advancing Astrophysics with the SKA*, PoS(AASKA14)094

Brentjens, M.A. & de Bruyn, A.G. 2005, A&A, 441, 1217

Condon, J. J. et al. 1998, AJ, 115, 1693

Falcke, H. et al. 2004, NewAR, 48, 1157

Fanaroff, B.L. & Riley, J.M., 1974, MNRAS, 1767, 31

Hammond, A. M., Robishaw, T., & Gaensler, B. M. 2012 (arXiv:1209.1438v3)

PoS(AASKA14)113

Heald, G. et al. 2015, "Magnetic Field Tomography in Nearby Galaxies with the Square Kilometre Array" in proc. *Advancing Astrophysics with the SKA*, PoS(AASKA14)093
Hopkins, A. M. et al. 2003, AJ, 125, 465
Mao, S. A., Gaensler, B. M., Haverkorn, M., et al. 2010, ApJ, 714, 1170
Mesa, D. 2002, A&A, 396, 463
O'Dea, C. 1998, PASP, 110, 493
Rudnick, L. and Owen, F.N., 2014, ApJ, 785, 45
Ryu, D., Kang, H., Cho, J., & Das, S. 2008, Science, 320, 909
Ryu, D., et al. 2012, Space Science Review, 166, 1
Schnitzeler, D. H. F. M. 2010, MNRAS, 409, 99
Shi, H. et al. 2010, MNRAS, 409., 821
Stil, J. M., Krause, M., Beck, R., & Taylor, A. R. 2009, ApJ, 693, 1392
Stil, J. M., Taylor, A. R., & Sunstrum, C. 2011, ApJ, 726, 4
Stil, J. M., Keller, B.W., George, S.J. and Taylor A.R. 2014, ApJ, 797, 99
Taylor, A. R., Stil, J.M., Grant, J.K. et al. 2007, ApJ, 666, 201
Taylor, A.R., Bhatnagar, S., Condon, J. et al., 2014, BASI, arXiv:1405.0117
Widraw, L., et al. 2012, Space Science Review, 166, 37
Wilman, R. J., Miller, L., Jarvis, M. J., Mauch, T., Levrier, F., Abdala, F. B., Rawlings, S., Klöckner, H.-R., Obreschkow, D., Olteanu, D. & Young, S. 2008, MNRAS, 388, 1335

PoS(AASKA14)113

PROCEEDINGS OF SCIENCE

Statistical methods for the analysis of rotation measure grids in large scale structures in the SKA era

Vacca V.[*a], **Oppermann N.**[b], **Enßlin T.**[a,c], **Selig M.**[a,c], **Junklewitz H.**[d], **Greiner M.**[a,c], **Jasche J.**[e], **Hales, C. A.**[f,g], **Reinecke M.**[a], **Carretti E.**[h], **Feretti L.**[i], **Ferrari C.**[j], **Giovannini G.**[i,k], **Govoni F.**[l], **Horellou C.**[m], **Ideguchi S.**[n], **Johnston-Hollitt M.**[o], **Murgia M.**[l], **Paladino R.**[i,k], **Pizzo R. F.**[p], **and Scaife A.** [q]

[a] *Max Planck Institute for Astrophysics, Karl-Schwarzschild-Str. 1, 85748 Garching, Germany;* [b] *Canadian Institute for Theoretical Astrophysics, University of Toronto, 60 St. George Street, Toronto ON, M5S 3H8, Canada;* [c] *Ludwig-Maximilians - Universität München, Geschwister-Scholl-Platz 1, 80539, MÃijnchen, Germany;* [d] *Argelander-Institut für Astronomie, Auf dem Hügel 71, 52121 Bonn, Germany;* [e] *CNRS, UMR 7095, Institut d'Astrophysique de Paris, 98 bis, boulevard Arago, F-75014 Paris, France;* [f] *Jansky Fellow of the National Radio Astronomy Observatory;* [g] *National Radio Astronomy Observatory, PO Box 0, Socorro, NM 87801, USA;* [h] *CSIRO Astronomy and Space Science PO Box 276. Parkes 2870;* [i] *INAF-Istituto di Radioastronomia, Via P.Gobetti 101, 40129 Bologna, Italy;* [j] *Université de Nice Sophia Antipolis, CNRS, Observatoire de la Côte d'Azur, Laboratoire Cassiopée, Nice, France;* [k] *Department of Physics and Astronomy, University of Bologna, V.le Berti Pichat 6/2, 40127 Bologna, Italy;* [l] *INAF-Osservatorio Astronomico di Cagliari, Strada 54, Loc. Poggio dei Pini, 09012 Capoterra (Ca), Italy;* [m] *Department of Earth and Space Sciences, Chalmers University of Technology, Onsala Space Observatory, SE-439 92 Onsala, Sweden;* [n] *University of Kumamoto, 2-39-1, Kurokami, Kumamoto 860-8555, Japan;* [o] *School of Chemical & Physical Sciences, Victoria University of Wellington, PO Box 600, Wellington 6014, New Zealand;* [p] *ASTRON, Postbus 2, 7990 AA, Dwingeloo, The Netherlands;* [q] *University of Southampton Highfield, Southampton SO17 1BJ, U.K.*

E-mail: vvacca@mpa-garching.mpg.de

To better understand the origin and properties of cosmological magnetic fields, a detailed knowledge of magnetic fields in the large-scale structure of the Universe (galaxy clusters, filaments) is crucial. We propose a new statistical approach to study magnetic fields on large scales with the rotation measure grid data that will be obtained with the new generation of radio interferometers.

Advancing Astrophysics with the Square Kilometre Array
June 8-13, 2014
Giardini Naxos, Italy

[*]Speaker.

PoS(AASKA14)114

1. Introduction

Magnetic fields have been detected in planets, stars, galaxies, and clusters of galaxies. Intracluster magnetic fields are characterized by a strength of $\sim \mu$G and fluctuations on scales from a few kpc to ~ 100 kpc (e.g., Enßlin & Vogt 2003, Vogt & Enßlin 2003, Vogt & Enßlin 2005, Murgia et al. 2004, Govoni et al. 2006, Guidetti et al. 2008, Bonafede et al. 2009, Bonafede et al. 2010, Vacca et al. 2010, Vacca et al. 2012). On larger scales, along galaxy filaments as well as in voids and sheets, a firm detection has not yet been possible. Cosmological magneto-hydro-dynamical simulations indicate that magnetic fields are present in intergalactic low-density environments (e.g., Dolag et al. 2008), while γ-ray observations suggest their presence in voids where a lower limit of ~ 1 fG has been derived (see Beck A. et al. 2013 and references therein). For more details of our current observational understanding of magnetic fields in low-density regions, see also the chapter by Giovannini et al. (2014) in these proceedings.

Magnetic fields can be studied using a variety of techniques, among which rotation measure (RM) observations are a powerful tool (e.g., Carilli & Taylor 2002, Govoni et al. 2004). The amount of Faraday rotation measured from radio observations along a given line of sight is the result of the contribution from the Milky Way, the radio source itself and other extragalactic environments. The distribution of matter in large-scale structures can be classified into four types (following Hahn et al. 2007, using a criterion of local stability of test particle orbits): voids, sheets, filaments and galaxy clusters. We will hereafter call these four types, as well as the sources responsible for the radio emission, *environments*.

Disentangling the contributions from different extragalactic environments is essential in order to study magnetic fields in large-scale structures, and consequently infer information about cosmic magnetism (e.g., Beck R. et al. 2013, Gaensler et al. 2004). However, this is a non-trivial task that demands a statistical approach. The first statistical studies to prove the existence of Faraday rotation from large-scale extragalactic environments (galaxy clusters) were published by Lawler & Dennison (1982) and Vallée et al. (1986). Later, an important statistical RM analysis on intracluster magnetic fields was performed by Clarke et al. (2001, 2004). Relevant contributions regarding intergalactic magnetic fields on even larger scales were done by Kolatt (1998), Stasyszyn et al. (2010), and Akahori et al. (2014).

A statistical theory for Bayesian inference on spatially distributed signals, *Information Field Theory*, was developed by Enßlin et al. (2009). Within the framework of this theory, Oppermann et al. (2012, 2014) reconstructed the Galactic Faraday rotation foreground and estimated the extragalactic contribution. In this chapter we take a step forward, with a new algorithm, able to statistically separate the different extragalactic contributions, by combining RMs with information about the large-scale structure of the cosmic web. This approach will make it possible to study magnetic fields on large scales with the RM grid data that will be obtained with the new generation of radio interferometers (see the chapter by Johnston-Hollitt et al. 2014 in these proceedings).

2. General description

The probability density distribution of the extragalactic Faraday rotation measure along a given

PoS(AASKA14)114

line of sight i can be described with a Gaussian of mean $\langle \phi_{\mathrm{e},i} \rangle$ and variance $\langle \phi^2_{\mathrm{e},i} \rangle$

$$\begin{aligned} \langle \phi_{\mathrm{e},i} \rangle &= 0 \\ \langle \phi^2_{\mathrm{e},i} \rangle &= a_0^2 \int_0^{x_i} \int_0^{x_i} \mathrm{d}x\mathrm{d}x' \frac{n_\mathrm{e}(x) n_\mathrm{e}(x') \langle B_x(x) B_x(x') \rangle}{(1+z(x))^2 (1+z(x'))^2} \end{aligned} \tag{2.1}$$

where a_0 is a constant, x_i is the proper distance of the source, z is the redshift, n_e is the electron density, and B_x is the component of the magnetic field along the line of sight. We can define a length scale λ_x, so that the auto-correlation tensor of the magnetic field $\langle B_x(x) B_x(x') \rangle$ on average gives significant contributions for $|x - x'| < \lambda_x$, but not for $|x - x'| \gg \lambda_x$. The strength of the magnetic field, its correlation length, and the electron density have a different value in each environment j, i.e., in voids, sheets, filaments, galaxy clusters, and the in radio source itself. If we define

$$\chi_x = a_0^2 n_\mathrm{e}(x)^2 \langle B_x(x)^2 \rangle \lambda_x, \tag{2.2}$$

which we assume to depend only on the environment, so that $\chi_x = \chi_{j(x)}$, and introduce l_{ij} as the length of the line of sight i through each environment j, the overall variance in Faraday rotation can be written as

$$\langle \phi^2_{\mathrm{e},i} \rangle \approx a_0^2 \int_0^{x_i} \frac{n_\mathrm{e}(x)^2 \langle B_x(x)^2 \rangle \lambda_x}{(1+z(x))^4} \mathrm{d}x \approx \chi_0 + \sum_j l_{ij} \chi_j. \tag{2.3}$$

The intrinsic contribution of the emitting source χ_0 is assumed to be on average the same for all sources. Since the intrinsic size of the emitting radio source is unknown, χ_0 is defined according to Eq. (2.2) but with the length l_{i0} factored in. Here, the auto-correlation function of the magnetic field has been approximated with a top-hat function of width λ_x. We assume that, within a correlation length λ_x, the redshift can be approximated to be constant. Moreover, we note that χ_j has been assumed to be independent of the redshift, meaning that the contribution to the Faraday rotation from a given environment does not change with redshift. The redshift dependence is totally absorbed by the term l_{ij}. Residual small-scale, uncorrelated Galactic contributions could be present in the estimate of the extragalactic Faraday rotation $\phi_{\mathrm{e},i}$. To properly take them into account, the inclusion of a latitude dependent contribution in Eq. (2.3) could be necessary.

To constrain the contribution from the different environments χ_j, an estimate of the extragalactic Faraday rotation $\phi_{\mathrm{e},i}$ for a collection of lines of sight, as well as a description of the cosmic web large-scale structure, summarized by l_{ij}, is required. With a Bayesian approach, Jasche et al. (2010) reconstructed the cosmic density field on the basis of optical data from the SDSS *Data Release 7*. Following the scheme proposed by Hahn et al. (2007), they give a three-dimensional classification of the density field posterior in terms of voids, sheets, filaments, and clusters of galaxies. For a source with known redshift, this reconstruction allows one to estimate the path covered by the radio signal through each environment, i.e., the elements l_{ij} in Eq. (2.3). Radio sources can sit in different structures, e.g. galaxy clusters or filaments. This effect can be taken into account statistically since it is possible to locate the radio source in the reconstruction of the large scale structure via redshift identification. The fractions of the line of sight that the different radio sources spend in the different environments varies (this is also the case for the same radio source when different reconstruction of the large scale structure are considered). The combination of this information with

PoS(AASKA14)114

the Faraday depth estimation for a collection of sources enables us therefore to statistically discriminate between the average contributions from the source itself, from galaxy clusters, filaments, voids, and sheets.

3. Bayesian approach

To infer information about the contribution from the different extragalactic environments, χ, to the extragalactic Faraday rotation on the basis of data d [1] obtained from a RM grid, we propose a Bayesian approach. Bayes theorem,

$$P(\chi|d) = \frac{P(d|\chi)P(\chi)}{P(d)}, \tag{3.1}$$

expresses our *a posteriori* knowledge $P(\chi|d)$ about the signal χ after the measurement process took place. The initial knowledge on the signal before the data have been acquired is described by the prior $P(\chi)$ and is modified by the data d through the likelihood $P(d|\chi)$. The evidence $P(d)$ is a normalization factor, obtained by marginalizing the joint probability $P(d,\chi) = P(d|\chi)P(\chi)$ over all the possible configurations of the signal χ.

In order to get a data-driven solution and to keep our assumptions as general as possible, we do not put constraints on the magnetic field strength and assume all values of magnetic field magnitudes to have equal probability. Such *a priori* knowledge can be well described by a flat prior on a logarithmic scale. Mathematically, it is expressed as an Inverse-Gamma distribution

$$P(\chi) \propto \prod_j \chi_j^{-\alpha_j} e^{-\frac{q_j}{\chi_j}} \tag{3.2}$$

where $\alpha_j = 1$ and $q_j = 0$ (Jeffreys' Prior).

The Faraday depths d_i coming from radio observations contain the Galactic and extragalactic contribution, $\phi_{\mathrm{g},i}$ and $\phi_{\mathrm{e},i}$, and the noise n_i of the measurement process

$$d_i = \phi_{\mathrm{g,i}} + \phi_{\mathrm{e,i}} + n_i. \tag{3.3}$$

Oppermann et al. (2012, 2014) developed an algorithm to reconstruct the Galactic Faraday rotation foreground and estimate the extragalactic contribution, given a catalog of Faraday RMs for different lines of sight. Their results are available as a collection of N random samples extracted from the posterior distribution

$$P(\phi_{\mathrm{e}}|d,\mathrm{Opp}) = \frac{P(d|\phi_{\mathrm{e}})P(\phi_{\mathrm{e}}|\mathrm{Opp})}{P(d|\mathrm{Opp})}, \tag{3.4}$$

which intrinsically depends on the assumption enclosed in their prior, as indicated by "Opp". In order to disentangle the different contributions that make up the overall observed extragalactic Faraday depth, this prior must be replaced with a new one.

[1] Here, d and χ are respectively vectors with elements d_i and χ_j with $i = 1,...,N_{\mathrm{los}}$ and $j = 0,...,N_{\mathrm{env}}$, where N_{los} and N_{env} are the total number of lines of sight and the total number of environments in between the source and the observer.

PoS(AASKA14)114

If in Eq. (3.1), we expand our likelihood

$$P(d|\chi) = \int \mathscr{D}\phi_{\rm e} P(d|\phi_{\rm e}) P(\phi_{\rm e}|\chi) \tag{3.5}$$

and insert the likelihood $P(d|\phi_{\rm e})$ from Oppermann et al. (2014), see Eq. (3.4), we obtain

$$P(\chi|d) = \int \mathscr{D}\phi_{\rm e} \frac{P(\phi_{\rm e}|d,{\rm Opp}) P(d|{\rm Opp})}{P(\phi_{\rm e}|{\rm Opp})} \frac{P(\phi_{\rm e}|\chi) P(\chi)}{P(d)}, \tag{3.6}$$

where $\int \mathscr{D}\phi_{\rm e}$ denotes the phase space integral over all the possible field configurations of $\phi_{\rm e}$. As the evidence is simply a normalization factor, this posterior no longer depends on the assumptions of Oppermann et al. (2014), which cancel out.

Under the assumption that the lines of sight are sufficiently separated, that is, the cross-correlation function of their magnetic field is zero, for each line of sight we can consider independent Gaussian distributions for the extragalactic Faraday depth given the cosmic web's large-scale structure

$$P(\phi_{\rm e}|\chi) = \int \mathscr{D}l P(l|{\rm Jasche}) \prod_i \mathscr{G}(\phi_{\rm e,i}, \sum_{\rm j} l_{ij}\chi_j), \tag{3.7}$$

where $P(l|{\rm Jasche})$ is the posterior of the cosmic web structure from Jasche et al. (2010), available in the form of N' samples. The notation $\mathscr{G}(x,X)$ indicates a one-dimensional Gaussian distribution for a variable x with zero mean and variance X. Moreover, since the prior $P(\phi_{\rm e}|{\rm Opp})$ from Oppermann et al. (2014) is

$$P(\phi_{\rm e}|{\rm Opp}) = \prod_i \mathscr{G}(\phi_{{\rm e},i}, \sigma_{\rm e}^2) \tag{3.8}$$

with a standard deviation $\sigma_{\rm e} \sim 6.4\,{\rm rad/m^2}$, it follows that

$$P(\chi, \phi_{\rm e}, l|d) \approx \frac{\prod_i \mathscr{G}(\phi_{{\rm e},i}, \sum_j l_{ij}\chi_j)}{\prod_i \mathscr{G}(\phi_{{\rm e},i}, \sigma_{\rm e}^2)} \prod_j \chi_j^{-1} P(\phi_{\rm e}|d,{\rm Opp}) P(l|{\rm Jasche}). \tag{3.9}$$

This probability density function can be marginalized over l and $\phi_{\rm e}$ by making use of the sample-representation available for the posterior of the large scale structure $P(l|{\rm Jasche})$ and of the extragalactic Faraday rotation $P(\phi_{\rm e}|d,{\rm Opp})$. To evaluate the posterior distribution for χ, we plan to use a Monte Carlo Markov Chain approach.

In this approximation the lines of sight are considered independent. This means that, if the assumption does not hold, a correlated component of the magnetic field could be missed. A proper modeling that takes into account possible cross-correlations between lines of sight is left for future works.

4. Current developments and applications with SKA

An application to archival *Very Large Array* (VLA) data is in progress. By reanalyzing 1.4 GHz data from the *NRAO VLA Sky Survey* (NVSS), Taylor et al. (2009) derived a catalog of RM values for 37543 linearly polarized radio sources, north of declination -40° - which corresponds to a

PoS(AASKA14)114

number density of approximately one source per square degree. Oppermann et al. (2014) evaluated the posterior distribution of the extragalactic Faraday rotation for all the lines of sight in this catalog.

By using optical data from on-line databases (NED and SIMBAD) as well as from surveys (SDSS, 6dFGS, 2dFGRS, 2QZ, 6QZ), Hammond et al. (2012) published a catalog of spectroscopic redshifts for 4003 linearly polarized sources from the NVSS. The sources in this sample have redshifts in the range $0.0007 < z < 5.3$. Only about 30 sources have $z < 0.02$, and the mean redshift of the sample is 0.89. The mean angular distance of the sources being equal to $\sim$1 degree, this implies a mean distance among sources larger than 1 Mpc for 99% of the sample, and on average larger than $\approx$30 Mpc. If $\lambda_x >> 30$ Mpc, the assumption of no cross-correlation is not valid anymore. As noted in the previous section, this would translate in an underestimate of the magnetic field for structures with such a length scale. By combining the reconstruction of the large-scale structure from Jasche et al. (2010) with this catalog of redshifts, it is possible to evaluate the path covered by the radio signal through each environment for each line of sight.

The catalog of Faraday rotation values in Taylor et al. (2009) was derived through a linear fit of the observed polarization angle versus λ^2 at two closely separated radio frequencies (1365 and 1435 MHz). When few data points are used, such λ^2-fits can suffer from an $n\pi$-ambiguity. Moreover, this approach is suitable only if no Faraday rotating plasma is mixed with the radio-emitting plasma. A better analysis of polarization properties of radio sources can be done with the RM synthesis (Brentjens & de Bruyn 2005) and the Faraday synthesis (Bell & Enßlin 2012) techniques if more frequencies are available. A continuous and broad frequency coverage is desirable, both to reduce the risk of $n\pi$-ambiguities and to reach a sufficiently high resolution in Faraday depth to distinguish nearby Faraday components (e.g., Farnsworth et al. 2011, Kumazaki et al. 2014).

In this respect, the *Square Kilometer Array* as well as its precursors will offer a great improvement. Broadband spectro-polarimetric surveys of the sky in combination with deep observations of specific targets will provide densely spaced RM grids. A RM catalog one hundred times denser than those currently existing (Taylor et al. 2009) will be obtained with POSSUM, the polarization survey planned with the SKA precursor ASKAP. POSSUM will observe the sky between 1130 and 1430 MHz with a sensitivity in U and Q of $\sim 10\,\mu$Jy/beam and a resolution of $10''$, giving an expected density of 70 polarized sources per square degree (Hales et al. 2014a). The uncertainty on the RM is lower than ≈ 6 rad/m^2 for a polarized signal with a $S/N > 5$ (Stepanov et al. 2008). The ultra-deep polarization survey CHILES Con Pol with the Jansky Very Large Array (Hales et al. 2014b) will reach a sensitivity of 400 nJy with sky area of a fraction of a square degree, providing a first look at the magnetic field science that can be performed with the SKA. The sky survey in polarization SKA1-SUR planned for SKA1 will go much further. Designed to cover the frequency range 650-1670 MHz, it will produce Stokes U and Q images over 30000 square degrees with a spatial resolution of $2''$. Within two years, a sensitivity in polarization of $\sim 1\mu$Jy/beam will be reached, with an uncertainty in RM lower than ≈ 1 rad/m^2 ($S/N > 5$). The high RM accuracy will make our approach viable for detecting magnetic fields with strengths $\sim$nG already during the early science phase of SKA1, when sensitivity will be at 50% of its full level. For weaker magnetic fields the full deployment of all the SKA1 baseline will be necessary. The resulting sky grid of Faraday rotation values will be 300-1000 times denser than the largest catalog available at the moment. The better resolution of $2''$, compared to the $45''$ of Taylor et al. (2009), will make it possible to identify optical counterparts uniquely and hence the source redshift. For fields of particular interest, e.g., regions

PoS(AASKA14)114

where galaxy filaments have been observed, deeper observations could be necessary to assess the presence of magnetic fields and their properties. In this case, the observations from the survey can be complemented by targeted SKA1-MID pointings over a continuous frequency band from 350 to 3050 MHz. This would imply a polarization sensitivity $\lesssim 1\,\mu$Jy/beam after one hour of integration time and an uncertainty in RM lower than $\approx 0.2\,\mathrm{rad/m^2}$ ($S/N > 5$). These targeted observations will be crucial, both to increase the resolution in Faraday depth and to detect a larger number of sources, allowing to distinguish nearby components in Faraday spectra and improve the statistics.

The even higher spatial and frequency resolution and the deeper sensitivity of SKA2 will make it possible to obtain RMs for an unprecedented number of background and intervening sources. It is therefore essential to develop and apply statistical approaches with the aim of interpreting the data correctly.

5. Conclusions

The origin and evolution of cosmological magnetic fields are still open questions. Magnetic fields are currently being studied in galaxy clusters but a firm detection is lacking in larger scale structures, such as galaxy filaments. The structure and the strength of magnetic fields in galaxy clusters are both deeply affected by the cluster formation processes (e.g., Dolag et al. 2005, Donnert et al. 2009, Xu et al. 2010), almost independently of the mechanism of generation of the seed magnetic field. This makes it difficult to discriminate between the different formation scenarios from galaxy cluster observations alone. The SKA's large bandwidth, high sensitivity and frequency resolution will permit a more reliable recovery of the Faraday depth for a large number of sources, and its high spatial resolution will allow a proper identification of the optical counterparts necessary for redshift assignment. Modern techniques based on the largest photometric all-sky surveys (2MASS, WISE and SuperCOSMOS) already provide catalogs of redshifts for millions of sources up to redshifts of 0.2 to 0.3 (e.g. Bilicki et al. 2014), and the next generation of redshift surveys will push those limits. We will investigate to what depths and accuracy redshifts are needed in order to apply the proposed method. The ultimate goal is to search for magnetic fields in large-scale structures like filaments, where magnetic field amplification is not yet saturated and therefore the field strength still depends on the seed field strength. This information will help to place firm constraints on the origin and evolution of cosmological magnetic fields.

Acknowledgments

We thank the anonymous referee for useful comments and suggestions. The implementation of the code makes use of the NIFTY package by Selig et al. (2013) and of the cosmology calculator by Ned Wright (www.astro.ucla.edu/∼wright). This research was supported by the DFG Forschengruppe 1254 "Magnetisation of Interstellar and Intergalactic Media: The Prospects of Low-Frequency Radio Observations".

REFERENCES

Akahori, T., Gaensler, B. M., & Ryu, D. 2014, ApJ, 790, 123

PoS(AASKA14)114

Beck, A. M., Hanasz, M., Lesch, H., Remus, R.-S., & Stasyszyn, F. A. 2013, MNRAS, 429, L60
Beck, R., Anderson, J., Heald, G., et al. 2013 334, 548
Bell, M. R., & Enßlin, T. A. 2012, A&A, 540, A80
Bilicki, M., Peacock, J. A., Jarrett, T. H., Cluver, M. E., & Steward, L. 2014, arXiv:1408.0799
Bonafede, A., Feretti, L., Giovannini, G., et al. 2009, A&A, 503, 707
Bonafede, A., Feretti, L., Murgia, M., et al. 2010, A&A, 513, A30
Brentjens, M. A., & de Bruyn, A. G. 2005, A&A, 441, 1217
Carilli, C. L., & Taylor, G. B. 2002, ARA&A, 40, 319
Clarke, T. E., Kronberg, P. P., Böhringer, H. 2001, ApJL, 547, L111
Clarke, T. E. 2004, Journal of Korean Astronomical Society, 37, 337
Dolag, K., Grasso, D., Springel, V., & Tkachev, I. 2005, JCAP, 1, 9
Dolag, K., Bykov, A. M., & Diaferio, A. 2008, SSRv, 134, 311
Donnert, J., Dolag, K., Lesch, H., Müller, E. 2009, MNRAS, 392, 1008
Enßlin, T. A., & Vogt, C. 2003, A&A, 401, 835
Enßlin, T. A., Frommert, M., & Kitaura, F. S. 2009, PhRvD, 80, 105005
Farnsworth, D., Rudnick, L., & Brown, S. 2011, AJ, 141, 191
Gaensler, B. M., Beck, R., & Feretti, L. 2004, NewAR, 48, 1003
Giovannini, G. et al. 2015, "Cluster magnetic fields through the study of polarized radio halos in the SKA era", in proc. *Advancing Astrophysics with the Square Kilometre Array*, PoS(AASKA14)105
Govoni, F., & Feretti, L. 2004, International Journal of Modern Physics D, 13, 1549
Govoni, F., Murgia, M., Feretti, L., et al. 2006, A&A, 460, 425
Guidetti, D., Murgia, M., Govoni, F., et al. 2008, A&A, 483, 699
Hahn, O., Porciani, C., Carollo, C. M., & Dekel, A. 2007, MNRAS, 375, 489
Hales, C. A., Norris, R. P., Gaensler, B. M., & Middelberg, E. 2014a, MNRAS, 440, 3113
Hales, C. A., & Chiles Con Pol Collaboration 2014b, Exascale Radio Astronomy, 50301
Hammond, A. M., Robishaw, T., & Gaensler, B. M. 2012, arXiv:1209.1438
Jasche, J., Kitaura, F. S., Li, C., & Enßlin, T. A. 2010, MNRAS, 409, 355
Johnston-Hollitt, M. et al. 2015, "Using SKA Rotation Measures to Reveal the Mysteries of the Magnetised Universe", in proc. *Advancing Astrophysics with the Square Kilometre Array*, PoS(AASKA14)092
Kolatt, T. 1998, ApJ, 495, 564
Kumazaki, K., Akahori, T., Ideguchi, S., Kurayama, T., & Takahashi, K. 2014, PASJ, 66, 61
Lawler, J. M., & Dennison, B. 1982, ApJ, 252, 81
Murgia, M., Govoni, F., Feretti, L., et al. 2004, A&A, 424, 429
Oppermann, N., Junklewitz, H., Robbers, G., et al. 2012, A&A, 542, A93
Oppermann, N., Junklewitz, H., Greiner, M., et al. 2014, arXiv:1404.3701
Selig, M., Bell, M. R., Junklewitz, H., et al. 2013, A&A, 554, A26
Stasyszyn, F., Nuza, S. E., Dolag, K., Beck, R., & Donnert, J. 2010, MNRAS, 408, 684
Stepanov, R., Arshakian, T. G., Beck, R., Frick, P., & Krause, M. 2008, A&A, 480, 45
Taylor, A. R., Stil, J. M., & Sunstrum, C. 2009, ApJ, 702, 1230
Vacca, V., Murgia, M., Govoni, F., et al. 2010, A&A, 514, A71
Vacca, V., Murgia, M., Govoni, F., et al. 2012, A&A, 540, A38

PoS(AASKA14)114

Vallée, J. P., MacLeod, M. J., & Broten, N. W. 1986, A&A, 156, 386
Vogt, C., & Enßlin, T. A. 2003, A&A, 412, 373
Vogt, C., & Enßlin, T. A. 2005, A&A, 434, 67
Xu, H., Li, H., Collins, D. C., Li, S., & Norman, M. L. 2010, ApJ, 725, 2152

PoS(AASKA14)114

The Hydrogen Universe

PROCEEDINGS OF SCIENCE

H I science with the Square Kilometre Array

Lister Staveley-Smith
(1) International Centre for Radio Astronomy Research (ICRAR), University of Western Australia, 35 Stirling Hwy, Crawley, WA 6009, Australia
(2) ARC Centre for All-sky Astrophysics (CAASTRO)
E-mail: Lister.Staveley-Smith@icrar.org

Tom Oosterloo
(1) Netherlands Institute for Radio Astronomy (ASTRON), PO Box 2, 7900 AA Dwingeloo, The Netherlands
(2) Kapteyn Astronomical Institute, Groningen University
E-mail: oosterloo@astron.nl

The Square Kilometre Array (SKA) will be a formidable instrument for the detailed study of neutral hydrogen (H I) in external galaxies and in our own Galaxy and Local Group. The sensitivity of the SKA, its wide receiver bands, and the relative freedom from radio frequency interference at the SKA sites will allow the imaging of substantial number of high-redshift galaxies in H I for the first time. It will also allow imaging of galaxies throughout the Local Volume at resolutions of < 100 pc and detailed investigations of galaxy disks and the transition between disks, halos and the intergalactic medium (IGM) in the Milky Way and external galaxies. Together with deep optical and millimetre/sub-mm imaging, this will have a profound effect on our understanding of the formation, growth and subsequent evolution of galaxies in different environments. This paper provides an introductory text to a series of nine science papers describing the impact of the SKA in the field of H I and galaxy evolution. We propose a nested set of surveys with phase 1 of the SKA which will help tackle much of the exciting science described. Longer commensal surveys are discussed, including an ultra-deep survey which should permit the detection of galaxies at $z = 2$, when the Universe was a quarter of its current age. The full SKA will allow more detailed imaging of even more distant galaxies, and allow cosmological and evolutionary parameters to be measured with exquisite precision.

Advancing Astrophysics with the Square Kilometre Array
June 8-13, 2014
Giardini Naxos, Italy

PoS(AASKA14)167

1. Introduction

The 1944 prediction of the existence of the 21-cm line of atomic hydrogen (H I; van de Hulst 1945), and its later detection from our Galaxy and other galaxies (Ewen & Purcell 1951; Muller & Oort 1951; Kerr, Hindman & Robinson 1954), was driven by the realisation of the huge scientific potential of observations of this spectral line. From the start, it was clear that atomic hydrogen is not only a fundamental constituent of galaxies whose role has to be studied and understood, but that observations of H I in galaxies can also be used as an important tool for understanding a wide range of phenomena, ranging from large-scale dynamics to the physics of the interstellar medium (ISM). The large amount of H I-related work over the years following has indeed shown that it is almost impossible to understand galaxies, their structure, the distribution of dark matter and their environmental interactions, without knowing about their H I properties. As a result, improving the observational capabilities in radio astronomy in order to extend the scope of 21-cm studies of galaxies in sensitivity, survey speed, resolution and redshift has always been one of the main science drivers for SKA. In the following chapters, the main issues the community hopes to address with future H I observations with SKA phase 1 (SKA1) and SKA are outlined. In these chapters, it will be clear that there are strong underlying connections and therefore that there are a number of important themes that can be addressed by a concerted approach involving observations of our own Galaxy (and its very nearest companions), detailed studies of nearby galaxies and statistical studies using surveys of a large number of galaxies, out to the highest redshifts available to SKA1 and SKA.

A key goal is to understand the role of H I in the life-cycle of galaxies and how this role evolved over time. How do galaxies acquire gas? What does the interface between galaxies and the intergalactic medium (IGM) look like? How is star formation controlled by gas accretion and, in turn, how does feedback from star formation affect the ISM? Similarly, how is the activity in active galactic nuclei (AGN) connected to H I and how do AGN affect the gas content of galaxies? What is the role of the environment, and of galaxy interactions? With SKA1 and SKA, important progress can be made on answering all these questions, and in particular, how the balance between all the different phenomena has evolved over time.

With current instruments, H I observations of very gas-rich galaxies are possible to redshifts $z \sim 0.2$, or look-back times up to around 2.4 Gyr, but only for a few objects and using long integration times (Zwaan, van Dokkum & Verheijen 2001; Catinella et al. 2008; Verheijen et al. 2007; Fernández et al. 2013). With the SKA Pathfinders, huge samples ($> 10^5$ galaxies) will be available locally, and significant samples ($> 10^4$ galaxies) will be detected to look-back times of ~ 5 Gyr. With the improved sensitivity and survey speed offered by SKA1 and SKA, the possibilities to detect and image larger samples of galaxies to even larger look-back times ($7-11$ Gyr) are dramatically improved. Importantly, the high sensitivity of SKA will allow the spatial resolution of the distribution and kinematics of the H I, as well as the measurement of global quantities, such H I mass and linewidth. This will open up many new ways of investigating the role of H I in galaxy evolution. We must not forget how important it will be to combine these H I data with large galaxy surveys in other wavebands to obtain a complete picture of galaxy evolution. Conversely, the interpretation of those other data sets will not be complete without the matching information available from the SKA H I surveys.

PoS(AASKA14)167

2. The life-cycle of galaxies

At a more detailed level, it is necessary to understand the gas cycle in galaxies: how galaxies acquire their gas to fuel star formation and how star formation affects the state of gas in galaxies and mediates the accretion of gas onto galaxies. It is important to understand the interplay between the various phases of the gas (ionised, atomic, molecular) and how this connects to star formation. To make progress with modelling galaxy evolution, the accurate physics of the ISM on the smallest scales has to be understood. With the widefield capability of the SKA (an individual beam is ~ 1 deg^2 at 1.4 GHz), this can be studied in the Galaxy and in the Magellanic Clouds in unprecedented detail. Detailed observations of nearby galaxies will also be required. With the sensitivity of the SKA1, finally we will be able to study the structure and the kinematics of the H I in nearby galaxies, and its relation to star formation and other constituents of the ISM, at spatial resolutions similar to that possible in other wavebands. This will be a major breakthrough. The synergy with other new facilities in the southern hemisphere, such as the Atacama Large Millimeter/sub-millimeter Array (ALMA), the Large Synoptic Survey Telescope (LSST), the multi-field IFU on the Anglo-Australian Telescope (HECTOR), the upcoming 30-m class optical/infrared telescopes, as well as space observatories such as Euclid and eROSITA will lead to significant advances in the field.

An exciting prospect for future SKA observations is having sufficient sensitivity and spatial resolution to detect, for the first time, how galaxies are embedded in the diffuse, low column-density IGM. All current models of galaxy evolution predict that galaxies are surrounded by large gaseous halos from which the galaxies accrete gas to feed their star formation. At column densities below roughly 10^{19} cm^{-2}, H I is not self-shielding against the intergalactic radiation field. Around this limit, when going from high to low column density, the ionisation balance quickly changes and the IGM goes from mainly neutral to mainly ionised and H I column densities quickly drop. Therefore, to observe these gaseous halos, we have to be able to detect H I column densities of 10^{18} cm^{-2} or lower at a spatial resolution matching the structure of the filaments. This has been a major barrier for studying the IGM near galaxies with current instruments. SKA1 with its dense, inner array configuration, has the potential to detect and image the gaseous interface between galaxies providing a major step forward in understanding galaxy evolution.

Finally, the low-RFI environment at the SKA sites provides unique observational capabilities to detect H I in emission at moderate redshifts ($z \sim 1$) in phase 1. However, for absorption studies, detections at higher redshifts will readily be possible with SKA1-MID for $z < 3$ and SKA1-LOW for $z > 3$. Absorption due to intervening H I clouds along the line-of-sight, as well as H I absorption associated with the ISM surrounding an AGN can be studied in this way. Studies of the intervening H I absorption will allow a blind study of the evolution in the properties of the ISM in galaxies from high redshift to the present. Studies of the associated H I absorption will show how feedback effects of AGN activity on the ISM of galaxies change with redshift. In local galaxies, this activity is often observed in the form of fast, AGN-driven outflows of large amounts of cold gas. Such feedback effects are thought to be important for regulating star formation as well as for the growth of super massive black holes.

PoS(AASKA14)167

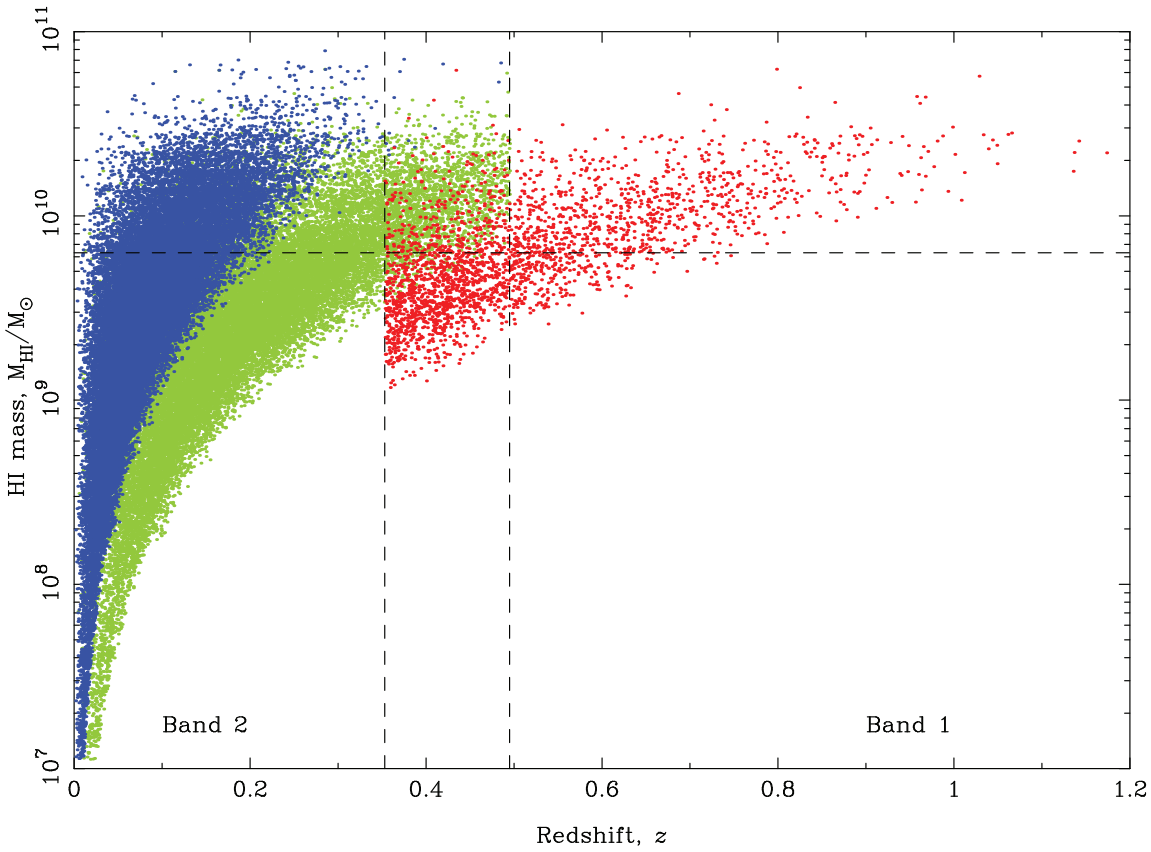

Figure 1: A simulation which shows the distribution with redshift of H I masses of galaxies likely to be detected in the representative tiered set of 1,000 hr surveys discussed in the text and in the following table. The 'medium wide' (blue), 'medium deep' (green) and 'deep' (red) surveys are plotted. The vertical dashed lines refer to the (overlapping) band edges, as specified in Dewdney et al. (2013). The horizontal line represents the value of M^*_{HI} at $z = 0$. A non-evolving 2-dimensional stepwise maximum likelihood (2DSWML) H I mass and velocity width function (Zwaan et al. 2005) is assumed for the purpose of this simulation.

3. The H I Science Case

The following chapters concentrate on the far-reaching impact of SKA1 on our understanding of the formation and evolution of galaxies (Blyth et al. 2015; Power et al. 2015; Meyer et al. 2015) including the build-up of angular momentum (Obreschkow et al. 2015), the accretion of gas into the outskirts of galaxies (Popping et al. 2015), the detailed understanding of the ISM of galaxies (de Blok et al. 2015), and the impact of AGN on the large-scale gas distribution in galaxies (Morganti et al. 2015). The impact of SKA1 on our understanding of the local Galactic ISM and halo is also explored, including detailed mapping via absorption-line studies of the density and temperature of the cold neutral medium (McClure-Griffiths et al. 2015; Oonk et al. 2015). This impressive set of science cases and chapters has been facilitated by the H I and Galaxy Evolution working group of the SKA Science Working Group. Strong links are noted with the Cosmology working group (Maartens et al. 2015) who have explored use of the SKA in measuring cosmological parameters

PoS(AASKA14)167

and exploring evolution through galaxy surveys and intensity mapping (Bull et al. 2015; Santos et al. 2015).

4. Possible SKA1 H I surveys

As with the SKA pathfinders, a major part of the science output of the SKA is likely to come from the allocation of significant amounts of telescope time (1,000 hrs, or greater) to Key Science Projects. In order to maximise the H I science output of the SKA, it is desirable for these to be complementary in nature between science cases. For example, a natural suite of surveys may include: (1) a wide area survey for studies of cosmology; (2) medium deep surveys for studies of environmental dependence and individual galaxies; and (3) a deep survey for studies of evolution. H I chapter authors have indicated their range of preferences based on the fiducial baseline design of Dewdney et al. (2013). The recent re-baseline only has a modest effect (less than a factor of two in observing time) on science goals best achieved with SKA1-MID, but a more dramatic effect on goals that require SKA1-survey. Nevertheless, on the basis that some SKA1-survey science can still be achieved with SKA1-MID, we retain the moniker as used in the individual science chapters.

In suggesting the nested set of surveys in Table 1 and Figure 1, we have referred to the individual chapters for guidance. We have used the simulations of Popping et al. (2015) as a guide to the SKA1 sensitivity as a function of resolution, taking into account a 're-baselining' scale factor of 1.3 and, for SKA1-MID band 1 only, a further band-average sensitivity loss of ~ 1.7 due to system temperature and antenna efficiency (Dewdney et al. 2013). We have accounted for the change of primary beam with frequency. In selecting surveys, we also need to be cognisant of the capabilities of the various SKA precursors and pathfinders, ASKAP, FAST, JVLA, MeerKAT and WSRT/APERTIF, some of which have sensitivities or survey speed not very different from SKA1 at lower angular resolutions. In particular, an all-sky emission-line survey with SKA1 will not be better than those currently planned for the pathfinders unless more integration time can be devoted than indicated in Table 1.

5. Commensal SKA1 Observations

With SKA1, greater sensitivities are possible for surveys that are commensal across science themes. Whereas Table 1 indicates that dedicated survey times of $\sim 1,000$ hrs will meet key H I science goals such as investigating the cosmic evolution of galaxies at high angular resolution to $z \sim 1$, a commensal survey could in principle have a factor of ~ 10 more integration time. This would permit a large-area H I survey, which cannot otherwise be undertaken with SKA1 in 1,000 hrs because of column density sensitivity limits. This would enable 'SKA1-survey' outcomes discussed by various chapter authors (Obreschkow et al. 2015; McClure-Griffiths et al. 2015; Meyer et al. 2015), as well as H I cosmology outcomes (Bull et al. 2015), and important commensal pulsar, continuum and magnetism science outcomes (e.g. Keane et al. 2015; Norris et al. 2014; Gaensler et al. 2015). Another possibility is an ultra-deep survey which would allow detection of H I emission from galaxies at $z \sim 2$ (Blyth et al. 2015) as well as allowing studies of continuum star formation rates in galaxies at the highest redshifts (Jarvis et al. 2014). Similarly, deep and highly resolved H I observations of nearby galaxies would also yield deep continuum and polarisation

PoS(AASKA14)167

data. These could be used to further explore the physics of the continuum-star formation rate relation, rotation measures, and magnetic field configuration. Such observations would also have very deep column density limits ($< 10^{18}$ cm^{-2}) at $1'$ resolution. We list a subset of three possible H I commensal surveys in Table 2. Although only one or two such commensal surveys are likely to be possible, they would be a significant step towards the full SKA.

Survey	Ω deg^2	Frequency[1] MHz	Resolution[2]	N	$< z >$ (z_{lim})	$N_{\rm HI}$ 10^{20} cm^{-2}	Science chapter
Galaxy/MS (absorption)	400	1418-1422	$5''$	4,000			McClure-Griffiths et al. (2015)
Extragalactic (absorption)	1000	350-1050	$2''$	5,000	1(3)		Morganti et al. (2015)
	1000	200-350[3]	$10''$	?	4(6)		”
Galaxy/MS	600	1418-1422	$10''$-$1'$			2	McClure-Griffiths et al. (2015); Oonk et al. (2015)
Medium wide	400	950-1420	$10''$	34,000	0.1 (0.3)	2	Meyer et al. (2015); Obreschkow et al. (2015); Popping et al. (2015)
Medium deep	20	950-1420	$5''$	25,000	0.2 (0.5)	0.6	Meyer et al. (2015); Obreschkow et al. (2015); Popping et al. (2015)
Deep	1	600-1050	$2''$	2,600	0.5 (1)	0.4	Blyth et al. (2015); Meyer et al. (2015); Obreschkow et al. (2015); Power et al. (2015)
Targeted	–	1400-1420	$3''$-$1'$	50	0.002 (0.01)	0.5	de Blok et al. (2015); Popping et al. (2015)

[1]SKA1-MID band definition is 350–1050 MHz (band 1) and 950–1760 MHz (band 2); SKA1-LOW band definition is 50–350 MHz.

[2]Typical angular resolution; value changes with frequency and (for H I emission) column-density sensitivity threshold.

[3]SKA1-LOW.

Table 1: Fiducial 1,000-hr SKA1 H I surveys and the science cases that they would facilitate. The list is not complete, but illustrates the tiered structure necessary to allow a comprehensive, multi-faceted study of galaxies and their evolution in a range of environments and over a range of redshifts. The SKA1 telescope parameters are those resulting from the 2015 re-baseline (see text for further details). For non-targeted emission-line surveys, the predicted number of galaxies N (column 5) assumes an invariant 2DSWML H I mass and velocity width function (Zwaan et al. 2005) and assumes a detection at 5-σ significance or higher, at $10''$ resolution. The mean sample redshift $<z>$ and redshift upper limit z_{lim} are indicated (column 6). The corresponding 5-σ column density sensitivity $N_{\rm HI}$ for extended objects at $<z>$ is also indicated (column 7), assuming a rest-frame velocity width of 20 km s^{-1}. Angular resolutions finer than $10''$ are available down to the approximate value indicated in column 4, but only for high column densities. The prediction follows methodology similar to that of Duffy et al. (2012).

PoS(AASKA14)167

Survey	Ω deg^2	Freq- ency MHz	Resol- ution	N	$< z >$ (z_{lim})	$N_{\rm HI}$ 10^{20} cm^{-2}	Science chapter
All-sky	20,000	950-1420	$15''$	550,000	0.06 (0.3)	2	McClure-Griffiths et al. (2015); Obreschkow et al. (2015); Bull et al. (2015)
Wide	5,000	950-1420	$10''$	340,000	0.1 (0.5)	2	Meyer et al. (2015); Obreschkow et al. (2015); Popping et al. (2015)
Ultra deep	1	450-1050	$2''$	23,000	0.7 (2)	0.2	Blyth et al. (2015); Meyer et al. (2015); Obreshkow et al. (2015); Power et al. (2015)

Table 2: Commensal 10,000 hr SKA1 surveys across science areas allow much greater observing times for a smaller number of surveys. Here we list some possible commensal surveys, each with a total integration time of 10,000 hrs. The scientific goals of such surveys extend well beyond the H I and cosmology science chapters listed here. The numbers of detectable galaxies and 5-σ column density limits at the mean redshift <z> are estimated at $15''$ resolution for the all-sky survey, and $10''$ otherwise. Column density limits at $1'$ resolution are ~ 33 times better (Popping et al. 2015).

6. The full SKA

One of the early headline science goals of the SKA was to image H I in a 'Milky Way-type' galaxy at a cosmologically significant ($z \sim 2$) redshift (Taylor & Braun 1999). In the updated science case edited by Carilli & Rawlings (2004), the possibility of retaining such sensitivity was emphasised (van der Hulst et al. 2004). However, it was also pointed out that with the large field-of-view of new-technology radio telescopes, it is possible to observe extremely large samples of galaxies at lower resolution to undertake 21cm cosmology. The so-called 'billion galaxy survey' (Abdalla & Rawlings 2005) was proposed to investigate the nature of dark energy over the crucial redshift range $1.5 > z > 0$. Although this remains a clear science goal for the full SKA, it receives less attention in this volume which focusses on SKA1. Furthermore, this needs re-evaluation in light of projects such as Euclid and DES which have been funded in the meantime, and the potential of other novel techniques that can be applied to SKA data such as Intensity Mapping (Chang et al. 2010). The full SKA would also transform our understanding of the galaxy evolution and dynamics over the range of redshifts even beyond that currently accessible to the largest optical telescopes.

For example, an ultra-deep single-pointing with an SKA of 10 times the sensitivity of SKA1 would be able to detect and resolve galaxies, or compact groups of galaxies, with H I masses in excess of 10^{10} M$_\odot$ out to the $z = 3$ redshift limit of band 1 in 1000 hrs, when the Universe was a sixth of its current age. Similarly, a hemispheric survey using an SKA with 100 times the survey speed of SKA1 would be able to detect around 2.5×10^7 galaxies in H I out to the $z = 0.5$ redshift limit of band 2 in 10,000 hrs, and almost a million galaxies in the redshift range $0.35 < z < 0.7$ with similar band 1 integration times. The more ambitious 'dark energy' evolution survey (Abdalla, Blake & Rawlings 2010) of a similar duration would require a telescope whose survey speed is over

PoS(AASKA14)167

4,000 times greater than the band 1 survey speed of SKA1, and would require large numbers of antennas, phased array feeds or aperture arrays. If feasible, such a survey could detect 10^8 galaxies with redshifts $z > 0.35$, of which over 2×10^6 would be at $z > 1$ in a no-evolution scenario.

7. Acknowledgments

It is a pleasure to thank the members of the SKA H I and Galaxy Evolution working group who have contributed to this overview and for writing the chapters contained within this science book.

References

Abdalla, F. B., Blake, C., Rawlings, S., 2010, MNRAS, 401, 743.

Abdalla, F. B., Rawlings, S., 2005, MNRAS, 360, 27.

Blyth, S.-L., van der Hulst, J. M., Verheijen, M. A. W., et al., 2015, "Exploring Neutral Hydrogen and Galaxy Evolution with the SKA", in proc. *Advancing Astrophysics with the Square Kilometre Array*, PoS(AASKA14)128

Bull, P., Camera, S., Raccanelli, A., et al., 2015, "Measuring baryon acoustic oscillations with future SKA surveys", in proc. *Advancing Astrophysics with the Square Kilometre Array*, PoS(AASKA14)024

Carilli C.L., Rawlings S. 2004, eds. "Science with the Square Kilometre Array", NewAR, 48, 979.

Catinella, B., Haynes, M. P., Giovanelli, R., Gardner, J. P., Connolly, A. J., 2008, ApJ, 685, L13.

Chang, T.-C., Pen, U.-L., Bandura, K., Peterson, J. B., 2010, Nature, 466, 463.

de Blok, W. J. G., Fraternali, F., Heald, G. H., et al., 2015, "The SKA view of the Neutral Interstellar Medium in Galaxies", in proc. *Advancing Astrophysics with the Square Kilometre Array*, PoS(AASKA14)129

Dewdney, P. E., Turner, W., Millenaar, R., McCool, R., Lazio, J., Cornwell, T. J., 2013, SKA1 System Baseline Design (SKA Office), SKA-TEL-SKO-DD-001 revision 1.

Duffy, A. R., Meyer, M. J., Staveley-Smith, L., et al., 2012, MNRAS, 426, 3385.

Ewen, H. I., Purcell, E. M., 1951, Nature, 168, 356.

Fernández, X., van Gorkom, J. H., Hess, K. M., et al., 2013, ApJ, 770, L29.

Gaensler, B. M., Agudo, I., Akahori, T., et al., 2015, "Broadband Polarimetry with the Square Kilometre Array: A Unique Astrophysical Probe", in proc. *Advancing Astrophysics with the Square Kilometre Array*, PoS(AASKA14)103

Jarvis, M. J., Seymour, N., Afonso, J., et al., 2015, "The star-formation history of the Universe with the SKA", in proc. *Advancing Astrophysics with the Square Kilometre Array*, PoS(AASKA14)068

Keane, E. F., Bhattacharyya, B., Kramer, M., et al., 2015, "A Cosmic Census of Radio Pulsars with the SKA", in proc. *Advancing Astrophysics with the Square Kilometre Array*, PoS(AASKA14)040

Kerr, F. J., Hindman, J. F., Robinson, B. J., 1954, AuJPh, 7, 297.

Maartens, R., Abdalla, F. B., Jarvis, M., et al., 2015, "Overview of Cosmology with the SKA", in proc. *Advancing Astrophysics with the Square Kilometre Array*, PoS(AASKA14)016

PoS(AASKA14)167

McClure-Griffiths, N. M., Stanimirovic, S., Murray, C. E., et al., 2015, "Galactic and Magellanic Evolution with the SKA", in proc. *Advancing Astrophysics with the Square Kilometre Array*, PoS(AASKA14)130

Meyer, M., Robotham, A., Obreschkow, D., Driver, S., Staveley-Smith, L., Zwaan, M., 2015, "Connecting the Baryons: Multiwavelength Data for SKA HI Surveys", in proc. *Advancing Astrophysics with the Square Kilometre Array*, PoS(AASKA14)131

Morganti, R., Sadler, E. M., Curran, S. J., 2015, "Cool Outflows and HI absorbers with SKA", in proc. *Advancing Astrophysics with the Square Kilometre Array*, PoS(AASKA14)134

Muller, C. A., Oort, J. H., 1951, Nature, 168, 357.

Norris, R. P., Basu, K., Brown, M., et al., 2015, "The SKA Mid-frequency All-sky Continuum Survey: Discovering the unexpected and transforming radio-astronomy", in proc. *Advancing Astrophysics with the Square Kilometre Array*, PoS(AASKA14)086

Obreschkow, D., Meyer, M., Popping, A., Power, C., Quinn, P., Staveley-Smith, L., 2015, "The SKA as a Doorway to Angular Momentum", in proc. *Advancing Astrophysics with the Square Kilometre Array*, PoS(AASKA14)138

Oonk, J. B. R., Morabito, L. K., Salgado, F., et al., 2015, "The Physics of the Cold Neutral Medium: Low-frequency Radio Recombination Lines with the Square Kilometre Array", in proc. *Advancing Astrophysics with the Square Kilometre Array*, PoS(AASKA14)139

Popping, A., Meyer, M., Staveley-Smith, L., Obreschkow, D., Jozsa, G. I., Pisano, D. J., 2015, "Observations of the Intergalactic Medium and the Cosmic Web in the SKA era", in proc. *Advancing Astrophysics with the Square Kilometre Array*, PoS(AASKA14)132

Power, C., Lagos, C. D. P., Qin, B., et al., 2015, "Galaxy Formation & Dark Matter Modelling in the Era of the Square Kilometre Array", in proc. *Advancing Astrophysics with the Square Kilometre Array*, PoS(AASKA14)133

Santos, M. G., Bull, P., Alonso, D., et al., 2015, "Cosmology from a SKA HI intensity mapping survey", in proc. *Advancing Astrophysics with the Square Kilometre Array*, PoS(AASKA14)019

Taylor, A. R., Braun, R., 1999, eds. 'Science with the Square Kilometer Array: a next generation world radio observatory'.

van de Hulst, H. C., 1945, Ned.Tijd.Natuurkunde, 11, 21.

van der Hulst J.M., Sadler E.M., Jackson C.A., Hunt L.K., Verheijen M., van Gorkom J.H. 2004, NewAR, 48, 1221.

Verheijen, M., van Gorkom, J. H., Szomoru, A., Dwarakanath, K. S., Poggianti, B. M., Schiminovich, D., 2007, ApJ, 668, L9.

Zwaan M. A., Meyer M. J., Staveley-Smith L., Webster R. L., 2005, MNRAS, 359, 30

Zwaan, M. A., van Dokkum, P. G., Verheijen, M. A. W., 2001, Sci, 293, 1800.

PoS(AASKA14)167

PROCEEDINGS OF SCIENCE

Exploring Neutral Hydrogen and Galaxy Evolution with the SKA

S. -L. Blyth[1], J. M. van der Hulst*[2], M.A.W. Verheijen[2], HI SWG Members[3], B. Catinella[4], F. Fraternali[5,2], M. P. Haynes[6], K. M. Hess[1,2,7], B.S. Koribalski[8], C. Lagos[9], M. Meyer[10], D. Obreschkow[10], A. Popping[10,11], C. Power[10], L. Verdes-Montenegro[12], and M. Zwaan[9]

[1]*University of Cape Town, South Africa;* [2]*Kapteyn Astronomical Institute, The Netherlands;* [3]*SKA HI Science Working Group;* [4]*Swinburne University of Technology, Australia;* [5]*University of Bologna, Italy;* [6]*Cornell University, USA;* [7]*Netherlands Institute for Radio Astronomy (ASTRON);* [8]*ATNF, CSIRO Astronomy and Space Science, Australia;* [9]*European Southern Observatory, Germany;* [10]*ICRAR, University of Western Australia;* [11]*ARC Centre of Excellence for All-sky Astrophysics (CAASTRO);* [12]*Instituto de Astrofisica de Andalucia (IAA/CSIC), Spain*
E-mail: sarblyth@ast.uct.ac.za

One of the key science drivers for the development of the SKA is to observe the neutral hydrogen, H I, in galaxies as a means to probe galaxy evolution across a range of environments over cosmic time. Over the past decade, much progress has been made in theoretical simulations and observations of H I in galaxies. However, recent H I surveys on both single dish radio telescopes and interferometers, while providing detailed information on global H I properties, the dark matter distribution in galaxies, as well as insight into the relationship between star formation and the interstellar medium, have been limited to the local universe. Ongoing and upcoming H I surveys on SKA pathfinder instruments will extend these measurements beyond the local universe to intermediate redshifts. We present here an overview of the H I science which will be possible with the the SKA and which will build upon the expected increase in knowledge of H I in and around galaxies obtained with the SKA pathfinder surveys. With the SKA1 the greatest improvement is the capability to image galaxies at reasonable linear resolution and good column density sensitivity to much higer redshifts ($0.2 < z < 1.7$). So one will not only be able to increase the number of detections to study the evolution of the H I mass function, but also have the sensitivity and resolution to study inflows and outflows to and from galaxies and the kinematics of the gas within and around galaxies as a function of environment and cosmic time out to previously unexplored depths. The increased sensitivity of SKA2 will allow us to image Milky Way-size galaxies out to redshifts of $z = 1$ and will provide the data required for a comprehensive picture of the H I content of galaxies back to $z \sim 2$ when the cosmic star formation rate density was at its peak.

Advancing Astrophysics with the Square Kilometre Array
June 8-13, 2014
Giardini Naxos, Italy

*Speaker

PoS(AASKA14)128

1. Introduction

How galaxies form and evolve is one of the fundamental questions in modern astrophysics. Over the past decade, multiwavelength observations of galaxies spanning a wide range of cosmic time have indicated that galaxy evolution seems to depend primarily on two parameters: a galaxy's stellar mass, and the environment in which it is located. In the Λ-cold dark matter (CDM) hierarchical structure formation picture, galaxies form through the successive mergers of smaller units (namely dark matter haloes) to form larger structures. Prior to the epoch of galaxy formation, baryons existed almost entirely in gaseous form, and it is through the infall of this material onto the filamentary structures of the cosmic web, its accretion into the deepest potential wells, and ultimate collapse into dense molecular clouds, that galaxies were able to start forming and producing stars. The ongoing influence of dark matter haloes, and complex feedback mechanisms between baryonic components, continue to regulate the gas content and evolution of galaxies today. In order to fully understand the build up of stellar mass in galaxies, we need to understand the role that neutral gas, the fuel for star formation, plays, along with the physical processes involved. Therefore we need to study the neutral gas distributions and kinematics of galaxies, in large numbers, in different environments, as a function of cosmic time to uncover the full picture of galaxy evolution and structure formation in the Universe. This is one of the main scientific drivers for the development of the SKA.

Along with recent progress in observations, there have been many theoretical advances in both semi-analytic modelling and full hydrodynamical modelling of galaxy evolution and, importantly, the role of neutral hydrogen gas, in both its atomic (H I) and molecular forms (see section 2.2). However, observations of neutral gas have lagged behind observations at other wavelengths; due to the intrinsic faintness of H I emission, unreasonably long observing times are required to probe to redshifts beyond $z \sim 0.25$ with existing facilities, although with the construction of SKA pathfinder instruments and significant upgrades to current facilities, deeper, more sensitive, observations will be possible in the very near future (see section 2.3). The SKA will allow us to probe HI emission in galaxies to previously unexplored depths and further back in cosmic history. The SKA2 will enable optical quality H I imaging of Milky Way size galaxies out to redshifts of $z = 1$

Analysis of thousands of galaxies in the Sloan Digital Sky Survey (SDSS) has shown that they follow a bimodal distribution in colour as a function of stellar mass (Baldry et al. (2004)); most galaxies are either located in the so-called blue cloud or on the red sequence, indicating that star formation is either still ongoing or was quenched billions of years ago. Furthermore, the galaxy 'main sequence' (star formation rate vs. stellar mass) shows a relatively smooth evolution over cosmic time from $z \sim 2.5$ to $z \sim 0$ while over the same period, the star formation rate density of the Universe has dropped by more than an order of magnitude since its peak at $z \sim 2-3$ (Madau et al. (1998); Hopkins & Beacom (2006)). Star formation also seems to have shifted from the more massive galaxies to less massive galaxies at later times, a pattern known as cosmic downsizing (Cowie et al. (1996)). Understanding the role of the neutral gas that fuels star formation and enables the build up of stellar mass as well as the role of the environment in enabling or quenching these processes, is vital to disentangle the physics involved in the evolution of galaxies. To move forward, a number of key questions related to the role of H I in galaxies need to be answered such as:

- What is the distribution and kinematics of the neutral (H I) gas within and around galaxies,

PoS(AASKA14)128

both as a function of environment (i.e. groups/clusters vs. the field) and over cosmic time?

- How much H I is there on average as a function of redshift?
- How does the M_{HI} of galaxies scale with their stellar/halo masses and other properties, e. g.,star formation rate, as a function of environment and redshift?
- How important is gas accretion vs. merging in terms of building stellar mass?

The process of star formation is intimately related to how individual galaxies evolve. On kpc-size scales, the Kennicutt-Schmidt law (Bigiel et al. (2008); Leroy et al. (2012); Calzetti et al. (2012)) describes the relationship between the star formation rate surface density and the molecular gas mass surface density. However, details of the conditions needed for star formation to begin at the scales of (molecular) clouds are as yet unclear. High resolution observations of the interstellar medium (ISM) in individual galaxies are required in order to clarify the astrophysical processes taking place at these scales. This topic will be more fully discussed in a separate chapter, *The Interstellar medium in Galaxies* (de Blok et al. (2014)). Further discussion of the interaction of galaxies with their environment, the IGM and the distribution of neutral hydrogen in the cosmic web will be presented in the chapter *The Intergalactic Medium and the Cosmic Web* (Popping et al. (2014)).

Observations of H I in absorption along lines of sight to strong radio sources can provide information on the neutral gas content of galaxies at higher redshifts than it is possible to reach directly with H I emission measurements. These are key measurements for studies of galaxy evolution at higher redshifts, and will be discussed further in a separate chapter, *Cool Outflows and HI absorbers* (Morganti et al. (2014))

2. H I observations and theory: the status quo

2.1 Recent observational results

2.1.1 The Local Universe

Recent years have ushered in a "golden age" of H I science that has seen a variety of H I surveys to study galaxy evolution take place. The recent single dish, large area blind H I surveys HIPASS (Barnes et al. (2001)) and ALFALFA (Giovanelli et al. (2005)) have shed light on the global H I properties of galaxies in general and provided the best estimates of the global H I mass function. Poor statistics at the very high H I mass end **and** the very low H I mass end ($< 10^7$ $M_\odot$) limit the current results and do not resolve questions such as whether the H I mass function depends on the local enviroment (Zwaan et al. (2005); Springob et al. (2005)). Yet these surveys have revealed that there is indeed an extreme paucity of H I objects without stellar counterparts when the H I mass detection limit is pushed well below 5×10^6 $M_\odot$, enabling the interesting discovery of a few local, gas-rich dwarf galaxies such as Leo T (Ryan-Weber et al. (2008)) and Leo P (Giovanelli et al. (2013)). In addition the surveys demonstrate the power of combining the H I survey information with data from other wavebands (optical, UV, IR) to address questions relevant to galaxy evolution (Catinella et al. (2010); Schiminovich et al. (2010); Wong et al. (2009)).

More detailed information about the kinematics and structure of the H I disks in individual galaxies has come from resolved observations using synthesis radio telescopes. Major surveys

PoS(AASKA14)128

carried out in the last decade are WHISP (van der Hulst et al. (2001)), THINGS (Walter et al. (2008)), LVHIS (Koribalski (2008)), Atlas-3D (Serra et al. (2012)), Little THINGS (Hunter et al. (2012)), VLA-ANGST (Ott et al. (2012)), VIVA (Chung et al. (2009)), SHIELD (Cannon et al. (2011)), FIGGS (Begum et al. (2008)), HALOGAS (Heald et al. (2011)) and BlueDisks (Wang et al. (2013)). Major results are the systematic inventory of the distribution of dark matter in galaxies, the prevalence of warps, tidal features, and signs of ram pressure stripping, and detailed relationships between star formation and the ISM including galactic fountains and the presence of extra-planar H I. A synopsis of results to date can be found in two recent reviews (Sancisi et al. (2008); van der Hulst & de Blok (2013)).

Observations of H I in galaxies in very dense environments (a well studied example is the Virgo cluster (Chung et al. (2009)) demonstrate the importance of the environment. The growing inventory of detailed H I observations of galaxies in different environments is mixed, but suggest that even intermediate density environments in galaxy groups (Hess & Wilcots (2013)), and on the outskirts of clusters (Jaffé et al. (2013)) impact the HI content of galaxies. Dense environments in small volumes, such as Hickson compact groups, also exhibit H I deficiencies (Verdes-Montenegro et al. (2001)) with a suggestion that a reservoir of low density H I might exist to feed the galaxies (Borthakur et al. (2011)). In very isolated environments, such as voids (Kreckel et al. (2012); Beygu et al. (2013)) there is a suggestion that accretion is an important process. Obtaining information for galaxies that are specifically selected to be extremely isolated will be very important (Espada et al. (2011)) provided detailed imaging is performed (Scott et al. (2014)). Having a good enough sample of H I in and around many galaxies in different enviroments to address the question of *nature versus nurture* will will be a prime goal for the SKA.

Three surveys are currently pushing the present technology to redshifts beyond $z = 0.2$; the HIGHz survey (Catinella et al. (2008)) with Arecibo and two interferometric surveys, BUDHIES (Verheijen et al. (2007); Jaffé et al. (2013)) and CHILES (Fernández et al. (2013)) which are using observing times approaching 1000 hours. To date, the most successful method of detecting H I emission beyond $z = 0.2$ with current instrumentation is stacking based on position and redshift information from optical surveys. In the following sections we will briefly describe the current status of H I observations and then focus on the important next steps to be addressed by SKA1 and SKA2.

2.1.2 Observations at low redshift ($z < 0.4$)

Exploiting the exquisite sensitivity of the Arecibo radio telescope, the HIGHz survey provides a glimpse into the H I properties of star-forming galaxies at $z \sim 0.2$ located in relatively isolated environments. The survey measured the H I content of 39 optically-selected galaxies with redshifts between $0.17 < z < 0.25$; these are all actively star-forming, disk-dominated systems with stellar and H I masses larger than 10^{10} $M_{\odot}$. This sample includes not only the highest-redshift detections of H I emission from individual galaxies to date, but also some of the most H I-massive systems known. Despite being exceptionally large, the H I reservoirs of these galaxies are consistent with what is expected from their UV and optical properties.This, and the fact that the galaxies lie on the baryonic Tully-Fisher relation, suggests that HIGHz systems are rare, scaled-up versions of gas-rich disks in the local Universe. These observations provide important insight into the properties

PoS(AASKA14)128

of the massive, H I -rich systems that will likely dominate the next-generation H I surveys with the SKA and its pathfinder telescopes.

Taking advantage of the upgraded Westerbork receiver system, a Blind, Ultra-Deep H I Environmental Survey (BUDHIES) has been carried out to image two cosmic volumes, both covering the redshift range z=0.164−0.224, centered on the galaxy clusters Abell 2192 at $z = 0.187$ and Abell 963 at $z = 0.206$. A963 is a massive, lensing, X-ray bright, Butcher-Oemler cluster with an unusual high fraction of blue galaxies in its center. The main scientific goal of BUDHIES is to characterize the gas content of these blue galaxies in relation to the gas content of galaxies in the cluster outskirts and the surrounding field in which this cluster is embedded. A 2192 is a less massive cluster that mainly serves as a control object. The clusters within their Abell radii occupy only ∼5% of the total surveyed volume, which also contains voids and galaxy overdensities in the fore- and background of both clusters.

Data were collected with the WSRT with $78\times12^{\rm hr}$ on A2192 and $117\times12^{\rm hr}$ on A963 to obtain a similar HI mass limit of 2×10^9 $M_\odot$. A total of 39 galaxies were detected in the volume containing A2192 and 120 galaxies in A963. First results from a pilot survey showed that none of the blue galaxies in A963 were detected, while stacking the HI spectra from galaxies of similar luminosity and color in the surrounding field showed a clear detection (Verheijen et al. (2007)). The full dataset is currently being analysed with a focus on the H I content of galaxies in the various substructures within and around the clusters (Jaffé et al. (2012, 2013)), as well as the H I-based Tully-Fisher relation at these redshifts.

The COSMOS H I Large Extragalactic Survey (CHILES) is an ongoing 1000 hour program designed to take advantage of the upgraded capabilities on the Karl G. Jansky Very Large Array (VLA). The upgrade enables continuous redshift coverage for H I in emission from $z = 0 - 0.5$, doubling the look-back time of existing H I measurements. A single pointing centered in the COSMOS field, CHILES is expected to detect and resolve Milky Way-like galaxies in H I ($M_{HI} = 3 \times 10^{10}$ $M_\odot$) at the most distant redshift accessible, and the most gas-rich galaxies that we know of at $z = 0$, totalling over 300 H I -rich objects in the roughly 4×10^5 Mpc^3 surveyed. The chosen field intersects with known large-scale structure at low, intermediate, and high redshifts, and COSMOS provides a wealth of complementary multi-wavelength photometry and optical spectroscopy enabling the study of galaxy evolution as a function of galaxy properties, environment, and cosmic time. CHILES will be the first survey to probe the H I content, growth, and morphology of galaxies over the same redshift range in which star formation undergoes "cosmic downsizing".

First results from 50 hours observing (Fernández et al. (2013)) produced 33 direct detections in observations covering a continuous redshift range $z = 0 - 0.193$ over a $34' \times 34'$ field of view, including three galaxies for which there were no previous spectroscopic redshifts. The most distant galaxy was detected at z=0.176 and has an HI mass of 8×10^9 $M_\odot$. Stacking the H I spectra of 80 galaxies in a "wall" between $z = 0.12 - 0.13$ produced a detection with an average HI mass of 1.8×10^9 $M_\odot$.

Recent results from H I stacking

H I observations have only begun to detect 21 cm line emission from individual galaxies beyond redshift $z \sim 0.1$. Although a number of galaxies will be individually detected at these and higher redshifts by the upcoming SKA pathfinder surveys (see Table 1), the most stringent constraints on

PoS(AASKA14)128

the H I content of galaxies across cosmic time will come from stacking of undetected sources.

Stacking has become a common tool to constrain the statistical properties of a population of objects that lack individual detections in a survey, and has been applied to a variety of different astrophysical data, including H I -line spectra (Chengalur et al. (2001); Lah et al. (2007); Verheijen et al. (2007); Lah et al. (2009); Fabello et al. (2011); Delhaize et al. (2013); Geréb et al. (2013)). This technique requires independent measurements of the redshifts of the galaxies, and yields an estimate of the average H I content of a sample of galaxies by co-adding their line emission (see description in Fabello et al. (2011)).

Over the past decade, in an effort to probe the evolution of H I gas with cosmic time, Lah et al. (2007), who used the Giant Metrewave Radio Telescope (GMRT) to estimate the H I content of star-forming galaxies at $z \sim 0.24$, and Rhee et al. (2013), who targeted field galaxies at redshift $z \sim 0.1$ and $z \sim 0.2$ with the Westerbork Synthesis Radio Telescope (WSRT), showed that it is possible to constrain the cosmic H I gas density, Ω_{HI}, of the Universe up to look-back times 2-4 Gyr with H I stacking. Intriguingly, these studies have begun to bridge the gap between high-z damped Lyman-α observations and blind 21-cm surveys at $z = 0$ (Fig. 1). Determining Ω_{HI} is especially critical at these intermediate redshifts when the cosmic star formation rate density plummeted.

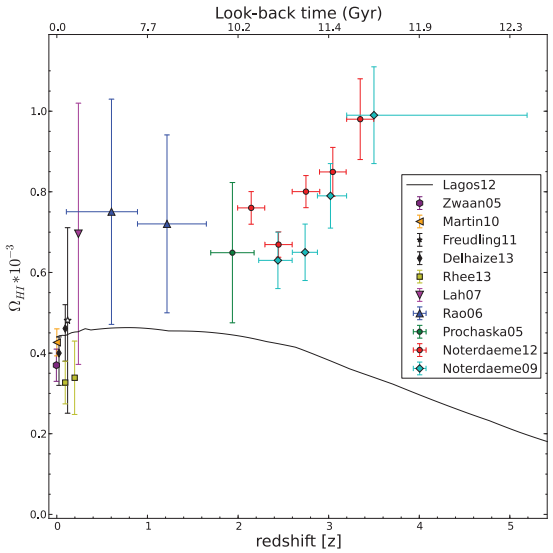

Figure 1: Recent compilation of cosmic H I gas density measurements as functions of redshift and look-back time. At z=0, the hexagon and triangle refer to direct observations from blind H I surveys (Zwaan et al. (2005); Martin et al. (2010)). All points above $z = 0.4$ are damped Ly-α measurements from HST and SDSS (Prochaska et al. (2005); Rao et al. (2006); Noterdaeme et al. (2009, 2012)). Bridging the gap between the two are the estimates from H I stacking of Parkes (diamonds)(Delhaize et al. (2013), WSRT (yellow squares) (Rhee et al. (2013)) and GMRT (magenta triangle) (Lah et al. (2007)) observations. The curve represents model predictions by Lagos et al. (2012).

Stacking is also extremely promising for galaxy evolution studies in general, as a means to investigate the connection between gas, star formation rate, and other galaxy properties across environment and time. Application of the stacking technique to a sample of ∼5000 optically-selected galaxies with H I observations from ALFALFA has successfully recovered the main scaling relations connecting the gas fractions of galaxies with their structural and star formation properties (Fabello et al. (2011)) and the effects of environment on gas content (Fabello et al. (2012)). Because of the large statistics needed for these studies, and because of the need to reach the gas-poor regime, this question is optimally addressed by H I stacking, rather than by individually detected galaxies. Environmental effects on the gas have also been investigated at much greater distances, using H I stacking at $z \sim 0.2$ (Verheijen et al. (2007)) and $z = 0.37$ (Lah et al. (2009)).

PoS(AASKA14)128

Clearly, the upcoming H I surveys with the SKA and its pathfinders will allow us to extend all these studies to significantly higher redshifts, and to vastly larger optically-selected samples than is possible today. H I stacking will be a very powerful technique to exploit the next-generation H I surveys, well beyond the limits imposed by individual detections.

2.2 Recent theoretical advances

The two most widely used techniques to study galaxy formation in a cosmological context are hydrodynamical simulations and semi-analytical models (SAMs). Hydrodynamical simulations follow the evolution of both the dark matter and baryons (gas and stars) simultaneously, while SAMs evolve the baryons in a pre-computed (usually by an *N*-body simulation) dark matter background. These approaches are complementary: both approximate the key physical processes that are fundamental to galaxy formation, such as star formation and feedback, but hydrodynamical simulations directly solve the equations of gas dynamics and the gravitational interactions between the gas, stars and dark matter, whereas SAMs must approximate them. SAMs are computationally inexpensive, can model galaxy populations in cosmological volumes over cosmic time, and can be used to explore the parameter space of galaxy formation rapidly. In contrast, hydrodynamical simulations are computationally expensive but can capture the detailed spatial, kinematical and dynamical structure of gas, stars, and dark matter in galaxies within individual systems or in small volumes, and can be used to inform the choice of physically motivated recipes used in SAMs. Both approaches have shown substantial progress in the treatment of gas phases in and outside galaxies in the last $\sim$5 years.

Hydrodynamical simulations have witnessed important advances in the treatment of the interstellar medium (ISM) in galaxies and in metal enrichment of the circumgalactic medium (CGM). *Non-cosmological simulations* of galaxy formation have been used to study in detail processes such as H_2 formation and destruction, the H I to H_2 transition in non-equilibrium chemistry, non-equilibrium thermal state, and variations in the strength of the radiation field (e.g. Pelupessy et al. 2006, 2009; (Robertson & Kravtsov (2008); Gnedin et al. (2009); Dobbs et al. (2011); Shetty & Ostriker (2012); Glover & Clark (2012); Christensen et al. (2012)). This work has allowed for physical interpretation of the observed relation between the SFR and the H_2 mass surface densities observed in local galaxies. Another important area of progress has been in exploration of the mechanisms that drive turbulence in the ISM. (Dobbs et al. (2011) simulated a large spiral galaxy and showed that stellar feedback is important in setting the scale height of the galaxy disk through its effect on the velocity dispersion. Similarly, Shetty & Ostriker (2012) find that supernovae are the primary source of turbulence in the dense environments of starburst galaxies. However, Bournaud et al. (2010) found in their simulation of a LMC-like dwarf galaxy that gravitational instabilities – which drive the velocity dispersion in their simulation – rather than stellar feedback set the scale height, while stellar feedback is necessary to maintain large-scale turbulence, which initiates cascades to small scales and suppresses the formation of very dense, small gas clumps (see also Hopkins et al. (2013) and Shetty & Ostriker (2012)). In *cosmological hydrodynamical simulations*, the transition from H I to H_2 has an important effect on the predicted number of large column density absorbers, $N_{\rm H} > 7 \times 10^{21}\,{\rm cm}^{-2}$ (Altay et al. (2011)). Extensive testing of the relation between galaxies and H I absorbers at high redshifts has been presented by Rahmati & Schaye (2014), who reach con-

PoS(AASKA14)128

clusions similar to SAMs (Lagos et al. (2011, 2014); Popping et al. (2014); Fu et al. (2012)), that a large fraction of the damped Ly-α absorbers are associated with galaxies with stellar masses $M_\star < 10^9 M_\odot$ (see also Davé et al. (2013); Bird et al. (2014); Rafieferantsoa et al. (2014)).

In *semi-analytical models* of galaxy formation, significant effort has focused on improving the modelling of the ISM in galaxies. Whereas previous generations of models followed the evolution of only a single cold gas phase (Obreschkow et al. (2009b); Power et al. (2010)), current models partition this cold gas phase into H I and H_2 phases and follow the evolution of these phases in a self-consistent manner (e.g. Cook et al. (2010); Fu et al. (2010); Lagos et al. (2011); Popping et al. (2014)). These models assume gas in hydrostatic and chemical equilibrium and use either the empirical relation of (Blitz & Rosolowsky (2006)), which relates the H_2/H I gas surface density ratio to the local hydrostatic pressure, or theoretical relations that calculate H_2 abundance as a result of the equilibrium between rates of destruction due to UV radiation and formation on dust grains (e.g. (Krumholz et al. (2009); Gnedin & Kravtsov (2011)). Models based on the empirical relation of Blitz & Rosolowsky appear to provide a better fit to the z=0 H I mass function (Zwaan et al. (2005); Martin et al. (2010)), with good agreement extending down to H I masses of $10^6 M_\odot h^{-2}$ (Lagos et al. (2011), and also reproduce the observed clustering of H I selected galaxies (Kim et al. (2012)).

One of the key results of SAMs is shown in Fig. 1, which shows the very mild evolution of Ω_{HI} from $z = 2$ to $z = 0$. This prediction relates to a key question in extragalactic astrophysics: what accounts for the dramatically different evolution of the star formation rate (SFR) and H I densities of the Universe. Lagos et al. (2011) and Lagos et al. (2014) argue that the steep decline observed in the SFR density with decreasing redshift is closely connected to the steep decline of the molecular gas density – because star formation is linked explicitly to the H_2 density in galaxies – whereas the H I density is predicted to evolve very weakly with redshift. Lagos et al. explain this trend as arising from a combination of decreasing gas fractions and increasing galaxy sizes with decreasing redshift, both of which act to reduce gas surface density and the hydrostatic pressure of the disk, which controls the rate at which stars form. Therefore, the SFR density evolution reflects the evolution of the surface density of gas in the galaxies that dominate the SFR in the universe as a function of cosmic time (see also Obreschkow & Rawlings (2009)). This interpretation also implies an increase in the molecular to dynamical mass ratios and H_2/H I mass ratio with increasing redshift, which is consistent with observations (Geach et al. (2011); Tacconi et al. (2013)).

Recent progress in the simulation and modelling of galaxy formation has been rapid, and has emphasized the critical role H I plays in driving galaxy formation and evolution. This work has also highlighted how *pivotal H I surveys on the SKA and its pathfinders will be* in revealing the full extent of this role, how they will make a crucial contribution to multi-wavelength surveys campaigns, and how they will provide – arguably – the most powerful tests of the predictions of our theories of galaxy formation and evolution. For example, simulations make clear predictions for the expected relation between galaxy properties (such as stellar mass and SFRs), environment (measured by halo mass and also clustering) and H I content (Lagos et al. 2011, 2014, Davé et al. (2013); Kim et al. (2013); Rahmati & Schaye (2014)), as well as the clustering of H I selected galaxies at different H I masses and cosmic times. These measurements will be partially accessible with the ASKAP and MeerKAT pathfinders, but it will be with SKA1 that the most complete and powerful tests will be made.

PoS(AASKA14)128

2.3 Upcoming SKA pathfinder H I surveys

Various H I surveys are planned for the SKA pathfinder instruments MeerKAT, ASKAP and APERTIF over the next 5–7 years, ranging from deep observations of particular galaxies or clusters to very wide-area, relatively shallow surveys to narrow, deep surveys. A summary of the science aims and specifications for those surveys focusing on galaxy evolution is presented in Table 1.

BLIND H I SURVEYS: WIDE-AREA vs. DEEP **Main aims:** To investigate: - Evolution of H I content (H I mass function) of galaxies vs. z and environment - Galaxy formation & missing satellite problem in Local Group - Correlation of H I properties of galaxies and with stellar/halo masses, star-formation rates, etc. - Physics governing cool gas distribution & evolution at low z - Baryonic Tully-Fisher relation vs. z - Cosmological parameters relating to gas-rich galaxies - Cosmic web	
CHILES (JVLA) [*ongoing*]	**Specifications:** Single pointing in COSMOS field, for $z < 0.45$
Medium-deep blind imaging (APERTIF) [*proposed*]	**Specifications:** $z < 0.25$ over 500 deg^2
Northern sky H I shallow survey (APERTIF) [*proposed*]	**Specifications:** $\delta > +27°$, $0 < z < 0.26$
WALLABY (ASKAP) [*approved*]	**Specifications:** $-90° < \delta < +30°$, $z < 0.26$
DINGO (ASKAP) [*approved*]	**Specifications:** 2 Phases: DEEP: $z < 0.26$ over 150 deg^2 UDEEP: $0.1 < z < 0.43$ over 60 deg^2
LADUMA (MeerKAT) [*approved*]	**Specifications:** Single pointing encompassing ECDF-S, $z < 1.4$ over $\sim$4 deg^2,
H I SURVEYS OF INDIVIDUAL GALAXIES / CLUSTERS **Main aims:** To investigate: - The range of conditions in ISM in local galaxies - The gas-cycle in nearby galaxies by probing high vs. low column density regions - The connection to local cosmic web - Gas-stripping processes in clusters - H I content vs. galaxy morphological type	
MHONGOOSE (MeerKAT) [*approved*]	**Specifications:** 30 nearby galaxies with $10^5 < M_{HI} < 10^{10} M_\odot$, $N_{HI}(5\sigma) \sim 10^{19}$ cm^{-2}
Fornax H I survey (MeerKAT) [*approved*]	**Specifications:** Fornax cluster galaxies over 11 deg^2 down to $M_{HI}(3\sigma) \sim 5 \times 10^5 M_\odot$, $N_{HI}(5\sigma) \sim 10^{19}$ cm^{-2}

Table 1: Overview of upcoming H I emission line surveys on SKA pathfinder facilities, APERTIF [Medium-deep blind imaging survey, Northern sky H I shallow survey (Verheijen et al. (2009))], ASKAP [WALLABY and DINGO] (Duffy et al. (2012)) and MeerKAT [LADUMA (Holwerda et al. (2012)), MHONGOOSE (mhongoose.astron.nl) and the Fornax H I survey (Serra (2011))].

PoS(AASKA14)128

This table is meant to be a summary of H I line work to be carried out in the next 5–10 years which will form a solid basis for further work (more detailed and sensitive studies of selected objects and areas and pushing knowledge of H I in and around galaxies to higher redshifts with the increased collecting area of SKA1 and eventually the SKA2). The SKA2 will not only be capable of providing optical quality ($\sim$ 1" resolution) H I images of Milky Way size galaxies at $z = 1$, but will also have the survey speed to carry out the billion galaxy survey that will chart out the large scale structure of the Universe from $z = 0$ to $z = 3$ and allow precision cosmology studies (Myers et al. (2009)).

3. Probing galaxy evolution with the SKA

Once SKA1 comes online, the various surveys mentioned above will have pushed our knowledge of H I in galaxies and its role in galaxy evolution to a situation where we have a good inventory of detailed knowledge of the nearby universe. Shallow surveys will have covered most of the sky out to $z \sim 0.25$ (Duffy et al. (2012)) and provided H I masses of half a million galaxies, of which several tens of thousands of galaxies will be reasonably well resolved. Deeper surveys will have pushed to $z \sim 0.6$, but lack the detailed information needed to characterize the physical processes that govern galaxy evolution from the H I point of view: gas accretion, gas removal by winds, ram pressure or tidal stripping. Such details are also an important ingredient for comparisons with and input to the advanced modelling described in section 2.2. The obvious next steps are to obtain more sensitive and more detailed observations in the nearby universe ($0 < z < 0.25$) for characterizing these processes and to push single-galaxy H I mass detections to larger distances and lower H I masses to explore the dependence on cosmic time and environment of the H I mass function and other scaling relations. In the following subsections, we briefly describe these science goals in more detail.

3.1 The H I mass function

The H I mass function (Rao & Briggs (1993)) is one of the most important statistical measures for gas-rich galaxy populations. It describes the volume density of galaxies as a function of H I mass and is therefore the neutral hydrogen equivalent of the optical luminosity function. One important use of the H I mass function in the context of galaxy evolution is its second moment, which gives the cosmic H I mass density: the number of neutral hydrogen atoms per unit volume. This is an important input into the understanding of the evolution of the cosmic star formation rate density. When combined with damped Ly α measurements at higher redshifts (e.g., Noterdaeme et al. 2012, and references therein), the evolution of the H I mass density can be charted and compared to models of gas and galaxy evolution. The H I mass density can be compared with the predictions of semi-analytic or hydrodynamic models in order to study the processes governing the distribution and evolution of cool gas (e.g., Obreschkow & Rawlings (2009), Lagos et al. 2011).

Of equal importance is the *shape* of the H I mass function. For example, Kim et al. (2012) demonstrate that the H I mass function is a more sensitive probe of cosmological reionization for galaxy formation than the optical galaxy luminosity function. For semi-analytic models, the H I mass function shape at $z = 0$ is an indispensable constraint (Obreschkow & Rawlings (2009), Lagos et al. 2010, Neistein et al. 2010, Kim et al. 2011). The H I mass function puts additional limits

PoS(AASKA14)128

on the models compared to, e.g., the stellar mass function because the correlation between halo mass and cold gas mass is very different from that between halo mass and stellar mass (the most gas-rich galaxies often have low halo mass). Furthermore, Kim et al. (2012) show how different star formation laws affect the shape of the H I mass function.

The H I mass function has been well measured for the Local Universe (Zwaan et al. (2005); Martin et al. (2010); however, controversy still surrounds the magnitude and sign of the environmental density dependence of the H I mass function, possibly due to depth and cosmic variance issues with existing shallow surveys (Zwaan et al. (2005); Springob et al. (2005)). Upcoming precusor surveys such as WALLABY, will detect galaxies over a $\sim$100 times larger volume and will therefore be much less sensitive to cosmic variance, enabling detailed study of the variation of the H I mass function with environmental density. The deeper HI pathfinder surveys such as DINGO and LADUMA will enable measurement of the H I mass function to intermediate redshifts, $z < 0.6$.

With the SKA, it will be possible to push measurements of the H I mass function to even higher redshifts ($z \sim 1$), which will in turn place even more stringent constraints on galaxy evolution models (see Fig. 2). It will also allow us to probe the evolution of the cosmic neutral gas density, Ω_{gas}, from H I emission into the redshift range where it is currently estimated using damped Ly-α and magnesium absorber measurements (Prochaska et al. (2005); Rao et al. (2006); Noterdaeme et al. (2009, 2012); Zafar et al. (2013)).

Many questions demanding measurements of the H I masses of galaxies can also be investigated with these observations. As functions of both environment (i.e., field vs group or cluster)(e.g., Hess & Wilcots (2013); Jaffé et al. (2013)) and cosmic time, we will be able to study, for lower H I masses than ever before, the relationships between H I mass and stellar mass, star formation rate, galaxy morphology, etc., as a means to uncover how galaxies evolve over time in different environments.

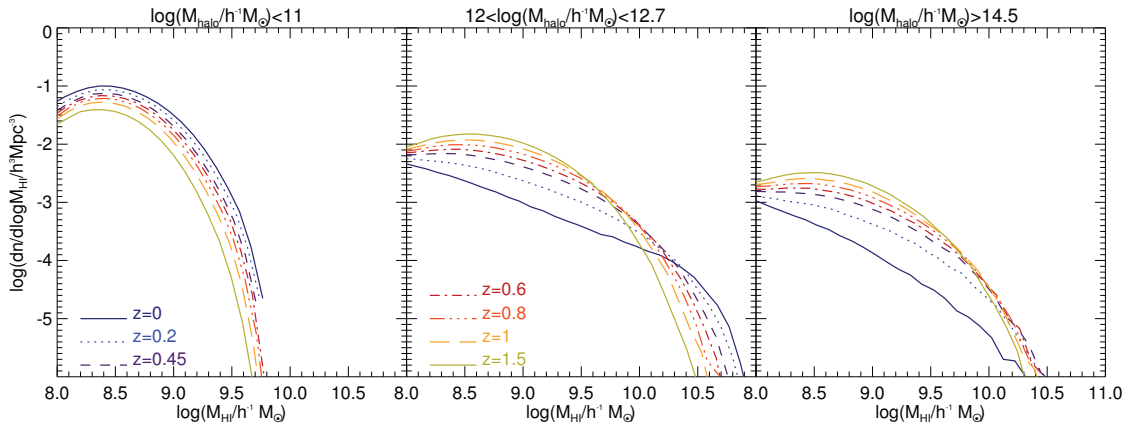

Figure 2: Models from Lagos et al. (2012) showing evolution of the H I mass function with redshift and halo mass. Halo mass bins correspond to field (left panel), group (middle panel), and cluster (right panel) environments.

PoS(AASKA14)128

3.2 Using H I to probe gas inflow and removal

Galaxies form and evolve via the acquisition of gas from the intergalactic medium (IGM). In star-forming (blue cloud) galaxies, gas infall is expected to occur over a Hubble time to keep them forming stars at a relatively high rate (Fraternali & Tomassetti (2012)). Indirect evidence for gas infall comes from estimates of gas depletion times (Bigiel et al. (2011)), the reconstruction of star formation histories (Panter et al. (2007)), and chemical evolution models of the Milky Way (Schönrich & Binney (2009). However, at present the observational evidence for gas inflow into galaxies is rather scant, and it is not clear how and in what form it takes place (Sancisi et al. (2008)).

Inflow of gas into galaxies has a long history dating back to the discovery of the high-velocity clouds (HVCs) in the Milky Way (Wakker & van Woerden (1997)). To date, the origin of these clouds remain a mystery, and their contribution to the feeding of the Galactic star formation is uncertain (Putman, et al. (2012)). Deep HI observations of external galaxies also show similar features in HI (Westmeier et al. (2005)). Fig. 3 shows examples of massive clouds/filaments observed in projection over the bright optical disk of three nearby galaxies. These filaments/complexes are well separated in velocity from the H I in their disks. These structures have H I masses similar to that of the Galactic HVC Complex C. It is unlikely that they result from a galactic fountain and they may be the signs of either minor mergers or the infall of cosmological filaments (Fernández, Joung, & Putman (2012)).

The typical sensitivities achieved with the current interferometers for deep HI observations like those of NGC 2403 (Fraternali et al. (2002)) are of order 10^{19}cm^{-2}. SKA will improve this sensitivity by 2 orders of magnitude, keeping the spatial resolution very high. This will have a tremendous impact on our understanding of gas inflow, as we will finally be able to trace the origin of these structures and detect gas falling into galaxies from the IGM. At present, the only information about low column density material around galaxies comes from absoption line studies towards AGNs. From the study of Lyα absorbers, it is clear that there are vast reservoirs of *cold* gas surrounding both star-forming and early type galaxies (Tumlinson et al. (2013)). However their origin, morphology, and fate are not clear; for instance whether they are gas clouds falling into the galaxies or simply floating in the galactic coronae remains ambiguous. This can be explored with the SKA.

Galaxies also eject gas from their disks as a consequence of stellar winds and supernova explosions. The ejected gas is likely multiphase but a large fraction of it is likely cold (Melioli et al. (2009)) or will cool rapidly (Houck & Bregman (1990)). Observations show HI at large distance from the Milky Way's disk associated with superbubble expansion (Pidopryhora et al. (2007)) and gas at high velocities escaping from holes in the disks of external galaxies (Boomsma et al. (2008)).

Such HI outflows produce large layers of extra-planar gas that contain typically 10% of the HI mass of a galaxy, reaching up to 25% in exceptional cases (Oosterloo et al. (2007); Sancisi et al. (2008)). The study of the kinematics of H I halos gives essential information about the exchange of material and angular momentum between galactic disks and the IGM (Marinacci et al. (2010)). However, at the moment, the overall picture is not understood, as these low column density features are not seen around all galaxies and in several cases are not very extended (Heald et al. (2011)). Going down to a sensitivity well below $\times 10^{18}$ cm^{-2} will provide unprecented information about gas escaping from galaxies and how this interacts with the surrounding medium. With SKA2 we

PoS(AASKA14)128

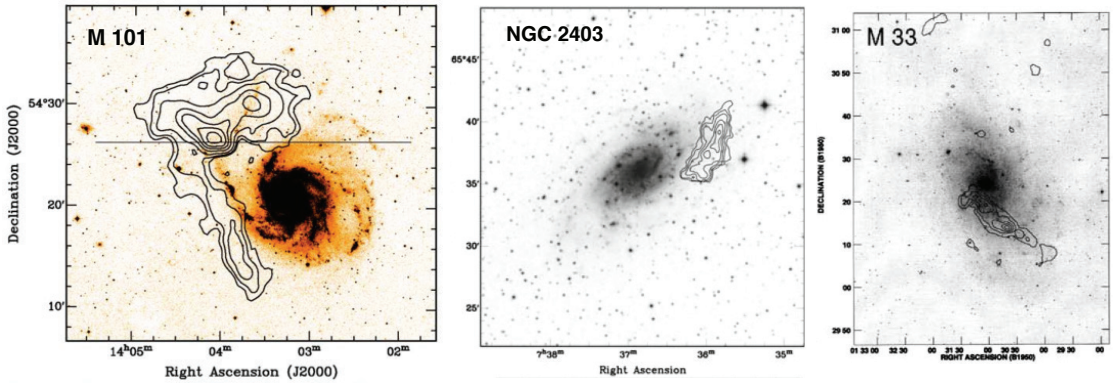

Figure 3: Three examples of possible accretion of H I in nearby spirals indicated by the presence of gas complexes at anomalous velocities: M 101 (van der Hulst & Sancisi (1988)), NGC 2403 (Fraternali et al. (2002)), and M 33 (Sancisi et al. (2008)).

will eventually be able to fully trace the gas cycle from disks to the IGM and understand its crucial role for the evolution of star-forming galaxies.

Gas can also be removed from galaxies via tidal interactions (Sancisi et al. (2008)) and ram pressure stripping in galaxy clusters (Kenney et al. (2004), see also Fig. 4). At the moment, these observations are limited to very few cases of mostly very massive structures (Oosterloo & van Gorkom (2005)) although H I deficiencies are also found in small but dense environments, such as Hickson compact groups (Verdes-Montenegro et al. (2001)). SKA will change this dramatically, giving the possibility to study tidal interactions and minor mergers in unprecentedly large galaxy samples. We will be able to investigate the prevalence of these phenomena, the accretion and removal rates from interaction and how all these properties change as a function of environment and time. The study of gas removed from galaxies in dense environments will also finally solve the problem of star formation quenching, something that is considered of fundamental importance for the migration of star-forming galaxies towards the red sequence (Blanton & Moustakas (2009)).

3.3 The TF relation

The Tully-Fisher relation (TFr), originally describing a correlation between a galaxy's intrinsic luminosity and the distance-independent width of its global H I profile (Tully & Fisher (1977)), is the most important observed scaling relation for gas-rich, late-type galaxies. Although the TFr is empirical in nature, it seems astrophysically plausible that a galaxy's luminosity, as a proxy for its stellar mass, should be related to its gravitational potential as traced by the rotation speed of its gas disk, observed through the Doppler-broadened width of its H I emission line. The presence of dark matter and the detailed distribution of the visible mass inside galaxies complicate this naive interpretation (Zwaan et al. (1995)). Nevertheless, the TFr serves as a valuable tool to obtain distances to galaxies in the local universe where peculiar velocities dominate over the Hubble flow (Tully & Courtois (2012)), while its statistical properties constrain semi-analytical and hydrodynamical simulations of galaxy formation and evolution. Studies of the detailed H I kinematics of regularly-rotating galaxies for which the extended H I gas disk is a proper tracer of the gravitational potential, and for which good estimates of their relative stellar masses are available, indicate that the TFr is

PoS(AASKA14)128

fundamentally a correlation between the maximum rotational velocity of the dark matter halo and the embedded total baryonic mass, regardless of how this baryonic mass is distributed (McGaugh et al. (2000); Verheijen (2001); McGaugh (2005)).

Major advances in photometric imaging technologies have significantly improved our measures and understanding of a galaxy's luminosity to an extent that, combined with spectroscopic information, it has become common practice to replace a galaxy's luminosity in the TFr by its derived stellar mass, or even its baryonic mass when taking the atomic and estimated molecular gas masses into account (McGaugh (2005); Zaritsky et al. (2014)). Improving our understanding of the width of the global H I line as a kinematic measure has received little attention so far, and even the most recent studies still use this quantity (Sorce et al. (2013); Zaritsky et al. (2014)). As galaxies are usually not spatially resolved by single-dish radio telescopes, the shape and width of the global H I profile is the result of a convolution of the detailed distribution of the H I gas in a galaxy with the detailed geometry and kinematics of the gas disk, including possible warps, streaming motions, asymmetries and the overall shapes of rotation curves, which may not always be monotonically rising to a constant circular velocity (Bosma (1981a,b); Begeman (1989); Casertano & van Gorkom (1991); Verheijen & Sancisi (2001); Noordermeer et al. (2007); Swaters et al. (2009)). Hence, the width of the global H I profile is only a proxy for the rotational speed of a galaxy, while the latter may not even be properly defined and identified for non-flat rotation curves, and trends in rotation curve shapes along the TFr may introduce significant biases in scatter and slope (Verheijen (2001); Noordermeer & Verheijen (2007)). Imaging the geometry and kinematics of a galaxy's extended H I disk with interferometers is the only observational avenue to identify the relevant kinematic measure for the TFr and to significantly improve our understanding of the underlying astrophysics.

It is expected that upcoming H I imaging surveys with ASKAP, WSRT/APERTIF and MeerKAT will further reduce the observed scatter in the TFr by spatially resolving the H I kinematics thereby improving TF-based distances to galaxies in the local universe. These imaging surveys will also establish the statistical properties of the TFr at modest redshifts ($z < 0.2$) using spatially resolved H I kinematics, and up to $z < 0.5$ using global H I line widths. It is unlikely that the SKA will significantly improve upon these studies. However, given the anticipated sensitivity and angular resolution of the SKA, it will be possible to exploit the TFr to study the evolution of galaxies over cosmic time by investigating the slope, scatter and zero-point as a function of redshift and cosmic environment, as well as global galaxy properties such as morphological type and (specific) star formation rate. This requires adequate angular resolution and column density sensitivity to image the H I kinematics in the outer gas disks of galaxies at higher redshifts, as well as survey volumes that encompass all cosmic environments with sufficient statistical significance to mitigate cosmic variance. In order to assess the kinematical state of the largest H I disks in M^*_{HI} galaxies at a redshift of $z = 0.5$, a spatial resolution of 10 kpc would be sufficient, corresponding to an angular resolution of 1.6 arcseconds at a frequency of 950 MHz. Based on studies of nearby galaxies, the required column density sensitivity at this angular resolution would need to be $\sim 5 \times 10^{20}$ [cm^{-2}]. This could be achievable with an ultra-deep survey using SKA1-MID but seems out of reach for SKA-SUR. The volume surveyed by a single SKA1-MID pointing at $z = 0.5$ at 950 MHz is large enough to sample all cosmic environments with a sufficient number of detections to provide adequate statistics on the TFr. Pushing TFr studies based on resolved H I kinematics to even higher redshifts would require the power of SKA2, in particular given the required column density sensitivities.

PoS(AASKA14)128

4. SKA HI Strawman Surveys

4.1 Survey scenarios and requirements

The science goals outlined in section 3 should lead us to define the most efficient observing strategies for obtaining the data, given the the technical capabilities of the SKA, in the first phase and eventual final form. A review of the science addressed in section 3 makes clear immediately that it is of the greatest importance not only to have a sufficiently large number of objects for statistical studies probing different regions of the universe, both spatially and in cosmic time, but also to have the appropriate linear resolution and column density sensitivity to probe the phenomena of interest. For studies involving the H I mass function, it is important to push the detection limit to objects with small H I masses ($< 10^7$ M$_\odot$) without having to resolve the H I distributions. For all other science goals it is extremely important to resolve the galaxies and be able to detect H I column densities to levels well below $N_{\rm HI} \sim 10^{21}$cm^{-2}. This is beautifully illustrated in Fig. 4.

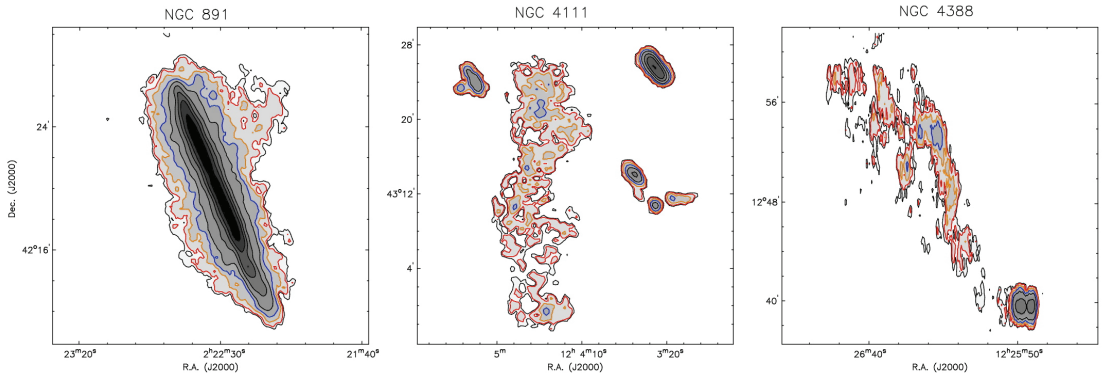

Figure 4: Three examples of galaxies undergoing gas accretion and gas removal events. From left to right: NGC891 (Oosterloo et al. (2007)), NGC4111 (Verheijen (2004)), and NGC4388 (Oosterloo & van Gorkom (2005)). The lowest contours levels are 2×10^{20}cm^{-2} (red), 5×10^{20}cm^{-2} (orange) and 10×10^{20}cm^{-2} (blue). It is clear that the signs of gas accretion (NGC891, NGC4111) and of gas stripping (NGC4388) require column density sensitivities of well below 10^{21}cm^{-2}.

Using the specifications of the SKA baseline design (Dewdney (2013)), one can derive the observing parameters required to reach a depth of $N_{\rm HI} \sim 10^{20}$cm^{-2} at reasonable resolution. Table 2 provides basic input to these considerations. The numbers are based on the latest sensitivity estimates for SKA1-MID, SKA1-SUR and SKA2. Table 2 provides information for four different resolutions because $N_{\rm HI}$ sensitivity scales with resolution. The corresponding linear resolution is given for two nominal distances. In addition, Table 2 gives the H I mass limits for a 10 hour integration assuming a profile width of 50 km s^{-1} for three nominal distances. For reference, the canonical value for $M^*_{\rm HI}$ is $\sim 8 \times 10^9$ M$_\odot$(Zwaan et al. (2003, 2005); Haynes et al. (2011)).

It is clear that in order to design the right surveys for the science described in this chapter, trade-offs need to be made between resolution, integration time, and area covered. Table 3 provides an attempt to do this for SKA1. Survey areas are chosen such that the total integration time remains realistic, while the appropriate resolution and column density are chosen to match the science goals outlined in the previous sections. For example, a survey of the entire southern sky to a depth of

PoS(AASKA14)128

Table 2: SKA sensitivity limits (5 sigma) for HI emission

SKA1-MID t=10h

Resolution (")	d (z=0.2) (kpc)	d (z=0.5) (kpc)	rms noise mJy dV=5 km/s	5 sigma N(HI) dV=5 km/s	5 sigma N(HI) dV=25 km/s	5 sigma M(HI) dV=50 km/s z=0.02	5 sigma M(HI) dV=50 km/s z=0.2	5 sigma M(HI) dV=50 km/s z=0.5
1	3.3	6.1	0.141	3.92E+21	1.96E+22	1.20E+07	1.56E+09	1.32E+10
3	9.8	18.4	0.118	3.65E+20	1.83E+21	1.00E+07	1.31E+09	1.10E+10
10	32.8	61.2	0.091	2.53E+19	1.26E+20	7.72E+06	1.01E+09	8.50E+09
30	98.3	183.7	0.095	2.95E+18	1.47E+19	8.11E+06	1.06E+09	8.92E+09

SKA1-SUR t=10h

Resolution (")	d (z=0.2) (kpc)	d (z=0.8) (kpc)	rms noise mJy dV=5 km/s	5 sigma N(HI) dV=5 km/s	5 sigma N(HI) dV=25 km/s	5 sigma M(HI) dV=50 km/s z=0.02	5 sigma M(HI) dV=50 km/s z=0.2	5 sigma M(HI) dV=50 km/s z=0.5
1	3.3	6.1	0.551	1.06E+22	5.28E+22	4.67E+07	6.11E+09	5.14E+10
3	9.8	18.4	0.361	9.96E+20	4.98E+21	3.06E+07	4.00E+09	3.37E+10
10	32.8	61.2	0.323	1.00E+20	5.01E+20	2.74E+07	3.58E+09	3.02E+10
30	98.3	183.7	0.588	1.88E+19	9.38E+19	5.00E+07	6.53E+09	5.50E+10

SKA2 t=10h

Resolution (")	d (z=0.2) (kpc)	d (z=0.8) (kpc)	rms noise mJy dV=5 km/s	5 sigma N(HI) dV=5 km/s	5 sigma N(HI) dV=25 km/s	5 sigma M(HI) dV=50 km/s z=0.02	5 sigma M(HI) dV=50 km/s z=0.2	5 sigma M(HI) dV=50 km/s z=0.5
1	3.3	6.1	0.009	2.53E+20	1.26E+21	7.64E+05	9.99E+07	8.41E+08
3	9.8	18.4	0.009	2.81E+19	1.40E+20	7.64E+05	9.99E+07	8.41E+08
10	32.8	61.2	0.009	2.53E+18	1.26E+19	7.64E+05	9.99E+07	8.41E+08
30	98.3	183.7	0.009	2.81E+17	1.40E+18	7.64E+05	9.99E+07	8.41E+08

Table 3: Strawman SKA1 surveys

	Shallow survey	**Medium deep survey**	**Deep survey**	**Ultra Deep Survey**
Area	10000 deq^2	2000 deq^2	150 deq^2	2 deq^2
Integration time	1 yr (Sur)	1 yr (Sur)	1 yr (Sur)	1 yr (Mid)
Resolution	10"	5"	3"	2"
***z* (M_{HI}*)**	0.27	0.37	0.69	1.7
mean *z*	0.08	0.11	0.19	0.37
nr. of detections	2.02E+06	1.20E+06	4.60E+05	4.20E+04

$N_{\rm HI} \sim 10^{20}$ at a resolution of 2" would take half a century with SKA1, so a better approach is to cover a smaller area at lower but still useful resolution, leaving substantial improvement on a large H I survey such as WALLABY to SKA2. Which surveys cover substantial gound in redshift space is very well illustrated in Fig. 5, showing the distribution over redshift of the four surveys from Table 3. The distributions represent five statistically independent realisations of a 100 deg^2 sky model, truncated to $z = 1.2$, based on the S3-SAX simulation (Obreschkow et al. (2009a,b)) using the telescope simulations of Popping et al. (2014) which are consistent with the sensitivity calculations used here. In other words SKA1 is the appropriate instrument for addressing follow-up science from the SKA pathfinders; SKA2 provides a major step towards pushing our observing capabilities to higher redshifts, i.e., look back times. In order to obtain a good census of galaxy evolution and the influence of the environment over cosmic time, one has to design surveys in such a way that SKA1 probes the epochs $0.1 < z < 0.5$ with similar linear resolution and $N_{\rm HI}$ sensitivity as APERTIF, ASKAP and MeerKAT will probe at $0.02 < z < 0.2$, while SKA2 will eventually provide the data required to get the full picture of H I evolution from the current epoch to $z \sim 2$ when the star formation rate density in the evolving universe is at its peak.

5. Summary and conclusions

Our current H I view of the universe is restricted to the Local Volume and hence only informs

PoS(AASKA14)128

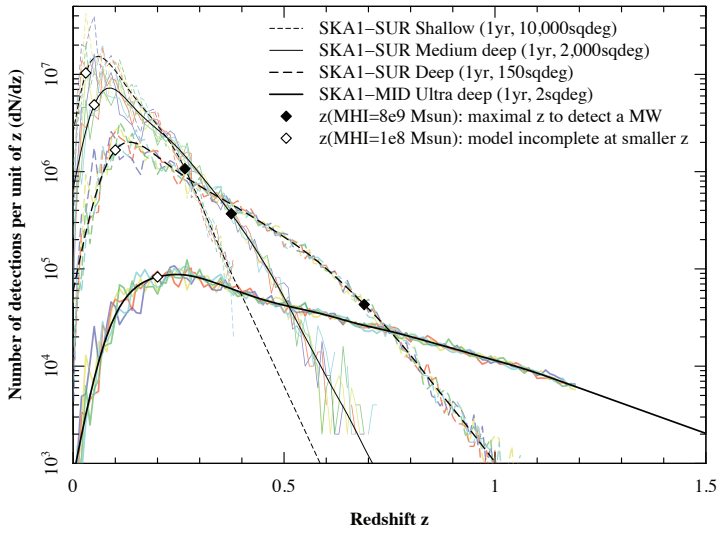

Figure 5: Distribution over redshift of the four surveys given in Table 3 based on the S3-SAX simulation (Obreschkow et al. (2009a,b))

us about gas-related processes in galaxies in a late state of their cosmic evolution. Semi-analytical and hydrodynamical models, however, suggest significant changes in the H I properties of galaxies beyond the Local Universe. We are poised to start testing these models with upcoming surveys on the SKA pathfinder instruments over the next few years. These facilities will provide much improved statistics on the H I properties of galaxies and will begin to open a window on the H I universe beyond the Local Volume. The SKA1 (and eventually SKA2) will truly revolutionise studies of H I in galaxies by enabling observations at higher angular resolutions and with sensitivities that are an order of magnitude greater than currently possible. Most importantly, the SKA1 will allow us to reach out to distances and lookback times spanning more than half the age of the universe. Combined with data at other wavelengths and detailed theoretical models, H I observations with the SKA1 will enable us to trace the baryon cycle in galaxies from the IGM and back out again in different environments. The SKA2 offers the exciting prospect of directly measuring the HI masses of the nearest Lyman limit systems and performing precision cosmology with the billion galaxy survey. Ultimately, we will reveal the evolution of the distribution and kinematics of gas in galaxies back to $z \sim 2$ when the cosmic star formation rate density was at its peak and an order of magnitude higher than the present, thereby building a comprehensive picture of galaxy evolution over cosmic time.

Acknowledgments

We thank various colleagues for valuable input to this chapter. JMvdH acknowledges support from the European Research Council under the European Union's Seventh Framework Programme (FP/2007-2013) / ERC Grant Agreement nr. 291531. BC is the recipient of an Australian Research Council Future Fellowship (FT120100660). MPH is supported by US-NSF/AST-1107390 and the Brinson Foundation. LVM has been supported by grants AYA2011-30491-C02-0S1 and TIC-114.

PoS(AASKA14)128

References

Acreman, D. M., Dobbs, C. L., Brunt, C. M., & Douglas, K. A. 2012, MNRAS, 422, 241
Altay, G., Theuns, T., Schaye, J., Crighton, N. H. M., & Dalla Vecchia, C. 2011, ApJ, 737, L37
Baldry, I. K., Glazebrook, K., Brinkmann, J., et al., 2004, ApJ, 600, 681
Barnes, D. G., Staveley-Smith, L., de Blok, W. J. G., et al., 2001, MNRAS, 322, 486
Begeman, K. G. 1989, A&A, 223, 47
Begum, A., Chengalur, J. N., Karachentsev, I. D., Sharina, M. E., & Kaisin, S. S., MNRAS, 386, 1667
Beygu, B., Kreckel, K., van de Weygaert, R., van der Hulst, J. M., & van Gorkom, J. H., AJ, 145, 120
Bigiel, F., Leroy, A., Walter, F., et al. 2008, AJ, 136, 2846
Bigiel, F., Leroy, A. K., Walter, F., et al., ApJ, 730, 2011, 13
Bird, S., Vogelsberger, M., Haehnelt, M., et al. 2014, MNRAS, 44, 2313
Blanton, M. R. and Moustakas, J., 2009, ARA&A, 47, 159
Blitz, L., & Rosolowsky, E. 2006, ApJ, 650, 933
Borthakur, S., Yun, M. S., & Verdes-Montenegro, L., 2011, ApJ, 729, 149
Bosma, A., 1981, AJ, 86, 1791
Bosma, A., 1981, AJ, 86, 1825
Bournaud, F., Elmegreen, B. G., Teyssier, R., Block, D. L., & Puerari, I. 2010, MNRAS, 409, 1088
Boomsma, R., Oosterloo, T. A., Fraternali, F., van der Hulst, J. M., and Sancisi, R., 2008, A&A, 490, 555
Calzetti, D., Liu, G., & Koda, J. 2012, ApJ, 752, 98
Cannon, J. M., Giovanelli, R., Haynes, M. P., et al., 2011, ApJ, 739, L22
Casertano, S., & van Gorkom, J. H., 1991,AJ, 101, 1231
Catinella, B., Haynes, M. P., Giovanelli, R., Gardner, J. P., & Connolly, A. J. 2008, ApJ, 685, L13
Catinella, B., Schiminovich, D., Kauffmann, G., et al., 2010, MNRAS, 403, 683
Chengalur, J. N., Braun, R., & Wieringa, M. 2001, A&A, 372, 768
Christensen, C., Quinn, T., Governato, F., et al. 2012, MNRAS, 425, 3058
Chung, A., van Gorkom, J. H., Kenney, J. D. P., Crowl, H., & Vollmer, B., 2009, AJ, 138, 1741
Cook, M., Evoli, C., Barausse, E., Granato, G. L., & Lapi, A. 2010, MNRAS, 402, 941
Cowie, L. L., Songaila, A., Hu, E. M., & Cohen, J. G. 1996, AJ, 112, 839
Davé, R., Katz, N., Oppenheimer, B. D., Kollmeier, J. A., & Weinberg, D. H. 2013, MNRAS, 434, 2645
de Blok, W.J.G., Fraternali, F., Heald, G.H., Adams, E.A.K., Bosma, A., Koribalski, B.S. & the H I Science Working Group, "The SKA view of the Neutral Interstellar Medium in Galaxies", in proc. *Advancing Astrophysics with the Square Kilometre Array*, PoS(AASKA14)129
Delhaize, J., Meyer, M. J., Staveley-Smith, L., & Boyle, B. J. 2013, MNRAS, 433, 1398
Dewdney, P., Turner, W., Millenaar, R., et al., 2013, *SKA1 System Baseline Design*, Document number SKA-TEL-SKO-DD-001 Revision 1
Dobbs, C. L., Burkert, A., & Pringle, J. E. 2011, MNRAS, 417, 1318
Duffy, A. R., Meyer, M. J., Staveley-Smith, L., et al., 2012, MNRAS, 426, 3385
Duffy, A. R., Kay, S. T., Battye, R. A., et al., 2012, MNRAS, 420, 2799

PoS(AASKA14)128

Espada, D., Verdes-Montenegro, L., Huchtmeier, W. K., et al., 2011, A&A, 532, A117
Fabello, S., Catinella, B., Giovanelli, R., et al. 2011, MNRAS, 411, 993
Fabello, S., Kauffmann, G., Catinella, B., et al. 2012, MNRAS, 427, 2841
Feldmann, R., Gnedin, N. Y., & Kravtsov, A. V. 2011, ApJ, 732, 115
Fernandez, X., Joung, M. R., and Putman, M. E., 2012, ApJ, 749, 181
Fernández, X., van Gorkom, J. H., Hess, K. M., et al., 2013, ApJ, 770, L29
Fu, J., Guo, Q., Kauffmann, G., & Krumholz, M. R. 2010, MNRAS, 409, 515
Fraternali, F., van Moorsel, G., Sancisi, R., & Oosterloo, T., 2002, AJ, 123, 3124
Fraternali, F. and Binney, J. J., 2008, MNRAS, 386, 935
Fraternali, F. and Tomassetti, M., 2012, MNRAS, 426, 2166
Freudling, W., Staveley-Smith, L., Catinella, et al., 2011, ApJ, 727, 40
Fu, J., Kauffmann, G., Li, C., & Guo, Q. 2012, MNRAS, 424, 2701
Geach, J. E., Smail, I., Moran, S. M., et al. 2011, ApJ, 730, L19
Geréb, K., Morganti, R., Oosterloo, T. A., Guglielmino, G., & Prandoni, I., 2013, A&A, 558, A54
Giovanelli, R., Haynes, M. P., Adams, E. A. K., et al., 2013, AJ, 146, 15
Giovanelli, R., Haynes, M. P., Kent, B. R., et al., 2005, AJ, 130, 2598
Glover, S. C. O., & Clark, P. C. 2012, MNRAS, 421, 9
Gnedin, N. Y., Tassis, K., & Kravtsov, A. V. 2009, ApJ, 697, 55
Gnedin, N. Y., & Kravtsov, A. V. 2011, ApJ, 728, 88
Haynes, M. P., Giovanelli, R., Martin, A. M., et al., 2011, AJ, 142, 170
Heald, G., Józsa, G., Serra, P., et al., 2011, A&A, 526, A118
Hess, K. M., & Wilcots, E. M. 2013, AJ, 146, 124
Holwerda, B. W., Blyth, S.-L., & Baker, A. J., 2012, IAU Symposium, 284, 496
Hopkins, A. M., & Beacom, J. F. 2006, ApJ, 651, 142
Hopkins, P. F., Hernquist, L., Cox, T. J., Dutta, S. N., & Rothberg, B. 2008, ApJ, 679, 156
Hopkins, P. F., Narayanan, D., Murray, N., & Quataert, E. 2013, MNRAS, 433, 69
Houck, J. C. and Bregman, J. N., 1990, ApJ, 352, 506
Hunter, D. A., Ficut-Vicas, D., Ashley, T., et al., 2012, AJ, 144, 134
Jaffé, Y. L., Poggianti, B. M., Verheijen, M. A. W., Deshev, B. Z., & van Gorkom, J. H., 2013, MNRAS, 431, 2111
Jaffé, Y. L., Poggianti, B. M., Verheijen, M. A. W., Deshev, B. Z., & van Gorkom, J. H., 2012, ApJ, 756, L28
Kenney, J. D. P., van Gorkom, J. H., and Vollmer, B., 2004, AJ, 127, 3361
Kim, H.-S., Lacey, C. G., Cole, S., et al. 2012, MNRAS, 425, 2674
Kim, H.-S., Power, C., Baugh, C. M., et al. 2013, MNRAS, 428, 3366
Koribalski, B. S., 2008, *Galaxies in the Local Volume*, 41
Kreckel, K., Platen, E., Aragón-Calvo, M. A., et al., 2012, AJ, 144, 16
Krumholz, M. R., McKee, C. F., & Tumlinson, J. 2009, ApJ, 699, 850
Lagos, C. D. P., Baugh, C. M., Lacey, C. G., et al. 2011, MNRAS, 418, 1649
Lagos, C. D. P., Lacey, C. G., Baugh, C. M., Bower, R. G., & Benson, A. J. 2011, MNRAS, 416, 1566
Lagos, C. d. P., Bayet, E., Baugh, C. M., et al. 2012, MNRAS, 426, 2142
Lagos, C. D. P., Baugh, C. M., Zwaan, M. A., et al. 2014, MNRAS, 440, 920

PoS(AASKA14)128

Lah, P., Chengalur, J. N., Briggs, F. H., et al. 2007, MNRAS, 376, 1357
Lah, P., Pracy, M. B., Chengalur, J. N., et al. 2009, MNRAS, 399, 1447
Leroy, A. K., Bigiel, F., de Blok, W. J. G., et al. 2012, AJ, 144, 3
Madau, P., Pozzetti, L., & Dickinson, M. 1998, ApJ, 498, 106
Marinacci, F., Binney, J., Fraternali, F., Nipoti, C., Ciotti, L., and Londrillo, P., 2010, MNRAS, 404, 1464
Martin, A. M., Papastergis, E., Giovanelli, R., et al. 2010, ApJ, 723, 1359
McGaugh, S. S., Schombert, J. M., Bothun, G. D., & de Blok, W. J. G., 2000, ApJ, 533, L99
McGaugh, S. S., 2005, ApJ, 632, 859
Melioli, C., Brighenti, F., D'Ercole, A., and de Gouveia Dal Pino, E. M., 2009, MNRAS, 399, 1089
Meyer, M. J., Zwaan, M. A., Webster, R. L., et al., 2004, MNRAS, 350, 1195
Morganti, R., Sadler, E., Curran, S.J. & the HI Science Working Group, "Cool Outflows and HI absorbers with SKA", in proc. *Advancing Astrophysics with the Square Kilometre Array*, PoS(AASKA14)134
Myers, S. T., Abdalla, F. B., Blake, C., et al., 2009, Astro2010: The Astronomy and Astrophysics Decadal Survey, Science White Papers, no. 219
Noordermeer, E., van der Hulst, J. M., Sancisi, R., Swaters, R. A., & van Albada, T. S., 2007, MNRAS, 376, 1513
Noordermeer, E., & Verheijen, M. a. W., 2007, MNRAS, 381, 1463
Noterdaeme, P., Petitjean, P., Ledoux, C., & Srianand, R., 2009, A&A, 505, 1087
Noterdaeme, P., Petitjean, P., Carithers, W. C., et al., 2012, A&A, 547, L1
Obreschkow, D., Klöckner, H.-R., Heywood, I., Levrier, F., & Rawlings, S., 2009, ApJ, 703, 1890
Obreschkow, D., Croton, D., De Lucia, G., Khochfar, S., & Rawlings, S., 2009, ApJ, 698, 1467
Obreschkow, D., & Rawlings, S. 2009, ApJ, 696, L129
Oosterloo, T., Fraternali, F., & Sancisi, R., 2007, AJ, 134, 1019
Oosterloo, T., & van Gorkom, J., 2005, A&A, 437, L19
Ott, J., Stilp, A. M., Warren, S. R., et al., 2012, AJ, 144, 123
Panter, B., Jimenez, R., Heavens, A. F., and Charlot, S., 2007, MNRAS, 378, 1550
Pelupessy, F. I., Papadopoulos, P. P., & van der Werf, P. 2006, ApJ, 645, 1024
Pelupessy, F. I., & Papadopoulos, P. P. 2009, ApJ, 707, 954
Pidopryhora, Y., Lockman, F. J., and Shields, J. C., 2007, ApJ, 656, 928
Pisano, D. J., Barnes, D. G., Gibson, B. K., et al., 2007, ApJ662, 959
Popping, A., Meyer, M., Staveley-Smith, L., Obreschkow, D., Jozsa, G.I., Pisano, D.J. & the HI Science Working Group, "Observations of the Intergalactic Medium and the Cosmic Web in the SKA era", in proc. *Advancing Astrophysics with the Square Kilometre Array*, PoS(AASKA14)132
Popping, G., Somerville, R. S., & Trager, S. C. 2014, MNRAS, 442, 2398
Popping, A., Davé, R., Braun, R., & Oppenheimer, B. D., 2009, A&A, 504, 15
Power, C., Baugh, C. M., & Lacey, C. G. 2010, MNRAS, 406, 43
Prochaska, J. X., Herbert-Fort, S., & Wolfe, A. M. 2005, ApJ, 635, 123
Putman, M. E., Peek, J. E. G., and Joung, M. R., 2012, ARA&A, 50, 2012, 491
Rafieferantsoa, M., Davé, R., Anglés-Alcazar, D., et al. 2014, arXiv:1408.2531
Rahmati, A., & Schaye, J. 2014, MNRAS, 438, 529

PoS(AASKA14)128

Rao, S., & Briggs, F., 1993, ApJ, 419, 515
Rao, S. M., Turnshek, D. A., & Nestor, D. B. 2006, ApJ, 636, 610
Rhee, J., Zwaan, M. A., Briggs, F. H., et al. 2013, MNRAS, 435, 2693
Robertson, B. E., & Kravtsov, A. V. 2008, ApJ, 680, 1083
Ryan-Weber, E. V., Begum, A., Oosterloo, T., et al., 2008, MNRAS, 384, 535
Sancisi, R., Fraternali, F., Oosterloo, T., & van der Hulst, T., 2008, ARA&A, 15, 189
Schiminovich, D., Catinella, B., Kauffmann, G., et al., 2010, MNRAS, 408, 919
Scott, T. C., Sengupta, C., Verdes Montenegro, L., et al., 2014, A&A, 567, A56
Serra, P. 2011, Fornax, Virgo, Coma et al., Stellar Systems in High Density Environments, 49P
Serra, P., Oosterloo, T., Morganti, R., et al., 2012, MNRAS, 422, 1835
Springob, C. M., Haynes, M. P., & Giovanelli, R. 2005, ApJ, 621, 215
Schönrich, R. and Binney, J., 2009, MNRAS, 396, 203
Shetty, R., & Ostriker, E. C. 2012, ApJ, 754, 2
Sorce, J. G., Courtois, H. M., Tully, R. B. et al., 2013, ApJ, 765, 94
Swaters, R. A., Sancisi, R., van Albada, T. S., & van der Hulst, J. M., 2009, A&A, 493, 871
Tacconi, L. J., Neri, R., Genzel, R., et al. 2013, ApJ, 768, 74
Tully, R. B., & Fisher, J. R., 1977, A&A, 54, 661
Tully, R. B.. & Courtois, H. M., 2012, ApJ, 749, 78
Tumlinson, J., Thom, C., Werk, J.K., Prochaska, J.X., Tripp, T.M., Katz, N. et al., 2013, ApJ, 777, 59
van der Hulst, T., & Sancisi, R., 1988, AJ, 95, 1354
van der Hulst, J. M., van Albada, T. S., & Sancisi, R., 2001, Gas and Galaxy Evolution, 240, 451
van der Hulst, J. M., & Blok, W. J. G. d., *The Cool ISM in Galaxies* 2013, Planets, Stars and Stellar Systems. Volume 6: Extragalactic Astronomy and Cosmology, 183
Verdes-Montenegro, L., Yun, M. S., Williams, B. A., et al., 2001, A&A, 377, 812
Verheijen, M. A. W., 2001, ApJ, 563, 694
Verheijen, M. A. W., & Sancisi, R., 2001, A&A, 370, 765
Verheijen, M. A. W., *Galaxy evolution in dense environments: a concise HI perspective* 2004, IAU Colloq. 195: *Outskirts of Galaxy Clusters: Intense Life in the Suburbs*, 394
Verheijen, M., van Gorkom, J. H., Szomoru, A., et al., 2007, ApJ, 668, L9
Verheijen, M., Oosterloo, T., Heald, G., & van Cappellen, W., 2009, Panoramic Radio Astronomy: Wide-field 1-2 GHz Research on Galaxy Evolution
Verheijen, M. et al. 2014, 7th International PHISCC Workshop, *The Challenges of the Upcoming H* I *Surveys*
Wakker, B. P. and van Woerden, H., 1997, ARA&A, 35, 217
Walter, F., Brinks, E., de Blok, W. J. G., et al., 2008, AJ, 136, 2563
Wang, J., Kauffmann, G., Józsa, G. I. G., et al. 2013, MNRAS, 433, 270
Westmeier, T., Braun, R., Thilker, D., 2005, A&A, 436, 101
Wong, O. I., Webster, R. L., Kilborn, V. A., Waugh, M., & Staveley-Smith, L., 2009, MNRAS, 399, 2264
Zafar, T., Péroux, C., Popping, A., et al. 2013, A&A, 556, A141
Zaritsky, D., Courtois, H., Muñoz-Mateos, J.-C. et al., 2014, AJ, 147, 134
Zwaan, M. A., van der Hulst, J. M., de Blok, W. J. G., & McGaugh, S.S., 1995, MNRAS, 273 L35

PoS(AASKA14)128

Zwaan, M. A., Staveley-Smith, L., Koribalski, B. S., et al., 2003, AJ, 125, 2842
Zwaan, M. A., Meyer, M. J., Staveley-Smith, L., & Webster, R. L., 2005, MNRAS, 359, L30
Zwaan, M. A., van der Hulst, J. M., Briggs, F. H., Verheijen, M. A. W., & Ryan-Weber, E. V., 2005, MNRAS, 364, 1467

PoS(AASKA14)128

PROCEEDINGS OF SCIENCE

The SKA view of the Neutral Interstellar Medium in Galaxies

W.J.G. de Blok[*abc], **F. Fraternali**[dc], **G.H. Heald**[ac], **E.A.K. Adams**[a], **A. Bosma**[e], **Bärbel S. Koribalski**[f] **and the H I Science Working Group**

[a] *ASTRON*
Postbus 2, 7990 AA, Dwingeloo, The Netherlands
[b] *Department of Astronomy, Astrophysics, Cosmology and Gravity Centre,*
University of Cape Town, Private Bag X3, Rondebosch, 7701 South Africa
[c] *Kapteyn Astronomical Institute, University of Groningen*
Postbus 800, 9700 AV, Groningen, The Netherlands
[d] *Department of Physics and Astronomy, University of Bologna,*
via Berti Pichat 6/2, I-40127 Bologna, Italy
[e] *Aix Marseille Universite, CNRS, LAM (Laboratoire d'Astrophysique de Marseille)*
UMR 7326, F-13388 Marseille, France
[f] *Australia Telescope National Facility, CSIRO Astronomy & Space Science*
P.O. Box 76, Epping, NSW 1710, Australia
E-mail: blok@astron.nl, filippo.fraternali@unibo.it, heald@astron.nl, adams@astron.nl, bosma@lam.fr, Baerbel.Koribalski@csiro.au, swg-higalaxy@skatelescope.org

Two major questions in galaxy evolution are how star-formation on small scales leads to global scaling laws and how galaxies acquire sufficient gas to sustain their star formation rates. H I observations with high angular resolution and with sensitivity to very low column densities are some of the important observational ingredients that are currently still missing. Answers to these questions are necessary for a correct interpretation of observations of galaxy evolution in the high-redshift universe and will provide crucial input for the sub-grid physics in hydrodynamical simulations of galaxy evolutions. In this chapter we discuss the progress that will be made with the SKA using targeted observations of nearby individual disk and dwarf galaxies.

Advancing Astrophysics with the Square Kilometre Array
June 8-13, 2014
Giardini Naxos, Italy

*Speaker.

PoS(AASKA14)129

1. The Galactic Gas Cycle

Galaxy evolution is driven by the flow of gas into galaxies, the transformation of gas into stars, and the expulsion of gas due to the subsequent stellar evolution processes. Atomic neutral hydrogen (H I) is an excellent tracer — and often the main constituent — of this gas, and can be observed readily in the 21-cm line. The SKA will be able to directly trace the gradual transformation from primordial hydrogen into galaxies over cosmic time. However, to correctly interpret this evolution, direct detailed observations of the sub-kpc-scale physical processes that cause this transformation are essential for understanding the astrophysics of galaxy evolution.

Two very important processes in this cosmic evolution are star formation and gas accretion. The first one enriches the interstellar medium (ISM) with metals, injects energy into it, and, through the ejection of gas, also enriches the intergalactic medium (IGM). The second process delivers gas from outside galaxies (either primordial or previously ejected) into the star-forming disks, which ensures galaxies can keep forming stars over a Hubble time.

Star formation thus plays a central role in galaxy evolution, yet little is known about the necessary conditions for star formation to occur. Global, kpc-scale relations, such as the Kennicutt-Schmidt Law (Kennicutt 1989, 1998), have established that there is a direct connection between the (molecular) gas surface density and the star formation rate (SFR) surface density. This relation has been found to hold for both spiral galaxies, as well as late-type dwarf galaxies (see, e.g., Leroy et al. 2008 and Bigiel et al. 2008 for a recent analysis). How the underlying astrophysics at the scales of individual gas clouds and cloud complexes leads to such a relation on more global scales remains, however, ill-understood.

The initial phase of this star-formation sequence will presumably be the cooling of gas to temperatures below $\sim 10^4$ K, where it can collapse and form clouds. Observing this cold, clumpy ISM and distinguishing it from the warmer, more diffuse phase requires imaging at high spatial and velocity resolution. To date, few H I observations of nearby galaxies resolve the individual cold gas complexes (see, e.g., Braun et al. 2009 and Kim et al. 2003 for examples in the Local Group). The SKA will have sufficient sensitivity at the required high resolution to do this for many galaxies. This enables studies of the properties of the cold gas in galaxies at the desired cloud-size resolution over a wide range of galaxy properties and environments. In addition, ALMA can observe the molecular components of these clouds and complexes, and this complementarity will lead to a revolutionary improvement in our understanding of star formation — and the conditions leading to it — in different environments.

A related question is: how can galaxies sustain their star formation over a Hubble time? In general, local galaxies only have enough gas to sustain their SFR for few Gyr, and they must thus acquire gas from somewhere else (see Sancisi et al. 2008 for a recent overview). Numerical simulations suggest gas flows in from the IGM (or "cosmic web"), through a process called "cold accretion" (e.g., Kereš et al. 2005). "Cold" in this context means that the gas has not been shock-heated as it entered the galaxy halo. This cold accretion process is discussed in more detail in the chapter by Popping et al. (2015) elsewhere in this volume. So far there is little direct observational evidence for significant cold accretion. The observed cold gas accretion in galaxies seems to be an order of magnitude too low to explain the current star formation rates (SFR) in galaxies (Sancisi et al. 2008; Putman et al. 2012). If cold accretion is the dominant process by which galaxies acquire

PoS(AASKA14)129

their gas, then current observational limits indicate it must happen at H I column densities below $\sim 10^{18}$ cm^{-2}. Only a limited number of galaxies have so far been explored at sufficient sensitivity and spatial resolution to probe this regime (Heald et al. 2011; Putman et al. 2012). SKA will be able to directly detect and map in detail the gas at these column densities and trace its connection with the cosmic web.

The galactic fountain process (Shapiro & Field 1976; Bregman 1980; Norman & Ikeuchi 1989) links the gas in the star forming disk and that in the halo. Massive stars, through supernova explosions and stellar winds, can push gas out of the disk and into the halo of a galaxy. This creates the holes and bubbles frequently observed in the gas disks of galaxies (Bagetakos et al. 2011). The expelled gas will cool and eventually rain back on the disk, most likely in the form of H I clouds (Putman et al. 2012). Such clouds have also been observed in a number of other galaxies as part of an extra-planar gas component (Sancisi et al. 2008), and presumably form the equivalent of the high and intermediate velocity clouds (HVCs and IVCs, respectively) in our Galaxy. It is thought that the process of these clouds moving through the hot gaseous halo of a galaxy provides an alternative mechanism for accretion of gas. Here, hot halo gas cools in a cloud's wake and is dragged along as the cloud moves back into the disk (Fraternali 2013).

While the galactic fountain clouds thus provide a possible means for the transportation of gas into the disk, they also hinder our ability to identify primordial gas clouds that are being accreted from the IGM. A small number can be identified as they are counter-rotating with respect to their host galaxy (Oosterloo et al. 2007), but a better census down to lower H I masses and column densities is needed to properly understand these accretion mechanisms. Prime targets for this are galaxies in the 'Local Volume', defined as the sphere of radius 10 Mpc centered on the Local Group (Karachentsev et al. 2004, 2013; Koribalski 2008). This volume includes around 900 galaxies, the majority of which are gas-rich. Distances to these galaxies are known with high accuracy. The H I contents and sizes of Local Volume galaxies cover more than two orders of magnitudes, ranging from low-mass dwarf galaxies with diameters of less than one kpc (e.g., Leo T; Ryan-Weber et al. 2008) to grand design spirals with H I diameters of $\sim$100 kpc (e.g., Circinus; For et al. 2012).

In summary, the SKA will be a unique instrument that will be able to track the gas in low-redshift galaxies as it accretes onto the disk, forms H I cloud complexes (which in turn produce stars through an intermediate, molecular phase), is expelled through feedback processes, and subsequently returns to the disk. Complemented by ALMA molecular line observations, the transformation from neutral atomic and molecular gas to the formation of stars can thus be investigated in exceptional detail over a large range in galaxy properties (see, e.g., Ott et al. 2008 and Fukui et al. 2009 for work on the LMC and Stanimirović et al. 2014 for our Galaxy). These processes can be studied in detail in a variety of environments at low redshift, thus establishing the astrophysical foundations that are needed to interpret observations of galaxies at higher redshifts, and to guide the implementation of 'sub-grid' physics into hydrodynamical simulations of galaxy formation and evolution.

In the rest of this section we calculate the H I column density and mass sensitivities of SKA, SKA1-MID and SKA1-SUR for a number of observing scenarios. This chapter specifically deals with high-resolution and high-sensitivity observations of individual objects, i.e., deep observations of limited areas of sky.

The remainder of this chapter then discusses the prospects for obtaining detailed, sensitive

PoS(AASKA14)129

observations of nearby, individual galaxies and the progress that will be made towards a better understanding of the link between star formation, accretion, and gas in these galaxies.

1.1 SKA column density and H I mass sensitivities

We calculate column density sensitivities for SKA, SKA1-MID and SKA1-SUR for a range of angular and velocity resolutions and three representative integration times. For the latter we choose:

• **10 hours**: representing a typical "single-track" observation (as motivated in Sect. 2.3). In terms of science, an observation like this can be used to characterise high-resolution structures in the star forming disks of galaxies, as well as (at lower spatial resolutions) the outer low-column density disk down to $N_{\rm HI} \sim 10^{18}$ cm^{-2};

• **100 hours**: this longer observation will typically result in detection of H I column densities down to $\sim 10^{17}$ cm^{-2} where accretion and faint outer gas can be directly studied;

• **1000 hours**: this extremely long observation allows detection of column densities well below 10^{17} cm^{-2} where one can directly explore the link of galaxies with the cosmic web.

For the angular resolutions we choose representative beam sizes between $1''$ and $30''$. For the velocity resolution we choose values between 1 and 20 km s^{-1}. Using these parameters we calculate the 5σ column density detection limits per velocity channel. Our basis for this are the SKA1-MID and SKA1-SUR natural sensitivities as listed in Table 1 of the SKA Baseline Design Document (Dewdney et al. 2013). For SKA1-MID we use the sensitivity listed for 190 SKA dishes combined with the 64 MeerKAT dishes. For SKA1-SUR the sensitivity of 60 SKA dishes combined with 36 ASKAP dishes is used. For SKA1-MID the 1σ sensitivity is given as 63 μJy beam^{-1} over 100 kHz for one hour of observing time. For SKA1-SUR this value is 263 μJy beam^{-1} over 100 kHz after one hour. We scale these sensitivities using the appropriate integration time and velocity resolution. For the sensitivity scaling as a function of angular resolution we use the noise scaling curve shown in the bottom panel of Figure 1 of the SKA1 Imaging Science Performance document (Braun 2014). These scalings take into account the effect of the spatial tapering needed to achieve the desired resolution. In addition, we apply an overall efficiency factor of 0.9 as listed in Appendix A of Braun (2014). At 1.4 GHz SKA1-MID will have a field of view of 0.5 square degrees. SKA1-SUR will be able to map 18 square degrees due to its wide-field phased array feeds.

The 5σ column density limits for SKA1-MID, SKA1-SUR and SKA are given in Table 1. These values agree well with those listed in Popping et al. (2015) which were derived using simulations. Note that a column density limit is defined as the flux density limit times the velocity width, so for a fixed observation time and angular resolution, observing with a larger velocity channel width will lead to a *higher* column density limit. This is therefore distinctly different from the case where an already detected signal is smoothed to a larger channel width giving an improved sensitivity (but at the cost of a coarser velocity resolution).

For SKA, we assume that it has 10 times the natural sensitivity of SKA1-MID, and apply a 50% correction factor to take into account tapering and weighting. We assume this factor is independent of angular resolution.

In addition to column densities, we also list in Table 2 the limiting H I masses that can be detected using the various setups. Here we assume the sources are unresolved and have a top-hat velocity profile with a peak flux equal to 5σ and a velocity width of 50 km s^{-1}. Optimal smoothing

PoS(AASKA14)129

(i.e., a channel width equal to the velocity width) is assumed. Mass limits for other velocity widths can be deduced by simply scaling with the width of the profile.

The science described here focuses on H I observations of low-redshift galaxies ($z < 0.1$) so only frequency band 2 (950-1760 MHz on SKA1-MID and 650-1760 MHz on SKA1-SUR) is needed.

2. Gas, Star Formation and Dark Matter at High Resolution

2.1 Gas and Stars

The transformation of gas into stars is one of the most important processes in galaxy evolution. Understanding the conditions that determine the efficiency of this process, and the associated physics, is the goal of many observational and theoretical studies. They also form important input into numerical models of galaxy formation and evolution. This requires knowledge of these processes over a large range in scales: from galaxy-sized scales where gas is transported from the disk of the galaxy into the halo and back, to kpc-sized scales where gas clouds are collapsing, via sub-kpc scales where neutral gas cools and turns molecular in Giant Molecular Clouds (GMC), to parsec scales where individual stars are formed. The latter, very small, scales can be directly observed in our Galaxy, while processes happening at galaxy scales can be studied in external galaxies. Tying together the processes happening at these two extreme scales is a major challenge: in our Galaxy we lack the overview, while in external galaxies we rarely have the required resolution and sensitivity to study these processes in detail.

Over the last decade the number of high-resolution, multi-wavelength studies of galaxies in the nearby universe has increased dramatically. The H I observations were obtained as part of dedicated surveys such as THINGS (Walter et al. 2008), Little THINGS (Hunter et al. 2012), VLA-ANGST (Ott et al. 2012), FIGGS (Begum et al. 2008), WHISP (van der Hulst et al. 2001), HALOGAS (Heald et al. 2011), SHIELD (Cannon et al. 2011), and LVHIS (Koribalski 2008). These surveys have made possible new studies of the conditions for star formation on kpc or even sub-kpc scales in a larger number of galaxies (see the chapter by Blyth et al. 2015 for a more extensive description of recent H I surveys). These have made it possible to make the first steps towards bridging the gap between the observations at the scales of stars and those at scales of galaxies. With the SKA the next step can be taken.

Kennicutt (1989) studied the gas and Hα content of a number of nearby galaxies and found a power-law relation between the total gas surface density and the Hα-derived SFR. Over the years, similar studies (see e.g., Calzetti et al. 2012; Calzetti 2013), using different measures for the gas surface density, and different star formation tracers (such as ultra-violet, Hα, infra-red or combinations of them) found similar relations, but with a large spread in the parameters. This may reflect actual variations in the physics, but a large part of this spread is very likely also due to choice of sample, analysis and star formation tracers.

Recent studies of the star-forming disks of nearby galaxies found a tight linear relation between the molecular gas surface density and the SFR surface density (Leroy et al. 2008; Bigiel et al. 2008). This can be interpreted as stars forming from the molecular ISM at a constant efficiency. Note though that these results do not say anything about the necessary conditions for star formation on

PoS(AASKA14)129

Table 1: 5σ H I column density limits (cm^{-2})

beam size	velocity resolution 1 km s^{-1}	5 km s^{-1}	10 km s^{-1}	20 km s^{-1}
		SKA1-MID		
$t = 10^h$				
$1''$	1.75E+21	3.91E+21	5.53E+21	7.83E+21
$3''$	1.63E+20	3.65E+20	5.16E+20	7.30E+20
$10''$	1.13E+19	2.52E+19	3.57E+19	5.05E+19
$30''$	1.31E+18	2.94E+18	4.16E+18	5.89E+18
$t = 100^h$				
$1''$	5.53E+20	1.23E+21	1.75E+21	2.47E+21
$3''$	5.16E+19	1.15E+20	1.63E+20	2.30E+20
$10''$	3.57E+18	7.99E+18	1.13E+19	1.59E+19
$30''$	4.16E+17	9.32E+17	1.31E+18	1.86E+18
$t = 1000^h$				
$1''$	1.75E+20	3.91E+20	5.53E+20	7.83E+20
$3''$	1.63E+19	3.65E+19	5.16E+19	7.30E+19
$10''$	1.13E+18	2.52E+18	3.57E+18	5.05E+18
$30''$	1.31E+17	2.94E+17	4.16E+17	5.89E+17
		SKA1-SUR		
$t = 10^h$				
$1''$	4.71E+21	1.05E+22	1.49E+22	2.11E+22
$3''$	4.45E+20	9.96E+20	1.40E+21	1.99E+21
$10''$	4.48E+19	1.00E+20	1.41E+20	2.00E+20
$30''$	8.38E+18	1.87E+19	2.65E+19	3.75E+19
$t = 100^h$				
$1''$	1.49E+21	3.33E+21	4.71E+21	6.67E+21
$3''$	1.40E+20	3.15E+20	4.45E+20	6.30E+20
$10''$	1.41E+19	3.16E+19	4.48E+19	6.33E+19
$30''$	2.65E+18	5.93E+18	8.38E+18	1.18E+19
$t = 1000^h$				
$1''$	4.71E+20	1.05E+21	1.49E+21	2.11E+21
$3''$	4.45E+19	9.96E+19	1.40E+20	1.99E+20
$10''$	4.48E+18	1.00E+19	1.41E+19	2.00E+19
$30''$	8.38E+17	1.87E+18	2.65E+18	3.75E+18
		SKA		
$t = 10^h$				
$1''$	1.13E+20	2.52E+20	3.57E+20	5.05E+20
$3''$	1.25E+19	2.80E+19	3.97E+19	5.61E+19
$10''$	1.13E+18	2.52E+18	3.57E+18	5.05E+18
$30''$	1.25E+17	2.80E+17	3.97E+17	5.61E+17
$t = 100^h$				
$1''$	3.57E+19	7.99E+19	1.13E+20	1.59E+20
$3''$	3.97E+18	8.87E+18	1.25E+19	1.77E+19
$10''$	3.57E+17	7.99E+17	1.13E+18	1.59E+18
$30''$	3.97E+16	8.87E+16	1.25E+17	1.77E+17
$t = 1000^h$				
$1''$	1.13E+19	2.52E+19	3.57E+19	5.05E+19
$3''$	1.25E+18	2.80E+18	3.97E+18	5.61E+18
$10''$	1.13E+17	2.52E+17	3.57E+17	5.05E+17
$30''$	1.25E+16	2.80E+16	3.97E+16	5.61E+16

PoS(AASKA14)129

Table 2: H I mass limits for unresolved sources

beam	$M_{\rm HI}/D^2_{\rm Mpc}$ for SKA1-MID			$M_{\rm HI}/D^2_{\rm Mpc}$ for SKA1-SUR		
	$t = 10^h$	$t = 100^h$	$t = 1000^h$	$t = 10^h$	$t = 100^h$	$t = 1000^h$
$1''$	2.6E+03	8.3E+02	2.6E+02	7.1E+03	2.2E+03	7.1E+02
$3''$	2.1E+03	7.0E+02	2.2E+02	6.0E+03	1.9E+03	6.0E+02
$10''$	1.7E+03	5.3E+02	1.7E+02	6.7E+03	2.1E+03	6.7E+02
$30''$	1.8E+03	5.6E+02	1.8E+02	1.1E+04	3.6E+03	1.1E+03

H I masses were calculated assuming a 5σ flux density limit and a velocity width of 50 km s^{-1}. Optimal smoothing is assumed.

the scales of GMCs or smaller. With the analysis performed at a resolution of 750 pc, any relation must be interpreted within the context of "counting clouds", i.e., one has to assume that the GMCs have uniform properties with the observed molecular surface density determined by the beam filling factor of these clouds. Higher resolutions are needed to go beyond this limitation.

Schruba et al. (2011) found that the linear relation between molecular gas and SFR surface densities extends into the H I-dominated regime of the outer disks of galaxies (see also Roychowdhury et al. 2014). This is supported by the realisation that star formation in the outer parts of disks is more widespread than originally thought. GALEX UV observations enabled direct detection of O and B stars which would otherwise have escaped detection due to their inability to excite the surrounding ISM enough to produce Hα emission. It is now thought that these extended UV (XUV) disks are found in $\sim 30\%$ of nearby disk galaxies (Thilker et al. 2007). A striking example is M83 (NGC 5236) as shown in Fig. 1. The outlying H I structures show up remarkably well in the UV, indicating that star formation is progressing there as well, albeit with a lower efficiency (Bigiel et al. 2011) than in the bright, inner region of the galaxy. An extreme example of this is the dwarf galaxy ESO215-G?009 (Warren et al. 2004). This galaxy has the highest gas-to-light ratio known for a galaxy in the low-redshift universe, yet, despite the large gas reservoir, star formation apparently has halted, is inhibited or lacks a trigger.

The above broad-brush picture illustrates the progress made in the last few years, and mentions some of the empirical relations that are now routinely used as input for numerical models that attempt to explain the variations of star formation efficiency with, e.g., redshift, environment or galaxy mass. It is however still difficult to link the observations with the actual physical processes driving the star formation rate. For example, Leroy et al. (2008) test a number of theoretical explanations proposed in the literature linking the gas density and the SFR. They looked at the disk free fall time, the orbital timescale, the effects of cloud-cloud collisions, the assumption of fixed GMC star formation efficiency, and the relation between pressure in the ISM and the phases of the ISM. Their conclusions were that none of these offers a unique explanation for the observed behavior. So, though large-scale relations can be identified (such as the Kennicutt-Schmidt Law), the actual physics is a lot more complicated, and happens below the resolutions achieved so far. Observationally, we will therefore have to probe the ISM at scales below that of GMCs and individual H I complexes. We also need to have a better understanding of the balance between warm and cold H I phases, the efficiency of H_2 formation and the effects of shocks and turbulence. Examples of the importance of high resolution and high sensitivity for the study of turbulence in H I are found in, e.g., Dutta et al. (2009, 2013).

PoS(AASKA14)129

Figure 1: Composite multi-wavelength image of M83. Near- and far-UV from GALEX are shown in blue. Optical *R*-band from SDSS in green, *J*-band from 2MASS in red, H I data from LVHIS is shown in pale-blue, and a combination of *B*, *R* and Hα have been used as the luminosity of the stellar disk. The field of view is $1.3^\circ \times 1.5^\circ$. (Picture courtesy B. Koribalski)

Young & Lo (1996, 1997), Young et al. (2003), de Blok & Walter (2006), Ianjamasimanana et al. (2012), Warren et al. (2012) and Stilp et al. (2013) all analyzed the H I emission velocity profiles of galaxies and found evidence for the presence of cold and warm H I components by decomposing the velocity profiles into components with a high and a low velocity dispersion. They found that the cold (low velocity dispersion) component is usually located near star-forming regions, whereas the warm (high velocity dispersion) component tends to be found along every line of sight. This presumably tells us something about the conditions for the warm H I to cool and turn molecular, but the key limitation of these studies was again spatial resolution. The improved capabilities of the SKA will enable these studies to be repeated but now resolving the individual gas complexes. (Equivalent absorption line studies are described in the chapters by Morganti et al. 2015 and McClure-Griffiths et al. 2015.) This should thus provide observations of a large number of galaxies at sufficient resolution to gauge the ability of and the conditions for the ISM to form GMCs over a wide range of galaxy conditions and environments.

An angular resolution of $1''$ allows 100 pc physical resolutions out to 20 Mpc (i.e., the distance of the Virgo cluster). The high-resolution observations of M31 by Braun et al. (2009) (shown in Fig. 2) have a maximum resolution of 50 pc, while the LMC observations by Kim et al. (2003) probe scales of 15 pc. Assuming SKA can observe efficiently up to $\delta \sim +35^\circ$, then gives access to ~ 800 galaxies within 20 Mpc that have independent distance measurements. Of these $\sim 80\%$ have H I detections. With the SKA these can therefore all be studied at a resolution close to that of the Braun et al. (2009) M31 observations. Out to 3 Mpc, we can study galaxies at the same resolution

PoS(AASKA14)129

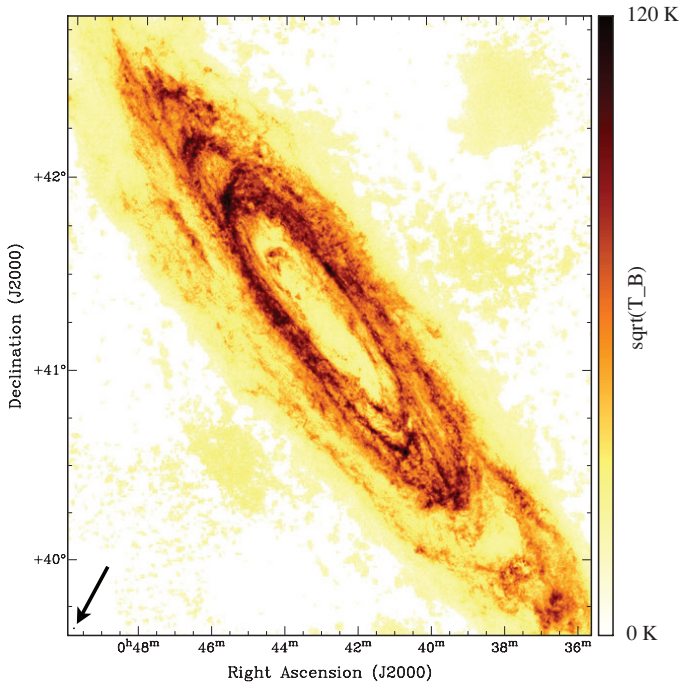

Figure 2: Integrated H I map of M31 from high-resolution observations by Braun et al. (2009). The resolution of these observations is $\sim$ 50 pc. The beam is indicated by the arrow in the bottom-left corner. SKA will enable highly detailed observations of this kind for hundreds of galaxies.

of the Kim et al. (2003) LMC observations. There are $\sim$ 75 galaxies with independent distance measurements within that distance in the part of the sky accessible to the SKA. This includes, for example, the Sculptor group.

There are therefore a significant number of galaxies out to these distances, and this opens up the exciting prospect of being able to characterize the properties and morphologies of individual H I clouds in other galaxies over a wide range of environments. Combination with high-resolution ALMA observations should provide a comprehensive picture of the condition for and first phases of star formation.

2.2 Dynamics and Dark Matter

The high angular resolution that can be achieved with SKA will also be of importance to studies of the internal dynamics of galaxies and the distribution of dark matter.

H I studies played a major role in the 1970s and 1980s to establish the presence of dark matter in gas rich galaxies, necessary to keep up the extended, flat (or rising) rotation curves at large radii. More recent work on late-type low surface brightness galaxies showed that pure ΛCDM models are in disagreement with observations, the so-called core-cusp controversy (de Blok 2010). Recent attempts to solve this problem concentrate on introducing feedback in the star formation recipes used in the numerical simulations of galaxy formation (Oh et al. 2011), so that an initially cuspy dark matter distribution can be modified sufficiently. Research on this problem can be expected to continue to progress, until a better understanding of these feedback mechanisms has been reached. At present, the predictions from these simulations seem to begin to work for small galaxies, but for

PoS(AASKA14)129

larger ones the answer is still open. This is an active area of research, and further improvements of the galaxy formation models can be expected (e.g., di Cintio et al. 2014).

In terms of further H I observations addressing this problem, surveys planned with the SKA precursors will enable the selection of an adequate sample of relatively unperturbed galaxies, for which far deeper H I observations can be done with the SKA, as well as molecular gas observations with ALMA. These data will yield detailed information on the circular and (equally important) non-circular motions in these galaxies. Combined with more extensive diagnostics of the stellar kinematics using optical integral-field units, this will yield crucial information about the galaxy kinematics, and hence can be used to study the dark matter problem. Moreover, they can also be used for the purposes of studying the star formation and gas accretion in disk galaxies, as discussed in this chapter.

2.3 SKA Prospects

Here we use the column density limits listed in Table 1 and explore how the increased resolution and sensitivity of SKA makes new science possible. We use the results from the THINGS survey (Walter et al. 2008) as a benchmark. THINGS observed 34 nearby disk galaxies with the combined VLA B, C and D array with a maximum angular resolution of $6''$, or $\sim$ 500 pc on average. For each galaxy, observing time was 7^h with the VLA B-array, 2.5^h with the C-array and 1.5^h with the D-array. A total of $\sim 10^h$ is therefore needed in this setup to produce a complete observation — this motivates our choice for 10^h as a typical observing time in Sect. 1.1. With these parameters, the column density sensitivity of the THINGS observations is $2.7 \cdot 10^{20}$ cm^{-2} for a 5σ detection over a 5 km s^{-1} channel at $6''$ resolution (Walter et al. 2008). This angular resolution is effectively also the highest that can be achieved with the VLA B-array at 1.4 GHz, and is currently the highest resolution at which H I can still be observed routinely.

To compare prospective SKA observations directly with THINGS, we focus here on limits derived with a channel width of 5 km s^{-1}. A 10^h integration time at $6''$ with SKA1-MID will achieve a column density limit of $8.1 \cdot 10^{19}$ cm^{-2}. This is close to the $4 \cdot 10^{19}$ cm^{-2} THINGS sensitivity at $30''$. A 10^h observation on SKA1-MID at $6''$ thus enables studies at the resolution of THINGS, but to column density limits that are a factor of 3 deeper, thus probing the H I well outside the star forming disks. The larger sensitivity of SKA1-MID allows tapering to spatial resolutions higher than used by THINGS. For 10^h and at $3''$, the sensitivity at is $3.7 \cdot 10^{20}$ cm^{-2}. This is comparable to the THINGS sensitivity at $6''$ and therefore allows study of the star-forming disk at twice the spatial resolution. For galaxies out to 10 Mpc the linear resolution corresponding to $3''$ is better than $\sim$ 145 pc, which is starting to resolve individual H I complexes.

With the current baseline design, $3''$ is an upper limit in terms of resolution on SKA1-MID. There is not enough sensitivity on the longer baselines to push the resolution higher. For example, performing the same 10^h observation described above at $1''$ gives a column density limit of $3.9 \cdot 10^{21}$ cm^{-2}, which is higher than the maximum face-on column densities typically found in galaxies at scales of hundreds of parsecs ($\sim 10^{21}$ cm^{-2}; Bigiel et al. 2008). It is possible that optical depth effects mask higher column densities at much smaller scales (e.g., Braun et al. 2009), but this has been tested only in a limited number of galaxies, and is the kind of project one would tackle with the SKA for a larger sample.

PoS(AASKA14)129

Using SKA1-MID to make a longer observation of 100^h, we reach column density limits of $1.2 \cdot 10^{20}$ cm^{-2} at $3''$ resolution (again using a channel spacing of 5 km s^{-1}). This is a factor of $\sim 2-3$ deeper than THINGS at twice the spatial resolution, and will enable high-resolution characterization of the ISM at scales better than 145 pc out to 10 Mpc.

Even with an increased observing time, resolutions of $1''$ remain challenging. At 100^h the limit is $1.2 \cdot 10^{21}$ cm^{-2} which is comparable to the highest column densities typically found in galaxies. At 1000 hours, the corresponding limit is around $3.9 \cdot 10^{20}$ cm^{-2}, and this would allow mapping of most of the H I disk. This seems, however, a large investment of time for a single galaxy. For high-resolution observations of H I in nearby galaxies using SKA1-MID, $3''$ thus seems to be the practical (design-imposed) limit.

For a 50% SKA1-MID, many aspects of the science mentioned above can still be done. The noise will be a factor two higher, but this still allows $3''$ resolution observations that, even at 10^h, lead to sensitivities that are better than THINGS at $6''$.

At 10^h observing time, the 5σ limits for SKA1-SUR at resolutions better than $5''$ are too high for mapping galaxies. For resolutions between $\sim 10''$ and $\sim 30''$ the sensitivities are high enough to perform THINGS-like observations. The strength of the SKA1-SUR observations will, however, be in their ability to characterize the environment due to its large instantaneous field-of-view of 18 square degrees.

The increased sensitivity of a full SKA means that an order of magnitude increase in column density sensitivity can be achieved with respect to SKA1-MID. A 10^h observation will reach down to $2.8 \cdot 10^{19}$ cm^{-2} at $3''$ and 5 km s^{-1} resolution. At $1''$ and 5 km s^{-1} resolution, the column density sensitivity that is achieved is comparable to that of THINGS (at $6''$), but with a spatial resolution that is a factor of 6 better.

At 100^h, $3''$ observations with SKA reach levels around $8.9 \cdot 10^{18}$ cm^{-2}, with even a $1''$ beam giving limits of $8.0 \cdot 10^{19}$ cm^{-2}, i.e., enough sensitivity to reach the levels typically found in the outer disks of galaxies. The Braun et al. (2009) observations of M31 (Fig. 2) have a linear resolution of 50 pc. With SKA at $1''$ we can thus reach similar resolutions out to 10 Mpc. This opens the exciting prospect of mapping galaxies at a physical resolution comparable to the M31 observations shown in Fig. 2. Furthermore, the SKA would make it possible to do this for hundreds of galaxies. Characterisation of the ISM at a resolution of tens of parsecs in such a large number of galaxies, each presumably with different physical conditions, would dramatically improve our knowledge of the ISM in other galaxies.

3. The Galactic Fountain and Accretion

3.1 Background

Galaxies are not isolated systems, as they continuously interact and exchange material with the environment in which they reside. Understanding how and in what form gas is transferred to galaxies from the IGM and vice-versa is a major challenge for current cosmological models. Star-forming galaxies are expected to accrete fresh gas to feed their star formation throughout the whole Hubble time. Evidence for gas accretion includes estimates of the gas depletion times (Bigiel et al. 2011), the study of the star formation histories (Panter et al. 2007) and chemical evolution models

PoS(AASKA14)129

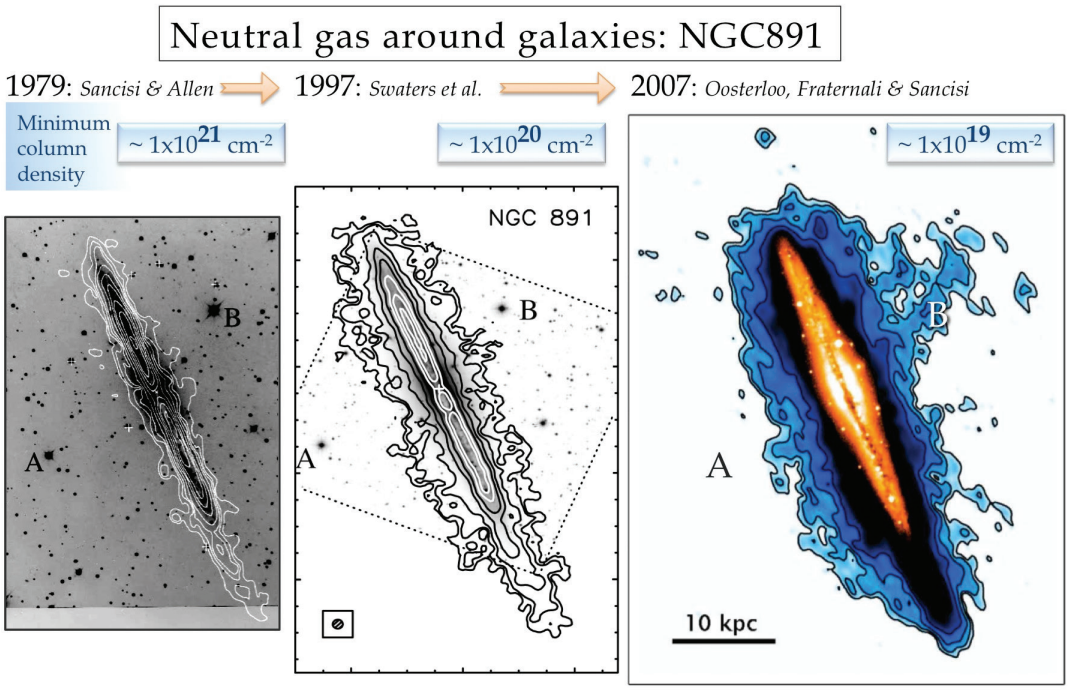

Figure 3: Three generations of neutral hydrogen observations of the edge-on spiral galaxy NGC 891, obtained with the Westerbork Synthesis Radio Telescope in 1979 (Sancisi & Allen 1979) (left panel), 1997 (Swaters et al. 1997) (middle panel) and 2007 (Oosterloo et al. 2007) (right panel). The improvement in sensitivity of only one order of magnitude between each observation led to the discovery of the H I halo (middle panel) and next to the realization that this halo comprises almost 30% of the H I mass of the gas and hosts gas filaments extending up to more than 20 kpc from the disk (right panel). SKA will go down two more orders of magnitude in column density, we can only wonder what we will find.

of the Milky Way (Chiappini et al. 1997; Schönrich & Binney 2009). Indirect determinations of the gas accretion rate show that it should closely follow the SFR in every galaxy (Hopkins et al. 2008; Fraternali & Tomassetti 2012). However, there is little evidence for the majority of the gas accretion taking place in the form of gas clouds infalling into local galaxies. In the Milky Way, the accretion rate from high velocity clouds is only 0.08 $M_\odot\,\mathrm{yr}^{-1}$ (Putman et al. 2012), more than an order of magnitude lower than the SFR ($1-3\ M_\odot\,\mathrm{yr}^{-1}$, Chmoiuk & Povich 2011). H I studies of nearby galaxies give similar discrepancies (Sancisi et al. 2008).

A possibility is that accretion takes place at very low column densities. At the moment the deepest H I observations of nearby disk galaxies obtained with an interferometer reach column densities slightly below 10^{19} cm^{-2} (Oosterloo et al. 2007; Walter et al. 2008; Westmeier et al. 2011; Heald et al. 2011). Fig. 3 shows three observations of the same galaxy, NGC 891, obtained in the last thirty years with the Westerbork Synthesis Radio Telescope (WSRT). The improvement in sensitivity from $\sim 1\cdot 10^{21}$ cm^{-2} (left panel; Sancisi & Allen 1979) to $\sim 1\cdot 10^{19}$ cm^{-2} (right panel; Oosterloo et al. 2007) has revealed a completely different picture of the H I distribution in this galaxy. The most recent data have shown the presence of an extended H I halo which everywhere extends up to $8-10$ kpc above the disk of NGC 891, and with a long filament extending up to 20 kpc. Most of this gas is likely to be produced by stellar feedback from the disk (Fraternali &

PoS(AASKA14)129

Binney 2008) but a fraction could come from accretion. The long filament is, however, likely due to a minor interaction (cf. Oosterloo et al. 2007; Mapelli et al. 2008). Clouds and filaments at similar column densities are observed also around other galaxies (Fraternali et al. 2002; Mundell et al. 2004; Westmeier et al. 2005; Sancisi et al. 2008). As an aside, a similar increase in the prominence of H I when going to lower column densities is also found for early-type galaxies. Here the H I detection rate outside clusters increases from $\sim 0\%$ to $\sim 40\%$ when going from $1 \cdot 10^{21}$ cm^{-2} to $1 \cdot 10^{19}$ cm^{-2} (Serra et al. 2012).

Gas at lower column densities is therefore certainly present around galaxies. This is indicated by deep single-dish observations (e.g., de Blok et al. 2014), and by the study of Lyman-α absorbers towards quasars and their association with the circumgalactic media of nearby galaxies (Tumlinson et al. 2013). The distribution of this ultra-low column density gas can only be directly measured by the SKA.

The presence of low-column density gas around galaxies is also predicted by models. For example, some recent cosmological simulations show *cold* gas filaments penetrating the hot halos of galaxies and reaching the disks to feed star formation (e.g., Fernandez et al. 2012), though the magnitude of the implied accretion is still a matter of some debate (Nelson et al. 2013). Finally, galactic fountain models predict that the hot gaseous halos of galaxies are polluted and cooled by stellar feedback from the galactic disks (Fraternali & Binney 2008; Marinacci et al. 2010). All these models make predictions on the presence and distribution of low column density material that can be directly tested by SKA (see also the chapter by Popping et al. 2015).

SKA will as well reveal the fate of the "missing" H I in more high-density environments such as Hickson Compact Groups (Verdes-Montenegro et al. 2001; Borthakur et al. 2010), which is suspected to be in the form of low-column density intra-group material extending to large relative velocities.

Given the dramatic difference which two orders of magnitude make, as illustrated in Fig. 3, it is difficult to anticipate what the full SKA will be able to see when going down to a sensitivity of below 10^{17} cm^{-2}. However, what is clear, is that with SKA we will obtain the full picture of H I around galaxies, characterize the properties and the kinematics of the H I halos, and derive precise estimates of gas accretion. SKA will provide a definitive answer on how gas falls into galaxies from intergalactic space.

3.2 Current Status

The WSRT Hydrogen Accretion in Local Galaxies (HALOGAS) survey (Heald et al. 2011) aims to catalogue accreting gas in nearby spiral galaxies, and to determine the ubiquity, properties, and origin of neutral gas halos such as the one associated with NGC 891 (Fig. 3). The HALOGAS survey observed 24 galaxies for 120 hours each to a column density limit of $\sim 1 \cdot 10^{19}$ cm^{-2} (assuming a 5σ limit and a linewidth of 12 km s^{-1}). As noted above, this level is suitable for confidently detecting and characterizing diffuse neutral extraplanar gas, and also for identifying isolated clouds around the target galaxies. The HALOGAS detection limit for unresolved cloud masses is approximately $M_{\rm HI} \approx 2.7 \cdot 10^5 \, (D/10\,{\rm Mpc})^2 \, M_\odot$. The HALOGAS observations with the WSRT attain the best compromise between angular resolution and sensitivity at around $30''$, meaning that for a galaxy at a typical distance of 10 Mpc, the linear resolution is around 1.5 kpc. While a higher resolution survey like THINGS is better suited for study of small-scale structure in the ISM and the

PoS(AASKA14)129

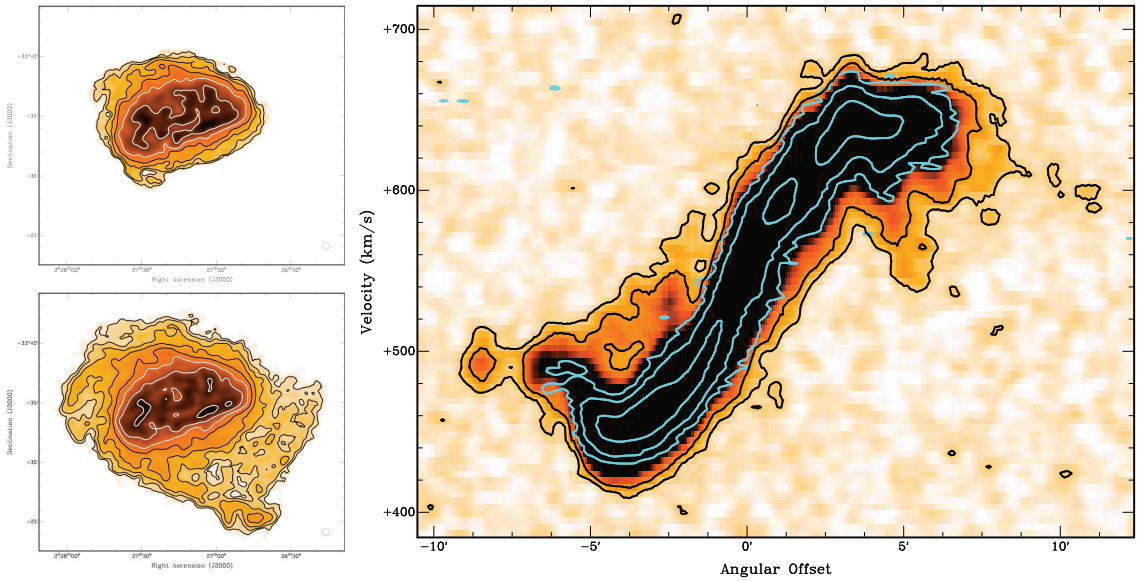

Figure 4: Comparison between THINGS and HALOGAS data for NGC 925. The THINGS data have been smoothed to the same resolution ($\sim 30''$) as the HALOGAS data. Top left: THINGS moment-0. The lowest contour is at $5 \cdot 10^{19}$ cm^{-2}, and contour levels increase by factors of two. Bottom left: HALOGAS moment-0; the lowest contour is $1 \cdot 10^{19}$ and levels increase by a ctor of two. Right: PV diagram near the major axis (grayscale and black contours from HALOGAS at $3, 9\sigma$, cyan from THINGS at $3, 9, 27\sigma$). This figure shows how the increased column density sensitivity of HALOGAS enables mapping of the low column density gas in and around galaxies.

connection to star formation (as discussed in the previous section), the HALOGAS observations are much more sensitive to diffuse structures (see as an example data for NGC 925 in Fig. 4).

HALOGAS provides the capability for a uniquely deep and uniform search for gas clouds and streams in the environment of the target galaxies. These clouds and streams, if present, could represent the most obvious signposts of ongoing cold accretion in the local Universe. A complete accounting of the potentially accreting gas is still being finalized (Jütte et al. 2015) but it can already be concluded that the total visible accretion rate attributable to such features is rather small. HALOGAS shows that a substantial population of gas clouds and streams in neutral gas is not present down to the $\sim 10^{19}$ cm^{-2} survey column density limit. There are clear consequences for the mechanisms that can be invoked to explain the continued fuelling of star formation and the column density levels at which these occur.

Crucially, the benefit of deep observations is not just the sensitivity to faint diffuse outer disk emission, but also to faint diffuse thick disk gas seen in projection against the inner thin (main) disk. Analysis of the HALOGAS sample shows that the key discriminating factor in determining the presence of such a thick H I disk is the star formation rate normalized by the disk area (Heald et al. 2015). These thick disks in many cases show rotation speeds which are smaller than those in the plane of the disk (e.g., Oosterloo et al. 2007). The dependence on star formation rate surface density points strongly toward the galactic fountain being the dominant factor in creating thick H I disks in galaxies. It looks consistent with the picture of galactic-fountain-driven positive feedback (Fraternali & Binney 2008; Marinacci et al. 2010). The presence and importance

PoS(AASKA14)129

of extra-planar material (such as a thick H I disk) would then be the relevant observational tracer of the gas accretion process for galaxies in the local Universe. This result bears confirmation and further investigation with the SKA.

3.3 SKA Prospects

The current configuration of SKA1-MID is heavily dominated by short baselines and therefore has an exquisite column density sensitivity at moderate resolutions. To compare its performance with existing observations we use the HALOGAS survey (Heald et al. 2011) as described above as a benchmark. HALOGAS reaches a typical 5σ column density sensitivity of $5 \cdot 10^{18}$ cm^{-2} per 4.1 km s^{-1} channel at a spatial resolution of $30''$. This beam size represents the optimal combination between resolution and sensitivity for these particular WSRT observations and is the standard resolution HALOGAS used.

We compare these numbers with those derived for the SKA as shown in Table 1. For a 10^h observation with SKA1-MID using a $30''$ beam and 5 km s^{-1} velocity resolution, the resulting 5σ column density limit is $2.9 \cdot 10^{18}$ cm^{-2} . In other words, a 10^h SKA1-MID observation already goes twice as deep as HALOGAS. This therefore opens the prospect of routinely obtaining deep observations of a large number of galaxies in a modest amount of time, and efficiently characterizing the presence of clouds, thick H I disks and other extra-planar features. This will lead to a more complete statistical description of the importance and mechanisms for accretion.

With 100^h of observing on SKA1-MID (again at $30''$ and 5 km s^{-1}), a column density limit of $9.3 \cdot 10^{17}$ cm^{-2} is reached. This is comparable to the column densities that deep H I observations of nearby galaxies with the Green Bank Telescope reach (Pisano 2014), but with a spatial resolutions that is almost a factor 20 better (from $9'$ to $30''$).

A 50% SKA1-MID will still be able to reach HALOGAS depth, but in 10^h per galaxy instead of 120^h. In terms of increasing the statistics of accretion processes these observations will therefore already be scientifically valuable.

For a fixed observing setup, the column density sensitivity of SKA1-SUR is lower by a factor of 2.7 (for $3''$) to 6.4 (for $30''$). Though observations will thus be less sensitive, the large field of view will help exploring the extended environment around nearby galaxies, and can help placing the SKA1-MID results in the context of the large-scale cosmic web.

For the full SKA, at a resolution of $30''$, the column density limits after 10^h are truly impressive, reaching $\sim 2.8 \cdot 10^{17}$ cm^{-2}, i.e., more than an order of magnitude deeper than HALOGAS. At 100^h, these numbers go down even further to $\sim 8.9 \cdot 10^{16}$ cm^{-2}. At these column densities one would be able to detect the 21-cm emission from Lyman Limit Systems. Further discussion on this and the cosmic web in general is presented in the chapter by Popping et al. (2015).

4. Accretion and external high-velocity clouds

4.1 HVCs as accretion probes

The previous section emphasised the importance of the extra-planar gas as a tracer of accretion. Here we discuss some of the properties of the clouds that form part of that extra-planar component. In our Milky Way (MW) these are observed as HVCs (see the chapter by McClure-Griffiths et al.

PoS(AASKA14)129

2015 elsewhere in this volume). Here we discuss the prospects of observing these clouds in other galaxies.

The physical properties of the HVCs around the MW span a large range; the large complexes are at distances of ~ 10 kpc, with similar heights above the Galactic plane, and have physical sizes of several kpc and masses of $1-50\times10^5$ $M_\odot$ (Putman et al. 2012; Wakker et al. 2008, 2007). Compact clouds near the disk-halo interface are $\lesssim 1$ kpc above the disk and have sizes and masses of ~ 700 $M_\odot$ and ~ 30 pc (Ford et al. 2010). In addition, there may be populations of clouds distributed throughout the halo of the MW. These compact high velocity clouds (CHVCs) appear to be circumgalactic and at distances of $\sim 50-150$ kpc with masses of $\sim 5\times10^4$ $M_\odot$ and sizes of ~ 0.8 kpc for an assumed distance of 100 kpc (Sternberg et al. 2002; Maloney & Putman 2003; Putman et al. 2002; de Heij et al. 2002). The difference in observed properties of the HVCs is a clue to their likely origins. The velocities of the large complexes and their low metallicities ($\sim 0.15 Z_\odot$) are consistent with accretion of gas onto the MW (Wakker et al. 2007). The spatial distribution and kinematics of the clouds at the disk-halo interface are consistent with a galactic fountain (Ford et al. 2010). The same phenomenon is traced by the IVCs. The CHVCs potentially provide information on the Galactic dark matter substructure (Sternberg et al. 2002).

HVCs are thus a probe of both accretion in galaxies and the recycling of gas through the hot halo as part of the galactic fountain. Observing and understanding these processes in our own Galaxy is hampered by the difficulty of constraining the distance to these systems. In external galaxies, we can directly determine the masses and sizes of the HVCs and have the opportunity to view the HVCs in relation to the galactic disks. Unfortunately, attempts to search for HVCs in external galaxies are often hampered by lack of resolution and sensitivity. HVCs are low column density structures with peak column densities of $\sim 10^{19}$ cm^{-2}. The compact clouds (disk-halo and CHVCs) will be point source detections for most extragalactic surveys with masses $< 10^5$ $M_\odot$ down to ~ 100 $M_\odot$ for clouds at the disk-halo interface.

Only a handful of nearby disk galaxies outside the Local Group have detections of discrete clouds of anomalous HI: NGC 891 with clouds of $1-3\times10^6$ $M_\odot$ (Oosterloo et al. 2007), NGC 2403 with clouds of $6-10\times10^6$ $M_\odot$ (Fraternali et al. 2001), NGC 2997 with clouds of $\sim 10^7$ $M_\odot$ (Hess et al. 2009) and NGC 55 with clouds of $2-40\times10^6$ $M_\odot$ (Westmeier et al. 2013). These anomalous H I clouds appear to be the analogs of the large HVC complexes in the MW with substantial H I masses, large extents of several kpcs and projected separations from the galactic disks of $\sim 10-20$ kpc. Other dedicated surveys of other nearby galaxies and galaxy groups reveal no HVC analogs down to $\sim 4\times10^5$ $M_\odot$ at larger distances from galaxies (Pisano et al. 2007; Irwin et al. 2009).

Further systematic studies of nearby galaxies are thus needed to determine the properties of the global HVC population. Observations much deeper than those that currently exist are needed to extend the extragalactic HVC population to the low mass clouds at the disk-halo interface that are associated with the galactic fountain mechanism.

4.2 Prospects for HVCs with the SKA

Table 3 summarizes the properties of HVCs. The large HVC complexes have physical sizes of ~ 10 kpc and will remain resolved with a $30''$ beam out to distances of ~ 30 Mpc, so observing requirements in the nearby Universe will be set by column density limits. For typical z-heights of

PoS(AASKA14)129

Table 3: Galactic and Extragalactic HVCs

Class	d_{HI} (kpc)	θ_{HI} (D^{-1}_{Mpc} kpc)	N_{HI} (cm^{-2})	M_{HI} ($M_\odot$)	z-height (kpc)	θ_z $D^{-1}_{Mpc}\sin(i)$	References
	(1)	(2)	(3)	(4)	(5)	(6)	
Complexes	$3-15$	$34'^a$	$\sim 10^{19}$	$1-50\times10^5$	$\lesssim 10$	$34'$	Putman et al. (2012)
CHVCs^b	0.78	$2.7'$	1.4×10^{19}	5×10^4	100	5.7°	Putman et al. (2002)
Disk-halo clouds	0.030	$6''$	1×10^{19}	700	0.66	$2.3'$	Ford et al. (2010)

^{a}Typical assumed size ~ 10 kpc. ^{b}Assumed distance from galaxy center of 100 kpc.
(1) diameter in kpc (2) angular diameter normalized for distance (3) column density in cm^{-2} (4) typical H I mass (5) height above the plane in kpc (6) projected separation from the plane normalized for distance.

~ 10 kpc, the HVC complexes should be spatially resolved from the disk out to 10 Mpc for all but the most face-on systems ($i > 20^\circ$) at $30''$ resolution. In more face-on systems they can however be detected because of their velocity separation from the main disk (e.g., in M101; Kamphuis et al. 1991). In a 10^h observation, SKA1-MID can achieve a 5σ column density sensitivity of $\sim 5\times10^{18}$ cm^{-2} in a 20 km s^{-1} channel (matched to the typical linewidth of the HVCs). This is a factor of 2 lower than the typical peak column density for MW HVCs; at this level a survey of nearby galaxies would be sensitive to the full range of MW HVC complexes rather that just the most massive systems with the highest peak column densities. The full SKA will offer greatly improved column density sensitivity. Increasing sensitivity to lower column density allows the tracing of the extended structure of the HVCs which can offer clues to the environment, including the pressure of the medium they are embedded in. Higher resolution observations trace the clumpiness and structure of the H I complexes.

The compact clouds at the disk-halo interface are physically very small and will be mostly unresolved point sources except at the highest resolutions in the closest galaxies. With a typical size of 30 pc they have angular sizes of $6''\ D^{-1}_{Mpc}$. For a 25 km s^{-1} channel (matched to the linewidth of HVCs; Table 2 scaled by velocity width), SKA1-MID with a $10''$ beam is sensitive to the typical disk-halo cloud of Ford et al. (2010) of $\sim 700\ M_\odot$ at 1 Mpc in a 100^h observation. Deep observations of very nearby galaxies ($D = 2$ Mpc) would be sensitive to the most massive disk-halo clouds ($M_{\rm HI} > 3000\ M_\odot$). With a sensitivity improvement of ~ 10 for the full SKA, the median disk-halo cloud population will be detectable in deep (100^h) observations out to ~ 3 Mpc.

SKA1-SUR lacks the column density sensitivity to efficiently detect the large HVC complexes in large surveys; neither does it have the point source sensitivity to detect the disk-halo clouds. However, its large field of view does make it ideal for deep surveys of nearby galaxies to search for an extended circumgalactic HVC population separated from the parent galaxy by multiple degrees. With a 10 hr observation at $30''$ and 20 km s^{-1}, SKA1-SUR has a column density sensitivity of $\sim 4\cdot10^{19}$ cm^{-2}. This would allow for the detection of the high-$N_{\rm HI}$ tail of the CHVC population. At 100^h the sensitivity is $\sim 1.2\cdot10^{19}$ cm^{-2}; this is well-matched to the median peak $N_{\rm HI}$ of the CHVC population.

5. Summary

Two of the main unanswered questions in galaxy evolution are: "how do the astrophysics at the scales of individual clouds and gas complexes lead to global star formation laws?" and "where

PoS(AASKA14)129

do galaxies acquire their gas from?" Much progress has been made on these questions in recent years, but the required combination of column density sensitivity and high spatial resolution that is needed to definitively answer these questions has so far been missing. For example, a proper study of the first problem has so far really only been possible in the MW and the nearest galaxies in the Local Group (see the chapter by McClure-Griffiths et al. 2015 elsewhere in this volume). Similarly, the second question has so far only been addressed for a limited number of galaxies with investment of a large amount of observing time. SKA will enable us to make great progress in both areas.

For studies of individual objects, SKA1-MID provides the highest resolution and sensitivity. With a maximum effective angular resolution of $3''$ SKA1-MID will go as deep as the highest-resolution existing H I surveys ($\sim 3 \cdot 10^{20}$ cm^{-2} at 5σ and 5 km s^{-1} — this limit definition applies to all values quoted here) in the same observing time (10^h per galaxy), but at a resolution that is at least twice as good. SKA1-SUR with its 18 square degree field of view will be able to instantaneously map the environment around the target galaxies. While (for a fixed observing time), its resolution and sensitivity will be more limited, this will nevertheless provide invaluable information on the context of the observed objects.

The full SKA will go an order of magnitude deeper than SKA1-MID and SKA1-SUR. SKA will allow mapping of individual galaxies at $1''$. After 10^h it will reach column densities of $2.5 \cdot 10^{20}$ cm^{-2}, while 100^h gives a 5σ limit of $8 \cdot 10^{19}$. This allows mapping of galaxies out to 10 Mpc at a spatial resolution that has so far only been possible in our Local Group.

SKA1-MID has an exquisite column density sensitivity, and at an angular resolution of $30''$ is extremely efficient in detecting low-column density H I. At 10^h it will reach limits of $2.9 \cdot 10^{18}$ cm^{-2}, which is twice as deep as the deepest existing observations at comparable resolutions. A 100^h integration gives limits of $9.3 \cdot 10^{17}$ cm^{-2}, comparable to what is achieved with the single-dish Green Bank Telescope, but at 20 times better resolution. SKA1-SUR will again be able to provide quantitative information on the environment and larger surroundings of any detections.

The full SKA will be truly ground-breaking: after 10^h its column density limit at $30''$ angular resolution is $\sim 2.8 \cdot 10^{17}$ cm^{-2}, after 100^h, $\sim 8.9 \cdot 10^{16}$ cm^{-2}. The latter will enable a direct exploration of the link between galaxies and the cosmic web, and should reveal accretion processes in great detail.

SKA will therefore revolutionize our understanding of star formation in other galaxies, the processes leading to it, as well as the ways by which galaxies acquire the necessary gas.

References

Bagetakos, I., Brinks, E., Walter, F., et al. 2011, AJ, 141, 23

Begum, A., Chengalur, J.N., Karachentsev, I.D., Sharina, M.E., Kaisin, S.S. 2008, MNRAS 386, 1667

Bigiel F., Leroy A., Walter F., Brinks E., de Blok W.J.G., Madore B., Thornley M.D., 2008, AJ, 136, 2846

Bigiel F. et al., 2011, ApJ, 730, L13

Blyth, S.-L., et al., 2015, "Exploring Neutral Hydrogen and Galaxy Evolution with the SKA", in proc. *Advancing Astrophysics with the Square Kilometre Array*, PoS(AASKA14)128

PoS(AASKA14)129

Borthakur, S., Yun, M. S., & Verdes-Montenegro, L. 2010, ApJ, 710, 385
Braun, R., Thilker, D. A., Walterbos, R. A. M., & Corbelli, E. 2009, ApJ, 695, 937
Braun, R., 2014, SKA-TEL-SKO-DD-XXX, Rev A DRAFT 5 (2014-06-02)
Bregman, J. N. 1980, ApJ, 236, 577
Calzetti, D., Liu, G., & Koda, J. 2012, ApJ, 752, 98
Calzetti, D. 2013, Secular Evolution of Galaxies, 419
Cannon, J. M., Giovanelli, R., Haynes, M. P., et al. 2011, ApJL, 739, L22
Chiappini, C., Matteucci, F., and Gratton, R. 1997, ApJ, 477, 765
Chomiuk, L. and Povich, M. S. 2011, AJ, 142, 197
de Blok, W.J.G., 2010, Advances in Astronomy, 2010, article id. 789293
de Blok, W. J. G. & Walter, F. 2006, AJ, 131, 363
de Blok, W. J. G., Keating, K. M., Pisano, D. J., et al. 2014, arXiv:1407.3648
de Heij, V., Braun, R., and Burton, W.B. 2002, A&A, 392, 417
Dewdney, P.E., et al., 2013, SKA-TEL-SKO-DD-001 (2013-03-13)
di Cintio, A., Brook, C., Dutton, A.A., Macciò, A.V., Stinson, G.S., Knebe, A. 2014, MNRAS, 441, 2986
Dutta, P., Begum, A., Bharadwaj, S., & Chengalur, J. N. 2009, MNRAS, 398, 887
Dutta, P., Begum, A., Bharadwaj, S., & Chengalur, J. N. 2013, New Astronomy, 19, 89
Fernandez, X., Joung, M. R., and Putman, M. E. 2012, ApJ, 749, 181
For, B.-Q., Koribalski, B.S., Jarrett, T.H. 2012, MNRAS 425, 1934
Ford, H.A., Lockman, F.J., and McClure-Griffiths, N.M. 2010, ApJ, 722, 367
Fraternali, F. and Binney, J. J. 2008, MNRAS, 386, 935
Fraternali, F. and Tomassetti, M. 2012, MNRAS, 426, 2166
Fraternali, F., Oosterloo, T., Sancisi, R., van Moorsel, G. 2001, ApJL, 562, L47
Fraternali, F., van Moorsel, G., Sancisi, R., and Oosterloo, T. 2002, AJ, 123, 3124
Fraternali, F. 2013, IAU Symp. 298 (arXiv:1310.2956)
Fukui, Y., Kawamura, A., Wong, T., et al. 2009, ApJ, 705, 144
Heald, G., Józsa, G., Serra, P., et al. 2011, A&A, 526, A118
Heald, G. et al. 2015, A&A, in prep
Hess, K.M., Pisano, D.J., Wilcots, E.M., and Chengalur, J.N., 2009, ApJ, 699, 76 2009.
Hopkins, A. M., McClure-Griffiths, N. M., and Gaensler, B. M. 2008, ApJ, 682, L13
Hunter, D. A., Ficut-Vicas, D., Ashley, T., et al. 2012, AJ, 144, 134
Ianjamasimanana, R., de Blok, W. J. G., Walter, F., & Heald, G. H. 2012, AJ, 144, 96
Irwin, J.A, Hoffman, G.L., Spekkens, K., et al., 2009, ApJ, 692, 1447
Jütte, E., Heald, G., et al. 2015, A&A, in prep.
Kamphuis, J., Sancisi, R., & van der Hulst, T. 1991, A&A, 244, L29
Karachentsev, I. D., Karachentseva, V. E., Huchtmeier, W. K., & Makarov, D. I. 2004, AJ, 127, 2031
Karachentsev, I. D., Makarov, D. I., & Kaisina, E. I. 2013, AJ, 145, 101
Kennicutt R. C., Jr., 1989, ApJ, 344, 685
Kennicutt R. C., Jr., 1998, ARA&A, 36, 189
Kereš, D., Katz, N., Weinberg, D. H., & Davé, R. 2005, MNRAS, 363, 2
Kim, S., Staveley-Smith, L., Dopita, M. A., et al. 2003, ApJS, 148, 473

PoS(AASKA14)129

Koribalski, B. S. 2008, in "Galaxies in the Local Volume", Astrophysics and Space Science Proceedings, eds. Koribalski & Jerjen, Springer Netherlands, p. 41
Leroy A. K., Walter F., Brinks E., Bigiel F., de Blok W. J. G., Madore B., Thornley M. D., 2008, AJ, 136, 2782
Maloney, P.R., and Putman, M.E., 2003, ApJ, 589, 270
Mapelli, M., Moore, B., & Bland-Hawthorn, J. 2008, MNRAS, 388, 697
Marinacci, F., Binney, J., Fraternali, F., Nipoti, C., Ciotti, L., and Londrillo, 2010, MNRAS, 404, 1464
McClure-Griffiths, N.M., et al., 2015 "Galactic and Magellanic Evolution with the SKA", in proc. *Advancing Astrophysics with the Square Kilometre Array*, PoS(AASKA14)130
Mundell, C. G., James, P. A., Loiseau, N., Schinnerer, E., & Forbes, D. A. 2004, ApJ, 614, 648
Nelson, D., Vogelsberger, M., Genel, S., Sijacki, D., Keres, D., Springel, V., Hernquist, L. 2013, MNRAS, 429, 3353
Norman, C. A., & Ikeuchi, S. 1989, ApJ, 345, 372
Oh, S.-H., Brook, C., Governato, F., Brinks, E., Mayer, L., de Blok, W.J.G., Brooks, A., Walter, F. 2011, AJ, 142, 24
Oosterloo, T., Fraternali, F., & Sancisi, R. 2007, AJ, 134, 1019
Ott, J., Wong, T., Pineda, J. L., et al. 2008, PASA, 25, 129
Ott, J., Stilp, A. M., Warren, S. R., et al. 2012, AJ, 144, 123
Panter, B., Jimenez, R., Heavens, A. F., & Charlot, S. 2007, MNRAS, 378, 1550
Pisano, D. J., Barnes, D. G., Gibson, B. K., et al. 2007, ApJ, 662, 959
Pisano, D. J. 2014, AJ, 147, 48
Popping, A., et al., 2015, "Observations of the Intergalactic Medium and the Cosmic Web in the SKA era", in proc. *Advancing Astrophysics with the Square Kilometre Array*, PoS(AASKA14)132
Putman, M. E., de Heij, V., Staveley-Smith, L., et al. 2002, AJ, 123, 873
Putman, M. E., Peek, J. E. G., & Joung, M. R. 2012, ARA&A, 50, 491
Roychowdhury, S., Chengalur, J. N., Kaisin, S. S., & Karachentsev, I. D. 2014, MNRAS, 445, 1392
Ryan-Weber, E., et al. 2008, MNRAS 384, 535
Morganti, R., et al., 2015, "Cool Outflows and HI absorbers with SKA", in proc. *Advancing Astrophysics with the Square Kilometre Array*, PoS(AASKA14)134
Sancisi, R., & Allen, R. J. 1979, A&A, 74, 73
Sancisi, R., Fraternali, F., Oosterloo, T., & van der Hulst, T. 2008, A&A Rev, 15, 189
Schönrich, R. and Binney, J. 2009, MNRAS, 396, 203
Schruba A., et al., 2011, AJ, 142, 37
Serra, P., Oosterloo, T., Morganti, R., et al. 2012, MNRAS, 422, 1835
Shapiro, P. R., & Field, G. B. 1976, ApJ, 205, 762
Stanimirović, S., Murray, C. E., Lee, M.-Y., Heiles, C., & Miller, J. 2014, ApJ, 793, 132
A. Sternberg, C. F. McKee, and M. G. Wolfire 2002, ApJS, 143, 419
Stilp, A. M., Dalcanton, J. J., Warren, S. R., et al. 2013, ApJ, 765, 136
Swaters, R. A., Sancisi, R., and van der Hulst, J. M. 1997, ApJ, 491, 140
Thilker D. A., et al., 2007, ApJS, 173, 538
Tumlinson, J., Thom, C., Werk, J. K., et al. 2013, ApJ, 777, 59

PoS(AASKA14)129

van der Hulst, J. M., van Albada, T. S., & Sancisi, R. 2001, Gas and Galaxy Evolution, 240, 451
Verdes-Montenegro, L., Yun, M. S., Williams, B. A., et al. 2001, A&A, 377, 812
Wakker, B. P., York, D. G., Howk, J. C., et al. 2007, ApJL, 670, L113
Wakker, B. P., York, D. G., Wilhelm, R., et al. 2008, ApJL, 672, 298
Walter, F., Brinks, E., de Blok, W. J. G., et al. 2008, AJ, 136, 2563
Warren, B. E., Jerjen, H., & Koribalski, B. S. 2004, AJ, 128, 1152
Warren, S. R., Skillman, E. D., Stilp, A. M., et al. 2012, ApJ, 757, 84
Westmeier, T., Braun, R., and Thilker, D., 2005, A&A, 436, 101
Westmeier, T., Braun, R., & Koribalski, B. S. 2011, MNRAS, 410, 2217
Westmeier, T., Koribalski, B.S., and Braun, R. 2013, MNRAS, 434, 3511
Young, L. M. & Lo, K. Y. 1996, ApJ, 462, 203
Young, L. M. & Lo, K. Y. 1997, ApJ, 490, 710
Young, L. M., van Zee, L., Lo, K. Y., Dohm-Palmer, R. C., & Beierle, M. E. 2003, ApJ, 592, 111

PoS(AASKA14)129

PROCEEDINGS OF SCIENCE

Galactic and Magellanic Evolution with the SKA

Naomi M. McClure-Griffiths*[1], Snežana Stanimirović[2], Claire E. Murray[2], Di Li[3], John M. Dickey[4], Enrique Vázquez-Semadeni[5], Josh E. G. Peek[6], Mary Putman[6], Susan E. Clark[6], Marc-Antoine Miville-Deschênes[7], Joss Bland-Hawthorn[8], Lister Staveley-Smith[9], on behalf of the H I Science Working Group

[1]*CSIRO Astronomy & Space Science, Australia;* [2]*University of Wisconsin-Madison, USA;* [3]*National Astronomical Observatories of China, China;* [4]*University of Tasmania, Australia;* [5]*Centro de Radioastronomía y Astrofísica, UNAM, Morelia, Mexico;* [6]*Columbia University, USA;* [7]*CNRS - Institut d'Astrophysique Spatiale, Université Paris-XI, Orsay, France;* [8]*Sydney Institute for Astrophysics, University of Sydney, Australia;* [9]*International Centre for Radio Astronomy Research , University of Western Australia, Australia*

E-mail: naomi.mcclure-griffiths@csiro.au

As we strive to understand how galaxies evolve it is crucial that we resolve physical processes and test emerging theories in nearby systems that we can observe in great detail. Our own Galaxy, the Milky Way, and the nearby Magellanic Clouds provide unique windows into the evolution of galaxies, each with its own metallicity and star formation rate. These laboratories allow us to study with more detail than anywhere else in the Universe how galaxies acquire fresh gas to fuel their continuing star formation, how they exchange gas with the surrounding intergalactic medium, and turn warm, diffuse gas into molecular clouds and ultimately stars. The λ21-cm line of atomic hydrogen (H I) is an excellent tracer of these physical processes. With the SKA we will finally have the combination of surface brightness sensitivity, point source sensitivity and angular resolution to transform our understanding of the evolution of gas in the Milky Way, all the way from the halo down to the formation of individual molecular clouds.

Advancing Astrophysics with the Square Kilometre Array
June 8-13, 2014
Giardini Naxos, Italy

*Speaker.

PoS(AASKA14)130

1. Introduction

The next decades offer us the opportunity to revolutionize our understanding of how galaxies form and evolve. The current paradigm is that galaxies form at the nexus between colliding streams of cold dark matter, where new stellar systems form through bursts of star formation (SF; e.g. Vogelsberger et al. 2014). Strong winds driven by SF can force gas out of galaxies (Veilleux et al. 2005) and conversely galaxies must accrete new material to sustain their SF rates. In addition, there is mounting evidence from numerical simulations that molecular clouds form at the interfaces of colliding streams of warm atomic gas, at least under conditions similar to those in the present Milky Way. Thus, there appears to exist a continuous gas flow from extragalactic scales down to stellar scales.

The Milky Way (MW) and Magellanic System are ideal laboratories for studying the evolution of gas in galaxies. These systems have a wide range of physical conditions, including high and low interstellar heavy element abundance and SF rates. They are close, so close that the SKA will achieve spatial resolution finer than one parsec, in some cases as small as an AU. With this extreme spatial resolution, in combination with high spectral resolution, we can resolve many of the open questions about galaxy evolution: how galaxies acquire fresh gas, how they feed gas to local environments and how they turn warm, diffuse gas into cold, dense gas and ultimately form stars. In addition, the Magellanic Stream (MS), Large Magellanic Cloud (LMC), and Small Magellanic Cloud (SMC) showcase how rapidly star-forming gas driven by tidal interactions gets out of dwarf galaxies, eventually being accreted into larger systems, in this case the MW. They also show how the physical conditions of the interstellar medium (ISM) vary with heavy element abundance, gravitational potential depth, and radiation field. The MW is in many ways an archetypal spiral galaxy, and so is an important point of comparison for extragalactic studies. In addition, there is some evidence from its star formation rate and global color that the MW is undergoing one of the most important transitions in galaxy evolution, leaving its period of rapid star formation and entering the so-called “green valley", and that it will have all but extinguished its star formation in less than 5 Gyr (Mutch et al. 2011). Studying the cold gas in the MW will elucidate how star formation is quenched during this pivotal era. Thus, it is of fundamental importance to characterize the gas flow into, within, and from the Galaxy.

The λ21-cm line is an excellent tracer of the neutral interstellar medium (ISM) in galaxies. Atomic hydrogen (H I) is found in a variety of environments, from dense clouds to the diffuse galactic halo and shows structure with size scales from kilo parsecs to a few tens of AU. Galactic H I spectral lines vary in width from ~ 1 km s^{-1} to ~ 60 km s^{-1}, tracing gas with temperatures from 20 K to 8000 K. The SKA will combine surface brightness sensitivity with the angular resolution provided by long baselines to deliver a MW gas survey machine. Combining SKA H I data with single-dish or auto-correlation data for the so-called “zero-spacing” will probe H I in the MW and Magellanic Clouds (MCs) over its full range of size scales and temperatures.

The combination of excellent H I surface brightness sensitivity and dense coverage of H I absorption measurements will enable measurements of the multiphase gas flows into and out of the Milky Way disk and MCs. In combination with tracers of molecular gas and dust, such as maps made by Planck and Herschel, these H I data will reveal the transitions between atomic and molecular material within interstellar clouds that are crucial for star formation. Only the SKA will be able

PoS(AASKA14)130

to capture these clouds in the MCs for the first time at sub-parsec resolution, providing important tests of the effect of metallicity and radiation field on molecular cloud formation and evolution. Over the next decade, GAIA and the Large Synoptic Survey Telescope (LSST) will provide stellar distance measurements for constructing 4D (3D plus velocity) maps of nearby nearby interstellar clouds. Moreover, the SKA will make it feasible to perform large-scale absorption surveys of the OH molecule. It has recently been realized that this molecule may be an ideal tracer of the so-called CO-free molecular gas, thus allowing us to investigate in detail the transformation of gas from atomic to molecular.

In this chapter we outline a number of areas where the SKA will transform our understanding of how the MW and Magellanic System work. This understanding will provide much of the physical underpinning for how large spirals and dwarf irregular galaxies evolve.

2. The Structure and Evolution of Gas in the Milky Way and Magellanic System

2.1 Understanding how gas accretes onto, moves within, and is lost from a galaxy

Galaxies are not closed systems. The evolution of the MW is significantly impacted by the two-way flow of gas and energy between the Galactic disk, halo, and intergalactic medium. We have long known that there is an extended halo of gas, both atomic and ionized, far beyond the disk of the Galaxy (e.g. Lockman 1984; Kalberla & Dedes 2008; Reynolds 1991; Gaensler et al. 2008). In recent years we have also come to realize that the atomic portion of the halo is a highly structured and dynamic component of the Galaxy. Despite these advances we are far from understanding the origin of the gaseous halo and its interaction with the disk of the Galaxy. There are two dominant sources of structure in the halo: one is the outflow of gas from the Galactic disk, and the second is the infall of gas from extragalactic space (Putman et al. 2012). The interplay of these sources and their relative importance on the global evolution of the MW, and MW-like galaxies, is not known.

2.1.1 Accretion

Cosmological simulations predict that gas accretion onto galaxies is ongoing into the present epoch (e.g Joung et al. 2012). Maintaining the star formation rate measured in galaxies across cosmic time requires significant amounts of gas infall (e.g. Hopkins et al. 2008). The Milky Way is a clear example of this. With $\sim 5 \times 10^9$ $M_\odot$ of gas in the disk and a current star formation rate of $1-3$ $M_\odot$ year^{-1}, it is clear that the Galaxy would exhaust its supply of star-forming gas in only a few Gigayears (Putman et al. 2012). The problem of providing new gas to facilitate star formation is not just limited to the current epoch. Measurements of stellar ages in disk stars show that they have formed continuously over the past ~ 12 Gyrs (e.g. Bensby et al. 2014) and chemical evolution models can only reproduce the abundances observed in old stars by assuming continuous accretion of low metallicity gas (e.g. Chiappini et al. 2001; Schönrich & Binney 2009).

An outstanding source of low-metallicity star formation material for disk galaxies is gas accretion from the disruption of neighboring dwarf galaxies. The Magellanic System, created from the interaction between the SMC, LMC and the MW, provides the closest example of galaxy fueling. While the Magellanic Leading Arm is believed to be closely interacting with the MW disk, the northern tip of the MS is furthest from the MW and contains a wealth of small scale structure (Stanimirović et al. 2008). Surrounding the neutral MS is a significant pool of ionized gas, indicated

PoS(AASKA14)130

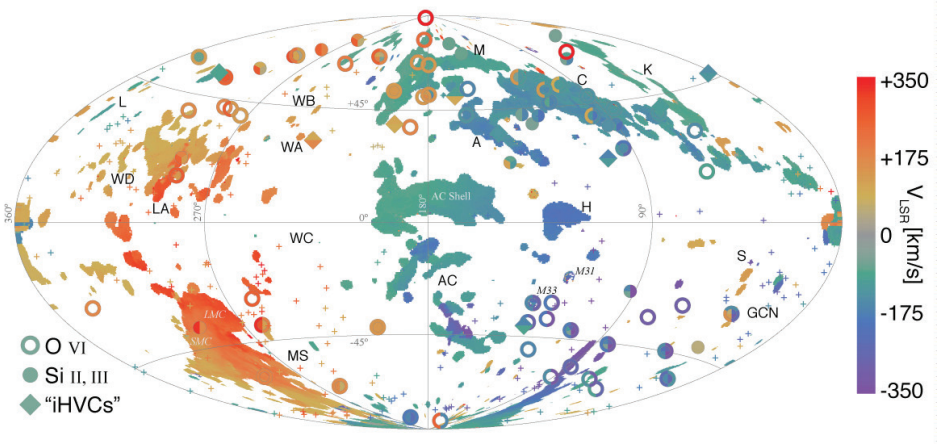

Figure 1: Distribution of high velocity clouds (HVCs) detected in H I and overlaid with measurements of low column density absorbers traced via ultraviolet metal lines (circles and diamonds). The plus symbols represent compact HI clouds, the distribution of which will change dramatically with SKA. The color scale indicates the local standard of rest velocity of the gas as shown in the bar at the right. From Putman, Peek & Joung (2012).

by UV absorption lines, which may account for as much as three times the mass of the neutral gas (Fox et al. 2014). By imaging both the neutral and the ionized gas we will be able to model how the gas is being broken down, and ultimately how it is accreting onto the MW. To image the neutral gas we will need the combination of surface brightness sensitivity, spatial coverage and angular resolution provided by the SKA. Detailed H I images to a low column density limit will allow us to study the physical and thermal structure of the Magellanic System throughout the halo and probe the interaction between the Magellanic H I features and the MW disk and halo. The H I images can be compared with three-dimensional maps of the warm, ionized gas made with large-area, high kinematic resolution integral field units on 8-m optical telescopes to show the flow of warm gas relative to the disk. These studies will reveal the dynamical and thermal instability processes that are essential for feeding external material into galaxies. The SKA will also allow us to trace cold gas throughout the Stream by resolving, spatially and spectrally, cold cores, and allowing us to search for absorption through the Stream. Finally, these studies will help us to probe the physical properties of the halo itself, using the Stream clouds as test particles in the halo.

Another potential source of accreted gas is the reservoir of H I in the form of high velocity clouds (HVCs, see Figure 1); however, these clouds fall about an order of magnitude short of what is needed (Putman et al. 2012). Some of the missing mass is in the form of ionized gas (e.g. Lehner et al. 2012; Fox et al. 2014) and another, undetermined, small fraction may be in the form of small, dense clumps of optically thick material. While the ionized gas is best traced by UV and optical absorption lines, gas at $T < 8000$ K is well-traced by H I. Our understanding of the link between the H I gas detected in emission and warm gas detected in ultraviolet absorption will change dramatically with the SKA. While high velocity H I gas detected in emission has been estimated to cover ∼35% of the sky, high velocity gas detected in absorption using metal lines is found to cover on the order of 80% of the sky. This indicates there is a large reservoir of gas in the Galaxy's halo with column densities of N(H I) $< 10^{18}$ cm^{-2} that remains to be detected in H I

PoS(AASKA14)130

emission (e.g. Lehner et al. 2012). This is consistent with what has been found in other galaxy halos (e.g. Werk et al. 2014). Very deep integrations of H I and spatial stacking have detected some of this diffuse (N(H I) $\sim 2 \times 10^{18}$ cm^{-2}) medium as HVC envelopes with FWHM ~ 60 km s^{-1} at the interface with the hot halo gas (Nigra et al. 2012). This diffuse low column density material could be important for cloud lifetimes and overall accretion onto the Milky Way. To detect this gas we require a combination of extremely high surface brightness sensitivity and "zero-spacing" observations for H I mapping of all angular scales. Combining these maps with sensitive H I absorption observations, the SKA will be able to *detect* and *map* both the cold and warm gas reservoirs of Milky Way star formation fuel.

We also know that cool ($T < 1000$ K) gas exists in the HVC population. In some cases, H I cores have been found to be associated with optical and UV absorption line systems when synthesis observations are completed (Ben Bekhti et al. 2009). Kalberla & Haud (2006) find that 24% of HVC sight-lines show narrow-line width ($\Delta v \sim 7$ km s^{-1}) components consistent with multiphase structure in the condensed halo. Evidence from higher resolution observations suggests that beam dilution hides some of this cool gas (Moss 2014). Furthermore, data from FUSE show H_2 absorption in more than a dozen high and intermediate velocity clouds (Richter et al. 2001). Unfortunately, most of what we know about the multiphase H I in the MW halo is derived from single dish observations, which lack the spatial resolution to clearly detect small, cold clumps of H I. We know very little about the temperature, distribution or quantity of cool H I in the halo. At present there are only two measurements of H I gas excitation, or *spin*, temperature in an HVC (Wakker et al. 1991; Matthews et al. 2009). Absorption line measurements with the SKA, with its resolution and sensitivity, will comprehensively determine the amount of condensed gas in the halo enabling direct comparisons with theoretical and numerical models (e.g. Wolfire et al. 1995, Joung et al. 2012). Furthermore, estimates of the mass of H I in HVCs rely on the assumption of optically thin gas when calculating column densities (Putman et al. 2002; Moss et al. 2013), leading to underestimates of the total HVC mass in the halo. Using NVSS continuum source counts (Condon et al. 1998) we estimate that with the SKA we will measure hundreds of absorption components through HVCs, giving estimates of H I spin temperatures and opacity in HVCs and estimates of the fraction of gas "missed" by optical depth assumptions.

2.1.2 Outflow

A significant fraction of the gas in the Galactic halo may also be attributed to the outflow of structures formed in the disk, but extending into the halo. Large-scale H I "chimneys" (e.g. McClure-Griffiths et al. 2006; Pidopryhora et al. 2007) supply hot, metal-enriched gas to the Galactic halo via the "Galactic Fountain" (Shapiro & Field 1976; Bregman 1980) and also may be a dominant source of multi-phase gas structure for the lower halo. Dense, cool condensations from expelled gas (e.g. de Avillez 2000) and the tops of H I chimneys that break at z-heights of $\sim$1 kpc (e.g. Mac Low et al. 1989) may populate the halo. Deriving the destruction timescales and physical properties (temperature, density) of multiphase fountain gas will inform our estimates of the survival times and journey histories for cold halo cloud populations. High sensitivity SKA observations of H I in emission and absorption, together with observations of molecular and ionized gas tracers, will reveal the multiphase structure of gas outflowing from the disk. Comparison of

PoS(AASKA14)130

multiphase gas properties with heating and cooling models (e.g. Wolfire et al. 1995) will determine the pressure and thermal structure of the lower halo of the MW.

Galactic fountain gas may even play an important role in seeding the halo to trigger gas accretion from so-called hot-mode accretion. Fraternali et al. (2013) have suggested that high-metallicity expelled gas mixes efficiently with hot halo gas and triggers the cooling of such gas in the lower halo. This cooled gas is observed as absorption features (e.g. Lehner et al. 2012) and can efficiently accrete onto the disk. Fraternali et al. estimate that supernova-driven fountain cooling produces a net gas accretion onto the disk at a rate of a few $M_\odot$ yr^{-1} and speculate that this mechanism explains how the hot mode of cosmological accretion feeds star formation in galactic disks. This intriguing suggestion can be tested by combining SKA H I observations with UV/optical absorption line measurements. A sensitive SKA survey of H I emission in the lower halo of the Milky Way will reveal the predicted low column density ($< 10^{19}$ cm^{-2}) tails of Galactic fountain material. These images, combined with H I absorption will directly associate cool and warm H I, measure temperatures, and trace its origins to the disk.

2.1.3 The SKA and Gas Tomography

The development of the SKA is happening in tandem with an ongoing explosion of stellar data. The gaseous properties can be linked to the dust and distance measurements made using detections of stars in the halo of the MW and LMC from future large optical surveys, such as Pan-STARRS and LSST. By measuring the colors of stars with enormous photometric surveys we are able to build 3D tomographic maps of the dust distribution in the Galaxy (Green et al. 2014; Schlafly et al. 2014). In many circumstances, especially in low-density environments, H I and dust trace the same underlying distribution of material. For example, by looking at absorption lines toward stars, there have been some measurements of distances to high velocity gas (e.g. Thom et al. 2008), and from those estimates of accretion rates onto the Galaxy (Putman et al. 2012). Thus, if we are able to combine our kinetic information from a high sensitivity SKA Galactic H I survey with the tomographic information from stellar surveys we will be able to produce truly 4D (3D plus velocity) kinetic tomography maps of gas flow to and from the Milky Way, revealing how feedback works in disk galaxies.

Within our Galaxy's disk, structures are formed through the collapse of diffuse material. By combining H I kinematics with information on the distance of gas, observations of H I represent a direct measurement of one of the most fundamental questions in all astronomy, "where did this come from"? To understand formation using observations of diffuse gas we look to the continuity equation, which relates the rate of change of density ($\delta\rho/\delta t$) to the spatial and kinematic state of the fluid. The position-position-velocity (or hyper-spectral) data provided by radio surveys is clearly incomplete for this task — we do not have access to distance information. This leads to highly model-dependent descriptions of the state of the Galaxy. As an example, maps of the H I surface density of the disk must rely on assumptions of a flat rotation curve to extrapolate into the third spatial dimension (e.g. Levine et al. 2006). Even with these assumptions, we lose information about flows of the gas beyond simple rotation, and thus are blind to the more complex dynamics at play. The high angular resolution H I data cubes that we will obtain with the SKA can be used in conjunction with deep photometric stellar surveys to finally enable 4D kinetic tomography maps of gas flow within the MW. Combining high angular resolution H I data, which provides the

PoS(AASKA14)130

information we need to isolate individual H I structures, with next-generation photometric surveys of tens of billions of stars which give us precision reddening information, will allow us to determine the distance to many Galactic H I structures enabling reconstruction of the detailed structure of the MW disk. With the full kinematic information, vertical oscillations and corrugations of the MW disk will be related for the first time to small-scale dynamical effects of spiral arms, giant molecular clouds, and/or sites of stellar energy injection.

2.2 Tracing the Life-cycle of Hydrogen from Diffuse to Molecular

The current paradigm is that gas in the MW is continually *flowing* between its various thermal states. The flow changes gas from its warm $T \sim 10^4$ K state, through an intermediate unstable phase, to its cold atomic form, with temperatures ranging from ~ 20 K to 500 K. How exactly atomic gas transitions into denser, colder clouds in which the hydrogen is mostly in molecular form and in which stars form, is still not understood.

The corollary of this hydrogen life-cycle is that the formation of stars ultimately destroys the molecular clouds, and a large fraction of the gas is returned to either ionized or atomic form. Part of understanding how a galaxy evolves is understanding how much hydrogen exists in its various states and the flow rates between states and scales. The SKA is the only instrument capable of providing direct and statistically significant measurements ($\sim 2 \times 10^5$ sources) of neutral gas states over the full temperature range from 20 to 10^4 K, while simultaneously probing diverse interstellar environments and spatial scales from AU to kiloparsecs.

2.2.1 Distribution of Mass and Temperature in the Cool, Unstable and Warm Atomic Medium

Interstellar gas is subject to strong radiative heating and cooling processes which, within certain density or temperature ranges, may cause a gas parcel to become depressurized when it is compressed (Field 1965; Field et al. 1969; Wolfire et al. 1995) leading to the so-called *thermal instability* and a runaway compression which lasts until the parcel exits the unstable range. This process tends to segregate the atomic gas into a warm/diffuse phase called the warm neutral medium (WNM) and a cold/dense phase called the cold neutral medium (CNM). The classical picture arising from this is that the medium should exist in two or three main stable phases (Field et al. 1969; McKee & Ostriker 1977) with very little gas in the thermally unstable range. However, both observational (e.g. Dickey et al. 1977; Kalberla et al. 1985; Heiles & Troland 2003) and numerical (e.g. Vázquez-Semadeni et al. 2000; Gazol et al. 2001, 2005; Audit & Hennebelle 2005; Hill et al. 2012) studies have suggested the presence of significant amounts of unstable gas. The existence of this unstable gas could be understood theoretically as a consequence of several physical processes. Small-scale changes in pressure caused by spiral arms or the distance from the Galactic mid-plane can alter the temperature range where stable gas is observed. Alternatively, the mixing action of turbulence, which causes the gas to flow from one phase to another, can produce gas in the traditionally unstable temperature range. However, the predicted fraction of thermally unstable gas varies hugely across numerical models. Direct comparison with observations over focused interstellar conditions are highly required to constrain the above physical processes and timescales on which they operate.

PoS(AASKA14)130

The mass fraction in each of the hydrogen phase regimes, including the unstable regime, is driven by the heating and cooling processes and therefore is highly sensitive to parameters such as metallicity, the interstellar radiation field and the strength of the turbulence (Wolfire et al. 2003). Surprisingly, even the fractions of the total H I mass in the CNM and WNM for most regions of the Galaxy are poorly known and almost nothing is known about how they vary with Galactic position. Our knowledge of the unstable gas fraction is even worse and the flow rates between stable and unstable phases are virtually unknown.

With the SKA we will achieve statistically meaningful measurements of the distribution of mass and temperature in the CNM and WNM, as well as the unstable phase. The SKA, with a deep survey of the Galactic plane and lower halo, will provide those measurements through detections of H I absorption, probing spiral arms, inter-arm regions and distance from the mid-plane. For the first time we will be able to measure gas spin temperature,distribution functions at all Galactocentric radii, as well as in and above the plane, and close to some major Giant Molecular Clouds (GMCs) with unprecedented spatial coverage of absorption sources. With this we can test the theoretical predictions on how the spin temperature varies with metallicity, interstellar radiation field and pressure for the first time.

2.2.2 Molecular cloud formation

Recent numerical studies suggest that cold, dense clouds of atomic hydrogen form by a phase transition from the WNM to the CNM induced by large-scale compressions in the warm gas (Ballesteros-Paredes et al. 1999; Audit & Hennebelle 2005; Heitsch et al. 2005, 2006; Vázquez-Semadeni et al. 2006). Such compressions may be a consequence of the general turbulence in the WNM or by large-scale instabilities that drive converging flows in this medium. Cold clouds formed by this mechanism can eventually develop column densities large enough for molecules to form, and ultimately form stars. Simulations of the formation of GMCs are rich and show that GMC formation can happen via many different avenues. One possibility is that cold clouds develop gravitational instabilities, which lead to contraction. Thus, molecular gas and stars may be the result of gravitational contraction starting in the atomic phase (e.g Vázquez-Semadeni et al. 2007; Heitsch et al. 2008; Heitsch & Hartmann 2008; Heitsch & Putman 2009; Banerjee et al. 2009) which, along the way, also produces complicated filamentary structures (Gomez & Vazquez-Semadeni 2013). As the gas flows from the WNM into the dense molecular structures, transitional regions that are mostly cold atomic in their outermost parts, then CO-free molecular, and finally CO-bearing molecular in their innermost parts are produced (Smith et al. 2014; Heiner et al. 2014). Alternatively, GMCs may develop from an agglomeration of small cold clouds, collected together by the sweeping action of spiral arms (Dobbs et al. 2012) or through the compressive action of superbubbles whose walls collect and compress small H I clouds (Ntormousi et al. 2011; Clark et al. 2012).

The detail apparent in the simulations is not yet matched by observational data. While undoubtedly most of the simulated physical processes are involved in forming molecular clouds, we do not have the observational handles to determine which processes dominate in different environments. Observing the flow pattern of cold atomic gas is difficult because of the confusion in the atomic gas along lines of sight inside our Galaxy. Dominated by turbulence and the overlay of structures, the spectral structure of Galactic H I line profiles is usually wider than 7 km s^{-1}. By

PoS(AASKA14)130

comparison, typical molecular line widths, although supersonic, are mostly on the order of ~ 1 km s^{-1}. This mismatch of spectral characteristics is the main reason why the atomic to molecular transition in ISM has not been mapped systematically, in spite of the existence of both large scale H I maps and large scale CO maps for more than three decades. The observational challenge lies in objectively associating flux in the H I line with a specific molecular structure, which is orders of magnitude smaller both in spatial extent and turbulence magnitude. SKA H I absorption measurements, combined with high surface brightness sensitivity data at high Galactic latitude and sub-arcminute resolution will generate a substantial catalogue of isolated H I clouds with simple Gaussian line profiles. These clouds can be observed with matching angular (~ 20") and velocity (0.3 km s^{-1}) resolutions in molecular tracers, such as OH, CO and HCO^+. The matching of molecules and atoms will enable quantitative analysis of important atomic to molecular transitions in many well-defined systems.

The SKA will finally give us the ability to observe the flow of cold H I onto molecular clouds and the mixture of phases within molecular clouds. One important tool in studies of cold gas flow is the wide-spread effect of H I Self-Absorption (HISA), which is observed when cold foreground H I absorbs background H I emission at similar velocities. Many of these features are completely without molecular counterparts (Gibson et al. 2005). Within molecular clouds, the collision with H_2 produces a much colder and generally narrower feature often called HI Narrow Self-Absorption (HINSA; Li & Goldsmith 2003). HISA and HINSA allow us to *map* the structure of cold gas, but because the temperature of the background emission is unknown we cannot know the temperature of the cold gas. By contrast, H I absorption toward continuum sources gives us the spin temperature of the gas, T_s, but not the spatial structure. Using the SKA we will finally be able to use a combination of HISA and H I continuum absorption to understand the *spatial* and *thermal* structure of cold H I. An SKA survey of the Milky Way will enable sensitive absorption studies toward background quasars giving opacity measurements with source density of > 10 deg^2. This survey will provide multiple absorption spectra across any given HISA feature, effectively providing a temperature gauge to calibrate the HISA optical depth. This powerful technique will provide accurate measurements of gas temperatures and column densities around and within molecular clouds. The SKA data will be combined with detailed studies of individual molecular clouds from ALMA for a complete picture of the flow of cold gas into and through molecular clouds.

The SKA will also enable essential complementary surveys of the hydroxyl (OH) molecule, whose emission is very weak, despite its probable ubiquity and large observed column densities. Recent evidence that a large fraction of molecular gas exists in the so-called "dark molecular gas" (or CO-free) form (Grenier et al. 2005; Planck Collaboration et al. 2011; Langer et al. 2010) amplifies the need to find other tracers of cold H_2. In models of photo-dissociation regions (PDRs), OH can form quickly in terms of extinction after H_2 becomes self-shielded (van Dishoeck & Black 1988). A series of charge exchange reactions facilitated by cosmic rays produces OH. Due to its low excitation temperature, however, large scale maps of OH emission has not been available. A systematic and large scale OH absorption survey, possible with the sensitivity afforded by the SKA, will quantify the amount of this potentially most abundant diatomic molecule after H_2 and lead to a Milky Way-wide measurement of dark molecular gas. The column densities and temperatures of OH will be the cornerstone to build models of H I-H_2 transition.

PoS(AASKA14)130

2.2.3 The multi-scale SKA meets the multi-scale ISM

Turbulence is a concept often applied to random variations in the density and velocity fields of the ISM. The term implies a stochastic process that transfers kinetic energy from larger to smaller scales in a cascade similar to the well known Kolmogorov process (Kolmogorov 1941, 1962, reviewed by Elmegreen and Scalo 2004, Falceta-Gonçalves et al. 2014), although only a few studies exist about the nature of the cascade in the strongly compressible case (e.g., Kritsuk et al. 2007). Interstellar turbulence affects many different kinds of observations, from spectral line cubes to pulsar scintillation. It is present in all phases of the ISM, yet its exact energy sources and sinks are still not identified. Interstellar turbulence can be measured quantitatively either through the structure function or power spectrum (Rickett 1977; Dickman & Kleiner 1985; Lazarian & Pogosyan 2000). The 21-cm line can be used in emission or absorption to trace turbulence in both the WNM and CNM over a broad range of scales. The SKA will connect the H I with turbulence in the warm ionized medium (WIM) on large-scales as traced by pulsars (Armstrong et al. 1995) and polarization observations of the magneto-ionic medium (Gaensler et al. 2011). On small scales the SKA will connect the CNM with turbulence in molecular clouds, where fluctuations in the density and velocity fields are generally thought to shape the processes of gravitational collapse and star formation (Larson 1981, Qian et al. 2012; see also the review by McKee and Ostriker 2007), although recently it has been proposed that, instead, these fluctuations are the result of global gravitational contraction in the clouds rather than the other way around (Ballesteros-Paredes et al. 2011).

Spectral line cubes of the 21-cm H I emission brightness over a large area with a small beam are used to characterize the turbulence spectrum over a range of scales, typically from $\sim$100 pc to $\sim$0.1 pc (Chepurnov et al. 2010; Pingel et al. 2013). The SKA will provide the high sensitivity and large numbers of independent emission spectra needed to compute the spatial power spectrum in the Galactic ISM down to AU scales and with precision and statistical confidence better than in previous studies (Crovisier & Dickey 1983; Green 1993; Dickey et al. 2001). In the Magellanic System, the sensitivity of a deep SKA survey will give a large improvement over the best existing data (Stanimirović & Lazarian 2001; Elmegreen et al. 2001; Muller et al. 2003). In nearby Galactic H I clouds, moments of the spectral line cubes give the velocity and density structure functions that can connect the turbulence spectrum in the H I to the very well known spectrum measured for the WIM (Armstrong et al. 1995). It will be particularly important to test whether the neutral medium has structure similar to the extreme scattering events (ESE) in the ionized gas (Fiedler et al. 1987; Walker & Wardle 1998), and to match structures in the H I with scattering screens deduced from pulsar scintillation (Bhat & Gupta 2002). Additional statistical measures such as those proposed by Burkhart et al. (2010) will probe deeper into the fluctuations of the ISM.

In the CNM, variations in the optical depth and line centre velocities among H I absorption spectra toward nearby background sources will provide a way of tracing turbulence independently of the H I emission that is dominated by WNM. The SKA will provide orders of magnitude more absorption spectra toward compact continuum sources, making it possible to use these data to map the variations in absorption on a wide range of scales. This is particularly important to connect with the "tiny scale structure" (Heiles 1997; Deshpande et al. 2000; Braun & Kanekar 2005) that is seen in similar variations of the absorption, particularly with VLBI (Roy et al. 2012). It will also be critical to link the turbulence in the CNM to that seen in molecular clouds using CO and

PoS(AASKA14)130

other molecular line tracers (Falgarone et al. 2009; Krčo et al. 2008; Li & Goldsmith 2012) using ALMA. Whether or not the turbulence in molecular clouds is "frozen-in" with the gas when it makes the transition from CNM atomic to molecular is an important question for understanding star formation. The multi-scale physics of the mass and energy cascade from large galactic scales down to the small scales on which molecular clouds shape the ISM is a challenge for our understanding of galaxy evolution. The SKA, with its inherent spatial dynamic range, is ideally designed to probe the multi-scale physics of the ISM.

2.3 Taking ISM evolution to The Magellanic Clouds

The MCs, including the SMC and LMC, offer a nearby example of a low-metallicity ($Z \sim 0.2$ $Z_\odot$ and 0.5, respectively; Dufour 1975, Olszewski 1996) environment with interstellar conditions that sharply contrast with what we find in the MW. Given their close proximity ($\sim$ 50–60 kpc Westerlund 1997), these are the only external galaxies where we can study the atomic and molecular content– from dense star-forming regions to diffuse accretion streams– at high (pc-scale) spatial resolution. In addition, the intense interstellar UV radiation field of the SMC and the LMC, $4-10$ times higher than that in the Solar neighborhood (Azzopardi et al. 1988), implies that heating and cooling rates, dust-to-gas ratios, and chemical abundances in the MCs represent the closest local examples of less-evolved systems common at high redshift.

2.3.1 Interstellar environment and the fraction of cold gas

The census of cold gas and its conversion into stars over cosmic time is one of several key parameters associated with galaxy evolution; however little is known about the cold atomic gas even in very nearby galaxies. As the "demography" of cold gas and the phase mix are largely driven by the heating and cooling processes – whose rates vary with metallicity, dust-to-gas ratio, and the strength of the interstellar radiation field – significant variations of the CNM/WNM properties and abundances are expected from a theoretical point of view (Wolfire et al. 2003). The reality is that, in our home neighborhood only 29 H I absorption measurements exist for the cold gas in the SMC (Dickey et al. 1994, 2000), the nearest metal-poor galaxy. Similarly, only a handful of H I absorption spectra exists for the LMC (Marx et al. 1997), M31 (Dickey & Brinks 1993), and M33 (Dickey & Brinks 1993; Braun 1997). The only recent attempt to study properties of cold gas in a lower-metallicity environment offered by the outer radii of the Milky Way resulted in a highly puzzling result. Dickey et al. (2009) suggest that the spin temperature of the CNM, and the CNM fraction, stay constant with Galactocentric radius. At a Galactocentric radius of 25 kpc, where the supernova rate, metallicity and interstellar radiation field are significantly lower than in the inner Galaxy, the temperature of cold gas, contrary to all theoretical predictions, is not different from what is found close to the Galactic centre (Strasser et al. 2007). The SKA will allow us to extend this test to lower metallicities within the LMC and SMC.

The SKA will revolutionize our understanding of the cold neutral gas in nearby galaxies, starting with the MCs. With 25 background radio continuum sources ($S > 20$ mJy) per square degree (Condon et al. 1998), $\sim$ 2000 H I absorption spectra with $\sigma_\tau < 10^{-2}$ will be obtained towards the MCs. This will allow us to measure the properties of the CNM in the Clouds and the mixture of warm and cool atomic gas, as well as their respective spatial distributions. A comparison

PoS(AASKA14)130

of the CNM/WNM statistics between the Milky Way and the MCs will show the variation of the heating and cooling rates with metallicity and how these processes affect the star formation rate.

2.3.2 Formation of H_2 in galaxies

Observational studies of galaxies (Kennicutt 1998; Bigiel et al. 2008; Schruba et al. 2011) show that the surface density of the star formation rate scales linearly with the surface density of molecular gas. This suggests that stars form in molecular clouds with a relatively similar efficiency and therefore the ability to form H_2 controls the evolution of individual galaxies. Another interesting observational result that came to light over the past few years is that the surface density of atomic gas (Σ_{HI}) on kpc-scales rarely exceeds ~ 10 $M_\odot$ pc^{-2} (e.g Bigiel et al. 2008). This saturation of Σ_{HI} provides important pointers for the physical conditions required to form molecular gas out of the atomic medium. For example, Krumholz et al. (2009) showed that in the case of equilibrium H_2 formation, a certain amount of H I surface density is required to shield H_2 against photodissociation, and this H I shielding surface density depends primarily on metallicity.

Lee et al. (2012) found a relatively uniform H I surface density of 6–8 $M_\odot$ pc^{-2} for several dark and star-forming regions in the Perseus molecular cloud in the MW and showed that Σ_{HI} and the H_2 fraction agree well with the equilibrium model predictions. However, the key test for understanding H_2 formation across galaxies requires observational probes of interstellar environments different from those we find in the MW. Extragalactic observations in the pre-SKA era cannot resolve individual molecular clouds. Only SKA observations of the MCs will provide crucial tests for the H I surface density and H_2 fraction in low metallicity and high-interstellar radiation field environments on pc-scales required to test both equilibrium and non-equilibrium (e.g. Glover & Mac Low 2007) models for H_2 formation and molecular cloud evolution.

2.3.3 The warm neutral medium and excitation of H I

The WNM is one of the least understood phases of the ISM. To constrain theoretical and numerical models of the ISM and its evolution over cosmic time, temperature distributions over the *full* temperature range from ~ 20 to $\sim 10^4$ K are essential. This requires extremely high-sensitivity observations due to the very low optical depth of the WNM, $\tau < 10^{-3}$. Only two direct measurements of WNM spin temperature exist for the MW so far (Carilli et al. 1998; Dwarakanath et al. 2002). Using the upgraded Very Large Array, Murray et al. (2014) detected statistically the presence of a widespread WNM population with $T_s = 7200$ K. This study was possible due to very deep integrations, detection and modeling of the CNM lines, and then stacking of the spectral residuals. This study demonstrates, for the first time, that the non-collisional excitation of H I is significant even at high Galactic latitudes. As Lyα scattering is the most likely candidate for additional excitation of H I, the Murray et al. results show that the fraction of Lyα photons, and/or the photon propagation through the ISM, are likely more complicated than what is currently assumed. For example, both a theoretical study by Liszt (2001) and recent numerical simulations by Kim et al. (2014) assume a uniform flux of Lyα photons throughout the ISM and result is the expected $T_s \lesssim 4000$ K. Clearly, this discrepancy between observations and theory needs to be understood.

The high sensitivity enabled by the SKA will allow direct measurements of WNM spin temperature and its spatial variations for the first time. As extremely high sensitivity is needed, the

PoS(AASKA14)130

MCs are perfect candidates for obtaining deep H I absorption spectra ($\sigma_\tau = 10^{-4}$ per 1 km s^{-1} velocity channels) to provide a statistically significant sample of the WNM. With thousands of H I spectra we will also be able to stack selectively to probe different interstellar environments (e.g. close to major star forming regions vs galaxy outskirts).

Finally, while the H I content of the MCs has been extensively studied alone and in synergy with other multi-wavelength observations (e.g. Kim et al. 1998; Stanimirović et al. 1999; Leroy et al. 2007; Meixner et al. 2013), the SKA will provide necessary sensitivity and angular resolution to match H I images with the resolution of Spitzer, Herschel ($18''$ and $12''$, respectively), and ALMA images.

2.4 The Milky Way as a Foreground for Cosmology

To properly measure the magnitudes and colors of populations of extragalactic objects, a correction for the extinction and reddening caused by dust in the MW is crucial. There are classically two ways of mapping this correction across the high Galactic latitude sky. The first is to measure the far-infrared (IR) emission from dust particles and make an assumption about the ratio of this emission to reddening and extinction. This method has been implemented by Schlegel et al. (1998, SFD). The second is to assume dust and neutral gas are well mixed, and that neutral gas dominates the column density, so that the H I column density can be used as a proxy for extinction (Burstein & Heiles 1978). It has recently been shown that known biases in the SFD dust map affect large-scale structure observations to the point of significantly biasing estimation of key cosmological parameters (Huterer et al. 2013), such as the evolution of the equation of state of dark matter (dw/dt) or cosmic non-Gaussianity. Thus, we require higher precision, less biased dust maps than are currently available to make best use of planned cosmological studies of large-scale structure. It has also recently been shown that better dust maps can be constructed by combining far-IR-based methods and H I-based methods (Peek 2013). Thus, a high-resolution H I column density map of the high-latitude sky is a crucial product of the SKA. At present it is not known whether the CNM and WNM phases of the ISM have significantly different ratios of reddening to integrated H I line intensity, but it is likely, as differing gas volume densities modify grain depletion (Wakker & Mathis 2000). If this is the case, it is crucial that a high latitude survey not only have high angular resolution and sensitivity, but also high spectral resolution to get independent estimates of CNM (narrow) and WNM (broad) columns for each line of sight.

3. Goals for SKA1

Significant advances in our understanding of the evolution of the H I in the MW and Magellanic System from kiloparsec to AU scales can be achieved through two surveys, both with high spectral and spatial resolution. One survey will be a shallow, high spectral resolution, all-sky survey of Galactic H I, which could be carried out commensally with an all-sky continuum survey covering 1420 MHz. The second will target the Galactic Plane and Magellanic System with high sensitivity, spectral resolution and angular resolution. The two surveys are described below. Critical to both surveys are the requirements for: a) high velocity resolution on the order of ~ 0.3 km s^{-1} to resolve narrow spectral lines of $\Delta v \sim 2$ km s^{-1}, b) excellent surface brightness sensitivity for imaging of diffuse H I emission, c) capacity to recover "zero-spacing" flux by combining

PoS(AASKA14)130

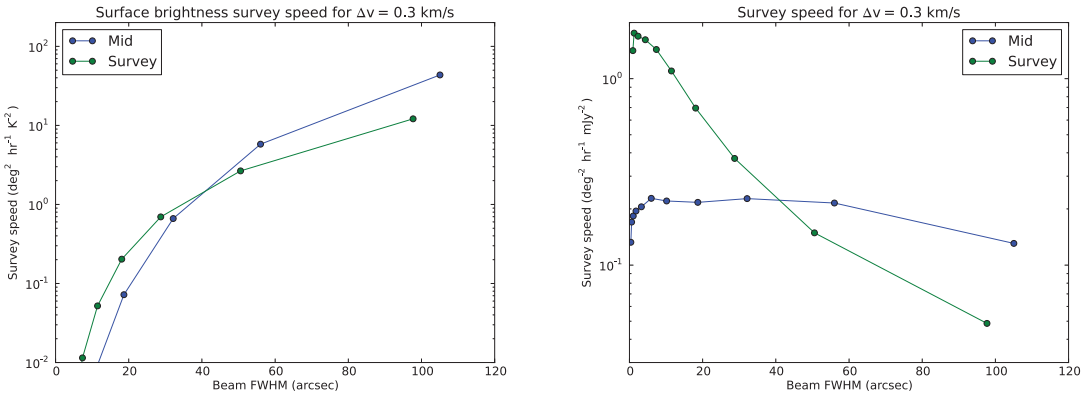

Figure 2: Comparison of H I line survey speeds for 0.3 km s^{-1} channels on SKA1-MID and SKA1-SUR for *left*): surface brightness limited survey and *right*): flux limited survey. These are derived from simulations using the latest SKA1-MID and SKA1-SUR baseline distributions and assuming uniform weighting (Popping et al. 2014) and agree with the Braun (2014) SKA performance document.

interferometric and single dish data and d) significant long baseline coverage to enable accurate H I absorption measurements.

Brightness temperature limited survey speed as a function of beam size for both SKA1-SUR and SKA1-MID is shown in Figure 2 (left) assuming a channel width of 0.3 km s^{-1}. Clearly for heavily tapered data at angular resolutions of > 40" the survey speed for SKA1-MID exceeds that of SKA1-SUR by up to a factor of a few. However, at the angular scales of interest for Galactic H I (< 30") the surface brightness limited survey speed for SKA1-SUR is about a factor of 1.5 times that for SKA1-MID. For measurements of H I absorption, the flux sensitivity at a spectral resolution of 0.3 km s^{-1} at the natural resolution of the array , ~ 5", is the important quantity. In Figure 2 (right) we see that for ~ 5" resolution the survey speed for SKA1-SUR is more than a factor of 10 faster than SKA1-MID. To achieve the simultaneous goals of Galactic H I emission and absorption SKA1-SUR is clearly the optimum instrument. Assuming SKA1-SUR we estimate the expected brightness temperature sensitivity, σ_T, with an angular resolution of 30" and flux density sensitivity, σ_S, at 5" per 0.3 km s^{-1} channel for three nominal integration times of 200 hr, 50 hr and 8 hr (dwell time) as given in Table 1.

Table 1: Sensitivities for various dwell times for SKA1-SUR

Dwell time	σ_T (30")	σ_S (5")	Absorption sources (deg^{-2})
200 hr	0.3 K	0.2 mJy	25
50 hr	0.7 K	0.5 mJy	14
8 hr	1.7 K	1.2 mJy	8

3.1 All-sky Survey of H I Emission and Absorption with SKA1

Using SKA1 we will study the interplay of warm and cold atomic gas in the disk and halo by conducting a two-year all-sky survey of H I emission and absorption with SKA1-SUR. We estimate the observing times required to achieve necessary sensitivities for the two components of

PoS(AASKA14)130

this survey on SKA1-SUR. Imaging of H I emission will probe the diffuse circumgalactic MW and MS, enabling many of the scientific goals outlined above. A 2-year survey (8 hours per pointing) will give a brightness temperature limit over the whole sky at $30''$ of about 1.7 K per 0.3 km s^{-1} channel, which is comparable to the most sensitive Galactic plane interferometric surveys but covers the whole sky, including the disk-halo interface and the Magellanic System, at a factor of six better angular resolution. This survey will probe the structure of the circumgalactic gas, the MS and gas at the interface between the disk and halo. Diffuse emission requires significant numbers of short baselines for surface brightness sensitivity and recovery of extended emission. Furthermore, to understand the nature of the diffuse H I, which fully covers the sky we will need to include "zero-spacing" information, as discussed in §3.3 below.

The transformative aspect of the SKA1 all-sky survey will be the most extensive study of H I absorption in the Galaxy and Magellanic System ever conducted, probing the physical properties of gas throughout the Galactic halo. A 2-year all-sky SKA1-SUR survey will give $\sigma_S = 1.2$ mJy in 0.3 km s^{-1} spectral channels. For H I absorption, the flux density sensitivity converts to optical depth sensitivity of $\sigma_\tau = \sigma_S/S_{bkg}$ for a given value of the background source flux density, S_{bkg}. Using Condon et al. (1998) continuum source counts we estimate the number of optical depth detections of $\sigma_\tau < 0.05$ per square degree in Figure 3. The density of sources is also given in column 4 of Table 3. We expect to obtain precision measurements of $\sigma_\tau < 0.05$ towards ~ 8 sources deg^{-2} or a total $\sim 2 \times 10^5$ sources.

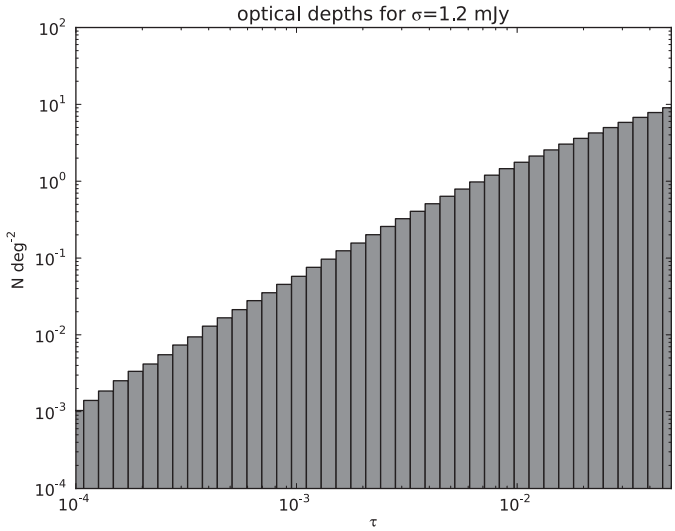

Figure 3: Cumulative distribution of expected H I optical depth measurements for an SKA1-SUR all-sky absorption survey. The histogram shows the number of optical depths per square degree we expect to measure to a given τ or smaller. These are based on detections in 0.3 km/s channels where $\sigma_S = 1.2$ mJy.

Figure 4 shows the expected sky density of H I absorption measurements based on σ_τ and weighted by the H I column density. The left panel shows an estimate of the expected number of WNM measurements with $T_s > 4000$ K overlaid on an H I total column density image and the right panel shows an estimate of the number of CNM measurements with $T_s < 500$ K. The accuracy of spin temperature measurements from H I absorption is limited by the error envelope imposed

PoS(AASKA14)130

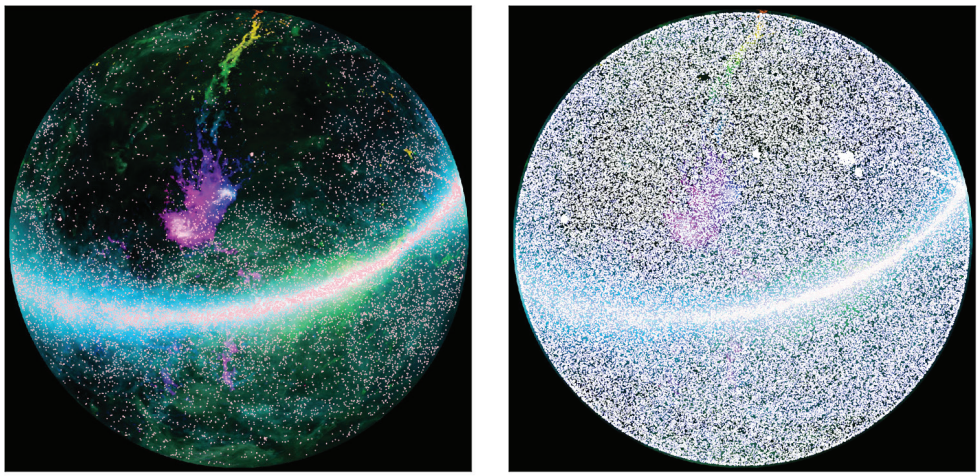

Figure 4: Source density of H I absorption measurements expected with SKA1 of the WNM (left) and the CNM (right). Each dot is an anticipated absorption measurement. The color image in the background is H I emission, where color represents velocity from the Parkes Galactic All-Sky Survey (McClure-Griffiths et al. 2009).

by emission fluctuations around a continuum source. It is therefore essential to have sufficient surface brightness sensitivity on angular scales < 30" to measure the fluctuations in emission. Extrapolating spatial power spectra currently measured in the Galactic plane and MCs (Elmegreen et al. 2001; Dickey et al. 2001) suggests that we will require $\sigma_T < 1.7$ K at 30" to fully take advantage of the sensitivity of the absorption measurements.

The average linewidth, even for cold H I, will be 2.5 km s^{-1}, so some gains can be achieved by averaging channels. Averaging to ~ 1 km s^{-1} channels will give $\sigma_\tau < 0.05$ towards more than 10 sources deg^{-2}. If $\tau = N_{HI}/(1.8 \times 10^{18}\ \mathrm{cm}^{-2}\, T_s * \Delta v)$, we can detect $N_{HI} = 5.6 \times 10^{18}$ cm^{-2} in a 2.5 km s^{-1} line, assuming $T_s = 100$ K. This will be an outstanding progression beyond the well known Millennium survey (Heiles & Troland 2003, 2005), which has been the gold-standard for our knowledge of the distribution of temperatures in the MW neutral ISM with its measurement of 202 cold neutral components toward 79 high Galactic latitude sources.

Furthermore, the all-sky SKA1 H I absorption survey will measure absorption in the WNM. While the 21-SPONGE survey (Murray et al. 2014) will undoubtedly directly measure several WNM temperatures, the numbers of measurements before the SKA1 are likely to be of the order of tens. The SKA1-SUR all-sky absorption survey will be able to directly detect this WNM component towards hundreds of sources, as shown in Figures 3 and 4. Measurements of H I absorption will extend to HVCs, where there are currently only two (Wakker et al. 1991; Matthews et al. 2009). Given the sky density of background sources and the column density distribution of known HVCs (Moss et al. 2013), a blind all-sky survey covering all HVCs should detect cold H I components in absorption towards most known HVCs ($\delta < +30°$) with narrow line components and measure their spin temperatures.

For maximal efficiency of SKA1-SUR time this project should be conducted commensally with an all-sky continuum or extra-galactic H I survey, provided the correlator can be configured to provide 1.5 kHz spectral channels over ~ 5 MHz around 1420 MHz. This could be achieved

PoS(AASKA14)130

through either a "zoom-mode" or through narrow spectral channels over the entire range PAF frequency range. In this case, the Galactic H I absorption survey comes for free with the extragalactic H I survey.

3.2 Targeted Galactic and Magellanic surveys

To achieve the scientific goals of understanding the transition from atomic to molecular gas described in §2 SKA1 should be used for a targeted survey of: (*i*) the MCs and (*ii*) the Galactic plane. The required sensitivity for these two regions is different, with the MCs requiring deeper integrations over a comparatively small area. Integrations of 200 hours on the MCs and 50-hours on the Galactic Plane will exceed current surveys and those and planned for the Australian SKA Pathfinder (ASKAP) by about an order of magnitude in sensitivity. The flux limits for these surveys are given in Table 3.

These surveys will deliver detailed H I emission images capable of measuring turbulence through the spatial power spectrum and probing the structure of H I flows around individual molecular clouds to AU scales in the MW and pc scales in the MCs. The data will be matched to the resolution of data available from space missions, such as Herschel, and molecular line measurements with ALMA. Imaging of all spatial scales, from $20''$ to many degrees, will be needed. To achieve this we will require short baselines as well as the ability to combine single dish data, as discussed below. With a spectral resolution of less than 1 km s^{-1} our spatially resolved H I images will trace velocity gradients in gas flow. As shown in Table 3 the survey will deliver 14 H I absorption sources per square degree across the Galactic plane and up to 25 per square degree in the MCs. These measurements will allow comprehensive measurements of the temperature distribution of gas across the Galaxy and MCs as well as detailed calibration of the H I self-absorption observed in H I emission images. To successfully remove the effects of H I emission fluctuations from the absorption spectra we will require $\sigma_T \sim 0.5$ K at 30".

To achieve the needed sensitivity on the MCs (100 deg^2) with 200 hours dwell time per point gives a total of 2×10^4 deg^2 hr. The Galactic plane area ($|b| < 2^\circ$), is 1100 deg^2 so for 50 hours dwell time per point the total is 5.5×10^4deg^2 hr. Dividing by the PAF FoV of SKA1-SUR at 1.4 GHz, FOV= 18 deg^2 gives a total survey time of about 125 days.

3.3 Zero-spacing information

Both the Galactic plane and all-sky surveys require the inclusion of so-called "zero-spacing", to recover the total flux and structure of the diffuse H I emission that fills the sky. The technical aspects of how this might be achieved with the SKA have to be considered carefully. Typically "zero-spacing" data are provided from single-dish surveys, which effectively sample baselines from 0m to the size of the single dish. Provided these data are matched in spectral resolution and brightness sensitivity to the interferometric data and the interferometer has sufficient baselines smaller than the size of the single dish to allow for cross-calibration, the two datasets can be combined to provide an image sensitive to all angular scales larger than the resolution limit of the interferometer. For SKA Phase 1 the surface brightness sensitivity expected by even the deep Galactic plane (0.3 K per 0.3 km s^{-1} channel) is at the level that can attained by large all-sky single dish surveys similar to GASS (McClure-Griffiths et al. 2009; Kalberla et al. 2010) and EBHIS (Winkel et al.

PoS(AASKA14)130

2010), which both reach ~ 50 mK sensitivities at 1 km s^{-1} spectral resolution. As SKA2 becomes available it may be necessary to use antennas of the SKA itself, through its autocorrelations or other means, to obtain short-spacings information at sufficient sensitivity. Although for SKA1 data can be obtained with existing single dish telescopes, it will be necessary to accommodate the data processing requirements of adding short-spacings in all stages of the SKA.

3.4 Phasing in of SKA1

Galactic fields will benefit from the sensitivity of a fully scoped SKA1 1. The Galactic demands pull the SKA design to its two extremes: short baselines for surface brightness sensitivity and long baselines for H I absorption. Given $\sim$50% less collecting area, it would be preferable to start with the shorter baselines as the survey speed for surface brightness sensitivity scales as the inverse of the square of the filling factor, or one over the longest baseline length to the fourth power. By contrast the survey speed for point source sensitivity has no dependence on baseline length and goes simply as the square of the collecting area. The scientific objectives are such that even for angular resolutions of 20" at 50% of its baseline collecting area SKA1 would be an advance over ASKAP. For a phased SKA1 working for some time without the longest baselines ($<$ 4000m) is satisfactory and could still provide an outstanding Galactic survey. Furthermore, emission line surveys of the targeted Galactic plane and MCs could be completed with worse angular resolution than the natural SKA1-SUR array, and still achieve more than a factor of five improvement in sensitivity at a factor of a few improvement in angular resolution over ASKAP.

4. All-sky H I Emission and Absorption with the SKA

The ultimate goal for SKA is a complete survey of Galactic H I in emission and absorption over 3π steradians. All-sky Galactic H I emission surveys have been limited to single-dish surveys with angular resolutions of typically 10-60$'$ (Winkel et al. 2010; Kalberla et al. 2010; McClure-Griffiths et al. 2009; Kalberla et al. 2005) and at best 3$'$(GALFA; Peek et al. 2011). From these all-sky surveys comes the bulk of our knowledge about the disk-halo interaction of the Milky Way, the overall structure of the Galaxy and the distribution of the phases. These provide essential foregrounds for interpreting observations of everything from X-ray sources to cosmological backgrounds. They have been essential to recent estimates of the total gas quantities in warm and cold H I and dust from comparisons with Planck (e.g. Planck collaboration 2013, Fukui et al. 2014). After very little improvement in angular resolution over the past 30 years, SKA offers us the first chance to conduct an all-sky MW survey at interferometric resolution, improving the angular resolution by more than an order of magnitude. A fully equipped SKA with 10 times the sensitivity of SKA1 will be almost unfathomably powerful, helping us to reach sub-Kelvin sensitivity over the whole local H I sky. Finally we will have the sensitivity to map the low-column density component of the high velocity sky in emission, while simultaneously measuring the fluctuations in H I emission necessary to interpret H I absorption spectra. With these observations we will be able to realize all of the goals outlined in §2.

Together with the all-sky H I emission survey SKA will obtain measurements of optical depths, $\tau < 10^{-2}$ towards half a million sources (~ 20 deg^{-2}; Figure 2), giving direct measurements of the

PoS(AASKA14)130

temperature and column density of the CNM throughout the Galactic disk and halo. Most excitingly, the SKA all-sky HI absorption survey will be ably to detect the warm WNM in absorption towards all > 700 mJy sources, giving $\sim$ 4000 direct measurements of the temperature of the WNM. With these we will be able to determine the fractions of thermally stable and unstable gas in differing galactic environments. Finally we will be able to move beyond mapping to actually *measuring* the physical properties of H I throughout the MW and Magellanic System on the angular scale that we currently observe H I emission, $15'$.

5. Summary

The SKA will revolutionize our knowledge of the evolution of the MW and the Magellanic System. As we move first through SKA1 towards SKA2 we will be able to image the structure and measure the physical properties of H I throughout the Milky Way, its halo and the Magellanic System. With these data we expect to reveal the multi-scale physics that determines structure formation in the MW, probe the transformation of atomic gas to molecular clouds and determine the gas accretion processes crucial to the long-term survival of the MW.

The nature of structure formation is a question that drives many fields of astrophysics, from the formation of galaxy clusters to the formation of planets. The processes driving structure formation are multi-scale by nature with sources and sinks of energy and mass at all scales. The multi-scale nature of the ISM spans more than eight orders of magnitude in spatial scale probing a tremendous range of physical processes (Armstrong et al. 1995). ISM studies with the multi-scale sensitivity of the SKA will provide hereto inaccessible insight into the detailed dynamical processes that govern the flux of mass and energy to and from various ISM phases. These are crucial to understanding the hydrogen cycle of galaxies, and in turn the evolution of structure in the Universe.

With the SKA we will have measurements of the thermal state, accretion rates and origins of gas traveling into and out of the MW. When combined with measurements of ionized gas we should finally be able to produce a full census of material in the halo of the MW, and relate the rate and efficiency of accretion to the rate of star formation within disk.

By studying H I in three different galactic laboratories (MW, Small and Large Magellanic Clouds) we will reveal how H I transforms into molecular clouds in regions with different metallicities and UV radiation fields. When compared with theoretical models of molecular cloud formation this will have important implications on the evolution of gas in a variety of cosmic environments.

References

Armstrong, J. W., Rickett, B. J., & Spangler, S. R. 1995, ApJ, 443, 209
Audit, E., & Hennebelle, P. 2005, A&A, 433, 1
Ballesteros-Paredes, J., Hartmann, L., & Vázquez-Semadeni, E. 1999, ApJ, 527, 285
Ballesteros-Paredes, J., Hartmann, L. W., Vázquez-Semadeni, E., Heitsch, F., & Zamora-Avilés, M. A. 2011, MNRAS, 411, 65
Banerjee, R., Vázquez-Semadeni, E., Hennebelle, P., & Klessen, R. S. 2009, MNRAS, 398, 1082
Ben Bekhti, N., Richter, P., Winkel, B., Kenn, F., & Westmeier, T. 2009, A&A, 503, 483
Bensby, T., Feltzing, S., & Oey, M. S. 2014, A&A, 562, A71

PoS(AASKA14)130

Bhat, N. D. R., & Gupta, Y. 2002, ApJ, 567, 342
Bigiel, F., Leroy, A., Walter, F., et al. 2008, AJ, 136, 2846
Braun, R. 1997, ApJ, 484, 637
Braun, R., 2014, "SKA1 Imaging Science Performance", Document number SKA-TEL- SKO-DD-XXX Revision A Draft 2
Braun, R., & Kanekar, N. 2005, A&A, 436, L53
Bregman, J. N. 1980, ApJ, 236, 577
Burkhart, B., Stanimirović, S., Lazarian, A., & Kowal, G. 2010, ApJ, 708, 1204
Burstein, D., & Heiles, C. 1978, ApJ, 225, 40
Carilli, C. L., Dwarakanath, K. S., & Goss, W. M. 1998, ApJL, 502, L79
Chepurnov, A., Lazarian, A., Stanimirović, S., Heiles, C., & Peek, J. E. G. 2010, ApJ, 714, 1398
Chiappini, C., Matteucci, F., & Romano, D. 2001, ApJ, 554, 1044
Clark, P. C., Glover, S. C. O., Klessen, R. S., & Bonnell, I. A. 2012, MNRAS, 424, 2599
Condon, J. J., Cotton, W. D., Greisen, E. W., et al. 1998, AJ, 115, 1693
Crovisier, J., & Dickey, J. M. 1983, A&A, 122, 282
de Avillez, M. A. 2000, MNRAS, 315, 479
Deshpande, A. A., Dwarakanath, K. S., & Goss, W. M. 2000, ApJ, 543, 227
Dickey, J. M., & Brinks, E. 1993, ApJ, 405, 153
Dickey, J. M., McClure-Griffiths, N. M., Stanimirović, S., Gaensler, B. M., & Green, A. J. 2001, ApJ, 561, 264
Dickey, J. M., Mebold, U., Marx, M., et al. 1994, A&A, 289, 357
Dickey, J. M., Mebold, U., Stanimirovic, S., & Staveley-Smith, L. 2000, ApJ, 536, 756
Dickey, J. M., Salpeter, E. E., & Terzian, Y. 1977, ApJL, 211, L77
Dickey, J. M., Strasser, S., Gaensler, B. M., et al. 2009, ApJ, 693, 1250
Dickman, R. L., & Kleiner, S. C. 1985, ApJ, 295, 479
Dobbs, C. L., Pringle, J. E., & Burkert, A. 2012, MNRAS, 425, 2157
Dwarakanath, K. S., Carilli, C. L., & Goss, W. M. 2002, ApJ, 567, 940
Elmegreen, B. G., Kim, S., & Staveley-Smith, L. 2001, ApJ, 548, 749
Elmegreen, B. G., & Scalo, J. 2004, ARA&A, 42, 211
Falceta-Gonçalves, D., Kowal, G., Falgarone, E., & Chian, A. C.-L. 2014, Nonlinear Processes in Geophysics, 21, 587
Falgarone, E., Pety, J., & Hily-Blant, P. 2009, A&A, 507, 355
Fiedler, R. L., Dennison, B., Johnston, K. J., & Hewish, A. 1987, Nature, 326, 675
Field, G. B. 1965, ApJ, 142, 531
Field, G. B., Goldsmith, D. W., & Habing, H. J. 1969, ApJL, 155, L149
Fox, A. J., Wakker, B. P., Barger, K. A., et al. 2014, ApJ, 787, 147
Fraternali, F., Marasco, A., Marinacci, F., & Binney, J. 2013, ApJ, 764, L21
Fukui, Y., Okamoto, R., Yamamoto, H., et al. 2014, ApJ, 796, 59
Gaensler, B. M., Tanna, A., Slane, P. O., et al. 2008, ApJ, 680, L37
Gaensler, B. M., Haverkorn, M., Burkhart, B., et al. 2011, Nature, 478, 214
Gazol, A., Vázquez-Semadeni, E., & Kim, J. 2005, ApJ, 630, 911
Gazol, A., Vázquez-Semadeni, E., Sánchez-Salcedo, F. J., & Scalo, J. 2001, ApJL, 557, L121
Gibson, S. J., Taylor, A. R., Higgs, L. A., Brunt, C. M., & Dewdney, P. E. 2005, ApJ, 626, 195

PoS(AASKA14)130

Glover, S. C. O., & Mac Low, M.-M. 2007, ApJ, 659, 1317
Gomez, G. C., & Vazquez-Semadeni, E. 2014, ApJ, 791, 124
Green, D. A. 1993, MNRAS, 262, 327
Green, G. M., Schlafly, E. F., Finkbeiner, D. P., et al. 2014, ApJ, 783, 114
Grenier, I. A., Casandjian, J.-M., & Terrier, R. 2005, Science, 307, 1292
Heiles, C. 1997, ApJ, 481, 193
Heiles, C., & Troland, T. H. 2003, ApJ, 586, 1067
—. 2005, ApJ, 624, 773
Heiner, J. S., Vázquez-Semadeni, E., & Ballesteros-Paredes, J. 2014, ArXiv e-prints
Heitsch, F., Burkert, A., Hartmann, L. W., Slyz, A. D., & Devriendt, J. E. G. 2005, ApJL, 633, L113
Heitsch, F., & Hartmann, L. 2008, ApJ, 689, 290
Heitsch, F., Hartmann, L. W., Slyz, A. D., Devriendt, J. E. G., & Burkert, A. 2008, ApJ, 674, 316
Heitsch, F., & Putman, M. E. 2009, ApJ, 698, 1485
Heitsch, F., Slyz, A. D., Devriendt, J. E. G., Hartmann, L. W., & Burkert, A. 2006, ApJ, 648, 1052
Hill, A. S., Joung, M. R., Mac Low, M.-M., et al. 2012, ApJ, 750, 104
Hopkins, A. M., McClure-Griffiths, N. M., & Gaensler, B. M. 2008, ApJ, 682, L13
Huterer, D., Cunha, C. E., & Fang, W. 2013, MNRAS, 432, 2945
Joung, M. R., Putman, M. E., Bryan, G. L., Fernández, X., & Peek, J. E. G. 2012, ApJ, 759, 137
Kalberla, P. M. W., Burton, W. B., Hartmann, D., et al. 2005, A&A, 440, 775
Kalberla, P. M. W., & Dedes, L. 2008, A&A, 487, 951
Kalberla, P. M. W., & Haud, U. 2006, A&A, 455, 481
Kalberla, P. M. W., Schwarz, U. J., & Goss, W. M. 1985, A&A, 144, 27
Kalberla, P. M. W., McClure-Griffiths, N. M., Pisano, D. J., et al. 2010, A&A, 521, 17
Kennicutt, Jr., R. C. 1998, ApJ, 498, 541
Kim, C.-G., Ostriker, E. C., & Kim, W.-T. 2014, ApJ, 786, 64
Kim, S., Staveley-Smith, L., Dopita, M. A., et al. 1998, ApJ, 503, 674
Kritsuk, A. G., Norman, M. L., Padoan, P., & Wagner, R. 2007, ApJ, 665, 416
Krumholz, M. R., McKee, C. F., & Tumlinson, J. 2009, ApJ, 693, 216
Krčo, M., Goldsmith, P. F., Brown, R. L., & Li, D. 2008, ApJ, 689, 276
Langer, W. D., Velusamy, T., Pineda, J. L., et al. 2010, A&A, 521, L17
Larson, R. B. 1981, MNRAS, 194, 809
Lazarian, A., & Pogosyan, D. 2000, ApJ, 537, 720
Lee, M.-Y., Stanimirović, S., Douglas, K. A., et al. 2012, ApJ, 748, 75
Lehner, N., Howk, J. C., Thom, C., et al. 2012, MNRAS, 424, 2896
Leroy, A., Bolatto, A., Stanimirovic, S., et al. 2007, ApJ, 658, 1027
Levine, E. S., Blitz, L., & Heiles, C. 2006, ApJ, 643, 881
Li, D., & Goldsmith, P. F. 2003, ApJ, 585, 823
Li, D., & Goldsmith, P. F. 2012, ApJ, 756, 12
Liszt, H. 2001, A&A, 371, 698
Lockman, F. J. 1984, ApJ, 283, 90
Mac Low, M.-M., McCray, R., & Norman, M. L. 1989, ApJ, 337, 141
Matthews, D., Staveley-Smith, L., Dyson, P., & Muller, E. 2009, ApJL, 691, L115

PoS(AASKA14)130

McClure-Griffiths, N. M., Ford, A., Pisano, D. J., et al. 2006, ApJ, 638, 196
McClure-Griffiths, N. M., Pisano, D. J., Calabretta, M. R., et al. 2009, ApJS, 181, 398
McKee, C. F., & Ostriker, E. C. 2007, ARA&A, 45, 565
McKee, C. F., & Ostriker, J. P. 1977, ApJ, 218, 148
Meixner, M., Panuzzo, P., Roman-Duval, J., et al. 2013, AJ, 146, 62
Moss, V. A. 2014, PhD Thesis
Moss, V. A., McClure-Griffiths, N. M., Murphy, T., et al. 2013, ApJS, 209, 12
Muller, E., Staveley-Smith, L., Zealey, W., & Stanimirović, S. 2003, MNRAS, 339, 105
Murray, C. E., Lindner, R. R., Stanimirović, S., et al. 2014, ApJ, 781, L41
Mutch, S. J., Croton, D. J., & Poole, G. B. 2011, ApJ, 736, 84
Nigra, L., Stanimirović, S., Gallagher, III, J. S., et al. 2012, ApJ, 760, 48
Ntormousi, E., Burkert, A., Fierlinger, K., & Heitsch, F. 2011, ApJ, 731, 13
Peek, J. E. G. 2013, ApJL, 766, L6
Peek, J. E. G., Heiles, C., Douglas, K. A., et al. 2011, ApJS, 194, 20
Pidopryhora, Y., Lockman, F. J., & Shields, J. C. 2007, ApJ, 656, 928
Pingel, N. M., Stanimirović, S., Peek, J. E. G., et al. 2013, ApJ, 779, 36
Planck Collaboration, Ade, P. A. R., Aghanim, N., et al. 2011, Astronomy and Astrophysics, 536, A19
Planck Collaboration, Abergel, A., Ade, P. A. R., et al. 2013, ArXiv e-prints
Putman, M. E., de Heij, V., Staveley-Smith, L., et al. 2002, AJ, 123, 873
Putman, M. E., Peek, J. E. G., & Joung, M. R. 2012, ARA&A, 50, 491
Qian, L., Li, D., & Goldsmith, P. F. 2012, ApJ, 760, 147
Reynolds, R. J. 1991, in IAU Symp. 144: The Interstellar Disk-Halo Connection in Galaxies, ed. H. Bloeman, 67–76
Richter, P., Sembach, K. R., Wakker, B. P., & Savage, B. D. 2001, ApJL, 562, L181
Rickett, B. J. 1977, ARA&A, 15, 479
Roy, N., Minter, A. H., Goss, W. M., Brogan, C. L., & Lazio, T. J. W. 2012, ApJ, 749, 144
Schlafly, E. F., Green, G., Finkbeiner, D. P., et al. 2014, ApJ, 789, 15
Schlegel, D. J., Finkbeiner, D. P., & Davis, M. 1998, ApJ, 500, 525
Schönrich, R., & Binney, J. 2009, MNRAS, 399, 1145
Schruba, A., Leroy, A. K., Walter, F., et al. 2011, AJ, 142, 37
Shapiro, P. R., & Field, G. B. 1976, ApJ, 205, 762
Smith, R. J., Glover, S. C. O., Clark, P. C., Klessen, R. S., & Springel, V. 2014, MNRAS, 441, 1628
Stanimirović, S., Hoffman, S., Heiles, C., et al. 2008, ApJ, 680, 276
Stanimirović, S., & Lazarian, A. 2001, ApJL, 551, L53
Stanimirović, S., Staveley-Smith, L., Dickey, J. M., Sault, R. J., & Snowden, S. L. 1999, MNRAS, 302, 417
Strasser, S. T., Dickey, J. M., Taylor, A. R., et al. 2007, AJ, 134, 2252
Thom, C., Peek, J. E. G., Putman, M. E., et al. 2008, ApJ, 684, 364
van Dishoeck, E. F., & Black, J. H. 1988, ApJ, 334, 771
Vázquez-Semadeni, E., Gazol, A., & Scalo, J. 2000, ApJ, 540, 271
Vázquez-Semadeni, E., Gómez, G. C., Jappsen, A. K., et al. 2007, ApJ, 657, 870

PoS(AASKA14)130

Vázquez-Semadeni, E., Ryu, D., Passot, T., González, R. F., & Gazol, A. 2006, ApJ, 643, 245
Veilleux, S., Cecil, G., & Bland-Hawthorn, J. 2005, ARA&A, 43, 769
Vogelsberger, M., Genel, S., Springel, V., et al. 2014, Nature, 509, 177
Wakker, B. P., & Mathis, J. S. 2000, ApJL, 544, L107
Wakker, B. P., Vijfschaft, B., & Schwarz, U. J. 1991, A&A, 249, 233
Walker, M., & Wardle, M. 1998, ApJL, 498, L125
Werk, J. K., Prochaska, J. X., Tumlinson, J., et al. 2014, ArXiv e-prints
Westerlund, B. E. 1997, The Magellanic Clouds (Cambridge University Press)
Winkel, B., Kalberla, P. M. W., Kerp, J., & Flöer, L. 2010, ApJS, 188, 488
Wolfire, M. G., Hollenbach, D., McKee, C. F., Tielens, A. G. G. M., & Bakes, E. L. O. 1995, ApJ, 443, 152
Wolfire, M. G., McKee, C. F., Hollenbach, D., & Tielens, A. G. G. M. 2003, ApJ, 587, 278

PoS(AASKA14)130

PROCEEDINGS OF SCIENCE

Connecting the Baryons: Multiwavelength Data for SKA HI Surveys

Martin Meyer[*1], **Aaron Robotham**[1], **Danail Obreschkow**[1], **Simon Driver**[1], **Lister Staveley-Smith**[1], **and Martin Zwaan**[2]

[1] *International Centre for Radio Astronomy Research (ICRAR)*
[2] *European Southern Observatory*
E-mail: martin.meyer@uwa.edu.au

The science achievable with SKA HI surveys will be greatly increased through the combination of HI data with that at other wavelengths. These multiwavelength datasets will enable studies to move beyond an understanding of HI gas in isolation to instead understand HI as an integral part of the highly complex baryonic processes that drive galaxy evolution.

As they evolve, galaxies experience a host of environmental and feedback influences, many of which can radically impact their gas content. Important processes include: accretion (hot and cold mode, mergers), depletion (star formation, galactic winds, AGN), phase changes (ionised/atomic/molecular), and environmental effects (ram pressure stripping, tidal effects, strangulation). Governing all of these to various extents is the underlying dark matter distribution. In turn, the result of these processes can significantly alter the baryonic states in which material is finally observed (stellar populations, dust, chemistry) and its morphology (galaxy type, bulge/disk ratio, bars, warps, radial profile). To fully understand the evolution of HI and the role it plays in galactic evolution requires the ability to quantify each of these separate processes, and hence to coordinate SKA HI surveys with extensive multi-band photometric and spectroscopic campaigns. In addition, multiwavelength data is essential for statistical methods of HI analysis such as HI stacking and intensity mapping cross-correlations.

In this chapter, we examine some of the principal science motivations for acquiring multiwavelength data to match that from the extragalactic SKA HI surveys, and review the currently planned capacity to achieve this (eg. LSST, Euclid, W-FIRST, SPICA, ALMA, and 4MOST).

Advancing Astrophysics with the Square Kilometre Array
June 8-13, 2014
Giardini Naxos, Italy

[*] Speaker.

PoS(AASKA14)131

1. Introduction

Our knowledge of galaxies and their evolution has been dominated by studies of the late-stage products of the evolutionary cycle, with extensive surveys in the optical and nearby wavelengths tracing the evolution of stellar material across large fractions of cosmic time. In contrast, our knowledge of the HI content of galaxies, the fundamental baryonic material out of which galaxies are made and a key tracer of their dynamics, remains rudimentary. Direct measurements of HI content in individual galaxies beyond the local universe are currently limited to galaxy samples of only hundreds out to z$\sim$0.2-0.3 (BUDHIES, Verheijen et al. 2007; CHILES, Fernández et al. 2013), compared to the multi-million object samples out to z$\sim$1 and beyond that will be possible with the SKA (more than half the history of the Universe). Linking these groundbreaking HI samples with matched multiwavelength tracers will provide transformational new datasets spanning all of the major galactic constituents, and provide unique insight into the evolution of galaxies across cosmic time.

In this chapter, we explore the needs and availability of multiwavelength data for extragalactic HI surveys with the SKA. Section 2 summarises some of the principal scientific drivers for ancillary multiwavelength data and the analysis techniques these enable, followed by an overview of upcoming multiwavelength survey facilities in Section 3. The implications for future SKA and multiwavelength survey design are discussed in Section 4. Finally, conclusions are given in Section 5, including a basic ranking of facilities and multiwavelength science products based on the degree to which well-matched multiwavelength data will be possible for SKA HI surveys, as known at the time of writing.

2. Need to Match HI Surveys with Multiwavelength Data

2.1 Characterising Different Baryonic States

Understanding the mass assembly of galaxies, and the evolution of material from one baryonic state to another, is at the heart of galaxy evolution studies. A large range of processes and scales are involved in this assembly, from the on-going gravitational collapse of gas into the filamentary structures of the cosmic web and its accretion into galactic halos, the cooling of gas into galactic disks and dense molecular clouds, to the subsequent star formation processes within these structures. In this simple picture, galactic HI acts as a bridge between the reservoir of gas in the cosmic web and the stellar material in galaxies. However, the full picture of HI content and its role in galaxy evolution is likely much more complex, with a host of mechanisms that can variously act to both add and remove HI from galaxies. Potentially important processes here include: accretion (hot and cold mode, mergers; eg. Keres et al. 2005), depletion (star formation, galactic winds, AGN; eg. Power et al. 2010; Kim et al. 2013), phase changes (ionised/atomic/molecular; eg. Hopkins et al. 2008), and environmental effects (eg. Gunn & Gott 1972; Moore et al. 1996). Each of these sources and sinks ideally needs to be quantified through multiwavelength observations to determine the relative importance of each, and the nature of the fundamental scaling relations that link them (eg. the Schmidt law, Schmidt 1959; Table 1 provides a summary of some of the central multiwavelength tracers and the physical processes and galactic components they measure). The SKA will provide an unprecedented window through which to study the role of HI in these rela-

PoS(AASKA14)131

Property	Tracers
atomic gas mass	HI
molecular gas mass	mm emission lines (eg. CO)
stellar mass	optical/NIR multiband photometry (eg. K, g-i), optical spectroscopy
dust mass/temperature	mid/far-IR multiband photometry, (sub)mm continuum
morphology	panchromatic high resolution imaging, fitted structural parameters and decomposition (bulge, disk, bar)
star formation rate	Hα, UV, radio continuum, mid-IR
supermassive black hole	optical emission line diagnostics, radio continuum
chemistry	optical/submm/mm spectroscopy via emission/absorption lines (high R)
dynamics	line fitting (optical, near-IR, CO, HI), spatially resolved (optical IFU, CO, HI)
environment	redshift surveys (low R) + group catalogues (membership, multiplicity, halo mass, central/satellite classification), photo-z (multiband optical/NIR, large scale structure), X-rays (clusters, hot groups, massive halos), radio SZ (clusters, high-z)
distance	redshift (Hubble flow), Tully-Fisher (HI+optical/NIR imaging), Faber Jackson/Fundamental Plane (optical/NIR imaging and spectroscopy)

Table 1: Physical quantities and their multiwavelength tracers

tions across a large fraction of the history of the Universe, and will do so on both a global and morphologically resolved basis.

2.2 Characterising Galaxy Dynamics

Along with mass, another key property in the evolution of galaxies are their kinematics and angular momenta. HI observations with the SKA will be a powerful addition to this field, with SKA1 alone expected to yield two orders of magnitude more good HI kinematic maps than the leading existing datasets (Obreschkow et al. 2015), and more than a million galaxies with spatially unresolved HI profiles. While a powerful diagnostic in their own right, with HI gas extending further into the dark matter haloes of galaxies than can be typically traced by stellar emission, the potential of these data will be best exploited through its combination with tracers at other wavelengths. At the most basic level, higher resolution optical photometry enables inclination corrected rotation velocities to be extracted from line-of-sight global HI profiles, along with improved morphological parameters such as disk scale lengths. At a more detailed level, matched optical/NIR spectroscopy and IFU data provide complimentary measurements of the stellar-phase and ionized gas-phase material, which combined with HI data will allow the full kinematic and angular momentum properties of galaxies to be studied, linking the often different evolutionary information encoded in the kinematics of gas and stars, and indeed tracing the dynamics of different morphological features such as disks and bulges. Through both joint and separate analyses, HI and multiwavelength data will enable the full suite of galactic dynamical scaling relations to be examined (eg. Tully & Fisher 1977; Faber & Jackson 1976; M_*-$S_{0.5}$ relation, Kassin et al. 2007), and their evolution, underlying physics, and observational biases to be understood.

PoS(AASKA14)131

2.3 Characterising Environment

Some of the most important external effects driving the distribution of galaxy properties we observe today are the environmental factors that can drastically impact HI content. For instance, the suppression of star formation in cluster environments is not due to an alteration in the actual processes of star formation, but rather due to a quenching of the HI supply (tidal influences, Moore et al. 1996; ram pressure stripping, Gunn & Gott 1972; strangulation, Balogh et al. 2000). However, the detailed processes by which environment affects HI remain only partially understood and will be an important area of research for the SKA. In the case of star formation quenching, for example, major optical surveys such as 2dFGRS find that star formation is suppressed at large distances from clusters, implying that evolutionary processes must be at work beyond these environments and the simple ram-pressure stripping of HI gas in their cores (Lewis et al. 2002). Existing studies also find contradictory results on the environmental dependence of the HI mass function (Zwaan et al. 2005; Springob et al. 2005).

A potential contributor to some of the observational uncertainties and disagreements in existing environmental effect results are difficulties associated with properly characterising environment and the variety of different methods that have been used (eg. HI vs. optical metrics). From an observational perspective, overcoming these challenges requires the combination of HI data with deep, well-sampled optical redshift samples to provide a full characterisation of environment (group membership, group multiplicity, parent halo mass, central/satellite status). Together, these datasets will sample a greater dynamic range of environment than is possible from examining the distribution of HI-rich galaxies alone, which are strongly anti-biased in the local Universe. Direct tracers of the intra-group/cluster medium, such as that provided by X-ray data, will also be a highly valuable addition to the group catalogues provided by redshift surveys. Interferometric HI observations with sufficient resolution to isolate emission from galaxies in close proximity will also be needed to mitigate confusion effects in these environments, a requirement that will be met over a large redshift range by the SKA.

2.4 Characterising Feedback

The feedback effects from local processes such as star formation and AGN activity can be equally as important as those on larger scales. For instance, recent simulation results find that feedback from supernovae impacts the overall normalisation of the HI mass function, while AGN feedback can impact its high mass slope, with increased activity decreasing the number of high HI mass galaxies observed (Kim et al. 2013). The strength of these feedback mechanisms is also found to have an inverse effect on the global clustering strength of the HI-rich galaxy population. Importantly, the various feedback mechanisms are also found to imprint differently on the distribution functions of the HI-rich galaxy population compared to that observed at other wavelengths, offering an improved diagnostic ability for understanding the role of feedback in galaxy evolution when HI datasets are combined with those selected, for instance, in the optical. Nevertheless, a great deal of progress remains to be made in this area, and favoured models still offer sometimes widely discrepant results with observations (Duffy et al. 2012). Large-scale HI surveys with the SKA, combined with matching multiwavelength data, will be essential for resolving these uncertainties, tracing the causes and varying effects of feedback across all of the major galactic constituents.

PoS(AASKA14)131

2.5 Enabling Alternative Analysis Techniques

Finally, multiwavelength data can also offer new ways of analysing HI datasets. Notably, the combination of HI data with independent optical redshift catalogues has been used to vastly increase the redshift range over which measurements of the cosmic HI density and gas fraction scaling dependencies can been made. In one technique, HI stacking, the rest frame HI spectra of a large number of sources - extracted from an HI datacube and shifted to rest frame on the basis of their known optical positions and redshifts - are combined to obtain a statistically significant average spectrum for the input galaxy sample. This method has now been used to successfully obtain high redshift determinations for $\Omega_{\rm HI}$ in both single-dish and interferometric observations (Lah et al. 2007; Delhaize et al. 2013; Rhee et al. 2013). The technique has also been demonstrated for absorption line studies (eg. Geréb et al. 2013, 2014). Another method is intensity mapping, which rather than trying to stack the emission from individual sources and correct for any confusion effects that may arise, instead analyses the intensity field of emission as a whole, through auto-correlation or cross-correlation of the HI intensity field with that derived from an optical spectroscopic catalogue. In the last decade, great strides have been made in the application of this technique to measure the global HI content of the Universe (Pen et al. 2009; Chang et al. 2010). Lastly, independent optical redshifts can be used to measure the HI properties of individual sources at a much lower significance level that would be possible from the blind HI data alone, significantly increasing sample sizes for galaxy-by-galaxy analyses.

3. Multiwavelength Facilities & Surveys

In this section, we review current and planned multiwavelength survey facilities, examining these by survey class (imaging, spectroscopic, IFU) and assessing their relative performance as a function of wavelength to identify those best suited to provide matching multiwavelength data for the strawman SKA HI surveys. Note that we have not differentiated between facilities with open data access policies and those with restricted proprietary periods. However, over the lifetime of the SKA it is expected that all of these datasets will become publicly available, as is normal astronomy practice.

Given inevitable variations in survey design, there is not a single figure of merit (FoM) that covers all scientific purposes. For instance, for spectroscopic surveys an experiment designed to cover a huge area of sky at low redshift will need a large field of view but not necessarily huge multiplexing or collecting area given the distribution of sources on the sky. Equally, a high redshift study might need good multiplexing and a large collecting area but not a huge field of view. To allow for these design variations in desired FoMs we have designed an interactive website where users can build their own FoM, amongst other interactive options. The aim is to keep this database up-to-date with a moving 10-year window. The current host location is at: https://asgr.shinyapps.io/ganttshiny/.

3.1 Optical/near-IR imaging surveys

From a multiwavelength standpoint, imaging surveys represent the base from which other, more detailed follow-up observations can follow independently of the HI selected dataset, and are

PoS(AASKA14)131

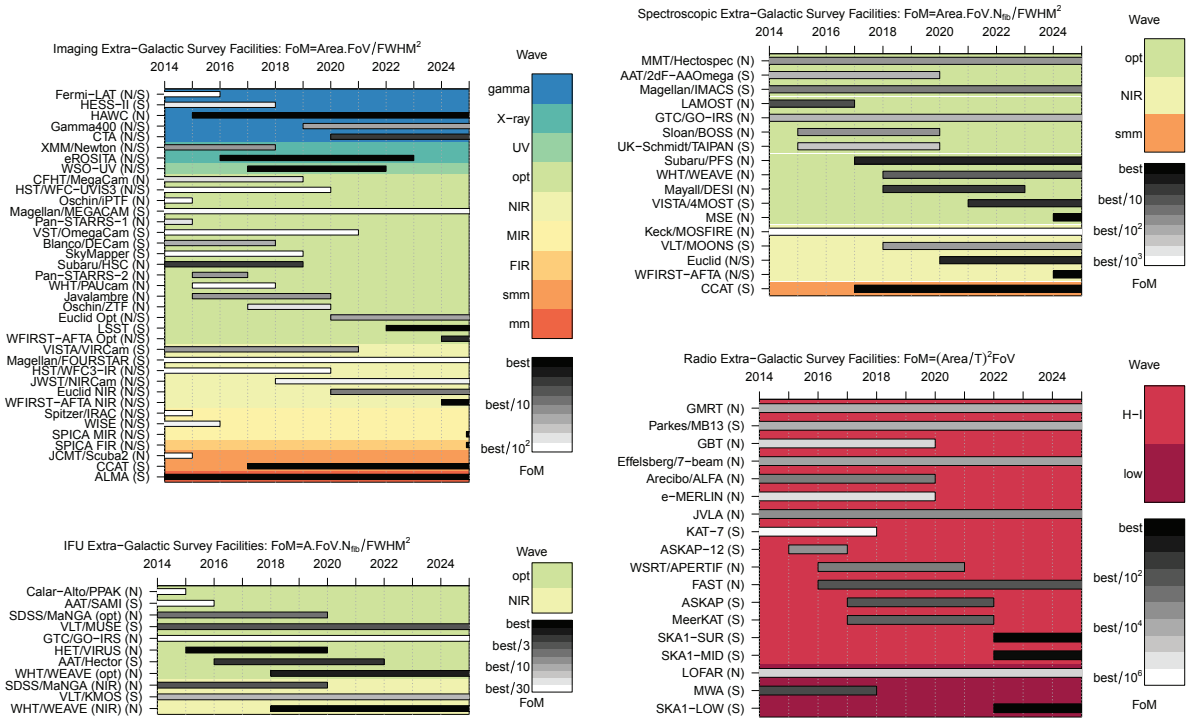

Figure 1: (top left) Comparison of various extra-galactic imaging survey facilities that will operate between now and 2025. Figure of merit (FoM) is calculated using Area.FoV/(FWHM^2). (top-right) Comparison of various extra-galactic spectroscopic survey facilities that will operate between now and 2025. FoM is calculated using Area.FoV.N$_{fib}$/(FWHM^2). (bottom-left) Comparison of various extra-galactic IFU survey facilities that will operate between now and 2025. FoM is calculated using Area.FoV.N$_{fib}$/(FWHM^2). (bottom-right) Comparison of various extra-galactic radio survey facilities that will operate between now and 2025. FoM is calculated using (Area/T)^2.FoV. 'HI' corresponds to facilities able to observe HI in the local Universe, i.e. they can observe at frequencies as high as 1.4 GHz. Note that in all panels FoM shading is scaled within a wavelength subset. The accompanying data for all charts is given in the Appendix. Versions of these charts and table data can be generated online using an interactive tool located at https://asgr.shinyapps.io/ganttshiny.

therefore a crucial starting point. The survey imaging needs to be competitive otherwise all that follows will be similarly limited.

There are a significant number of imaging facilities that have recently come online or will come online in the next decade. The top-left panel of Figure 1 is a Gantt-Chart representation of when these facilities might become available, and how 'fast' they are at surveying the extra-galactic sky. The chosen metric provides an insight into depth (telescope area) and sky coverage (FoV) per unit time, and data quality (FWHM image resolution). The majority of facilities will operate in the optical and there are two clear front-runners: Subaru Hyper-SuPrime-Cam, and towards the end of the decade, LSST. In the near-IR, arguably the more obvious band for sample selection as it most closely follows stellar mass, the obvious winner is VISTA, moving to Euclid towards the end of the decade.

The SKA will be largely accommodated by the huge Southern sky survey area and depth of LSST (at least in the optical). For this reason we have confidence that a large fraction of the

PoS(AASKA14)131

imaging side of the SKA multiwavelength data will be either in place, or appearing, by the time SKA begins operations. This is one part of the multiwavelength equation the SKA will not need to worry about going forward, but it should be noted that near-IR surveys will be less well matched in both depth and area.

3.2 Massively multiplexed spectroscopic surveys

Moving into the next generation of surveys, there will need to be a natural synergy with optical and NIR spectroscopic campaigns. There are a number of multi-object spectroscopic (MOS) facilities available currently, and that are scheduled to come online between 2015–2025. Figure 1 (top-right) is a Gantt-Chart representation of when these facilities might become available, and how fast they are at spectroscopically surveying extra-galactic objects.

One of the fastest MOS facilities available is AAT/AAOmega. This has been used to conduct a number of multiple hundred thousand sized extra-galactic surveys: 2dFGRS, WiggleZ and GAMA. Looking forward, there are a huge number of next generation MOS facilities scheduled to start operating in the Northern hemisphere before between 2017–2019, however only VISTA/4MOST will be operating in the South (i.e. overlapping substantially with ASKAP, MeerKAT and SKA). For this reason alone it would be a compelling next generation MOS facility for the SKA to become involved in. It is worth noting that these next-generation MOS facilities are all comparably fast, and the reality is the faster extra-galactic surveys will be conducted on the most dedicated facilities.

3.3 Spatially resolved spectroscopic surveys

An equally important direction for next generation survey science is spatially resolved spectroscopy through the development of novel and pioneering instrumentation (e.g. AAT/SAMI, VLT/MUSE, VLT/KMOS). A key power of these instruments is their ability to spatially resolve the chemistry and dynamics of galaxies – star-formation, metallicity, stellar population ages, angular momenta and stellar dispersions. Current spatially resolved surveys are at the thousand galaxy mark (the Spain-led CALIFA, the Australian-led SAMI and the US-led MANGA surveys). ATLAS^{3D} has also compiled a large sample of IFU and HI measurements for early-type galaxies with WHT and WSRT.

The AAT/SAMI facility is the only multi-object IFU facility currently available, but others are scheduled to come online between 2015–2025. Figure 1 (bottom-left) is a Gantt-Chart representation of when these facilities might become available and how fast they are at surveying extra-galactic objects with IFUs. Simultaneously probing gas and stellar kinematics through the combination of SKA and optical/NIR IFU data will be a huge science lever in the near future. Beyond this, high S/N chemistry can provide great insight into the conversion of HI and molecular gas into stars and metals, but a full understanding will require large numbers of galaxies in huge spatial and multiwavelength detail.

4. Optimal Matching of HI and Multiwavelength Datasets

The minimal obvious requirement to maximise scientific return from SKA HI surveys is to ensure that multiwavelength survey programs are carried out in the same regions of sky as those proposed for HI. Beyond that, there are clearly pragmatic considerations regarding the depth and

PoS(AASKA14)131

area of such overlapping multiwavelength surveys, with consideration needed for likely source densities, survey times and expense. We perform a basic assessment of the optimal required depth for multiwavelength data as a function of SKA survey area and integration time by analysing simulated data from S3-SAX (Obreschkow et al. 2009; Obreschkow & Meyer 2014). This data spans the redshift range $0 < z < 1.2$ in a 100 deg^2 volume-limited light-cone containing galaxy cold gas masses, HI and H_2 masses, stellar masses, luminosities, and apparent magnitudes. We apply apparent HI, r-band and CO detection thresholds to assess the degree of overlap between a range of simulated observed galaxy datasets. For the detection of HI sources by the SKA in this analysis, a 5σ (optimal) threshold is applied. A synthesised beam size of 5" is used for all surveys, with the point source signal-to-noise value of galaxies being adjusted according to their size relative to the beam (SNR $\propto 1/\sqrt{1+A_{\rm galaxy}/A_{\rm beam}}$).

The first metric we consider is the simple fraction of HI sources detected in a simulated HI SKA survey (sample A) that will have a counterpart in an r-magnitude limited dataset (sample B): $F = \frac{A \cap B}{A}$. r-band selection is used for redshift surveys such as GAMA due to the presence of Hα (for higher redshift samples a longer observed frame wavelength selection may be preferable). The results of this analysis are shown in Figure 2, with separate panels given for SKA1 (50%), SKA1 and SKA2. We also include a plot for the match between SKA1 and a CO(1-0) flux limited dataset. For SKA1 and its 50% early deployment option, four separate y-axis are included for the four nominal reference surveys considered by the HI Science Assessment Workshop (September 2013): 3 deg^2 (SKA1-MID and 50% option), 300 deg^2 (SKA1-SUR and 50% option), 3000 deg^2 (SKA1-SUR and 50% option) and 30000 deg^2 (SKA1-SUR and 50% option). For SKA2, three survey areas are examined: 60 deg^2, 600 deg^2 and 6000 deg^2. A horizontal dashed line indicates the reference integration times for each survey: 2000 hours for the 3 deg^2 survey with SKA1-MID and the 60-6000 deg^2 SKA2 surveys, and 2 years for the 300-30000 deg^2 surveys with SKA1-SUR. The vertical intersect for each dashed survey line then corresponds to the required r-band limit for 90% of the HI sample to have an optical counterpart.

While achieving high completeness (well-suited eg. for tasks such as optically motivated source finding, or an indicative limit for where HI stacking gains interest), the above identified r-band samples will be comparatively inefficient when viewed from an optical standpoint, containing many sources that will have no HI counterpart. To assess the optimal r-band (and CO) depth at which the mutual overlap between HI and multiwavelength samples is maximised, we consider a second metric $E = \left(\frac{A \cap B}{A}\right)\left(\frac{A \cap B}{B}\right)$, where a value of 0 indicates that the two selected populations are disjoint, and a value of 1 indicates the selected populations are identical. The results of this analysis are shown in Figure 3, with panels arranged as for Figure 2. We note that the S3-SAX simulations used become incomplete for stellar/gas masses below $\sim 10^8 M_{\odot}$, a mass limit that may lead to an overestimate of survey overlap in the top-right portions of these diagrams compared to the full-mass distribution of galaxies in the Universe. The dashed lines now indicate the r-band and CO flux thresholds corresponding to the optimal identified limits where the mutual overlap between the HI and ancillary datasets are largest. The redshift and stellar mass distributions for the resultant HI and r-band limited samples are shown in Figure 4.

From these plots it can be seen that the optical imaging depth requirements for all the examined SKA surveys (up to, and including the full SKA2) will be well met by surveys such as those proposed for LSST. Only the very deepest small-area HI surveys may wish to coordinate with the

PoS(AASKA14)131

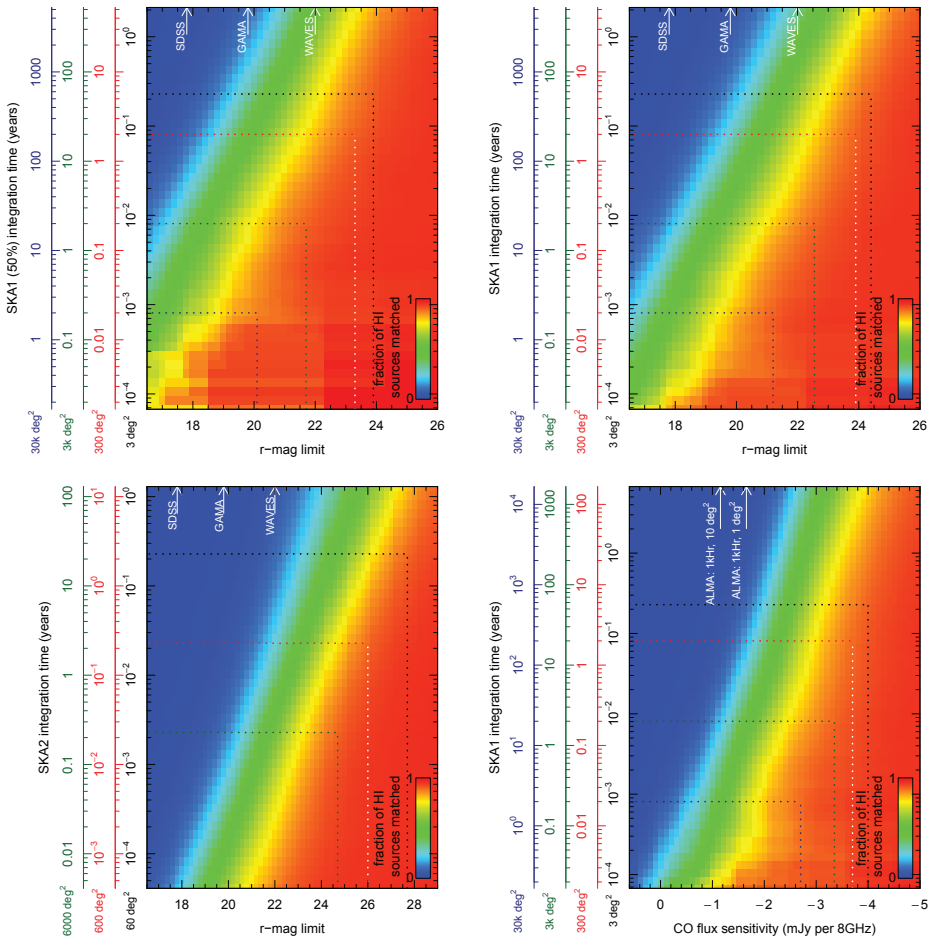

Figure 2: (top-left, top-right, bottom-left) Fraction of HI SKA survey sources (SKA1 50%, SKA1, SKA2 respectively; as a function of integration time) that are detected in an r-band apparent magnitude-limited sample (down to a given magnitude). The colour-scale indicates the value of the metric $F = \frac{A \cap B}{A}$. Different y-axis give the integration time scales for different survey areas. For SKA1 50% and SKA1, four surveys are considered: 3 deg^2 using SKA1-MID (and 50%; black), 300 deg^2 using SKA1-SUR (and 50%; red), 3000 deg^2 using SKA1-SUR (and 50%; green), and 30000 deg^2 using SKA1-SUR (and 50%; blue). For SKA2, three surveys are considered: 60 deg^2 (black), 600 deg^2 (red), and 6000 deg^2 (green). Dotted lines indicate the r-magnitude limit needed to achieve matches for 90% of sources in each SKA survey area (given 2000 hrs of integration for SKA1-MID & SKA2 surveys, and 2 years of telescope time for SKA1-SUR surveys). (bottom-right) Fraction of HI SKA1 survey sources that are detected in a CO(1-0) flux sensitivity limited sample, with colour-scale, colour-axes and indication lines as before.

LSST deep fields rather than the main survey (r $\sim$ 28 mag vs. $\sim$26.5 mag). Black/white arrows are also included in the r-band plots to indicate the depths of some existing and planned low-SNR optical redshift surveys (SDSS, GAMA, WAVES). These show that the optimal redshift sample depth requirements for SKA1-SUR and SKA1-SUR 50% HI surveys will be met by programs such as the WAVES design-reference survey on 4MOST (within its proposed $\lesssim$ 1000 deg^2 area). However, for SKA2, suitably matched redshift samples will require the development of a new class of multiplexed spectroscopic survey facility compared to the current generation of existing (and

PoS(AASKA14)131

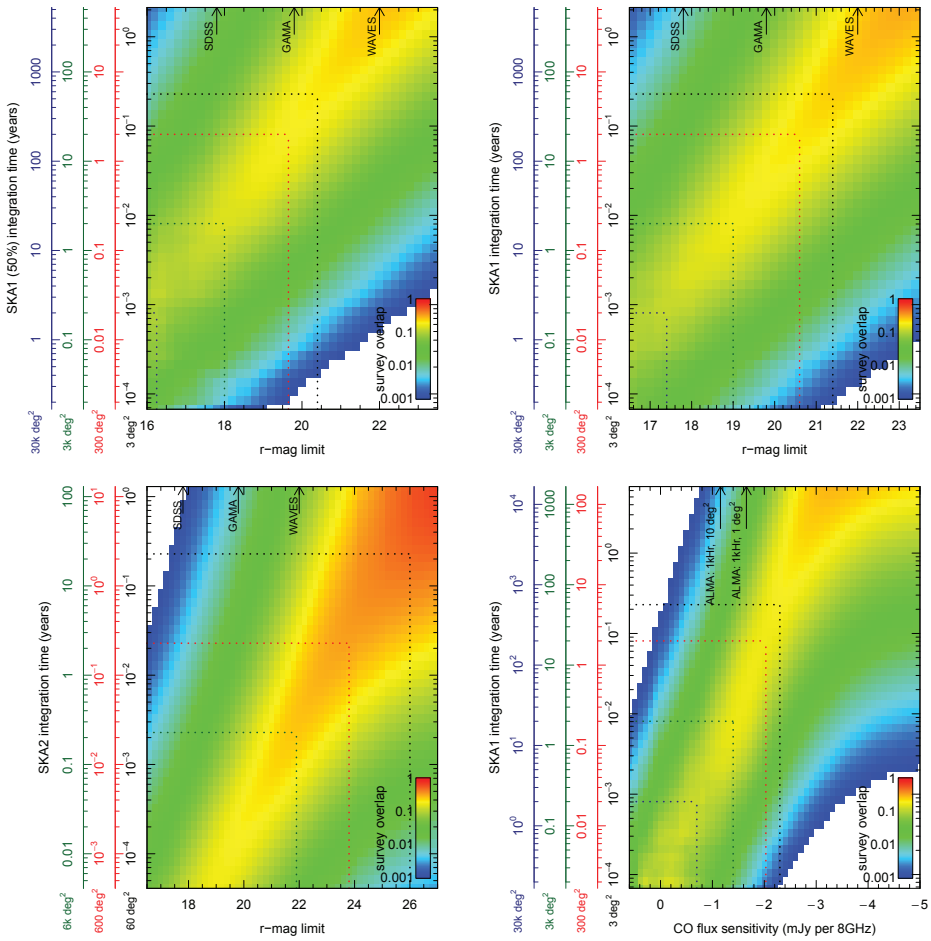

Figure 3: (top-left, top-right, bottom-left) Degree of mutual overlap between the HI sources detected by SKA telescopes (SKA1 50%, SKA1, SKA2 respectively; as a function of integration time) and an optically selected r-band sample (down to a given magnitude). The colour-scale indicates the value of the metric $E = \left(\frac{A \cap B}{A}\right)\left(\frac{A \cap B}{B}\right)$, where $E = 0$ indicates that the two selected populations are disjoint, and $E = 1$ indicates the selected populations are identical. Different y-axis give the integration time scales for different survey areas. For SKA1 50% and SKA1, four surveys are considered: 3 deg^2 using SKA1-MID (and 50%; black), 300 deg^2 using SKA1-SUR (and 50%; red), 3000 deg^2 using SKA1-SUR (and 50%; green), and 30000 deg^2 using SKA1-SUR (and 50%; blue). For SKA2, three surveys are considered: 60 deg^2 (black), 600 deg^2 (red), and 6000 deg^2 (green). Dotted lines show the optimal r-magnitude matching limit for each SKA survey area (given 2000 hrs of integration for SKA1-MID & SKA2 surveys, and 2 years of telescope time for SKA1-SUR surveys). (bottom-right) Degree of mutual overlap between the HI sources detected by SKA1 and a CO(1-0) flux sensitivity limited sample, with colour-scale, colour-axes and indication lines as before.

planned) 4m telescopes. From the black arrows in the CO plots, showing example blind surveys that could be achieved with ALMA, it can be seen that the vast difference in survey speeds between ALMA and the SKA mean that ALMA observations will largely be restricted to targeting HI sub-samples.

PoS(AASKA14)131

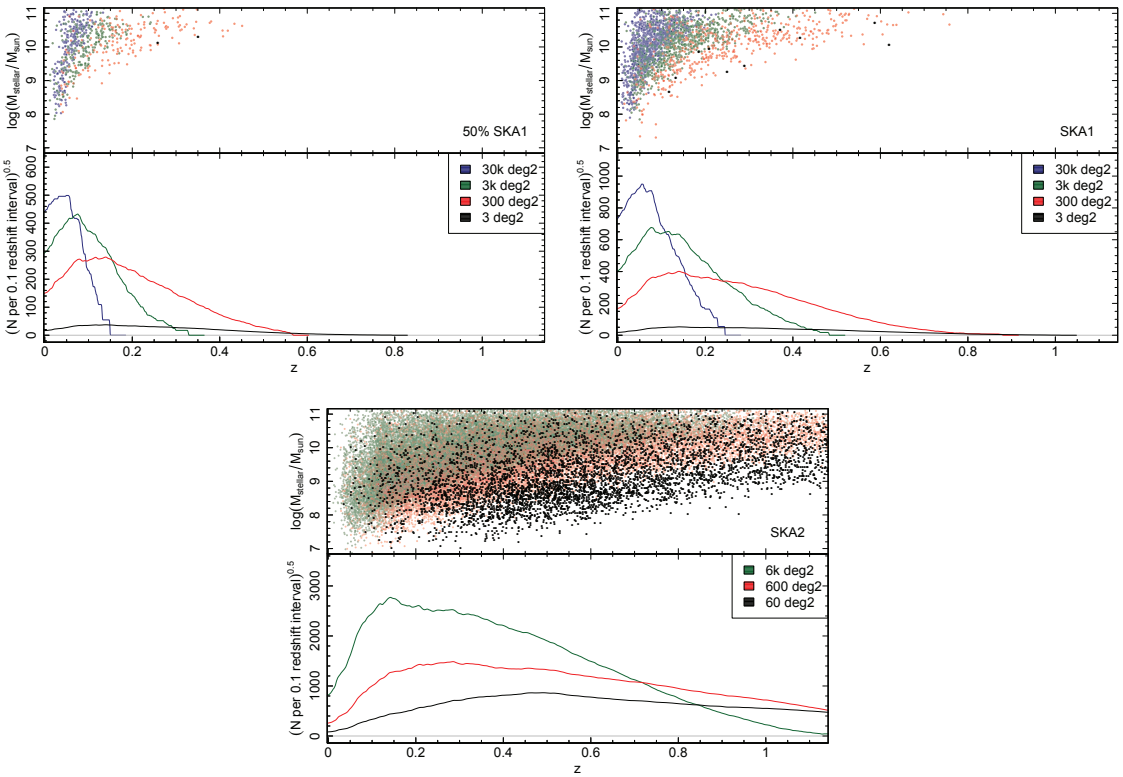

Figure 4: Stellar mass and redshift distributions of the optimal HI and r-band limited samples as identified by the dashed lines in Figure 3 for SKA1 (50%; top-left), SKA1 (top-right) and SKA2 (bottom). Redshift distributions reflect the full number counts for each HI and r-band limited survey, while one thousandth of each sample is plotted in the stellar mass distributions. HI survey integration times are: 2000hrs (SKA1-MID, SKA1-MID 50%: 3 deg^2; SKA2: 60, 600 and 6,000 deg^2); and 2 years (SKA1-SUR, SKA1-SUR 50%: 300, 3000 and 30,000 deg^2).

5. Conclusion

The SKA offers a unique opportunity to understand the evolution of galaxies through large-scale surveys of the most fundamental baryonic building block of the Universe: HI. The scientific opportunity provided by this capacity will be maximised by linking these data to that at other wavelengths, shedding light on the host of regulatory processes that govern the transfer and conversion of material from one baryonic state to another. At present, the planned capability for the acquisition of appropriate multiwavelength data for extragalactic HI surveys varies significantly as a function of frequency and required survey area for SKA1. Excellent optical/NIR imaging will be available through facilities such as LSST, Euclid and W-FIRST (indeed also extending to depths suitable for SKA2), caveat any issues that may arise through a need to coordinate target areas, or that potentially arise from restricted access to proprietary data. However, there is a comparative lack of planned capacity to carry out complementary imaging surveys at other wavelengths. This will restrict the ability to trace important physical quantities such as star formation and dust content. Molecular line observations are similarly constrained with only targeted follow-up observations currently possible over larger areas with facilities such as ALMA, rather than blind surveys

PoS(AASKA14)131

of matching regions. The landscape for optical spectroscopy is significantly better, with suitable surveys expected to be possible with facilities such as VISTA/4MOST, Subaru/PFS, Mayall/DESI etc. However, the sensitivity of these facilities will likely only be good enough to provide redshift information, and not the required 10+ S/N spectra required to trace chemistry which will need the development of 10+m dedicated spectroscopic survey facilities. The availability of these various required multiwavelength data products can loosely be broken down into five categories as summarised below.

Facility grades:

1. Planned capacity exists, and blind ancillary survey data is expected to exist without coordination of target areas: optical imaging (LSST).

2. Planned capacity exists, and blind ancillary survey data could exist with coordination of target areas: NIR imaging (Euclid: < 8000 deg^2, W-FIRST); redshift emission spectra ($S/N \sim 2$).

3. Planned capacity exists, and fully sampled ancillary data could exist, but only in a targeted follow-up mode of worthwhile sources: optical IFU; gas-phase emission spectra ($S/N \sim 10$).

4. Planned capacity exists, and significantly sampled ($\sim$ 1–10%) ancillary data could exist, but only in a targeted follow-up mode: mm (ALMA), FIR imaging (SPICA).

5. Little capacity is expected to be available in the coming decade, and only poorly sampled ($< 1\%$) ancillary data are possible: UV imaging; stellar-phase absorption spectra ($S/N \sim 100+$).

References

Balogh, M. L., et al., 2000, ApJ, 540, 113
Chang, T.-C., et al., 2010, Nature, 466, 463
Delhaize, J., et al., 2013, MNRAS, 433, 1398
Dewdney, P., et al., 2013, "SKA1 System Baseline Design", Document number SKA-TEL-SKO-DD-001 Revision 1
Duffy, A. R., et al., 2012, MNRAS, 420, 2799
Faber, S. M., Jackson, R. E., 1976, ApJ, 204, 668
Fernández, X., et al., 2013, ApJL, 770, L29
Geréb, K., et al., 2013, A&A, 558, A54
Geréb, K., et al., 2014, A&A, 569, A35
Gunn, J. E., Gott, J. R. I., 1972, ApJ, 176, 1
Hopkins, A. M., et al., 2008, ApJ, 682, L13
Kassin, S. A., et al., 2007, ApJ, 660, L35
Keres, D., et al., 2005, MNRAS, 363, 2
Kim, H.-S., et al., 2013, MNRAS, 428, 3366

PoS(AASKA14)131

Lah, P., et al., 2007, MNRAS, 376, 1357
Lewis, I., et al., 2002, MNRAS, 334, 673
Moore, B., et al., 1996, Nature, 379, 613
Obreschkow, D., Meyer, M., 2014, arXiv, 1406.0966O
Obreschkow, D., et al., 2009, ApJ, 703, 1890
Obreschkow, D., Meyer, M., Popping, A., et al., 2015, "The SKA as a Doorway to Angular Momentum" in proc. *Advancing Astrophysics with the Square Kilometre Array*, PoS(AASKA14)138
Pen, U.-L., et al., 2009, MNRAS, 394, L6
Popping, A., Meyer, M., Staveley-Smith, L., et al., 2015, "Observations of the Intergalactic Medium and the Cosmic Web in the SKA era" in proc. *Advancing Astrophysics with the Square Kilometre Array*, PoS(AASKA14)132
Power, C., et al., 2010, MNRAS, 406, 43
Rhee, J., et al., 2013, MNRAS, 435, 2693
Schmidt, M., 1959, ApJ, 129, 243
Springob, C. M., et al., 2005, ApJ, 621, 215
Tully, R. B., Fisher, J. R., 1977, A&A, 54, 661
Verheijen, M., et al., 2007, ApJ, 668, L9
Zwaan, M. A., et al., 2005, MNRAS, 359, L30

PoS(AASKA14)131

Appendix A: Multiwavelength Facilities

Data used for the Gantt charts presented in Figure 1 are given below. We note these numbers were compiled on a best-effort basis, with a degree of uncertainly or arbitrariness existing in some of the parameters (eg. dates). The exact specifications for a number of future facilities will no doubt also evolve with time.

Facility	Start	End	Wave	Hemi	Area (m^2)	A_{eff}/T (m^2/K)	FoV (deg^2)	FWHM (")	Reference
GMRT	1995	20??	HI	N	47,713	250	7.5E-02	2.0	Ananthakrishnan S. & Rao A.P., 2001, AP-RASC '01, 237
Parkes/MB13	1997	20??	HI	S	3,217	100	4.8E-01	830	Staveley-Smith L., et al., 1996, PASA, 13, 243
GBT	2002	2020	HI	N	7,854	276	1.5E-02	531	Jewell P.R & Prestage R.M., 2004, SPIE, 5489, 312
Effelsberg/7-beam	2009	20??	HI	N	7,854	262	1.1E-01	531	Keller R., et al., 2006, Technical Report
Arecibo/ALFA	2010	2020	HI	N	35,633	1150	2.4E-02	249	Giovanelli, R., et al., 2005, AJ, 130, 2598
e-MERLIN	2012	2020	HI	N	9,073	60	2.4E-01	0.24	Garrington S.T., et al., 2004, SPIE, 5489, 332
JVLA	2012	20??	HI	N	13,254	265	2.4E-01	1.5	Perley R.A., et al., 2011, ApJL, 739, LL1
KAT-7	2012	2018	HI	S	792	18	1.1E+00	287	Booth R.S. & Jonas J.L., 2012, AfrSk, 16, 101
ASKAP-12	2015	2017	HI	S	1,357	22	3.0E+01	24	Schinckel A.E., et al., 2012, SPIE, 8444
WSRT/APERTIF	2016	2021	HI	N	5,890	63	8.0E+00	19	Oosterloo T., et al., 2009, PoS(SKADS 2009), 70
FAST	2016	20??	HI	N	70,686	2000	3.2E-02	177	Nan R., et al., 2011, IJMPD, 20, 989
ASKAP	2017	2022	HI	S	4,072	65	3.0E+01	8.9	Schinckel A.E., et al., 2012, SPIE, 8444
MeerKAT	2017	2022	HI	S	9,161	321	8.4E-01	6.6	Booth R.S. & Jonas J.L., 2012, AfrSk, 16, 101
SKA1-SUR	2022	2027	HI	S	14,674	391	1.8E+01	1.1	Dewdney P., 2013, SKA-TEL-SKO-DD-001
SKA1-MID	2022	2027	HI	S	42,737	1630	6.7E-01	0.27	Dewdney P., 2013, SKA-TEL-SKO-DD-001
LOFAR	2012	20??	low	N	2,048	61	3.4E+00	0.33	van Haarlem M.P., et al., 2013, A&A, 556, AA2
MWA	2013	2018	low	S	2,752	55	6.1E+02	120	Tingay S.J., et al., 2013, PASA, 30, 7
SKA1-LOW	2022	2027	low	S	876,485	1000	2.7E+01	11	Dewdney P., 2013, SKA-TEL-SKO-DD-001

Table 2: Table comparing various extra-galactic radio survey facilities that will operate between now and 2025. In the 'Wave' column, 'HI' corresponds to facilities able to observe HI in the local Universe, i.e. they can observe at frequencies as high as 1.4 GHz. Most of the A_{eff}/T values come from Dewdney et al. (2013) which contains a good summary of radio facilities. For a more detailed comparison of radio telescope performance characteristics beyond the first order approach used here, the reader is referred to Popping et al. (2015) in this volume.

PoS(AASKA14)131

Facility	Start	End	Wave	λ_{low} (nm)	λ_{hi} (nm)	Spec. Res.	Hemi	Area (m^2)	FoV (deg^2)	FWHM (")	N_{fibre}	Reference
MMT/ Hectospec	2003	20??	opt	360	920	1,000	N	33.2	7.9E-01	0.7	300	Fabricat D., et al., 2005, PASP, 117, 1411
AAT/ 2dF-AAOmega	2006	20??	opt	370	950	1,300	S	11.9	3.1E+00	1.5	400	Saunders W., et al., 2004, SPIE 5492
Magellan/IMACS	2008	20??	opt	500	900	20	S	31.2	2.0E-01	0.7	2500	Alison L. Coil, 2011, ApJ, 741, 8
LAMOST	2012	2017	opt	370	900	1,000	N	12.6	2.0E+01	3.0	4000	Wang X., et al., 2009, MNRAS, 394, 1775
GTC/GO-IRS	2014	20??	opt	370	991	2,000	N	84.9	4.9E-02	0.8	1000	Caballero J.A., 2011, HSA6 SEA, 769
Sloan/BOSS	2015	2020	opt	360	1,000	1,560	N	4.9	7.1E+00	1.4	1000	Gunn J.E., et al., 2006, AJ, 131, 2332
UK-Schmidt/ TAIPAN	2015	2020	opt	400	800	2,000	S	1.1	2.8E+01	1.5	300	Kuehn K., et al., 2014, SPIE, 9147
Subaru/PFS	2017	20??	opt	380	1,300	2,300	N	52.8	1.3E+00	0.7	2400	Ian S., et al., 2012, SPIE 8446
WHT/WEAVE	2018	20??	opt	370	1,000	5,000	N	13.9	3.1E+00	0.8	1000	Balcells M., et al., 2010, SPIE, 7735
Mayall/DESI	2018	2023	opt	360	980	2,000	N	12.6	7.1E+00	1.5	5000	Flaugher B. & Bebek C., 2014, SPIE, 9147
VISTA/4MOST	2021	20??	opt	390	1,050	5,000	S	12.6	4.2E+00	0.7	2400	de Jong R., et al., 2012, SPIE, 8446
MSE	2024	2029	opt	370	1,300	2,000	N	78.5	1.8E+00	0.7	3200	McConnachie A., et al., 2014, SPIE, 9145E
Keck/MOSFIRE	2012	20??	NIR	970	2,400	3,310	N	76.0	2.8E-03	0.7	46	McLean I.S., et al., 2012, SPIE, 8446
VLT/MOONS	2018	20??	NIR	800	1,800	4,000	S	50.3	1.3E-01	0.8	1000	Cirasuolo M., et al., 2014, SPIE. 9147
Euclid	2020	2026	NIR	1,100	2,000	250	N/S	1.1	5.0E-01	0.2	1700	Beaulieu J.P., 2010, ASPC, 430, 266
WFIRST-AFTA	2024	2030	NIR	1,100	2,000	200	N/S	2.4	2.8E-01	0.1	1000	Green J., et al., 2012, arXiv, 1208.4012G
CCAT	2017	20??	smm	577,000	1,538,000	400	S	491.0	7.9E-01	2.5	100	Woody D., et al., 2012, SPIE, 8444

Table 3: Table comparing various extra-galactic spectroscopic survey facilities that will operate between now and 2025.

Facility	Start	End	Wave	λ_{low} (nm)	λ_{hi} (nm)	Spec. Res.	Hemi	Area (m^2)	FoV (deg^2)	FWHM (")	N_{fibre}	Reference
Calar-Alto/ PPAK	2010	2015	opt	370	700	850	N	9.6	2.8E-04	1.5	400	S.F.Sanchez et al., 2012, A&A, 538, 8
AAT/SAMI	2013	2016	opt	370	950	1,300	S	11.9	7.9E-01	1.5	400	Croom S.M., et al., 2012, MNRAS, 421, 872
SDSS/MaNGA (opt)	2014	2020	opt	360	1,000	2,000	N	4.9	7.1E+00	1.5	1423	Law D.R., et al., 2014, AAS, 22325431
VLT/MUSE	2014	20??	opt	460	930	2,000	S	50.3	2.8E-04	0.2	90000	Bacon R., et al., 2010, SPIE, 7735
GTC/GO-IRS	2014	20??	opt	370	991	2,000	N	84.9	7.1E-04	0.8	1600	Caballero J.A., 2011, HSA6 SEA, 769
HET/VIRUS	2015	2020	opt	350	550	550	N	64.2	1.1E-01	1.5	33600	Hill G.J., et al., 2008, ASP conf, 399, 115
AAT/Hector	2016	2022	opt	370	950	1,300	S	11.9	3.1E+00	1.5	3050	Bland-Hawthorn J, 2014, arXiv, 1410.3838
WHT/WEAVE (opt)	2018	20??	opt	370	1,000	5,000	N	13.9	3.1E+00	0.8	1000	Balcells M., et al., 2010, SPIE, 7735
SDSS/MaNGA (NIR)	2014	2020	NIR	360	1,000	2,000	N	4.9	7.1E+00	1.5	1423	Law D.R., et al., 2014, AAS, 22325431
VLT/KMOS	2014	20??	NIR	800	2,500	1,800	S	50.3	1.1E-02	0.7	4704	Sharples R.M., et al., 2004, SPIE, 5492
WHT/WEAVE (NIR)	2018	20??	NIR	370	1,000	5,000	N	13.9	3.1E+00	0.8	1000	Balcells M., et al., 2010, SPIE, 7735

Table 4: Table comparing various extra-galactic IFU survey facilities that will operate between now and 2025.

PoS(AASKA14)131

Facility	Start	End	Wave	Hemi	Area (m^2)	FoV (deg^2)	FWHM (")	Reference
Fermi-LAT	2008	2016	gamma	N/S	2.5	2.8E+03	360	Atwood W.B., et al., 2009, ApJ, 697, 1071
HESS-II	2012	2018	gamma	S	50,000	8.0E+00	900	Becherini Y., et al., 2008, AIPC, 1085, 738
HAWC	2015	2030	gamma	N	10,000	2.5E+04	2,700	Abeysekara A.U., et al., 2012, AsPaP, 35, 641
Gamma400	2019	20??	gamma	N/S	0.8	2.8E+03	36	Galper A.M., 2013, AdSpR, 51, 297
CTA	2020	2030	gamma	N/S	500,000	2.0E+01	900	Gibney E, 2014, Nat, 508, 297
XMM/Newton	2000	2018	X-ray	N/S	0.4	2.0E-01	50	Kirsch M.G.F., et al., 2004, SPIE, 5488
eROSITA	2016	2023	X-ray	N/S	0.4	7.9E-01	25	Chon G. & Bohringer H., 2013, AN, 334, 478
WSO-UV	2017	2022	UV	N/S	2.3	2.0E-01	0.2	Shustov B., et al., 2009, Ap&SS, 320, 187
CFHT/MegaCam	2003	2019	opt	N	10.2	9.5E-01	0.7	Aune S., et al., 2003, SPIE 4841
HST/WFC-UVIS3	2009	2020	opt	N/S	4.5	1.3E-04	0.1	Windhorst R., et al., 2011, ApJS, 193, 27
Oschin/iPTF	2009	2015	opt	N	1.1	7.1E+00	1.5	Law N.M., et al., 2009, PASP, 121, 1395
Magellan/MEGACAM	2009	20??	opt	S	31.2	2.0E-01	0.7	Szentgyorgyi A., et al., 2012, SPIE, 8446
Pan-STARRS-1	2010	2015	opt	N	2.5	7.1E+00	1.0	Morgan J.S., et al., 2014, SPIE, 914
VST/OmegaCam	2011	2021	opt	S	5.3	7.9E-01	0.7	Iwert O., et al., 2006, SPIE 6276
Blanco/DECam	2013	2018	opt	S	12.6	3.8E+00	1.0	Hand E., 2012, Nat, 489, 190
SkyMapper	2014	2019	opt	S	1.4	5.7E+00	1.6	Keller S.C., et al., 2007, PASA, 24, 1
Subaru/HSC	2014	2019	opt	N	52.8	1.8E+00	0.5	Miyazaki S., et al., 2012, SPIE, 8446
Pan-STARRS-2	2015	2017	opt	N	5.1	1.4E+01	1.0	Morgan J.S., et al., 2014, SPIE, 914
WHT/PAUcam	2015	2018	opt	N	13.9	7.9E-01	1.2	Madrid F., et al., 2010, SPIE, 7735
Javalambre	2015	2020	opt	N	4.9	7.1E+00	0.7	Abramo L., et al., 2012, MNRAS, 423, 4
Oschin/ZTF	2017	2020	opt	N	1.1	3.6E+01	1.5	Bellm E., 2014, htu conf, 27
Euclid Opt	2020	2026	opt	N/S	1.1	5.0E-01	0.2	Beaulieu J.P., 2010, ASPC, 430, 266
LSST	2022	2032	opt	S	55.4	9.6E+00	0.7	Krabbendam V.L., 2008, SPIE, 7012
WFIRST-AFTA Opt	2024	2030	opt	N/S	4.5	2.8E-01	0.1	Green J., et al., 2012, arXiv, 1208.4012G
VISTA/VIRCam	2009	2021	NIR	S	13.2	2.1E+00	0.6	Dalton G.B., et al., 2006, SPIE 6269
Magellan/FOURSTAR	2009	20??	NIR	S	31.2	7.9E-03	0.7	Persson S.E., 2008, SPIE, 7014
HST/WFC3-IR	2009	2020	NIR	N/S	4.5	1.3E-04	0.1	Windhorst R., et al., 2011, ApJS, 193, 27
JWST/NIRCam	2018	2028	NIR	N/S	33.2	7.9E-05	0.04	Beichman C.A., et al., 2012, SPIE, 8442
Euclid NIR	2020	2026	NIR	N/S	1.1	5.0E-01	0.2	Beaulieu J.P., 2010, ASPC, 430, 266
WFIRST-AFTA NIR	2024	2030	NIR	N/S	4.5	2.8E-01	0.1	Green J., et al., 2012, arXiv, 1208.4012G
Spitzer/IRAC	2003	2015	MIR	N/S	0.6	7.5E-03	1.7	Fazio, G.G., et al., 2004, ApJSS, 154, 10
WISE	2010	2016	MIR	N/S	0.1	5.0E-01	5.0	Wright E.L., et al., 2010, AJ, 140, 1868
SPICA MIR	2025	20??	MIR	N/S	9.6	2.0E-01	1.0	Nakagawa T., et al., 2014, SPIE, 9143
SPICA FIR	2025	20??	FIR	N/S	9.6	2.0E-01	5.0	Nakagawa T., et al., 2014, SPIE, 9143
JCMT/Scuba2	2011	2015	smm	N	176.7	1.8E-02	14	Holland W.S., et al., 2013, MNRAS, 430, 2513
CCAT	2017	20??	smm	S	491	7.9E-01	2.5	Woody D., et al., 2012, SPIE, 8444
ALMA	2013	20??	mm	S	6,569	2.8E-05	0.01	Brown R.L., 2004, AdSpR, 34, 555

Table 5: Table comparing various extra-galactic imaging survey facilities that will operate between now and 2025.

PoS(AASKA14)131

PROCEEDINGS OF SCIENCE

Observations of the Intergalactic Medium and the Cosmic Web in the SKA era

A. Popping[*1,2], **M. Meyer**[1,2], **L. Staveley-Smith**[1,2], **D. Obreschkow**[1,2], **G. I. Józsa**[3,4], **D.J. Pisano**[5,6] **and HI SWG Members**

[1] *ICRAR, The University of Western Australia*
[2] *ARC Centre of Excellence for All-sky Astrophysics (CAASTRO)*
[3] *SKA South Africa*
[4] *Rhodes University*
[5] *Dept. of Physics & Astronomy, West Virginia University*
[6] *NRAO-Green Bank.*

E-mail: attila.popping@icrar.org

The interaction of galaxies with their environment, the Intergalactic Medium (IGM), is a very important aspect of galaxy formation. One of the most fundamental, but unanswered questions in the evolution of galaxies is how gas circulates in and around galaxies and how it enters the galaxies to support star formation. We have several lines of evidence that the observed evolution of star formation requires gas accretion from the IGM at all times and on all cosmic scales. This gas remains largely unaccounted for and the outstanding questions are where this gas resides and what the physical mechanisms of accretion are. The gas is expected to be embedded in an extended cosmic web made of sheets and filaments. Such large-scale filaments of gas are expected by cosmological numerical simulations, which have made significant progress in recent years. Such simulations do not only model the large scale structure of the cosmic web, but also investigate the neutral gas component. To truly make significant progress in understanding the distribution of neutral hydrogen in the IGM, column densities of $N_{HI} \sim 10^{18}$ cm^{-2} and below have to be probed over large areas on the sky at sub-arcminute resolution. These are the densities of the faintest structures known today around nearby galaxies, though mostly found with single dish telescopes which do not have the resolution to resolve these structures and investigate any kinematics. Existing interferometers lack the collecting power or short baselines to achieve brightness sensitivities typically below $N_{HI} \sim 10^{19}$ cm^{-2}. Reaching lower column densities with current facilities is feasible, however requires prohibitively long observing times. The SKA will for the first time break these barriers, enabling interferometric observations an order of magnitude deeper than current interferometers and with an order of magnitude better linear resolution than single-dish telescopes.

Advancing Astrophysics with the Square Kilometre Array
June 8-13, 2014
Giardini Naxos, Italy

[*] Speaker.

PoS(AASKA14)132

1. Introduction

The Intergalactic Medium contains a large fraction of the Universal baryon budget and is a key aspect in galaxy formation. This chapter focuses on recent observational results and progress in simulations of the cosmic web. We will motivate the new insights in cosmology and galaxy evolution that the SKA will bring and we will assess the detectability of the IGM at low column densities with SKA1 and SKA2.

Currently almost everything that is known about the structure of the IGM has been derived from the Lyman resonance scattering lines in the optical and ultraviolet (UV). Although this will continue to be an important method, there will be a significant change in the near future when radio telescopes will be used for the detection of intergalactic gas. New arrays, such as the LOw Frequency ARray (LOFAR), the Murchison Widefield Array (MWA) and the Precision Array to Probe the Epoch of Reionisation (PAPER) will be used in an effort to detect the 21-cm signature of the IGM at the epoch of reionization (EoR). Current efforts at different wavelenghts (UV, optical and IR) search for the first galaxies at high redshift and are complementary to the EoR detection experiments with the SKA and its precursors. In studies of the evolution of the luminosity function, redshifts in the range of $z = 7$ - 8 are reached, where it is expected that the 21-cm signature of neutral hydrogen will be seen at slightly higher redshift.

In this chapter we make predictions for observations that can be performed with SKA1-MID and SKA1-SUR at redshift $z \sim 0$ and that will directly detect faint neutral hydrogen gas in emission. Simulations expect that intergalactic gas is accreting onto galaxies, one of the 'holy grails' in understanding galaxy formation is to detect this infalling gas. This has been proven to be extremely difficult, partly due to the interface of outflowing gas caused by galactic fountains which are associated with regions of star formation (Fraternali & Binney 2006). To fully understand and test our cosmological model a crucial step is to detect the infalling gas between galaxies and measure its physical properties. This gas can be detected in the local Universe by using the 21-cm line of neutral hydrogen. Apart from some tentative detections (e.g. Popping (2010); Wolfe et al. (2013)), there has not been clear evidence for the existence of the diffuse gas filaments and infalling gas. New telescopes such as the Australian SKA Pathfinder (ASKAP), the Meer-Karoo Array Telescope (MeerKAT), the Five hundred meter Aperture Spherical Telescope (FAST) and the SKA will be able to probe the neutral fraction and kinematics of the IGM in the Local Universe at significantly lower column densities compared to what has been done before in HI 21-cm emission.

This low column density gas, residing in filamentary structures, is the reservoir that fuels future star formation, and could provide a direct signature of smooth cold-mode accretion predicted to dominate gas acquisition in star-forming galaxies today (Kereš et al. (2005); Dekel et al. (2009); Kereš et al. (2009)). Furthermore, the trace neutral fraction in this phase may provide a long-lived fossil record of tidal interactions and feedback processes such as galactic winds and AGN-driven cavities.

In the following section of this chapter we will give a short overview of the distribution of low column density HI gas in the cosmic web and around galaxies. In section two and three we discuss the current status of observations and simulations, that probe these low column densities. We have conducted very detailed performance simulations of the SKA baseline design (Dewdney et al.

PoS(AASKA14)132

2013), which will be discussed in section four. Based on the results of these simulations, we make predictions for several science projects that can be performed with SKA1-MID or SKA1-SUR. In section six we discuss the prospects of SKA1, the development phase of SKA1 and eventually the full SKA (SKA2). We end with a short conclusion.

2. Background

2.1 Cosmic Web

Theories of structure formation predict that matter in the IGM and in galaxies is embedded in a "cosmic web" of walls, sheets and filaments. (e.g. Davis et al. (1985); Frenk et al. (1985); Miralda-Escudé et al. (1996)). This web contains large filaments and structures with sizes that range up to several megaparsecs. Galaxies reside in the high density regions of the cosmic web, at the intersection of sheets and filaments. This large scale galaxy structure has been discovered by redshift surveys (e.g. de Lapparent et al. (1986)), however the gas that is associated with the filaments has been known much longer and has been detected using the absorption lines in spectra of high redshift quasars (Gunn & Peterson (1965); Lynds (1971)). The spectral density of these Lymanα lines indicate that at redshift $z = 3$, nearly all baryons in the Universe were in a cool phase with temperatures of $T \sim 10^4$ K. (Rauch et al. 1997). As time evolves this cool gas is being shock heated during the gravitational collapse of dark matter within the filaments, resulting in a Warm Hot Intergalactic Medium (WHIM) (Bregman (2007)). A part of this gas accretes rapidly onto the virialized dark matter halos of galaxies. Numerical simulations of structure formation support the picture of a cosmic web containing baryonic matter that aligns with the underlying dark matter structure. (e.g. Cen et al. (1994); Cen & Ostriker (2006); Fukugita & Peebles (2004)). An example is shown in Fig 1. from Popping et al. (2009) where the total hydrogen component (HII + HI) and neutral hydrogen component (HI) of the cosmic web are reconstructed. In the regions of very high over-density, in the centres of galaxies, the neutral gas density is roughly equivalent to the total gas density, indicating that the gas is fully neutral. However at the edges of galaxies and in the filaments the neutral fraction of the gas decreases rapidly resulting in HI column densities well below $N_{HI} \sim 10^{18}$ cm^{-2}.

2.2 Gas Accretion

The formation and evolution of galaxies is expected to be intimately connected to the IGM. Stars in galaxies are formed from molecular gas and after the galaxies have been formed, the stellar mass that is locked in galaxies keeps increasing with time (e.g. Marchesini et al. (2009)). This means that to maintain star-formation, the molecular phase needs to be re-supplied over cosmic time. The molecular gas gets replenished from atomic gas, therefore the next question is whether there is enough gas in the dense atomic reservoir directly surrounding the galaxy to explain the continuous star formation. An overview of galaxies with surrounding neutral hydrogen gas is given by Sancisi et al. (2008)

We have several lines of evidence that the observed evolution of star formation requires gas accretion from the intergalactic medium at all times and on all cosmic scales. Until today, this gas has been unaccounted for and the outstanding question is where this gas resides and what the physical mechanisms of accretion are

PoS(AASKA14)132

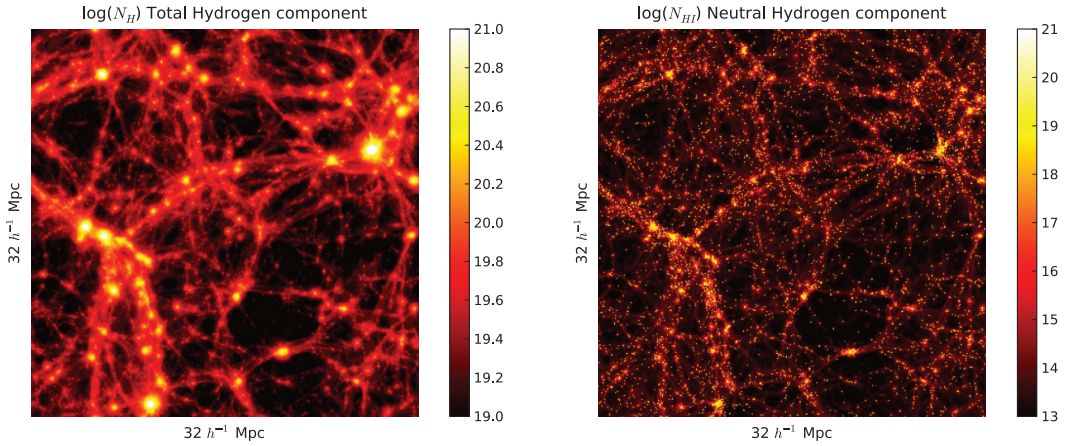

Figure 1: Simulation of the cosmic web from Popping et al. (2009), left panel shows column densities of the total Hydrogen gas component (HII + HI), the right panel shows the neutral gas component (HI) that can potentially be detected by radio telescopes using the 21-cm line.

When looking at the density of neutral hydrogen 10 billion years ago above redshift $z \sim 2$ (e.g. Prochaska & Wolfe (2009)), the total amount of gas that is locked in galaxies is less than the mass which is locked in stars today. Recent simulations support this picture of continuous gas accretion. Due to the gravitational collapse of dark matter dense structures and filaments are created. The primordial atomic gas falls into the gravitational potential wells of the dark matter. There are two modes in which gas falls onto galaxies, dubbed hot-mode and cold-mode accretion (Kereš et al. 2005). In the case of hot mode accretion the gas falling on the dark matter filaments is shock heated to temperatures up to 10^7 Kelvin and forms a quasi hydrostatic equilibrium halo; the warm-hot intergalactic medium (WHIM) (e.g. Davé et al. (2001)). At some evolutionary stage this hot virialized gas cools rapidly while loosing its pressure support and settles into the centrifugally supported disks or the spiral arms of a galaxy. In the case of cold mode accretion the gas is never heated to these high temperatures, but smoothly accretes directly into the galaxies. The empirical deviation between the two accretion modes is around 2×10^5 K. Recently simulations have converged to a cosmological model where cold mode accretion dominates gas infall at all cosmic times and hot mode accretion is mostly relevant for galaxies that reside in halos with masses above 10^{12} solar masses (Kereš et al. 2009; Dekel et al. 2009).

2.3 The Circumgalactic Medium

Surrounding the direct environment of galaxies is the circumgalactic medium (CGM) which is the interplay between galaxies and the IGM. The gaseous haloes of 44 galaxies between $z = 0.15$ and 0.35 has been investigated using background QSOs observed with the Cosmic Origins Spectrograph (Tumlinson et al. 2013). The galaxies span both early and late types and the sight-lines of the QSO spectra pass within 150 kpc of the galaxies. The authors find that the circumgalactic medium exhibits strong HI, with a 100% covering fraction for star-forming galaxies and 75% covering for passive galaxies. The kinematics of this gas indicate that it is bound to the host galaxy and the bulk of the detected HI arises in a bound, cool, low-density photoionized diffuse medium. This gas may

PoS(AASKA14)132

act as fuel for future star formation (Werk et al. 2013) and for star forming galaxies intervening gas is found up to 75% of the virial radius of the galaxy. The total mass of gas in the CGM is expected to be responsible for at least half of the missing baryons purported to be missing from dark matter halos at the 10^{12} $M_{\odot}$ scale (Werk et al. 2014).

2.4 Low Column Density of the Intergalactic neutral gas

The single biggest challenge in detecting neutral hydrogen gas in the IGM is that extremely low brightness sensitivities have to be achieved, well below 10^{19} and possibly 10^{18} cm^{-2}. Unfortunately, emission from intergalactic baryons is difficult to observe, because current interferometers result in a detection limit of column densities typically $N_{HI} \gtrsim 10^{19}$ cm^{-2}. These densities are the realm of damped Lyα (DLA) systems and sub-DLAs. Below column densities of $N_{HI} \sim 10^{20}$ cm^{-2}, the neutral fraction of hydrogen decreases rapidly because of the transition from optically-thick to optically-thin gas ionised by the metagalactic ultraviolet flux. At lower densities, the gas is no longer affected by self-shielding and the atoms are mostly ionised (e.g. Rauch (1998)). This sharp decline in neutral fraction from almost unity to less than a percent happens within a few kpc. Below $N_{HI} \sim 3 \cdot 10^{17}$ cm^{-2}, the gas is optically thin and the decline in neutral fraction with total column is much more gradual. A consequence of this rapid decline in neutral fraction is a plateau in the HI column density distribution function between $N_{HI} \sim 10^{18}$ and $N_{HI} \sim 10^{20}$ cm^{-2}, where the relative surface area at these columns shows only modest growth. This behaviour is confirmed in QSO absorption line studies tabulated by Corbelli & Bandiera (2002) and in HI emission by Braun & Thilker (2004). This plateau in the distribution function is a critical issue for observers of neutral hydrogen in emission and the flattening in the distribution function near $N_{HI} \sim 3 \cdot 10^{19}$ cm^{-2} has limited the ability of even deeper observations to detect hydrogen emission from a larger area. This behaviour is demonstrated in Fig. 2 from Popping et al. (2009), where the distribution on neutral hydrogen gas is simulated. By establishing that a steeper distribution function is again expected below about $N_{HI} \cdot 10^{18}$, it provides a clear technical target for what the SKA needs to achieve to effectively probe diffuse gas. Exploration of the $N_{HI} < 10^{18}$ cm^{-2} regime is essential for gaining a deeper understanding of the repository of baryons that drive galaxy formation and evolution.

3. Current Status of observations and simulations

3.1 Observations

Detecting the gas in the cosmic web in HI and understanding the relation between galaxies and the IGM has proven to be very challenging, because the neutral fraction of this gas is very low. At redshifts above $z \sim 2$ HI clouds are visible as intervening structures in Lyman-alpha absorption lines of QSO spectra which are able to probe very low column densities. However these are indirect detections and are confined to a very small number of locations where there is a sufficiently bright background quasar. As a result the Lyman-α lines are generally not suitable to either image the intergalactic gas, or measure any kinematics. Nevertheless, studies with especially the Cosmic Origins Spectograph (Tumlinson et al. 2013) have shown very substantial indications for the existence of large amounts of gas surrounding galaxies out to 75% of the virial radius.

PoS(AASKA14)132

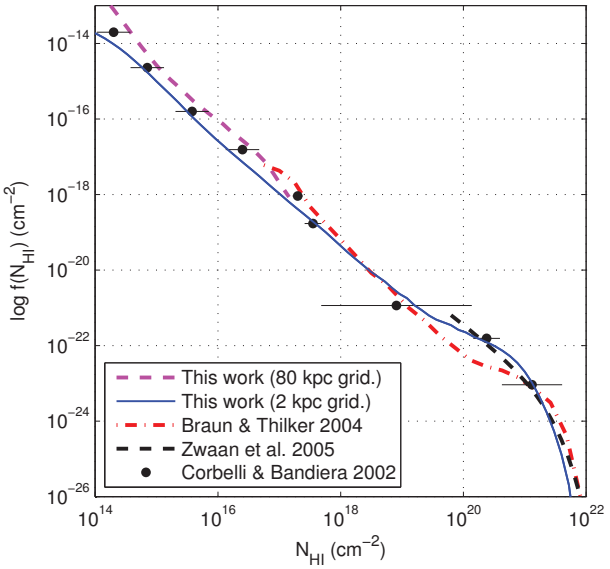

Figure 2: Simulated N_{HI} distribution function from Popping et al. (2009) at redshift $z = 0$. Around column densities of $N_{HI} \sim 10^{19}$ cm^{-2} there is a flattening plateau in the distribution, as the gas densities are getting lower as the gas is not protected anymore against ionisation by self shielding.

At low redshifts HI observations have been pushing the limits of existing telescopes, to trying to image the extended environment of galaxies at very low column densities and to detect gas filaments connecting the galaxies. The best known example is a filament of HI gas that has been detected between M31 and M33 by Braun & Thilker (2004) using the Westerbork telescope as an array of single dish telescopes rather than an interferometer. The large beam size of the Westerbork telescope when used as a single dish telescope results in a a very good brightness sensitivity, however is limited to very nearby objects such as M31 or the Magellanic clouds. Continuing on this concept Popping & Braun (2011b) performed a survey of the filament connecting the Local Group with the Virgo cluster, again using the WSRT as a single dish telescope. Some tentative detections have been made for which confirmations were sought in the cross correlation data of the survey Popping & Braun (2011c) and re-reduced data from the HIPASS survey covering the same area Popping & Braun (2011a). More recently the connecting bridge between M31 and M33 has been confirmed by Lockman et al. (2012), which until today remains the most convincing example of a very extended, low column density HI filament connecting two galaxies.

Several other attempts have been made to detect gas between galaxies at very low column densities, e.g. Wolfe et al. (2013) and Pisano (2014). Both these papers detect some gas features with column densities of $\sim 10^{18}$ cm^{-2}. Wolfe et al. (2013) report clumpy structures of gas, however they lack the resolution to resolve most of the kinematics. A very deep observation on Arecibo was conducted by Irwin et al. (2009), looking for companions of NGC 2903 and reaching column densities of $N_{HI} = 2 \cdot 10^{17}$ cm^{-2}. The galaxy is found to have a very large HI envelope and two companions that are most likely dwarf galaxies. In a very different approach Chang et al. (2010) have attempted to map the cosmic web in HI at redshift $z \sim 0.8$ using intensity mapping with the

PoS(AASKA14)132

GBT. Noteworthy is that all very low column density detections have been made with single dish telescopes such as the GBT and Arecibo. Existing interferometers lack the sensitivity to detect very low column density gas within a reasonable integration times and have been unable to confirm detections made by single dish telescope. An exception may be a survey of the Virgo area presented in Popping & Braun (2011c), where the WSRT has been used at very extreme hour angles. Because of the extreme observing conditions this resulted in a large number of projected short baselines and a low spatial resolution that enabled the detection of low column density gas.

Interferometric telescopes have been used to map the extended environment of single galaxies in great detail. Indeed, observations of a few nearby large spirals (e.g. NGC 891 (Oosterloo et al. 2007), NGC 2403 (Fraternali et al. 2004; de Blok et al. 2014) and NGC 6946 (Boomsma et al. 2008)) and the nearby dwarf galaxy UGCA 105 (e.g. Schmidt et al. (2014)) have shown large amounts of cold gas in their extended halos. In a review article by Sancisi et al. (2008) many examples of galaxies are shown with extended neutral hydrogen emission that are caused by a combination of gas infall and feedback. The authors conclude however that this is not the directly detected infalling gas that fuels the galaxies, because even if all the observed gas would be attributed to gas accretion, an order of magnitude more gas infall is needed to sustain the observed star formation rates.

Accretion of intergalactic matter does not only affect the inner portions of galactic disks, but also the outer, extended, HI disks. At large radii (typically beyond r_{25}), the spin vectors of outer galactic HI disks often appear to be tilted with respect to the inner disks, i. e., galactic disks become warped where the stellar component is fading. The warp, the transition from one orientation to the other, often appears in a confined radial range, indicating a two-regime structure of an inner bright disk and a faint, inclined outer disk (e.g. Briggs (1990); van der Kruit (2007); Józsa (2007)). At the transition radius, a sudden drop in surface brightness occurs frequently (García-Ruiz et al. 2002; van der Kruit 2007; Józsa 2007). These specific features have been interpreted as a signature of accretion from the IGM with misaligned angular momentum (van der Kruit 2007).

However, among other scenarios, warps may also be excited through a backreaction of the dark matter halo and the disk disk on accreted dark matter (e.g. Ostriker & Binney (1989); Shen & Sellwood (2006)) or by accretion of the IGM onto the - already existing - corona or disk (e.g. Kahn & Woltjer (1959), López-Corredoira et al. (2002)), which becomes more susceptible to disturbances with increasing radius (see van der Kruit (2007), Józsa (2007) for more comprehensive reviews). Using the warp structure as a tracer of the IGM is hence an indispensible ingredient in future studies of galaxy evolution, but it requires a good overview of the channels through which galaxies acquire their angular momentum. A more detailed overview about the angular momentum of galaxies is given in Obreschkow et al. (2015)

Currently the HALOGAS survey (Heald et al. 2011) gives the largest inventory of extended gas in nearby galaxies mapping 22 galaxies down to column densities of a few time 10^{19} cm^{-2} at a resolution of 15 arcsec. Results of this survey show that an extended HI disk is not common for galaxies (e.g. Zschaechner et al. (2012)) and that the best example is NGC 891.

Apart from targeted observations to achieve low column densities, currently existing all-sky

PoS(AASKA14)132

surveys such as HIPASS and ALFALFA also have a good brightness sensitivity. These all-sky surveys have been performed with single dish telescopes, that generally give a much better brightness sensitivity than interferometric observations due to the low resolution of the beam. HIPASS has a typical column density sensitivity of $N_{HI} \sim 4 \cdot 10^{17}$ cm^{-2} over 26 km s^{-1} (Barnes et al. 2001) , this can be slightly improved upon by reducing data in a different way compared to the original product, for example Popping & Braun (2011a) achieve a brightness sensitivity of $3 \cdot 10^{17}$ cm^{-2} over 26 km s^{-1} in the northern part of the survey, which is typically less sensitive than the rest of the survey. ALFALFA has a better flux sensitivity compared to HIPASS, but due to the smaller beam it has a very similar brightness sensitivity of $\sim 5 \cdot 10^{17}$ cm^{-2} over 26 km s^{-1} (Giovanelli et al. 2005). Despite the very good brightness sensitivities of these surveys, neither of them show a large amount of column density gas in the realm of a few times $N_{HI} \sim 10^{18}$ cm^{-2} that should be apparent in these surveys. This lack of observational results could support the predicted plateau in the HI distribution function as predicted by simulations. A disadvantege of the surveys performed with single dish telescopes is the very large beam size of up to 15 arcmin the case of HIPASS, that can dilute any structures with physical scales that are smaller than the beam size. The simulations in Popping et al. (2009) predict the extended gas clumps or filaments to have widths of the order of ~ 25 kpc. At the resolution of the HIPASS this corresponds to physical distance of only 6 Mpc.

3.2 Predictions from simulations

In view of the observational difficulties in probing the low HI column density regime, it is particularly important to have reliable numerical simulations to aid in planning new observational campaigns, and eventually to help interpret such observations within a structure formation context. The most widely used methods to make predictions are semi-analytical models and hydrodynamical simulations. In semi-analytical models the evolution of baryons is based on the dark matter distribution of the simulation, hydrodynamical simulations follow the distribution of both baryons and dark matter independently. While simulations of galaxy formation are challenging, historically they have had much success predicting the more diffuse baryons residing in the cosmic web (e.g. Davé et al. (1999)).

The drawback of most numerical simulations is that they concentrate on the total baryon or total gas budget (e.g. Obreschkow et al. (2009); Power et al. (2010)), but do not focus on the neutral hydrogen component. Only recently the first papers have appeared that make an effort to extract the HI component from hydrodynamical simulations at low redshift (e.g. (Popping et al. 2009; Duffy et al. 2012; Cunnama et al. 2014)). The most significant uncertainty in modelling the neutral hydrogen distribution arises from our need to model a self-shielding correction in moderate density regions Duffy et al. (2012). The papers listed here all use a simple prescription to extract the neutral gas component, based on the thermal pressure of the gas. Although these predictions have been relatively successful, they do not justify the true physics of the gas and a lot of effort is going on to model the radiative processes that determine the phase of the gas more realistically. It also remains a large challenge to understand the interplay between gas in galaxies and the surrounding environment. Although many simulation predict the accretion of gas from the IGM, a significant fraction of the gas in the CGM may be due to feedback mechanisms as a result of supernovae explosion. Very recently Crain et al. (2013) have found that in their simulations at $z \sim 0$ the electron density of hot coronae around galaxies is dominated by the metal-poor gas accreted from the IGM, they

PoS(AASKA14)132

infer that the hot CGM observed via X-ray emission is the outcome of both hierarchical accretion and stellar recycling.

Both (Popping et al. 2009) and (Duffy et al. 2012) have attempted to model the gas clumps and filaments around galaxies and both papers show small over-densities of HI gas with physical scales in the range between 10 and 50 kpc. Unfortunately it is very difficult to assess the reliability of the neutral hydrogen distribution in these simulations as there is a complete lack of observational support at these low column densities. Nevertheless it seems that to align with predictions from simulations, future observations of neutral hydrogen gas in the CGM and IGM should aim to achieve physical resolutions of the order of 10 kpc to be able to resolve the gas. Lower resolution observations might dilute the emission making it harder to detect.

4. Performance of the SKA1 baseline design

In order to assess the potential of phase 1 of the SKA, we have performed detailed simulations to model observations realistically, using different scenarios. For both SKA1-SUR and SKA1-MID we have simulated observations and compare their performance to that of ASKAP, MeerKAT and the VLA. ASKAP and MeerKAT are the main precursors of SKA1-SUR and SKA1-MID respectively, while the recently upgraded VLA provides the benchmark of what can be achieved with an existing interferometer.

4.1 Simulated observations

We have created visibility-datasets using the MIRIAD software package, for eight hour synthesis observations with a cycle time of 10 minutes. A continuous integration time of eight hours is considered to be a typical length for observations with SKA1-SUR and SKA1-MID, although shorter integration times are possible and longer integration times can be achieved by combining multiple observations. For each telescope datasets are generated at declinations of 0, -30 and -60 degrees. Beam size, brightness sensitivity and survey speed are dependent on the observing frequency, all simulations have been performed at three different frequencies, relevant to SKA science; 0.6, 1.0 and 1.4 GHz, using a constant bandwidth of 50 kHz. The visibility data is used to generate noise maps and beam-point spread functions (PSF). For all the simulations the telescope parameters have been extracted from table 1,9 and 16 of the SKA1 Baseline Design (Dewdney et al. 2013). For clarification relevant parameters that have been used are listed in table 1. The effective field of view is given in the last row at 1.42 GHz and gives the noise equivalent area of the beam, which can be calculated by:

$$\mathrm{FoV}_{beam} = (\pi/8)(1.3\lambda/D)^2 \tag{4.1}$$

To be able to quantify the performance at different resolutions, in the imaging step a tapering function is applied to the visibilities. Both a Gaussian taper and top-hat filter have been applied. The Gaussian taper is the default in MIRIAD, a top-hat filter is a sharp cutoff filter that is applied to the visibility data, to only use *uv*-points within a certain length $q = (u^2 + v^2)^{1/2}$. The top-hat filter gives better control over the maximum baseline length and the corresponding resolution when using uniform weighting. We compare the performance of the telescope for a large range of q values, up to baseline lengths of 128 kilometers, or angular resolutions of sub-arcsecond up to several

PoS(AASKA14)132

	VLA	**ASKAP**	**MeerKAT**	**SKA1-SUR**	**SKA1-MID**
$\mathbf{A}_{eff}/\mathbf{T}_{sys}$	265	65	321	391	1630
Receptor Size	25	12	13.5	15	15
$\mathbf{T}_{sys}$	25	50	20	30	20
Efficiency	0.5	0.8	0.7	0.8	0.78
$\mathbf{FoV}_{beam}$	0.16	30	0.53	18	0.43

Table 1: Telescope parameters used in the simulations to model observations

arcminutes. Different maps are created using weighting schemes ranging from uniform to natural using 5 robustness parameters (-2,-1,0,1,2), where uniform weighting is equivalent ro robust=-2 and natural weighting corresponds to robust=+2.
For every single simulation we have created an overview panel, showing the most relevant information. Two examples are shown in Fig. 3 and 4 for SKA1-SUR and SKA1-MID, where the different panels show different features of the simulated observation, including *uv*-distribution, the beam point spread function and UVGAP. The last panel lists the actual numbers to quantify the performance of a certain telescope configuration and observations setup, listed are:
- RMS: the 1σ noise value in the image maps.
- Beam size: the average is taken of the major a minor axis of the synthesized beam
- HI column density (N_{HI}), the 1σ brightness sensitivity is determined at the observing frequency over a 50 kHz bandwidth, taking into account redshift dependence Fernández et al. (2013):

$$N_{HI} = \frac{2.34 \cdot 10^{20}}{b_{min} b_{maj}} (1+z)^4 S d\nu \tag{4.2}$$

- UVGAP: This parameter gives an impression of how optimal the *uv* distribution is, it calculates the fraction between the gap between two baselines and the baseline length. UVGAP is a function of baseline-length and polar angle, a full description is given in Millenaar & Bolton (2010) which is defined as:

$$uvgap = \frac{1}{q_{max}} \sum_{k=1}^{n} \partial q_k \times (q_k - q_{k-1}), \text{ with } q_0 = 0 \text{ and } q_n = q_{max} \tag{4.3}$$

The mean and median values of UVGAP as mentioned in the plots are calculated using the top 75 percent of the values in the UVGAP panel (second panel on the bottom), not taking into account the shortest q-values.

- Survey Speed: defined here as field of view, divided by the noise squared and scaled with the integration time, (FoV/rms^2/t_{int})

4.2 Performance results

Comparing the performance of the SKA to existing telescopes is very relevant to demonstrate where the main differences are and to understand in which parameter space the biggest gain in science can be achieved. In Fig. 5 we have plotted the flux rms, brightness sensitivity and survey speed as a function of beam size or resolution for the different telescopes at a declination of -30 degrees, at an observing frequency of 1.42 GHz and using uniform weighting.

PoS(AASKA14)132

In the current configuration the flux sensitivity of SKA1-MID remains roughly constant for resolutions smaller than 100 arc sec, while the sensitivity for SKA1-SUR remains stable below ~ 20 arcsec. This indicates that the distribution of telescopes is close to logarithmic and gives roughly constant flux sensitivity at different scales. The sensitivity of SKA1-MID is about a factor three better compared to SKA1-SUR for the typical resolution range between 1 and 10 arcsecond. This implies, that if the highest possible sensitivity is required, SKA1-MID is the superiour instrument. The same behaviour is reflected in the brightness sensitivity; when using SKA1-MID, a brightness sensitivity of $N_{HI} \sim 10^{19}$ cm^{-2} can be achieved at a resolution of 10 arcsecond after 8 hours of observing.
The survey speed relates to the inverse of the noise squared, times the field of view, divided by the integration time and shows a very different behaviour. For the nominal observing resolution of a few arcsecond, SKA1-SUR is five or six times faster compared to SKA1-MID. This indicates that when observing at low redshift, any area on the sky larger than three or four degrees squared can be observed faster down to a given sensitivity using SKA1-SUR. This area of three degrees squared is based on a field of view of 18 degrees squared for SKA1-SUR and the factor six difference in survey speed. Obviously this number will change when observing at higher redshift, as the primary beam of SKA1-MID will increase with lower frequency, also increasing the survey speed. For clarification the performance results of SKA1-MID sand SKA1-SUR at 1.42 GHz are listed in table 2.

In Fig. 6 we have kept all the observing parameters constant, but changed the robustness parameter when making the image cubes using values of -2 (uniform), 0 and 2 (natural). Please note that the x-axis is slightly different in the three rows, because the range in beam sizes is slightly different due to the different weightings. Interestingly the performance of SKA1-MID and SKA1-SUR changes quite significantly at high resolution, but the choice of weighting is not very relevant at low resolution. Low resolution images are mostly affected by the short baselines in the core of the array. Since the core of both SKA1-MID and SKA1-SUR is dense compared to the distribution of antennas in the outer spiral arms, different weighting schemes do not result in significantly different results.

5. Science projects

Image maps that are created using uniform weighting have the best predictable behaviour and as can be seen in the previous section the flux sensitivity remains relatively constant for SKA1-MID over the full resolution range and for SKA1-SUR for beam sizes below ~ 20 arcsec. The same is true for the survey speed of the telescopes.
A great benefit of the current configurations is that no special observations are required with the aim of achieving a good brightness sensitivity. Basically any spectral line observation can be used and the choice of tapering and weighting when making the image cubes will determine the resolution.

5.1 Imaging the extended environment of galaxies

SKA1-MID has a large number of antennas and an effective observing area that is significantly

PoS(AASKA14)132

Performance of SKA1-MID			
Beam (arcsec)	rms (mJy)	N_{HI} (cm^{-2})	SS (deg^2 mJy^{-2} s^{-1})
0.43	0.0883	5.47e+21	1923.82
0.70	0.0902	2.16e+21	1843.64
1.33	0.0850	5.59e+20	2075.57
2.59	0.0799	1.39e+20	2347.72
3.83	0.0762	6.04e+19	2581.77
6.24	0.0721	2.15e+19	2883.57
8.44	0.0720	1.18e+19	2895.60
12.1	0.0726	5.82e+18	2844.01
14.5	0.0729	4.01e+18	2822.98
18.4	0.0728	2.52e+18	2829.19
24.6	0.0723	1.39e+18	2869.23
30.6	0.0715	8.87e+17	2933.78
36.6	0.0711	6.18e+17	2971.89
48.2	0.0720	3.62e+17	2896.40
59.5	0.0751	2.47e+17	2657.91
70.6	0.0798	1.87e+17	2356.55
87.3	0.088	1.35e+17	1937.84
103.1	0.0964	1.06e+17	1612.83
133.2	0.1134	7.46e+16	1166.96
161.6	0.1306	5.83e+16	879.83
188.7	0.1481	4.86e+16	684.18
Performance of SKA1-SUR			
Beam (arcsec)	rms (mJy)	N_{HI} (cm^{-2})	SS (deg^2 mJy^{-2} s^{-1})
0.83	0.2509	4.19e+21	9928.39
0.93	0.2393	3.20e+21	10914.27
1.62	0.2115	9.37e+20	13972.02
3.30	0.2132	2.28e+20	13750.09
4.95	0.2174	1.03e+20	13223.94
8.01	0.2303	4.18e+19	11783.98
10.9	0.2472	2.40e+19	10227.82
14.9	0.2758	1.44e+19	8216.59
17.3	0.2954	1.15e+19	7162.42
20.6	0.3248	8.88e+18	5924.45
25.7	0.3728	6.58e+18	4497.05
30.6	0.4215	5.26e+18	3517.91
35.5	0.471	4.36e+18	2817.33
45.6	0.5723	3.22e+18	1908.24
55.9	0.6773	2.53e+18	1362.44
66.7	0.7838	2.06e+18	1017.35
82.7	0.9406	1.61e+18	706.43
99.0	1.095	1.30e+18	521.26
142.8	1.412	8.01e+17	313.48
213.3	1.736	4.02e+17	207.39

Table 2: Performance of SKA1-MID and SKA1-SUR at an declination of -30 degrees and observing frequency of 1.42 GHz for an 8 hour observation with a simulated cycle time of 10 minutes and using uniform weighting to generate the image cubes.

PoS(AASKA14)132

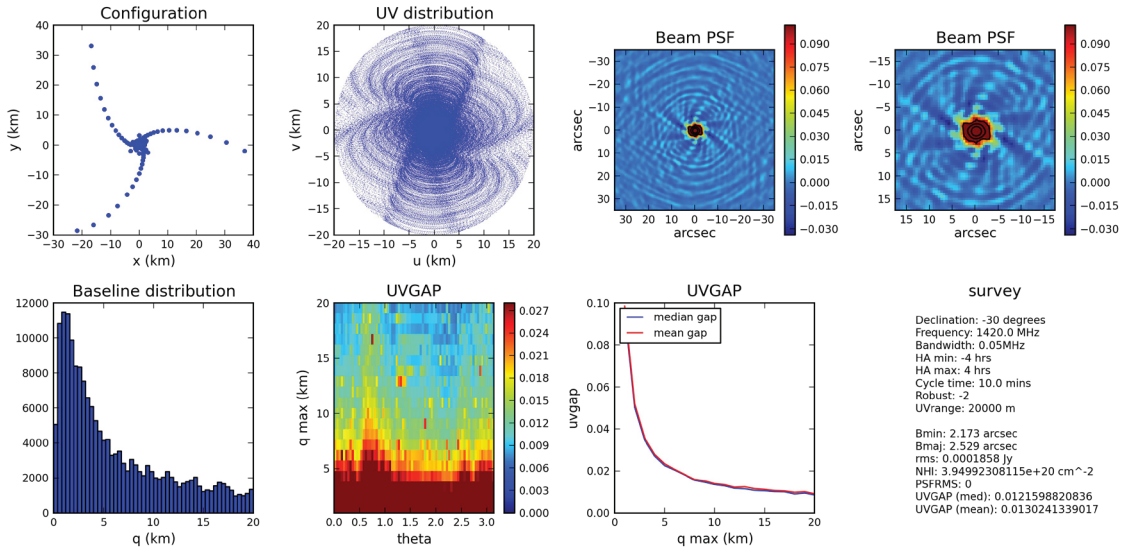

Figure 3: Overview panel of the performance results of SKA1-SUR for an 8 hour observation at 1.42 GHz using baselines shorter than 20 km. The top panels show the array configuration, the uv distribution and the beam PSF. The bottom panels show a histogram of the baseline distribution, UVGAP values as function of baseline length and polar angle. The third panel at the bottom shows the mean and median uvgap at a certain baseline length. The last panel lists the observation setup and typical numbers that represent the performance of the simulation.

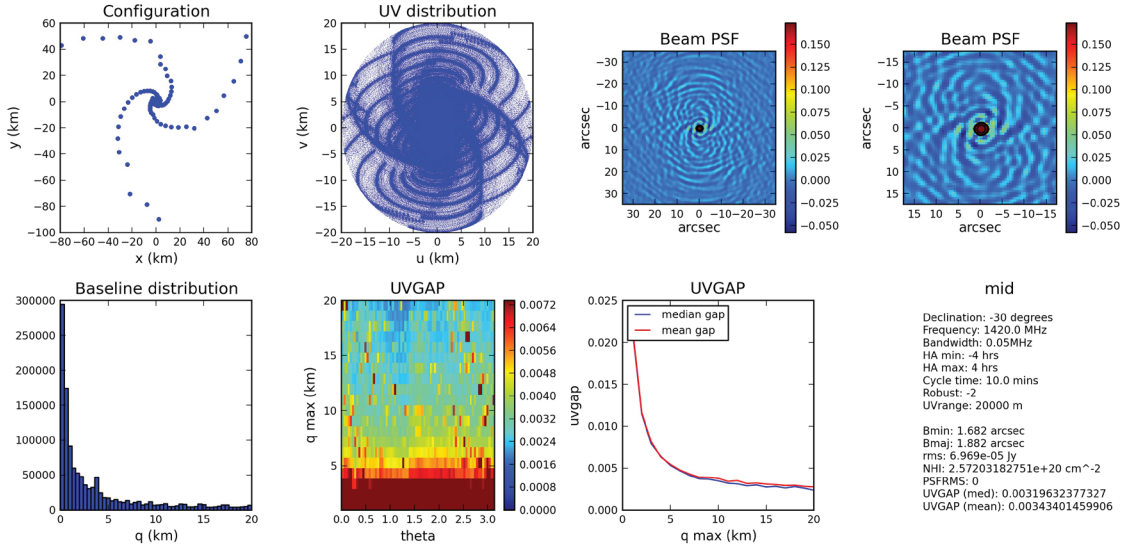

Figure 4: Same as figure 2, but now for a simulation representing SKA1-MID

PoS(AASKA14)132

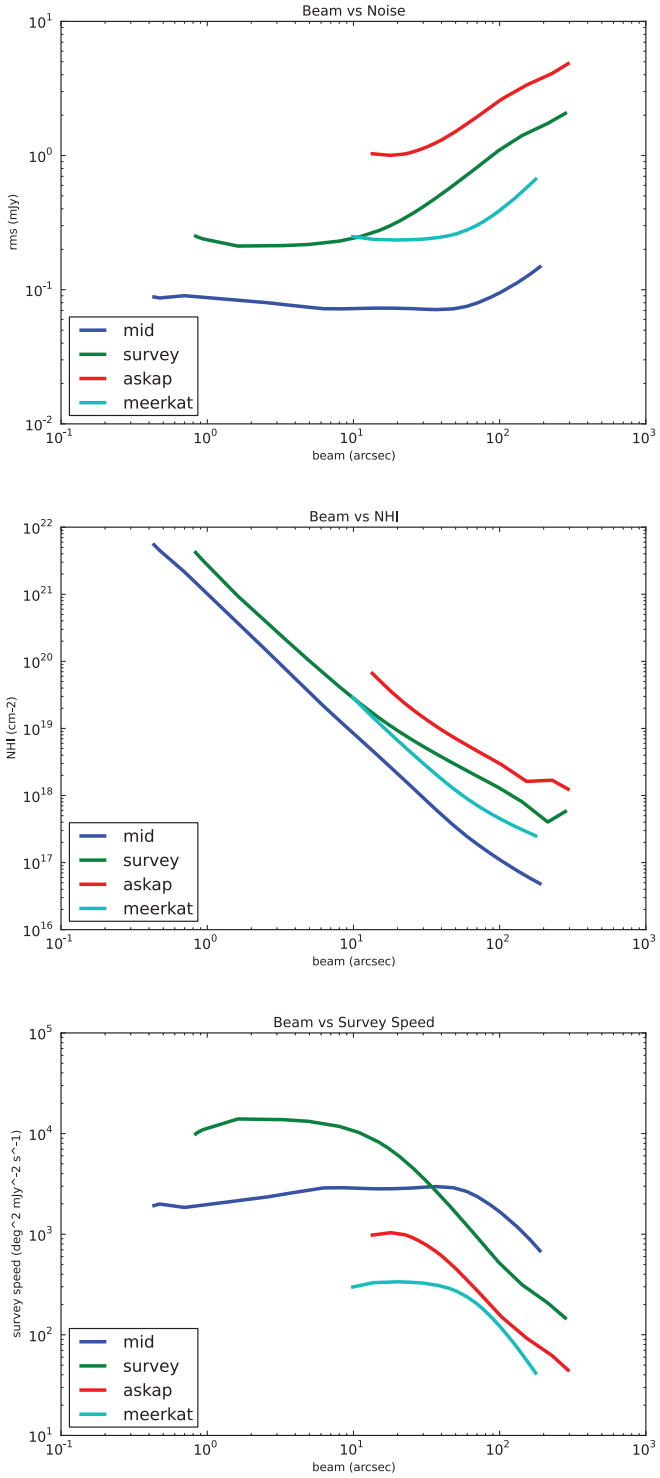

Figure 5: Simulated noise, brightness sensitivity and survey speed are plotted as function of angular resolution for different telescopes. All simultaions are performed for an integration time of eight hours, at a declination of -30 degrees and observing frequency of 1.42 GHz, using uniform weighting to generate the image cubes.

PoS(AASKA14)132

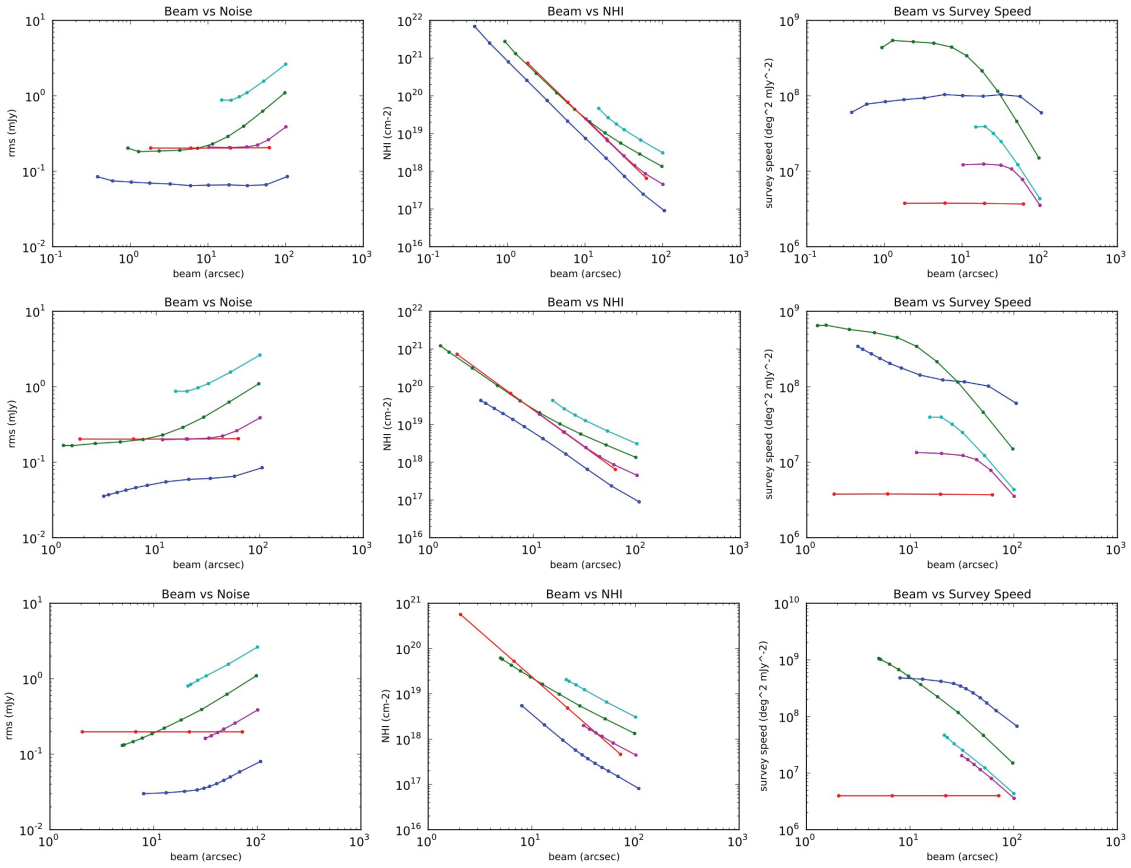

Figure 6: Similar as Figure 5, but now different robustness parameters are tested. All simulations are performed at 1.42 GHz, with top panels showing uniform weighting (robust=-2), middle horizontal panels show weighting using robust=0 and the bottom panel represent natural weighting (robust=2). The different lines corresond to SKA1-MID (blue), SKA1-SUR (green), ASKAP (turquoise) and meerkat (purple). For comparison the perfomance of the JVLA is shown as well (red line).

larger than any existing interferometer. As a result it can achieve brightness sensitivities over small areas that are orders of magnitude better than before and really explore new territory. The HALOGAS survey observed individual galaxies for 10x12 hours with the WSRT. Characteristic one sigma column densities of this survey ar $N_{HI} \sim 10^{19}$ cm^{-2} at a resolution of 15". We will use this number as a benchmark of what is possible in large projects and propose to observe selected nearby galaxies for a period of up to 100 hours with SKA1-MID. Such observations will achieve brightness sensitivities of $N_{HI} \sim 7 \cdot 10^{16}$ cm^{-2} over 10 km s^{-1} at a resolution of 1 arcmin, or $N_{HI} \sim 5 \cdot 10^{17}$ cm^{-2} over 10 km s^{-1} at a resolution of 20 arcsec. Compared to existing deep observations on single dish telescopes such as the GBT, these observations have a roughly similar brightness sensitivity, however over a beam area that is about a factor 1000 smaller. Not only should such observations confirm the existing detections from single dish telescopes, but also resolve these structures kinematically. Compared to a project such as HALOGAS, these observations have roughly the same resolution, however with a sensitivity that is more than ten times deeper and over an area that is larger due to the larger primary beam size of SKA compared to the WSRT. Both

PoS(AASKA14)132

in sensitivity and resolution these observations will open up complete new parameter space. They will provide unprecedented sensitivity to investigate gas accretion and will be able to resolve the clumps or substructure in the extended environment of galaxies.

5.2 All sky survey of the IGM

Given that SKA1-SUR is a survey instrument, we assume that this telescope will be used to perform a large area survey on the sky, possibly an all sky survey. Typical integration times for an all sky survey would be 10 hours per pointing which is sufficient to get the full *uv*-coverage and this number is also very similar to the integration time of the anticipated WALLABY survey on ASKAP. Doing such a survey, a brightness sensitivity can be achieved of $N_{HI} \sim 10^{19}$ cm^{-2} over 10 km s^{-1} at a resolution of 15-20 arc sec. This is almost a factor two improvement in brightness sensitivity over WALLABY at a linear resolution that is two times smaller, or four times smaller in beam area. These resolutions correspond to a physical beam size of about 10 kpc at a luminosity distance of 130 Mpc and therefore should be able to detect and possibly resolve faint clumps or filaments up to these distances.
The brightness sensitivity of such a survey is very comparable to the sensitivity of the HALOGAS, which is currently the deepest survey of individual galaxies limited to a sample of 22 galaxies. A large area survey with SKA1-SUR will provide extended image maps for not only all galaxies in the local universe but also for all positions across the entire sky. Such a survey will provide unprecedented information of the distribution of faint gas at very high resolution and can shed a light on the different modes of gas accretion. Another major difference compared to HALOGAS is that such a survey will map the environment of galaxies out to the virial radius where gas is still expected to reside. Since all galaxies in the Local Universe will be mapped, these observations will also demonstrate whether galaxies with halo masses below $M_{sun} \sim 10^{12}$ have more extended gas and are more prone to cold gas accretion as is predicted by the simulations.

As mentioned in section 3, studies of the HI structure of the outer warped disks of galaxies are a major ingredient in investigating the interplay of the IGM and the ISM, although the theory has to be understood well. An all-sky HI survey with SKA1-SUR down to a sensitivity where warps are easily detected [see e.g. García-Ruiz et al. (2002), Józsa (2007)] makes comprehensive warp statistics, studies of the structure of the IGM in different environments (Haan & Braun 2014), as well as studies of large-scale alignment of outer disk material, possible. Tracing the IGM through spin alignment of outer disks has been attempted using optical observations (Battaner et al. 1990; López-Corredoira et al. 2008). The wide-field access to the much better suited tracer HI, which is often detected far beyond the optical disk and including the kinematical information, will, however, mean an observational quantum step for studies of the ISM-IGM interface.

The mechanism of IGM accretion onto the disc produces warps (López-Corredoira et al. 2008). The ubiquity of the warp phenomenon might be used to reconstruct both the IGM density profile and the individual member orbits within galaxy groups (Haan & Braun 2014). Several groups have sought systematically aligned warps within galaxy samples as a probe of large scale accretion signatures. When probing column densities of $N_{HI} \sim 10^{19}$ cm^{-2} at a resolution of $\sim$15 arcsec, we can detect and resolve the disks and warps of a large number of galaxies.

PoS(AASKA14)132

6. SKA prospects

6.1 SKA Phase 1

Phase 1 of the SKA can make a major step in helping us understand the distribution of very low column density gas around and between galaxies as outlined in the previous section. We have modelled the performance of SKA1-SUR and SKA1-MID in very high detail. Compared to existing observations we can achieve orders of magnitude improvement in either resolution or sensitivity which will enable us to explore a new area in parameter space.

6.2 SKA Early science operations

Development of the SKA is a long process and final completion of even Phase 1 will be preceded by a period of commissioning, testing and early science operations. Nevertheless studies of the IGM and the cosmic web are an excellent test case for the SKA as the technical requirements are relatively modest.

Most likely the inner core of the SKA will be constructed first, representing the majority of the short baselines. To detect very faint and diffuse gas, the shorter baselines in interferometric arrays are most relevant. Also computing requirements are relatively modest as low resolution cubes are required to study the faint IGM. These cubes are much easier to process than science projects that rely on high resolution and the longest baselines in the array. Because of these arguments we anticipate that when 50% of SKA1 is constructed, we will be able to achieve more than 50% of the science performance, relevant to low resolution images.

When assuming an early science phase with 50% of the final sensitivity of Phase 1, still very relevant science can be done when 50% percent of the brightness sensitivity is achieved. When using the numbers as calculated in the previous section, for SKA1-MID we predict a 5σ brightness sensitivity of $N_{HI} \sim 2 \cdot 10^{18}$ cm^{-2} over 10 km/s at 15" resolution after 100 hours of integration time over 0.46 deg^2 at 1.42 GHz. For SKA Survey we predict $N_{HI} \sim 10^{19}$ cm^{-2} over 10 km/s at 15" resolution after 10 hours of integration over an area of 18 deg^2 at the full frequency range of the telescope. The integration times of 100 and 10 hours for respectively SKA1-MID and SKA1-SUR are chosen in the same way as for the science project of SKA 1 but can easily be scaled to any other integration time. The estimated sensitivities are still a very major improvement compared to all currently available data.

6.3 Full SKA

Phase 1 of the SKA will improve upon existing observations by several orders of magnitude. The low column density gas that can be detected is predicted by simulations but apart from that largely unknown. Completion of Phase 2 of the SKA will improve the sensitivities by another order of magnitude. Assuming similar integration times as in previous sections, an all sky survey will be able to achieve a brightness sensitivity of $N_{HI} \sim 10^{17}$ cm^{-2} over 10 km s^{-1} at a resolution of 10 arc sec. Targeted observation of single galaxies will be able to detect HI emission down to column densities of $N_{HI} \sim 10^{16}$ cm^{-2} at 1 arcmin resolution.

PoS(AASKA14)132

7. Conclusion

The interplay of gas between galaxies and the surrounding IGM is a key aspect in galaxy formation. The cosmic web holds the large reservoir of gas that eventually accretes into galaxies and supports the formation of stars. For the imaging of the diffuse gas filaments in the cosmic web, HI column densities are required in the range $N_{HI} \sim 10^{15} - 10^{18}$ cm^{-2} which is mostly the realm of the full SKA. Nevertheless already Phase 1 of the SKA can provide much better understanding about the IGM. Observations with the SKA1 will not only be able to detect low column density gas over very large areas much deeper than ever before, for the first time they will be able to resolve this gas at sub-arcminute resolution.

Studies of the IGM do not require additional observations and can completely rely on observations performed for other HI projects. Due to the close to logarithmic distribution of telescopes in the current baseline design, the noise remains relatively constant as function of resolution. For any existing observations we can make cubes at a lower resolution to enhance the brightness sensitivity.

Using SKA1-MID, brightness sensitivities can be reached that are 10 times better compared to current observations, and this can be achieved within a realistic integration time of 100 hours. These integration times align very well with the integration times that are needed to image the ISM in individual galaxies at high spatial resolution (see de Blok et al. (2015)). Targeted observations of individual galaxies will improve our sensitivity limits and already with SKA1 column densities of $N_{HI} \sim 10^{17}$ cm^{-2} can be detected. Such observations will image and resolve the clumps and substructure in the environment of galaxies that are predicted by simulations, and these observations might start to probe the cosmic web filaments in which galaxies reside.

Using SKA1-SUR with an integration time of ten hours per pointing, brightness sensitivities can be achieved equivalent to the best datasets we currently have, however for very large areas on the sky, rather than a small sample of individual galaxies. The SKA will for the first time give column densities of $N_{HI} \sim 10^{19}$ cm^{-2} at an angular scale of 15" over very large areas of the sky. This will not only image the extended environment of galaxies to study disks and gas accretion, but will also provide an unbiased search for diffuse intergalactic gas.

References

Barnes, D. G., Staveley-Smith, L., de Blok, W. J. G., et al. 2001, MNRAS, 322, 486

Battaner, E., Florido, E., & Sanchez-Saavedra, M. L. 1990, A&A, 236, 1

Boomsma, R., Oosterloo, T. A., Fraternali, F., van der Hulst, J. M., & Sancisi, R. 2008, A&A, 490, 555

Braun, R., & Thilker, D. A. 2004, A&A, 417, 421

Bregman, J. N. 2007, ARAA, 45, 221

Briggs, F. H. 1990, ApJ, 352, 15

Cen, R., Miralda-Escudé, J., Ostriker, J. P., & Rauch, M. 1994, ApjL, 437, L9

Cen, R., & Ostriker, J. P. 2006, ApJ, 650, 560

Chang, T.-C., Pen, U.-L., Bandura, K., & Peterson, J. B. 2010, Nature, 466, 463

Corbelli, E., & Bandiera, R. 2002, ApJ, 567, 712

Crain, R. A., McCarthy, I. G., Schaye, J., Theuns, T., & Frenk, C. S. 2013, MNRAS, 432, 3005

PoS(AASKA14)132

Cunnama, D., Andrianomena, S., Cress, C. M., et al. 2014, MNRAS, 438, 2530
Davé, R., Hernquist, L., Katz, N., & Weinberg, D. H. 1999, ApJ, 511, 521
Davé, R., Cen, R., Ostriker, J. P., et al. 2001, ApJ, 552, 473
Davis, M., Efstathiou, G., Frenk, C. S., & White, S. D. M. 1985, ApJ, 292, 371
de Blok, E., Fraternali, F., Heald, G., et al. 2015, in "The SKA view of the Neutral Interstellar Medium in Galaxies" in proc. *Advancing Astrophysics with the Square Kilometre Array*, PoS(AASKA14)129
de Blok, W. J. G., Keating, K. M., Pisano, D. J., et al. 2014, ArXiv e-prints, arXiv:1407.3648
de Lapparent, V., Geller, M. J., & Huchra, J. P. 1986, ApjL, 302, L1
Dekel, A., Birnboim, Y., Engel, G., et al. 2009, Nature, 457, 451
Dewdney, P., Turner, W., Millenaar, R., et al. 2013, SKA1 System Baseline Design, Document number SKA-TEL-SKO-DD-001 Revision 1
Duffy, A. R., Kay, S. T., Battye, R. A., et al. 2012, MNRAS, 420, 2799
Fernández, X., van Gorkom, J. H., Hess, K. M., et al. 2013, ApjL, 770, L29
Fraternali, F., & Binney, J. J. 2006, MNRAS, 366, 449
Fraternali, F., Oosterloo, T., & Sancisi, R. 2004, A&A, 424, 485
Frenk, C. S., White, S. D. M., Efstathiou, G., & Davis, M. 1985, Nature, 317, 595
Fukugita, M., & Peebles, P. J. E. 2004, ApJ, 616, 643
García-Ruiz, I., Sancisi, R., & Kuijken, K. 2002, A&A, 394, 769
Giovanelli, R., Haynes, M. P., Kent, B. R., et al. 2005, AJ, 130, 2598
Gunn, J. E., & Peterson, B. A. 1965, ApJ, 142, 1633
Haan, S., & Braun, R. 2014, MNRAS, 440, L21
Heald, G., Józsa, G., Serra, P., et al. 2011, A&A, 526, A118
Irwin, J. A., Hoffman, G. L., Spekkens, K., et al. 2009, ApJ, 692, 1447
Józsa, G. I. G. 2007, A&A, 468, 903
Kahn, F. D., & Woltjer, L. 1959, ApJ, 130, 705
Kereš, D., Katz, N., Fardal, M., Davé, R., & Weinberg, D. H. 2009, MNRAS, 395, 160
Kereš, D., Katz, N., Weinberg, D. H., & Davé, R. 2005, MNRAS, 363, 2
Lockman, F. J., Free, N. L., & Shields, J. C. 2012, AJ, 144, 52
López-Corredoira, M., Betancort-Rijo, J., & Beckman, J. E. 2002, A&A, 386, 169
López-Corredoira, M., Florido, E., Betancort-Rijo, J., et al. 2008, A&A, 488, 511
Lynds, R. 1971, ApjL, 164, L73
Marchesini, D., van Dokkum, P. G., Förster Schreiber, N. M., et al. 2009, ApJ, 701, 1765
Miralda-Escudé, J., Cen, R., Ostriker, J. P., & Rauch, M. 1996, ApJ, 471, 582
Obreschkow, D., Croton, D., De Lucia, G., Khochfar, S., & Rawlings, S. 2009, ApJ, 698, 1467
Obreschkow, D., Meyer, M., Popping, A., et al. 2015, in "The SKA as a Doorway to Angular Momentum" in proc. *Advancing Astrophysics with the Square Kilometre Array*, PoS(AASKA14)138
Oosterloo, T., Fraternali, F., & Sancisi, R. 2007, AJ, 134, 1019
Ostriker, E. C., & Binney, J. J. 1989, MNRAS, 237, 785
Pisano, D. J. 2014, AJ, 147, 48
Popping, A. 2010, PhD thesis, University of Groningen
Popping, A., & Braun, R. 2011a, A&A, 533, A122
—. 2011b, A&A, 527, A90

PoS(AASKA14)132

—. 2011c, A&A, 528, A28
Popping, A., Davé, R., Braun, R., & Oppenheimer, B. D. 2009, A&A, 504, 15
Power, C., Baugh, C. M., & Lacey, C. G. 2010, MNRAS, 406, 43
Prochaska, J. X., & Wolfe, A. M. 2009, ApJ, 696, 1543
Rauch, M. 1998, ARAA, 36, 267
Rauch, M., Miralda-Escude, J., Sargent, W. L. W., et al. 1997, ApJ, 489, 7
Sancisi, R., Fraternali, F., Oosterloo, T., & van der Hulst, T. 2008, AAPR, 15, 189
Schmidt, P., Józsa, G. I. G., Gentile, G., et al. 2014, A&A, 561, A28
Shen, J., & Sellwood, J. A. 2006, MNRAS, 370, 2
Tumlinson, J., Thom, C., Werk, J. K., et al. 2013, ApJ, 777, 59
van der Kruit, P. C. 2007, A&A, 466, 883
Werk, J. K., Prochaska, J. X., Thom, C., et al. 2013, ApJS, 204, 17
Werk, J. K., Prochaska, J. X., Tumlinson, J., et al. 2014, ApJ, 792, 8
Wolfe, S. A., Pisano, D. J., Lockman, F. J., McGaugh, S. S., & Shaya, E. J. 2013, Nature, 497, 224
Zschaechner, L. K., Rand, R. J., Heald, G. H., Gentile, G., & Józsa, G. 2012, ApJ, 760, 37

PoS(AASKA14)132

PROCEEDINGS OF SCIENCE

Galaxy Formation & Dark Matter Modelling in the Era of the Square Kilometre Array

C. Power[a⋆], C.D.P. Lagos[⋆b†], B. Qin[c‡], C.M. Baugh[d], D. Cunnama[e], J. Fu[f], H.S. Kim[g], C.G. Lacey[d], L. Li[c], D. Obreschkow[a], J. Wang[c], Y. Wang[c] and M. Zhu[c]

[a] *International Centre for Radio Astronomy Research,The University of Western Australia, 35 Stirling Highway,Crawley, WA 6009, Australia*

[b] *European Southern Observatory,Karl-Schwarzschild-Str. 2, 85748 Garching bei München, Germany*

[c] *National Astronomical Observatories, Chinese Academy of Science, A20 Datun Road, Beijing 100012, China*

[d] *Institute for Computational Cosmology, Durham University, Science Laboratories, South Road, Durham DH1 3LE, United Kingdom*

[e] *Department of Physics, University of Western Cape, Bellville 7535, Republic of South Africa*

[f] *Shanghai Astronomical Observatory, Chinese Academy of Sciences, 80 Nandan Road, Shanghai 200030, China*

[g] *School of Physics, The University of Melbourne, Parville, Vic 3010, Australia*

E-mail: ⋆chris.power@icrar.org, †clagos@eso.org, ‡qinbo@bao.ac.cn

Theoretical galaxy formation models are an established and powerful tool for interpreting the astrophysical significance of observational data, particularly galaxy surveys. Such models have been utilised with great success by optical surveys such as 2dFGRS and SDSS, but their application to radio surveys of cold gas in galaxies has been limited. In this chapter we describe recent developments in the modelling of the cold gas properties in the models, and how these developments are essential if they are to be applied to cold gas surveys of the kind that will be carried out with the SKA. By linking explicitly a galaxy's star formation rate to the abundance of molecular hydrogen in the galaxy rather than cold gas abundance, as was assumed previously, the latest models reproduce naturally many of the global atomic and molecular hydrogen properties of observed galaxies. We review some of the key results of the latest models and highlight areas where further developments are necessary. We discuss also how model predictions can be most accurately compared with observational data, what challenges we expect when creating synthetic galaxy surveys in the SKA era, and how the SKA can be used to test models of dark matter.

Advancing Astrophysics with the Square Kilometre Array
June 8-13, 2014
Giardini Naxos, Italy

*Speaker.

PoS(AASKA14)133

1. Introduction

Neutral hydrogen, both in its atomic (HI) and molecular (H_2) forms, plays a fundamental role in galaxy formation, principally as the raw material from which stars are made. At any given time, the fraction of a galaxy's mass that is in the form of neutral hydrogen will be determined by the competing rates at which it is depleted (by e.g. star formation, photo-ionization, expulsion via winds) and replenished (by e.g. recombination, accretion from galaxy's surroundings) – physical processes that are the foundations of any viable theory of galaxy formation.

Most of what we know currently about HI in galaxies derives from 21-cm surveys of the nearby Universe ($z \lesssim 0.05$) such as HIPASS (HI Parkes All Sky Survey; cf. Barnes et al., 2001) and ALFALFA (Arecibo Legacy Fast ALFA; cf. Giovanelli et al., 2005). Efforts are ongoing to complement these data with results from higher redshifts, using innovative techniques to estimate statistically typical galaxy HI content (e.g. stacking, cf. Lah et al. 2007 and Delhaize et al. 2013). These efforts will accelerate dramatically over the coming decade, with the advent of next generation radio telescopes such as the Australian Square Kilometre Array Pathfinder (ASKAP Johnston et al., 2008), MeerKAT (de Blok et al., 2009), and ultimately the Square Kilometre Array (SKA) itself. The SKA and its shorter wavelength counterpart the Atacama Large Millimetre Array (hereafter ALMA) offer the technical capability to chart the evolution of neutral hydrogen in galaxies over the last $\sim$12 billion years of cosmic time. This is a significant fraction of the assembly history of present-day galaxies, and the results of these observations will provide a stringent test of our theories of galaxy formation and evolution.

These theories of galaxy formation and evolution have undergone some timely and fundamental changes over the last $\sim$5 years. Signficantly for forthcoming HI and H_2 galaxy surveys, there has been particular emphasis on model predictions for the cold gas content of galaxies, which has led to some important conceptual changes in, for example, the treatment of star formation in the models. In the remainder of this chapter, we review briefly the essential features of the theoretical galaxy formation models, in particular the semi-analytical approach (§2); discuss the recent developments in these models, explaining why they were necessary (§3) and what the consequences are (§4 to §7); and indicate where further developments will be necessary (§8). Finally, we explore the potential of the SKA as a testbed for our theories of dark matter (§9).

2. Galaxy Formation Modelling: Hydrodynamical and Semi-Analytical Approaches

The two most widely used techniques to study galaxy formation in a cosmological context are *hydrodynamical N-body simulations* and *semi-analytical models*. Both follow the formation and evolution of dark matter halos over cosmic time using cosmological *N*-body simulations. However, hydrodynamical models compute the formation and evolution of the baryonic structures (e.g. hot gaseous halos, galaxy discs) at the same time as the dark matter, whereas semi-analytical models use the results of the pre-computed *N*-body simulation to guide the formation and evolution of the baryonic structures subsequently.

The methods should be viewed as complementary, each with their own advantages and disadvantages. Briefly, these are as follows.

PoS(AASKA14)133

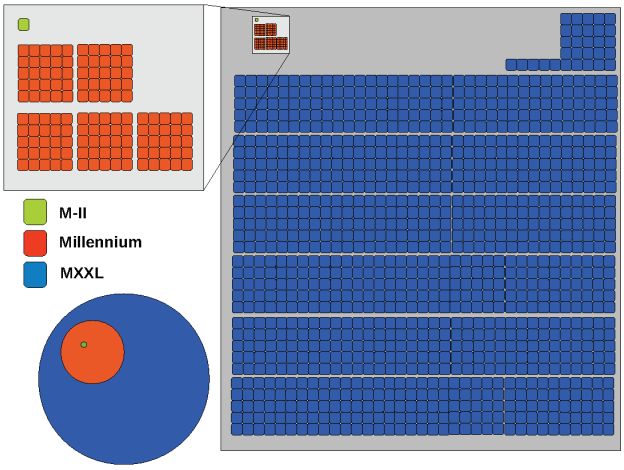

Figure 1: Schematic figure showing the difference in volume between the Millennium-I, II and XXL simulations (courtesy of Raul Angulo). The volume of Millennium-I exceeds that of Millennium-II by a factor of 125 times, while it is dwarfed by XXL by more than a factor of 200 in volume. The particle mass of Millennium-II is ≈ 1225 times smaller than the XXL simulation. Galaxy formation models for the SKA will require Millennium-II resolution in Millennium-I or XXL volumes.

- *Hydrodynamical N-body simulations* capture the complexity of gas and stellar dynamics in a way that semi-analytical models cannot, which is invaluable when studying, for example, the details of gas accretion onto galaxies. They are, however, computationally expensive when compared to semi-analytical models, and usually employed when studying galaxy formation on the scale of individual systems or in small-to-intermediate cosmological volumes.

- *Semi-analytical models* are computationally inexpensive when compared to hydrodynamical simulations, requiring only the *N*-body simulation and derived merger histories for the host dark matter halos of galaxies. While they sacrifice capturing the complex dynamical and structural properties of galaxies, they are ideally suited to the study of statistical samples of galaxies in cosmological volumes over many cosmic epochs. The models are such that they can be parameterised and calibrated to reproduce a set of standard observations (e.g. the galaxy luminosity function, and the Tully-Fisher relation) in a relatively straightforward manner (see Baugh 2006 for a comprehensive review), a process that is comparatively unwieldy for hydrodynamical simulations.

Therefore, it is in the detailed dynamical and structural properties of baryons within galaxies and in the surrounding haloes that the methods differ[1]; otherwise both approaches treat the physics of galaxy formation – star formation, stellar winds and supernovae, black hole growth and outburst of feedback – using similar simplified prescriptions that parameterise physical processes on spatial scales much smaller than can be resolved in the simulations.

This distinction is important when considering the kinds of volumes ($1\,\mathrm{Gpc}^3$ and larger) that the SKA will be probing. To date, the state-of-the-art in cosmological hydro-dynamical galaxy

[1] Although we note that efforts are underway in the semi-analytical models to capture, for example, the effect of baryon displacement highlighted by e.g. van Daalen et al. (2014) in hydrodynamical simulations

PoS(AASKA14)133

formation simulations probe volumes of order 100 Mpc^3 (Vogelsberger et al. 2014; Schaye et al. 2014). Contrast with semi-analytical models, which have been applied to the Millennium series of simulations. These are some of the largest cosmological N-body (i.e. dark matter only) simulations ever run, both in terms of particle number and volume – spanning the Millennium-I Simulation (Springel et al. 2005; with particle mass of $1.2 \times 10^9\, h^{-1}\mathrm{M}_\odot$ and box size of $500h^{-1}$Mpc), the Millennium-II Simulation (Boylan-Kolchin et al. 2009; with particle mass of $6.9 \times 10^6\, h^{-1}\mathrm{M}_\odot$ and box size of $100h^{-1}$Mpc) and Millennium XXL (Angulo et al. 2012; with particle mass of $8.5 \times 10^9\, h^{-1}\mathrm{M}_\odot$ and box size of $3000h^{-1}$Mpc). Fig. 1 shows these three simulations in a way that emphasises the differences in volumes modelled.

Fig. 1 also encapsulates the challenge facing galaxy formation modelling in the SKA era. The SKA will probe enormous volumes, in excess of those modelled in the Millennium-I and comparable to those in Millennium XXL, but most HI in the Universe is concentrated in low-mass galaxies and dark matter halos; this requires high mass resolution, comparable to that of the Millennium-II. This combination of high mass resolution and enormous volume demands a semi-analytical rather than a hydrodynamical approach. Hydrodynamical simulations will play a vital role in informing semi-analytic models, both about the limitations of assumptions as well as improvements and approximations that can be made (some aspects of which we discuss in Section 8). However, it is semi-analytical models that we expect to underpin the theoretical framework supporting the SKA and it is this approach that we focus on in the remainder of this chapter.

3. Semi-Analytical Modelling of HI in Galaxies

As noted already, semi-analytical models offer a simplified physically motivated treatment of the processes that control the amount of cold gas[2] in a galaxy: namely the rate at which it cools radiatively within its host dark matter halo; the rate at which it is accreted in galaxy mergers; the rate at which it is consumed in star formation; and the rate at which it is reheated or expelled from galaxies by sources of feedback (e.g. photo-ionisation, stellar winds, supernovae and active galactic nuclei, AGN, heating).

A visual impression of the results of a semi-analytical calculation is given in Fig. 2, which shows the stellar and HI content of galaxies in a cluster drawn from the Millennium-I Simulation, as predicted by the Lagos et al. (2011a) model. The Lagos et al. (2011a) model was one of the first to predict the HI and H_2 content of galaxies explicitly and self-consistently, tracking individual gas phases over the duration of the calculation; prior to this, HI and H_2 masses in galaxies were obtained by post-processing cold gas masses at the end of the calculation. We consider briefly the results of these older *post-processed* models, and the physics underpinning the newer *self-consistent* models.

Post-processed models predicted galaxy populations with cold gas properties in broad agreement with observations. Baugh et al. (2004) and Rawlings et al. (2004) showed that semi-analytical mass functions of HI in galaxies (hereafter HIMF) were in satisfactory agreement with observations (HIPASS; cf. Zwaan et al., 2003) and semi-empirical fits. They converted between cold gas mass and HI mass by using the observationally measured global densities of HI and H_2 (Zwaan et al. 2003 and Keres et al. 2003 respectively) and splitting the cold gas mass into HI, H_2 and He phases.

[2]Here cold gas refers to gas that has cooled radiatively from a hot phase to below 10^4K, is predominately HI, H_2 and helium (He), and is available for star formation.

PoS(AASKA14)133

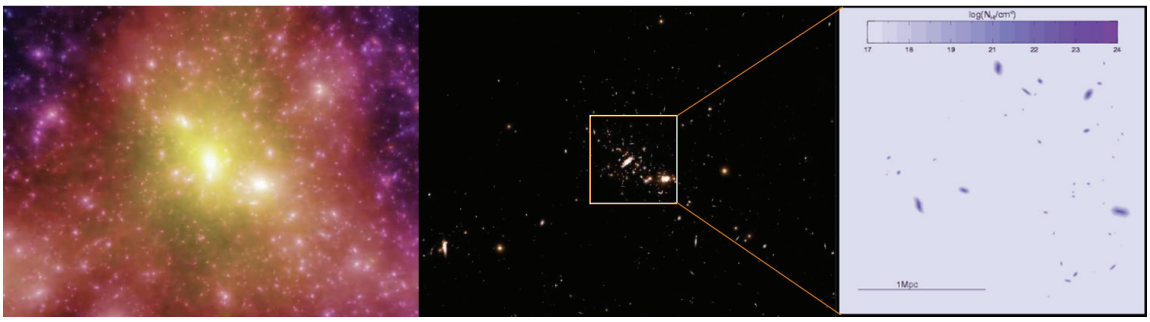

Figure 2: A massive galaxy cluster drawn from the Millennium-I Simulation, showing colour coded projected dark matter density, galaxy optical light and HI content (left, middle and right panels respectively). Galaxy properties were calculated using the GALFORM semi-analytical model of Lagos et al. (2011a). Image of dark matter distribution courtesy of Volker Springel.

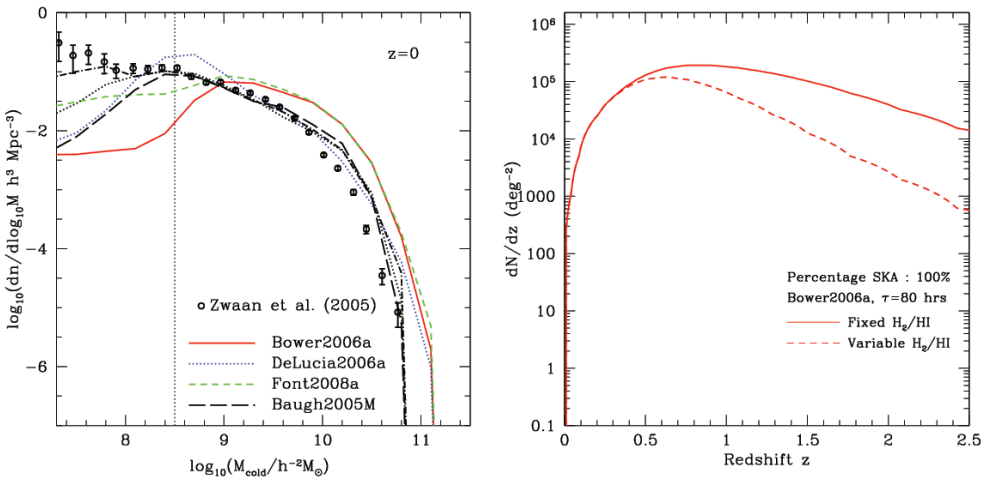

Figure 3: *Left Panel:* Cold gas mass function at $z = 0$ in 4 different galaxy formation models applied to the Millennium-I Simulation (see legend); data points are observational estimates derived from HIPASS (Zwaan et al., 2005) obtained by rescaling HI masses by a factor of $\sim$1.85; see text for further details. Dotted vertical line corresponds to the resolution limit of the models. *Right Panel:* Predicted number counts of galaxies per square degree per unit redshift for peak flux limited 1-year survey on a fiducial SKA with effective area 1 km^2 and integration time of τ=80 hrs, based on Bower et al. (2006). Solid (dashed) curves correspond to a fixed (variable) conversion factor from cold gas to H_2/HI. Both figures from Power et al. (2010).

Obreschkow & Rawlings (2009) and Obreschkow et al. (2009) adopted a more sophisticated approach to conversion, using the empirical relation between the HI/H_2 ratio and midplane pressure in galaxies (cf. Blitz & Rosolowsky, 2006) to predict the HI, H_2 and He phases on a galaxy-by-galaxy basis. Power et al. (2010) compared results from four then favoured models (Baugh et al., 2005; Bower et al., 2006; De Lucia & Blaizot, 2007; Font et al., 2008) applied to the Millennium-I Simulation for the mass function (MF) of cold neutral gas (atomic and molecular) in galaxies as a function of redshift. Despite different implementations of galaxy formation physics, the predictions were found to be broadly consistent with one another; key differences reflected how the models treated AGN feedback and the timescale for star formation as a function of redshift. The

PoS(AASKA14)133

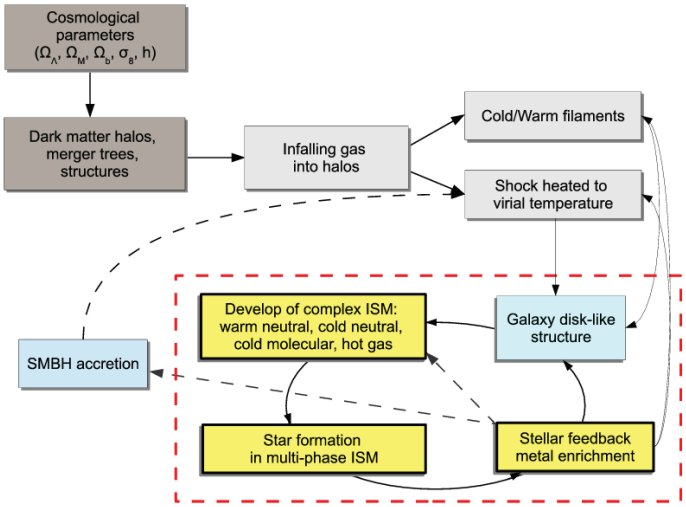

Figure 4: Schematic of the Physics of Disc Galaxy Formation and the ISM. Galaxies form within the potential wells of dark matter halos, whose formation is governed by the cosmological parameters and dark matter model, from baryons; these baryons either shock-heated upon infall and cooled or fell directed onto the galaxy along filaments. This emphasises the impact modelling of the ISM and SF has on galaxy components and the circum- and inter-galactic medium.

predicted MF of cold gas in galaxies agreed well with that inferred from HI surveys at z=0 (see left panel of Fig. 3)[3].

However, consideration of how the HIMF evolves with cosmic time and what this implies for future HI surveys highlighted that uncertain conversions from cold gas mass to HI and H_2 masses translate into large variations in model predictions. The right panel of Fig. 3 shows how predicted HI number counts are influenced by the choice of conversion factor – the solid (dashed) curve assumes Baugh et al. (2004) (Obreschkow et al. 2009) approaches. Number counts differ negligibly for $z \lesssim 1$, but grow to a factor of $\sim$10 by $z \sim 2.5$, reflecting the increasing proportion of cold gas in the form of H_2 with increasing z, as galaxies become more gas-rich and more compact.

Self-consistent models have addressed the question of how to convert from a cold gas mass to HI and H_2 mass by focusing on improved modelling of the interstellar medium (ISM), and, in particular, the relationship between star formation (SF) and neutral hydrogen phases; this has been the pivotal area of development in semi-analytical models over the last $\sim$5 years. Post-processed models treated the ISM as a single star-forming phase (e.g. Cole et al. 2000), but this is at odds with both empirical evidence and theoretical expectation. Observationally, there is evidence that a galaxy's SF rate (SFR) per unit area and molecular gas surface density correlate linearly, $\Sigma_{\rm SFR} \propto \Sigma_{\rm mol}$ (Wong & Blitz 2002; Bigiel et al. 2008). Theoretically, recent hydrodynamical simulations of star forming clouds suggests that the physical conditions necessary for SF – high density and low temperature gas – are also necessary for formation of H_2 and CO, but these conditions are driven by the presence of dust shielding, which prevents photo-dissociation by energetic UV photons, and

[3]Here the HIPASS HIMF of Zwaan et al. 2005 was converted to a cold gas MF by an empirically-motivated rescaling of HI masses by a factor of $\sim$1.85. This accounts for the 24% helium and assumes that HI and H_2 are split such that the global HI and H_2 densities are consistent with the observational estimates of Zwaan et al. (2003) and Keres et al. (2003).

PoS(AASKA14)133

CII cooling (Glover & Clark, 2012a,b). In other words, the presence of H_2 correlates naturally with SF (see also the arguments of Schaye 2004 and recent numerical work by Gnedin & Kravtsov 2011; Feldmann et al. 2011; Glover & Clark 2012b; Krumholz 2013).

This has led to the development of semi-analytical models that implement a fully self-consistent treatment of the ISM and SF (cf. Cook et al. 2010; Fu et al. 2010; Lagos et al. 2011b; also Robertson & Kravtsov 2008; Dutton et al. 2010). Fig. 4 encapsulates the complex interplay of physical processes in the ISM and their influence on galaxy formation, ranging from star formation in high density regions (e.g. Bigiel et al. 2008), to supernovae-driven turbulence (e.g. Dobbs et al. 2011), to chemical enrichment of the inter-galactic medium via outflows (e.g. Putman et al. 2012), and it provides a template for the treatment of the ISM in the models.

Two of the first models to implement this self-consistent approach – Lagos et al. (2011b) and Fu et al. (2010) – each explored two approaches to estimating the HI and H_2 content of the ISM[4]. The first was the *empirical relation* of Blitz & Rosolowsky (2006), which relates the molecular-to-atomic surface density ratio to hydrostatic pressure within the disc, estimating the SFR from the molecular gas surface density using the well measured molecular depletion timescale Bigiel et al. (2008) (also used by Cook et al. 2010). The second was the *theoretical relation* of Krumholz et al. (2009), which models SF as taking place in turbulent, marginally stable clouds, estimating the molecular abundance from the balance between the dissociating radiation flux and the formation of molecules on the surface of dust grains. Both Lagos et al. (2011b) and Fu et al. (2010) favoured the empirical relation of Blitz & Rosolowsky (2006), which provides a better fit to the HIMF at $z = 0$ (Zwaan et al. 2005; Martin et al. 2010) and predicts a clustering of HI selected galaxies in good agreement with observations (cf. Kim et al. 2013b); in contrast, the theoretical model of Krumholz et al. (2009) overpredicts the number density of intermediate HI mass galaxies.

In the remainder of this chapter, we assume self-consistent models that derive from Lagos et al. (2011b) and later. Model parameters are calibrated to reproduce the z=0 K- and b_j band luminosity functions (hereafter LFs), which govern AGN and stellar feedback, and UV LFs at z=2-6, which limit the duration of starbursts; no gas properties were used.

4. Insights into Global Star Formation Rates over Cosmic Time

The more realistic treatment of the ISM in the newer self-consistent models leads naturally to predictions that can explain trends in observational data.

First, the observed steep decline of SFR density with decreasing redshift is a consequence of the steep decline in the underlying molecular gas mass density with redshift (see left and middle panels of Fig. 5; see also Lagos et al. 2011a); in contrast, HI mass density evolves very weakly with redshift (right panel of Fig. 5). This arises from a combination of decreasing gas fractions and increasing galaxy sizes with decreasing redshift, which both act to reduce the gas surface density and the hydrostatic pressure of the disc. The redshift evolution of SFR density tracks that of the gas surface density of galaxies dominating the SFR in the Universe at a given epoch.

Increasing hydrostatic pressure in galaxy discs and increasing gas fractions with increasing redshift also leads to increasing molecular to dynamical mass ratios, which is consistent with ob-

[4]The Lagos et al. (2011b) and Fu et al. (2010) follow similar prescriptions, the key difference being that Fu et al. (2010) follow the radial gas profile of the galaxy disc explicitly.

PoS(AASKA14)133

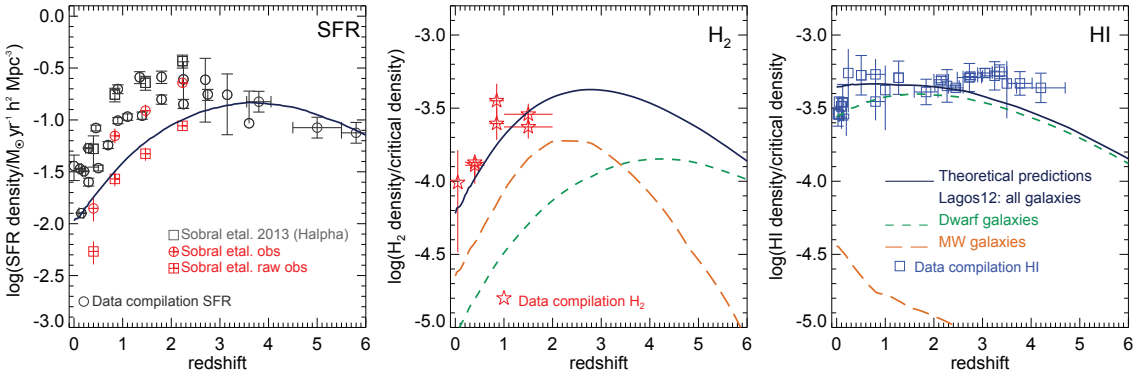

Figure 5: Global densities (solid lines) of the SFR in units of $M_\odot\,\mathrm{yr}^{-1}\,h^3\,\mathrm{Mpc}^{-3}$ (left hand panel), the estimated molecular hydrogen (middle panel) and the atomic hydrogen (right hand panel) in units of the critical density, as a function of redshift for the Lagos et al. (2012) model. The circles, stars and squares correspond to a data compilation of observations presented in Lagos et al. (2014) for the SFR, H_2 and HI densities, and are taken from Sobral et al. (2013). We also show the predicted contribution from dwarf galaxies (those with stellar masses $< 10^9\,M_\odot$; dashed lines) and Milky-Way (MW) type galaxies (those with stellar masses in the range $10^{10}\,M_\odot - 10^{11}\,M_\odot$; long-dashed lines).

servations of normal galaxies in the Universe up to $z \sim 2.5$ (see Geach et al. 2011). Note, however, that the increase in the SFR density is $2-3$ times higher than that of the H_2 density; this reflects the greater efficiency of star formation in starbursts, which is not accounted for in the normal star-forming discs assumed in the model (Lagos et al. 2014). Lagos et al. (2011a) showed that the shape of the relation between molecular gas fraction (i.e. $M_{\rm mol}/M_{\rm mol}+M_*$) and redshift depends on galaxy environment, such that, on average, galaxies with low mass host halos have larger molecular gas fractions than those with more massive hosts. Gas dynamical simulations agree qualitatively with this prediction (e.g. Davé et al. 2011).

The offset between the observational data points and model prediction evident in the left panel of Fig. 5 is well known in galaxy formation models, which tend to under-predict the SFR density by factors of ∼2-3. This discrepancy has been explored in some depth in Lagos et al. (2014) and is driven by a number of factors, including extrapolation of observed luminosity functions to account for the contribution of faint, undetected galaxies; the adopted stellar initial MF; and uncertainties in the SFRs of individual galaxies, which are of order 0.3-0.4 dex, as found by Speagle et al. (2014).

Second, the molecular-to-atomic gas ratio correlates with stellar mass, and so the low-mass end of the HIMF is steeper than the low-mass end of the stellar and H_2 MFs. We show in Fig. 5 the predicted contribution to the HI and H_2 densities from low mass galaxies (dwarfs) and more massive, Milky-Way like galaxies; the contribution from Milky-Way like galaxies to HI density is negligible except at very low redshifts, while dwarf galaxies dominate over the entire redshift range. For H_2, we see that Milky Way like galaxies dominate at lower redshifts but dwarfs make a significant contribution at higher redshifts, when the contribution from Milky Way like galaxies declines sharply. Note that these estimates are derived from the observations of Keres et al. (2003) and Berta et al. (2013) and required a number of assumptions to be made in their estimation (e.g. correlation between $A_{\rm UV}$ and H_2). Fig. 5 suggests that the SKA will provide new and interesting insights into dwarf galaxies, which at present are only partially accessible optical and near infrared

PoS(AASKA14)133

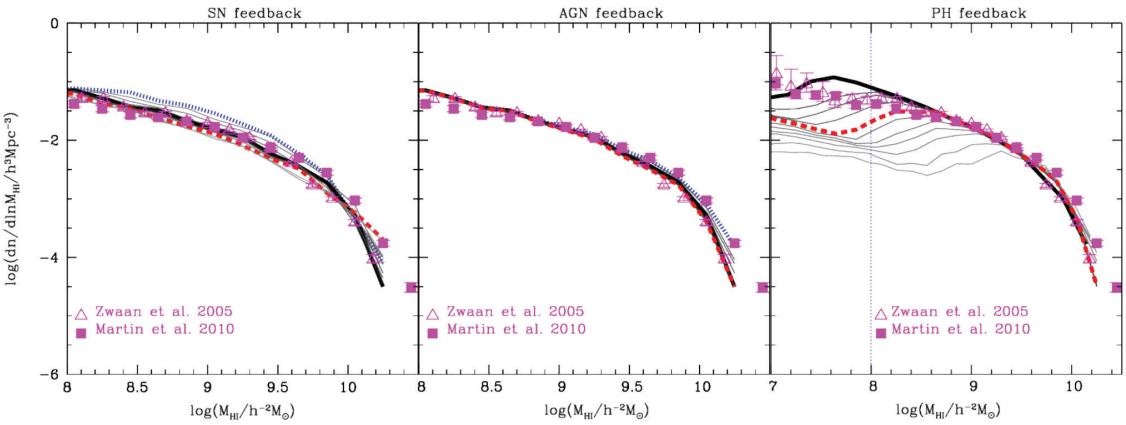

Figure 6: Impact of feedback from supernovae (SNe), AGN and the photoionising background (PH; left to right panels) on the HIMF in the Lagos et al. (2011a) model. Open triangles (filled squares) represent observational data from the HIPASS Zwaan et al. (2005)) and ALFALFA Martin et al. (2010) surveys. SNe strength varies in the range of $V_{\rm hot} = 300{\rm km/s}$ to $V_{\rm hot} = 700{\rm km/s}$; AGN strength varies in the range of $\alpha_{\rm cool} = 0.4 - 0.8$; photoionisation strength in the range of $30{\rm km/s} \leq V_{\rm cut} \leq 90{\rm km/s}$. Dark solid lines correspond to the default models values; red dashed and blue dotted curves correspond strong and weak feedback limits, respectively.

telescopes.

5. Probing the Physics of Feedback with HI Surveys

Semi-analytical models include a range of physical processes that either prevent hot gas from cooling onto a galaxy or heat up neutral gas and expel it from a galaxy (cf. Baugh, 2006). Simple physical arguments to detailed numerical calculations demonstrate that supernovae are responsible for expelling large amounts of gas from galaxies in low mass halos ($M_{\rm halo} <$ few $\times 10^{11} M_{\odot}$), shaping the faint-end of the LF. Similarly, the photo-ionising background present during cosmological reionization quenches low-mass galaxy formation, influencing the faint-end of the LF (e.g Benson et al., 2002). AGN appear necessary to suppress excessive star formation in high stellar mass galaxies and so regulate the amplitude and shape of the bright-end of the LF (cf. Bower et al., 2006; Croton et al., 2006).

The effect of different feedback mechanisms on optical and near infrared LFs have been explored with semi-analytical models Benson et al. (2003); Baugh et al. (2005); Bower et al. (2006); Croton et al. (2006), and this has been extended to the HIMF by Kim et al. (2013b) using the Lagos et al. (2011a) model. These authors studied the influence of varying the strength of supernovae (SNe), AGN and photo-ionizing (PH) feedback on both the (optical) b_j-band LF and the HIMF; we focus on the HIMF in Fig. 6. As the Figure reveals, SNe feedback (left panel) affects the HIMF uniformly across the entire range of HI masses; weaker feedback boosts the amplitude of the HIMF, and vice versa. AGN (middle panel) have little impact on the HIMF except at the very highest HI masses, with weaker feedback reducing the slope. Interestingly, photo-ionization (PH; right panel) has a significant effect at lower HI masses, driven by the sensitivity of the low-mass end slope to

PoS(AASKA14)133

the halo mass scale below which galaxy formation is suppressed at reionization. Here the caveat is that particular models for feedback were assumed.

6. Clustering of HI-Selected Galaxies

Both the older post-processed models and the newer self-consistent ones predict clustering of HI-selected galaxies that are broadly consistent with observations, which indicate that the clustering strength of HI-selected galaxies is weaker than that of their optically-selected counterparts (cf. Meyer et al., 2007; Martin et al., 2012). For example, Kim et al. (2011) and Kim et al. (2013b) demonstrated that the post-processed Bower et al. (2006) and Font et al. (2008) models[5] and the self-consistent Lagos et al. (2011a) model, all variants of the GALFORM model of Cole et al. (2000), make predictions that are in good agreement with the observed 2-point correlation functions (cf. left panel of Fig. 7, with data points drawn from Meyer et al. 2007). The models suggest that it is the central galaxies of halos with masses $\approx 10^{11}h^{-1}\mathrm{M}_{\odot}$, which are more likely to be HI-rich, that determine the shape of the 2-point correlation function.

Interestingly, the Font et al. (2008) model, which seeks to capture the effects of ram-pressure stripping on the ISM of satellites and the consequences of this for their observed colours, predicts stronger clustering on small scales than the Bower et al. (2006) and Lagos et al. (2011a) models, which provide a better description of the observed data points. This suggests that treating the ISM of a galaxy either explicitly in its HI and H_2 phases or simply as a monolithic cold gas phase has little effect on predicted clustering. Physically we expect how the ISM is modelled to influence how it is stripped – lower column density HI should be stripped preferentially while higher column density H_2 should resist stripping, which is what is found in hydrodynamical simulations (e.g. Quilis et al., 2000; Bekki, 2014) – although it is plausible that the behaviour of a single phase cold gas ISM and a multiphase ISM in which H_2 is retained is similar. Nevertheless, the treatment of the ISM in even the newer models is too coarse-grained to capture this, and ram pressure stripping modelling requires further development (e.g. Book & Benson, 2010).

The models also predict that the halo occupation distribution (HOD) for HI galaxies (the mean number of galaxies with a given HI mass per host dark matter halo as a function of host halo mass; cf. right hand panel of Fig. 7, based on the Lagos et al. 2011a model) has a functional form that is distinct from that usually employed for optically selected galaxies (e.g. Wyithe & Brown, 2010). We show Fig. 7 the HOD for HI-selected galaxies (heavy solid curve) split into centrals (heavy long-dashed curve) and satellites (heavy short-dashed curve); for comparison we show also the HOD for optically-selected (*r*-band) galaxies (light solid curve), with light long- and short-dashed curves indicating centrals and satellites respectively. The contribution to the HI-selected HOD from centrals is negligible at higher halo masses ($\gtrsim 10^{13}h^{-1}\mathrm{M}_{\odot}$), whereas the measured HOD in the *r*-band is consistent with the usual functional form assumed in the literature. Reconstructing the HOD of HI-selected galaxies will provide an important test of the treatment of ram pressure stripping of the models.

[5]Their cold gas masses were converted to HI masses using the approach of Baugh et al. (2004), which is tuned to recover the global densities of HI and H_2 at z=0.

PoS(AASKA14)133

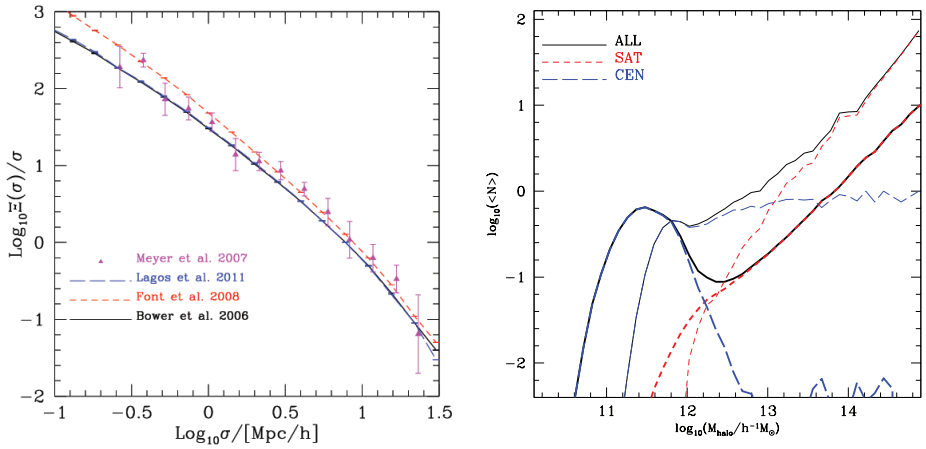

Figure 7: Predicted spatial clustering of HI galaxies. The left panel shows the projected 2-point correlation function of HI-rich galaxies at z=0, with symbols and errorbars indicating observational data from Meyer et al. (2007). Lines show predictions from three different models, as labelled, for galaxies with HI masses $M_{\rm HI} > 10^{9.25}\,h^{-2}\,M_\odot$, which is consistent with threshold assumed in the observational measurement. The right panel shows the halo occupation distribution for HI-rich galaxies (heavy curves) and r-band selected galaxies (light curves) in the Lagos et al. (2011a) model, using the same data as in the left panel. ALL, SAT and CEN refer to all, satellite and central galaxies respectively.

7. Probing Galaxy Kinematics with HI

The baryonic content of galaxies in the local Universe can be probed using the Tully-Fisher relation between galaxy velocity width measured by HI in emission and baryonic mass (see left panel of Fig. 8). The dramatic increase in the number of galaxies with good quality HI emission lines measured by the SKA will allow us to test our understanding of galaxy kinematics for statistical samples of galaxies as a function of epoch with the most stringent data ever available. Semi-analytical models have proven to be particularly useful in modelling HI-derived kinematics, with work presented in Obreschkow et al. (2009), Obreschkow & Rawlings (2009) and most recently Obreschkow et al. (2013) making it possible to build catalogues including complete HI emission lines (with velocity width, peak flux, and integrated flux) for millions of galaxies in a semi-analytic model derived from the Millennium-I Simulation (cf. Obreschkow et al., 2009).

Using this catalogue, the consistency of the galaxy velocity function (i.e. comoving number density of galaxies with a given rotational velocity) predicted in a Cold Dark Matter (CDM) universe with observations has been assessed.Obreschkow et al. (2013) replicated selection effects and completeness of observed galaxies to show that the reported discrepancy between the predicted and observed velocity functions claimed in the literature (e.g. Zwaan et al., 2010) is more apparent than real, arising from observational incompleteness and erroneous corrections to the observed data to recover galaxy velocities. The right panel of Fig. 8 shows the distribution of HI velocity widths predicted by the model of Obreschkow et al. (2009) after taking into account sky coverage, completeness and blending of sources, compared to observations. The excellent agreement suggests that comparison of predicted and observed velocity functions must be to directly model HI

PoS(AASKA14)133

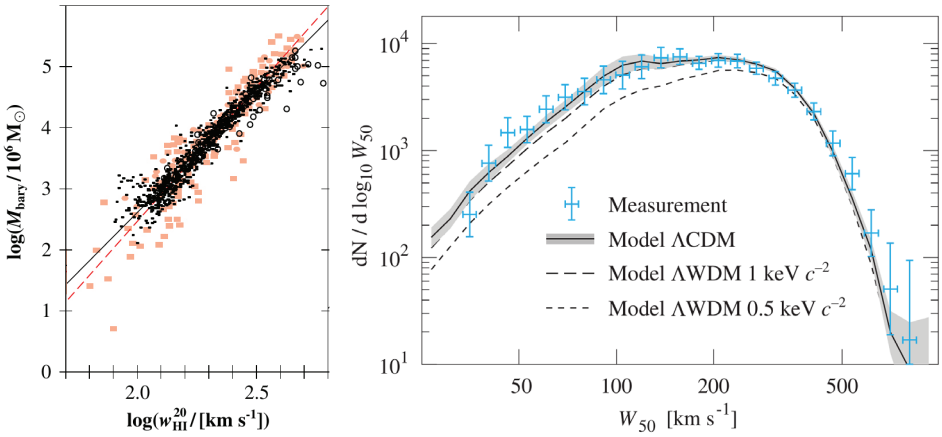

Figure 8: The left panel shows the baryonic mass as a function of HI velocity width measured at 0.2 of peak flux, w_{20}. Simulated spirals and elliptical galaxies from Obreschkow et al. (2009) are shown as filled and empty circles, respectively, while observations from McGaugh et al. (2000) are shown as solid squares. The right panel shows the distribution of HI velocity widths measured at 0.5 of peak flux, w_{50} for the simulation of Obreschkow et al. (2009). Observations from Zwaan et al. (2010) are shown as symbols.

emission lines using predicted galaxy properties and to replicate observations using model data.

The ability to study evolution in the internal kinematics of galaxies offer new and powerful insights into a property of galaxies that has traditionally been difficult to study but which plays a crucial role in shaping not only a galaxy's morphology but also the distribution of gas, the impact of feedback, the growth of its supermassive black hole, etc... namely angular momentum. This will be an area in which the SKA can have a transformational impact.

8. Future Developments

We now survey anticipated developments in the models, focussing on three key areas. First, the distribution of gas in the circum- and inter-galactic media (CGM and IGM respectively); second, feedback within galaxies; and third next generation synthetic surveys.

Distribution of Gas in the CGM and IGM. Large HI 21 cm emission line surveys of local galaxies (Zwaan et al., 2005) and absorption-line measurements in the spectra of quasi-stellar objects (Noterdaeme et al., 2012) have allowed accurate measurement of the evolution of the global density of atomic hydrogen over the redshift range $0 \leq z \lesssim 4$, and these suggest little evolution of the global density of atomic hydrogen, $\Omega_{\rm HI}$, with time. The latest semi-analytics models account for HI in galaxies and can account for evolution of $\Omega_{\rm HI}$ over the range $0 \leq z \lesssim 2.5$, but predict lower values than observed at higher redshifts by a factor of ~ 2, suggesting a large reservoir of neutral hydrogen outside of galaxies (Lagos et al., 2011a). This neutral gas does not need to be outside of the galaxy's halo, but instead it could be in the CGM. Indeed, observations indicate that it is within $\approx$ 20-40 kpc of the galaxy (Krogager et al., 2012).

The interpretation of the results in Lagos et al. (2012) are consistent with the results of recent hydro-dynamical simulations (van de Voort et al., 2012; Davé et al., 2013; Rahmati & Schaye, 2014). The challenge for semi-analytical models is to account for gas in the CGM and IGM in a

PoS(AASKA14)133

self-consistent way. One approach will be to couple semi-analytical models to a hydrodynamical description of the IGM. Such a technique has been recently applied by Moster et al. (2014) to idealised galaxy mergers. On larger scales, work is already underway (by some of the authors) to characterise the sensitivity of the IGM to the choice of cooling and feedback prescriptions adopted in hydrodynamical simulations, to develop a simple predictive model for IGM properties based on the underlying dark matter density field. A complementary approach is to use state-of-the-art gas dynamical simulations to study the distribution of neutral gas in haloes combined with semi-analytical calculations of the neutral gas distribution at cosmological reionization (Kim et al., 2013a). Both techniques will lead to an ultimate answer to what is the predicted density of HI all the way from $z = 0$ to $z = 12$ including all possible sources of neutral gas in an ab-initio galaxy formation simulation. A natural by-product of this work will be predictions for HI absorption.

Impact of Stellar Feedback. Feedback, the process by which stars and accreting compact objects interact with and modify their environment, is what makes galaxy formation modelling particularly challenging. In particular, feedback from supernovae (SNe) represents a long standing problem. Traditionally it has been parametrized to reproduce the faint-end of the luminosity function (Guo et al., 2011), but ignored physical properties of the galaxy such as the density of the ISM or the amount of energy released. Recent models (Creasey et al., 2013; Hopkins et al., 2012; Lagos et al., 2013) now incorporate a treatment of SNe-driven outflows that account for the physical properties of the galaxy, and have, for example, revealed the importance of gas surface density in regulating mass entrained in the outflows, which was ignored in previous models.

This improved description gives predictions of mass entrainment and outflow velocities in good agreement with observations. However, the development of a galaxy-wide outflow does not necessarily imply long-term disruption of the galaxy's gas reservoir, and improvements are necessary to calculate the evolution of such outflows – when are they confined by the galaxy's halo, and when do they escape? These question also relate to the condition for gas expelled from the galaxy to be reincorporated into it. Whether or not gas that is expelled from the disc returns to the galaxy or is lost to the gaseous halo is one of the key unknowns in galaxy formation, which lead to very different star formation histories of galaxies. For example, Henriques et al. (2013) showed that a different parametric form for reincorportation will help the build-up of the stellar mass predicted by models to get closer that what is inferred from observations. Resolving this problem will require not only extensions of the models but careful comparison with gas-dynamical simulations of galaxies in both a controlled non-cosmological setting and in cosmological simulations.

Next Generation Synthetic Surveys. The importance of the models in the design and astrophysical interpretation of future surveys means that the creation of synthetic surveys is central to future developments of the models. We focus on two aspects. First, *radio continuum emission*. The SKA is predicted to detect hot, diffuse gas in the cosmic web, undetectable with current instruments, through its emission in the radio continuum. At the same time, these surveys will detect radio continuum emission from galaxies, driven by star formation and AGN. Some of the framework to calculate radio continuum emission is already in place, e.g. the work of Fanidakis et al. (2011) on the mass and spin growth of black hole engines of AGN. However, further development is required to account for emission from star forming regions and the cosmic web, involving e.g. hybrid

PoS(AASKA14)133

hydrodynamical and semi-analytical modelling. Second, *molecular line emission*. The SKA will survey molecular emission from the high-redshift Universe (Geach & Papadopoulos, 2012) using the novel technique of intensity mapping (Carilli, 2011). This gives two-dimensional spatial information about the emission line at a given redshift; imaging is obtained by aggregating emission from thousands of galaxies on very large scales to produce the summed signal of galaxies that are not individually detected. Future models must account for e.g. thermalisation of the ISM of galaxies by the cosmic microwave background and e.g. the full spectral line energy distribution of the most used molecular emission line, carbon monoxide (CO).

9. Testing Dark Matter Models with the SKA

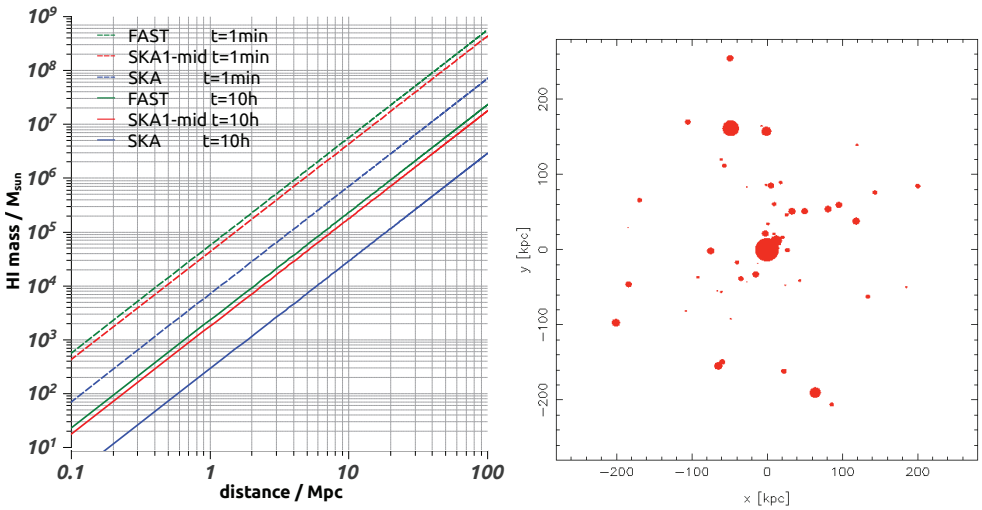

Figure 9: *Left Panel*: HI detection limits of FAST (green), SKA1-MID (red), and SKA2 (blue). Dashed and solid lines show 1min and 10h integrations. *Right Panel*: A preliminary result of the HI distributions of a Milky Way-like galaxy from the Aquarius simulation. The HI mass limit is $10^4 M_\odot$.

The CDM model for cosmological structure formation is well established. However, accumulating evidence during the past 15 years has revealed that its predictions are at odds with observations on galactic and sub-galactic scales. Numerical simulations of the CDM model predict abundances of substructure halos (subhalos) that are an order of magnitude larger than the numbers of satellite galaxies observed around nearby galaxies. This has led to modifications of CDM to be proposed, ranging from coupling between CDM and radiation (Bœhm et al., 2014) to self-interacting dark matter (Spergel & Steinhardt, 2000; Qin & Wu, 2001) to Warm Dark Matter (WDM; cf. Bode et al., 2001), all of which suppress the abundance of subhalos. For example, Lovell et al. (2014) have shown that the subhalo abundance in a WDM galaxy-mass halo at $M_{sub} > 10^7 M_\odot$ is approximately a factor of 10 smaller than in the corresponding CDM halo, and Kennedy et al. (2014) have shown that the magnitude of the effect depends strongly on WDM particle mass.

HI observations may reveal optically invisible satellite galaxies around nearby galaxies. For example, the Arecibo ALFALFA HI survey of the local Universe (Haynes et al., 2011) has found more than $15,000$ extragalactic HI sources within $\sim$250 Mpc, with the lowest HI mass of a few

PoS(AASKA14)133

$10^6 M_\odot$. SKA1-MID will have higher sensitivity and a much larger field of view (FoV, 0.7 deg $\times$ 0.7 deg) than Arecibo; SKA2 will 10 times higher sensitivity and 20 times larger FoV. The left panel of Fig. 9 shows the HI detection limits for the planned 500-m FAST (Nan et al., 2011), SKA1-MID, and SKA2, at 1 min and 10 hours integrations, with velocity linewidth of 200 km/s and signal-to-noise of 6. SKA1-MID (SKA2) will be able to detect HI masses of a few $10^6 M_\odot$ ($10^5 M_\odot$) respectively at a distance of 50Mpc and with a 10-hour integration; this corresponds to host halo masses of order $\sim 10^7 - 10^8 M_\odot$, assuming that these halos contain a few percent of HI mass. This implies that the SKA can potentially discriminate between the CDM and WDM models by detecting the difference in predicted subhalo abundance.

The right panel of Fig. 9 shows the predicted distribution of HI gas in satellites in a Milky Way-type halo, taken from the Aquarius Simulation (Springel et al., 2008) coupled to the semi-analytical model of Fu et al. (2010), with an HI cutoff mass of $10^4 M_\odot$; the influence of reionization is accounted for, and dot size is proportional to HI mass. This indicates that the optically invisible satellite haloes of nearby galaxies may be visible by the SKA, if they contain enough HI gas. By surveying $\sim$ 100 nearby galaxies within a few tens Mpc, and comparing with the results of numerical simulations such as the Aquarius Simulation, the SKA may be able to provide independent limits on dark matter particle candidates and, in doing so, guide experimental astro-particle physicists in their efforts to detect the dark matter particle directly in the lab.

10. Summary

Neutral hydrogen plays a fundamental role in galaxy formation, as the raw material from which stars form and galaxies are built, yet much of what we know about the HI and H_2 content of galaxies derives from the local Universe. The SKA will change this dramatically, revolutionising our understanding of neutral hydrogen in galaxies over cosmic time and its role in galaxy formation and evolution. Recognition of this has led to rapid developments in theoretical galaxy formation models over the last $\sim$ 5 years, which we have reviewed. Key has been a radical rewriting of the way star formation is modelled (Lagos et al., 2011b), linking explicitly a galaxy's star formation rate to its H_2 abundance, in agreement with both high resolution observations of star-forming regions in galaxies (e.g. Bigiel et al. 2008) and the results of detailed numerical simulations (e.g. Glover & Clark 2012b).

This has resulted in pleasing consistency between model predictions (e.g. Lagos et al. 2011a; Kim et al. 2011) and observations of HI in galaxies in the local Universe (e.g. Zwaan et al. 2005; Meyer et al. 2007; Martin et al. 2010), as well as providing insights into how gas is distributed in the high redshift Universe (e.g. Lagos et al. 2012). At the same time the models have indicated the kind of observations that are necessary to better understand the physical processes that drive galaxy formation, most notably feedback (Kim et al., 2013b), and to constrain dark matter particle physics by placing limits on the abundance of low-mass dark matter halos containing cold gas.

The models are still evolving, however, and we have highlighted key areas where further developments, including the development of hybrid schemes in which semi-analytics and gas dynamical simulations are coupled to better capture the distribution of gas outside of galaxies and how this gas accretes onto galaxies; the modelling of feedback from supernovae; and more realistic synthetic galaxy surveys. These are topics where the authors will be focussing their collective efforts in the coming years.

PoS(AASKA14)133

References

Angulo, R. E., Springel, V., White, S. D. M., et al. 2012, MNRAS, 426, 2046
Barnes, D. G., Staveley-Smith, L., de Blok, W. J. G., et al. 2001, MNRAS, 322, 486
Baugh, C. M. 2006, Reports on Progress in Physics, 69, 3101
Baugh, C. M., Lacey, C. G., Frenk, C. S., et al. 2004, New Astron. Rev., 48, 1239
—. 2005, MNRAS, 356, 1191
Bekki, K. 2014, MNRAS, 438, 444
Benson, A. J., Bower, R. G., Frenk, C. S., et al. 2003, ApJ, 599, 38
Benson, A. J., Lacey, C. G., Baugh, C. M., Cole, S., & Frenk, C. S. 2002, MNRAS, 333, 156
Berta, S., Lutz, D., Nordon, R., et al. 2013, ArXiv:1304.7771, arXiv:1304.7771
Bigiel, F., Leroy, A., Walter, F., et al. 2008, AJ, 136, 2846
Blitz, L., & Rosolowsky, E. 2006, ApJ, 650, 933
Bode, P., Ostriker, J. P., & Turok, N. 2001, ApJ, 556, 93
Bœhm, C., Schewtschenko, J. A., Wilkinson, R. J., Baugh, C. M., & Pascoli, S. 2014, MNRAS, 445, L31
Book, L. G., & Benson, A. J. 2010, ApJ, 716, 810
Bower, R. G., Benson, A. J., Malbon, R., et al. 2006, MNRAS, 370, 645
Boylan-Kolchin, M., Springel, V., White, S. D. M., Jenkins, A., & Lemson, G. 2009, MNRAS, 398, 1150
Carilli, C. L. 2011, ApJ L, 730, L30
Cole, S., Lacey, C. G., Baugh, C. M., & Frenk, C. S. 2000, MNRAS, 319, 168
Cook, M., Evoli, C., Barausse, E., Granato, G. L., & Lapi, A. 2010, MNRAS, 402, 941
Creasey, P., Theuns, T., & Bower, R. G. 2013, MNRAS, 429, 1922
Croton, D. J., Springel, V., White, S. D. M., et al. 2006, MNRAS, 365, 11
Davé, R., Katz, N., Oppenheimer, B. D., Kollmeier, J. A., & Weinberg, D. H. 2013, ArXiv:1302.3631, arXiv:1302.3631
Davé, R., Oppenheimer, B. D., & Finlator, K. 2011, MNRAS, 415, 11
de Blok, E., Booth, R., & Frank, B. 2009, in Panoramic Radio Astronomy: Wide-field 1-2 GHz Research on Galaxy Evolution
De Lucia, G., & Blaizot, J. 2007, MNRAS, 375, 2
Delhaize, J., Meyer, M., Staveley-Smith, L., & Boyle, B. 2013, ArXiv:1305.1968, arXiv:1305.1968
Dobbs, C. L., Burkert, A., & Pringle, J. E. 2011, MNRAS, 417, 1318
Dutton, A. A., van den Bosch, F. C., & Dekel, A. 2010, MNRAS, 405, 1690
Fanidakis, N., Baugh, C. M., Benson, A. J., et al. 2011, MNRAS, 410, 53
Feldmann, R., Gnedin, N. Y., & Kravtsov, A. V. 2011, ApJ, 732, 115
Font, A. S., Bower, R. G., McCarthy, I. G., et al. 2008, MNRAS, 389, 1619
Fu, J., Guo, Q., Kauffmann, G., & Krumholz, M. R. 2010, MNRAS, 409, 515
Geach, J. E., & Papadopoulos, P. P. 2012, ApJ, 757, 156
Geach, J. E., Smail, I., Moran, S. M., et al. 2011, ApJ L, 730, L19+
Giovanelli, R., Haynes, M. P., Kent, B. R., et al. 2005, AJ, 130, 2598
Glover, S. C. O., & Clark, P. C. 2012a, MNRAS, 421, 116
—. 2012b, MNRAS, 421, 9

PoS(AASKA14)133

Gnedin, N. Y., & Kravtsov, A. V. 2011, ApJ, 728, 88
Guo, Q., White, S., Boylan-Kolchin, M., et al. 2011, MNRAS, 413, 101
Haynes, M. P., Giovanelli, R., Martin, A. M., et al. 2011, AJ, 142, 170
Henriques, B. M. B., White, S. D. M., Thomas, P. A., et al. 2013, MNRAS, 431, 3373
Hopkins, P. F., Quataert, E., & Murray, N. 2012, MNRAS, 421, 3522
Johnston, S., Taylor, R., Bailes, M., et al. 2008, Experimental Astronomy, 22, 151
Kennedy, R., Frenk, C., Cole, S., & Benson, A. 2014, MNRAS, 442, 2487
Keres, D., Yun, M. S., & Young, J. S. 2003, ApJ, 582, 659
Kim, H.-S., Baugh, C. M., Benson, A. J., et al. 2011, MNRAS, 414, 2367
Kim, H.-S., Power, C., Baugh, C. M., et al. 2013a, MNRAS, 428, 3366
Kim, H.-S., Wyithe, J. S. B., Raskutti, S., Lacey, C. G., & Helly, J. C. 2013b, MNRAS, 428, 2467
Krogager, J.-K., Fynbo, J. P. U., Møller, P., et al. 2012, MNRAS, 424, L1
Krumholz, M. R. 2013, MNRAS, 436, 2747
Krumholz, M. R., McKee, C. F., & Tumlinson, J. 2009, ApJ, 699, 850
Lagos, C. D. P., Baugh, C. M., Lacey, C. G., et al. 2011a, MNRAS, 418, 1649
Lagos, C. D. P., Baugh, C. M., Zwaan, M. A., et al. 2014, MNRAS, 440, 920
Lagos, C. d. P., Bayet, E., Baugh, C. M., et al. 2012, MNRAS, 426, 2142
Lagos, C. d. P., Lacey, C. G., & Baugh, C. M. 2013, MNRAS, 436, 1787
Lagos, C. D. P., Lacey, C. G., Baugh, C. M., Bower, R. G., & Benson, A. J. 2011b, MNRAS, 416, 1566
Lah, P., Chengalur, J. N., Briggs, F. H., et al. 2007, MNRAS, 376, 1357
Lovell, M. R., Frenk, C. S., Eke, V. R., et al. 2014, MNRAS, 439, 300
Martin, A. M., Papastergis, E., Giovanelli, R., et al. 2010, ApJ, 723, 1359
Martin, C. L., Shapley, A. E., Coil, A. L., et al. 2012, ApJ, 760, 127
McGaugh, S. S., Schombert, J. M., Bothun, G. D., & de Blok, W. J. G. 2000, ApJ L, 533, L99
Meyer, M. J., Zwaan, M. A., Webster, R. L., Brown, M. J. I., & Staveley-Smith, L. 2007, ApJ, 654, 702
Moster, B. P., Macciò, A. V., & Somerville, R. S. 2014, MNRAS, 437, 1027
Nan, R., Li, D., Jin, C., et al. 2011, International Journal of Modern Physics D, 20, 989
Noterdaeme, P., Petitjean, P., Carithers, W. C., et al. 2012, A&A, 547, L1
Obreschkow, D., Croton, D., De Lucia, G., Khochfar, S., & Rawlings, S. 2009, ApJ, 698, 1467
Obreschkow, D., Ma, X., Meyer, M., et al. 2013, ApJ, 766, 137
Obreschkow, D., & Rawlings, S. 2009, MNRAS, 394, 1857
Power, C., Baugh, C. M., & Lacey, C. G. 2010, MNRAS, 406, 43
Putman, M. E., Peek, J. E. G., & Joung, M. R. 2012, ARA&A, 50, 491
Qin, B., & Wu, X.-P. 2001, Physical Review Letters, 87, 061301
Quilis, V., Moore, B., & Bower, R. 2000, Science, 288, 1617
Rahmati, A., & Schaye, J. 2014, MNRAS, 438, 529
Rawlings, S., Abdalla, F. B., Bridle, S. L., et al. 2004, New Astronomy Reviews, 48, 1013
Robertson, B. E., & Kravtsov, A. V. 2008, ApJ, 680, 1083
Schaye, J. 2004, ApJ, 609, 667
Schaye, J., Crain, R. A., Bower, R. G., et al. 2014, ArXiv e-prints, arXiv:1407.7040
Sobral, D., Smail, I., Best, P. N., et al. 2013, MNRAS, 428, 1128

PoS(AASKA14)133

Speagle, J. S., Steinhardt, C. L., Capak, P. L., & Silverman, J. D. 2014, ApJS, 214, 15
Spergel, D. N., & Steinhardt, P. J. 2000, Physical Review Letters, 84, 3760
Springel, V., White, S. D. M., Jenkins, A., et al. 2005, Nat, 435, 629
Springel, V., Wang, J., Vogelsberger, M., et al. 2008, MNRAS, 391, 1685
van Daalen, M. P., Schaye, J., McCarthy, I. G., Booth, C. M., & Vecchia, C. D. 2014, MNRAS, 440, 2997
van de Voort, F., Schaye, J., Altay, G., & Theuns, T. 2012, MNRAS, 421, 2809
Vogelsberger, M., Genel, S., Springel, V., et al. 2014, Nat, 509, 177
Wong, T., & Blitz, L. 2002, ApJ, 569, 157
Wyithe, J. S. B., & Brown, M. J. I. 2010, MNRAS, 404, 876
Zwaan, M. A., Meyer, M. J., & Staveley-Smith, L. 2010, MNRAS, 403, 1969
Zwaan, M. A., Meyer, M. J., Staveley-Smith, L., & Webster, R. L. 2005, MNRAS, 359, L30
Zwaan, M. A., Staveley-Smith, L., Koribalski, B. S., et al. 2003, AJ, 125, 2842

PoS(AASKA14)133

PROCEEDINGS OF SCIENCE

Cool Outflows and HI absorbers with the SKA

Raffaella Morganti[*†1,2], **Elaine M. Sadler**[3], **and Stephen J. Curran**[4]

[1]*ASTRON, the Netherlands Institute for Radio Astronomy, PO Box 2, 7990AA Dwingeloo, The Netherlands;* [2]*Kapteyn Astronomical Institute, University of Groningen, P.O. Box 800, 9700 AV Groningen, The Netherlands;* [3]*University of Sydney/CAASTRO, SIfA, School of Physics A28, University of Sydney, NSW 2006, Australia;* [4]*School of Chemical and Physical Sciences, Victoria University of Wellington, New Zealand*

E-mail: morganti@astron.nl

HI 21-cm absorption spectroscopy provides a unique probe of the cold neutral gas in normal and active galaxies from redshift z > 6 to the present day. We describe the status of HI absorption studies, the plans for pathfinders/precursors, the expected breakthroughs that will be possible with SKA1, and some limitations set by the current design.

Advancing Astrophysics with the Square Kilometre Array
June 8-13, 2014
Giardini Naxos, Italy

* Speaker

† On behalf of the HI SWG Members (*E-mail: sqg-higalaxy@skatelescope.org*)

PoS(AASKA14)134

1. Introduction

One of the main goals of SKA is to trace the neutral phase of hydrogen, the most abundant element in the Universe, out to high redshift and connect this to the formation and evolution of galaxies across cosmic time. Observing the neutral hydrogen (HI 21cm) line in emission can achieve part of this task, but an important and complementary study uses the HI 21cm line detected in absorption against strong radio continuum sources.

Studies of *associated HI 21cm absorption* (HI located in and around the host galaxy of a radio source) allow us to understand the HI content of individual galaxies (as a function of their morphological properties, redshift and environment), the structure of the central regions and the feeding and feedback of active galactic nuclei (AGN).

Studies of *intervening HI 21cm absorption* (HI absorption toward radio-loud background sources, see e.g. Wolfe, Gawiser & Prochaska 2005, Kanekar & Briggs 2004), allow us to measure the number density of 21-cm absorbers and constrain the evolution of cold gas in normal galaxies over more than 12 billion years of cosmic time. HI 21cm absorption lines can also be used to probe fundamental constant evolution, by comparing the HI redshifts to those of redshifted ultraviolet lines (e.g. Wolfe et al. 1976; Kanekar et al. 2010), mm-wave rotational lines (e.g. Drinkwater et al. 1998, Carilli et al. 2000, Murphy et al. 2001), and OH lines (e.g. Chengalur & Kanekar 2003, Kanekar et al. 2012).

Below we briefly review the status of HI 21cm absorption studies and the most important perspectives that will be opened up by SKA1. HI absorption studies have both advantages and disadvantages compared to HI emission studies. The detectability of an absorption line is essentially independent of redshift, since it depends only on the strength of the background continuum source, so HI absorption measurements can probe the presence of neutral hydrogen in high-redshift galaxies where the HI emission line is far too weak to be detectable. HI 21cm absorption can also be detected and studied at very high spatial resolution (including at milli-arcsecond scales with VLBI if the background source remains bright enough), which is not possible for HI emission studies. Thus associated HI absorption has been used to probe the circumnuclear regions of radio-loud AGN on very small scales. Furthermore, given that the absorbing gas *has to be located in front* of the radio source, the kinematics of the gas can be more easily disentangled, therefore making studies of infall/outflows less affected by ambiguities.

The observed HI 21cm optical depth τ is related to the HI column density N_{HI} by the expression

$$N_{\rm HI} = 1.823 \times 10^{18} \, [Ts / f] \int \tau \, dV \quad (1)$$

where T*s* (K) is the harmonic mean spin temperature of the HI gas, *f* is the covering factor (i.e. the fraction of the background radio source that is covered by intervening gas) and ΔV the line width in km s^{-1}. If the HI column density can be measured independently (e.g. using the optical damped Ly α absorption profile), then the 21cm optical depth provides information on the spin

PoS(AASKA14)134

temperature and filling factor of the neutral gas. Conversely, if some reasonable assumptions about the spin temperature and filling factor can be made (e.g. Braun 2012), then an HI column density can be estimated even without optical Ly α measurements. As can be seen from equation (1), at fixed HI column density the observed optical depth rises as the mean spin temperature decreases, so HI 21cm absorption measurements are most sensitive to the cold neutral gas within galaxies (Rao & Briggs 1993) – in contrast to HI 21cm emission-line studies, which are sensitive to both warm and cold gas.

One disadvantage of HI 21cm absorption studies is that their view of the HI distribution is limited to the regions where the background continuum is present. To partly compensate for this, it is important to take advantage of other gas diagnostics (i.e. multiwaveband data) and information about other gas phases (ionized and molecular) where possible.

2. Associated absorption

2.1 Motivation and previous work

HI 21cm absorption in radio AGN has been detected and studied for many years, starting with the detection against the core of the radio source Centaurus A (Roberts 1970) and the nearby spiral galaxy NGC 4945 (Whiteoak & Gardner 1976). This associated HI absorption has been used to trace the gas in central regions of radio AGN, as well as to probe the extreme physical conditions due to the interplay between the energy released by the active black hole (BH) and the ISM.

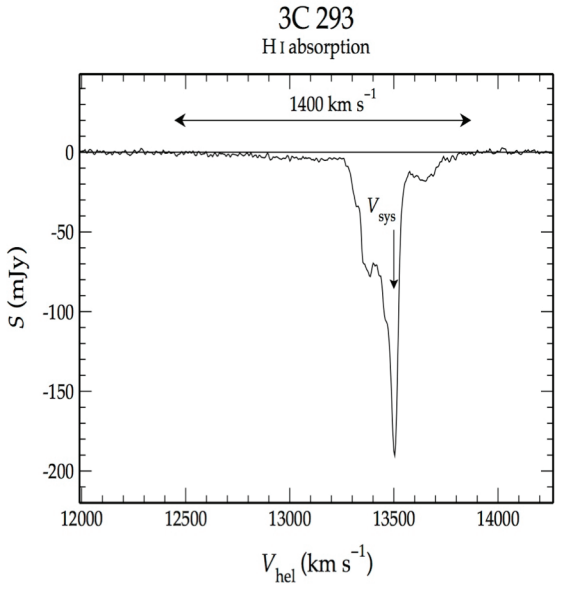

Figure 1 – HI absorption in 3C293, as detected by the WSRT. A broad, shallow HI absorption is detected as well as a deep, narrower component. The latter is associated with the circumnuclear disk/dust-lane while the former represent gas associated to a fast outflow (~1400 km s^{-1}, Morganti et al. 2003). Because of its location (~0.5kpc from the nucleus) the outflow appears to be driven by the radio jet/lobe. This profile shows the need for a stable instrumental bandpass as discussed in Sec.2.

The detection of HI 21cm absorption in active galaxies has been often considered a **tracer of circumnuclear disks**. Several such cases have been studied, e.g. Beswick et al. 2004, Struve & Conway 2010, 2012, Peck & Taylor 2001, Morganti et al. 2008. However, even more intriguing has been the discovery that HI can also be associated with kinematically extreme phenomena. Fast ($\geq$ 1000 km s^{-1}) and massive (up to 50 M$\odot$ yr^{-1}) **outflows** have been found traced by HI (Morganti et al. 2005, Teng et al. 2013, Morganti et al. 2013 and ref. therein). Gas outflows driven by AGN and supernovae (SNe) are a key ingredient in current models of galaxy evolution (e.g. Croton et al. 2006; Hopkins & Elvis 2010; Schaye et al. 2015), since they can efficiently heat up or even expel gas from a galaxy. This feedback

PoS(AASKA14)134

process regulates galaxy growth over cosmic time by stopping or regulating further star-formation and nuclear accretion through feedback processes. Feedback therefore appears to be a fundamental process that affects the bulk of the baryons in the universe, and more detailed observations of gas outflows are needed to build a coherent picture of their role in shaping galaxies over time. High spatial resolution observations (sub-arcsec and VLBI) have shown that outflows can be co-spatial with bright radio components, suggesting the radio jets are the driver of such outflows (Morganti et al. 2013, Tadhunter et al. 2014). The fast outflows have been traced using different phases of the gas (including molecular gas, e.g. Feruglio et al. 2010, Alatalo et al. 2011) showing that they are truly multi-phase structures and that cold gas can live in a harsh environment. HI and molecular gas represent the dominant component of the outflows and, therefore, their detection is highly relevant to quantify the impact of feedback and the relevance of radio plasma in this process. Even low power radio emission can provide the driver for gas outflows (e.g. Nyland et al. 2013, Combes et al. 2013), opening possibilities for many more cases to be discovered by more sensitive radio telescopes and in particular SKA1.

Finally, the gas in the nuclear regions can have an important role triggering the nuclear activity. For example, **infalling** gas, whether from an accretion disk or an advective flow, is an essential ingredient of AGN activity, as it can feed the central engine, turning a dormant super-massive black hole into an active one. Suggestions that this can be traced by HI 21cm absorption have been presented e.g. in van Gorkom et al. (1989) and Morganti et al. (2009). However, the search for infalling gas has been, so far, less successful. This could suggest that the HI does not always provide the fuelling or that the amplitude of the infalling gas is not large enough to be easily isolated from the regularly rotating gas or fast outflowing component.

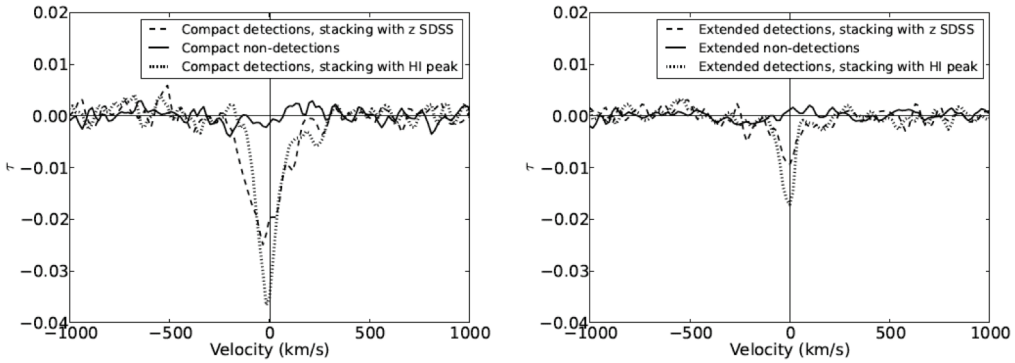

Figure 2 - Stacked HI profiles for compact (left) and extended (right) sources (from Gereb et al. 2014). The profiles show the higher optical depth and the broader width of the stacked profiles of the former, suggesting differences in the medium in which the two groups of objects are embedded.

Gereb et al. (2014a,b) present an overview of the HI content, detection rate and kinematics of associated HI 21cm absorption in a large sample of nearby radio galaxies. To date, this work most closely mimics the kind of *"blind survey"* which will be done with SKA pathfinders and precursors and, to even higher sensitivity, with SKA1. The Gereb et al. (2014a,b) work expanded the search for HI 21cm absorption down to 50 mJy radio sources and made use of stacking techniques not previously used for extragalactic absorption studies. This survey found a high detection rate of HI absorption (~ 30 %), which does not appear to be biased towards

PoS(AASKA14)134

brighter continuum sources. This is an important result, because it suggests that HI 21cm absorption studies can be extended to even lower radio fluxes, which is important input for future surveys. The stacked profiles of detections and non-detections reveal a clear dichotomy in the presence of HI, with the detections showing an average peak optical depth $\tau = 0.02$ corresponding to an estimated HI column density $N_{HI} \sim 7 \times 10^{20}$ cm^{-2} (for T_{spin}= 100 K and covering factor $f = 1$), while the non-detections remain undetected with a peak optical depth upper limit $\tau < 0.002$ corresponding to $N_{HI} < 2.26 \times 10^{19}$ (Ts/100 K) (dV/FWHM km s^{-1}) cm^{-2}.

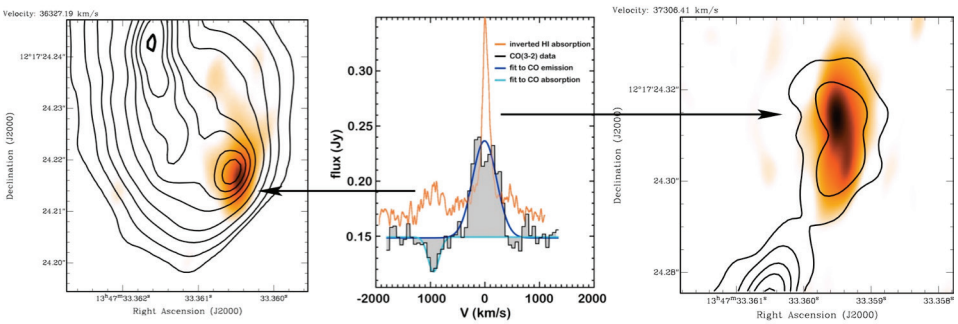

Figure 3 - Illustrating the importance of locating the absorbing gas, the case of 4C12.50 (Morganti et al. 2013). The central image shows the integrated HI profile (orange) superimposed on a CO emission profile for comparison, while the two outer plots show the location of two HI clouds based on 21cm absorption measurements made at high angular resolution.

Thus, 30% is a representative detection rate of HI in AGN. Comparing these results with what obtained in the study of HI for nearby early-type galaxies (e.g. Serra et al. 2012), one can conclude that HI 21cm absorption can be used to trace the HI content of these galaxies, and so could be used to trace the presence of gas in high-*z* objects (instead of HI emission for which there will not be enough sensitivity). Orientation effects due to the distribution of HI in a disk-like structure can be partly responsible for the observed dichotomy in optical depth, although some galaxies must be genuinely depleted of cold gas. Young, compact radio sources show a higher HI detection rate, confirming and expanding the results from smaller samples (e.g. Gupta et al. 2006, Chandola et al. 2011). The HI 21cm absorption lines in these compact sources also show higher optical depth and large FWHM compared to extended sources, strengthening the idea that the compact sources are richer in nuclear gas.

Finally, it is important to emphasise the crucial advantage that high spatial resolution provide for disentangling all these structures. HI 21cm absorption observations have revealed regularly rotating structures in a number of compact sources (Struve & Conway 2010, 2012, Peck & Taylor 2001). However, extremely important is also that VLBI observations have confirmed, in a number of cases, the key role that radio jets are playing in outflow of cold gas by locating (at the end of the radio jet) the fast outflowing gas. The most impressive case is 4C12.50, shown in Fig. 3 (Morganti et al. 2013).

PoS(AASKA14)134

2.2 Associated HI 21cm absorption in high-redshift radio sources

Detections of associated HI 21cm absorption in the high redshift Universe remain extremely rare, with only two detections to date at $1 < z < 2$ (Ishwara-Chandra et al. 2003; Curran et al. 2013) and two at $z \geq 2$ (Uson et al., 1991; Moore et al., 1999). In contrast, more than 40 associated HI 21cm absorption systems are known at $0.1 < z < 1$ (e.g. Carilli et al. 1998; Vermuelen et al. 2003), and the detection rate for compact radio sources is typically ~30% in this redshift range (e.g. Vermeulen et al. 2003; Gereb et al. 2014).

Curran et al. (2008) have proposed that the low detection rate of associated HI absorption at $z > 1$ is due at least in part to the selection of bright radio sources with known optical redshifts as targets for an HI search, since most of these objects are powerful QSOs with a rest-frame ultraviolet luminosity above $L_{UV} \sim 10^{23}$ W Hz^{-1} (see Figure 4) in which the interstellar gas is likely to be completely ionised (Curran & Whiting 2012). The broad frequency coverage and large instantaneous bandwidth of SKA1 will remove this problem by making it possible to carry out genuinely blind HI 21cm absorption surveys out to $z > 6$ without the need for optical pre-selection of targets.

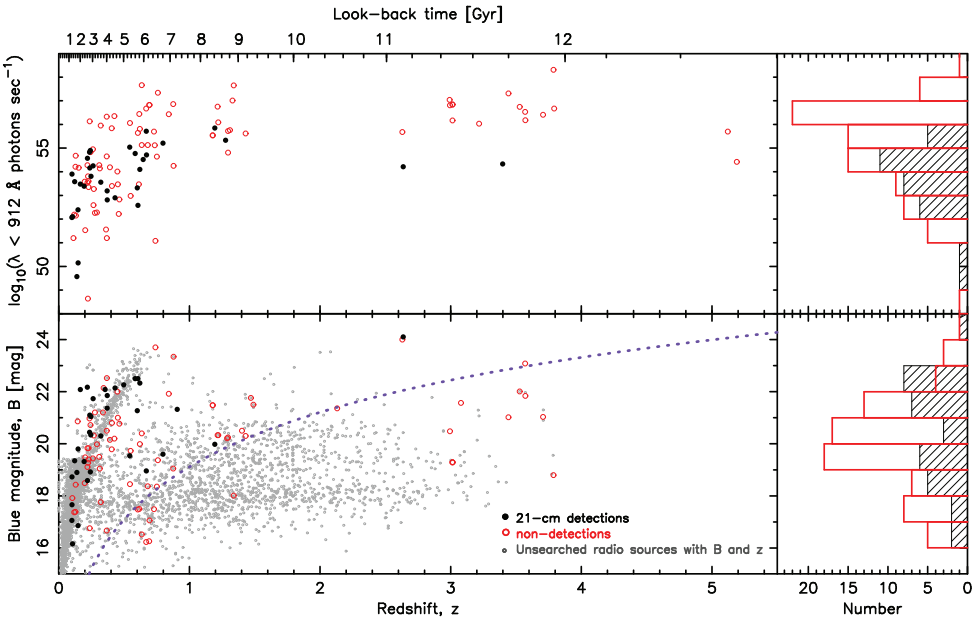

Figure 4: Top: The ionising photon rate versus the redshift for the $z \geq 0.1$ galaxies and quasars searched for HI 21cm absorption (Curran & Whiting 2012). Filled symbols/histogram show the detections and unfilled symbols/histogram the non-detections. Bottom: The corresponding optical blue magnitudes (updated from Curran et al. 2013). The dotted line shows the B magnitude corresponding to the critical UV luminosity identified by Curran & Whiting 2011. In objects below this line, all the gas in the galaxy is expected to be ionised rather than neutral (assuming a spectral slope of $\alpha = -1.5$).

2.3 Upcoming surveys with SKA pathfinders and precursors

Most of the work in the next few years will be focused on exploiting the large field of view of some of the SKA pathfinder and precursor telescopes, along with the uniform frequency coverage enabled by the radio-quiet SKA sites. This will make it possible to carry out blind searches that can probe the HI distribution in radio sources in a more systematic way. At this

PoS(AASKA14)134

stage, the sensitivity of the pathfinders (at least for searches up to redshift z~0.2) will only be comparable to that of existing telescopes, though the available redshift range will be larger. These pathfinder observations will only be able to use relatively bright radio sources, telling us about gas in the central region of radio AGN with continuum flux > 50mJy (where we will be able to probe optical depth down to a few %).

Automated search techniques for HI absorption in blind surveys have already been developed (Allison et al. 2012, 2014; Koribalski 2012), along with techniques for stacking (Gereb et al. 2014a) and profile characterisation (Gereb et al. 2014b). The pathfinder and precursor surveys will allow us to expand the use of stacking techniques and derive general properties of group of objects (e.g. young/old/restarted, compact/extended and exploring trends with redshift, optical properties etc.). Furthermore, some of the new surveys will give us a first census of what to expect at higher redshift. The possibility of extending the search to redshift z~1 using ASKAP (FLASH survey, PI E. Sadler), with improved sensitivity and bandwidth compared to previous searches (with GMRT and WSRT) will be a first step in the study of evolution of HI content and its properties.

3. **Intervening absorption**

The SKA will be a uniquely powerful instrument for studying neutral gas in the distant universe through HI surveys for *intervening absorbers,* which will provide large samples of HI-selected galaxies spanning a huge range in redshift. Figure 5 shows the profile of intervening HI 21cm absorption detected along the line of sight to the bright continuum source PKS 1830-211 with the WSRT (Chengalur et al. 1999), and more recently with the first three ASKAP antennas.

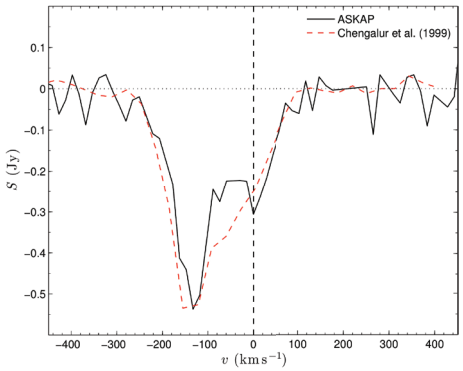

Figure 5: An early ASKAP spectrum of intervening HI 21cm absorption at z = 0.89 along the line of sight to the strong radio source PKS 1830-211, a gravitationally-lensed QSO at z = 2.51. The line profile from the original detection by Chengalur et al. (1999) is shown in red for comparison.

Almost all the currently-known intervening HI 21cm absorption-line systems were found through pointed observations of pre-selected targets, but SKA1 (and some of its precursor and pathfinder telescopes) will be able to carry out genuinely blind HI 21cm absorption surveys of large areas of sky, detecting many thousands of HI absorption systems and providing new insights into the role of neutral hydrogen in galaxy evolution across cosmic time.

3.1 Motivation and previous work

Cold neutral gas is central to understanding how galaxies and their star-formation rates evolve over cosmic time, yet we currently lack a clear picture of how much neutral gas is present in

PoS(AASKA14)134

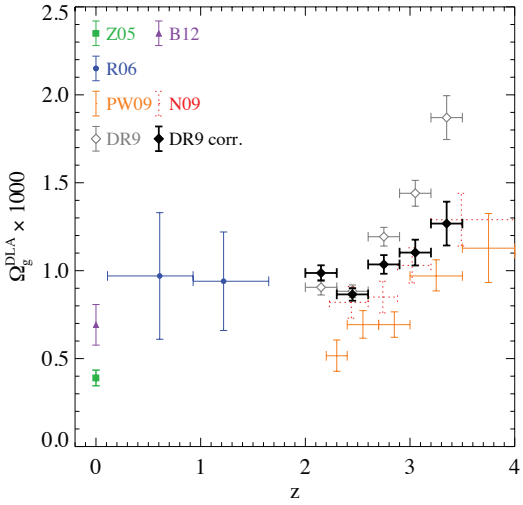

Figure 6: Cosmological mass density of neutral gas in DLAs as a function of redshift, from Noterdaeme et al. (2012). Data points are coded as follows: Z05: Zwaan et al. (2005), B12: Braun (2012), R06: Rao et al. (2006), PW09: Prochaska & Wolfe (2009), DR9:

the Universe at different epochs or how this gas is distributed in dark halos of different mass. Almost all our current measurements of HI in the distant universe come from optical observations of Lyman α (Ly α) absorption by gas clouds along the line of sight to distant quasars (e.g. Wolfe et al. 1986; Lanzetta et al. 1991; Wolfe et al. 1995; Storrie-Lombardi, Irwin & McMahon 1996; Peroux et al. 2005; Wolfe, Gawiser & Prochaska 2005; Rao et al. (2006), Prochaska & Wolfe 2009; Noterdaeme et al. 2012). With the exception of the study by Rao et al. (2006), these observations have mainly been carried out at redshift $z > 2$ where the UV Ly α line is redshifted to optical wavelengths and can be observed by ground-based telescopes. As a result, we currently have more accurate estimates of the cosmic mass density of HI at $z > 2$ than at lower redshifts (see Figure 6).

Studies of the 21cm HI line in absorption along the line of sight to distant radio galaxies and quasars can provide a direct tracer of both the distribution of neutral hydrogen in distant galaxies and the physical conditions in the neutral gas (Kanekar & Chengalur 2003). Radio measurements of HI 21cm absorption offer some advantages over the existing optical Ly α surveys. There is no redshift limit for line detection, other than that set by the frequency coverage of the telescope and the availability of suitable bright background continuum sources. Radio observations are unaffected by extinction and can probe objects with a high dust content, in contrast to optical surveys for damped Ly α absorbers (Kanekar & Briggs 2004; Kanekar et al. 2009). In addition, optical/IR identification and follow-up of HI-detected galaxies is likely to be easier if the background source is an optically-faint radio galaxy rather than a bright quasar (which generally overwhelms the light of a fainter intervening galaxy). On the other hand, because a 21cm absorption survey provides a measurement of HI optical depth rather than HI column density as discussed below (see also Braun 2012), interpretation of the data also presents some novel challenges.

Kanekar & Briggs (2004) laid out a detailed science case for HI 21cm absorption studies with the SKA. They showed that blind SKA 21-cm surveys will yield large, unbiased absorber samples, tracing the evolution of normal galaxies and active galactic nuclei from $z > 6$ to the local universe. Such surveys will make it possible to directly measure the physical size and mass of typical galaxies as a function of redshift, and will provide new tests of hierarchical models of structure formation.

The Kanekar & Briggs (2004) paper remains an essential reference document for SKA studies, and our focus here is on developments over the past decade. There are three areas in particular where rapid progress has been made:

PoS(AASKA14)134

(1) Our understanding of **neutral molecular gas in distant galaxies** has advanced in recent years through observations with new mm and sub-mm interferometers. This opens up new opportunities to combine information about both the atomic and molecular phases of neutral gas in distant galaxies, providing a much more complete picture of their gas

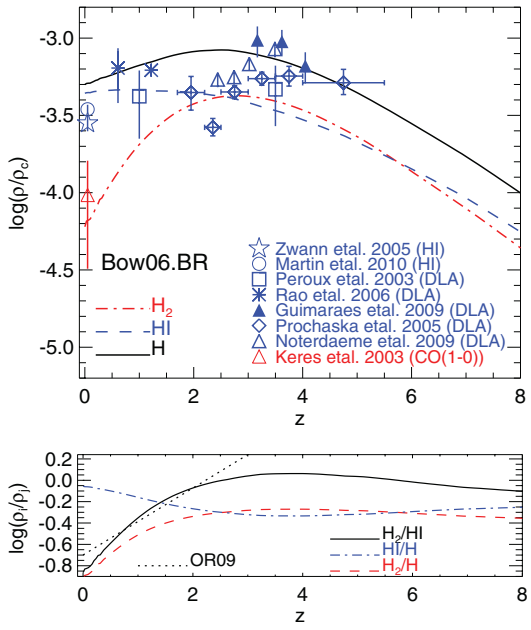

Figure 7: (top) Global density of all forms of neutral hydrogen (solid line), atomic HI (dashed) and molecular H_2 (dot– dashed) in units of the critical density at z = 0, as a function of redshift; (bottom) evolution of the global H_2 /H I (both plots from Lagos et al. 2011).

content as well as more rigorous constraints on theoretical models. A methodology for large "blind" mm-wave surveys for molecular absorption has been laid out, and the first such survey carried out with the GBT (Kanekar et al. 2014a). Such absorption surveys with ALMA and EVLA are likely to provide an important complementary view of the neutral ISM in high-z galaxies to that provided by HI 21cm absorption studies.

In a targeted study, Tacconi et al. (2010) found that the molecular gas content of spiral galaxies (as measured from the CO emission line) was three to ten times higher at redshift z=1-2 than it is today, and molecular gas has now been detected in QSO host galaxies out to z > 6 (e.g. Wang et al. 2011). Although these studies focused on bright objects, rapid progress in understanding the molecular gas properties of distant galaxies seems certain to continue as ALMA comes into full operation in the near future. There is already evidence that the overall molecular gas content of galaxies evolves more rapidly with redshift than their neutral hydrogen content over the redshift range 0 < z < 2 (Lagos et al. 2011; see Figure 7), but we still have almost no observational constraints on the relative amounts of atomic and molecular gas in individual galaxies except in the very local universe.

(2) New HI absorption measurements of radio-loud QSOs have advanced our understanding of the **typical spin temperature and filling factor** in intervening HI 21cm absorption systems, particularly at z > 2 (Kanekar et al. 2014b and references therein). In particular, large GMRT and GBT studies of HI-21cm absorption in MgII-selected samples at z<1.7 (e.g. Gupta et al. 2007; Kanekar et al. 2009; Gupta et al. 2012) have significantly increased the number of known HI 21cm absorbers in the redshift desert, and provide a new route to finding DLAs at z<1.7, where the Lyman-alpha line is not observable from the ground. Around 200 QSO DLAs have now been studied in detail with optical telescopes, allowing the metallicity, elemental abundances and kinematics to be measured. The results of these studies imply that the number of absorbers with high spin temperature (Ts > 1000 K) increases with redshift (though Curran & Webb (2006) argue that part of this difference may be due to changes in the covering factor *f*). An important new result is the spin temperature - metallicity anti-correlation found in DLAs

PoS(AASKA14)134

(Kanekar & Chengalur 2001; Kanekar et al. 2009). This anti-correlation is important for SKA1 searches at high redshift because it implies that galaxies with low metallicities are likely to have high spin temperatures, and so may be more difficult to detect in HI 21cm absorption.
(3) There have also been significant advances in **modelling the evolution of cold atomic and molecular gas** in distant galaxies, using both semi-analytic and hydrodynamical approaches. A detailed discussion of these models is presented in the chapter on *Neutral Hydrogen and Galaxy Evolution* (Blyth et al., this volume).

3.2 Forthcoming surveys with SKA pathfinders

As with the associated HI absorption case outlined in section 2.3, forthcoming surveys with SKA pathfinder telescopes will carry out the first large blind imaging radio surveys for intervening HI 21cm absorption. ASKAP, with its 30 deg^2 field of view, and frequency coverage down to 700 MHz (i.e. redshift z ~ 1 for the HI line), will open up a large area of new parameter space for HI 21cm absorption studies, and Apertif and MEERKAT will also do important work. The ASKAP FLASH survey will cover the whole southern sky, searching more than 150,000 sightlines to bright (> 50 mJy) continuum sources for intervening HI absorbers in the redshift range $0.5 < z < 1$. The 5-sigma detection limit in HI optical depth for the planned integration time of 2 hours/field is expected to range from $\tau < 0.01$ for the brightest (> 1 Jy) background continuum sources to $\tau \sim 0.3$ for the faintest (50 mJy) sources. Thus the FLASH survey will mainly target the rare, high-column density absorbers expected to occur on < 1% of sightlines (Braun 2012). Deeper integrations with e.g. Apertif and MEERKAT (PI N. Gupta) will cover smaller areas of sky but probe to deeper HI optical-depth limits.

An important feature of all these pathfinder surveys is that unlike previous HI 21cm absorption studies, they will use all the strong continuum sources in the field (both radio galaxies and QSOs) to search for absorption lines. The angular size of these background sources will depend on several factors, including the source type and redshift, and many of them are likely to have resolved structures on sizes smaller than the angular resolution of the pathfinder telescopes (at 843 MHz, roughly 10% of continuum sources brighter than 50 mJy are expected to be QSOs; Jackson et al. 1998). Braun (2012) notes that the highest column-density HI gas in galaxy disks is likely to reside in discrete clumps with a characteristic scale size of ~100 pc (angular size 15 mas at z ~ 1), which will have a low filling factor if observed at arcsec resolution against a background radio galaxy several kpc in extent. As well as providing a large 'HI-selected galaxy sample' out to z ~1, high-resolution follow-up studies of HI 21cm absorption systems detected in these first blind surveys will provide important pathfinder results to guide and refine the design of future large HI absorption surveys with SKA1.

4. Expected science outcomes from SKA Phase 1

4.1 Planned observations

Table 1 outlines a set of three planned surveys for HI 21cm absorption with SKA1. These surveys are complementary to the strawman HI emission surveys proposed by Blyth et al. (this volume) but the use of absorption lines allows us to span a far larger redshift range than will be possible with the SKA1 emission-line studies (or even the range covered by HI emission studies

PoS(AASKA14)134

with SKA2, which will reach to z ~2). Survey 1 is expected to take 1-2 months to complete, and will extend the pathfinder studies out to higher redshift by providing a detailed inventory of both intervening and associated HI 21cm absorption for galaxies in the redshift range $1 < z < 3$.

Survey	**SKA1**	**Redshift range**	**Receiver**	**Spatial res.**	**Sky area**	**Spectral-line rms**	**Optical depth τ**	**Expected detections**
1. Inventory of HI in distant galaxies	SUR or MID	To z=3	Band 1	~1 arcsec	1,000 deg^2	<0.1 mJy	<0.01 (10mJy source)	~5000 associated, several hundred intervening
2. (i) Cold outflows (assoc.), (ii) Evolution of HI in galaxies (interven.)	SUR or MID	To z=3	Band 1	~1 arcsec	10,000 deg^2	<0.1 mJy	0.001 to 0.005 (20mJy source)	A few hundred outflows, several thousand intervening absorbers
3. HI at very high redshift	LOW	3 < z < 8	220 MHz band	~5 arcsec	>1,000 deg^2	<0.5 mJy	<0.05 (10mJy source)	Unknown, new discovery space.

Table 1: Specifications of three proposed HI 21cm absorption surveys with SKA1.

This will provide exciting new scientific results in its own right, but can also be used to refine the observing strategy for a larger-area survey (Survey 2 in Table 1) which would take ~1 year to complete and provide breakthrough science for understanding both galaxy feedback processes at high redshift and the co-evolution of cold gas and star formation across cosmic time. The third survey, with SKA1-LOW, will open new discovery space at $z > 3$, where the volume density of powerful radio galaxies is currently poorly known. This survey will be able to identify high-redshift radio galaxies and quasars through the 21cm line, with no requirement for optical pre-selection, and will connect the lower-redshift HI results to future studies of the HI '21cm forest' at $z > 7$ with SKA1 and SKA2 (e.g. Furlanetto & Briggs 2005; Ciardi et al. this volume).

4.2 Associated absorption

The main breakthroughs expected (for associated HI absorption) from SKA1 will be:

1) the use of absorption to trace the presence and properties of HI in active galaxies out to z~3 and beyond, as a function of galaxy properties and redshift;

2) tracing the presence of neutral gas outflows in sources below 100 mJy in flux, therefore increasing dramatically the numbers of potential candidates;

3) tracing the evolution of outflows (occurrence and characteristics) as a function of redshift, providing crucial information for this important ingredient in the feedback scenario;

4) making use of serendipitous detections of HI absorption to derive new redshifts (also for weak radio sources, i.e. not dominated by a radio AGN).

For studies of associated absorption with SKA1, we will be using Bands 1 and 2. This allows us to observe from redshift 0 (1421MHz, the HI 21cm rest frequency) to 350 MHz

PoS(AASKA14)134

corresponding to redshift z~3 with MID and SUR. We will also use SKA1-LOW to probe associated absorption at z > 3, noting that associated systems are likely to have higher metallicity than intervening systems at these high redshifts (since they are close to a bright AGN) so cold gas may be easier to detect.

The success of searches for HI absorption will depend on the available sensitivity (see below). This will be combined with high spatial resolution observations because, as discussed above, pinpointing the location of the absorption is key for the interpretation. We will need at least arcsec/sub-arcsec resolution for this work, but possibly VLBI-like capabilities. This appears to be not well covered by the capabilities described in the Level 0 requirements (Dewdney et al. 2013; see also the chapter on *Very Long Baseline Interferometry with the SKA* by Paragi et al. this volume). Bandpass stability is also an extremely important parameter to allow the detection, also in weak radio sources, of shallow components and signatures of outflows (the stability of the bandpass is required to a level of 10^5).

Present and near-future surveys can provide an inventory of HI 21cm absorption down to ~50 mJy for a typical optical depth (τ) of a few %. The big step forward provided by SKA1 is the possibility of extending the search and characterisation of the HI to higher redshifts (z > 1).

To make a substantial step forward and explore the presence of HI against radio sources down to the 10 mJy level, we will need to reach noise levels (per channel) < 100 μJy.
Given the relatively high density of sources at this low flux level (around 15 per deg^2) it would not be necessary to cover a huge area: an area of roughly 1000 deg^2 would give ~15,000 sources, and if the detection rate holds to 30% (Gereb et al. 2014b) we will have ~5000 absorption systems to study in different redshift bins and to divide in different groups. The stacking will be done using weaker sources in the field as well.

Covering even larger areas would have the advantage that, for a large number of objects, we will be able to use HI 21cm absorption to derive the redshift of the host galaxy. For example, in the 3π sr survey from Fig. 5 and 7 of the Level 0 document, sources of ~30mJy can be searched for absorption down to ~ 2 % optical depth. An important goal is to trace the presence of outflows of cold gas as function of the radio power (i.e. exploring the low flux/radio power range). In order to trace these outflows with τ = 0.001-0.005 (typical of the known cases, Morganti et al. 2005) in sources of 100 mJy we will need to reach ~30 – 170 μJy. Reaching these sensitivities will substantially increase the number of candidate sources that can be searched, allowing us to derive the statistics of the occurrence of cold gas outflows as a function of flux and of redshift.

To reach this level, we will need to go at least a factor of two deeper than the proposed SKA1 MID/survey 3π sr (Figs 5 and 7 in the Level 0 document) and cover at least 10,000 deg^2 of sky (from source counts we expect about 2 sources per deg^2 above 100 mJy) to allow enough sources to be explored. If the detection rate of outflows is about 10% of the overall HI 21cm absorption *detections* (as found for powerful sources by Gereb et al. 2014b), this would give ~ 600 potential outflows to use for derive the statistics of their characteristics and evolution in different redshift bins. However, for this particular science case, the full velocity resolution of 30 km s^{-1} will not strictly be required, and therefore the observing time can also be slightly reduced. A shallow all-sky survey will not provide, for this topic, a comparably interesting step

PoS(AASKA14)134

forward. The expected spatial resolution of SKA1 is higher than 1arcsec only up to 1 GHz. This is likely to limit our ability to pinpoint the location of the absorbing HI gas and outflows.

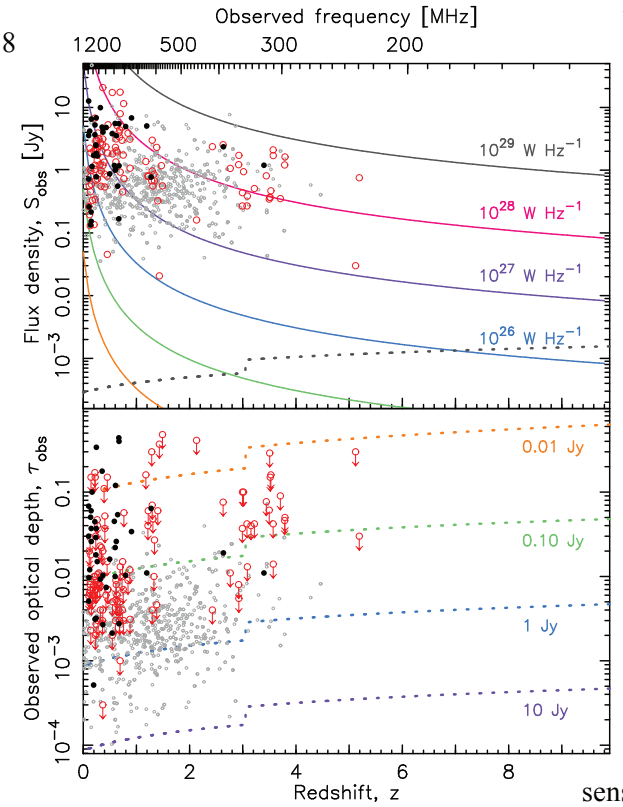

Figure 8: (Top): Flux densities of sources at z > 0.1 which have so far been searched for HI absorption. As in Fig. 4, filled symbols show detections and open symbols non-detections. The small grey circles show Parkes Quarter-Jansky (Jackson et al. 2002) sources with known redshifts. Current z > 0.1 searches range from 10^{24} - 10^{29} W Hz^{-1} (Curran et al. 2008), and the dashed line shows the rms noise level of SKA1–MID and SKA1–Low in a 1 km s^{-1} channel in a 1 hour integration. (Bottom): The corresponding optical depths and 3σ limits. Dashed lines show the sensitivity of SKA1 for the corresponding flux density at 1 km s^{-1} resolution after 1 hour.

For studies of distant radio galaxies, Figure 8 (top) shows the flux densities of the sources currently searched for associated HI absorption at z > 0.1. There are two decades of unexplored space between these observations and the SKA1 sensitivity. SKA1–MID and –Low will cover the entire frequency range from 50 to 1420 MHz in just a few tunings, means that there is no need to preselect targets using an optical redshift. This opens up unexplored territory at high redshift, possibly uncovering a population of obscured gas-rich radio galaxies and QSOs that are hidden at optical wavelengths.

Synergy with other facilities. The SKA1 studies will provide extremely interesting targets for follow up with the optical and mm facilities that also available in the southern hemisphere. In particular, the study of the HI outflows will be relevant and complementary to the molecular studies. The wider field of view of HI observations will allow blind searches and provide targets for ALMA. Future large-area spectroscopic surveys in the southern hemisphere will also be an important complement to the HI data.

4.3 Intervening absorption

HI 21cm absorption-line surveys with SKA1 will provide an **HI-selected galaxy sample** extending out to z ~3 with SKA1-MID/SUR, and potentially at z >> 3 with LOW. Follow-up observations with ALMA will allow us to link HI and CO along the same sightline for galaxies over a wide range in redshift, and follow-up optical/IR studies will also be possible for many objects out to at least z ~ 1.5 to 2. At redshifts above z ~ 2, there will be a significant overlap with radio-loud QSOs for which optical spectra of the Ly α line are already available. An

PoS(AASKA14)134

SKA1 HI 21cm absorption survey will also be able to find heavily reddened and dust-obscured QSOs that have been missed by optical surveys.

At z > 1, SKA1 HI absorption studies will open up a new parameter space not explored by the pathfinder surveys. SKA1 will provide detailed information on the HI properties of individual galaxies at z = 1 and higher. A wide field of view is an advantage for these studies, because the surface density of sufficiently distant background radio sources is low, and decreases out to higher redshift (e.g. the expected surface density of continuum sources brighter than 30 mJy is roughly 2.5 per deg^2 for sources with z > 1 and 1 per deg^2 for sources at z > 3; see Kanekar & Briggs 2004 and Wilman et al. 2008). Figure 9 shows the expected distribution of HI column densities at different redshifts, as discussed by Braun (2012).

A large-area survey of ~10,000 deg^2, as outlined in Table 1, would allow 5-σ detection of HI absorption lines with an optical depth of τ ~ 0.015 against background sources stronger than about 30 mJy, and of stronger lines against weaker sources (e.g. τ ~ 0.05 lines against sources stronger than ~10 mJy and τ ~ 0.1 lines against sources stronger than ~ 2-3 mJy). The HI column densities probed by these lines would depend on the spin temperature and filling factor of the neutral gas, but such a survey would probe at least

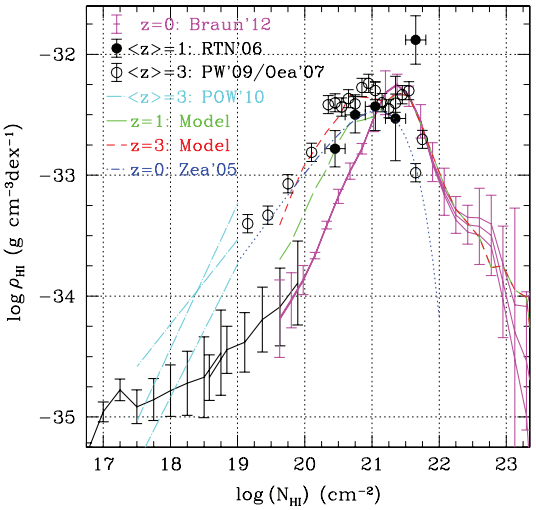

Figure 9: HI mass density function for intervening HI absorption systems over the redshift range 0 < z < 3, from Braun (2012). Filled circles show the ⟨z⟩ = 1 QSO absorption line data of Rao et al. (2006), and open circles the ⟨z⟩ = 3 QSO absorption line data of Prochaska & Wolfe (2009) and O'Meara et al. (2007). The relation at z=0 is derived from 21cm HI emission surveys

50,000 sightlines to background sources at z > 1, and might be expected to detect several thousand intervening HI absorption systems out to redshift z = 3.

Longer integration times could also be built up over smaller regions of sky to push to lower optical depth and provide better coverage of absorbers linked to warmer gas with spin temperatures above 200-300 K, providing a unique probe of the warm neutral medium in high-redshift DLA systems.

Synergy with other facilities. HI 21cm absorption surveys with HI will provide data for an exciting range of follow-up programs with other facilities. Current optical/UV DLA samples are dominated by systems at redshift z > 1.7, with over 10,000 DLAs known at z > 2 and only about 50 at z < 1.7 (e.g. Noterdaeme et al. 2009; Lee et al. 2013). Redshifted HI-21cm absorption surveys with the SKA1-SUR and –MID will therefore have a huge impact on studies of neutral gas in galaxies at z < 1.7, both through blind surveys and by targeting QSOs with known MgII

PoS(AASKA14)134

absorbers. In particular, blind HI 21cm absorption surveys with SKA1 will allow us to assemble large and unbiased samples of HI-selected galaxies across a wide range in redshift. We can then probe the nature of "typical" galaxies as a function of redshift, via follow-up optical/IR imaging with large ground-based telescopes and JWST, and spectroscopy using optical/near-IR integral field spectrographs to study the Lyman-alpha and H-alpha lines in emission, and CO studies with ALMA.

SKA1 will also have an impact at $z > 1.8$, where large ground-based studies of QSO absorption have already been carried out with optical telescopes. At least 10% of the powerful radio sources used to search for HI 21cm absorption with SKA1 are expected to be bright optical QSOs, and combining optical and radio measurements for these objects will provide new insights into the physical properties of the interstellar medium at high redshift through measurements of the spin temperature and metallicity for large samples of HI absorption systems (Kanekar et al. 2014).

The other place where HI 21cm absorption surveys will have an important impact is at $z > 5$, where it becomes difficult to identify DLAs at optical/IR wavelengths because the Lyman-alpha forest becomes extremely dense. The limiting factor here is the low surface density of bright radio continuum sources at $z > 5$, but HI absorption surveys with SKA1-LOW should yield at least a modest number of detections which can be followed up at other wavelengths (though we note that ALMA CO emission studies may be challenging at $z > 5$, since the CO-to-H2 conversion factor is likely to be very high in small, low-metallicity galaxies at high redshift).

Over the full SKA 1 redshift range, blind HI 21cm absorption surveys will also find dusty absorbers that could be followed up to search for OH/CO/HCO+ absorption. Such observations would provide tests of fundamental constant evolution, as well as allowing us to study molecular gas in normal galaxies over a wide range in redshift. In addition, optical measurements of molecular hydrogen (H_2) absorption along the sightline to 21cm HI absorption systems will allow a direct comparison of the atomic and molecular phases of the neutral ISM at high redshift (Ledoux et al. 2003; Hirashita et al. 2003). ALMA observations of CO emission within distant galaxies identified through intervening HI absorption will also allow us to study correlations between the 21cm optical depth or spin temperature, H_2 absorption and CO emission within the same objects, making it possible to link the physical conditions derived from HI absorption-line studies (with SKA and optical telescopes) and molecular emission-line studies with ALMA.

5. Expected outcomes from early science (50% SKA1)

The main breakthrough enabled by SKA1 is the opening-up of new parameter space for studies of HI absorption at redshift $1 < z < 3$ (350-700 MHz), a redshift range not covered by the SKA pathfinder and precursor telescopes. Existing telescopes have probed some regions of this redshift space, but bandwidth limitations and the effects of radio-frequency interference (RFI) have strongly limited their redshift coverage. The radio-quiet site of SKA1 offers an important advantage for work in this frequency range. Although a 50% SKA1 instrument will be less sensitive (in terms of Ae/Tsys) than existing large telescopes like GMRT and GBT, it will still open up an exciting new parameter space for HI 21cm absorption surveys in the distant

PoS(AASKA14)134

universe. For example, a 50% SKA1 instrument would have a survey speed roughly 25 times faster than the GMRT for blind HI absorption surveys at 350-700 MHz. HI absorption studies are an excellent early science project because the strongest lines have high optical depth and can be detected in fairly short integrations. Since SKA1 opens up a new frequency range below 700 MHz, new science can be done even with much less than 50% of the final collecting area.

6. Anticipate the science outcomes of SKA 2

For intervening HI 21cm absorption, a key focus for SKA2 will be the evolution of cold gas in galaxies across cosmic time, including direct measurements of the physical size and mass of typical galaxies as a function of redshift out to $z > 6$, as discussed in detail by Kanekar & Briggs (2004). Beyond $z \sim 6$, HI 21cm absorption measurements potentially provide a unique measurement of the HI density power spectrum on small scales (Ciardi et al., this volume). For associated HI absorption, SKA2 will provide two main steps forward. The enhanced sensitivity at low frequencies will allow us to trace the evolution of radio galaxies (not only the powerful one) and, in particular, the inflow and outflow of cold gas with their host galaxies, over almost the whole of cosmic time. The higher spatial resolution offered by SKA2 will also be a major advantage for the interpretation of associated HI detections and their links to the nuclear activity and the evolution of the host galaxy.

References

Alatalo et al. 2011 ApJ 735, 88
Allison J.R., Sadler E.M., Meekin A.M., 2014, MNRAS, 440, 696
Allison J.R., et al., 2012, MNRAS, 423, 2601
Beswick R.J., Peck A.B., Taylor G.B., Giovannini G., 2004, MNRAS, 352, 49
Braun R., 2012, ApJ, 87, 749
Carilli C.L., Dwarakanath K.S., Goss W.M., 1998, ApJ, 502, L79
Carilli C.L., et al., 2000, PhRvL, 85, 5511
Chandola Y., Sirothia S. K., Saikia D. J. 2011, MNRAS, 418, 1787
Chengalur J. N., de Bruyn A. G., Narasimha D., 1999, A&A, 343, L79
Chengalur J.N., Kanekar N., 2003, PhRvL, 91, 1302
Combes F., et al., 2013, A&A, 558, 124
Croton D.J., et al., 2006, MNRAS, 367, 864
Curran S. J., et al. 2008, MNRAS, 391, 765
Curran S. J., Whiting M. T., 2010, ApJ, 712, 303
Curran S. J., Whiting M. T., 2012, ApJ, 759, 117
Curran S. J., Whiting M. T., Tanna A., Sadler E. M., Athreya R., 2013, MNRAS, 429, 3402
Dewdney, P., Turner, W., Millenaar, R., McCool, R., Lazio, J., Cornwell, T., 2013, "SKA1 System Baseline Design", Document number SKA-TEL-SKO-DD-001 Revision 1
Drinkwater M.J., Webb J.K., Barrow J.D., Flambaum V.V., 1998, MNRAS, 295, 457
Feruglio C., Maiolino R., Piconcelli E., Menci N., Aussel H. et al. 2010, A&A, 518, L155
Gereb K., Morganti R., Oosterloo T. 2014a, A&A 569, 35
Gereb K., Maccagni F.M., Morganti R., Oosterloo T.A., 2014b, A&A in press (arXiv:1411.0361)
Gupta N., Salter C. J., Saikia D. J., Ghosh T., Jeyakumar S. 2006, MNRAS, 373, 972
Gupta N., Srianand R., Petitjean P., Khare P., Saikia D.J., York D.G., 2007, ApJ, 654, L111
Gupta N., et al., 2012, A&A, 544, 21

PoS(AASKA14)134

Hirashita H., Ferrara A., Wada K., Richter P., 2003, MNRAS 341, L18
Hopkins P.F., Elvis M., 2010, MNRAS, 401, 7
Ishwara-Chandra C.H., Dwarakanath K.S., Anantharamaiah K.R., 2003, JAstrophysAstr 24, 37
Jackson C.A., Wall J.V., 1998, wfsc.conf, 153
Kanekar N., Chengalur J.N., 2003, A&A, 399, 857
Kanekar N., Briggs F.H., 2004, NewAR, 48, 1259
Kanekar N., Prochaska J.X., Ellison S L., Chengalur J. N., 2009, MNRAS, 396, 385
Kanekar N., Prochaska J.X., Ellison S.L., Chengalur J. N., 2010, ApJ, 712, L148
Kanekar N., Langston G.I., Stocke J.T., Carilli C.L., Menten K.M., 2012, ApJ, 746, L16
Kanekar N., Gupta A., Carilli C. L., Stocke J. T., Willett K. W., 2014a, ApJ, 782, 56
Kanekar N., et al., 2014b, MNRAS, 438, 2131
Koribalski B.S., 2012, PASA, 29, 213
Lagos C.D.P., Baugh C.M., Lacey C.G. et al., 2011, MNRAS, 418, 1649
Lanzetta K.M., Wolfe A.M., Turnshek D.A., Lu L., McMahon R.G., Hazard C., 1991, ApJS, 77, 1
Ledoux, C., Petitjean, P., Srianand, R., 2003, MNRAS 346, 29
Lee, K.-G., et al., 2013, ApJ, 145, 69
Moore, C.B., Carilli, C.L., Menten, K.M., 1999, ApJ 510, L87
Morganti, R., et al. 2005, A&A, 444, L9
Morganti R., Peck A. B., Oosterloo T. A., et al. 2009, A&A, 505, 559
Morganti R., Oosterloo T., Struve C., Saripalli L., 2008, A&A, 485, L5
Morganti R., Fogasy J., Paragi Z., Oosterloo T., Orienti M., 2013, Sci, 341, 1082
Murphy M.T., et al., 2001, MNRAS, 327, 1244
Noterdaeme P., et al., 2012, A&A, 547, L1
Nyland K., et al., 2013, ApJ, 779, 173
Peck A.B., Taylor G.B. 2001, ApJ 554, L147
Peroux C., Dessauges-Zavadsky M., D'Odorico S., Sun Kim T., McMahon R.G., 2005, MNRAS, 363, 479
Prochaska J.X., Wolfe A.M., 2009, ApJ, 696, 1543
Rao S., Briggs F., 1993, ApJ, 419, 515
Rao, S.M., Turnshek D.A., Nestor D.B., 2006, ApJ, 636, 610
Roberts M.S., 1970, ApJ, 161, L9
Schaye J., et al., 2015, MNRAS, 446, 521
Serra P., et al., 2012, MNRAS, 422, 1835
Storrie-Lombardi L.J., Irwin M.J., McMahon R.G., 1996, MNRAS, 282, 1330
Struve C., Conway J.E., 2010, A&A, 513, A10
Struve C., Conway J.E., 2012, A&A, 546, A22
Tacconi L.J., et al., 2010, Natur, 463, 781
Tadhunter C., Morganti R., et al. 2014, Nature 511, 440
Teng S,H., Veilleux, S., Baker, A.J., 2013, ApJ, 765, 95
Uson J.M., Bagri D.S., Cornwell T.J., 1991, PhRvL, 67, 3328
van Gorkom J. H., Knapp G. R., Ekers R. D., et al. 1989, AJ, 97, 708
Vermeulen R.C., et al., 2003, A&A, 404, 861
Wang R., et al. 2011, AJ, 142, 101
Whiteoak J.B., Gardner F.F., 1976, PASA 3, 71
Wiklind T., Combes, F., 1995, A&A, 315, 86
Wilman R.J., et al., 2008, MNRAS, 388, 1335
Wolfe, A. M., Brown, R.L., Roberts, M.S., 1976, PhRvL 37, 179
Wolfe A.M., Lanzetta K.M., Foltz C.B., Chaffee F.H., 1995, ApJ, 454, 698
Wolfe A.M., Gawiser E., Prochaska J.X., 2005, ARA&A, 43, 861

PoS(AASKA14)134

Zwaan, M. A., Meyer, M. J., Staveley-Smith, L., Webster, R. L., 2005, MNRAS, 359, 30

PoS(AASKA14)134

PROCEEDINGS OF SCIENCE

The SKA as a Doorway to Angular Momentum

D. Obreschkow[*1], **M. Meyer**[1], **A. Popping**[1], **C. Power**[1], **P. Quinn**[1], **and L. Staveley-Smith**[1]

[1] *International Centre for Radio Astronomy Research (ICRAR)*
E-mail: danail.obreschkow@icrar.org

Angular momentum is one of the most fundamental physical quantities governing galactic evolution. Differences in the colours, morphologies, star formation rates and gas fractions amongst galaxies of equal stellar/baryon mass M are potentially widely explained by variations in their specific stellar/baryon angular momentum j. The enormous potential of angular momentum science is only just being realised, thanks to the emergence of the first simulations of galaxies with converged spins, paralleled by a dramatic increase in kinematic observations. Such observations are still challenged by the fact that most of the stellar/baryon angular momentum resides at large radii. In fact, the radius that maximally contributes to the angular momentum of an exponential disk ($3R_\mathrm{e} - 4R_\mathrm{e}$) is twice as large as the radius that maximally contributes to the disk mass; thus converged measurements of angular momentum require either extremely deep IFS data or, alternatively, kinematic measurements of neutral atomic hydrogen (H I), which naturally resides at the large disk radii that dominate the angular momentum. The SKA has a unique opportunity to become the world-leading facility for angular momentum studies due to its ability to measure the resolved and/or global HI kinematics in very large and well-characterised galaxy samples. These measurements will allow, for example, (1) a very robust determination of the two-dimensional distribution of galaxies in the (M, j)-plane, (2) the largest, systematic measurement of the relationship between M, j, and tertiary galaxy properties, and (3) the most accurate measurement of the large-scale distribution and environmental dependence of angular momentum vectors, both in terms of norm and orientation. All these measurements will represent exquisite tools to build a next generation of galaxy evolution models.

Advancing Astrophysics with the Square Kilometre Array
June 8-13, 2014
Giardini Naxos, Sicily, Italy

[*] Speaker.

PoS(AASKA14)138

1. Introduction

1.1 Importance of angular momentum

Understanding how galaxies form and evolve is one of the central topics in explaining the Universe we observe today. Pioneering studies (Fall & Efstathiou 1980; Mo et al. 1998; Quinn & Zurek 1988) have long stressed that galaxy properties are primarily driven by two physical quantities: mass and angular momentum (spin). Two recent advances have significantly increased our ability to understand the role of angular momentum. First, increased computing power and enhanced modelling of stellar feedback finally allow the simulation of galaxies with realistic angular momenta (Agertz et al. 2011; Brooks et al. 2011; Governato et al. 2010; Guedes et al. 2011). Second, enormous progress in kinematic observations, via optical integral field spectroscopy (IFS, see Glazebrook 2013) and radio/millimetre interferometry (e.g. using the VLA and ALMA), now yield the first precision-measurements of spin in controlled galaxy samples.

The new fields of research now accessible via angular momentum studies range from sub-galactic astrophysics (i.e., the study of angular momentum feedback, spin alignment of individual components, warped disks) to global galaxy evolution studies and large-scale cosmology. The next two paragraphs discuss two fruitful examples that are by no means meant to be exhaustive.

In the context of galaxy evolution studies, a major result of recent kinematic observations is that the shape of galaxies is tightly linked to their angular momentum and that the historical classification of galaxies by stellar or baryon mass M and Hubble type can instead be substituted for a more physically motivated classification by M and baryon/stellar angular momentum J (Cappellari et al. 2011; Obreschkow & Glazebrook 2014; Romanowsky & Fall 2012). This is illustrated

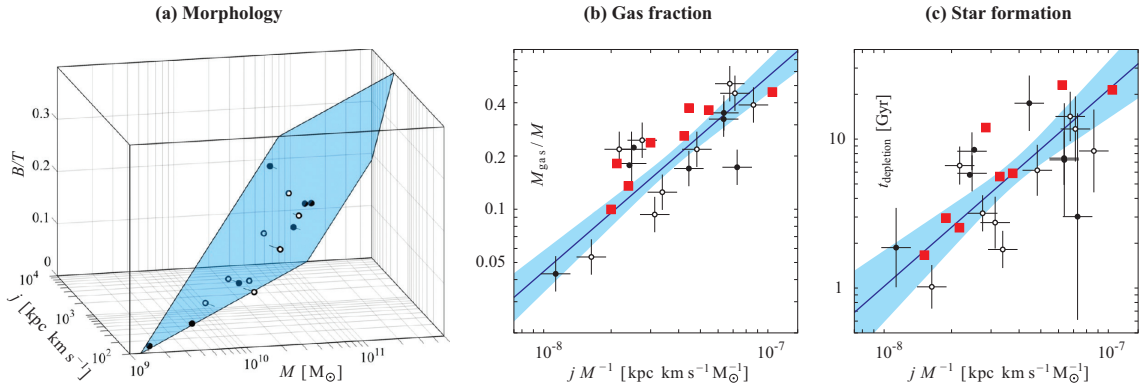

Figure 1: [from Obreschkow & Glazebrook (2014) and forthcoming work] Empirical evidence for the fundamental importance of the specific baryon angular momentum j, measured 10-times more accurately than so far, using kinematic maps of atomic hydrogen (Leroy et al. 2008). These high-precision data uncover strong correlations between j, baryon mass M and tertiary galaxy properties: (a) shows the M-j-morphology relation, where morphology is measured by the bulge mass fraction B/T; (b) and (c) show the relations between j/M and the cold gas fraction and depletion time (gas mass per star-formation rate), respectively. Black dots denote measurements for barred (open dots) and unbarred (filled dots) spiral galaxies. The blue plane in panel (a) and lines in panels (b) and (c) are regressions to the data, with the blue shades in panels (b) and (c) representing the uncertainty of these fits. Red squares are theoretical predictions from high-resolution hydrodynamic simulations [courtesy of C. Brook].

PoS(AASKA14)138

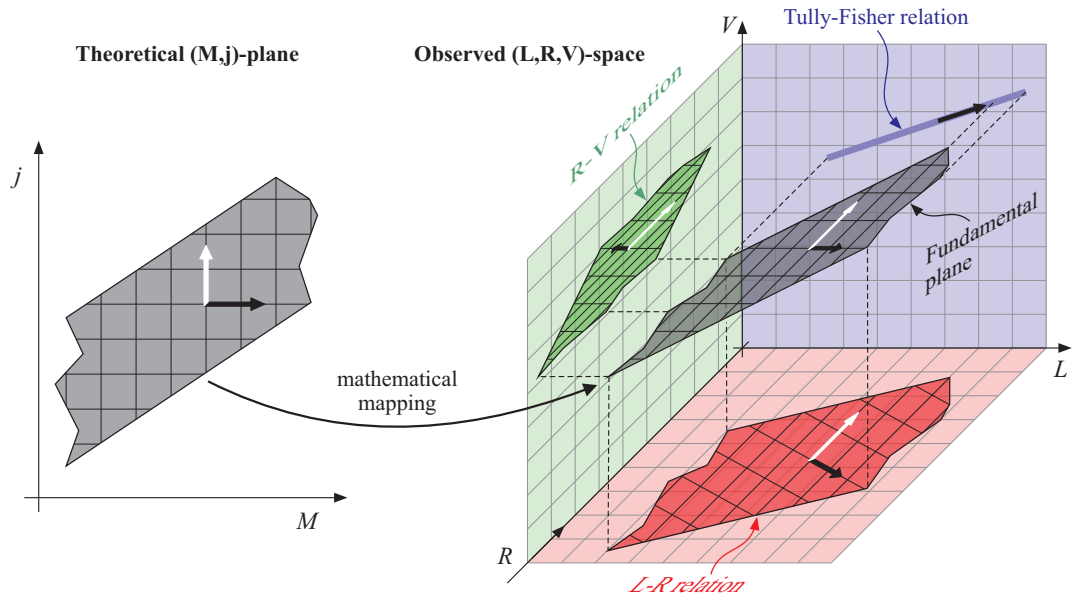

Figure 2: [Obreschkow & Glazebrook (2014)] In the model of an exponential disk inside a spherical halo, galaxies lie on a plane in the space spanned by luminosity L, disk radius R, and rotation velocity V. This plane can be explained as a mapping of the (M,j)-plane into (L,R,V)-space. Projections onto the planes (L,R), (R,V), and (V,L) give rise to classical scaling relations, whose dependence on morphology is then explained by the M-j-morphology relation.

in Fig. 1a for spiral galaxies, where we have introduced the *specific* angular momentum $j \equiv J/M$ (not to be confused with variations of the spin parameter λ, also sometimes called 'specific angular momentum'). Moreover, theoretical models reveal that the most important scaling relations of spiral galaxies, the mass-size-velocity scalings, can be understood as mappings of the (M,j)-plane into three dimensions (Fig. 2). Finally, angular momentum must play a fundamental role in star formation, since it sets the disk pressure, regulating the conversion of atomic gas to molecular gas and stars. The preliminary analysis in Figs. 1b and 1c confirms that in star-forming galaxies j/M is significantly correlated with the cold gas fraction and gas depletion time. This correlation had to be expected, to first order, because $j/M = J/M^2$ is inversely proportional to the disk surface density (details in Obreschkow & Glazebrook), which affects the conversion rate of H I to H_2 and stars.

In a cosmological context, much progress is to be made by analysing the large-scale (>Mpc, comoving) distribution of galaxies as a function of kinematic properties, in simulated and observed datasets. In fact, the large-scale distribution of angular momentum, both in terms of norm and orientation, contains information on the mechanisms of angular momentum growth by cosmic tides (White 1984) and the redistribution of angular momentum by galaxy coalescence. Empirical investigations using the SDSS survey revealed that spiral and elliptical galaxies obey opposite correlations with filaments (Jones et al. 2010), hinting at the importance of the orbital angular momentum involved in the merger-based formation of ellipticals. As for the norm of j, Fig. 3 shows a state-of-the-art analysis of the galaxy-galaxy correlation function for two samples of low and high j, relative to the mean M-j relation. Although the models (lines) appear consistent with the observations (points) within the observational uncertainties, the latter are currently too large to verify the predicted enhanced clustering of the low-j, subsample.

PoS(AASKA14)138

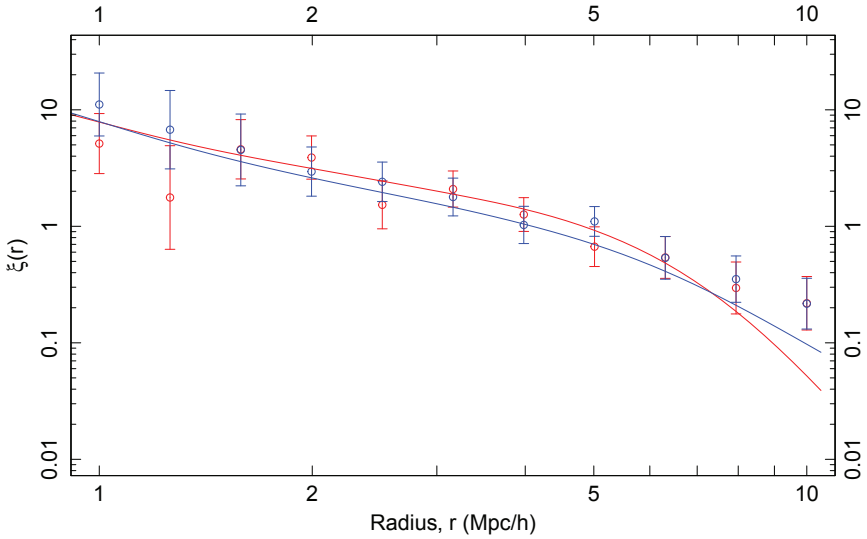

Figure 3: Preliminary analysis of the 2-point correlation function of spiral galaxies split in two samples of low (red) and high (blue) specific angular momentum j, relative to the mean M-j relation. Points with (correlated) error bars are observational data from the HIPASS catalog with optical counterparts from SuperCOSMOS (Doyle & Drinkwater 2006). Lines are model results from the S^3-SAX model (Obreschkow et al. 2009a). Observations and simulation are consistent within the observational uncertainties, but the latter are currently too large to verify the predicted enhanced clustering of low-j galaxies.

1.2 Objective of this paper

Having illustrated some of the importance of angular momentum in galaxies (Section 1.1), the remaining objective of this paper is to demonstrate the world-leading potential of the SKA in this field due to its unprecedented ability to detect neutral atomic hydrogen (H I) via 21cm interferometry. In fact, kinematic maps of H I combined with optical images allow the stellar/baryon j of disk galaxies to be measured within $\lesssim 5\%$ (Obreschkow & Glazebrook 2014) – the most accurate measurements to-date. *The advantage of H I data relies in the fact that H I naturally resides at large disk radii (about twice as large as stars), such that the radii that maximally contribute to the H I mass are similar to those that maximally contribute to angular momentum* ($3R_\mathrm{e} - 4R_\mathrm{e}$).

Section 2 explains how both spatially resolved kinematic H I maps and unresolved H I line profiles can be used to measure the angular momentum in disk galaxies. Simulation-based modelling in Section 3 reveals that already the SKA1 will increase the numbers of good kinematic H I maps and unresolved H I detections by about two orders of magnitude relative to the current state-of-the-art (e.g. THINGS, HIPASS, ALFALFA). Explicit numbers of angular momentum measurements are calculated for different benchmark survey scenarios with well-defined observing parameters. A brief discussion and summary are presented in Section 4.

2. Methods of Measuring Angular Momentum

This chapter presents different ways of measuring the stellar/baryon angular momentum **J** of disks using 21cm radio data. We will restrict this discussion to the measurement of the norm

PoS(AASKA14)138

$J \equiv |\mathbf{J}|$, however, using the inclination+chirality of the disk (from images or kinematic maps), the norm J can be converted to the vector $\mathbf{J}$. With respect to the centre of mass, J is defined as

$$J = \left| \int dM\, \mathbf{r} \times \mathbf{v} \right|, \tag{2.1}$$

where $\mathbf{r}$ is the position vector of the mass element dM relative to the centre of mass and $\mathbf{v}$ denotes the velocity in an inertial frame. In principle, J can be measured for different baryonic components, including the atomic and molecular material of the disk, but often only the stellar component is considered due to its dominance of the disk angular momentum in nearby galaxies (e.g. Obreschkow & Glazebrook 2014, Table 1).

Method 1: Precision Measurement (requiring 21cm maps and resolved optical images)

In the approximation of a disk with circular orbits, the norm of the angular momentum relative to the centre of gravity can be rewritten as

$$J = 2\pi \int_0^\infty dr\, r^2\, \Sigma(r)\, v(r) \tag{2.2}$$

and the specific angular momentum as

$$j \equiv \frac{J}{M} = \frac{\int_0^\infty dr\, r^2\, \Sigma(r)\, v(r)}{\int_0^\infty dr\, r\, \Sigma(r)}, \tag{2.3}$$

where $v(r)$ is the norm of the circular velocity at $r = |\mathbf{r}|$, and $\Sigma(r)$ is the azimuthally averaged mass surface density of the considered baryonic component. Note that r, v and Σ have to be deprojected (i.e., reconstructed from observations of an *inclined* disk) assuming circular orbits. The use of axially averaged surface densities $\Sigma(r)$ has the advantage of increasing the signal-to-noise in the faint outer part of the disk. This axial averaging, does *not*, in fact, lead to errors if the surface density were not axially symmetric, as long as the velocity field is axially symmetric.

In practice, the surface density $\Sigma(r)$ is measured from optical images (for stellar Σ) or from more complex multi-wavelength images (for baryon Σ). In turn, $v(r)$ can be measured from kinematic maps. In 16 regular disk galaxies of the THINGS survey (Leroy et al. 2008), axially averaged data of the stellar and baryon $\Sigma(r)$ (from optical+CO+H I imaging) and $v(r)$ (from H I maps) is available at sub-kpc resolution out to ~ 14 exponential disk scales. This extremely deep data enabled us to study the convergence of the stellar and baryon J as a function of r in detail (see Fig. 4). For these 16 galaxies J and j are converged to much less than 1%, reducing the overall uncertainties of j to 3%-5%.

Figure 4 highlights the key challenge of such precision measurements of angular momentum: the exquisite surface brightness sensitivity requirement. The data reveals that local disk galaxies need to be kinematically mapped to galactocentric radii of $3.6R_e$, on average, in order to capture 90% of the stellar angular momentum. For IFS surveys, this is an extreme requirement, given that the majority of galaxies in current IFS surveys are mapped to less than $2R_e$. Pushing from $2R_e$ to $3.6R_e$ corresponds to an increase of the surface brightness sensitivity by ~ 3 magnitudes, i.e. a ~ 200-times increase in observing time. In turn, H I maps almost by default extend to at least $4R_e$, because the H I gas is naturally situated at larger radii than the stars.

PoS(AASKA14)138

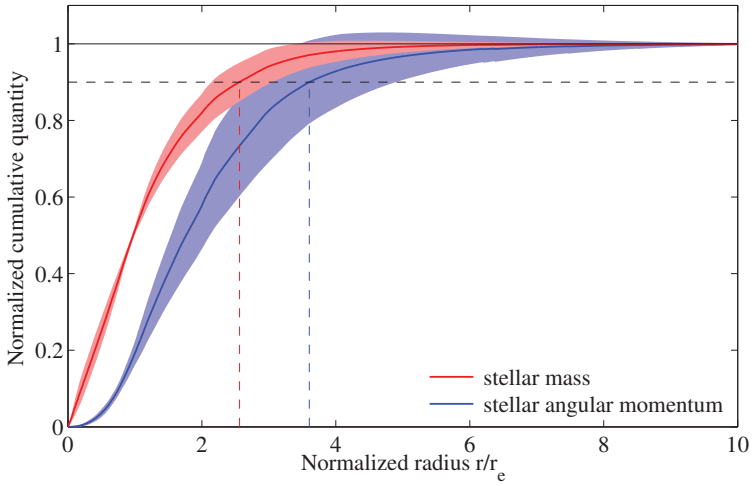

Figure 4: Cumulative mass (red) and angular momentum (blue) as a function of the normalised radius for 16 nearby disk galaxies of the THINGS survey (see Obreschkow & Glazebrook 2014 for details).

Method 2: Approximation (requiring global 21cm profiles and optical images)

If H I kinematic maps are unavailable, the simplest assumption to use is that galactic disks are objects rotating at constant velocity V with exponentially declining surface density of scale length R. In this model, the specific angular momentum is exactly $j = 2RV$ according to Equation (2.3). In practice, the scale radius $R_* \approx R_e/1.68$ of the stellar disk can be estimated from optical images, and for non-dwarf galaxies the asymptotic circular velocity (now considered the sole velocity) is well approximated as half the H I linewidth W_{50}, corrected for the inclination i. Thus,

$$j = R_* \, W_{50} \, \sin^{-1} i. \tag{2.4}$$

A detailed comparison of this approximation against high-precision measurements of the stellar j from the sub-kpc kinematic maps of the THINGS sample revealed that Eq. (2.4) recovers the 'true' j with an observational error of about 40% (standard deviation, see Section 2.4 in Obreschkow & Glazebrook 2014). Romanowsky & Fall (2012) demonstrated that this is just good enough to evidence a systematic angular momentum dependence of morphology within regular late-type galaxies. However, at this stage it is not yet clear to what extent this conclusion holds for galaxies with poorly defined or inexistent asymptotic velocities.

Method 3: Approximation (requiring global 21cm profiles and IFS velocity maps)

The biggest drawback of the approximation method 2 is that the errors of j are correlated with the stellar/baryon mass M as a result of the rotation curve shape being correlated to M (de Blok et al. 2008). To bypass this limitation, the assumption of a constant rotation velocity can be substituted for a variable velocity model $v(r) = V[1 - \exp(-r/R_{\rm flat})]$ (Boissier et al. 2003), where V now denotes the asymptotic velocity at large radii r, and $R_{\rm flat}$ is the scale-length of the rotation curve. Since most H I is generally situated at radii much larger than $R_{\rm flat}$, the velocity V remains well approximated by $V = \frac{1}{2} W_{50} \, \sin^{-1} i$ in this model. Convolving $v(r)$ with an exponential surface

PoS(AASKA14)138

density $\Sigma(r) \propto \exp(-r/R_*)$ in Equation (2.3), results in

$$j = R_* \, W_{50} \, \sin^{-1} i \, \frac{(1+x)^3 - 1}{(1+x)^3}. \tag{2.5}$$

This equation differs from Equation (2.4) by the right-most factor that depends on $x \equiv R_*/R_{\rm flat}$. Thus, this method requires a measurement of $R_{\rm flat}$, representing the characteristic scale of the inner part of the rotation curve. Velocity maps from optical IFS data are well-suited for this measurement, even if limited to radii of $1R_{\rm e} - 2R_{\rm e}$. Obreschkow & Glazebrook (2014) showed that Equation (2.5) increases the accuracy relative to Equation (2.4) by a factor $2-3$, to a relative error on j of $\sim 20\%$ with no significant correlation to M. Like in method 2, it is not yet fully established to what extent this method works for galaxies with poorly defined or inexistent asymptotic velocities, such as dwarfs.

3. Assessment of SKA Capabilities

3.1 Modelling of galaxies and detection rates

For the following performance calculations we draw a 100 deg^2 mock cone from the S^3-SAX simulation (Obreschkow et al. 2009a,b), truncated radially to redshifts below $z = 1.2$, the distance limit for H I set by the 650 MHz lower limit of SKA1-SUR band 2. This simulation is publicly available and has been verified against local observations in terms of the H I mass function (Obreschkow et al. 2009a), the H I velocity function (Obreschkow et al. 2013), the Tully-Fisher relation (Obreschkow et al. 2009a), and the H I large-scale clustering (Fig. 3).

A galaxy in the mock cone is considered detected sufficiently well to measure linewidths W_{50} if its peak flux density $s_{\rm peak}$ – the flux density at the horns of a typical H I profile – exceeds 5-times the RMS channel noise ($10\,{\rm km\,s^{-1}}$ channels in observer-frame). Out of all the galaxies detected in this sense, we determine the subsample for which a GAMA-like survey can detect and spatially resolve the optical counterparts to measure the disk radius and inclination. Explicitly, this subsample is defined by the additional selection criteria $m_{\rm R} < 20$ and $R_{\rm e} > 1''$. These are the minimal criteria required for an approximate angular momentum measurement via 'Method 2'. Tables 1–3 show the numbers of galaxies in this subsample, as well as their median redshift.

Of particular interest for angular momentum science are those galaxies with kinematic H I maps that are good enough to allow precision measurements of angular momentum via Method 1. Here, we say that a galaxy has a 'good kinematic map', if two criteria are met:

1. The H I-half-mass radius spans more than 5 synthesised beams, i.e. the H I disk is resolved in $\gtrsim 100$ beams. (Velocity measurements in 5 galactocentric rings are roughly the minimum requirement for a robust fit of kinematic models.)

2. The average flux per beam inside the H I-half-mass radius exceeds 10-times the RMS beam noise ($10\,{\rm km\,s^{-1}}$ channels). (This condition approximately corresponds to a 5-sigma column sensitivity limit of $2 \cdot 10^{20}\,{\rm cm^{-2}}$, although the exact value depends slightly on the H I surface density profiles of the galaxies detected in the respective survey scenarios.)

PoS(AASKA14)138

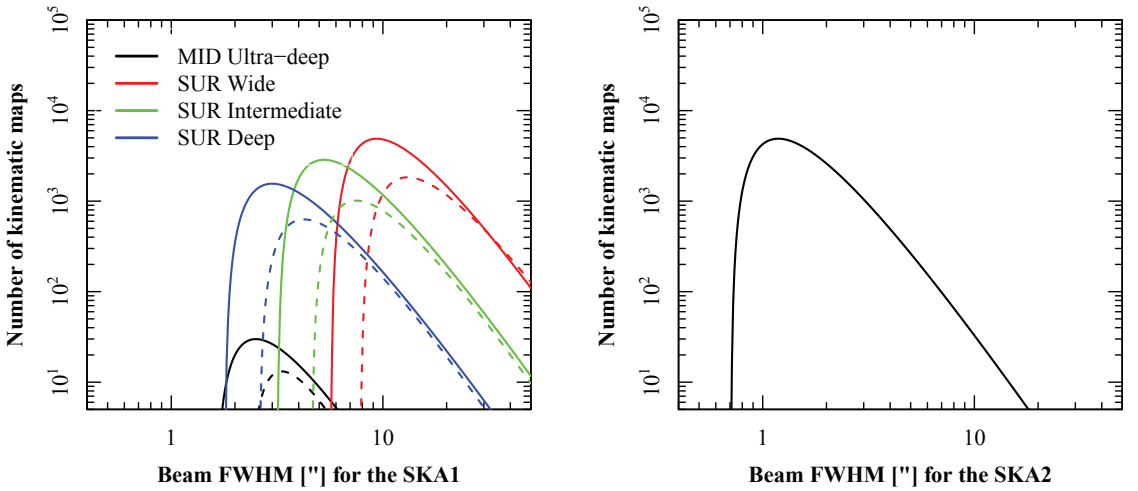

Figure 5: Number of galaxies with good kinematic H I maps (as defined in §3.1), as a function of the FWHM of the synthesised beam (pixel). The left panel represents the SKA1 (solid lines) and the Early phase 50% SKA1 (dashed lines); the right panel represent the SKA2. The competing criteria that galaxies must be spatially resolved, but still yield enough signal per pixel causes these functions to peak. The increased sensitivity of the SKA2 allows kinematic maps to be obtained for galaxies at greater distances, hence requiring smaller pixels. All these functions assume channels of $10\,\mathrm{km\,s^{-1}}$ (observer-frame) with an RMS noise per beam that is independent of the beam FWHM – an assumption that is approximately verified for the 'logarithmic' antenna distribution of the System Baseline Design.

This definition of a 'good kinematic map' ensures a measurement of the stellar/baryon specific angular momentum at less than 10% uncertainty (down to 3%-5% for THINGS-like quality), provided stellar surface density maps from optical imaging. A subtle aspect is the choice of the synthesised beam size (i.e. the weighting of the baselines). The resolution-criterion (1) favours small beams, whereas the signal/noise-criterion (2) demands large beams. To optimise the case, we have determined the number of good kinematic maps as a function of the beam FWHM (see Fig. 5). Table 1 shows the maximally achievable number of good kinematic maps and the corresponding beam FWHM. These FWHM are consistent with those found by De Blok et al. (2015) for a H I column sensitivity of $2\cdot 10^{20}\,\mathrm{cm^{-2}}$ (5-sigma level with $10\,\mathrm{km\,s^{-1}}$ channels).

3.2 SKA1

To predict the capabilities of the SKA1, as specified in the System Baseline Design (Dewdney et al. 2013), we adopt the reference survey scenarios considered at the H I Science Assessment Workshop (September 2013), but ignore the surveys dedicated to H I absorption and to the local ISM. Our sensitivity estimations build on a telescope simulation (described in Popping et al. 2015), assuming observations at a declination of $-30°$. The respective RMS noise levels per beam for an 8h integration with $10\,\mathrm{km\,s^{-1}}$ channels (observer-frame) are approximately 0.1 mJy (SKA1-MID) and 0.25 mJy (SKA1-SUR). These noise levels are reasonably constant ($\sim 50\%$ variations) across the ranges of frequency and beam size relevant to this analysis. The resulting sensitivities of the reference surveys are listed in Table 1.

PoS(AASKA14)138

Telescope	SKA1-MID	SKA1-SUR		
Survey mode	Ultra-deep 2000 h, 3 deg^2	Wide 2 yr, $3\cdot10^4$ deg^2	Intermediate 2 yr, $3\cdot10^3$ deg^2	Deep 2 yr, 300 deg^2
FoV [deg^2]	$0.49\cdot(1+z)^2$	18	18	18
Number of pointings	6	1,700	170	17
Effective int. time [h]	$330\cdot(1+z)^2$	10	100	1,000
Beam noise σ [mJy] at fixed rest-frame ΔV of 10 km s^{-1}	$0.016(1+z)^{-\frac{1}{2}}$	$0.22(1+z)^{\frac{1}{2}}$	$0.071(1+z)^{\frac{1}{2}}$	$0.022(1+z)^{\frac{1}{2}}$
Number of line detections, $S_{\rm int}>5\sigma$	22,000	6,000,000	2,500,000	1,100,000
Median z	0.25	0.06	0.11	0.19
Number of line detections, $s_{\rm peak}>5\sigma$	9,300	2,200,000	980,000	440,000
Median z	0.20	0.04	0.09	0.14
... $s_{\rm peak}>5\sigma$ and $m_{\rm R}<20,\ R_{\rm e}>1''$	2,100	1,800,000	650,000	160,000
Median z	0.19	0.04	0.09	0.16
Number of good kinematic maps	30	3,900	3,600	1,900
Optimal beam FWHM ["]	2.5	9.3	5.3	3.0

Table 1: Predicted capabilities of different reference surveys with the SKA1, as specified in the System Baseline Design (Dewdney et al. 2013). The reference survey scenarios are adopted from the H I Science Assessment Workshop (September 2013). The values chosen for the beam FWHM are the 'sweet spots', where the number of kinematic H I maps sufficient for a precision-measurement of j is maximal (see Fig. 5). For smaller synthesised beams, the signal per beam becomes so low that most kinematic maps are no longer useable, while larger synthesised beams lead to insufficient spatial resolution.

Table 1 confirms that wide-field surveys detect a larger number of sources than deep surveys. The wide-field survey with SKA1-SUR will increase both the number of global H I line detections and the number of 'good kinematic maps' by about two orders of magnitude with respect to the state-of-the-art (e.g. THINGS, HIPASS, ALFALFA). Explicitly, about 3,900 galaxies will be useable for a precision angular momentum measurement via method 1, while 1,800,000 galaxies will be useable for an approximate angular momentum measurement via method 2 – provided sufficient optical counterparts.

PoS(AASKA14)138

3.3 Early phase SKA1 (50% SKA1)

Table 2 shows the results for the same analysis as in §3.2, but assuming half the sensitivity for the SKA1. Halving the sensitivity of the SKA1 reduces the number of useable line detections, as well as the number of good kinematic maps by about a factor two, depending on the survey strategy.

Telescope	50%-SKA1-MID	50%-SKA1-SUR		
Survey mode	Ultra-deep 2000 h, 3 deg^2	Wide 2 yr, $3\cdot10^4$ deg^2	Intermediate 2 yr, $3\cdot10^3$ deg^2	Deep 2 yr, 300 deg^2
FoV [deg^2]	$0.49\cdot(1+z)^2$	18	18	18
Number of pointings	6	1,700	170	17
Effective int. time [h]	$330\cdot(1+z)^2$	10	100	1,000
Beam noise σ [mJy] at fixed rest-frame ΔV of 10 km s^{-1}	$0.031(1+z)^{-\frac{1}{2}}$	$0.45(1+z)^{\frac{1}{2}}$	$0.14(1+z)^{\frac{1}{2}}$	$0.045(1+z)^{\frac{1}{2}}$
Number of line detections, $S_{\rm int}>5\sigma$	9,600	2,400,000	1,100,000	440,000
Median z	0.19	0.04	0.09	0.13
Number of line detections, $s_{\rm peak}>5\sigma$	3,700	850,000	410,000	180,000
Median z	0.14	0.04	0.06	0.10
... $s_{\rm peak}>5\sigma$ and $m_{\rm R}<20,\ R_{\rm e}>1''$	1,500	740,000	320,000	99,000
Median z	0.16	0.04	0.06	0.11
Number of good kinematic maps	13	2,400	930	670
Optimal beam FWHM ["]	3.3	13	7.4	4.2

Table 2: Same as Table 1, but for the Early phase SKA1 (50% SKA1).

PoS(AASKA14)138

3.4 SKA2

Finally, we consider the SKA2, consisting of a MID array with 5-times[1] the sensitivity of SKA1-MID (above 350 MHz) and 20-times the instantaneous field-of-view (FoV). This results in a FoV of 9.8 deg^2 at $z = 0$, larger than the 3 deg^2 of the ultra-deep reference survey for SKA1-MID. Hence, we increase this survey area by a factor 20 to 60 deg^2. The fact that the SKA2 also allows much higher spatial resolution than SKA1-MID is relevant, since the analysis of the optimal beam size in Fig. 5 indeed favours SKA2 to work at higher spatial resolution than SKA1-MID to maximise the number of good kinematic H I maps.

Telescope	SKA2
Survey mode	Ultra-deep 2000 h, 60 deg^2
FoV [deg^2]	$9.8 \cdot (1+z)^2$
Number of pointings	6
Effective int. time [h]	$330 \cdot (1+z)^2$
Beam noise σ [mJy] at fixed rest-frame ΔV of 10 km s^{-1}	$0.0031(1+z)^{-\frac{1}{2}}$
Number of line detections, $S_{\rm int} > 5\sigma$	2,800,000
Median z	0.47
Number of line detections, $s_{\rm peak} > 5\sigma$	1,500,000
Median z	0.41
... $s_{\rm peak} > 5\sigma$ and $m_{\rm R} < 20,\ R_{\rm e} > 1''$	53,000
Median z	0.21
Number of good kinematic maps	5,700
Optimal beam FWHM ["]	1.2

Table 3: Same as Table 1, but for the SKA2.

[1]For SKA2, a sensitivity increase of a factor of 10 is assumed, but this refers to the natural sensitivity. A sensitivity loss of 50% has to be applied in addition due to the tapering used (see Braun, 2014, imaging document).

PoS(AASKA14)138

4. Discussion and Conclusions

This paper demonstrates that the SKA will be the *best* machine to conduct world-leading angular momentum science. In fact, kinematic H I maps from 21cm interferometry, combined with optical images, allow the specific angular momentum j of disks to be measured within 3%-5% uncertainty (Obreschkow & Glazebrook 2014) – the most accurate measurements to-date. It is important to emphasise that H I maps outperform optical IFS maps due to the fact that only H I (not stars) resides where most of the stellar/baryon angular momentum resides. This feature also allows us to measure j to a lesser precision from spatially unresolved H I emission lines combined with spatially resolved optical images.

Already the SKA1 will increase the number of kinematic H I maps, as well as the number of global H I line profiles useable for angular momentum measurements by two orders of magnitude compared to the state-of-the-art. It will be challenging to match the millions of unresolved H I detections with sufficiently many and sufficiently resolved optical counterparts. Our analysis suggests that a seeing-limited ($\sim 0.''5$ resolution) 3π-sky imaging+redshift survey at the depth of the GAMA survey provides enough optical counterparts to determine the specific angular momenta of millions of galaxies (using Method 2) and thousands of galaxies (using Method 1).

Some science examples enabled by angular momentum measurements with the SKA include

- a very robust determination of the two-dimensional distribution in the (M, j)-plane of galaxy samples with well-described completeness,
- the largest, systematic measurement of the relationship between M, j, and tertiary galaxy properties (morphology, gas fraction, depletion time),
- the most accurate measurement of the large-scale distribution, including environment-dependence, of angular momentum, both in terms of norm and orientation.

These examples are by no means exhaustive, but they are good illustrations of powerful future measurements to test and improve hydrodynamical simulations of galaxies and to build a next generation of models of galaxy evolution.

Acknowledgements

We thank the referees, Erwin de Blok and Paolo Serra, for very insightful and helpful comments.

References

Agertz, O., Teyssier, R., & Moore, B. 2011, MNRAS, 410, 1391
Boissier, S., Prantzos, N., Boselli, A., & Gavazzi, G. 2003, MNRAS, 346, 1215
Brooks, A. M., Solomon, A. R., Governato, F., *et al*. 2011, ApJ, 728, 51
Cappellari, M., Emsellem, E., Krajnović, D., *et al*. 2011, MNRAS, 413, 813

PoS(AASKA14)138

De Blok, W., Fraternali, F., Heald, G., *et al*. 2015, in "The SKA view of the Neutral Interstellar Medium in Galaxies" in proc. *Advancing Astrophysics with the Square Kilometre Array*, PoS(AASKA14)129

De Blok, W. J. G., Walter, F., Brinks, E., *et al*. 2008, AJ, 136, 2648

Dewdney, P., Turner, W., Millenaar, R., McCool, R., Lazio, J., Cornwell, T., 2013, "SKA1 System Baseline Design", Document number SKA-TEL-SKO-DD-001 Revision 1, SKA Organisation

Doyle, M. T. & Drinkwater, M. J. 2006, MNRAS, 372, 977

Fall, S. M. & Efstathiou, G. 1980, MNRAS, 193, 189

Glazebrook, K. 2013, Publications of the Astronomical Society of Australia, 30, 56

Governato, F., Brook, C., Mayer, L., *et al*. 2010, Nat, 463, 203

Guedes, J., Callegari, S., Madau, P., & Mayer, L. 2011, ApJ, 742, 76

Jones, B. J. T., van de Weygaert, R., & Aragón-Calvo, M. A. 2010, MNRAS, 408, 897

Leroy, A. K., Walter, F., Brinks, E., *et al*. 2008, AJ, 136, 2782

Mo, H. J., Mao, S., & White, S. D. M. 1998, MNRAS, 295, 319

Obreschkow, D., Croton, D., DeLucia, G., Khochfar, S., & Rawlings, S. 2009a, ApJ, 698, 1467

Obreschkow, D. & Glazebrook, K. 2014, Astrophys. J., 784, 26

Obreschkow, D., Klöckner, H., Heywood, I., Levrier, F., & Rawlings, S. 2009b, ApJ, 703, 1890

Obreschkow, D., Power, C., Bruderer, M., & Bonvin, C. 2013, ApJ, 762, 115

Popping, A., Meyer, M., Staveley-Smith, L., *et al*. 2015, in "Observations of the Intergalactic Medium and the Cosmic Web in the SKA era" in proc. *Advancing Astrophysics with the Square Kilometre Array*, PoS(AASKA14)132

Quinn, P. J. & Zurek, W. H. 1988, ApJ, 331, 1

Romanowsky, A. J. & Fall, S. M. 2012, ApJS, 203, 17

White, S. D. M. 1984, ApJ, 286, 38

PoS(AASKA14)138

PROCEEDINGS OF SCIENCE

The Physics of the Cold Neutral Medium: Low-frequency Carbon Radio Recombination Lines with the Square Kilometre Array

J. B. R. Oonk[*1,2], **L. K. Morabito**[1], **F. Salgado**[1], **M. C. Toribio**[2], **R. J. van Weeren**[3], **A. G. G. M. Tielens**[1], **and H. J. A. Röttgering**[1]

[1] *Leiden Observatory, Leiden University, PO Box 9513, NL-2300 RA Leiden, the Netherlands*
[2] *Netherlands Institute for Radio Astronomy (ASTRON), Postbus 2, NL-7990 AA Dwingeloo, the Netherlands*
[3] *Harvard-Smithsonian Center for Astrophysics, 60 Garden Street, Cambridge, MA 02138, USA*
E-mail: oonk@astron.nl

The Square Kilometre Array (SKA) will transform our understanding of the role of the cold, atomic gas in galaxy evolution. The interstellar medium (ISM) is the repository of stellar ejecta and the birthsite of new stars and, hence, a key factor in the evolution of galaxies over cosmic time. Cold, diffuse, atomic clouds are a key component of the ISM, but so far this phase has been diffcult to study, because its main tracer, the HI 21 cm line, does not constrain the basic physical information of the gas (e.g., temperature, density) well.

The SKA opens up the opportunity to study this component of the ISM through a complementary tracer in the form of low-frequency (<350 MHz) carbon radio recombination lines (CRRL). These CRRLs provide a sensitive probe of the physical conditions in cold, diffuse clouds. The superb sensitivity, large field of view, frequency resolution and coverage of the SKA allows for efficient surveys of the sky, that will revolutionize the field of low-frequency recombination line studies.

By observing these lines with the SKA we will be able determine the thermal balance, chemical enrichment, and ionization rate of the cold, atomic medium from degree-scales down to scales corresponding to individual clouds and filaments in our Galaxy, the Magellanic Clouds and beyond. Furthermore, being sensitive only to the cold, atomic gas, observations of low-frequency CRRLs with the SKA will aid in disentangling the warm and cold constituents of the HI 21 cm emission.

Advancing Astrophysics with the Square Kilometre Array
June 8-13, 2014
Giardini Naxos, Italy

[*] Speaker.

PoS(AASKA14)139

1. The cold neutral medium

The ISM is central to the evolution of galaxies as the birth site of new stars and the repository of processed stellar ejecta. Star formation slowly consumes matter from the ISM and later returns it to the ISM via winds and explosions, enriched by the nucleosynthetic products of stellar interiors. Over cosmic time, this constant recycling and enrichment drives galaxy evolution. Stars also control the radiative energy budget of the ISM and its emission characteristics. Photons from massive stars with energies above 13.6 eV ionize hydrogen creating HII regions. Less energetic photons couple to the gas through photoelectrons from large molecules and small dust grains that heat atomic gas in PhotoDissociation regions (PDRs) surrounding HII regions and – on a much larger scale – in diffuse interstellar clouds. Through their winds and explosions, stars also stir up the ISM dynamically, sweeping up gas and forming large bubbles. This injection of mechanical energy into the ISM is a source of turbulent pressure, supporting the gas disk and the clouds therein against galactic- and self-gravity. Radiative and mechanical interaction of stars with their environment results in a number of distinct phases in the ISM; e.g., a phase of cold, neutral atomic hydrogen – diffuse clouds or Cold Neutral Medium (CNM) – and a phase of warm, neutral atomic hydrogen – the Warm Neutral Medium (WNM).

Clearly, there is a complex feedback between stars and the ISM that determines the structure, composition, chemical evolution, and observational characteristics of the ISM in the Milky Way and other galaxies all the way back to the first galaxies. Understanding this interaction has to start with characterizing the phases of the ISM and linking these to stellar and galactic energy sources and physical processes that couple interstellar gas to the mechanical and radiative energy inputs from stars and the large scale motions in the galaxy.

Over the last decades, our understanding of the ISM and its role in the evolution of galaxies has increased dramatically, but in leaps, driven, in particular, by the opening up of new observational windows by unique observatories. While the molecular medium has been well characterized and its role in star formation is well documented, analyzing and interpreting the atomic phase from the HI 21 cm line data in terms of the density and temperature has been challenging and has sofar only be done in a very limited number of cases (e.g. Heiles & Troland 2003). The main difficulty here is to accurately separate the warm and cold components that both contribute to the observed HI 21 cm signal. A consequence of this is that the thermal balance of the cold, atomic ISM and its role in starformation is poorly understood.

A promising, complementary method is to observe low-frequency CRRLs. These CRRLs have been found to be a good tracer of cold atomic gas (e.g. Payne et al. 1989, Anantharamaiah et al. 1994, Kantharia & Anantharamaiah 2001, Anish-Roshi et al. 2001). Their observed properties, i.e. line strength and width, as a function of frequency provides a convenient method to determine the physical conditions of this gas. The unprecedented sensitivity and bandwidth of the SKA will revolutionize the field of low-frequency, i.e. $< 350\ MHz$, CRRLs. In Sect. 2 we give a brief overview of the current status of the field. In Sect. 3 we discuss the models necessary to interprete CRRL observations. In Sect. 4 we describe how SKA-LOW will impact and transform the field of low-frequency CRRL studies. We focus our discussion here on two prime targets, the Galactic center and the Magellanic Clouds. In Sect.'s 5 and 6 we discuss the capabilities of SKA-LOW in phase 1 and 2 respectively, and finally we present a brief summary in Sect. 7.

PoS(AASKA14)139

2. Low-frequency CRRLs

Radio recombination lines (RRL) result from atoms recombining with electrons in an ionised plasma and can broadly be separated in to two classes: discrete and diffuse (e.g. see Gordon & Sorochenko 2009 for a recent overview). Discrete RRLs from hydrogen (HRRL), helium (HeRRL) and carbon (CRRL) are typically observed above about 1 GHz. Here the RRL spectrum is dominated by HRRL and HeRRL lines that are found to be excellent tracers of the dense, warm, ionized gas (e.g. Palmer & Zuckerman 1966). Discrete RRLs are described in more detail by M. Thompson et al. (2015) and R. Beswick et al. (2015) in this volume.

In this chapter we focus on the lower-frequency, i.e. $<$350 MHz, diffuse RRLs. At these frequencies we predominantly observe RRLs from carbon and hydrogen (e.g. Konovalenko & Sodin 1981, Anantharamaiah 1985.). HeRRLs have not been detected at these frequencies. Recent overviews of low-frequency RRLs and the instruments that are able to observe them are given in Peters et al. (2011) and Gordon & Sorochenko (2009). Below we will briefly summarize the current status of low-frequency RRL observations.

2.1 Galactic CRRLs

Large-scale studies: A summary of CRRL observations below 200 MHz is presented in Peters et al. (2011). Two large-scale Galactic surveys below 200 MHz were done at 76 MHz (Erickson et al. 1995) and 34.5 MHz (Kantharia & Anantharamaiah 2001). These low-resolution (beam FWHM $\geq$2 deg) studies find that CRRL absorption is widespread throughout the inner Galatic plane with typical peak optical depths in the range 0.5×10^{-3} to 1×10^{-3} and typical line widths in the range 10 to 50 km/s. HRRLs were not detected by these surveys.

Two other low resolution (beam FWHM $\sim$2 deg) surveys were conducted near 330 MHz by Anantharamaiah (1985) and Roshi et al. (2000). These surveys also find widespread RRL emission, from hydrogen and carbon, in the inner Galactic plane with peak optical depths in the range -0.5×10^{-3} to -2×10^{-3} for HRRL and -0.5×10^{-3} to -1×10^{-3} for CRRL (the minus sign indicates emission). The CRRLs are found to have typical linewidths in the range 15-30 km/s, about a factor 2 narrower than the corresponding HRRLs with typical linewidths 30-60 km/s.

The broader HRRLs likely arise in the warm ionized medium (WIM) (e.g. Anantharamaiah 1985, Heiles et al. 1996, Anish-roshi et al. 2001, Kantharia et al. 2007). The CRRLs are more likely associated with the CNM as shown by their good correspondence with HI 21 cm absorption (e.g. Anish-Roshi et al. 2001, Anantharamaiah et al. 1994, Oonk et al. 2014). Theoretical models of CRRL emission are consistent with this picture (see Sect. 3).

Kantharia & Anantharamaiah (2001) made an attempt at modelling the large-scale CRRL emission by combining the above mentioned surveys. They found that the observed CRRLs are consistent with arising in the CNM. However, their analysis was limited by the low resolution, poor spatial overlap and narrow frequency sampling of these surveys. Especially the unknown beam dilution due to the low resolution affected their investigation. Higher spatial resolution observations are therefore essential to make further progress in this field.

Small-scale studies: The only source that has been studied with sufficient spatial resolution, spectral coverage and sensitivity to allow for detailed CRRL modeling are the cold clouds along the line

PoS(AASKA14)139

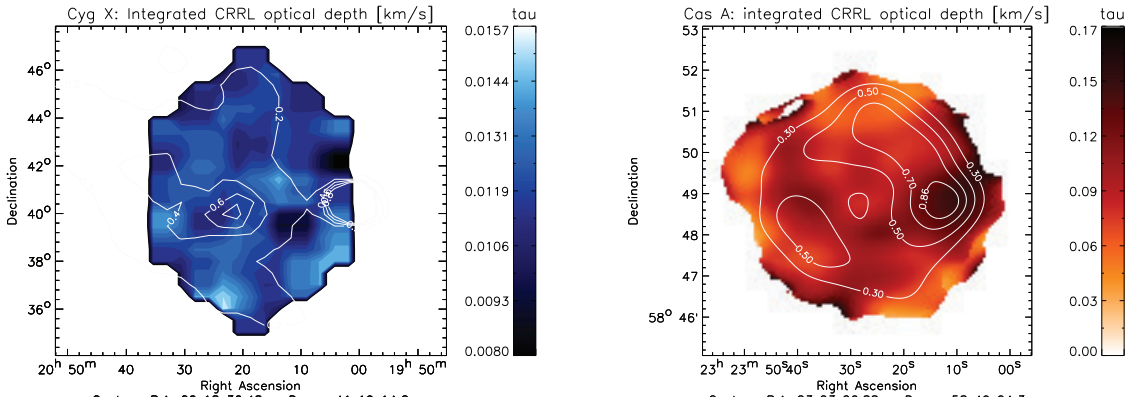

Figure 1: Observations of CRRL absorption in the Milky Way near 50 MHz (Oonk et al. in prep.). *(Left)* LOFAR 4 hr observation of degree-scale CRRLs in the Cygnus X region. Shown is a map of the integrated CRRL absorption in units of optical depth with radio continuum contours overlaid in white. The map shows structure down to the 1 degree limit of this observation. *(Right)* LOFAR 8 hr observation of arcmin-scale CRRLs along the line of sight to Cas A. Shown is a map of the integrated CRRL absorption in units of optical depth with radio continuum contours overlaid in white. The CRRL absorption is resolved in several filamentary structures that agree well with the corresponding HI 21 cm absorption (e.g. Bieging et al. 1991).

of sight towards Cassiopeia A (Cas A). The CRRLs towards this source can reach a peak optical depth of almost 10^{-2} (e.g. Kantharia et al. 1998). This is a factor of a few brighter than seen on large scales in other regions, although this could simply a consequence of the low spatial resolution used in the studies of these other regions. The CRRL line width observed towards Cas A varies from about 4 km/s at 350 MHz to about 10 km/s at 50 MHz (Payne et al. 1989; Oonk et al. in prep.).

Modeling shows that the CRRLs observed towards Cas A arise in the CNM (e.g. Payne et al. 1989; Kantharia et al. 1998). Cas A is an example of a bright Galactic source that can be used for detailed high-resolution CRRL 'pinhole' studies of the CNM. Similarly extragalactic sources can also be used to perform such pinhole studies, as shown by our recent detection of CRRL absorption from the Milky Way against the bright extragalactic source Cygnus A (Oonk et al. 2014).

With LOFAR we are conducting a Galactic survey to establish the physical scales on which CRRLs are present. Some preliminary results are shown in Fig. 1. These and previous observations show that CRRLs are widespread in our Galaxy with typical peak optical depths of a few times 10^{-4} to a few times 10^{-3} and typical line widths from a few to a few tens of km/s.

2.2 Extragalactic CRRL studies

The first detection of extragalactic low-frequency CRRLs has recently been achieved with LOFAR. In Morabito et al. (2014) we report CRRL absorption from M82 near 60 MHz with a peak optical depth of about 3×10^{-3} and we find a good correspondence with HI 21 cm absorption. This first detection shows the potential that with increasing sensitivity and bandwidth it is now becoming possible to detect CRRLs in other galaxies. In the upcoming years we will use LOFAR to carry out a flux limited, i.e. $F_\nu > 10$ Jy at 160 MHz, survey for extragalactic CRRLs. The primary aim of this survey will be to establish what type and fraction of bright extragalactic radio

PoS(AASKA14)139

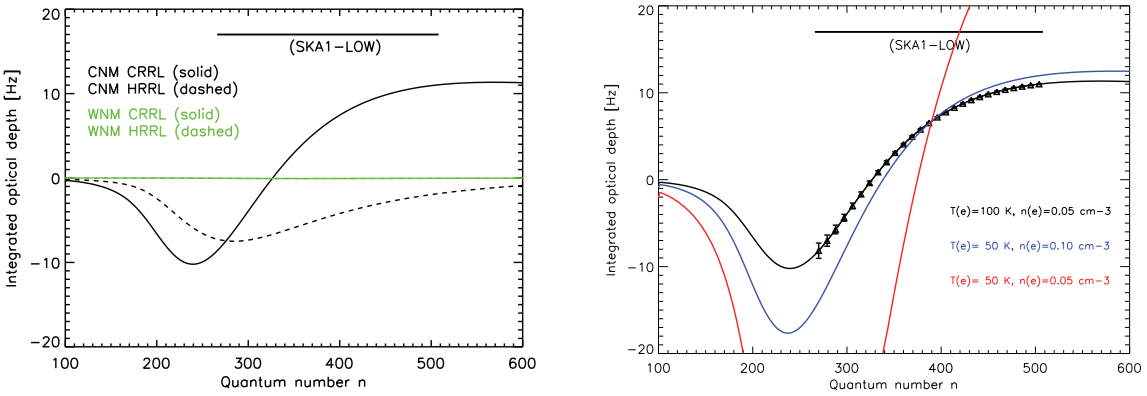

Figure 2: RRLs and the diffuse neutral ISM. Model results are given for the CNM (n_H=50 cm^{-3}, n_e=0.05 cm^{-3}, T_e=100 K) and WNM (n_H=0.1 cm^{-3}, n_e=0.01 cm^{-3}, T_e=10000 K). For both the CNM and the WNM a hydrogen column density N(HI)=10^{21} cm^{-2} is used.*(Left)* Integrated optical depth vs. quantum number for CRRL (solid) and HRRL (dashed) for the CNM (black) and WNM (green). The WNM optical depth is neglible and as such the HRRL and CRRL curves for the WNM overlap on this plot. *(Right)* The CRRL curve for the CNM model with error bars simulated for a 8 hr single pointing core SKA1-LOW observation in the inner Galactic plane with a continuum temperature of 140 K at 408 MHz. The integrated optical depth depends linearly on the column density. In red and blue we overplot two lower temperature models that are scaled to reproduce the optical depth for the black reference model at n=390.

sources show detectable CRRL signals and how the CRRLs compare to other properties of these systems.

3. CRRL models & methods

Low-frequency CRRLs originate in the partially ionized ($X_e \simeq 10^{-4}$), dense atomic phases of diffuse clouds and PDRs. This can be understood as singly ionized carbon has an ionization potential below that of hydrogen and this is therefore the dominant ionization state of carbon in the ISM. The observed properties of CRRLs, i.e. line strength and width, provide a convenient probe of the physical conditions of the gas. However, low-frequency CRRLs are not in local thermal equilibrium (LTE), and therefore non-LTE models are necessary to analyze the observations in terms of electron temperature, electron density and carbon column density (e.g. Shaver 1975; Brocklehurst & Salem 1977; Walmsley & Watson 1982; Ponomarev & Sorochenko 1992; Storey & Hummer 1995; Salgado et al. in prep.). A comprehensive literature exists on the topic of non-LTE models for low-frequency RRL emission and for further details we refer the interested reader to the above references and references therein. Here we show a few examples of such models in Fig. 2 and we briefly discuss how these models can be used to obtain the physical conditions of the CRRL emitting gas.

Electron temperature and density: The optical depth of CRRLs is affected by departure coefficients from LTE. For a given temperature T_e and density n_e these coefficients trace out a unique curve as function of frequency (or equivalently quantum number n), see Fig. 2. Therefore by measuring the CRRLs over a range of frequencies and comparing with models we can obtain T_e and n_e

PoS(AASKA14)139

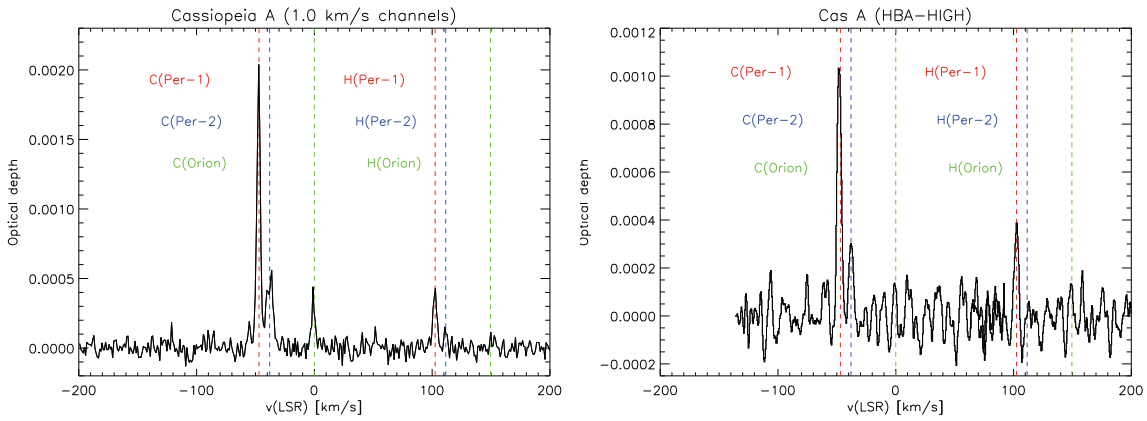

Figure 3: LOFAR and WSRT observations of CRRL and HRRL emission in the cold clouds towards Cas A. *(Left)* WSRT 12 hr 350 MHz observation. The RRL spectrum showing matching narrow HRRL and CRRL emission. For both the WSRT and LOFAR spectrum the velocity scale has been centered on the local standard rest for CRRLs. on this scale the corresponding HRRLs are offset by +150 km/s. *(Right)* LOFAR 3 hr HBA-HIGH observation at 220 MHz. This spectrum was obtained using only the LOFAR core stations. The HRRLs in both the LOFAR and WSRT spectra are likely associated with hydrogen that has been ionized by cosmic rays and the HRRL/CRRL ratio implies a cosmic ray hydrogen ionization rate $\zeta_H \sim 10^{-16}$ s^{-1} (Oonk et al. in prep.).

(e.g. Kantharia et al. 1998). Additional constraints on both of these parameters can be obtained by measuring how the pressure broadening affects the line width of the CRRLs (e.g. Kantharia et al. 1998; Oonk et al. 2014).

Thermal pressure: Once the electron temperature and density of the CRRL emitting gas has been obtained one can estimate the associated thermal pressure by invoking a carbon to hydrogen abundance [C/H]. The thermal pressure is then given by $p_{th} \sim n_e \times T_e$/[C/H] (e.g. Payne et al. 1989, Kantharia et al. 1998).

Carbon abundance: A systematic uncertainty in deriving hydrogen densities from CRRLs and thus thermal pressures is related to the carbon abundance [C/H]. Typically [C/H] has an uncertainty of about a factor 2 in our Galaxy. However, [C/H] can be determined by comparing, for the same line of sight, the carbon column density obtained from CRRLs with the cold hydrogen column density obtained from HI 21 cm absorption studies.

WNM to CNM fraction: Fig. 2 shows that low-frequency CRRLs only trace cold, atomic gas, i.e. the CNM. This means that CRRLs can be used as a tracer of this phase in terms of temperature and distribution. To also obtain the hydrogen density it is necessary to invoke a carbon to hydrogen abundance [C/H]. A Galactic [C/H] grid can be created by comparing CRRL and HI 21 cm absorption measurements (e.g. this work; McClure-Griffiths et al. 2015 in this volume). If [C/H] does not vary strongly between the HI 21 cm absorption measurements then the CRRLs can be used to also determine the CNM hydrogen density between absorption measurements.

WWW

Hydrogen ionization: Hydrogen in diffuse clouds can only be ionized through cosmic rays. Therefore the HRRL to CRRL ratio, if they measure the same gas, is a measure of the cosmic ray

PoS(AASKA14)139

ionization rate (e.g. Sorochenko & Smirnov 1987). Recently, using observations from the WSRT at 350 MHz and LOFAR at 220 MHz, we have found a weak, narrow HRRL component in the cold clouds towards Cas A. These HRRLs have the same width and velocity as the corresponding CRRLs indicating that the arise from the same gas and thus can be used to determine the hydrogen ionization rate, see Fig 3.

4. Square Kilometre Array

The properties of the low-frequency CRRLs discussed in Sect. 2 & 3 show that these originate in the CNM where they are associated with cold, diffuse clouds and PDRs. Here we propose to use SKA-LOW to perform a survey of Carbon Radio Recombination Lines (CRRLs) originating from cold atomic gas in diffuse interstellar clouds and in PDRs associated with regions of massive star formation in the Milky Way as well as with AGN and starburst activity in other galaxies. This CRRL survey can help answer a number of important open questions related to the ISM, such as;

(1) What is the morphology of CRRL emitting regions and how do they relate with the neutral, molecular, star forming and hot gas, as well as the large-scale structure of the Milky Way?

(2) What is the thermal, pressure balance for cold, diffuse clouds?

(3) What is the C abundance in the diffuse gas and how does this vary with galactic radius?

(4) What is the ionization rate for the cold ISM?

(5) What are the physical conditions of the cold, atomic gas in other galaxies and how do these compare to other properties like jets, winds, and stellar, molecular & dust mass?

Instead of attempting to summarize here all of the possible science topics that can be pursued with CRRLs and the many interesting regions that can be investigated we have chosen to limit our discussion in this section to two prime targets in the southern hemisphere, the Galactic center and the Magellanic clouds. In the Sect.'s 5 and 6 we will then discuss the technical details for studying these objects with SKA-LOW in phase 1 and phase 2.

SKA & Galactic Center. The center of the Milky Way shares many properties with other, often more spectacular nuclei of galaxies. Indeed, at a distance of only 8 kpc, the nucleus of our galaxy is a unique laboratory for studies of global phenomena – e.g., accretion, mass flow, star formation – and the physical and chemical conditions and the micro-physics processes at work in the interstellar medium in the nuclei of galaxies. The few parsecs surrounding the massive black hole in the center of our Milky Way contain a dense and luminous star cluster, as well as various components of neutral, ionized and hot gas.

The central parsec region contains mostly ionized gas (the HII region Sgr A West) and hot, X-ray emitting gas. This low density, ionized 'central cavity' is pervaded by a set of orbiting ionized gas filaments, which in turn are surrounded by orbiting, dense molecular cloud streamers at $\sim$1.5 to

PoS(AASKA14)139

4 pc (the circum-nuclear disk). The outer edge of the circum nuclear disk is bordered by the young supernova remnant, Sgr A East, and surrounded by a number of dense molecular clouds on a scale of 5 to 100 pc (see the reviews by Genzel et al. 2010; Morris & Serabyn 1996, and references therein). This central molecular zone is embedded in a more extensive HI nuclear disk. The high surface density and total mass content likely reflect inflow from larger radii.

Because of the high pressures and strong tidal shearing effects, the average properties of the molecular clouds in the Galactic Center differ significantly from those in the outer Galaxy with elevated gas temperatures, high average densities and strong turbulent velocity fields. Magnetic fields with mG field strength have been reported, that – at least locally – control the dynamics of the gas. A number of gas heating mechanisms are important in this nuclear environment including far-UV radiation emitted by the OB stars near the center responsible for the HII regions and the surrounding photo-dissociation regions at the edges of the cavities blown by the hot stars. Clouds compressed at the edges of the expanding bubbles are shock heated. The dense gas phase in shielded cloud cores is heated by turbulent dissipation and magnetic viscous heating. The interrelationship of these structures and the processes that drive them will be an important testbed for our general understanding of what drives the evolution of galactic nuclei.

Low-frequency CRRLs can provide a unique information on the central region of our galaxy specifically on the physical conditions in and the dynamics of the dense photodissociation regions that separate the ionized and molecular gas (Wyrowski et al. 1997, 2000; Natta et al. 1994). On a larger scale, the carbon radio recombination lines can probe the interrelationship of the molecular gas and the wider atomic H layer.

The Magellanic Clouds. The Large Magellanic Cloud (LMC) and Small Magellanic Cloud (SMC) are irregular galaxies in orbits around the Milky Way that have experienced several tidal encounters with each other and with the Galaxy. The Large Magellanic Cloud contains a bright stellar bar which together with regions of star formation and the patchy dust obscuration dominates its optical appearance. In HI, on scales of 15 to 500 pc, the morphology is dominated by HI filaments with numerous shells and holes. The turbulent and fractal nature of the ISM on these scales is the result of dynamical feedback into the ISM from star formation processes. On larger scales, (200 pc to 10 kpc), the HI distribution is very patchy. The reduced metallicity implies lower dust shielding and higher photodissociation rates. Hence, the Magellanic Clouds are a more hostile environment for molecular gas. Indeed, while – because of self-shielding – much of the hydrogen may be in molecular form in the clouds, carbon may be largely in the form of C^+. In general, this so-called CO-dark gas may be an important reservoir of gas in low metallicity environments.

The LMC is home to the most luminous and best known massive star-forming region in the Local Group, the Tarantula nebula, powered by the super star cluster 30 Dor, which contains some 1000 bright O stars. The Magellanic Clouds serve as excellent laboratories for the study of the process of star formation in an environment that, in many ways (such as metallicity, dust content, and star formation rate), resembles the extreme conditions of the early universe and distant star-forming regions.

The LMC and SMC are also excellent astrophysical laboratories for studying the life cycle of the interstellar medium (ISM). Located at 50 and 60 kpc, their proximity permits detailed studies of resolved ISM clouds and their relation to stellar populations on global scales, which in the

PoS(AASKA14)139

MilkyWay are obfuscated by line-of-sight crowding and distance ambiguity. The SMC and LMC (and Milky Way) span an interesting range in their global properties (metallicity, molecular gas content, and gas-to-dust ratio) that make them interesting testbeds for galaxy evolution studies. In terms of galaxy evolution, the LMC–SMC pair is well suited for studying how the agents of evolution, the ISM and stars, operate as a whole in two galaxies that are tidally interacting with each other and with the Milky Way.

Low frequency carbon recombination lines will provide a unique tool specifically geared towards tracing CO-dark gas and its relationship to, on one hand, HI clouds and molecular gas and, on the other hand, the regions of active star formation. In addition, CRRLs can be used to study the physical conditions in the photodissociation regions associated with regions of massive star formation. In particular, the 30 Dor region will allow a study of the characteristics of PDRs in a super star cluster environment. Finally, we like to highlight that the many bright HII regions and supernova remnants will provide convenient bright background sources for detailed studies of the carbon and hydrogen recombinations that can probe the cosmic ray ionization rate on a galaxy-wide scale and relate them to their likely sources.

5. SKA Phase 1

The technical details of SKA-LOW in phase 1, SKA1-LOW, are described in the SKA1 Imaging Science Performance document (hereafter SKA1-ISP) by R. Braun. SKA1-LOW provides an increase in sensitivity, relative to its precursors and pathfinders, by up to 2 orders of magnitude. The proposed configuration offers a dense core, with a filling factor close to unity. Outside the core the stations are arranged in three outwards extending spiral arms. The core dominates the angular resolution versus sensitivity and the sweetspot is in range 1-5 arcmin at 140 MHz. SKA1-LOW will have a large bandwidth from 50-350 MHz where up to 243 α-transition CRRLs (n=266-508) can be observed simultaneously. Comparing with the models in Fig. 2 shows that this range is well suited to study the low density, low temperature CRRL emitting gas.

Galactic survey. The overall goal of a Galactic CRRL survey with SKA1-LOW is to determine the physical conditions of the cold, diffuse clouds and their role in the process of starformation in the inner Galactic plane (l<50 deg, b<|5| deg). In Sect. 2 we showed that, at frequencies below 350 MHz, on degree-scales Galactic CRRLs have typical line widths in the range from 10 to 50 of km/s and typical peak optical depths in the range of a few times 10^{-4} to a few times 10^{-3}.

Table 1 shows that upon stacking the CRRLs in sets of 9 lines that the SKA1-LOW sensitivity in 8 hours with 1 kHz resolution is sufficient to detect CRRLs down to a peak optical depth level of $\sim 10^{-4}$ throughout the entire inner Galactic plane on scales from 1.5 arcmin at 350 MHz to 10 arcmin at 50 MHz. The arcmin-scale resolution is well suited to study the cold, diffuse clouds in the Milky Way and the peak optical depth limit corresponds to a HI column density of about 1×10^{20} cm^{-2}.

Stacking CRRLs in sets of 9 does not affect our science goals as the lines are spaced very closely. In this way we obtain 27 stacked CRRL α transition measurements for each line of sight across the full frequency range. In Fig. 2 we give an example of what such a measurement with SKA1-LOW simulated noise could look like. The poorest sensitivity, in units of optical depth, is

PoS(AASKA14)139

Frequency	$\sigma_{T,rms,extended}$	$\tau_{T,peak,extended}$	$\sigma_{\nu,rms,point}$	$F_{\nu,point}$
[MHz]	[mK]	$\times(10^{-4})$	[mJy]	[Jy]
60	980	(0.5-0.05)	1.9	1.9
160	140	(1.0-0.10)	0.4	0.4
220	140	(2.1-0.21)	0.2	0.2
350	154	(7.5-0.75)	0.2	0.2

Table 1: CRRL sensitivity with SKA1-LOW. Column (1) Observing frequency. Column (2) Core SKA1-LOW 5σ spectral sensitivity for extended sources, in units of mK, for an effective baseline B_{eff}=2 km with 1 kHz channels, 8 hr integration and stacking 9 lines. Column (3) Corresponding 5σ peak optical depth range for extended sources. These ranges are calculated for the inner Galactic plane with continuum temperatures between 140 and 1400 K at 408 MHz (Haslam et al. 1982) and using a $\lambda^{2.5}$ scaling (e.g. Rogers et al. 2008). Column (4) Full SKA1-LOW 5σ point source spectral sensitivity, in units of flux, for 30 km/s channel width, 8 hr integration, 200 arcsec FWHM beam and stacking 9 lines. Column (5) Corresponding limiting point source continuum flux $F_{\nu,lim}$ to obtain a 5σ CRRL detection with τ_{peak}=10^{-3}. Comparing to the S3 simulation (Wilman et al. 2008) and the 7C survey (Riley et al. 1999) shows that on average there are about 5 extragalactic sources per deg^2 brighter than these limiting fluxes. For both the extended and point source cases SKA1-LOW is typically about a factor 10 more sensitive than LOFAR at 160 MHz and a factor 100 more sensitive than LOFAR at 60 MHz. The above sensitivities are derived from the SKA-ISP document.

obtained at 350 MHz. However, by convolving the higher frequency maps to the spatial resolution of the lowest frequency maps at 50 MHz the noise will be similar at all frequencies. By comparing the SKA1-LOW noise levels with our models this means that we can determine the electron temperature and density on arcmin-scales in diffuse clouds to better than a factor 2 down to a limiting HI column density of about 1×10^{20} cm^{-2}.

Additional constraints on the electron temperature and density of the cold gas can be obtained from the CRRL line width (e.g. Kantharia et al. 1998). However, the currently planned 1 kHz channel width in phase 1 is not sufficient to resolve the narrowest CRRLs measured towards Cas A (e.g. Fig. 3; Payne et al. 1989) and Cygnus A (Oonk et al. 2014). To resolve these lines would require a channel width of about 0.3 kHz.

A 500 deg^2 survey of the inner Galactic plane requires 13 pointings at 50 MHz and 500 pointings at 350 MHz. For 8 hr pointings this would take about 10^2 hrs at 50 MHz and 4×10^3 hrs at 350 MHz and is therefore limited by the small field of view at 350 MHz. If a beamformer becomes part of the SKA1-LOW design this time requirement can be reduced by scanning the sky in smaller frequency chunks with more beams.

One of the prime targets of a Galactic CRRL survey with SKA1-LOW is the Galactic center. At the distance of the Galactic center (8 kpc) the 1.5 arcmin resolution at 350 MHz means that we can resolve CRRL emitting structures down to 4 pc at 350 MHz. To study the physical properties of these structures we are limited to the 10 arcmin resolution at 50 MHz corresponding to about 25 pc. This means that in phase 1 we can study the interaction of the molecular gas with the wider atomic H layers. Smaller scale structures such as the PDRs and the HI nuclear disk require the capabilities of SKA-LOW in phase 2.

To derive the carbon abundance and convert our carbon column densities to hydrogen column densities we aim to combine our CRRL measurements with the planned Galactic HI absorption grid

PoS(AASKA14)139

survey, see McClure-Griffiths et al. (2015) in this volume. We estimate that this can be done on average in the Galactic plane for about 5 extragalactic background sources per deg^2 (e.g. Wilman et al. 2008; Riley et al. 1999). This number should be considered a lower limit for measuring the carbon abundance in the galactic center given the many bright Galactic radio sources that are located in this region and which can also be used for this purpose.

The models in Fig. 2 and the Cas A spectra in Fig. 3 show that with with the spatial resolution and sensitivity of SKA1-LOW it should be possible to detect the narrow HRRL component from diffuse clouds and separate it from the broader HRRL components associated with the WIM. The models show that this is best done at higher frequency range of SKA1-LOW. In combination with the corresponding CRRLs this will allow us to determine the hydrogen ionization rate due to cosmic rays in these clouds. Presently, this rate in the CNM has only been measured through molecular observations in the infrared or submillimeter (e.g. Indriolo et al. 2007; Shaw et al. 2008). However, these observations have been limited to a small number of bright sources and the analysis is hampered by the complex molecular physics involved. Cosmic ray ionization, especially in the Galactic center, may play an important role in heating of diffuse clouds.

Extragalactic survey. The overall goal of an extragalactic CRRL survey with SKA1-LOW is to determine the presence of CRRLs in other galaxies and use these lines to trace the physical conditions of the CNM in these objects. Our CRRL models show that we can expect a peak optical depth of about 10^{-3} for a HI column density of about 10^{21} cm^{-2} (Salgado et al. in prep.). This is consistent with our recent detection of CRRLs in M82 (Morabito et al. 2014). Furthermore the known frequency spacing of RRLs can be used to determine redshifts for extragalactic objects. This is particularly useful for those optically faint objects where it is difficult to identify the HI 21 cm line.

Table 1 shows that upon stacking the CRRLs in sets of 9 lines that the limiting point source sensitivity is about 0.4 Jy at 160 MHz for an 8 hr observation with SKA1-LOW and a resolution of about 3 arcmin. A 2π sr survey to this depth would enable a CRRL search in up to 10^5 galaxies, spanning a redshift range from z=0 to 5 (Wilman et al. 2008). This sample size would represent an increase of almost 3 orders magnitude relative to our planned LOFAR survey.

The time requirement for such a 2π sr survey varies between 4×10^3 hrs at 50 MHz and a staggering 1.6×10^5 hrs at 350 MHz. At the high frequencies this is clearly too long to be realistic. If a beamformer becomes part of the SKA1-LOW design then these time requirements can be reduced significantly. Alternatively, one could first perform a blind CRRL detection survey near 100 MHz and then only follow-up the detected galaxies with wider frequency coverage using pointed observations.

Of particular interest in an extragalactic SKA1-LOW survey are nearby galaxies. We estimate that for 8 hr integrations about 400 nearby galaxies are bright enough to be detected CRRLs and that in about 100 of these the CRRLs can be spatially resolved (e.g. Israel 1990, Negrello et al. 2013). A pointed survey for nearby galaxies over the full frequency range would therefore take about 4×10^3 hrs.

Two prime targets in a nearby galaxy survey are the Magellanic Clouds. They contain large quantities of cold, atomic gas (e.g. Stanimirovic et al. 1999; Dickey et al. 2000) and have a 408 MHz background radio continuum temperature of about 30-120 K with an approximate $\lambda^{2.6}$

PoS(AASKA14)139

scaling to lower frequencies (Haslam et al. 1982; Israel et al. 2010). Table 1 then shows that in an 8 hr single pointing we can reach peak optical depths of few times 10^{-3} at 350 MHz to a few times 10^{-4} at 60 MHz. This is suffienct to detect CRRLs for hydrogen column densities down a few times 10^{20} cm^{-2} on 10 arcmin scales.

At the distance of the Magellanic Clouds a 10 arcmin scale corresponds to 200 pc. This means that we will be able to resolve the CRRLs associated with larger scale patchy HI distribution and HI supershells. The smaller scale HI shells and PDRs require the capabilities of SKA-LOW in phase 2. Just as for the inner Galactic plane survey we estimate there are on average 5 extragalactic background sources per deg^2 for which HI 21 cm absorption and CRRL measurements can be compared to derive the carbon abundance in these systems.

5.1 SKA Phase 1: Early science

For early science (ES) it is expected that SKA1-LOW will have about half of its final sensitivity. The CRRL science that can be done during ES depends the array configuration. If the filling factor of core of the array during ES remains similar to that of the final array configuration then the inner Galactic plane survey, as outlined above, can be carried out. Given the high HI column densities and high background continuum radiation the survey can then start at the Galactic center during ES and progress outwards in Galactic longitude as the array builds up to its full phase 1 sensitivity.

For an extragalactic CRRL survey the lower sensitivity during ES has different effects for different source populations. For the bright, distant FR I and FR II radio galaxies the number of objects that can be searched for CRRLs down to a peak optical depth of 10^{-3} decreases with about a factor of two (Wilman et al. 2008). For nearby galaxies the effect is more severe. We estimate a decrease by about a factor 4, such that at most 100 nearby galaxies are bright enough to be searched for CRRLs and that only about 20 of these are sufficiently bright and large that the CRRLs within can be spatially resolved (Negrello et al. 2013, Israel et al. 1990).

For the Magellanic Clouds the lower sensitivity during early science will primarily affect the limiting column density. Therefore for a fixed observing time of 8 hrs per pointing we will start to miss the more diffuse clouds starting at a HI column density of about 5×10^{20} cm^{-2}.

6. SKA Phase 2

In phase 2 SKA-LOW is expected to have 4 times the sensitivity of SKA1-LOW over a wide range of angular scales and up to 20 times the angular resolution. For both a Galactic and an extragalactic survey this increase in resolution is very important. In the Galactic center we will be able to spatially resolve the HI nuclear disk and connect its kinematical and thermal properties to that of wider inflow of cold gas. Similar this increase in resolution is essential to spatially resolve PDRs and HI shells, as tracers of stellar feedback, over a wide range of environments in both our own Galaxy and the Magellanic Clouds.

For a larger extragalactic survey the increased sensitivity and resolution of SKA-LOW in phase 2 would allow us spatially resolve CRRLs in up to 3×10^3 nearby galaxies and search for CRRLS in up to half a million $>$0.1 Jy radio sources spanning a range in redshift from z=0 to 5. This will provide important input on how the physical properties of the CNM evolve with time and

PoS(AASKA14)139

environment. If redshift information is available then the average CNM properties for well-defined samples of even fainter radio sources can be studied by employing stacking techniques.

7. Summary

SKA observations of low-frequency CRRLs, in combination with HI 21 cm absorption measurements, will provide a comprehensive and unprecedented inventory of the low-density, cold ISM in our Galaxy, the Magellanic Clouds and beyond. This will enable us to quantify its role in the overall pressure, mass and energy balance of the interstellar medium and how it relates to the cycles of star formation and death.

In addition, for studies of the Epoch of Reionization and the HI dark ages it is important to quantify the distribution of the Milky Way CNM, in terms of strength and velocity, as a potential foreground signal. Deep, high spectral resolution, low-frequency RRL observations with SKA-LOW can help provide this quantification and by doing this with the same instrument at the same frequencies one can minimize the uncertainties due to instrumental systematics and extrapolation from higher to lower frequencies.

In order to spectrally resolve CRRLs associated with the coldest, atomic gas structures on small scales a channel width of about 0.3 kHz will be required, instead of the 1 kHz that is currently planned in the SKA1 design. Another important element that could significantly speed up large low-frequency surveys is a beamformer. The change in field of view with frequency for SKA-LOW means these surveys can be done much more efficiently by trading bandwidth against beams.

References

Anantharamaiah, K. R. 1985, JApA, 6, 177
Anantharamaiah, K. R., Erickson, W. C., Payne, H. E, et al., 1994, ApJ, 430, 682
Asgekar, A., Oonk, J. B. R., Yatawatta, S., et al., 2013, A&A, 551L, 11
Anish Roshi, D., Kantharia, N. G., Anantharamaiah, K. R., 2001, arXiv:astro-ph/0110121
Beswick, R., Brinks, E., Pérez-Torres, M.A., et al., 2015, "SKA studies of nearby galaxies: star-formation, accretion processes and molecular gas across all environments", in proc. *Advancing Astrophysics with the Square Kilometre Array*, PoS(AASKA14)070
Bieging, J. H, Goss, W. M., Wilcots, E. M., 1991, ApJ, 379, 271
Braun R., 2013, SKA1 Imaging Science Performance (SKA1-ISP)
Brocklehurst M., Salem M., 1977, CoPhC, 13, 39
Erickson, W. C., McConnell, D., Anantharamaiah, K. R., 1995, ApJ, 454, 125
Dickey, J. M., Mebold, U., Stanimirovic, S., et al., 2000, ApJ, 536, 756
Genzel, R., Eisenhauer, F., Gillessen, S., 2010, RvMP, 82, 3121
Gordon, M. A., Sorochenko, R. L., 2009, Radio Recombination Lines, Springer
Haslam, C. G. T., Salter, C. J., Stoffel, H., et al., 1982, A&AS, 47, 1
Heiles, C., Reach, W. T., Koo, B.-C., 1996, ApJ, 466, 191
Heiles, C., Troland, T. H., 2003, ApJS, 145 329
Indriolo, N., Geballe, T. R., Oka, T., et al., 2007, ApJ, 671 1736
Israel, F. P., Mahoney, M. J., 1990, ApJ, 352, 30

PoS(AASKA14)139

Israel, F. P., Wall, W. F., Raban, D., et al., 2010, A&A, 519, 67
Kantharia, N. G., Anantharamaiah, K. R., Payne, H. E., 1998, ApJ, 506, 758
Kantharia, N. G., Anantharamaiah, K. R., 2001, JApA, 22, 51
Kantharia, N. G., Goss, W. M., Roshi, D. A., Mohan, N. R., Viallefond, F., 2007, JApA, 28, 41
Konovalenko, A. A., Sodin, L. G., 1980, Nature, 283, 360
McClure-Griffiths, N. M., Stanimirović, S., Murray, C.E., et al., 2015, "Galactic and Magellanic Evolution with the SKA", in proc. *Advancing Astrophysics with the Square Kilometre Array*, PoS(AASKA14)130
Morabito, L. K., Oonk, J. B. R., Salgado, F., et al., 2014, ApJ, 795L, 33
Morris, M., Serabyn, E., 1996, 1996, ARA&A, 34, 645
Natta, A., Walmsley, C. M., Tielens, A. G. G. M., 1994, ApJ, 428, 209
Negrello, M., Clemens, M., Gonzalez-Nuevo, J., et al., 2013, MNRAS, 429, 1309
Oonk, J. B. R., van Weeren, R. J., Salgado, F., et al., 2014, MNRAS, 437, 3506
Palmer, P., Zuckerman B., 1966, Nature, 209, 1118
Payne, H. E., Anantharamaiah, K. R., Erickson, W. C., 1989, ApJ, 341, 890
Peters, W. M., Lazio, T. J. W., Clarke, T. E., et al., 2011, A&A, 525, 128
Ponomarev, V. O., Sorochenko, R. L., 1992, SvAL, 18, 215
Riley, J. M. W., Waldram, E. M., Riley, J. M., 1999, MNRAS, 306, 31
Rogers, A. E. E., Bowman, J. D., 2008, AJ, 136, 641
Roshi, D. Anish; Anantharamaiah, K. R., ApJ, 535, 231
Shaver, P. A., 1975, Pramana, 5, 1
Shaw, G., Ferland, G. J., Srianand, R., et al., 2008, ApJ, 675, 405
Sofia, U. J., Cardelli, J. A., Guerin, K. P., et al., 1997, ApJ, 482, L105
Sorochenko R. L., 1989, AN, 310, 389
Sorochenko R. L., Smirnov G. T., 1987, SvAL, 13, 77
Stanimirovic, S., Staveley-Smith, L., Dickey, J. M., et al., 1999, MNRAS, 302, 417
Storey, P. J., Hummer, D. G., 1995, MNRAS, 272, 41
Thompson, M. A., Beuther, H., Dickinson, C., et al., 2015, "The ionised, radical and molecular Milky Way: spectroscopic surveys with the SKA", in proc. *Advancing Astrophysics with the Square Kilometre Array*, PoS(AASKA14)126
Walmsley, C. M., Watson, W. D., 1982, ApJ, 260, 317
Wilman, R. J., Miller, L., Jarvis, M. J., et al., 2008, MNRAS, 388, 1335
Wyrowski, F., Walmsley, C. M., Goss, W. M., Tielens, A. G. G. M., 2000, ApJ, 543, 245
Wyrowski, F., Schilke, P., Hofner, P., Walmsley, C. M., 1997, ApJ, 487L, 171

PoS(AASKA14)139

The Transient Universe

PROCEEDINGS OF SCIENCE

Transient Astrophysics with the Square Kilometre Array

Rob Fender*
Oxford Astrophysics
E-mail: rob.fender@astro.ox.ac.uk

Adam Stewart
Oxford Astrophysics
E-mail: adam.stewart@astro.ox.ac.uk

Jean-Pierre Macquart
ICRAR/Curtin
E-mail: J.Macquart@curtin.edu.au

Immacolata Donnarumma
IAPS/INAF Rome
E-mail: immacolata.donnarumma@iaps.inaf.it

Tara Murphy
University of Sydney
E-mail: tara@physics.usyd.edu.au

Adam Deller
ASTRON
E-mail: deller@astron.nl

Zsolt Paragi
Joint Institute for VLBI in Europe
E-mail: zparagi@jive.nl

Shami Chatterjee
Cornell
E-mail: shami@astro.cornell.edu

This chapter provides an overview of the possibilities for transient and variable-source astrophysics with the Square Kilometre Array. While subsequent chapters focus on the astrophysics of individual events, we focus on the broader picture, and how to maximise the science coming from the telescope. The SKA as currently designed will be a fantastic and ground-breaking facility for radio transient studies, but the scientifc yield will be dramatically increased by the addition of (i) near-real-time commensal searches of data streams for events, and (ii) on occasion, rapid robotic response to Target-of-Opprtunity style triggers.

Advancing Astrophysics with the Square Kilometre Array
June 8-13, 2014
Giardini Naxos, Italy

*Speaker.

PoS(AASKA14)051

1. Introduction

Radio transients are both the sites and signatures of the most extreme phenomena in our Universe: e.g. exploding stars, compact object mergers, black holes and ultra-relativistic flows. They also have the potential to act as probes of the intervening medium on all scales, up to and including cosmological distances. As such they are invaluable probes for subjects as diverse as stellar evolution, relativistic astrophysics and cosmology.

The majority of such transients can be broadly divided into:

- **Incoherent synchrotron events**, which are associated with all explosive kinetic feedback and particle acceleration in the Universe, from relativistic jets to supernova explosions. Such emission is limited, in a steady state, to a brightness temperature of $T_{\rm B} \leq 10^{12}$K, and therefore the most luminous events (observable at cosmological distances) vary rather slowly (days to years).

  This timescale is often longer than that of a typical observation, and variability is usually determined by comparing images made at different epochs. As noted below, synchrotron flares can generally be used as a measure of the kinetic feedback associated with an event, and as such allow us to understand the flow of energy in the most extreme astrophysical environments.

- **Coherent bursts**, which can achieve much higher brightness temperature (up to at least 10^{30}K) and hence can be of very short durations. Such events can be intrinsically much shorter than the timescales imposed by scattering and dispersion in the intervening interstellar and intergalactic medium, and so can be used as unique probes of these environments. These events are generally observed in 'pulsar mode' beamformed data.

The correspondence between emission mechansim and observing modes is not exact, however, and very fast imaging (on millisecond timescales) and strong scattering can blur the boundaries between the two. Furthermore, while the above constitute the majority of radio transients, strong variability can also be observed associated with thermal emission (e.g. novae), gravitational lensing and scattering, all of which can be picked up by the revised approaches outlined here. In all cases, transient science benefits greatly from monitoring the sky frequently. As such, commensal observing alongside other projects is a powerful strategy.

1.1 Examples of important science associated with radio variables

There are many examples of unexepected and/or extreme astrophysical phenomena being revealed or better understood via observations of radio variability. These include:

- Radio bursts from Jupiter (Burke & Franklin 1955).
- The discovery of neutron stars via their pulsed radio emission (Hewish et al. 1968).
- Discovery of apparent superluminal motion in relativistic jets in variable extragalactic (Cohen et al. 1971) and Galactic ('microquasars', Mirabel & Rodriguez 1994) sources (black holes).

PoS(AASKA14)051

- Extreme scattering events caused by small scale structures in the ISM (Fiedler et al. 1987).
- The powerful, beamed, jet-like nature of gamma-ray bursts, and their probable association with unusual supernovae (Kulkarni et al. 1998).
- Elucidation of the relation between accretion states and feedback in accreting black holes (Fender et al. 2004).
- Discovery of Fast Radio Bursts (Lorimer et al. 2007).
- Highly relativistic jet-like flows associated with the tidal disruption and accretion of a star (Zauderer et al. 2011).

Wilkinson (2015, this volume) discusses other cases of serendipitous discoveries made in the radio band.

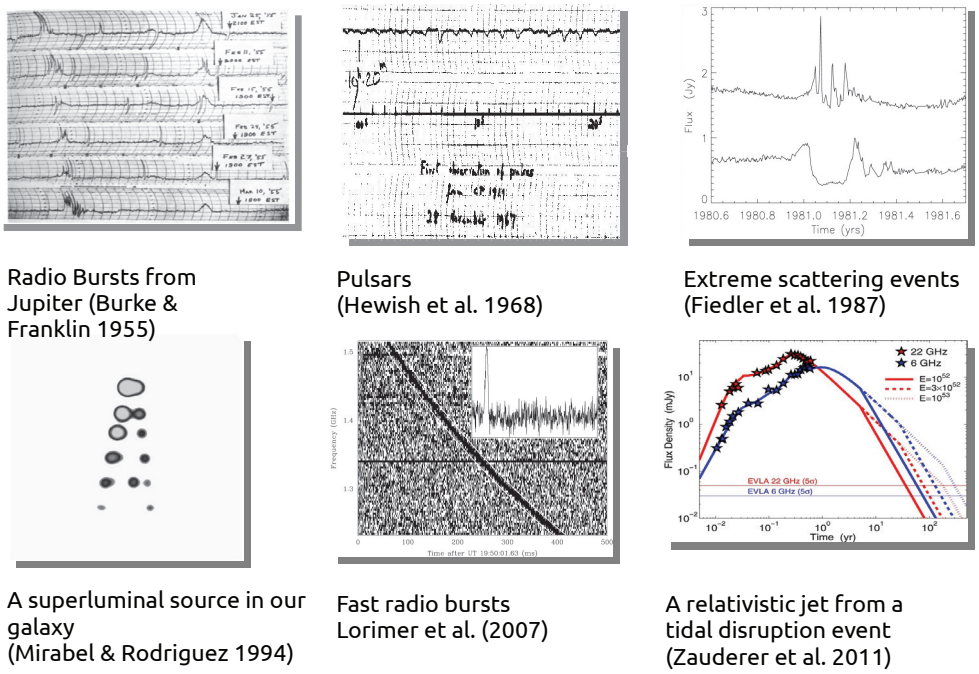

Figure 1: Some, but by no means all, of the major astrophysical discoveries associated with variable radio emission. Major discoveries have been made entirely serendipitously (e.g. pulsars), by searching parameter space (e.g. Fast Radio Bursts) and by rapidly following-up events discovered at other wavelengths (e.g. Microquasars, jetted Tidal Disruption Events).

Of course transient studies are given high priority in other wavelength bands. X-ray astronomy has a rich history of discovering variable and transient X-ray sources as well as reporting them in real time to the global community (e.g. RXTE All-Sky Monitor, Levine et al. 1996; *Swift*, Gehrels & Cannizzo 2015). Transient science is undergoing a golden age in the optical band (e.g. the

PoS(AASKA14)051

Palomar Transients Factory, Law et al. 2009) and is key science for the LSST in the 2020s (Abell et al. 2009).

The key advantages and complementarity of radio emission compared to other wavelengths include:

- **Measuring kinetic feedback, which often originates in relativistically moving ejecta:** radio emission uniquely traces the feedback of kinetic energy, via relativistic jets or more isotropic explosions. Such explosions result in the acceleration of particles and compression of magnetic fields, resulting in synchrotron emission from which the minimum injected energy can be directly estimated.

- **Probing the properties of the intervening ionised media:** radio waves are scattered, dispersed and have their plane of polarisation rotated as they propagate through various media along the line of sight. These effects deliver more and complementary information about the properties of intergalactic and interstellar space than do the absorption and reddening observed at higher frequencies.

- **Precise localisation across very wide fields of view:** the beauty of radio interferometers is the ability to use small dishes or even dipoles to survey very large areas of sky whilst simultaneously having high angular resolution (the downside of this being the very large computational resource required to image huge numbers of pixels). The wide fields of view ($\rightarrow$ high survey speed) are essential for fast and efficient searches, the excellent potential localisation important for selecting candidates at other wavelengths in crowded fields (e.g. globular clusters or galaxies).

2. Incoherent (image plane) transients

Essentially all explosive events in astrophysics are associated with incoherent synchrotron emission, resulting from ejections at velocities in excess of the local sound speed which compress ambient magnetic fields and accelerate particles. These events range from relatively low-luminosity flares from stars, to the most powerful events in the Universe, associated with gamma-ray bursts and relativistic jets from super-massive black holes in active galactic nuclei. Fig 2 presents a set of synchrotron flares associated with different types of object and different timescales: more luminous objects evolve more slowly. This is expected because incoherent synchrotron emission in a steady state is limited to a (rest-frame) brightness temperature of $T_{\rm B} \sim 10^{12}$K, and so the more luminous sources must be physically larger and hence vary more slowly.

The best-fit relation between peak radio luminosity and flare timescale for a (biased) sample of sources with known distances (and hence radio luminosities) is presented in Fig 3 and is approximately of the form

$$L_{\rm radio} \propto \tau^5$$

where τ is the exponential rise timescale (Pietka, Fender & Keane 2015). The results are very similar for decays.

PoS(AASKA14)051

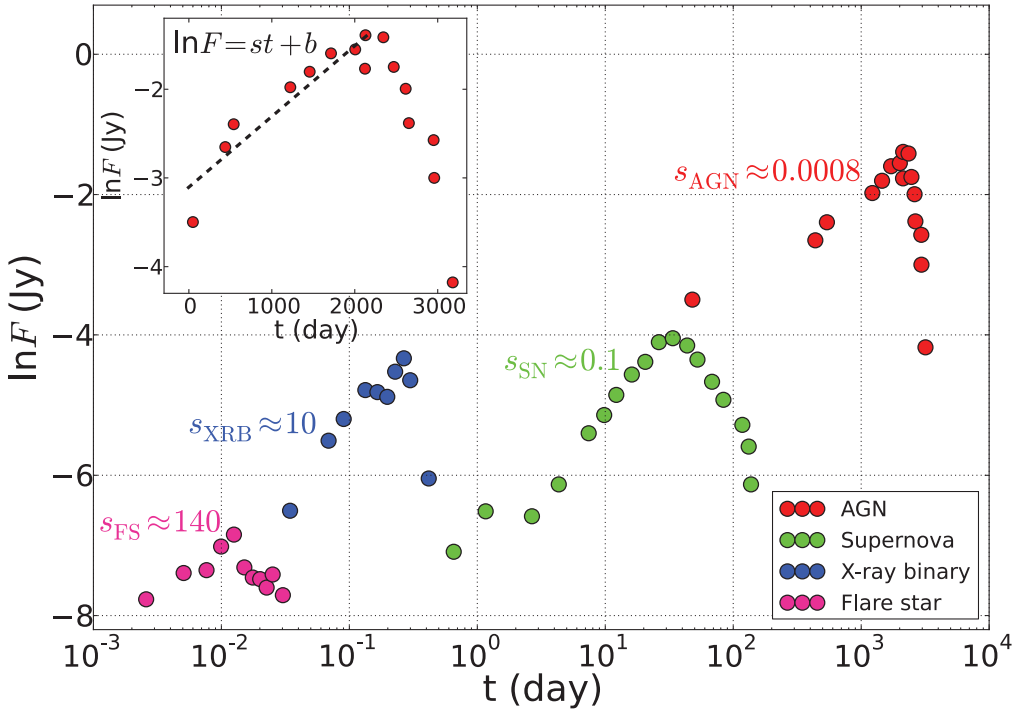

Figure 2: Incoherent synchrotron flares on a range of timescales from different objects. The fitted constant s, corresponds to τ^{-1}, where τ is the exponential rise time of the events. The evolution is often adequately described (in terms of the reliably extracted astrophysics) by the simple expanding-blob model of van der Laan (1966). From Pietka, Fender & Keane (2015).

Such synchrotron events typically have rich multiwavelength counterparts, and can be associated with explosions and accretion events which are visible at optical, X-ray and gamma-ray wavelengths. Combining these data sets can provide unique insights with, as noted earlier, the radio providing both a key estimate of kinetic feedback and, in some cases, more precise localisation and resolved ejecta. There is also usually a delay in the sense that the highest-energy emission escapes while the synchrotron source is still optically thick at most radio wavelengths and hence the radio emission peaks much later. For many sources the timescale of the trigger event will be much shorter than the timescale for the source to evolve to an optically thin phase at radio wavelengths, and so the delay between event and radio peak will be approximately the same as τ (See Figs 2, 3). There may be exceptions to this however, such as relatively slowly-evolving internal shocks in the jets of variable velocities.

For more details on the important science and exciting prospects for these kinds of events, we refer the interested reader to Corbel et al. (2015, this volume) and Yu et al. (2015, this volume) for radio emission from accreting binaries and related systems, Donnarumma et al. (2015, this volume) for jetted tidal disruption events, Burlon et al. (2015, this volume) for gamma-ray bursts, Perez-Torres et al. (2015, this volume) and Wang et al. (2015, this volume) for supernovae. Variable radio emission (both intrinsic and propagation-induced) associated with AGN is discussed in Bignall et al. (2015, this volume), and radio emission from thermal sources such as novae in O'Brien et al.

PoS(AASKA14)051

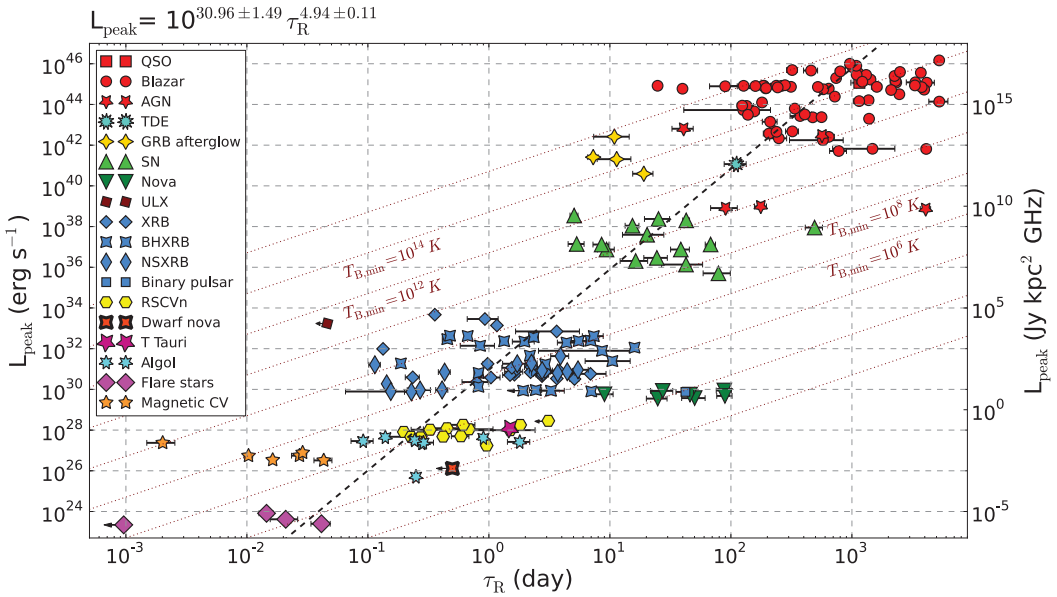

Figure 3: Comparison of radio luminosity with rise time for a (biased) sample of sources for which the distance is known. The peak radio luminosity is a function of of the flare rise timescale. The diagonal (red) lines correspond to a fixed minimum brightness temperature (which would imply $L \propto \tau^2$), and so we see that the more luminous objects also have higher (minimum) brightness temperatures. This result is biased, at least partially, by the beaming of some of the most luminous sources. From Pietka, Fender & Keane (2015), which includes a more comprehensive discussion of these biases.

(2015, this volume).

2.1 Coherent (beamformed) transients

Coherent radio emission can have a much higher brightness temperature than incoherent synchrotron emission (see Fig 4), and is exemplified by pulsars which typically have $T_B \geq 10^{20}$K (see Kramer & Stappers, 2015; this volume, and references therein for the exciting prospects for pulsar science with the SKA); other physical mechanisms include cyclotron masers. Coherent flares are not, typically, associated with energy release on the scale of the most luminous synchrotron events, and are more commonly used as precise probes of the physical conditions at the emission site as well as propagation effects in the intervening ISM/IGM.

Fig 4 expands the parameter space explored in Fig 3 to include also coherent events, including Solar and Jovian events from within our own solar system, the shortest timescale events observed from pulsars, and Fast Radio Bursts.

3. Rates

The rate of transient events at a given depth, cadence and observing frequency is not well measured in the radio band (in fact it is not well reported in most bands of the electromagnetic spectrum). The overwhelming majority of radio sources observed by the SKA will be distant galaxies, a large fraction of which will be AGN. Low-level variability of these AGN, both intrinsic

PoS(AASKA14)051

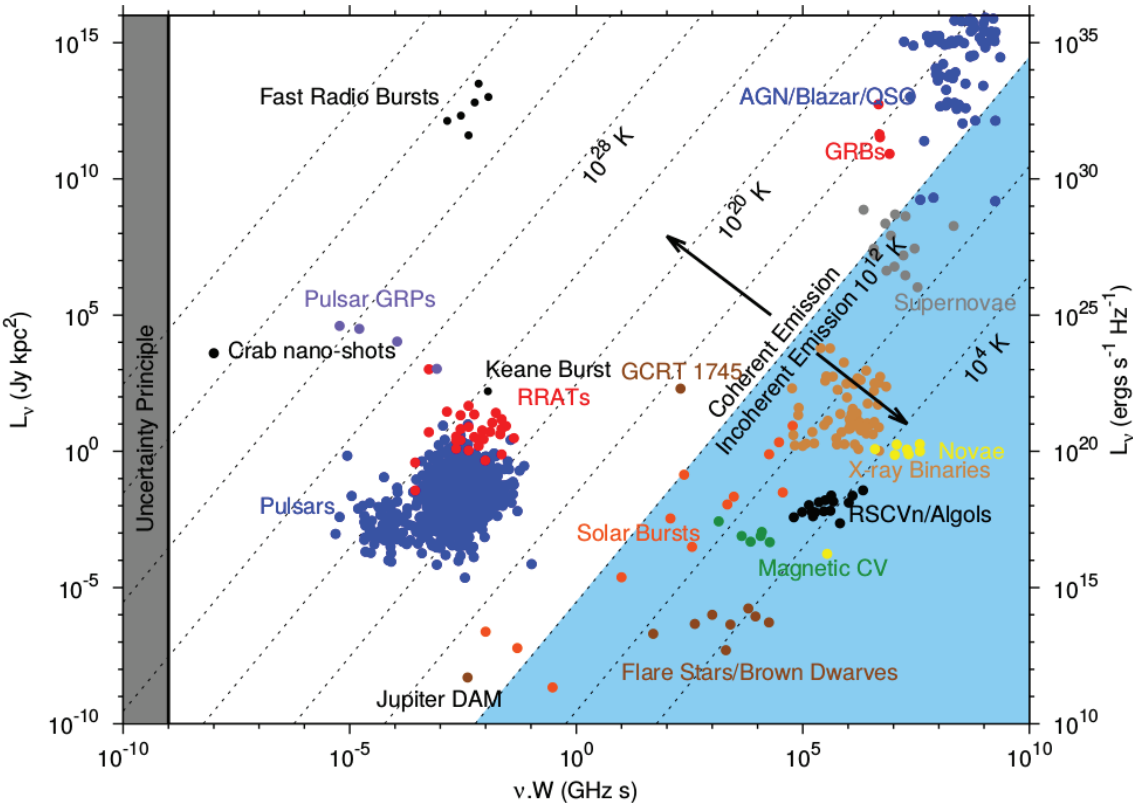

Figure 4: Transients parameter space expanded to include coherent sources. From Pietka, Fender & Keane (2015), following a long line of similar plots (e.g. Cordes, Lazio & McLaughlin 2004).

and via scintillation (see also Bignall et al. 2015, this volume) will result in at least 1% of radio sources being variables at the tens of percent level (e.g. Deller & Middelberg 2014).

However, relatively low-level AGN activity, while interesting, is not our main target. In searching for, and following up, radio transients, we wish both to study populations we know to exist (for example GRBs) and to search for new and unexpected populations. In terms of the known populations, we choose to use, as an indicator of the likely success rate of the SKA, two topical and exciting classes of object, the Fast Radio Bursts (FRBs) and the (jetted) Tidal Disruption Events (TDEs). We should be clear that we are focussing on these two classes of object simply as examples: transient science is too diverse to devote space to a dedicated discussion to all of the very interesting astrophysics under study (e.g. X-ray binaries, GRBs, stellar flares).

3.1 Fast Radio Bursts

Fast Radio Bursts (FRBs) are very short ($\leq$ 15 ms), apparently coherent, bursts which show large excess dispersion when compared to that expected for the line of sight within our galaxy. First discovered by Lorimer et al. (2007), if the excess dispersion is associated with the IGM, they could lie at cosmological distances (the current sample may be probing to redshift $z \sim 1$), be the tracers of new astrophysical phenomena and acts as probes of the missing baryons (see discussion in Macquart et al. 2015, this volume).

PoS(AASKA14)051

Initial estimates placed the FRB rate at $1.0^{+0.6}_{-0.5} \times 10^4$ events sky^{-1}day^{-1} for bursts above the flux density threshold of the Parkes radio telescope, whose 10σ sensitivity reaches 460 mJy in 1 ms (Thornton et al. 2013). However, subsequent FRB detections in the High Time Resolution Universe survey (HTRU; Keith et al. 2010) reveal a significant disparity in the detection rate between events detected above and below a Galactic latitude of 30°, with the event rate being ≈ 4 times higher at high latitudes (Petroff et al. 2014).

Uncertainties in the FRB flux density distribution and spectrum render the estimation of event detection rates for other telescopes uncertain by several orders of magnitude (but see Lorimer et al. 2013 & Trott et al. 2013). However, a simple estimate of the event detection rate at observing frequencies comparable to those at which FRB detections are made (i.e. 1.2-1.7 GHz, as probed by SKA1-MID) is possible based on reasonable estimates of the slope of the differential flux density distribution (i.e. the log N-log S distribution). The cumulative event rate scales as $\Omega S_0^{-3/2}$ for events that are distributed homogeneously throughout a Universe in which spacetime curvature is neglected.

SKA1-MID should be a potent FRB detection machine. With an SEFD of 1.7 Jy and a bandwidth of 720 MHz over the 900-1670 MHz observing band, SKA1-MID reaches a 10σ sensitivity of $S_0 = 14$ mJy in 1 ms. This represents a factor of 33 sensitivity advantage over Parkes. For an SKA1-MID comprised of 15 m diameter dishes, it possesses a field of view (Ω) advantage of a factor of 1.4 over the Parkes multibeam receiver. Thus, if SKA1-MID is able to conduct a tied-array beam search for FRBs over the entire field of view out to the half-power point of the primary beam, this represents a factor $\Omega S_0^{-3/2} \approx 260$ advantage over the Parkes HTRU survey.

However, recent critical examination of the cause of the FRB event rate dependence on Galactic latitude suggests that such simple estimates are in error (Macquart & Johnston, submitted). Diffractive interstellar scintillation of FRB radiation can enhance common, weaker events at high Galactic latitudes to a point where they are detectable, thus enhancing the apparent even rate under certain circumstances. If this effect is the correct explanation of the FRB latitude event rate disparity, it also implies that the FRB differential flux density distribution is much steeper than expected, with the cumulative event rate scaling between $\Omega S_0^{-2.4}$ and $\Omega S_0^{-2.8}$.

Applying the foregoing considerations implies SKA1-MID should detect FRBs at a rate $(6-25) \times 10^3$ higher than the Parkes rate.

3.2 Tidal Disruption Events

Tidal disruption events (TDEs) are accretion events onto a central galactic black hole (e.g. dormant AGN) which result from the tidal disruption and accretion of (approximately half of) a star which passes close to the black hole. The events are faster and of higher amplitude than typical AGN activity, and may be our closest analogues to the instability-induced outbursts in stellar mass black hole binaries, which had led to a new understanding of the connection between relativistic accretion and ejection. Zauderer et al. (2011) reported the detection of a radio flare from such an event, likely to have been associated with the production of a relativistic jet (for more discussion see Donnarumma et al. 2015, this volume). SKA / SKA1-MID will have great potential to discover and follow up large numbers of such events. This is achievable by means of a commensal search in all SKA observations, or by carrying out a near real-time transient search in a high cadence dedicated survey. The latter is preferred to detect TDEs early on in order to allow for the necessary

PoS(AASKA14)051

high energy follow-ups aimed at confirming the TDE origin of the transient event. In the following, we discuss both real-time and commensal search for the discovery.

In the first case, we define a trade-off between sky coverage and sensitivity, favoring short integration times in order to allow for detection at higher energies and then enable the identification of the transient at higher redshift (see Donnarumma et al. 2015). We assume a multiple cadence half-sky survey, comparable to the shallow surveys proposed by the 'continuum' working group (Prandoni et al. 2015, this volume). By assuming an half sky coverage with a 2-day cadence at a $5-\sigma$ flux limit of 90 μJy, we estimate a number between ~ 300 and ~ 800 yr^{-1} (a bulk Lorentz factor $\Gamma = 2$ is assumed). This is because the 1.4 GHz light curve of the prototype event, Sw J1644 increases with time at least up to 600 days (Zauderer et al. 2013), therefore a multiple cadence survey with longer integration times (~ 8 days) needed to achieve the same flux limit of our strategy should not result in a significant loss of radio detections. However, radio triggers at late times could be problematic for follow-up observations, because sources would get fainter in both optical and X-rays, preventing the identification of higher redshift TDEs. Nevertheless, the bulk of the sample expected to be at $z \lesssim 0.5$ should still be successfully followed up at higher frequencies. On the basis of these considerations, TDEs can be commensally searched for by exploiting the SKA1 all-sky surveys (31,000 deg^2 at 2 μJy beam^{-1} at 1.5-2 arcsec resolution) proposed in the framework of both the Magnetism and Continuum science cases (see Johnston-Hollit et al. 2015, this volume; Prandoni et al. 2015, this volume). By carrying out multiple visits of the fields, with a cadence of ~ 10 days over the two year period, it will be very efficient in finding extra-galactic transients down to $\sim$90 μJy beam^{-1} .

3.3 Implications: rich science

For each of the two chosen example classes of objects we see, therefore, that the rates for detection for SKA1-MID are rather high, indicating a very high scientific yield from radio transients searches, simply for known objects, *as long as we commensally search all data sets (see below)*. Of course we can also estimate rates for many other types of object, such as X-ray binaries (Corbel et al. 2015), GRBs (Burlon et al. 2015) or supernovae (Perez-Torres et al. 2015, Wang et al. 2015), but the above are already sufficient to demonstrate the high scientific return likely from the SKA in this area.

For both TDEs and FRBs the predicted rates are between 1 and 1000 per week for SKA1-Mid. As noted above, this will be on top of a sea of other, less dramatic, but scientifically interesting variability. A good comparison area to TDEs and FRBs, and indeed one which has attracted similar researchers, is GRB afterglows: transient events which were for a long time mysterious in their origin (and to some extent still are), are associated with the most extreme astrophysical conditions, and can be seen to cosmologically significant distances. GRB afterglows have generated a very large number of high profile papers and citations, and continue to do so ~ 15 years after their discovery, have motivated major space missions (e.g. *Swift*) and are a major area of interest for the LSST. Furthermore, multiple high-profile papers are still being written about *individual* events. It is therefore entirely reasonable to surmise that many major papers per year could arise from radio transient studies, and be one of the main sources of early SKA publications (certainly while the deepest surveys are still being built up).

PoS(AASKA14)051

For SKA1-Low the rates are less certain. Large numbers of FRBs *might* be detectable, but this depends strongly on the scattering and also on the spectra of the objects (rates calculated in the 1 GHz band for SKA1-Mid do not suffer from these uncertainties). LOFAR is probably the best facility against which to compare rates, although LW(D)A (Lazio et al. 2010) and MWA (Bell et al. 2014) rates are also relevant. Variability searches with LOFAR across ~ 1500 deg^2 as part of the LOFAR Transients Key Science Project have shown that the sky is essentially static at flux densities above a few mJy (at 140 MHz) on timescales of weeks – months. However, there is good evidence for one or more bright ($\geq$ Jy) $\sim$ 10-minute transients in a high-cadence shallow monitoring of the north celestial pole at 60 MHz (Stewart et al. 2014). If SKA1-Low can really achieve a continuum sensitivity of a few μJy in an hour across 27 deg^2 (although source confusion may be a major issue here), and the LOFAR transient reported by Stewart et al. is part of a population which follows $N(>F) \propto F^{-3/2}$ relation (as expected for an isotropic homogeneous distribution of sources throughout a flat space), then we would expect to find 1000s of such events per day. We note that completely independent of the SKA Transients SWG (and therefore of the authors of this paper), Metzger, Williams & Berger (2105) have predicted that SKA surveys at 0.1–1 GHz should detect thousands of radio transients associated with GRBs, TDEs and neutron star mergers associated with magnetar remnants.

3.4 Existing rates and limits from blind searches

Complementary to the rates estimated for specific classes of object such as those given for the FRBs and TDEs given above, we can also consider the rates and limits set by existing blind searches for radio transients. In the following we attempt to provide a comprehensive summary of the published rates and limits. We separate these into slow/image-plane and fast/beamformed, although – as noted earlier – the boundary between the regimes is rather blurred.

3.4.1 Transient rates and limits from imaging

A large number of image-plane surveys have been performed at a range of frequencies, observation timescales and cadences. Such rates are typically quoted as a surface density (limit), and these can be compiled and plotted as a function of flux density (corresponding to the sensitivity of the survey). A compilation of such limits, from image-plane surveys, presented in this way, is given in Table 1, and Figs 5, 6. We caution that presenting the limits and rates in 2D plots such as these can be very misleading: observation timescales and cadence are also very important parameters for such surveys. We have tried presenting the data from Table 1 in a 3D form (such as that envisaged by Fender & Bell 2011) but it is our feeling that the resulting plots confuse more than they clarify. Clearly in the future multi-dimensional analysis and Monte Carlo simulations will be required to determine how well parameter space has been explored.

3.4.2 Transient rates and limits from beamformed/pulsar modes

Table 2 lists a sample of the largest beam-formed searches which have been previously performed and/or are currently ongoing. We caution that sensitivity estimates in this table were derived on the basis of nominal telescope characteristics and average sky characteristics in some cases, and that choices made during processing can have a substantial impact on the completeness of searches

PoS(AASKA14)051

Survey/Paper	Flux Limit (mJy)	ρ (deg^{-2})	δt	Δt	ν (GHz)	N_e
Stewart et al. (in prep)(A)	2.25×10^4	4.1×10^{-7}	30 sec	cont - 4 months	0.060	41 350
Stewart et al. (in prep)(B)*	4 100	1.4×10^{-5}	11 min	4 min - 4 months	0.060	1 897
Stewart et al. (in prep)(C)	1 400	5.3×10^{-4}	297 min	4 min - 4 months	0.060	32
Lazio et al. (2010)	2.5×10^6	9.5×10^{-8}	5 min	2 min - 5 min	0.074	$\sim$1 272
Obenberger et al. (2014)*	1.44×10^6	2.2×10^{-9}	5 sec	cont - year	0.074	$\sim$43 056
Cendes et al. (2014)	500	10^{-2}	11 min	min - months	0.149	26
Carbone et al. (2014)	500	10^{-3}	11 min	min - months	0.150	151
Bell et al. (2014)	5 500	7.5×10^{-5}	5 min	min - 1 year	0.154	51
Hyman et al. (2009)*[a]	30	0.034	$\sim$3 hr	days - months	0.235, 0.330	-
Jaeger et al. (2012)*	2.1	0.12	12 hr	1 day - 1 month	0.325	6
Bannister et al. (2011a,b)*	14	1.5×10^{-3}	12 hr	1 day - 20 yr	0.843	2
Ofek et al. (2010)*	6	1.5	days	-	1.4	2
ATATS I/Croft et al. (2010)	40	0.004	months	1 month	1.4	2
ATATS II/Croft et al. (2011)	350	6.0×10^{-4}	1 day	min - days	1.4	12
Bower & Saul (2011)(A)	3000	9.0×10^{-4}	2 min	$>$ 1 min	1.4	1 852
Bower & Saul (2011)(B)	70	3.0×10^{-3}	2 min	1 day - yrs	1.4	1 852
Bell et al. (2011)	8	0.032	5 min	4 - 45 days	1.4, 4.9, 8.4	5037
Aoki et al. (2014)*	3000	2.0×10^{-6}	4 min	day	1.4	1 200
ASGARD/Williams et al. (2013)	16	0.14	1 hr	days - years	3	29
PiGSS I/Bower et al. (2010)(A)	1	1	months	months	3.1	2
PiGSS I/Bower et al. (2010)(B)	5	0.3	months	mins	3.1	2
PiGSS II/Bower et al. (2011)(A)	15	0.025	hours	days	3.1	78
PiGSS II/Bower et al. (2011)(B)	5	0.18	month	month	3.1	5
PiGSS III/Croft et al. (2013)(A)	10	0.009	hours	days	3.1	379
PiGSS III/Croft et al. (2013)(B)	10	0.02	months	months	3.1	-
PiGSS III/Croft et al. (2013)(C)	10	0.08	months	years	3.1	2
Bower et al. (2007)	0.9	6	20 min	years	4.8, 8.4	17
Frail et al. (2012)(A)	0.2	3	20 min	month	4.8, 8.4	-
Frail et al. (2012)(B)	0.37	0.6	20 min	mins - days	4.8, 8.4	-
Ofek et al. (2011)	1.8	0.039	50 seconds	day - month	4.9	16
Alexander et al. (2014)	0.5	17	15 mins	days - months	4.9	31
SKA-Shallow	1.0×10^{-3}	3.0×10^{-8}	4 hr	-	1.4	$\sim$5000
SKA-Deep	2.0×10^{-5}	6.0×10^{-3}	5 hr	-	1.4	$\sim$500

* Limit derived from a transient detection.

[a] Using approximate rate derived in Williams et al. (2013) which is inclusive of Hyman et al. (2005,2006,2009).

Table 1: Summary of image-plane radio transient surface densities, ρ, as found in the literature. Columns: Keeping with the format set by Ofek et al. (2011), δt is the timescale of each individual epoch, Δt is the timescale(s) between epochs and N_e is the total number of epochs. The first block in the main section of the table is considered the low-frequency portion of surface densities, which incorporates surveys conducted at frequencies $\leq$ 330 MHz. The second block are the densities defined at mainly GHz frequencies. The second section of the table provides estimates of transient surface densities that will be achievable with the SKA. An entry containing '-' signifies that we were not confident in identifying the respective value from the literature. All these values are those used in Figures 5 and 6.

PoS(AASKA14)051

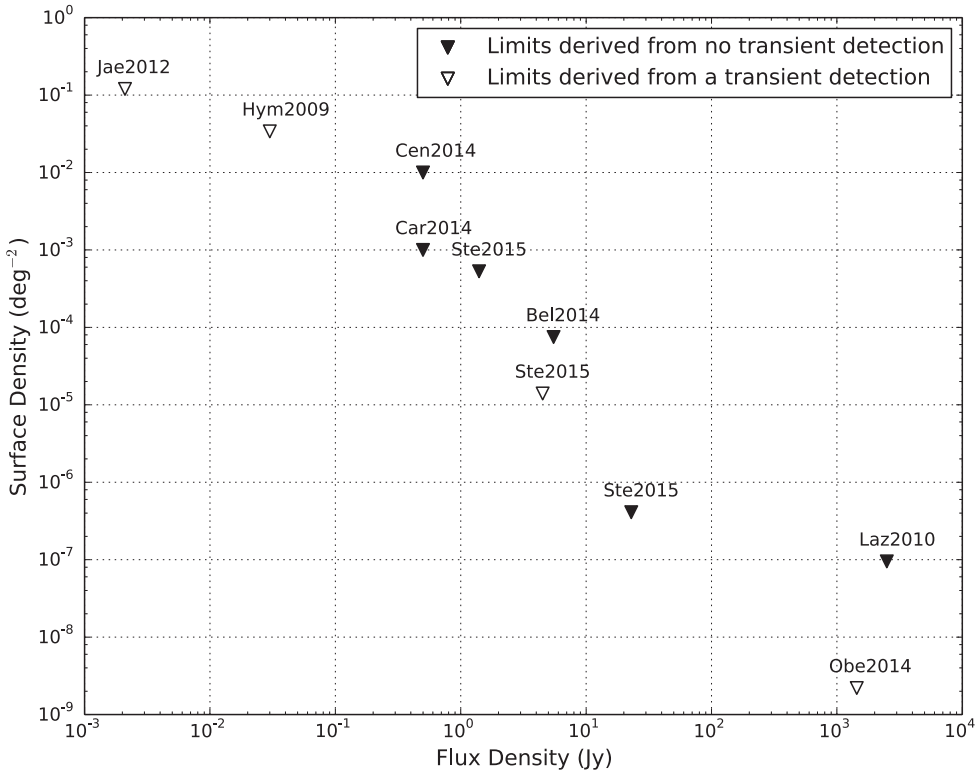

Figure 5: A compilation of rates and upper limits for blind searches for radio transients at MHz frequencies. The surveys included in this plot are: Bell et al. (2014) (Bel2014); Carbone et al. (2014) (Car2014); Cendes et al. (2014) (Cen2014); Hyman et al. (2005,2006,2009) (Hym2009); Jaeger et al. (2012) (Jae2012); Lazio et al. (2010) (Laz2010), Obenberger et al. (2014) (Obe2014); and Stewart et al. (in prep) (Ste2015).

for short-duration, dispersed events Keane et al. (2015). Given the wide range of parameters encapsulated in these surveys we do not attempt to present them graphically. However, as noted above, the detection rate of FRBs should be more than a thousand times higher with SKA1-MID than Parkes, which has discovered the majority of FRBs to date.

4. Optimising the SKA for transients

In a set of meetings and discussions between 2013 – 2015, the radio transients community concluded that while the telescope should be a superb facility for detecting radio transients, the major drawback of the existing designs was the lack of a requirement for (i) automatic, near real-time searching of data streams for transients, (ii) very fast (robotic) response modes for transients found in other ways.

4.1 Commensality

It is important to define commensal transient searches, and how we would want these to be implemented in the SKA system. By 'commensal', we mean having no effect on (i) the original

PoS(AASKA14)051

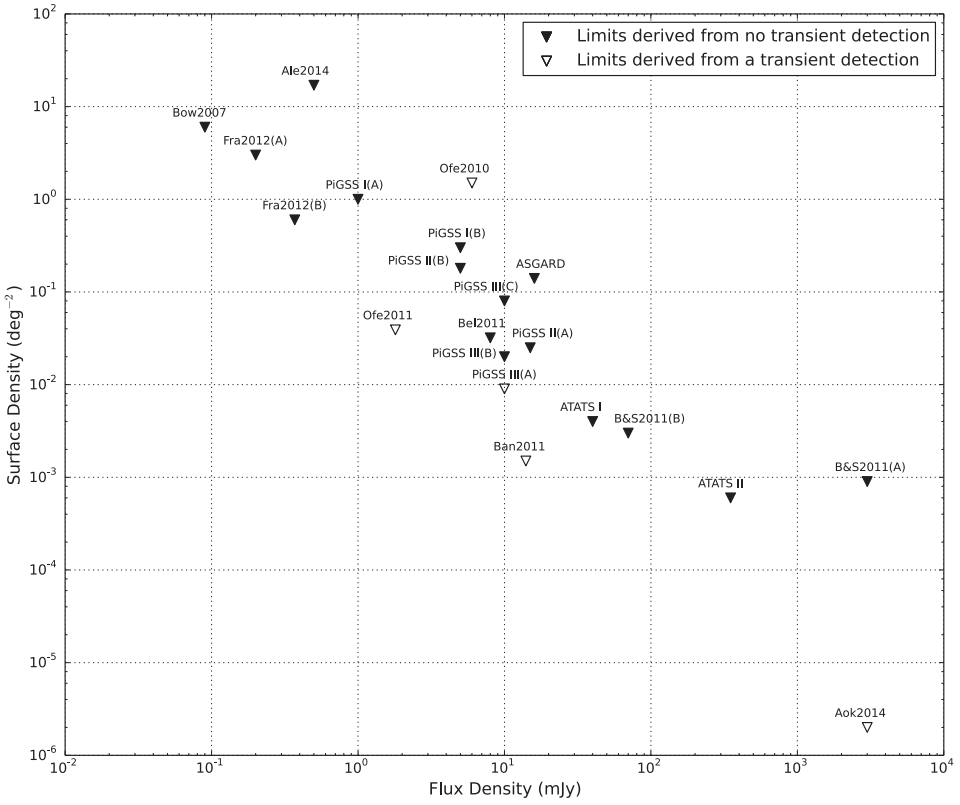

Figure 6: A compilation of rates and upper limits for blind searches for radio transients at GHz frequencies. Multiple rates derived from the same survey are denoted by (A), (B) and (C). The surveys included in this plot are: Alexander et al. (2014) (Ale2014); Aoki et al. (2014) (Aok2014); Bannister et al. (2011a,b) (Ban2011); Bell et al. (2011) (Bel2011); Bower et al. (2007) (Bow2007); Bower et al. (2010) (PiGSS I); Bower et al. (2011) (PiGSS II); Bower & Saul (2011) (B&S2011); Croft et al. (2010) (ATATS I); Croft et al. (2011) (ATATS II); Croft et al. (2013) (PiGSS III); Frail et al. (2012) (Fra2012); Ofek et al. (2010) (Ofe2010); Ofek et al. (2011) (Ofe2011); and Williams et al. (2013) (ASGARD).

scientific goals and (ii) proposed observing strategy of an accepted proposal. Clause (i) is very strong and should be considered inviolate (of course we also hope that observations can be over-ridden by T-o-O style triggers but that is dealt with in the next section). Clause (ii) should be considered a default position but could potentially be modified at some stage if it increased the secondary science without harming the primary (consider a scenario in which we have discovered that transients which vary on ∼day timescales are extremely interesting – it would then make sense to schedule a deep 8-hr pointing of some field as two 4-hr observation separated by one day). The implementation of commensal searches should, in our view, be part of the default SKA system and is not associated with custom instrumentation or 'spigots'[1].

How can we compare the likely scientific harvest of 'normal' (a.k.a. 'conservative' or '20th

[1] spigots have a particular definition within the SKA system design and should be not used lightly

PoS(AASKA14)051

Survey/ Telescope	Freq. (MHz)	B/width (MHz)	Int. time (μs)	Freq. res. (MHz)	σ_{1-ms} (Jy)	Beamsize (sq. deg.)	Dwell time (sec)	$N_{\rm beams}{}^{A}$	$N_{\rm FRBs}$	Refs
LOTAAS* (coh.) / LOFAR	135	32	0.495	0.012	1.4	0.28	3600	119133	0	1
LOTAAS* (incoh.) / LOFAR	135	32	0.495	0.012	2.4	34	3600	1953	0	1
GBNCC* / GBT	350	100	0.082	0.024	0.065	0.41	120	30000	0	2
PALFA / Arecibo	1440	100	0.064	0.39	0.011	0.0027	176	35067	1	3,4
Parkes-MB (Gal.) / Parkes	1370	288	0.25	3	0.07	0.043	2100	34710	1	5
Parkes-MB (Int. lat.) / Parkes	1370	288	0.125	3	0.07	0.043	265	155142	1	6,7
HTRU-N* / Effelsberg	1400	300	0.054	0.59	0.036	0.017	90^{B}	1260000	0	8
HTRU-S / Parkes	1350	340	0.064	0.39	0.064	0.043	270^{C}	554333	5	9
SKA1-MID^{D}	1400	400	0.064	0.2	0.007	0.00027	600	11000000	-	10,11
SKA1-LOW^{E}	300	100	0.064	0.024	0.02	0.004	600	5000000	-	10,11

^{A}Given by the number of beams per pointing, multiplied by the number of pointings.
^{B}For the all-sky section of the survey; longer dwells are used of 180 and 1500 seconds are used at intermediate and low Galactic latitudes respectively.
^{C}For the all-sky section of the survey; longer dwells are of 540 and 4200 seconds are used at intermediate and low Galactic latitudes respectively.
^{D}Assumes 2000 tied array beams (including stations within 900m diameter) and a survey of the Galactic plane covering a total of ∼3000 square degrees.
^{E}Assumes 500 tied array beams (including stations within 1200m diameter) and a total sky area of ∼20000 square degrees.
*Survey is ongoing, observations and/or analysis are not completed.
REFS: 1: Unpublished, see Coenen et al. (2014) for pilot project, also **www.astron.nl/lotaas/**, 2:Stovall et al. (2014), 3:Deneva et al. (2009), 4:Spitler et al. (2014), 5:Manchester et al. (2001), 6:Edwards et al. (2001), 7:Jacoby et al. (2009), 8:Ng and the HTRU collaboration (2013), 9:Keith et al. (2010), 10:Keane & Petroff (2015), 11:Macquart et al. (2015)

Table 2: Overview of beamformed searches for radio transients. The $\sigma_{\rm 1ms}$ column gives the nominal 1-σ sensitivity of the survey to a transient of duration 1 millisecond with a dispersion measure at which intra-channel smearing is negligible.

century') observing with that of 'fully commensal' (i.e. efficiently searching all data streams for transient events)? Considering briefly the 'wedding cake' approach of most proposed/envisaged surveys (different tiers, with the shallowest being the widest), these are not very different from the search strategies a transients team would develop for the telescope if it had 100% of the observing time. How much time is a transient programme likely to get in reality? We could imagine, optimistically, that this might be 10%. Therefore, *if an efficient commensal transient search can be performed on all data streams*, then the rate of events increases by at least one order of magnitude. Fig 7 is plotted in the form of Fig 6 but showing the rates/limits which would be achieved by piggybacking on the deep-and-narrow and wide-and-shallow continuum surveys which have been proposed for SKA1-MID (and would take place over the first few years of operation of SKA phase 1). These are vast improvements on current limits, which could be achieved 100% commensally. The FRB and TDE searches discussed above could also be achieved almost entirely commensally. Facilitating the rapid commensal search of these data, as they are taken, for transients would not only maximise the scientific yield on the telescope, it would also reduce the proposal time pressure.

Of course this is a big if, as is the associated design and implementation cost. Nevertheless, it is our judgement right now that such an addition to the telescope design would not incur a large fractional cost (and certainly much less than the rescope associated with the decisions taken in March 2015).

Two scenarios might be considered for commensal searching:

- **Slow commensal:** searching of data for transients some time after the data have been taken,

PoS(AASKA14)051

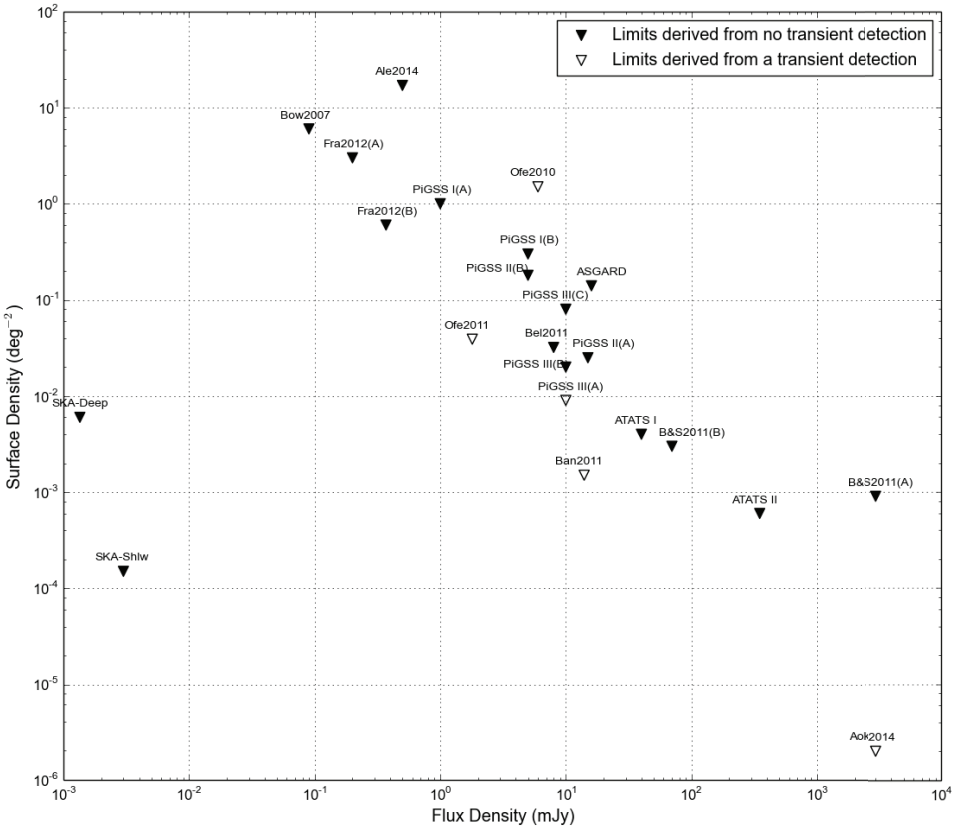

Figure 7: Same as Fig 6 with the survey sensitivities which would be achieved by searching commensally through the planned SKA-1 wide-and-shallow and narrow-and-deep continuum surveys. These limits correspond to one, and only one, way of searching these data: the same data can be searched on a variety of timescales in such a way theat they move more steeply than $-3/2$ in this representation. Specifically, for the estimated wide-and-shallow survey we consider two one-hour pointings, reaching $\sim 1\mu$Jy r.m.s., at each of 20 000 square degrees (one pointing per square degree). For narrow-and-deep we consider 500 pointings of $\sim$ 5hr each on the same field, reaching an rms of about 450 nJy per pointing (ultimately giving ~ 20 nJy sensitivity across one square degree).

possibly when they have been moved from the current 'live' data store to the archive. In many cases this timescale would be much longer than the timescale of the event and so, while easier to implement, this would have a lower scientific yield. Nevertheless, for many luminous synchrotron events, timescales (for both latency and imaging) of $\sim$days, would not seriously damage the programme. The computational demand of such a programme would be entirely minimal.

- **Fast commensal:** Ideally, to fully explore parameter space and catch the fastest transients while counterparts at other wavelengths were still detectable, a near-real-time system could be implemented into the SKA *from the design phase* which was able to make a search for

PoS(AASKA14)051

transients in data streams in close to real time (which here probably means timescales of ∼seconds for latency and imaging). The computational demand for such a system would be moderate, although the storage associated with continuously-generated 1sec, full-field full-resution images would be significant and would mean that the transient search algorithms would have to be working very fast to prevent a backlog.

The conceptual parallel paths for near-real-time commensal transients searches and regular observing are illustrated in Fig 8. We remain convinced that it would be a missed opportunity not to include a fast-commensal system in the design of the SKA (certainly SKA1-Mid).

Of course the latter, fast commensal, system is the goal of our community, and we remain convinced that – against the scale of the ∼ 30% project 'rescope' in March 2015 – it is entirely possible for it to be accommodated within a new baseline design.

The politics of data ownership is also of course an issue here. Traditionally, but not exclusively, in astronomy, telescopes have awarded all the science in a data set to the proposers, for some proprietary period (typically 12 months). It is not obvious, however, that this is the right approach for facilities with very wide fields of view where multiple, distinct, science goals can be explored with the same data. In some such cases proposers are limited to certain science within a given data set – such a system has been previously implemented for the gamma-ray observatory INTEGRAL. Specifically, for the first decade of INTEGRAL operations, a two-round system was used. In the first round, proposers could request certain fields to be observed, and define (and reserve) the primary science drivers for the proposal. In the second round, 'data rights proposals' could be used to obtain proprietary rights on other sources within the selected fields if they have not been reserved by the primary proposal. This system has now been dropped, and a more traditional one-round system adopted, but this is primarily as a cost-cutting measure and the original system was widely considered to be successful with little evidence of gaming. However, a weakness of this system for dealing with transients was identified – there was no guarantee that they would be spotted or acted upon in a timely manner (as with most telescopes), depending on the scientific inclinations and resources of the primary observers.

There is also a concern from some parts of the community that a small group would get to 'own all the transients' and that this would be unfair. This is not the thrust of what we are proposing; rather we wish for the SKA to incorporate a generally-implemented and open system which delivers public alerts. Who then owns the data related to the follow-ups may be a question for a programme committee, but the global scientific community can only gain from immediate alerting to astrophysical transients. As noted above, this is precisely the policy adopted by several space missions, such as the enormously successful *Swift*, and is the planned policy for the LSST. How people deal with very large rates of transients, including how to select those which are potentially interesting and which to follow up with other facilities is another question.

Specifically, therefore, we propose that the commensal system itself be transparent (i.e. publically available, up-to-date, documents and code) and that automatic alerts resulting from it are made globally and publicly, probably using the *VOEvent* framework. Of course there would be a commissioning/training phase in which alerts were only shared with trusted partners, but it should be possible to complete such a phase on a timescale of ∼year. Furthermore, we note that some groups (Armstrong et al. *in prep*) are already beginning to design a system for MeerKAT, which

PoS(AASKA14)051

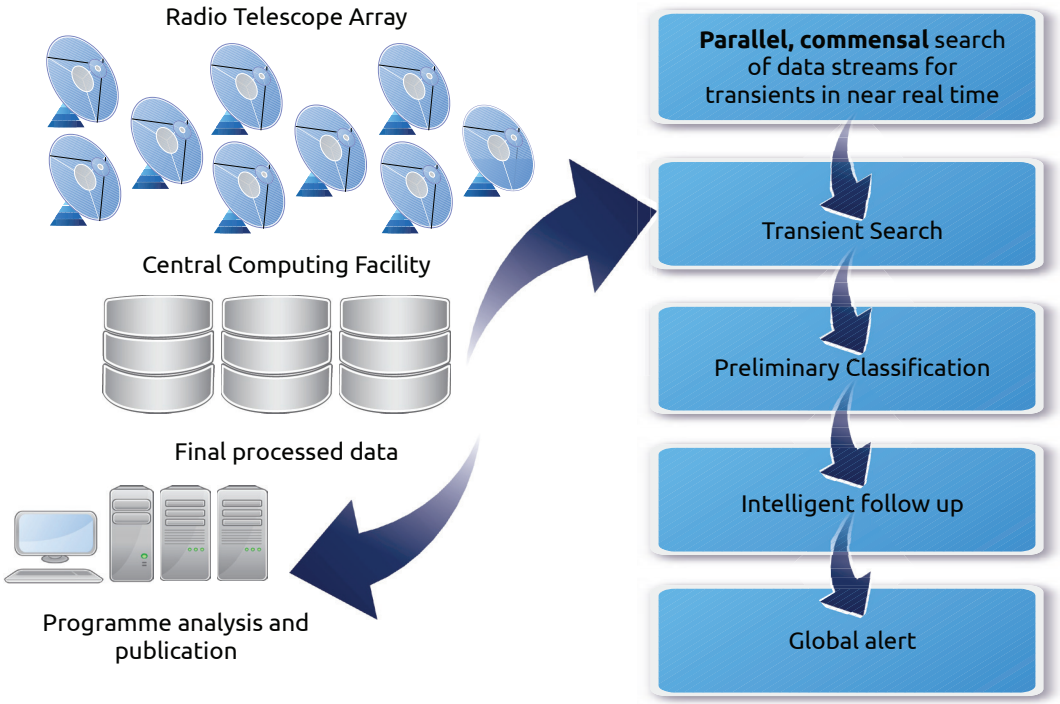

Figure 8: Schematic of 'traditional' and near-real-time transient searches occurring commensally, in parallel.

should be well-tested by the time SKA1-Mid is being deployed. For SKA1-Low, with its rather different family of transients (coherent vs synchrotron) and response modes, it would be desirable to be able to test such a mode on LOFAR (or maybe MWA), but this has not yet been implemented.

Such concepts, while not at present embedded in the SKA design, are not radical. Several projects within the radio domain have attempted to achieve similar goals, for example VFASTR (Wayth et al. 2011), European VLBI Network is (partially) implementing a robotic rapid-response system, the JVLA is implementing a real-time commensal fast transient detection system (Law et al. 2014), the Allen Telescope Array searched many of its data sets commensally for transients (e.g. ASGARD, Williams et al. 2013), the SUPERB programme at Parkes is making near-real-time searches for FRBs, NASA's Deep Space Network is searching for radio transients (O'Dea et al. 2014). The first steps towards a commensal image-plane transient search system for MeerKAT are also under design (Armstrong et al.*in prep*).

4.2 Rapid Response

Rapid response to transient astrophysical events, so called Target-of-Opportunity (T-o-O) modes, is of great importance in astrophysics. As an example, the NASA *Swift* space mission was designed explicitly for very rapid slewing in response to GRB triggers; the most expensive array of optical telescopes in the world, ESO's Very Large Telescope, has had a Rapid Response Mode implemented. Such observations always cause inconvenience for the observing programme that they

PoS(AASKA14)051

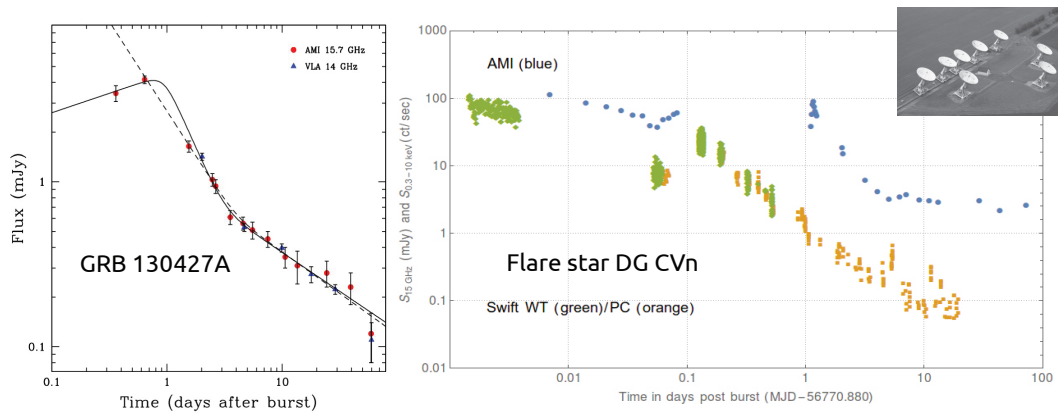

Figure 9: Results from the ALARRM programme (see **4pisky.org**) in which the AMI-LA radio telescope has been configured to respond robotically (with no human interaction) to automatically-generated alerts from the *Swift* gamma-ray satellite. **Left panel:** AMI-LA observations of radio emission from Gamma Ray Burst GRB130427A, which at the moment of trigger was unobservable from AMI. Override observations were automatically scheduled and performed when the source was next at sufficient elevation, all without human intervention. The early time radio detections are amongst the earliest ever and probably detect the reverse shock in the early phases of the jet evolution (from Anderson et al. 2014). **Right panel:** Very early time radio flaring during a gamma-ray superflare from the young M dwarf binary DG CVn. In this case AMI-LA was observing within six minutes of the burst alert, and caught a $\sim$ 100mJy flare which was already decaying (from Fender et al. 2015). The inset in the top-right hand corner is an aerial photo of AMI-LA.

interrupt, but this has been shown time and again to be acceptably manageable by replacing lost time ASAP, something that is easy to do in an automatically queue-scheduled system.

Before 2012, no robotic override system, in which T-o-Os were implemented without human intervention, had ever been operated on a radio telescope (although the scientific utility of such modes had been demonstrated in the optical and X-ray bands). However, such a system has now been implemented on the AMI-LA telescope, an array of eight 12.8m radio dishes, operating in the 15 GHz band, and located in the UK. The array now routinely begins slewing to automatically-generated triggers based upon *Swift* alerts (transmitted using the *VOEvent* protocol) on timescales of less than a minute, taking data on-target within five minutes (Staley et al. 2013; part of the '4 PI SKY' project). This AMI-LA Rapid Response Mode, ALARRM, has been extremely successful both as a demonstrator and for doing real science, including possibly the earliest-ever detection of reverse shock radio emission from a GRB (Anderson et al. 2014; see Fig 2) and a prompt radio transient associated with a gamma-ray superflare from a nearby young binary system (Fender et al. 2015). An extension of the system, including *Fermi* alerts, has been occasionally implemented on the LOFAR-UK station at Chilbolton (Breton, Karastergiou *private communication*), and there are hopes that it could eventually be deployed for the entire LOFAR array. Similar in concept to the ALARRM programme, but using a single dish in pulsar mode, Bannister et al. (2012) also followed up several *Swift* GRBs without human intervention.

PoS(AASKA14)051

In addition, the European VLBI Network (EVN) currently has two mechanisms for implementing rapid response observations. Besides the classical T-o-Os, the EVN has introduced a scheme of triggering proposals. In this case sources are observed if certain trigger condition (based on either an increase in the radio flux density, or changes e.g. in X-ray properties) are fulfilled. These projects can be triggered up to 1 day before real-time electronic VLBI (e-VLBI) observing sessions. There have been a number of automated trigger tests in 2013/2014 to aim for much shorter timescale triggers, to be implemented in the near future.

In summary, rapid response can be done, fast and efficiently, without human intervention, and we consider it essential that the SKA implement such modes.

5. Summary

The Square Kilometre Array has the potential to be a superb machine for the discovery of radio transients, yielding an extremely rich harvest of relativistic explosions, exotic astrophysics and previously unknown phenomena. As redesigned in 2015, the collecting area, wide bandwidth and spectral flexibility mean that the prospects for transients are extremely good. Nevertheless, a great opportunity would be missed, and the scientific harvest greatly reduced, if the following are not integrated into the system design:

- **Fast commensal searches for transients:** technically achievable, politically surmountable, this would increase the transient harvest by an order of magnitude, provide alerts for a global community hungry for interesting targets, and reduce the observer time pressure on the telescope.

- **Fast (robotic) response to transient alerts:** A further step forward can be made if the SKA can – at times – respond very rapidly to alerts generated either by other facilities or its own monitoring programmes (e.g. the commensal search, above). So much of the exciting astrophysics occurs early on in these phenomena that getting on source as early as possible (in reality, seconds to minutes) must be a high priority (for *some*, not all, events).

We believe that the combination of the existing SKA design with these two features would make it a truly transformational facility for both stand-alone radio transients astrophysics and as part of a broad multiwavelength suite of telescopes exploring the most extreme phenomena the universe has to offer.

Acknowledgements

Much of the knowledge in this work was distilled from countless meetings, telecons and email exchanges with the full and wide membership of the SKA Transients Science Working Group. We would like to specifically thank Tyler Bourke for assistance and patience in preparing this manuscript, and Evan Keane and Casey Law for useful comments and suggestions.

PoS(AASKA14)051

REFERENCES

Abell P.A. and the LSST Science Collaboration, LSST Science Book, Version 2.0 (arXiv:0912.0201)

Alexander K. D., Soderberg A. M., Chomiuk L. B., 2014, ApJ, submitted (arXiv:1405.0228)

Anderson G. et al., 2014, MNRAS, 440, 2059

Aoki T., Tanaka T., Niinuma K., et al., 2014, ApJ, 781, 10

Bannister K. W., Murphy T., Gaensler B. M., Hunstead R. W., Chatterjee S., 2011a, MNRAS, 412, 634

Bannister K. W., Murphy T., Gaensler B. M., Hunstead R. W., Chatterjee S., 2011b, MNRAS, 418, 2813

Bell M. E., Fender R. P., Swinbank J., et al., 2011, MNRAS, 415, 2

Bell M.E., Murphy T., et al., 2014, MNRAS, 438, 352

Bignall H., et al., 2015, "Time domain studies of Active Galactic Nuclei with the Square Kilometre Array", in Advancing Astrophysics with the Square Kilometre Array, PoS(AASKA14)058

Bower G. C., Saul D., Bloom J. S., Bolatto A., Filippenko A. V., Foley R. J., Perley D., 2007, ApJ, 666, 346

Bower G. C., Croft S., Keating G., et al., 2010, ApJ, 725, 1792

Bower G. C., Saul D., 2011, ApJ, 728, L14

Bower G. C., Whysong D., Blair S., Croft S., Keating G., Law C., Williams P. K. G., Wright M. C. H., 2011, ApJ, 739, 76

Burlon D. et al., 2015, "The SKA View of Gamma-Ray Bursts", in Advancing Astrophysics with the Square Kilometre Array, PoS(AASKA14)052

Carbone D., van der Horst A. J., Wijers R. A. M. J., et al., 2014, MNRAS submitted (arXiv:1411.7928)

Carilli, C. L., & Rawlings, S., 2004, New Astronomy Reviews, 48, 979

Cendes Y., Wijers R. A. M. J., Swinbank J. D., et al., 2014, MNRAS submitted (arXiv:1412.3986)

Coenen T., et al., 2014, A&A, 570, 60

Cohen M.H., Cannon W., Purcell G.H., Shaffer D.B., Broderick J.J., Kellermann K.I., Janucey D.L., 1971, ApJ, 170, 207

Corbel, S., et al., 2015, "Incoherent transient radio emission from stellar-mass compact objects in the SKA era", in Advancing Astrophysics with the Square Kilometre Array, PoS(AASKA14)053

Croft S., Bower G. C., Ackermann R., et al., 2010, ApJ, 719, 45

Croft S., Bower G. C., Keating G., Law C., Whysong D., Williams P. K. G., Wright M., 2011, ApJ, 731, 34

Croft S., Bower G. C., Whysong D., 2013, ApJ, 762, 93

Deller A.T., Middelberg E., 2014, AJ, 147, 14

Deneva J.S. et al., 2009, ApJ, 703, 2259

Edwards R.T, Bailes M., van Straten W., Britton M.C., 2001, MNRAS, 326, 358

Donnarumma I., et al., 2015, "SKA as a powerful hunter of jetted Tidal Disruption Events", in Advancing Astrophysics with the Square Kilometre Array, PoS(AASKA14)054

Fender R.P., Belloni T.M., Gallo E., 2004, MNRAS, 355, 1105

PoS(AASKA14)051

Fender R.P., Bell M.E., 2011, BASI, 39, 315
Fiedler R.L., Dennison B., Johnston K.J., Hewish A., 1987, Nature, 326, 675
Frail D. A., Kulkarni S. R., Ofek E. O., Bower G. C., Nakar E., 2012, ApJ, 747, 70
Gehrels N., Cannizzo J.K., 2015, Journal of Hugh Energy Astrophysics, in press (arXiv:1502.03064)
Hewish A., Bell S.J., Pilkington J.D.H., Scott P.F., Collins R.A., 1968, Nature, 217, 709
Hyman S. D., Lazio T. J. W., Kassim N. E., Ray P. S., Markwardt C. B., Yusef-Zadeh F., 2005, Nature, 434, 50
Hyman S. D., Lazio T. J. W., Roy S., Ray P. S., Kassim N. E., Neureuther J. L., 2006, ApJ, 639, 348
Hyman S. D., Wijnands R., Lazio T. J. W., Pal S., Starling R., Kassim N. E., Ray P. S., 2009, ApJ, 696, 280
Jacoby B.A., et al., 2009, ApJ, 699, 2009
Jaeger T.R., Hyman S.D., Kassim N.E., Lazio T.J.W., 2012, AJ, 143, 96
Keane E., Petroff E., 2015, MNRAS, 447, 2852
Keith, M., Jameson, A., van Straten, W., Bailes, M., Johnston, S. et al. 2010, MNRAS, 409, 619
Kulkarni S.R. et al., 1998, Nature, 395, 663
Law C., Bower G.C., Burke-Spolaor S., Butler B., Lawrence E., Lazio T.J.W., Mattmann C., Rupen M., Siemion A., Van der Wiel S., 2014, In: The Third Hot-wiring the Transient Universe Workshop, p 85-92
Law C.J., Bower G.C., Burke-Spolaor S., Butler B., Lawrence E., Lazio T.J.W., Mattman C.A., Rupen M., Siemion A., Van der Wiel S., 2014, ApJ, submitted (arXiv:1412.7536)
Law N.M., Kulkarni S.R., et al., 2009, PASP, 121, 1395
Lazio T.J., et al., 2010, AJ, 140, 1995
Levine A.M., Bradt H., Cui W., Jernigan J.G., Morgan E.H., Remillard R., Shirey R.E., Smith D.A., 1996, 469, L33
Lorimer D.R., Bailes M., McLaughlin M.A., Narkevic D.J., Crawford F., 2007, Science, 318, 777
Macquart J.P. et al., 2015, "Fast Transients at Cosmological Distances with the SKA", in Advancing Astrophysics with the Square Kilometre Array, PoS(AASKA14)055
Manchester R.N. et al., 2001, MNRAS, 328, 17
Metzger B.D., Williams P.K., Berger E., 2015, ApJ, submitted (arXiv:1502.01350)
Mirabel I.F., Rodríguez L.F., 1994, Nature, 371, 46
Ng C. and the HTRU Collboration, in IAU Symposium, Vol. 291, IAU Symposium, ed. J. van Leeuwen, 53, 56
O'Brien T., et al., 2015, "Thermal radio emission from novae & symbiotics with the Square Kilometre Array", in Advancing Astrophysics with the Square Kilometre Array, PoS(AASKA14)062
Obenberger K. S., Hartman J. M., Taylor G. B., et al., 2014, ApJ, 785, 27
O'Dea J.A., Jenet F.A., Cheng T-H., Buu C.M., Beroiz M., Asar S.W., Armstrong J.W., 2014, ApJ, 147, 100
Ofek E. O., Breslauer B., Gal-Yam A., Frail D., Kasliwal M. M., Kulkarni S. R., Waxman E., 2010, ApJ, 711, 517
Ofek E. O., Frail D. A., Breslauer B., Kulkarni S. R., Chandra P., Gal-Yam A., Kasliwal M. M.,

PoS(AASKA14)051

Gehrels N., 2011, ApJ, 740, 65
Perez-Torres M. et al., 2015, "Core-collapse and Type Ia supernovae with the SKA", in Advancing Astrophysics with the Square Kilometre Array, PoS(AASKA14)060
Petroff, E. et al. 2014, ApJ, 789, L26
Spitler L.G. et al., 2014, ApJ, 790, 101
Staley T. et al., 2013, MNRAS, 428, 3114
Stewart A., Fender R., et al., 2015, "LOFAR MSSS: Detection of a Low Frequency Radio Transient in 400 hrs of Monitoring of the North Celestial Pole", in prep
Stovall K. et al., 2014, ApJ, 791, 67
Thornton, D. et al. 2013, Science, 341, 53
Trott, C.M., Tingay, S.J. & Wayth, R.B. 2013, ApJ, 776, L16
van der Laan H., 1966, Nature, 211, 1131
Wang L., et al., 2015, "Investigations of supernovae and supernova remnants in the era of SKA", in Advancing Astrophysics with the Square Kilometre Array, PoS(AASKA14)064
Wayth R.B., Brisken W.F., Deller A.T., Majid W.A., Thompson D.R., Tingay S.J., Wagstaff K.L., 2011, ApJ, 735, 97
Wilkinson P., 2015, "The SKA and the Unknown Unknowns", in Advancing Astrophysics with the Square Kilometre Array, PoS(AASKA14)065
Williams P.K.G., Bower G.C., Croft S., Keating G.K., Law C.J., Wright M.C.H., 2013, ApJ, 762, 85
Yu W., et al., 2015, "Early Phase Detection and Coverage of Extragalactic and Galactic Black Hole X-ray Transients with SKA", in Advancing Astrophysics with the Square Kilometre Array, PoS(AASKA14)066
Zauderer B.A. et al., 2011, Nature, 476, 425
Zauderer B.A., Berger E., et al., 2013, ApJ, 767, 152

PoS(AASKA14)051

PROCEEDINGS OF SCIENCE

The SKA view of Gamma-ray Bursts

Davide Burlon[*,1,2], **Giancarlo Ghirlanda**[3], **Alexander van der Horst**[4], **Tara Murphy**[1,2], **Ralph Wijers**[4], **Bryan Gaensler**[1,2], **Gabriele Ghisellini**[3], **Isabella Prandoni**[5]

[1] *Sydney Institute for Astronomy, The University of Sydney, NSW 2006, Australia,*
[2] *ARC Centre of Excellence for All-sky Astrophysics (CAASTRO),*
[3] *INAF – Osservatorio Astronomico di Brera, via E. Bianchi 46, I-23807 Merate (LC) - Italy,*
[4] *Anton Pannekoek Institute, University of Amsterdam, Science Park 904, 1098 XH Amsterdam, The Netherlands,*
[5] *INAF – IRA, Via P. Gobetti 101, 40129 Bologna, Italy*
Email: davide.burlon@sydney.edu.au

Gamma-ray bursts (GRBs) are some of the most extreme events in the Universe. As well as providing a natural laboratory for investigating fundamental physical processes, they might trace the cosmic star formation rate up to extreme redshifts and probe the composition of the intergalactic medium over most of the Universe's history. Radio observations of GRBs play a key part in determining their physical properties, but currently they are largely limited to follow-up observations of γ-ray-detected objects.

The SKA will significantly increase our ability to study GRB afterglows, following up several hundred objects in the high frequency bands already in the "early science" implementation of the telescope. SKA1-MID Bands 4 (4 GHz) and 5 (9.2 GHz) will be particularly suited to the detection of these transient phenomena. The SKA will trace the peak of the emission, sampling the thick-to-thin transition of the evolving spectrum, and follow-up the afterglow down to the time the ejecta slow down to non-relativistic speeds. The full SKA will be able to observe the afterglows across the non-relativistic transition, for $\sim 25\%$ of the whole GRB population. This will allow us to get a significant insight into the true energy budget of GRBs, probe their surrounding density profile, and the shock microphysics. The SKA will also be able to routinely detect the elusive "orphan afterglow" emission, from the population of GRBs whose jets are not pointed towards the Earth. We expect that a deep all-sky survey such as SKA1-SUR will see around 300 orphan afterglows every week. We predict these detection to be $\gtrsim$1000 when the full SKA telescope will be operational.

Advancing Astrophysics with the Square Kilometre Array
June 8-13, 2014
Giardini Naxos, Italy

*Speaker.

PoS(AASKA14)052

1. Introduction

Gamma-ray bursts (GRBs) are among the most extreme events in the Universe. they provide a laboratory for investigating fundamental physical processes, trace the cosmic star formation up to very high redshifts, and probe the composition of the intergalactic medium over most of the Universe's history. Radio observations of GRBs play a key part in determining their physical properties by complementing the broadband spectrum and providing information unique to the radio regime.

The origin of GRBs remained elusive for three decades after their initial discovery (Klebesadel et al. 1973), but this changed with the discovery of their afterglows at X-ray (Costa et al. 1997), optical (van Paradijs et al. 1997), and radio (Frail et al. 1997) frequencies. GRBs occur at cosmological distances (Meegan et al. 1992; Metzger et al. 1997), and are generally thought to be caused by either the collapse of a massive star (Woosley 1993), or the binary merger of two neutron stars or a neutron star and a black hole (Eichler et al. 1989; Narayan et al. 1992). The former are the progenitors of so-called long GRBs, while the latter are associated with short GRBs. Long and short refer to the GRB duration in gamma-rays, and the divide between the two classes is at ~ 2 s (Kouveliotou et al. 1993), albeit it should be noted that the measured duration is energy-dependent. In both cases, the rapid accretion of material onto the compact object that is formed in these catastrophic events is thought to produce a pair of highly collimated relativistic jets, which decelerate and eventually evolve into a roughly isotropic blast wave. The isotropic equivalent kinetic energy released in a GRB is of order 10^{53-54} ergs, which is similar to that seen in supernova explosions when corrected for collimation and radiative efficiency (van Paradijs et al. 2000). However, GRB jets have bulk Lorentz factors of order of hundreds, and therefore relativistic beaming makes them some of the most luminous events in the Universe.

By studying the broadband emission of GRBs, from low-frequency radio waves to high-energy gamma-rays, we can determine the physical properties of the jet and its surroundings, and also the microphysics of the emission we observe. GRBs are amongst the highest redshiftobject known: the current highest spectroscopic redshift is $z = 8.23$ (Tanvir et al. 2009), and the photometric record-holder is $z = 9.2$ (Cucchiara et al. 2011). Therefore they can be used as probes of the early Universe, of the host galaxies (see e.g. Stanway et al. 2014; Perley & Perley 2013), and of the medium in between their host galaxies and us. Furthermore, GRBs are excellent laboratories for studying particle acceleration physics, because they are not only accelerating electrons to extreme relativistic velocities to produce the observed emission, but are also prime candidates for producing ultra-high energy cosmic rays. In this chapter we first focus on the role of radio observations in GRB studies (Section 2) and the progress that has been made in this field over the decade since the original SKA science case was written (Section 3). We have performed simulations to give prospects for GRB studies in the SKA era, for GRBs whose jets point towards the Earth (Section 4), and also those which are pointed away and from which we can detect late-time emission when the GRB outflow enters our line of sight (Section 5). For a more comprehensive review on radio observations of GRBs and their role in GRB jet studies we refer to Granot & van der Horst (2014).

PoS(AASKA14)052

2. Radio observations of GRBs

Almost all GRBs have been detected first with γ-ray instruments and then followed up at other wavelengths (see e.g. the interesting case reported by Cenko et al. 2013). Since the discovery of the first radio afterglow (Frail et al. 1997) roughly one third of all GRBs with accurate locations has been detected at radio frequencies (Chandra & Frail 2012). This rate is much lower than at higher observing frequencies, where for instance 93% of GRBs detected in gamma-rays by the *Swift* satellite are also detected at X-ray frequencies and 75% have been detected in optical. This difference is due to the fact that GRBs have radio flux densities typically at the sub-mJy level, which for a long time has been close to the sensitivity limits of even the largest radio observatories. Besides the sample of radio detected GRBs being sensitivity limited (Chandra & Frail 2012), it has been claimed that there are in fact two populations of radio-bright and radio-faint GRBs (Hancock et al. 2013). The latter has been found by stacking radio visibility data of many GRB follow-up observations. This could be tested with the upgraded Very Large Array and ultimately with the SKA. If there are indeed two populations of radio afterglows, the cause of this can be resolved by broadband modelling of a large sample of individual GRBs.

In the standard model for GRBs, the afterglow is thought to be emission from the blast wave at the front of the relativistic jet pointing towards us. As this shock sweeps up the ambient medium, it accelerates electrons (and protons) and amplifies the magnetic field, both necessary for the observed synchrotron radiation. Deceleration of the blast wave results in the peak of the spectrum moving from high to low observing frequencies over time (Sari et al. 1998). This spectral peak is typically already below optical frequencies when the first observations commence, resulting in declining light curves at optical and X-ray frequencies, but rising light curves in the radio at early times, up to the peak occurring days or weeks after the initial gamma-ray trigger (see Figure 1). Multi-frequency radio observations at later times can follow the evolution of both the peak frequency and peak flux. Furthermore, the radio regime is affected by synchrotron self-absorption, which makes early radio detections challenging, but when detected, time evolution of the self-absorption frequency provides important constraints on the blast wave physics. Therefore, the radio regime plays an important role in constructing the full broadband spectrum, to constrain both the macrophysics of the jet, i.e. the energetics and ambient medium density, and the microphysics of the electrons and magnetic fields necessary for synchrotron emission (Wijers & Galama 1999).

Radio afterglow emission peaks much later than at higher frequencies, and it also lasts much longer, for months or even years (Figure 1; e.g., Frail et al. 2000; Berger et al. 2004; van der Horst et al. 2008). Late-time observations can be used to study the GRB jet as it decelerates into the non-relativistic phase. This provides a unique probe for the dynamics of the jet, in particular for determining the true total kinetic energy in the blast wave; at late times the outflow is almost spherical and energy estimates are not complicated by relativistic effects (see Section 4.1 for a more detailed discussion). In addition to these late-time studies, the radio regime is also well suited for studying early-time phenomena which may go undetected at high frequencies, for instance emission from the reverse shock. When the blast wave at the front of the jet is formed, there is not only a shock moving forward into the ambient medium, but also a shock moving backwards into the ejecta (Sari & Piran 1999). Under the right conditions this reverse shock will result in an optical flash in the first tens of seconds after the gamma-ray trigger (Akerlof et al. 1999), which can

PoS(AASKA14)052

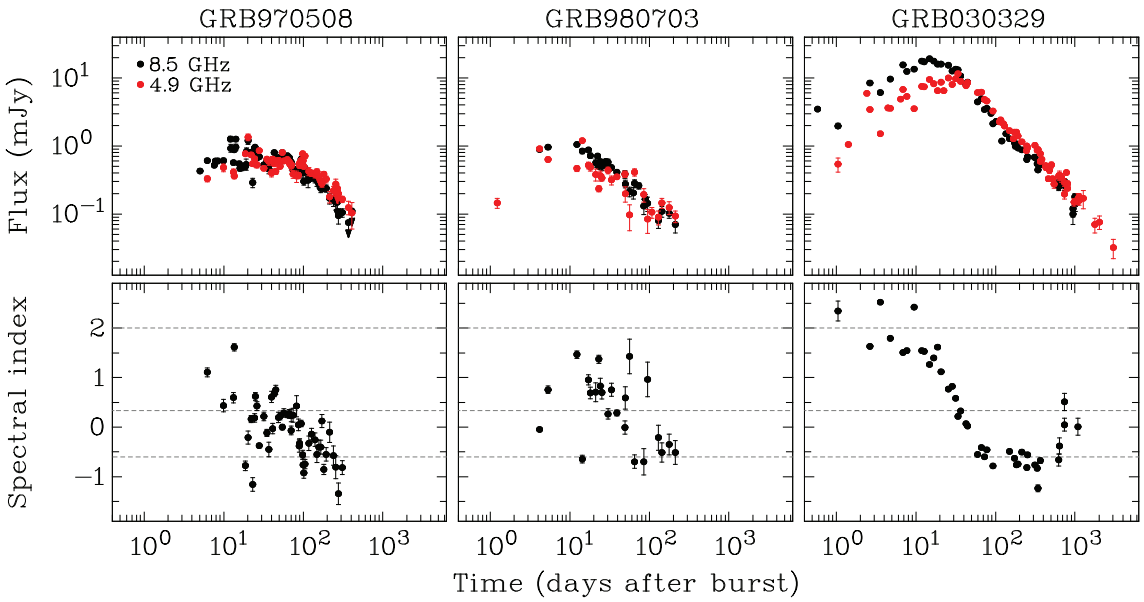

Figure 1: Radio light curves at 4.9 and 8.5 GHz (top panels) and spectral indices (bottom panels) for the well-sampled, long-lasting GRBs 970508, 980703 and 030329 (Granot & van der Horst 2014). The spectral index α (where $F_\nu \propto \nu^\alpha$) between 4.9 and 8.5 GHz varies significantly due to the spectral evolution and scintillation effects. The dashed lines in the bottom panels indicate spectral indices of 2, $1/3$ and -0.6, which are expected below the self-absorption frequency, between the self-absorption and peak frequency, and above the peak frequency, respectively.

only be detected if robotic telescopes are on target fast enough. However the peak of this emission moves to lower frequencies over time and can be probed at radio frequencies on a time-scale of hours to days (Kulkarni et al. 1999). Multi-frequency observations of this reverse shock provide crucial information regarding the particle content of the jet and its internal magnetic field (e.g. Perley et al. 2014; Anderson et al. 2014, and references therein).

Another way in which radio observations play a key role in GRB studies is by providing evidence for the relativistic expansion of the jet. The source size and its evolution can be estimated either directly by means of Very Long Baseline Interferometry (VLBI), or indirectly by utilising the effects of interstellar scintillation. The former method has only been possible for one nearby GRB (Taylor et al. 2004), and the source size measurements have been combined with its light curves to better constrain the physical parameters (Granot et al. 2005; Mesler & Pihlström 2013). Indirect source size measurements are possible because of scintillation due to the local interstellar medium, which modulates the radio flux (Goodman 1997). While the angular size of the blast wave is initially smaller than the characteristic angular scale for interstellar scintillation, it grows with time until it eventually exceeds this scale and the modulations quench. This can be utilised in determining the source size and the expansion speed of the blast wave, which impose constraints on the modelling of GRB afterglows (Frail et al. 1997). The future possibilities of VLBI observations of GRBs in the SKA era are discussed elsewhere in this book; see the Chapter by Paragi et al., "Very Long Baseline Interferometry with the SKA", in proceedings of "Advancing Astrophysics

PoS(AASKA14)052

with the Square Kilometre Array", PoS(AASKA14)143.

All the observational characteristics at radio frequencies discussed so far are for GRBs in which the jet is oriented along our line of sight. Since the initial Lorentz factors of the shocks are of the order of a few hundred, relativistic beaming causes the initial γ-ray emission to go undetected if we are not observing a GRB within the jet opening angle. Therefore, we only detect a small fraction of the total number of events (Rhoads 1997). Estimates of collimation for individual GRBs are usually derived from the afterglow light curve: an achromatic break to a steeper decay indicates a transition across the jet opening angle. The time at which this 'jet break' occurs, combined with the ambient medium density and the energetics of the GRB, leads to an estimate of the jet opening angle (Sari et al. 1999). This approach is limited by the difficulty in identifying an unambiguous jet break in the light curve and yields a wide variation of jet angles, but typically a few to a few tens of degrees. An alternative way to obtain a handle on jet opening angles, and on the total GRB rate whether beamed towards us or not, is to carry out a survey for GRB afterglows at very late times when the outflow is (quasi-)spherical and only detectable at radio frequencies. Since a large fraction of GRBs are associated with supernovae of Type Ib/c, it has been suggested to search for radio counterparts of relatively nearby supernovae of that type (Paczynski 2001; Granot & Loeb 2003). Attempts to find such orphan radio afterglows have been unsuccessful thus far (Berger et al. 2003; Soderberg et al. 2006a; Bietenholz et al. 2014).

3. Progress in the Last Decade

Our understanding of GRBs has increased significantly over the past decade, mainly because of improvements in observational capabilities across the electromagnetic spectrum. For instance, the *Swift* satellite has revealed very interesting X-ray behavior in the first minutes to hours (Nousek et al. 2006), robotic telescopes have done the same at optical frequencies (e.g., Racusin et al. 2008), and the *Fermi Gamma-ray Space Telescope* has opened the high-energy gamma-ray regime for GRBs, including emission at GeV energies (Ackermann et al. 2013). Furthermore, the GRB-supernova association has been further established for long GRBs (Woosley & Bloom 2006), while afterglows of short GRBs have been discovered (Gehrels et al. 2005), and strong indications for their connection with binary mergers of compact objects have been found (Tanvir et al. 2013).

From the radio perspective, GRB 030329 had a major impact: the first high-luminosity GRB at low redshift, which also satisfied the GRB-supernova connection. It is the only GRB up to now for which the source size has been measured with VLBI, and the radio afterglow was so bright and long-lasting that it has been detected for almost a decade at low radio frequencies (van der Horst et al. 2008; Mesler et al. 2012). The multi-frequency light curves have made it possible to follow the evolution of the blast wave from the ultra-relativistic to the non-relativistic phase and perform broadband modeling in the different phases. This has led to tight constraints on the physical parameters, and also a consistent picture together with modeling of the VLBI measurements (Granot et al. 2005; Mesler & Pihlström 2013). The puzzle that still remains is that all the modeling work points to the ambient medium being homogeneous, and in that case a signature from the counter-jet (the jet originally pointed away from the Earth) should have been observed (De Colle et al. 2012). This did not happen, questioning the existance and properties of this counter-jet.

PoS(AASKA14)052

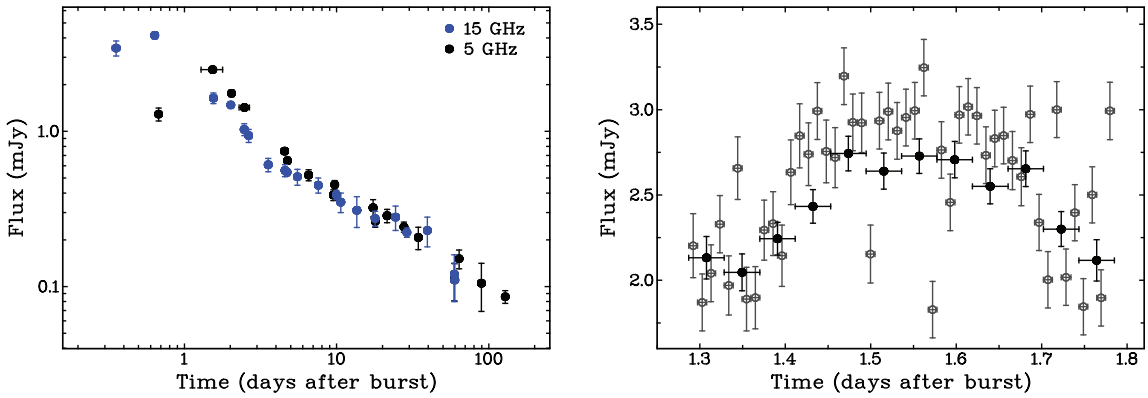

Figure 2: The left panel (Anderson et al. 2014) shows the radio light curves of the bright GRB 130427A at 5 and 15 GHz (see also Laskar et al. 2013; Perley et al. 2014; van der Horst et al. 2014), showing the evolution of the radio peak moving from high to low frequencies at early times. The right panel shows strong variability at the peak of the 5 GHz light curve on a timescale of hours (solid symbols), and perhaps even shorter (15 minutes; open symbols), due to interstellar scintillation (van der Horst et al. 2014).

Radio observations have played an important role in the broadband modeling of a larger sample of GRBs, e.g., very energetic GRBs detected by *Swift* (Cenko et al. 2010) and those for which high-energy gamma-rays have been detected by *Fermi* (Cenko et al. 2011). These studies indicate that there is a large spread in the physical parameters, which has implications for models of GRB progenitors, particle acceleration, and magnetic field amplification by shocks (Granot & van der Horst 2014). A striking example is GRB 130427A, another nearby, high-luminosity event with extremely good temporal and spectral coverage, over 10 orders of magnitude in time and 16 orders of magnitude in observing frequency (Ackermann et al. 2014; Maselli et al. 2014). A bright radio flare was observed in the first days, with the peak moving from high to low radio frequencies over time (left hand panel of Figure 2; Laskar et al. 2013; Anderson et al. 2014; Perley et al. 2014; van der Horst et al. 2014). The earliest clear detection at 8 h and subsequent observations at high cadence have shown how early-time radio observations can contribute significantly to our understanding of the physics of both the forward and reverse shocks. This was also the second GRB for which radio variability on the timescale of hours has been reported (right hand panel of Figure 2; van der Horst et al. 2014), and in this case, as well as for GRB 070125 (Chandra et al. 2008), the variability strength and timescale are both consistent with interstellar scintillation effects.

An important probe for getting a better understanding of the jet and magnetic field structure is polarization measurements. In the optical, linear polarization of the order of a few percent has been observed in emission from the forward shock (Covino et al. 1999; Wijers et al. 1999), while this can be tens of percent for the reverse shock (Mundell et al. 2013). Optical circular polarization has recently been discovered, at a level of only a few tenths of a percent (Wiersema et al. 2014). At radio frequencies the most stringent constraints have been obtained for GRB 030329 at late times (Taylor et al. 2005), and for GRB 130427A at early times (van der Horst et al. 2014). The upper limits are only a few percent in both linear and circular polarization, and thus getting close to the optical detections. Deeper radio polarization measurements for bright GRBs, preferably at early

PoS(AASKA14)052

times and for GRBs with optical polarization detections as well, will provide more insight into the magnetic field strength and structure inside the GRB jet.

Coherent radio emission has been predicted at earlier times than from the reverse shock, which peaks at a timescale of hours to days at radio frequencies. In these models the jet is magnetically dominated (Usov & Katz 2000; Sagiv & Waxman 2002; Moortgat & Kuijpers 2006), and detecting this emission would uniquely constrain the jet production and collimation mechanism. The first searches have not resulted in any firm detections (Bannister et al. 2012; Obenberger et al. 2014), but surveys with large field-of-view telescopes are vital for this research. Such studies should also clarify if (some of) the recently discovered fast radio bursts (Lorimer et al. 2007; Thornton et al. 2013) are connected to GRBs (Zhang 2014).

Radio surveys with sufficient sensitivity and sky coverage are not only important for prompt radio emission searches, but also for detecting orphan afterglows. Such studies would let us directly constrain the overall beaming fraction of GRBs, and yield the rate of the events that generate this phenomenon. Furthermore, since radio emission is unaffected by extinction, and a significant fraction of GRBs are thought to occur in highly obscured regions (Perley et al. 2009), radio surveys can provide a new picture of the GRB population unbiased by their local environments. This ties in with studies of dark bursts, i.e. GRBs for which the optical afterglow is much dimmer than expected from the observed X-ray emission. These GRBs are either at a high redshift or there is significant optical extinction in the host galaxy. The latter is the most common explanation, and the amount of extinction can be estimated by modeling of the X-ray and radio light curves (Rol et al. 2007; Zauderer et al. 2013).

4. The GRB population pointing to Earth

In this section we focus on GRBs that can be studied by the SKA after a trigger has been produced by γ-ray detectors, as now happens with *Swift* and *Fermi* providing the high energy trigger and initiating the follow-up campaign. These are the GRBs that have their jets pointed towards the Earth.

Substantial advances in breaking the degeneracies of the physical parameters of the afterglow emission process and, globally, of the GRB itself can only be possible through a considerable increase of the detection rate of GRBs coupled to the ability to follow the radio emission from early to very late times (i.e. at extremely faint flux densities).

The key questions we will address are:

1. What are the prospects for the detection and follow up of GRBs by the SKA?
2. What is the expected rate of GRBs that can be observed by the SKA?
3. What is the best observational strategy, considering the wide frequency range covered by the SKA and the behaviour of the GRB emission at radio frequencies as a function of time?

In order to answer these questions, we first characterised the radio afterglow light curves of a synthetic population of GRBs constructed so that its γ-ray properties (flux distributions, energetics/luminosities) match those of the real populations of GRBs detected by CGRO/BATSE, *Swift* and *Fermi*. GRBs are distributed in redshift between $z = 0$ and 10 according to the GRB formation

PoS(AASKA14)052

rate (see Salvaterra et al. 2012, for the different components that are used). For each simulated burst, the radio afterglow emission was simulated using a hydrodynamic numerical code (for full details we refer the reader to van Eerten & MacFadyen 2011, and van Eerten et al. 2012). The micro-physical parameters (how much energy is distributed to the electrons and magnetic fields, the slope of the electron distribution, and the density of the homogeneous ambient medium) were set in order to reproduce the typical fluxes of the afterglows observed in the optical (Melandri et al. 2014) and radio (Ghirlanda et al. 2013a) bands of a carefully selected sample of bright GRBs observed by *Swift* (the so-called BAT6 sample of Salvaterra et al. 2012). These are the brightest GRBs detected by *Swift*/BAT and they have typical flux densities between 1 and 5 days distributed between 0.1 and 2 mJy at 8.4 GHz (Chandra & Frail 2012). The micro-physical parameters were tuned to reproduce these flux levels (as shown by the red points in the right panel of Fig. 3). This approach is discussed in detail by Ghirlanda et al. (2013b). A caveat is the lack of the possible contribution of the reverse shock component, which might dominate the emission at early times. Estimates on the detection rates at early times should hence be conservative lower limits. Another caveat is that the simulations do not consider the possible supernova contribution, nor the effects of scintillation.

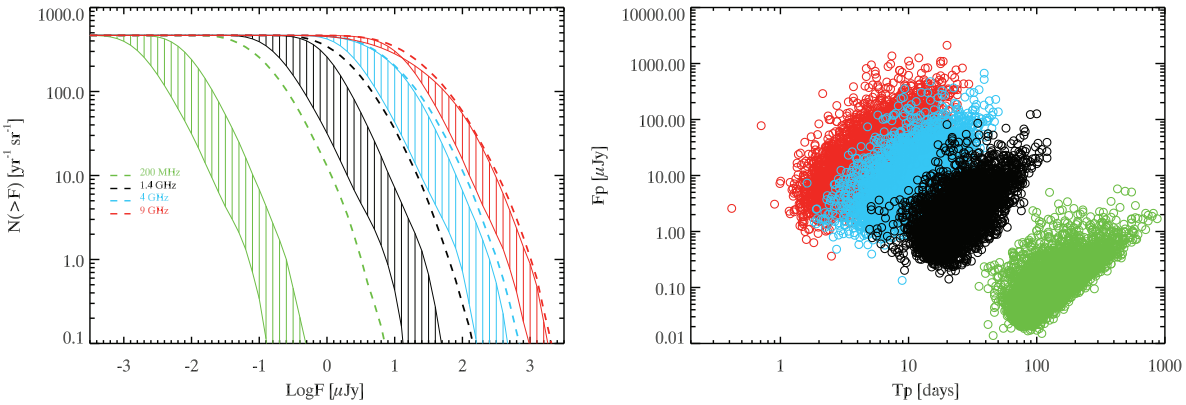

Figure 3: *Left*: Cumulative flux distribution of afterglows at SKA1-LOW and SKA1-MID observing bands 2, 4, and 5 (from left to right). The shaded area represents the span between 2 and 10 days (left and right boundary respectively). The dashed line represent the flux at the peak time. *Right:* Afterglow peak flux vs. observed time of the peak (which happens at the time the peak of the spectrum crosses the observed band) for different SKA frequencies. The colours (red, blue, black, and green) represent bands 5, 4, 2 of SKA1-MID and SKA1-LOW, i.e. 9.2, 4, 1.4 and 0.2 GHz respectively.

At early times (days after the burst), the emission from the forward shock is suppressed by synchrotron self-absorption, and therefore the flux density due to this component is expected to rise until a *spectral peak* is produced by the passage of the frequency (be it the injection frequency or the self-absorption frequency) corresponding to the peak of the spectrum in the telescope observing band. This effectively means that the observing strategy should consider the available frequencies and the typical behaviour of the flux of the afterglow at those frequencies. For instance, the detection rate is maximised if the observations are performed close to the time when the peak of the afterglow is reached at a certain frequency. On the other hand, early time observations, which are critical for the multi-wavelength study of the GRB emission (coupling radio with

PoS(AASKA14)052

optical/NIR, and X-rays), should be planned considering that the radio spectrum of the afterglow is still self-absorbed. Therefore, a successful detection is optimised if performed at relatively high radio frequencies[1].

In Fig. 3 (left) we show the cumulative flux distribution of the simulated sample of GRBs. The different colours represent different bands of the SKA. The shaded regions represent the cumulative flux distributions if observations are performed between 2 and 10 days after the GRB trigger. The peak flux distributions are shown by the dashed lines. Two behaviours are clearly visible. Firstly, the highest flux is always at the time of the second observation (i.e. the emission is still in the self-absorbed region of the spectrum). Secondly, the width of the region decreases with increasing frequency, because observing in a higher radio band will bring the observation closer to the region in the spectrum where most of the flux is emitted, and where the evolution is faster. SKA1-MID band 5 (9.2 GHz) is clearly the band that tends to pick a radio afterglow between 2 and 10 days closest to the time of the peak. Another way of looking at the distance of the dashed line from the corresponding shaded area (which again, is maximum for SKA1-LOW, and minimum for the highest SKA1-MID band shown), is a measure of how long to delay an observation in order to maximise the chance of detection in each SKA band.

Table 1: SKA detection rates of radio afterglows independent from high-energy triggers. For each band we report the 5σ sensitivity limit. A standard observation of 12 hours is assumed. [a] Refers to "early science", an initial implementation with half the sensitivity across all bands. [b] The sensitivity is assumed to be $4\times$ better in the LOW band, and $10\times$ otherwise.

	SKA1-MID			SKA1-MID E.S.[a]	SKA2[b]
Band	Freq. [GHz]	$F_{\rm lim}$ [μJy]	Rate [# sr^{-1} yr^{-1}]	Rate [# sr^{-1} yr^{-1}]	Rate [# sr^{-1} yr^{-1}]
LOW	0.2	3	0	0	2
Band 2	1.4	1.39	300	170	465
Band 4	4.0	0.65	465	450	465
Band 5	9.2	0.75	465	465	465

Alternatively, one can visualise this behaviour by investigating the flux density at which a GRB afterglow peaks when the transition from optically thick-to-thin happens. Fig. 3 (right) shows a plot of the peak fluxes versus the time at which the frequency corresponding to the peak of the spectrum crosses the band (different colours represent the simulated SKA bands). The more energetic GRBs peak at later times, with the lower frequencies lagging the high ones. The brighter bursts populate the upper right part of the distributions, and can indeed be brighter than 0.1 mJy at 1.4 GHz even months after the prompt emission has disappeared. However they are very rare, representing less than 1% of the whole population. We note that this is probably a lower limit on the actual fraction of these highly luminous afterglows, given that small number statistics dominate the tail of the simulated distributions. We have calculated the rates of GRB afterglows that we expect to be able to observe at the time of their peak, depending on the level of sensitivity[2] the SKA1 and SKA2

[1] Conversely, the chance of detection of the reverse shock component is maximised in the first day.

[2] Sensitivities are calculated from the SKA1 system baseline design documents, see Dewdney et al. (2013).

PoS(AASKA14)052

will reach in each band. Table 1 summarises these results for the whole synthetic population of afterglows (i.e. regardless of their γ-ray properties). Given that the logN-logF is almost flat at sub-μJy levels, in particular for the high frequency bands, there is no big improvement in expected rates from SKA1 to SKA2. The catch is that in order to detect a GRB pointed to Earth, we will always need a trigger. On the other hand, for the GRBs that we will be able to detect, the SKA will be able to sample to lightcurve down to the μJy level, producing finely sampled lightcurves, that current facilities are able to produce just for the very close-by GRBs.

In the past, the observation strategy for GRB afterglows was driven more by the goal of having coeval multi-wavelength observations across the spectrum. The need of being on target as soon as possible in the optical, NIR, and X-rays possibly drove the attempt of having a detection in the very first few days. A small number of bursts were detected and followed-up to extremely late times (see Frail et al. 1997, 2004; Berger et al. 2004; van der Horst et al. 2005, 2008), but the large majority ($> 70\%$) of radio observations resulted in non-detections overall. Note that when just the (γ-ray) brighter population of bursts was considered, the ratio of positive detections rose to $\sim 50\%$ (Ghirlanda et al. 2013a), which hints that the SKA will indeed be able to probe the hidden population of radio afterglows (Anderson et al., 2014 –in preparation– will present the first systematic radio follow-up of *Swift* GRBs at GHz frequencies).

4.1 GRB calorimetry: accessing the true energy budget

One of the key characteristics of the GRB phenomenon that has eluded direct measurements is the estimate of the true energy budget of the central engine that powers the explosion. The isotropic equivalent energy emitted in γ-rays ($E_{\gamma,\mathrm{iso}}$) is just a proxy of the true GRB energy. Indeed, due to the collimated structure of GRBs, the energy E_γ emitted just in γ-rays is a factor $\approx \theta_{\mathrm{jet}}{}^2/2$ smaller than that derived assuming isotropy, where θ_{jet} is the jet angle. Moreover, the measure of the jet angle can be marred by observational biases and possibly by additional components at play in the external shock emission. Additionally, the energy emitted in the high-energy band is a fraction of the kinetic energy ($E_{\mathrm{kin,iso}}$), initially available.

According to the standard model, the fireball becomes non-relativistic (NR) at a time t_{NR}, which is long after the prompt emission has faded away. The theoretical prediction of when this transition should occur is subject to debate, and consequently there is roughly an order of magnitude in the range of values that t_{NR} can take, from hundreds (e.g. Livio & Waxman 2000; Sironi & Giannios 2013) to thousands of days (e.g. Piran 2004; Zhang & MacFadyen 2009; Wygoda et al. 2011; van Eerten et al. 2012). For this Chapter, we have adopted the "best case" scenario, with the caveat that this is subject to further improvements. Following Livio & Waxman (2000), the transition happens at $t_{\mathrm{NR}} \sim 275(1+z)(n/1\ \mathrm{cm}^{-3})^{-1/3}(E_{\mathrm{kin,iso}}/10^{53}\ \mathrm{erg})^{1/3}$ days. The advantage of performing energetic estimates (calorimetry) at such late times is that the afterglow emission becomes independent from the bulk Lorentz factor (which becomes ≈ 1). This allows us to derive the true GRB kinetic energy (e.g. Frail et al. 2000; Shivvers & Berger 2011), which is directly related to the energy emitted in γ-rays during the prompt phase through a radiative efficiency factor η. This is related to the measurable $E_{\gamma,\mathrm{iso}}$ by $E_{\mathrm{kin,jet}} \approx [\theta_{\mathrm{jet}}{}^2/(2\eta)] \times E_{\gamma,\mathrm{iso}}$. This is where the power of these observations becomes evident: assuming the efficiency η of the shocks will give us an independent measure of the jet opening angle; conversely for the cases in which there will be a measure of the

PoS(AASKA14)052

jet opening angle (e.g. from the achromatic break in the X-ray and optical afterglow), we will be able to compute the shock efficiency.

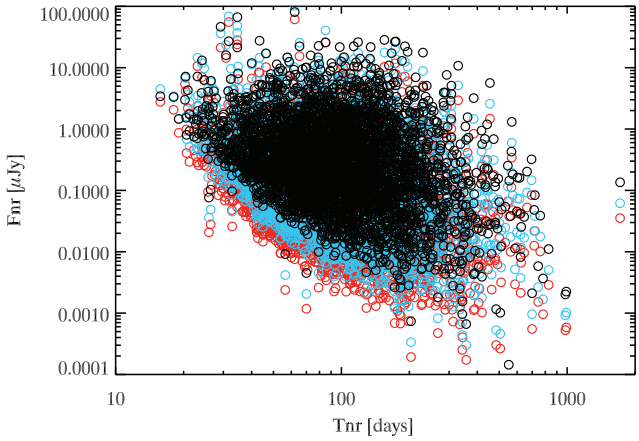

Figure 4: Transition to the NR regime: the flux is calculated at time of the crossing to the NR regime, calculated as per Livio & Waxmann, 2001. The colour code is as per Fig. 3.

In addition, observations before and after $t_{\rm NR}$ are probes of the ambient medium profile. In the simple case of a homogeneous density ambient medium, a peculiar flattening of the lightcurve is predicted by the standard model. In the simple case of uniform density ISM, a flattening of $\Delta\alpha = (21-5p)/10$ is expected for the lightcurve across this transition (Frail et al. 2005), for the standard values of the electron distribution slope p. Interestingly, a steepening could also potentially be observed at times after $t_{\rm NR}$, and that would also help us constrain the microphysical parameter p. In the case of a wind-like medium, the transition is expected at later times, with a distinct slope variation of the lightcurve. Therefore observing across the NR transition is a powerful diagnostic of the circumburst medium density profile.

We have computed the expected flux density at the NR transition for the SKA bands 2, 4, and 5, see Fig. 4. Consistently with the observations available so far, only a handful of objects reach the sensitivity limit of current facilities (a few μJy at best). We foresee that SKA1-MID will be able to observe a minor fraction of these (of the order of 2–5%, down to 0.9–2% for the "early science" phase), but that the full SKA will routinely observe a significant fraction (15–25%) of the whole GRB afterglow population at the NR transition.Even for the full SKA though, a substantial (75–85%) fraction of sources will be undetectable. We calculated the fractions based on the number of afterglows above a 12-hour-long observation (5σ), over the total population.

4.2 The case for a very sensitive high–energy telescope

The sensitivity of the SKA will allow us to observe almost the complete population of GRBs, provided that a γ-ray instrument, more sensitive than *Swift* will be operational in the SKA era, and provided that a GRB localisation to a few arcsec spatial resolution will be available. We have explored the case of a burst monitor with a ($\sim 5\times$) greater sensitivity than that of the *Swift*/BAT. As can be seen in Fig. 5, the bursts that can be seen in band 5 (9.2 GHz) of SKA1-MID are a larger

PoS(AASKA14)052

fraction of the whole population with respect to the ones that will trigger *Swift* provided that a γ-ray trigger is supplied.

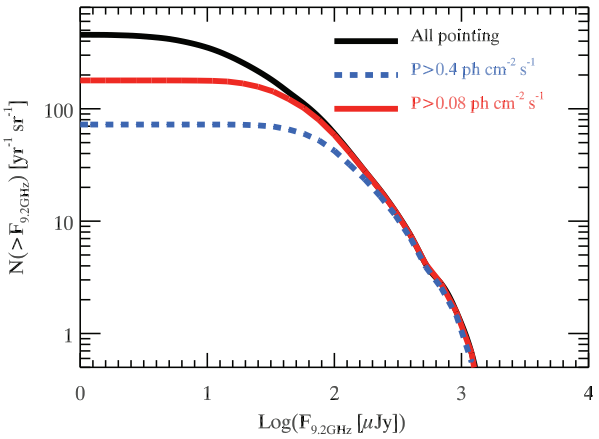

Figure 5: LogN–logF of SKA1-MID band 5 (9.2 GHz) showing the flux at the peak of the light curve for the population of simulated GRBs. The red solid and blue dashed lines represent the population of GRBs that have a γ-ray photon peak flux (P) greater than 0.08 and 0.4 ph cm^{-2} s^{-1}, respectively. The latter represents the synthetic population of bursts that can trigger *Swift*. The improvement of radio flux sensitivity assured by the SKA can be exploited only if a γ-ray detector more sensitive (in the case shown, we assume a five-fold improvement in trigger sensitivity) than *Swift* will be operating in the SKA era. The distance between the red and blue line shows how many GRB afterglows, whose radio flux density is accessible by the SKA, we will miss out unless there is a GRB trigger. The black line shows all GRBs pointing to the Earth, irrespectively of the their γ-ray flux.

In short, the future absence of a burst monitor with an improved sensitivity than that of the *Swift*/BAT, would imply that the rate of GRB afterglows that are observable at the μ-Jy level is comparable to the the ones we can already observe today (i.e. ~ 50 sr^{-1} yr^{-1}). In conclusion, while trigger-dependent detection rates might not dramatically improve in the SKA era, the sampling of the lightcurves of the GRBs that will produce a γ-ray trigger will be far better than that available today.

5. Revealing the orphan afterglow population

Most GRBs do not have their jets pointing towards us. As a result they are undetectable in the γ-ray band but should be detectable as 'orphan afterglow (OA)'. Given the typical jet opening angles of GRBs, the population of OAs should outnumber the pointing GRB population by two orders of magnitude.

Jet opening angles have been derived by the afterglow light curve break (Frail et al. 2001; Ghirlanda et al. 2004) and have a distribution clustered at $\theta_{\rm jet} \sim 5$ deg. It is expected that, purely by geometric arguments, for each GRB pointing towards the Earth that can potentially trigger a γ-ray instrument, there are $\sim 2(\theta_{\rm jet}/0.1)^{-2} \approx 260$ events directed in all other directions in the sky. More realistically, Ghirlanda et al. (2014) have estimated that — given that $\theta_{\rm jet}$ has a distribution

PoS(AASKA14)052

of values — the ratio of OAs to GRBs pointing to us is ~ 40. These bursts are undetectable in the high energy band because are viewed at angles $\theta_{\rm view} > \theta_{\rm jet}$, but are expected to be potentially observable at optical and radio wavelengths from the time when, during the afterglow evolution, their Lorentz factors slows down to $\Gamma \sim {\theta_{\rm view}}^{-1}$. These events should therefore lack their prompt emission (and hence have been dubbed 'orphan afterglows') and should show up in deep optical and radio transient surveys. The characterisation of their properties, the feature of their lightcurves, the typical timescales and peak fluxes are of particular interest for the deep, large surveys of the future facilities like SKA1-SUR, since this class of transients could (i) be difficult to disentangle from other classes of transients, and (ii) constitute a considerable fraction of transient events in the sky. Up until today the quest for their discovery has resulted in upper ($\theta_{\rm jet} \lesssim 22^\circ$ Levinson et al. 2002) or lower ($\theta_{\rm jet} \gtrsim 0.8^\circ$ Soderberg et al. 2006b) limits on the GRB opening angles. Some peculiar transients in past surveys could have been genuine OAs both in the optical (Rau et al. 2006; Zou et al. 2007; Malacrino et al. 2007) and radio (for a recent reveiw on blind surveys see Murphy et al. 2013) regime, but none have been confirmed so far.

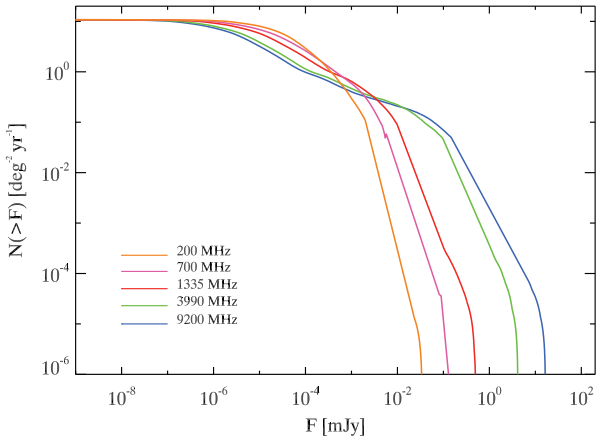

Figure 6: Cumulative flux distribution of orphan afterglows at the frequencies of SKA1-MID/SKA1-SUR and SKA1-LOW are shown. To compute the number of expected OA detections, as detailed in the text, we assumed a deep (1000 hour), all-sky (3π) survey. The rates can be rescaled easily since they are linearly proportional to the sky fraction covered.

The evolution of the OA lightcurve differs from that of a normal afterglow before reaching its peak flux. In fact, an OA should start to be potentially observable[3] when the edge of the jet intercepts the line of sight of the observer: this happens when the fireball has decelerated to $\Gamma = 1/\sin(\theta_{\rm view} - \theta_{\rm jet})$. In this respect, the OA is driven by geometry because it is a *dynamical peak*, not a spectral peak generated by the passage of the peak of the spectrum through the observing band. This happens at $\Gamma = 1/\sin(\theta_{\rm view})$, and the afterglow evolves like that of a standard GRB thereafter. Ghirlanda et al. (2014) have estimated that the distribution of peak times is very broad and peaks at ~ 1000 days. In addition, we show in Fig. 6 the cumulative flux distribution of a simulated sample of OAs in the SKA1 bands. The rates are expressed in units of deg^{-2} yr^{-1}, so that the conversion

[3]Under the simplified assumption of a sharp edged cone shape for the jet.

PoS(AASKA14)052

to the prediction for different fields of view will be straightforward. The high (low) flux tail of the logN-logF are consistent with a slope of -1.7 (-0.4) roughly in all bands. The GRBs with small opening angles dominate the logN-logF in the high flux tail; conversely the low flux tail is due to the cumulative contribution of GRBs with progressively large opening angles. We calculated from Fig. 6 how many OAs an all-sky survey with SKA1-SUR should be able to detect each week in every PAF band. This result is summarised in Table 2.

Table 2: SKA1-SUR detection rates of orphan afterglows in the SKA1-SUR bands. The rates are derived from the flux density distributions shown in Fig. 6, assuming 1000 hours of integration time, all-sky (3π), 5σ and given in units of $3\pi^{-1}$ week^{-1}. $F_{\rm lim}$ is in units of μJy. [a] Refers to "early science", an initial implementation with half the sensitivity. [b] The sensitivity is assumed to be 10 $\times$ better for SKA2.

		SKA1-SUR		SKA1-SUR E.S.[a]		SKA2[b]	
Band	Freq. [GHz]	$F_{\rm lim}$	Rate	$F_{\rm lim}$	Rate	$F_{\rm lim}$	Rate
PAF band 1	0.7	1.54	357	3.08	178	0.2	1190
PAF band 2	1.4	0.92	387	1.84	297	0.9	1011
PAF band 3	4.0	1.23	297	2.46	237	0.6	892

The possibility of revealing the population of orphan afterglows by SKA through its survey is tantalizing. Our estimates suggests that at radio frequencies orphan afterglows should be relatively long-term transients with typical duration above the expected flux limit of the SKA survey of hundreds of days. The challenge will be to distinguish the population of orphans from other possible sources (non-GRBs) that produce such slow transients. The unique possibility offered by the SKA multifrequency observations will be to study the radio spectrum of these transients. Moreover, as discussed more in detail in the Chapter on the VLBI capabilities of the SKA (Paragi et al., "Very Long Baseline Interferometry with the SKA", in proceedings of "Advancing Astrophysics with the Square Kilometre Array", PoS(AASKA14)143), the longest baselines will secure sub-mas resolution. This is turn will mean that, at least for the OAs with sufficient signal-to-noise we will be able to measure the expansion velocity of the ejecta. This will be an additional tool to distinguish transients powered by a central engine from radio SNe.

6. Conclusion and the road to the SKA

The SKA era will be transformational for the study of GRBs, because it will allow us to observe close to 100% of the detected GRBs directed towards the Earth. In addition to very high detection *rates*, if compared to the state of the art, it will be able to produce well-sampled radio lightcurves, bringing radio-astronomy to the same level of completeness obtained in the last decade at higher (optical, X-ray) frequencies.

For a quarter of all GRBs with a jet pointing to the Earth, the SKA will be able to trace the lightcurve up to very late times, even across the non-relativistic transition. We will get an unprecedented insight into the true energy budget of GRB engines by means of these very late-time observations. Additionally, these observations will probe both the macrophysics of the ambient medium (e.g. the density profile) and the microphysics of the shocks, which are believed to be at the basis of afterglow emission.

PoS(AASKA14)052

The ability to both increase the sheer rate of detections, and to follow the afterglow lightcurve to very late times will naturally depend on the availability of a γ-ray trigger with arcsecond resolution.

Finally we will be able to observe the so far elusive class of "orphan afterglows", which are predicted to exceed the standard afterglow rate by orders of magnitude. The full SKA telescope should detect up to $\gtrsim$1000 of these slowly evolving transients *every week*.

On the way to the SKA1, the "early science" phase will roughly triple the rate of observed afterglows from GRBs pointed towards Earth. The next steps forward will be taken by surveys on SKA pathfinder instruments such as the Australian SKA Pathfinder (ASKAP; Johnston et al. 2007). The VAST survey (Murphy et al. 2013) at GHz frequencies will be first of its kind to reach a uniform sub-mJy sensitivity in the whole southern hemisphere. VAST will not have the sensitivity to target the bulk of the afterglow population, but it will be the benchmark for the SKA era blind surveys of slow transients.

Acknowledgments

TM and DB acknowledge the support of the Australian Research Council (ARC) through Discovery Project DP110102034, and, with BMG, through the ARC Centre of Excellence for All-sky Astrophysics (CE110001020). GG acknowledges INAF PRIN 2011. AJvdH and RAMJW acknowledge support from the European Research Council via Advanced Investigator Grant no. 247295

References

Ackermann, M., Ajello, M., Asano, K., et al. 2013, ApJS, 209, 11
—. 2014, Science, 343, 42
Akerlof, C., Balsano, R., Barthelmy, S., et al. 1999, Nature, 398, 400
Anderson, G. E., van der Horst, A. J., Staley, T. D., et al. 2014, MNRAS, 440, 2059
Bannister, K. W., Murphy, T., Gaensler, B. M., & Reynolds, J. E. 2012, ApJ, 757, 38
Berger, E., Kulkarni, S. R., & Frail, D. A. 2004, ApJ, 612, 966
Berger, E., Kulkarni, S. R., Frail, D. A., & Soderberg, A. M. 2003, ApJ, 599, 408
Bietenholz, M. F., De Colle, F., Granot, J., Bartel, N., & Soderberg, A. M. 2014, MNRAS, 440, 821
Cenko, S. B., Frail, D. A., Harrison, F. A., et al. 2010, ApJ, 711, 641
—. 2011, ApJ, 732, 29
Cenko, S. B., Kulkarni, S. R., Horesh, A., et al. 2013, ApJ, 769, 130
Chandra, P., & Frail, D. A. 2012, ApJ, 746, 156
Chandra, P., Cenko, S. B., Frail, D. A., et al. 2008, ApJ, 683, 924
Costa, E., Frontera, F., Heise, J., et al. 1997, Nature, 387, 783
Covino, S., Lazzati, D., Ghisellini, G., et al. 1999, A&A, 348, L1
Cucchiara, A., Levan, A. J., Fox, D. B., et al. 2011, ApJ, 736, 7
De Colle, F., Ramirez-Ruiz, E., Granot, J., & Lopez-Camara, D. 2012, ApJ, 751, 57

PoS(AASKA14)052

Dewdney, P., Turner, W., Millenaar, R., et al. 2013, SKA Documents, “SKA1 System Baseline Design", Document number SKA-TEL-SK0-DD-001, Revision 1
Eichler, D., Livio, M., Piran, T., & Schramm, D. N. 1989, Nature, 340, 126
Frail, D. A., Kulkarni, S. R., Nicastro, L., Feroci, M., & Taylor, G. B. 1997, Nature, 389, 261
Frail, D. A., Metzger, B. D., Berger, E., Kulkarni, S. R., & Yost, S. A. 2004, ApJ, 600, 828
Frail, D. A., Soderberg, A. M., Kulkarni, S. R., et al. 2005, ApJ, 619, 994
Frail, D. A., Waxman, E., & Kulkarni, S. R. 2000, ApJ, 537, 191
Frail, D. A., Kulkarni, S. R., Sari, R., et al. 2001, ApJL, 562, L55
Gehrels, N., Sarazin, C. L., O’Brien, P. T., et al. 2005, Nature, 437, 851
Ghirlanda, G., Ghisellini, G., & Lazzati, D. 2004, ApJ, 616, 331
Ghirlanda, G., Salvaterra, R., Burlon, D., et al. 2013a, MNRAS, 435, 2543
Ghirlanda, G., Ghisellini, G., Salvaterra, R., et al. 2013b, MNRAS, 428, 1410
Ghirlanda, G., Burlon, D., Ghisellini, G., et al. 2014, PASA, 31, 22
Goodman, J. 1997, Nature, 2, 449
Granot, J., & Loeb, A. 2003, ApJL, 593, L81
Granot, J., Ramirez-Ruiz, E., & Loeb, A. 2005, ApJ, 618, 413
Granot, J., & van der Horst, A. J. 2014, PASA, 31, 8
Hancock, P. J., Gaensler, B. M., & Murphy, T. 2013, ApJ, 776, 106
Johnston, S., Bailes, M., Bartel, N., et al. 2007, PASA, 24, 174
Klebesadel, R. W., Strong, I. B., & Olson, R. A. 1973, ApJ, 182, L85
Kouveliotou, C., Meegan, C. A., Fishman, G. J., et al. 1993, ApJL, 413, L101
Kulkarni, S. R., Frail, D. A., Sari, R., et al. 1999, ApJL, 522, L97
Laskar, T., Berger, E., Zauderer, B. A., et al. 2013, ApJ, 776, 119
Levinson, A., Ofek, E. O., Waxman, E., & Gal-Yam, A. 2002, ApJ, 576, 923
Livio, M., & Waxman, E. 2000, ApJ, 538, 187
Lorimer, D. R., Bailes, M., McLaughlin, M. A., Narkevic, D. J., & Crawford, F. 2007, Science, 318, 777
Malacrino, F., Atteia, J.-L., Boër, M., et al. 2007, A&A, 464, L29
Maselli, A., Melandri, A., Nava, L., et al. 2014, Science, 343, 48
Meegan, C. A., Fishman, G. J., Wilson, R. B., et al. 1992, Nature, 355, 143
Melandri, A., Covino, S., Rogantini, D., et al. 2014, A&A, 565, A72
Mesler, R. A., & Pihlström, Y. M. 2013, ApJ, 774, 77
Mesler, R. A., Pihlström, Y. M., Taylor, G. B., & Granot, J. 2012, ApJ, 759, 4
Metzger, M. R., Djorgovski, S. G., Kulkarni, S. R., et al. 1997, Nature, 387, 878
Moortgat, J., & Kuijpers, J. 2006, MNRAS, 368, 1110
Mundell, C. G., Kopač, D., Arnold, D. M., et al. 2013, Nature, 504, 119
Murphy, T., Chatterjee, S., Kaplan, D. L., et al. 2013, PASA, 30, 6
Narayan, R., Paczynski, B., & Piran, T. 1992, ApJL, 395, L83
Nousek, J. A., Kouveliotou, C., Grupe, D., et al. 2006, ApJ, 642, 389
Obenberger, K. S., Hartman, J. M., Taylor, G. B., et al. 2014, ApJ, 785, 27
Paczynski, B. 2001, AcA, 51, 1
Perley, D. A., & Perley, R. A. 2013, ApJ, 778, 172
Perley, D. A., Cenko, S. B., Bloom, J. S., et al. 2009, AJ, 138, 1690

PoS(AASKA14)052

Perley, D. A., Cenko, S. B., Corsi, A., et al. 2014, ApJ, 781, 37
Piran, T. 2004, Reviews of Modern Physics, 76, 1143
Racusin, J. L., Karpov, S. V., Sokolowski, M., et al. 2008, Nature, 455, 183
Rau, A., Greiner, J., & Schwarz, R. 2006, A&A, 449, 79
Rhoads, J. E. 1997, ApJL, 487, L1
Rol, E., van der Horst, A., Wiersema, K., et al. 2007, ApJ, 669, 1098
Sagiv, A., & Waxman, E. 2002, ApJ, 574, 861
Salvaterra, R., Campana, S., Vergani, S. D., et al. 2012, ApJ, 749, 68
Sari, R., & Piran, T. 1999, A&AS, 138, 537
Sari, R., Piran, T., & Halpern, J. P. 1999, ApJL, 519, L17
Sari, R., Piran, T., & Narayan, R. 1998, ApJL, 497, L17
Shivvers, I., & Berger, E. 2011, ApJ, 734, 58
Sironi, L., & Giannios, D. 2013, ApJ, 778, 107
Soderberg, A. M., Nakar, E., Berger, E., & Kulkarni, S. R. 2006a, ApJ, 638, 930
Soderberg, A. M., Berger, E., Kasliwal, M., et al. 2006b, ApJ, 650, 261
Stanway, E. R., Levan, A. J., & Davies, L. J. M. 2014, MNRAS, 444, 2133
Tanvir, N. R., Levan, A. J., Fruchter, A. S., et al. 2013, Nature, 500, 547
Tanvir, N. R., Fox, D. B., Levan, A. J., et al. 2009, Nature, 461, 1254
Taylor, G. B., Frail, D. A., Berger, E., & Kulkarni, S. R. 2004, ApJL, 609, L1
Taylor, G. B., Momjian, E., Pihlström, Y., Ghosh, T., & Salter, C. 2005, ApJ, 622, 986
Thornton, D., Stappers, B., Bailes, M., et al. 2013, Science, 341, 53
Usov, V. V., & Katz, J. I. 2000, A&A, 364, 655
van der Horst, A. J., Rol, E., Wijers, R. A. M. J., et al. 2005, ApJ, 634, 1166
van der Horst, A. J., Kamble, A., Resmi, L., et al. 2008, A&A, 480, 35
van der Horst, A. J., Paragi, Z., de Bruyn, A. G., et al. 2014, MNRAS, 444, 3151
van Eerten, H., van der Horst, A., & MacFadyen, A. 2012, ApJ, 749, 44
van Eerten, H. J., & MacFadyen, A. I. 2011, ApJL, 733, L37
van Paradijs, J., Kouveliotou, C., & Wijers, R. A. M. J. 2000, ARA&A, 38, 379
van Paradijs, J., Groot, P. J., Galama, T., et al. 1997, Nature, 386, 686
Wiersema, K., Covino, S., Toma, K., et al. 2014, Nature, 509, 201
Wijers, R. A. M. J., & Galama, T. J. 1999, ApJ, 523, 177
Wijers, R. A. M. J., Vreeswijk, P. M., Galama, T. J., et al. 1999, ApJL, 523, L33
Woosley, S. E. 1993, ApJ, 405, 273
Woosley, S. E., & Bloom, J. S. 2006, ARA&A, 44, 507
Wygoda, N., Waxman, E., & Frail, D. A. 2011, ApJL, 738, L23
Zauderer, B. A., Berger, E., Margutti, R., et al. 2013, ApJ, 767, 161
Zhang, B. 2014, ApJL, 780, L21
Zhang, W., & MacFadyen, A. 2009, ApJ, 698, 1261
Zou, Y. C., Wu, X. F., & Dai, Z. G. 2007, A&A, 461, 115

PoS(AASKA14)052

PROCEEDINGS OF SCIENCE

Incoherent transient radio emission from stellar-mass compact objects in the SKA era

S. Corbel[*1†], **J. C. A. Miller-Jones**[2‡], **R. P. Fender**[3], **E. Gallo**[4], **T. J. Maccarone**[5], **T. J. O'Brien**[6], **Z. Paragi**[7], **M. P. Rupen**[8], **A. P. Rushton**[3], **S. Sabatini**[9], **G. R. Sivakoff**[10], **J. Strader**[11] **and P. A. Woudt**[12]

[1]*University Paris Diderot & CEA Saclay,* [2]*ICRAR, Curtin University,* [3]*Oxford University,* [4]*University of Michigan,* [5]*Texas Tech University,* [6]*University of Manchester,* [7]*JIVE,* [8]*NRAO,* [9]*INAF,* [10]*University of Alberta,* [11]*Michigan State University,* [12]*University of Cape Town*

E-mail: stephane.corbel@cea.fr, james.miller-jones@curtin.edu.au

The universal link between the processes of accretion and ejection leads to the formation of jets and outflows around accreting compact objects. Incoherent synchrotron emission from these outflows can be observed from a wide range of accreting binaries, including black holes, neutron stars, and white dwarfs. Monitoring the evolution of the radio emission during their sporadic outbursts provides important insights into the launching of jets, and, when coupled with the behaviour of the source at shorter wavelengths, probes the underlying connection with the accretion process. Radio observations can also probe the impact of jets/outflows (including other explosive events such as magnetar giant flares) on the ambient medium, quantifying their kinetic feedback. The high sensitivity of the SKA will enabling the monitoring of accreting stellar-mass compact objects from their bright, Eddington-limited outburst states down to the lowest-luminosity quiescent levels, whose intrinsic faintness has to date precluded detailed studies. A census of quiescently accreting black holes will constrain binary evolution processes. By extending existing investigations of black hole jets to the fainter jets from neutron star and white dwarf systems, the SKA will permit comparative studies to determine the role of the compact object in jet formation. Further, the SKA will enable the detection and monitoring of all bright flaring transients in the observable local Universe (within $\sim$ 15 Mpc), including the radio counterparts of ultraluminous X-ray sources, improving our understanding of accretion and jet ejection at the highest rates, with important implications for the growth of the first quasars. As synchrotron events peak earlier at higher frequencies, and with higher flux densities, such studies will be best enabled by SKA1-MID. SKA1-MID will probe isolated quiescent black holes undergoing Bondi-Hoyle accretion from the nearby environment, both stellar-mass black holes in the field and the putative population of intermediate black holes in globular clusters. Detecting the latter would confirm the existence of the black hole seeds that must have existed in the early Universe.

This chapter reviews the progress that will be made by the SKA in studying incoherent synchrotron emission from accreting compact objects. We also discuss the potential of the astrometric and imaging observations that would be possible should a significant VLBI component be available for SKA.

Advancing Astrophysics with the Square Kilometre Array
June 8-13, 2014
Giardini Naxos, Italy

[*]Speaker.
[†]Co-chair of the chapter.
[‡]Co-chair of the chapter.

PoS(AASKA14)053

1. Introduction and context

Stellar-mass compact objects provide important laboratories for studying the fundamental coupling between the accretion process and the launching of energetic outflows, which often take the form of highly-collimated jets (Hughes 1991). A theoretical picture has been developed where the jets are composed of an electron/positron or electron/proton plasma (e.g. Bonometto & Rees 1971), which is magnetically collimated as it flows away from the compact object. These jets may be powered either by tapping the energy of a rotating black hole (Blandford & Znajek 1977), or by extracting energy from the accretion flow (Blandford & Payne 1982). However, many basic aspects of jet physics are uncertain, including their composition and structure, as well as the mechanisms that power and collimate them. Relativistic jets are relevant in almost all fields of astrophysics, and in some cases may be the dominant output channel for the accretion power from black holes (Fender et al. 2003). They provide an important source of feedback to the surrounding environment, being able to either trigger or suppress star formation, accelerate cosmic rays, and seed the surrounding medium with magnetic fields. They have even been suggested to play a role in the reionisation of the Universe (e.g. Mirabel et al. 2011).

Despite their relative proximity, the lower masses of stellar-mass compact objects imply that they are observed at lower angular resolution (in terms of gravitational radii) than nearby AGN, yet they evolve through their duty cycles on human timescales, typically undergoing entire outbursts over periods of days to months. Thus, they provide unique insights into the coupling between accretion and outflow. Furthermore, comparative studies of the different classes of compact object can provide important insights into the necessary and sufficient ingredients for the jet launching processes.

The non-thermal radio emission from stellar-mass compact objects typically arises via synchrotron emission from relativistic particles spiraling around the magnetic field lines of the jets. While significant progress has been made over the past few decades in understanding the nature of the jets and their coupling to the accretion flow (see Fender 2006, for a review), investigations have been hampered by the limited sensitivity of past and current facilities (see also Fender et al. 2015). We detail in this chapter how the sensitivity improvement brought about by the SKA will allow us to study black hole outbursts throughout the Galaxy and out into the Local Group, determine the role of jets in the low-luminosity quiescent state, and extend our existing studies of black holes to the analogous yet fainter neutron star and white dwarf systems.

2. Galactic black holes

From an observational standpoint, black hole transients spend most of their time in a quiescent state, at very low mass accretion rates. They occasionally undergo outbursts that last from a few months to $\sim$ a year, during which the flux rises by several orders of magnitude across the whole electromagnetic spectrum (McClintock & Remillard 2006). These outbursts are associated with global changes in three main components: the jets, the accretion disk and the corona. The luminous outburst phase, with a luminosity $>$ 10–30% of the Eddington luminosity (the "soft state"), is dominated by thermal emission from the accretion disk. During the rise and decay phases of the outburst (the "hard" state), the bolometric luminosity of the source is dominated by non-thermal

PoS(AASKA14)053

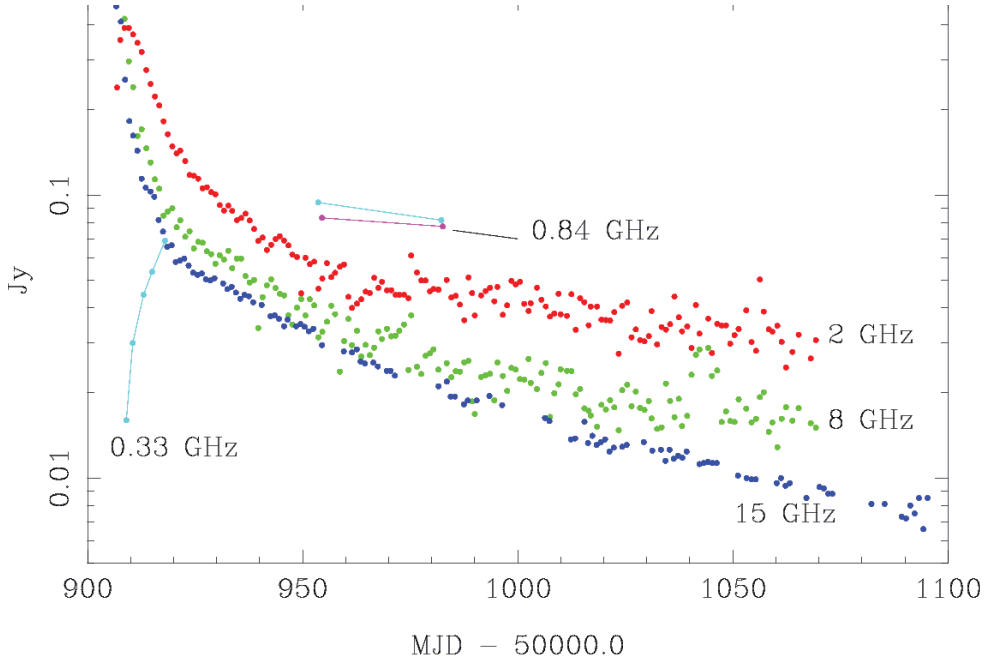

Figure 1: Radio lightcurve of CI Cam (a B[e] X-ray transient, also called XTE J0421+560) following its discovery. As for all incoherent synchrotron transients, the lower-frequency radio emission peaks later and with lower amplitude (Figure from Fender et al. 2008). Depending on the rate at which a source evolves through its X-ray spectral states, such radio flares typically occur a few days to months following the detection of the X-ray outburst.

emission (synchrotron or inverse Compton emission from either the jets or the corona) extending up to the hard X-ray band. Following recent results with high-resolution X-ray spectroscopy, accretion disk winds are now recognized as ubiquitous in black hole X-ray binaries, and may carry away a significant fraction of the inflowing energy (Miller et al. 2006; Neilsen & Lee 2009; Ponti et al. 2012; Díaz Trigo et al. 2013).

Observations of typical Galactic black holes have indicated two forms of jets associated with these primary accretion states; the slowly-varying, partially self-absorbed compact jets (with radio emission usually $\leq$ 30-50 mJy for distances of a few kpc, and a flat or slightly inverted radio spectrum) observed in the hard state (Corbel et al. 2000; Fender et al. 2000; Dhawan et al. 2000; Stirling et al. 2001), and the bright (0.1–10 Jy, with an optically thin radio spectrum), strongly variable transient jets (occasionally showing apparent superluminal motion) detected during the transition from the hard to the soft state (Corbel et al. 2004; Fender et al. 2004b). The core radio emission is then strongly quenched during the soft state (Fender et al. 1999; Coriat et al. 2011). Relic radio emission can also be detected in some cases when the jets interact with the ambient medium, either as large-scale lobes (Gallo et al. 2005), or as faint, transient hot spots (Corbel et al. 2002), depending on the duty cycle of the central black hole.

As is characteristic of expanding synchrotron sources, the bright radio flares from the transient jets display a characteristic frequency dependence of the transition (see Fig. 1) from optically-thick to optically-thin emission, which is consistent with an expanding plasmon model such as the one described by van der Laan (1966). Thus, the low-frequency radio emission ($<$ 1 GHz) will peak later (usually by a few days to weeks) and at lower fluxes (by at least an order of magnitude)

PoS(AASKA14)053

compared to the emission at higher frequencies (> 3 GHz). To study the transient radio emission, it is therefore of the utmost importance for the initial deployment of SKA1-MID to include band 4 (2.80-5.18 GHz) or (preferably) band 5 (4.6-13.8 GHz). This is also important to constrain the energy budget of the compact jets seen in the hard state, which can be strongly affected by opacity effects at lower frequencies. Bands 4 and 5 have higher intrinsic sensitivity than bands 1–3 (see Table 7 of the SKA1 System Baseline Design Document; band 1 = 0.35-1.05 GHz, band 2 =0.95-1.76 GHz, band 3 = 1.65-3.05 GHz), as well as lower confusion limits and higher intrinsic levels of radio emission at the peak of an outburst (see Fig. 1 or any textbook example of a synchrotron flare; e.g. van der Laan 1966). This allows them to probe a larger observing volume than the lower frequency bands, by factors of between 6 (comparing band 4 to band 3) and 200 (comparing band 4 to band 1), thereby extending the maximum distance we can probe by factors of 2–6. The brighter peak emission in band 5 would increase these numbers still further.

There is a strong correlation between the radio and X-ray emission in the hard and quiescent states (Corbel et al. 2003, 2013b; Gallo et al. 2003, 2012), indicating a possible coupling between the launch of the jets and the dynamics of the flow close to the accreting black hole (Fig. 2). It can be used to determine the expected source behaviour at the lowest radio luminosities, which remain relatively poorly explored owing to the limited sensitivity of current instruments (Miller-Jones et al. 2011). It is, for example, not clear whether quiescent black holes do host jets as in the brighter states. Current observations seem to indicate weak jet activity even in quiescence (Gallo et al. 2006, 2014), but it is not known what fraction of the liberated accretion power is carried away in the jets rather than being advected across the black hole event horizon (Fender et al. 2003). Furthermore, understanding the recently-discovered dichotomy in the radio/X-ray correlation (Coriat et al. 2011; Gallo et al. 2012) could provide a new way to explore the possibility of different couplings between accretion and ejection in black hole transients. With a sensitivity as good as 30 μJy s$^{-1/2}$ in band 4/5 (Dewdney et al. 2013), SKA1-MID is the ideal instrument to monitor all detected black hole outbursts (up to a few tens per year) all the way down to quiescence. Furthermore, a long observation (10 hrs) with SKA1-MID could detect all quiescent black hole binaries up to a distance of 5 kpc. These transient black holes could either be discovered by targetted monitoring or a blind radio survey with SKA (Fender et al. 2015), or by any active multi-wavelength monitoring facility.

The brightest phases of black hole outbursts (the hard to soft state transitions) can easily be studied via snapshot observations, even for the most distant systems in our Galaxy, meaning that SKA (even in phase 1) will probe a significant fraction of the outburst activity for almost all black holes in our Galaxy, including the very faint, sub-Eddington transients, which have rarely been observed at radio frequencies. With a resolution on the order of a few tenths of an arcsecond – if SKA1-MID is equipped with band 4 or 5 receivers – the bright radio emission associated with the transient jets (Mirabel & Rodriguez 1994) could also be resolved from a week after the onset of the radio flare, as typical proper motions are on the order of 15–20 mas day^{-1} (see Section 5 for the additional benefits of VLBI). Good polarization measurements (linear and circular) from SKA1-MID, associated with good signal purity, will provide key probes of the composition and geometry of the jets, and the structure of their magnetic fields.

The high sensitivity and ability to dump the visibilities on rapid ($\lesssim 1$ s) timescales would allow us to probe any short-timescale variability of the jets, should it be present (shortest timescales of ~ 10 minutes up to now, e.g. Corbel et al. (2000); Middleton et al. (2013)). Casella et al. (2010)

PoS(AASKA14)053

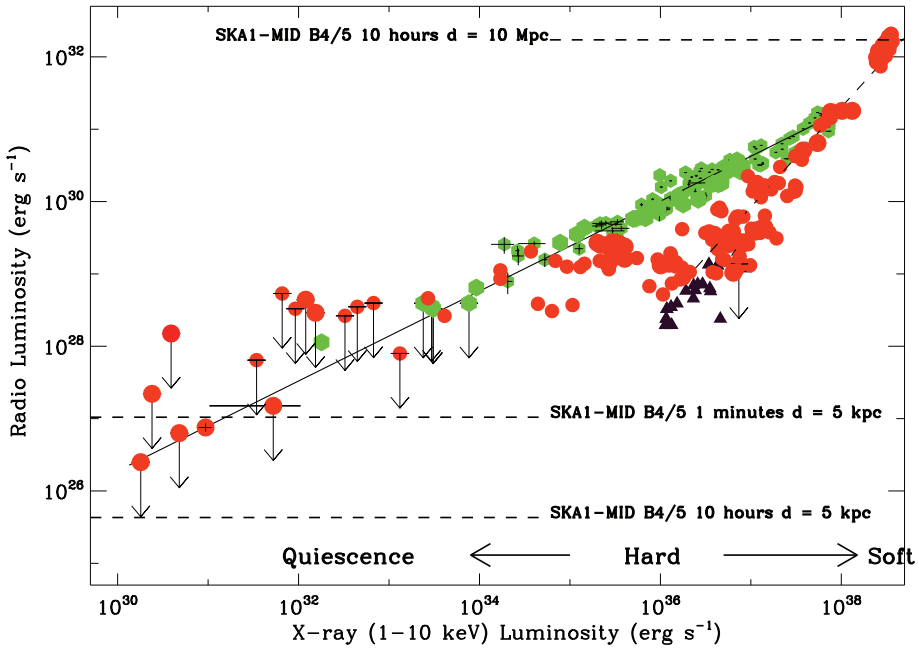

Figure 2: Radio and X-ray (1-10 keV) luminosities for Galactic accreting binary black holes in the hard and quiescent states (see arrows at bottom for approximate luminosity levels). It illustrates the standard correlation (defined by sources such as GX 339−4 or V404 Cyg with index ~ 0.6; green points) and the new correlation for the so-called "outliers" (defined by e.g. H 1743−322 or Swift J1753.5−0127 with index ~ 1.4; a significant fraction of the red points). Black triangles represent neutron star binaries. The solid line illustrates the fit to the whole 1997–2012 sample of GX 339−4 (Corbel et al. 2013b) with an extrapolation to the quiescent state. The dotted line corresponds to the fit to the data for H 1743−322, one of the representatives for the outliers (Coriat et al. 2011). Upper limits are plotted at the 3σ confidence level. The horizontal dashed lines represent some sensitivity levels for SKA1-MID as discussed in the text.

detected rapid (sub-second) infrared variability from the jets of GX 339−4, which was correlated with the observed X-ray variability. Observing these variations at multiple frequencies as they propagate downstream in the jets would allow us to directly measure the speeds and sizes of the compact jets, providing the best observational constraints on their Lorentz factors.

An X-ray binary by nature includes several emission components (star, compact object, accretion disk, corona, jets, and nearby environment), all emitting over a wide energy range (the jets themselves can be observed to emit up to the gamma-ray band), meaning that SKA observations would greatly benefit from coordinated and simultaneous observations with multi-wavelength facilities (e.g. Rodriguez et al. 2008; Corbel et al. 2013a). Some obvious new facilities for transient black holes in the next decade include (but are not limited to) X-ray observatories (e.g. *SVOM, ASTROSAT*), ground-based all-sky optical telescopes such as LSST, or a sensitive new high-energy gamma-ray observatory (CTA). Furthermore, all SKA1 components have the potential to act as radio "all-sky monitors" (if commensal transient search capability is implemented in the early phases; see Fender et al. 2015). This would be of prime importance, allowing SKA to provide alerts to multi-wavelength facilities. Such a radio sky monitor could be crucial for detecting new outbursts should no X-ray all-sky monitor be available in the coming decades.

PoS(AASKA14)053

With a reduced sensitivity of 50% during the deployment of SKA1-MID, a significant fraction of the above scientific goals could still be achieved as long as band 4 or 5 is included in the early phase. If we consider the improved performance of SKA2, with broadband frequency access up to 24 GHz, then it is likely that almost all transient black holes located up to the distance of the Galactic Centre could be studied in great detail, as outlined above.

3. Neutron star binaries

Comparisons between accreting neutron stars and black holes are ideal for determining which effects seen from accreting black holes are fundamentally related to the presence of an event horizon, instead of being generic to accretion onto objects with deep gravitational potential wells. Largely speaking, the phenomenology of accretion onto neutron stars is similar to that onto black holes (e.g. Psaltis 2006). Many of the known differences can be explained in a straightforward manner by the presence of a solid surface for neutron stars and the lack of one for black holes.

Studies of accreting neutron stars will be bolstered by the enhanced sensitivity of the SKA. Systematic studies of the radio luminosities of accreting neutron stars as a function of their X-ray luminosities are far sparser than those for black holes. This is in part because the characteristic timescales on which accretion disks change scales inversely with the accretor mass, so that "typical" outbursts of accreting neutron stars are shorter than those for accreting black holes; and partly because both the peak X-ray luminosities of neutron star transients and the ratio of radio to X-ray flux for neutron stars are both lower than for black holes (Fender & Kuulkers 2001; Wu et al. 2010; Migliari & Fender 2006). As a result of these factors, most soft X-ray transients with neutron star accretors peak at flux densities of about 1 mJy or less (for typical distances of several kpc). Until recently it was not feasible to probe flux densities significantly fainter than 100 μJy, and even with the upgraded VLA, the sensitivity of short target-of-opportunity (ToO) observations is limited to a few μJy. Thus, it has traditionally been difficult to span more than a factor of 10 in radio luminosity for neutron stars, and even now it is nearly impossible to span much more than a factor of 100. Furthermore, since the outbursts progress quickly, scheduling a large number of epochs places strong pressure on the ToO scheduling of existing arrays. Finally, since many of these sources are located in the Galactic Bulge, or elsewhere in the Southern Hemisphere, often only short observations are possible. Despite these problems, some progress has still been made on understanding the radio emission of neutron star X-ray binaries. A few things seem clear: the high magnetic field X-ray pulsars are not strong radio emitters (Migliari & Fender 2006); the radio and X-ray fluxes are correlated (see Fig. 2) for neutron star X-ray binaries that emit at less than about 10% of the Eddington luminosity (Migliari et al. 2003; Tudose et al. 2009); and the reduction of the radio power of neutron stars in accretion states dominated by thermal emission is less extreme than the same turn-down for black holes (Migliari et al. 2004).

The enhanced sensitivity of the SKA should allow more quantitative statements on these topics. For example, Migliari et al. (2003) find that $L_R \propto L_X^{1.4}$ for the neutron star 4U 1728-34 in hard spectral states, while Tudose et al. (2009) looked at Aql X-1 and found $L_R \propto L_X^{0.4}$, albeit while including data from a range of X-ray spectral states. The finding of Migliari et al. (2003) made for nice agreement with a theoretical picture in which the bulk power put into the jet scales with the

PoS(AASKA14)053

mass accretion rate, and the radio power of the jet scales with its bulk power to the 1.4, and also bolsters the suggestion that most hard states of black hole X-ray binaries are in radiatively inefficient states where $L_X \propto \dot{m}^2$. Developing a sample of sources that has both many objects, and which spans a few orders of magnitude in radio luminosity would bring the data quality into line with that from the black hole transients at the present time (Fig. 2). It also opens the door to making robust determinations of whether the spin period of a neutron star affects the normalization of its radio/X-ray relation (Migliari et al. 2011).

Additional studies of the thermal X-ray states of neutron stars in the radio may also hold important clues to understanding how jets are launched. In these systems, by analogy with the black holes, the accretion disks themselves are unlikely to supply much power to an accretion flow. On the other hand, the boundary layers, where the neutron star's accretion disk dissipates its excess rotational energy, should have the large scale height thought to be needed to power jets, and may interact with the magnetic field of the neutron star itself. Studies of a large sample of these soft states rather than merely the two that have been detected already (Migliari et al. 2004), may help us to understand jet production in this environment.

A final class of systems that can probe the relationship between the accretion flow and the launching of jets are the recently-discovered class of transitional binary pulsars, which switch between accretion-powered and rotation-powered states on timescales of just weeks (e.g. Archibald et al. 2009; Papitto et al. 2013; Bassa et al. 2014). These systems have been shown to emit flat or inverted-spectrum radio emission in their accretion-powered states, which is consistent with partially-self absorbed synchrotron jets (Papitto et al. 2013; Bassa et al. 2014). Intensive radio monitoring of the transitions between these two states would provide unique insights into how the jets are formed and destroyed, and, together with simultaneous X-ray monitoring, would highlight the connection between the jets and the evolving accretion flow.

A second point, unrelated to the disk-jet connection, which can be addressed with neutron star observations is whether particles can be launched in a jet at speeds significantly greater than the escape speed of the accretor. To date, one example has been identified, Cir X-1 (Fender et al. 2004a). In this system an apparent speed of the jet of $15c$ has been inferred from the appearance of radio emission far from the neutron star itself relatively soon after X-ray flaring episodes. Since the escape speed from a neutron star is typically $\sim 0.3c$ this would imply that the bulk jet speed must be larger than the escape speed for a neutron star by a large factor; however, what has not yet been seen, due to lack of sensitivity and angular resolution with existing Southern radio facilities, is actual motion of the radio-emitting structures at an apparent speed larger than the speed of light. As distances and inclination angles for many neutron star X-ray binaries will be directly measurable with the SKA, the combination of two-sided proper motions and detections of the counterjets should allow for a clean test of whether the pattern speeds and the bulk motions of jets are equal. If e.g. the jets are dominated by Poynting flux close to the neutron star, then it would not be surprising for them to appear to move very close to the speed of light, even if the particles energized by the jet move at much slower speeds. Such measurements represent a unique opportunity to test a major hypothesis from theoretical work that cannot be tested with black holes, where the jet speeds are expected to be close to the speed of light.

PoS(AASKA14)053

4. Cataclysmic variables and related objects

The occurrence of jets and fast collimated outflows is by no means restricted to accreting black holes or neutron stars. Through sensitive and timely observations in the last decade, numerous accreting white dwarfs (in cataclysmic variables, symbiotic stars and supersoft X-ray sources) have shown strong evidence for jets and jet-like shocked, collimated outflows, observed at radio frequencies and interpreted as synchrotron emission. However, the brightness temperatures of the radio emission from cataclysmic variables are small enough that thermal and/or cyclotron emission are still viable possibilities, and given the multiple possible mechanisms, there may be some heterogeneity in emission mechanisms. Better spectral measurements, and searches for circular polarization, which should be possible with SKA, can help resolve these issues.

Perhaps the most striking (and encouraging) aspect is that these transient radio jets have all occurred in the prototypes of subclasses of accreting white dwarfs – the symbiotic star Z And (Brocksopp et al. 2004), the recurrent nova[1] RS Oph (Rupen et al. 2008) and the dwarf nova SS Cyg (Körding et al. 2008), suggesting they are more common in white dwarf accretors than previously assumed. Persistent jets are also thought to occur in nova-like variables (Körding et al. 2011); these are systems in a regime of steady high mass transfer rate ($\sim 10^{-9} - 10^{-8}$ $M_\odot$ yr^{-1}) where accretion onto the white dwarf occurs via a standard thin α-disc (see e.g. Potter & Balbus 2014).

In close analogy to transient jets in X-ray binaries, the non-magnetic dwarf nova SS Cyg repeatedly exhibits radio outbursts associated with its disc instability outburst cycle (Körding et al. 2008). The outbursts in dwarf novae are described by a thermal-viscous instability in the accretion disc, leading to a brief period (days to weeks) of enhanced mass transfer ($\sim 10^{-8}$ $M_\odot$ yr^{-1}) onto the white dwarf. Even though radio luminosities are low compared to X-ray binaries – peak flux densities of $\sim$ 1 mJy at 1–10 GHz for a system at 114 pc (SS Cyg; Miller-Jones et al. 2013) – these systems provide an important link in understanding how accretion is coupled to the outflow of matter across a range of compact accretors. With the expected sensitivities achieved by SKA1-MID we can extend the sample of dwarf novae observed at radio frequencies out to kiloparsec distances, where optical transient surveys such as CRTS and iPTF (and LSST in the SKA era) are finding thousands of new dwarf novae; see Drake et al. (2014) for an overview of dwarf novae in CRTS. The sheer numbers of systems, the accessible time scales of the disc instability cycle in cataclysmic variables (weeks to months), and the reasonably well-understood accretion discs around white dwarfs provide an excellent laboratory for the SKA to study accretion physics with targeted (and target-of-opportunity) observations.

Whilst thermal emission is the dominant component of radio emission in novae (Seaquist & Bode 2008; O'Brien et al. 2015b), a significant number of novae exhibit non-thermal (synchrotron) emission associated with collimated bipolar and jet-like outflows (e.g., RS Oph: O'Brien et al. 2006; Rupen et al. 2008; V445 Pup: Woudt et al. 2009; V959 Mon: Chomiuk et al. 2014a). As recurrent novae are prime candidates for the progenitors of type Ia supernovae, questions surrounding the nature and energetics of the outflow of material during a nova outburst are at the core of the debate as to whether a white dwarf grows in mass during successive nova cycles. Regular,

[1]For more on classical and recurrent novae and the SKA, see also the chapter on thermal emission from novae (O'Brien et al. 2015b).

PoS(AASKA14)053

multi-frequency monitoring of Galactic novae with the VLA (an SKA1-MID pathfinder in terms of sensitivity) and e-MERLIN (a pathfinder in terms of angular resolution) is ongoing and will be complemented by deep observations with MeerKAT ahead of SKA1-MID. At the moment we are likely only picking up the tip of the iceberg in terms of synchrotron-emitting novae, i.e. those with significant circumstellar medium (e.g. from red giant secondary winds) to provide strong shock interactions, or those sufficiently nearby. A representative census of Galactic novae observed at the sensitivity of SKA1-MID (including band 4 or 5) is required to determine what fraction of novae show evidence for synchrotron emission and to fully understand the processes that lead to the formation of collimated jets following a thermonuclear runaway on the surface of the white dwarf.

5. Imaging and astrometry with VLBI

High-cadence, high-resolution imaging using SKA-VLBI (Paragi et al. 2015) during rare outburst events can provide a wealth of information about the jets in stellar-mass compact objects, and their coupling to the accretion process. Daily imaging during and after state transitions can determine the proper motions (and any observed deceleration) of the approaching and receding jet ejecta, allowing us to track them back to zero-separation, and hence determine the exact timing of the ejection event. By comparison with X-ray spectral and timing signatures, this enables us to establish the causal connection between changes in the accretion flow and the ejection of relativistic jets. Since structural changes in the accretion flow occur on timescales of hours to days, such information cannot be gleaned from radio light curves alone, as both opacity effects and time delays between ejection and shock formation cause a lag between an ejection event and the associated peak in the integrated radio light curve.

From such observations, we can determine the product of the jet speed and inclination angle, $\beta\cos\theta$, which can then be decoupled if the distance can be well constrained. Should we detect deceleration, we can constrain both the power of the jets and the density of the surrounding medium. Spatially resolving the polarisation of the jets can provide information on the magnetic field structure, helping to distinguish shocks from steady flow. Polarization observations of stellar-mass synchrotron sources on mas scales have been very rare because these objects are usually very faint ($\sim$mJy or below), and sensitive VLBI networks have not been easy to arrange at short notice during outbursts (but see Tudose et al. 2007). A flexible SKA-VLBI array will therefore play an important role here, even during the initial deployment phase of SKA1-MID (cf. Paragi et al. 2015). To date, intensive VLBI monitoring has only been carried out for a small number of outbursts (e.g. Yang et al. 2011; Miller-Jones et al. 2012a; Paragi et al. 2013). However, the peculiarities of the individual sources, together with scheduling considerations and sensitivity limitations have so far precluded the identification of which changes in the accretion flow give rise to the major jet events.

The great sensitivity and resolving power of SKA-VLBI will also be invaluable for the particularly interesting lower-mass neutron star and white dwarf systems, which show similar patterns of behaviour (Maitra & Bailyn 2004; Körding et al. 2008) but are typically significantly fainter than black holes. The lower radio luminosities of these two classes of system have meant that they have not been as intensively studied to date. Comparative studies of accretion-ejection coupling across different classes of compact object can provide important insights into the process of jet forma-

PoS(AASKA14)053

tion and collimation, determining how the jet properties depend on the depth of the gravitational potential well, and the presence or absence of a stellar surface and magnetic field.

The high-precision astrometry enabled by SKA-VLBI can also play an important role in compact object studies. Compact, partially self-absorbed synchrotron jets show distinct structural properties on (sub-)mas scales (see Paragi et al. 2013, and references therein). While flat-spectrum compact jets are typically observed in the hard state of black hole binaries (see Section 2), the first (and only well-established) observation of the expected frequency-dependent position shift in the jet peak-brightness distribution (the "core shift") – due to the different optical depths at different frequencies – was in SS433 (Paragi et al. 1999). Since the synchrotron optical depth depends on jet parameters (e.g. magnetic field strength and relativistic particle density), the jet peak position will also change as the source gets brighter or fainter (see Rushton et al. 2012; Paragi et al. 2013). SKA-VLBI will be sufficiently sensitive to reliably measure core shifts for a large number of Galactic black hole binaries, given the astrometric accuracy of a few μarcsec for sources as faint as $\sim$1 mJy. This will provide information on the structural properties of the jets, but also has the potential to constrain the accretion physics, as has recently been shown for AGN (Zamaninasab et al. 2014).

SKA-VLBI astrometry would be important for measuring accurate parallaxes of Galactic transient sources. Distances to X-ray binaries are typically uncertain by a factor of ~ 2 (Jonker & Nelemans 2004), rendering relatively uncertain our measurements of luminosities, jet speeds and even black hole spin. As faint, persistent, yet unresolved radio sources, X-ray binaries detected in the hard or quiescent states make ideal astrometric targets (e.g. Bradshaw et al. 1999; Reid et al. 2011; Miller-Jones et al. 2009). The high astrometric accuracy feasible with VLBI currently enables the measurement of a trigonometric parallax distance out to several kpc. While *Gaia* will provide accurate distances for relatively bright quiescent systems that are not highly absorbed, VLBI will remain the only feasible alternative for distance determinations for optically-faint systems in the Galactic Plane, and the only means to accurately measure distances for transients discovered after the end of the *Gaia* mission lifetime.

Even for systems that are either too distant or too faint for parallax measurements, proper motions can be measured over a time baseline as short as the few-month duration of an individual outburst. When combined with the line-of-sight radial velocity (from optical or infrared observations) and an estimate of the source distance, the full three-dimensional space velocity of the system can be determined (e.g. Mirabel et al. 2001). This can shed light on whether it received a natal kick in a supernova, and hence place observational constraints on the formation of black holes and neutron stars. Subtracting the measured parallax and proper motion signatures from astrometric observations of a given system can provide additional constraints on the physical dimensions of the binary. With sufficient astrometric accuracy, we can measure the orbital signature of high-mass binary systems, and the size scale of the unresolved jets, from the scatter of the astrometric residuals perpendicular and parallel to the jet axis (see Miller-Jones 2014 for more details).

6. Isolated black holes

There are likely to be $\sim 10^8$ stellar-mass black holes in our Galaxy (Samland 1998), which, while not in a binary system, are still accreting at some low level from the interstellar medium. If the correlation between radio and X-ray luminosities that is observed for stellar-mass black

PoS(AASKA14)053

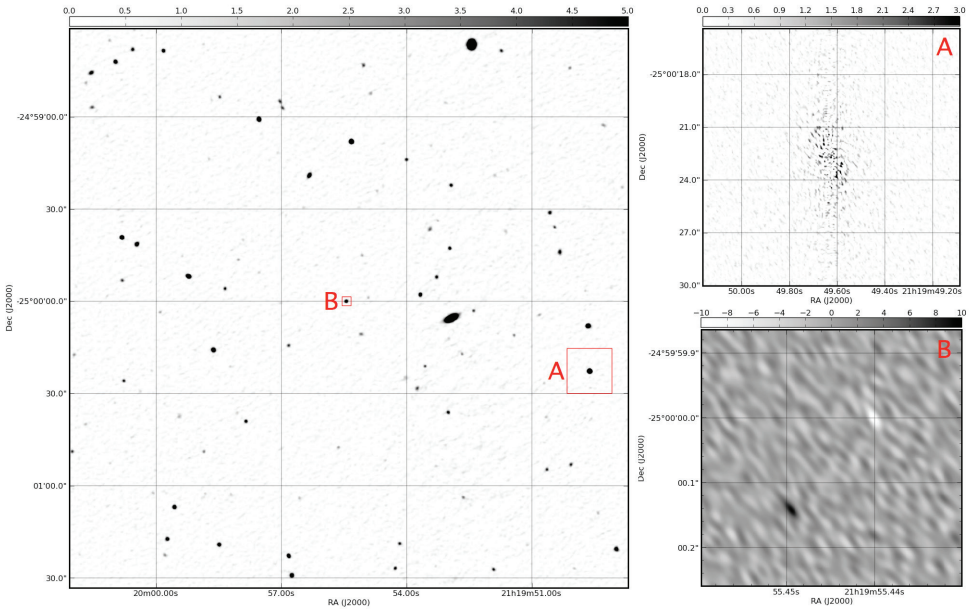

Figure 3: The main panel shows one of the two simulated SKA2 observations, at 1-2 GHz. Panel A shows the residual emission around a bright source due to incomplete removal of the differing PSFs. Panel B shows a difference image of the region around the IBH, with positive-negative emission due to the motion of the source between the observations. Pixel values are shown with a scale bar above the panel in all cases, the units of which are in μJy.beam^{-1}. See Fender et al. (2013) for more details.

holes in X-ray binaries continues to such low luminosities, then it has been suggested that such sources might be detectable in radio surveys (Maccarone 2005). In Fender et al. (2013), a detailed simulation was performed of a sphere of radius 250 pc centered on the Sun, which is estimated to contain $\sim$ 35000 isolated black holes (IBH), combining our latest understanding of the relation between accretion rate and radio luminosity with the best estimates of the distribution of phases in the ISM. It was found that although the majority of sources would be too faint, a small but significant fraction should be detectable by the SKA as radio point sources with flux densities of a few μJy. Such sources would be distinguishable from faint background radio sources (AGN and starburst galaxies) by their relatively high proper motions, which could be up to 100 mas yr^{-1}. Such an approach may be the best method of finding the closest black holes to the Earth. Figure 3 shows a full simulation of an SKA observation of a field containing such a nearby black hole, demonstrating how it can be identified via its proper motion. Similarly, a population of floating intermediate-mass black holes may also be detectable with the SKA, when they traverse the disk of our Galaxy (Wang & Loeb 2014).

7. Gamma-ray binaries

With the advent of very high energy (e.g. MAGIC, HESS) and high energy (e.g. HESS or Fermi) observatories, a new class of binary systems has been brought to light. These these so-called “gamma-ray binaries" are characterized by having most of their radiative power above 1 MeV (Dubus 2013). Their non-thermal gamma-ray emission is driven by rotation-powered pulsars and likely originates from the particles accelerated at the shock front between the wind of a pulsar and the wind of the massive companion. They constitute ideal testbeds for pulsar physics

PoS(AASKA14)053

and the acceleration of particles up to very high energies. Variable continuum radio emission has been reported in all of the 5 detected gamma-ray binaries, likely due to synchrotron emission from electrons accelerated at the shock. Furthermore, in three of these systems, the radio source was resolved on milli-arcsecond scales (Dhawan et al. 2006; Moldón et al. 2011a,b, 2012), illustrating a cometary tail with a changing morphology along the course of the orbit, a key expectation in the pulsar wind scenario. However, radio pulsations have only been detected in the system with the longest orbital period, PSR B1259-63. The sensitivity of the SKA (even with SKA1-MID 50%) will not only allow searches for very faint pulsations in these systems, but also reveal in great detail the properties of the radio flare (i.e. the onset of particle acceleration) when the neutron star is close to periastron passage. Furthermore, direct imaging by the SKA-VLBI of the evolution of the morphology of the cometary tails will be a complementary tool for understanding the environment of the binary and fundamental issues such as particle acceleration.

8. Magnetars

Magnetars are isolated neutron stars with very large ($\gtrsim 10^{13}$G) magnetic fields, often identified by their association with short bursts of gamma-rays. These systems occasionally undergo giant outbursts, probably powered by reconfiguration of the magnetic field, which can be associated with radio flares and spatially-resolved, mildly-relativistic ejecta. The best example to date is that of the magnetar SGR 1806−20, which on Dec 27 2004 underwent probably the largest outburst within our Galaxy, observed by humans, since Kepler's supernova. The outburst was associated with a flare that peaked at over 100 mJy at 1.4 GHz, which originated in relativistic ejecta expanding at ≥ 0.3c (Gaensler et al. 2005; Fender et al. 2006). Since this source lies at $\sim$ 10kpc, the $\sim 10\mu$Jy sensitivity of the SKA1-SUR and -MID (in hours) could potentially detect such events at Mpc distances, i.e. surveys of the local group. Such a survey could also be conducted with SKA1-LOW, as the radio flare from SGR 1806−20 was already optically thin and bright at low frequencies ($\sim$ 500 mJy at 250 MHz) very early in the outburst. See Tauris et al. (2015) for more details of isolated neutron stars.

9. Extragalactic binaries and ultraluminous X-ray sources

As discussed above, studies of Galactic X-ray binaries have significantly improved our understanding of the coupling between the processes of accretion and ejection. However, as the accretion rate approaches the Eddington limit, the increased radiation pressure changes both the structure of the accretion flow and the nature of the associated outflows (both winds and jets; Ohsuga & Mineshige 2011). Owing to the relatively small number of Galactic sources reaching such high luminosities, our understanding of this regime is less well advanced, which is unfortunate given its important implications for the rapid growth of the most massive quasars in the early Universe. It has even been demonstrated that Eddington-rate accretion onto low-mass black holes could play a significant role in the reionisation of the Universe (Mirabel et al. 2011; Fragos et al. 2013).

The population of ultraluminous X-ray sources (ULXs) in external galaxies provides potential laboratories for studying accretion at the highest rates. With X-ray luminosities $\geq 1 \times 10^{39}$ erg s^{-1},

PoS(AASKA14)053

these sources (recently reviewed by Feng & Soria 2011) may be ordinary X-ray binaries accreting at or above the Eddington rate, massive stellar-mass black holes ($M \lesssim 100 M_{\odot}$), or, more exotically, intermediate-mass black holes (IMBHs; $10^2 < M/M_{\odot} < 10^4$). Radio emission has been detected from several such sources, either as jet-blown bubbles around powerful, persistent sources (e.g. Kaaret et al. 2003; Soria et al. 2014), or (in rare cases) as compact, transient emission from powerful jets during outbursts of flaring ULXs (Webb et al. 2012; Middleton et al. 2013). Nebulae inflated by powerful jets can be used as calorimeters, providing the only method of measuring the unseen mechanical power of the jets, averaged over the source lifetime. To date, such nebulae have been detected out to distances of ~ 10 Mpc, but with typical radio luminosities of 10^{35} erg s^{-1}, they could be detected out as far as 100 Mpc with SKA1-MID in just a few hours of time. With typical sizes of 200 pc, sub-arcsecond resolution would be required to ascertain whether the sources were extended, implying a need for observations in bands 4 or 5. With sufficient resolution, individual jet ejecta can be resolved within the nebulae, placing constraints on the source duty cycle (e.g. Cseh et al. 2014). Such high -resolution imaging may also be crucial to properly image the nebulae in order to understand their origin (e.g. jets, disk winds).

The existence of a correlation among radio luminosity, X-ray luminosity and mass of accreting black holes (the "Fundamental Plane of Black Hole Activity; Merloni et al. 2003; Falcke et al. 2004) implies that measurements of the X-ray and radio luminosities of an accreting ULX can be used to infer its mass, assuming that it is in the equivalent of the hard X-ray spectral state. Thus, should IMBHs exist, their masses can be measured (to within a factor of a few) via deep radio and X-ray observations. As an example, the lower limit of $9000 M_{\odot}$ on the mass of HLX-1 (Farrell et al. 2009) would imply a radio luminosity of 1.3 μJy beam^{-1} at 5 GHz at an X-ray luminosity of $0.02 L_{\rm Edd}$, which would be detected at a 5σ level by SKA1-MID in 3 hours of time (see also Wolter et al. 2015 for more details on ULXs).

Galactic studies of Eddington-rate accretion are typically hindered by the uncertain source distances, large absorbing columns in the Galactic plane, and the small number of sources reaching the Eddington luminosity. Since the low-mass X-ray binary population traces the total stellar mass, extending such studies to nearby massive galaxies will provide new insights into the nature of jet-disc coupling at Eddington accretion rates. A recent transient ULX in M31 showed luminous, compact radio emission, with evidence for multiple discrete flaring events and variability on timescales as short as a few minutes, reminiscent of that seen in the Eddington-rate Galactic source GRS 1915+105 (Middleton et al. 2013). The sensitivity of SKA1-MID will allow us to detect such events out to the Virgo cluster.

10. Black holes in globular clusters

Globular clusters are extremely efficient at forming X-ray binaries relative to other Galactic environments, due to the additional formation channels of tidal capture or three-body interactions. However, the several dozen black holes formed from the collapse of massive stars early in the cluster lifetime were initially thought to efficiently eject one another via mutual gravitational interactions (Kulkarni et al. 1993; Sigurdsson & Hernquist 1993), such that clusters were not thought to be rich hunting grounds for black holes. This picture has recently been revised by new theoretical and observational results, finding that old clusters could still contain many black holes.

PoS(AASKA14)053

The first good evidence for cluster black holes was the detection of highly variable X-ray sources in extragalactic globular clusters, whose luminosities exceeded 10^{39} erg s^{-1} (Maccarone et al. 2007). More recently, deep radio observations with the newly-upgraded VLA detected flat-spectrum radio sources in the cores of the Galactic globular clusters M22 and M62 (Strader et al. 2012a; Chomiuk et al. 2013), which were interpreted as quiescent accreting black holes in binary systems. With two such sources detected in M22 alone, the total black hole population in that cluster was estimated as 5–100 (Strader et al. 2012a).

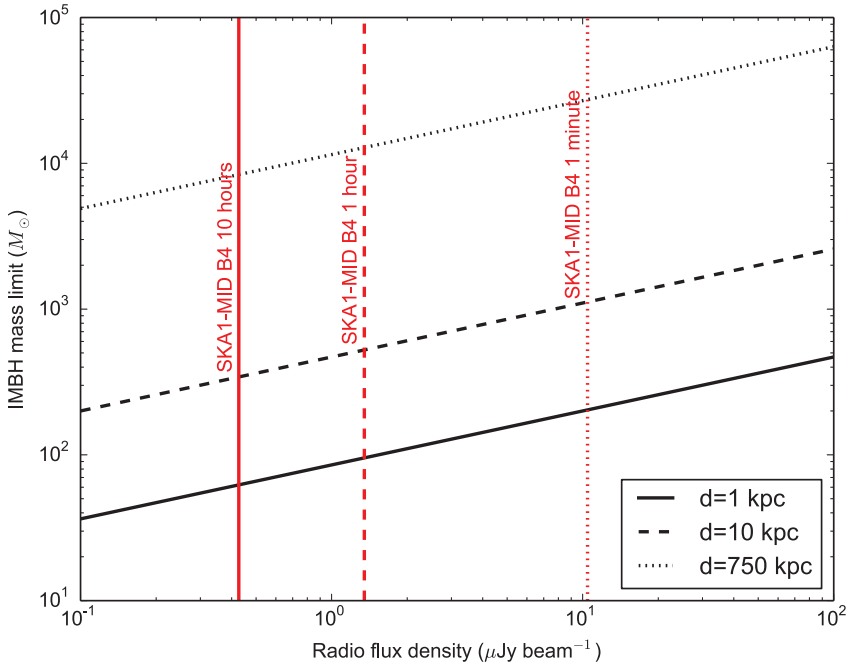

Figure 4: A summary of all globular clusters in our Galaxy (with declination $< 10^\circ$) that could be observed with SKA1-MID. A mass cut of 10^5 M$_\odot$ is applied to allow enough black holes to form early in the cluster lifetime. The green symbols show the detected candidates to date (see references in text), and the red symbols show the observed clusters with no indication of the existence of a black hole. The lines illustrate the distance cut corresponding to the distance out to which we can detect the most radio-luminous of our candidate black holes (stellar mass or intermediate mass) at the 5-sigma level for the ATCA (dashed line) or SKA1-MID (full line). This is ~ 8 kpc for ATCA, and ~ 23kpc for SKA1-MID, for a comparable integration time ($\sim$ 20h observing). Higher-mass clusters at larger distances are also included, as the best candidates to host IMBHs.

The presence of stellar-mass black holes in globular clusters has also been supported by theoretical work, with *N*-body simulations showing that the interactions between the black hole subsystem in the core and the rest of the cluster would allow a significant number of black holes to persist in the core after a Hubble time (Sippel & Hurley 2013; Morscher et al. 2013; Breen & Heggie 2013). The additional formation channels for X-ray binaries in clusters implies that these cluster black holes could well be more massive than those in the field, since the progenitor star, if not in a binary system, would have avoided the strong mass loss associated with the common envelope phase of binary evolution. Thus, in addition to providing new accretion laboratories, these cluster

PoS(AASKA14)053

black holes could provide new observational constraints on black hole formation mechanisms. Finally, the presence of multiple black holes within a cluster core raises the prospect of gravitational wave signals from black hole mergers.

Globular clusters have also been suggested as likely hosts for the elusive IMBHs, which can form in cluster centres from successive mergers of stellar-mass black holes, or via runaway collision of massive stars. If present, accretion onto these black holes from the intracluster gas should produce detectable radiative signatures (Maccarone 2005). However, while analysis of stellar dynamics has provided some evidence for IMBHs at the centres of several clusters (Gebhardt et al. 2002; Gerssen et al. 2002), there has to date been no good radiative evidence supporting the presence of IMBHs in globular clusters, down to upper limits of several hundred solar masses (Miller-Jones et al. 2012b; Strader et al. 2012b).

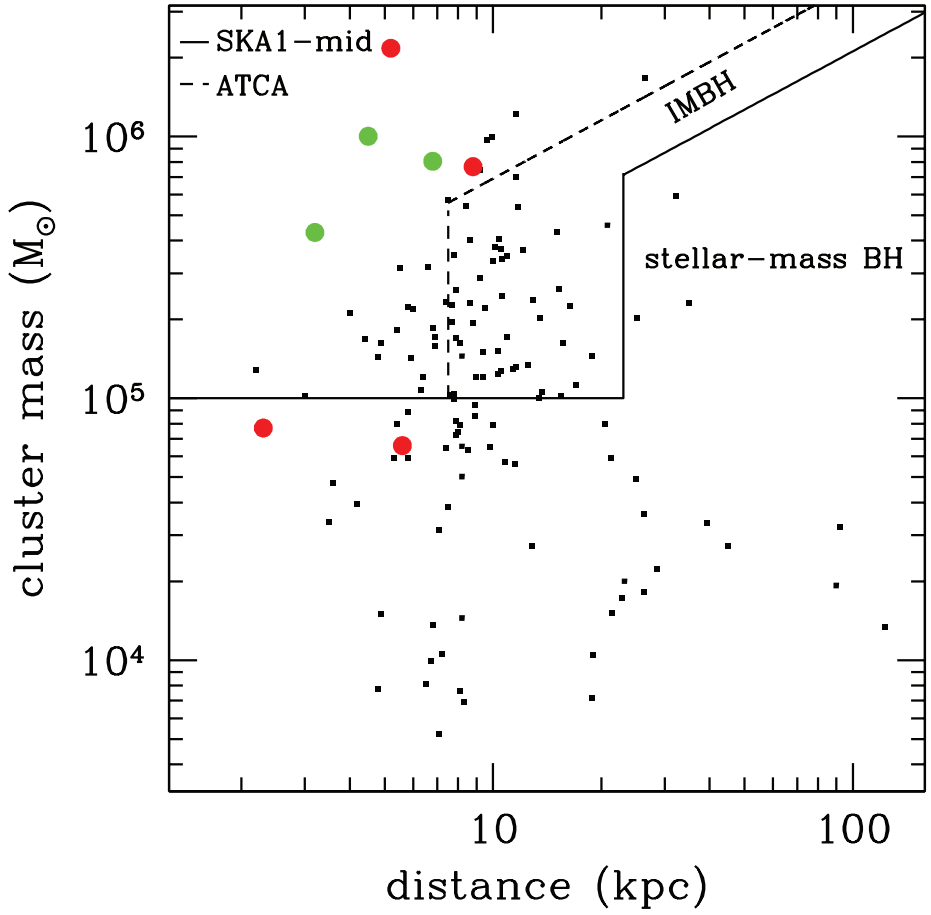

Figure 5: The SKA can place stringent upper limits on the masses of IMBHs in globular clusters, assuming that the black holes accrete via Bondi-Hoyle accretion from the cluster gas. Assuming that the accretion leads to the production of jets, we use the formalism of Strader et al. (2012b) to calculate the upper limit on the mass as a function of radio luminosity for distances of 1, 10 and 750 kpc (corresponding to M31).

With sufficient resolution, the high sensitivity of the SKA can make significant contributions to this field. The three quiescent black holes detected in M22 and M62 were the first radio-selected stellar-mass black holes. The well-established, non-linear correlation between radio and X-ray

PoS(AASKA14)053

luminosities of accreting stellar-mass black holes in the hard and quiescent X-ray spectral states implies that radio surveys may be more efficient at finding quiescent accreting black holes than X-ray searches (Maccarone 2005), as well as providing a way to discriminate between black holes and the less radio-bright neutron star and white dwarf systems. The most sensitive current radio facility, the VLA, can only reach radio luminosities of $\sim 10^{28}$ erg s^{-1} in Galactic clusters, enabling the detection of the brightest quiescent systems (giant donors or ultracompact sources). A 10-hour run in band 4 using SKA1-MID could drop this limit by an order of magnitude, extending our sensitivity to fainter and more distant quiescent systems (see Fig. 4), and reducing the upper limit on putative IMBH masses to $< 150 M_{\odot}$ for the most nearby clusters (see Fig. 5). Equivalently, the radio outburst of an Eddington-rate X-ray binary flare in an extragalactic cluster could be detected out to the Virgo cluster. However, sub-arcsecond resolution is required to associate any detected radio sources with the known locations of either X-ray sources (in Galactic clusters) or extragalactic globular clusters. Sufficiently attenuating confusing steep-spectrum sources such as pulsars or background AGN also strongly motivates conducting such observations in bands 4 or (preferably) 5 on SKA1-MID.

11. Summary of requirements for the SKA

As discussed in the previous sections, the most important component of SKA1 for the field of incoherent transients is SKA1-MID, because of its high-frequency capability, implying improved angular resolution, a lower confusion limit, and brighter intrinsic synchrotron emission. The performance of SKA1-MID (even at 50% capacity during initial deployment) will largely supersede the current generation of radio interferometers for studies in this field (especially in the Southern hemisphere). However, we stress a number of critical considerations for the final design of SKA1 and its extension to SKA2.

- Because most of the incoherent transients will initially be optically thick at low frequencies, we emphasise the importance of having band 4 or (preferably) 5 incorporated in the initial deployment of SKA1-MID. This may imply initially dropping band 3, as bands 1 and 2 will be needed to assure continuity with SKA1-LOW and SKA1-SUR, and for the study of the hydrogen in the local Universe.

- In addition to having band 4 or 5 included in the initial design, SKA1-MID should be able to operate simultaneously in at least two different frequency bands (possibly via sub-arrays) in order to identify transient radio sources and measure their spectral evolution. Good polarization capabilities (linear and circular) are also needed to probe the structure and composition of the jets. It is important to have well-sampled daily radio light curves (with high time resolution) on timescales of weeks–months, meaning that having sub-arrays or multi-beaming capabilities will greatly enhance the SKA scientific return.

- Whereas incoherent transients are not the fastest transients in the sky, it is important to stress that they do show huge variations on timescales of the order of hours (and smaller). It is therefore crucial that SKA1-MID should be able to respond quickly (few hours/days) in the event of (un)expected transients. Such a response could be triggered either by SKA itself, or

PoS(AASKA14)053

from an external source, as these transients (and also GRBs, SNe, ...) are powerful emitters across the entire electromagnetic spectrum. Relatively short-timescale co-ordination of SKA observations with multi-wavelength facilities should be envisaged and facilitated.

- We also stress the importance of commensal searches for radio transients with all SKA components. A dedicated monitoring of the Galactic plane/bulge or selected portions of the sky (perhaps via a radio "all sky monitor") would facilitate the SKA triggering observations at external observatories, especially if no X-ray all sky monitor is available in the next decade. All new transients should be made public immediately to enable rapid multi-wavelength response.

- Angular resolution is crucial for imaging the radio structures associated with those transients, filtering out extended emission to avoid confusion, or studying faint sources in crowded regions of sky such as globular clusters or external galaxies. This can be achieved only if SKA1-MID is equipped with band 4 or 5, with the antennas spread over an area of radius a few hundred km. Phasing the SKA dish arrays alone or with existing/planned new VLBI arrays would be a key feature of the SKA, enabling vastly more sensitive imaging and astrometric studies with SKA-VLBI.

References

Archibald, A. M., Stairs, I. H., Ransom, S. M., et al . 2009, Science, 324, 1411
Bassa, C. G., Patruno, A., Hessels, J. W. T., et al . 2014, MNRAS, 441, 1825
Blandford, R. D. & Payne, D. G. 1982, MNRAS, 199, 883
Blandford, R. D. & Znajek, R. L. 1977, MNRAS, 179, 433
Bonometto, S. & Rees, M. J. 1971, MNRAS, 152, 21
Bradshaw, C. F., Fomalont, E. B., & Geldzahler, B. J. 1999, ApJ, 512, L121
Breen, P. G. & Heggie, D. C. 2013, MNRAS, 436, 584
Brocksopp, C., Sokoloski, J. L., Kaiser, C., et al . 2004, MNRAS, 347, 430
Casella, P., Maccarone, T. J., O'Brien, K., et al . 2010, MNRAS, 404, L21
Chomiuk, L., Linford, J. D., Yang, J., et al . 2014a, Nature, 514, 339
Chomiuk, L., Strader, J., Maccarone, T. J., et al . 2013, ApJ, 777, 69
Corbel, S., Aussel, H., Broderick, J. W., et al . 2013a, MNRAS, 431, L107
Corbel, S., Coriat, M., Brocksopp, C., et al . 2013b, MNRAS, 428, 2500
Corbel, S., Fender, R. P., Tomsick, J. A., Tzioumis, A. K., & Tingay, S. 2004, ApJ, 617, 1272
Corbel, S., Fender, R. P., Tzioumis, A. K., et al . 2000, A&A, 359, 251
—. 2002, Science, 298, 196
Corbel, S., Nowak, M. A., Fender, R. P., Tzioumis, A. K., & Markoff, S. 2003, A&A, 400, 1007
Coriat, M., Corbel, S., Prat, L., et al . 2011, MNRAS, 414, 677
Cseh, D., Kaaret, P., Corbel, S., et al . 2014, MNRAS, 439, L1
Dewdney, P., Turner, W., Millenaar, R., et al. 2013, SKA Documents, "SKA1 System Baseline Design", Document number SKA-TEL-SK0-DD-001, Revision 1
Dhawan, V., Mioduszewski, A., & Rupen, M. 2006, in VI Microquasar Workshop: Microquasars and Beyond

PoS(AASKA14)053

Dhawan, V., Mirabel, I. F., & Rodríguez, L. F. 2000, ApJ, 543, 373
Díaz Trigo, M., Miller-Jones, J. C. A., Migliari, S., Broderick, J. W., & Tzioumis, T. 2013, Nature, 504, 260
Drake, A. J., Gänsicke, B. T., Djorgovski, S. G., et al . 2014, MNRAS, 441, 1186
Dubus, G. 2013, AA Rv., 21, 64
Falcke, H., Körding, E., & Markoff, S. 2004, A&A, 414, 895
Farrell, S. A., Webb, N. A., Barret, D., Godet, O., & Rodrigues, J. M. 2009, Nature, 460, 73
Fender, R. 2006, Compact stellar X-ray sources (Cambridge University Press), 381–419
Fender, R. et al . 1999, ApJ, 519, L165
Fender, R., Wijers, R., Stappers, B., & LOFAR Transients Key Science Project, t. 2008, in Proceedings of "Bursts, Pulses and Flickering: wide-field monitoring of the dynamic radio sky", PoS(Dynamic)030
Fender, R., Wu, K., Johnston, H., et al . 2004a, Nature, 427, 222
Fender, R. et al 2015, "The Transient Universe with the Square Kilometre Array", in Proceedings of "Advancing Astrophysics with the Square Kilometre Array", PoS(AASKA14)051
Fender, R. P., Belloni, T. M., & Gallo, E. 2004b, MNRAS, 355, 1105
Fender, R. P., Gallo, E., & Jonker, P. G. 2003, MNRAS, 343, L99
Fender, R. P. & Kuulkers, E. 2001, MNRAS, 324, 923
Fender, R. P., Maccarone, T. J., & Heywood, I. 2013, MNRAS, 430, 1538
Fender, R. P. et al . 2006, MNRAS, 367, L6
Fender, R. P., Pooley, G. G., Durouchoux, P., Tilanus, R. P. J., & Brocksopp, C. 2000, MNRAS, 312, 853
Feng, H. & Soria, R. 2011, New Astron. Rv., 55, 166
Fragos, T., Lehmer, B. D., Naoz, S., Zezas, A., & Basu-Zych, A. 2013, ApJ, 776, L31
Gaensler, B. M., Kouveliotou, C., Gelfand, J. D., et al . 2005, Nature, 434, 1104
Gallo, E., Fender, R., Kaiser, C., et al . 2005, Nature, 436, 819
Gallo, E., Fender, R. P., Miller-Jones, J. C. A., et al . 2006, MNRAS, 370, 1351
Gallo, E., Fender, R. P., & Pooley, G. G. 2003, MNRAS, 344, 60
Gallo, E., Miller, B. P., & Fender, R. 2012, MNRAS, 423, 590
Gallo, E., Miller-Jones, J. C. A., Russell, D. M., et al . 2014, MNRAS, 445, 290
Gebhardt, K., Rich, R. M., & Ho, L. C. 2002, ApJ, 578, L41
Gerssen, J., van der Marel, R. P., Gebhardt, K., et al . 2002, AJ, 124, 3270
Hughes, P. A. 1991, Beams and jets in astrophysics (Cambridge University Press)
Jonker, P. G. & Nelemans, G. 2004, MNRAS, 354, 355
Kaaret, P., Corbel, S., Prestwich, A. H., & Zezas, A. 2003, Science, 299, 365
Körding, E., Rupen, M., Knigge, C., et al . 2008, Science, 320, 1318
Körding, E. G., Knigge, C., Tzioumis, T., & Fender, R. 2011, MNRAS, 418, L129
Kulkarni, S. R., Hut, P., & McMillan, S. 1993, Nature, 364, 421
Maccarone, T. J. 2005, MNRAS, 360, L30
Maccarone, T. J., Kundu, A., Zepf, S. E., & Rhode, K. L. 2007, Nature, 445, 183
Maitra, D. & Bailyn, C. D. 2004, ApJ, 608, 444
McClintock, J. E. & Remillard, R. A. 2006, Black hole binaries (Compact stellar X-ray sources), 157–213

PoS(AASKA14)053

Merloni, A., Heinz, S., & di Matteo, T. 2003, MNRAS, 345, 1057
Middleton, M. J., Miller-Jones, J. C. A., Markoff, S., et al . 2013, Nature, 493, 187
Migliari, S. & Fender, R. P. 2006, MNRAS, 366, 79
Migliari, S., Fender, R. P., Rupen, M., et al . 2003, MNRAS, 342, L67
—. 2004, MNRAS, 351, 186
Migliari, S., Miller-Jones, J. C. A., & Russell, D. M. 2011, MNRAS, 415, 2407
Miller, J. M., Raymond, J., Fabian, A., et al . 2006, Nature, 441, 953
Miller-Jones, J. C. A. 2014, PASA, 31, 16
Miller-Jones, J. C. A., Jonker, P. G., Dhawan, V., et al . 2009, ApJ, 706, L230
Miller-Jones, J. C. A., Jonker, P. G., Maccarone, T. J., Nelemans, G., & Calvelo, D. E. 2011, ApJ, 739, L18
Miller-Jones, J. C. A., Sivakoff, G. R., Altamirano, D., et al . 2012a, MNRAS, 421, 468
Miller-Jones, J. C. A., Sivakoff, G. R., Knigge, C., et al . 2013, Science, 340, 950
Miller-Jones, J. C. A., Wrobel, J. M., Sivakoff, G. R., et al . 2012b, ApJ, 755, L1
Mirabel, I. F., Dhawan, V., Mignani, R. P., Rodrigues, I., & Guglielmetti, F. 2001, Nature, 413, 139
Mirabel, I. F., Dijkstra, M., Laurent, P., Loeb, A., & Pritchard, J. R. 2011, A&A, 528, A149
Mirabel, I. F. & Rodriguez, L. F. 1994, Nature, 371, 46
Moldón, J., Johnston, S., Ribó, M., Paredes, J. M., & Deller, A. T. 2011a, ApJ, 732, L10
Moldón, J., Ribó, M., & Paredes, J. M. 2011b, A&A, 533, L7
—. 2012, A&A, 548, A103
Morscher, M., Umbreit, S., Farr, W. M., & Rasio, F. A. 2013, ApJ, 763, L15
Neilsen, J. & Lee, J. C. 2009, Nature, 458, 481
O'Brien, T. J., Bode, M. F., Porcas, R. W., et al . 2006, Nature, 442, 279
O'Brien, T., Rupen, M., Chomiuk, L., & et al. 2015, "Thermal radio emission from novae & symbiotics with the Square Kilometre Array", in Proceedings of "Advancing Astrophysics with the Square Kilometre Array", PoS(AASKA14)062
Ohsuga, K. & Mineshige, S. 2011, ApJ, 736, 2
Papitto, A., Ferrigno, C., Bozzo, E., et al . 2013, Nature, 501, 517
Paragi, Z., Godfrey, L., Reynolds, C., & et al., 2015, "Very Long Baseline Interferometry with the SKA", in Proceedings of "Advancing Astrophysics with the Square Kilometre Array", PoS(AASKA14)143
Paragi, Z., van der Horst, A. J., Belloni, T., et al . 2013, MNRAS, 432, 1319
Paragi, Z., Vermeulen, R. C., Fejes, I., et al . 1999, A&A, 348, 910
Ponti, G., Fender, R. P., Begelman, M. C., et al . 2012, MNRAS, 422, L11
Potter, W. J. & Balbus, S. A. 2014, MNRAS, 441, 681
Psaltis, D. 2006, Accreting neutron stars and black holes: a decade of discoveries (Cambridge University Press), 1–38
Reid, M. J., McClintock, J. E., Narayan, R., et al . 2011, ApJ, 742, 83
Rodriguez, J., Hannikainen, D. C., Shaw, S. E., et al . 2008, ApJ, 675, 1436
Rupen, M. P., Mioduszewski, A. J., & Sokoloski, J. L. 2008, ApJ, 688, 559
Rushton, A., Miller-Jones, J. C. A., Campana, R., et al . 2012, MNRAS, 419, 3194
Samland, M. 1998, ApJ, 496, 155
Seaquist, E. R. & Bode, M. F. 2008, Cambridge University Press (Classical Novae), 141

PoS(AASKA14)053

Sigurdsson, S. & Hernquist, L. 1993, Nature, 364, 423
Sippel, A. C. & Hurley, J. R. 2013, MNRAS, 430, L30
Soria, R., Long, K. S., Blair, W. P., et al . 2014, Science, 343, 1330
Stirling, A. M., Spencer, R. E., de la Force, C. J., et al . 2001, MNRAS, 327, 1273
Strader, J., Chomiuk, L., Maccarone, T. J., Miller-Jones, J. C. A., & Seth, A. C. 2012a, Nature, 490, 71
Strader, J., Chomiuk, L., Maccarone, T. J., et al . 2012b, ApJ, 750, L27
Tauris, T. M., Kaspi, V. M., Breton, R. P., & et al. 2015, "Understanding the Neutron Star Population with the SKA", in Advancing Astrophysics with the Square Kilometre Array, Proceedings of Science, PoS(AASKA14)039
Tudose, V., Fender, R. P., Garrett, M. A., et al . 2007, MNRAS, 375, L11
Tudose, V., Fender, R. P., Linares, M., Maitra, D., & van der Klis, M. 2009, MNRAS, 400, 2111
van der Laan, H. 1966, Nature, 211, 1131
Wang, X. & Loeb, A. 2014, MNRAS, 441, 809
Webb, N. et al . 2012, Science, 337, 554
Wolter, A., Rushton, A., Mezcua, M., & et al. 2015, "Radio investigation of Ultra-Luminous X-ray (ULX) Sources in the SKA Era", in Proceedings of "Advancing Astrophysics with the Square Kilometre Array", PoS(AASKA14)091
Woudt, P. A., Steeghs, D., Karovska, M., et al . 2009, ApJ, 706, 738
Wu, Y. X., Yu, W., Li, T. P., Maccarone, T. J., & Li, X. D. 2010, ApJ, 718, 620
Yang, J., Paragi, Z., Corbel, S., et al . 2011, MNRAS, 418, L25
Zamaninasab, M., Clausen-Brown, E., Savolainen, T., & Tchekhovskoy, A. 2014, Nature, 510, 126

PoS(AASKA14)053

PROCEEDINGS OF SCIENCE

SKA as a powerful hunter of jetted Tidal Disruption Events

I. Donnarumma[*1], **E. M. Rossi**[2], **R. Fender**[3], **S. Komossa**[4], **Z. Paragi**[5], **S. Van Velzen**[6], **I. Prandoni**[7]

[1] *INAF-IAPS, via Fosso del Cavaliere 100, 00133, Rome, Italy;* [2] *Leiden Observatory, Leiden University;* [3] *Physics and Astronomy, University of Southampton, Southampton SO17 1BJ, UK.;* [4] *Max-Planck-Institut fuür Radioastronomie, Auf dem Hügel 69, 53121 Bonn, Germany;* [5] *Joint Institute for VLBI in Europe, Postbus 2, NL-7990 AA Dwingeloo, the Netherlands;* [6] *IMAPP, Radbound University, PO Box 9010, 6500 GL Nijmegen, The Netherlands;* [7] *IRA Bologna, Via P. Gobetti 101, 40129 Bologna, Italy;*

E-mail: immacolata.donnarumma@iaps.inaf.it

Observational consequences of the tidal disruption of stars (TDEs) by supermassive black holes (SMBHs) can enable us to discover quiescent SMBHs and constrain their mass function. Moreover, observing jetted TDEs (from previously non-active galaxies) provides us with a new means of studying the early phases of jet formation and evolution in an otherwise "pristine" environment. Although several (tens) TDEs have been discovered since 1999, only two jetted TDEs have been recently discovered in hard X-rays, and only one, Swift J1644+57, has a precise localization which further supports the TDE interpretation. These events alone are not sufficient to address those science issues, which require a substantial increase of the current sample. Despite the way they were discovered, the highest discovery potential for *jetted* TDEs is not held by current and up-coming X-ray instruments, which will yield only a few to a few tens events per year. In fact, the best strategy is to use the Square Kilometer Array to detect TDEs and trigger multi-wavelength follow-ups, yielding hundreds candidates per year, up to $z \sim 2$. Radio and X-ray synergy, however, can in principle constrain important quantities such as the absolute rate of jetted TDEs, their jet power, bulk Lorentz factor, the black hole mass function, and perhaps discover massive black holes (MBH) with $< 10^5 M_{\odot}$. Finally, when comparing SKA results with information from optical surveys like LSST, one can more directly constrain the efficiency of jet production.

Advancing Astrophysics with the Square Kilometre Array
June 8-13, 2014
Giardini Naxos, Italy

*Speaker.

PoS(AASKA14)054

1. Introduction

Mounting observational evidence is supporting a scenario where most galactic nuclei host supermassive black holes (SMBHs). Gas inflow from larger scales causes a small ($\sim 1\%$) fraction of SMBHs to accrete continuously for millions of years and shine as quasars. Most of them are instead "quiescent", accreting –if at all– at a highly sub-Eddington rate. Observationally, it is therefore hard to assess the presence and measure the mass of most of SMBHs, beyond the local universe. Occasionally, however, a sudden increase of the accretion rate may occur, if a large mass of gas, e.g. a star, falls into the tidal sphere of influence of the black hole and find its-self torn apart and accreted. We call these events "tidal disruption events" (TDEs). TDEs can result in sudden flares: these can reach the luminosity of a quasar but they are rare ($\sim 10^{-5}\mathrm{yr}^{-1}$ per galaxy) and last for only a few up to several months. We will show in this Chapter how the SKA sensitivity and its large field of view could increase the TDE sample and have a large discovery potential.

The detection and study of these flares can deliver other important astrophysical information, beyond flagging the presence of a SMBH. The theoretical expectation is that TDE flares would be caused by sudden accretion of the star debris. If the star is completely disrupted, its debris is accreted at a decreasing rate of $\dot{M} \propto t^{-5/3}$ (Rees 1988; Phinney 1989). Therefore, TDEs allow us to study the formation of a transient accretion disc and its continuous transition through different accretion states. As the accretion rate decreases, we can in principle observe a disc in an initial super-Eddington phase, lasting several months; the disc then would become *slim* and later enter in a *thin* disc regime, finally ending its life, years later, in a radiative *inefficient* state. The super-Eddington phase — which occurs only for SMBH masses $M \lesssim 10^7$ $\mathrm{M}_\odot$ — is theoretically uncertain, but it may be associated with a powerful radiative driven wind (Rossi & Begelman 2009), which thermally emits $\sim 10^{41} - 10^{43}$ erg s^{-1}, mainly at optical frequencies (Strubbe & Quataert 2009; Lodato & Rossi 2011). The disc luminosity ($\sim 10^{44} - 10^{46}$ erg s^{-1}), instead, peaks in the far-UV/soft X-rays (Lodato & Rossi 2011). Of great theoretical importance would also be the possibility to observe the formation and evolution of an associated jet, powered by this sudden accretion episode.

The first TDEs were discovered in *ROSAT* surveys of the X-ray sky (e.g., Komossa & Bade 1999; Grupe et al. 1999) — see Komossa (2002) for a review. Later, *GALEX* allowed for the selection of TDE at UV frequencies (Gezari et al. 2009, 2012); many of the most recent TDE candidates are now found in optical transient surveys (van Velzen et al. 2011a; Cenko et al. 2012; Chornock et al. 2014; Arcavi et al. 2014). An alternative method to select TDE candidate is to look for optical spectra with extreme coronal lines (Komossa et al. 2008; Wang et al. 2012). These "thermal" features are believed to be associated with emission from the disc or the radiative driven wind.

Moreover, recently the *Swift* Burst Alert Telescope (BAT) instrument (Burrows et al. 2011; Cenko et al. 2012), triggered two TDE candidates in the hard X-ray band. A multi-frequency follow-up from radio to γ-rays revealed a new class of non-thermal TDEs. It is widely believed that emission from a relativistic jet is responsible for the hard X-ray spectrum (with power-law photon index $\beta \sim 1.6 - 1.8$) and the increasing radio activity (Levan et al. 2011), detected a few days after the trigger. The best studied of the two events is Swift J1644+57 (Sw J1644 in short), whose radio lightcurve (see next section) is used in this Chapter to estimate detection rates in the

PoS(AASKA14)054

radio band. The two main features that support the claim that Sw J1644 is a tidal disruption event are i) the X-ray lightcurve behaviour, that follows $\propto t^{-5/3}$ after a few days from the trigger, and ii) the radio localization of the event within 150 pc from the centre of a known quiescent galactic nucleus (Zauderer et al. 2011).

1.1 Radio emission of jetted TDEs

In 2011, BAT discovered a peculiar gamma-ray burst, now known as Sw J1644. What first caught the attention was the flaring activity, which caused multiple BAT triggers, followed by an X-ray light curve that extended to much longer timescales than any known GRB (Levan et al. 2011). The source was confirmed to be of extragalactic origin, its peak luminosity ~ 100 times higher than bright active galactic nuclei (Burrows et al. 2011; Levan et al. 2011). Follow-up radio observations revealed a transient radio counterpart (Zauderer et al. 2011) and the multi-wavelength SED of the source resembled that of BL Lac objects (Bloom et al. 2011). Key evidence that Sw J1644 is, in fact, a newly launched jet, is the rapid X-ray variability implying Doppler-beamed emitting regions (Bloom et al. 2011). A second BAT-triggered TDE candidate, Swift 2058+05, that also has a transient radio counterpart was discovered by Cenko et al. (2012).

A rich dataset of radio follow-up observations of Sw J1644 is presented in Berger et al. (2012); Zauderer et al. (2013). At 5 GHz, the peak in the light curve occurs about 100 days after the first gamma-ray trigger, at $F_\nu = 15$ mJy ($\nu L_\nu = 4 \times 10^{41}$ erg s) (cf. Fig. 3 in Zauderer et al. 2013). During the first years the self-absorption frequency is around 10 GHz; at 2 GHz the peak of the light curve is expected to occurs about 500 days after the stellar disruption. The lightcurve at 1.4 GHz is shown in Fig. 3.2. Data were collected from 5 days after the Swift trigger, with a flux of $F_\nu \geq 0.2$ mJy. The radio light curve of the second relativistic TDE, Swift 2058+05, has been sampled for only a few epochs (at 5 GHz the flux is 0.9 mJy). Its luminosity is similar to Sw J1644, but the spectrum is rather flat ($F_\nu \propto \nu^0$) from 4.5 GHz up to 22.5 GHz Cenko et al. (2012).

The light curve of Sw J1644 can be modeled as synchrotron emission from the forward shock (Giannios & Metzger 2011; Metzger, Giannios & Mimica 2012), although this model requires an increase of the isotropic-equivalent jet kinetic energy (Berger et al. 2012), which is much stronger than what is expected from the fallback rate of stellar debris (see also Kumar et al. 2013). Interestingly, the X-ray light curve Sw J1644, shows a very steep drop when the (theoretically estimated) fallback rate crosses the Eddington limit (Zauderer et al. 2013). This could imply that the jet engine has switched off due to a state change of the accretion disk, as suggested by the first models of TDE jets (Giannios & Metzger 2011; van Velzen, Körding & Falcke 2011).

2. Constraints on TDE jets from past and present radio surveys

So far, surveys of radio transients have yielded a few events (e.g, Gal-Yam et al. 2006; Bannister et al. 2011) — see Frail et al. (2012) for a review. However, due to the lack of follow-up observations it has been difficult to test if these are TDE jets. For a given light curve model of the radio emission from TDE jets, the upper limits on the event rate from these surveys can be used to constrain the rate of these events.

As shown in van Velzen et al. (2013), the observed light curve of Sw J1644 can be used to make an order of magnitude estimate of snapshot rate of events that have a similar light curve.

PoS(AASKA14)054

Input to this estimate are the per-galaxy rate of tidal disruption jets ($\dot{N}_{\rm TDE}$) and the mean volume density of black holes $\rho_{\rm BH}$ that create observable TDE jets. If we assume that only jets with an inclination smaller than $1/\Gamma_j$ are visible, we arrive at the following expression for the snapshot rate above a given flux limit $F_{\nu,\rm lim}$:

$$R(F_{\nu,\rm lim}) \sim 8\times10^{-3}\,\Gamma_j^{-2}\left(\frac{F_{\nu,\rm Sw}}{F_{\nu,\rm lim}}\right)^{3/2}\frac{\Delta T\dot{N}_{\rm TDJ}}{10^{-5}}\frac{\rho_{\rm BH}}{5\times10^{-3}\ {\rm Mpc}^{-3}}\ {\rm deg}^{-2} \quad . \tag{2.1}$$

Here ΔT denotes the time interval along which Sw J1644 flux is above $F_{\nu,\rm lim}$. Here we normalized snapshot rate assuming that the rate of jetted TDE $\dot{N}_{\rm TDJ}$ is similar to the rate of thermal TDE (we return to this assumption below). The rate of thermal TDE can be estimated from soft X-ray (Donley et al. 2002) or optical (van Velzen & Farrar 2014) surveys, a conservative value is $\dot{N}_{\rm TDE}\sim10^{-5}\,{\rm yr}^{-1}$.

For $\Delta T = 1$ yr, the light curve of Sw J1644 implies $F_{\nu,\rm Sw} = 10$ mJy, 2 mJy at 5 and 1 GHz, respectively. Adopting $\Gamma_j = 2$ as estimated from modelling the late-time radio emission of Sw J1644 (Berger et al. 2012), we obtain our estimate of snapshot rate as shown in Fig. 1. This rate is close to the existing upper limits of radio transient surveys.

In Fig. 1 we also show the predicted rate at 1 GHz based on the model of van Velzen, Körding & Falcke (2011). In the optimistic scenario of these authors, 20% of the accretion power is converted into jet power (i.e., in analogy with AGNs, tidal disruption jets are always radio-loud). The synchrotron luminosity is computed using the conical equipartition jet model (Blandford & Königl 1979; Falcke & Biermann 1995), which yields a peak luminosity (for on-axis events) that is lower than the peak of Sw J1644 (hence the predicted snapshot rate is also lower). In the conservative scenario of van Velzen, Körding & Falcke (2011), tidal disruption jets are only radio-loud when the fallback rate drops below 2% of the Eddington limit.

3. SKA as the best hunter of *jetted* TDEs

In this section we report on the rate of TDEs expected to be detected with SKA operating in survey mode. The SKA1-survey (SKA1-SUR) provides us with an optimal tool to catch and discover jetted TDEs. We adopted a strategy which relies on a trade-off between sky coverage and sensitivity, fully compliant with the SKA1-SUR science requirements reported in the Baseline Design Document (Dewdney et al. 2013). We request to achieve an half sky coverage (20,000 deg^2) with a 2-day cadence at a $5-\sigma$ flux limit of 90 μJy. This can be achieved by SKA1-SUR. SKA1-SUR can cover this area with 1111 pointings at 1.4 GHz (the SKA1-SUR field of view at this frequency is 18deg^2) at a sensitivity of 3.72 microJy hr$^{-1/2}$ (see Table 1 in Dewdney et al. 2013), or at a flux limit of 90 μJy in 2 days.

3.1 Snapshot rate estimate

We first make a rough estimate based on Eq. 2.1. At 1 GHz, the observed light curve of Sw J1644 is above 2 mJy for less than one year ($\Delta T \approx 0.8$yr) (Zauderer et al. 2013), for a flux limit 90 μJy we thus obtain a snapshot rate of 0.2 deg^{-2} (Fig. 1), implying ≈ 4000 events for the SKA transient survey adopted here if $\Gamma_j = 2$ is assumed.

PoS(AASKA14)054

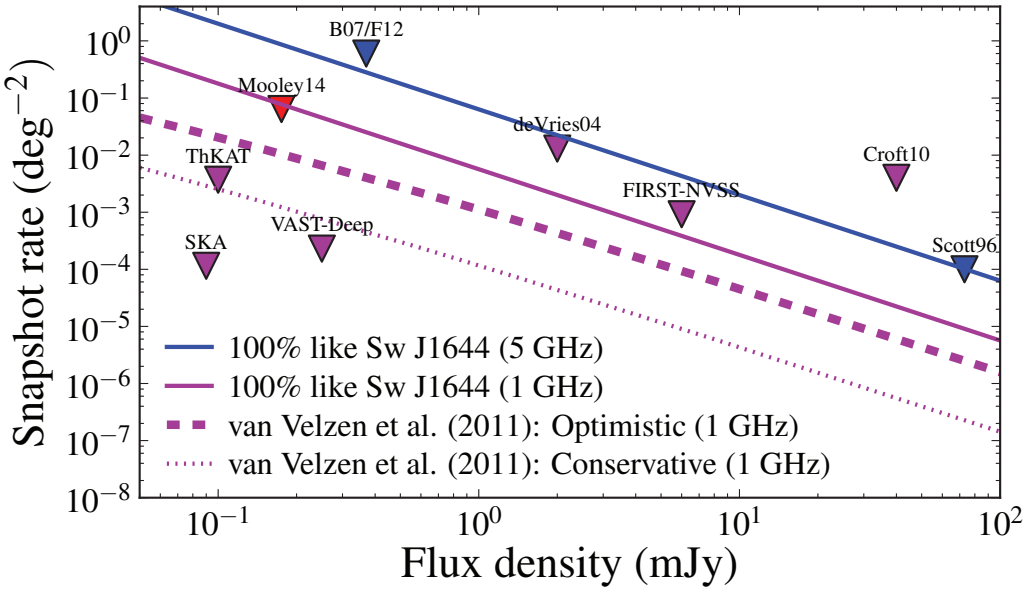

Figure 1: Predicted snapshot rate and upper limits from current and future radio surveys. The predicted rate for Sw J1644 is based on eq. 2.1 and assumes a 100% jet production efficiency, i.e., every TDE makes a jet with a light curve similar to Sw J1644. The blue, red, and magenta triangles show (potential) 2-σ upper limits at 5, 3 and 1 GHz, respectively. References: B7/F12: Bower et al. (2007); Frail et al. (2012); de Vries et al. (2004), FIRST-NVSS: Gal-Yam et al. (2006); Croft et al. (2010); Scott (1996); Mooley et al. (2014).

3.2 Radio Lightcurve and Monte Carlo simulations

We here extend our rate calculations to explicitly account for redshift, BH mass M and stellar mass m_* dependences, using Monte Carlo simulations (see Donnarumma & Rossi 2014, for details). The radio lightcurve at 1.4 GHz of Sw J1644 is plotted in Fig. 3.2. To investigate the detection capability of SKA1-SUR, we assume that all events have the same light curve shape as Sw J1644. We model the mission as synchrotron radiation and use the peak flux and characteristic frequencies measured at different times by Berger et al. (2012, see their eq.4 and dash-dotted line in our Fig.3.2) extended at late epochs by Zauderer et al. (2013). The lightcurve behaviour in the first ≈ 8 days (where there are no data) has been extrapolated from later epochs. The result is a quite sharp rise, that can be considered a conservative assumption: a more gentle rise would ensure more detections. Note that ours is *not a fit* to the data, but *it is a modelling*. From Fig. 2 it is clear that the radio flux does not show the temporal characteristic behaviour $\propto t^{-5/3}$ of a tidal disruption event, that it is present in the X-ray band. Therefore, a follow up strategy at higher frequency is required for identification (see Section 3.5).

An appropriate spectral correction can describe events which explode at different redshifts than Sw J1644 [1]. Rescaling the flux for different BH and stellar masses requires instead to assume a jet model. A first possibility is to describe the jet evolution with a Blandford McKee solution

[1] We here assume that all jets have approximately the same Doppler factor $\delta \approx \Gamma_j \simeq 2$, as measured in radio for Sw J1644

PoS(AASKA14)054

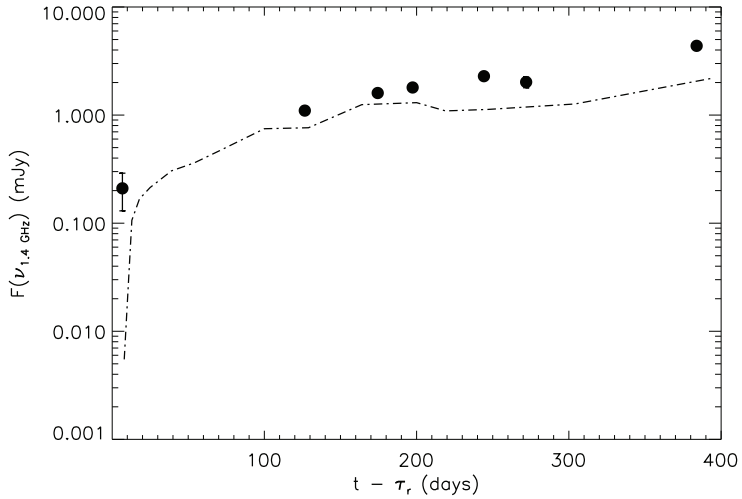

Figure 2: The radio (1.4 GHz) light curve of Sw J1644: data (black circles) from Berger et al. (2012); Zauderer et al. (2013), modelling (dash-dotted black line) from Donnarumma & Rossi (2014). Figure adapted from Donnarumma & Rossi (2014). Note that the black line is not a fit. We trace it by assuming synchrotron emission and the characteristic frequencies and peak flux measured by Berger et al. (2012); Zauderer et al. (2013) at different times. The result slightly underpredicts the data, but recovers the overall temporal behaviour which is rather flat.

(Blandford & Mckee 1977), usually adopted for γ-ray burst afterglows. In this case, the radio flux does *not* explicitly depend on the BH mass. A second approach is to assume that the luminosity is proportional to the peak of the jet power, which in turn is proportional to the peak fall-back rate $L_{\rm j,p} \propto \dot{M}_{\rm p}$. This introduces a mass dependence in the luminosity as $L_\nu \propto L_{\rm j,p} \propto M^{-1/2} m_*^{1/2}$. Hereafter we will focus on this second BH mass dependent lumimosity (MDL) model and we refer the readers to Donnarumma & Rossi (2014) for a comparison with the Blandford Mckee solution. The stellar mass distribution in galactic nuclei may vary, but there is no solid observational evidence. We therefore assume a "universal" Kroupa initial mass function Kroupa (2001), as observed in our Galaxy. The BH mass function is instead explained more in detail in the following section.

3.3 Black hole mass functions

The mass distribution of black holes as a function of redshift is a key ingredient to calculate TDE rates. We adopt the BH mass function (MF) predictions according to the models labeled *G* and $G(z)$ in Shankar, Weinberg & Miralda-Escudé (2013). In practice, we consider the two accretion models which yield the largest and the lowest MF predictions in order to reflect the uncertainty due to the black hole mass distribution on our expected TDE rates. The "intrinsic" TDE rate as a function of redshift is defined by

$$R(z) = \int_{M_{\rm min}}^{M_{\rm max}} \phi(M,z) \dot{N}_{\rm TDE} V(z) dM, \tag{3.1}$$

where $\dot{N}_{\rm TDE} = 10^{-5}$ yr^{-1} is as our fiducial *intrinsic* TDE rate, $\phi(M,z)$ is the black hole comoving number density and $V(z)$ the comoving cosmological volume. In our calculations, we consider

PoS(AASKA14)054

only BH masses above $M_{\rm min} = 10^6$ M$_\odot$, because MFs are not observationally constrained below that mass.

3.4 Monte Carlo simulations

Assuming the radio modellings described in section 3.2, we performed Monte Carlo simulations (MCs) to derive the rate of jetted TDEs expected to be detected by SKA1-SUR operating in wide survey mode .

The intrinsic rate $R(z)$ (eq. 3.1) is reduced by a factor of $1/2\ \Gamma_j^2$ for the relativistic beaming. Our fiducial value is $\Gamma_j = 2$ (Zauderer et al. 2013; Berger et al. 2012), but our results may be easily rescaled by assuming different values of Γ_j. Finally, a further scaling factor accounts for the fraction of the sky accessible at each time by the instrument. As already discussed in section 3.3, we will provide a range of rates whose limits reflect the uncertainty in the BH MF predictions.

The specific observational strategy for SKA1-SUR explained at the beginning of this section assumes an half sky coverage (20,000 deg^2) with a 2-day cadence at a $5-\sigma$ flux limit of 90 μJy.

For each event, with given redshift, BH and stellar mass, the light curve is predicted as described in section 3.1. We extract the trigger time randomly from a 1 year uniform distribution, and we calculate the average flux over 2 days since the trigger and then we compare it with the SKA1-SUR flux limit fixed for our strategy.

We show in Fig. 3, the distribution of the TDE rate as a function of z (right panel) and the corresponding BH mass distribution (left panel) for the two BH MFs assumed (solid and dotted blue lines). In the right panel, we overplot the rate distributions for TDEs with BH masses lower than 10^7 M$_\odot$ (solid and dotted red lines). The total rate distribution peaks around $z \sim 0.5$ and it is dominated by light SMBHs locally and for z above the peak. The maximum redshift that SKA can attain is close to $z \sim 2$.

The total number of objects obtained by integrating these distributions in z and M$_{BH}$ is ~ 300 and ~ 800 yr^{-1} for the G and G(z) models, respectively. We note that our integrated rates are significantly lower than the first simple estimates reported in section 3. This is mainly due to the fact that we accounted for the stellar mass dependence, that introduces a large variation in the intrinsic luminosity of these events. Nevertheless, our results imply that a significant increase in the number of detected jetted TDEs can be achieved thanks to our strategy in the framework of SKA1-SUR. However, as mentioned before, the TDE signature seems to appear at higher frequencies. We therefore proceed to consider X-ray facilities.

3.5 Radio and X-ray synergy

Future X-ray surveys can detect much fewer candidates than SKA. The e-Rosita all sky survey (Merloni et al. 2012) is expected to trigger a few jetted TDEs by using its “hard" X-ray band ($2-10$ keV). Calculations based on the Swift statistics (by using SW 2058 as a prototype) predicted 1 object to be detected per scan (6-month long) probing the universe up to $z \sim 4.5$ (Khabibullin et al. 2014).

We also envisage the use of X-ray telescopes to follow up radio candidates and confirm their nature. To quantitatively explore this possibility, we model the X-ray emission of Sw J1644 in the 1-10 keV band, assuming that the X-ray luminosity scales as the fall back rate, $L_{\rm X} \propto \dot{M}$. (see

PoS(AASKA14)054

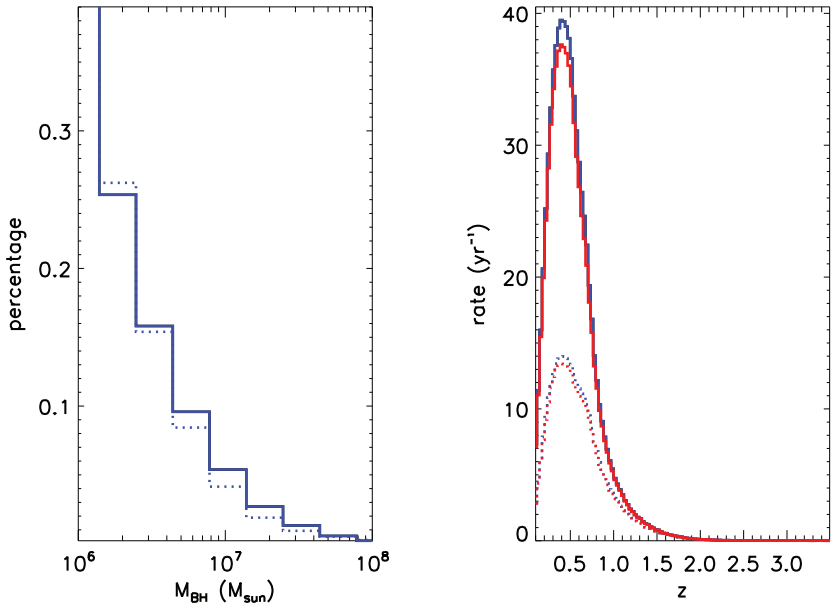

Figure 3: Rate of events detected by SKA as a function of redshift (right panel) and their mass distribution (expressed in percentage, left panel), for two different black hole mass distribution functions (solid and dotted blue lines). The rates for BH masses lower than 10^7 $M_\odot$ are also shown (red lines, right panel). Figure adapted from Donnarumma & Rossi (2014).

Donnarumma & Rossi 2014, for a full description of the methodology). In our estimates, we assumed that a follow-up can be arranged within 1 day from the radio trigger. To claim detection, we require that the observed flux can be detected with a signal to noise of at least 10 during four pointings, spread over four days. This requirement implies that a flux threshold (unabsorbed flux) of $\sim 5 \times 10^{-12}$ erg cm^{-2} s^{-1} in the 1-10 keV band is in principle enough to identify all the SKA selected candidates.

Therefore, given their sensitivity, future X-ray experiments like Athena (Nandra et al. 2013) and a LOFT-like mission (Feroci et al. 2012) could offer a unique chance to follow-up and characterize SKA-triggered TDEs. If Athena will have a follow-up efficiency of 50% associated with the sky accessibility, it will be able to identify about 50% of all the radio sample. For a LOFT-like mission, we would expect that a sub-sample of radio TDEs between $\simeq 100$ and $\simeq 350$ will be detected per year up to $z \sim 1.2$ by observing with its main instrument, the Large Area Detector.

4. Constraints on the jet production efficiency

As recalled above, only two jetted TDEs have been detected, while detections of the thermal candidates, related to the presence of an accretion disk, have been more numerous. The question then arises whether this is due to observational biases or to a small jet opening angle or to an intrinsic low efficiency of transient accretion disks to produce (luminous) jets.

PoS(AASKA14)054

To answer this question, one may first compare predictions in the Swift/BAT bands with the observed rate of ≈ 0.3 yr^{-1}. It turns out that the most pessimistic predictions by Donnarumma & Rossi (2014) are still a factor of tens higher than observed and it would be tempting to reconcile this discrepancy by invoking a jet production efficiency of a few percent. However, it has been shown that this inference *cannot* be confidently drawn (Donnarumma & Rossi 2014). On the one hand, other uncertain parameters –like the value of the beaming factor in the X-ray emitting region – can mitigate the discrepancy. On the other, the modelling of the characteristics (e.g. flux limit and sky coverage) of an effective Swift/BAT survey (in fact, Swift is *not* operating in survey mode) it is not at all straightforward and does not allow for firm predictions. Plus, with just two events, the Poisson uncertainty is very large.

Another approach for estimating the jet production efficiency is to use instead the observed thermal candidates. Thermal TDEs may also contain jets. In fact, based on an analogy with X-ray binaries, one may anticipate that each TDE is accompanied by a jet (see van Velzen, Körding & Falcke 2011, and references therein). Because they are observed off-axis, these jets are less luminous and will not trigger *Swift*, but they can be detected through radio or X-ray follow-up observations.

The existing radio follow-up observations of known thermal TDEs are summarized in van Velzen et al. (2013). So far, none of the optical/UV-selected TDE have been detected at radio frequencies (see also Arcavi et al. 2014). Using a simple model to scale the observed light curve of Sw J1644 for off-axis observed we find that the current radio observations are deep enough to detect jets similar to Sw J1644 to an inclination of $i < 70^\circ$ (van Velzen et al. 2013). We thus know that the jet production efficiency has to be less than 100%.

Two of the seven TDE candidates that were detected by ROSAT or XMM have been detected at 5 GHz in follow-up observation by Bower et al. (2013), namely IC 3599 (Komossa & Bade 1999) and RX J1420+5334 (Greiner et al. 2000). The radio observations were obtained about ten years after the estimated time of disruption, their transient nature remains to be confirmed (in fact one of the radio-detected sources, IC 3599, is more likely to be an AGN).

We can thus conclude that none of the thermal TDE show strong evidence for relativistic jets. This could imply that the fraction of TDE that launch jets similar to Sw J1644 less than $\approx 10\%$, although currently is not clear if the detection of optical/UV emission implies a bias against the detection of radio emission. To be able to detect optical or UV emission, one requires a circum-nuclear environment with little absorption by dust, while the radio luminosity can be boosted by a high density circumnuclear gas.

Present constraints on the jet production efficiency suffer of the poor statistics due to the small X-ray and radio samples. The radio rates of jetted TDEs predicted in this work, will help to overcome the present limitation due to the very large sample expected to be triggered by the SKA. Besides serving as a trigger, the high survey speed of the SKA implies that it will be possible to have near-simultaneous observations with LSST surveys. The detection rate of optical TDE with LSST is ~ 1000yr^{-1} (e.g., Gezari et al. 2009; van Velzen et al. 2011a), hence the SKA observations will be able to measure a jet production efficiency for thermal TDE as small as 0.1%. Comparing the SKA-triggered TDEs with the SKA observations of thermal TDE discovered by LSST will provide a new window to study the jet physics of massive black holes.

PoS(AASKA14)054

5. Implications for the cosmological growth of SMBHs

The observed properties of central SMBH and their hosts show evidence for a strong link between SMBH and galaxy formation (Ferrarese & Merritt 2000; Gebhardt et al. 2000). Outstanding questions include how the massive black hole seeds (MBH, $\sim 10^2 - 10^5\ M_\odot$) were initially formed, and their successive mass growth, which determine their mass functions (Volonteri 2010). TDEs will provide a great opportunity in this quest.

Fig.3 shows that SKA will more easily detect light ($< 10^7 M_\odot$) MBHs locally and at z > 1. Since the lighter the more luminous, this result suggests the possibility to observe BHs in the elusive "intermediate mass regime" in the distant Universe.

As described in section 3, in this Chapter we focused our work on BHs with masses $\geq 10^6 M_\odot$. This because of the very high uncertainties affecting the lower mass side of the BH mass functions. However, the recently reported TDE candidate from a $\sim 10^{5.5}\ M_\odot$ black hole (Donato et al. 2014) shows the great potential to exploit TDEs to seek out MBHs in the mass range of $\sim 10^2 - 10^5\ M_\odot$, with important consequences for BH formation models. These black holes must exist in low-mass dwarf galaxies or perhaps as remnants inside massive galaxies. Alternatively, they may have formed in the centre of globular clusters[2] (Maccarone 2004).

We would like to point out, that the high-precision location of the radio-TDE with respect to the galaxy core will be of great relevance in the understanding of both SMBH and IMBH formation. TDEs might reveal recoiling black holes (e.g. Komossa 2012) that have wandered slightly away from the nucleus, off-nuclear SMBH due to ongoing merger activity (Comerford & Greene 2014), or for example black holes that were formed in the centre of globular clusters (Maccarone 2004). In the case of galaxy mergers, the stellar tidal disruption rate can be temporarily strongly enhanced (e.g., Chen et al. 2009). Such TDE would point us to an ongoing merger, but would likely be off-set from the geometrical center of the merging system. In the case of recoiling BHs due to e.g. SMBH coalescence, gravitational wave recoil will insert a kick velocity on the newly formed single black hole, which will carry a retinue of stars with it, as it is ejected from the core of its host galaxy. These bound stars will undergo tidal disruption (Komossa & Merritt 2008), leading to a radio event offset from the galaxy core.

6. Observational strategies

As showed in Section 3, SKA can play an important role in discovering jetted TDEs. To achieve this, it will be necessary to find TDEs by means of a commensal search in all SKA observations, or by carrying out a near real-time transient search in a high cadence dedicated survey observations. The latter is preferred since our goal is to detect TDEs early on in order to allow for the necessary follow-ups (to confirm the TDE origin). The real advantage of this strategy is that it will be able to build up a large sample of jetted TDEs up to $z \sim 2$, where the low-mass population of SMBHs could dominate, providing a unique opportunity to constrain the low mass end of the SMBH mass function in the far Universe.

[2]Off-nuclear BH in the mass range $\sim 10^2 - 10^5\ M_\odot$, as a likely power source of the most extreme ultra-luminous X-ray sources, and the ones that are believed to have formed in the centre of globular clusters are often referred to as intermediate-mass black holes (IMBH) in the literature.

PoS(AASKA14)054

The SKA1-SUR will provide us with an optimal instrument to detect transient events as TDEs. Our strategy, explained in Section 3, is compliant with the Baseline Design Document (Dewdney et al. 2013) and predicts a few hundred detections with X-ray follow up for identification. However, a significant sample could also be collected, assuming a 50% reduction in sensitivity due to re-baselining. This is because the 1.4 GHz light curve of Sw J1644 increases with time at least up to 600 days (Zauderer et al. 2013), therefore a multiple cadence survey with longer integration times (~ 8 days) needed to achieve the same flux limit of our strategy should not result in a significant loss of radio detections. However, radio triggers at late times could be problematic for follow-up observations, because sources would get fainter in both optical and X-ray energy range, preventing the identification of higher redshift TDEs. Nevertheless, the bulk of the sample at $z \lesssim 0.5$ should still be successfully followed up at higher frequencies.

On the basis of these considerations, TDE can be commensally searched for, by exploiting the SKA1-SUR all-sky survey ($31,000$ deg^2 at 2 μJy beam^{-1} at 1.5-2 arcsec resolution) proposed in the framework of both the Magnetism and Continuum science cases (see Johnston-Hollit et al. 2015; Prandoni et al. 2015). If carried out by visiting individual fields multiple times with a cadence of ~ 10 days over the two year period, it will be very efficient in finding extra-galactic transients down to $\sim$90 μJy beam^{-1} .

As mentioned before, the 1.4 GHz light curve of our prototype TDE does not bear any specific footprints of a TDE nature. Thus we cannot use only its properties or variability to distinguish a TDE candidate from neither a slowly variable AGN or a GRB. However, we can account for AGN contamination by cross-correlating the transient positions with deep AGN catalogues. A significant advance in this direction will be achieved by the large amount of data that LSST will provide in the near future together with those collected after one year of SKA and SKA precursor (ASKAP) observations. On the other hand, precise localization of the radio transient in the core of galactic nuclei will help assessing the nuclear origin: the better the localisation, the stronger is the case for a TDE.

This means that a rapid optical follow-up aimed at determining the host galaxy has to be foreseen. Once the host galaxy is found, thanks to a resolution of about 2 arcsec (SKA1-SUR) and 0.6 arcsec or better (SKA1-MID) (Dewdney et al. 2013) it will be possible to localize the brighter transients with a precision of ~ 100 milliarcsecond (mas), essential to separate nuclear transients from other phenomena (e.g., GRB). This angular localization is at the current alignment accuracy level of radio and optical reference frames (Orosz & Frey 2013), corresponding to linear scales of 0.5–0.8 kpc at $z > 0.3$.

We note that by detecting radio emission associated with star formation, pre-flare SKA observations can help to identify jetted TDEs. By combining the individual snapshot obtained *after* ~ 1 year of observations, we expect to be able to see typical star-forming galaxies ($L \sim 10^{20}$ W/Hz; Condon (1992)) up to $z \approx 0.5$. At this redshift we also expect to see most of our detected jetted TDEs (see Fig. 2), hence most TDEs that occur in star-forming galaxies will have a detected host galaxy. These host detections will allow for an accurate localization of the radio transient with respect to the center of its host galaxy, which will help to reject SNe and GRBs (TDE from SMBHs occur in the nucleus of the galaxy, while SNe/GBRs track the stellar density). The identification of nuclear radio transients will allow for faster triggers for follow-ups in X-rays (by avoiding the need for the optical follow-up for the host identification), which will give us a firm signature of the TDE

PoS(AASKA14)054

nature if the trigger occur within 1 year from the beginning of the event (see section 3). A synergy with SKA and VLBI will help to characterize the jet formation in the pristine environment of the TDE hosts (Paragi et al. 2015).

Given the huge amount of TDE candidates predicted and the *expensive* strategy, we do not need to know immediately for all hundreds of events, what they are. In the first stage, we could concentrate the efforts on the brightest events (tens of objects) and for them activate follow-up observations at higher energies. The rest of those events could be analyzed later by means of commensal search in SKA observations.

Finally, SKA will play an important role even for the follow-up of all TDEs detected by the *Gaia* mission (expected to end soon before SKA1-MID early operations) thanks to the SKA1-MID sub-arcsec angular resolution. Immediate follow-up observations of TDEs detected in the X-rays and by LSST in the optical will be important to constrain the jet production efficiency at low redshift. This will require flexible operations and the ability to respond to triggers from other instruments (see Fender 2015).

7. Conclusions

In this Chapter, we have shown how SKA alone, thanks to its combination of survey speed (SKA1-SUR, for transient searches) and sub-arcsec angular resolution (SKA1-MID, for TDE identifications), and in synergy with coeval instruments at higher energies, can play a leading role in discovering jetted TDEs and allowing for the first time statistical studies of their features. We predict a sample of hundreds, up to redshift ~ 2. It is however, important to be able to communicate the detection promptly, so that an immediate campaign to localize the event and trigger higher frequency instruments may be launched within a week from the TDE discovery. A lot of relevant information will be gathered from TDE discoveries thanks to the synergy among future radio, optical and X-ray surveys, allowing to:

- make the estimate of the jet production efficiency more reliable
- differentiate different theories of jets production onto supermassive black holes, e.g., spin-powered versus accretion-disk powered
- discover quiescent SMBHs in the distant Universe
- probe the BH mass function at low masses.

References

Arcavi, I., Gal-Yam, A., Sullivan, M., et al. 2014, ArXiv e-prints, arXiv:1405.1415

Bannister, K. W., Murphy, T., Gaensler, B. M., Hunstead, R. W., & Chatterjee, S. 2011, Mon. Not. Roy. Astro. Soc., 412, 634

Barth, A. J., Ho, L. C., Rutledge, R. E. & Sargent, W. L. W. 2004, Ap. J., 607, 90

Berger, E., Zauderer, A., Pooley, G. G., et al. 2012, Ap. J., 748, 36

Blandford, R. D., & Königl, A. 1979, Ap. J., 232, 34

PoS(AASKA14)054

Blandford, R.. D., & McKee, C. F., 1977, Mon. Not. Roy. Astro. Soc., 180, 343
Bloom, J. S., Giannios, D., Metzger, B. D., et al. 2011, Sci, 333, 203
Bower, G. C. 2011, Ap. J., 732, L12
Bower, G. C., Metzger, B. D., Cenko, S. B., et al. 2013, Ap. J., 763, 84
Bower, G. C., Saul, D., Bloom, J. S., et al. 2007, Ap. J., 666, 346
Burrows, D. N., Kennea, J. A., Ghisellini, G., et al. 2011, Nat, 476, 421
Campana, S., Lodato, G., D'Avanzo, P., et al. 2011, Nat, 480, 69
Cannizzo, J. K., Troja, E., & Lodato, G. 2011, Ap. J., 742, 32
Carilli, C. L., Rawlings, S. 2004, New Astronomy Reviews, 48, 979
Cenko, S. B., Krimm, H. A., Horesh, A., et al. 2012, Ap. J., 753, 77
Chen, X., Madau, P., Sesana, A., Liu, F. K.. 2009, Ap. J., 697, 149
Chornock, R., Berger, E., Gezari, S., et al. 2014, Ap. J., 780, 44
Comerford, J. M., & Greene, J. E. 2014, Ap. J., 789, 112C
Condon, J. J. 1992, ARA& A, 30, 575
Croft, S., Bower, G. C., Ackermann, R., et al. 2010, Ap. J., 719, 45
de Vries, W. H., Becker, R. H., White, R. L., & Helfand, D. J. 2004, Astron. J., 127, 2565
Dewdney, P., Turner, W., Millenaar, R., McCool, R., Lazio, J., Cornwell, T., 2013, "SKA1 System Baseline Design", Document number SKA-TEL-SKO-DD-001 Revision 1
Donato, D., Cenko, S. B., Covino, S., et al. 2014, Ap. J., 781, 59
Donley, J. L. ,Brandt, W. N., Eracleous, M., & Boller, T. 2002, Ap. J., 124, 1308
Donnarumma, I., & Rossi, E. M. 2014, Ap. J., submitted
Fender, R. P., et al. 2015, "The Transient Universe with the Square Kilometre Array", in proceedings of "Advancing Astrophysics with the Square Kilometre Array", PoS(AASKA14)051
Feroci, M., Stella, L., van der Klis, M., et al. 2012, Experimental Astronomy, 34, 415
Ferrarese, L., & Merritt, D. 2000, Ap. J., 539, L9
Filippenko, A. V., & Ho, L. C. 2003, Ap. J., 588, L13
Frail, D. A., Kulkarni, S. R., Ofek, E. O., Bower, G. C., & Nakar, E. 2012, Ap. J., 747, 70
Gal-Yam, A., Ofek, E. O., Poznanski, D., et al. 2006, Ap. J., 639, 331
Gebhardt, K., Bender, R., Bower, G., et al. 2000, Ap. J., 539, L13
Gezari, S., Heckman, T., Cenko, S. B., et al. 2009, Ap. J., 698, 1367
Gezari, S., Chornock, R., Rest, A., et al. 2012, Nat, 485, 217
Giannios, D., & Metzger, B. D. 2011, Mon. Not. Roy. Astro. Soc., 416, 2102
Granot, J., & Sari, R. 2002, Ap. J., 568, 820
Greene, J. E., & Ho, L. C. 2004, Ap. J., 610, 722
Greiner, J., Schwarz, R., Zharikov, S., & Orio, M. 2000, Astron. Astrophys., 362, L25
Grupe, D., Thomas, H.-C., & Leighly, K. M. 1999, Astron. Astrophys., 350, L31
Guillochon, J., & Ramirez-Ruiz, E. 2013, Ap. J., 767, 25
Hayasaki, K., Stone, N., & Loeb, A. 2013, Mon. Not. Roy. Astro. Soc., 434, 909
Hodge, J. A., Becker, R. H., White, R. L., & Richards, G. T. 2013, Ap. J., 769, 125
Johnston-Hollitt, M., et al., 2015, "Using the SKA Rotation Measure Grid to Reveal the Mysteries of the Magnetised Universe", in "Advancing Astrophysics with the Square Kilometre Array", PoS(AASKA14)092
Kauffmann, G., & Haehnelt, M. 2000, Mon. Not. Roy. Astro. Soc., 311, 576

PoS(AASKA14)054

Kesden, M. 2012, PhRvD, 85, 4037
Khabibullin, I., Sazonov, S., & Sunyaev, R. 2014, Mon. Not. Roy. Astro. Soc., 437, 327
Komossa, S. 2002, Reviews in Modern Astronomy, 15, 27
Komossa, S., & Merritt, D. 2008, ApJ, 683, L21
Komossa, S., et al. 2008, ApJ, 678, L13
Komossa, S. 2012, Advances in Astronomy, 2012, id. 364973
Komossa, S., & Bade, N. 1999, Astron. Astrophys., 343, 775
Krimm, H. A., Kennea, J. A., Holland, S. T., et al. 2011, ATel #3384
Krimm, H. A., Holland, S. T., Corbet, R. H. D., et al. 2013, Ap. J. Suppl., 209, 14
Kroupa, P. 2001, Mon. Not. Roy. Astro. Soc., 322, 231
Levan, A. J, Tanvir, N. R., Cenko, S. B., et al. 2011, Sci, 333, 199
Levan, A. 2012, "Relativistic tidal disruption events", in R. Saxton & S. Komossa (eds.) "Tidal Disruption Events and AGN Outbursts", EPJ Web of Conferences, 39, 2005
Lien, A., Sakamoto, T., Gehrels, N., et al. 2014 Ap. J., 783, 24
Falcke, H., & Biermann, P. L. 1995, Astron. Astrophys., 293, 665
Kumar, P. and Barniol Duran, R. and Bosnjak, Z., et al., 2013, Mon. Not. Roy. Astro. Soc., 434, 3078
Lodato, G., King, A. R., & Pringle, J. E. 2009, Mon. Not. Roy. Astro. Soc., 392, 332
Lodato, G. & Rossi, E. M. 2011, Mon. Not. Roy. Astro. Soc., 410, 359
Loeb, A. 2007, Phys. Rev. D, 99, Issue 4, id. 041103
Maccarone, T. J. 2004, Mon. Not. Roy. Astro. Soc., 351, 1049
Merloni, A., Predehl, P., Becker, W., et al. 2012, ArXiv e-prints, arXiv1209.3114M
Merritt, D., 2009, ApJ, 694, 959
Metzger, B. D., Giannios, D., & Mimica, P. 2012, Mon. Not. Roy. Astro. Soc., 420, 3528
Mooley, Kunal P., Myers, S. T., Hallinan, G., et al. 2014, in AAS Meeting Abstracts, 223
Narayan, R., Igumenshchev, I. V., & Abramowicz, M. A. 2003, Pub. Astron. Soc. Japan, 55 L69
Nandra P., et al., 2013, arXiv1306.2307N
Orosz, G. & Frey, S. 2013, Astron. Astrophys., 553, A13
Paragi, Z., Frey, S., Kaaret, P., et al. 2014, Ap. J., 791, 2
Paragi, Z., Godfrey, L., Reynolds, C., et al. 2015, "Very Long Baseline Interferometry with the SKA", in proceedings of "Advancing Astrophysics with the Square Kilometre Array", PoS(AASKA14)143
Peterson, B. M., Bentz, M. C., Desroches, L.-B., et al. 2005, Ap. J., 632, 799
Phinney, E. S. 1989, Nat, 340, 595
Prandoni, I., et al. 2015, "Revealing the Physics and Evolution of Galaxies and Galaxy Clusters with SKA Continuum Surveys", in proceedings of "Advancing Astrophysics with the Square Kilometre Array", PoS(AASKA14)067
Rees, M. J. 1988, Nat, 333, 523
Reis, R. C., Miller, J. M., Reynolds, M. T., et al. 2012, Sci, 337, 949
Rossi, E. M. & Begelman, M. C. 2009, Mon. Not. Roy. Astro. Soc., 392, 1451
Sadowski, A., Narayan, R., McKinney, J., & Tchekhovskoy, A. 2014, Mon. Not. Roy. Astro. Soc., 439, 503
Sari, R., Kobayashi, S., & Rossi, E. M. 2010, Ap. J., 708, 605

PoS(AASKA14)054

Saxton, C. J., Soria, R., Wu, K., & Kuin, N. P. M. 2012, Mon. Not. Roy. Astro. Soc., 422, 1625
Scott, W. K. 1996, PhD thesis, University Of British Columbia
Shankar, F., Weinberg, D. H., & Miralda-Escudé, J. 2013, Mon. Not. Roy. Astro. Soc., 428, 421
Stone, N., Sari, R., & Loeb, A. 2013, Mon. Not. Roy. Astro. Soc., 435, 1809
Strubbe, L. E., & Quataert, E. 2009, Mon. Not. Roy. Astro. Soc., 400, 2070
Tchekhovskoy, A., Metzger, B. D., Giannios, D., & Kelley, L. Z. 2013, Mon. Not. Roy. Astro. Soc., 437, 2744
Thornton, C. E., Barth, A. J., Ho, L. C., Rutledge, R. E., & Greene, J. E. 2008, Ap. J., 686, 892
van Velzen, S., Farrar, G. R., Gezari, S., et al. 2011, Ap. J., 741, 73
van Velzen, S., Körding, E., & Falcke, H. 2011, Mon. Not. Roy. Astro. Soc., 417, 51
van Velzen, S., & Farrar, G. R. 2014, Ap. J., in press
van Velzen, S., Frail, D., Körding, E., & Falcke, H. 2013, Astron. Astrophys., 552, A5
Volonteri, M. 2010, Astron. Astrophys. Rev., 18, 279
Wang, T.-G., Zhou, H.-Y., Komossa, S., et al. 2012, Ap. J., 749, 115
Zauderer, B. A., Berger, E., Margutti, R., et al. 2013, Ap. J., 767, 152
Zauderer, B. A., Berger, E., Soderberg, A. M., et al. 2011, Nat, 476, 425

PoS(AASKA14)054

PROCEEDINGS OF SCIENCE

Fast Transients at Cosmological Distances with the SKA

Jean-Pierre Macquart[*1], **Evan Keane**[2], **Keith Grainge**[3] **Matthew McQuinn**[4], **Robert Fender**[5], **Jason Hessels**[6], **Adam Deller**[6], **Ramesh Bhat,**[1], **René Breton**[7], **Shami Chatterjee**[8], **Casey Law**[4], **Duncan Lorimer**[9], **Eran O. Ofek**[10], **Malgorzata Pietka**[5], **Laura Spitler**[11], **Ben Stappers**[3], **Cathryn Trott**[1]

[1]*ICRAR/Curtin Institute of Radio Astronomy, Bentley, WA 6845, Australia*
E-mail: J.Macquart@curtin.edu.au
[2]*Swinburne University of Technology*
[3]*University of Manchester*
[4]*UC Berkeley*
[5]*University of Oxford*
[6]*ASTRON*
[7]*University of Southampton*
[8]*Cornell University*
[9]*West Virginia University*
[10]*Weizmann Institute of Science*
[11]*MPIfR*

Impulsive radio bursts that are detectable across cosmological distances constitute extremely powerful probes of the ionized Inter-Galactic Medium (IGM), intergalactic magnetic fields, and the properties of space-time itself. Their dispersion measures (DMs) will enable us to detect the "missing" baryons in the low-redshift Universe and make the first measurements of the mean galaxy halo profile, a key parameter in models of galaxy formation and feedback. Impulsive bursts can be used as cosmic rulers at redshifts exceeding 2, and constrain the dark energy equation-of-state parameter, $w(z)$ at redshifts beyond those readily accessible by Type Ia SNe. Both of these goals are realisable with a sample of $\sim 10^4$ fast radio bursts (FRBs) whose positions are localized to within one arcsecond, sufficient to obtain host galaxy redshifts via optical follow-up. It is also hypothesised that gravitational wave events may emit coherent emission at frequencies probed by SKA1-LOW, and the localization of such events at cosmological distances would enable their use as cosmological standard sirens.

To perform this science, such bursts must be localized to their specific host galaxies so that their redshifts may be obtained and compared against their dispersion measures, rotation measures, and scattering properties. The SKA can achieve this with a design that has a wide field-of-view, a substantial fraction of its collecting area in a compact configuration (80% within a 3 km radius), and a capacity to attach high-time-resolution instrumentation to its signal path.

Advancing Astrophysics with the Square Kilometre Array
June 8-13, 2014
Giardini Naxos, Italy

*Speaker.

PoS(AASKA14)055

1. Observational Phenomenology of Fast Radio Bursts

Before discussing the cosmological science that can be achieved by observing fast radio bursts (FRBs), it is important to describe them as an observational phenomenon. Radio pulsar surveys sample the sky at high time resolution (typically 100-μs samples) and search in dispersion measure (DM) space. The dedispersed time-frequency data are searched for both periodic signals as well as individual impulsive events, i.e. single pulses, with durations from the sampling time up to at least tens of milliseconds. The single-pulse searches are sensitive to bright pulsars and those that emit only sporadically, such as the sub-class known as the rotating radio transients (RRATs; McLaughlin et al. 2006). Individual pulses can be differentiated from radio frequency interference (RFI) because they are localized on the sky (appearing in only one beam of a multi-beam system, or imaged using fast-imaging techniques); broadband; and have DMs that indicate that the signal has been dispersed by an intervening ionized material with a delay proportional to ν^{-2} (cold plasma dispersion). RFI almost never exhibits similar dispersive properties. When combined with a model for the free electron distribution of the Galaxy, the DM can also be used to estimate the distance to the emitting source (e.g. Cordes & Lazio 2002, the NE2001 model).

Recent pulsar surveys have discovered close to a hundred RRATs[1], almost all of which have shown multiple detected pulses, and have DMs that are less than the maximum Galactic DM expected from the NE2001 model along that line-of-sight. It appears likely that all the RRATs are sporadically-emitting neutron stars. Interestingly, such searches have also discovered a small number of individual pulses that are now commonly referred to as FRBs. What distinguishes FRB signals from those of pulsars/RRATs is that they are apparently non-repeating and have DMs that are well in excess of the maximum Galactic contribution predicted by NE2001. The high DMs in particular have led to the conclusion that these signals are likely of extragalactic origin and the dispersive delay results from the combined interstellar medium of our Galaxy, the intergalactic medium and that of a potential host galaxy. The apparently non-repeating nature of the signal also suggest some kind of cataclysmic event, though there is no way to conclusively show that the signal will never repeat.

Determining the sources of the FRB signals, and definitely proving that they are of extragalactic origin has been hampered by their relatively poor sky localization. The positional uncertainty of the known FRBs is on the order of arcminutes, while arcsecond localization is needed to associate them with a known optical source or host galaxy. Such localization requires at least several kilometer baselines, which are not currently used in ongoing pulsar surveys.

In this paper we discuss the utility of FRBs — the events originally termed "Lorimer bursts" — and other as yet undiscovered impulsive extragalactic phenomena as cosmological probes. Our discussion is limited purely to their cosmological applications, and does not address the mystery of their origin. Although understanding the origin of FRBs is highly compelling, the overwhelming abundance of suggested explanations makes it difficult to specify the astrophysical implications of their identification. The layout of the remainder of this paper is as follows. In §2 we describe the various facets of cosmology that are potentially addressed using observations of FRBs. In §3 we describe the requirements driven by the science goals motivated in the previous section, while in

[1] see http://astro.phys.wvu.edu/rratalog/

PoS(AASKA14)055

§4, §5 and §6, we describe respectively the portions of the science case that can be addressed with SKA1, a reduced-sensitivity SKA1 and, finally, the full SKA. Our conclusions are presented in §7.

2. Extragalactic Transients as cosmological probes

Two key questions facing early twenty-first century cosmology are the nature of the mysterious dark energy that appears to pervade 70% of the mass-energy of the Universe, and the distribution of the large reservoir of missing baryonic matter in the present Universe. The detection of impulsive bursts at cosmological distances offers an entirely new means of solving both of these problems.

Over the past seven years the realization has grown that cosmological bursts may be common and bright. The class of events known as Fast Radio Bursts (FRBs), discovered with the Parkes and Arecibo multibeam receivers (Lorimer et al. 2007; Thornton et al. 2013; Spitler et al. 2014), represents the first of a new category of radio transients detected at apparently cosmological distances. These events are bright ($> 1\,\mathrm{Jy\,ms}$), and their millisecond durations make it possible to directly measure the column density of ionized plasma in intergalactic space via their frequency-dependent time of arrival (i.e. their dispersion measure). The dispersion measures of these bursts place them *prima facie* at redshifts out to > 1.

The short durations of these bursts makes them exquisite probes of the dispersion measure, enabling us to account for every single ionized baryon that lies between the burst and the Earth to high precision, and to measure the curvature of spacetime through which the radiation propagates on its way to Earth. This unique attribute has led to a spate of recent suggestions (Macquart & Koay 2013; Deng & Zhang 2014; Zhou et al. 2014; McQuinn 2014) describing their utility as cosmological probes. These fall into several categories:

- Locators of the "missing" baryons in the low ($z \leq 2$) redshift universe (Ioka 2003; Inoue 2004; Deng & Zhang 2014; McQuinn 2014);
- High-redshift cosmic rulers which have the potential to determine the equation-of-state parameter w over a large fraction of the history of the Universe (Zhou et al. 2014) and
- Potential probes of primordial (intergalactic) magnetic fields and turbulence (Macquart & Koay 2013).

In this paper we discuss each of these science cases below in detail. For the purposes of illustration we shall primarily frame the discussion in terms of FRBs, but we stress that such investigations would be possible using any class of impulsive extragalactic transients. With the modest sensitivity and narrow field of view of the telescopes with which they were detected, FRBs likely represent only a tiny fraction of all the classes of new transient phenomena awaiting discovery in the SKA-era.

2.1 Missing Baryons

The "missing" baryon problem refers to the fact that most baryons in the low-redshift Universe remain undetected (Cen & Ostriker 1999, 2007; Bregman 2007; Shull, Smith & Danforth 2012; McQuinn 2014; Sullivan et al. 2011). Only 5% of the cosmic baryons at $z \sim 0$ lie within galaxies,

PoS(AASKA14)055

another 5% are detected in X-ray coronae in massive groups and clusters, and 30% reside in a warm intergalactic phase observed in Lyα absorption. The constraints on the remaining 60% of the baryons are weaker, and they are believed to reside at temperatures and densities that are difficult to detect via traditional spectral line absorption and emission diagnostics (Cen & Ostriker 1999, however see Gnat (2011)).

Most dark matter is found within massive galaxy halos, but most baryonic matter is outside this scale ($\gtrsim 100\,$kpc). Since baryonic matter is more sensitive than dark matter to star formation and AGN feedback in galaxies, the baryon distribution in cosmological simulations is very sensitive to the feedback implementation. The location of these missing baryons constitutes an important element of galaxy halo accretion and feedback models. Although half of the Universe's dark matter lies within halo masses $> 10^{10}\mathrm{M}_\odot$, less than half of the baryonic matter lies within these halos. The unseen baryons associated with halos below $\sim 10^{13}\,\mathrm{M}_\odot$ likely must lie outside of the halo virial radius because a hot atmosphere containing these baryons would be thermally unstable, which would lead to a cooling flow that would cause an (unobserved) excess of star formation in these galaxies.

The dispersion measures of FRBs can resolve the origin of these missing baryons. The distribution of dispersion measures is sensitive to the locations of these baryons, and can determine whether they lie within the virial radius of 10^{11}-$10^{13}\,\mathrm{M}_\odot$ halos, or whether they lie further out in an intra-halo medium.

The basis of this determination is the variation in dispersion measure for a set of FRBs at similar redshifts. The sightline-to-sightline scattering in dispersion measure observed is predicted to be primarily caused by the scatter in the number of collapsed systems encountered along the ray path to an FRB. The measured DM of an FRB contains four contributions,

$$\mathrm{DM_{tot}} = \mathrm{DM_{MW}} + \mathrm{DM_{IGM}} + \mathrm{DM_{host}} + \mathrm{DM_{FRB}}, \tag{2.1}$$

namely from the Milky Way, the IGM, the host galaxy and the circum-burst shell (if any) respectively. The Milky Way contribution is often known from pulsar models and is small (typically $\sim 50\,\mathrm{pc\,cm^{-3}}$ off the Galactic plane), and the host contribution is likely similarly small for all bursts not located near the centres of their host galaxies. Moreover, both the host and FRB contributions[2] to the DM decrease as $1/(1+z)$ relative to local contributions, where z is the FRB host galaxy redshift.

A key observable quantity is the DM probability distribution function. For a set of FRBs at the same redshift, the shape of the DM distribution function depends sensitively on the extent of the distribution of the baryons around the halos. Figure 1 shows how the DM distribution function of a sample of 1000 FRBs at $z = 1$ depends on the nature of the distribution of baryons around their halos. Note that all models predict a high-DM tail in the distribution. A general property is that the distribution function is more centrally peaked if the gas around the halo is more diffuse or if the halos capable of retaining their gas are rarer.

[2]The FRB DM contribution is limited by the fact that it cannot be so dense as to prevent propagation of the radiation (i.e. the plasma frequency must not exceed the radiation frequency), which limits the emission to regions with densities $\lesssim 10^{10}\,\mathrm{cm^{-3}}$.

PoS(AASKA14)055

Another method of exploring the baryon distribution involves stacking FRBs based on their angular proximity to galaxies in order to measure the mean baryon profile of galaxies to large radii (McQuinn 2014). This technique requires sub-arcminute (or better) localization of each FRB.

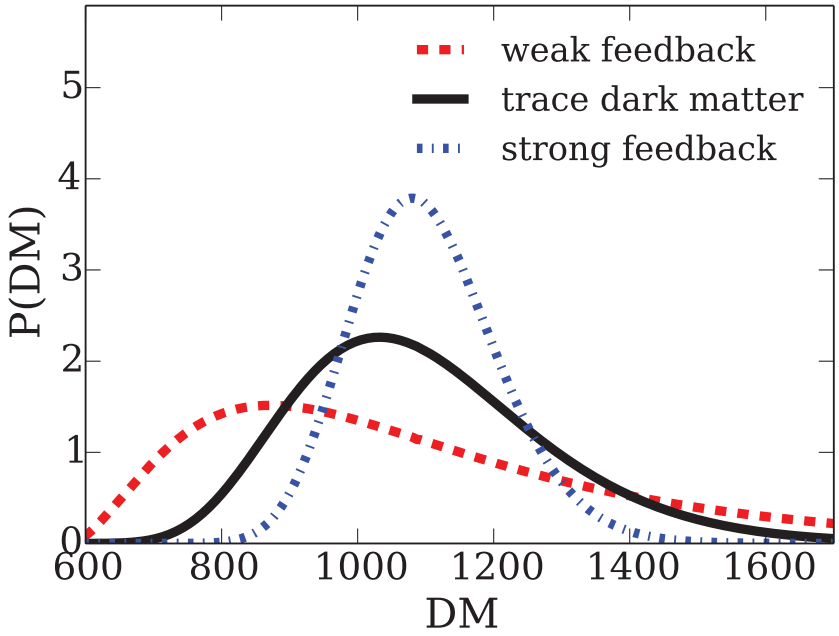

Figure 1: Possible probability distributions of FRB dispersion measures for bursts located at $z = 1$. The distribution depends on how the baryons are distributed near the halos of galaxy clusters along the line of sight. The more diffuse the gas, the more concentrated is the probability density around its central value. Here, strong feedback corresponds to a scenario in which the baryonic extent of each galaxy cluster halo extends to 2 virial radii, while the weak feedback corresponds to one in which the halo extends to only half the cluster virial radius. (See McQuinn (2014) for more details.)

2.2 Cosmic Rulers

Measurements of Type Ia SNe out to $z \sim 1.5$ have been used to determine the dark energy content of the Universe. The opportunity exists to make much more detailed measurements of the geometry of the Universe using impulsive transients at redshifts > 2, where their DM contribution is dominated by the IGM. FRBs are much brighter relative to telescope sensitivity than Type Ia SNe and are potentially easily detectable to much higher redshifts, especially with high-sensitivity, wide-field telescopes. FRBs offer access to the dark energy equation of state parameter $w(z) = p/\rho$ (Zhou et al. 2014).

The basis for using transients as cosmic rulers is that its average DM at a redshift z depends on the geometry of the Universe in a specific manner. Transients are usable as cosmic rulers in the sense that a comparison of their DM to their redshift, when coupled with a model for the average electron density of the Universe as a function of redshift, enables one to measure the time of flight of the photons and hence the *path length*. It is in this sense that transients represent cosmic rulers[3].

[3]The essence of the argument is that, in the integral over path length $\int n_e dl$, one writes $dl = cdt = c|dt/dz|dz$.

PoS(AASKA14)055

The exact relation between DM and z is (Zhou et al. 2014):

$$\langle \mathrm{DM_{IGM}}(z) \rangle = \Omega_b \frac{3H_0 c}{8\pi G m_p} \int_0^z \frac{(1+z') f_{\mathrm{IGM}} \left[\frac{3}{4} X_{e,H}(z') + \frac{1}{8} X_{e,He}(z')\right]}{\left[\Omega_{\mathrm{M}}(1+z')^3 + \Omega_{\mathrm{DE}}(1+z')^{3[1+w(z')]}\right]^{1/2}} dz' \tag{2.2}$$

where Ω_b, Ω_{M} and Ω_{DE} are the baryonic, matter and dark energy densities, respectively, relative to the critical density, $\rho_c = 3c^2 H_0^2 / 8\pi G$. $X_{e,H}$ and $X_{e,He}$ are, respectively, the ionization fractions of Hydrogen and Helium.

The determination of cosmological parameters relies upon the detection of a sufficient number of FRBs that it is possible to measure the *average* DM of FRBs as a function of redshift. Figure 2 shows the expected scaling of DM with redshift for a concordance cosmology. The main contaminant is the uncertain contribution $\mathrm{DM_{host}}$ and $\mathrm{DM_{FRB}}$ to the total dispersion measure. However, these contributions diminish relative to the local contribution as $1/(1+z)$ and rapidly decrease relative to an IGM whose mean density increases as $(1+z)^3$. This makes the technique viable for FRBs at $z \gtrsim 2$. Zhou et al. (2014) estimate that $\sim 10^3$ FRBs must be detected in order to place significant cosmological constraints on w, as demonstrated in Figure 2.

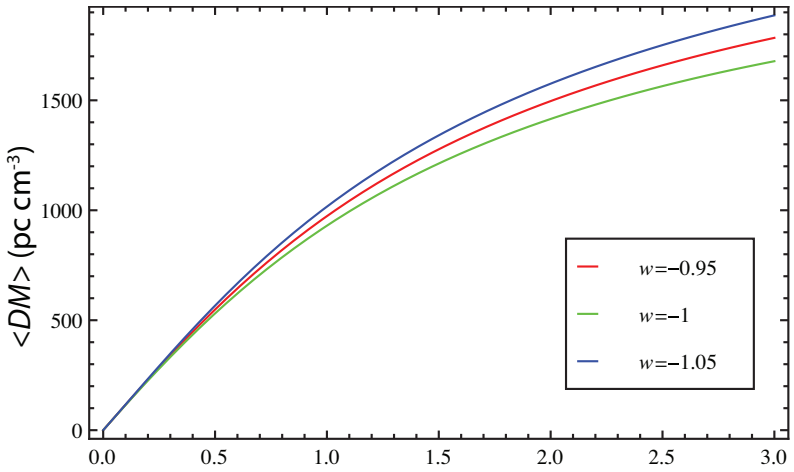

Figure 2: The mean DM contribution to the IGM of an FRB as a function of redshift based on eq.(2.2) for a concordance ΛCDM Universe with $\Omega_{\mathrm{M}} = 0.318$, $\Omega_\Lambda = 0.682$, $\Omega_b = 0.049$ and $H_0 = 70\,\mathrm{km\,s^{-1}Mpc^{-1}}$.

2.3 Intergalactic Magnetic Fields and Turbulence

Two of the seven FRBs reported in the literature so far exhibit clear evidence for temporal smearing caused by scattering. The observed few-millisecond timescale of the smearing however, cannot be accounted for by the interstellar medium of the Milky Way, whose maximum expected contribution is at most microseconds for the lines of sight through which these bursts were detected. The origin of this scattering therefore lies in the turbulent intergalactic medium, or in the turbulent interstellar medium of the burst host galaxy. The IGM and host-galaxy scattering scenarios can be distinguished on the basis of the redshift dependence of the magnitude of the scattering (Macquart & Koay 2013).

PoS(AASKA14)055

If the scattering is inherent to the IGM, the effect affords a means of probing the evolution of energy deposition in the IGM. The sources invoked to explain reionization of the Universe and feedback associated with galaxy formation inject energy into the IGM on large scales, driving a turbulent cascade that should drive the evolution of inhomogeneity in the IGM. Sources of energy input include the radiative and mechanical energy of AGN and their jets, the UV and X-ray emission and stellar winds from young stars and the flows driven by supernovae (Cen & Ostriker 1999, 2007, and references therein).

The combination of DM and scattering information affords the possibility of tomographically reconstructing the structure and turbulent properties of the Universe's baryonic content, similar to the manner in which pulsar measurements have been used to map out the structure of the Milky Way's interstellar medium (e.g. Armstrong, Rickett & Spangler 1995; Taylor & Cordes 1993; Cordes & Lazio 2002).

However, there are arguments that the observed scattering may not be inherent to the IGM unless it is highly clumped in relatively dense regions, or the physics of the turbulent cascade is far from that envisaged in simple models (Macquart & Koay 2013; Luan & Goldreich 2014). In this case, the temporal smearing must originate in the ISM of the host galaxy or in intervening dense, gravitationally collapsed systems, and the smearing provides a rare opportunity to probe turbulence in external galaxies.

Most coherent mechanisms that generate extremely bright emission of the sort observed in FRBs generate radiation that is partially polarized (e.g. pulsar emission). If FRB emission contains a significantly linearly polarized component, it affords a means of probing intergalactic magnetic fields. Comparison of the DM and rotation measure (RM; see e.g. Kulkarni et al. 2014) of the transient will enable measurements of the mean magnetic field of the IGM, in much the same way that RM measurements of pulsars enable measurements of the in situ magnetic field of our own Galaxy (Noutsos et al. 2008; Han & Qiao 1994).

2.4 The future of Fast Transients Research in the SKA era

Figure 3 shows the transient parameter space often used to characterise the known sources in the transient radio sky. One can see that the known sources span 25 orders of magnitude in radio (pseudo-)luminosity and 18 orders of magnitude in terms of $\nu * W$, covering timescales ranging from weeks, for AGN, to nanoseconds, which is the Nyquist rate for giant pulses from the Crab pulsar. Despite this, the parameter space is mostly devoid of sources. While past discoveries are no guarantee of future successes, it is nonetheless remarkable that whenever we have probed a new area in this parameter space we have found new sources, each bringing their own astrophysical applications, as well as the huge potential for discovery that the SKA has within the key projects of the Transients SWG. Several design aspects of the SKA render it an exceptionally potent transients exploration machine: aside from its high sensitivity, and thus ability to probe to large distances, it will have a hugely increased likelihood of detection by virtue of its large field-of-view and observing-time product. This is a result of the multi-beaming capabilities of SKA-LOW and SKA-MID, and the fact that transient detection systems will operate in a 'piggyback' mode on all SKA projects 24/7/365. This alone increases the equal-sensitivity rate of detection, by many orders of magnitude, and will ensure that the SKA will operate as an unprecedented all-sky all-timescale monitor.

PoS(AASKA14)055

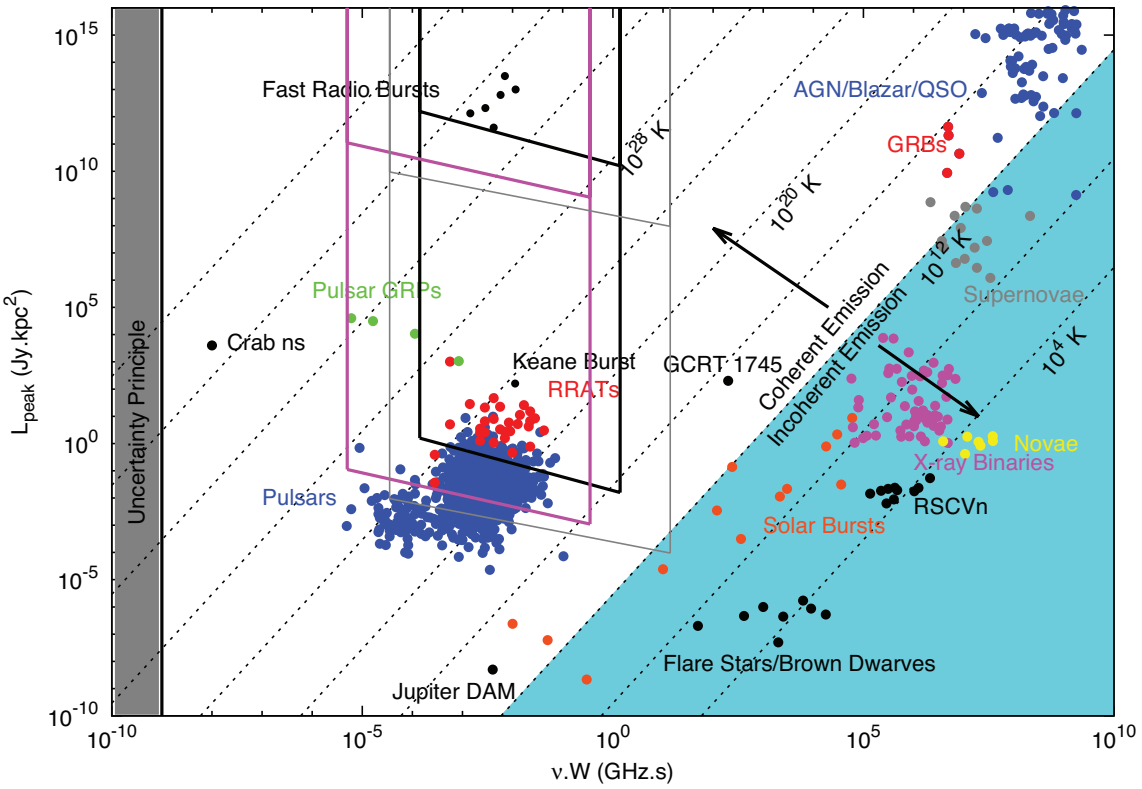

Figure 3: Transient parameter space of specific luminosity versus the product of observing frequency and transient duration. All the known sources of transient radio emission are shown. Overplotted are 1 kpc and 1 Gpc sensitivity curves for Parkes (black), SKA1-LOW (pink) and SKA1-MID (grey). This figure illustrates the depth to which SKA1 can probe the transient radio sky. For example the published FRBs are all just above the Parkes 1 Gpc sensitivity limit (black line). These sensitivity limit curves are for beamformed searches. Fast imaging transient searches extend the RHS boundary of these curves all the way to the far right extent of the plot. This Figure is based on a representation of parameter space originally made by Cordes, Lazio & McLaughlin (2004).

3. Science-driven Telescope Requirements

The basic requirements resulting from the science cases mentioned above are as follows:-

- For the missing baryon science we need to detect of order 10^2 events per redshift bin. This translates to requiring the detection of order 10^4 events in total (depending on their redshift distribution.)

- It is estimated that the cosmic ruler science requires at least 10^3 events. The exact number greatly depends on the dispersion of FRB DM values about the mean as a function of redshift. It also depends on the contribution of the host galaxy to the overall DM which is, as yet, undetermined.

- The science depends crucially on our ability to determine FRB redshifts, requiring event localization to within $\sim$0.1-0.5$''$ for events at $z \gtrsim 1$. The Dark Energy Survey (DES) and

PoS(AASKA14)055

surveys with LSST will enable us to obtain redshifts for these counterparts[4]. We elaborate on this point in §4.5.

A crucial point is that a large amount of time on sky is necessary to achieve the large numbers of event detections needed to prosecute the cosmological investigations outlined above. This argues strongly that surveys for FRBs need to operate commensally with other telescope projects. One could expect at most 10% of the telescope time to be allocated to a dedicated survey for FRBs, whereas a survey capable of operating in conjunction with other projects could feasibly achieve close to 100% efficiency, and could build up a sufficiently large FRB sample much more rapidly.

To put this remark in perspective, we note the estimated event rate based on Parkes detections is $10^{+6}_{-4} \times 10^3$ events sky^{-1}day^{-1} (at a centre frequency of 1340 MHz and with an effective 1 ms timescale 10σ detection threshold of 0.46 Jy). Parkes therefore detects a single FRB on average once every 10 days of telescope time. Even if this telescope were dedicated solely to FRB surveys, the detection rate is three orders of magnitude too small to successfully the pursue cosmological studies with FRBs. Though the expected event detection rate on SKA1 is higher (e.g. we see below that SKA1-SUR's detection rate is ~ 200 times higher than that of Parkes), only a fully commensal survey is capable of detecting FRBs in sufficient numbers.

4. Science with SKA1

Here we outline several ways in which the detection *and follow-up* of cosmological events may be prosecuted with SKA1. At present a great deal of important information, such as FRB spectral indices and source counts, are unknown. The effect of scatter broadening due to turbulence in intervening plasmas, which scales as ν^{-4} if it is relevant, is the biggest unknown in determining the optimum survey frequency for cosmological transients. As a result, it is difficult to design a survey strategy for FRBs – or any other type of yet-undiscovered cosmological transients – so we advocate a flexible approach and investigate several different means of pursuing this science.

4.1 SKA1-LOW

The primary advantages of using SKA1-LOW for fast transients detection are its large field of view and the fact that many coherent emission mechanisms are brighter at lower frequencies. SKA1-LOW would be the instrument of choice for FRB detection if their spectra are not flat below 1 GHz and intergalactic scattering does not significantly broaden their pulse widths.

Incoherent search with SKA1-LOW: An initial survey is most plausibly conducted over the range extending from 200-350 MHz, where the lowest frequency is limited to a relatively high value so that the effects of dispersion (and possibly scattering) are not so deleterious as to place onerous demands on computational capacity (and sensitivity). If pulse scatter-broadening is large at these frequencies, a plausible alternative survey could be conducted over the frequency range 350-650 MHz, if available.

[4]Experience at sub-mm wavelengths suggest that $0.1''$ localization is necessary to achieve unambiguous galaxy identifications. The point spread functions of DES and LSST have sizes of $0.9''$ and $0.7''$ respectively; localization to $0.1''$ is possible with sufficient S/N as long as confusion is not an issue.

PoS(AASKA14)055

Events can be detected by dedispersing and searching the co-added station beam powers. (The sensitivity in 5 ms for a 150 MHz bandwidth is 72 mJy.) Upon detection of an event, this would trigger the automated dump of station voltages since the detected start time of the event; this mandates the presence of voltage buffering for a sizable fraction of each of SKA1-LOW's 1024 stations. A DM 2000 pc cm^{-3} event would have a dispersion sweep lasting 140 s for frequencies over the range 200-350 MHz. These data can either be processed online or offline to verify the event and determine its position; the volume of data to be dumped is not as large as might be supposed since one need extract only the subset of relevant frequency channels at the relevant times in which the signal will occur for a given dispersion measure. Verification is made possible by the fact that a coherent summing of the station voltages at the time and dispersion measure of the event should yield a detection with far greater significance than that in the incoherent data stream. Since detection rate is linearly proportional to FoV, this survey approach would benefit enormously from the capability to form multiple independent station beams. For instance, a transients detection system would capitalize on a system in which it were possible to trade beams for bandwidth. Assuming a detection rate scaling as FoV $\times S_{\rm min}^{-3/2}$, one sees that a halving (an $n-th$ing) of the bandwidth but doubling of the FoV results in a net increase in the detection rate of $2^{1/4}$ ($n^{1/4}$). A more moderate dependence on rate of FoV $\times S_{\rm min}^{-1}$ results in a detection rate increase of $2^{1/2}$ ($n^{1/2}$).

An alternative scenario is as above, but instead the initial search is performed over a large ($\gtrsim 100$) number of tied-array beams formed from antennas in the dense central core (such as will be used for pulsar surveys). This approach has the advantage that it would achieve a sensitivity ~ 32 times better than that of the incoherent search above at the possible expense of a smaller FoV. This approach is superior to (1) if a sufficiently large number of tied-array beams are available that they cover more than 1/180th of the primary FoV[5], assuming a detection rate that scales as FoV$\times S_{\rm min}^{-3/2}$.

A shallow all-sky search with SKA1-LOW: An ultra-widefield search for transients would be capable of detecting events near the 1 Jy ms level at which they are currently detected by Parkes. This mode would involve summing the powers of all 250000 antennas to search for events over the entire antenna FoV (roughly equivalent to 1/7th of the sky). This yields an rms sensitivity of 800 mJy in 5 ms with 300 MHz bandwidth. Coherent follow-up of these events could be performed by accessing the voltage data from just 1024 individual antennas. Detection of an event triggers the capture of the voltage streams of 1024 single antennas, with an associated sensitivity of 400 mJy (5 ms, 300 MHz) in order to perform event verification and localization. However, calibration of the array in the presence of strong ionospheric fluctuations would present a challenge; one would need at least 256 antennas in the array to be closely-packed in order to perform ionospheric calibration, with the remainder providing the long baselines necessary to perform event localization.

4.2 SKA1-SUR

The attractiveness of SKA1-SUR is that it potentially permits searches over a range of different frequency bands, depending on which turns out to be optimal for FRB searches, though we note that at present only Band 2, covering 650-1670 MHz, is expected to be deployed in Phase 1 of construction.

[5]If the tied-array beams are formed from the core only, the necessary number of tied-array beams is $(2000/35)^2/180 = 18$.

PoS(AASKA14)055

Incoherent search with SKA1-SUR: a wide-field search for transients is effective with SKA1-SUR by searching the total powers for each PAF beam summed over all telescopes. Upon detection of an event, the voltage buffers would be dumped and used to verify the event with a factor of $\sqrt{96} = 9.7$ better S/N than the initial detection, and to localize it. A buffer of duration >4 s is required: for a DM=2000 pc cm^{-3} event, the dispersion sweep across 300 MHz from 1.0 GHz to 1.3 GHz is 3.4s. We note that this is the approach advocated by the CRAFT survey consortium for detecting fast transients on ASKAP.

Fast imaging search with SKA1-SUR: the method above represents a relatively computationally light method of detecting FRBs that capitalizes on the full FoV of SKA1-SUR, but not its full sensitivity. The ultimate capability would be provided by a fast (1ms-timescale) imaging mode, which would be capable of simultaneously detecting and localizing any FRBs. However, we note that the requirement of searching each image pixel over a large range of trial dedispersions likely renders this approach computationally intractable at present. This requirement is moderated by the fact that there is a factor 9.7 sensitivity advantage in an imaging survey relative to an incoherent survey. An imaging survey would still be superior to an incoherent survey if one were able to integrate more coarsely in time and frequency with 50 ms integration maps with 30×10 MHz channels. The advantage of initially implementing a fast imaging mode is that one can improve resolution and thus sensitivity as computational power increases in future.

We note that such fast-imaging transient detection pipelines are already feasible and in use at present. One such pipeline runs on data from the VLA. The code is parallelized to run in a multi-core, multi-node CPU environment simply by using tools available in Python. This system produces images at a rate of 20 images/s/core with a size of 1024×1024 pixels (for 27 antennas, 2 polarizations and 256 MHz of bandwidth). This parallelizes well, so when running it on a cluster with 15 nodes of 15 cores, it sustains an imaging rate of 4500 images/s, enabling a survey which images 100 DM trials with ~ 25 ms integrations in real time. Based on experience acquired at the VLA, this pipeline is feasible only for compact arrays; the current pipeline runs for VLA B-array configurations and smaller, namely 13000 m^2 of collecting area within 10 km.

4.3 SKA1-MID

The smaller instantaneous FoV of SKA1-MID compared to SKA1-LOW and SKA1-SUR puts it at a disadvantage in the detection of relatively rare and bright transient events. Its nominal survey speed is at least a factor of two lower than that of SKA1-SUR. However, this disadvantage can be partially mitigated if the backend hardware can exploit the full sensitivity of the array over its entire $\sim$ 1sq.deg. field of view. This may be possible if a pulsar backend proposed for SKA1-MID is constructed: this machine would be capable of forming ≈ 2200 tied-array beams, covering the entire primary FoV of the antennas out to the half-power point of the beam. This would give SKA1-MID an advantage over SKA1-SUR for more common, dimmer events.

4.4 Relative detection rates of SKA1 variants

It is instructive to compare the expected FRB detection rates of SKA1-LOW, SKA1-MID and SKA1-SUR. In Table 1 we compare the relative detection rates of various components of SKA1. The absolute detection rate is obtained by noting that the Parkes detection rate is 1 FRB

PoS(AASKA14)055

per ≈ 10 days, and that an incoherent survey mode with SKA1-SUR is expected to detect FRBs at a rate 6.5 times higher than Parkes, and a coherent (e.g. full sensitivity, full field of view) survey mode would detect them at a rate 197 times higher than Parkes.

Survey Metric	ΩS_0^{-1}	$\Omega S_0^{-3/2}$	ΩS_0^{-2}
SKA1-SUR/MID (coherent)	8.8	4.3	2.1
SKA1-SUR/MID (incoherent)	15	9.7	6.2
SKA1-LOW/SKA1-SUR (coherent)	3.8	6.3	10
SKA1-LOW/SKA1-SUR (incoherent)	1.2	1.1	0.9

Table 1: The relative detection rate of various components of SKA1 according to various possible scaling relations for the detection rate with sensitivity. Here S_0 is the threshold detection flux density (for a given unspecified time interval) and Ω is the field of view. In a Euclidean universe with no cosmological evolution of the FRB population the event rate scales as $\Omega S_0^{-3/2}$. Flatter or steeper dependences on S_0 correspond to various plausible scenarios for the evolution of the FRB population throughout cosmic time. The values computed here are derived on sensitivity and field of view figures tabled in the baseline design. In making comparisons between various frequencies a flat spectral index is assumed and the possible effects of pulse smearing are neglected. The contribution of $T_{\rm sky}$ to the system temperature below ≈ 200 MHz for SKA1-LOW is ignored, since FRBs are feasibly detected in the range 200-350 MHz with this telescope. A coherent survey mode corresponds to one in which one is capable of surveying the entire instrument primary FoV with the full array sensitivity, while the incoherent survey mode corresponds to one in which the total powers from each station/antenna are summed only. It should be noted that this table forms only a part of the comparison between telescopes: the ability to implement a coherent detection mode is easier on telescopes such as SKA1-MID and SKA1-LOW relative to SKA1-SUR, and this makes SKA1-SUR less effective a transients detection instrument than first may be supposed.

It would seem from Table 1 that SKA1-SUR is potentially inherently more effective at detecting FRBs at cm-wavelengths than SKA1-LOW, but that, if FRBs are detectable at low frequencies, a coherent survey mode on SKA1-LOW is at least half an order of magnitude more potent as a survey machine than SKA1-SUR.

However, the comparison does not capture the ease of accessing the entire field of view at full sensitivity in the coherent survey mode; this is especially impractical for SKA1-SUR, with its low array filling factor, unless it is possible to implement a fast imaging mode. Barring this eventuality, the most appropriate comparison at centimetre wavelengths is between an incoherent detection mode on SKA1-SUR and a coherent detection mode on SKA1-MID, for which a beamformer capable of tiling the approximately half the primary FoV is planned. In this case the ratio of the expected detection rate on SKA1-MID relative to SKA1-SUR is either 0.9, 1.7 or 2.6, respectively for a detection rate that scales as either S_0^{-1}, $S_0^{-3/2}$ or S_0^{-2}.

In summary, SKA1-MID appears to be the immediate instrument of choice for FRB studies for three reasons: (1) it observes at the frequencies where FRBs have already been detected, (2) it has a compact core, so that its FoV can be utilized effectively, and (3) it has a planned pulsar backend capable of performing single-pulse searches.

4.5 The necessity of localization

In many instances, the scientific payoff from the detection of an astrophysical event is only

PoS(AASKA14)055

realized once it is localized. Event localization is paramount in the characterisation of one-off transient events, where the position is necessary to associate the event with a specific object or host galaxy. This is necessary to determine its distance and thus energetics, and, through multi-wavelength follow-up, its origin. The determination of burst positions has historically been central to the transients field, a key example being the use of accurate positions from the BeppoSAX satellite to resolve the thirty-year mystery of the origin of gamma-ray bursts.

Much of the transients science proposed for the SKA hinges upon its ability to localize events to sufficient accuracy to permit unambiguous association with a particular object. In particular, the science case for FRBs hinges on the ability to localize them sufficiently well to identify their host galaxies and hence redshifts. This requires event localization to within $\sim 0.1-0.5''$ for $z > 1$ events. Coeval photometric surveys such as DES and LSST will make host galaxy redshift determinations easy given their intention to identify most $z \leq 1.5$ galaxies over $\sim 50\%$ of the sky. We note that any detection today could be followed up with a 4m-class optical telescope to find a counterpart and get a redshift; the difficulty so far has been to obtain positions precise enough to merit optical follow-up.

FRBs are but one class of fast transient object that require accurate localization. The localization problem applies to every other fast transient that the SKA will detect. For imaging surveys, applicable to slow transients the position is determined as part of the detection process. However, this is not the case for fast transients, whose emission occurs below the integration timescale of the correlator.

Searching for short, highly dispersed signals in the imaging domain is computationally infeasible, as the image cubes require not only millisecond time resolution but also 1-100 kHz frequency resolution to avoid intra-channel smearing. This implies $\sim 10^5$ images at every millisecond timestep. The resultant 10^8 images each second must then still be tested over many DM trials. The most computationally feasible way to search for events on these timescales is to search station beam outputs or tied-array beams from the core of the array, which seek to maximize FoV and sensitivity, but not resolution. Thus there is a fundamental disparity between the requirements of the transients search, which requires large FoV but poor resolution in order to be computationally tractable, and the event localization, which requires high resolution and only small FoV.

These computational realities necessitate the use of a transients buffer. The role of the buffer is to store either station voltages from outer stations or high time-resolution correlation products on long baselines. Once an event is detected in the low-resolution search, the corresponding information from the buffer, at the time of the event, is frozen. A detailed search of the detection region is then performed at the specific epoch of the transient event in order to localize the event.

The use of a transients buffer fulfills a secondary role of event verification. By including information from multiple distant stations, it is possible to verify that the event does not represent spurious emission from a local source of RFI.

We emphasise that there will be many instances in which the localization of the emission from fast transients can be performed only in the radio domain. This is because the emission from fast transients need not have an counterpart in any other part of the electromagnetic spectrum. For emission of durations less than ~ 1 s, the sensitivity of the SKA is such that for objects at >1kpc only objects with brightness temperatures well in excess of the inverse Compton limit for incoherent synchrotron emission are detectable. Thus the emission from fast transients is necessarily coherent

PoS(AASKA14)055

emission. Coherent emission mechanisms operate most effectively at low frequencies, and usually do not extend above the radio wavelength regime.

These buffers would also add the important additional capability of enabling the telescope to follow-up possible triggers from transient events identified by telescopes in other wavebands.

5. Early Science at Reduced Sensitivity

It is difficult to precisely assess the impact of reduced sensitivity on the FRB detection rate because the flux density distribution of FRBs is currently unknown. However, several remarks are in order. 1. The event rate likely scales in the range between ΩS_0^{-1} and ΩS_0^{-2}. Thus a 50% reduction in the array sensitivity will cause a decrease in the event detection rate between a factor of two and a factor of four. Even with this reduction, the telescope will be much more sensitive than Parkes, so there will be no problem detecting FRBs. 2. We still require the commensal transients capability in this early phase and the ability to localize the events.

6. Science for the Full SKA

There is currently so much important information lacking about the nature of FRBs that it is difficult to assess the impact of the transition from SKA1 to the full SKA, other than to say that the increased sensitivity, coherent field-of-view and processing power will open up for investigation huge new volumes of parameter space; new discoveries are almost bound to occur. Early results from SKA-precursors (e.g. Trott, Tingay & Wayth 2013) and SKA1 will determine the source count and spectrum of FRBs and so will allow critical design decisions for the full SKA to reflect FRB search requirements. One such driver to be assessed will be the importance of the intrinsic hemispherical sensitivity offered by the Mid-Frequency Aperture Array for identifying fast transient events in the Universe.

7. Conclusions

The occurrence of impulsive radio transients at cosmological distances, as embodied by FRBs, offers enormous scope for addressing a number of cosmological questions of fundamental significance. This includes direction detection and characterisation of the "missing" baryons in the Inter-Galactic Medium. The prospect of probing the dark energy equation of state will be possible if these events can be detected at redshifts $z \gtrsim 2$.

The ability to perform this science is contingent upon several facets of the design of the SKA. The telescope must be able to detect events in sufficient numbers (i.e. $> 10^3$), and to do this it must be able to access a large field of view for long periods of time (i.e. as part of a commensal survey). It must be able to localize events with sufficient accuracy to enable the measurement of redshifts at optical wavelengths; this facility is most easily provided by transient buffers, which can localize an event after each burst is detected. This also entails the provision of the ability to trigger the localization through the telescope signal path.

Finally, we remark that the relative infancy of this field means that it is likely that many more significant discoveries await, and it is not possible to specify precisely telescope all the requirements that best suit this future science. However, by adopting a modular design approach which

PoS(AASKA14)055

ensures access to key points in the telescope signal path are not designed out will greatly increase the scope to exploit future discoveries as they are made over the fifty year lifetime of the telescope.

References

Armstrong, J.W., Rickett, B.J. & Spangler, S.R. 1995, ApJ, 443, 209
Bregman, J.N. 2007, Ann. Rev. Astron. & Astrophys., 45, 221
Cen, R. & Ostriker, J.P. 1999, ApJ, 514,1
Cen, R. & Ostriker, J.P. 2007, ApJ, 650, 560
Cordes, J.M. & Lazio, T.J.W. 2002, arXiv:astro-ph/0207156 [NE2001]
Cordes, J.M., Lazio, T.J.W. & McLaughlin, M.A., New Astronomy Reviews, 48, 1459
Deng, W. & Zhang, B. 2014, ApJL, 783, L35
Gnat, O. 2011, ApJ, 729, 82
Han & Qiao, 1994, A&A, 288, 759
Inoue, S. 2004, MNRAS, 348, 999
Ioka, K. 2003, ApJ, 598, L79
Kulkarni, S.R., Ofek, E.O., Neill, J.D., Zheng, Z. & Juric, M. 2014, ApJ, submitted (arXiv:1402.4766)
Lorimer, D.R., Bailes, M., McLaughlin, M.A., Narkevic, D.J. & Crawford, F. 2007, Science, 318, 777
Luan, J. & Goldreich, P. 2014, ApJ, 785, L26
Macquart, J.-P. & Koay, J.Y. 2013, ApJ, 776, 125
McLaughlin, M.A., Lyne, A. G., Lorimer, D. R. et al. 2006, Nature, 439, 817
McQuinn, M. 2014, ApJ, 780, L33
Noutsos, A., Johnston, S., Kramer, M. & Karastergiou, A 2008, MNRAS, 386, 1881
Shull, J.M., Smith, B.D. & Danforth, C.W. 2012, ApJ, 759, 23
Spitler, L.G, Cordes, J.M., Hessels, J.W.T. et al. 2014, ApJ, 790, 101
Sullivan, M., Guy, J., Conley, A., et al. 2011, ApJ, 737, 102
Taylor & Cordes 1993, ApJ, 411, 675
Thornton, D., Stappers, B., Bailes, et al. 2013, Science, 341, 53
Trott, C.M., Tingay, S.J. & Wayth, R.B. 2013, ApJ, 776, L16
Zhou, B., Li, X., Wang, T., Fan, Y.-Z. & Wei, D.-M. 2014, Phys. Rev. D., 89(10), 107303

PoS(AASKA14)055

PROCEEDINGS OF SCIENCE

The SKA contribution to GRB cosmology

Lorenzo Amati[1,2], **Alan Cosimo Ruggeri**[3,4], **Giulia Stratta**[5], **Salvatore Capozziello**[3,4], **Mariafelicia De Laurentis**[3,4], **Massimo Della Valle**[2,6], **Orlando Luongo**[3,4]

[1]*INAF - IASF Bologna, via P. Gobetti 101, Bologna (Italy)* [2]*ICRANet, Piazzale della Repubblica 10, Pescara (Italy)* [3]*Università di Napoli Federico II, Via Cinthia, Napoli (Italy)* [4]*INFN Sez. di Napoli, Monte S. Angelo, Via Cinthia, Napoli (Italy)* [5]*Universitá degli Studi di Urbino "Carlo Bo", Urbino (Italy)* [6]*INAF - Osservatorio di Capodimonte, Salita Moiariello 16, Napoli (Italy)*
E-mail: amati@iasfbo.inaf.it

Although they are not standard candles, the use of Gamma–Ray Bursts (GRBs) as a tool for measuring the geometry and expansion rate of the Universe is strongly motivated by their unique combination of huge luminosities, up to more than 10^{53} erg/s, with a redshift distribution extending up to more than $z = 9$. Several attempts to exploit the correlation between the photon energy at which the spectral energy distribution peaks (*peak energy*) and the radiated energy (or luminosity) for standardizing GRBs and to use them to estimate cosmological parameters have been made. These studies show that with the present data–set, GRBs can provide a significant and independent confirmation of $\Omega_M \sim 0.3$ for a flat ΛCDM. The SKA, through its unprecedented capabilities of characterizing the radio afterglow light-curve from the peak emission up to the transition to non–relativistic regime for a significant fraction of GRBs, and in combination with measurements from next generation GRB experimens, will provide unique clues on the collimation angles and energy budget of these events, thus reducing significantly the dispersion of the *peak energy – radiated energy* correlation and improving its reliability and accuracy in investigating dark energy properties and evolution.

Advancing Astrophysics with the Square Kilometre Array,
June 8-13, 2014
Giardini Naxos, Sicily, Italy

PoS(AASKA14)056

1. Introduction

The evidence that we are living in a flat Universe undergoing accelerated expansion and in which the baryonic matter contributes only a small fraction (∼4–5%) of the total matter–energy density is mostly based on combined observations of high redshift type Ia supernovae (SNe Ia) and of the Cosmic Microwave Background (CMB). Other complementary probes like Galaxy Clusters and Baryonic Acoustic Oscillations (BAO) further support this scenario.

Each of these probes is affected by specific systematics, which may significantly bias the estimate of cosmological parameters, like the matter density Ω_M, the dark energy density Ω_Λ and the equation of state (EoS) of the dark energy. More probes are now available and more cross–checks among the results obtained with each of them can be done, thus minimizing the effects of the systematics of single probes. In addition, each different class of probe has a different "sensitivity" to cosmological parameters depending on its redshift distribution. Thus, the search for more classes of sources that can be used as standard candles to study the geometry and the evolution of the expansion rate of the Universe is highly motivated.

With an observed redshift distribution extending from 0.0085 (GRB 980425) up to 8.26 (GRB 090423) or ∼9.2 if we include photometric redshift (GRB 090429B) and isotropic-equivalent radiated energies up to more than $\sim 10^{54}$ erg, released typically in a few tens or hundreds of seconds, Gamma–Ray Bursts (GRBs) are the brightest cosmological sources in the Universe (Fig. 1). In addition, they emit most of their radiation in the hard X–rays, thus, contrary to SNe Ia, they are not affected by dust absorption. Unfortunately, they are not standard candles, given that their radiated energies, or luminosities, span several orders of magnitude. However, as we discuss in the next Sections, the evidence for a strong correlation between the photon energy at which the spectral energy distribution (SED) peaks and the GRB intensity has opened the possibility of using them as cosmological probes.

2. The correlation between GRB spectral peak energy and intensity.

GRBs show non thermal spectra which can be modeled with broken power laws with 3 pa-

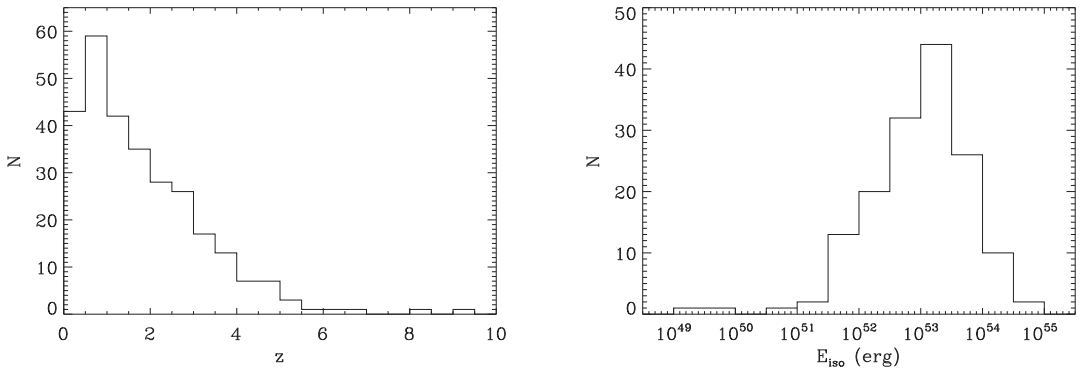

Figure 1: Distributions of redshift and isotropic–equivalent radiated energy, E_{iso}, of long GRBs (as of end of 2013).

PoS(AASKA14)056

rameters: the low–energy spectral index α, the high energy spectral index β and the "roll–over" energy E_0 . The peak of the spectral energy distribution (Fig. 2) is a characteristic quantity in GRB emission models and is called *peak energy*, $E_{\rm p}$. Converting the observed spectrum into a rest-frame spectrum via optical redshift measurements for a small fraction of GRBs has enabled the estimate of two key intrinsic quantities: the total radiated energy computed by integrating the spectrum in a standard (1–10000 keV) energy band and assuming isotropic emission, $E_{\rm iso}$, and the peak energy of the cosmological rest–frame νF_ν spectra of GRBs, $E_{\rm p,i} = E_{\rm p} \times (1+z)$. As of the end of 2013, the number of GRBs with measurements of the redshift and of the spectral parameters accurate enough to allow a reliable computation of $E_{\rm p,i}$ and $E_{\rm iso}$, is $\sim$160. The distribution of $E_{\rm p,i}$ for these events is approximately a Gaussian centered at a few hundreds of keV and with a low energy extension down to a few keV, corresponding to the so–called X–Ray Flashes (XRFs) or X–Ray Rich (XRR) events. Whether this distribution is significantly biased by instrumental effects or is an intrinsic properties of GRBs is still unclear, in particular concerning the real fraction of XRFs and XRRs with respect to "normal GRBs". The distribution of $E_{\rm iso}$ is somewhat similar, extending from $\sim 10^{51}$ to more than $\sim 10^{54}$ erg, peaking at $\sim 10^{53}$ erg and with a few peculiar weak events ($\sim 10^{48}$ - $\sim 10^{50}$ erg).

In 2002, based on a small sample of *Beppo*SAX GRBs with known redshift and spectral parameters, it was discovered (Amati et al., 2002) that $E_{\rm p,i}$ is significantly correlated with $E_{\rm iso}$. This correlation has the form

$$\log E_{\rm p,i}({\rm keV}) = m \log E_{\rm iso}(10^{52}{\rm erg}) + q\,,$$

with $m \sim 0.5$ and $q \sim 2$, and is characterized by an extra–Poissonian scatter normally distributed with a $\sigma_{\rm ext}$ of $\sim$0.2 dex around the best–fit law. Subsequent observations with various detectors and spectrometers confirmed and extended the $E_{\rm p,i} - E_{\rm iso}$ correlation, showing that it holds for all long GRBs and XRFs with well measured redshift and spectral parameters (Amati, 2006; Amati et al., 2008). The present distribution of long GRBs and XRFs in the $E_{\rm p,i} - E_{\rm iso}$ plane is shown in Fig. 2 (see caption for details). The existence, properties (slope and dispersion) and extension over several orders of magnitude in both $E_{\rm p,i}$ and $E_{\rm iso}$ of the correlation provide observational challenges for the models of the physics and geometry of the prompt emission of GRBs (e.g., Zhang & Mészáros, 2002; Lamb et al., 2004; Amati, 2006).

3. GRB cosmology through the $E_{\rm p,i}$-intensity correlation

Since the $E_{\rm p,i} - E_{\rm iso}$ correlation correlates the quantity $E_{\rm p,i}$(which is independent of cosmological model), with the quantity $E_{\rm iso}$(whose computation requires the luminosity distance D_L), then it could theoretically be used to "standardize GRBs", in a way similar to the use of the Phillips relation (Phillips, 1993) to standardize SNe Ia. However, the scatter of the correlation (Amati et al., 2008) and the lack of a sufficient number of very low redshift GRBs allowing a cosmological–independent calibration has been a challenge to its use for this purpose.

The investigations of GRBs as cosmological probes started in 2004, when it was found that the $E_{\rm p,i} - E_{\rm iso}$ correlation tightens by substituting $E_{\rm iso}$ with the collimation–corrected radiated energy $E_\gamma = (1-\cos\theta_{jet}) \times E_{\rm iso}$ (Ghirlanda et al., 2004; Dai et al., 2004). This result was based on a small sub–sample of GRBs with known $E_{\rm p,i}$ and $E_{\rm iso}$ for which it was possible to infer the jet opening angle θ_{jet} from the *break time*, t_b , at which the decay index of the light curve of the optical

PoS(AASKA14)056

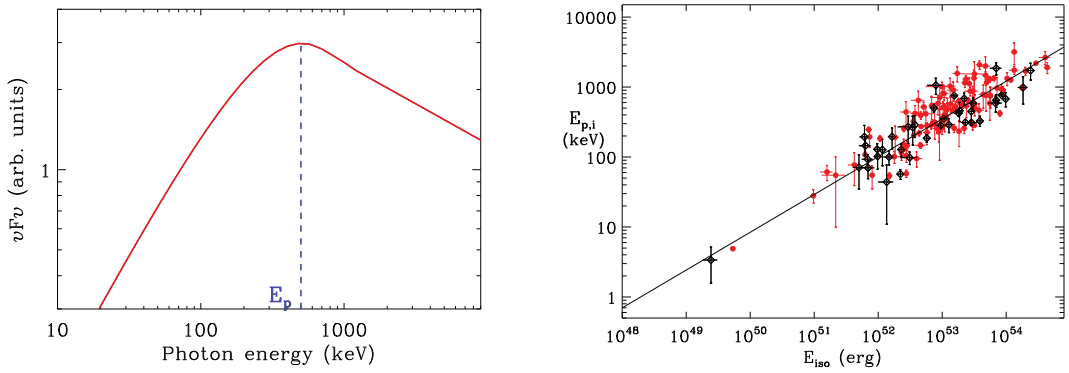

Figure 2: Left: typical νF_ν (energy) spectrum of a GRB in its cosmological rest–frame. Right: the $E_{\rm p,i}$ – $E_{\rm iso}$ correlation in long GRBs (as of the end of 2013). The black line shows the best–fit power law. Data from Amati et al. (2008), Amati et al. (2009) and citetAmdv13. These values are based on spectral data and fluences reported in official catalogs and in the GCN Circulars (gcn.gsfc.nasa.gov/gcn3_archive.html) by following the method outlined, e.g., in Amati et al. (2002) and Amati (2006).

afterglow sharply changes to a steeper one, under the assumption of a simple jet and afterglow model (Sari et al., 1999). With this improvement it was possible to derive, within the standard ΛCDM cosmological model, estimates of $\Omega_{\rm M}$ and Ω_Λ consistent with the "concordance" values mostly coming from the analysis of SNe Ia and the CMB (see review by Ghirlanda et al. (2006)). These results prompted other studies aimed at deriving a GRB Hubble diagram, based, e.g., on the joint use of the $E_{\rm p,i} - E_\gamma$ correlation together with other weaker correlations between luminosity and observed properties (Schaefer, 2007), or the calibration of the $E_{\rm p,i} - E_\gamma$ correlation with SNe Ia (e.g., Kodama et al., 2008; Demianski et al., 2008). In recent years, the simple jet model assumed to compute θ_{jet} from the break time of the optical afterglow light curve has been seriously challenged by the observation that in several cases the the X–ray afterglow light curves show no *jet–break* or show a break not simultaneous to the optical one. This makes the determination of E_γ, and thus the characterization and use of the $E_{\rm p,i} - E_\gamma$ correlation, less firm.

This uncertainty has led to a re-evaluation of the simple $E_{\rm p,i} - E_{\rm iso}$ correlation as a cosmological tool, as it has many advantages, e.g., a sample size four times larger, is based on only two variables, and avoids model-dependent assumptions (Amati et al., 2008). By assuming a flat ΛCDM Universe, the χ^2 obtained by fitting this correlation with a simple power law is a function of the value of $\Omega_{\rm M}$ assumed in the computation of $E_{\rm iso}$. [1] In particular, as can be seen in Fig. 3, the function $\chi^2(\Omega_{\rm M})$ shows a parabolic shape with a minimum at $\Omega_{\rm M}\sim$0.25–0.30. This is a simple but relevant result: a) it shows that the $E_{\rm p,i} - E_{\rm iso}$ correlation can indeed be used to extract information on cosmological parameters; b) it provides evidence, independently from SNe Ia or other probes, that, if we live in a flat Universe as predicted by many inflationary models and supported by CMB measurements, the density of the Universe is dominated by an unknown component (e.g., dark energy).

The simple χ^2 method cannot be used to obtain reliable confidence levels on both the parameters of the correlation (normalization and slope) and the cosmological parameters. Instead a

[1] This result was originally based on the sample of 70 long GRBs with known $E_{\rm p,i}$ and $E_{\rm iso}$published by Amati et al. (2008).

PoS(AASKA14)056

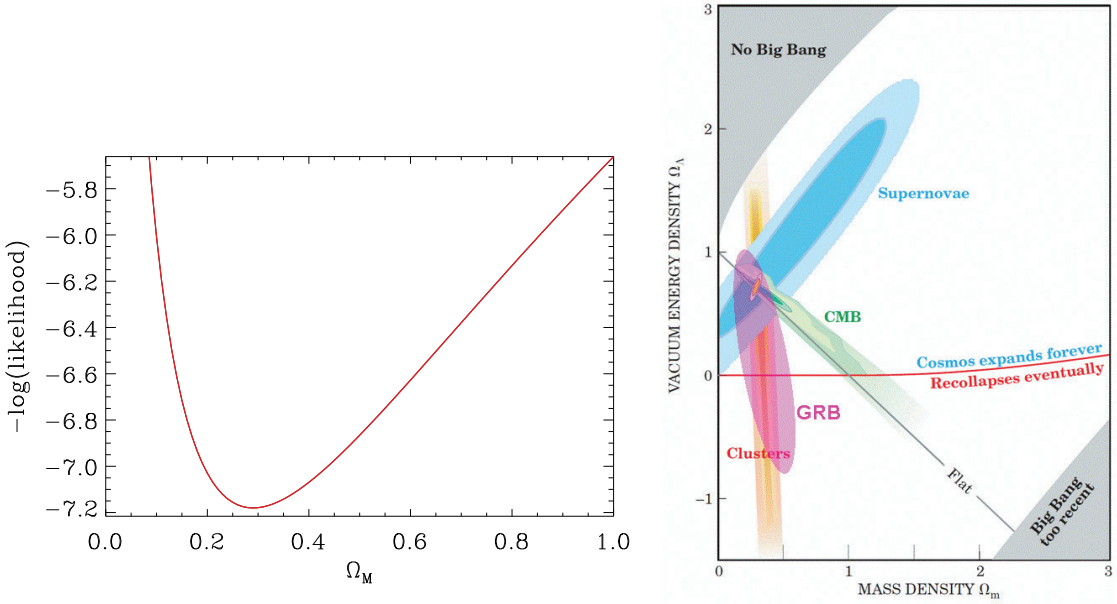

Figure 3: Left: goodness of fit of the $E_{p,i}$ – E_{iso} correlation of long GRBs, expressed in terms of $-log$(likelihood), as a function of the value of Ω_M used to compute the E_{iso} values in a standard ΛCDM flat universe (for a sample of 156 GRBs available as of the end of 2012). Right: 68% confidence level contour in the Ω_M – Ω_Λ plane obtained by releasing the flat Universe assumption and assuming a sample of sample of 250 GRBs expected in the near future (see Table 1 and text) compared to those from other cosmological probes (adapted from a figure by the Supernova Cosmology Project; Suzuki et al. 2012). From Amati & Della Valle (2013).

maximum likelihood method accounting for the uncertainties on both the X and Y quantities and the extra variance σ_{ext} is adopted (Amati et al., 2008). In Table 1, we show the 68% and 90% confidence level intervals for Ω_M, in the assumption of a flat Universe, obtained in this way with samples of 70 GRBs (Amati et al., 2008) and 156 GRBs (Amati & della Valle, 2013). As can be seen, by increasing the number of GRBs in the sample the accuracy of the estimate of Ω_M improves. This is confirmed also by the investigation of the confidence contours in the Ω_M – Ω_Λ plane computed by following the same method as above but releasing the flat Universe assumption (Fig. 3.).

Broad energy band spectroscopy of GRBs (from ∼10-15 keV up to several MeVs) is required to obtain reliable estimates of $E_{p,i}$ and E_{iso}. The main contribution to the number of GRBs that populate the $E_{p,i}$ – E_{iso} plane comes from joint detections by *Swift* the *Fermi*/GBM and/or Konus–WIND. Hopefully, these missions will continue to operate for at least a few years, providing ∼15–20 GRBs/year, to increase the $E_{p,i}$ – E_{iso} sample and refine the present estimates of cosmological parameters (Fig. 3 and Table 1). A further improvement should come from next generation (after 2018) missions capable of performing both the task of prompt accurate localization and broad–band spectroscopy of GRBs, like the French–Chinese Space Variable Objects Monitor (SVOM) or the proposed Ultra-Fast Flash Observatory (UFFO) mission, an international project led by Korea and Taiwan.

PoS(AASKA14)056

Table 1: Comparison of the 68% confidence intervals on Ω_M and w_0 (Ω_M=0.3, w_a=0.5; a standard parametrization of the dark energy equation of state: $w = w_0 + w_a z/(1+z)$ was assumed) for a flat Friedmann-Lemaître-Robertson-Walker (FLRW) universe obtained with the sample of 70 GRBs by Amati et al. (2008), the sample of 156 GRBs available as of the end of 2012 (Amati & della Valle, 2013) and simulated samples of 250 and 500 GRBs (see text). In the last three lines we also show the results obtained for the same samples by assuming that the dispersion of the correlation between $E_{p,i}$ and radiated energy is reduced by a factor of 2 thanks to the measurements by the SKA allowing inferences on the kinetic energy and collimation angle of the emitting plasma.

GRB #	Ω_M (flat)	w_0 (flat,Ω_M=0.3,w_a=0.5)
70 (real) GRBs (Amati et al., 2008)	$0.27^{+0.38}_{-0.18}$	< -0.3 (90%)
156 (real) GRBs (Amati & della Valle, 2013)	$0.29^{+0.28}_{-0.15}$	$-0.9^{+0.4}_{-1.5}$
250 (156 real + 94 simulated) GRBs	$0.29^{+0.16}_{-0.12}$	$-0.9^{+0.3}_{-1.1}$
500 (156 real + 344 simulated) GRBs	$0.29^{+0.10}_{-0.09}$	$-0.9^{+0.2}_{-0.8}$
156 (real) GRBs, SKA	$0.30^{+0.06}_{-0.06}$	$-1.1^{+0.25}_{-0.30}$
250 (156 real + 94 simulated) GRBs, SKA	$0.30^{+0.04}_{-0.05}$	$-1.1^{+0.20}_{-0.20}$
500 (156 real + 344 simulated) GRBs, SKA	$0.30^{+0.03}_{-0.03}$	$-1.1^{+0.12}_{-0.15}$

4. Improving GRB cosmology with the SKA

The improvement in the accuracy of the estimate of cosmological parameters with the $E_{p,i}$ – E_{iso} correlation obtained by enlarging the sample on which the analysis is performed (Tab. 1), confirms that the method is reliable and promising. However, a real breakthrough in these field would be obtained if the dispersion of the correlation between $E_{p,i}$ and radiated energy or luminosity could be reduced by at least a factor of 2 (e.g., Ghirlanda et al. 2004). In particular, the accuracy in the estimate of cosmological parameters and dark energy properties with GRBs is presently limited by the large uncertainties affecting our knowledge of the truly radiated energy, which forces us to use the isotropic–equivalent quantity E_{iso}. This conservative assumption, while accounting for our ignorance on the true energy budget, is expected to contribute at least 50% of the correlation dispersion. In this section we show that, in this respect, the radio measurements that will be provided initially by the SKA1–MID and then by the full SKA2 will be fundamental. Indeed, as detailed below, the measurements of the radio afterglow emission that the SKA will perform for most of the GRBs detected and localized at high energies will allow to infer both the jet opening angle and the fireball kinetic energy. As we are going to discuss, these quantities enable to obtain more accurate estimates of the truly radiated energy with respect to E_{iso}, thus substantially reducing the dispersion of the radiated energy – $E_{p,i}$ correlation and improving its reliability and power for cosmology.

4.1 Radio emission from GRBs: perspectives with the SKA

Accretion onto a black hole formed during a GRB event produces two jets along which matter is ejected at relativistic velocities (fireball). Part of the fireball kinetic energy is converted into electromagnetic (synchrotron) radiation producing the afterglow emission while the ejecta gradually slows down to a non-relativistic regime (e.g. Panaitescu, 1999). The photon energy corresponding

PoS(AASKA14)056

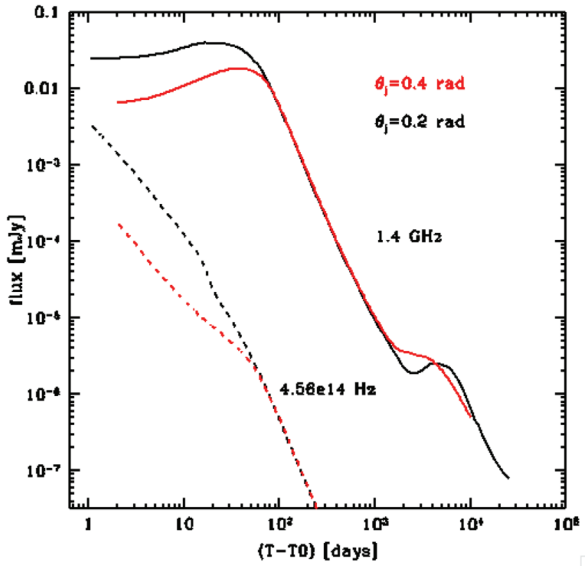

Figure 4: Simulated afterglow light curves in radio (solid line) and optical (dashed line) bands from Van Eerten et al. (2010), obtained assuming two possible jet opening angle ($\theta_{jet} = 0.2$ radian plotted in red, and $\theta_{jet} = 0.4$ radian plotted in black). The light curves clearly show different behaviour up to about tens of days after the trigger in both energy bands depending on the jet opening angle. The simulation assumes a GRB at a luminosity distance of 10^{28} cm, with energy 10^{50} erg, and a surrounding interstellar matter density of 10^{-3} cm^{-3}.

to peak of the spectral energy distribution evolves with time towards longer wavelengths and at days up to months from the burst onset (depending on the frequency), it is expected to appear at radio frequencies.

In the *Swift* era, radio afterglow emission is being detected only for about 30% of accurately ($<$ a few arcmin) localized GRBs, compared with $\sim$93% in X–rays and $\sim$75% in optical/NIR. Most measurements have been made with the Very Large Array (VLA) and Expanded Very Large Array (EVLA), although other telescopes have contributed (Westerbork Synthesis Radio Telescope (WSRT), the Australia Telescope Compact Array (ATCA), the Giant Metrewave Radio Telescope (GMRT), a few by the Very Long Baseline Array (VLBA)). The canonical long–duration GRB radio light curve at 8.5 GHz peaks at three to six days in the source rest frame, with a median peak luminosity of 10^{31} erg s^{-1} Hz^{-1}. The typical mean fluxes at 8.5 GHz in 5–10 days from the GRB range from $\sim$100 to $\sim$900 μJy. Peak fluxes may occasionally reach 10 mJy. See, e.g., Chandra & Frail (2012) and Granot & Van del Horst (2014) for a review.

As discussed, e.g., by Chandra & Frail (2012), the small range of peak flux densities between the radio detection and non-detections suggests that the detection fraction of radio afterglows is largely determinated by the instrumental sensitivities. The SKA, already in its Phase 1, will shed light on this fundamental issue, given that the current upper limits set by VLA and EVLA observations are of the order of a few tens of μJy (8.5 GHz) and the foreseen SKA1–MID continuum sensitivity is of the order of 0.72 μJy-hr$^{-1/2}$ (Dewdney et al., 2013).

GRB population synthesis codes show that all GRBs with gamma-ray peak flux above the

PoS(AASKA14)056

Swift/BAT flux threshold (0.4 ph cm^{-2} s^{-1}) have a peak flux in radio above 1μJy, thus already detectable by the SKA Phase 1. The major difference between present/forthcoming SKA precursors and the final SKA can be appreciated considering the entire population of GRBs, thus including those GRBs with gamma-ray flux well below the present detector sensitivity. For example, it is foreseen that the SKA will be able to detect at radio frequencies all the bursts, with a detection rate of 480 GRBs yr^{-1} sr^{-1} (Ghirlanda et al., 2013).

The combination of high sensitivity, high angular resolution, short reaction time and broad band of the SKA (initially with the SKA1 and then with the full SKA) will allow to achieve important and partly unprecedented goals for GRB science. These include: measurements of GRB source size and expansion velocities through ISM scintillation; accurate localization of GRBs in host galaxies; measurement of host galaxy radio emission; early radio afterglow: physics (reverse shock, transition from optically thick to optically thin synchrotron emission, etc.), estimate of kinetic energy and jet opening angle from the SED and light curve fitting. In the next sections we show how the two latters measurements are fundamental for the role of GRBs in cosmology.

4.2 Impact on measuring cosmological parameters with GRBs

Concerning GRB cosmology, the high sensitivity of the SKA will allow accurate radio calorimetry for a large number of GRBs. In the following sections we show how a significant improvement in using GRBs to measure cosmological parameters would come from a more reliable way to estimate the jet opening angle and, thus, the true radiated energy and/or the kinetic energy of the fireball in non-relativistic regime. Only observations of a large number of radio afterglows offer this opportunity.

4.2.1 SKA Phase 1: measuring the jet collimation angle

In the simplest modelling of the afterglow light curve, after reaching its maximum intensity, the radiative flux decays following a power law function with decay index ~ 1. "Achromatic" steepening (i.e. a steepening not dependent from the photon energy) to a decay index ~ 2.2 is expected when the relativistic collimation angle $1/\Gamma(t)$ within which the expanding fireball radiates, becomes greater than jet collimation angle θ_j because of the fireball deceleration when interacting with the ISM (Sari et al., 1998; Sari & Piran, 1999). The achromatic break epoch (*jet break*) observed in the light curve is a function of the jet aperture angle, thus measuring this time it is possible to inferr θ_j. However, as mentioned already in Section 3, in the last years this simple jet model has been seriously challenged by the observed different behavior of the X-ray afterglow light curves, which, in several cases, show no jet break or show a break not simultaneous to the optical one. This makes the determination of θ_j through observations of jet breaks uncertain in several cases. In addition, for jet opening angles larger than few degrees, achromatic jet breaks are expected days or weeks after the trigger when the optical and X-ray afterglow are typically well below the instrumental detection thresholds.

A more promising method to estimate θ_j may reside in the comparison of the observed multi-wavelength light curves with synthetic light curves obtained from relativistic hydrodynamical simulations (e.g. Van Eerten et al. 2010). The simulated light curves represent a more realistic description of the observed afterglow phenomenology. In Figure 4 is shown an example of synthetic light curve of the optical and radio afterglows, obtained from relativistic hydrodinamic simulations

PoS(AASKA14)056

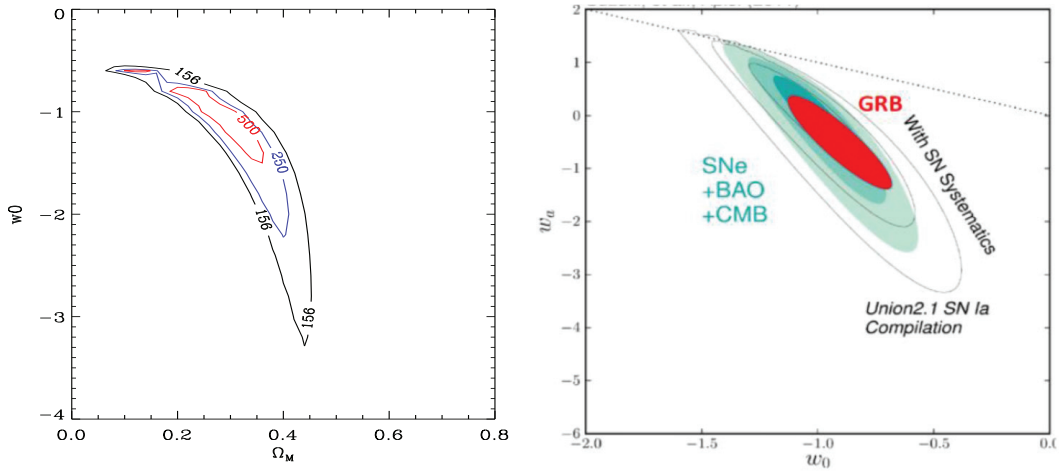

Figure 5: 68% confidence level contours in the Ω_M–w_0 and w_0–w_a planes (by assuming a standard parametrization of the dark energy equation of state: $w = w_0 + w_a z/(1+z)$) for a flat FLRW universe derived from the expected future samples by assuming that the scatter of the $E_{p,i}$ – radiated energy correlation is reduced by a factor of 2 thanks to the measurements by the SKA. In the right panel, we show only the contour obtainable with 500 GRBs, compared to those form other cosmological probes combined together (adapted from Suzuki et al. 2012).

joined with radiative transfer code (van Eerten et al. 2010) of two GRBs with identical energetics, ISM densities and distances, but with two different jet opening angles. The plot clearly show how the overall behaviour of the light curve depends on the jet opening angle and thus can constrain it by comparison with observations.

With a sensitivity of $\sim 1\mu$Jy, almost all the GRB detected today with *Swift* could be not only detected but monitored in time for days up to weeks already with the SKA in Phase 1 (see for example Figure 4 in Ghirlanda et al. 2013) thus complementing the multi-wavelength picture of the afterglow and, by comparison with synthetic light curves, constraining the jet opening angle and ultimately the true radiated energy budget $E = E_{iso}(1 - cos\theta_j)$.

4.2.2 SKA Phase 2: measuring the fireball kinetic energy

Another more challenging way to estimate the radiated energy content of GRBs relies on late time monitoring. At about 100 days after the burst (but theoretical predictions are still compatible with a range that goes from 10 to 1000 days), the decelerating fireball is expected to reach a non-relativistic expansion velocity (Livio & Waxman, 2000) and an isotropic geometry due to the increasing lateral spreading of the jet (Frail et al., 2000). Radiation at this time is expected only in the radio frequencies. Radio emission marks this transition with an expected flattening of its power law decaying light curve. The non-relativistic regime transition epoch, t_{NR}, depends from the fireball kinetic energy E_K (Frail et al., 2001) that consequentely can be derived once t_{NR} has been measured. Therefore, by assuming a kinetic-to-radiated energy conversion efficiency η, from the kinetic energy it is possible to estimate the true radiated energy in an independent way from the collimation angle estimate as $E = \eta E_K$. In those cases where θ_j is also known, together with E_K, a complete picture can be obtained by estimating the conversion efficiency η.

PoS(AASKA14)056

Flux levels at t_{NR} are expected to be < 10 μJy. While SKA in Phase 1 is expected to measure t_{NR} for about 30% of the Swift/BAT GRBs sample, this number will increase to about 70% with the SKA at the end of Phase 2 assuming a 10-fold improved sensitivity (see for example Figure 5 in Ghirlanda et al. 2013).

4.2.3 Expected accuracy for dark energy investigation

The strong impact of the reduction of the dispersion of the $E_{\rm p,i}$ – $E_{\rm iso}$ correlation by a factor of $\sim$2 thanks to the estimate of the jet opening angle and, possibly, the kinetic energy of the blastwave, on the accuracy in the measurement of cosmological parameters with GRBs can be seen by comparing the first and second part of Table 1 (see also the simulations performed by Ghirlanda et al. 2004). Of particular interest is the perspective capability of GRBs of contributing to the characterization of dark energy and its evolution, one of the most relevant open issues in modern science, as illustrated in Figure 5. The start of the SKA Phase 1 early science will coincide with the launch of the Chinese-French SVOM space mission dedicated to GRBs (Godet et al., 2012). This mission, combined with the follow-up observations by the large optical and IR facilities that will be operating at that epoch, is expected to provide us with the measure of redshift and spectral peak energy (the basic information required to use a GRB for cosmology through the $E_{\rm p,i}$ – $E_{\rm iso}$ correlation) for about 50 GRBs/year. Based on the SKA phase 1 capabilities (early science and nominal) summarized above and by taking into account that the sensitivity of SVOM will be worse with respect to that of Swift/BAT (i.e. it will detect brighter GRBs), we expect that SKA1, already in its early science phase, will be capable of detecting and characterizing the radio afterglow emission of most SVOM GRBs with measured redshift and peak energy. By combining the SKA measurements with those at other wavelengths, it will then be possible, as discussed in previous section, to get a reliable estimate of the true radiated energy of $40-50$ GRB year^{-1}. This means that the accuracy on the estimates of $\Omega_{\rm M}$, Ω_Λ and on the parameters of the equation of state of dark energy reported in Table 1 and Figure 5 for 156, 250 and 500 GRBs will be reachable in about 3, 5 and 10 years of operation of SKA Phase 1. Actually, such results may be obtained even in shorter times, if we take into account that, in addition to SVOM, it is likely that other satellites with GRB detection and location capabilities will be flying in the next decade (several projects are under study and being proposed).

As can be inferred from the expected performances summarized in previous subsection, the coming of operative SKA Phase 2 at the end of next decade, combined with large GRB facilities with sensitivities significantly better than Swift and SVOM and autonomous optical / IR follow-up capabilities (e.g., as proposed to ESA, Amati et al. 2013), may provide us with accurate measurements of redshift, spectral peak energy, radio afterglow light curve and kinetic energy for hundreds of GRBs in a few years, thus pushing the investigation of dark energy with GRBs at its extreme (e.g., the study of the evolutionary properties of dark energy shown in the right panel of Fig. 5 may be obtained in 8-10 years of the SKA Phase 1 and $\sim$3 years of the SKA Phase 2).

5. Summary and conclusions

Given their huge radiated energies and redshift distribution extending from ~ 0.01 up to 9.2, GRBs are potentially a very powerful cosmological probe, complementary to other probes (e.g.,

PoS(AASKA14)056

SNe Ia, galaxy clusters, BAO). As demonstrated by several works, the most promising tool allowing the use of GRBs for measuring cosmological parameters and, in perspective, characterizing the properties of "dark energy" is the correlation between the burst radiated energy $E_{\rm iso}$ and the spectral peak energy $E_{\rm p,i}$. The main limit of the use of the $E_{\rm p,i} - E_{\rm iso}$ correlation in cosmology so far comes from its large scatter, that is in part due to our ignorance on the emission processes at play during a burst and partly to the unknown collimation factor of the ejecta (forcing us to use the isotropic emission approximation). Radio observations with the SKA Phase 1 and the full SKA (Phase 2) will provide an important step forward in the attempt of estimating the true radiated energy of GRBs and, hence, reducing significantly the dispersion of the correlation between $E_{\rm p,i}$ and radiated energy (or luminosity). More specifically, with SKA Phase 1 this goal will be mostly achieved by getting reliable estimates of the jet opening angle, and therefore of the collimation corrected radiated energy, for a large sample of GRBs, through the monitoring the afterglow flux evolution with time from the early up to late epochs and by comparing it with simultaneous multiwavelength observations and synthetic light curves. With the Phase 2 of SKA there will be also the possibility of estimating, for about 50% of the GRBs detectable by space detectors, the true energy budget through the fireball kinetic energy (from which $E = \eta \times E_K$ where η is assumed to be typically 0.1) by very late epochs radio monitoring of the fireball in its non-relativistically expanding regime. Simultaneous observations from high-energy satellites expected to be operative at the time the SKA will reach its full sensitivity, will continue to provide measures of the burst spectrum peak energy. As supported by previous studies (e.g., Ghirlanda et al., 2004) and simulations here reported, the expected reduction of the correlation scatter by using a better proxy to the true radiated energy of GRBs (Ghirlanda et al., 2004) will provide substantial improvement in the accuracy of the estimate of cosmological parameters with GRBs.

References

Amati, L., Frontera, F., Tavani, M., et al., 2002, A&A, 390, 81
Amati, L., 2006, MNRAS, 372, 233
Amati, L., Della Valle, M., Frontera F. et al., 2007, A&A, 463, 913
Amati, L., Guidorzi, C., Frontera F. et al., 2008, MNRAS, 391, 577
Amati, L., Frontera, F. & Guidorzi, C., 2009, A&A, 508, 173
Amati, L. & Della Valle, M., 2013, IJMPD, 22, 1330028
Burlon, D., Ghirlanda, G., van der Horst, A., et al., 2015, “The SKA View of Gamma-Ray Bursts”, in "Advancing Astrophysics with the Square Kilometre Array", Proceedings of Science, PoS(AASKA14)052 (arXiv:1501.04629)
Chandra, P. & Frail, D.A., 2012, ApJ, 746, 156
Dai, Z.G., Liang, E.W. & Xu, D., 2004, ApJ, 612, L101
Demianski, M., Piedipalumbo, E., Rubano, C, Scodellaro, P., 2008, A&A, 481, 279
Dewdney, P., Turner, W., Millenaar, R., McCool, R., Lazio, J., Cornwell, T., 2013, "SKA1 System Baseline Design", Document number SKA-TEL-SKO-DD-001 Revision 1
Frail, D. A., Waxman, E. and Kulkarni, S.R., 2000, ApJ, 537, 191
Frail, D. A., et al., 2001, ApJ, 562, L55

PoS(AASKA14)056

Ghirlanda, G., Ghisellini, G., Lazzati, D., 2004, ApJ, 616, 331 Gamma-Ray Burst Energies Correlate with the Peak Energy of Their νF_ν Spectrum
Ghirlanda, G., Ghisellini, G., Firmani, 2006, New J. Phys., 8, 123 candles to constrain the cosmological parameters
Ghirlanda, G., Salvaterra, R., Burlon, D. et al., 2013, MNRAS, 435, 2543
Godet, O., Paul, J., Wei ,J.Y., et al., 2012, SPIE Conf. Ser. 8443, p. 1
Granot, J. & van der Horst, A. J., 2014, PASA, 31, 8
Kodama, Y., Yonetoku, D., Murakami, T. et al., 2008, MNRAS, 391, L1
Lamb, D. Q., Ricker, G. R., Atteia, J.-L. et al., 2004 NewAR, 48, 423
Livio, M & Waxman, E., 2000, ApJ, 538, 187
Panaitescu, A. and Meszaros, P. 1999, ApJ, 526, 707
Phillips, M.M., 1993, ApJ, 413, L105
Sari, R., Piran, T., & Narayan, R., 1998, ApJ, 497, L17
Sari R. & Piran, T. 1999 ApJ, 520, L641
Sari, R., Piran, T. & Halpern, J.P., 1999, ApJ, 519, L17
Schaefer, B.E., 2007, ApJ, 660, 16
Suzuki, N., Rubin, D., Lidman, C. et al., 2012, ApJ, 746, 85
Zhang, B. & Mészáros, P., 2002, ApJ, 581, 1236

PoS(AASKA14)056

PROCEEDINGS OF SCIENCE

Time domain studies of Active Galactic Nuclei with the Square Kilometre Array

Hayley Bignall,[1] **Steve Croft**[*,2] **Talvikki Hovatta,**[3,4] **Jun Yi Koay,**[5] **Joseph Lazio,**[6] **Jean-Pierre Macquart**[1,7] **and Cormac Reynolds**[1]

[1]*ICRAR/Curtin University*
[2]*University of California, Berkeley*
[3]*California Institute of Technology*
[4]*Aalto University, Metsähovi Radio Observatory*
[5]*DARK, Niels Bohr Institute, University of Copenhagen*
[6]*Jet Propulsion Laboratory, California Institute of Technology*
[7]*ARC Centre of Excellence for All-Sky Astrophysics (CAASTRO)*
E-mail: H.Bignall@curtin.edu.au, scroft@astro.berkeley.edu

Variability of radio-emitting active galactic nuclei can be used to probe both intrinsic variations arising from shocks, flares, and other changes in emission from regions surrounding the central supermassive black hole, as well as extrinsic variations due to scattering by structures in our own Galaxy. Such interstellar scattering also probes the structure of the emitting regions, with microarcsecond resolution. Current studies have necessarily been limited to either small numbers of objects monitored over long periods of time, or large numbers of objects but with poor time sampling. The dramatic increase in survey speed engendered by the Square Kilometre Array will enable precision synoptic monitoring studies of hundreds of thousands of sources with a cadence of days or less. Statistics of variability, in particular concurrent observations at multiple radio frequencies and in other bands of the electromagnetic spectrum, will probe accretion physics over a wide range of AGN classes, luminosities, and orientations, as well as enabling a detailed understanding of the structures responsible for radio wave scattering in the Galactic interstellar medium.

Advancing Astrophysics with the Square Kilometre Array
June 8-13, 2014
Giardini Naxos, Italy

[*]Speaker.

PoS(AASKA14)058

1. Introduction

The limited survey speed of existing radio telescopes means that active galactic nucleus (AGN) variability has been studied in detail only for $\sim 10^3$ relatively bright objects, or in only a few epochs for larger numbers of sources down to lower flux density limits. However, AGN dominate the radio sky at flux densities above a milliJansky (Seymour et al. 2008), and synoptic surveys with SKA Phase 1 will provide radio variability information with a cadence of days or less for hundreds of thousands of AGN.

The characteristic timescales of the inner regions of the AGN central engine are accessible on human timescales, from hours to days to years, and enable processes occuring close to the supermassive black hole (SMBH) to be probed. Understanding variability on these timescales, and correlating variability over a range of radio frequencies with that seen across the electromagnetic spectrum, can provide a powerful probe of the connection between disks and jets, inflow and outflow, turbulence and shocks, and activity and quiescence.

In addition to source-intrinsic processes, propagation effects also play an important role in observed variability at centimetre wavelengths. Interstellar scintillation (ISS) in the strong refractive and weak scattering regimes produces apparent intensity variations for sufficiently compact sources on timescales of typically days, but sometimes as short as minutes to hours. ISS gives access to microarcsecond (μas) scales (Lovell et al. 2008), allowing the study of changes in intrinsic source structure with resolution beyond that achievable with VLBI. Extreme scattering events (ESEs) are transient events in which sources undergo large, week- to months-long time-symmetric flux density excursions, due to refractive lensing potentially by discrete structures in the interstellar medium (ISM). While these effects have been known for decades, several significant questions remain, both with respect to the characteristics of sources that vary and the interstellar structures that produce the variation.

In this Chapter we discuss the contribution that SKA will make to various outstanding questions in time domain studies of AGN, through observations of both intrinsic and extrinsic variability. Although a broad range of specific science outcomes is addressed, similar or identical survey strategies are involved, and disentangling intrinsic and extrinsic causes of observed variability will be important in order to achieve the desired goals: increased understanding of the physics both of AGN and of the intervening media.

2. Science from time domain studies of AGN: state of the art

In §2.1 below we discuss direct observations of intrinsic AGN variability, with reference to many recent studies. In §2.2 we discuss variability due to scattering in the interstellar medium, including results from the extensive MASIV VLA Survey and follow-up observations, and still-mysterious ESEs. Monitoring of ISS probes intrinsic source changes, as well as small-scale structures in the ISM. In §2.3 we discuss methods for disentangling variations due to intrinsic and extrinsic mechanisms.

2.1 AGN physics from intrinsic variability

Variability of both total intensity and polarization is a common characteristic of AGN, and

PoS(AASKA14)058

occurs with multiple characteristic timescales in individual objects. Variations between different bands of the electromagnetic spectrum are often related, with early emission at short wavelengths—X-rays or γ-rays—eventually propagating to longer wavelengths, including radio, and longer timescales. Emission at different wavelengths probes a range of processes occuring in different regions of the AGN central engine, and a panchromatic view can help to answer questions of how relativistic AGN jets are launched, and how inflow and outflow are coupled. In some cases (e.g. Thyagarajan et al. 2011) variable radio emission is the only indicator of AGN activity, and can provide a powerful probe of buried AGN which show no evidence of an accreting black hole at other wavelengths.

AGN intrinsic variability exhibits both red and white noise components, as well as quasi-periodic oscillations in some cases (King et al. 2013; Wiita 2011), corresponding to variations in accretion rate, flares and shocks in disks and jets, transitions between high and low states (Krauß et al. 2013), changes in Doppler boosting and jet precession, and other processes taking place near the black hole. Long-term monitoring observations are required to sample the full range of timescales, to compare to observations at other wavelengths, and to catch rare events such as large flares and outbursts. The correlation delay between X-ray and radio can be hundreds of days, so long duration campaigns (at least several years) are required for adequate sampling. Day to year timescales for AGN variability correspond to the light crossing, viscous, and infall timescales of the black hole and accretion disk. Several ongoing programs (e.g. Hughes et al. 1992; Hovatta et al. 2007; Lister et al. 2009a; Richards et al. 2011) have monitored a few hundred sources for significant periods of time. A few other surveys (e.g. Thyagarajan et al. 2011) have obtained data over a handful of epochs for large numbers of sources. But until now, the primary limitation for this exercise has been the absence of dedicated radio instruments with the combination of field of view and sensitivity to partner with high energy facilities. SKA will open new parameter space by providing precision flux measurements as a function of time for almost all of the hundreds of thousands of compact sources typical of previous large-area single-epoch surveys. By providing high-cadence synoptic monitoring without the potential biases of small sample selections, SKA will produce an archive of variability information for a huge range of AGN.

The launch of the *Fermi* Space Telescope in 2008 revolutionized gamma-ray studies of AGN by providing the first instrument that monitors the entire gamma-ray sky every three hours (Atwood et al. 2009). It has become possible to do population studies of gamma-ray loud, and quiet, AGN and compare the gamma-ray emission to their radio properties. For example, gamma-ray detected AGN have larger variability amplitudes in radio (Richards et al. 2011), faster apparent jet speeds (Lister et al. 2009b), and higher Doppler beaming factors (Savolainen et al. 2010) than non-detected objects. Some studies have also reported that radio and gamma-ray luminosities are correlated (Ackermann et al. 2011; Nieppola et al. 2011). All of the above imply a connection between radio and gamma-ray variations in the sources. The next generation very high energy Cherenkov Telescope Array (CTA), in combination with SKA, will in turn open the possibility to study the connection between TeV and radio emission in a large number of sources, probing the acceleration of particles up to the highest energies (Giroletti et al. 2015).

Many existing surveys have focused on blazars, where relativistic beaming and the compact sizes of emitting regions produce more variability than in sources oriented further from the line of sight. The wide field monitoring capabilities of SKA, however, will enable lightcurves from all classes of AGN to be studied, refining unification schemes and our understanding of the geometry

PoS(AASKA14)058

of the emitting regions. One caveat is that most, but by no means all (e.g. Kedziora-Chudczer et al. 2001; Ojha et al. 2010; Stevens et al. 2012), of the existing monitoring surveys were undertaken in the northern hemisphere, so not all of the sources from these surveys will be accessible for continued monitoring with SKA.

The details of accretion, and its connection to jet launching in radio-loud sources, as well as a wide range of other AGN phenomena, are still not well understood. Radio flares may occur at time intervals corresponding to the formation of shocks in the jets, which could be due to interaction with the ISM or torus (Brunthaler et al. 2005), or to changes in accretion rate propagating to changes in the jet (Chatterjee et al. 2011). The most commonly used models for flares in blazars are so called shock-in-jet models where the variations are caused by shocks propagating down the jet and emitting synchrotron radiation (Marscher & Gear 1985; Hughes et al. 1985). Multifrequency radio observations can be used to model the shock propagation and jet properties in detail, giving insights into the jet geometry and magnetic field (Fromm et al. 2011). Radio flares seen in III Zw 2 (Fig. 1) and Mrk 348 suggest that jets in Seyferts can accelerate from non-relativistic to relativistic speeds during an outburst, but larger samples are required to confirm this (Mundell et al. 2009). Interestingly, narrow-line Seyfert I galaxies are an unexpected group of gamma-ray emitting AGN. Fermi has detected a handful of NLS1 galaxies, confirming that they indeed can also emit high energy electrons, and have prominent relativistic jets (Abdo et al. 2009). Modeling these variations can probe jet acceleration mechanisms and central engine physics (Kudryavtseva et al. 2011). Understanding jet production is also critical in studying galaxy formation, since jets play a key role in regulating galaxy growth (Hopkins & Elvis 2010).

Another promising avenue for understanding accretion and jet launching is the study of tidal disruption events (TDEs), posited to result from stars that are shredded after passing close to SMBH event horizons. The sudden increase in accretion rate results in SMBHs transitioning from a quiescent state to a short-lived, typically months-long, AGN-like phase. In some cases radio emission is thought to result from the formation of a jet, which interacts with the dense ISM of the galaxy (Metzger et al. 2012; Zauderer et al. 2011; Burrows et al. 2011), and produces a radio afterglow that peaks around a year after the star is tidally disrupted and lasts for around a year. A large sample of TDEs would allow us to address the unanswered question of how jets evolve when accretion rates undergo a sudden dramatic increase. By looking for common features in TDEs that are radio loud versus radio quiet, their role in AGN radio loudness in general could be constrained (van Velzen et al. 2011). TDEs are expected to occur in an average galaxy about once every 10^5 yr, so large surveys such as those that will be undertaken by SKA are required to see them in significant numbers. Further discussion of the role of SKA in finding TDEs can be found elsewhere in this volume (Donnarumma et al. 2015).

A recent study (MacLeod et al. 2010) found a dependence of AGN variability on black hole mass, luminosity, and Eddington ratio, as well as larger variability amplitudes for radio-loud objects than for radio-quiet. However, the relationship between variability and the properties of the host galaxy and black hole, and the accretion dynamics, are by no means clear (Zuo et al. 2012). Recently, it was shown that the jet magnetic field and accretion disk luminosity are tighly correlated in blazars (Zamaninasab et al. 2014). This result was obtained by comparing black hole mass estimates to the jet magnetic flux, calculated using radio interferometric observations. This result shows that it is possible to obtain information about the detailed physics near the black hole, by

PoS(AASKA14)058

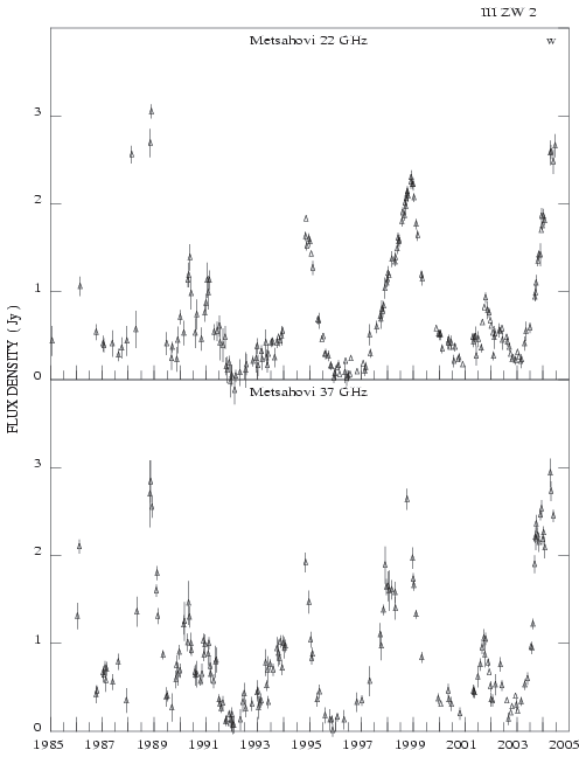

Figure 1: Lightcurve of III Zw 2 at 22 and 37 GHz from the Metsähovi Radio Observatory, showing flaring activity suggestive of acceleration of jets from non-relativistic to relativistic speeds during outbursts. Credit: Teräsranta et al., A&A, 440, 409, 2005, reproduced with permission © ESO.

relating observations further out in the jet to the smallest scales near the black hole.

VLBI observations provide direct evidence for relativistic outflows from AGN, and have been used to monitor the motion of jet components on parsec scales (e.g. Lister et al. 2013). It is possible to determine jet compositions, magnetic fields, variations in jet orientation, ages and densities of components, interplay between the jet and ambient medium, as well as other physical conditions in the jet and close to the black hole by comparing parsec-scale variations with spectral energy distributions, polarization and Faraday rotation, as well as observations at other wavelengths and relativistic MHD simulations (Hovatta et al. 2012, 2014). VLBI components are by their very nature intrinsically variable (Lister et al. 2009a), but are also subject to variability due to interstellar scattering (§2.2). Flares and superluminal blobs may be connected to changes in magnetic field on timescales of years, or to current-driven instabilities, tangled magnetic fields, or reconnection events, and SKA can help probe this (Agudo et al. 2015).

AGN activity appears to be enhanced during galaxy mergers (Manzer & De Robertis 2014) and in overdense environments (Croft et al. 2007). However, the relationship between mergers and the triggering of various kinds of AGN, including those selected at different frequencies, is still not clear (Kocevski et al. 2012; Karouzos et al. 2014). The details of what happens to SMBHs after mergers are also not yet well understood. In some instances, AGN pairs (or multiple AGNs) with an offset in position and / or velocity are seen in galaxies at various stages of mergers (e.g. Komossa et al. 2003; Comerford et al. 2011). With large area, sensitive, high resolution SKA

PoS(AASKA14)058

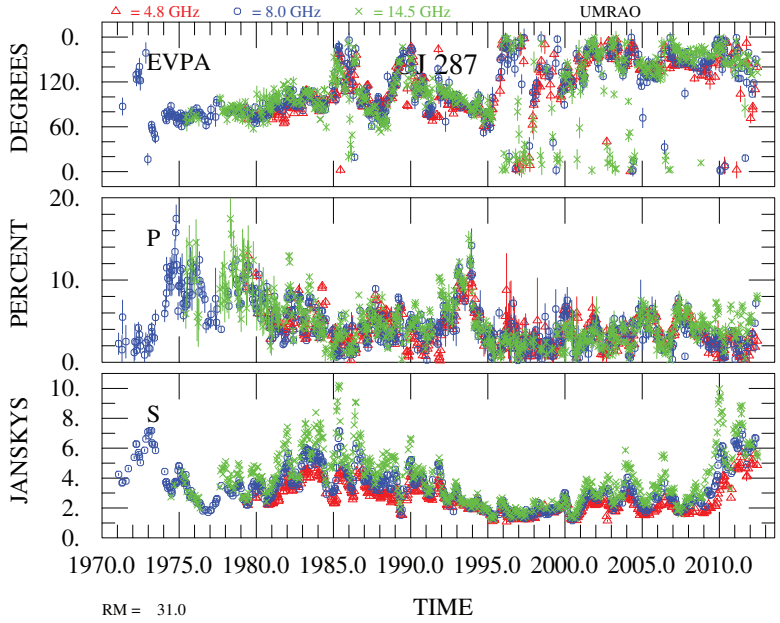

Figure 2: Centimetre-band lightcurves of BL Lac object OJ 287 from the University of Michigan Radio Telescope. Optical lightcurves of this source, including archival data dating back over 100 years, show a 12 year periodicity interpreted as the orbital period of a secondary SMBH intercepting the accretion disk of the primary. The radio lightcurves shown here (from Aller et al. 2014, reproduced by permission of the AAS) show flaring activity on shorter timescales. From top to bottom, the panels show total flux density, fractional linear polarization, and polarization electric vector position angle.

surveys, many more dual AGN (including binary AGN, where the AGN are clearly orbiting each other, e.g. Rodriguez et al. 2006; Deane et al. 2014) or systems containing an AGN and a quiescent SMBH (e.g. Comerford & Greene 2014), should be detected at various stages in their evolution. In at least one case known to date, the blazar OJ 287, variability of optical emission is proposed to arise as a secondary black hole plunges through the accretion disk of the primary (Valtonen et al. 2008). The optical lightcurve shows periodic outbursts every 12 years, corresponding to the proposed orbital period, and radio monitoring (Fig. 2) shows evidence of long term cycles of radio activity as well as periodic variability associated with flares and jet features (Hughes et al. 1998).

For closer binaries, the "final parsec problem"—the ineffectiveness of dynamical friction with stars near SMBHs in shrinking their separation to < 1 pc (Milosavljević & Merritt 2001)—remains unsolved, and likely requires a more detailed understanding of accretion disk dynamics. Periodic variability due to jet precession, a signature of gravitational wave dominated inspiral of SMBHs during the final stage of mergers (Haiman et al. 2009), can be used to search for merging systems containing a radio-loud AGN. A detection of this signal, which should be within reach of SKA and its precursors (O'Shaughnessy et al. 2011), could be used to probe the physics of viscous orbital decay as a function of black hole mass, and confirm that inspiral is driven by gravitational wave emission.

By probing the inner regions of AGN central engines, studies of AGN intrinsic variability with SKA will inform two Key Science Projects: "Strong Field Tests of Gravity Using Pulsars and

PoS(AASKA14)058

Black Holes", and through the connections between infall and outflow in AGN, and feedback on surrounding gas, "Galaxy Evolution, Cosmology, and Dark Energy".

2.2 Science from interstellar scattering

Radio wave propagation effects and implications for SKA, applying to studies of both pulsars and AGN, were discussed in some detail by Lazio et al. (2004). Here we provide an updated overview specifically related to AGN variability due to interstellar scattering, and outline the currently outstanding questions that can be addressed with SKA.

2.2.1 Interstellar scintillation

Over the past two decades, evidence has accumulated to demonstrate that rapid—intra-day and inter-day—flux density variations of AGN at centimetre wavelengths are predominantly caused by ISS rather than intrinsic variability. This evidence includes the frequency dependence of the observed variability (Kedziora-Chudczer et al. 1997), measurement of variability pattern arrival time delays of several minutes between widely separated telescopes for the most rapid variations (Jauncey et al. 2000; Dennett-Thorpe & de Bruyn 2002; Bignall et al. 2006), annual cycles in the characteristic timescale of variability (e.g. Dennett-Thorpe & de Bruyn 2001; Rickett et al. 2001; Jauncey & Macquart 2001; Qian & Zhang 2001; Bignall et al. 2003) and a strong correlation between cm-wavelength intraday variability (IDV) and Galactic Hα emission measure along the line-of-sight, showing that this IDV is related to the ionized Galactic ISM (Lovell et al. 2008; Koay et al. 2011).

Observed ISS implies the presence of high brightness temperature compact components, no larger than tens of μas in angular size (e.g. Lovell et al. 2008). ISS, with an adequate model of the scattering parameters, can thus be used to estimate source angular size and compact fraction, as well as investigate frequency- and polarization-dependent sub-structure, at resolutions beyond those achievable with ground-based VLBI. Angular scales of this order are presently being probed directly on baselines to the RadioAstron Space Radio Telescope (Kardashev et al. 2013), but the sensitivity is limited to bright sources. Studies of ISS of fainter sources over wide bandwidths probe a fundamentally different, much weaker, regime of AGN jet power.

The MASIV VLA Survey at 5 GHz (Lovell et al. 2003, 2008) found that more than half of all compact, flat-spectrum sources > 100 mJy exhibited rms variations $\geq 2\%$ on timescales ≤ 3 days due to ISS, with increased fractional variability towards lower flux densities. This trend is as expected for brightness temperature-limited sources, where angular size is expected to scale as $\sqrt{S}$ assuming no change in the Doppler boosting factor. The majority of MASIV sources have firm spectroscopic identifications—all AGN, with almost 80% being flat-spectrum radio quasars and most of the remaining fraction BL Lac objects (Pursimo et al. 2013).

A suppression of ISS towards higher redshift sources (Lovell et al. 2008) has been proposed as a possible indicator of angular broadening due to scattering in the turbulent intergalactic medium (IGM), making the high redshift sources appear too large to scintillate through the Galactic ISM. However, a careful analysis of the MASIV Survey and follow-up VLA data at 5 and 8 GHz found no conclusive evidence for IGM scatter-broadening of the high redshift MASIV sources. After accounting for a steepening with redshift of average spectral index between 5 and 8 GHz, the decrease in amplitude of ISS with redshift was found to be no longer significantly in excess of

PoS(AASKA14)058

that expected if angular size $\theta \propto \sqrt{1+z}$, as expected for a brightness temperature and flux limited sample of sources (Koay et al. 2012).

The statistics of short timescale radio variability for a larger and much fainter source sample, obtainable with SKA1, will allow tighter limits to be placed on extragalactic scatter-broadening through the suppression of ISS. As lower flux density AGN cores can have smaller intrinsic source sizes, they are more likely to be dominated by scatter-broadening. Observations of large numbers of faint sources in fields at high Galactic latitudes would provide a means of determining the ISM contribution to scattering; source redshifts are also required in order to measure, or obtain limits on, intergalactic scattering. Koay & Macquart (2014) have recently shown that while scatter-broadening in the warm-hot component of the IGM is not expected to be detectable, intergalactic scatter broadening can be significant, $\sim 100\mu$as at 1 GHz and $\sim 3\mu$as at 5 GHz, for sight-lines intersecting within a virial radius of at least one galaxy halo. Targeted, multi-frequency ISS surveys of compact sources behind rich clusters, galaxies or Damped Lyman-Alpha Systems may provide the best chance of detecting extragalactic scatter-broadening through the predicted angular size scaling as $\nu^{-2.2}$, providing a unique probe of the turbulent properties of these regions. Evidence for scatter-broadening in an intervening galaxy has been found from VLBI observations of AGN behind M31 (Morgan et al. 2013).

A handful of sources have been found which exhibit unusually rapid variability on timescales < 1 hour (Kedziora-Chudczer et al. 1997; Dennett-Thorpe & de Bruyn 2000; Bignall et al. 2003), which is modelled as ISS in the weak scattering regime due to very nearby scattering plasma, within tens of parsec of the Sun (Rickett et al. 2002; Dennett-Thorpe & de Bruyn 2003; Bignall et al. 2006). The scattering is determined to be highly anistropic, as has been found also for a number of pulsars displaying diffractive "scintillation arcs" in their secondary spectra (Walker et al. 2008; Brisken et al. 2010, and references therein). This suggests scattering in thin "screens" in which the electron density fluctuations are subject to extreme magnetic stresses (Tuntsov et al. 2013). The specific nature of the material responsible is still unknown. Despite two of the three exemplary "intrahour variables" being discovered serendipitously, the MASIV Survey found no more examples of such rapid, large-amplitude ISS, implying that the covering factor of nearby screens is very small; $\ll 1\%$ of compact sources would be expected to vary on intra-hour timescales.

The correlation between H-alpha and short-term variability from MASIV suggests that in general, the more typical slower, low-amplitude ISS is probably related to the overall amount of ionized material in the ISM along the line-of-sight, but this is not the case for the intrahour variables. Because AGN angular sizes are typically larger than the Fresnel scale at interstellar distances, they are "resolved" by ISS. The smaller the screen distance L from the observer, the larger the angular Fresnel scale, so nearby scattering will tend to dominate the observed variability; not only is the ISS less quenched, but nearby screens also induce faster variations compared with more distant scattering material, since the Fresnel zone crossing time which sets the timescale for weak ISS scales as $\sqrt{L}$ for a given scintillation velocity. ISS behaviour is often observed to be episodic, which can be due to a combination of intermittency in interstellar turbulence and intrinsic changes in source structure, although the relative importance of the two effects remains poorly constrained. This problem can be addressed by comparing longer term source-intrinsic changes in spectral index, flux density, polarization and VLBI structure, with changes in ISS behaviour for a large source sample.

PoS(AASKA14)058

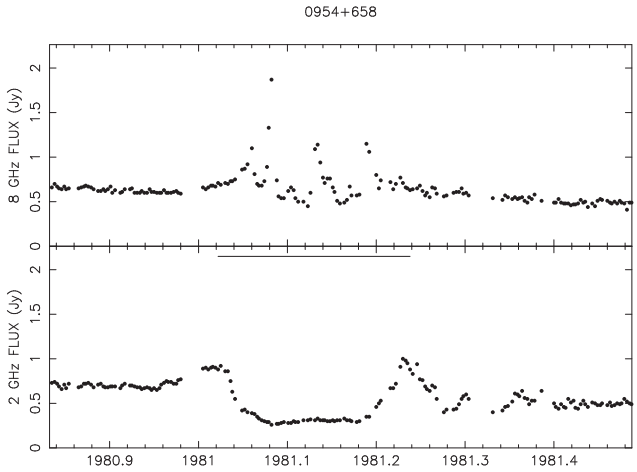

Figure 3: The extreme scattering event toward QSO 0954+658, the prototypical and exemplar ESE. The top panel shows the 2 GHz flux densities measured by the Green Bank Interferometer, and the bottom panel shows the 8 GHz flux densities. Data are from Rickett et al. (2006).

Finding a large number of rapid intraday variables through SKA Surveys will help to determine the nature of the local scattering plasma in the ISM. While fast intra-day variability can be picked up in undersampled data, extracting useful science would require detailed follow-up observations, either with (a sub-array of) SKA or with other instruments. Well-sampled ISS light-curves across a broad bandwidth, ideally several GHz, can be used to determine the detailed polarization- and frequency-dependent structure of the ultracompact jet with μas precision. This information can be used to model the magnetic field configuration, geometry, particle density and pressure in the jet (Rickett et al. 2002; Macquart et al. 2013).

2.2.2 Extreme Scattering Events

Extreme scattering events (ESE) are a class of dramatic changes in the flux density of radio sources (Fiedler et al. 1994). They are typically marked by a decrease, as large as $\gtrsim 50\%$, in the flux density near 1 GHz for a period of several weeks to months, bracketed by substantial increases, viz. Figure 3. Because of the simultaneity of the events at different wavelengths, the time scales of the events, and light travel time arguments, ESEs are likely due to strong scattering by ionized structures in the Galactic ISM (Fiedler et al. 1987a; Romani et al. 1987, but see Walker & Wardle 1998). First identified in the light curves of extragalactic sources, ESEs have since been observed during a timing program of the pulsars PSR B1937+21 (Cognard et al. 1993; Lestrade et al. 1998) and PSR J1643−1224 (Maitia et al. 2003).

While the focus of this chapter is on the variability of AGN, ESEs probably are related to "strong fringing events" observed in dynamic spectra from pulsars (Hill et al. 2005). In those events, the dynamic spectra—intensity as a function of time and frequency—show "fringes," consistent with the interference from multiple images of a pulsar resulting from strong lensing along the line of sight to the pulsar.

Modeling of ESE light curves leads to inferred densities $n_e \gtrsim 10^2$ cm^{-3} within these ionized structures (Romani et al. 1987; Clegg et al. 1998). In turn, these densities imply pressures $nT \sim$

PoS(AASKA14)058

10^6 K cm^{-3} or more, well in excess of the "average" interstellar pressure $nT \sim 3000$ K cm^{-3} (Kulkarni & Heiles 1988).

Outstanding issues related to ESEs include the following:

- What is the mechanism by which they occur? Most models predict that ESEs arise from strong refraction through relatively isolated structures. Observational support for this prediction is mixed. Pulse times of arrival from the pulsars that have undergone an ESE do show an increased scatter, but no increase in the pulse width—as would be expected from the extra path length caused by the refraction. However, VLBI observations of the source B1741−038 while it was undergoing an ESE show its angular diameter to *increase*, contrary to expectations from a purely refractive model (Lazio et al. 2000). One obvious resolution is to model the ESE structures as being internally turbulent, but largely refracting structures. The serendipitous detection of multiple imaging of the quasar 2023+335 observed with VLBI during an ESE was recently reported, and found to be consistent with strong refraction through a turbulent plasma structure (Pushkarev et al. 2013).

- What is the relationship of ESE structures to other phases of the ISM? or are ESE structures even interstellar? ESE structures may represent relatively isolated structures, perhaps in pressure balance with a lower density, higher temperature "background" phase (Clegg et al. 1988); they may represent manifestations of the most extreme pressure ranges within the ISM and thereby trace energy input into the ISM (Jenkins & Tripp 2001); they may result from a low level of cosmic-ray ionization within an otherwise neutral tiny scale atomic structure (TSAS; Heiles 1997); or they may not be interstellar at all, but due to photoionized molecular clouds in the Galactic halo (Walker & Wardle 1998). H I absorption measurements during the ESE of B1741−038 show no statistically significant change in the H I line during the ESE (Lazio et al. 2001a). However, the limits on the changes in optical depth, and therefore H I column density, only marginally rule out a connection between ESE structures and TSAS in the ISM. Any change in the H I column density is limited to be $\Delta N_H < 10^{18}$ cm^{-2}, while TSAS has a typical column density of 3×10^{18} cm^{-2}. Geometrical factors (e.g., the line of sight did not pass through the center of the cloud) could easily account for this difference. Conversely, the velocity range of the H I absorption measurements was no more than 250 km s^{-1}. If ESE structures are halo objects, the allowed velocity range could approach 1000 km s^{-1}. Thus, the existing H I absorption observations cannot constrain significantly either of the two competing models.

- What is the frequency with which ESEs occur and what is their sky distribution? The Green Bank Interferometer (GBI) monitored approximately 30 sources for over a decade and an additional 120 sources for five years. A total of 12 ESEs were found in this monitoring program. However, a six-month monitoring program with the NRAO 300 ft telescope found a comparable number of ESEs (R. Fiedler 1998, private communication). The 12 ESEs observed in the GBI program appear to be located near the edges of radio Loops I–IV (Fiedler et al. 1994), structures thought to be old supernova remnants. If this is correct, old supernova remnants could provide the high-pressure environment in which ESE lenses could survive

PoS(AASKA14)058

(Clegg et al. 1988). However, the radio Loops cover a large fraction of the sky, and the sky distribution might also be consistent with a halo population of objects.

Since the cessation of the GBI monitoring program in 1994 (Fiedler et al. 1987b; Waltman et al. 1991; Lazio et al. 2001b), there has been no monitoring program observing a sufficiently large number of sources, at a low enough radio frequency, and with frequent enough time sampling to have a realistic chance of detecting the requisite number of ESEs to address these questions. Although some new programs aim to tackle this in the lead-up to SKA Phase 1, e.g. the ASKAP VAST project (Murphy et al. 2013), these cannot match the efficiency of potential SKA surveys to detect a sufficient number of ESEs to address their statistics (§3.1).

Identification of ESEs as they occur is critical in order to determine the nature of the refracting "lenses" responsible. Multiple imaging on milliarcsecond scales is predicted at strong caustics, and VLBI monitoring of ESEs will differentiate between competing models for ESEs (Pen & King 2012). Detailed radio follow-up over a broad frequency range, and observations at other wavelengths, including optical/infrared, will also help to rule out or support various models.

2.3 Determining the origin of AGN radio variability

Observations at multiple frequencies and classification of light curves based on their structure function, power spectral density, and other statistics will help to disentangle intrinsic and extrinsic causes of variability. Ofek & Frail (2011) argued that a large fraction of variability at 1.4 GHz must be RISS, based on a flat structure function between $\sim 200 - 1800$ days for a sample of 43 variables. Rickett et al. (2006), in an analysis of GBI monitoring data for 146 sources, applied a simple filter on the time series to separate slow intrinsic variations from fast ISS, confirming that both processes are important at the observed frequencies near 2 and 8 GHz (see Figure 4).

It is expected that propagation effects may dominate at low frequencies, below ~ 2 GHz, while large-amplitude variations at higher frequencies, > 8 GHz are more likely intrinsic — at least on timescales of weeks to months and longer, although both ISS (Savolainen & Kovalev 2008; Kara et al. 2012) and ESEs (Pushkarev et al. 2013) have been observed at 15 GHz. However, a test shows no statistical correlation between line-of-sight Galactic Hα emission and 15 GHz variability on timescales of months to years from published OVRO data, indicating intrinsic variability dominates, whereas there is a strong correlation between Hα emission measure and inter-day variability at 5–8 GHz, indicating that the latter is predominantly ISS. At these intermediate frequencies, both intrinsic and ISS-induced variability are likely to be important. Concurrent lightcurves, including polarization information, for large numbers of AGN, using Band 5, 4.6–13.8 GHz, of SKA1-MID—and MeerKAT's X-band receivers—along with two lower frequency bands, will provide a powerful discriminant between intrinsic and extrinsic variability. AGN lightcurves from SKA1-LOW, at 50–300 MHz, and SKA1-SUR, at 650–1670 MHz (PAF Band 2), will likely be dominated by extrinsic variability, although the panchromatic view provided by the wide frequency coverage of SKA, in conjunction with instruments such as the Large Synoptic Survey Telescope (LSST) and high energy facilities, will provide a powerful discriminant of the source of variability for a range of objects.

The largest amplitude variations due to ISS are usually seen close to the transition between weak and strong scattering, which is dependent on Galactic latitude but typically ~ 5 GHz (Kedziora-

PoS(AASKA14)058

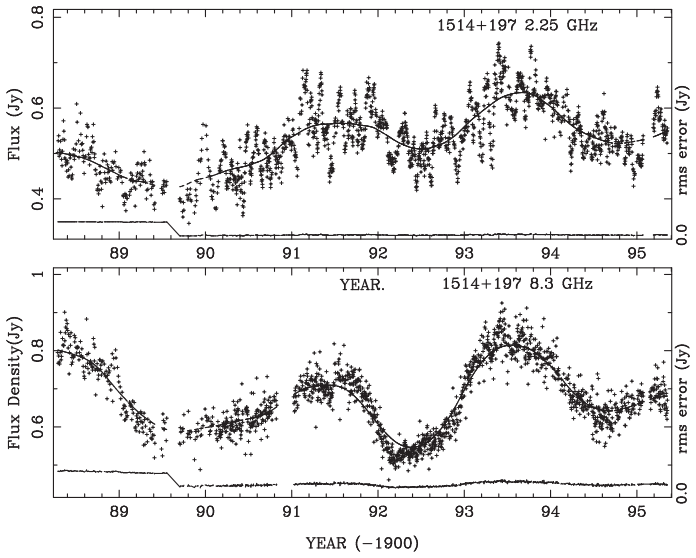

Figure 4: Flux density at 2 and 8 GHz for 1514+197 from the Green Bank Interferometer monitoring program, analysed by Rickett et al. (2006) (figure reproduced with permission). The solid curve is the time series (Jy) smoothed over 365 days with a truncated cosine function. It is interpreted to be dominated by intrinsic variation in the synchrotron radiation from the source. The short-term deviations from the line are due to ISS. The trace below each curve gives the rms error in a single measurement (on the same scale) relative to the horizontal axis. This demonstrates the value of long-term, multi-frequency monitoring with high cadence to determine the origin of variability.

Chudczer et al. 1997; Walker 1998). When the source is much larger than the angular size of the first Fresnel zone at the scattering screen distance, then weak ISS will be suppressed, but slower refractive ISS may still be observed at lower frequencies in the strong scattering regime. Intrinsic variability at centimetre wavelengths will typically have longer timescales and larger amplitude than scintillation. A preliminary comparison of modulation indices from four years of OVRO data (Richards et al. 2014) at 15 GHz — predominantly intrinsic variability — and short-timescale (2 day) modulation indices from the MASIV Survey at 5 GHz — predominantly ISS — for sources common to both samples shows a significant correlation: sources which show the largest amplitude ISS are also more intrinsically variable. This finding, yet to be published, indicates that intrinsic source compactness, core dominance and beaming are important factors for ISS, in addition to the properties of the ISM on a particular line of sight.

ESEs may be distinguished from intrinsic variability or "normal" ISS through their strong frequency dependence, the presence of caustics at frequencies of at least a few GHz, and the overall time-symmetric behaviour in the light curves, including a sharp flux density decrease (see Figure 3). As discussed in Section 2.2.2, identifying ESEs as they occur is critical to address the nature of the lensing structures responsible, by obtaining detailed follow-up observations at high angular resolution and at other wavelengths.

Observations of variability, both intrinsic and due to ISS, may additionally provide a means of distinguishing between emission due to AGN and star formation for large samples of the faint radio source population. The survey speed of SKA will enable high cadence monitoring of sample sizes vastly in excess of what is achievable with existing telescopes.

PoS(AASKA14)058

3. Time domain studies of AGN with the SKA

3.1 Source statistics - expected rates of variability

The VLA FIRST Survey (Becker et al. 1995) measured an average source density of ~ 90 per square degree down to 1 mJy at 1.4 GHz, the vast majority of which are AGN. Below this flux density, star forming galaxies become more numerous, although a significant fraction of sources are found to be AGN-driven (see e.g. Figure 4 of Norris et al. 2011, and references therein). The mJIVE-20 VLBA Survey of FIRST sources (Deller & Middelberg 2014) found an increasing fraction of compact components down to 1 mJy, with 30-35% of sources being core-dominated and $\sim 10\%$ being completely compact. Such compact sources are likely to be variable. Deller & Middelberg (2014) obtained a lower limit on the highly variable source fraction at 1.4 GHz based on the number of sources which showed an increase in the VLBI flux density over the VLA FIRST Survey flux density measured some 10–15 years earlier. This number is an underestimate of the true number of variables because the different resolutions of the VLA and the VLBA mean that only a relatively large increase in flux density of core-dominated sources could be measured, since an observed decrease in flux density could be entirely due to resolution effects rather than variability. Based on this, a conservative lower limit to the variable fraction at 1.4 GHz, for $> 25\%$ variability on timescales of years, is 0.7% of *all* radio sources in the 1–20 mJy range. This is in agreement with results from comparing flux densities for sources detected in multiple epochs of the FIRST survey, where around 0.6% of sources vary by 25% or more (Thyagarajan et al. 2011). Down to flux density levels of 40 μJy, Mooley et al. (2013) found 1% of unresolved sources variable at the 4σ level on timescales from 1 day to 3 months, with no evidence that the fractional variability changes along with the known transition of radio-source populations below 1 mJy. Optical identifications showed the variable radio emission to be associated with the central regions of an AGN or star-forming galaxy.

The fraction of sources identified as variable naturally increases as source lightcurves are measured with higher precision and over a wider range of timescales and frequencies. Close to the detection threshold of any survey, it is difficult to determine whether a source is variable or not (see, e.g. fig. 26 of Croft et al. 2013, for a quantitative example for the case of the Allen Telescope Array). A strawman survey with SKA1-SUR or SKA1-MID in band 2, ~ 1.2 GHz, would be capable of surveying the entire visible sky every day to an RMS sensitivity of around 100 μJy beam^{-1}, enabling 10σ detections of variability at the 50% level for sources brighter than ~ 2 mJy. Almost all of these sources will be AGN. Of order 10^6 sources, similar to the entire catalogs of previous surveys such as FIRST and NVSS, could be monitored for such variability on a daily basis, or larger numbers of fainter sources by binning data. For bright sources, high-precision lightcurves in total as well as polarized flux density will enable measurements of variability with an order of magnitude or more better precision than is possible with existing facilities. The accuracy and stability of calibrated flux density measurements is a critical parameter here; as an example, the MASIV VLA Survey achieved $< 1\%$ rms stability over each observing session. Because of the large number of available in-beam calibrators, many of which will be steep-spectrum and not significantly variable, in principle SKA instruments should be able to achieve at least this level of precision for flux density measurements, but careful implementation of calibration procedures will be required.

PoS(AASKA14)058

At flux densities $\lesssim 1$ mJy, the population begins to transition from AGN-dominated to starburst-dominated, although even at 1.4 GHz flux densities of $\sim 50\mu$Jy, AGN still make up $\sim 25\%$ of radio sources (Seymour et al. 2008). Starburst galaxies are not expected to be variable at radio wavelengths, with the exception of rare transient events such as radio supernovae, but low-luminosity AGN—including those that are technically classified as "radio-quiet" but nevertheless have low-power radio emission—will still be present, both in ordinary galaxies and in some of the starburst galaxies themselves. The high resolution—tens of milliarcseconds—enabled by SKA2 will help to distinguish nuclear point sources from emission due to a surrounding disk, but variability will also be an important clue to the presence of AGN whose emission might otherwise be swamped by the host galaxy. Variability may also be key in identifying and classifying counterparts to sources found by CTA or other high energy facilities, where positional coincidence alone may be insufficient (Giroletti et al. 2015).

3.2 Frequency coverage

Intrinsic AGN variability is more extreme towards higher frequencies. Therefore SKA1-MID band 5, covering 4.6–13.8 GHz, along with two lower frequency bands, would be extremely useful for distinguishing intrinsic from extrinsic changes. While not critical for this work, an expansion to 24 GHz as part of SKA2 would enable monitoring observations at similar frequencies to existing long-term surveys focusing on intrinsic variability (e.g., Fig. 1).

The inclusion of SKA1-MID or SKA1-SUR band 2, covering 1.4 GHz, would allow measurements of H I absorption towards sources undergoing ESEs (section 2.2.2). The optimal frequency range for ESE searches is not yet well determined. Refractive effects are stronger towards lower frequencies, and the "cross-section" for events occurring may also be higher due to larger source sizes, however larger source sizes are also a problem as they result in the ESE light curves being "smeared out". ESEs have also been seen at frequencies as high as 15 GHz (Pushkarev et al. 2013). Ideally, monitoring would be done over a wide range of frequencies; this could be facilitated by the use of sub-arrays observing simultaneously in different frequency bands. The appearance of caustics at frequencies of a few GHz helps to unambiguously identify ESEs (see Figure 3).

For ISS, the largest amplitude variations may be observed close to the transition frequency between weak and strong scattering, typically a few GHz. Weak ISS occurs on shorter timescales than refractive ISS. In general, AGN components are too large to exhibit the narrow-band, short-timescale diffractive ISS observed for pulsars in the strong scattering regime (Dennison & Condon 1981, but see Macquart & de Bruyn 2006).

3.3 Modeling intrinsic variations

In the brightest AGN, blazars, the variability is often modeled with shock-in-jet models (Marscher & Gear 1985; Hughes et al. 1985). Recently, detailed modeling of blazar variability during high activity periods was conducted using 4.8, 8 and 15 GHz total intensity and linear polarization archival data from the University of Michigan Radio Astronomy Observatory (Aller et al. 2014). The variations were modeled with shocks moving down the jet, and the results showed that no extreme jet conditions are required to form the shocks. The jet and shock parameters obtained were also very similar in all sources modeled. Multiple frequencies providing spectral index information and

PoS(AASKA14)058

inclusion of linear polarization were essential for constraining the model parameters. The higher frequencies of SKA1-MID will provide information about the intrinsic variability of a much larger set of AGN, and modeling of a large sample of sources will become possible. In particular, SKA will have unprecedented ability to monitor changes in the weak, typical $V/I < 1\%$, but highly variable circular polarization (CP) component (Homan et al. 2006), a powerful probe of the evolution of magnetic fields in relativistic jets (Agudo et al. 2015). CP is associated with the most compact components of AGN, which are also subject to ISS. Unusually strong and intra-day variable CP has been observed for the BL Lac object PKS 1519−273, with the variability readily explained as ISS of a component with up to 3.8% CP, although the origin of the CP itself is unclear (Macquart et al. 2000).

The great sensitivity of SKA will enable the extension of variability modeling to lower luminosity sources. Monitoring of broad absorption line (BAL) QSOs and other radio quiet objects, such as Mrk 231, has already revealed variations similar to blazars. Although large scale jets and lobes do not develop in these objects, likely due to local environmental conditions—perhaps the presence of the BAL wind, highly energetic flares can still occur close to the core (Reynolds et al. 2009, 2013). However, with few examples, it is difficult to establish if the flaring is a common property in so-called radio quiet AGN. With SKA, the number of low luminosity AGN monitored will be extremely large, allowing detailed studies of the variability and comparison to blazars. This will give insights into the jet formation processes and bridge the gap between variations in jetted systems around stellar-mass black holes and the most extreme blazars.

Another interesting group of fainter AGN that have recently received a lot of attention are the Narrow-Line Seyfert I Galaxies (NLS1). Only 7% of NLS1s are formally radio loud (Komossa et al. 2006), but interestingly the radio loud ones show many similar properties to blazars, for example, several of them are detected in gamma rays by *Fermi* (Abdo et al. 2009). They also show fast variations in their radio light curves, similar to blazars (Foschini et al. 2011; D'Ammando et al. 2012). With SKA we will be able to probe the variability in both radio loud and radio quiet NLS1 objects, shedding light on why some of them are radio loud and others not. If no significant variability is detected, it implies that the sources are not Doppler beamed and are viewed at larger angles to the line of sight.

In general, the large number of AGN observed by SKA will allow statistical analysis of AGN variability over large populations. By calculating the power spectral densities of the light curves, we can gain understanding of the nature of the variations. In cases where significant polarization is detected, we obtain information about the underlying magnetic field structure in these objects. For example, if the polarization angle is stable over a long time period, it implies that large-scale ordered magnetic fields play a role (Aller et al. 2003). The strength of SKA will be the ability to study the variations in a large number of sources over a large luminosity range, shedding light on AGN unification.

3.4 Use case: synoptic surveys with outer antennas of SKA1-MID

It is anticipated that a number of SKA1-MID projects will not make use of the longest available baselines. Using the outer antennas to conduct a monitoring programme while the inner antennas conduct other observational programmes will be an extremely valuable operational mode. The outer antennas could be used for monitoring sufficiently bright targets in order to study their ISS

PoS(AASKA14)058

and intrinsic variability, as well as searching for ESEs (and other transient events). Flexible sub-arraying to allow simultaneous observations at multiple frequencies, and/or of multiple targets, would be an important capability. The value of sub-arraying for time domain work was successfully demonstrated by the MASIV Survey, which used the VLA split into 5 subarrays to monitor ~ 700 fields with two-hourly cadence (Lovell et al. 2003).

3.5 Capabilities of SKA1 with 50% reduced sensitivity

The early science phase of SKA deployment, although not reaching full SKA1 sensitivity, nevertheless represents a huge leap over existing surveys, and a transition between those possible with MWA, MeerKAT, and ASKAP, and the full SKA1. The main effect of 50% reduced sensitivity relative to SKA1 on the surveys discussed here would be a decrease of a factor ~ 3 in the number of sources that could be monitored to a given flux density precision. For programmes where sub-arraying is the desired observing mode, the early science phase would simply use fewer sub-arrays. Limited instantaneous (u,v) coverage of the early roll-out phase may pose problems for the type of snap-shot monitoring observations discussed here; in any case an accurate sky model to sufficient depth will be required to search for variability.

3.6 Prospects for SKA2

Current VLBI surveys reach milliarcsecond resolutions, corresponding to parsec scales in AGN. Resolution of the baseline SKA-MID is an order of magnitude or so poorer. Including sufficient sensitivity on long baselines as part of SKA2 (see Paragi et al. 2015) would enable the expansion of existing monitoring programs to much larger numbers of sources. Polarization capabilities will be particularly important in enabling identification and tracking of jet components, characterizing changes in magnetic fields and their connection to flares, and shedding light on jet composition and the interaction of jets with the ambient medium. Simultaneous monitoring of large numbers of sources in conjunction with high-energy all-sky instruments will enable us to constrain the dissipation of energy during rare AGN outbursts.

One of the limitations of AGN monitoring at high frequencies is the decrease of survey speed with the square of the frequency, assuming single pixel feeds, constant sensitivity, and flat spectrum sources. A factor 20 increase in field of view with SKA2-MID would enable survey speeds at 6 GHz comparable to those with SKA1-MID at 1.4 GHz, enabling the kind of surveys discussed above to be undertaken at these higher frequencies, where intrinsic variability becomes increasingly important.

4. Summary

Variability of AGN provides a powerful probe of the physics of accretion and outflow, as well as the dynamics and structure of our own Galaxy's interstellar medium. The huge leap in survey speed engendered by SKA will enable a precision synoptic view of variability for hundreds of thousands of AGN, an archive of variability statistics for comparison to LSST and other large surveys, and a huge expansion into unexplored parameter space as the study of radio AGN truly enters the wide-field time-domain era. These data will allow us to move from the phenomenology and statistics of radio variability to understanding the physical mechanisms responsible for the

PoS(AASKA14)058

large range of observed variability behaviour. Key capabilities for this work are broad frequency coverage—it is particularly desirable to include the 4.6-13.8 GHz Band 5 on SKA-MID; flexible, independent sub-arrays which can cover different frequency bands; and high angular resolution capability.

Acknowledgments

SDC acknowledges support from the Theodore Dunham, Jr. Grant of the F.A.R. and from the NSF via AST-1009421. TH acknowledges support from the Academy of Finland project number 267324. JYK acknowledges support by a research grant (VKR023371) from VILLUM FONDEN. The Dark Cosmology Centre (DARK) is funded by the Danish National Research Foundation. Part of this research was carried out at the Jet Propulsion Laboratory, California Institute of Technology, under a contract with the National Aeronautics and Space Administration. We thank the reviewers for helpful feedback to improve the manuscript.

References

Abdo, A. A., Ackermann, M., Ajello, M., et al. 2009, *ApJL*, 707, L142

Ackermann, M., Ajello, M., Allafort, A., et al. 2011, *ApJ*, 741, 30

Agudo, I., Böttcher, M., Falcke, H., et al. 2015, "Studies of Relativistic Jets in Active Galactic Nuclei with SKA", in Advancing Astrophysics with the Square Kilometre Array, PoS(AASKA14)093

Aller, M. F., Aller, H. D., & Hughes, P. A. 2003, *ApJ*, 586, 33

Aller, M. F., Hughes, P. A., Aller, H. D., Latimer, G. E., & Hovatta, T. 2014, *ApJ*, 791, 53

Atwood, W. B., Abdo, A. A., Ackermann, M., et al. 2009, *ApJ*, 697, 1071

Becker, R. H., White, R. L., & Helfand, D. J. 1995, *ApJ*, 450, 559

Bignall, H. E., Jauncey, D. L., Lovell, J. E. J., et al. 2003, *ApJ*, 585, 653

Bignall, H. E., Macquart, J.-P., Jauncey, D. L., et al. 2006, *ApJ*, 652, 1050

Brisken, W. F., Macquart, J.-P., Gao, J. J., et al. 2010, *ApJ*, 708, 232

Brunthaler, A., Falcke, H., Bower, G. C., et al. 2005, *A&A*, 435, 497

Burrows, D. N., Kennea, J. A., Ghisellini, G., et al. 2011, *Nature*, 476, 421

Chatterjee, R., Marscher, A. P., Jorstad, S. G., et al. 2011, *ApJ*, 734, 43

Clegg, A. W., Chernoff, D. F., & Cordes, J. M. 1988, in American Institute of Physics Conference Series, Vol. 174, Radio Wave Scattering in the Interstellar Medium, ed. J. M. Cordes, B. J. Rickett, & D. C. Backer, 174–178

Clegg, A. W., Fey, A. L., & Lazio, T. J. W. 1998, *ApJ*, 496, 253

Cognard, I., Bourgois, G., Lestrade, J.-F., et al. 1993, *Nature*, 366, 320

Comerford, J. M., & Greene, J. E. 2014, *ApJ*, 789, 112

Comerford, J. M., Pooley, D., Gerke, B. F., & Madejski, G. M. 2011, *ApJL*, 737, L19

Croft, S., Bower, G. C., & Whysong, D. 2013, *ApJ*, 762, 93

Croft, S., de Vries, W., & Becker, R. H. 2007, *ApJL*, 667, L13

D'Ammando, F., Orienti, M., Finke, J., et al. 2012, *MNRAS*, 426, 317

Deane, R. P., Paragi, Z., Jarvis, M. J., et al. 2014, *Nature*, 511, 57

PoS(AASKA14)058

Deller, A. T., & Middelberg, E. 2014, *AJ*, 147, 14
Dennett-Thorpe, J., & de Bruyn, A. G. 2000, *ApJL*, 529, L65
Dennett-Thorpe, J., & de Bruyn, A. G. 2001, in Astronomical Society of the Pacific Conference Series, Vol. 250, Particles and Fields in Radio Galaxies Conference, ed. R. A. Laing & K. M. Blundell, 133
—. 2002, *Nature*, 415, 57
—. 2003, *A&A*, 404, 113
Dennison, B., & Condon, J. J. 1981, *ApJ*, 246, 91
Donnarumma, I., et al. 2015, "Cross correlation surveys with the Square Kilometre Array", in Advancing Astrophysics with the Square Kilometre Array, PoS(AASKA14)054
Fiedler, R., Dennison, B., Johnston, K. J., Waltman, E. B., & Simon, R. S. 1994, *ApJ*, 430, 581
Fiedler, R. L., Dennison, B., Johnston, K. J., & Hewish, A. 1987a, *Nature*, 326, 675
Fiedler, R. L., Waltman, E. B., Spencer, J. H., et al. 1987b, *ApJ Suppl*., 65, 319
Foschini, L., Ghisellini, G., Kovalev, Y. Y., et al. 2011, *MNRAS*, 413, 1671
Fromm, C. M., Perucho, M., Ros, E., et al. 2011, *A&A*, 531, A95
Giroletti, M., et al. 2015, "The connection between radio and high energy emission in black hole powered systems in the SKA era", in Advancing Astrophysics with the Square Kilometre Array, PoS(AASKA14)153
Haiman, Z., Kocsis, B., & Menou, K. 2009, *ApJ*, 700, 1952
Heiles, C. 1997, *ApJ*, 481, 193
Hill, A. S., Stinebring, D. R., Asplund, C. T., et al. 2005, *ApJL*, 619, L171
Homan, D. C., Kovalev, Y. Y., Lister, M. L., et al. 2006, *ApJL*, 642, L115
Hopkins, P. F., & Elvis, M. 2010, *MNRAS*, 401, 7
Hovatta, T., Aller, M. F., Aller, H. D., et al. 2014, *AJ*, 147, 143
Hovatta, T., Lister, M. L., Aller, M. F., et al. 2012, *AJ*, 144, 105
Hovatta, T., Tornikoski, M., Lainela, M., et al. 2007, *A&A*, 469, 899
Hughes, P. A., Aller, H. D., & Aller, M. F. 1985, *ApJ*, 298, 301
Hughes, P. A., Aller, H. D., & Aller, M. F. 1992, *ApJ*, 396, 469
Hughes, P. A., Aller, H. D., & Aller, M. F. 1998, *ApJ*, 503, 662
Jauncey, D. L., Kedziora-Chudczer, L. L., Lovell, J. E. J., et al. 2000, in Astrophysical Phenomena Revealed by Space VLBI, ed. H. Hirabayashi, P. G. Edwards, & D. W. Murphy, 147–150
Jauncey, D. L., & Macquart, J.-P. 2001, *A&A*, 370, L9
Jenkins, E. B., & Tripp, T. M. 2001, *ApJ Suppl*., 137, 297
Kara, E., Errando, M., Max-Moerbeck, W., et al. 2012, *ApJ*, 746, 159
Kardashev, N. S., Khartov, V. V., Abramov, V. V., et al. 2013, Astronomy Reports, 57, 153
Karouzos, M., Jarvis, M. J., & Bonfield, D. 2014, *MNRAS*, 439, 861
Kedziora-Chudczer, L., Jauncey, D. L., Wieringa, M. H., et al. 1997, *ApJL*, 490, L9
Kedziora-Chudczer, L. L., Jauncey, D. L., Wieringa, M. H., Tzioumis, A. K., & Reynolds, J. E. 2001, *MNRAS*, 325, 1411
King, O. G., Hovatta, T., Max-Moerbeck, W., et al. 2013, *MNRAS*, 436, L114
Koay, J. Y., & Macquart, J.-P. 2014, *MNRAS*, accepted. arXiv:1410.7612 [astro-ph]
Koay, J. Y., Macquart, J.-P., Rickett, B. J., et al. 2012, *ApJ*, 756, 29
—. 2011, *AJ*, 142, 108

PoS(AASKA14)058

Kocevski, D. D., Faber, S. M., Mozena, M., et al. 2012, *ApJ*, 744, 148
Komossa, S., Burwitz, V., Hasinger, G., et al. 2003, *ApJL*, 582, L15
Komossa, S., Voges, W., Xu, D., et al. 2006, *AJ*, 132, 531
Krauß, F., Müller, C., Kadler, M., et al. 2013, ArXiv e-prints
Kudryavtseva, N. A., Gabuzda, D. C., Aller, M. F., & Aller, H. D. 2011, *MNRAS*, 415, 1631
Kulkarni, S. R., & Heiles, C. 1988, Neutral hydrogen and the diffuse interstellar medium, 95–153
Lazio, T. J. W., Cordes, J. M., de Bruyn, A. G., & Macquart, J.-P. 2004, *New A Rev.*, 48, 1439
Lazio, T. J. W., Fey, A. L., Dennison, B., et al. 2000, *ApJ*, 534, 706
Lazio, T. J. W., Gaume, R. A., Claussen, M. J., et al. 2001a, *ApJ*, 546, 267
Lazio, T. J. W., Waltman, E. B., Ghigo, F. D., et al. 2001b, *ApJ Suppl.*, 136, 265
Lestrade, J.-F., Rickett, B. J., & Cognard, I. 1998, *A&A*, 334, 1068
Lister, M. L., Aller, H. D., Aller, M. F., et al. 2009a, *AJ*, 137, 3718
Lister, M. L., Aller, M. F., Aller, H. D., et al. 2013, *AJ*, 146, 120
Lister, M. L., Homan, D. C., Kadler, M., et al. 2009b, *ApJL*, 696, L22
Lovell, J. E. J., Jauncey, D. L., Bignall, H. E., et al. 2003, *AJ*, 126, 1699
Lovell, J. E. J., Rickett, B. J., Macquart, J.-P., et al. 2008, *ApJ*, 689, 108
MacLeod, C. L., Ivezić, Ž., Kochanek, C. S., et al. 2010, *ApJ*, 721, 1014
Macquart, J.-P., & de Bruyn, A. G. 2006, *A&A*, 446, 185
Macquart, J.-P., Godfrey, L. E. H., Bignall, H. E., & Hodgson, J. A. 2013, *ApJ*, 765, 142
Macquart, J.-P., Kedziora-Chudczer, L., Rayner, D. P., & Jauncey, D. L. 2000, *ApJ*, 538, 623
Maitia, V., Lestrade, J.-F., & Cognard, I. 2003, *ApJ*, 582, 972
Manzer, L. H., & De Robertis, M. M. 2014, *ApJ*, 788, 140
Marscher, A. P., & Gear, W. K. 1985, *ApJ*, 298, 114
Metzger, B. D., Giannios, D., & Mimica, P. 2012, *MNRAS*, 420, 3528
Milosavljević, M., & Merritt, D. 2001, *ApJ*, 563, 34
Mooley, K. P., Frail, D. A., Ofek, E. O., et al. 2013, *ApJ*, 768, 165
Morgan, J. S., Argo, M. K., Trott, C. M., et al. 2013, *ApJ*, 768, 12
Mundell, C. G., Ferruit, P., Nagar, N., & Wilson, A. S. 2009, *ApJ*, 703, 802
Murphy, T., Chatterjee, S., Kaplan, D. L., et al. 2013, *PASA*, 30, 6
Nieppola, E., Tornikoski, M., Valtaoja, E., et al. 2011, *A&A*, 535, A69
Norris, R. P., Hopkins, A. M., Afonso, J., et al. 2011, *PASA*, 28, 215
Ofek, E. O., & Frail, D. A. 2011, *ApJ*, 737, 45
Ojha, R., Kadler, M., Böck, M., et al. 2010, *A&A*, 519, A45
O'Shaughnessy, R., Kaplan, D. L., Sesana, A., & Kamble, A. 2011, *ApJ*, 743, 136
Paragi, Z., et al. 2015, "Very Long Baseline Interferometry with the SKA", in Advancing Astrophysics with the Square Kilometre Array, PoS(AASKA14)143
Pen, U.-L., & King, L. 2012, *MNRAS*, 421, L132
Pursimo, T., Ojha, R., Jauncey, D. L., et al. 2013, *ApJ*, 767, 14
Pushkarev, A. B., Kovalev, Y. Y., Lister, M. L., et al. 2013, *A&A*, 555, A80
Qian, S.-J., & Zhang, X.-Z. 2001, *ChJAA*, 1, 133
Reynolds, C., Punsly, B., Kharb, P., O'Dea, C. P., & Wrobel, J. 2009, *ApJ*, 706, 851
Reynolds, C., Punsly, B., O'Dea, C. P., & Hurley-Walker, N. 2013, *ApJL*, 776, L21
Richards, J. L., Hovatta, T., Max-Moerbeck, W., et al. 2014, *MNRAS*, 438, 3058

PoS(AASKA14)058

Richards, J. L., Max-Moerbeck, W., Pavlidou, V., et al. 2011, *ApJ Suppl.*, 194, 29
Rickett, B. J., Kedziora-Chudczer, L., & Jauncey, D. L. 2002, *ApJ*, 581, 103
Rickett, B. J., Lazio, T. J. W., & Ghigo, F. D. 2006, *ApJ Suppl.*, 165, 439
Rickett, B. J., Witzel, A., Kraus, A., Krichbaum, T. P., & Qian, S. J. 2001, *ApJL*, 550, L11
Rodriguez, C., Taylor, G. B., Zavala, R. T., et al. 2006, *ApJ*, 646, 49
Romani, R. W., Blandford, R. D., & Cordes, J. M. 1987, *Nature*, 328, 324
Savolainen, T., Homan, D. C., Hovatta, T., et al. 2010, *A&A*, 512, A24
Savolainen, T., & Kovalev, Y. Y. 2008, *A&A*, 489, L33
Seymour, N., Dwelly, T., Moss, D., et al. 2008, *MNRAS*, 386, 1695
Stevens, J., Edwards, P. G., Ojha, R., et al. 2012, ArXiv e-prints
Teräsranta, H., Wiren, S., Koivisto, P., Saarinen, V., & Hovatta, T. 2005, *A&A*, 440, 409
Thyagarajan, N., Helfand, D. J., White, R. L., & Becker, R. H. 2011, *ApJ*, 742, 49
Tuntsov, A. V., Bignall, H. E., & Walker, M. A. 2013, *MNRAS*, 429, 2562
Valtonen, M. J., Lehto, H. J., Nilsson, K., et al. 2008, *Nature*, 452, 851
van Velzen, S., Farrar, G. R., Gezari, S., et al. 2011, *ApJ*, 741, 73
Walker, M., & Wardle, M. 1998, *ApJL*, 498, L125
Walker, M. A. 1998, *MNRAS*, 294, 307
Walker, M. A., Koopmans, L. V. E., Stinebring, D. R., & van Straten, W. 2008, *MNRAS*, 388, 1214
Waltman, E. B., Fiedler, R. L., Johnston, K. J., et al. 1991, *ApJ Suppl.*, 77, 379
Wiita, P. J. 2011, Journal of Astrophysics and Astronomy, 32, 147
Zamaninasab, M., Clausen-Brown, E., Savolainen, T., & Tchekhovskoy, A. 2014, *Nature*, 510, 126
Zauderer, B. A., Berger, E., Soderberg, A. M., et al. 2011, *Nature*, 476, 425
Zuo, W., Wu, X.-B., Liu, Y.-Q., & Jiao, C.-L. 2012, *ApJ*, 758, 104

PoS(AASKA14)058

PROCEEDINGS OF SCIENCE

Core-collapse and Type Ia supernovae with the SKA

M.A. Pérez-Torres[*1,2,3], **A. Alberdi**[1], **R. J. Beswick**[4], **P. Lundqvist**[5], **R. Herrero-Illana**[1], **C. Romero-Cañizales**[6,7], **S. Ryder**[8], **M. della Valle** [9], **J. Conway**[10], **J.M. Marcaide**[11,12], **S. Mattila**[13], **T. Murphy**[14], **E. Ros**[15,11,16]

[1] *Instituto de Astrofísica de Andalucía (IAA-CSIC), E-18008 Granada, Spain*
[2] *Centro de Estudios de la Física del Cosmos de Aragón, E-44001 Teruel, Spain*
[3] *Depto. de Física Teórica, Facultad de Ciencias, Universidad de Zaragoza, E-50009, Spain*
[4] *Jodrell Bank Centre for Astrophysics/e-MERLIN, The University of Manchester, M13 9PL, UK*
[5] *Stockholms Observatorium, Sweden*
[6] *Instituto de Astrofísica, Pontificia Universidad Católica de Chile, Macul, Santiago, Chile*
[7] *Millennium Institute of Astrophysics, Vicuña Mackenna 4860, 7820436 Macul, Santiago, Chile*
[8] *Australian Astronomical Observatory, P.O. Box 915 North Ryde NSW 1670, Australia*
[9] *Osservatorio Astronomico di Capodimonte - INAF, 80131 Napoli, Italy*
[10] *Onsala Space Observatory, Chalmers, Tekniska Högskola, SE-439 92 Onsala, Sweden*
[11] *Dept. Astronomia i Astrofisica, Universitat de València, E-46100 Burjassot, Spain*
[12] *DIPC, Paseo Manuel Lardizabal, Donostia-San Sebastián, Spain*
[13] *Finnish Centre for Astronomy with ESO (FINCA), University of Turku, FI-20014, Finland*
[14] *The University of Sydney, 44 Rosehill Street, NSW 2006, Australia*
[15] *Max-Planck-Institut für Radioastronomie, Auf dem Hügel 69, D-53121 Bonn, Germany*
[16] *Observatori Astronòmic, Universitat de València, E-46980 Paterna, Valéncia, Spain*
E-mail: torres@iaa.es

Core-collapse SNe (CCSNe): Systematic searches of radio emission from CCSNe are still lacking, and only targeted searches of radio emission from just some of the optically discovered CCSNe in the local universe have been carried out. Optical searches miss a significant fraction of CCSNe due to dust obscuration; CCSN radio searches are thus more promising for yielding the complete, unobscured star-formation rates in the local universe. The SKA yields the possibility to piggyback for free in this area of research by carrying out commensal, wide-field, blind transient survey observations. SKA1-SUR should be able to discover several hundreds of CCSNe in just one year, compared to about a dozen CCSNe that the VLASS would be able to detect in one year, at most. SKA, with an expected sensitivity ten times that of SKA1, is expected to detect CCSNe in the local Universe by the thousands. Therefore, commensal SKA observations could easily result in an essentially complete census of all CCSNe in the local universe, thus yielding an accurate determination of the volumetric CCSN rate. **Type Ia SNe:** We advocate for the use of the SKA to search for the putative prompt (∼first few days after the explosion) radio emission of any nearby type Ia SN, via target-of-opportunity observations. The huge improvement in sensitivity of the SKA with respect to its predecessors will allow to unambiguously discern which progenitor scenario (single-degenerate vs. double-degenerate) applies to them.

Advancing Astrophysics with the Square Kilometre Array,
June 8-13, 2014
Giardini Naxos, Sicily, Italy

PoS(AASKA14)060

1. Why CCSN searches in the radio?

The limited sensitivity of pre-eMERLIN/VLA interferometric arrays has biased past radio observations of CCSNe towards the brightest events, preventing any systematic radio follow-up of CCSNe of all types. The exception has been that of Type Ib/c SNe, which due to their GRB link have been the subject of a systematic monitoring with the VLA (see, e.g., Bietenholz et al. 2014; Soderberg et al. 2006). All this makes the currently existing radio observations of CCSNe of rather limited use

In this chapter, we argue that a commensal, wide-field, transient survey with the SKA could potentially allow us to obtain a complete census of CCSNe in the local universe, and therefore will permit us to determine the true CCSN rate and thus the star-formation rate of the population of massive stars in the local universe. In addition, some specific, relevant questions that will be tackled by those observations include the following:

- *Obtaining an accurate estimate of the true volumetric CCSN rate in the local universe*, $\Re$. Wide-field SKA observations covering a significant area of the sky will discover many CCSNe in the nearby universe, and therefore will allow us to determine this relevant parameter (see Fig. 1).

- *Probing the SN-CSM interaction for all CCSN types*, from the relatively faint Type IIP to the extremely radio bright Type IIn SNe (Fig.2). Probing the SN-CSM interaction for all CCSN types will allow us to obtain basic, crucial information to characterize their progenitors, including mass-loss rates and, for synchrotron-self-absorbed SNe, the shock radius and the magnetic field–directly from the light curves (see, e.g., Chevalier 1998).

- *Bridging the gap between Type Ibc SNe and (long) γ-ray bursts*. Type Ibc are arguably the CCSNe that show the highest blastwave speeds, yet most of them are energetically much less powerful than GRBs. Recently, however, cases like SN 2009bb, with $\beta \sim 0.9$ and energy $\sim 10^{49}$ erg seem to be intermediate cases. These "engine-driven" CCSNe could be detected with the high-sensitivity offered by the SKA, thus filling this gap in the energy-blastwave velocity parameter space of SNe-GRBs (see, e.g., Gal-Yam et al. (2006) and references therein).

- *Typing CCSNe from their radio behaviour.* A systematic monitoring could permit us to type CCSNe from their radio emitting properties. This is crucial for the study of the hidden SN population in (Ultra)Luminous Infra-Red Galaxies, where a spectroscopical classification, or even an optical discovery, is essentially impossible (see, e.g., Mattila et al. (2012) and Fig.1).

- *Unveiling the hidden CCSN population.* Horiuchi et al. (2011) found out an apparent mismatch between the measured CCSN rate (mostly from optical observations) and the cosmic massive star formation rate, which was twice as large as the measured one. However, Mannucci et al. (2007) and Mattila et al. (2012) have shown that a significant fraction of the exploding CCSNe in the local universe are hidden behind dust, and that this fraction seems to increase significantly as one goes back in the history of the universe (see Fig. 1, left panel),

*Speaker.

PoS(AASKA14)060

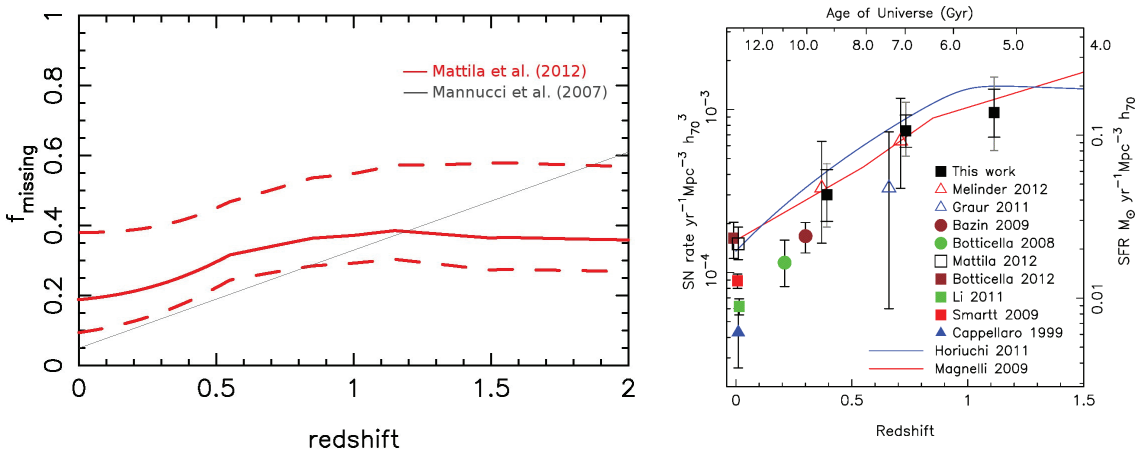

Figure 1: *Left:* Fraction of CCSNe missed by rest-frame optical searches as a function of redshift. The red lines show the best estimate (solid line) together with the upper and lower bounds of the missing fraction as dashed lines. The solid black line corresponds to the missing fraction from Mannucci et al. (2007). (Figure from Mattila et al. 2012.) *Right:* Core-Collapse Supernova rate as a function of redshift. (Figure from Dahlen et al. 2012.) The use of the SKA as a CCSN discovery machine willl reduce the relatively large uncertainty in the missing fraction of CCSNe in the local universe (left figure), as well as in the volumetric CCSN rate (right figure).

i.e., there seems to be no mismatch when the *hidden CCSNe* are taken into account. The results obtained by Mattila et al. (2012) were mostly based on high spatial resolution near-IR and radio observations of the local LIRG Arp 299, and showed that the combination of near-IR and radio observations with high angular resolution are very useful to study CCSNe in LIRGs (e.g. Kankare et al. 2014; Romero-Cañizales et al. 2014). Radio observations have the advantage over both optical and near-IR that the emission from CCSNe is not hampered by dust, and thus offers an excellent opportunity to determine the true core-collapse supernova rate in the local universe. In fact, most of the the CCSNe that explode in the compact, central regions of luminous and ultra-luminous infrared galaxies can essentially be found only at radio wavelengths, e.g. SN 2000ft in NGC 7469 (Alberdi et al. 2006; Colina et al. 2001), or the many CCSNe unveiled by radio observations in Arp 299A (Bondi et al. 2012; Pérez-Torres et al. 2009a), Arp 299B (Romero-Cañizales et al. 2011), or Arp 220 (Batejat et al. 2011; Parra et al. 2007).

- *Correlating optical and radio properties.* The combined use of optical information for both SN and host galaxy, together with the obtained peak (radio) luminosities will allow us to check whether there is a correlation between the optical and radio properties of CCSNe, as well as with their host galaxies. This will be possible by, e.g., making a combined, commensal, use of wide-field surveys programmed at radio wavelengths with SKA, and at optical wavelengths with, e.g., the LSST or similar telescopes. Obviously, the most interesting cases will likely be subject of targeted, monitoring observations with these and other facilities. For example, Gal-Yam et al. (2006) clearly showed the impact of carrying radio and optical follow-up observations of all possible radio transients discovered in surveys covering a

PoS(AASKA14)060

significant fraction of the sky area, in terms of GRBs and SNe studies.

2. Radio emission from CCSNe

In this section we give account of the radio emitting properties, which are crucial to understand the technical issues discussed in the remaining sections.

CCSNe result from both single and binary massive star systems, with initial masses $\gtrsim 8$ $M_\odot$, and include a diversity of spectroscopically divided subtypes (Type IIP/L, IIn, IIb, Ib/c; see e.g. Eldridge et al. 2013). Upon gravitational collapse of the core, the outer parts of the shell are ejected at very high speeds, $v \approx 10000\,(E_{\rm in}/10^{51}{\rm erg})^{1/2}\,(M_{\rm ej}/1{\rm M}_\odot)^{-1/2}$ km s^{-1}, and the interaction with the outer, much less dense, material of the progenitor star, drives a blastwave that propagates at speeds as high as $v_s \simeq (0.1-0.3)c$ (e.g., Matzner & McKee 1999). This high-speed shock heats the circumstellar material to temperatures of $\sim 10^9$ K. In addition, a reverse shock propagates back into the stellar envelope at speeds of 500-1000 km s^{-1} relative to the expanding ejecta.

When the supernova shock-wave ploughs through the circumstellar gas, a high-energy density shell forms. Within this shell, electrons are accelerated to relativistic speeds and significant magnetic fields are generated, giving rise to the production of the observed radio emission. The radio emission from supernovae is essentially non-thermal synchrotron emission from relativistic electrons, and is due to circumstellar interaction (e.g., Chevalier 1982). In the framework of the SN-circumstellar interaction scenario, the optically thin radio emission from CCSNe scales with the mass-loss wind parameter, $\mathscr{M} = \dot{M}/v_w$, where $\dot{M}$ and v_w are the pre-supernova mass-loss rate and wind speed, respectively. Thus, for the radio emission to be appreciable, the progenitor star must have lost a significant amount of mass via a stellar wind and/or stripping due to a close companion. The presupernova stellar wind speed plays an equally important role: the smaller the wind speed, the more mass is retained in the vicinities of the SN progenitor, and the stronger the circumstellar interaction will be. According to their $\mathscr{M}$ value, CCSNe can be divided into two basic groups: Type Ib/c SNe, which have expelled fast winds ($v_w \approx 1000$ km s^{-1}), have $\mathscr{M} \sim 10^{-8}\,{\rm M}_\odot\,{\rm yr}^{-1}/\,{\rm km\,s}^{-1}$, thus implying $\dot{M} \sim 10^{-5}\,{\rm M}_\odot\,{\rm yr}^{-1}$ during their blue supergiant phase. Type II SNe are characterized by significantly slower ($v_w \approx 10$ km s^{-1}) winds, although the large differences in mass-loss rates $\dot{M} \sim (10^{-4}-10^{-6})\,{\rm M}_\odot\,{\rm yr}^{-1}$ result in a large scatter in $\mathscr{M} \sim (10^{-5}-10^{-7})\,{\rm M}_\odot\,{\rm yr}^{-1}/\,{\rm km\,s}^{-1}$ during their red supergiant phase, which affects the time at which they reach their peak radio luminosity.

This pre-supernova wind, made of thermal electrons, has a power-law density profile, which for a steady, spherically symmetric wind has the following form: $\rho_{\rm CSM} \propto r^{-2}$. This circumstellar wind is the main responsible for the partial suppression of synchrotron radio emission from supernovae (e.g., Chevalier 1982), so that the radio flux density evolution of many CCSNe can be well described by the following equation (e.g., Weiler et al. 2002)

$$S_\nu(t) = K_1 \left(\frac{\nu}{5{\rm GHz}}\right)^\alpha \left(\frac{t-t_0}{1{\rm day}}\right)^\beta e^{-\tau_\nu}, \qquad (2.1)$$

where τ_ν is the optical depth due to external absorption, which for the sake of simplicity is taken to be due only to the (thermal) electrons of the pre-supernova wind and of a possible distant H II region. The optical depth can then be written as

PoS(AASKA14)060

Table 1: Radio parameters of core-collapse supernovae

SN Type	$f_{\rm CCSN}$	α	β	δ	$t_{\rm peak(days)} \times (\nu/5\ {\rm GHz})$	$L_{\nu,{\rm peak}}/(10^{27}{\rm erg\,s^{-1}\,Hz^{-1}})$
Ib/c	26.0%	-1.1	-1.4	-2.5	2 - 100	0.02 – 20
IIb	12.1%	-1.1	-1.0	-2.0	180	2 – 5
IIP	55.5%	-0.7	$-(0.7$ - $1.2)$	-3.0	30 – 500	0.2 – 1
IIL	3.0%	-0.7	-0.8	$-(2.7$ - $3.0)$	100 – 800	1 – 30
IIn	2.4%	-0.7	$-(1.3$ - $1.7)$	-3.0	$\gtrsim 800$	10 – 20
87A-like	1.0%	-1.0	...	-3.0	$\sim$2	0.004

$$\tau_\nu = \left(\frac{\nu}{5{\rm GHz}}\right)^{-2.1}\left[K_2\left(\frac{t-t_0}{1{\rm day}}\right)^{\delta}+K_3\right], \tag{2.2}$$

where the first term accounts for the time varying external absorption, which continuously decreases (since $\rho_{\rm CSM} \propto r^{-2}$), and the second term allows for a non-varying absorber, i.e., a distant H II region. The former term is usually the one that dominates in most CCSNe, but cases where the latter term dominates also exist, e.g., SN 2000ft in NGC 7469 (Alberdi et al. 2006; Pérez-Torres et al. 2009b), or some of the SNe in Arp 299A (Pérez-Torres et al. 2009a, 2010). (Synchrotron self-absorption seems to be the dominant mechanism in many Type Ib/c SNe; however, this does not affect the discussion below, so for the sake of simplicity we only consider here external absorbers.)

In Table 1 we present typical values for the relevant radio emission parameters in Eqs. 2.1 and 2.2, based on those published in Weiler et al. (2002) and Romero-Cañizales et al. (2014) for a sample of CCSNe. Stripped-envelope SNe (i.e., Type Ib/c and, to some extent, their cousins, Type IIb SNe) have an optically thin spectral index, α ($S_\nu \propto \nu^\alpha$), which is steeper than the spectral index of Type II SNe. The combination of high blastwave speed and stripped envelope in Type Ib/c events (and also in Type IIbc supernovae) explains their very short times to peak and their swift radio evolution (steep values of β), compared to the rest of CCSNe.

The tabulated fraction of each CCSN type is taken from Eldridge et al. (2013), which used CCSNe discovered between 1998.00 and 2012.25 (14.25yr) in galaxies with recessional velocities less than 2000 km s^{-1}. Type Ibc SNe make up $\sim$ 26% of all CCSNe in the local universe. $\sim$57% of all CCSNe are faint radio SNe, i.e., the Type IIP SNe and the peculiar Type II SNe, e.g., SN 1987A; $\sim$15% are the moderately bright Type IIb and Type IIL SNe, and only $\lesssim$ 3% are type IIn SNe, the brightest radio events (see Table 1 and Figure 2).

Type IIn SNe show peak luminosities $L_{\rm peak} \gtrsim (1-2)\times 10^{28}$ erg s^{-1} Hz^{-1}, while Type Ib/c and Type IIb SNe peak at values of a few times 10^{27} erg s^{-1} Hz^{-1}. Together, these bright CCSNe account for less than 30% of all radio supernovae. Most of the remaining $\sim$70% are type IIP SNe, which are significantly fainter radio supernovae, with peak luminosities $\lesssim$ few times 10^{26} erg s^{-1} Hz^{-1}(see Fig. 2).

3. CCSN searches with the SKA

In this section, we discuss in detail the advantages of a commensal, wide-field, transient survey with the SKA with respect to currently envisioned efforts with other facilities.

PoS(AASKA14)060

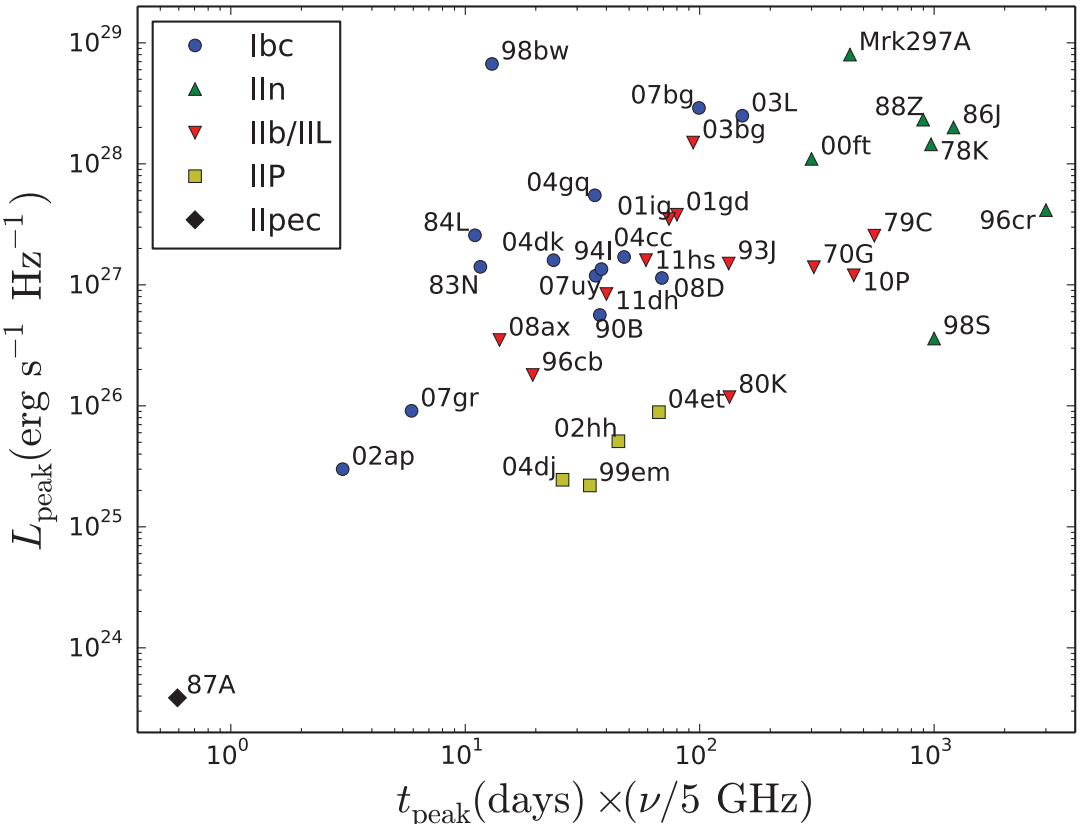

Figure 2: *Peak spectral radio luminosity of CCSNe vs. time to peak, times the observing frequency. There is a clear correlation between time to the peak and the luminosity at the peak; in this parameter space, each subtype of CCSNe are located in specific areas; CCSNe show typical peak radio luminosities above* 10^{26} *erg* s^{-1} *Hz*$^{-1}$*, except Type IIP SNe, which usually peak at a few times* 10^{25} *erg* s^{-1} *Hz*$^{-1}$*, and the very rare 87A-like events. Figure adapted from Chevalier et al. (2006) and Romero-Cañizales et al. (2014).*

In fact, several wide-field sky surveys will be carried out with the SKA pathfinders MeerKAT and ASKAP, as well as with the upgraded Very Large Array. Those surveys can be used commensally for transient studies, by profitting from programmed wide-field observations. For example, the planned Very Large Array Sky Survey (VLASS) is contemplating the possibility of observing wide field areas (a few hundreds to about one thousand of square degrees) with nominal sensitivities of $1\sigma \simeq 100\mu$Jy/beam per epoch, aiming at reaching r.m.s. values of $\simeq (40-70)\mu$Jy/beam after stacking multi-epoch observations. However, those sensitivities are just too shallow to be of any real use for CCSN studies. Indeed, a 5σ figure of merit corresponds to 500 μJy/beam per epoch, so that the maximum distance to detect a type IIP event would be $\sim$9 Mpc (see Table 3). Unless sky areas close to the full celestial sphere are surveyed–which is very unlikely– VLASS will only pick up a handful of CCSNe after one year of observations (see Sect. 3.1 below). Most likely, this handful of CCSNe will be discovered first by optical searches, and some of them will

PoS(AASKA14)060

Table 2: Relevant observational parameters for the proposed SKA1 designs and comparable telescopes

	eMERLIN	VLA[†]	MeerKAT	ASKAP	SKA1-SUR	SKA1-LOW	SKA1-MID
FoV (deg^2)	0.25	0.25	0.86	30	18	27	0.49
Fiducial Freq. (GHz)	1.4	1.4	1.4	1.4	1.67	0.11	1.67
Resolution (arcsec)	0.15	1.4	11	7	0.9	11	0.22
Baseline/size (km)	220	35	4	6	50	50	200
Bandwidth (MHz)	400	1000	1000	300	500	250	770
Sensitivity (μJy-hr$^{-1/2}$)	27.1	3.9	3.2	28.9	3.7	2.1	0.7

[†]The VLASS 1-σ figure is $\gtrsim 10$ times worse than obtained with one hr of VLA observing time.

be subject of targeted radio observations anyway, given their vicinity. Thus, deeper sensitivies are needed to make a substantial contribution to the field.

3.1 SKA survey strategy for commensal CCSN searches

The best strategy for transient studies with the SKA is one that combines good angular resolution ($\lesssim 1.5$ arc sec) and large field of view, (FoV $\gtrsim$10 deg^2), at frequencies around and above $\sim$1.5 GHz. The SKA1-SUR, which should provide an approximate survey sensitivity of $\lesssim 4.2\mu$Jy/beam after 1-hr of on-source integration (assuming a bandwidth of 500 MHz) for a FoV of $\simeq$18 deg^2, with an angular resolution of $\sim$0.9 arc sec at a fiducial frequency of 1.7 GHz, meets such requirements (see Table 2).

SKA1-SUR is likely to observe the sky for $\gtrsim 1000$ hr in its first year of operations. Thus, depending on the specific observing band (or bands), the surveyed area will lie in the range of $\sim 9000 - 18000$ deg^2. As we explain below, to be of use for CCSNe searches, each field of view should be visited five times (each time for an on-source time of 12 minutes), at a cadence of one visit every $\lesssim$ 90d. The r.m.s. attained per pointing will be of 9.3 μJy/beam per pointing, and the r.m.s. for stacked images will be 4.2 μJy/beam, according to the SKA1-SUR specifications. Such a commensal strategy is likely to result in the largest sample of radio supernovae ever detected in the nearby universe.

3.2 Expectations for CCSN discoveries with wide surveys

Table 3 summarizes the expectations for detecting CCSNe using the VLASS, SKA1-SUR, SKA-50% and SKA. More specifically, we show the maximum distance to which a CCSN is expected to be detected above 5σ, for the nominal r.m.s. values of VLASS ($\sim 100\mu$Jy/beam/pointing) and SKA1-SUR ($\sim 9.3\mu$Jy/beam/pointing), as well as for SKA1-50% (i.e., only half of the bandwidth of SKA1-SUR will be available), and SKA (ten times more sensitive than SKA1). Here, we took the approximate median value of the peak luminosity of each CCSN type. In practice, this means that only half of the quoted values in Table 3 will be detected. The other half would lie below our 5 σ cut and are expected to be missed. In its currently assumed specifications, VLASS will detect Type Ib/c SNe only up to a distance of $\lesssim$58 Mpc, less than half the value quoted in Kamble et al. (2014). SKA1-SUR, on the other hand, will be able to detect Type Ib/c SNe up to $\sim$ 188 Mpc, i.e., a volume $\sim$35 times larger than the volume where the VLASS will be sensitive to Type Ib/c SNe.

PoS(AASKA14)060

For an all-sky survey, the total number of detections in one year can be written as $N_{\rm all-sky} = \Re \times V \times \min[\Delta t_{\rm bright}/\Delta t_{\rm cadence}, 1]$, where $\Re$ is the volumetric rate of CCSNe, $\Delta t_{\rm bright}$ is the time that a CCSN of a given type remains bright above the survey sensitivity, and $\Delta t_{\rm cadence}$ is the cadence time of the observations, respectively. As long as $\Delta t_{\rm bright} \gtrsim \Delta t_{\rm cadence}$, one can be sure that all CSSNe are detected. Since $\Delta t_{\rm bright} \simeq \Delta t_{\rm peak}\, \nu_5^{-1}$ days (see col. 6 in Table 3), then $\Delta t_{\rm cadence} \lesssim \Delta t_{\rm peak}\, \nu_5^{-1}$ days, where $\nu_5 = \nu/5$GHz. The volumetric rate of CCSNe in the local universe ($z \lesssim 0.1$) is $\Re \sim 10^{-4}$ SNe yr^{-1} Mpc^{-3} within a factor of $\sim$2, while at $z \gtrsim 1.0$ the volumetric CCSN rate is $\Re \sim 10^{-3}$ SNe yr^{-1} Mpc^{-3} (see Dahlen et al. 2012 and the right panel of Fig. 1). The total number of CCSNe expected to be detected in one year over the whole sky, in the local universe ($z \lesssim 0.1$), where $\Re \sim 10^{-4}$ SNe yr^{-1} Mpc^{-3} is then $N_{\rm all-sky} \approx 420\, (D_{\rm max}/100\,{\rm Mpc})^3\, \left(\Re/10^{-4}{\rm SNe\,yr^{-1}Mpc^{-3}}\right)$, and the expected number of detections of each CCSN type is $f_{\rm CCSN} \times N_{\rm all-sky}$, where $f_{\rm CCSN}$ is the fraction of each CCSN type (see Table 1). The cadence time is set up by the need to detect the fast-evolving type Ib/c SNe. For a fiducial frequency of 1.7 GHz, the cadence time should thus be no more than $\sim$90 days. Note the huge difference in the number of expected CCSNe to be detected by the VLASS and by SKA1-SUR, which is due to the VLASS being $\simeq$10.8 times less sensitive than SKA1-SUR. Since $N_{\rm det} \propto D_{\rm max}^3 \propto S_\nu^{-3/2}$, the expected number of detections in SKA1-SUR is $\simeq$ 35.3 times larger than for the VLASS.

We used the above expression for $N_{\rm all-sky}$, and combined it with the fraction of SNe from each type (second column in Table 1) to obtain the expected number of detected CCSNe in one year, for a survey covering 10,000 deg^2 (see Table 3). We also took into account the limiting detectable volumes for each CCSN type, according to their approximated median luminosities. The main limitation is due to the relatively small value of the maximum distance that will allow a detection of a type IIP SN, which is why so few detections of them are expected. (Note that the VLASS will need to sample a 10,000 deg^2 area for 25 years to blindly discover just one single type IIP event.) On the contrary, the extremely bright Type IIn supernovae would be detectable, in principle, up to a distance of $\sim$422 Mpc ($z \sim 0.1$) with SKA1, and up to $\sim$1350 Mpc ($z \sim 0.25$) with SKA, assuming a tenfold increment in sensitivity (see Table 3). The relatively high luminosity of spirals at those frequencies ($\sim 7 \times 10^{27}$ erg s^{-1} Hz^{-1}) may prevent unambiguous detection of even Type IIn at those distances with SKA1, as the synthesized beam of 1.0$''$corresponds to 2.1 kpc, which could pick up a significant amount of the galaxy luminosity, thus the need for high angular resolution. This limitation will be overcome once SKA is completed, as is foreseen to have a twentyfold better angular resolution. In addition, one has to take into account that around 10% of the massive star-formation already at $z \sim 0.1$ will come from Luminous Infrared Galaxies (Magnelli et al. 2011). While those galaxies are prolific CCSN factories, their detection with SKA1, or even with SKA, will not be possible in general, as the compact starburst (size $\lesssim$ 500 pc) will have a typical 1.4 GHz brightness well in excess of our 5-σ sensitivity limit. For the sake of simplicity, and to stay on the conservative side, we assume here that we recover all Type IIn SNe up to an effective distance of 250 Mpc with SKA1-SUR and SKA1-50% (see Table 3).

We advocate for SKA1-SUR transient observations at 1.7 GHz, which should provide a survey speed of $\simeq$18 deg^2/hr. Thus, 10,000 deg^2 can be covered in 556 hr, which easily accomodates into surveys like SKA1-SUR. Indeed, the only requirement for such a programme to be successful under SKA1-SUR is that a minimum number of visits are done to the same field to secure the discovery of recently exploded CCSNe by means of their variability. The cadence time would be limited by

PoS(AASKA14)060

Table 3: Expectations for CCSN detections in the local Universe from commensal radio surveys from the VLASS (5-σ = 500 μJy/beam), SKA1-SUR (5-σ = 46.5 μJy/beam), SKA1-50% (5-σ = 66.4 μJy/beam), and SKA (5-σ = 4.65 μJy/beam) assuming each survey observes at a nominal frequency of 1.7 GHz and covers an area of 10,000 deg^2 in one year. $L_{\nu,26} = L_{\nu,\rm peak}/10^{26}$ erg/s/Hz; $\nu_5^{-1} = \nu/5$ GHz

SN Type	$\Delta t_{\rm peak}\,\nu_5^{-1}$	$L_{\nu,26}$	VLASS		SKA1-SUR		SKA1-50%		SKA	
	[days]		$D_{\rm max}$	$N_{\rm det}$	$D_{\rm max}$	$N_{\rm det}$	$D_{\rm max}$	$N_{\rm det}$	$D_{\rm max}$	$N_{\rm det}$
Ib/c	30	20	58	5.1	189	177	159	106	596	5618
IIb, IIL	$\sim$150	10	41	0.8	133	29	112.2	17.4	422	924
IIP	40	0.5	9	0.04	30	1.5	25	0.9	94	47
IIn	1000	100	129	6.6	422	104	355	80	1334	7247
87A	2	0.04	2.6	$\sim 10^{-5}$	8.4	$\sim 10^{-3}$	9	$\sim 10^{-3}$	26.7	0.05
Total				$\sim$13		$\sim$311		$\sim$204		$\sim$13800

peculiar Type II SNe, e.g., SN 1987A, peaking very early after the explosion, but since we will miss them anyway (see Table 3), the cadence time is actually constrained to $\sim$ 90 days by the type Ib/c SNe turnover. This requirement can be easily fulfilled by carrying out five equally spaced 12-min visits of the same field during one year, resulting in an r.m.s. of 9.3 μJy/beam per visit and thus reaching the specified 4.2μJy/beam after five visits (=1 hr on-source).

While the VLASS will detect only $\sim$13 CCSNe after surveying 10,000 deg^2 after one year, SKA1-SUR is expected to detect over 300 CCSNe in one year (see Table 3). SKA1-SUR, unlike VLASS, will not need to cover an extremely huge area to ensure a large number of detections. In fact, Table 3 shows that the VLASS needs to cover an area of $\gtrsim$ 13,000 deg^2 to detect just one single IIb/IIL event in one year; the detection of a single Type IIP from a blind radio survey within the VLASS, would require about six years of observations of the whole sky (or 25 years of the same 10,000 deg^2 field). In short, the handful of radio SNe expected to be detected by the VLASS will most likely be detected anyway by nearby optical searches. Clearly, VLASS-class blind radio surveys will not add much to our knowledge of CCSN radio properties and/or statistics. On the contrary, SKA1-SUR, carried out over $\sim$ 10000 deg^2 with a cadence time of 90 days, should detect about 177 type Ibc SNe, 29 type IIb/IIL, $\sim$1-2 type IIP, and 104 type IIn CCSNe, for a total of $\sim$311 CCSNe in just one year, or about 26 CCSNe per month, for a total on-source time of 556 hr. Assuming a 33% overhead time, the total time needed is of $\sim$740 hr, or 2.0 hr/day for such a commensal, transient survey to be successful.

There are several reasons for the unrealistic predictions made by Kamble et al. (2014) regarding expectations of CCSN detections within the VLASS. Kamble et al. (2014) mimicked the approach of Lien et al. (2011), who fitted the distribution of radio luminosity peaks of about 20 well observed radio supernovae, concluding that the average peak radio luminosity of *all* CCSNe was $\gtrsim 10^{27}$ erg s^{-1} Hz^{-1}. However, as Fig. 2 shows, different types of CCSNe peak at significantly different luminosities, so the predictions of both Lien et al. (2011) and Kamble et al. (2014) were too optimistic. Indeed, Kamble et al. (2014) considered all CCSNe to be type Ib/c, i.e., $f_{\rm Ib/c} = f = 1.0$, while type Ib/c in the local Universe make up about 26% ($f_{\rm Ib/c} = 0.26$) of all CCSNe. Finally, Kamble et al. (2014) assumed that CCSNe are detected at the 1-σ level, which clearly cannot be the case. Actually, for a clear detection, a minimum threshold of five times the off-source r.m.s. will be needed, since the number of independent beams within the 1.7 GHz FoV

PoS(AASKA14)060

will be of several millions with SKA1, and this number will be much larger with the SKA. Therefore, artificial sources above 3σ and approaching a $\sim 5\sigma$ level should be expected, which may result in a substantial fraction of false detections even with a 3 σ threshold.

When the characteristic radio luminosity of each CCSN type is taken into account, as well as their fraction, and a realistic 5-σ detection threshold, numbers get dramatically lower for the intended VLASS in terms of (blind) CCSN radio discoveries. Even for SKA1-SUR, Achille's heel remains the expected low-number statistics for Type IIP SNe, so large areas need to be covered (see Table 3).

3.3 Impact of a "poor man's" SKA1

We now quantify the impact of a decrement by a 50% in the SKA1-SUR specifications (SKA1 50%). If the angular resolution is degraded, this is expected to have a minor effect in terms of CCSN discovery, as most of the SNe in normal, spiral galaxies, will be far from the galaxy nucleus, and therefore should be easily discerned. However, the impact due to a poorer array sensitivity is very relevant. Since $N_{\rm det} \propto S_\nu^{-3/2}$, then a decrement of the available bandwidth by 50% implies a sensitivity decrement by $\sqrt{2}$, and thus a decrement in the number of CCSN detections of almost 40%, if the initial specifications are not observed.

Although the preferred frequencies are $\gtrsim 1.7$ GHz, which optimizes FoV, sensitivity, and angular resolution, as well as permits a cadence time significantly larger than at higher frequencies, any of the currently deep, very wide continuum surveys will have a profound, extremely positive impact in the number of CCSN discoveries. In particular, any of the two All-Sky referenced surveys for SKA1 at band 2 will be very beneficial for CCSN searches. Indeed, both surveys propose to image an area of 31000 deg^2, at $\sim$1.4 GHz, reaching r.m.s. sensitivities of 2 (3) μJy/beam after two years with an angular resolution of $\sim$0.5 ($\sim$2) arcsec resolution. If any of those surveys is performed, observing the cadence-time of $\sim$90 days, this would yield increments in the number of CCSNe expected to be detected with respect to the nominal values in Table 3 for SKA1-SUR by factors of 6 and 11, for the All-Sky surveys with 2μJy/beam and 3μJy/beam sensitivities.

Once SKA is completed, the sensitivity will be about 10 times better than for SKA1, the angular resolution will be about 20 times better, and the FoV around 20 times larger. Therefore, the number of detections is expected to be very close to the number of explosions of all CCSNe in the local universe (see Table 3), and the close to milliarcsecond angular resolution could permit to detect CCSNe even in the dusty environments on (U)LIRGs, thus allowing us to obtain a dust-free, complete census of CCSNe in the local universe. In addition, devoted CCSNe surveys of smaller fields (several degrees to a hundred) with sensitivities of $\sim$ 100 nJy/beam (1 σ) will be possible with very modest observing times. This will allow us to precisely determine the value and evolution of the fundamental parameter $\Re$ as a function of redshift in the relevant redshift range from $z = 0$ to at $z \simeq 1.0$ from radio observations, and compare them with existing estimates (see right panel in Fig. 1).

4. Type Ia supernovae with the SKA

Type Ia SNe are the end-products of white dwarfs (WDs) with a mass approaching, or equal to, the Chandrasekhar limit, which results in a thermonuclear explosion of the star. While it is well

PoS(AASKA14)060

acknowledged that the exploding WD dies in close binary systems, it is still unclear whether the progenitor system is composed of a C+O white dwarf and a non-degenerate star (single-degenerate scenario), or both stars are WDs (double-degenerate scenario). In the single-degenerate scenario, a WD accretes mass from a hydrogen-rich companion star before reaching a mass close to the Chandrasekhar mass and going off as supernova, while in the double-degenerate scenario, two WDs merge, with the more-massive WD being thought to tidally disrupt and accrete the lower-mass WD (see, e.g., Maoz et al. 2013, and references therein). This lack of knowledge makes it difficult to gain a physical understanding of the explosions, and to model their evolution, thus also compromising their use as distance indicators.

4.1 Radio and X-ray observations of SNe Ia

Radio and X-ray observations can potentially discriminate between the progenitor models of SNe Ia. For example, in all scenarios with mass transfer from a companion, a significant amount of circumstellar gas is expected (see, e.g., Branch et al. 1995), and therefore a shock is bound to form when the supernova ejecta are expelled. The situation would then be very similar to circumstellar interaction in core-collapse SNe (see above), where the interaction of the blast wave from the supernova with its circumstellar medium results in strong radio and X-ray emission (Chevalier 1982). On the other hand, the double-degenerate scenario will not give rise to any circumstellar medium close to the progenitor system, and hence essentially no prompt radio emission is expected. Nonetheless, we note that the radio emission increases with time in the double-degenerate scenario, contrary to the single-degenerate scenario. This also opens the possibility for confirming the double-degenerate channel in Type Ia SNe via sensitive SKA observations of decades-old Type Ia SNe.

Radio (e.g., Hancock et al. 2011; Panagia et al. 2006) and X-ray (e.g., Hughes et al. 2007; Russell & Immler 2012) observations of SNe Ia resulted in upper limits on the wind density around SN Ia progenitors of the order of $\dot{M} = 1.2 \times 10^{-7}$ $M_\odot\,yr^{-1}$, assuming a wind velocity of 10 km s^{-1}. At the moment, the deepest radio limits on circumstellar gas come from SNe 2011fe and 2014J. The limits on mass-loss rate from the progenitor system of SN 2011fe are $\dot{M} = 6 \times 10^{-10}$ $M_\odot\,yr^{-1}$ and $\dot{M} = 2 \times 10^{-9}$ $M_\odot\,yr^{-1}$ from radio (Chomiuk et al. 2012) and X-rays (Margutti et al. 2012), respectively, assuming a wind velocity omass-lossf 100 km s^{-1}. Similarly, the mass-loss rate limits for the progenitor system of SN 2014J are $\dot{M} = 7 \times 10^{-10}$ $M_\odot\,yr^{-1}$ and $\dot{M} = 1.2 \times 10^{-9}$ $M_\odot\,yr^{-1}$ from radio (Pérez-Torres et al. 2014) and X-rays (Margutti et al. 2014), respectively, for a wind velocity of 100 km s^{-1}. The above limits permit to rule out all symbiotic systems and the majority of the parameter space associated with stable nuclear burning WDs, as viable progenitor systems for either SN 2011fe or SN 2014J. Recurrent novae with main sequence or subgiant donors cannot be ruled out completely, yet most of their parameter space is also excluded by those radio observations (see Fig. 3.)

4.2 Unveiling the progenitor scenarios of type Ia SNe with the SKA

With the advent of the SKA, we will be able to obtain significantly deeper radio limits, or an eventual detection, for SNe Ia exploding at the distance of M 82. For more distant supernovae, we will be able to obtain similar or even more constraining limits to those obtained for SNe 2011fe

PoS(AASKA14)060

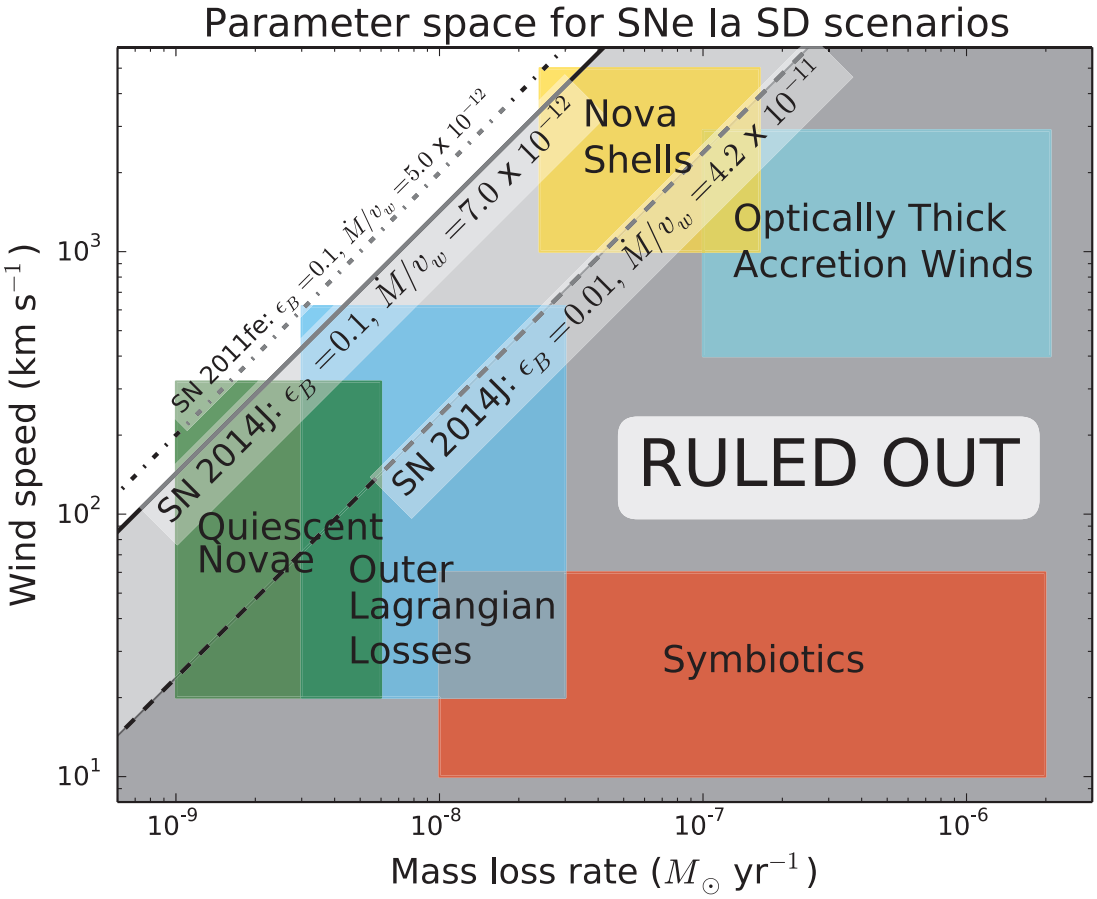

Figure 3: *Constraints on the parameter space (wind speed vs. mass-loss rate) for single degenerate scenarios for SN 2014J (see Pérez-Torres et al. 2014 for details). Progenitor scenarios are plotted as schematic zones, following Chomiuk et al. (2012). We indicate our 3σ limits on $\dot{M}/v_w$, assuming ε_B = 0.1 (solid line) and the conservative case of ε_B = 0.01 (dashed line). Mass loss scenarios falling into the gray-shaded areas should have been detected by the deep radio observations, and therefore are ruled out for SN 2014J. For a comparison, we have included also the limit on SN 2011fe (dash-dotted line) for the same choice of parameters as the solid line for SN 2014J, which essentially leaves only room for quiescent nova emission as a viable alternative among the single-degenerate scenarios for SN 2011fe (see Pérez-Torres et al. (2014) for details).*

and 2014J, which will allow us to build a picture from a larger statistical sample of observed SNe Ia.

The first phase of SKA considers three different surveys: SKA1-LOW, -mid, and -sur (see also Table 2). SKA1-MID, promises to yield 1σ sensitivities of $\sim 0.7\mu$Jy/beam in one hour at a fiducial frequency of 1.7 GHz. This figure is five times better than currently provided by the most sensitive array, the VLA. SKA1-MID will be able to either detect the putative radio emission of SN 2014J-like objects up to distances $\lesssim 8$ Mpc in less than one hour, or put significantly better constraints on the parameter space of single-degenerate scenarios for the next Type Ia SN that explodes at a distance no larger than that to M 82. However, the expected number of SNe Ia per

PoS(AASKA14)060

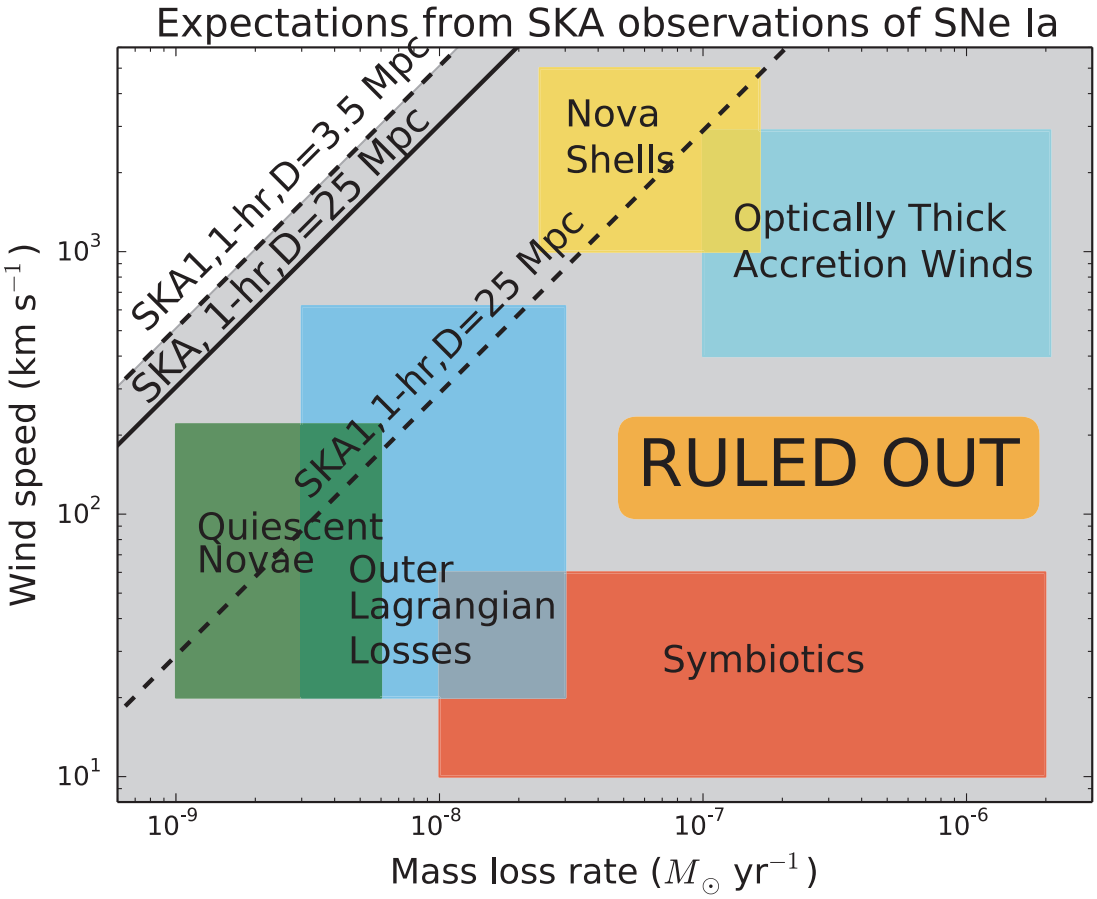

Figure 4: *Constraints on the parameter space (wind speed vs. mass-loss rate) for the same single-degenerate scenarios as in Fig. 3, as expected with SKA1 (dashed lines) and the full SKA (solid line). SKA1 will be able to unambiguously probe all single degenerate scenarios for SNe Ia exploding at distances similar to that of M 82 (3.5 Mpc), and will be more sensitive than current state of the art, deep radio observations of SN 2014J in M 82, up to a distance of 25 Mpc, or even larger. When SKA is completed, we will be able to unambiguously probe the prompt radio emission within the single degenerate scenario up to distances of* $\geq$ *25 Mpc. All lines correspond to 3-*σ.

year in such a volume of the local universe is small. Since the volumetric rate of Type Ia SNe is $\sim 3 \times 10^{-5}$ SN yr^{-1} Mpc^{-3} (Dilday et al. 2010), we should expect on average one Type Ia SN every $\sim$15 yr within a distance of $\lesssim$ 8 Mpc (more than twice the distance to M 82), which is a depressingly small value to get any statistical improvement in a sensible amount of time. Smartt (2009) found 26 Type Ia SNe out of 132 SNe from a 10.5 year-long survey within 28 Mpc. This figure corresponds to about 1 SN Ia every 13 yr within a distance of 8 Mpc, in agreement with the value found by Dilday et al. (2010).

To obtain a statistically significant sample of SNe Ia observed in radio and with similar upper limits to those obtained for SNe 2011fe and 2014J, we need to sample significantly larger volumes and need much more sensitive radio observations. For example, by sampling out to a distance of 25 Mpc, we can expect $\sim$2 SNe Ia per year within this sampled volume, which in 10 years would result

PoS(AASKA14)060

in a total of ∼20 SNe Ia, enough to extract statistical results. At this maximum distance, we need a sensitivity ∼50 times better than obtained by the deep radio observations discussed in Chomiuk et al. (2012) and Pérez-Torres et al. (2014), i.e., 80 nJy/beam (1-σ), to be as constraining. The fiducial 1-σ sensitivity of SKA should be 10 times better than that of SKA1-MID, or about ~ 70 nJy/beam in one hour, which will allow to obtain deep radio limits (or eventually the detection) of type Ia SNe in a short amount of time and out to 25 Mpc, or even further. To get a more clear idea of what can be reached with SKA1 and SKA, we plot in Fig. 4 the constraints on the mass-loss rate parameter for an upper limit of 3-σ ($3\times0.7\mu$Jy/beam for SKA1, or 3×70 nJy/beam for SKA) for a Type Ia SN exploding at the distance of M 82 and at 25 Mpc. It is evident that, at this level of sensitivity, a non-detection would be essentially as meaningful as a detection, since the former would imply that only the double-degenerate scenario is viable, while the latter would tell us which of the single-degenerate channels results in Type Ia SNe. The overall time needed to carry out such a target-of-opportunity programme will require no more than about $12-24$ hr/year, overheads included, for an average of two targets/year within a radius of 25 Mpc. Such modest time requests can be easily accommodated within a sensible period of time.

5. Summary

We have presented the prospects for advancing our understanding of the physics of supernovae via their study at radio wavelengths with the SKA. Our suggested approach for core-collapse supernovae is a commensal one, taking advantage of the deep, sensitive surveys that are planned with SKA1. We have discussed the expectations for CCSN studies under the specific case of SKA1-SUR (∼1000 hr in one year, rms=4.2 μJy/beam in 1-hr, FoV=18 deg^2, bandwidth=500 MHz). In particular, we assumed a fiducial frequency of 1.7 GHz and a covered area of 10000 deg^2 in one year. The expected number of new CCSNe discovered after one year would be $\gtrsim 310$. For SKA, the expected number of expected CCSN discoveries is well over 10,000 in one year. Therefore, the number of detections is expected to approach the number of explosions of all CCSNe in the local universe, thus allowing us to obtain a dust-free, complete census of CCSNe. The only request from such a programme is a multi-epoch approach, observing a cadence-time of $\lesssim 90\nu_{1.7}^{-1}$ days, where $\nu_{1.7} = \nu/1.7$ GHz. We also note that the proposed programme can be carried out as well at higher frequency bands, as long as an adequate cadence time is observed.

We have also discussed the prospects for probing Type Ia SNe progenitor scenarios with the SKA. The SKA can be used at very low time-cost for searching the putative prompt radio emission arising, in the single-degenerate scenario, from the circumstellar medium around Type Ia SN progenitors in the nearby universe. Complementarily, since the radio emission of Type Ia SNe is expected to increase with time in the double-degenerate scenario, the SKA should observe decades-old, nearby Type Ia SNe, which can potentially confirm the double-degenerate scenario in them. In conclusion, the huge improvement in sensitivity of the SKA with respect to their predecessors should allow us to unambiguously discern which progenitor scenario (single-degenerate vs. double-degenerate) applies to them, thus solving this long-standing issue.

PoS(AASKA14)060

6. Acknowledgments

MAPT, AA, RHI, JMM, and ER acknowledge support from the Spanish Ministry of Economy and Competitiveness (MINECO) through grants AYA2012-38491-C02-01 and AYA2012-38491-C02-02. PL acknowledges support from the Swedish Research Council. JMM and ER also acknowledge support from the Generalitat Valenciana through grants PROMETEO/2009/104 and PROMETEOII/2014/057. CRC acknowledges financial support from the ALMA-CONICYT FUND Project 31100004. CRC is also supported by the Ministry of Economy, Development, and Tourism's Millennium Science Initiative through grant IC120009, awarded to The Millennium Institute of Astrophysics, MAS.

References

Alberdi, A., Colina, L., Torrelles, J. M., et al. 2006, ApJ, 638, 938
Batejat, F., Conway, J. E., Hurley, R., et al. 2011, ApJ, 740, 95
Bietenholz, M. F., De Colle, F., Granot, J., Bartel, N., & Soderberg, A. M. 2014, MNRAS, 440, 821
Bondi, M., Pérez-Torres, M. A., Herrero-Illana, R., & Alberdi, A. 2012, A&A, 539, A134
Branch, D., Livio, M., Yungelson, L. R., Boffi, F. R., & Baron, E. 1995, PASP, 107, 1019
Chevalier, R. A. 1982, ApJ, 259, 302
Chevalier, R. A. 1998, ApJ, 499, 810
Chevalier, R. A., Fransson, C., & Nymark, T. K. 2006, ApJ, 641, 1029
Chomiuk, L., Soderberg, A. M., Moe, M., et al. 2012, ApJ, 750, 164
Colina, L., Alberdi, A., Torrelles, J. M., Panagia, N., & Wilson, A. S. 2001, ApJ, 553, L19
Dahlen, T., Strolger, L.-G., Riess, A. G., et al. 2012, ApJ, 757, 70
Dilday, B., Smith, M., Bassett, B., et al. 2010, ApJ, 713, 1026
Eldridge, J. J., Fraser, M., Smartt, S. J., Maund, J. R., & Crockett, R. M. 2013, MNRAS, 436, 774
Gal-Yam, A., Ofek, E. O., Poznanski, D., et al. 2006, ApJ, 639, 331
Hancock, P. J., Gaensler, B. M., & Murphy, T. 2011, ApJ, 735, L35
Horiuchi, S., Beacom, J. F., Kochanek, C. S., et al. 2011, ApJ, 738, 154
Hughes, J. P., Chugai, N., Chevalier, R., Lundqvist, P., & Schlegel, E. 2007, ApJ, 670, 1260
Kamble, A., Soderberg, A., Berger, E., et al. 2014, arXiv:1401.1221
Kankare, E., Mattila, S., Ryder, S., et al. 2014, MNRAS, 440, 1052
Lien, A., Chakraborty, N., Fields, B. D., & Kemball, A. 2011, ApJ, 740, 23
Magnelli, B., Elbaz, D., Chary, R. R., et al. 2011, A&A, 528, A35
Mannucci, F., Della Valle, M., & Panagia, N. 2007, MNRAS, 377, 1229
Maoz, D., Mannucci, F., & Nelemans, G. 2013, arXiv:1312.0628
Margutti, R., Soderberg, A. M., Chomiuk, L., et al. 2012, ApJ, 751, 134
Margutti, R., Parrent, J., Kamble, A., et al. 2014, ApJ, 790, 52
Mattila, S., Dahlen, T., Efstathiou, A., et al. 2012, ApJ, 756, 111
Matzner, C. D., & McKee, C. F. 1999, ApJ, 510, 379
Panagia, N., Van Dyk, S. D., Weiler, K. W., et al. 2006, ApJ, 646, 369
Parra, R., Conway, J. E., Diamond, P. J., et al. 2007, ApJ, 659, 314

PoS(AASKA14)060

Pérez-Torres, M. A., Alberdi, A., Colina, L., et al. 2009, MNRAS, 399, 1641
Pérez-Torres, M. A., Romero-Cañizales, C., Alberdi, A., & Polatidis, A. 2009, A&A, 507, L17
Pérez-Torres, M. A., Alberdi, A., Romero-Cañizales, C., & Bondi, M. 2010, A&A, 519, L5
Pérez-Torres, M. A., Lundqvist, P., Beswick, R. J., et al. 2014, ApJ, 792, 38
Romero-Cañizales, C., Mattila, S., Alberdi, A., et al. 2011, MNRAS, 415, 2688
Romero-Cañizales, C., Herrero-Illana, R., Pérez-Torres, M. A., et al. 2014, MNRAS, 440, 1067
Russell, B. R., & Immler, S. 2012, ApJ, 748, L29
Smartt, S. J. 2009, ARA&A, 47, 63
Soderberg, A. M., Nakar, E., Berger, E., & Kulkarni, S. R. 2006, ApJ, 638, 930
Weiler, K. W., Panagia, N., Montes, M. J., & Sramek, R. A. 2002, ARA&A, 40, 387

PoS(AASKA14)060

PROCEEDINGS OF SCIENCE

Thermal radio emission from novae & symbiotics with the Square Kilometre Array

Tim O'Brien[1], **Michael Rupen***[2], **Laura Chomiuk**[3], **Valerio Ribeiro**[4,5], **Michael Bode**[6] **Jennifer Sokoloski**[7], **Patrick Woudt**[4]

[1] *University of Manchester;* [2] *NRC/CNRC-Canada;* [3] *Michigan State University;* [4] *University of Cape Town;* [5] *Radboud University;* [6] *Liverpool John Moores University;* [7] *Columbia University.*
E-mail: tim.obrien@manchester.ac.uk

Thermal radio emission is a fundamental tracer of outflows from stellar systems. Novae and symbiotic stars are interacting binary systems incorporating accretion and nuclear burning on white dwarfs. They share several distinct observational features during their outbursts: higher flux densities at higher radio frequencies, variability on a range of (unpredictable) timescales, and locations largely confined to the Galactic plane. Physical insights drawn from free-free radiation are distinct and complementary to the more commonly sought after radio synchrotron emission, and high-quality observations of thermal processes draw on different SKA capabilities.

The thermal radio emission of novae during outburst enables us to derive fundamental quantities such as the ejected mass, kinetic energy, and density profile of the ejecta. Recent observations with newly-upgraded facilities such as the VLA and e-MERLIN are just beginning to reveal the incredibly complex processes of mass ejection in novae (ejections appear to often proceed in multiple phases and over prolonged timescales). Symbiotic stars can also exhibit outbursts, which are sometimes accompanied by the expulsion of material in jets. However, unlike novae, the long-term thermal radio emission of symbiotics originates in the wind of the giant secondary star, which is irradiated by the hot white dwarf. The effect of the white dwarf on the giant's wind is strongly time variable, and the physical mechanism driving these variations remains a mystery (possibilities include accretion instabilities and time-variable nuclear burning on the white dwarf's surface).

The exquisite sensitivity of SKA1 will enable us to survey novae throughout the Galaxy, unveiling statistically complete populations. With SKA2 it will be possible to carry out similar studies in the Magellanic Clouds. This will enable high-quality tests of the theory behind accretion and mass loss from accreting white dwarfs, with significant implications for determining their possible role as Type Ia supernova progenitors. Observations with SKA1-MID in particular, over a broad range of frequencies, but with emphasis on the higher frequencies, will provide an unparalleled view of the physical processes driving mass ejection and resulting in the diversity of novae, whilst also determining the accretion processes and rates in symbiotic stars.

Advancing Astrophysics with the Square Kilometre Array
June 8-13, 2014
Giardini Naxos, Sicily, Italy

*Speaker.

PoS(AASKA14)062

1. Introduction

Novae and symbiotic stars are interacting binary star systems in which a hot white dwarf orbits a companion main-sequence or red giant star. Material is accreted onto the white dwarf, via Roche-lobe overflow (typically in the case of novae) or directly from the wind of the companion. They are excellent laboratories for studying a number of very important astrophysical phenomena, for example: binary evolution; accretion; ionization of circumstellar material; mass ejection; jet formation; thermonuclear burning and explosions. Those with massive white dwarfs may eventually lead to Type Ia supernovae.

Novae are the most common stellar thermonuclear explosions (Bode & Evans 2008). They result from a thermonuclear runaway (TNR) in material accreted from a main sequence or red giant star onto the surface of a white dwarf. In the explosion, $10^{-8} - 10^{-3}$ solar masses are ejected at speeds ranging from a few hundred to several thousand km s^{-1}. The white dwarf is not destroyed so accretion begins again, leading to repeated explosions with recurrence periods ranging from a year (for recurrent novae in which more than one outburst has been observed, Tang et al. 2014) to millions of years (in the case of so-called classical novae, Yaron et al. 2005). If all the mass accreted since the previous outburst is not ejected, then novae with massive CO white dwarfs will evolve towards explosion as a Type Ia supernova.

Radio observations are particularly useful in studies of novae as they provide a direct view of the ejected mass by tracking the free-free photosphere as it moves back through the outflow over months to years (Seaquist & Bode 2008; Roy et al. 2012). The mass ejected can be estimated using standard models assuming free-free emission from instantaneous ejection of spherical shells (e.g. Hjellming et al. 1979; Seaquist & Palimaka 1977; Seaquist et al. 1980). Radio imaging can of course also resolve the ejecta throughout the outburst, aiding distance estimates and determinations of ejection geometry (Taylor et al. 1988; Eyres et al. 1996).

Recent observations of novae (see below) have resulted in discoveries which present challenges to the orthodox interpretation: nova ejecta are often aspherical, with some even showing evidence for jets (Rupen et al. 2008; Sokoloski et al. 2008); light curves indicate that there is frequently more than one major ejection (Krauss et al. 2011; Nelson et al. 2014); some novae show evidence for non-thermal radio emission (Chomiuk et al. 2014b); observational mass estimates tend to exceed predictions from models of the TNR by an order of magnitude (Roy et al. 2012); and several novae have now been detected as high-energy gamma-ray sources, suggesting large-scale particle acceleration in shocks (Ackermann et al. 2014).

Symbiotic stars are wide binary systems where mass is accreted onto the surface of a white dwarf from a red giant star. These systems have high mass loss rates in the red giant wind, of order 10^{-7} to 10^{-6} solar masses per year (Seaquist et al. 1984; Seaquist & Taylor 1990). Unlike typical novae, thermal radio emission arises in symbiotics primarily from this wind ionised by the white dwarf. Its study therefore allows us to explore the circumstellar environment of these systems, the mass-loss history of the central system, and the luminosity of the white dwarf. Symbiotic stars undergo occasional outbursts in which the optical brightness increases and sometimes even thermonuclear-powered nova events (see below). During these outbursts, some symbiotic stars have shown evidence for collimated jets (Dougherty et al. 1995; Crocker et al. 2001; Karovska et al. 2010). Mass accretion and nuclear burning on the white dwarf leads to the suggestion that

PoS(AASKA14)062

they could be one class of progenitors of Type Ia supernovae (Munari & Renzini 1992; Di Stefano 2010).

Progress in understanding the nova phenomenon and its wider links to binary evolution is challenged by the heterogeneous nature of the population, particularly as revealed in recent observations with the VLA (Roy et al. 2012). SKA will enable a statistically complete survey of novae and symbiotic stars in our Milky Way, providing multi-frequency light curves and resolved images of individual objects which will help us answer several major outstanding questions, including:

– How much mass is ejected in nova outbursts and what system parameters determine the ejecta mass?

– What is the geometry of mass ejection and what is its relation to the properties of the binary system?

– What are the physical mechanisms driving mass loss during the nova outburst?

– What is the density and distribution of circumbinary material?

– What is the true galactic population of novae and symbiotic stars?

– How do symbiotic stars transfer mass? Is it via a wind, Roche lobe overflow or a combination of both?

– What proportion of symbiotic systems have "jets"?

– How do novae and symbiotic stars relate to the progenitors of Type Ia supernovae?

2. Recent observations

2.1 Novae

The 2006 outburst of the recurrent nova RS Ophiuchi was the target of an extensive multi-frequency campaign of observations which included: the first resolution of the expanding shock wave from a nova explosion using the VLBA, EVN & MERLIN (O'Brien et al. 2006); detection of X-ray emission from the expanding shock wave using RXTE & Swift (Sokoloski et al. 2006; Bode et al. 2006); the discovery of jet-like radio emission using the VLA & VLBA (Sokoloski et al. 2008; Rupen et al. 2008; Eyres et al. 2009); and extensive coverage of the super-soft phase of X-ray emission using Swift (Osborne et al. 2011).

Following the successful campaign on RS Oph, two large collaborations were formed: Swift-nova-cv uses Swift to study super-soft and shock X-ray emission from novae, whilst the E-Nova team (many of whom are also members of Swift-nova-cv) concentrates on exploiting new radio facilities such as the upgraded VLA and e-MERLIN to monitor novae in outburst. Both projects are resulting in far more extensive observational databases. Several examples of recent results are summarised below before we go on to discuss the future role of SKA.

T Pyx is a recurrent nova whose most recent outburst was in 2011. The VLA radio light curve showed several surprises (Nelson et al. 2014). No detections for the first two months after the optical outburst were followed by a dramatic rise after day 65, and surprisingly high peak luminosities, requiring an ejection of significantly more mass than expected from the high-mass white dwarfs thought to host recurrent novae. To explain the rapid rise, this needs to be combined with significant cooling/reheating and/or delayed ejection (a hypothesis supported by the *Swift* X-ray light curve, Chomiuk et al. 2014b).

PoS(AASKA14)062

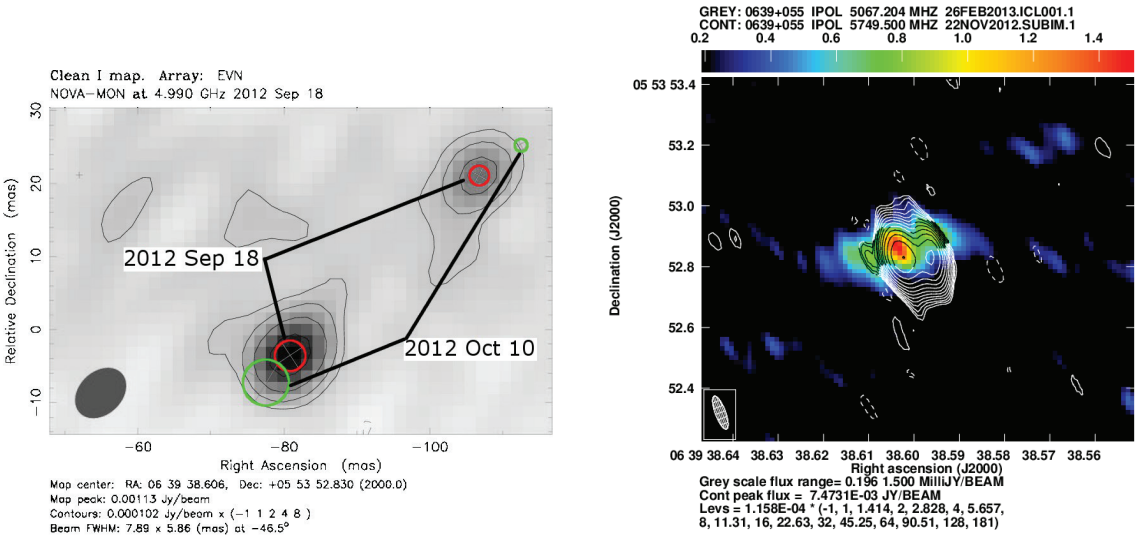

Figure 1: Left: EVN image of V959 Mon on 2012 Sep 18 (91 days after *Fermi* discovery; 5.8 GHz). Components in this image are labelled by red circles, with the positions of components 22 days later (Oct 10; day 113) labelled with green circles (see Chomiuk et al. 2014a). Right: e-MERLIN images on Nov 23 (day 157; 5.8 GHz) in contours and 2013 Feb 26 (day 252; 5.1 GHz) in colour scale (Healy et al. in prep).

V959 Mon is a classical nova which went into outburst in 2012. This was the third nova to be detected in GeV gamma-rays (Ackermann et al. 2014), this time detected by *Fermi* before it was identified as a nova due to its proximity to the Sun during outburst. VLA detected V959 Mon within a week or so of outburst, but three months later the source brightened significantly. Target-of-opportunity observations were obtained with e-EVN, e-MERLIN and VLBA (O'Brien et al. 2012; Chomiuk et al. 2014a), revealing two compact VLBI components moving away from each other and a larger-scale thermal bipolar structure (Figure 1).

Since V959 Mon has a main sequence companion (Munari et al. 2013), and is therefore not an embedded nova like RS Oph (i.e. with no dense pre-existing circumstellar medium), the gamma-ray and synchrotron radio emission must arise as a result of internal shocks between fast and slow-moving material ejected in the outburst. Radio imaging of V959 Mon (Chomiuk et al. 2014a) shows the structure evolve from an east-west structure to a larger north-south structure. One possibility is that interaction of the expanding nova ejecta with the binary in a common-envelope phase expels material at different rates. This leads to the shock interactions visible as non-thermal emission with VLBI, and sculpts the expanding ejected shell, which is visible in thermal radio emission.

2.2 Symbiotic stars

To date the largest radio survey of symbiotic stars is that from Seaquist et al. (1993), detecting 50 stars (out of 99 observed) with a sensitivity of 110 μJy. These were single-epoch observations, so much information was missed. For example, Brocksopp et al. (2004) observed Z And over several epochs and frequencies, revealing variable radio emission and jet ejection. Jet-like, collimated, or bipolar outflows have also been observed at radio frequencies in CH Cyg (Crocker et al. 2001) and R Aqr (Dougherty et al. 1995). In CH Cyg, there is evidence for an episodic precessing jet (visible in the optical, X-ray and radio) interacting with the ambient medium (Karovska et al. 2010).

PoS(AASKA14)062

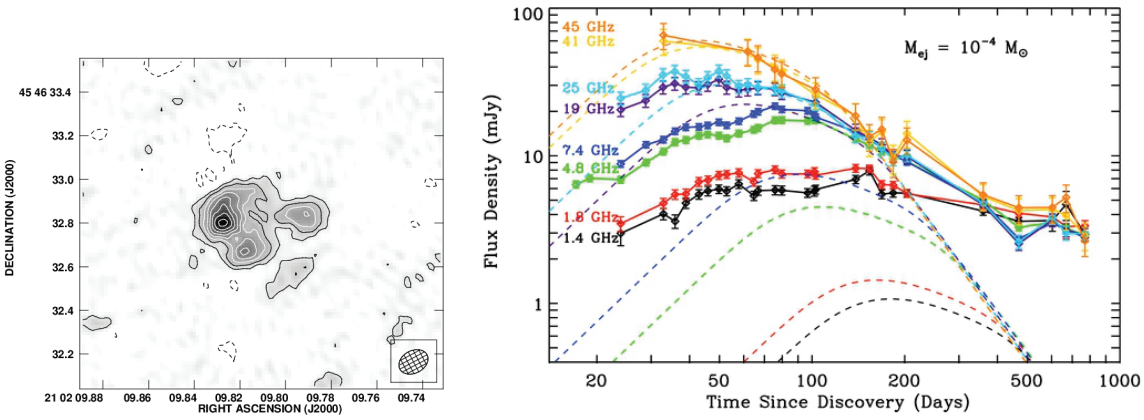

Figure 2: Left: 5 GHz MERLIN image of V407 Cyg, 11 days after outburst, showing extended emission from the Mira giant wind. Right: VLA light curve showing how standard models of thermal radio emission from novae (dashed lines) fail to fit observations (points and solid lines) (Chomiuk et al. 2012).

The timescales, amplitude, and mechanism of radio variability remain poorly explored in symbiotic stars, but certainly contains information about the accretion, nuclear burning, and outflows that power these systems.

Perhaps even more fundamentally, recent detections of strong hard X-ray emission (E > 2 keV) from symbiotic stars that have weak signatures of mass transfer in their optical spectra (e.g. Bird et al. 2007; Nichols et al. 2007; Luna & Sokoloski 2007; Kennea et al. 2009; Luna et al. 2013) suggest that past surveys of symbiotic stars have been subject to severe selection biases. Since quasi-steady nuclear shell burning releases approximately 50 times more energy per nucleon than accretion alone, symbiotic white dwarfs powered by accretion alone are typically much less luminous – with much lower fluxes of ionizing photons, weaker optical emission lines, and lower radio fluxes – than symbiotic white dwarfs with shell burning. Thus the strength of optical emission lines, which have been considered the defining feature of symbiotic stars, is not necessarily a good proxy for the rate of mass transfer. Since most known symbiotic stars have been identified because of their strong optical emission lines, the Galactic population of symbiotic stars might actually be much larger than previously appreciated. Sensitive radio observations with SKA1 could both characterize the radio properties of accretion-powered symbiotic stars and also provide a new measure of the true Galactic population of these important interacting binaries.

The symbiotic system V407 Cyg, composed of a white dwarf and a Mira giant, underwent a nova outburst in 2010 and was the first nova to be detected in gamma rays (Abdo et al. 2010). Radio observations were made with the VLA, MERLIN and EVN. MERLIN resolved the emission region within the first few weeks after outburst (Fig. 2), and showed that it was too extended to be from material ejected in the outburst and rather appears to be flash-ionized circumstellar medium. As the later VLA light curve showed (Fig. 2, Chomiuk et al. 2012), the subsequent radio emission appears to originate from the extended wind of the Mira companion, increasing in luminosity as the wind is ionized, and fading as the wind is heated from within by the expanding nova shock wave (Nelson et al. 2012)—the first time such a phenomenon has been observed.

PoS(AASKA14)062

3. The role of SKA in studies of novae and symbiotic stars

The first novae to be detected in the radio were HR Del and FH Ser in 1970 (Hjellming & Wade 1970). But as Seaquist & Bode (2008) pointed out, as of 2008 only 17 classical novae had been detected in outburst and of these, only four had so-called first class data with multiple epochs and observing frequencies. Hence, novae with high-quality radio observations are too dissimilar and too few in number to know which behaviours are odd and which common, let alone to connect the mass ejection histories to the details of the host system. Novae are famously heterogeneous with a wide range of behaviour seen in the optical, including light curves whose decline times range from 4 to 900 days. Factor in the variation in circumstellar environments (e.g. whether the nova is embedded in a dense wind from the secondary) and the viewing angle and it becomes clear that a fuller understanding will require study of a statistically significant sample.

Excellent progress is being made with current VLA monitoring programmes led by authors on this chapter, but even here we are limited to only a small subset of new novae, typically up to four new targets each year out of around ten discovered optically (current rate). Note, it is estimated that there are ~ 35 nova outbursts in the Milky Way each year (Shafter 1997) with the majority passing unnoticed in the optical, presumably because of distance, short duration at peak, high extinction, or proximity to the Sun at outburst. Even the outbursts of naked eye novae have gone unnoticed for weeks to months in recent times (Hounsell et al. 2010). In the era of LSST and SKA, this will change.

In a very simple model of thermal radio emission from expanding ejecta (Seaquist & Bode 2008), the emission is initially optically thick and the flux rises as the solid angle increases. As its density decreases it becomes optically thin, first at higher frequencies, and the nova fades. This simple model (for a shell with mass M_{ej}, velocity V_{ej} and electron temperature, assumed isothermal, T_e) leads to estimates for the maximum flux density f_{max} at time t_{max} when the angular diameter is θ_{max} :

$$f_{max} \approx 6.7 \left(\frac{\nu}{\mathrm{GHz}}\right)^{1.16} \left(\frac{T_e}{10^4\ \mathrm{K}}\right)^{0.46} \left(\frac{M_{ej}}{10^{-4}\ \mathrm{M}_\odot}\right)^{0.80} \left(\frac{D}{\mathrm{kpc}}\right)^{-2} \quad \mathrm{mJy}\ ; \tag{3.1}$$

$$t_{max} \approx 2.6 \left(\frac{\nu}{\mathrm{GHz}}\right)^{-0.42} \left(\frac{T_e}{10^4\ \mathrm{K}}\right)^{-0.27} \left(\frac{M_{ej}}{10^{-4}\ \mathrm{M}_\odot}\right)^{0.40} \left(\frac{V_{ej}}{10^3\ \mathrm{km\ s^{-1}}}\right)^{-1} \quad \mathrm{years}\ ; \tag{3.2}$$

$$\theta_{max} \approx 1.1 \left(\frac{\nu}{\mathrm{GHz}}\right)^{-0.42} \left(\frac{T_e}{10^4\ \mathrm{K}}\right)^{-0.27} \left(\frac{M_{ej}}{10^{-4}\ \mathrm{M}_\odot}\right)^{0.40} \left(\frac{D}{\mathrm{kpc}}\right)^{-1} \quad \mathrm{arcsec}\ . \tag{3.3}$$

Slightly more complex models include a density gradient in a thick shell of ejecta, while continuing to assume that the ejecta are isothermal and spherically symmetric. These models describe mass ejection in either an impulsive, homologous explosion with a range of velocities (also known as a 'Hubble flow'; Seaquist & Palimaka 1977) or a prolonged wind (Kwok 1983). As with the simple model, flux density during the optically thick and thin phases is time dependent and is proportional to $\nu^2 t^2$ and $\nu^{-0.1} t^{-3}$, respectively.

In Figure 3 we show 'Hubble flow' model light curves at various frequencies along with SKA1-SUR, -LOW, and -MID 5-σ sensitivities at 1 second, 1 minute and 1 hour integrations (Dewdney et al. 2013; Braun 2013). What is immediately evident from this figure is that we can detect nearby novae with very short integration times within a few weeks of the outburst. One minute

PoS(AASKA14)062

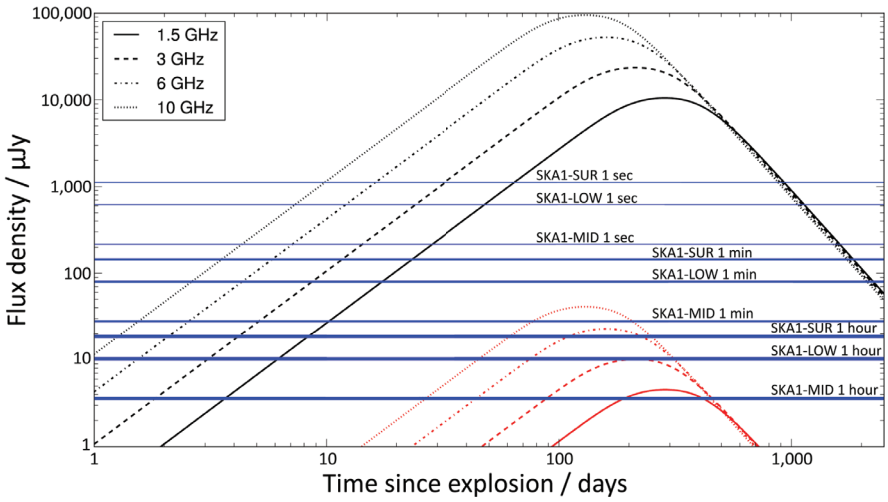

Figure 3: Synthetic light curves at several radio frequencies for a nova with $M_{\rm ej} = 1 \times 10^{-4}$ M$_\odot$, maximum ejecta velocity V_{max} = 3,000 km s^{-1}, $T_{\rm e}$ = 17,000 K, and the ratio of the inner to outer radius of the shell of 0.25. The upper set of curves (black) are for a nova at a distance of 1 kpc whilst the lower set (red) are for the distance of the LMC. The horizontal blue lines are the 5-σ sensitivity limits for SKA1 observations at 1 sec, 1 min, and 1 hour integrations.

integrations would allow us to characterise much of the light curve for novae within about 10 kpc. In addition, SKA1 will enable detection of novae out to 50 kpc (i.e., the Magellanic Clouds) with 1 hour integrations. It is clear from this figure that the most natural match to nova science is SKA1-MID at the higher frequency bands.

We will be able to carry out a complete survey of novae throughout the Galaxy, exploring the entire range of ejecta masses and timescales. SKA1 will probe not only the nearest and brightest novae, but the full population—i.e., ∼35 novae per year (compare with our current *total* of ∼20 with high-quality data). Radio surveys with SKA1 will see through the dust of the Galactic plane to reveal well-defined, complete samples of Milky Way novae, enabling detailed modeling of novae as an evolving population. Searches for novae can piggy back on wide-field surveys, with a focus on the Galactic plane ($|b| < 10^\circ$; if the Galactic plane were observed every few weeks, we could in principle detect every nova in the Galaxy visible from SKA latitudes). With SKA1, it will be possible to map out complex ejection histories for complete samples, comparing radio evolution for different speed classes, sources with and without narrow optical lines, sources with and without hard X-ray and gamma-ray emission, etc. By using complementary observations at other wavebands we will be able to tie ejection mass, velocity, and evolution to properties of the white dwarf (e.g. composition, mass) and binary system (e.g. orbital period, companion mass, companion wind).

SKA1 will enable, for the first time, detection of radio emission from novae in the Magellanic Clouds. The SKA1-MID 1-hour sensitivity of a few μJy rms at 50 kpc is equivalent to several 10's of μJy rms at the Galactic Centre, or around 0.1 mJy at a few kpc (Figure 3). By observing the LMC and SMC for 1 hour per pointing every month, we should easily detect most Magellanic Cloud novae with radio light curves comparable to those studied in the Milky Way today, allowing

PoS(AASKA14)062

us to compare nova populations as a function of host metallicity.

In addition to the significant advantages of full population surveys, SKA1 will provide completely new information on individual novae. Sensitive early observations will allow us to look for rapidly-recombining emission from the surrounding circumbinary emission (as in the one example so far, V407 Cyg; Fig. 2). We will be able to detect sources when they have very small angular diameters and/or very low ejected mass, thereby determining exactly when the first mass is ejected and relating mass ejection to models of the TNR (e.g., Hillman et al. 2014). This early faint radio emission will be detected when the hard X-ray and gamma-ray emission is also being detected, probing the mechanism for producing strong shocks in novae.

Excellent light curves will be obtained with very little commitment of observing time so we can increase cadence to daily or weekly observations and carry on observations for years. Such unprecedented time coverage will enable us to see exactly what is happening without theoretical bias (cf. the early rapid rise in RS Oph seen by MERLIN and the multi-peaked behaviour seen in recent VLA observations of several novae; Eyres et al. 2009; Krauss et al. 2011; Nelson et al. 2014).

Detection of radio recombination lines will allow us to map out the full 3D structure of novae. At the very least we could measure the strength and velocity structure of the lines. Simple estimates (e.g. following Condon & Ransom 2010, Gordon & Sorochenko 2002), suggest that the lines could be up to around 0.5% of the continuum at the higher frequency bands. If the nova is spatially resolved while still optically thick, then 3D imaging with direct density and filling factor measures is possible. Sources at tens of mJy should provide measurements of HI and OH absorption, enabling distance constraints and direct measurements of the evolving neutral and molecular circumbinary medium.

The $\sim$100 km baselines at 10 GHz for SKA1-MID provides 60 mas resolution, better than VLA in A configuration (albeit with few baselines) and similar to e-MERLIN. This *uv* coverage will provide superb imaging 12 months a year at the higher frequencies (rather than only one quarter of the time with VLA).

Imaging with SKA1 will enable consistent observation of the evolving ejecta structure and direct measurement of the ejecta brightness temperature. The high sensitivity of SKA1 means we can robustly compare radio images with, for example, JWST images, probing the nova structure with high time and angular resolution across the electromagnetic spectrum, and revealing the properties of the ejecta in unprecedented detail.

Currently we only detect one old nova via shock interaction with circumstellar material (GK Per; Seaquist et al. 1989). This interaction in GK Per has enabled us to piece together the binary's history and probe the common envelope ejection that created the current binary system. We will be able to explore GK Per itself in extreme detail, with high sensitivity and at 60 mas resolution, and we will also be able to search for emission from other old novae to probe their circumstellar environments.

For symbiotic stars, we will be able to determine why some systems experience quasi-steady shell burning, and the pervasiveness of this phenomenon. Nuclear shell burning could be the result of continuous accretion onto the white dwarf at a rate of a few times $10^{-8} - 10^{-7}$ $M_\odot$ yr^{-1}, as in the persistent supersoft X-ray sources (e.g. van den Heuvel et al. 1992). The range of accretion rates required to produce quasi-steady shell burning, however, is quite narrow (Fujimoto 1982). Given

PoS(AASKA14)062

the diversity of symbiotic systems with shell burning (orbital periods range from hundreds of days to decades), it is a challenge to explain how they could all accrete within the required narrow range of rates. Alternatively, shell burning could be residual nuclear burning from a previous nova explosion. In either case, ubiquitous steady burning would mean that most symbiotics can avoid full-scale nova explosions in which the entire accreted envelope is ejected, allowing symbiotic white dwarfs to accumulate material efficiently. Such efficient mass accumulation would increase the likelihood that they can gain enough material to explode as Type Ia supernovae. Since we expect accretion-powered symbiotics to produce $\sim$100 times less radio emission than symbiotics powered by nuclear shell burning, a sensitive radio survey like that which can be provided by SKA1 is required to find accretion-powered symbiotics and reveal the prevalence of shell burning.

With the reduced sensitivity of 50% during the early phase of SKA1-MID, we will still be able to achieve a good part of the science case. However, we emphasise that Band 5 capabilities are crucial for studies of novae and symbiotic stars.

4. Optimising SKA for Thermal Transients

Here, we address aspects of SKA1 design which will enable us to meet our science goals described above.

Most importantly, studies of novae and symbiotics require a high frequency band (as high as possible). The most efficient band for observing optically-thick thermal emission, by far, will be Band 5. In addition, the radio spectral energy distribution holds critical information, so quasi-simultaneous multi-band observations are key. Such observations may lend themselves to the use of sub-arrays or multiple beams.

Observations of thermal transients requires efficient, short (seconds to minutes), and frequent (daily or weekly) observations over the lifetime of an outburst lasting months to years. Observations with the VLA have illustrated how unpredictable and poorly understood the radio light curves of novae are on timescales of days to weeks (Roy et al. 2012), so it is important to be able to trigger on short timescales (within hours), particularly given that SKA will open up a new parameter space of low flux density observations early in the outburst. In addition, longer sensitive observations will enable study of short timescale variability, an aspect of accreting white dwarfs which remains completely unexplored in the radio (but may be expected, as such behaviour is seen at other wavebands; e.g. X-ray and optical).

To probe the complex evolving structures of novae and symbiotics, the angular resolution of SKA1 needs to be high, demanding Band 5 and antennas spread over several hundred kilometres. In addition, a number of novae have been imaged now with VLBI (e.g. RS Oph and V959 Mon) so SKA-VLBI will be key to imaging and tracking non-thermal components of emission resulting from the shocks now known to be present in many novae. A combination of lower-resolution imaging of the thermal ejecta and VLBI imaging of non-thermal components will be crucial for developing models to explain the evolution and ultimate fate of novae, helping us answer questions regarding the ejected mass, its geometry, and the role of shock interactions.

Study of radio recombination lines and disentangling multiple spectral components demands wide bandwidths with well-behaved bandpasses. In addition, a consistent flux density scale is

PoS(AASKA14)062

needed to allow assessment of the reality of small changes in flux density caused by, for example, variations in ejection properties or other evolution of these dynamic sources.

During the era of SKA2—with its dramatic sensitivity improvements on SKA1—we will be able to efficiently survey for novae across the Milky Way and explore a full sample of novae in the Magellanic Clouds (Figure 3). Furthermore, with the improved angular resolution and sensitivity of SKA2, we will be able to resolve the ejecta of novae much earlier in outburst and at even greater distances.

5. Tackling the big science questions in the era of SKA

First, we would like to test the theory of mass accretion onto white dwarfs and nova explosions by measuring the ejected mass and explosion energetics for a substantial sample of novae. This will be made possible in the era of SKA because we will have a sample of radio-observed novae with well understood selection effects (and selection effects that should mostly be a simple function of distance and ejected mass), enabling us to model novae as populations. High quality radio light curves complemented by observations at other wavelengths will allow us to finally measure the distribution of ejecta masses and energetics, and compare these with predictions from cataclysmic variable and nova theory. For example, theory makes predictions for the relative numbers of novae with low ejecta mass and high ejecta mass (the massive white dwarfs and high accretion rates that produce novae with low ejecta mass should be rare by number but have short recurrence time, and so should be relatively over-represented in the population), and this prediction will be tested with SKA-detected nova samples.

Second, exquisite multi-frequency light curves from the SKA will enable us to determine the mechanisms of mass ejection in novae, exploring why novae appear so diverse and how the mass-loss mechanism shapes nova ejecta. Novae are famous for their complexity, often showing plateaus, dips, and multiple peaks in their optical light curves (Strope et al. 2010), and recent data are showing that their behaviour at radio wavelengths is similarly rich—implying multiple episodes and processes of mass ejection that can act for months. Physically, mass loss in novae may be powered by the impulsive thermonuclear runaway, prolonged optically thick winds, common-envelope like interaction with the binary, jets, or ablation of the companion star/accretion disk. Radio light curves and imaging are powerful tools for disentangling these possibilities, by tracing the bulk of the ejected mass in a simple and straightforward way.

Finally, radio observations of both novae and symbiotics will allow us to map the density and distribution of circumbinary material, enabling a direct comparison between observations of Type Ia supernovae and these proposed progenitor systems. Radio surveys for symbiotic stars will reveal the prevalence of nuclear-burning white dwarfs approaching the Chandrasekhar mass.

In all of the above cases, the real advance of the SKA is that it will give us complete and well-understood samples of novae and symbiotics, so that the field can be transformed from a series of case studies to an understanding of these systems as populations. We will finally be able to answer questions such as: What is the dominant mechanism of mass loss in novae? How aspherical is the typical wind surrounding a symbiotic star? How well do novae adhere to theoretical expectations? Can white dwarfs really grow in mass by accreting non-degenerate matter?

PoS(AASKA14)062

References

Abdo, A. A., Ackermann, M., Ajello, M., et al. 2010, Science, 329, 817
Ackermann, M., Ajello, M., Albert, A., et al. 2014, Science, 345, 554
Bird, A. J., Malizia, A., Bazzano, A., et al. 2007, ApJS, 170, 175
Bode, M. F., & Evans, A., eds. 2008, Classical Novae, 2nd Edition (Cambridge: Cambridge University Press)
Bode, M. F., O'Brien, T. J., Osborne, J. P., et al. 2006, ApJ, 652, 629
Braun, R. 2013, "SKA1 Imaging Science Performance", Document number SKA-TEL-SKO-DD-XXX Revision A Draft 2
Brocksopp, C., Sokoloski, J. L., Kaiser, C., et al. 2004, MNRAS, 347, 430
Chomiuk, L., Krauss, M. I., Rupen, M. P., et al. 2012, ApJ, 761, 173
Chomiuk, L., Linford, J. D., Yang, J., et al. 2014a, Nature, 514, 339
Chomiuk, L., Nelson, T., Mukai, K., et al. 2014b, ApJ, 788, 130
Condon, J. J., & Ransom, S. M. 2010, http://www.cv.nrao.edu/course/astr534/ERA.shtml, Essential Radio Astronomy
Crocker, M. M., Davis, R. J., Eyres, S. P. S., et al. 2001, MNRAS, 326, 781
Dewdney, P., Turner, W., Millenaar, R., et al. 2013, "SKA1 System Baseline Design", Document number SKA-TEL-SKO-DD-001 Revision 1
Di Stefano, R. 2010, ApJ, 719, 474
Dougherty, S. M., Bode, M. F., Lloyd, H. M., Davis, R. J., & Eyres, S. P. 1995, MNRAS, 272, 843
Eyres, S. P. S., Davis, R. J., & Bode, M. F. 1996, MNRAS, 279, 249
Eyres, S. P. S., O'Brien, T. J., Beswick, R., et al. 2009, MNRAS, 395, 1533
Fujimoto, M. Y. 1982, ApJ, 257, 767
Gordon, M. A., & Sorochenko, R. L., eds. 2002, Astrophysics and Space Science Library, Vol. 282, Radio Recombination Lines. Their Physics and Astronomical Applications
Hillman, Y., Prialnik, D., Kovetz, A., Shara, M. M., & Neill, J. D. 2014, MNRAS, 437, 1962
Hjellming, R. M., & Wade, C. M. 1970, ApJLett, 162, L1
Hjellming, R. M., Wade, C. M., Vandenberg, N. R., & Newell, R. T. 1979, AJ, 84, 1619
Hounsell, R., Bode, M. F., Hick, P. P., et al. 2010, ApJ, 724, 480
Karovska, M., Gaetz, T. J., Carilli, C. L., et al. 2010, ApJLett, 710, L132
Kennea, J. A., Mukai, K., Sokoloski, J. L., et al. 2009, ApJ, 701, 1992
Krauss, M. I., Chomiuk, L., Rupen, M., et al. 2011, ApJLett, 739, L6
Kwok, S. 1983, MNRAS, 202, 1149
Luna, G. J. M., & Sokoloski, J. L. 2007, ApJ, 671, 741
Luna, G. J. M., Sokoloski, J. L., Mukai, K., & Nelson, T. 2013, A&A, 559, A6
Munari, U., Dallaporta, S., Castellani, F., et al. 2013, MNRAS, 435, 771
Munari, U., & Renzini, A. 1992, ApJLett, 397, L87
Nelson, T., Donato, D., Mukai, K., Sokoloski, J., & Chomiuk, L. 2012, ApJ, 748, 43
Nelson, T., Chomiuk, L., Roy, N., et al. 2014, ApJ, 785, 78
Nichols, J. S., DePasquale, J., Kellogg, E., et al. 2007, ApJ, 660, 651
O'Brien, T. J., Bode, M. F., Porcas, R. W., et al. 2006, Nature, 442, 279
O'Brien, T. J., Yang, J., Paragi, Z., et al. 2012, The Astronomer's Telegram, 4408, 1

PoS(AASKA14)062

Osborne, J. P., Page, K. L., Beardmore, A. P., et al. 2011, ApJ, 727, 124
Roy, N., Chomiuk, L., Sokoloski, J. L., et al. 2012, Bulletin of the Astronomical Society of India, 40, 293
Rupen, M. P., Mioduszewski, A. J., & Sokoloski, J. L. 2008, ApJ, 688, 559
Seaquist, E. R., & Bode, M. F. 2008, in Classical Novae, 2nd Edition, ed. M. F. Bode & A. Evans (Cambridge: Cambridge University Press), 141–166
Seaquist, E. R., Bode, M. F., Frail, D. A., et al. 1989, ApJ, 344, 805
Seaquist, E. R., Duric, N., Israel, F. P., et al. 1980, AJ, 85, 283
Seaquist, E. R., Krogulec, M., & Taylor, A. R. 1993, ApJ, 410, 260
Seaquist, E. R., & Palimaka, J. 1977, ApJ, 217, 781
Seaquist, E. R., & Taylor, A. R. 1990, ApJ, 349, 313
Seaquist, E. R., Taylor, A. R., & Button, S. 1984, ApJ, 284, 202
Shafter, A. W. 1997, ApJ, 487, 226
Sokoloski, J. L., Luna, G. J. M., Mukai, K., & Kenyon, S. J. 2006, Nature, 442, 276
Sokoloski, J. L., Rupen, M. P., & Mioduszewski, A. J. 2008, ApJLett, 685, L137
Strope, R. J., Schaefer, B. E., & Henden, A. A. 2010, AJ, 140, 34
Tang, S., Bildsten, L., Wolf, W. M., et al. 2014, ApJ, 786, 61
Taylor, A. R., Hjellming, R. M., Seaquist, E. R., & Gehrz, R. D. 1988, Nature, 335, 235
van den Heuvel, E. P. J., Bhattacharya, D., Nomoto, K., & Rappaport, S. A. 1992, A&A, 262, 97
Yaron, O., Prialnik, D., Shara, M. M., & Kovetz, A. 2005, ApJ, 623, 398

PoS(AASKA14)062

PROCEEDINGS OF SCIENCE

Investigations of supernovae and supernova remnants in the era of SKA

Lingzhi Wang, Xiaohong Cui, Hui Zhu, Wenwu Tian
National Astronomical Observatory of China, Chinese Academy of Sciences, Beijing 100012, China
E-mail: wanglingzhi@bao.ac.cn, tww@bao.ac.cn

Xiaofeng Wang
Department of Physics, Tsinghua University, Beijing 100084, China

Supernovae are extremely luminous and can outshine an entire galaxy for a period of days. Two main physical mechanisms are used to explain supernova explosions: thermonuclear explosion of a white dwarf (Type Ia) and core collapse of a massive star (Type II and Type Ib/Ic). Type Ia supernovae serve as distance indicators that led to the discovery of the accelerating expansion of the Universe. The exact nature of their progenitor systems however remain unclear. Radio emission from the interaction between the explosion shock front and its surrounding circumstellar medium (CSM) or interstellar medium (ISM) provides an important probe into the progenitor star's last evolutionary stage. No radio emission has yet been detected from Type Ia supernovae by current telescopes. The SKA will hopefully detect radio emission from Type Ia supernovae due to its much better sensitivity and resolution.

There is a 'supernovae rate problem' for the core collapse supernovae because the optically dim ones are missed due to being intrinsically faint and/or due to dust obscuration. A number of dust-enshrouded optically hidden supernovae should be discovered via SKA1-MID/survey, especially for those located in the innermost regions of their host galaxies. Meanwhile, the detection of intrinsically dim SNe will also benefit from SKA1. The detection rate will provide unique information about the current star formation rate and the initial mass function.

A supernova explosion triggers a shock wave which expels and heats the surrounding CSM and ISM, and forms a supernova remnant (SNR). It is expected that more SNRs will be discovered by the SKA. This may decrease the discrepancy between the expected and observed numbers of SNRs. Several SNRs have been confirmed to accelerate protons, the main component of cosmic rays, to very high energy by their shocks. This brings us hope of solving the Galactic cosmic ray origin's puzzle by combining the low frequency (SKA) and very high frequency (Cherenkov Telescope Array: CTA) bands' observations of SNRs.

Advancing Astrophysics with the Square Kilometre Array
June 8-13, 2014
Giardini Naxos, Italy

PoS(AASKA14)064

1. Introduction

The SKA will be a giant radio imaging and survey telescope array that will have an effective collecting area of one-million square meters and will be operated in the wide band range between 70 MHz to 10 GHz. The combination of its unprecedented sensitivity and resolution will start a new era of exploring the electromagnetic and other windows into the Universe. One of its key sciences (radio transients) will involve looking at vast swathes of the radio sky and making a detailed map as the thousands of telescopes work together in unison. Radio surveys have already recorded many transient events which exhibit rapid changes and large amounts of energy over short periods of time, e.g., supernovae (SNe) and their SN remnants (SNRs). With its higher sensitivity and broader field of view, the SKA will bring a revolution in the field of SNe and SNRs.

The low-frequency part (SKA1-LOW & SKA1-SUR) of SKA will be built in Western Australia where it will be merged with its precursor ASKAP, while the mid- and high-frequency part (SKA1-MID) of SKA will be built in South Africa where it will be merged with its precursor MeerKAT. Table 1 shows the parameters of SKA phase 1 and its precursors, and also includes parameters for the Cherenkov Telescope Array (CTA) for comparison.

Table 1: Parameters for SKA phase 1 telescopes (SKA1-LOW, SKA1-MID, & SKA1-SUR) and their precursors (ASKAP & MeerKAT), together with the Cherenkov Telescope Array.

Parameter	Resolution[a] (arcsec)	FoV[a] (deg^2)	Bandwidth (MHz)	Sensitivity (μJy $hr^{-1/2}$)
SKA1-LOW	11	$\sim$30	250	$\sim$2
SKA1-MID	0.22	$\sim$0.5	770	$\sim$1
SKA1-SUR	0.9	18	500	$\sim$4
ASKAP	7	30	300	$\sim$30
MeerKAT	11	0.86	1000	$\sim$3
CTA	0.04-0.05 deg	6-8 deg		10^{-13}erg cm^{-2} s^{-1}

[a]Fiducial Frequencies assumed: 110 MHz for SKA1-LOW; 1.4 GHz for SKA1-MID and SKA1-SUR; 1.4 GHz for ASKAP and MeerKAT (Dewdney et al., 2013); 1 TeV for CTA.

The SKA offers an excellent opportunity to systematically study the radio emissions from SNe and SNRs thanks to its higher sensitivity and wide FOV. The paper is organized as follows: §2 presents the radio SNe and their applications; §3 is the research of SNRs and cosmic rays; §4 draws our conclusions.

2. Radio SNe Investigations in the era of SKA1

Two main physical mechanisms are used to explain the SNe observations. One is thermonuclear explosion of a white dwarf in a binary system i.e., Type Ia SNe; the other is core collapse of a massive star ($M_{MS} \gtrsim 8\ M_{\odot}$), e.g., Type II, Ib/c SNe and their subtypes (Filippenko, 1997; Smith, 2014). SNe play a critical role in galactic evolution, via explosive nucleosynthesis and chemical enrichment, energy injection into the CSM & ISM, long γ-ray bursts and the origin and acceleration of cosmic rays. Moreover, Type Ia SNe are used as cosmological distance indicators due to

PoS(AASKA14)064

their nearly homogeneous intrinsic luminosities. Understanding the progenitor stars and explosion mechanisms for the different SNe types are the primary goal of SN investigation, which spans optical, X-rays, and radio observations. Radio emission from SNe involves the acceleration of relativistic electrons and amplified magnetic field necessary for synchrotron radiation, producing from the SN shock interactions with a relatively high-density CSM, which is assumed to be formed by the mass loss in the late stages of the progenitor's evolution. Intriguingly, the mass loss rate can potentially be used to probe different types of SN progenitor stars, see Table 2 (Smith, 2014). Therefore, radio emission from SNe plays a critical role in studying their progenitors' properties and final stages of evolution.

Radio SNe have been extensively studied for decades and detected at multiple radio frequencies with facilities including the Very Large Array (VLA; Weiler et al., 2007). The radio light curves can be fit by the parameterized model developed by Weiler et al. (2002, 1990, 1986), which can be used to compute the ratio of the mass loss rate to the stellar wind velocity. Different SN progenitor stars have their own characteristic mass loss rates (Table 2), shaping different CSM environments and thus leading to a diversity of radio light curves (Weiler et al., 2002; Wellons et al., 2012). Radio flux modulations are likely attributed to the CSM density modulations, which can be used to trace the mass loss rate variations of pre-SNe late evolutionary stages, and the influence of binaries. This method has been applied to Type II (Weiler et al., 2002) and Ibc SNe (Wellons et al., 2012) to constrain SNe CSM environments.

Table 2: Mapping of SN types to their likely progenitor star properties. Taken from Smith (2014)

SN	Progenitor Star	M_{ZAMS}	$\dot{M}$	V_{wind}
...	...	($M_\odot$)	($M_\odot$ yr^{-1})	(km s^{-1})
II-P	RSG	8–20	10^{-6}–10^{-5}	10-20
II-L	RSG/YSG	20–30 (?)	10^{-5}–10^{-4}	20-40
II-pec	BSG (b)	15–25	10^{-6}–10^{-4}	100-300
IIb	YSG (b)	10–25	10^{-5}–10^{-4}	20-100
Ib	He star (b)	15–25 (?)	10^{-7}–10^{-4}	100-1000
Ic	He star (b)/WR	25–?	10^{-7}–10^{-4}	1000
Ic-BL	He star (b)/WR	25–?	10^{-6}–10^{-5}	1000
IIn (SL)	LBV	30–?	(1–10)	50-600
IIn	LBV/B[e] (b)	25–?	(0.01-1)	50-600
IIn	RSG/YHG	25–40	10^{-4}–10^{-3}	30-100
IIn-P	super-AGB	8–10	0.01-1	10-600
Ibn	WR/LBV	40–?	10^{-3}–0.1	1000
Ia-CSM	WD (b)	5-8 (?)	0.01-1	50-100

RSG: Red supergiant; YSG: Yellow supergiant; BSG: Blue supergiant; WR: Wolf-Rayet star; LBV: Luminous blue variable; B[e]: B-type stars; YHG: Yellow hypergiant; WD: white dwarf (b) indicates probably a binary channel.

2.1 Progenitors of Type Ia SNe via SKA1

Two scenarios of single degenerate (SD) and double degenerate (DD) progenitor systems dom-

PoS(AASKA14)064

inate the current SNe explosion models. The post-explosion radio detection of the blastwave impact with the CSM would not only favor the SD model, but also provide the density and structure of the CSM. Due to extremely low mass loss rates, no radio emission has yet been detected from Type Ia SNe (Hancock et al., 2011; Panagia et al., 2006), even for the closest SNe 2011fe (Chomiuk et al., 2012) and 2014J (Pérez-Torres et al., 2014), which have set tight upper limits on radio luminosity, hence placing some constraints on the mass loss rate and wind velocity from its progenitor system. The lack of a radio detection from either SN 2011fe (d $\sim$ 6.4 Mpc) or SN 2014J (d $\sim$ 3.5 Mpc) all but rules out a symbiotic progenitor system and also a system with high accretion rate onto the white dwarf (Chomiuk et al., 2012; Pérez-Torres et al., 2014).

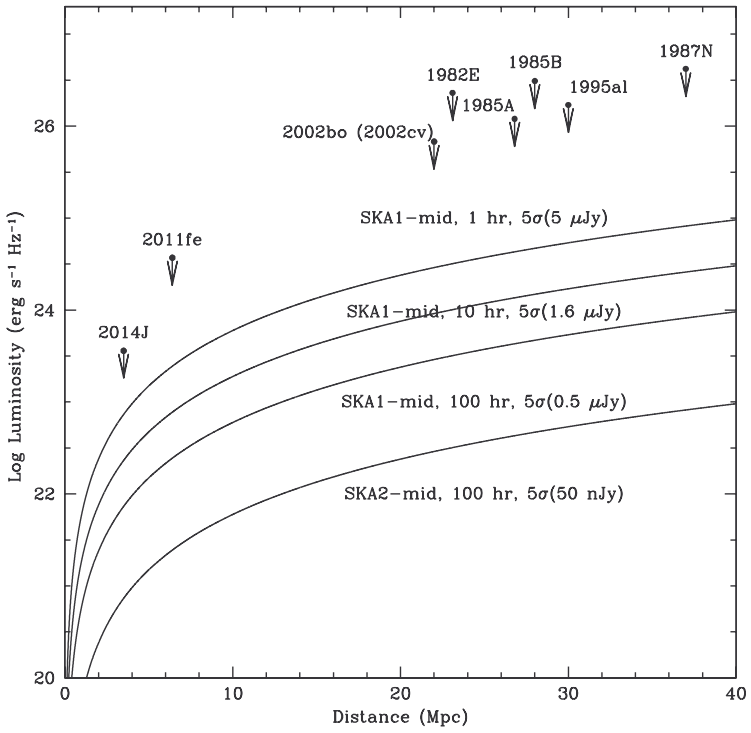

Figure 1: Log luminosity VS distance plot for Type Ia SNe by SKA1-MID in 1, 10, 100 hr and SKA2-mid in 100 hr observations. Eight close Ia SNe were indicated by downward arrows.

Due to their intrinsic faintness in the radio and their low volumetric rate, blind detection of Type Ia SNe is unfeasible (Lien et al., 2011; Panagia et al., 2006). SKA1-MID will hopefully carry out targeted follow-up observations to detect the first radio light from nearby Type Ia SNe ($\lesssim$20 Mpc) due to its much better sensitivity and resolution (Figure 1). Otherwise, no radio detection from Ia SN will place stronger constraint on its last evolutionary stage of progenitor system (e.g. lower mass loss rate upper limit). Since the sensitivy of SKA1-MID will be improved to 10 $\times$ higher (0.1μJy hr$^{-1/2}$) than the current one at phase 2, radio luminosity from a Type Ia SN could be detected as low as 2.4×10^{22} erg s^{-1}Hz^{-1}, out to the Virgo Cluster ($\sim$20 Mpc) after 100 hr integrations as a 5σ detection, as shown by the bottom solid line from Figure 1.

PoS(AASKA14)064

2.2 CCSNe survey

CCSNe represent the core collapse death of massive stars. The cosmic CCSNe rate can be determined by multiplying cosmic star formation rate (SFR) by the efficiency of forming CCSNe. Horiuchi et al. (2011) raised the "SN rate problem": the measured cosmic CCSNe rate is a factor of $\sim$2 smaller than that predicted from the cosmic massive-star formation rate. The "missing" percentage of optical CCSNe surveys can reach up to $\sim$30% at $Z = 1$ and increase to $\sim$60% at $Z = 2$ (Mannucci et al., 2007; Mattila et al., 2012). Many CCSNe are missed due to being intrinsically dim or due to obscuration. Radio techniques have great potential to find more "missing" CCSNe, especially CCSNe hidden in the inner regions of their host galaxies, because radio photons are not influenced by dust. SKA1-SUR provides a good chance to discover more faint "missing" CCSNe to yield a better sample because of its higher sensitivity and larger field (Table 1).

Typical radio luminosities of CCSNe are 10^{27} erg s^{-1} Hz^{-1} (Kamble et al., 2014; Lien et al., 2011). Luminosity distance is $D_L(z) = (1+z)\ c/H_0\ \int_0^z dz'\ [\Omega_{\rm m}(1+z')^3 + \Omega_\Lambda]^{-1/2}$, where the cosmological parameters were adopted from Planck Collaboration et al. (2014). SKA1-SUR will reach to Z = 0.14 (225 Mpc) in one hour, and to Z = 0.25 (0.43) in 10 (100) hr observations, refer to Figure 2. For a more complete outline of a CCSNe survey, also refer to Perez-Torres & et al. (2015).

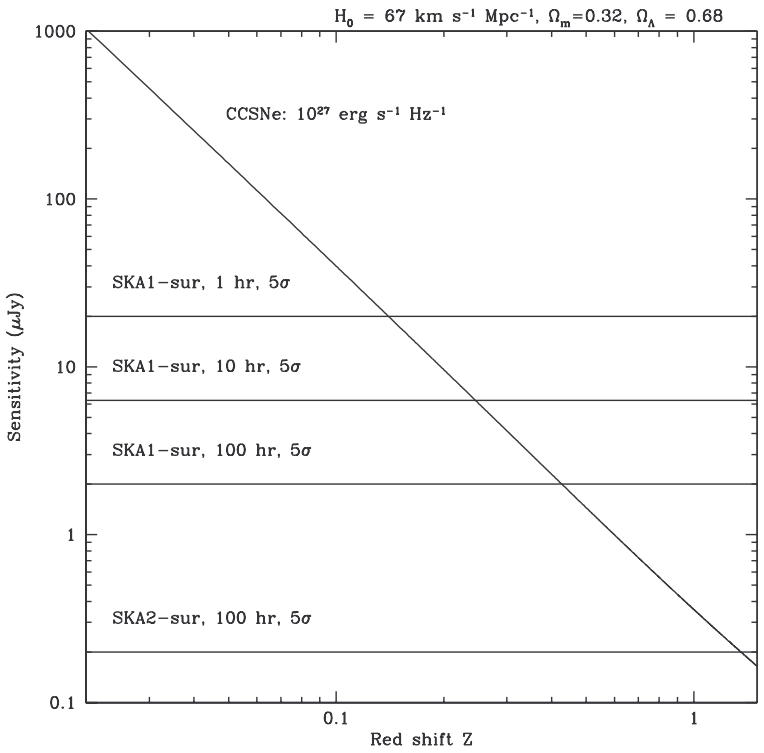

Figure 2: Sensitivity VS redshift plot for CCSNe with typical average radio luminosity of 10^{27} erg s^{-1} Hz^{-1} at 1.67 GHz.

PoS(AASKA14)064

2.3 SNe and SNRs connections

The transition from SNe to SNRs, or young SNRs to old SNRs are very critical for understanding SNe evolution and their interactions with CSM and ISM. Currently there are gaps between young SNRs and old SNRs. Bridging this gap will help to understand the spectra index variation and the magnetic field direction variation in SNRs. For example, the magnetic field in young SNR Tycho shells is predominantly radially oriented, while that in evolved SNR CTB1 shells is largely tangential to the shock front (Fürst & Reich, 2004).

3. SNRs investigations in the era of SKA

After SNe exploding, the results of interaction between ejected steller material and the ambient gas, form SNRs, refer to the review Woltjer (1972). Four-zone structure of a SNR are constituted with the freely expanding ejecta, the shocked ejecta, the shocked ambient medium (AM including CSM & ISM) and the unperturbed ambient gas. The SNRs have four evolutional stages, see Table 3. More mass the exploding ejecta swept up, slower shock velocity expanded and bigger size the SN remnants evolved. During the evolution process, the ejectors inject the huge energy into the AM. The feedback machanism of the exploding energy ($\sim 10^{51}$ erg) and matter leads to metals richening and heating in the AM. SNRs represent the last evolution stage of massive stars, which can be taken as agents of testing massive stellar evolution theory.

Table 3: The evolution phases of SN remnants

	Mass swept up $M_\odot$	Velocity kms^{-1}	Radius pc	Age yrs	Phase
I	<5	<10,000	<1	<2,000	ejecta-dominated (free expansion)
II	tens	~ 200	~ 10	~40,000	Sedov-Taylor(adiabatic)
III	$\sim 1{,}000$	~ 20	~ 30	~100,000	pressure-driven-snow-plow
IV					momentum-conserving (merging)

3.1 SNRs' discovery

SNRs play a key role in massive stellar evolution, thus the number of SNRs in a galaxy can be used as a diagnostic tool to test the current star formation. Taking our Galaxy for example, about 300 SNRs have been detected. Most of them were discovered by radio surveys. (Green, 2009a,b). However, the predicted number of SNRs is more than one thousand (Li et al., 1991). The reason existing the big gap is likely due to selection effects acting against the discovery of old, faint, large remnants (<0.3 Jy), as well as young, small remnants (<1 arcmin) in previous limited-sensitivity and/or -resolution Galactic radio surveys. In addition, the missing SNRs are likely concentrated toward the inner Galaxy, where thermal HII regions cause the most confusion due to their shell-like morphologies. The previous methods of seeking SNRs are based on their radio continuum data from high frequency and low sensitivity and skews the statistics, therefore only the bright and big SNRs can be detected (Green 2009). More sensitive, higher resolution surveys of the inner Galaxy at low radio frequencies are perhaps the key to determine how many SNRs are missing or to test current predicted SNRs rates.

PoS(AASKA14)064

SKA has a sensitivity of A_{eff}/T_{sys}=10000 and resolution of less than 1 arcsec. The fiducial sensitivity can reach as low as 50 nJy with 100 hours exposure time at 1.4 GHz. The radio emissions of SNRs are nonthermal and follow power law flux density as a function of frequency with a typical spectral index -0.5. The SKA1-LOW, with frequency range of between 50 MHz to 350 MHz, hosts great potentials to discover a large amount of 'missing' SNRs in Galaxy at the sensitivity of $\sim$2 μJy hr$^{-1/2}$ with a FOV of $\sim$30 deg^2, see Table 1.

3.2 High energy Cosmic rays origin via SKA & CTA

The work of identifying two SNRs as Cosmic Rays (CRs)' accelerators was selected as the Breakthough of the Year 2013 by the magazine <Science>. <Science> claimed that astronomers traced high-energy particles called cosmic rays back to their birthplaces in the debris clouds of SNe (Ackermann et al., 2013). The research in complex particle acceleration in an SNR is undergoing notable growth recently. The multi-wavelength observations of SNRs, especially the high-energy γ-rays observations from ground-based and space-based telescopes, play a powerful tools to probe the particle acceleration machanism in SNRs. Shell-type SNRs (e.g. young: G347.3-0.5; see Enomoto et al. (2002) and old: G353.6-0.7, see Tian et al. (2008)) are the major component of the five Galactic populations to generate very high energy γ-rays, i.e., pulsar wind nebulae (PWNe), X-ray binaries, shell SNRs, young stellar cloud, and giant molecular cloud.

Magnetic field amplification is needed to accelerate cosmic rays to very high energy in SNRs. Meanwhile, the density perturbations come up and are most rapid for the smaller scales or filaments, when passing through the shock. Observations of filaments of non-thermal X-ray emission in all young SNRs provide strong evidences of magnetic field amplification in the shock regions (Vink, 2012). Therefore, filamentary emissions are very important to study the particle acceleration. Taking figure 3 for example, only higher resolutions telescopes can map the filaments' details. Theoretical calculations and simulations reveal that the amplification usually happens on the scale of $<$0.1 pc. SKA will host great potentials to observe these structures due to its high resolution of less than 1 arcsec which could distinguish the structures of about 0.02 pc at a distance of 5 kpc and reduce the depolarization caused by small scale distortion of magnetic field.

Cosmic rays are mainly composed of charged particles which are deflected in the magnetic fields, thus, direct observations on the charged particles carry little information on their origin. However, observations of γ-ray photons, as small component of the CRs ($<$1%) play a key role in solving this issue due to two reasons: γ-rays have straight line propagation; γ-rays may be produced by relativistic particles' interactions (Tian & Zhang, 2013). Theoretical exploration has indicated two major emission mechanisms for γ-rays from Galactic objects: hadrons and leptons origin. When accelerated protons interact with interstellar material they generate neutral pions, which in turn decay into γ-rays (hadron origin). However, the high-energy electrons also generate γ-rays by means of inverse Compton scattering and bremsstrahlung.

The low-frequency synchrotron emission ($\lesssim$2 GHz) tracks the Mev-Gev part of electrons' spectra. For example, supposing a typical Galactic magnetic field of 10 μG, electrons with 2.9 GeV energy will have their peak radio emission at a frequency 408 MHz; electrons of 5.4 GeV energy will have peak emission at 1420 MHz; and electrons of 7.5 GeV energy will have peak emission at 2695 MHz (Leahy & Tian, 2009). The relativistic electrons are generally understood to be accelerated by the Fermi mechanism in fast moving shock fronts. There is strong evidence

PoS(AASKA14)064

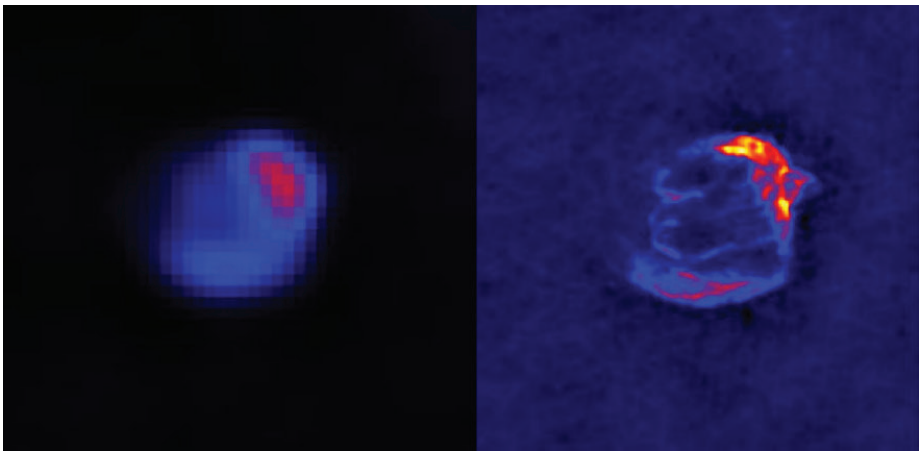

Figure 3: 1.4 GHz continuum observations of SNR W49B with two resolutions: Left, ∼1 arcmin (Stil et al., 2006); right, ∼6 arcsec (Helfand et al., 2006). Filaments are seen in right panel, while not in left panel.

of electron acceleration based on the detection of synchrotron X-rays from shell of young SNRs (Koyama et al., 1995). For old SNRs with an age of around 10^5 yr, theoretical calculations show that primary electrons could not be accelerated to high energy enough to emit obvious γ rays. But proton acceleration is still efficient to produce γ-ray emission. In lower frequency, non-thermal emissions from the secondary electrons generated in pp collisions dominate the spectrum. The energy spectrum of such secondary electrons starts to deviate from a pure power below ∼1 GeV and finally to cut off below ∼100 MeV. In turn, the radio continuum synchrotron spectrum from the secondary electrons will start to diverge from the pure power at frequencies below 100 MHz in case of typical B of 10 μG (Aharonian et al., 2013). Therefore, The SKA1-LOW with frequency range of between 50 MHz to 350 MHz, provides an excellent opportunity to distinguish the spectrum features of old SNRs produced from protons or secondary electrons. Obviously the low frequency radio spectrum serves as the proxy of the GeV energy particles. For high energy TeV particles, X-rays synchrotron spectrum (KeV) features are a powerful diagnostic tool to probe the TeV particles. In the coming golden era, observation of both sensitive γ-ray and low frequency radio telescopes, i.e., CTA and SKA1-LOW, will simultaneously trace the emissions produced by high energy GeV & TeV particles from SNRs so help solving the CR's origin issue. In addition, the high sensitivity of SKA is very useful to search for the radio counterpart of unidentified γ-ray source.

4. Summary

SNe and SNRs play a key role from stellar scale (for stellar evolutions) to galaxy scale (for galaxy chemical evolution), and out to cosmological scale (as distance candles). Radio emission from SNe will probe the last evolutionary stages of their progenitor systems and test the stellar evolutionary theory. The radio and γ-ray emission from SNRs will hopefully address the cosmic rays' origin. SKA1 will open a new era for investigations of SNe and SNRs, thanks to its higher sensitivity and better resolution.

PoS(AASKA14)064

References

Ackermann, M., Ajello, M., Allafort, A., et al. 2013, Science, 339, 807
Aharonian, F., Arshakian, T. G., Allen, B., et al. 2013, ArXiv e-prints, arXiv:1301.4124
Chomiuk, L., Soderberg, A. M., Moe, M., et al. 2012, ApJ, 750, 164
Dewdney, P., Turner, W., Millenaar, R., et al. 2013, SKA Documents, "SKA1 System Baseline Design", Document number SKA-TEL-SK0-DD-001, Revision 1
Enomoto, R., Tanimori, T., Naito, T., et al. 2002, Nature, 416, 823
Filippenko, A. V. 1997, ARA&A, 35, 309
Fürst, E., & Reich, W. 2004, in The Magnetized Interstellar Medium, ed. B. Uyaniker, W. Reich, & R. Wielebinski, 141–146
Green, D. A. 2009a, VizieR Online Data Catalog, 7253, 0
—. 2009b, Bulletin of the Astronomical Society of India, 37, 45
Hancock, P. J., Gaensler, B. M., & Murphy, T. 2011, ApJL, 735, L35
Helfand, D. J., Becker, R. H., White, R. L., Fallon, A., & Tuttle, S. 2006, AJ, 131, 2525
Horiuchi, S., Beacom, J. F., Kochanek, C. S., et al. 2011, ApJ, 738, 154
Kamble, A., Soderberg, A., Berger, E., et al. 2014, ArXiv e-prints, arXiv:1401.1221
Koyama, K., Petre, R., Gotthelf, E. V., et al. 1995, Nature, 378, 255
Leahy, D. A., & Tian, W. W. 2009, 13th International Symposium on Antenna Technology and Applied Electromagnetics and the Canadian Radio Science Meeting
Li, Z., Wheeler, J. C., Bash, F. N., & Jefferys, W. H. 1991, ApJ, 378, 93
Lien, A., Chakraborty, N., Fields, B. D., & Kemball, A. 2011, ApJ, 740, 23
Mannucci, F., Della Valle, M., & Panagia, N. 2007, MNRAS, 377, 1229
Mattila, S., Dahlen, T., Efstathiou, A., et al. 2012, ApJ, 756, 111
Panagia, N., Van Dyk, S. D., Weiler, K. W., et al. 2006, ApJ, 646, 369
Perez-Torres, M. A., & et al. 2015, "Core-collapse and Type Ia supernovae with the SKA", in proceedings of "Advancing Astrophysics with the Square Kilometre Array", PoS(AASKA14)060
Pérez-Torres, M. A., Lundqvist, P., Beswick, R. J., et al. 2014, ApJ, 792, 38
Planck Collaboration, Ade, P. A. R., Aghanim, N., et al. 2014, A&A, 571, A16
Smith, N. 2014, ARA&A, 52, 487
Stil, J. M., Taylor, A. R., Dickey, J. M., et al. 2006, AJ, 132, 1158
Tian, W., & Zhang, J. 2013, Science China Physics, Mechanics, and Astronomy, 56, 1443
Tian, W. W., Leahy, D. A., Haverkorn, M., & Jiang, B. 2008, ApJL, 679, L85
Vink, J. 2012, A&ARv, 20, 49
Weiler, K. W., Panagia, N., Montes, M. J., & Sramek, R. A. 2002, ARA&A, 40, 387
Weiler, K. W., Panagia, N., & Sramek, R. A. 1990, ApJ, 364, 611
Weiler, K. W., Sramek, R. A., Panagia, N., van der Hulst, J. M., & Salvati, M. 1986, ApJ, 301, 790
Weiler, K. W., Williams, C. L., Panagia, N., et al. 2007, ApJ, 671, 1959
Wellons, S., Soderberg, A. M., & Chevalier, R. A. 2012, ApJ, 752, 17
Woltjer, L. 1972, ARA&A, 10, 129

PoS(AASKA14)064

PROCEEDINGS OF SCIENCE

The SKA and the Unknown Unknowns

Peter Wilkinson*[1]
[1]*Jodrell Bank Centre for Astrophysics, School of Physics and Astronomy, The University of Manchester, Manchester, UK;*

E-mail: peter.wilkinson@manchester.ac.uk

As new scientists and engineers join the SKA project and as the pressures come on to maintain costs within a chosen envelope it is worth restating and updating the rationale for the "Exploration of the Unknown" (EoU). Maintaining an EoU philosophy will prove a vital ingredient for realizing the SKA's discovery potential. Since people make the discoveries enabled by technology a further axis in capability parameter space, the "human bandwidth" is emphasised. Using the morphological approach pioneered by Zwicky, a currently unexploited region of observational parameter space can be identified viz: time variable spectral patterns on all spectral and angular scales – one interesting example would be "spectral transients". We should be prepared to build up to 10% less collecting area for a given overall budget in order to enhance the ways in which SKA1 can be flexibly utilized.

Advancing Astrophysics with the Square Kilometre Array
June 8-13, 2014
Giardini Naxos, Sicily, Italy

*Speaker.

PoS(AASKA14)065

1. Introduction

The 2014 SKA Science Case has become impressively wide-ranging. Perhaps the most significant change in perception over recent years has been the increased importance afforded to transient science, which can be viewed as an emerging response to the "6th KSP" the Exploration of the Unknown (EoU). Nonetheless the main science imperatives for SKA1 can be traced back to the 2004 Science Case (Carilli & Rawlings 2004) – and quite often back to the arguments for the "Hydrogen Array" (Wilkinson 1991). The rationale for the SKA has firm foundations.

Despite the growth in breadth and depth of the science case over the past ten years we can still be certain that the SKA's place in astronomical history will not all be found within its pages. As the authors of EoU (Wilkinson et al. 2004) in the 2004 Science Case put it "If history is any example, the excitement of the SKA will not be in the old questions which are answered, but the new questions which will be raised by the new types of observations it alone will permit. The SKA is a tool for as-yet-unborn users and there is an onus on its designers to allow for the exploration of the unknown." More recently Kulkarni (2012) has noted: "discovery is important in astronomy because we are not sufficiently imaginative to construct the Universe and its constituents from first principles..."

The question is how to respond. In 2004 when considering the potential Key Science Programmes the SKA Level Zero Science Committee stated: "... the topic of 'serendipity' does not meet the [level-0] definitions... The recommendation... is therefore that serendipitous discoveries and the expansion of phase space not be included as level-0 science but that serendipity be explicitly included in the science case as an additional motivation for building the SKA." As Carilli put it in his science retrospective to AASKA14 "unknowns were a hard sell in 2004 since physics had torqued astronomy towards experiments but the pendulum is swinging... and general facilities may be back in vogue".

Recent SKA planning documents show that indeed the arc of history is bending in the right direction. In the SKA Concept of Operations Document (Bock et al. 2013) for example: "the primary success metric for the SKA Observatory will be the significance of its role in making fundamental scientific discoveries" and "recognizing the long history of discovery at radio wavelengths... the telescope will be designed in a manner to affordably allow flexibility and evolution of its capabilities to probe new parameter space (e.g., time variable phenomena that current telescopes are not well-equipped to detect)". While in the SKA Level 0 Science Requirements Document (Braun 2014) three of the general scientific requirements of SKA1 are given as:

- to provide the capability to carry out small-scale, experimental observations that utilise the outputs of tied-array beams from one or more sub-arrays.

- to be capable of rapid reconfiguration of their observing mode in response to internal or externally generated, pre-defined triggers.

- to enable commensal observations. It is apparent that many scientific applications can make effective use of the same basic observing campaign to multiply the scientific productivity of the facilities by a large factor.

PoS(AASKA14)065

Explicit realizations of these philosophies are captured in the specifications of the SKA1 Level 1 System Requirements (Cornwell et al. 2014). This is all greatly to be welcomed. But as pressures come on to keep costs within a chosen ceiling good intentions may fall victim to bean counting.

2. Discovery in Radio Astronomy – Lessons from History

In 2007 I assembled a personal list of important discoveries made with classical radio astronomy instruments working from deca to centimetre wavelengths – as is appropriate for SKA (Wilkinson 2007). Space prevents me from presenting a complete updated list here, instead additions to the 2007 list (with thanks to colleagues) are given in Table 1. What are the lessons to be learned?

1. In this region of the spectrum the large telescopes of their day have been at the forefront of discovery. This can be ascribed to the inherently low signal-to-noise ratio of observations indeed it is only with a radio telescope the size of the SKA that one can expect to detect the radio emission from most objects detected in other wavebands.

2. The rate of discovery has slowed in the last ten years (see Table 2) despite the rapid improvement in digital technology which has been well harnessed by the pulsar community. This was the period when LOFAR was being constructed and the VLA was being upgraded to the JVLA so we can hope to recover from this discovery "recession" over the course of this decade. But to me Table 2 is a prima facie argument for the SKA.

3. The designers of did not anticipate what they would be "known for" – a failing shared with HST as pointed out by Norris et al. (2015).

4. In many cases, the people involved had access to lots of telescope time and were not testing any particular theoretical model (not evidenced in the Table).

3. Discovery with SKA

3.1 Parameter Space

The SKA's place in astronomical history will not all be anticipated within the pages of the 2014 Science Case – so what do we do about it? We start by recognizing that discovery can be planned. As Harwit (1984) noted technology innovation allows the exploration of new areas of capability parameter space whose axes are, broadly:

- sensitivity;
- spatial coverage and or resolution;
- temporal coverage and or resolution;
- spectral coverage and or resolution;
- availability of past observations.

PoS(AASKA14)065

Discovery	**Instrument**	**Design Purpose**	**Forseen by Designers?**
Interplanetary Scintillation (1955)	Special purpose interferometer	Solar radio astronomy	Partly
Ordered Magnetic Fields in External Galaxies (1970s)	Westerbork SRT and Effelsberg	High resolution imaging General purposes	No
Laing-Garrington effect (1988)	Cambridge 5km and Very Large array	High resolution imaging	No
IDV is interstellar scintillation (1992)	Very Large Array Westerbork SRT	High resolution imaging	No
Spinning Dust (1996/97)	COBE and OVRO 40m	CMB and general purpose	No
Geodetic (GR) Precession in a binary pulsar (1998)	Effelsberg	General purpose	No
Winds on Titan (2004)	Global VLBI	Mapping compact sources	No
RRATs–intermittent pulsars (2006)	Jodrell Bank Lovell Telescope	General Purpose	No
Fast Radio Bursts (2006)	Parkes	General purposes	No
Neutron stars above 2Msun (2010)	GBT	General purposes	No

Table 1: Discoveries in deca-centimetric radio astronomy – an update to the list in Wilkinson (2007)

Decade	**Number of discoveries**
1930-9	1
1940-9	2
1950-9	4
1960-9	8
1970-9	6
1980-9	5
1990-9	8
2000-9	4

Table 2: Rate of discovery in the deca-centimetric radio band

Note that the last one is already an addition to Harwit's original thinking. The ready access to archive data has become a major factor in many modern scientific projects. A recent highlight in radio astronomy was the discovery of Fast Radio Bursts (FRBs) in the Parkes pulsar archive some years after the data were taken (Lorimer et al. 2007). Other pulsar discoveries are mentioned below.

In terms of these technologically-driven axes the future looks bright. Even SKA1 will offer a huge boost in sensitivity coupled with a wide field of view for survey throughput plus the ability to sample with high resolutions in the time, frequency and spatial domains. Flexible archiving is also seen as a priority. Thus in terms of technical capability we should expect SKA1 to be able to find

PoS(AASKA14)065

unexpected phenomena– but only if "the system" allows its users the maximum chance to do so. To encapsulate this idea let us identify a new, more abstract, axis in capability parameter space

- human bandwidth.

Technological innovation alone will not be enough to unlock SKA's full discovery potential. There should be scope for many as many people as possible to gain access to SKA data and for the expression of curiosity in its use.

3.2 Types of discovery

The International SKA SWG (Cordes et al. 2006) put it succinctly: "One might think that all of the combinations of key variables have been probed with existing telescopes. This is far from being the case because the so-defined parameter space has been investigated only in very compartmentalized sub-volumes." They went on to extend the rather general arguments adduced by Wilkinson et al. (2004) and introduced a wide range of potential areas for discovery:

1. New objects in known classes.
2. Targeted known phenomena e.g.
    - the EoR;
    - magnetic fields in structures covering a range of physical scales
    - coherent emission from extrasolar planets
3. New Classes of Sources and Phenomena Based on Known Physics, Biology e.g.
    - transient sources of many kinds
    - new structures e.g in the Cosmic Web
4. The totally unexpected

For the "rare events" under heading 1) the path forward is simple - find more objects. The amount of "surprise" in a data set rises only as the logarithm of the number of independent data elements within it. In the context of astronomical discovery this "logarithmic surprise" idea was first used by Disney (1998). Wilkinson (2007) particularized it for pulsar-related discoveries and the pulsar story was extended by Kramer (2014). For the targeted known phenomena under heading 2) the way forward is basically via the KSPs and PI science – after all these are the "known unknowns". However when we come to headings 3) and 4) new classes of sources and "allowed" phenomena and the complete surprises we need to look in regions of parameter space not previously explored. As Cordes et al. (2006) recognized, the problem arises in defining these areas and so we now turn to this issue.

3.3 Are there unexplored regions of parameter space?

As outlined by Wilkinson (2007) a purely phenomenological approach can offers a complement to the thinking described by Cordes et al. (2006) and by Cordes (2007). This is the basis of Zwicky's "morphological" methodology which he developed to a high art in astronomy and other fields (e.g. Zwicky (1969)). Its basis is that all volume elements in parameter space - as long as

PoS(AASKA14)065

they are not explicitly prohibited – should be considered. Identifying these elements involves freeing one's mind of prejudice and being willing to contemplate unorthodox comparisons. A start for assessing the reach of SKA1 Level 0 science can be made by constructing a cross-linking matrix with the following broad-brush parameters:

- Observing time: short & long
- Total intensity: high & low SNR
- Polarised intensity: high & low SNR
- Spectral patterns: small scale & large scale
- Spectral resolution: high & low
- Spatial patterns: small scale & large scale
- Spatial resolution: high & low
- Temporal patterns: short term & long term
- Temporal resolution: high & low

This leads to a matrix with 18 rows and columns and 144 independent boxes. This matrix is not shown here for reasons of space but the SKA1 Level 0 Science programmes (Braun 2014) do a good job in filling the boxes. There is, however, a set of boxes involving time variable spectra on all angular and spectral scales which is not filled. One example would be "spectral transients".

3.4 Operational flexibility

In order to explore observational parameter space as widely as possible some broad flexibility principles were laid out by Wilkinson et al. (2004). It is encouraging that many of these principles are represented, in one form or another, in the Level 0 Science Specifications and the steadily solidifying technical design. However, the cardinal point of this paper is that people make discoveries not technology. The problem is that no one can forecast which right people are going to be in the right place at the right time. The only response must be to seek ways to allow some people access to lots of telescope time and to allow as many different people as possible to gain some access to the data. The essence of the human bandwidth axis is maximising the "brain multiplexing factor". With this in mind let us look at the range of operational modes identified in SKA documents (Bock et al. 2013; Braun 2014; Cornwell et al. 2014). Reduced to their simplest they are:

- Normal
  - PI
  - Legacy survey
- Targets of Opportunity
- Custom Experiments
- Commensal Observing

A few comments seem worthwhile. First, the normal and TOO modes will be evolutions of existing practice but there is always scope for adding flexibility. For example when the data are being taken for the Legacy Surveys can one open the "collection window" more than is strictly necessary so

PoS(AASKA14)065

as to add depth to the archived data set and hence increase the post-observation discovery potential? Second, the most radical of the suggestions made by Wilkinson et al. (2004) was to allow a fraction of observing time for high-risk or unproven new-style observations which may be tentative or based on a hunch and hence hard to justify in the formal sense. Here the availability of independent beams and commensal observing will help without compromising conventional observing programs. Custom experiments must be considered on a case-by-case basis – but don't become prey to the criticism " knows the price of everything and the value of nothing". Finally, a constant theme of the SKA should be to seek constructive ways of establishing parallel access to the data. Wider public access is only briefly mentioned in Bock et al. (2013) but it could well be crucial in EoU. "Citizen Science" is a proven route to maximising the "reach" and the recent run of successes of Einstein@home in finding new pulsars (Allen et al. 2013; Knispel et al. 2013; Pletsch 2013) provides graphic evidence. The SKA was born global – so let it be a globally accessible source of data!

3.5 Synergy with other telescopes

The sensitivity of the SKA means that for the first time in the history of astronomy, an object detected in any waveband in the electromagnetic spectrum is also likely to be detected in the radio. The opportunities for data linkages with other with ground- (e.g. LSST; ELT; TMT; GMT) and space-based (e.g. JWST; GAIA; EUCLID) telescopes will be enormously greater than with any previous radio telescope. As well as specific bilateral comparisons SKA scientists should make a major commitment to getting the most out of international Virtual Observatories and hence to maximise professional and public access to multi-wavelength data. There was plenty of evidence from talks at AASKA14 that this message is understood by the SKA community.

3.6 Conclusions

"The known knowns" – read the literature;
"The known unknowns" – write a proposal;
"The unknown unknowns" – hold on to a vision.

The current community which is planning and implementing the first phase of the SKA should maintain faith with the scientists of the future by ensuring that the SKA system is prepared for the EoU. This capability will come from a holistic vision of its:

- Large data collecting power: from raw sensitivity and large field-of-view plus multiple beams some of which can be dedicated to specific tasks.
- Some freedom to take risks: from use of independent beams plus new time allocation paradigms.
- Large human bandwidth: allowed by commensal observing; multiple independent beam capability; an in depth data archive coupled with a coordinated strategy for the use of international Virtual Observatories and the citizens of the world.

Much is this is there in present thinking. But the system is not yet built and the flexibility required for the EoU is likely to impose an additional cost burden and hence is vulnerable. What price is

PoS(AASKA14)065

reasonable? I propose that we should be prepared to build up to 10% less collecting area for a given overall budget in order to enhance the ways in which this area can be utilized. The penalty may be up to 20% longer to carry out some projects but this is a graceful degradation and the upside is opening up "opportunity space". I believe that this is likely to prove a good bargain.

References

Allen B., Knispel B., Cordes, J. et al., Ap.J., 773, 91 (2013)

Bock, D., Dewdney P., Garrington S., et al "Concept of Operations for the SKA Observatory", Document Number SKA.TEL.SE.OPS-SKO-COO-001-0-A, revision B (2013)

Braun, R., "SKA1 Level 0 Science Requirements" Document Number SKA-TEL.SCI-SKO-SRQ-001 Revision 1 (2014)

Cornwell, T., McPherson A. & Diamond, P., "SKA Phase 1 System (Level 1) Requirements Specification" Document Number SKA-OFF.SE.ARC-SKO-SCI-001-3 Revision (2014)

Carilli, C & Rawlings, S. eds; "Science with the Square Kilometre Array" New Astronomy Reviews (2004)

Cordes J. et al., SKA Memo 85 (2006)

Cordes, J., SKA Memo 97 (2007)

Disney, M., "The comparative discovery potential of any astronomical instrument – or how to make discoveries", unpublished manuscript, (1998).

Harwit, M., "Cosmic Discovery", pub. MIT Press, Cambridge, (1984)

Lorimer, D., Bailes, M., McLaughlin, M., et al., Science, 318, 777 (2007).

Knispel, B., Eatough., R., Kim, H., et al., ApJ, 774, 93 (2013)

Kramer, M., "Pulsar Science with the SKA and its precursors – an overview": in "Transformational Science with the SKA" Stellenbosch (2014)

Kulkarni, S., arXiv:1202.2738v1 [astro-ph.IM] (2012)

Norris, R., Basu, K., Brown, M. et al., 2015, "The SKA Mid-frequency All-sky Continuum Survey: Discovering the unexpected and transforming radio-astronomy", in "Advancing Astrophysics with the Square Kilometre Array", PoS(AASKA14)086

Pletsch, H., Guillemot, L., Allen, B., et al., Astrophys J. Lett. 779, L11, (2013)

Wilkinson, P., in IAU/URSI Symposium 131, "Radio Interferometry - Theory, Techniques and Applications", ed. T.J. Cornwell, Publ. astr. Soc. Pacific, Conference Series Vol. 19, p. 428-432, (1991).

Wilkinson, P., Kellermann, K., Cordes, J. et al., in "Science with the Square Kilometre Array", eds C. Carilli and S. Rawlings, New Astronomy Reviews, 48, p1551. (2004)

Wilkinson, P., in "From Planets to Dark Energy The Modern RadioUniverse", Proceedings of Science (2007).

Zwicky, F.,"Discovery, Invention, Research – Through the Morphological Approach", pub. Macmillan, Toronto, (1969)

PoS(AASKA14)065

PROCEEDINGS OF SCIENCE

Early Phase Detection and Coverage of Extragalactic and Galactic Black Hole X-ray Transients with the SKA

Wenfei Yu[*†], **Hui Zhang, Zhen Yan and Wenda Zhang**
Shanghai Astronomical Observatory
80 Nandan Road, Shanghai 200030, China
E-mail: wenfei@shao.ac.cn

SKA's large field of view and high sensitivity at low frequencies will provide almost a complete coverage of the very early rising phase of extragalactic and Galactic transients which undergoes a flare or outburst due to an abrupt accretion onto either supermassive (such as tidal disruption events, TDEs) or stellar mass black holes (such as black hole LMXB) transients, when their broadband emission is supposed to be jet-dominated at low luminosities, allowing SKA to be the first facility to make source discoveries and to send out alerts for follow-up ground or space observations as compared with the sensitivity of future X-ray wide-field-view monitoring. On the other hand, due to extremely large rate-of-change in the mass accretion rate during the rising phase of TDE flares or transient outbursts, SKA will be able to cover an extremely large ranges of the mass accretion rate as well as its rate-of-change during the rising phase not accessible with observations in persistent black hole systems, which will shape our understanding of disk-jet coupling in accreting black holes in the non-stationary accretion regimes.

Advancing Astrophysics with the Square Kilometre Array
June 8-13, 2014
Giardini Naxos, Italy

[*]Speaker.
[†]We acknowledge support by the National Natural Science Foundation of China under grant No. 11333005.

PoS(AASKA14)066

1. Scientific background

Wide field-of-view (FOV) astronomical monitors and survey telescopes are very important to the time-domain astronomy, a rapidly developing field with the advances of space and ground telescopes equiped with either fast response or wide FOV monitoring or survey capabilities across a broad range of the electromagnetic wavelength. Diverse time domain phenomena, such as gamma-ray bursts, supernova explosions, tidal disruption flares, X-ray nova, giant flares from soft gamma repeater, transient pulsars or fast radio bursts, and so on, can only be efficiently detected with sensitive monitoring or wide FOV surveying telescopes. Wide FOV monitoring and surveying telescopes will bring a great impact on future astronomy.

All-sky or wide FOV X-ray monitoring has led such time domain studies on high energy transients for several decades. The success can be dated back as early as the discovery of gamma-ray bursts which was about 50 years ago. Current X-ray monitors remain at the frontier of time-domain astronomy on high energy transients. For instance, new scientific discoveries continue to occur from monitoring or survey observations made with current space observatories such as Swift, MAXI, and INTEGRAL. However, newly built or currently planned multi-wavelength time-domain ground facilities, such as the Palomer Transient Factory (PTF), the Pan-SSTARs, the LSST, and the LOFAR etc., will bring time domain astrophysics to a golden era, allowing almost simultaneous broadband coverage of those transient events, including potential transient events associated with strong gravitational waves. Here we emphasize that wide FOV monitoring observations with the SKA have significant advantages in observing Galactic and extragalactic black hole transients in the early rising phase, a great potential to take over future space X-ray monitors in monitoring Galactic and extragalactic black hole transients based on what we have learnt about disk and jet emission from accreting black holes and neutron stars. A wide FOV monitoring in the SKA1 towards the central Galactic Bulge region can demonstrate these advantages in the early phase of SKA.

1.1 Monitoring of Extragalactic and Galactic X-ray transients

Most of the high energy transients, such as GRBs and black hole transients, are of the nature of rapid accretion onto compact objects in a large range of mass accretion rate, from below 10^{-5} Eddington luminosity to super-Eddington luminosity. X-ray monitoring observations in the past few decades have usually reached a daily sensitivity of mCrab level, unable to alert transient activities at earlier times when the X-ray flux is substantially lower. At lower mass mass accretion rate regimes, the observed electromagnetic flux is probably dominated by jet emission rather than from the emission of the accretion flow itself, as suggested by the observations of microquasars and the prediction of the accretion theory such as advection-dominated accretion flow (ADAF) model for the accretion flows in the lower mass accretion rate regimes (Esin et al. 1996). This unambiguously highlights that the most sensitive and effective probe of activities in black holes accreting at low mass accretion rate is through the observations of their jet emission. Observations have shown that jet emission in microquasars contribute to a broad wavelength from the infrared (e.g., Russel et al. 2007) all the way up to at least ultra-violet (e.g., Yan & Yu 2012; Degenaar et al. 2014). However, these jets are usually detected in the radio band since only the most energetic ones could extend

PoS(AASKA14)066

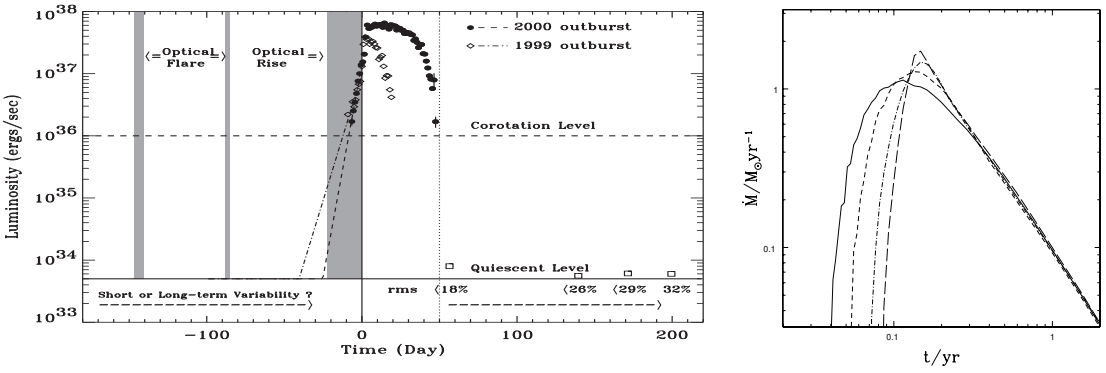

Figure 1: Examples of X-ray outbursts from a Galactic X-ray binary transient and the evolution of the fall-back rate expected from theory during typical tidal disruption events (TDEs). **Left:** An example of the X-ray outbursts of the neutron star soft X-ray transient Aquila X-1 as observed with the RXTE/ASM (2–12 keV). Typical rise time scale for black hole transients are about twice longer. A linear extrapolation of the rising trend in the X-ray flux back in time implies that outbursts started about 10–30 days from quiescent level before they were detected by the ASM on board the RXTE. Future X-ray monitoring with Lobster-Eye instrument would reach an X-ray sensitivity at the level of an X-ray luminosity of about 5×10^{34} ergs/s for this source, while SKA1 and SKA2 will be able to monitoring this source immediately after the source rose from quiescence, at the equivalent X-ray luminosity level of 1×10^{34} ergs/s (corresponding to about 25 microJy in radio band at 8.5 GHz) following the trend established from previous observations of a slope 0.6 (Miglari et al. 2011), and can detect such outbursts about a week before any possible detections with the next generation all-sky monitors, leading to a major step forward for the broadband monitoring of Galactic XRB transients. **Right:** The evolution of fall-back rate during typical tidal disruption flares (from Lodato, King & Pringle 2009). The typical rise time is on the time scales of about 20 days (0.5 T_m as calculated in Evans & Kochanek 1989) and the rate-of-increase of the mass accretion rate onto the supermassive black hole would be dramatic. Towards lower fall-back rate during the rising phase back in time during the rise, jet emission is expected to dominate when the corresponding mass accretion rate is low (Yuan, Cui & Narayan 2005). The SKA 2 has the sensitivity and large-enough FOV to detect these events about a week before they reach the maximum fall-back rates. Since typical peak luminosity of a TDE flare will be super-Eddington for typical SMBHs of the order of 10^6 solar masses, the coverage of almost the entire rising phase with the SKA 2 will be revolutionary.

to shorter wavelengths. This makes sensitive radio observations the most promising probe of the activities of black holes accretion at mass accretion rates.

Besides observing transients in the radio wavelength, there are quite some ambitious optical surveys with large FOV optical telescopes undergoing or planned, which will bring significant progress on transient science for the time domain astronomy. Among them, iPTF has carried out optical survey with different cadences, from a 5-day cadence down to 90 seconds. Its followup project ZWICKY will have a FOV of 47 square degrees with a survey speed of 3760 square degrees per hour. In its survey mode, Pan-SSTARS will cover 6000 square degrees per night, reaching a limiting magnitude of 24 in each exposure of tens of seconds. LSST has a field-of-view of 9.6 square degrees and will detect 10^6 transients per day. All these optical survey telescopes will bring tremendous data on transients and persistent sources. SKA's monitoring and survey capability

PoS(AASKA14)066

provide opportunities of source discoveries and synergetic multi-wavelength campaigns on newly discovered transients and persistent sources.

2. New discovery window with the SKA: the early rising phase

Space X-ray monitoring has been extremely successful in the past few decades on high energy transients of Galactic and extragalactic origins. Some examples of discoveries made with X-ray monitoring observations include gamma-ray bursts and soft gamma-ray repeaters, soft X-ray transient outbursts, supernova explosion during shock breakout, jetted tidal disruption events, etc. Most often these all sky or large FOV X-ray monitors are onboard satellites or space stations with a typical earth orbit of 1.5 hours or so, and usually serves to send out alerts while detailed X-ray spectral and short-term variability can not be simply acquired. Detailed spectral and timing properties rely on follow-up target-of-opportunity observations with dedicated space or ground telescopes or experiments. In the past decades, space X-ray monitors have reached a daily sensitivity at about the mCrab level. In the next decade the sensitivity of X-ray monitors would reach a flux level of about two orders of magnitude lower, with the development of large field-of-view Lobster-eye X-ray optics (Schmidt 1975; Angel 1979).

When approaching black hole transients at lower luminosities, large FOV radio facilities like SKA, in phase 2, will impose major challenge of the role of X-ray all-sky of wide FOV monitoring, and will likely take the lead instead according to our current knowledge of black hole accretion at low luminosities. Gallo et al. (2003) showed that there is a correlation between the radio flux and the X-ray flux in black hole X-ray binaries in the hard state, with the power-law index of the radio flux being 0.7 of that of the X-ray flux. The most updated data shows some obvious deviation and large scatters from this correlation (e.g., Gallo et al. 2014). However, black hole transients are still much more radio loud than neutron star low mass X-ray binary transients (Migliari & Fender 2006). It is found that even in the NS LMXBs the radio-X-ray correlation may follow different pow-law slopes (Migliari et al. 2011). The transient NS LXMB Aquila X-1 is typical for NS LMXBs showing a slope of 0.6, thus the slope for Aquila X-1 type NS LMXBs can be used to give conservative estimate of the LMXB transients as a whole. Together with the overall correlation in black hole X-ray binaries, this implies that the radio flux decrease slower than the X-ray flux when we approach lower luminosities. Therefore opportunities with radio observations will start to arise; sensitive radio observations will be able to surpass X-ray monitoring observations towards lower mass accretion rates. Taking Aquia X-1 as the example (see Figure 1 left). The empirical correlation with a power-law index of 0.6 gives that at an X-ray luminosity of 10^{34} ergs/s, which is just a little above its quiescent luminosity, the corresponding radio flux at 8.5 GHz would be 25 microJy. This radio flux level is well above the sensitivity of SKA1-SUR or SKA1-LOW for 20 minutes observations or so while an X-ray Lobster-Eye instrument can only reach the X-ray luminosity level of 5×10^{34} ergs/s with similar exposure time, which means the next generation X-ray monitor is not able to detect it in the same period of time. The same applies to accreting supermassive black holes. Merloni et al. (2003) found that there is fundamental plane of black hole activity. Similarly, the power-law index of the radio luminosity vs. the X-ray luminosity relation is about 0.6. Again, this indicates towards lower luminosities black hole accretors are relatively more radio bright compared with their X-ray brightness, and therefore radio observations with the SKA1-

PoS(AASKA14)066

SUR or SKA1-LOW, and SKA2, will be more sensitive to source activities at low luminosities (see Dewdney et al. 2013 for the SKA1 parameters). This means SKA observations in radio is able to lead X-ray monitoring campaigns on black hole transients of both Galactic and extragalactic origin, and therefore SKA has the chance to change the way of black hole monitoring. Sensitive wide FOV monitoring in radio band with SKA hence opens a new discovery window inaccessible with the X-ray monitoring of both stellar mass black hole and supermassive black hole transients in the decades to come.

For stellar mass black hole transients in our Galaxy, the quiescent X-ray luminosity in the 0.5–10 keV band is about 10^{30-31} ergs/s (e.g., Garcia et al. 2001). During the rising phase of black hole or neutron star LXMB transient outbursts, the e-folding rise time scales in the X-ray band measured with current X-ray monitors is about 3-5 days (Yan & Yan 2014, see early results of X-ray monitors in Chen et al. 1997). With an equivalent X-ray sensitivity of 1-2 orders of magnitude better, the SKA1 (and the SKA2) design will be able to send out alerts of black hole transient outbursts about a week ahead of X-ray monitoring detections if we assume the rises of either X-ray binary outbursts are of a simple monotonic form. This can be seen in an example shown in Figure 1. Similarly, extragalactic black hole transients such as tidal disruption events (i.e., solar-like star disrupted by the previous dormant supermassive black holes at the centers of normal galaxies) should also start to accrete matter from the debris flow of a disrupted star from very low mass accretion rate to super Eddington rate (Rees 1988; Evans & Kochanek 1989; Lodato, King & Pringle 2009), although the exact accretion process in the early stages is yet not well-studied. According to simple theoretical estimates, the fall-back rate increases from quiescent level undetectable with current X-ray satellites to super-Eddington fall-back rate up to more than 100 Eddington rate in about two-week's time during the rising phase of typical TDE flares (Rees 1988; Evans & Kochanek 1989; Lodato, King & Pringle 2009). Taking a conservative estimate of the quiescent luminosity level of supermassive black holes at centers of normal galaxies as 10^{34} ergs/s (note: Chandra observations of the supermassive black hole source Sgr A* at the center of our Galaxy gives such a value, see Baganoff et al. 2003; Nelsen et al. 2013), the mass accretion rate would rise by up to 10 orders of magnitude in about two weeks' time (Evans & Kochanek 1989). The e-folding rise time scale is then on the time scale of about 0.5–2 days, which can be ten time shorter than those seen during the rising phase of outbursts from Galactic black hole LMXB transients. Therefore TDE flares are cases of extreme non-stationary black hole accretion.

SKA has a very large field of view. For example, at 1 GHz, its field-of-view of SKA2 is around 200 square degrees. Both SKA1 and SKA2 are also very sensitive. For instance, SKA1-SUR's 20 minute sensitivity at 1 GHz is at 0.01 mJy level, and SKA2's 20 minute sensitivity at 1 GHz is at the μJy level. Due to its high sensitivity, its convenience for observations of our Galaxy and its large FOV, SKA is the best astronomical facility to catch the rising phase of outbursts or flares from accreting stellar mass black holes and supermassive black holes. Little is known about the early rising phase of these outbursts or flares from previous observations due to insufficient sensitivity of current and past space X-ray monitors. SKA1-SUR and the SKA Phase 2 will open a huge discovery window in catching the very early rising phase of those black hole transient flares and outbursts from, including both black hole binary transients and tidal disruption flares. Our estimates based on current knowledge of soft X-ray transient outbursts and TDEs suggest that SKA1, through a dedicated Galactic Bulge program, is able to detect black hole binary transients in our Galaxy;

PoS(AASKA14)066

while SKA2 is able to detect extragalactic tidal disruption events during the early rising phase about a week ahead of the most sensitive X-ray monitors in the next decades immediately after the accretion of matter just starts (see Figure 1 left and right).

3. Accretion physics and jet activity in extreme non-stationary accretion regimes

Observations of X-ray spectral states and transitions in Galactic X-ray binaries have shown that the primary parameter - the mass accretion rate is not the only parameter which drives spectral state transitions (Miyamoto et al. 1995; Homan et al. 2001; Maccaroni & Coppi 2003). The hard-to-soft spectral state transition usually observed during the rising phase of outbursts actually occurs at luminosities which correlates with the peak flux of an outburst or flare (Yu et al. 2004; Yu et al. 2007; Yu & Dolence 2007), due to the rate-of-increase in the mass accretion rate, which is not negligible, and in most of the spectral state transitions seen in bright Galactic X-ray binaries the effect of the rate-of-change of the mass accretion rate on the transition luminosity dominates (Yu & Yan 2009; Tang, Yu & Yan 2011). These studies indicate that the accretion properties are set up early and one can predict the spectral state transition ahead of time by measuring the rate-of-increase of the X-ray luminosity (Yu & Yan 2009). It is worth noting that our current knowledge of accretion regimes are actually based on stationary accretion theories. The non-stationary regimes are largely not explored. The studies of the hysteresis effect implies that there is actually accretion regimes specifically to the non-stationary regime, e.g., there is an actual black hole hard state regime corresponding to non-stationary accretion which exists above the mass accretion threshold below which the classical hard state sits as explained by existing theory (e.g., Esin et al. 1997). Because there is certain complex correlation between the radio flux and the X-ray flux in the hard spectral state (Gallo et al. 2003; but with so-called outliers), there is evidence that non-stationary accretion plays an important role in powering the radio jet. This is also suggested by a possible detection of the correlation between the rate-of-change of the mass accretion rate and the episodic jet power (Zhang & Yu, 2014, see Figure 2). Since both TDE flares and black hole binary transients can be detected by the SKA at much earlier times and at much lower luminosities, SKA will provide the opportunity to probe jet activity in the non-stationary accretion regimes over a radio flux range by more than 4 orders of magnitude, which roughly corresponds to an X-ray flux range by about 7 orders of magnitude in Galactic black hole transients. Stronger effect of non-stationary accretion is expected in extragalactic X-ray transients associated with tidal disruption events due to their much shorter e-folding rise time scale. Our conservative estimate suggest that TDE flares rise in luminosity as large as 10 orders of magnitude on the time scale of 20 days, accompanied by an extremely large rate-of-change of the mass accretion rate inaccessible in other black hole systems.

4. Recommended campaigns on extragalactic and Galactic black hole X-ray transients

As we described above, wide FOV sensitive observations in the wavelength have great advantages in detecting stellar mass and supermassive black hole X-ray transients during the very early rising phase of their outbursts or flares. Using SKA1-SUR band 2 with a FOV of 18 and a sensitivity of $0.351\mathrm{mJy/s}^{(}-1/2)$, in order to reach 0.01 mJy/beam per field, we would need 20.5 minutes

PoS(AASKA14)066

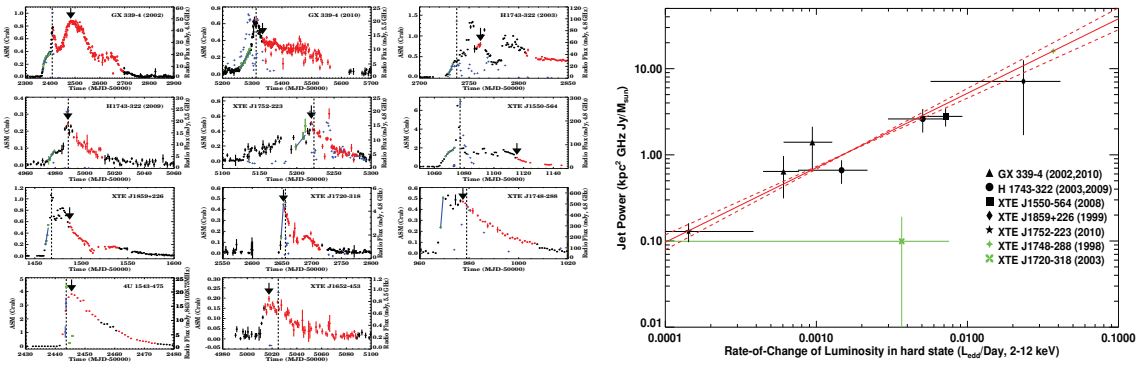

Figure 2: Evidence of the role of non-stationary accretion on the power of episodic jets in microquasars (figures adapted from Zhang & Yu 2014). **Left:** X-ray outbursts of black hole transients with radio observations of the episodic jets. Data shown in blue are radio measurements, data shown in red correspond to black hole soft state. Data marked in green correspond to the segments from which the rate-of-increase of the X-ray luminosity is measured for the rising phase of the corresponding outburst. **Right:** The relation between the episodic jet power and the rate-of-change of the X-ray luminosity measured before the hard-to-soft state transition during black hole transient outbursts (see Figure on the left). The dark points corresponding to sources with good measurements or estimates of mass, distance, X-ray and radio fluxes, while the green points indicate sources with large uncertainties.The best curve is over-plotted in red, with the ranges of uncertainty shown as dotted lines.

observation. The predicted SKA2 sensitivity is about 10 times sensitive than SKA1, which means we can reach the same sensitivity per field in only 12 seconds. WIth increasing FOV for SKA2, an all-sky survey down to 0.01 mJy/beam per field is applicable.

In Phase 1, SKA1-SUR has a FOV of about 18 square degrees in PAF band 2. For Galactic black hole or neutron star transients, in order to cover the very early phase of any future outbursts of Galactic black holes as well as neutron star LMXB transients, most of which reside in the Galactic bulge, a dedicated monitoring campaign of the Galactic bulge is recommended on the daily basis with the SKA1-SUR at 1 GHz. Past X-ray observations of the Galactic bulge indicate that there are about 80 known persistent and transient X-ray binaries in the central 25 x 25 degrees of the Galactic bulge, and probably hundreds to discover in the future. In a smaller central Bulge region of 8 x 8 squared degrees, there are 35 known persistent and transient X-ray binaries. In order to cover this region, we recommend that SKA1-SUR performs more than 4 short observations of the 8 x 8 square degrees of the Bulge down to 0.01 mJy flux level. According to the empirical relation established from radio flux vs. X-ray flux correlation, these SKA1-SUR observations will be able to detect outbursts of Galactic black hole or neutron star LMXB transients before they are visible to current or future X-ray monitors, and will be especially successful in detecting accretion-powered millisecond pulsars which is usually radio-louder than the Atoll type neutron star LMXBs. After the implementation of the full version of the SKA, because the FOV would reach 200 square degrees at 1 GHz, three observations will be able to cover the central Bulge region.

With full SKA's capability of a FOV of about 200 square degrees, SKA is a powerful machine to detect new tidal disruption events at very early times. This will bring tremendous opportunities for Target-of-Opportunities (ToO) with space X-ray observatories such as Athena+ and ground

PoS(AASKA14)066

optical telescopes on the scale of tens of meters, since there will be plenty time for both ground and space observatories to respond (about 10 days' earlier than current X-ray monitoring can provide), which will push time domain astrophysics on black hole transients, especially the tidal disruption events, to the extreme regimes. However, there are difficulties for the SKA1-SUR or the SKA1-LOW to sufficiently detect some extra-Galactic transients such as tidal disruption events due to their limited FOV, but still there are occasions when tidal disruption events occur in the SKA1-SUR or the SKA1-LOW's FOV. A better strategy during SKA1 for black hole transient science is to use SKA1-SUR and SKA1-LOW to perform quasi-simultaneous observations of the same field of view of optical surveys or X-ray all-sky monitoring, such as the LSST's FOV as much as possible. In this way, due to broadband measurements, empirical classification of transient events could be made straight forward. This would allow SKA-MID to perform sensitive follow-up observations of some candidate tidal disruption events timely.

In summary, the motivations of SKA1 and SKA2 campaigns on Galactic and extragalactic black hole X-ray transients are 1) the coverage of the very early rising phase of outbursts or flares and sending out extremely early alerts; and 2) provide rather complete data of jet activities in non-stationary accretion regimes corresponding to a large range of the mass accretion rate and its rate-of-change, which are inaccessible in other black hole accreting sources.

5. Scientific outcomes of SKA1 and SKA2

We expect the following outcomes of the SKA1 and SKA2 on the science of black hole transients containing both stellar mass or supermassive black holes.

In the SKA1, a Galactic Bulge monitoring campaign with SKA1-SUR in the central 8 x 8 squared degrees for 1.5 hours on the daily basis will be able to cover the very early rising phase of nearly half of the stellar mass black hole and neutron star LMXB transient outbursts, which will lead the detection in the X-rays by sensitive X-ray monitoring observations. Such a Galactic Bulge campaign will also detect some APMSP outbursts. Such a monitoring campaign will answer how jet is powered in the non-stationary regimes in a large range of mass accretion rate at the same time of the significant rate-of-change in the mass accretion rate, which will address accretion and jet physics in the non-stationary accretion regimes in LMXB transients. The program will also make SKA1-SUR likely the first facility to detect new black hole and neutron star LMXB transients in the Galactic Bulge at unprecedented low flux level and will be able to send out alerts on new BH or NS transients or outbursts to other ground or space observatories. On the other hand, only coordinated or follow-up SKA1 observations of extragalactic TDE flares are possible in SKA1.

In the SKA2, an efficient monitoring of the Galactic Bulge of a 25 x 25 FOV can be achieved at 1 GHz. Additionally, SKA2 will provide the best opportunity to study extragalactic SMBH transients such as TDEs. The most significant scientific impact on the study of black hole transients would come from the detection of a lot extragalactic TDE flares in the early rising phase with SKA. The SKA2's sensitivity allows detections of such events at the very early times, which is mostly unknown in both theory and observation. SKA2 would provide a complete coverage of their jet activities over an extremely large range of mass accretion rate and its rate-of-change, and is able to send out alerts extremely early for the largest ground and space observatories to respond. Thus

PoS(AASKA14)066

SKA will provide the golden opportunity to solve important astrophysical questions associated with black holes transients in binaries and at the centers of normal galaxies.

REFERENCES

Angel, J. R. P. 1979, ApJ, 233, 364
Bloom, J. S., Giannios, D., Metzger, B. D., et al. 2011, Science, 333, 203
Burrows, D. N., Kennea, J. A., Ghisellini, G., et al. 2011, Nature, 476, 421
Chen, W., Shrader, C. R., & Livio, M. 1997, ApJ, 491, 312
Corbel, S., Coriat, M., Brocksopp, C., et al. 2013, MNRAS, 428, 2500
Dewdney, P., Turner, W., Millenaar, R., McCool, R., Lazio, J., Cornwell, T., 2013, "SKA1 System Baseline Design", Document number SKA-TEL-SKO-DD-001 Revision 1
Evans, C. R., & Kochanek, C. S. 1989, ApJ, 346, L13
Fender, R. 2004, New Astronomy Reviews, 48, 1399
Gallo, E., Fender, R. P., & Pooley, G. G. 2003, MNRAS, 344, 60
Gallo, E., Miller-Jones, J. C. A., Russell, D. M., Jonker, P. G., Homan, J., Plotkin, R. M., Markoff, S., Miller, B. P., Corbel, S., Fender, R. P. 2014.MNRAS, 445, 290.
Garcia, M. R.; Murray, S. S.; McClintock, J. E.; Narayan, R. 2001, ApJ, 553, L47
Lodato, G., Nayakshin, S., King, A. R., & Pringle, J. E. 2009, MNRAS, 398, 1392
Merloni, A., Heinz, S.; Di Matteo, T. 2005, APSS, 300, 45
Merloni, A., Heinz, S.; di Matteo, T. 2003, MNRAS, 345, 1057
Migliari, S., Fender, R. P. 2006.MNRAS, 366, 79.
Migliari, S., Miller-Jones, J. C. A., Russell, D. M. 2011.MNRAS, 415, 2407.
Rees, M. J. 1988, Nature, 333, 523
Russell, D. M., Maccarone, T. J., Körding, E. G., Homan, J. 2007.MNRAS, 379, 1401
Schawinski, K., Justham, S., Wolf, C., et al. 2008, Science, 321, 223
Schmidt, W. K. H. 1975, Nucl. Inst. Methods, 127, 285
Tang, J., Yu, W.-F., & Yan, Z. 2011, Research in Astronomy and Astrophysics, 11, 434
Yan, Z. & Yu, W. 2014, submitted to ApJ (aarXiv: 1408.5146)
Yu, W., & Dolence, J. 2007, ApJ, 667, 1043
Yu, W., Lamb, F. K., Fender, R., & van der Klis, M. 2007, ApJ, 663, 1309
Yu, W., van der Klis, M., & Fender, R. 2004, ApJ, 611, L121
Yu, W., & Yan, Z. 2009, ApJ, 701, 1940
Yuan, F., Cui, W., Narayan, R. 2005. ApJ, 620, 905.
Zhang, H. & Yu, W., 2014, submitted to MNRAS

PoS(AASKA14)066

PROCEEDINGS OF SCIENCE

Lunar detection of ultra-high-energy cosmic rays and neutrinos with the Square Kilometre Array

J.D. Bray*[1], J. Alvarez-Muñiz[2], S. Buitink[3], R.D. Dagkesamanskii[4], R.D. Ekers[5], H. Falcke[3,6], K.G. Gayley[7], T. Huege[8], C.W. James[9], M. Mevius[10], R.L. Mutel[7], R.J. Protheroe[11], O. Scholten[10], R.E. Spencer[12] and S. ter Veen[3]

[1]*Univ. of Southampton;* [2]*Univ. de Santiago de Compostela;* [3]*Radboud Univ. Nijmegen;* [4]*Lebedev Physical Institute;* [5]*CSIRO ATNF;* [6]*ASTRON;* [7]*Univ. of Iowa;* [8]*KIT;* [9]*Univ. of Erlangen-Nuremberg;* [10]*Univ. of Groningen;* [11]*Univ. of Adelaide;* [12]*Univ. of Manchester*
E-mail: j.bray@soton.ac.uk

The origin of the most energetic particles in nature, the ultra-high-energy (UHE) cosmic rays, is still a mystery. Only the most energetic of these have sufficiently small angular deflections to be used for directional studies, and their flux is so low that even the 3,000 km^2 Pierre Auger detector registers only about 30 cosmic rays per year of these energies. A method to provide an even larger aperture is to use the lunar Askaryan technique, in which ground-based radio telescopes search for the nanosecond radio flashes produced when a cosmic ray interacts with the Moon's surface. The technique is also sensitive to UHE neutrinos, which may be produced in the decays of topological defects from the early universe.

Observations with existing radio telescopes have shown that this technique is technically feasible, and established the required procedure: the radio signal should be searched for pulses in real time, compensating for ionospheric dispersion and filtering out local radio interference, and candidate events stored for later analysis. For the Square Kilometre Array (SKA), this requires the formation of multiple tied-array beams, with high time resolution, covering the Moon, with either SKA1-LOW or SKA1-MID. With its large collecting area and broad bandwidth, the SKA will be able to detect the known flux of UHE cosmic rays using the visible lunar surface — millions of square km — as the detector, providing sufficient detections of these extremely rare particles to address the mystery of their origin.

Advancing Astrophysics with the Square Kilometre Array,
June 8-13, 2014
Giardini Naxos, Sicily, Italy

*Speaker.

PoS(AASKA14)144

1. Introduction

Cosmic rays are extraterrestrial high-energy particles with a spectrum (Amsler et al. 2008; Gaisser 2006) ranging from around 10^9 eV up to at least 10^{20} eV. The most energetic, ultra-high-energy (UHE) cosmic rays have an incredible amount of energy for a single particle — comparable to a well-served tennis ball — and their origin is unknown. The usual mechanism invoked for producing cosmic rays is the acceleration of charged particles by magnetic fields around shocks in the interstellar medium, via the Fermi process. However, the ability of a shock or other region of magnetic turbulence to accelerate a particle up to the highest energies is limited by its ability to keep the particle confined as it accelerates (Hillas 1984), and the observed UHE cosmic rays have energies around the limit achievable by known astrophysical objects such as active galactic nuclei, starburst galaxies, and gamma-ray bursts (Torres & Anchordoqui 2004), suggesting that other mechanisms may need to be invoked to overcome this limit (Protheroe et al. 2003). Alternatively, UHE cosmic rays could originate from the decay of hypothetical supermassive particles, which could either constitute dark matter, or be produced by topological defects such as kinks and cusps in cosmic strings formed in the early universe (Berezinsky et al. 2011; Lunardini & Sabancilar 2012). Identifying the source of UHE cosmic rays would improve our understanding of the most extreme astrophysical objects in the universe and the particle acceleration mechanisms they can support, and potentially establish the existence of hitherto-unknown exotic particles.

The study of UHE cosmic rays is difficult because of their extremely low flux: the cosmic ray spectrum follows a power-law of approximately $E^{-2.7}$, and at the highest energies the flux drops so low that less than one particle is detected per km^2 per century. Associating them with specific sources is also difficult because, as charged particles, they are deflected by intervening magnetic fields, so their direction of arrival does not correspond to the direction of their source. Furthermore, at energies exceeding $\sim 6 \times 10^{19}$ eV, they can interact with photons of the cosmic microwave background, either through photopion interactions (for cosmic-ray protons) or photodisintegration (for cosmic-ray nuclei); this GZK effect (Greisen 1966; Zatsepin & Kuzmin 1966) causes attenuation of the cosmic-ray flux at the highest energies, preventing many of them from reaching us. Studies of the few UHE cosmic rays that reach us have found them to be weakly correlated with the distribution of matter in the nearby universe (Abraham et al. 2007), which establishes that they are anisotropic, but the statistics are not sufficient to clearly link them to a specific class of source.

The observations proposed herein explore two major avenues for improving our understanding of the origin of UHE cosmic rays. The first is to observe more cosmic rays of even higher energy. As the energy increases, the magnetic deflection is reduced, and it becomes easier to link a particular cosmic ray with a specific source; together with an increase in the number of detected particles, correlation studies will be greatly improved. Also, the presence or absence of cosmic rays at higher energies will establish whether the observed cutoff in the spectrum (Abraham et al. 2008b; Settimo et al. 2012) is due to the GZK effect, in which case there will be a contribution at higher energies from sources within the GZK horizon; or from an inherent limit on the cosmic-ray energy which can be attained by their sources, in which case the cutoff will be sharp.

The second option is to search for UHE neutrinos, which should be produced both by UHE cosmic ray sources and in GZK interactions. Since neutrinos are uncharged, they travel in straight lines, and point directly back to their original source. Exotic-particle-decay models for the origin

PoS(AASKA14)144

of UHE cosmic rays also predict hard neutrino spectra up to extremely high energies, which would be a clear indication that these models were correct.

Due to the reduced cosmic ray flux at higher energies, and because neutrinos interact only weakly, both these methods benefit from extremely large detectors, significantly greater than even the $3,000$ km^2 Pierre Auger Observatory (Abraham et al. 2008a) and 700 km^2 Telescope Array (Abu-Zayyad et al. 2012). The resulting strategy is to remotely monitor a large fraction of the Earth's surface from a high-altitude balloon (Gorham et al. 2009) or from space (Takahashi et al. 2009). An alternative approach (Dagkesamanskii & Zheleznykh 1989) is to use the Moon as the detector, searching for the radio Askaryan pulse (Askaryan 1962) produced when a UHE cosmic ray or neutrino interacts in the dense lunar regolith. The visible lunar surface has an area of $19,000,000$ km^2; even with limited efficiency and angular acceptance, it still constitutes a very large UHE particle detector.

Since this idea was proposed, a series of experiments has been conducted by multiple teams with a range of radio telescopes: Parkes (Hankins et al. 1996), Goldstone (Gorham et al. 2004), Kalyazin (Beresnyak et al. 2005), the ATCA (James et al. 2010), Lovell (Spencer et al. 2010), the EVLA (Jaeger et al. 2010), Westerbork (Buitink et al. 2010), Parkes again (Bray 2013), and Parkes and the ATCA in combination (Bray et al. 2011), with preparatory work under way with LOFAR (Singh et al. 2012). These experiments have overcome a range of technical challenges specific to this type of experiment and, together with associated theoretical work, have established the viability of this technique for detecting UHE particles. The upcoming Square Kilometre Array (SKA) is an international radio telescope that will have greater sensitivity than any previous instruments. With SKA1 it will be able to achieve the first lunar-target particle detection, while SKA2 will be a powerful instrument for addressing the mystery of the origin of cosmic rays.

2. Particle astronomy with a radio telescope

In this section, we describe the physical mechanism — the Askaryan effect — by which the interaction of high-energy particles produces radio emission, and the methods by which a radio telescope such as the SKA could detect that emission.

2.1 Particle cascades and radio emission

A UHE particle interacting in a dense medium will initiate a particle cascade, with the total energy being distributed over an increasing number of particles as the cascade progresses. Due primarily to entrainment of electrons in the medium, the cascade develops a net negative charge (Askaryan 1962), causing it to radiate coherently at wavelengths greater than the width of the cascade ($\lambda \gtrsim 10$ cm; frequencies up to a few GHz). This radiation is beamed forward as a hollow cone around the cascade axis at the Cherenkov angle ($\sim 55^\circ$), at which it manifests as a single pulse with a duration given by the inverse bandwidth ($\lesssim 1$ ns). For directions away from the Cherenkov angle, the pulse is weaker, and more extended in time. The emission is more broadly beamed at lower frequencies, with the radiation pattern extending to perpendicular to the cascade axis (Scholten et al. 2006), and stronger at higher frequencies, as shown in Fig. 1 (left).

If the primary particle is a cosmic ray, then the cascade consists predominantly of hadrons, and develops (in a dense medium such as the lunar regolith) quite quickly, reaching a length of

PoS(AASKA14)144

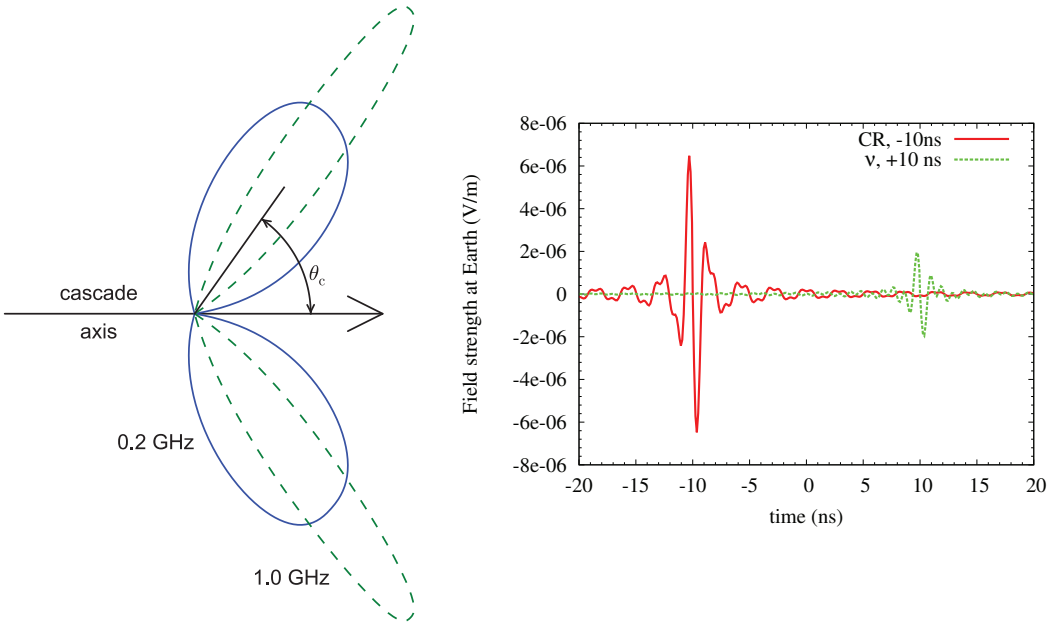

Figure 1: Left: Askaryan emission from a hadronic particle cascade in regolith. The emission is directed forward along the cascade axis as a hollow cone at the Cherenkov angle θ_c. The radiation pattern depends on the frequency, as shown. Right: time-domain pulses (excluding dispersive effects) from 10^{20} eV cosmic ray (CR) and neutrino (ν) interactions with typical geometries, as might be recorded at Earth over a 350 MHz to 1.05 GHz bandwidth. The pulses have been offset by $\pm$10 ns for display purposes.

only $\sim$ 3 m (Alvarez-Muñiz et al. 2006). If the primary particle is a neutrino, it initiates a hadronic cascade carrying $\sim$ 20% of the primary energy, which behaves in a similar fashion. Depending on the neutrino flavour and interaction type, the remaining energy may go into an electromagnetic cascade, containing only electrons/positrons and photons, but at ultra-high energies these cascades are highly elongated, suppressing their radio emission, and are not generally detectable (James & Protheroe 2009).

A cosmic ray interacts as soon as it enters the regolith, so all such cascades occur close to the lunar surface. At higher frequencies, where the radiation is strongly beamed forward, and refracted further forward as it escapes the lunar surface, the cascade is only detectable if the cosmic ray interacts in a shallow, skimming trajectory, allowing the radiation to escape rather than being directed downward into the Moon. At lower frequencies, where emission sideways from the cascade is coherent (ter Veen et al. 2010), detection is possible over a greater range of interaction geometries.

Neutrinos interact less strongly than do cosmic rays, and may occasionally pass through the bulk of the Moon and interact while steeply upgoing relative to the local surface, but at ultra-high energies their interaction cross-section is increased, and they are most likely instead to be detected in a skimming trajectory similar to cosmic rays. They may, however, be well below the lunar surface when they interact, and may be detected at depth up to a few times the radio attenuation length in the lunar regolith (a few tens of metres, depending on frequency). Because many of them will interact too deeply in the Moon to be detected, neutrinos are less likely to be detected than are

PoS(AASKA14)144

cosmic rays (Jeong et al. 2012).

The radiated pulse manifests as a transient bipolar fluctuation in the electric field measured by a radio receiver, as seen in Fig. 1 (right), and confirmed in laboratory measurements at SLAC (see e.g. Miočinović et al. 2006). As the components of the pulse at different frequencies combine coherently in the voltage domain, the signal-to-noise ratio in power scales linearly with bandwidth, in contrast to the square-root law typical in other fields of radio astronomy. The sensitivity of a radio telescope defines a minimum detectable pulse amplitude, which in turn defines a minimum detectable particle energy; the SKA, with its superior sensitivity, will probe down to lower particle energies than has previously been possible with this technique. As the pulse has a spectrum which increases in amplitude with increasing frequency, up to an angle-dependent turnover at a few GHz or below due to either decoherence or absorption, observations aiming to minimise the detection threshold tend to favour higher frequencies. Above the threshold energy, the sensitivity of an experiment to a particle flux is defined by the geometric aperture, with units of area times solid angle. The radio pulse at low frequencies is more broadly beamed, covering a larger solid angle, which favours lower frequencies for observations significantly above the detection threshold.

This complex dependence of sensitivity on frequency means that both SKA1-LOW and SKA1-MID are useful and complementary in this role, and explore different regions of the energy-flux phase space. (SKA1-SUR, despite its larger field of view, offers no advantage over SKA1-MID, as the field of view of the latter is sufficient to see the entire Moon.) The discussion below, except where noted, applies to both instruments.

2.2 Observational requirements

The observational requirements for detecting a nanosecond-scale pulse from the Moon are different from those of other areas of radio astronomy. Such a short pulse is only detectable in the original time-domain voltages sampled by the receiver, at their full native time resolution. Storing this quantity of data is usually impractical, so it is generally necessary to maintain a buffer of data and search for a pulse in real time, triggering the storage of the buffer only when a candidate event is found; the proposed signal path is shown in Fig. 2. The trigger criteria need not be perfectly optimised in real time, but they must be good enough that all plausible events are stored so that they can be analysed retrospectively.

As an array, the SKA is only fully sensitive to a transient signal when it is combined to form a tied-array beam. Buffered data can (and should) be kept from individual dishes/stations of the SKA so that they can be combined retrospectively, but for triggering purposes it is necessary to form beams with at least the core of the array in real time, to have sufficient sensitivity to detect candidate events. The specifications for SKA1-MID include such a beamformer (Dewdney et al. 2013), and a proposal for a similar feature for SKA1-LOW is under consideration (Stappers et al. 2014). The SKA1-MID beamformer, for bands 1 and 2, will have the capacity to form sufficient beams to tile across the visible surface of the Moon (~ 0.2 deg^2), and to tile in frequency to cover the entire band.

For a nanosecond-scale pulse to be detected, the signal for each beam should consist of a single sequence of voltage samples, with inverse-bandwidth time resolution, so that a pulse — which might comprise a single high-amplitude sample — can be identified. This presents a problem, as the beamformer acts on the signal after it has passed through a polyphase filterbank, which

PoS(AASKA14)144

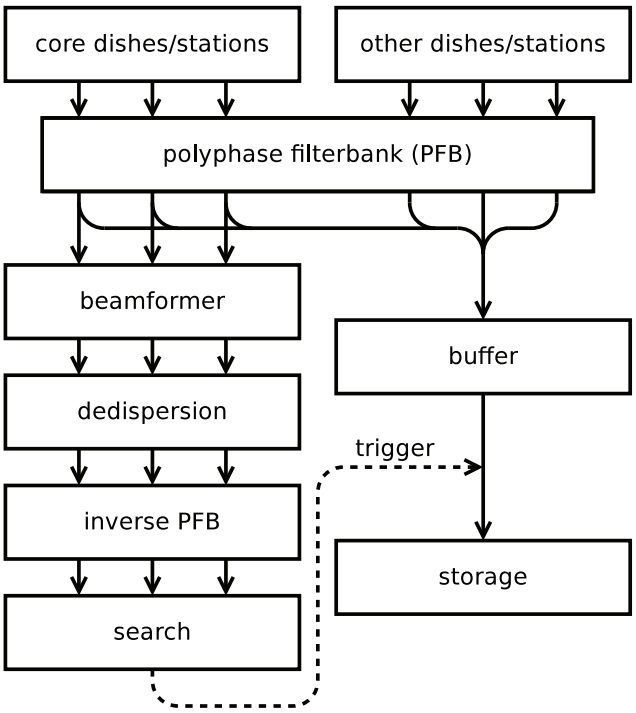

Figure 2: Proposed signal path as described in Sec. 2. The signals from the core dishes (SKA1-MID) or stations (SKA1-LOW) are, after being channelised by the polyphase filterbank, formed into sufficient beams to tile across the visible surface of the Moon. While still channelised, they are dedispersed to compensate for the effects of the ionosphere, and then converted back to pure time-domain signals by an inverse polyphase filterbank. The resulting signals are then searched searched for a nanosecond-scale pulse meeting several RFI-rejection criteria. If one is found, it is used to trigger the storage of buffered data from all dishes/stations, which can be retrospectively processed to analyse the pulse with the full sensitivity of the entire array.

separates it into frequency channels with inverse-channelwidth time resolution. Fortunately, it is possible to invert a polyphase filterbank to restore the time-domain signal for each beam, with a minor loss of efficiency (Singh et al. 2012).

A lunar-origin nanosecond-scale radio pulse is dispersed as it passes through the ionosphere. The degree of dispersion is minor compared to that for interstellar signals but, due to the extremely short pulse, it still causes a significant loss of amplitude, and must be corrected. Because the signal is channelised during the beamforming stage, it is relatively simple to dedisperse it by applying an appropriate phase factor, but it may be necessary to test the signal for a trigger condition at multiple dispersion measures, depending on how precisely the dispersion can be predicted. Current techniques are based on ionosonde measurements or GPS-based global electron content maps; improvements are possible through direct measurements of dispersion to GPS satellites from a ground station at the telescope site (currently on trial at Parkes) or through measurements of the Faraday rotation of polarised thermal emission from the Moon itself (McFadden et al. 2011).

As transient detection experiments aim to detect single, unrepeated events, they are highly susceptible to radio-frequency interference (RFI): it is necessary to reliably exclude every single instance of nanosecond-scale impulsive RFI to be certain that any remaining events are true lunar-

PoS(AASKA14)144

origin Askaryan pulses. The simplest way to achieve this is to require a coincident detection on multiple independent antennas (e.g. Gorham et al. 2004), but this limits the sensitivity of the experiment. In experiments which have used the full coherent sensitivity of a telescope's entire collecting area, the most effective technique is to exclude pulses that are detected with multiple beams directed at different parts of the Moon, as employed with the WSRT (Buitink et al. 2010) and the Parkes telescope (Bray 2013). In the latter case, RFI was successfully excluded with high fidelity in real time, and completely in retrospective processing. The SKA will have the further advantages of a less active RFI environment and a greater number of beams on the Moon, and we are confident that RFI triggers can be excluded with sufficient reliability that they will not dominate the real-time trigger rate, and those which do cause a trigger can be eliminated in retrospective processing.

If RFI is excluded, then the trigger rate will be dominated by thermal fluctuations in the voltage. As each trigger causes the current contents of the buffers to be stored to disk, the speed with which these data can be stored will determine the supportable trigger rate, and hence how low the trigger threshold can be set. Assuming a trigger condition of a global OR over all the on-Moon beams, so that a pulse can be detected from anywhere on the Moon, a trigger threshold of $\sim 7\sigma$ (relative to the thermal noise) would suffice to keep the background trigger rate around 1 Hz. Assuming a buffer length of 10 μs, primarily to assist in characterising RFI, and 8-bit sampling, this results in a manageable data-storage rate of ~ 10 MB/s. This value applies to both SKA1-LOW and SKA1-MID: the former has more stations and the latter has a higher sampling rate, but these effects approximately cancel out.

Retrospective analysis will achieve greater sensitivity than the real-time beams, due to the use of the entire array rather than just the beamformed core, resynthesising the beam directly on the source position, more precise dedispersion, etc. These effects are typically of the order of a few tens of percent. Combined, they might allow retrospective analysis to reach a sensitivity $\sim 2\times$ that available in real time; i.e. the real-time sensitivity would be worse than the theoretical sensitivity by a factor of 2, or $\sqrt{2}$ in the voltage domain. This means that a 7σ threshold in the real-time trigger would ensure that any pulse exceeding $7\sqrt{2}\sigma \sim 10\sigma$ with the full theoretical sensitivity would be stored and detected. We use this 10σ threshold when calculating the sensitivity in Sec. 3. At this level, the false detection rate is less than one per century.

3. SKA performance

Simulations of the SKA sensitivity to UHE particles using the lunar Askaryan technique were performed by a detailed Monte Carlo code (James & Protheroe 2009). This code simulates particle propagation and interactions in the Moon, radio-wave production according to Alvarez-Muñiz et al. (2006), its subsequent absorption in and transmission through lunar rock, and signal detection based upon an assumed instrumental sensitivity and the calculated pulse strength. The accuracy of this simulation has been verified by comparisons with (semi-)analytic calculations in limiting cases (Gayley et al. 2009; Scholten et al. 2006).

The dominant uncertainties in the simulation are the interaction cross-sections for UHE neutrinos and the effects of lunar surface roughness. The former have an uncertainty at 10^{20} eV of $\sim 20\%$ within the standard model (Cooper-Sarkar et al. 2011), and exotic extra-dimensional models suggest that they could be larger by 1–2 orders of magnitude (Connolly et al. 2011); we use the

PoS(AASKA14)144

			SKA1		SKA2	
Band	f_{min} (MHz)	f_{max} (MHz)	$A_{\mathrm{eff}}/T_{\mathrm{beam}}$ m^2/K	E_{thresh} V/m/MHz	$A_{\mathrm{eff}}/T_{\mathrm{beam}}$ m^2/K	E_{thresh} V/m/MHz
LOW	100	350	1000	1.4×10^{-9}	4000	7.2×10^{-10}
MID 1	350	1050	143	2.3×10^{-9}	844	9.4×10^{-10}
MID 2	950	1760	143	2.1×10^{-9}	844	8.7×10^{-10}

Table 1: Estimated sensitivities ($A_{\mathrm{eff}}/T_{\mathrm{beam}}$, including lunar thermal emission) and signal detection threshold thresholds (V/m/MHz) for SKA observation bands. SKA1-MID treats both 64 MeerKAT and 190 SKA antennas identically, while SKA2 uses 1,500 SKA antennas.

PoS(AASKA14)144

standard-model cross-sections of Gandhi et al. (1998). For the lunar surface, we use the self-affine model of Shepard et al. (1995), implementing it by randomly deviating the lunar surface on length scales corresponding to the characteristic size of the radiation transmission region on the surface.

Due to the broadband nature of the signal, the optimal frequency range for lunar observations with the SKA can only be determined by simulating all frequency bands up to the highest-frequency band for which beamforming across the entire Moon is practical. We therefore consider the SKA1-LOW band as well as the two lowest-frequency receivers for SKA1-MID (SKA1-MID 1 and 2). As described in Sec. 2, the sensitivity of these SKA bands to lunar signals must be calculated relative to the lunar thermal emission which, at approximately 225 K (Troitskij & Tikhonova 1970), is brighter than the sky at frequencies above approximately 168 MHz. Averaged over the SKA1-LOW band, both the lunar emission and the sky background will have similar strengths, so the SKA1-LOW sensitivity from Dewdney et al. (2013) is used unchanged. In the case of SKA1-MID, the lunar emission will dominate, and is added to the system temperature. The resulting sensitivities are given in Table 1, where the signal detection thresholds correspond to 10 times the effective beam root-mean-square noise voltage σ, under the assumption that the observational requirements — dedispersion, triggering, RFI discrimination, etc. — are satisfied.

We perform these simulations with a simple 10σ threshold, and with additional restrictions on the pulse amplitude, polarisation and point of origin on the Moon, as described below. Based on the results, we determine the effective aperture to cosmic rays and neutrinos, and the resolution in the energy and arrival direction of a detected cosmic ray. We neglect any constraints on the interaction geometry that could be obtained by measuring the radio pulse spectrum, or (for SKA2) the radiation pattern over the Earth, which would further improve the resolutions shown here. The prospects for determining the mass of a detected cosmic ray (as in e.g. Abraham et al. 2010b) are effectively nil.

3.1 Aperture

The geometric apertures for detection of cosmic rays and neutrinos are shown in Fig. 3. The general trends are as expected from previous work: observing at lower frequency results in a larger aperture, due to the larger beaming angle, while observing at higher frequency results in sensitivity down to lower energies, due to the more intense radio emission. Unlike cosmic rays, neutrinos may interact deep in the lunar regolith, which preferentially attenuates higher-frequency radio emission,

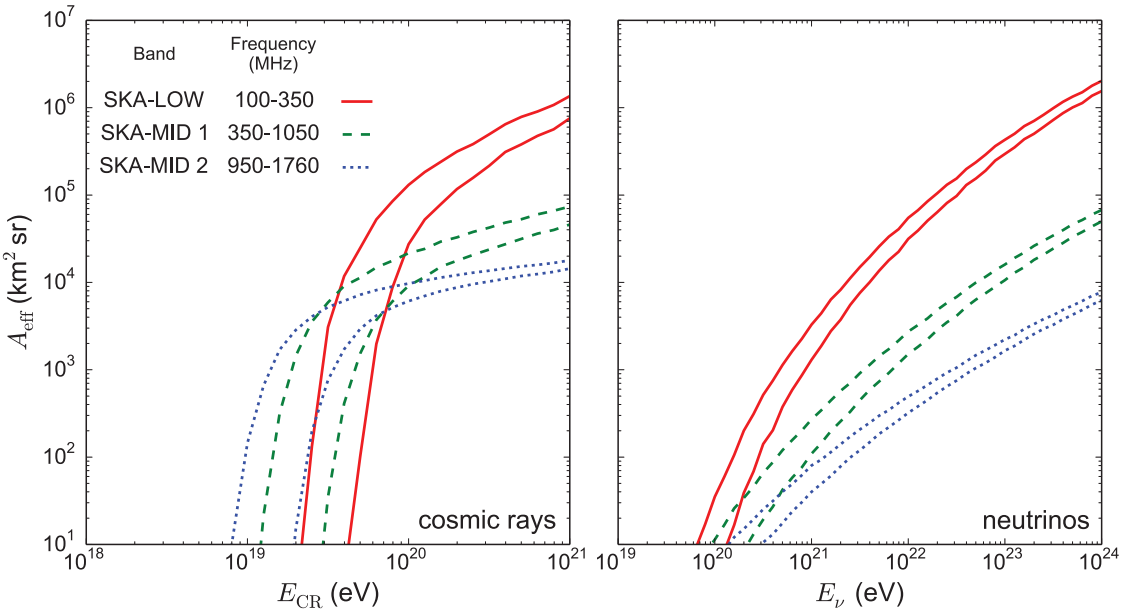

Figure 3: Effective apertures $A_{\rm eff}$ of the SKA to cosmic rays (left) and neutrinos (right). In each case, SKA1 is given by the lower curves, and SKA2 by the upper curves. Estimates for SKA1-LOW and SKA1-MID are shown, indicating the frequency range of each band.

so lower frequencies are more strongly prefered for the detection of neutrinos.

Fig. 4 (left) shows the expected energy-dependent detection rates for cosmic rays, based on these apertures and an empirical parameterisation of the UHE cosmic ray spectrum from Abraham et al. (2010a). The expected detection rates for SKA2 are much greater than those for SKA1: SKA2 at low frequencies would detect 165 cosmic rays above the 56 EeV threshold used for anisotropy studies by Abraham et al. (2008a) per year of observing time, although such a long exposure would require a parallel beamforming capacity to allow commensal observations.

3.2 Energy resolution

The interaction of a UHE particle can be observed as a radio pulse with an amplitude up to some energy-dependent maximum value, which is attained under an optimal observing geometry. A detected pulse therefore establishes a minimum bound on the energy of the original particle. A soft upper bound is placed by the steep cosmic ray spectrum: a low-amplitude pulse is more likely to originate from a lower-energy particle than from a rarer higher-energy particle observed in a suboptimal geometry. These two bounds allow us to establish an effective energy resolution for detected cosmic rays (similar to Scholten & van Vliet 2008).

Fig. 4 (right) shows the expected energy distribution of detected cosmic rays for all pulses in the range 10σ–12σ, with further constrains on location and polarisation (see Sec. 3.3). This effectively shows the expected posterior distribution in energy E for a cosmic ray detected with an amplitude uncertainty of $\pm 1\sigma$. Taking the root-mean-square variation in $\ln E$ gives values in the range 0.27–0.37 for the different frequency bands, with little variation from this with the different

PoS(AASKA14)144

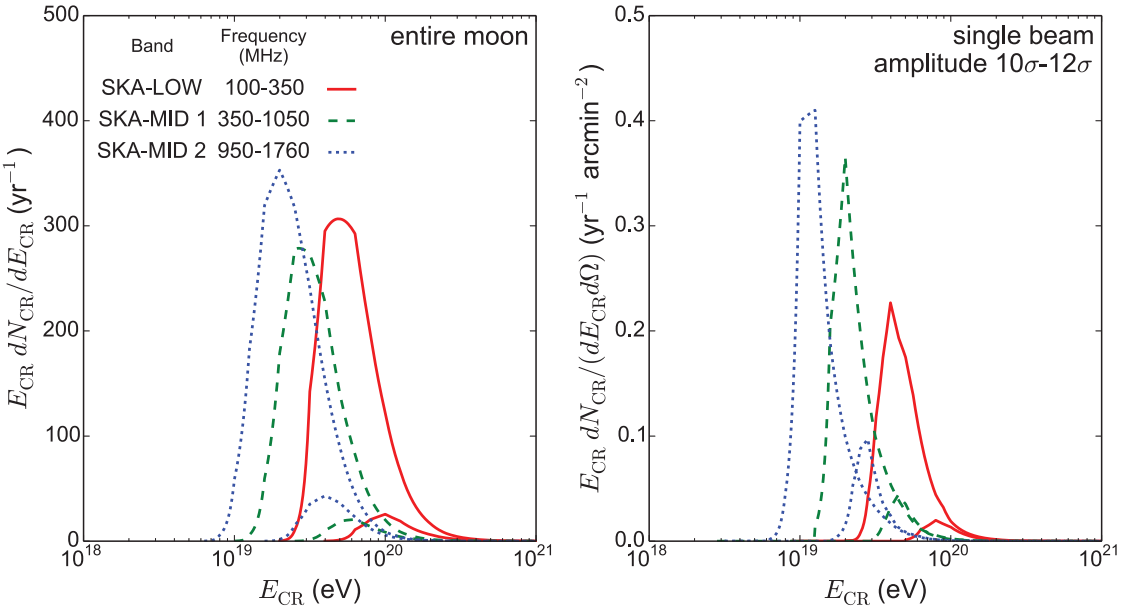

Figure 4: Expected energy distribution of detected cosmic rays, assuming the parameterised cosmic ray spectrum from Abraham et al. (2010a), for (left) coverage of the entire Moon, using the apertures from Fig. 3, and (right) for a single beam placed 0.97 lunar radii from the centre of the Moon, requiring detected events to have an amplitude in the range 10σ–12σ and polarisation within 5° of radial to the Moon. The latter curve is also scaled by the beam size, and acts as a measure of the energy resolution attainable with these constraints on the position, amplitude and polarisation of the pulse. As in Fig. 3, the lower curves correspond to SKA1, and the upper curves correspond to SKA2. With the scaling and normalisation used here, the number of detected cosmic rays is proportional to the area under the curve.

flux models considered in Sec. 4.1. This corresponds to an uncertainty factor in E of 1.31–1.45, which provides an indicative figure for the energy resolution. Note that, since the derivation of this value assumes the cosmic ray spectrum to be known, it is not a true energy resolution suitable for detecting spectral features, but it may still be used for selecting events for directional studies (see Sec. 4.3).

3.3 Angular resolution

The field of view from which a cosmic ray can be detected is an annular zone around the Moon, as shown in Fig. 5 (left). The origin of a cosmic ray within this zone can be determined from the point of origin of the pulse on the Moon and the polarisation of the pulse, which is linear and radial to the particle cascade. We perform simulations with restrictions placed on these characteristics in order to determine the angular resolution with which this origin can be determined.

We assume the origin of a detected pulse to be localised with an effective baseline of 10 km, a diameter which contains 90–95% of the antennas of SKA1-LOW or SKA1-MID. In practice, for a 10σ pulse, it should be possible to do better than this by measuring the phase slope across the array, but further improvements have only a small marginal benefit. For the purposes of the simulation, based on this baseline and the central frequency of each band, we require the pulse to

PoS(AASKA14)144

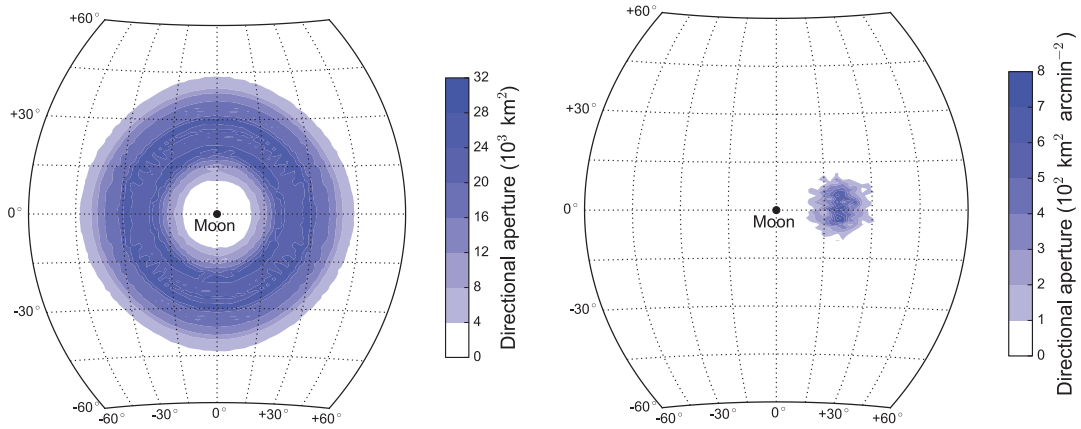

Figure 5: Directional aperture at 10^{20} eV to cosmic rays around the Moon with SKA1-LOW for (left) coverage of the entire Moon, and (right) for a single beam placed 0.97 lunar radii from the centre of the Moon, with the polarisation required to be within 5° of radial to the Moon, scaled by the beam size. The former indicates the field of view, while the latter indicates the angular resolution in the cosmic ray arrival direction, given these constraints on the detected pulse.

originate within a disk of radius 0.55 arcmin for SKA1-LOW, 0.17 arcmin for SKA1-MID band 1, or 0.08 arcmin for SKA1-MID band 2. Detectable pulses are expected to be clustered near the limb of the Moon; for our simulation, we place this disk 0.97 lunar radii from the centre of the Moon.

The polarisation of a pulse can be measured with a precision of $1/n_\sigma$ radians, where $n_\sigma \geq 10$ is the pulse amplitude. In our simulation we require the pulse polarisation to fall within the range $\pm 5°$, corresponding to a pulse near the detection threshold and neglecting the improved precision possible with pulses of larger amplitude. We centre the accepted polarisation range on an orientation radial to the Moon, which is the expected polarisation for a majority of detected pulses.

With the above constraints on the point of origin and polarisation angle of the pulse, our simulation produces directional apertures as shown in Fig. 5 (right). In Fig. 6, we show the root-mean-square variation of the directional aperture around the mean, in directions radial and tangential to the Moon. For comparison, we also show an estimate of the magnetic deflection of cosmic rays, based on the localised excesses seen by previous experiments (see Sec. 4.3).

4. Initial prospects with SKA1

Here we consider the objectives that could be addressed with 1,000 hours of lunar observations with SKA1. The primary objective of these initial observations would be to verify the lunar Askaryan technique by successfully detecting a lunar particle cascade, but there are also prospects to study the spectrum and anisotropy of UHE cosmic rays, and to search for UHE neutrinos.

4.1 Verification of the technique

The prospects for a successful detection depend on the UHE cosmic ray spectrum, which is not well constrained. Table 2 shows the expected number of detections in 1,000 hours of observations

PoS(AASKA14)144

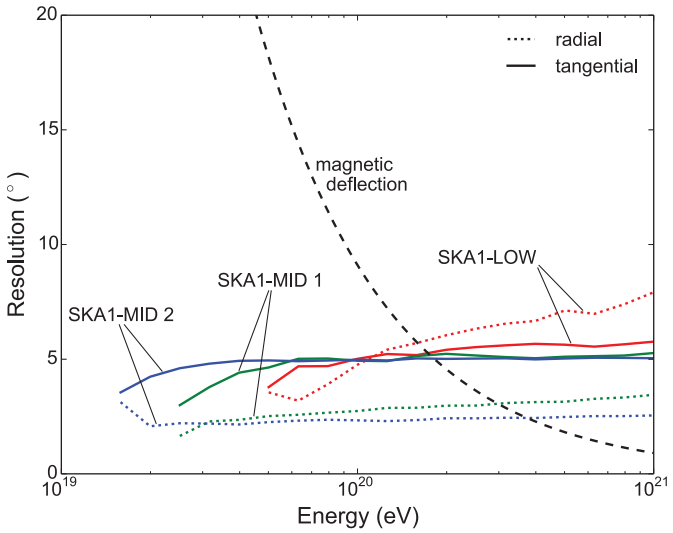

Figure 6: Angular resolution in cosmic ray arrival direction, calculated as the root-mean-square variation of the aperture distribution as in Fig. 5 (right), in the directions radial and tangential to the Moon. The results shown are for SKA1, but the results for SKA2 for the corresponding bands are similar. The dashed line corresponds to the derived deflection of cosmic rays in magnetic fields if the observed large-scale anisotropies in cosmic ray arrival directions are due to individual nearby sources; see Sec. 4.3 for details. At the energy of most expected detections (see Fig. 4, left), this magnetic deflection dominates the angular resolution.

	Scenario A (100% Fe) $E_{\max} = 10^{21}$ eV, $\alpha = 1.8$		Scenario B (100% Si) $E_{\max} = 10^{20.5}$ eV, $\alpha = 1.6$	
$L_{\min} =$	0 Mpc	27 Mpc	0 Mpc	27 Mpc
LOW	9.4	5.1	2.8	0.7
MID 1	4.9	3.8	2.6	1.6
MID 2	7.8	6.8	5.4	4.4

Table 2: Expected numbers of cosmic rays detected in 1,000 hours of observations with SKA1, under different scenarios considered by Taylor et al. (2011): for sources emitting a pure iron or silicon composition, with best-fit values for the cutoff energy $E_{\max}$ and spectral index α. A local void of radius $L_{\min}$ is assumed to exist in the distribution of cosmic ray sources; $L_{\min} = 0$ corresponds to a continuous distribution. SKA1-LOW shows the most potential for discriminating between scenarios, while SKA1-MID band 2 is most reliable for detecting at least one event, to allow verification of the technique.

for different theoretically-motivated models of the UHE cosmic ray spectrum from Taylor et al. (2011). SKA1-MID 2 would most reliably detect at least one cosmic ray, with 4.4 events expected in the most pessimistic case, or a 99% chance of one or more detections.

4.2 Measuring the cosmic ray spectrum

As seen in Table 2, the number of expected cosmic ray detections depends on the assumed model for the cosmic ray spectrum, which offers the prospect of discriminating between these models. The greatest discriminating power is provided by SKA1-LOW: neglecting the case of a

PoS(AASKA14)144

local void in cosmic ray sources, SKA1-LOW would detect an expected 9.4 events in scenario A and 2.8 events in scenario B. These are not an exhaustive sample of possible models, and synergies with other cosmic-ray experiments are complicated by the requirement to establish a common energy scale, but this indicates that event counts, even with no energy resolution, provide some discriminating power.

Further analysis of the prospects for spectral measurements will require more detailed simulations of the radio spectra of detected pulses, and the information they provide on the original particle energy. It is likely that SKA2, with its capacity for higher-significance detections and thus more precise measurements of the radio spectrum, will be particularly important in this application.

4.3 Identification of cosmic ray sources

The two major UHE cosmic ray detectors, the Pierre Auger Observatory (in the southern hemisphere) and Telescope Array (in the northern hemisphere), have each detected a large-scale localised excess of UHE cosmic rays. Catalogued events from the Pierre Auger Observatory (Abreu et al. 2010) show an excess aligned with the nearby active galactic nucleus Centaurus A, with 13 UHE cosmic rays detected within an 18° radius of this object against an isotropic expectation of 3.2 (Abreu et al. 2011), although the significance of the result has been reported to decline in more recent data (Revenu et al. 2013). Similarly, Telescope Array observed 19 UHE cosmic rays against an isotropic expectation of 4.5 originating within 20° of R.A. 146.7° Dec. +43.2°, although this hotspot does not correspond to any similarly prominent astronomical object (Abbasi et al. 2014). Increased statistics would allow these two positions to be identified or excluded as sources of UHE cosmic rays.

Taken at face value, and allowing for the relative directional exposure of each detector, these results imply Centaurus A to be responsible for 7.4% of the all-sky UHE cosmic ray flux, and the hotspot detected by Telescope Array to be responsible for a further 9.5%. Lunar observations to test these possible sources could be scheduled while the Moon is closest to them: 10% of the lunar orbit is within 36° of Centaurus A, or within 28° of the hotspot, which would allow 1,000 hours of targeted observations to be carried out over 2–3 years. At these angular offsets from the Moon, the directional aperture for SKA1-LOW is 5–15 times the all-sky average aperture, depending on energy, allowing a correspondingly increased exposure. Consequently, lunar observations with SKA1-LOW would expect to detect 5.3 (1.6) cosmic rays originating from Centaurus A or 9.4 (3.1) from the hotspot in scenarios A (B) considered above; these numbers are in addition to those listed in Table 2. We have neglected here the case of a local void in cosmic ray sources, because the existence of a single resolvable source implies that it lies within the local universe. We have also assumed the putative source to have the same spectrum as the cosmic ray background, which is pessimistic, because cosmic rays from a nearby source should be less affected by GZK attenuation.

From the mean energy and root-mean-square angular deviation of the events detected around Centaurus A, normal random magnetic deflection of $8.3^\circ \times (10^{20}\mathrm{eV}/E)$ would be sufficient to explain the distribution of the excess. The corresponding figure for the northern-hemisphere hotspot is $9.9^\circ \times (10^{20}\mathrm{eV}/E)$. We use the mean of these two similar values to obtain the empirical representation of the magnetic deflection shown in Fig. 6. By taking this simple dependence on energy, we have effectively assumed the cosmic ray composition to remain constant in this energy range.

PoS(AASKA14)144

Using the above assumptions, we perform a simple simulation to determine the expected significance of a detection of the hotspot, as the easier to test of the two putative sources. We apply an increased weight to higher-energy cosmic rays, using as our figure of merit the sum over detected cosmic rays

$$M = \sum \theta^{-2}\,\Omega^{-1} \tag{4.1}$$

where θ is the angular displacement of a detected cosmic ray from the putative source and

$$\Omega = \pi\,(\sigma_{\mathrm{rad}}^2 + \sigma_{\mathrm{tan}}^2 + \sigma_{\mathrm{mag}}^2) \tag{4.2}$$

is a field of view based on the angular displacements in Fig. 6. To represent the limited energy resolution, when determining the weighting factor Ω we randomise the energy with a log-normal distribution with half-width 0.37 in $\ln E$, taking the pessimistic end of the range in Sec. 3.2.

Performing this simulation for both scenarios considered above, with an isotropic background only, we find that a threshold of $M = 5000$ rad^{-2} will be exceeded in $< 5\%$ of trials in either case, allowing a 95%-confidence result. With the hotspot included as described above, this threshold is exceeded in 76% of trials in scenario A, but only 16% of trials with the softer spectrum of scenario B. This simplified simulation indicates that the lunar observations considered here have the potential to provide independent confirmation of the hotspot in cosmic rays, but this will depend on the behaviour of their spectrum. More sophisticated simulations (e.g. those of Rouillé d'Orfeuil et al. 2014) would find the expected results across a wider range of scenarios.

4.4 Detection of UHE neutrinos

UHE neutrinos are expected to be produced by GZK interactions as well as, in exotic top-down models, directly alongside UHE cosmic rays. Top-down models generally predict much harder neutrino spectra than those from GZK interactions, and are commonly constrained by limits on the fluxes of UHE neutrinos and photons (e.g. Abraham et al. 2009; Gorham et al. 2010). Families of predicted neutrino spectra for both cases are shown in Fig. 7, alongside existing and projected limits. No band of SKA1 is sensitive to the GZK neutrino flux, but some top-down models could be detected with SKA1-LOW. Due to the extreme energies of the neutrinos predicted in this case, they should be clearly distinguishable from the expected lower-energy cosmic rays, so even a single detection could provide strong support for a top-down model.

4.5 Effects of reduced SKA performance

The primary characteristic of the SKA which determines its performance in this application is the point-source sensitivity, proportional (for the detection of coherent pulses) to the product of the collecting area and the beamformed bandwidth. If this sensitivity is decreased by 50%, the expected detection rates in Table 2 are reduced typically by a factor ~ 3, requiring a corresponding increase in observing time to compensate. If the observing time is held at 1,000 hours, the identification of a cosmic ray source considered in Sec. 4.3 is unlikely to be significant, and there is effectively zero capacity to discriminate between the model spectra considered in Sec. 4.2. Even the probability of achieving a single successful detection of a cosmic ray to verify the technique, as described in Sec. 4.1, is decreased to $\lesssim 80\%$ for a pessimistic cosmic ray spectrum. The only goal not strongly affected is the testing of exotic top-down neutrino models described in Sec. 4.4, as the stringency

PoS(AASKA14)144

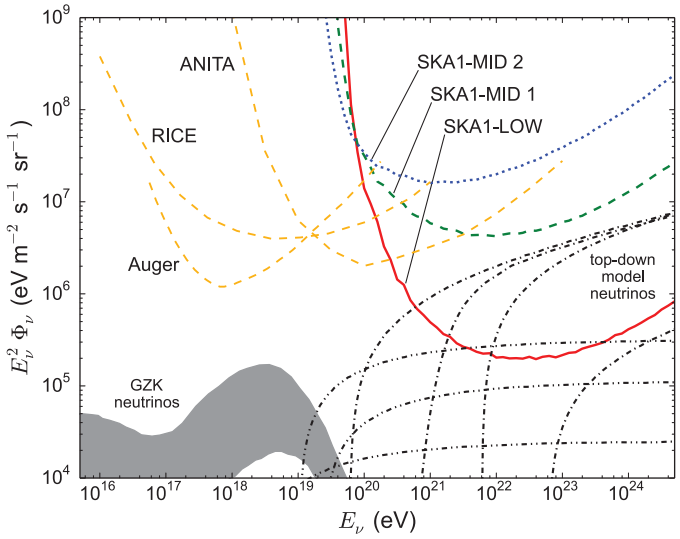

Figure 7: Projected 90%-confidence limits on the UHE neutrino flux from 1,000 hours of observations with different bands of SKA1. Predictions are shown for the neutrino flux from GZK interactions (Allard et al. 2006, shaded), and from top-down models involving the production of UHE neutrinos from kinks (Lunardini & Sabancilar 2012, dash-dotted) and cusps (Berezinsky et al. 2011, dot-dash-dotted) in cosmic strings. Limits set by other experiments — the Pierre Auger Observatory (Abreu et al. 2013), RICE (Kravchenko et al. 2012) and ANITA (Gorham et al. 2010, 2012) — are also shown.

of the limits in this extremely high-energy regime depends more on raw observation time than on radio sensitivity.

5. Conclusion

The use of the lunar Askaryan technique offers a new way to study ultra-high-energy cosmic rays. Compared to other forms of radio astronomy, this technique has an unusual set of technical requirements, with full-time-resolution beamforming, real-time dedispersion and a sophisticated buffering and triggering algorithm required in order to detect a nanosecond-scale radio pulse from a particle interaction in the Moon. A thorough understanding of these challenges, and the means to overcome them, has been developed through a series of previous experiments.

SKA1 will be the first radio telescope with sufficient sensitivity to successfully apply this technique to detect an ultra-high-energy cosmic ray. It will also probe a range of astrophysical models: neutrinos from exotic top-down models, and the flux and anisotropy at the top end of the cosmic ray spectrum. Finally, it will develop this technique for use with SKA2, which will act as an even larger detector for studying the most extreme particles in the universe.

References

Abbasi et al. (Telescope Array Coll.), 2014, ApJ, 790, L21
Abraham, J. et al. (Pierre Auger Coll.), 2007, Science, 318, 938

PoS(AASKA14)144

Abraham, J. et al. (Pierre Auger Coll.), 2008a, Astropart. Phys., 29, 188
Abraham, J. et al. (Pierre Auger Coll.), 2008b, Phys. Rev. Lett., 101, 061101
Abraham, J. et al. (Pierre Auger Coll.), 2009, Astropart. Phys., 31, 399
Abraham, J. et al. (Pierre Auger Coll.), 2010, Phys. Lett. B, 685, 239
Abraham, J. et al. (Pierre Auger Coll.), 2010, Phys. Rev. Lett., 104, 091101
Abreu, P. et al. (Pierre Auger Coll.), 2010, Astropart. Phys., 34, 314
Abreu, P. et al. (Pierre Auger Coll.), 2011, JCAP, 6, 22
Abreu, P. et al. (Pierre Auger Coll.), 2013, Proc. 33rd ICRC, Rio de Janeiro
Abu-Zayyad, T. et al. (Telescope Array Coll.), 2012, ApJ, 757, 26
Allard, D., Ave, M., Busca, N. et al., 2006, JCAP, 9, 005
Alvarez-Muñiz, J., Marqués, E., Vázquez, R.A., & Zas, E., 2006, Phys. Rev. D, 74, 023007
Amsler, C., Doser, M., Antonelli, M. et al., 2008, Phys. Lett., B667, 1
Askaryan, G.A., 1962, Sov. Phys. JETP, 14, 441
Beresnyak, A.R., Dagkesamanskii, R.D., Zheleznykh, I.M. et al., 2005, Astron. Rep., 49, 127
Berezinsky, V., Sabancilar, E. & Vilenkin, A., 2011, Phys. Rev. D, 84, 085006
Bray, J.D., Ekers, R.D., James, C.W. et al., 2011, Proc. 32nd ICRC, Beijing
Bray, J.D., 2013, PhD thesis, University of Adelaide
Buitink, S., Scholten, O., Bacelar, J. et al., 2010, A&A, 521, A47
Connolly, A., Thorne, R.S. & Waters, D., 2011, Phys. Rev. D, 83, 113009
Cooper-Sarkar, A., Mertsch, P. & Sarkar, S., 2011, JHEP, 2011, 42
Dagkesamanskii, R.D. & Zheleznykh, I.M., 1989, Sov. Phys. JETP Lett., 50, 259
Dewdney, P.E., Turner, W., Millenaar, R. et al., 2013, "SKA1 System Baseline Design", Document number SKA-TEL-SKO-DD-001
Gaisser, T.K., 2006, J. Phys.: Conf. Ser., 47, 15
Gayley, K.G., Mutel, R.L. & Jaeger, T.R., 2009, ApJ, 706, 1556
Gandhi, R., Quigg, C., Reno, M.H. & Sarcevic, I., 1998, Phys. Rev. D, 58, 039009
Gorham, P.W., Hebert, C.L., Liewer, K.M. et al., 2004, Phys. Rev. Lett., 93, 041101
Gorham, P.W. et al. (ANITA Coll.), 2009, Astropart. Phys., 32, 10
Gorham, P.W. et al. (ANITA Coll.), 2010, Phys. Rev. D, 82, 022004
Gorham, P.W. et al. (ANITA Coll.), 2012, Phys. Rev. D, 85, 049901
Greisen, K., 1966, Phys. Rev. Lett., 16, 748
Hankins, T.H., Ekers, R.D. & O'Sullivan, J.D., 1996, MNRAS, 283, 1027
Hillas, A.M., 1984, Ann. Rev. Astron. Astrophys., 22, 425
Jaeger, T.R., Mutel, R.L. & Gayley, K.G., 2010, Astropart. Phys., 43, 293
James, C.W., Ekers, R.D., Alvarez-Muñiz, J. et al., 2010, Phys. Rev. D, 81, 042003
James, C.W. & Protheroe, R.J., 2009, Astropart. Phys., 30, 318
Jeong, Y.S., Reno, M.H. & Sarcevic, I., 2012, Astropart. Phys., 35, 383
Kravchenko, I., Hussain, S., Seckel, D. et al., 2012, Phys. Rev. D, 85, 062004
Lunardini, C. & Sabancilar, E., 2012, Phys. Rev. D, 86, 085008
McFadden, R.A., Ekers, R.D. & Bray, J.D., 2011, Proc. 32nd ICRC, Beijing
Miočinović, P., Field, R.C., Gorham, P.W. et al., 2006, Phys. Rev. D, 74, 043002
Protheroe, R.J., Donea, A.-C. & Reimer, A., 2003, Astropart. Phys., 19, 559
Revenu, B. et al. (Pierre Auger Coll.), 2013, Proc. 33rd ICRC, Rio de Janeiro

PoS(AASKA14)144

Rouillé d'Orfeuil, B., Allard, D., Lachaud, C. et al., 2014, A&A, 567, A81
Scholten, O., Bacelar, J., Braun, R. et al., 2006, Astropart. Phys, 26, 219
Scholten, O. & van Vliet, A.R., 2008, JCAP, 6, 15
Settimo, M. et al. (Pierre Auger Coll.), 2012, Eur. Phys. J. Plus, 127, 87
Shepard, M.K., Brackett, R.A. & Arvidson, R.E., 1995, J. Geophys. Res., 100, 11709
Singh, K., Mevius, M., Scholten, O. et al. (LOFAR Coll.), 2012, NIMA, 664, 171
Spencer, R.E., Macfarlane, A., Mills, O. & Piccirillo, L., 2010, Proc. 10th EVN Symposium, 097
Stappers, B. et al. (Pulsar SWG), 2014, "Enabling Beamforming and Time Domain Processing for SKA1_LOW", Document number ECP140006
Takahashi, Y. et al. (JEM-EUSO Coll.), 2009, New J. Phys., 11, 065009
Taylor, A.M., Ahlers, M. & Aharonian, F.A., 2011, Phys. Rev. D, 84, 105007
ter Veen, S., Buitink, S., Falcke, H. et al., 2010, Phys. Rev. D, 82, 103014
Torres, D.F. & Anchordoqui, L.A., 2004, Rep. Prog. Phys., 67, 1663
Troitskij, V.S. & Tikhonova, T.V., 1970, Izv. Vyssh. Uchebn. Zaved. Radiofiz., 13, 1272
Zatsepin, G. & Kuzmin, V., 1966, Pis'ma Zh. Eksp. Teor. Fiz., 4, 114

PoS(AASKA14)144

PROCEEDINGS OF SCIENCE

Precision measurements of cosmic ray air showers with the SKA

T. Huege[1], J.D. Bray[2], S. Buitink[3], R. Dallier[4,5], R.D. Ekers[6], H. Falcke[3,7], C.W. James[8], L. Martin[4,5], B. Revenu[4], O. Scholten[9] and F.G. Schröder[1]

[1]*KIT;* [2]*Univ. of Southampton;* [3]*Radboud Univ. Nijmegen;* [4]*Subatech, Nantes;* [5]*Station de radioastronomie de Nançay;* [6]*CSIRO ATNF;* [7]*ASTRON;* [8]*Univ. of Erlangen-Nuremberg;* [9]*Univ. of Groningen*

E-mail: tim.huege@kit.edu

Supplemented with suitable buffering techniques, the low-frequency part of the SKA can be used as an ultra-precise detector for cosmic-ray air showers at very high energies. This would enable a wealth of scientific applications: the physics of the transition from Galactic to extragalactic cosmic rays could be probed with very high precision mass measurements, hadronic interactions could be studied up to energies well beyond the reach of man-made particle accelerators, air shower tomography could be performed with very high spatial resolution exploiting the large instantaneous bandwith and very uniform instantaneous *u-v* coverage of SKA1-LOW, and the physics of thunderstorms and possible connections between cosmic rays and lightning initiation could be studied in unprecedented levels of detail. In this article, we describe the potential of the SKA as an air shower radio detector from the perspective of existing radio detection efforts and discuss the associated technical requirements.

Advancing Astrophysics with the Square Kilometre Array,
June 8-13, 2014
Giardini Naxos, Sicily, Italy

PoS(AASKA14)148

1. Introduction

One hundred years after the discovery of cosmic radiation, the sources of the highest energy particles are still a mystery. Previously observed correlations of cosmic-ray arrival directions with catalogued positions of active galactic nuclei at energies beyond $5 \cdot 10^{19}$ eV (Abraham et al. 2007) have by now diminished in significance (Abreu et al. 2010). At the same time, there are indications for a mixed proton-iron composition up to the highest energies (Abraham et al. 2010), but better detectors will be needed to test this scenario. Also, the transition from Galactic to extragalactic cosmic rays, expected at energies between 10^{17} and 10^{19} eV, is not yet understood (Blasi 2013), in spite of decades of intense research.

One reason for these many unsolved questions is the fact that there are a great many unknown factors acting together: the physics of the acceleration at the sources, the mass composition of the particle distributions from which cosmic rays are accelerated, the propagation through the little-known extragalactic and Galactic magnetic fields, and in fact even the mass composition of the high-energy particles arriving at Earth. The last problem is due to the fact that cosmic rays at very high energies arrive with an extremely low flux. They can thus only be detected with ground-based detectors which do not measure the actual primary particle, but an extensive air shower initiated by it. Determining the mass of the primary cosmic ray from such indirect measurements, prone to uncertainties of hadronic interactions at energies beyond the reach of man-made accelerators, has proven to be very difficult. Those detection techniques that do provide a good determination of the primary particle mass, in particular detection of optical fluorescence light, suffer from low duty cycles, limiting the badly needed statistics.

Radio detection of cosmic rays has the potential to provide high-precision mass-sensitive measurements with nearly 100% duty cycle, as has recently been demonstrated with LOFAR (Schellart et al. 2013). The low-frequency part of the SKA will allow us to push these measurements to a new level, measuring cosmic-ray masses and studying hadronic interaction physics with unprecedented precision up to energies as high as 10^{19} eV, cf. Fig. 1. However, a number of technical requirements need to be fulfilled to use the SKA for cosmic-ray air shower detection. In the following, we briefly lay out the current state of the field of radio detection of cosmic rays, then describe the science goals for air shower detection with the SKA and afterwards describe the technical requirements that would need to be fulfilled to reach these science goals.

2. The state of cosmic ray radio detection

Driven by the prospect of a precise and cost-effective detection technique for cosmic-ray air showers which measures with a duty cycle of nearly 100%, digital radio detection of cosmic rays has matured from small prototype installations to experiments spanning several km^2 in the past decade (Huege 2014). Experiments such as LOPES (Falcke et al. 2005) and CODALEMA (Torres-Machado et al. 2013) have delivered the proof of principle for radio detection of cosmic rays, and have established the basic properties of the radio signal. The emission can be coherent up to GHz frequencies for specific geometries and is generally coherent in the frequency range up to $\sim$ 100 MHz. It is dominated by radiation associated with the time-variation of geomagnetically induced transverse currents. In parallel with the experimental activities, sophisticated Monte

PoS(AASKA14)148

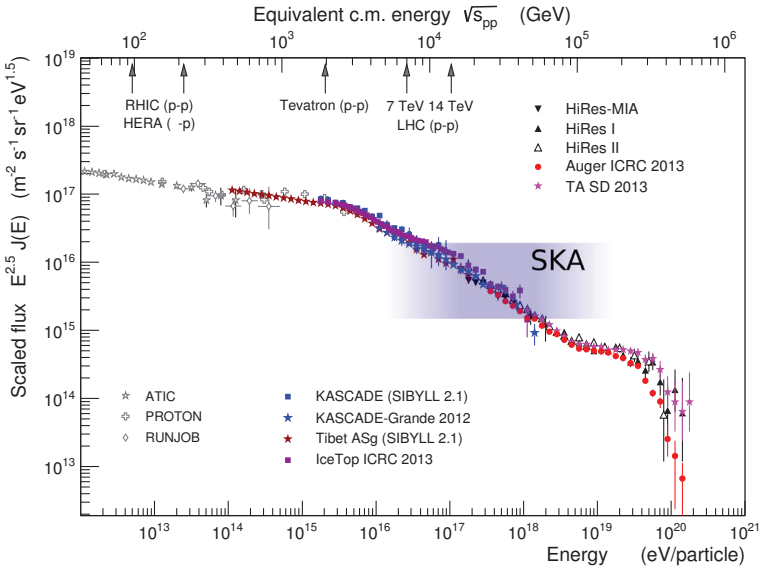

Figure 1: The energy spectrum of the highest energy cosmic rays as updated and adapted from Engel et al. (2011). The energy range accessible to SKA1-LOW is indicated. This is the region in which the transition from Galactic to extragalactic cosmic rays is expected. Mass-composition-sensitive measurements with the SKA could determine the details of the transition with unprecedented accuracy. In addition, hadronic interactions can be studied up to energies much higher than those reachable with the Large Hadron Collider (LHC).

Carlo simulation codes (Alvarez-Muñiz et al. 2012; Huege et al. 2012; Marin & Revenu 2012) as well as macroscopic models (Scholten et al. 2008) have been developed to study the radio emission physics. Today, we have a very good understanding of the emission mechanisms, down to sub-dominant contributions such as the time-varying charge-excess radiation (Askaryan effect; Askaryan 1962). Building on this understanding, it has been demonstrated that all important properties of extensive air showers can be deduced from radio measurements, in particular the arrival direction, energy, and mass-sensitive observables for individual cosmic rays (Apel et al. 2014).

The major players in the current generation of experiments are the Auger Engineering Radio Array (AERA; Fuchs et al. 2012) and LOFAR. AERA is focused at scaling the detection technique to much larger areas and thus energies and has by now instrumented an area of ~ 6 km^2 with a sparse array of autonomous antenna stations. One of its goals is to cross-check the mass sensitivity of the radio measurements directly with the Auger Fluoresence Detectors. In contrast, LOFAR features a very dense core of radio antennas over an area of ~ 0.2 km^2 allowing us to study the radio emission of individual air showers with much higher precision than any other experiment. It has recently been demonstrated that with these high-precision measurements, LOFAR is able to gather very high precision information on the mass of individual cosmic rays (Buitink et al. 2014). A comparison of the scales and antenna densities of AERA, LOFAR and SKA1-LOW is shown in Fig. 2. With its very dense, uniformly instrumented core and its large instantaneous bandwidth, SKA1-LOW will be able to study individual air showers even more precisely than LOFAR, opening up the potential to address a number of long-standing questions in cosmic ray physics.

PoS(AASKA14)148

2.1 LSS/NenuFAR as a pathfinder

The project "NenuFAR" — the LOFAR Super Station (LSS) in Nançay (Zarka et al. 2012) — will be installed at the Nançay Radio Observatory, which hosts a regular international LOFAR station (FR606), completely surrounded by the 57 radio detection stations of CODALEMA as well as 43 particle detectors. This environment provides a unique opportunity to test and improve techniques for cosmic ray radio detection, acting as a pathfinder for air shower detection with the SKA.

LSS/NenuFAR consists of an extension to the standard LOFAR local station including 96 mini-arrays of 19 crossed-dipole antennas (hereafter MA_{19}), analogically phased in the $\sim 10-87$ MHz frequency window. These will be connected to the 96 dual-polarization receivers of the LOFAR backend. The 3648 dipoles will be positioned within a circle of 400 m diameter (~ 5 LOFAR station diameters). NenuFAR will be used both as part of the LOFAR network in LSS, and as a standalone instrument with large instantaneous sensitivity ($\sim 2\times$ LOFAR's core) and wide frequency band. Standalone measurements will be possible due to a dedicated receiver, allowing NenuFAR to be used *simultaneously* in both modes, within the instantaneous field of view of the beam formed at the MA_{19} scale (10 to 50° from 10 to 87 MHz). As beam-forming is disfavoured for cosmic ray detection (see section 4), a dedicated acquisition channel will be implemented to extract the signal from one single antenna of each of the 96 MA_{19} before beam-forming, and an external trigger input will be available to trigger NenuFAR by CODALEMA during regular astronomical operation. Beside this first cosmic ray detector operating mode, during dedicated standalone observations, NenuFAR can also be used in a "radio fly's eye" mode by phasing each of the 96 MA_{19} in a different direction of the sky, thus covering the 2π sr with 96 beams. The sensitivity will be 19 times higher than that reached with single antennas. The large field of view of each MA_{19} ensures an overlap between adjacent beams and thus detection of distant showers by several MA_{19}.

3. Science goals for air shower detection with SKA1-LOW

3.1 Ultra-high resolution mass composition

The SKA will have a densely populated core of > 1 km^2, which makes it an excellent observatory for air showers in the energy regime of 10^{16} eV to 10^{19} eV. The detection rate will be $\sim 25,000$ showers above 10^{17} eV per year. Because of the steep drop-off of the cosmic-ray flux as a function of energy, there will be several hundreds of showers per year above 10^{18} eV. Below 10^{17} eV, the radio detection efficiency of current-generation experiments is small because the signal strength becomes weak compared to the Galactic background noise. At the SKA, however, the sensitivity at low energies can be improved by beam-forming techniques and by exploiting the wide instantaneous bandwidth. Consequently, the detection threshold can likely be lowered well below 10^{17} eV.

The energy range of 10^{17}–10^{19} eV probably harbors the transition from a Galactic to an extragalactic cosmic-ray component. While some models interpret the ankle feature in the all-particle spectrum at $10^{18.2}$ eV as the transition energy, other models predict that the extragalactic component already becomes dominant at lower energies. In the latter class of models the ankle is caused

PoS(AASKA14)148

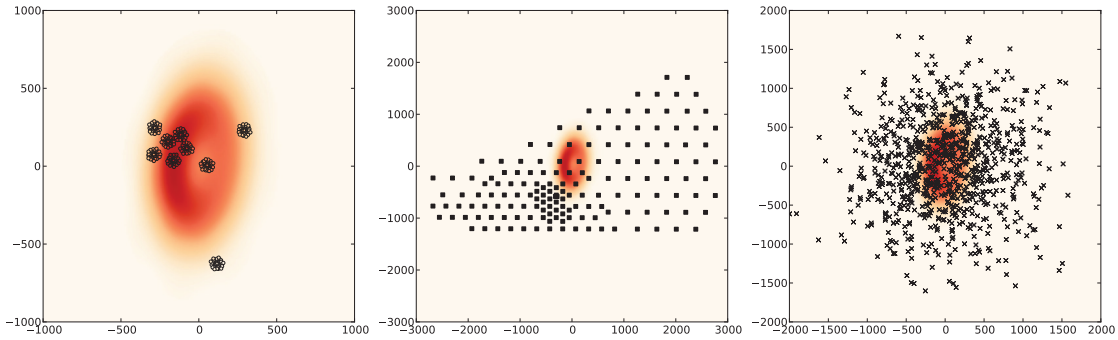

Figure 2: Antenna layouts for several observatories (axes denote distances in metres). The antennas of LOFAR (left) are clustered in stations of 48 antennas each. Six of these stations lie in a dense core, additional stations are positioned at increasing distances. The background colors represent the radio footprint of an air shower simulated with CoREAS. The shape is elongated because the shower has a zenith angle of 55°. The same footprint is shown in comparison with the AERA layout (middle), and the layout of SKA1-LOW (right), approximated by a Gaussian distribution of 866 antennas (i.e. a very small fraction of the actual number of antennas in the dense core). Both LOFAR and SKA sample the footprint with hundreds of antennas simultaneously, but at SKA the coverage is much more uniform. The instrumented area of SKA1-LOW is slightly smaller than AERA.

by pair production of cosmic rays on the cosmic microwave and infrared background radiation (Berezinskii & Grigoreva 1988). Furthermore, there may be a secondary Galactic component due to very energetic sources or re-acceleration of cosmic rays in the Galactic halo. To investigate how and at what energy the transitions between components take place, accurate mass composition measurements are crucial.

The main observable to study the mass of the primary particles initiating extensive air showers is the atmospheric depth (in g/cm^2) at which an air shower has evolved to its maximum particle number, the "shower maximum" $X_{\rm max}$. LOFAR has demonstrated that with a dense antenna array, $X_{\rm max}$ can be measured with a precision below 20 g/cm^2 by fitting simulated two-dimensional radio power profiles to the data (Buitink et al. 2014). For showers with a particularly advantageous geometry, i.e. when the radiation profile on the ground is sufficiently well-sampled by antennas, the precision can be as good as 8 g/cm^2. More advanced analysis techniques that incorporate the polarization, spectrum and arrival time of the radio pulse will improve the reconstruction quality further. We expect that the application of such advanced techniques to the SKA will yield a mean precision of 10 g/cm^2. This is significantly better than the $X_{\rm max}$ resolution achievable to date: The highest quality $X_{\rm max}$ measurements are made with Fluorescence Detectors which achieve a resolution of ~ 20 g/cm^2, but with a duty cycle of only $\sim 10\%$. With the $X_{\rm max}$ precision achievable with the SKA, it will be possible to measure the energy spectra of individual chemical elements or groups of elements with unprecedented precision. In particular, it will be possible to cleanly separate proton showers from other nuclei. This will allow the identification of the different source components between the second knee and the ankle.

3.2 Hadronic physics beyond the LHC scale

The longitudinal development of air showers depends on several important features of hadronic

PoS(AASKA14)148

interactions which are currently known only up to the energy that can be reached by the LHC ($\sim 10^{13}$ eV equivalent center-of-mass energy). Above this energy, several hadronic interaction models exist that provide extrapolated values based on phenomenological models, but the correct values cannot be calculated from first principles. The predictions that advanced models like QGSJET-II, EPOS and SYBILL make for shower properties such as $X_{\rm max}$ and the muon-to-electron ratio diverge at super-LHC energies. Ulrich et al. (2011) made a detailed study on how various shower properties are affected by the p-air cross section, the secondary particle multiplicity, the elasticity and the muon charge ratio. Accurate air shower measurements can thus probe hadronic physics at energies unreachable by man-made accelerators.

A clean separation of protons from other cosmic ray particles (with a contamination at percent-level) allows measurement of the inclusive cross section for protons (p-air). At the Pierre Auger Observatory, the p-air cross section has been derived at a center-of-mass energy of $5.7 \cdot 10^{13}$ eV, by measuring the tail of the $X_{\rm max}$ distribution for protons (Abreu et al. 2012). Their systematic uncertainty is dominated by the helium contamination of the shower sample. The SKA can measure $X_{\rm max}$ with a higher resolution than Auger, allowing more precise measurements of the p-air cross section.

In addition, it is expected that radio measurements can provide more information on the longitudinal development than only the depth of the shower maximum. The radiation is strongest when the number of charged particles in the shower changes most rapidly, at an early stage in the shower development. In general, the observed radio pulse contains information on all stages of the shower development. Near the shower core the signal is relativistically compressed but at larger distances the pulses are wider and the information is conserved. The information can be extracted by using a near-field imaging technique, for which the SKA is exceptionally well-suited due to its excellent instantaneous coverage of the *u*-*v* plane (cf. Fig. 2). Thus, "air shower tomography" can be used to extract more hadronic parameters. For example, the distance between the first interaction and the shower maximum depends critically on the secondary multiplicity and elasticity. Furthermore, shower imaging can be used to probe air-shower universality up to very high precision.

3.3 Wide-band air shower measurements extending to high frequencies

SKA1-LOW will have an instantaneous bandwidth of 50 to 350 MHz, which is much broader than current air-shower radio detectors. LOPES and AERA measure showers at frequencies below 100 MHz. LOFAR has both a low frequency (30–80 MHz) and high frequency window (110–250 MHz), but these cannot currently operate simultaneously. Recently, LOFAR has observed radio Cherenkov rings of $\sim$ 100 m radius in the high band (Nelles et al. 2014). CROME (Šmída et al. 2014) has detected GHz emission from air showers which was also found at typical distances of $\sim$ 100 m to the shower core. The ANITA balloon experiment (Hoover et al. 2010) has picked up signals at frequencies from 300 to 900 MHz which are also likely to come from air showers; from their polarization mode it can be inferred that the signals do not originate from neutrino cascades inside the Antarctic ice, but are reflected off the ice surface and must originate from the atmosphere.

Broad-band air shower measurements at the SKA can test air shower radiation models at frequencies up to 350 MHz with an unprecedented level of detail. Although various models are converging towards similar results at low frequencies, uncertainties remain at high frequencies. One reason for this is that the shorter wavelengths probe the shower on smaller scales and are

PoS(AASKA14)148

thus more sensitive to small variations. In combination with the very uniform *u*-*v* coverage, measurements up to 350 MHz will thus provide a tremendous advantage for the shower tomography technique described above. Another reason for an increased complexity of the radio emission at high frequencies is that additional emission mechanisms may start to contribute, like synchrotron radiation or molecular bremsstrahlung. A thorough understanding of the high-frequency emission will provide a calibration in particular for the events measured by ANITA.

3.4 Cosmic rays and lightning initiation

The severe thunderstorms that occur on the Australian mainland provide an additional research opportunity. It has been shown that atmospheric electric fields can influence the air-shower emission mechanism (Buitink et al. 2007). The strong fields present inside thunderclouds accelerate the shower electrons and positrons, and can strongly amplify the radio pulse. These effects also leave an imprint on the polarization, which can be used to infer the direction and possibly the strength of the atmospheric electric field. This provides a unique way to study the otherwise hard-to-measure electric fields in thunderclouds.

In addition, potential connections between air shower physics and lightning initiation can be studied with the SKA: air showers leave behind a trail of ionization electrons. Under normal weather conditions the electrons quickly attach to oxygen molecules, but inside electric fields they start to drift. If the field strength is high enough, the electrons will gain enough energy to ionize their environment further and create an electron avalanche. This process, known as runaway breakdown, may play an important role in the initiation of lightning (Gurevich & Karashtin 2013). Radio arrays have the distinct advantage that they can measure both the air shower signal and the electrical processes in a thunderstorm. With the SKA, the possible connection between air showers and lightning initiation can be explored with an unprecedented level of detail.

Furthermore, the SKA can be used as a lightning mapping array which can make high-resolution 3D movies of the initiation of lightning and the electrical processes ultimately leading to a discharge. Because of the low attenuation of radio waves, the SKA can also search for high-altitude phenomena like sprites and discharges to the ionosphere.

4. Technical requirements

Detection of extensive air showers with SKA1-LOW has specific technical requirements which are significantly different from those of astronomical observations. The signal emitted by cosmic-ray air showers is a very short transient with a length of ten nanoseconds up to a few hundred nanoseconds. As the emission source is in the atmosphere, there is no dispersion to longer timescales as is the case for astronomical sources. It is also important to note that the area on the ground which is illuminated typically has a diameter of only 500 to 1000 metres.

As the arrival direction of the cosmic-ray particles is unknown a priori, detection of air shower pulses in pre-beamformed data imaging only a limited field-of-view is strongly disfavoured. Instead, the best strategy is to read out the raw waveform information of individual antennas. These raw waveform data need to be read out with high-resolution sampling of at least 700 MSPS and with a dynamic range of at least 8 effective bits above the noise level, i.e. ideally a raw dynamic range of 12 bits. The high dynamic range is needed because the amplitude of the radio signal

PoS(AASKA14)148

emitted by air showers varies very significantly over the illuminated area and in addition increases linearly with the primary particle energy. Thus, the waveform data has to be read out before any channelising or conversion to 2-bit dynamic range.

As also the arrival time is unknown a priori, it is necessary to buffer the individual antenna raw data for the time that is needed to wait for an external trigger to initiate read-out and storage of the raw waveform data. This external trigger would need to be provided by an array of particle detectors that would need to be installed within SKA1-LOW. Particle detectors are used routinely for cosmic ray shower detection and they do not generate any RFI, as has been successfully demonstrated at LOFAR. The time-scale on which the trigger signal could be delivered, i.e. the required buffer depth, would be of order a few milliseconds.

To limit the memory needed for buffering, only a small fraction of the SKA1-LOW antennas would need to be buffered. Buffering antennas on a grid of order a few meters would be sufficient.[1] Once the trigger signal arrives, it is also possible to only read out a subset of the buffers: using information about the location of the illuminated area (the so-called "shower core"), only antennas in an area with a radius of 500 to 1000 metres need to be read out and stored. To keep the buffer scheme flexible, the best strategy would be to feed all individual antenna signals to a central location and provide a defined interface to access the unchannelised raw data of a user-defined subset of antennas for buffering purposes.

In summary, EAS detection with the SKA would require: access to high dynamic range raw waveform data of a user-defined subset of individual antennas, buffering capability for this subset of antennas for a few milliseconds, a particle detector array for triggering purposes, and the ability to read out and store the raw waveform data of a subset of buffered antennas upon reception of a trigger signal. Suitable approaches will be tested on a reduced scale at NenuFAR, as mentioned in section 2.1.

5. Conclusions

The SKA provides a unique opportunity to perform cosmic ray studies with very high precision using radio measurements in the 50-350 MHz band. In particular, ultra-high precision measurements of the mass composition of cosmic rays in the energy range from 10^{17} to 10^{19} eV would allow us to address the long-standing problem of the transition from Galactic to extragalactic cosmic rays. Furthermore, hadronic interactions could be studied up to energies well beyond the reach of the LHC, in particular if high-frequency air shower tomography using near-field imaging is exploited. Lastly, the physics of thunderstorms and the possible connections between cosmic ray physics and lightning initiation can be studied with the SKA. To enable these studies, millisecond-scale buffering of the high-sampling-rate, high dynamic range raw data of a subset of the individual SKA1-LOW antennas in the dense core is required.

[1] Consequently, even in the early deployment of SKA1-LOW with 50% of the design sensitivity air shower detetection would be feasible to its full potential, provided that the instantaneous *u-v* coverage of the buffered subset of antennas remains similar.

PoS(AASKA14)148

References

Abraham, J., Abreu, P., Aglietta, M. et al. (Pierre Auger Coll.), 2007, Science, 318, 938
Abraham, J., Abreu, P., Aglietta, M. et al. (Pierre Auger Coll.), 2010, Phys. Rev. Lett., 104, 091101
Abreu, P., Aglietta, M., Ahn, E.J. et al. (Pierre Auger Coll.), 2010, Astropart. Phys., 34, 314
Abreu, P., Aglietta, M., Ahn, E.J. et al. (Pierre Auger Coll.), 2012, Phys. Rev. Lett., 109, 062002
Alvarez-Muñiz, J., Carvalho, W.R. & Zas, E., 2012, Astropart. Phys., 35, 325
Apel, W.D., Arteaga-Velazquez, J.C., Bähren, L. et al. (LOPES Coll.), 2014, Phys. Rev. D., 90, 062001
Askaryan, G.A., 1962, Sov. Phys. JETP, 14, 441
Berezinskii, V. & Grigoreva, S., 1988, A&A, 199, 1
Blasi, P., 2013, Nucl. Phys. B Proc. Suppl., 239, 140
Buitink, S., Apel, W.D., Asch, T. et al. (LOPES Coll.), 2007, A&A, 467, 385
Buitink, S., Corstanje, A., Enriquez, J.E. et al., 2014, Phys. Rev. D., 90, 082003
Engel, R., Heck, D. & Pierog, T., 2011, Annu. Rev. Nucl. Part. Sci., 61, 467
Falcke, H., Apel, W.D., Badea, A.F. et al. (LOPES Coll.), 2005, Nature, 435, 313
Fuchs, B. for the Pierre Auger Coll., 2012, NIMA, 692, 93
Gurevich, A.V. & Karashtin, A.N., 2013, Phys. Rev. Lett., 110, 185005
Hoover, S., Nam, J., Gorham, P.W. et al. (ANITA Coll.), 2010, Phys. Rev. Lett., 105, 151101
Huege, T., 2014, Brazilian J. Phys., 44, 520
Huege, T., Ludwig, M. & James, C.W., 2012, AIP Conf. Proc., 1535, 128
Marin, V. & Revenu, B., 2012, NIMPA, 662, 171
Nelles, A., Schellart, P., Buitink, S. et al. (LOFAR Coll.), 2014, Astropart. Phys., in press, doi:10.1016/j.astropartphys.2014.11.006
Schellart, P., Nelles, A., Buitink, S. et al. (LOFAR Coll.), 2013, A&A, 560, A98
Scholten, O., Werner, K. & Rusydi, F., 2008, Astropart. Phys., 29, 94
Šmída, R., Werner, F., Engel, R. et al. (CROME Coll.), 2014, Phys. Rev. Lett., 113, 221101
Torres-Machado, D. for the CODALEMA Coll., 2013, Proc. 33rd ICRC, Rio de Janeiro
Ulrich, R., Engel, R. & Unger, M., 2011, Phys. Rev. D, 83, 054026
Zarka, P., Girard, J.N., Tagger, M. et al. (LSS team), 2012, Proc. SF2A-2012, 687–694

PoS(AASKA14)148